frontiers | Research Topics

Molecular biomarkers in the prediction, diagnosis, and prognosis of neurodegenerative diseases

Edited by
Yuzhen Xu, Jun Xu, Shenfeng Qiu and Wen-Jun Tu

Published in
Frontiers in Aging Neuroscience
Frontiers in Neuroscience

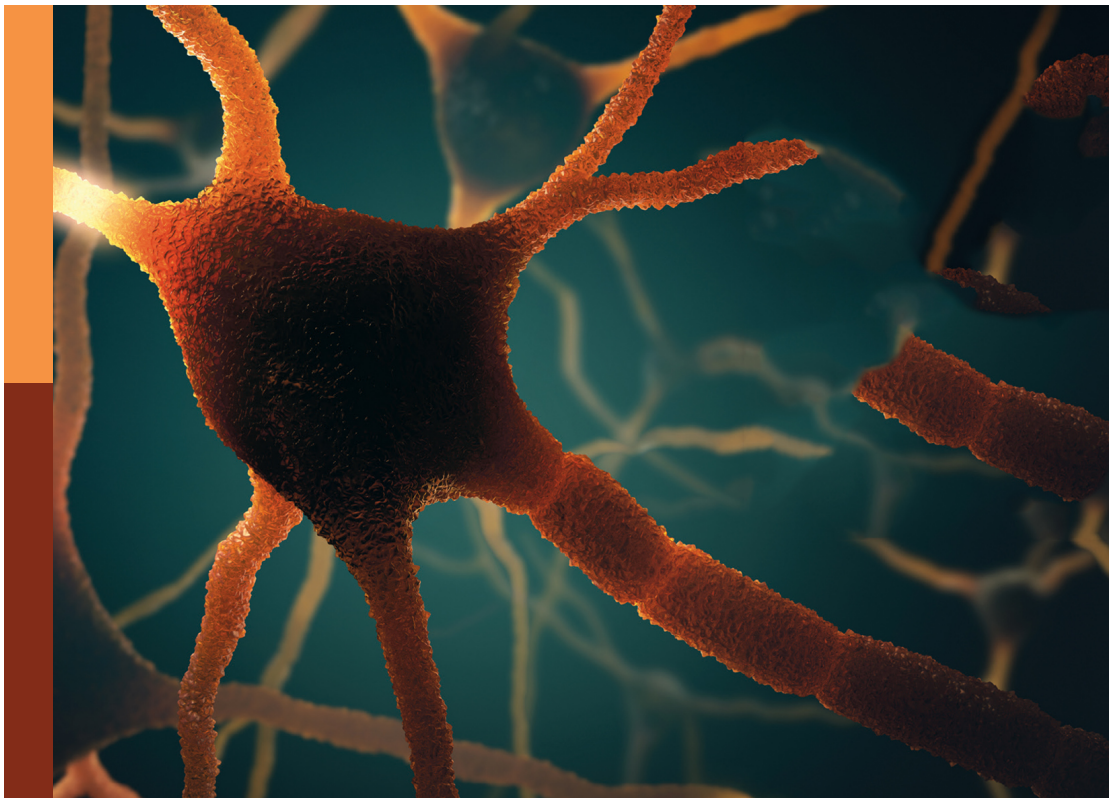

FRONTIERS EBOOK COPYRIGHT STATEMENT

The copyright in the text of individual articles in this ebook is the property of their respective authors or their respective institutions or funders. The copyright in graphics and images within each article may be subject to copyright of other parties. In both cases this is subject to a license granted to Frontiers.

The compilation of articles constituting this ebook is the property of Frontiers.

Each article within this ebook, and the ebook itself, are published under the most recent version of the Creative Commons CC-BY licence. The version current at the date of publication of this ebook is CC-BY 4.0. If the CC-BY licence is updated, the licence granted by Frontiers is automatically updated to the new version.

When exercising any right under the CC-BY licence, Frontiers must be attributed as the original publisher of the article or ebook, as applicable.

Authors have the responsibility of ensuring that any graphics or other materials which are the property of others may be included in the CC-BY licence, but this should be checked before relying on the CC-BY licence to reproduce those materials. Any copyright notices relating to those materials must be complied with.

Copyright and source acknowledgement notices may not be removed and must be displayed in any copy, derivative work or partial copy which includes the elements in question.

All copyright, and all rights therein, are protected by national and international copyright laws. The above represents a summary only. For further information please read Frontiers' Conditions for Website Use and Copyright Statement, and the applicable CC-BY licence.

ISSN 1664-8714
ISBN 978-2-8325-2786-3
DOI 10.3389/978-2-8325-2786-3

About Frontiers

Frontiers is more than just an open access publisher of scholarly articles: it is a pioneering approach to the world of academia, radically improving the way scholarly research is managed. The grand vision of Frontiers is a world where all people have an equal opportunity to seek, share and generate knowledge. Frontiers provides immediate and permanent online open access to all its publications, but this alone is not enough to realize our grand goals.

Frontiers journal series

The Frontiers journal series is a multi-tier and interdisciplinary set of open-access, online journals, promising a paradigm shift from the current review, selection and dissemination processes in academic publishing. All Frontiers journals are driven by researchers for researchers; therefore, they constitute a service to the scholarly community. At the same time, the *Frontiers journal series* operates on a revolutionary invention, the tiered publishing system, initially addressing specific communities of scholars, and gradually climbing up to broader public understanding, thus serving the interests of the lay society, too.

Dedication to quality

Each Frontiers article is a landmark of the highest quality, thanks to genuinely collaborative interactions between authors and review editors, who include some of the world's best academicians. Research must be certified by peers before entering a stream of knowledge that may eventually reach the public - and shape society; therefore, Frontiers only applies the most rigorous and unbiased reviews. Frontiers revolutionizes research publishing by freely delivering the most outstanding research, evaluated with no bias from both the academic and social point of view. By applying the most advanced information technologies, Frontiers is catapulting scholarly publishing into a new generation.

What are Frontiers Research Topics?

Frontiers Research Topics are very popular trademarks of the *Frontiers journals series*: they are collections of at least ten articles, all centered on a particular subject. With their unique mix of varied contributions from Original Research to Review Articles, Frontiers Research Topics unify the most influential researchers, the latest key findings and historical advances in a hot research area.

Find out more on how to host your own Frontiers Research Topic or contribute to one as an author by contacting the Frontiers editorial office: frontiersin.org/about/contact

Molecular biomarkers in the prediction, diagnosis, and prognosis of neurodegenerative diseases

Topic editors
Yuzhen Xu — Tongji University, China
Jun Xu — Capital Medical University, China
Shenfeng Qiu — University of Arizona, United States
Wen-Jun Tu — Chinese Academy of Medical Sciences and Peking Union Medical College, China

Citation
Xu, Y., Xu, J., Qiu, S., Tu, W.-J., eds. (2023). *Molecular biomarkers in the prediction, diagnosis, and prognosis of neurodegenerative diseases*. Lausanne: Frontiers Media SA. doi: 10.3389/978-2-8325-2786-3

Table of contents

06 Editorial: Molecular biomarkers in the prediction, diagnosis, and prognosis of neurodegenerative diseases
Yuzhen Xu, Shenfeng Qiu, Wenjun Tu and Jun Xu

09 Elevated homocysteine levels, white matter abnormalities and cognitive impairment in patients with late-life depression
Huarong Zhou, Xiaomei Zhong, Ben Chen, Qiang Wang, Min Zhang, Naikeng Mai, Zhangying Wu, Xingxiao Huang, Xinru Chen, Qi Peng and Yuping Ning

18 Sexual dimorphism in the relationship between *Forkhead-Box P2* and BMI with cognitive deficits in schizophrenia
Mi Yang, Ying Cui, Mei Xue, Mattew T. Forster, Xiaoe Lang, Meihong Xiu, Zezhi Li and Xiangyang Zhang

27 Is liquid biopsy mature enough for the diagnosis of Alzheimer's disease?
Xun Gong, Hantao Zhang, Xiaoyan Liu, Yi Liu, Junlin Liu, Funmilayo O. Fapohunda, Peng Lü, Kun Wang and Min Tang

49 Crosstalk between regulatory non-coding RNAs and oxidative stress in Parkinson's disease
Hantao Zhang, Xiaoyan Liu, Yi Liu, Junlin Liu, Xun Gong, Gang Li and Min Tang

69 Abnormal regional homogeneity in right caudate as a potential neuroimaging biomarker for mild cognitive impairment: A resting-state fMRI study and support vector machine analysis
Yujun Gao, Xinfu Zhao, JiChao Huang, Sanwang Wang, Xuan Chen, Mingzhe Li, Fengjiao Sun, Gaohua Wang and Yi Zhong

77 A neglected neurodegenerative disease: Adult-onset globoid cell leukodystrophy
Guode Wu, Zhenhua Li, Jing Li, Xin Li, Manxia Wang, Jing Zhang, Guangyao Liu and Pengfei Zhang

92 Altered regional homogeneity of spontaneous brain activity in patients with toothache: A resting-state functional magnetic resonance imaging study
Jun Yang, Yi Shao, Bin Li, Qiu-Yue Yu, Qian-Min Ge, Biao Li, Yi-Cong Pan, Rong-Bin Liang, Shi-Nan Wu, Qiu-Yu Li and Yu-Lin He

103 Blunted superior temporal gyrus activity to negative emotional expression after mindfulness-based cognitive therapy for late-life depression
Weijian Liu, Hui Li, Xiao Lin, Peng Li, Ximei Zhu, Sizhen Su, Jie Shi, Lin Lu, Jiahui Deng and Xinyu Sun

114 Elevated serum nuclear factor erythroid 2-related factor 2 levels contribute to a poor prognosis after acute supratentorial intracerebral hemorrhage: A prospective cohort study
Chuan-Liu Wang, Xin-Jiang Yan, Cheng-Liang Zhang and Yan-Wen Xu

127 The identification of the key residues E829 and R845 involved in transient receptor potential melastatin 2 channel gating
Yuhuan Luo, Shijia Chen, Fei Wu, Chunming Jiang and Marong Fang

136 Association of cognitive function with Neurofilament light chain in the aqueous humor of human eye
Jianhao Bai, Zhongqi Wan, Minli Wang, Xue Wu, Tianyu Wang, Yuanyuan Zhang, Yawen Xue, Hong Xu and Qing Peng

147 Potential blood biomarkers for chronic traumatic encephalopathy: The multi-omics landscape of an observational cohort
Xintong Ge, Mengtian Guo, Meimei Li, Shishuang Zhang, Junlian Qiang, Luoyun Zhu, Lu Cheng, Wenzhu Li, Yan Wang, Jinwen Yu, Zhenyu Yin, Fanglian Chen, Wen Tong and Ping Lei

160 Identifying crosstalk genetic biomarkers linking a neurodegenerative disease, Parkinson's disease, and periodontitis using integrated bioinformatics analyses
Shaonan Hu, Simin Li, Wanchen Ning, Xiuhong Huang, Xiangqiong Liu, Yupei Deng, Debora Franceschi, Anthony Chukwunonso Ogbuehi, Bernd Lethaus, Vuk Savkovic, Hanluo Li, Sebastian Gaus, Rüdiger Zimmerer, Dirk Ziebolz, Gerhard Schmalz and Shaohong Huang

188 Proteomic profiling reveals the potential mechanisms and regulatory targets of sirtuin 4 in 1-methyl-4-phenyl-1,2,3,6-tetrahydropyridine-induced Parkinson's mouse model
Huidan Weng, Wenjing Song, Kangyue Fu, Yunqian Guan, Guoen Cai, En Huang, Xiaochun Chen, Haiqiang Zou and Qinyong Ye

212 Signature of miRNAs derived from the circulating exosomes of patients with amyotrophic lateral sclerosis
Yang-Fan Cheng, Xiao-Jing Gu, Tian-Mi Yang, Qian-Qian Wei, Bei Cao, Yang Zhang, Hui-Fang Shang and Yong-Ping Chen

226 Association between bilirubin levels with incidence and prognosis of stroke: A meta-analysis
Kun Zhao, Rui Wang, Rongrong Chen, Jialei Liu, Qing Ye, Kai Wang and Juebao Li

236 Mechanisms of abnormal adult hippocampal neurogenesis in Alzheimer's disease
Yujuan Zhou, Xu Wang, Yingying Liu, Yulu Gu, Renjun Gu, Geng Zhang and Qing Lin

248 Serum glial cell line-derived neurotrophic factor (GDNF) a potential biomarker of executive function in Parkinson's disease
Shu-Yan Tong, Rui-Wen Wang, Qian Li, Yi Liu, Xiao-Yan Yao, De-Qin Geng, Dian-Shuai Gao and Chao Ren

257 Analysis of gene expression profiles in Alzheimer's disease patients with different lifespan: A bioinformatics study focusing on the disease heterogeneity
Ji Zhang, Xiaojia Li, Jun Xiao, Yang Xiang and Fang Ye

269 Pattern of prefrontal cortical activation and network revealed by task-based and resting-state fNIRS in Parkinson's disease's patients with overactive bladder symptoms
Miaomiao Hou, Xiaowei Mao, Yarong Wei, Jiali Wang, Yu Zhang, Chen Qi, Lu Song, Ying Wan, Zhihua Liu, Jing Gan and Zhenguo Liu

279 Six mitophagy-related hub genes as peripheral blood biomarkers of Alzheimer's disease and their immune cell infiltration correlation
Kun Zhao, Yinyan Wu, Dongliang Zhao, Hui Zhang, Jianyang Lin and Yuanwei Wang

frontiers | Frontiers in Neuroscience

TYPE Editorial
PUBLISHED 08 June 2023
DOI 10.3389/fnins.2023.1226675

Check for updates

OPEN ACCESS

EDITED AND REVIEWED BY
Einar M. Sigurdsson,
New York University, United States

*CORRESPONDENCE
Jun Xu
✉ neurojun@126.com

RECEIVED 22 May 2023
ACCEPTED 26 May 2023
PUBLISHED 08 June 2023

CITATION
Xu Y, Qiu S, Tu W and Xu J (2023) Editorial: Molecular biomarkers in the prediction, diagnosis, and prognosis of neurodegenerative diseases. *Front. Neurosci.* 17:1226675. doi: 10.3389/fnins.2023.1226675

COPYRIGHT
© 2023 Xu, Qiu, Tu and Xu. This is an open-access article distributed under the terms of the Creative Commons Attribution License (CC BY). The use, distribution or reproduction in other forums is permitted, provided the original author(s) and the copyright owner(s) are credited and that the original publication in this journal is cited, in accordance with accepted academic practice. No use, distribution or reproduction is permitted which does not comply with these terms.

Editorial: Molecular biomarkers in the prediction, diagnosis, and prognosis of neurodegenerative diseases

Yuzhen Xu[1], Shenfeng Qiu[2], Wenjun Tu[3] and Jun Xu[4]*

[1]Department of Rehabilitation, The Second Affiliated Hospital of Shandong First Medical University, Taian, China, [2]Basic Medical Sciences, University of Arizona College of Medicine-Phoenix, Phoenix, AZ, United States, [3]Peking Union Medical College, Chinese Academy of Medical Sciences, Beijing, China, [4]Department of Neurology, China National Clinical Research Center for Neurological Diseases, Beijing Tiantan Hospital, Capital Medical University, Beijing, China

KEYWORDS

molecular mechanism, biomarkers, prediction, diagnosis, prognosis, neurodegenerative diseases

Editorial on the Research Topic
Molecular biomarkers in the prediction, diagnosis, and prognosis of neurodegenerative diseases

Neurodegenerative diseases including Alzheimer's disease (AD), Parkinson's disease (PD), stroke, mental illness and amyotrophic lateral sclerosis (ALS) are characterized by the progressive loss of structure and function of neurons in the central nervous system and has posed a significant burden on individuals, families, and societies worldwide. There has been a growing interest in the identification and utilization of molecular biomarkers as valuable tools in the prediction, diagnosis, and prognosis of neurodegenerative diseases. Molecular biomarkers encompass various biological molecules, such as proteins, nucleic acids, lipids, metabolites, and extracellular vesicles, which can be measured in biological samples, including blood, cerebrospinal fluid (CSF), and even urine. These biomarkers exhibit specific alterations in their expression patterns or structural characteristics that are associated with the underlying neurodegenerative processes (Hansson, 2021). In addition, the emergence of advanced technologies, such as genomics, proteomics, metabolomics, and high-throughput screening platforms, has enabled the identification and validation of numerous molecular biomarkers with potential clinical applications. In recent years, the field of molecular biomarkers has emerged as a promising avenue for enhancing the prediction, diagnosis, and prognosis of neurodegenerative diseases. This topic explores the potential of molecular biomarkers and their transformative role in improving patient outcomes.

AD is usually a slow onset, progressive neurodegenerative disease that accounts for about 70% of all dementias (Zvěrová, 2019). The main reason for the significant difference in lifespan of AD patients may be due to the presence of genetic and clinical heterogeneity in AD, which deserves further studies. To investigate the potential drivers, Zhang et al. identified differentially expressed genes (DEGs) that affect the lifespan of AD patients by bioinformatics analysis. The results suggest genes that exhibit parallel regulatory orientations in cancer, inflammation and AD, and their use as promising targets may help in developing prevention and treatment strategies in further studies. Zhou Y. et al. summarized the pathogenic mechanism of hippocampal neuroregeneration in AD, which will help to

further identify the targets regulating neurogenesis and provide new promising therapeutic approaches. Gong et al. described is a rapid, low-cost and simple method for the diagnosis of AD, namely liquid biopsy, which is maturing and improving. In addition, Gao et al. found in a resting-state functional MRI (fMRI) study that abnormal regional homogeneity in the right caudate nucleus is a potential neuroimaging biomarker for the diagnosis of mild cognitive impairment. Interestingly, the study by Bai et al. found a negative correlation between human ocular atrial aqueous (AH) neurofilament light chain and MMSE, suggesting that AH could play a role in screening individuals at high risk for AD.

PD is the second most common neurodegenerative disease after AD. A study by Tong et al. found that decreased serum Glial cell line-derived neurotrophic factor (GDNF) concentrations in PD patients were associated with impaired executive function, and that a complex synergistic mechanism between GDNF and HVA may partially explain the executive dysfunction in PD patients. Overactive bladder (OAB) symptoms are a common complication in patients with PD affecting the quality of survival. Hou et al. investigated the relationship between OAB and prefrontal cortex (PFC) activation patterns and networks in PD patients using fMRI, suggesting that OAB is associated with decreased PFC function, particularly with overactivation of the left dorsolateral prefrontal cortex (DLPFC). Weng et al. used bioinformatics to predict the substrates of SIRT4 in PD, and the results showed that the peroxisome proliferator-activated receptor (PPAR) signaling pathway is one of its most promising targets, offering new possibilities for drug development in PD. Similarly, Hu et al. used bioinformatics to predict crosstalk gene biomarkers for PD and periodontitis, identifying five potential crosstalk genes namely FMNL1, MANSC1, PLAUR, RNASE6 and TCIRG1, suggesting immunological involvement in the association of the two diseases.

The role of exosomes and miRNAs in neurodegenerative diseases is receiving more attention (Juzwik et al., 2019). Cheng et al. identified more differential miRNAs in the microarrays of amyotrophic lateral sclerosis (ALS) patients and finally determined that hsa-miR-34a-3p, hsa-miR-1306-3p, hsa-miR-199a-3p, and hsa-miR-30b-5p were significantly different in both SOD1-mutated ALS and C9orf72-mutated ALS, suggesting their possible involvement in the mechanism of ALS pathogenesis. Although it is still controversial whether stroke is a neurodegenerative disease, it is generally accepted that stroke can cause secondary neurodegenerative lesions. In a Meta-analysis, Zhao et al. showed that serum bilirubin levels correlated with stroke severity and there were gender differences, but the current study did not clarify the causal relationship between bilirubin and stroke prognosis and further studies are still warranted. A prospective cohort study by Wang et al. found elevated levels of serum Nuclear factor erythroid 2-related factor 2 (Nrf2) in patients after cerebral hemorrhage, suggesting that Nrf2 could be used as a biomarker to predict the prognosis of cerebral hemorrhage.

Neurodegeneration is considered to be one of the etiologies of mental disorders (Wingo et al., 2022). Liu et al. found that Mindfulness-based cognitive therapy (MBCT) improved mood and facial emotion recognition in patients with late-life depression (LLD), with the left superior temporal gyrus (L-STG) playing an important role in this process. And Zhou H. et al. found that high homocysteine levels and white matter abnormalities were all involved in the development of cognitive impairment in patients with LLD. Cognitive impairment is also present in schizophrenic patients. A study by Yang et al. showed that forkhead box P2 gene polymorphism, BMI and gender are factors that influence cognitive impairment in schizophrenia, suggesting that hermaphroditism and FOXP2 rs10447760 may be involved in the effect of BMI on cognitive deficits in schizophrenic patients.

In conclusion, the integration of molecular biomarkers into clinical practice has the potential to revolutionize the field of neurodegenerative disease management. By enabling early detection, accurate diagnosis, and reliable prognostic information, these biomarkers have the capacity to facilitate personalized therapeutic interventions, improve patient outcomes, and advance our understanding of these complex and devastating disorders.

Author contributions

YX drafted the manuscript. All authors contributed to the article and approved the submitted version.

Funding

The present study was funded by the Shandong Medical and Health Technology Development Fund (202103070325), the Shandong Province Traditional Chinese Medicine Science and Technology Project (M-2022216), the Natural Science Foundation of Shandong Province (ZR2022MH124), the Nursery Project of the Shandong First Medical University Youth Science Fund Cultivation Funding Program (202201-105), the National Key Research and Development Program of China (2021YFC2500103), the National Natural Science Foundation (Grant Nos. 82071187, 81870821, and 81471215), and Beijing Youth Talent Team Support Program (2018000021223TD08).

Acknowledgments

We would like to thank all the authors who participated in the subject collection and all the reviewers who were involved in the review process, and we are very grateful to all the editors who assisted us in processing the manuscripts.

Conflict of interest

The authors declare that the research was conducted in the absence of any commercial or financial relationships that could be construed as a potential conflict of interest.

Publisher's note

All claims expressed in this article are solely those of the authors and do not necessarily represent those of their affiliated organizations, or those of the publisher,

the editors and the reviewers. Any product that may be evaluated in this article, or claim that may be made by its manufacturer, is not guaranteed or endorsed by the publisher.

References

Hansson, O. (2021). Biomarkers for neurodegenerative diseases. *Nat. Med.* 27, 954–963. doi: 10.1038/s41591-021-01382-x

Juzwik, C. A., Drake, S. S., Zhang, Y., Paradis-Isler, N., Sylvester, A., Amar-Zifkin, A., et al. (2019). microRNA dysregulation in neurodegenerative diseases: a systematic review. *Progr. Neurobiol.* 182, 101664. doi: 10.1016/j.pneurobio.2019.101664

Wingo, T. S., Liu, Y., Gerasimov, E. S., Vattathil, S. M., Wynne, M. E., Liu, J., et al. (2022). Shared mechanisms across the major psychiatric and neurodegenerative diseases. *Nat. Commun.* 13, 4314. doi: 10.1038/s41467-022-31873-5

Zvěrová, M. (2019). Clinical aspects of Alzheimer's disease. *Clinic. Biochemistr.* 72, 3–6. doi: 10.1016/j.clinbiochem.2019.04.015

frontiers | Frontiers in Aging Neuroscience

TYPE Original Research
PUBLISHED 18 July 2022
DOI 10.3389/fnagi.2022.931560

Check for updates

OPEN ACCESS

EDITED BY
Yuzhen Xu,
Shandong First Medical University,
China

REVIEWED BY
Shuwei Xie,
University of Nebraska Medical Center,
United States
Shen Li,
Tianjin Medical University, China

*CORRESPONDENCE
Yuping Ning
ningjeny@126.com

†These authors have contributed equally to this work and share first authorship

SPECIALTY SECTION
This article was submitted to Cellular and Molecular Mechanisms of Brain-aging,
a section of the journal
Frontiers in Aging Neuroscience

RECEIVED 29 April 2022
ACCEPTED 30 June 2022
PUBLISHED 18 July 2022

CITATION
Zhou H, Zhong X, Chen B, Wang Q, Zhang M, Mai N, Wu Z, Huang X, Chen X, Peng Q and Ning Y (2022) Elevated homocysteine levels, white matter abnormalities and cognitive impairment in patients with late-life depression.
Front. Aging Neurosci. 14:931560.
doi: 10.3389/fnagi.2022.931560

COPYRIGHT
© 2022 Zhou, Zhong, Chen, Wang, Zhang, Mai, Wu, Huang, Chen, Peng and Ning. This is an open-access article distributed under the terms of the Creative Commons Attribution License (CC BY). The use, distribution or reproduction in other forums is permitted, provided the original author(s) and the copyright owner(s) are credited and that the original publication in this journal is cited, in accordance with accepted academic practice. No use, distribution or reproduction is permitted which does not comply with these terms.

Elevated homocysteine levels, white matter abnormalities and cognitive impairment in patients with late-life depression

Huarong Zhou[1†], Xiaomei Zhong[1†], Ben Chen[1], Qiang Wang[1], Min Zhang[1], Naikeng Mai[2], Zhangying Wu[1], Xingxiao Huang[1], Xinru Chen[3], Qi Peng[1] and Yuping Ning[1,3,4]*

[1]Center for Geriatric Neuroscience, The Affiliated Brain Hospital of Guangzhou Medical University, Guangzhou, China, [2]Department of Neurology, The Affiliated Brain Hospital of Guangzhou Medical University, Guangzhou, China, [3]The First School of Clinical Medicine, Southern Medical University, Guangzhou, China, [4]Guangdong Engineering Technology Research Center for Translational Medicine of Mental Disorders, Guangzhou, China

Background: Cognitive impairment in late—life depression (LLD) is considered to be caused by neurodegenerative changes. Elevated homocysteine (Hcy) levels may be linked to cognitive abnormalities associated with LLD. The important role of white matter (WM) damage in cognitive impairment and pathogenesis in patients with LLD has been widely reported. However, no research has explored the interrelationships of these features in patients with LLD.

Objective: The goal of the study was to examine the interrelationship between Hcy levels, cognition, and variations in WM microstructure detected by diffusion tensor imaging (DTI) in patients with LLD.

Methods: We recruited 89 healthy controls (HCs) and 113 patients with LLD; then, we measured the plasma Hcy levels of participants in both groups. All individuals performed a battery of neuropsychological tests to measure cognitive ability. Seventy-four patients with LLD and 68 HCs experienced a DTI magnetic resonance imaging (MRI) scan.

Results: Patients with LLD showed significantly lower fractional anisotropy (FA) values in the bilateral inferior longitudinal fasciculus than those of healthy participants. Only in LLD patients was Hcy concentration inversely associated to FA values in the forceps minor. Finally, multiple regression analyses showed that an interaction between Hcy levels and FA values in the right cingulum of the cingulate cortex and right inferior longitudinal fasciculus were independent contributors to the executive function of patients with LLD.

Conclusion: Our results highlight the complex interplay between elevated homocysteine levels and WM abnormalities in the pathophysiology of LLD-related cognitive impairment, consistent with the neurodegeneration hypothesis.

KEYWORDS

late-life depression, cognitive impairment, elevated homocysteine levels, white matter abnormalities, interaction

Introduction

Late-life depression (LLD) is related to a number of neurocognitive deficits, including impaired global cognition, executive functioning, memory, attention, and visuospatial perception (Reinlieb et al., 2014; Zhang et al., 2021). It was stated that cognitive impairment in LLD is thought to be related to neurodegenerative changes (Invernizzi et al., 2021; Rhodes et al., 2021). Cognitive impairments have been identified as essential features of LLD, as they persist even after depressive symptoms have subsided and are strongly linked to poor functional and therapeutic results (Bhalla et al., 2006). Furthermore, according to the findings of two large-sample prospective cohort studies, older people with indications of depression had an estimated twofold greater risk of developing dementia (Katon et al., 2015; Kaup et al., 2016). Therefore, knowing the pathogenic cause of cognitive deficits in patients with LLD is critical for dementia prevention and for effective therapy.

According to an increasing number of studies, elevated homocysteine (Hcy) levels are associated with cognitive impairments and dementia (Setien-Suero et al., 2016; Smith and Refsum, 2016; Kim et al., 2019). Furthermore, a prospective cohort study meta-analysis identified that each 5 μmol/L rise in homocysteine level increased the comparative Alzheimer's disease risk by 15 percent (Zhou and Chen, 2019). Since both LLD and elevated Hcy levels make individuals susceptible to cognitive deficits, comorbidity between these two disorders may lead to an increased prevalence and extent of cognitive deficits. A recent community-based cohort study discovered that there was a significant inverse correlation between Hcy levels and cognitive capability in elderly people with depressive symptoms (Ford et al., 2013).

Our recent report demonstrated that LLD patients had higher plasma Hcy levels and worse cognitive performance than those of controls. Furthermore, in LLD patients, plasma Hcy concentrations were observed to be negatively related to global cognition, visual space, attention, and executive function. More interestingly, when compared to those with LLD or high Hcy concentrations alone, elderly people with both high Hcy concentrations and LLD had more severe cognitive impairment (Zhou et al., 2020). However, the mechanisms behind the additive cognitive deficits caused by LLD and increased Hcy levels are not fully understood.

Recently, numerous investigations have indicated that abnormal white matter (WM) microstructure detected by means of diffusion tensor imaging (DTI) is significantly associated with LLD (Wen et al., 2014) and cognitive impairment (Li et al., 2013). Fractional anisotropy (FA) values are susceptible to changes in WM structure, such as axonal injury, myelin loss, edema, and cell death (Tae et al., 2018). Many studies have demonstrated that the FA value of LLD patients decreases in a large variety of fiber bundles and brain areas, indicating that the WM network of patients with LLD may be damaged, potentially leading to poor connectivity with gray matter (Wen et al., 2014; Harada et al., 2018). Moreover, WM fiber bundles maintain high-speed signal connections across various areas of the brain, and diminished WM integrity may contribute to cognitive impairment and clinical symptoms in patients with LLD (Shen et al., 2019; Rashidi-Ranjbar et al., 2020). Recently, numerous DTI researches have shown that the integrity of the WM was positively correlated with cognitive function in patients with LLD (Shimony et al., 2009; Yuan et al., 2010; Alves et al., 2012; Mettenburg et al., 2012). For instance, researchers have identified that abnormal WM microstructure in patients with LLD is connected with impairments in cognitive functions, including cognitive processing speed (Shimony et al., 2009), memory (Mettenburg et al., 2012), language (Alves et al., 2012), and executive function (Mettenburg et al., 2012). These findings imply that unconnected WM bundles or tracts may be involved in cognitive abnormalities in patients with LLD.

Interestingly, numerous investigations have shown an association between Hcy levels and WM abnormalities (Wright et al., 2005; Feng et al., 2013; Lee et al., 2017; Tan et al., 2018; Nam et al., 2019). For example, in people over 40 years old, Hcy level is a potential risk for WM injury (Wright et al., 2005). Another study showed that Alzheimer's disease patients with high Hcy levels had lower FA values of WM bundles (Lee et al., 2017). Furthermore, a recent study illustrated that higher Hcy level was related to decreased WM volume and cognitive deterioration in healthy elderly individuals (Feng et al., 2013), implying that higher Hcy levels can affect cognitive performance and WM structure.

All of the above evidence indicates that either elevated Hcy levels or WM abnormalities may be correlated with cognitive impairment in LLD patients. However, to the best of our knowledge, the collaborative consequence of homocysteine and WM microstructure on cognitive performance in this specific population has not been investigated. Therefore, the current investigation was aimed to ascertain (1) whether FA values of WM fibers were altered in LLD patients and (2) the correlation between Hcy concentration and the FA value of WM bundles, as well as their combined effect on cognition in both patients with LLD and healthy controls.

Materials and methods

Participants

Patients with LLD were enrolled at the Affiliated Brain Hospital of Guangzhou Medical University. Advertisements in the public were used to attract healthy elderly people. All participants signed a written informed consent form after getting a comprehensive overview of the study. The Ethics Committee of the Affiliated Brain Hospital of Guangzhou Medical University approved the study.

The inclusion and exclusion criteria have been described in previous studies (Zhou et al., 2020). Briefly, the inclusion criteria were the following: (1) A DSM-IV Structured Medical Interview-based diagnosis of major depressive disorder and (2) age ≥ 60 years. The following were the exclusion criteria: (1) A history of other serious mental illnesses; (3) a family history of schizophrenia and/or bipolar disorder; (4) transcranial magnetic stimulation and any electroconvulsive treatment in the last 6 months; (5) neurological disorders, for instance, brain tumor and stroke; and (6) physical disorders, such as hypothyroidism and anemia, that may cause emotional problems. Healthy control (HC) individuals who were not depressed, who were at least 60 years old and who had normal cognition were included. They were all found to be free of psychiatric disease and had 17-item Hamilton Depression Rating Scale (HAMD-17) scores of less than 7 (Zimmerman et al., 2013). Other criteria for exclusion were identical to those used for individuals in the LLD group.

A total of one hundred thirteen patients with LLD and eighty-nine HCs were recruited. The demographic information of the patients has been described in our previous studies (Zhou et al., 2020). Briefly, no significant differences were found in sex, age, or educational years between participants in the HC and LLD groups.

Neuropsychological evaluations

All of the participants completed a comprehensive battery of neuropsychological examinations as described in previous studies (Zhou et al., 2020). Briefly, the tests included the following six cognition domains: (1) Mini-Mental State Examination (MMSE) for global cognition; (2) Rey-Osterrieth Complex Figure (ROCF)-Delay Recall test and Auditory Verbal Learning Test (AVLT) for memory; (3) Trail Making Test (TMT)-B and Stroop Color and Word Test (SCWT)-C for executive function; (4) TMT-A and Symbol Digit Modalities Test (SDMT) for attention; (5) Verbal Fluency Test (VFT) and Boston Naming Test (BNT) for language ability; (6) Clock Drawing Test 4 (CDT4) and ROCF-Copy for visual space. The cognitive domain scores were determined by converting each test result to a standardized z score and taking the average of the total. Particularly, low scores implied high performance on exams that evaluate timing, such as SCWT-C, TMT-B, and TMT-A. As a result, before being transformed to the standard score, the scores were converted to the reciprocal (Shu et al., 2016).

Plasma homocysteine concentration measurements

The Hcy measurements have been described in previous studies (Zhou et al., 2020). Briefly, fasting plasma Hcy concentrations were assessed using the enzyme cycling assay by automatic testers (AU5800 testers, Beckman Coulter, Brea, CA). All of the samples were analyzed by a research assistant who was blinded to the status of the subjects.

Magnetic resonance imaging acquisition

Seventy-four patients with LLD and 68 HCs underwent MRI scans. MRI data were collected within 1 month of completing the neuropsychological evaluations. MRI data were obtained by means of a 3.0-Tesla Philips Achieva scanner (Philips, Best, Netherlands). Before DTI scanning, a T2weight image was taken to rule out major white matter lesions, tumors, and cerebral infarction. The participants were subjected to DTI with the following settings: Direction = 32, b0 = 1,000 s/mm^2, echo time (TE) = 92 ms, repetition time (TR) = 10,015 ms, flip angle = 90°, field of view (FOV) = 256*256 mm^2, imaging matrix = 128*128, voxel dimension of 2*2*2 mm^3, and 75 contiguous slices.

Data processing

All of the DTI images were obtained *via* the standard procedure PANDA software (a pipeline tool for analyzing brain diffusion images).[1] PANDA is a MATLAB toolbox that incorporates FSL,[2] Diffusion Toolkit[3] and MRIcron[4] (Cui et al., 2013). Each subject's diffuse tensor data were skull-stripped and subjected to eddy current and head movement rectification. The directions of the diffusion gradients were adjusted. After that, each subject's FA was calculated on a voxel-by-voxel basis. Individual FA pictures in native space were non-linearly registered to the FA template in Montreal Neurological Institute (MNI) space by means of the FNIRT command of FSL for normalization. After that, the mean of all aligned FA pictures was computed. We used an atlas-based segmentation strategy to examine diffusion changes in the major WM tracts. The FA maps of each subject were registered into the JHU WM Tractography Atlas (Hua et al., 2008). Twenty WM pathways were examined.

Statistical analysis

The 20 WM tracts' mean FA values of the were compared using analysis of variance (ANOVA), with age, education, and sex included as covariates. Partial correlation was used to discover the interrelationships between Hcy levels, cognition

1 http://www.nitrc.org/projects/panda/
2 https://fsl.fmrib.ox.ac.uk/fsl/fslwiki
3 http://www.trackvis.org/dtk
4 https://www.nitrc.org/projects/mricron

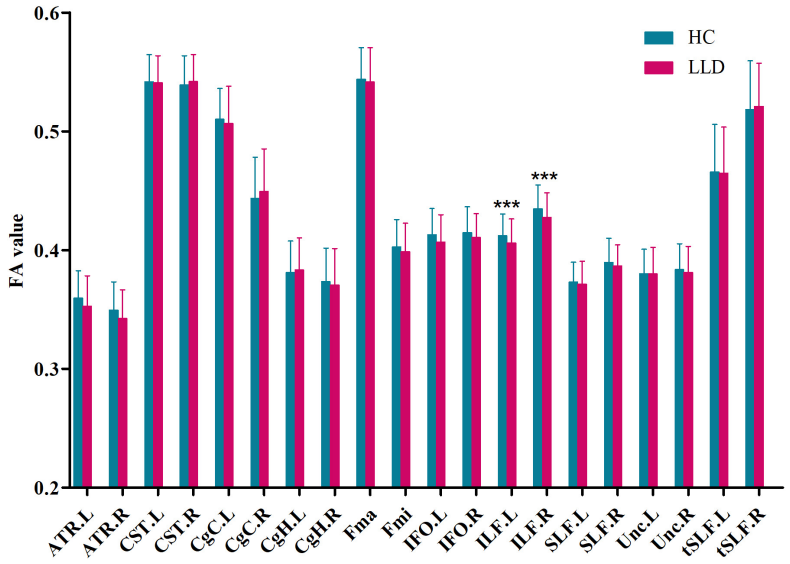

FIGURE 1
Group comparisons of the mean FA value of each tract in HCs and LLD patients. Each bar represents the mean ± SD. Analysis of covariance (ANCOVA) using age, sex, and education as covariates. *** indicates $q < 0.05$ after FDR correction. HC, healthy control; LLD, late-life depression; FA, fractional anisotropy; L, left, R, right; ATR, anterior thalamic radiation; CST, corticospinal tract; CgC, cingulum of the cingulate cortex; CgH, cingulum of the hippocampus; Fma, forceps major; Fmi, forceps minor; IFO, inferior fronto-occipital fasciculus; ILF, inferior longitudinal fasciculus; SLF, superior longitudinal fasciculus; Unc, uncinate fasciculus; tSLF, superior longitudinal fasciculus (temporal part).

and FA values of the WM tracts, and control variables included age, sex, and years of education. Furthermore, stepwise multiple regression analysis was performed to explore the associations between Hcy levels, FA values, their interaction (Hcy × FA values) and cognitive functioning after adjusting for education, sex, age, and HAMD-17 scores. All data were examined by means of SPSS version 23.0 (IBM, Chicago, Illinois, United States). The significance levels were set at 0.05, and two-tailed significance values were used. False discovery rate (FDR) corrections described by Benjamini and Hochberg (1995) were used for multiple test corrections. After utilizing the Benjamini and Hochberg (1995) procedure, FDR-corrected p-values (i.e., q-values) lower than 0.05 were considered statistically significant.

RESULTS

Group differences in fractional anisotropy values of atlas-based tracts

Participants in the LLD group had significantly lower FA values in the left inferior longitudinal fasciculus ($F = 6.17$, $p = 0.014$, $q = 0.014$) and right inferior longitudinal fasciculus ($F = 5.75$, $p = 0.018$, $q = 0.019$) after adjusting for age, sex, and education than those of controls (**Figure 1**). However, there were no significant differences in the bilateral anterior thalamic radiation, bilateral corticospinal tract, bilateral cingulum of the cingulate cortex, bilateral cingulum of the hippocampus, forceps major, forceps minor, bilateral inferior fronto-occipital fasciculus, bilateral superior longitudinal fasciculus, bilateral uncinate fasciculus, or bilateral superior longitudinal fasciculus (temporal part) between participants in the HC and LLD groups (all $q > 0.05$).

Relationships between cognitive deficits, homocysteine levels and fractional anisotropy values in healthy controls and patients with late–life depression

Hcy levels were significantly inversely correlated with FA values in the forceps major (Fma) only in patients with LLD after controlling for age, sex, and education ($r = -0.31$, $p = 0.009$, $q = 0.009$) (**Table 1**).

As shown in **Figure 2A**, the left cingulum of the cingulate cortex ($r = 0.32$, $p = 0.008$, $q = 0.008$) displayed positive associations with global cognition in patients with LLD after adjusting for age, sex, education, and HAMD-17 scores. As shown in **Figure 2B**, the forceps major ($r = 0.26$, $p = 0.033$, $q = 0.034$) displayed positive associations with global cognition in patients with LLD after controlling for age, sex, education, and HAMD-17 scores. The left anterior thalamic radiation ($r = 0.26$, $p = 0.029$, $q = 0.030$) displayed positive associations with executive function in patients with LLD after adjusting for

covariates (Figure 2C). The right anterior thalamic radiation (r = 0.27, p = 0.024, q = 0.025) displayed positive associations with executive function in patients with LLD after adjusting for covariates (Figure 2D). There was no correlation between FA values and other cognitive domains.

Furthermore, no correlation between FA values and Hcy levels or between FA values and cognitive performance was found in HCs (all $q > 0.05$).

Interaction of homocysteine level and fractional anisotropy values with cognition in patients with late–life depression and healthy controls

Multiple regression analysis displayed that the Hcy × FA interactions in the right cingulum of the cingulate cortex (beta = −0.24, t = −2.06, p = 0.043, q = 0.044) and right inferior longitudinal fasciculus (beta = -0.24, t = -2.12, p = 0.038, q = 0.038) were independent predictors for executive function only in patients with LLD. No association between the Hcy level × FA interaction in any of the 20 WM fiber tracts and other cognitive domains was found in patients with LLD (all $q > 0.05$).

Furthermore, no association between the Hcy level × FA interaction in any of the 20 WM fiber tracts and cognition was found in HCs (all $q > 0.05$).

Discussion

The findings from the current study showed (1) significantly lower FA values in the bilateral inferior longitudinal fasciculus in patients with LLD than those in HCs; (2) disruption of WM structure was linked to elevated Hcy concentrations and cognitive impairments in global cognition and executive function in LLD patients; and (3) the interaction between elevated Hcy concentrations and structural destruction of WM may affect executive deficits in patients with LLD.

Elevated homocysteine concentrations and white matter abnormalities in patients with late–life depression

Our previous report demonstrated that LLD patients had higher plasma Hcy levels and worse cognitive performance than those of healthy controls. Furthermore, higher plasma homocysteine levels were associated with poorer cognition in patients with LLD (Zhou et al., 2020). In the current study, we discovered lower FA values in the bilateral inferior longitudinal fasciculus in LLD patients, which is consistent with the majority of prior findings on FA values in patients with LLD (Alves et al., 2012; Mettenburg et al., 2012; Guo et al., 2014; Li et al., 2014, 2020; Wen et al., 2014; Emsell et al., 2017), confirming the LLD disconnection theory. Furthermore, we recognized a reverse relationship between plasma Hcy concentrations and FA values in the forceps minor in patients with LLD, suggesting that Hcy level is related to the WM structure. Because this is the first study to explore the increased homocysteine level and WM abnormalities of patients with LLD, any causal inferences are speculative.

TABLE 1 Correlation of Hcy levels with FA values of WM tracts in patients with LLD.

	Hcy				Hcy		
	r	*p*	*q*		*r*	*p*	*q*
ATR.L	−0.13	0.281	0.468	IFO.L	−0.11	0.348	0.773
ATR.R	−0.13	0.301	0.602	IFO.R	−0.08	0.527	2.108
CST.L	−0.11	0.363	0.908	ILF.L	−0.14	0.241	0.321
CST.R	−0.14	0.263	0.376	ILF.R	−0.13	0.267	0.411
CgC.L	−0.18	0.139	0.164	SLF.L	−0.19	0.110	0.116
CgC.R	−0.17	0.173	0.216	SLF.R	−0.10	0.406	1.160
CgH.L	0.00	0.998	19.960	Unc.L	−0.06	0.602	3.010
CgH.R	−0.18	0.125	0.139	Unc.R	−0.05	0.674	4.493
Fma	−0.08	0.49	1.633	tSLF.L	−0.01	0.937	9.370
Fmi	−0.31	0.009	0.009	tSLF.R	−0.13	0.290	0.527

The false discovery rate (FDR) was adjusted using the Benjamini–Hochberg procedure, and q-values are reported; q-values less than 0.05 were considered significant. Adjusted for age, sex, and years of education. Hcy, homocysteine; L, left; R, right; ATR, anterior thalamic radiation; CST, corticospinal tract; CgC, cingulum of the cingulate cortex; CgH, cingulum of the hippocampus; Fma, forceps major; Fmi, forceps minor; IFO, inferior fronto-occipital fasciculus; ILF, inferior longitudinal fasciculus; SLF, superior longitudinal fasciculus; Unc, uncinate fasciculus; tSLF, superior longitudinal fasciculus (temporal part).

Previous reports revealed that high Hcy concentrations inhibit mitochondrial activity in brain cells (Zhang et al., 2020), which might explain the link between hyperhomocysteinemia and cognitive impairment. In the developing brain, homocysteine induces cell cycle disruption and reactive gliosis (Cecchini et al., 2019). Data from animal studies demonstrate that even a slight increase in serum homocysteine levels upregulates matrix metalloproteinase-9 expression levels and disrupts blood–brain barrier integrity (Chu et al., 2021). In addition, endothelial dysfunction may result from an elevation in Hcy levels by enhancing oxidation and endothelial cell activation (Faverzani et al., 2017), increasing levels of adhesion molecules and proinflammatory cytokines (Barroso et al., 2016), and decreasing vascular wall integrity (Jakubowski, 2001). Endothelial cell damage causes a disruption in the tissue milieu, which leads to subsequent myelin injury and neurodegeneration. Moreover, a recent study demonstrated that increased Hcy levels were related to the imaging burden of cerebral small vessel disease (Cao et al., 2021). Taken together, animal and human research has suggested that high Hcy levels may affect adult neurogenesis as well as neuronal structure and function.

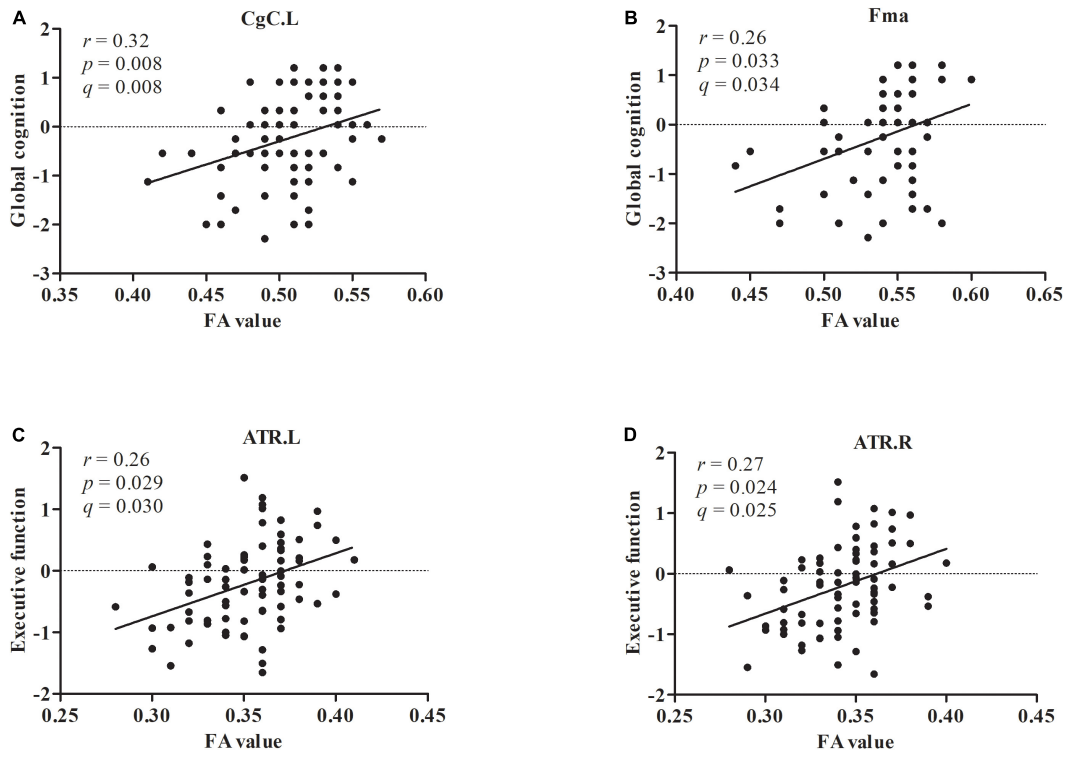

FIGURE 2
The FA value in CgC.L and Fma displayed positive associations with global cognition **(A,B)**. The FA value in ATR.L and ATR.R displayed positive associations with executive function **(C,D)**.

Interaction of elevated homocysteine levels and white matter abnormalities in cognitive deficits in patients with late–life depression

Our findings revealed a negative relationship between plasma Hcy levels and FA values in the forceps minor in patients with LLD, which reflects the interaction between elevated Hcy levels and abnormal WM structure as the pathogenic mechanism of LLD. Moreover, we found that the Hcy × FA interaction in the right cingulum of the cingulate cortex and right inferior longitudinal fasciculus contributed to executive dysfunction in patients with LLD. Executive deterioration is common in patients with LLD and predicts a worse response to antidepressant therapy as well as a greater recurrence risk (Alexopoulos et al., 2005). Growing evidence has shown that high levels of homocysteine and WM degeneration are associated with cerebrovascular disease (Kynast et al., 2018; Cao et al., 2021). Therefore, elevated Hcy levels and WM abnormalities support vascularity impairment in patients with LLD. Although these correlations do not provide proof of causality in pathophysiology, it is speculated that high Hcy levels may disrupt WM microstructural connections and induce cognitive impairment. Additionally, our findings showed that there was a positive association between global cognition and FA values in the left cingulum of the cingulate cortex or the forceps major, as well as between executive function and FA values in the bilateral anterior thalamic radiation in patients with LLD. Several investigations have described that neurocognitive impairment is related to WM abnormalities in LLD (Charlton et al., 2014; Respino et al., 2019; Wang et al., 2020). These findings support the hypothesis that damaged WM connections are related to cognitive abnormalities in patients with LLD.

Limitations

This research investigation had several limitations that must be noted. First, this was a case-control study. Thus, the causal relationship between elevated Hcy levels, WM injury and cognitive deficits in LLD patients is still uncertain. Therefore, in the future, a longitudinal investigation with a larger sample size will be required to obtain more persuasive and accurate results. Second, our research only investigated changes in WM structure; however, whether the change in WM structure is related to a change in function must be further explored. Third, the study did not assess diet, physical activity or lifestyle. All of these factors may influence Hcy levels and WM, but they were not controlled for in the present analysis.

Conclusion

In conclusion, both increased Hcy levels and the disturbance of WM structure may be involved in the cognitive impairment observed in patients with LLD. Only in the patient group was a negative relation between plasma Hcy levels and WM disconnectivity identified, implying pathogenic processes underlying the interaction between increased Hcy levels and WM disconnection. Furthermore, because our current investigation used a case-control methodology, a larger longitudinal sample is needed to identify the causal relationship among aberrant Hcy metabolism, WM disconnection, and cognitive deficits in patients with LLD.

Data availability statement

The raw data supporting the conclusions of this article will be made available by the authors, without undue reservation.

Ethics statement

The studies involving human participants were reviewed and approved by the Ethics Committee of Affiliated Brain Hospital of Guangzhou Medical University. The patients/participants provided their written informed consent to participate in this study.

Author contributions

YN conceived and designed the study. HZ and XZ performed testing and data collection and drafted the manuscript. BC, QW, MZ, NM, ZW, XH, XC, and QP performed the data analysis and interpretation. All authors contributed to the article and approved the submitted version.

Funding

This study was supported by the National Natural Science Foundation of China (Nos. 81701341, 82101508, and 82171533), the Key Laboratory for Innovation Platform Plan, Science and Technology Program of Guangzhou, China, Science and Technology Plan Project of Guangdong Province (No. 2019B030316001), the Guangzhou Municipal Psychiatric Diseases Clinical Transformation Laboratory (No. 201805010009), Medical Scientific Technology Research Foundation of Guangdong Province of China (No. A2020446), Key Medical Specialty Construction Project of Traditional Chinese Medical Science in the 13th 5-Year Plan of Guangdong Province, Key Medical Specialty Construction Project of Traditional Chinese Medical Science of Guangzhou (2020–2022), and the National Key Research and Development Program of China (No. 2016YFC0906300). The funders had no role in the study design, data collection and analysis, decision to publish or preparation of the manuscript.

Acknowledgments

We thank Cong Ouyang, Weiru Zhang, Wanruan Liang, and Chunying Dai for their assistance in data collection.

Conflict of interest

The authors declare that the research was conducted in the absence of any commercial or financial relationships that could be construed as a potential conflict of interest.

Publisher's note

All claims expressed in this article are solely those of the authors and do not necessarily represent those of their affiliated organizations, or those of the publisher, the editors and the reviewers. Any product that may be evaluated in this article, or claim that may be made by its manufacturer, is not guaranteed or endorsed by the publisher.

References

Alexopoulos, G. S., Kiosses, D. N., Heo, M., Murphy, C. F., Shanmugham, B., and Gunning-Dixon, F. (2005). Executive dysfunction and the course of geriatric depression. *Biol. Psychiatry* 58, 204–210. doi: 10.1016/j.biopsych.2005.04.024

Alves, G. S., Karakaya, T., Fußer, F., Kordulla, M., O'Dwyer, L., Christl, J., et al. (2012). Association of microstructural white matter abnormalities with cognitive dysfunction in geriatric patients with major depression. *Psychiatry Res.* 203, 194–200. doi: 10.1016/j.pscychresns.2011.12.006

Barroso, M., Kao, D., Blom, H. J., Tavares de Almeida, I., Castro, R., Loscalzo, J., et al. (2016). S-adenosylhomocysteine induces inflammation through NFkB: a possible role for EZH2 in endothelial cell activation. *Biochim. Biophys. Acta* 1862, 82–92. doi: 10.1016/j.bbadis.2015.10.019

Benjamini, Y., and Hochberg, Y. (1995). Controlling the False Discovery Rate: a Practical and Powerful Approach to Multiple Testing. *J. R. Stat. Soc. Series B* 57, 289–300.

Bhalla, R. K., Butters, M. A., Mulsant, B. H., Begley, A. E., Zmuda, M. D., Schoderbek, B., et al. (2006). Persistence of neuropsychologic deficits in the remitted state of late-life depression. *Am. J. Geriatr. Psychiatry* 14, 419–427. doi: 10.1097/01.jgp.0000203130.45421.69

Cao, Y., Su, N., Zhang, D., Zhou, L., and Yao, M. (2021). Correlation between total homocysteine and cerebral small vessel disease: a Mendelian randomization study. *Eur. J. Neurol.* 28, 1931–1938. doi: 10.1111/ene.14708

Cecchini, M. S., Bourckhardt, G. F., Jaramillo, M. L., Ammar, D., Müller, Y. M. R., and Nazari, E. M. (2019). Exposure to homocysteine leads to cell cycle damage and reactive gliosis in the developing brain. *Reprod. Toxicol.* 87, 60–69. doi: 10.1016/j.reprotox.2019.05.054

Charlton, R. A., Lamar, M., Zhang, A., Yang, S., Ajilore, O., and Kumar, A. (2014). White-matter tract integrity in late-life depression: associations with severity and cognition. *Psychol. Med.* 44, 1427–1437. doi: 10.1017/s0033291713001980

Chu, M., Teng, J., Guo, L., Wang, Y., Zhang, L., Gao, J., et al. (2021). Mild hyperhomocysteinemia induces blood-brain barrier dysfunction but not neuroinflammation in the cerebral cortex and hippocampus of wild-type mice. *Can. J. Physiol. Pharmacol.* 99, 847–856. doi: 10.1139/cjpp-2020-0507

Cui, Z., Zhong, S., Xu, P., He, Y., and Gong, G. (2013). PANDA: a pipeline toolbox for analyzing brain diffusion images. *Front. Hum. Neurosci.* 7:42. doi: 10.3389/fnhum.2013.00042

Emsell, L., Adamson, C., De Winter, F. L., Billiet, T., Christiaens, D., Bouckaert, F., et al. (2017). Corpus callosum macro and microstructure in late-life depression. *J. Affect. Disord.* 222, 63–70. doi: 10.1016/j.jad.2017.06.063

Faverzani, J. L., Hammerschmidt, T. G., Sitta, A., Deon, M., Wajner, M., and Vargas, C. R. (2017). Oxidative Stress in Homocystinuria Due to Cystathionine ß-Synthase Deficiency: findings in Patients and in Animal Models. *Cell. Mol. Neurobiol.* 37, 1477–1485. doi: 10.1007/s10571-017-0478-0

Feng, L., Isaac, V., Sim, S., Ng, T. P., Krishnan, K. R., and Chee, M. W. (2013). Associations between elevated homocysteine, cognitive impairment, and reduced white matter volume in healthy old adults. *Am. J. Geriatr. Psychiatry* 21, 164–172. doi: 10.1016/j.jagp.2012.10.017

Ford, A. H., Flicker, L., Singh, U., Hirani, V., and Almeida, O. P. (2013). Homocysteine, depression and cognitive function in older adults. *J. Affect. Disord.* 151, 646–651. doi: 10.1016/j.jad.2013.07.012

Guo, W., Liu, F., Xun, G., Hu, M., Guo, X., Xiao, C., et al. (2014). Disrupted white matter integrity in first-episode, drug-naive, late-onset depression. *J. Affect. Disord.* 163, 70–75. doi: 10.1016/j.jad.2014.03.044

Harada, K., Ikuta, T., Nakashima, M., Watanuki, T., Hirotsu, M., Matsubara, T., et al. (2018). Altered Connectivity of the Anterior Cingulate and the Posterior Superior Temporal Gyrus in a Longitudinal Study of Later-life Depression. *Front. Aging Neurosci.* 10:31. doi: 10.3389/fnagi.2018.00031

Hua, K., Zhang, J., Wakana, S., Jiang, H., Li, X., Reich, D. S., et al. (2008). Tract probability maps in stereotaxic spaces: analyses of white matter anatomy and tract-specific quantification. *Neuroimage* 39, 336–347. doi: 10.1016/j.neuroimage.2007.07.053

Invernizzi, S., Simoes Loureiro, I., Kandana Arachchige, K. G., and Lefebvre, L. (2021). Late-Life Depression, Cognitive Impairment, and Relationship with Alzheimer's Disease. *Dement. Geriatr. Cogn. Disord.* 50, 414–424. doi: 10.1159/000519453

Jakubowski, H. (2001). Protein N-homocysteinylation: implications for atherosclerosis. *Biomed. Pharmacother.* 55, 443–447. doi: 10.1016/s0753-3322(01)00085-3

Katon, W., Pedersen, H. S., Ribe, A. R., Fenger-Gron, M., Davydow, D., Waldorff, F. B., et al. (2015). Effect of depression and diabetes mellitus on the risk for dementia: a national population-based cohort study. *JAMA Psychiatry* 72, 612–619. doi: 10.1001/jamapsychiatry.2015.0082

Kaup, A. R., Byers, A. L., Falvey, C., Simonsick, E. M., Satterfield, S., Ayonayon, H. N., et al. (2016). Trajectories of Depressive Symptoms in Older Adults and Risk of Dementia. *JAMA Psychiatry* 73, 525–531. doi: 10.1001/jamapsychiatry.2016.0004

Kim, S., Choi, B. Y., Nam, J. H., Kim, M. K., Oh, D. H., and Yang, Y. J. (2019). Cognitive impairment is associated with elevated serum homocysteine levels among older adults. *Eur. J. Nutr.* 58, 399–408. doi: 10.1007/s00394-017-1604-y

Kynast, J., Lampe, L., Luck, T., Frisch, S., Arelin, K., Hoffmann, K. T., et al. (2018). White matter hyperintensities associated with small vessel disease impair social cognition beside attention and memory. *J. Cereb. Blood Flow Metab.* 38, 996–1009. doi: 10.1177/0271678x17719380

Lee, C. C., Hsu, S. W., Huang, C. W., Chang, W. N., Chen, S. F., Wu, M. K., et al. (2017). Effects of Homocysteine on white matter diffusion parameters in Alzheimer's disease. *BMC Neurol.* 17:192. doi: 10.1186/s12883-017-0970-7

Li, H., Liang, Y., Chen, K., Li, X., Shu, N., Zhang, Z., et al. (2013). Different patterns of white matter disruption among amnestic mild cognitive impairment subtypes: relationship with neuropsychological performance. *J. Alzheimers Dis.* 36, 365–376. doi: 10.3233/jad-122023

Li, H., Lin, X., Liu, L., Su, S., Zhu, X., Zheng, Y., et al. (2020). Disruption of the structural and functional connectivity of the frontoparietal network underlies symptomatic anxiety in late-life depression. *Neuroimage Clin.* 28:102398. doi: 10.1016/j.nicl.2020.102398

Li, W., Muftuler, L. T., Chen, G., Ward, B. D., Budde, M. D., Jones, J. L., et al. (2014). Effects of the coexistence of late-life depression and mild cognitive impairment on white matter microstructure. *J. Neurol. Sci.* 338, 46–56. doi: 10.1016/j.jns.2013.12.016

Mettenburg, J. M., Benzinger, T. L., Shimony, J. S., Snyder, A. Z., and Sheline, Y. I. (2012). Diminished performance on neuropsychological testing in late life depression is correlated with microstructural white matter abnormalities. *Neuroimage* 60, 2182–2190. doi: 10.1016/j.neuroimage.2012.02.044

Nam, K. W., Kwon, H. M., Jeong, H. Y., Park, J. H., Kwon, H., and Jeong, S. M. (2019). Serum homocysteine level is related to cerebral small vessel disease in a healthy population. *Neurology* 92, e317–25. doi: 10.1212/wnl.0000000000006816

Rashidi-Ranjbar, N., Miranda, D., Butters, M. A., Mulsant, B. H., and Voineskos, A. N. (2020). Evidence for Structural and Functional Alterations of Frontal-Executive and Corticolimbic Circuits in Late-Life Depression and Relationship to Mild Cognitive Impairment and Dementia: a Systematic Review. *Front. Neurosci.* 14:253. doi: 10.3389/fnins.2020.00253

Reinlieb, M., Ercoli, L. M., Siddarth, P., St Cyr, N., and Lavretsky, H. (2014). The patterns of cognitive and functional impairment in amnestic and non-amnestic mild cognitive impairment in geriatric depression. *Am. J. Geriatr. Psychiatry* 22, 1487–1495. doi: 10.1016/j.jagp.2013.10.010

Respino, M., Jaywant, A., Kuceyeski, A., Victoria, L. W., Hoptman, M. J., Scult, M. A., et al. (2019). The impact of white matter hyperintensities on the structural connectome in late-life depression: relationship to executive functions. *Neuroimage Clin.* 23:101852. doi: 10.1016/j.nicl.2019.101852

Rhodes, E., Insel, P. S., Butters, M. A., Morin, R., Bickford, D., Tosun, D., et al. (2021). The Impact of Amyloid Burden and APOE on Rates of Cognitive Impairment in Late Life Depression. *J. Alzheimers Dis.* 80, 991–1002. doi: 10.3233/jad-201089

Setien-Suero, E., Suarez-Pinilla, M., Suarez-Pinilla, P., Crespo-Facorro, B., and Ayesa-Arriola, R. (2016). Homocysteine and cognition: a systematic review of 111 studies. *Neurosci. Biobehav. Rev.* 69, 280–298. doi: 10.1016/j.neubiorev.2016.08.014

Shen, X., Adams, M. J., Ritakari, T. E., Cox, S. R., McIntosh, A. M., and Whalley, H. C. (2019). White Matter Microstructure and Its Relation to Longitudinal Measures of Depressive Symptoms in Mid- and Late Life. *Biol. Psychiatry* 86, 759–768. doi: 10.1016/j.biopsych.2019.06.011

Shimony, J. S., Sheline, Y. I., D'Angelo, G., Epstein, A. A., Benzinger, T. L., Mintun, M. A., et al. (2009). Diffuse microstructural abnormalities of normal-appearing white matter in late life depression: a diffusion tensor imaging study. *Biol. Psychiatry* 66, 245–252. doi: 10.1016/j.biopsych.2009.02.032

Shu, H., Shi, Y., Chen, G., Wang, Z., Liu, D., Yue, C., et al. (2016). Opposite Neural Trajectories of Apolipoprotein E 4 and 2 Alleles with Aging Associated with Different Risks of Alzheimer's Disease. *Cereb. Cortex* 26, 1421–1429. doi: 10.1093/cercor/bhu237

Smith, A. D., and Refsum, H. (2016). Homocysteine, B Vitamins, and Cognitive Impairment. *Annu. Rev. Nutr.* 36, 211–239. doi: 10.1146/annurev-nutr-071715-050947

Tae, W. S., Ham, B. J., Pyun, S. B., Kang, S. H., and Kim, B. J. (2018). Current Clinical Applications of Diffusion-Tensor Imaging in Neurological Disorders. *J. Clin. Neurol.* 14, 129–140. doi: 10.3988/jcn.2018.14.2.129

Tan, B., Venketasubramanian, N., Vrooman, H., Cheng, C. Y., Wong, T. Y., Ikram, M. K., et al. (2018). Homocysteine and Cerebral Atrophy: the Epidemiology of Dementia in Singapore Study. *J. Alzheimers Dis.* 62, 877–885. doi: 10.3233/jad-170796

Wang, Z., Yuan, Y., You, J., and Zhang, Z. (2020). Disrupted structural brain connectome underlying the cognitive deficits in remitted late-onset depression. *Brain Imaging Behav.* 14, 1600–1611. doi: 10.1007/s11682-019-00091-x

Wen, M. C., Steffens, D. C., Chen, M. K., and Zainal, N. H. (2014). Diffusion tensor imaging studies in late-life depression: systematic review and meta-analysis. *Int. J. Geriatr. Psychiatry* 29, 1173–1184. doi: 10.1002/gps.4129

Wright, C. B., Paik, M. C., Brown, T. R., Stabler, S. P., Allen, R. H., Sacco, R. L., et al. (2005). Total homocysteine is associated with white matter hyperintensity volume: the Northern Manhattan Study. *Stroke* 36, 1207–1211. doi: 10.1161/01.str.0000165923.02318.22

Yuan, Y., Hou, Z., Zhang, Z., Bai, F., Yu, H., You, J., et al. (2010). Abnormal integrity of long association fiber tracts is associated with cognitive deficits in patients with remitted geriatric depression: a cross-sectional, case-control study. *J. Clin. Psychiatry* 71, 1386–1390. doi: 10.4088/JCP.09m05313gry

Zhang, M., Chen, B., Zhong, X., Zhou, H., Wang, Q., Mai, N., et al. (2021). Neuropsychiatric Symptoms Exacerbate the Cognitive Impairments in Patients With Late-Life Depression. *Front. Psychiatry* 12:757003. doi: 10.3389/fpsyt.2021.757003

Zhang, T., Huang, D., Hou, J., Li, J., Zhang, Y., Tian, M., et al. (2020). High-concentration homocysteine inhibits mitochondrial respiration function and production of reactive oxygen species in neuron cells. *J. Stroke Cerebrovasc. Dis.* 29:105109. doi: 10.1016/j.jstrokecerebrovasdis.2020.105109

Zhou, F., and Chen, S. (2019). Hyperhomocysteinemia and risk of incident cognitive outcomes: an updated dose-response meta-analysis of prospective cohort studies. *Ageing Res. Rev.* 51, 55–66. doi: 10.1016/j.arr.2019.02.006

Zhou, H., Zhong, X., Chen, B., Wu, Z., Zhang, M., Mai, N., et al. (2020). Interactive effects of elevated homocysteine and late-life depression on cognitive impairment. *J. Affect. Disord.* 277, 212–217. doi: 10.1016/j.jad.2020.08.022

Zimmerman, M., Martinez, J. H., Young, D., Chelminski, I., and Dalrymple, K. (2013). Severity classification on the Hamilton Depression Rating Scale. *J. Affect. Disord.* 150, 384–388. doi: 10.1016/j.jad.2013.04.028

frontiers | Frontiers in Aging Neuroscience

TYPE Original Research
PUBLISHED 03 August 2022
DOI 10.3389/fnagi.2022.920352

Check for updates

OPEN ACCESS

EDITED BY
Yuzhen Xu,
Shandong First Medical University,
China

REVIEWED BY
Qin Xu,
National Institute of Allergy and
Infectious Diseases (NIH), United States
Yu Wang,
Tianjin Medical University General
Hospital, China

*CORRESPONDENCE
Zezhi Li
biolpsychiatry@126.com
Meihong Xiu
xiumeihong97@163.com
Xiangyang Zhang
zhangxy@psych.ac.cn

SPECIALTY SECTION
This article was submitted to
Cellular and Molecular Mechanisms of
Brain-aging,
a section of the journal
Frontiers in Aging Neuroscience

RECEIVED 14 April 2022
ACCEPTED 06 July 2022
PUBLISHED 03 August 2022

CITATION
Yang M, Cui Y, Xue M, Forster MT,
Lang X, Xiu M, Li Z and Zhang X
(2022) Sexual dimorphism in the
relationship between *Forkhead-Box
P2* and BMI with cognitive deficits in
schizophrenia.
Front. Aging Neurosci. 14:920352.
doi: 10.3389/fnagi.2022.920352

COPYRIGHT
© 2022 Yang, Cui, Xue, Forster, Lang,
Xiu, Li and Zhang. This is an
open-access article distributed under
the terms of the Creative Commons
Attribution License (CC BY). The use,
distribution or reproduction in other
forums is permitted, provided the
original author(s) and the copyright
owner(s) are credited and that the
original publication in this journal is
cited, in accordance with accepted
academic practice. No use, distribution
or reproduction is permitted which
does not comply with these terms.

Sexual dimorphism in the relationship between *Forkhead-Box P2* and BMI with cognitive deficits in schizophrenia

Mi Yang[1], Ying Cui[2], Mei Xue[2], Mattew T. Forster[3], Xiaoe Lang[4], Meihong Xiu[5]*, Zezhi Li[6,7]* and Xiangyang Zhang[6,8]*

[1]The Fourth Hospital of Chengdu, Chengdu, China, [2]Qingdao Mental Health Center, Qingdao, China, [3]Department of Psychiatry and Behavioral Sciences, University of Texas Health Science Center at Houston, Houston, TX, United States, [4]Department of Psychiatry, First Hospital/First Clinical Medical College of Shanxi Medical University, Taiyuan, China, [5]Beijing HuiLongGuan Hospital, Peking University, Beijing, China, [6]Department of Psychiatry, The Affiliated Brain Hospital of Guangzhou Medical University, Guangzhou, China, [7]Guangdong Engineering Technology Research Center for Translational Medicine of Mental Disorders, Guangzhou, China, [8]Department of Psychology, University of Chinese Academy of Sciences, Beijing, China

FOXP2, cognitive deficits, and schizophrenia are associated with neurodegenerative pathophyisiology. Mounting evidence suggests that body mass index (BMI) and *FOXP2* may contribute to cognitive deficits in schizophrenia. However, the sex difference in the contribution of *FOXP2* and BMI, as well as their potential interaction with cognitive deficits in schizophrenia, have not been investigated. A total of 867 schizophrenia patients and 402 controls were recruited. Cognitive function was assessed using the Repeatable Battery for the Assessment of Neuropsychological Status (RBANS). The polymorphism rs10447760 of the *FOXP2* gene was genotyped. Male schizophrenia patients had superior language performance compared to female patients ($F = 17.83$; $p_{\text{Bonferroni}} < 0.0001$). BMI was positively associated with language scores in male patients with schizophrenia ($SS = 0.60$, $t = 3.30$, $p = 0.001$), as well as in patients with schizophrenia who carried the *FOXP2* rs10447760 CC genotype ($SS = 0.53$, $t = 3.16$, $p = 0.002$). Interestingly, this association was only found in male patients with schizophrenia who also carried the *FOXP2* rs10447760 CC genotype ($SS = 0.63$, $t = 3.44$, $p = 0.001$). Our study reveals a sex difference in the language deficits of schizophrenia patients and shows sexual dimorphism in the contribution of *FOXP2*, BMI, and their interaction to cognitive deficits in patients with schizophrenia.

KEYWORDS

sexual dimorphism, *FOXP2*, BMI, cognitive deficit, schizophrenia

Introduction

Cognitive deficits, including in aspects of attention, memory, learning, language, and executive function, are an essential feature of schizophrenia—being displayed in 98% of patients (Keefe et al., 2005; Tripathi et al., 2018). These cognitive deficits can impinge on patient prognosis and quality of life (Harvey et al., 2009). Previous evidence has shown that cognitive deficits in schizophrenia may be an innate trait, as they can occur in the initial episode as well as in patients with chronic schizophrenia (Gerretsen et al., 2017). Cognitive deficits can also occur in the prodromal stages and throughout the illness course, despite the alleviation of symptoms with pharmacological therapy (Hughes et al., 2003; Kahn and Keefe, 2013).

Although it is recognized that certain patients are predisposed to cognitive deficits, the underlying multi-faceted cause of cognitive deficits in schizophrenia remains largely obscure (Toulopoulou et al., 2007). However, accumulating evidence suggests a genetic contribution to cognitive deficits in schizophrenia patients (Harvey et al., 2016). For instance, cognitive deficits have even been observed in the unaffected relatives of schizophrenia patients (Snitz et al., 2006). Currently, a primary hypothesis is that neurodevelopmental and neurodegenerative dysfunction underlies the etiology of both cognitive deficits and schizophrenia (Li et al., 2020). The forkhead-box P2 (*FOXP2*) gene, located on chromosome 7q31, which contributes to brain development and neuronal processes, was first identified as being involved in language and speech (Lai et al., 2001). It is well established that disturbances of speech and language processes are central components of both schizophrenia and cognitive deficits (Li et al., 2009). Furthermore, *FOXP2* has been associated with schizophrenia in genome-wide association studies (Hagenaars et al., 2016). Our previous studies have reported that one of the *FOXP2* polymorphisms, rs10447760 within the 5' regulatory region, is associated with clinical outcomes and cognitive deficits in chronic schizophrenia (Rao et al., 2017; Lang et al., 2019). Additionally, *FOXP2* has been associated with obesity in a genome-wide association study (Glessner et al., 2010; Clifton et al., 2018). Collectively, this evidence suggests that *FOXP2* contributes to both cognitive deficits and obesity in patients with schizophrenia.

In addition, it is now well established that critical, non-genetic aspects, such as metabolic syndrome and obesity, also contribute to cognitive deficits in schizophrenia patients (Rashid et al., 2013; Bora et al., 2017). Prior studies have also suggested a relationship between body mass index (BMI) and cognitive deficits (Smith et al., 2011). The frequency of higher BMI and obesity are greater in schizophrenic patients overall (Li et al., 2017), and the association of BMI with cognitive deficits in schizophrenia has also been established (Bora et al., 2017). However, other studies have reported inconsistent findings (Friedman et al., 2010; Takayanagi et al., 2012).

The above-mentioned inconsistent results may be due to the possible confounding interactions of sex, BMI, and genetic background. Increasing evidence has indicated that there are sex differences in clinical characteristics and outcomes, especially cognitive deficits, among schizophrenia patients across (Leger and Neill, 2016). Sex differences in brain structure and function, as well as sexually dimorphic steroid hormones, may contribute to the sex-specific effects on cognitive deficits in schizophrenic patients (Mendrek and Mancini-Marie, 2016). Previous studies have demonstrated different cognitive deficits between male and female patients with schizophrenia during their first and/or chronic episodes that were not observed in healthy controls (Leger and Neill, 2016; Mendrek and Mancini-Marie, 2016). However, the results are still equivocal. For example, several studies did not find an association between sex and cognitive deficits in patients with schizophrenia (Mendrek and Mancini-Marie, 2016).

Although our previous study has shown that *FOXP2* polymorphisms (rs10447760) is associated with cognitive deficits in chronic schizophrenia (Lang et al., 2019), it remains unclear whether there are sex differences in the degree of contribution of genetic factors to cognitive deficits in schizophrenia; whether there are sex differences in the influences of BMI on cognitive deficits in schizophrenia; and/or whether there are sex differences in the effects of genetic contributions and BMI on cognitive deficits in schizophrenia. These interesting questions prompt a need for further investigation.

Some previous evidence has demonstrated that sex differences in cognitive performance are associated with certain genetic backgrounds (Zhang et al., 2010; Jancke, 2018). Additionally, recent studies have shown that cognitive function and BMI may share a common genetic pathway (Davies et al., 2015; Marioni et al., 2016). Prior research has also suggested the existence of a shared genetic mutation that is associated with both BMI and cognitive performance (Marioni et al., 2016). Frazier-Wood et al. (2014) found that shared genetic factors contributed to cognitive function and BMI in a study of 1,312 twins. Additionally, Laitala et al. (2011) performed a study with a large sample of 2,606 twins which also showed a significant shared genetic influence on the correlation between cognitive decline and midlife BMI. The above evidence suggests that interactions between sex, genetic contribution, and BMI are involved in the pathophysiology of cognitive deficits.

Therefore, to the best of our knowledge, this study is the first to investigate: (1) whether the *FOXP2* polymorphism rs10447760 affects cognition differently as a function of sex; (2) whether BMI was associated with cognitive deficits in schizophrenia patients; (3) and whether any relationship

between BMI and cognitive deficits in schizophrenia was further altered by sex.

Materials and methods

Subjects

The protocol was approved by the ethics committee of the Beijing Huilongguan Hospital (No. BJ-7072035; Date: July 10th, 2016). Each subject or guardian signed a written informed consent prior to being enrolled in the study. The inclusion criteria have been described in previous studies (Lang et al., 2019), but, briefly, include: (1) patients must be between 18 and 75 years old; (2) patients must be of Han Chinese descent; (3) patients met diagnostic criteria for schizophrenia, as defined by the Diagnostic and Statistical Manual of Mental Disorders, Fourth Edition (DSM-IV); (4) patients experienced disease courses of at least 5 years; (5) patients had been treated mainly with monotherapy of an antipsychotic drug for at least 12 months.

Healthy controls without a family history of psychotic disorders were recruited through local advertisements. Individuals were excluded if they had any other major Axis I disorders.

Any patients who were pregnant or experiencing severe physical diseases, such as cardiovascular disease, cerebrovascular disease, cancer, infection, or unstable diabetes, were excluded. Any patient who had alcohol or drug abuse/dependence, as determined by laboratory urine tests, was excluded.

A total of 867 patients and 402 healthy controls were recruited. The demographic information of patients has been described in our previous studies. Briefly, there were differences in sex, BMI, and education between patients and healthy controls (Lang et al., 2019).

The antipsychotics that patients received have been described in our previous study but included clozapine, risperidone, quetiapine, chlorpromazine, sulpiride, aripiprazole, perphenazine, olanzapine, haloperidol, and other antipsychotics. The antipsychotic doses were calculated by being equivalent to chlorpromazine (Lang et al., 2019).

Clinical interview assessments

All participants were interviewed independently by two psychiatrists using the Structured Clinical Interview for DSM-IV (SCID-I/P). We also used the Positive and Negative Symptoms Scale (PANSS) to assess clinical symptoms. Cognitive performance was evaluated using the Chinese version of the Assessment of Neuropsychological Status (RBANS, Form A).

DNA isolation and SNP genotyping

Peripheral venous blood was sampled, and DNA was extracted using a salting-out method followed by preservation at −80°C (Rao et al., 2017).

The polymorphism rs10447760 of *FOXP2* was genotyped using the methods described before (Rao et al., 2017). 5% of the samples were randomly selected for repeated genotyping as a quality control measure.

Statistical analyses

The normality of variable distribution was assessed using the Kolmogorov-Smirnov test. Chi-square tests and student's *t*-tests were used, for categorical variables and continuous variables, respectively. Hardy–Weinberg equilibrium was detected using a goodness of fit of χ^2 test.

To investigate the effects of differing antipsychotics on cognitive scores in patients, we conducted a multiple analysis of covariance (MANCOVA). We chose this approach to address the overall *p*-value because we thought it would reduce type I error, while also adjusting for age, BMI, smoking, education, onset age, illness duration, hospitalization times, antipsychotic duration, and daily dose. Then, an analysis of covariance (ANCOVA) was performed to examine the effects of different antipsychotics on the cognitive score, while adjusting for the same parameters as in the primary MANCOVA.

To identify the effects of sex on cognitive scores in patients and healthy controls, a 2 × 2 MANCOVA (sex × diagnosis) was conducted. All of the RBANS subscores were dependent variables, and diagnosis and sex were fixed factors. We also adjusted for age, BMI, smoking, and education level. Then, an ANCOVA was performed with individual RBANS scores as the dependent variable. In this model, sex and diagnosis were the fixed factors, and we adjusted for age, BMI, smoking, and education in the control group, and for onset age, hospitalization time, antipsychotic types (atypical or typical antipsychotics), duration of treatment with antipsychotics and antipsychotics dose in the patient group. Stepwise multivariate regression analyses were conducted with each RBANS score as a dependent variable, where sex was an independent variable, and the same confounding covariates were controlled for patients.

To identify the effects of the *FOXP2* genotype on the relationship between sex and cognitive scores in patients and healthy controls, we used 2 × 2 MANCOVAs (genotype × sex) separately in patient and control groups. All RBANS scores were set as dependent variables, with the genotype and sex as the independent variables, and adjustment for confounding covariates. We then used an ANCOVA with each RBANS score as a dependent variable, genotype, and sex as independent variables, and with separate adjustments for confounding covariates in the patient and control groups.

To explore the association between BMI and cognitive scores in the patients and controls separately, as well as in the different sex and genotypic groupings, we used partial correlations which adjusted for demographic and clinical covariates. We also carried out multivariate regression analyses, with each cognitive domain as a dependent variable, BMI as an independent variable, and controlling for confounding variables.

Bonferroni corrections were performed for multiple tests. The power of the sample in the present study was calculated using Quanto Software under dominant, log additive, and recessive models, and setting the prevalence of schizophrenia as 1% in the population. The statistical analyses were applied using SPSS version 25.0, and statistical significance was identified as a 2-tailed p-value that was less than 0.05.

Results

The effect of different antipsychotics on cognitive performance in patients

The MANCOVA demonstrated that there were no significant effects of differing antipsychotics on cognitive function (Wilks' Lambda, $F = 0.94$, $p = 0.61$). Furthermore, the ANCOVA demonstrated that differing antipsychotics did not have different effects on immediate memory ($F = 1.46$, $p = 0.16$), visual space/structure ($F = 0.85$, $p = 0.56$), language ($F = 0.51$, $p = 0.89$), attention ($F = 1.03$, $p = 0.42$), delayed memory ($F = 1.18$, $p = 0.31$), or total RBANS scores ($F = 1.13$, $p = 0.34$).

Sex difference in cognitive scores of patients and controls

The 2 × 2 MANCOVA analysis (sex × diagnosis), which adjusted for age, BMI, and educational years, showed a main effect of sex on cognitive performance (Wilks' lambda $F = 8.01$; $p < 0.0001$). Then, as shown in Table 1, after adjustments for age, BMI, and educational years, ANCOVA showed a main effect of sex on language performance ($F = 25.13$; corrected $p < 0.0001$). There was a significant effect of diagnosis × sex on language scores ($F = 16.71$, $p < 0.001$) which also survived Bonferroni correction. Further ANCOVA analysis of the patient group showed male patients with schizophrenia had better language performance than female patients ($F = 17.83$; $p < 0.0001$), after adjusting for confounding variables. This result also persisted after Bonferroni correction ($p < 0.0001$). Further multivariate regression analysis demonstrated that sex was correlated with language performance in patients ($SS = -7.69$, $t = 4.22$, $p < 0.0001$); that is, female patients performed worse than males did. In the control group, there were no significant differences in any of the RBANS subscale scores, or the total RBANS scores, between males and females ($p > 0.05$).

Sex differences in the effects of *FOXP2* rs10447760 on cognitive scores in patients and controls

The 2 × 2 MANCOVA demonstrated no effects of genotype (Wilks' lambda $F = 1.41$; $p = 0.21$), sex (Wilks' lambda $F = 1.71$; $p = 0.12$), or genotype × sex (Wilks' lambda $F = 0.56$; $p = 0.77$) on cognitive performance. ANCOVA analysis showed that there were genotype effects on immediate memory scores ($F = 4.14$, $p = 0.04$) and language scores ($F = 4.89$, $p = 0.03$; Table 2) in the patient group. However, the results did not persist after Bonferroni correction ($p = 0.24$, $p = 0.18$). No sex differences in the genotypic effects on BMI was found.

In the control group, there were no effects of sex, genotype, or sex × genotype on any of the RBANS scores (all $p > 0.05$).

Sex difference in BMI of patients and healthy controls

There were no significant effects of sex or diagnosis × sex effects on BMI ($F = 0.96$, $p = 0.33$; $F = 0.16$, $p = 0.69$). Furthermore, there were no significant sex differences in BMI in any of the subjects, whether they were patients or healthy controls (all p's > 0.05), which suggested that sex had no effects on BMI in patients or controls.

Sex difference in the association between BMI and cognitive scores in patients and controls

To further investigate whether BMI was associated with cognitive scores in different sexes, we further divided the patients into a male patient group and a female patient group. Additional multivariate regression analysis demonstrated a positive association of BMI with language performance in the male patient group ($SS = 0.60$, $t = 3.30$, $p = 0.001$), while other cognitive subscale scores and total scores showed no significant differences after adjusting for confounding variables and performing Bonferroni corrections (all p's > 0.05).

In the healthy control group, BMI was negatively correlated with attention performance in the male control group ($r = -0.26$, $p = 0.001$), including after controlling confounding covariables (partial $r = -0.21$, partial $p = 0.009$). However, this did not persist after Bonferroni correction. Other cognitive subscale scores and total scores showed no significant associations with BMI after adjusting for confounding variables (all p's > 0.05).

TABLE 1 Comparisons among the RBANS total and five subscale scores by diagnostic and sex groupings (Mean ± SD).

RBANS scores	Patients		Controls		Diagnosis		Sex		Diagnosis × Sex	
	Male (N = 684)	Female (N = 183)	Male (N = 158)	Female (N = 244)	F	p	F	p	F	p
Immediate memory	56.88 ± 15.58	60.02 ± 18.38	75.56 ± 15.79	75.77 ± 18.27	256.95	<0.001	3.69	0.06	0.17	0.68
Attention	64.19 ± 17.87	64.21 ± 20.45	89.28 ± 18.34	86.24 ± 21.52	420.86	<0.001	1.78	0.18	0.36	0.55
Language	76.11 ± 17.31[a]	69.25 ± 19.96[a]	95.07 ± 11.41	93.12 ± 14.04	444.23	<0.001	25.13	<0.001[b]	16.71	<0.001[a]
Visuospatial/construction	76.56 ± 18.23	76.86 ± 17.95	81.26 ± 15.61	78.55 ± 15.52	13.19	<0.001	1.93	0.17	0.04	0.85
Delayed memory	63.48 ± 19.09	66.72 ± 20.91	86.72 ± 14.24	85.94 ± 15.91	323.84	<0.001	0.24	0.62	0.04	0.85
Total score	60.88 ± 13.79	61.58 ± 16.66	80.64 ± 14.90	79.31 ± 16.12	436.776	<0.001	0.48	0.49	0.92	0.34

[a]There was a significant effect of diagnosis X Gender on language score after a Bonferroni correction ($F = 16.71$, $p < 0.001$). Male patients had higher language performance than female patients. [b]Furthermore, there was a significant effect of gender on language score after a Bonferroni correction ($F = 25.13$, $p < 0.001$). The language score was higher in male than in female patients with schizophrenia ($F = 17.83$; $p < 0.0001$), while no difference was found in language score between males and females in controls ($p > 0.05$).

TABLE 2 Comparisons among the RBANS total and five subscale scores by gender and genotypic groupings in patient group (Mean ± SD).

RBANS scores	Male		Female		Sex		Genotype		Sex × Genotype	
	CC (N = 658)	CT (N = 26)	CC (N = 178)	CT (N = 5)	F	p	F	p	F	p
Immediate memory	57.05 ± 15.63	52.54 ± 14.00	60.45 ± 18.42	44.80 ± 8.04	0.003	0.96	4.14	0.04[a]	0.17	0.69
Attention	64.32 ± 18.00	60.96 ± 13.83	64.29 ± 20.58	61.40 ± 16.42	0.07	0.80	0.09	0.76	0.03	0.86
Language	76.19 ± 17.31	74.19 ± 17.53	69.50 ± 19.99	60.20 ± 18.21	4.89	0.03[a]	0.86	0.36	0.19	0.67
Visuospatial/construction	76.58 ± 18.27	75.92 ± 17.35	77.02 ± 17.93	71.20 ± 19.73	0.06	0.81	0.003	0.96	0.18	0.67
Delayed memory	63.50 ± 19.09	62.88 ± 19.33	66.95 ± 20.95	58.60 ± 19.41	0.02	0.88	0.09	0.77	<0.0001	0.99
Total score	60.97 ± 13.90	58.65 ± 10.76	61.79 ± 16.77	54.20 ± 10.92	0.23	0.63	0.86	0.36	0.02	0.90

[a]The p-value did not survive after a Bonferroni correction.

10.3389/fnagi.2022.920352

Sex differences in the association of BMI with cognitive performance: adjusted by *FOXP2* rs10447760

To further explore the association between BMI and cognitive performance in different *FOXP2* rs10447760 genotypes, we divided the patients into two genotypic groups: patients carrying CC and patients carrying CT. Multivariate regression analysis demonstrated a positive association between BMI and language scores in the patient group carrying the CC genotype ($SS = 0.53$, $t = 3.16$, $p = 0.002$). Interestingly, this positive association was found only in male patients ($SS = 0.63$, $t = 3.44$, $p = 0.001$), not in female patients ($p > 0.05$).

In the healthy control group, no association was found between BMI and any of the five RBANS subscale scores or total scores in either *FOXP2* genotypic subgroup, after adjusting for confounding variables and performing Bonferroni corrections (all p's > 0.05).

Discussion

The main findings of this study were: (1) male schizophrenia patients had better language performance than female patients; (2) the *FOXP2* rs10447760 genotype did not show an interaction with sex on cognitive performance in schizophrenia patients; (3) there was a positive correlation between BMI and language performance only in male schizophrenia patients; (4) after stratification by *FOXP2* rs10447760 genotype, there was a positive correlation between BMI and language performance only in schizophrenia patients carrying the CC genotype.

Considering differences in hormonal status, psychosocial stress, and brain structure and function between male and female patients with schizophrenia, previous evidence has documented sex-specific effects on cognitive deficits in schizophrenia (Han et al., 2012). However, these results are still controversial. Most prior studies have shown that male schizophrenia patients have relatively worse performances on various cognitive dimensions (Han et al., 2012; Leger and Neill, 2016), but some studies have shown opposite results (Gogos et al., 2010; Leger and Neill, 2016). Additionally, other studies have shown that sex has no effect on cognitive changes in schizophrenia (Karilampi et al., 2011; Kao et al., 2013). Our results demonstrated better language cognitive performance in males compared to female patients with chronic schizophrenia. Previously, Lewine et al. (1996) found greater deficits in verbal and spatial memory in female patients with schizophrenia. They also found the worse performance of the right hemisphere than that of the left hemisphere, consistent with previous evidence showing right-hemispheric brain activation contributes to language function (van Ettinger-Veenstra et al., 2010).

We have previously reported that *FOXP2* rs10447760 affects immediate memory in chronic schizophrenia (Lang et al., 2019). However, we did not find any effects of *FOXP2* rs10447760 on any cognitive scores across sexes, indicating that there were no interactive effects of *FOXP2* rs10447760 and sex on cognitive scores in schizophrenia. Few prior studies have explored the interplay of sex and gene polymorphism on cognitive deficits in schizophrenia. One previous study found significant sex interactions when assessing the relationship between BDNF AL66Met polymorphism, another neurotrophic factor, and cognitive performance (Kim et al., 2016). This evidence suggests that different genes, or even different polymorphisms in the same gene, can lead to different sex-specific interactions on cognitive functioning.

Higher BMI and obesity are common in schizophrenia patients. However, any effects of BMI on cognitive performance within schizophrenia patients are unknown (Bora et al., 2017). Previous findings have suggested that the influence of BMI on cognitive deficits in schizophrenia is complex (Friedman et al., 2010; Takayanagi et al., 2012; Rashid et al., 2013; Hidese et al., 2018). Other aspects, including sex and genetic background, may be involved in the association between BMI and cognitive deficits in schizophrenia patients (Rashid et al., 2013). A previous study by our group also showed that NRG3 polymorphism altered the effect of BMI on cognitive deficits of patients with schizophrenia (Zhou et al., 2020). Here, we showed that there was a positive association between BMI and language performance in schizophrenia patients, even after adjusting for demographic and clinical covariables. Interestingly, this positive association was found in male patients, but not in female patients. It seems likely that BMI affects cognitive deficits as a function of sex in schizophrenia. Previously, one study demonstrated that increased BMI correlated with worse executive function and attention in male patients with heart failure, but not in female patients, which also indicated an interacting sex effect on the relationship between BMI and cognitive function (Hawkins et al., 2014).

FOXP2 plays a critical role in the neuronal processes that contribute to language and speech performance (Liegeois et al., 2003; Vernes et al., 2007), and its polymorphisms have been reported to be involved in the pathophysiology of cognitive function and language phenotypes in schizophrenia (Tolosa et al., 2010; Mozzi et al., 2017). However, we did not find any associations between the *FOXP2* rs10447760 genotype and language scores in our previous study (Lang et al., 2019), and a recent meta-analysis also showed no association between *FOXP2* variations and language deficits in schizophrenia (McCarthy et al., 2019). These inconsistent findings might be the result of foregoing consideration of other crucial demographic or clinical

characteristics, including BMI and sex. In this study, although we did not observe an interactive effect between sex and *FOXP2* rs10447760 on cognitive deficits, we did find that *FOXP2* rs10447760 interplayed with BMI to affect cognitive changes in schizophrenia patients: There was a positive correlation of BMI with language function only in schizophrenia patients with the *FOXP2* rs10447760 CC genotype. This suggests that BMI might affect cognitive deficits in schizophrenia as a condition of specific *FOXP2* genotypes. *FOXP2* has also been associated with obesity in previous studies (Glessner et al., 2010; Xia and Grant, 2013; Clifton et al., 2018). Accumulating evidence indicates there is a shared genetic pathway or system for cognitive performance and BMI (Marioni et al., 2016). Marioni et al. (2016) demonstrated that individual genetic mutations correlating with BMI account for a critical component of the variance in cognitive performance, and *vice versa*. They also showed that genetic variants leading to higher cognitive performance correlated with lower BMI (Marioni et al., 2016). In addition, some studies have also suggested that genetic factors contribute highly to cognitive function and BMI phenotypes. For example, Frazier-Wood et al. (2014) reported between 20% and 30% shared genetic variance of cognitive function and BMI of 20%–30% (Laitala et al., 2011). Additionally, these shared genetic pathways or systems appear to display overlapping gene expression profiles in specific areas of the brain (Locke et al., 2015). Our present results provide further evidence of the shared genetic influences underlying BMI and cognitive function.

The present study has some limitations. First, we recruited patients with chronic schizophrenia and with different antipsychotic treatment regimens. However, several lines of evidence indicate that the style and severity of cognitive deficits are fundamentally stable. In addition, cognitive deficits were independent of illness duration and remained relatively stable without changes over time (Harvey et al., 1990; Bowie and Harvey, 2006). Furthermore, the different antipsychotics used all converted to chlorpromazine. Second, although we recruited relatively larger samples, unequal sample sizes between the patient and control groups, as we had here, may cause type II error. Furthermore, there were unequal sample sizes between males and females within patient or healthy controls, and unequal sample sizes between *FOXP2* CC and *FOXP2* CT genotypes within the patient group. Further studies in first episode drug naïve schizophrenia patients, and studies with equal sample sizes between patients and controls, should be conducted to validate our results. With regard to the unequal sample sizes between *FOXP2* C and T alleles within subjects, *FOXP2* rs10447760 has the rare variant allele T in the Asian population. Thus, a small number of subjects with CT genotype may dramatically change the significance of p-value. Last but not least, the differences in sex, BMI, and education between patients and healthy controls might influence the results, although these factors have been adjusted for.

In conclusion, the present study showed sex differences in language deficits in schizophrenia patients. Furthermore, sexual dimorphism and *FOXP2* rs10447760 may impact the influence of BMI on language-based cognitive deficits in schizophrenia patients.

Data availability statement

The datasets presented in this study can be found in online repositories. The names of the repository/repositories and accession number(s) can be found below: https://ngdc.cncb.ac.cn/gsub/submit/bioproject/list,subSAM098688.

Ethics statement

The studies involving human participants were reviewed and approved and the protocol was approved by the ethics committee of the Beijing Huilongguan Hospital (No. BJ-7072035). The patients/participants provided their written informed consent to participate in this study.

Authors contributions

ZL, MXi, and XZ designed the study. ZL, MF, MXu, and YC wrote the article. MY and XL did the statistical analysis. All authors contributed to the article and approved the submitted version.

Funding

This research was funded by National Natural Science Foundation of China (81401127, 62073058), Chengdu Municipal Health Commission (2021057), Open Project Program of State Key Laboratory of Virtual Reality Technology and Systems, Beihang University (No. VRLAB2022 B02), and Shanghai Key Laboratory of Psychotic Disorders Open Grant (21-K03). Funding had no role in study design, data analysis, or the decision to submit the article for publication.

Acknowledgments

We thank all of the patients and healthy volunteers who participated in this research. We also thank Dr. Dachun Chen,

Song Chen, and Gui Gang Yang for all of their hard work and significant contributions to this study.

Conflict of interest

The authors declare that the research was conducted in the absence of any commercial or financial relationships that could be construed as a potential conflict of interest.

Publisher's note

All claims expressed in this article are solely those of the authors and do not necessarily represent those of their affiliated organizations, or those of the publisher, the editors and the reviewers. Any product that may be evaluated in this article, or claim that may be made by its manufacturer, is not guaranteed or endorsed by the publisher.

References

Bora, E., Akdede, B. B., and Alptekin, K. (2017). The relationship between cognitive impairment in schizophrenia and metabolic syndrome: a systematic review and meta-analysis. *Psychol. Med.* 47, 1030–1040. doi: 10.1017/S0033291716003366

Bowie, C. R., and Harvey, P. D. (2006). Cognitive deficits and functional outcome in schizophrenia. *Neuropsychiatr. Dis. Treat.* 2, 531–536. doi: 10.2147/nedt.2006.2.4.531

Clifton, E. A. D., Perry, J. R. B., Imamura, F., Lotta, L. A., Brage, S., Forouhi, N. G., et al. (2018). Genome-wide association study for risk taking propensity indicates shared pathways with body mass index. *Commun. Biol.* 1:36. doi: 10.1038/s42003-018-0042-6

Davies, G., Armstrong, N., Bis, J. C., Bressler, J., Chouraki, V., Giddaluru, S., et al. (2015). Genetic contributions to variation in general cognitive function: a meta-analysis of genome-wide association studies in the CHARGE consortium (N=53949). *Mol. Psychiatry* 20, 183–192. doi: 10.1038/mp.2014.188

Frazier-Wood, A. C., Carnell, S., Pena, O., Hughes, S. O., O'Connor, T. M., Asherson, P., et al. (2014). Cognitive performance and BMI in childhood: shared genetic influences between reaction time but not response inhibition. *Obesity (Silver Spring)* 22, 2312–2318. doi: 10.1002/oby.20862

Friedman, J. I., Wallenstein, S., Moshier, E., Parrella, M., White, L., Bowler, S., et al. (2010). The effects of hypertension and body mass index on cognition in schizophrenia. *Am. J. Psychiatry* 167, 1232–1239. doi: 10.1176/appi.ajp.2010.09091328

Gerretsen, P., Voineskos, A. N., Graff-Guerrero, A., Menon, M., Pollock, B. G., Mamo, D. C., et al. (2017). Insight into illness and cognition in schizophrenia in earlier and later life. *J. Clin. Psychiatry* 78, e390–e397. doi: 10.4088/JCP.16m10741

Glessner, J. T., Bradfield, J. P., Wang, K., Takahashi, N., Zhang, H., Sleiman, P. M., et al. (2010). A genome-wide study reveals copy number variants exclusive to childhood obesity cases. *Am. J. Hum. Genet.* 87, 661–666. doi: 10.1016/j.ajhg.2010.09.014

Gogos, A., Joshua, N., and Rossell, S. L. (2010). Use of the repeatable battery for the assessment of neuropsychological status (RBANS) to investigate group and gender differences in schizophrenia and bipolar disorder. *Aust. N. Z. J. Psychiatry* 44, 220–229. doi: 10.3109/00048670903446882

Hagenaars, S. P., Harris, S. E., Davies, G., Hill, W. D., Liewald, D. C., Ritchie, S. J., et al. (2016). Shared genetic aetiology between cognitive functions and physical and mental health in UK Biobank (N=112 151) and 24 GWAS consortia. *Mol. Psychiatry* 21, 1624–1632. doi: 10.1038/mp.2015.225

Han, M., Huang, X. F., Chen, D. C., Xiu, M. H., Hui, L., Liu, H., et al. (2012). Gender differences in cognitive function of patients with chronic schizophrenia. *Prog. Neuropsychopharmacol. Biol. Psychiatry* 39, 358–363. doi: 10.1016/j.pnpbp.2012.07.010

Harvey, P. D., Aslan, M., Du, M., Zhao, H., Siever, L. J., Pulver, A., et al. (2016). Factor structure of cognition and functional capacity in two studies of schizophrenia and bipolar disorder: implications for genomic studies. *Neuropsychology* 30, 28–39. doi: 10.1037/neu0000245

Harvey, P. D., Docherty, N. M., Serper, M. R., and Rasmussen, M. (1990). Cognitive deficits and thought disorder: II. An 8-month followup study. *Schizophr. Bull.* 16, 147–156. doi: 10.1093/schbul/16.1.147

Harvey, P. D., Keefe, R. S., Patterson, T. L., Heaton, R. K., and Bowie, C. R. (2009). Abbreviated neuropsychological assessment in schizophrenia: prediction of different aspects of outcome. *J. Clin. Exp. Neuropsychol.* 31, 462–471. doi: 10.1080/13803390802251386

Hawkins, M. A., Gunstad, J., Dolansky, M. A., Redle, J. D., Josephson, R., Moore, S. M., et al. (2014). Greater body mass index is associated with poorer cognitive functioning in male heart failure patients. *J. Card. Fail.* 20, 199–206. doi: 10.1016/j.cardfail.2013.12.014

Hidese, S., Matsuo, J., Ishida, I., Hiraishi, M., Teraishi, T., Ota, M., et al. (2018). Relationship of handgrip strength and body mass index with cognitive function in patients with schizophrenia. *Front. Psychiatry* 9:156. doi: 10.3389/fpsyt.2018.00156

Hughes, C., Kumari, V., Soni, W., Das, M., Binneman, B., Drozd, S., et al. (2003). Longitudinal study of symptoms and cognitive function in chronic schizophrenia. *Schizophr. Res.* 59, 137–146. doi: 10.1016/s0920-9964(01)00393-0

Jancke, L. (2018). Sex/gender differences in cognition, neurophysiology and neuroanatomy. *F1000Res* 7:F1000 Faculty Rev-805. doi: 10.12688/f1000research.13917.1

Kahn, R. S., and Keefe, R. S. (2013). Schizophrenia is a cognitive illness: time for a change in focus. *JAMA Psychiatry* 70, 1107–1112. doi: 10.1001/jamapsychiatry.2013.155

Kao, Y. C., Liu, Y. P., Lien, Y. J., Lin, S. J., Lu, C. W., Wang, T. S., et al. (2013). The influence of sex on cognitive insight and neurocognitive functioning in schizophrenia. *Prog. Neuropsychopharmacol. Biol. Psychiatry* 44, 193–200. doi: 10.1016/j.pnpbp.2013.02.006

Karilampi, U., Helldin, L., and Archer, T. (2011). Cognition and global assessment of functioning in male and female outpatients with schizophrenia spectrum disorders. *J. Nerv. Ment. Dis.* 199, 445–448. doi: 10.1097/NMD.0b013e318221413e

Keefe, R. S., Eesley, C. E., and Poe, M. P. (2005). Defining a cognitive function decrement in schizophrenia. *Biol. Psychiatry* 57, 688–691. doi: 10.1016/j.biopsych.2005.01.003

Kim, S. W., Lee, J. Y., Kang, H. J., Kim, S. Y., Bae, K. Y., Kim, J. M., et al. (2016). Gender-specific associations of the brain-derived neurotrophic factor Val66Met polymorphism with neurocognitive and clinical features in schizophrenia. *Clin. Psychopharmacol. Neurosci.* 14, 270–278. doi: 10.9758/cpn.2016.14.3.270

Lai, C. S. L., Fisher, S. E., Hurst, J. A., Vargha-Khadem, F., and Monaco, A. P. (2001). A forkhead-domain gene is mutated in a severe speech and language disorder. *Nature* 413, 519–523. doi: 10.1038/35097076

Laitala, V. S., Kaprio, J., Koskenvuo, M., Raiha, I., Rinne, J. O., and Silventoinen, K. (2011). Association and causal relationship of midlife obesity and related metabolic disorders with old age cognition. *Curr. Alzheimer Res.* 8, 699–706. doi: 10.2174/156720511796717186

Lang, X., Zhang, W., Song, X., Zhang, G., Du, X., Zhou, Y., et al. (2019). FOXP2 contributes to the cognitive impairment in chronic patients with schizophrenia. *Aging (Albany NY)* 11, 6440–6448. doi: 10.18632/aging.102198

Leger, M., and Neill, J. C. (2016). A systematic review comparing sex differences in cognitive function in schizophrenia and in rodent models for schizophrenia, implications for improved therapeutic strategies. *Neurosci. Biobehav. Rev.* 68, 979–1000. doi: 10.1016/j.neubiorev.2016.06.029

Lewine, R. R., Walker, E. F., Shurett, R., Caudle, J., and Haden, C. (1996). Sex differences in neuropsychological functioning among schizophrenic patients. *Am. J. Psychiatry* 153, 1178–1184. doi: 10.1176/ajp.153.9.1178

Li, Q., Du, X., Zhang, Y., Yin, G., Zhang, G., Walss-Bass, C., et al. (2017). The prevalence, risk factors and clinical correlates of obesity in Chinese patients

with schizophrenia. *Psychiatry Res.* 251, 131–136. doi: 10.1016/j.psychres.2016.12.041

Li, X., Branch, C. A., and DeLisi, L. E. (2009). Language pathway abnormalities in schizophrenia: a review of fMRI and other imaging studies. *Curr. Opin. Psychiatry* 22, 131–139. doi: 10.1097/YCO.0b013e328324bc43

Li, Z., Liu, L., Lin, W., Zhou, Y., Zhang, G., Du, X., et al. (2020). NRG3 contributes to cognitive deficits in chronic patients with schizophrenia. *Schizophr. Res.* 215, 134–139. doi: 10.1016/j.schres.2019.10.060

Liegeois, F., Baldeweg, T., Connelly, A., Gadian, D. G., Mishkin, M., and Vargha-Khadem, F. (2003). Language fMRI abnormalities associated with *FOXP2* gene mutation. *Nat. Neurosci.* 6, 1230–1237. doi: 10.1038/nn1138

Locke, A. E., Kahali, B., Berndt, S. I., Justice, A. E., Pers, T. H., Day, F. R., et al. (2015). Genetic studies of body mass index yield new insights for obesity biology. *Nature* 518, 197–206. doi: 10.1038/nature14177

Marioni, R. E., Yang, J., Dykiert, D., Mottus, R., Campbell, A., Group, C. C. W., et al. (2016). Assessing the genetic overlap between BMI and cognitive function. *Mol. Psychiatry* 21, 1477–1482. doi: 10.1038/mp.2015.205

McCarthy, N. S., Clark, M. L., Jablensky, A., and Badcock, J. C. (2019). No association between common genetic variation in *FOXP2* and language impairment in schizophrenia. *Psychiatry Res.* 271, 590–597. doi: 10.1016/j.psychres.2018.12.016

Mendrek, A., and Mancini-Marie, A. (2016). Sex/gender differences in the brain and cognition in schizophrenia. *Neurosci. Biobehav. Rev.* 67, 57–78. doi: 10.1016/j.neubiorev.2015.10.013

Mozzi, A., Riva, V., Forni, D., Sironi, M., Marino, C., Molteni, M., et al. (2017). A common genetic variant in *FOXP2* is associated with language-based learning (dis)abilities: evidence from two Italian independent samples. *Am. J. Med. Genet. B Neuropsychiatr. Genet.* 174, 578–586. doi: 10.1002/ajmg.b.32546

Rao, W., Du, X., Zhang, Y., Yu, Q., Hui, L., Yu, Y., et al. (2017). Association between forkhead-box P2 gene polymorphism and clinical symptoms in chronic schizophrenia in a Chinese population. *J. Neural Transm. (Vienna)* 124, 891–897. doi: 10.1007/s00702-017-1723-x

Rashid, N. A., Lim, J., Lam, M., Chong, S. A., Keefe, R. S., and Lee, J. (2013). Unraveling the relationship between obesity, schizophrenia and cognition. *Schizophr. Res.* 151, 107–112. doi: 10.1016/j.schres.2013.09.020

Smith, E., Hay, P., Campbell, L., and Trollor, J. N. (2011). A review of the association between obesity and cognitive function across the lifespan: implications for novel approaches to prevention and treatment. *Obes. Rev.* 12, 740–755. doi: 10.1111/j.1467-789X.2011.00920.x

Snitz, B. E., Macdonald, A. W., 3rd, and Carter, C. S. (2006). Cognitive deficits in unaffected first-degree relatives of schizophrenia patients: a meta-analytic review of putative endophenotypes. *Schizophr. Bull.* 32, 179–194. doi: 10.1093/schbul/sbi048

Takayanagi, Y., Cascella, N. G., Sawa, A., and Eaton, W. W. (2012). Diabetes is associated with lower global cognitive function in schizophrenia. *Schizophr. Res.* 142, 183–187. doi: 10.1016/j.schres.2012.08.034

Tolosa, A., Sanjuan, J., Dagnall, A. M., Molto, M. D., Herrero, N., and de Frutos, R. (2010). *FOXP2* gene and language impairment in schizophrenia: association and epigenetic studies. *BMC Med. Genet.* 11:114. doi: 10.1186/1471-2350-11-114

Toulopoulou, T., Picchioni, M., Rijsdijk, F., Hua-Hall, M., Ettinger, U., Sham, P., et al. (2007). Substantial genetic overlap between neurocognition and schizophrenia: genetic modeling in twin samples. *Arch. Gen. Psychiatry* 64, 1348–1355. doi: 10.1001/archpsyc.64.12.1348

Tripathi, A., Kar, S. K., and Shukla, R. (2018). Cognitive deficits in schizophrenia: understanding the biological correlates and remediation strategies. *Clin. Psychopharmacol. Neurosci.* 16, 7–17. doi: 10.9758/cpn.2018.16.1.7

van Ettinger-Veenstra, H. M., Ragnehed, M., Hallgren, M., Karlsson, T., Landtblom, A. M., Lundberg, P., et al. (2010). Right-hemispheric brain activation correlates to language performance. *Neuroimage* 49, 3481–8. doi: 10.1016/j.neuroimage.2009.10.041

Vernes, S. C., Spiteri, E., Nicod, J., Groszer, M., Taylor, J. M., Davies, K. E., et al. (2007). High-throughput analysis of promoter occupancy reveals direct neural targets of FOXP2, a gene mutated in speech and language disorders. *Am. J. Hum. Genet.* 81, 1232–1250. doi: 10.1086/522238

Xia, Q., and Grant, S. F. (2013). The genetics of human obesity. *Ann. N Y Acad. Sci.* 1281, 178–190. doi: 10.1111/nyas.12020

Zhang, K., Gao, X., Qi, H., Li, J., Zheng, Z., and Zhang, F. (2010). Gender differences in cognitive ability associated with genetic variants of NLGN4. *Neuropsychobiology* 62, 221–228. doi: 10.1159/000319948

Zhou, Y., Li, Y., Meng, Y., Wang, J., Wu, F., Ning, Y., et al. (2020). Neuregulin 3 rs10748842 polymorphism contributes to the effect of body mass index on cognitive impairment in patients with schizophrenia. *Transl. Psychiatry* 10:62. doi: 10.1038/s41398-020-0746-5

frontiers | Frontiers in Aging Neuroscience

TYPE Review
PUBLISHED 05 August 2022
DOI 10.3389/fnagi.2022.977999

Check for updates

OPEN ACCESS

EDITED BY
Jun Xu,
Capital Medical University, China

REVIEWED BY
Weinan Zhou,
University of Illinois
at Urbana-Champaign, United States
Feng Wang,
Emory University, United States

*CORRESPONDENCE
Kun Wang
wktawx@163.com
Min Tang
mt3138@ujs.edu.cn

SPECIALTY SECTION
This article was submitted to
Cellular and Molecular Mechanisms
of Brain-aging,
a section of the journal
Frontiers in Aging Neuroscience

RECEIVED 25 June 2022
ACCEPTED 18 July 2022
PUBLISHED 05 August 2022

CITATION
Gong X, Zhang H, Liu X, Liu Y, Liu J, Fapohunda FO, Lü P, Wang K and Tang M (2022) Is liquid biopsy mature enough for the diagnosis of Alzheimer's disease?
Front. Aging Neurosci. 14:977999.
doi: 10.3389/fnagi.2022.977999

COPYRIGHT
© 2022 Gong, Zhang, Liu, Liu, Liu, Fapohunda, Lü, Wang and Tang. This is an open-access article distributed under the terms of the Creative Commons Attribution License (CC BY). The use, distribution or reproduction in other forums is permitted, provided the original author(s) and the copyright owner(s) are credited and that the original publication in this journal is cited, in accordance with accepted academic practice. No use, distribution or reproduction is permitted which does not comply with these terms.

Is liquid biopsy mature enough for the diagnosis of Alzheimer's disease?

Xun Gong[1], Hantao Zhang[2], Xiaoyan Liu[2], Yi Liu[2,3], Junlin Liu[2], Funmilayo O. Fapohunda[2], Peng Lü[2], Kun Wang[4]* and Min Tang[2]*

[1]Department of Rheumatology and Immunology, Affiliated Hospital of Jiangsu University, Zhenjiang, China, [2]School of Life Sciences, Jiangsu University, Zhenjiang, China, [3]Institute of Animal Husbandry, Jiangsu Academy of Agricultural Sciences, Nanjing, China, [4]Children's Center, The Affiliated Taian City Central Hospital of Qingdao University, Taian, China

The preclinical diagnosis and clinical practice for Alzheimer's disease (AD) based on liquid biopsy have made great progress in recent years. As liquid biopsy is a fast, low-cost, and easy way to get the phase of AD, continual efforts from intense multidisciplinary studies have been made to move the research tools to routine clinical diagnostics. On one hand, technological breakthroughs have brought new detection methods to the outputs of liquid biopsy to stratify AD cases, resulting in higher accuracy and efficiency of diagnosis. On the other hand, diversiform biofluid biomarkers derived from cerebrospinal fluid (CSF), blood, urine, Saliva, and exosome were screened out and biologically verified. As a result, more detailed knowledge about the molecular pathogenesis of AD was discovered and elucidated. However, to date, how to weigh the reports derived from liquid biopsy for preclinical AD diagnosis is an ongoing question. In this review, we briefly introduce liquid biopsy and the role it plays in research and clinical practice. Then, we summarize the established fluid-based assays of the current state for AD diagnostic such as ELISA, single-molecule array (Simoa), Immunoprecipitation–Mass Spectrometry (IP–MS), liquid chromatography–MS, immunomagnetic reduction (IMR), multimer detection system (MDS). In addition, we give an updated list of fluid biomarkers in the AD research field. Lastly, the current outstanding challenges and the feasibility to use a stand-alone biomarker in the joint diagnostic strategy are discussed.

KEYWORDS

Alzheimer's disease, liquid biopsy, blood, CSF, biomarkers

Introduction

Alzheimer's disease (AD) is a neurologic condition in which the brain shrinks and brain cells necrotize, which is characterized by a progressive loss of cognitive, behavioral, and social abilities (Soria Lopez et al., 2019). In the United States, AD is recognized as the most common cause of dementia, which affects about 5.1 million people aged 65 and up,

impairing their ability to work and live independently (Lane et al., 2018). Memory loss, intellectual disability, various cognitive abnormalities, and disorientation are among the symptoms of AD, and risk factors include age, sex, down syndrome, familial inheritance, and poor sleeping habits (Silva et al., 2019). Furthermore, the death rate from AD has been growing substantially, with a 71% increase from 2000 to 2013 (Cass, 2017; Tiwari et al., 2019). In the regions of the brain affected by this disease, the accumulation of intracellular neurofibrillary tangles (NFT) and extracellular amyloid plaques was found. These plaques are mainly comprised of neurotoxic amyloid-beta protein 40 (Aβ40) and amyloid-beta protein 42 (Aβ42), which would have a devastating effect on neuronal cells (Hodson, 2018; Breijyeh and Karaman, 2020). Though AD remains a major public health problem, there are only two classes of pharmacologic therapy available for treating patients with AD, which include inhibitors to cholinesterase enzyme and antagonists to *N*-methyl-D-aspartate (NMDA). It was proved that these two classes can only be used to treat the symptoms of AD but not to cure it (Chu, 2012; Birks and Harvey, 2018; Atri, 2019). Due to the difficulty of treating AD, special attention should be paid to developing methods for accurate and timely diagnosis.

Normally, the diagnosis of AD is based on clinical evaluation, with several tests required for a conclusive diagnosis, including neuropsychological examination, magnetic resonance imaging (MRI) or computed tomography (CT) for neurons, and serum vitamin B12 level test (Hane et al., 2017). However, early diagnosis of AD is also complicated since early symptoms are shared by several diseases with similar neuropathological features (Weller and Budson, 2018). The identification of measurable, non-invasive, and reliable biomarkers for AD early diagnosis must help address this problem. Biological markers, or biomarkers, are widely used in human pathology for both diagnosis and disease monitoring. They are parameters determined by biological methods and primarily used to determine whether a certain disease exists or not, as well as the likelihood of contracting it (Wu and Qu, 2015). Actually, in the fields of lung cancer, colorectal cancer, and pancreatic, research has already been conducted to discover liquid biopsy biomarkers for cancer prognosis (Vaidyanathan et al., 2018). Unlike tumor tissue biopsy, liquid biopsy is a non-invasive detection method that can enable researchers to get information from body fluid samples by sampling and analyzing these samples and monitoring the patient condition in real-time (Poulet et al., 2019). In addition, tumor tissue biopsy is rather difficult to conduct in several cases. Because liquid biopsy is easier, quicker, and less painful than conventional biopsy, it is a promising alternative to existing surgical biopsies (Mader and Pantel, 2017).

Given the breakthrough nature of liquid biopsy in Oncology, there is a promising rationale for trans-fertilization and validation of blood-based liquid biopsy in AD (Hampel et al., 2019). Since there are no specific signs or symptoms associated with AD, the discovery of blood biomarkers for AD allows for a less invasive and more precise diagnosis, which may aid in identifying patients at risk before clinical symptoms and complications occur and defining disease stages (Lashley et al., 2018). The liquid biopsy would be especially useful in identifying people with preclinical AD, namely those with AD neuropathology but no clinical symptoms (Markesbery et al., 2006). In this review, we introduced liquid biopsy and the role it plays in disease diagnosis. We also reviewed diversified liquid biopsy tools which sensitively reflect a person's health status and would be used for AD diagnosis. Finally, we discussed challenges and envisioned the future of liquid biopsy.

What is liquid biopsy?

Biopsy is a set of processes that include removing cells or tissues from the primary or metastatic mass and analyzing these samples to find out the causes of patients (De Rubis et al., 2019). In a traditional biopsy, the acquisition of specimens requires a biopsy needle or surgical procedure (see **Figure 1**). Given their invasive nature, tissue biopsy presents several limitations, which include patient risk, procedural costs, and invasive testing (Chen et al., 2020). In this regard, liquid biopsy can overcome these disadvantages and provide patients with a minimally invasive approach capable of cancer diagnosis (Smania, 2020).

Liquid biopsy is defined by the National Cancer Institute (NCI) as "a test done on a sample of blood to look for cancer cells from a tumor that are circulating in the blood or for pieces of DNA from tumor cells that are in the blood" (Underwood et al., 2020). Though blood is most commonly used, the use of other kinds of body fluids such as CSF, urine, saliva, and stool are also involved in liquid biopsy (Blanco and Wolfgang, 2019). Compared with samples taken from the primary tumor, body fluid reflects a much broader range of tumor properties. The tumor circulome is defined as a portion of circulating components shed from tumor tissue that can be collected from body fluid (Mader and Pantel, 2017). Analysis of elements of tumor circulome including tumor circulome comprises of circulating tumor cells (CTCs), circulating tumor DNA (ctDNA), circulating tumor RNA (ctRNA), and extracellular vesicles (EVs) serves as a superb way for screening, diagnosis, and prognosis of many cancer types (Rohanizadegan and Kulkarni, 2018; Poulet et al., 2019). The number of free CTCs and EVs can both inform the presence of malignant disease and tumor burden (Kloten et al., 2019). Similarly, ctDNA can be used for the early detection of cancer. Besides, nearly all known classes of ctRNA have the potential to serve as biomarkers in cancer diagnosis (Pessoa et al., 2020).

The idea of liquid biopsy is not restricted to oncology but applies to AD diagnosis. Though a definitive method of AD diagnosis is brain tissue evaluation, it is impossible

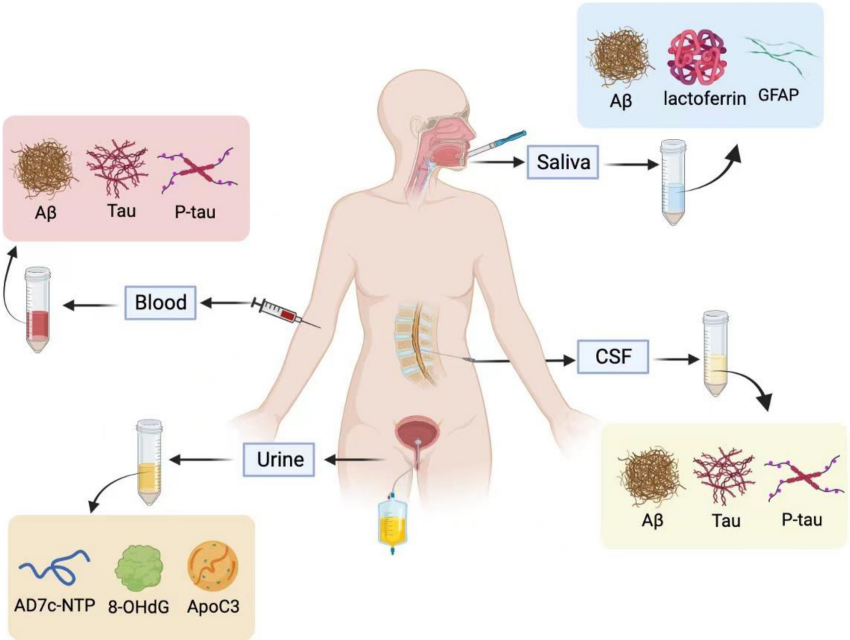

FIGURE 1
Saliva, blood, cerebrospinal fluid (CSF), and urine are used for Alzheimer's fluid biopsy. In the CSF and blood, Aβ, T-tau, and P-tau are used as biochemical indicators for the early diagnosis of Alzheimer's disease. The specific biomarkers in the urine are AD7c-NTP, 8-OHdG, and ApoC3, and salivary biomarkers are Aβ, Lactoferrin, and GFAP. Illustrations were generated using BioRender.

to take samples of living patients' brain tissue (Weller and Budson, 2018). Biomarkers derived from CSF analysis have been used for *in vivo* AD detection (Hampel et al., 2021). Because it is generally believed that the onset of AD relates to the deposition of amyloid-β (Aβ) in extracellular plaques, aggregation of tau into neurofibrillary tangles in neurons, and abnormal phosphorylation of tau, the measurements of Aβ1–42, hyperphosphorylated tau, and total tau proteins are options for AD early diagnosis (Hersi et al., 2017; Park et al., 2020). However, this method is risky and inconvenient due to the invasive nature of its lumbar puncture procedure (Li et al., 2019). It often takes weeks to obtain final results due to the deficiency of laboratory facilities, which makes CSF analysis unsuitable for broad clinical implementation (Delgado-Peraza et al., 2021). Blood-based liquid biopsy is an ideal substitute for CSF-based liquid biopsy since it is non-invasive and cost-effective (Abdel-Haq, 2020).

Blood-based liquid biopsy for preclinical or clinical AD diagnosis is a multistep work-up (Baldacci et al., 2019). For example, EVs are regarded as attractive tools for non-invasive diagnosis since they are stable and contain diverse molecules from their parental cells. To use blood-derived EVs to determine if a person suffers from AD, blood samples should be obtained through venipuncture, and EVs should be isolated from blood (Mustapic et al., 2017). The major isolation strategies include ultracentrifugation, polymer precipitation, ultrafiltration, size-exclusion chromatography, affinity isolation, and microfluidics-based techniques. Finally, clinicians can gain a view of an individual's health status by detecting the neurogranin level in blood-derived EVs, since it is downregulated in AD patients (Liu J. et al., 2021).

While liquid biopsy is a minimally invasive and cost-effective method that could be used to detect disease before patients have symptoms, many problems still need to be solved before liquid biopsy become a great alternative to tissue biopsy (De Rubis et al., 2019; Smania, 2020). First and foremost, the sensitivity and specificity of liquid biopsy assays need to be refined (Underwood et al., 2020). Meanwhile, protocols, pre-analytical, and analytical procedures need to be standardized (Blanco and Wolfgang, 2019). These procedures may include sample collection, liquid biopsy components isolation, analysis, data organization, and sharing (Poulet et al., 2019).

The cutting-edge liquid biopsy technologies for Alzheimer's disease

Blood sampling may be preferable to CSF sampling due to its convenient, inexpensive, safe, and minimally invasive nature, but measuring brain disease biomarkers in the blood presents a variety of challenges. Since the blood-brain barrier prevents molecules from freely passing between the central

nervous system (CNS) and blood, brain-derived biomarkers are usually found in low concentrations in blood (Lista et al., 2013). Also, biomarkers linked to AD pathology are rarely concentrated in non-cerebral tissues, making blood measurements challenging. Even though certain biomarkers linked to Alzheimer's disease pathology are expressed in non-cerebral tissues, their measurement in the blood could be muddled (Blennow and Zetterberg, 2018a; Liu L. et al., 2021). To solve this problem, several ultra-high-sensitivity technologies capable of quantifying concentrations of biomarkers not only in CSF but also in blood have been developed. These innovative technologies can be applied to the early stage diagnosis of AD (Kulichikhin et al., 2021).

Stable isotope labeling kinetics

The Stable Isotope Labeling Kinetics (SILK) technique has been widely used to measure the protein turnover in human plasma and CSF such as three Aβ peptides (Aβ38, Aβ40, and Aβ42), tau and/or p-tau, superoxide dismutase 1 (SOD1) and three ApoE isoforms (ApeE2, ApoE3, ApoE4) (Crisp et al., 2015; Paterson et al., 2019; Dincer et al., 2020; Li et al., 2021; Elbert et al., 2022). In the process of using this technique, the different Aβ were immunoprecipitated simultaneously via monoclonal anti-Aβ mid-domain antibodies and later quantified by the liquid chromatography mass spectrometry (LC-MS/MS). In amyloid positive individuals, the Aβ42 concentrations and Aβ42/Aβ40 concentration ratios are significantly lower than those in amyloid negative individuals, which is consistent with that in CSF. Though the differences in plasma Aβ42/Aβ40 ratios between amyloid positive and negative individuals are of lesser magnitude compared to CSF, the LC-MS/MS ensures specificity and precision of results, which makes SILK a reliable tool for AD diagnosis (Potter et al., 2013; Baker-Nigh et al., 2016; Ovod et al., 2017). In the early stages, Basak et al. (2012) successfully measured the clearance rates of ApoE and Aβ in the mouse brain pulse-labeled by $^{13}C_6$-leucine. Combining with the nanoscale secondary ion mass spectrometry (NanoSIMS) imaging technique, Wildburger et al. (2018) proposed a strategy termed SILK-SIMS to detect plaque dynamics in human AD brains. On the cellular level, the SILK technique can also be employed to measure tau kinetics with multiple isoforms and fragments in the induced pluripotent stem cell (iPSC)-derived neurons (Sato et al., 2018). The big limitation of this technique is the high labeling costs.

Fully automated assays

With the rapid development of technology, fully automated immunoassays such as Elecsys immunoassays (Roche Diagnostics) are now available to measure the CSF or plasma biomarkers with high precision and stability (Asberg et al., 2019; Blennow and Zetterberg, 2019). Using this newly developed Elecsys immunoassay (Palmqvist et al., 2019) examined the Aβ42, Aβ40, total levels of tau protein (T-tau), and phosphorylated tau (P-tau) in the CSF and plasma in two cohorts. It was found that plasma Aβ42 and Aβ40 detected by the fully automated Elecsys platform could be used to predict brain Aβ positivity. Furthermore, additional analysis of other blood biomarkers such as ApoE genotype, T-tau, and neurofilament light chain (NFL) can increase the accuracy of Aβ status prediction (Palmqvist et al., 2019). Meanwhile, the fully automated immunoassay system termed High Sensitivity Chemiluminescence Enzyme Immunoassay (HISCL^{TM} series) based on the plasma biomarkers has been emerging in the diagnosis market (Goto et al., 2019; Miura et al., 2020; Watanabe et al.; Noda et al., 2021).[1] Yamashita et al. (2021) declared that they had developed Aβ40 and Aβ42 immunoassays using the HISCL^{TM} series, which has higher reproducibility, wider dynamic range, and less reaction time compared with the conventional enzyme-linked immunosorbent assays (ELISA). Hence, the fully automated plasma assays as a high-throughput and highly reliable screening tool might be used for clinical AD trials, which would help the patients get rid of unnecessary lumber punctures and save the expanse of examination.

Superconducting quantum interference device-based immunomagnetic reduction (SQUID IMR)

The immunomagnetic reduction (IMR) biomarker detection system was established in the early 2000s (Yang et al., 2017). Magnetic nanoparticles used in IMR are particles whose core comprises Fe3O4 and surface consists of bio-probes and hydrophilic surfactants. The phosphate-buffered saline (PBS) solution where these particles are suspended presents a magnetic property under external alternative-current (ac) magnetic fields, which is termed as *x*ac. When magnetic nanoparticles and target molecules bond together, these particles will become larger and result in a reduction in *x*ac. IMR (%) is the percentage of the reduction in magnetic signals during immune reaction divided by magnetic signals before immune reaction. The reduction in *x*ac could be quite low, which requires magnetic sensors with high sensitivity (Lue et al., 2019). The superconducting-quantum interference-device (SQUID) magnetometer is capable of measuring IMR. The biomarker concentrations can be calculated from IMR via standard curves. Because SQUID IMR can be applied to quantify molecules of any size in human plasma, researchers

1 https://www.sysmex.co.jp/en/rd/report/index.html

have utilized this technology to predict the progression of dementia in high-risk groups. They found that the plasma Aβ42 level is an intriguing index for early detection of cognitive decline in patients with Down syndrome, stroke, or amnestic mild cognitive impairment (aMCI). In addition, the SQUID IMR technology is suitable for predicting Aβ status and brain atrophy (Yang et al., 2020).

Multimer detection system—Oligomerized amyloid beta (MDS-OAβ)

Meng et al. (2019) and Youn et al. (2019) presented the association between Aβ oligomerization in blood and AD neurodegeneration. An et al. (2017) found that Aβ oligomerization was significantly higher in AD patients than in normal people. Plus, the high correlations between Aβ oligomerization levels and other AD biomarkers, such as phosphorylated tau protein (pTau), amyloid positron emission tomography (PET) imaging, CSF biomarkers for Aβ42, total tau, and brain magnetic resonance imaging (MRI) were confirmed in many studies (Choi et al., 2021; Cheng et al., 2022).

Multimer detection system (MDS) is a traditional analytical platform based on modified ELISA to measure Aβ oligomerization tendency (An et al., 2010; Lim et al., 2015; Pyun et al., 2021). The epitope-overlapping detection antibodies applied in MDS are specifically designed for the N-terminus of Aβ for the selection of oligomerized formation over monomeric formation (Wang et al., 2017). Since the Aβ monomers have only one epitope available, once it has associated with a capturing antibody, it has no exposed epitopes to react with the antibodies (see **Figure 2**). Rather, the Aβ multimers with overlapping epitopes which bind the antibodies can be easily detected (An et al., 2010). Because of the ability to screen multimers, MDS has been utilized to differentiate the oligomeric Aβs (OAβ) from the monomeric Aβ in blood. Specific antibodies are used in MDS, and the level of OAβ can be obtained by using a spectrophotometer. As the OAβ test has the potential for distinguishing between AD patients and healthy controls, MDS would be a promising method for AD diagnosis, for example, AlphalLISA assay and the Blood^{TM} OAβ test (PeopleBio Inc., South Korea) (Lee et al., 2020; Babapour Mofrad et al., 2021; Dominguez et al., 2022).

Single molecule array

The single molecule array (Simoa), also known as the single molecule enzyme-linked immunosorbent assay, is a bead-based immunoassay with the ability to detect protein biomarkers in blood at subfemtomolar concentrations (Cohen and Walt, 2017). The specific steps of this approach are as follows: Firstly,

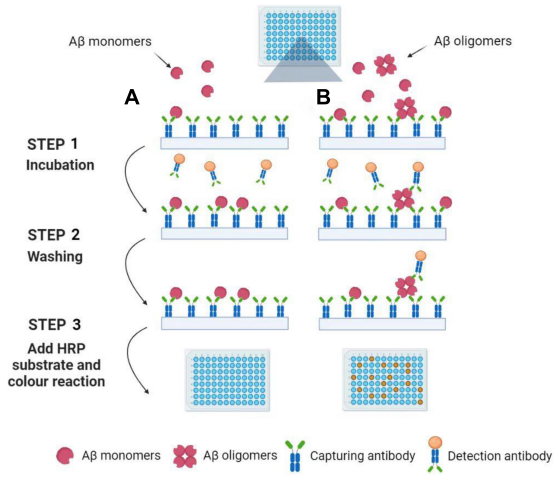

FIGURE 2
Detection of Aβ oligomers using the Multimer Detection System. **(A)** Aβ oligomers do not exist in blood plasma samples. Aβ monomers can be captured by an antibody attached to the ELISA plate's surface. After incubation and washing, the detection antibodies are not present in the well because the capture antibodies have already occupied the single epitope. Finally, the color reaction can be not observed with the addition of HRP substrate. **(B)** Aβ oligomers exist in blood plasma samples. Aβ monomers and oligomers can be captured by an antibody attached to the ELISA plate's surface. After incubation and washing, the detection antibodies are still present in the well because the Aβ oligomers have a lot of epitopes. Finally, the color reaction can be observed with the addition of HRP substrate. Illustrations were generated using BioRender.

paramagnetic beads coated with capture antibodies are added to a sample. The amount of these capture beads is far beyond the number of target analytes contained in a sample so that each capture bead binds to zero or one target analyte. Next, each capture bead is incubated with a biotinylated detection antibody and an enzyme, streptavidin-β-galactosidase (SβG), to form an enzyme-labeled immunocomplex. Thirdly, the beads are suspended in a fluorogenic substrate solution and then loaded into an array (see **Figure 3**). Finally, fluorescence images of the assay are utilized to determine the concentration of a protein biomarker (Cohen et al., 2018, 2020).

Many studies verify that the Simoa assays examining different P-tau isoforms (P-tau181, P-tau217, P-tau231) have high accuracy and specificity to detect early Alzheimer's pathology (Barthelemy et al., 2020b; Karikari et al., 2020, 2021a,b; Palmqvist et al., 2020; Suarez-Calvet et al., 2020; Thijssen et al., 2020; Janelidze et al., 2021; Keshavan et al., 2021; Rauchmann et al., 2021; Ashton et al., 2022). Barthelemy et al. (2020a) and Janelidze et al. (2020b) declared that P-tau217 has higher accuracy than P-tau181 in CSF. Also, Palmqvist et al. (2020) believed that P-tau217 was a better biomarker than P-tau181 in a comparative plasma study, while it was not reproductive with an updated assay (Brickman et al., 2021). In an overall study, Bayoumy et al. (2021) constructed another

comparative plasma study to test three P-tau181 assays (Eli Lilly, ADx, and Quanterix), a P-tau217 assay (Eli Lilly), and two P-tau231 assays (ADx, Gothenburg). All of the six Simoa assays showed robust clinical performance and high-sensitive. Notably, Lantero-Rodriguez et al. (2021) developed a new immunoassay targeting P-tau235 for staging preclinical AD. Currently, the Simoa NF-light Advantage Kit comes on the market, which quantifies the Neurofilament Light (Nf-L) in serum and plasma with high sensitivity (Hendricks et al., 2019; Ashton et al., 2020; Benussi et al., 2020; Manouchehrinia et al., 2020). The blood Nf-L level is becoming a supplemental biomarker of AD, there is little doubt that Simoa is a practical tool for AD diagnosis (Illan-Gala et al., 2021; Leuzy et al., 2021; Zetterberg and Blennow, 2021).

Immunoprecipitation–mass spectrometry

Immunoprecipitation combined with matrix-assisted-laser desorption/ionization time of flight mass spectrometry, or called immunoprecipitation–mass spectrometry (IP–MS) for short, to examine the truncated Aβ peptides is an approach for characterizing protein and peptide mixtures in body fluid (Portelius et al., 2006; Guard et al., 2019). During the IP, target proteins or peptides at low concentrations are enriched using antibodies (see **Figure 4**). Then MS allows an accurate analysis of levels of these proteins or peptides (Uljon et al., 2000; Campbell et al., 2021). Richard et al. (2019) proposed a simplified ad detailed protocol for robust immunoprecipitation of Aβ before mass spectrometric detection. They clarified that the employment of murine monoclonal and rabbit polyclonal antibodies can yield reproducible and high-resolution pictures with low background noise (Richard et al., 2019). The IP–MS method is commonly used to analyze the Aβ38, Aβ40, and Aβ42 levels in plasma, and companies with SILK method in CSF (Ovod et al., 2017). To reduce the amount of lab workload and accelerate the SILK studies, Mawuenyega et al. (2013) developed an efficient and specific quantitative isoform characterization and kinetics method. Plenty of studies adopting the IP-MS method elucidated that plasma Aβ42 concentration and Aβ42/Aβ40 rate are promising biomarkers for predicting Aβ status in individuals (Portelius et al., 2006, 2015; Ovod et al., 2017; Cheng et al., 2022). Furthermore, immunoprecipitation together with SampleStream mass spectrometry (SampleStream-MS) was established. The streamlined workflow could be used to profile protein products of genes efficiently (Santos Seckler et al., 2021).

In sum, a huge development has taken place in the liquid biopsy platform in the past two decades. Researchers used to apply the traditional ELISA to detect and measure core CSF biomarkers, including Aβ42, T-tau, and P-tau (Yoo et al., 2018). While CSF possesses the advantage of being continuous with the brain extracellular fluid, there is little doubt that blood is a more ideal subject for liquid biopsy. However, studying biomarkers in the blood is more challenging than in CSF, for blood only contains a tiny amount of brain protein (Blennow and Zetterberg, 2018b). The advancements in the field of ultra-high-sensitivity technologies provided a solution to this problem. Although these screening tools can accurately quantify biomolecules at ultralow levels, some shortcomings limit their utility in AD biomarker studies (Hampel et al., 2021). For example, due to the spectral overlap of fluorescent dyes, they cannot be used for the simultaneous detection of multiple analytes. In addition, interactions between non-target molecules during the assay can generate erroneous signals, thereby having a negative effect on their sensitivity and specificity (Cohen and Walt, 2017).

Histologic origin used in liquid biopsy and biological markers involved

A biological marker, or biomarker (Cedazo-Minguez and Winblad, 2010), is an indication of normal biological processes, pathogenic processes, or pharmacological responses to a therapeutic intervention that is objectively assessed and evaluated. The most important factors that determine a biomarker's diagnostic utility are its sensitivity, specificity, and ease of use. Since the cognitive symptoms of AD are often diffuse and overlap with other disorders, and the clinical progression is intermittent and variable even among patients with the same disease, biomarkers for AD are extremely important. Biomarkers representing various forms of pathophysiology in the brain can be used for clinical diagnosis, particularly in the early stages of the disorder, to forecast progression, to observe the effects of novel drug candidates in clinical trials, and finally, to further our understanding of the disease's pathogenesis in clinical science (**Table 1**, Blennow et al., 2010). Aiming to gain an insight into biomarkers for the early diagnosis of AD, molecules in CSF and blood have been intensively studied.

Cerebrospinal fluid

CSF can be obtained by lumbar puncture, a diagnostic technique in which a needle is inserted into the subarachnoid space in the lumbar area (L3/L4 or L4/L5), securely below the spinal cord's end.

Since CSF is in indirect contact with the brain's extracellular space, biochemical changes in the brain are expressed in the CSF. In neurodegenerative diseases, neurovascular and blood-brain barrier dysfunction may occur. As a result, CSF is the best source of AD biomarkers (Molinuevo et al., 2014; Ferreri et al., 2021).

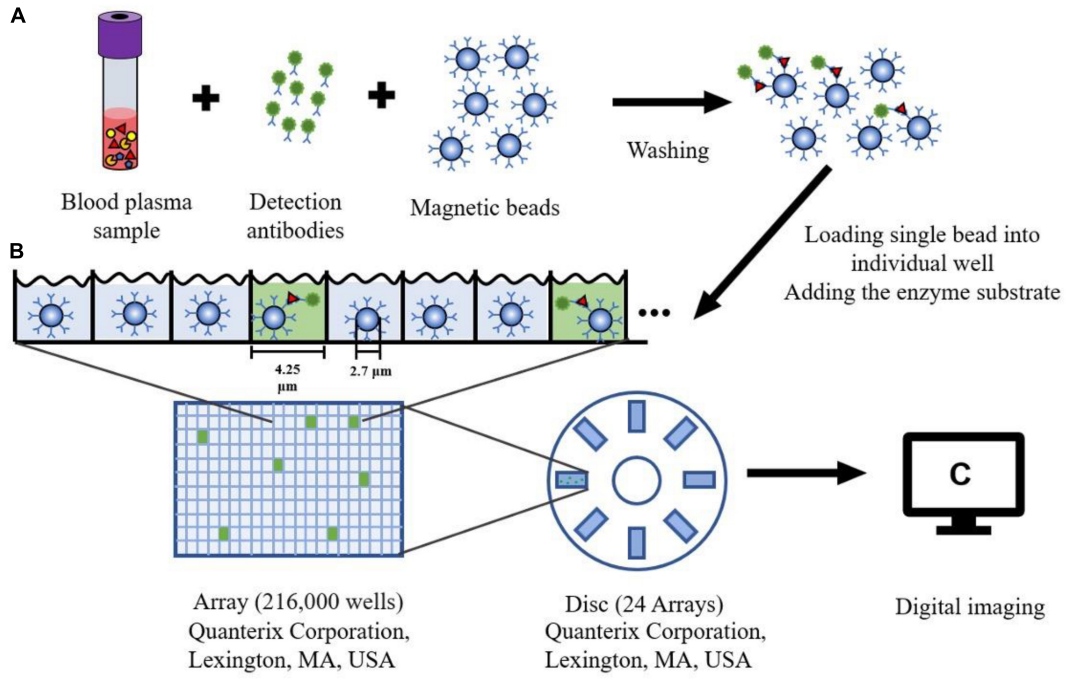

FIGURE 3
The schematic diagram of Single Molecule Array. **(A)** Blood plasma sample is mixed with the magnetic microbeads (2.7 µm) with capture antibodies and detection antibodies. After washing the beads three times, the protein can be captured specifically bound by the antibody. **(B)** Each Single magnetic bead is loaded into one well (4.25 µm diameter, 3.25 µm depth) of the array (216,000 wells). The substrate for the enzyme is added to the well sealing with oil. **(C)** After fluorescence detection of each well, a single molecule signal image can be obtained on this array.

T-tau, P-tau, and the 42-amino acid long amyloid beta peptide (Aβ42) are the most common AD CSF biomarkers.

In cognitively normal people, Aβ is formed in the brain and diffuses into the CSF, where it appears in moderate concentrations with multiple forms. Among them, the levels of Aβ42 and Aβ40 are relatively high. The former is a major component of amyloid plaques, which is regarded as an abnormal pathological lesion (Tiwari et al., 2019). The first step of amyloid pathogenesis is the generation of insoluble Aβ fibrils from amyloid precursor protein (APP) via cleavage. After oligomerization and subsequent polymerization, they transform into amyloid plaques (O'Brien and Wong, 2011). The toxicity of these plaques is associated with some mechanisms, including microglia infiltration, oxidative stress, and synaptic damage (Reiss et al., 2018).

The earliest studies of Aβ being secreted into the CSF date back to 1992, which encouraged researchers to develop corresponding immunoassays (Nitsch et al., 1992). Subsequently, decreased Aβ42 levels in the CSF of AD patients were revealed and validated, yet the cause was unknown for a long time (Gouras et al., 2015). In 2003, an autopsy study discovered a connection between low postmortem ventricular CSF Aβ42 levels and high plaque counts (Strozyk et al., 2003), a finding that was later confirmed in a study revealing a link between reduced CSF Aβ42 measured in ante mortem lumbar CSF samples and amyloid plaque counts measured autopsy (Tapiola et al., 2009). CSF Aβ42 levels can increase and then begin to decline 25 years before the onset of AD symptoms, according to a FAD cohort study from the Dominantly Inherited Alzheimer Network, while amyloid deposition measured with PET and Pittsburgh compound B, as well as an increased concentration of T-tau in the CSF, can be detected 15 years before expected symptom onset (Bateman et al., 2012). These results suggest that a decrease in CSF Aβ42 may be the first sign of preclinical Alzheimer's disease. Low CSF Aβ42 levels have been linked to cognitive impairment in older women (Gustafson et al., 2007). CSF Aβ42 can also be used to predict cognitive impairment in healthy elderly people (Stomrud et al., 2007). In most cases, CSF Aβ42 and amyloid PET status have a high degree of concordance (Blennow et al., 2015). With sensitivity and precision of over 80%, a significant decrease in CSF Aβ42 and a significant increase in CSF t-tau and p-tau can be used to distinguish symptomatic AD patients (Blennow and Hampel, 2003). Hence, in 2012, the utility of CSF Aβ42 in predicting preclinical Alzheimer's disease was verified in cognitively normal individuals with inherited AD genes.

In the brain (Suzuki et al., 1994), CSF (Portelius et al., 2006), and plasma (Zhang et al., 2018), Aβ40 is the most common

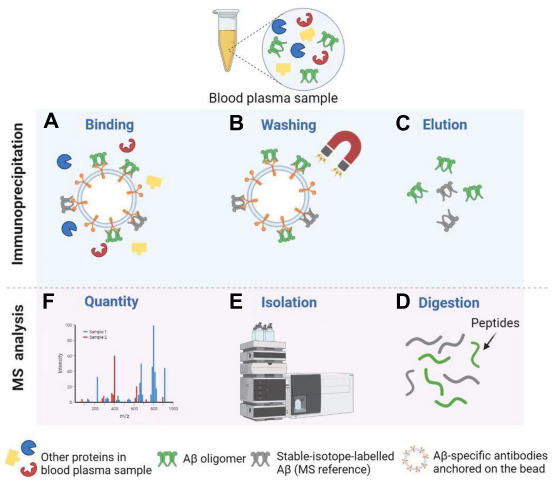

FIGURE 4
Detection of Aβ oligomers using Immunoprecipitation and Mass Spectrometry (IP-MS). **(A)** Aβ oligomers and stable-isotope-labeled Aβ (MS reference) can be captured by Aβ-specific antibodies anchored on the bead. **(B)** After washing, other proteins in the blood plasma sample are removed from the solution. **(C)** Next, Aβ oligomers and MS reference can be separated from the bead for further MS analysis. **(D,E)** After enzymatic digestion, peptides are isolated by High Performance Liquid Chromatography (HPLC). **(F)** Finally, MS profiles can be obtained to carry out the Aβ oligomer quantity. Illustrations were generated using BioRender.

source of Aβ peptide, although it does not appear to be as pathogenic as Aβ42 (McGowan et al., 2005). The CSF Aβ40 level in Alzheimer's patients is higher than in patients with Parkinson's disease dementia (PDD) or with dementia with Lewy bodies (DLB), implying that the Aβ42/Aβ40 ratio will help distinguish AD from PDD and DLB (Nutu et al., 2013). Also, the Aβ42/Aβ40 ratio could be used to differentiate AD from non-AD dementias better than CSF Aβ42 alone (Janelidze et al., 2016). The ratio of CSF Aβ42/Aβ40 is a better indicator of Aβ-positive PET than CSF Aβ42 alone (Pannee et al., 2016; Lewczuk et al., 2017), and is comparable to the ratios of t-tau/Aβ42 and p-tau/Aβ42 (Racine et al., 2016). Currently, fluid-based assays of Aβ40 and Aβ42 are commercially available.

Tau proteins are found in neuronal axons and play roles in preserving the cohesion of microtubules in neurons of the CNS. Tau proteins in the human brain are composed of six soluble isoforms and various phosphorylation sites (Khan and Bloom, 2016). Western blotting was used to classify tau proteins of Alzheimer's disease in CSF in 1987 (Wolozin and Davies, 1987). The development of quantitative immunoassays made the measurement of tau proteins in CSF easier. ELISA method was used to quantify tau in CSF, this method was based on the sandwich format of a monoclonal anti-tau antibody against the mid-domain combined with a polyclonal anti-tau antiserum (Vandermeeren et al., 1993). Apart from acute brain trauma, T-tau CSF levels are emphatic, rising within days of injury and then remaining rapt for weeks before homogenization (Zetterberg et al., 2006). CSF T-tau levels are highest in diseases with the most severe neurodegeneration, such as Creutzfeldt–Jakob disease, Alzheimer's disease, DLB, and frontotemporal dementia (FTD). Since it predicts more rapid clinical disease progression, CSF T-tau has been used as a biomarker for the severity of neurodegeneration (Buchhave et al., 2012; Hansson et al., 2018).

Tau is a phosphoprotein, indicating that its biological activity is completely regulated by its phosphorylation state (Gao et al., 2018). Highly phosphorylated tau proteins tend to form tangles rather than bind to microtubules, which may affect inter-synaptic signaling in brain neurons (Naseri et al., 2019). Since they were found in large numbers in neurofibrillary tangles in the brains of AD patients, they have been believed to be a reliable biomarker for AD (Lindwall and Cole, 1984; Bramblett et al., 1993). For different phosphorylated epitopes of tau proteins, ELISA methods have been established for threonine 181 and 231 (Blennow et al., 1995), threonine 181 (Vanmechelen et al., 2000), threonine 231 and serine 235 (Ishiguro et al., 1999), serine 199 [54], threonine 231 (Kohnken et al., 2000), and serine 396 and 404 (Hu et al., 2002). The phosphorylation state of tau in the brain is reflected in the concentration of phosphorylated tau protein in the CSF. The concentration of phosphorylated tau protein does not alter after an acute stroke, unlike the overall concentration of tau protein (Hesse et al., 2001). Sandwich ELISA was used to detect P-tau 181 in CSF in 2000, and it was discovered that levels were higher in AD patients relative to age-matched controls, but lower in FTD patients, indicating that CSF P-tau 181 may be a more specific marker for AD (Vanmechelen et al., 2000). Another sandwich ELISA for detecting P-tau threonine 231 was produced the same year, with 85 percent sensitivity and 97 percent specificity for distinguishing AD from non-AD controls (Kohnken et al., 2000).

Aβ42, T-tau, and P-tau levels are all considered practical biomarkers for AD (Lee et al., 2019). Moreover, the combined use of the three biomarkers in the diagnosis of AD has provided excellent results. For example, mild cognitive impairment (MCI) is the earliest clinical stage of AD, which is characterized by episodic memory problems. During clinical follow-up, MCI patients who progress to AD with dementia have the standard AD CSF biomarker profile (decreased CSF Aβ42 with increased T-tau and P-tau) already at this stage of the disease (Andreasen et al., 1999).

Blood (plasma/serum)

Blood sampling would be preferable to CSF sampling when taking fluid samples to measure AD biomarkers, both for clinical diagnosis or screening and for repeated sampling in clinical trials, since blood is more accessible than CSF. However,

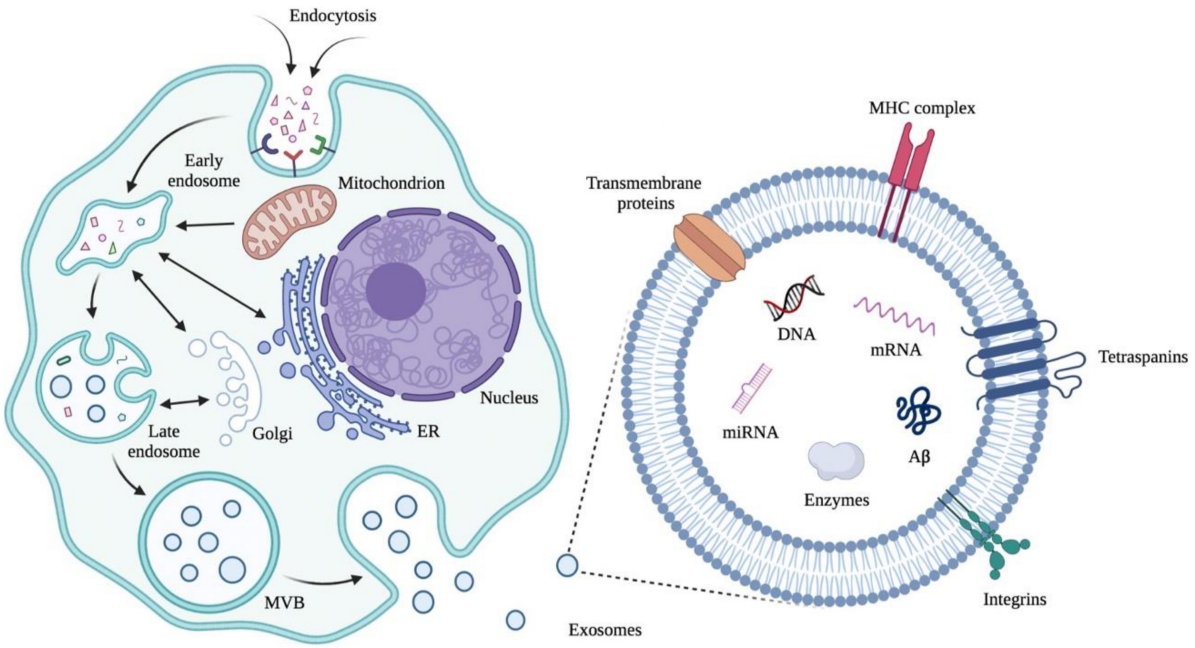

FIGURE 5
Early endosomes are generated from extracellular cargos as well as cell surface proteins through endocytosis. Mitochondria, endoplasmic reticulum (ER), and Golgi are involved in the formation of multivesicular bodies (MVBs) from early endosomes through fusion. MVBs can fuse with plasma membranes and release exosomes, which are membrane nanovesicles that contain plasma-membrane- and cytosol-associated molecules such as nuclear acids and proteins both inside and outside the vesicles. Illustrations were generated using BioRender.

blood-based biomarkers, on the other hand, encounter some challenges. Firstly, blood is a complicated fluid containing many cellular compartments as well as a constantly evolving environment of proteins, lipids, and other biochemical entities, which may intensify issues of reproducibility and necessitate concerted efforts to match methodology throughout studies (Thambisetty and Lovestone, 2010). Secondly, since the blood-brain barrier prevents molecules from freely passing between the CNS and the blood compartments, brain-derived biomarkers are found in low concentrations in the blood. Furthermore, certain biomarkers linked to Alzheimer's disease pathology are expressed in non-cerebral tissues, which may make blood measurements difficult. Consequently, the quantities of brain proteins entering the blood must be calculated in a matrix containing extremely high levels of plasma proteins, posing a significant risk of analytical method intervention (Blennow and Zetterberg, 2015). Thirdly, brain proteins released into the bloodstream can be degraded by proteases, metabolized in the liver, or cleared by the kidneys, resulting in a variation that is unrelated to brain changes and difficult to control. Finally, heterophilic antibodies (endogenous antibodies which respond with the antibodies of the immunochemical test to measure the biomarker) can be present in the blood, resulting in falsely high or low performance. In CSF, where antibody levels are much lower, these types of antibodies are much less of a concern. Despite all the aforementioned issues that limit the possibility of discovering blood biomarkers for AD (O'Bryant et al., 2015), several biomarkers for AD diagnosis have been discovered.

The most widely studied blood markers for the diagnosis of symptomatic and prodromal AD are Aβ42 and Aβ40. Plasma Aβ42 levels are higher than plasma Aβ40 levels in AD patients at baseline and in those who develop AD within 3 years in a follow-up analysis (Mayeux et al., 2003). Individuals with elevated plasma Aβ42 had a more than twofold increased chance of AD onset relative to those with low plasma Aβ42 (Mayeux et al., 2003). A high plasma Aβ40 concentration has also been linked to an increased risk of dementia (van Oijen et al., 2006). Discovered that a lower plasma Aβ42/Aβ40 ratio is linked to greater cognitive impairment in elderly people without dementia over 9 years. The clinical stage of the examination and/or the combination of other forms of dementia can cause this dissimilitude. When compared to age-matched standard controls, Aβ42 levels are lower and Aβ43 levels are higher in the serum of AD patients, indicating that a lower Aβ42/Aβ43 ratio may be used as a blood marker for AD diagnosis (Zou et al., 2013).

Plasma tau concentrations, as determined by ultrasensitive assays, are higher in dementia patients than in cognitively normal controls, but not as significantly as in CSF (Pereira et al., 2021). Plasma tau has become a candidate blood marker for AD diagnosis due to the invasiveness and high costs of testing CSF tau, and several studies have concentrated on the quantitation of

tau in AD, MCI, and normal classes. Since tau levels in plasma are much lower than in CSF (Karikari et al., 2020), ultrasensitive assays were created, which can be used to discover higher levels of T-tau in plasma from AD patients compared to control or MCI patients. However, there is no difference between MCI patients who developed AD and stable MCI patients.

Tau phosphorylated at threonine 181 (P-tau181) in blood has been widely recognized as a simple, accessible, and highly specific biomarker for AD diagnosis (Moscoso et al., 2021). Normally, plasma P-tau181 is higher in Alzheimer's patients compared to people with normal cognitive and will increase as the disease progresses. Therefore, it may be used to estimate the likelihood of people AD in the future, regardless of disease stage (Brickman et al., 2021). Since the increase in plasma P-tau181 is related to Aβ and tau pathologies, it could also be utilized as a screening tool to study the pathophysiology of AD *in vivo* (Janelidze et al., 2020a). Of all the promising clinical applications for plasma P-tau181, the most important one might be to differentiate AD from other neurodegenerative disorders (Simrén et al., 2021). Another likely application for plasma P-tau181 is to determine whether patients need more detailed tau diagnostics testing with PET scans (Thebault et al., 2020).

Neurofilaments (Nfs) are the structural proteins of the neural cytoskeleton (Thebault et al., 2020). The constitutions of Nfs can be divided into three categories according to their molecular weight, which are Nf light (NfL), Nf medium (NfM), and Nf heavy (NfH) chains (Hendricks et al., 2019). Among the three subunits of Nfs, NfL is the most promising biomarker for the diagnosis of neurodegenerative diseases, which plays important role in neuron growth (Bacioglu et al., 2016). Because of the fairly low concentration of NfL in blood, it was not until the development of highly sensitive assays such as Simoa that researchers were able to perform NfL evaluations in blood (Mattsson et al., 2019). Dynamic changes in plasma NfL concentrations are correlated with neurodegeneration in AD, as Alzheimer's patients had higher plasma NfL levels compared to healthy individuals (Mattsson et al., 2017; Preische et al., 2019). While plasma NfL cannot be used to distinguish AD from other dementias, it may serve as a practical tool for neurodegeneration detection. In addition, it could be used in combination with other available AD biomarkers for AD diagnosis (Blennow and Zetterberg, 2018b).

Urine and saliva

Urine is a desired substitute for blood since it can be collected in large quantities easily and non-invasively (Hartmann and Kist, 2018). Although the composition of organic compounds in urine is less complex than that of CSF and blood, changes in metabolites and hormones among these compounds can reflect the metabolic and pathophysiological state of a person (Sancesario and Bernardini, 2019). At the same time, the relatively low compositional complexity means that fewer proteins capable of interfering with measurements are present in the urine (Bălașa et al., 2020; Buccellato et al., 2021). Some AD biomarkers have already been identified in urine.

Alzheimer-associated neuronal thread protein (AD7c-NTP) has attracted a great deal of attention from researchers because of the correlation between its concentration changes in urine and the severity of AD (Wang et al., 2019; Ausó et al., 2020). Elevated urinary AD7c-NTP levels can be used in the early diagnosis of AD with high accuracy (Li Y. et al., 2020; Seol et al., 2020). Monocyte chemoattractant proteinx (MCP-1) also showed promise as a biomarker for AD. Its concentration in the urine of AD patients was discovered to be significantly higher than that of cognitively normal individuals (Xu et al., 2020). In addition, Watanabe et al. (2020) found that the AD group had significantly higher levels of apolipoprotein C3 (ApoC3) in urine than the control group did. Therefore, it could be utilized to differentiate patients with AD. Recently, Yao et al. (2018) applied a combination of computational and experimental methods to identify three differentially expressed proteins. To be specific, in the urine of AD patients, secreted phosphoprotein 1 (SPP1) was downregulated, whereas gelsolin (GSN) and insulin-like growth factor-binding protein-7 (IGFBP7) were upregulated, which made them promising biomarkers for AD.

In addition to the aforementioned proteins, several indicators of other disorders in urine can be considered candidates to be biomarkers for AD early detection. For example, the levels of formaldehyde and 8-hydroxy-2′-deoxyguanosine (8-OHdG) can be used to access the status of formaldehyde metabolism and oxidative DNA damage, respectively. They were significantly higher in the urine of AD patients compared to cognitively normal controls (Pena-Bautista et al., 2019; Wang et al., 2022). AD would interact with osteoporosis during its progression. Pu et al. (2020) found that urinary biomarkers reflecting osteoporosis and bone loss, such as deoxypyridinoline (DPD), creatinine (Cr), and calcium (Ca), can also be used in the early diagnosis of AD in male populations.

Similar to urine sampling, saliva sampling is non-invasive, stress-free, and easy to obtain (Lee et al., 2019; Veerabhadrappa et al., 2020; Francois et al., 2021). The origin of AD-related molecules in the saliva is unknown. It is speculated that they are secreted by the salivary glands or transported from the blood (Schepici et al., 2020). In addition, the flow and composition of saliva are directly regulated by the glossopharyngeal nerve and the facial nerve (Farah et al., 2018; Pawlik and Blochowiak, 2021). Given their proximity and relation, biomarkers may be secreted from the nerves into the salivary glands (Gleerup et al., 2019; Paraskevaidi et al., 2020). These characteristics may render saliva a promising matrix for biomarker discovery. Although saliva has quite a few unique advantages, the relatively low concentration of analytes in saliva makes detection more difficult (Reale et al., 2020). In recent years, developments in

TABLE 1 Statistics of biomarkers in saliva, CSF, blood, Serum, and Urine.

Biofluids	Common biomarkers	Unique biomarkers	miRNA biomarkers	References
CSF	Aβ40, Aβ42, P-tau, T-tau, NFL	Neurogranin, BACE1, PSEN1, synaptotagmin, SNAP-25, GAP-43, synaptophysin, sTREM2, YKL-40, ICAM1, Secretogranin-2, Neuronal pentraxin 1, Neurofascin, Myelin basic protein, α-Synuclein, VILIP-1, Ferritin, hFABP, p-T181 tau, HSPA1A, NPEPPS, PTGFRN, FABP3, IL-6, IL-8, IL-10, MCP-1, MIP-1β	miR-342-3p, miR-125a-5p, miR-125b-5p, miR-451a, miR-23a-3p, ex-let-7i-5p, ex-miR-126-3p, ex-miR-151a-3p, miR-223, miR-29a, miR-193b, miR-342-3p, miR-3065-5p, miR-let-7d-5p, miR-let-7g-5p, miR-26b-5p, miR-191-5p, miR-125a-5p, miR-126-3p, miR-23a-3p, miR-151a-3p, miR-135b, miR-181a, miR-194-5p, miR-19b-3p, miR-29c-3p, miR-125b-3p, miR-31, miR-93miR-3613-3p, miR-3916, miR-4772-3p, miR-185-5p, miR-20b-3p, miR-501-3p, miR-545-3p, miR-181c, miR-139-5p, miR-141-3p, miR-150-5p, miR-152-3p, miR-23b-3p, miR-24-3p, miR-338-3p, miR-342-3p, miR-125b-5p, miR-342-5p, miR-1306-5p, miR-143, miR-15b, miR-15b-3p, miR-193b, miR-223, miR-451a, miR-29, miR-125b, miR-146a, miR-3065-5p, let-7i-5p, miR-106a-5p, miR-20-5p, miR-425-5p, miR-18b-5p, miR-582-5p, miR-106b-3p, miR-20b-5p, miR-146a-5p, miR-195-5p, miR-497-5p, miR-455-3p, miR-4668-5p, miR-5001-3p, miR-519, miR-548at-5p, miR-590-5p, miR-101-3p, miR-106b-5p, miR-143-3p, miR-335-5p,miR-361-5p, miR-138-5p, miR-155, miR-15a-5p, miR-659-5p, miR-93-5p, miR-101, miR-132, miR-212, miR-200c, miR-9, miR-30e-5p, miR-29a, miR-206, miR-142-5p, miR-384, miR-135a, miR-29b, MALAT1	Hansson et al., 2006; Lukiw, 2007; Ewers et al., 2008; Hu et al., 2010; Lukiw et al., 2012b; García-Ayllón et al., 2013; Dubois et al., 2014; Liu C. G. et al., 2014; Cheng et al., 2015; Dong et al., 2015; Kester et al., 2015; Lugli et al., 2015; Suarez-Calvet et al., 2016; Zetterberg et al., 2016; Rani et al., 2017; Bettcher et al., 2018; Molinuevo et al., 2018; Tariciotti et al., 2018; Wei et al., 2018; Dhiman et al., 2019; Jia et al., 2019; Ausó et al., 2020; Bălaşa et al., 2020; Knapskog et al., 2020; Muraoka et al., 2020; Zhuang et al., 2020; Pawlik and Blochowiak, 2021; Rastogi et al., 2021
Plasma	Aβ40, Aβ42, P-tau (p-T181 tau, P-S396-tau), T-tau	BACE1, PSEN1, TREM2, neurogranin, synaptotagmin, SNAP-25, GAP-43, synaptophysin, sTREM2, YKL-40, VILIP-1, HSPA1A, NPEPPS, PTGFRN, MIP-1β, cytokine I-309, interferon-γ, TNF-α, clusterin, TDP-43, YKL-40, BACE1, NFL, VILIP-1, sAPPβ, γ-secretase, soluble APP α, GDNF, GAP43, SNAP-25, synapsin 1, REST, IL-1, IL-4, IL-6, and IL-10, IL-8, IP-10, MCP-1, MIP-1β, cytokine I-309, Lamp 1, cathepsin D, ubiquitinylated proteins, HSP70, Synaptophysin, synaptopodin, synaptotagmin-2, neurogranin, Autolysosomal proteins, C1q and C4b, Factor D, Fragment Bb, C5b, C3b, C5b-C9, IRS-1, P-Serine-312-IRS-1, P-pan-tyrosine-IRS-1, HGF, FGF-2, FGF-13, IGF-1	miR-342-3p, miR-125a-5p, miR-125b-5p, miR-451a, miRNA23a-3p, ex-let-7i-5p, ex-miR-126-3p, ex-miR-151a-3p, miR-223, miR-29a, miR-193b, miR-342-3p, miR-3065-5p, miR-let-7d-5p, miR-let-7g-5p, miR-26b-5p, miR-191-5p, miR-125a-5p, miR-126-3p, miR-23a-3p, miR-151a-3p, miR-135b, miR-181a, miR-194-5p, miR-19b-3p, miR-29c-3p, miR-125b-3p, miR-31, miR-93, miR-3613-3p, miR-3916, miR-4772-3p, miR-185-5p, miR-20b-3p, miR-501-3p, miR-545-3p, miR-181c, miR-139-5p, miR-141-3p, miR-150-5p, miR-152-3p, miR-23b-3p, miR-24-3p, miR-338-3p, miR-342-3p, miR-125b-5p, miR-342-5p, miR-1306-5p, miR-143, miR-15b, miR-15b-3p, miR-193b, miR-223, miR-451a, miR-29, miR-125b, miR-146a, miR-3065-5p, let-7i-5p, miR-106a-5p, miR-20-5p, miR-425-5p, miR-18b-5p, miR-582-5p, miR-106b-3p, miR-20b-5p, miR-146a-5p, miR-195-5p, miR-497-5p, miR-455-3p, miR-4668-5p, miR-5001-3p, miR-519, miR-548at-5p, miR-590-5p, miR-101-3p, miR-106b-5p, miR-143-3p, miR-335-5p, miR-361-5p, miR-138-5p, miR-155, miR-15a-5p, miR-659-5p, miR-93-5p, miR-101, miR-132, miR-212, miR-200c, miR-9, miR-30e-5p, miR-29a, miR-206, miR-142-5p, miR-384, miR-135a, miR-29b, BACE1-AS, GAS5, has-Circ-0003391	Cogswell et al., 2008; Shioya et al., 2010; Lukiw et al., 2012a; Femminella et al., 2015; Goetzl et al., 2015b, 2016; Jia and Liu, 2016; Sorensen et al., 2016; Winston et al., 2016; Zhang et al., 2016; Cosin-Tomas et al., 2017; Hara et al., 2017; Mullins et al., 2017; Wu et al., 2017; Kumar and Reddy, 2018; Yang et al., 2018; Cha et al., 2019; Fotuhi et al., 2019; Gamez-Valero et al., 2019; Goetzl et al., 2019; Kenny et al., 2019; Winston et al., 2019; Ausó et al., 2020; Bălaşa et al., 2020; Barbagallo et al., 2020; Liu L. et al., 2020; Pawlik and Blochowiak, 2021; Rastogi et al., 2021; Chen et al., 2022

(Continued)

TABLE 1 (Continued)

Biofluids	Common biomarkers	Unique biomarkers	miRNA biomarkers	References
Serum		BDNF, PHGDH	miR-31, miR-93, miR-143, miR-146a, miR-206, miR-135a, miR-193b, miR-384	Platenik et al., 2014; Dong et al., 2015; Goetzl et al., 2015a; Ausó et al., 2020; Yan et al., 2020; Rastogi et al., 2021
Saliva	Aβ40, Aβ42, T-tau, P-tau	Lactoferrin, AChE		Jann, 2000; Carro et al., 2017; Ausó et al., 2020; Bălaşa et al., 2020; Pawlik and Blochowiak, 2021
Urine	Aβ40, Aβ42, P-S396-tau	AD7c-NTP, MCP-1, ApoC3, SPP1, GSN, IGFBP7, Annexin2, Clusterin		Monte and Wands, 2001; Sancesario and Bernardini, 2019; Sun et al., 2019; Song et al., 2020; Watanabe et al., 2020; Xu et al., 2020; Rastogi et al., 2021

Aβ, Amyloid-beta; P-tau, phosphorylated-tau; T-tau, Total-tau; NFL, neurofilament light polypeptide; AChE, Acetylcholinesterase; BACE1, β-site amyloid precursor protein cleaving enzyme 1; PSEN1, Presenilin 1; GAP-43, Growth associated protein-43; TREM2, triggering receptor expressed on myeloid cells 2; sTREM2, soluble TREM2; YKL-40, Chitinase-3-like protein 1; ICAM1, intercellular adhesion molecule 1; VILIP-1, visinin-like protein-1; hFABP, heart-type fatty acid-binding protein; HSPA1A, Heat shock 70 kDa protein 1A; NPEPPS, Puromycin-sensitive aminopeptidase; PTGFRN, Prostaglandin F2 receptor negative regulator; FABP3, fatty acid-binding protein; MCP-1, monocyte chemoattractant protein 1; GSK-3β, glycogen synthase kinase 3β; DYRK1A, dual-specificity tyrosine-phosphorylation regulated kinase A; TNF-α, tumor necrosis factor α; TDP-43, transactive response DNA-binding protein 43; GDNF, glial-derived neurotrophic factor.

detection methods have provided a tempting opportunity to use saliva to diagnose diseases (Ashton et al., 2019). A growing number of researchers have been working to explore the association between salivary biomarkers and AD.

In exploring urinary biomarkers for AD diagnosis, many researchers have focused on Aβ42 quantification. A collection of studies has illustrated the potential use of salivary Aβ42 as a diagnostic tool for AD. Bermejo-Pareja et al. (2010), Kim et al. (2014), and Sabbagh et al. (2018) found that the salivary Aβ42 was significantly higher in AD patients than in healthy participants, although controversy exists regarding changes in Aβ42 secretion with the development of AD. In addition, according to the study by McGeer et al. (2018) salivary Aβ42 levels can be used to predict the likelihood of future AD onset. Furthermore, Lee et al. (2017) revealed that salivary Aβ42 concentrations in patients with Parkinson's disease were identical to those in healthy subjects, indicating that Aβ42 was specific for AD. However, Shi et al. (2011) and Lau et al. (2015) found that Aβ42 in saliva was undetectable, whereas the finding of Tvarijonaviciute et al. (2020) showed that salivary Aβ42 levels were significantly lower in AD patients than in controls. The inconsistency between these experimental results may be due to differences in saliva collection, storage, and testing methods, as well as differences in the subjects screened.

Lactoferrin is an iron-binding glycoprotein that is abundantly expressed in saliva. It has been considered a potential biomarker for AD because of two properties, namely anti-microbial and Aβ-binding (Zhang et al., 2021). Carro et al. (2017) measured salivary lactoferrin levels in some healthy individuals, patients with AD, patients with MCI, and patients with PD. The results showed that salivary lactoferrin concentrations were highest in PD patients, while patients with AD or MCI had lower salivary lactoferrin concentrations than the controls did. Low lactoferrin concentration in saliva was hypothesized to be associated with the risk of developing AD or MCI. In addition, Gonzalez-Sanchez et al. (2020) found that participants with FTD did not experience a significant decrease in salivary lactoferrin concentrations. These two studies demonstrate the value of this biomarker in diagnosing the early clinical stages of AD.

Glial fibrillar acidic protein (GFAP) is a component of the cytoskeleton of astrocytes, which plays an important role in modulating neuronal inflammation (Yang and Wang, 2015). According to the study of Katsipis et al. (2021) two different immunological assays, namely ELISA and Dot Blot, were applied to detect GFAP levels in the saliva of participants in the experiment. The results obtained by both methods showed a decrease in GFAP levels in patients with AD or MCI compared to healthy subjects. In addition, GFAP levels in the saliva of AD patients are significantly lower than those of MCI patients. The possible reason for this was that GFAP were susceptible to several post-transcriptional modifications, which would hinder their transfer from the brain to the saliva and reduce their solubility (Katsipis et al., 2021). Since salivary GFAP can be used to differentiate between healthy individuals, people suffering from MCI, and AD patients, it may present as a reliable biomarker for the screen of the neurological status of people.

Although researchers have uncovered these urinary and salivary biomarkers that are of value for the early diagnosis of AD, there is still much work to be done in the future. Firstly, standards for sampling, processing, storage, and analysis methods need to be developed (Bouftas, 2021; Goldoni et al., 2022). Secondly, before these novel biomarkers can be in the clinic, large-scale as well as longitudinal research is needed to further determine their reliability in detecting AD pathology (Liang and Lu, 2019). Finally, to test their specificity for AD, it is imperative to study the levels of the biomarkers in other neurodegenerative conditions (Ashton et al., 2021).

Exosomes (extracellular vesicles)

The application of exosomes derived from human cells to examine an individual's health status is an emerging molecular diagnostic (**Figure 5**, Trams et al., 1981; Johnstone et al., 1987; Sokolova et al., 2011; van der Pol et al., 2014; Greening et al., 2015; Pegtel and Gould, 2019). The focus of the published papers is related to cancer to parse the roles of exosomes in pathophysiology, autophagy, diagnosis, and therapeutic applications (Colletti et al., 2020; Jafari et al., 2021; Kugeratski and Kalluri, 2021; Lakshmi et al., 2021; Liu T. et al., 2021; Sandua et al., 2021; Xu et al., 2021; Zhou et al., 2021). As the exosomes are also synthesized and released from brain cells to blood or CSF through the BBB, alterations in the contents of exosomes may serve as biomarkers to detect the pathological progress of the CNS (Kanninen et al., 2016; Jiang et al., 2019; Vandendriessche et al., 2020; Pinnell et al., 2021). Structurally, exosomes are rich in certain tetraspanin proteins such as CD81, CD82, CD37, and CD63, which mediate the other protein inclusion, including immunoglobulin superfamily member 8 (IGSF8) major histocompatibility complex (MHC) class II proteins, syndecans (SDC1–4) and integrins (Raposo et al., 1996; Escola et al., 1998; Hemler, 2003; Segura et al., 2005; Liang et al., 2014; Kalluri and LeBleu, 2020). Notably, a growing number of studies certify that some inclusions in exosomes are RNAs in functional form with the ability to influence other cells and tissues (Ratajczak et al., 2006; Valadi et al., 2007; Skog et al., 2008; Pegtel et al., 2010). In addition, the exosomes cover a variety of DNAs which can be used to infer tissue-of-origin and molecular classification (Balaj et al., 2011; Kahlert et al., 2014; Thakur et al., 2014; Sansone et al., 2017). Taken together, exosomes have the potential to expand the central paradigm of liquid biopsy for preclinical AD diagnosis and the biomarker library (Yin et al., 2020; Guo et al., 2021).

In addition to biomarkers, clinical, physiological, and neuropsychological tests are also an important part of detecting clinically symptomatic persons. However, waiting periods for specialist appointments in hospitals can be very lengthy, causing severe and sometimes life-threatening delays for AD patients (Patterson et al., 2004). Besides, due to a lack of experience and skill, cognitive tests are often performed, scored, and interpreted inappropriately in primary care centers (Cannon and Larner, 2016), which gives rise to differences in diagnosis, evaluation, and assistance between primary care and specialty care systems (Garcia-Ptacek et al., 2017). Consequently, both physicians and patients will benefit a lot from a relatively simple first-line test determining which patients require more detailed diagnostics testing by measuring biomarkers in body fluid. Such a procedure would reduce the number of needless referrals and diagnostic tests and thus decrease the total pressure on healthcare systems (Hampel et al., 2017; O'Bryant et al., 2017). Furthermore, improvements in AD diagnosis produced by liquid biopsy could in turn promote symptomatic treatment (Hampel et al., 2021).

Conclusion

Undoubtedly, fluid-based biomarkers are crucial in the preclinical diagnosis of AD. For patients with cognitive problems, particularly those with mild memory loss as the only objective symptom, the current diagnostic method is incapable of predicting whether the end is Alzheimer's disease or not (Tan et al., 2014). Having outlined a huge collection of the literature, a good deal of analytes that had been claimed to have the diagnosis value for AD were revealed. As we summarized above, accompanying the theory innovation, the liquid biopsy technologies including the equipment and kits emerge in endlessly. However, the practice has proven that the relentless efforts worldwide have not reached a satisfactory conclusion. In other words, no one strategy has "saved" the doctors and researchers from the current plight. The cause is varied and super-complicated.

First of all, the etiology of AD has many risk factors or heterogeneity, including but not limited to smoking, drinking, aging, education, and underlying medical conditions (obesity, smoking, diabetes, hypertension, and cardiac disease). Importantly, the principal cause has not been deduced. Even the well-established suspicious loci only account for 15∼20% of the AD pathology, which was often obtained from population-based studies and taken as the fluid biomarkers. As a result, the model in mathematical statistics is hard to build because of too many variables, especially the unknowns.

Secondly, none of the current technologies in liquid biopsy can perfectly meet the clinical demand. On one hand, the CSF biomarkers Aβ42, total tau, P-tau181, P-tau217, and P-tau231 show a high diagnostic accuracy for AD, even for prodromal AD patients with MCI. Therefore, they are increasingly being used in the clinic and valued as a similar gold standard. However, the procedure for acquiring CSF is expensive and the individuals should suffer a lumbar puncture and extra risk. On the other hand, fluid-based biomarkers significantly boost AD diagnosis by lowering expense and increasing ease of testing. As opposed to CSF markers, they may provide a minimally invasive, time- and cost-effective method of early detection and diagnosis of AD (Olsson et al., 2016). Taking the three aforementioned phosphor-tau in blood as an example, only in specific scenarios, they can show good performance by independent use.

Thirdly, several joint diagnostic strategies have been applied to reveal the full view of AD pathologies. The biomarker-based amyloid-tangle-neurodegeneration (A-T-N) framework proposed by Jack et al. (2016) and updated by NIA-AA (Jack et al., 2018) can capture the whole spectrum pathophysiological features of AD. By which, AD can be distinguished from other neurodegenerative diseases. Even so, in this scheme, not all of the pathologies and related biomarkers are included. Therefore, Huang et al. (2022) suggested adding an X to form the A-T-N-X framework, focusing on the CNS and periphery biomarkers associated with inflammation, systemic immunity, metabolism,

and synaptic damage, neuroinflammation, glial cells. In the mid-to-long-term future, these frameworks should be validated in many clinical trials.

Lastly, many studies predict that faulty autophagy occurs before the formation of the fluid biomarkers such as Aβ or senile plaques, in the development of AD (Li W. et al., 2020; Lee et al., 2022). If in that case, the overwhelming majority of the aforementioned biomarkers cannot be employed in the routine clinical diagnostic for the very early stage of AD.

For now, it is foreseeable that an increasing number of blood-based biomarkers would be incorporated into diagnostic criteria and research frameworks for AD, in combination with current CSF biomarkers, to improve the preclinical and clinical diagnosis of AD, the world's most common age-related neurodegenerative disease.

Author contributions

MT and HTZ designed the study. JL performed the data analysis. YL and XG wrote the manuscript All authors made a direct and intellectual contribution to this topic and approved the article for publication.

Funding

This work was financially supported by grants from the National Natural Science Foundation of China (32002235) and the Natural Science Foundation of Shandong Province (No. ZR2020MH141).

Acknowledgments

We thank all the individuals who have helped us in this study. We acknowledge the valuable work of the many investigators whose published articles we were unable to cite owing to space limitations.

Conflict of interest

The authors declare that the research was conducted in the absence of any commercial or financial relationships that could be construed as a potential conflict of interest.

Publisher's note

All claims expressed in this article are solely those of the authors and do not necessarily represent those of their affiliated organizations, or those of the publisher, the editors and the reviewers. Any product that may be evaluated in this article, or claim that may be made by its manufacturer, is not guaranteed or endorsed by the publisher.

References

Abdel-Haq, H. (2020). The potential of liquid biopsy of the brain using blood extracellular vesicles: The first step toward effective neuroprotection against neurodegenerative diseases. *Mol. Diagn. Ther.* 24, 703–713. doi: 10.1007/s40291-020-00493-4

An, S. S., Lim, K. T., Oh, H. J., Lee, B. S., Zukic, E., Ju, Y. R., et al. (2010). Differentiating blood samples from scrapie infected and non-infected hamsters by detecting disease-associated prion proteins using Multimer Detection System. *Biochem. Biophys. Res. Commun.* 392, 505–509. doi: 10.1016/j.bbrc.2010.01.053

An, S. S. A., Lee, B. S., Yu, J. S., Lim, K., Kim, G. J., Lee, R., et al. (2017). Dynamic changes of oligomeric amyloid beta levels in plasma induced by spiked synthetic Abeta42. *Alzheimers Res. Ther.* 9:86. doi: 10.1186/s13195-017-0310-6

Andreasen, N., Minthon, L., Vanmechelen, E., Vanderstichele, H., Davidsson, P., Winblad, B., et al. (1999). Cerebrospinal fluid tau and Aβ42 as predictors of development of Alzheimer's disease in patients with mild cognitive impairment. *Neurosci. Lett.* 273, 5–8. doi: 10.1016/S0304-3940(99)00617-5

Asberg, A., Lofblad, L., Felic, A., and Hov, G. G. (2019). Measuring calprotectin in plasma and blood with a fully automated turbidimetric assay. *Scand. J. Clin. Lab. Invest.* 79, 50–57. doi: 10.1080/00365513.2018.1550810

Ashton, N. J., Benedet, A. L., Pascoal, T. A., Karikari, T. K., Lantero-Rodriguez, J., Brum, W. S., et al. (2022). Cerebrospinal fluid p-tau231 as an early indicator of emerging pathology in Alzheimer's disease. *EBioMedicine* 76:103836. doi: 10.1016/j.ebiom.2022.103836

Ashton, N. J., Blennow, K., and Zetterberg, H. (2021). Spitting image: Can saliva biomarkers reflect Alzheimer's disease? *EBioMedicine* 68:103437. doi: 10.1016/j.ebiom.2021.103437

Ashton, N. J., Hye, A., Rajkumar, A. P., Leuzy, A., Snowden, S., Suarez-Calvet, M., et al. (2020). An update on blood-based biomarkers for non-Alzheimer neurodegenerative disorders. *Nat. Rev. Neurol.* 16, 265–284. doi: 10.1038/s41582-020-0348-0

Ashton, N. J., Ide, M., Zetterberg, H., and Blennow, K. (2019). Salivary biomarkers for Alzheimer's disease and related disorders. *Neurol. Ther.* 8, 83–94. doi: 10.1007/s40120-019-00168-1

Atri, A. (2019). The Alzheimer's disease clinical spectrum: Diagnosis and management. *Med. Clin. North Am.* 103, 263–293. doi: 10.1016/j.mcna.2018.10.009

Ausó, E., Gómez-Vicente, V., and Esquiva, G. (2020). Biomarkers for Alzheimer's disease early diagnosis. *J. Pers. Med.* 10:114. doi: 10.3390/jpm10030114

Babapour Mofrad, R., Scheltens, P., Kim, S., Kang, S., Youn, Y. C., An, S. S. A., et al. (2021). Plasma amyloid-beta oligomerization assay as a pre-screening test for amyloid status. *Alzheimers Res. Ther.* 13:133.

Bacioglu, M., Maia, L. F., Preische, O., Schelle, J., Apel, A., Kaeser, S. A., et al. (2016). Neurofilament light chain in blood and CSF as marker of disease progression in mouse models and in neurodegenerative diseases. *Neuron* 91, 56–66. doi: 10.1186/s13195-021-00873-w

Baker-Nigh, A. T., Mawuenyega, K. G., Bollinger, J. G., Ovod, V., Kasten, T., Franklin, E. E., et al. (2016). Human Central Nervous System (CNS) ApoE isoforms are increased by age, differentially altered by amyloidosis, and relative amounts reversed in the CNS compared with plasma. *J. Biol. Chem.* 291, 27204–27218. doi: 10.1074/jbc.M116.721779

Balaj, L., Lessard, R., Dai, L., Cho, Y. J., Pomeroy, S. L., Breakefield, X. O., et al. (2011). Tumour microvesicles contain retrotransposon elements and amplified oncogene sequences. *Nat. Commun.* 2:180. doi: 10.1038/ncomms1180

Bălaşa, A. F., Chircov, C., and Grumezescu, A. M. (2020). Body fluid biomarkers for Alzheimer's disease-an up-to-date overview. *Biomedicines* 8:421. doi: 10.3390/biomedicines8100421

Baldacci, F., Lista, S., Vergallo, A., Palermo, G., Giorgi, F. S., and Hampel, H. (2019). A frontline defense against neurodegenerative diseases:the development of early disease detection methods. *Expert Rev. Mol. Diagn.* 19, 559–563. doi: 10.1080/14737159.2019.1627202

Barbagallo, C., Mostile, G., Baglieri, G., Giunta, F., Luca, A., Raciti, L., et al. (2020). Specific signatures of serum miRNAs as potential biomarkers to discriminate clinically similar neurodegenerative and vascular-related diseases. *Cell. Mol. Neurobiol.* 40, 531–546. doi: 10.1007/s10571-019-00751-y

Barthelemy, N. R., Li, Y., Joseph-Mathurin, N., Gordon, B. A., Hassenstab, J., Benzinger, T. L. S., et al. (2020b). A soluble phosphorylated tau signature links tau, amyloid and the evolution of stages of dominantly inherited Alzheimer's disease. *Nat. Med.* 26, 398–407. doi: 10.1038/s41591-020-0781-z

Barthelemy, N. R., Bateman, R. J., Hirtz, C., Marin, P., Becher, F., Sato, C., et al. (2020a). Cerebrospinal fluid phospho-tau T217 outperforms T181 as a biomarker for the differential diagnosis of Alzheimer's disease and PET amyloid-positive patient identification. *Alzheimers Res. Ther.* 12:26. doi: 10.1186/s13195-020-00596-4

Basak, J. M., Kim, J., Pyatkivskyy, Y., Wildsmith, K. R., Jiang, H., Parsadanian, M., et al. (2012). Measurement of apolipoprotein E and amyloid β clearance rates in the mouse brain using bolus stable isotope labeling. *Mol. Neurodegener.* 7:14. doi: 10.1186/1750-1326-7-14

Bateman, R. J., Xiong, C., Benzinger, T. L., Fagan, A. M., Goate, A., Fox, N. C., et al. (2012). Clinical and biomarker changes in dominantly inherited Alzheimer's disease. *N. Engl. J. Med.* 367, 795–804. doi: 10.1056/NEJMoa1202753

Bayoumy, S., Verberk, I. M. W., Den Dulk, B., Hussainali, Z., Zwan, M., Van Der Flier, W. M., et al. (2021). Clinical and analytical comparison of six Simoa assays for plasma P-tau isoforms P-tau181, P-tau217, and P-tau231. *Alzheimers Res. Ther.* 13:198. doi: 10.1186/s13195-021-00939-9

Benussi, A., Karikari, T. K., Ashton, N., Gazzina, S., Premi, E., Benussi, L., et al. (2020). Diagnostic and prognostic value of serum NfL and p-Tau181 in frontotemporal lobar degeneration. *J. Neurol. Neurosurg. Psychiatry* 91, 960–967. doi: 10.1136/jnnp-2020-323487

Bermejo-Pareja, F., Antequera, D., Vargas, T., Molina, J. A., and Carro, E. (2010). Saliva levels of Abeta1-42 as potential biomarker of Alzheimer's disease: A pilot study. *BMC Neurol.* 10:108. doi: 10.1186/1471-2377-10-108

Bettcher, B. M., Johnson, S. C., Fitch, R., Casaletto, K. B., Heffernan, K. S., Asthana, S., et al. (2018). Cerebrospinal Fluid and Plasma Levels of Inflammation Differentially Relate to CNS Markers of Alzheimer's Disease Pathology and Neuronal Damage. *J. Alzheimers Dis.* 62, 385–397. doi: 10.3233/JAD-170602

Birks, J. S., and Harvey, R. J. (2018). Donepezil for dementia due to Alzheimer's disease. *Cochrane Database Syst. Rev.* 6:CD001190. doi: 10.1002/14651858.CD001190.pub3

Blanco, B. A., and Wolfgang, C. L. (2019). Liquid biopsy for the detection and management of surgically resectable tumors. *Langenbecks Arch. Surg.* 404, 517–525. doi: 10.1007/s00423-019-01788-9

Blennow, K., and Hampel, H. (2003). CSF markers for incipient Alzheimer's disease. *Lancet Neurol.* 2, 605–613. doi: 10.1016/S1474-4422(03)00530-1

Blennow, K., Hampel, H., Weiner, M., and Zetterberg, H. (2010). Cerebrospinal fluid and plasma biomarkers in Alzheimer disease. *Nat. Rev. Neurol.* 6, 131–144. doi: 10.1038/nrneurol.2010.4

Blennow, K., Mattsson, N., Schöll, M., Hansson, O., and Zetterberg, H. (2015). Amyloid biomarkers in Alzheimer's disease. *Trends Pharmacol. Sci.* 36, 297–309. doi: 10.1016/j.tips.2015.03.002

Blennow, K., Wallin, A., Ågren, H., Spenger, C., Siegfried, J., Vanmechelen, E. J. M., et al. (1995). Tau protein in cerebrospinal fluid. *Mol. Chem. Neuropathol.* 26, 231–245. doi: 10.1007/BF02815140

Blennow, K., and Zetterberg, H. (2015). Understanding biomarkers of neurodegeneration: Ultrasensitive detection techniques pave the way for mechanistic understanding. *Nat. Med.* 21, 217–219. doi: 10.1038/nm.3810

Blennow, K., and Zetterberg, H. (2018a). Biomarkers for Alzheimer's disease: Current status and prospects for the future. *J. Intern. Med.* 284, 643–663. doi: 10.1111/joim.12816

Blennow, K., and Zetterberg, H. (2018b). The past and the future of Alzheimer's disease fluid biomarkers. *J. Alzheimers Dis.* 62, 1125–1140. doi: 10.3233/JAD-170773

Blennow, K., and Zetterberg, H. (2019). Fluid biomarker-based molecular phenotyping of Alzheimer's disease patients in research and clinical settings. *Prog. Mol. Biol. Transl. Sci.* 168, 3–23. doi: 10.1016/bs.pmbts.2019.07.006

Bouftas, M. (2021). A systematic review on the feasibility of salivary biomarkers for Alzheimer's disease. *J. Prev. Alzheimers Dis.* 8, 84–91. doi: 10.14283/jpad.2020.57

Bramblett, G. T., Goedert, M., Jakes, R., Merrick, S. E., Trojanowski, J. Q., and Lee, V. M. (1993). Abnormal tau phosphorylation at Ser396 in Alzheimer's disease recapitulates development and contributes to reduced microtubule binding. *Neuron* 10, 1089–1099. doi: 10.1016/0896-6273(93)90057-x

Breijyeh, Z., and Karaman, R. (2020). Comprehensive review on Alzheimer's disease: Causes and treatment. *Molecules* 25:5789. doi: 10.3390/molecules25245789

Brickman, A. M., Manly, J. J., Honig, L. S., Sanchez, D., Reyes-Dumeyer, D., Lantigua, R. A., et al. (2021). Plasma p-tau181, p-tau217, and other blood-based Alzheimer's disease biomarkers in a multi-ethnic, community study. *Alzheimers Dement.* 17, 1353–1364. doi: 10.1002/alz.12301

Buccellato, F. R., D'anca, M., Fenoglio, C., Scarpini, E., and Galimberti, D. (2021). Role of oxidative damage in Alzheimer's disease and neurodegeneration: From pathogenic mechanisms to biomarker discovery. *Antioxidants* 10:1353. doi: 10.3390/antiox10091353

Buchhave, P., Minthon, L., Zetterberg, H., Wallin, Å. K., Blennow, K., and Hansson, O. J. (2012). Cerebrospinal fluid levels of β-amyloid 1-42, but not of tau, are fully changed already 5 to 10 years before the onset of Alzheimer dementia. *Arch. Gen. Psychiatry* 69, 98–106. doi: 10.1001/archgenpsychiatry.2011.155

Campbell, L., Simpson, D., Ramasamy, K., and Sadler, R. (2021). Using quantitative immunoprecipitation mass spectrometry (QIP-MS) to identify low level monoclonal proteins. *Clin. Biochem.* 95, 81–83. doi: 10.1016/j.clinbiochem.2021.05.012

Cannon, P., and Larner, A. J. (2016). Errors in the scoring and reporting of cognitive screening instruments administered in primary care. *Neurodegener. Dis. Manag.* 6, 271–276. doi: 10.2217/nmt-2016-0004

Carro, E., Bartolome, F., Bermejo-Pareja, F., Villarejo-Galende, A., Molina, J. A., Ortiz, P., et al. (2017). Early diagnosis of mild cognitive impairment and Alzheimer's disease based on salivary lactoferrin. *Alzheimers Dement.* 8, 131–138. doi: 10.1016/j.dadm.2017.04.002

Cass, S. P. (2017). Alzheimer's disease and exercise: A literature review. *Curr. Sports Med. Rep.* 16, 19–22. doi: 10.1249/JSR.0000000000000332

Cedazo-Minguez, A., and Winblad, B. (2010). Biomarkers for Alzheimer's disease and other forms of dementia: Clinical needs, limitations and future aspects. *Exp. Gerontol.* 45, 5–14. doi: 10.1016/j.exger.2009.09.008

Cha, D. J., Mengel, D., Mustapic, M., Liu, W., Selkoe, D. J., Kapogiannis, D., et al. (2019). miR-212 and miR-132 are downregulated in neurally derived plasma exosomes of Alzheimer's patients. *Front. Neurosci.* 13:1208. doi: 10.3389/fnins.2019.01208

Chen, D., Xu, T., Wang, S., Chang, H., Yu, T., Zhu, Y., et al. (2020). Liquid biopsy applications in the clinic. *Mol. Diagn. Ther.* 24, 125–132. doi: 10.1007/s40291-019-00444-8

Chen, X., Ren, G., Li, Y., Chao, W., Chen, S., Li, X., et al. (2022). Level of LncRNA GAS5 and hippocampal volume are associated with the progression of Alzheimer's disease. *Clin. Interv. Aging* 17, 745–753. doi: 10.2147/CIA.S363116

Cheng, L., Doecke, J. D., Sharples, R. A., Villemagne, V. L., Fowler, C. J., Rembach, A., et al. (2015). Prognostic serum miRNA biomarkers associated with Alzheimer's disease shows concordance with neuropsychological and neuroimaging assessment. *Mol. Psychiatry* 20, 1188–1196. doi: 10.1038/mp.2014.127

Cheng, L., Li, W., Chen, Y., Lin, Y., Wang, B., Guo, Q., et al. (2022). Plasma Abeta as a biomarker for predicting Abeta-PET status in Alzheimer's diseasea systematic review with meta-analysis. *J. Neurol. Neurosurg. Psychiatry* 93, 513–520. doi: 10.1136/jnnp-2021-327864

Choi, Y., Joh, Y., Ryu, J. S., Kim, K., Seo, D., and Kim, S. (2021). Endogenous Abeta peptide promote Abeta oligomerization tendency of spiked synthetic Abeta in Alzheimer's disease plasma. *Mol. Cell. Neurosci.* 111:103588. doi: 10.1016/j.mcn.2021.103588

Chu, L. W. (2012). Alzheimer's disease: Early diagnosis and treatment. *Hong Kong Med. J.* 18, 228–237.

Cogswell, J. P., Ward, J., Taylor, I. A., Waters, M., Shi, Y., Cannon, B., et al. (2008). Identification of miRNA changes in Alzheimer's disease brain and CSF yields putative biomarkers and insights into disease pathways. *J. Alzheimers Dis.* 14, 27–41. doi: 10.3233/jad-2008-14103

Cohen, L., Keegan, A., and Walt, D. R. (2020). Single-molecule arrays for ultrasensitive detection of blood-based biomarkers for immunotherapy. *Methods Mol. Biol.* 2055, 399–412. doi: 10.1007/978-1-4939-9773-2_18

Cohen, L., and Walt, D. R. (2017). Single-molecule arrays for protein and nucleic acid analysis. *Annu. Rev. Anal. Chem.* 10, 345–363. doi: 10.1146/annurev-anchem-061516-045340

Cohen, L., Xie, L., Xylas, M. E., and Walt, D. R. (2018). Single Molecule Arrays for ultra-sensitive detection of rat cytokines in serum. *J. Immunol. Methods* 452, 20–25. doi: 10.1016/j.jim.2017.10.002

Colletti, M., Ceglie, D., Di Giannatale, A., and Nazio, F. (2020). Autophagy and exosomes relationship in cancer: Friends or foes? *Front. Cell Dev. Biol.* 8:614178. doi: 10.3389/fcell.2020.614178

Cosin-Tomas, M., Antonell, A., Llado, A., Alcolea, D., Fortea, J., Ezquerra, M., et al. (2017). Plasma miR-34a-5p and miR-545-3p as early biomarkers of Alzheimer's disease: Potential and limitations. *Mol. Neurobiol.* 54, 5550–5562. doi: 10.1007/s12035-016-0088-8

Crisp, M. J., Mawuenyega, K. G., Patterson, B. W., Reddy, N. C., Chott, R., Self, W. K., et al. (2015). *In vivo* kinetic approach reveals slow SOD1 turnover in the CNS. *J. Clin. Invest.* 125, 2772–2780. doi: 10.1172/JCI80705

De Rubis, G., Rajeev Krishnan, S., and Bebawy, M. (2019). Liquid biopsies in cancer diagnosis, monitoring, and prognosis. *Trends Pharmacol. Sci.* 40, 172–186. doi: 10.1016/j.tips.2019.01.006

Delgado-Peraza, F., Nogueras-Ortiz, C. J., Volpert, O., Liu, D., Goetzl, E. J., Mattson, M. P., et al. (2021). Neuronal and astrocytic extracellular vesicle biomarkers in blood reflect brain pathology in mouse models of Alzheimer's disease. *Cells* 10:993. doi: 10.3390/cells10050993

Dhiman, K., Blennow, K., Zetterberg, H., Martins, R. N., and Gupta, V. B. (2019). Cerebrospinal fluid biomarkers for understanding multiple aspects of Alzheimer's disease pathogenesis. *Cell. Mol. Life Sci.* 76, 1833–1863. doi: 10.1007/s00018-019-03040-5

Dincer, A., Gordon, B. A., Hari-Raj, A., Keefe, S. J., Flores, S., Mckay, N. S., et al. (2020). Comparing cortical signatures of atrophy between late-onset and autosomal dominant Alzheimer disease. *Neuroimage Clin.* 28:102491. doi: 10.1016/j.nicl.2020.102491

Dominguez, J. C., Yu, J. R. T., De Guzman, M. F., Ampil, E., Guevarra, A. C., Joson, M. L., et al. (2022). Multimer detection system-oligomerized amyloid beta (MDS-OAbeta): A plasma-based biomarker differentiates Alzheimer's disease from other etiologies of dementia. *Int. J. Alzheimers Dis.* 2022:9960832. doi: 10.1155/2022/9960832

Dong, H., Li, J., Huang, L., Chen, X., Li, D., Wang, T., et al. (2015). Serum MicroRNA profiles serve as novel biomarkers for the diagnosis of Alzheimer's disease. *Dis. Markers* 2015:625659. doi: 10.1155/2015/625659

Dubois, B., Feldman, H. H., Jacova, C., Hampel, H., Molinuevo, J. L., Blennow, K., et al. (2014). Advancing research diagnostic criteria for Alzheimer's disease: The IWG-2 criteria. *Lancet Neurol.* 13, 614–629. doi: 10.1016/S1474-4422(14)70090-0

Elbert, D. L., Patterson, B. W., Lucey, B. P., Benzinger, T. L. S., and Bateman, R. J. (2022). Importance of CSF-based Abeta clearance with age in humans increases with declining efficacy of blood-brain barrier/proteolytic pathways. *Commun. Biol.* 5:98. doi: 10.1038/s42003-022-03037-0

Escola, J. M., Kleijmeer, M. J., Stoorvogel, W., Griffith, J. M., Yoshie, O., and Geuze, H. J. (1998). Selective enrichment of tetraspan proteins on the internal vesicles of multivesicular endosomes and on exosomes secreted by human B-lymphocytes. *J. Biol. Chem.* 273, 20121–20127. doi: 10.1074/jbc.273.32.20121

Ewers, M., Zhong, Z., Burger, K., Wallin, A., Blennow, K., Teipel, S. J., et al. (2008). Increased CSF-BACE 1 activity is associated with ApoE-epsilon 4 genotype in subjects with mild cognitive impairment and Alzheimer's disease. *Brain* 131, 1252–1258. doi: 10.1093/brain/awn034

Farah, R., Haraty, H., Salame, Z., Fares, Y., Ojcius, D. M., and Said Sadier, N. (2018). Salivary biomarkers for the diagnosis and monitoring of neurological diseases. *Biomed. J.* 41, 63–87. doi: 10.1016/j.bj.2018.03.004

Femminella, G. D., Ferrara, N., and Rengo, G. (2015). The emerging role of microRNAs in Alzheimer's disease. *Front. Physiol.* 6:40. doi: 10.3389/fphys.2015.00040

Ferreri, A. J. M., Calimeri, T., Lopedote, P., Francaviglia, I., Daverio, R., Iacona, C., et al. (2021). MYD88 L265P mutation and interleukin-10 detection in cerebrospinal fluid are highly specific discriminating markers in patients with primary central nervous system lymphoma: Results from a prospective study. *Br. J. Haematol.* 193, 497–505. doi: 10.1111/bjh.17357

Fotuhi, S. N., Khalaj-Kondori, M., Hoseinpour Feizi, M. A., and Talebi, M. (2019). Long non-coding RNA BACE1-AS may serve as an Alzheimer's disease blood-based biomarker. *J. Mol. Neurosci.* 69, 351–359. doi: 10.1007/s12031-019-01364-2

Francois, M., Karpe, A., Liu, J. W., Beale, D., Hor, M., Hecker, J., et al. (2021). Salivaomics as a potential tool for predicting Alzheimer's disease during the early stages of neurodegeneration. *J. Alzheimers Dis.* 82, 1301–1313. doi: 10.3233/JAD-210283

Gamez-Valero, A., Campdelacreu, J., Vilas, D., Ispierto, L., Rene, R., Alvarez, R., et al. (2019). Exploratory study on microRNA profiles from plasma-derived extracellular vesicles in Alzheimer's disease and dementia with Lewy bodies. *Transl. Neurodegener.* 8:31. doi: 10.1186/s40035-019-0169-5

Gao, Y., Tan, L., Yu, J. T., and Tan, L. (2018). Tau in Alzheimer's disease: Mechanisms and therapeutic strategies. *Curr. Alzheimer Res.* 15, 283–300. doi: 10.2174/1567205014666170417111859

García-Ayllón, M.-S., Campanari, M.-L., Brinkmalm, G., Rábano, A., Alom, J., Saura, C. A., et al. (2013). CSF Presenilin-1 complexes are increased in Alzheimer's disease. *Acta Neuropathol. Commun.* 1:46. doi: 10.1186/2051-5960-1-46

Garcia-Ptacek, S., Modéer, I. N., Kåreholt, I., Fereshtehnejad, S.-M., Farahmand, B., Religa, D., et al. (2017). Differences in diagnostic process, treatment and social Support for Alzheimer's dementia between primary and specialist care: Resultss from the Swedish Dementia Registry. *Age Ageing* 46, 314–319. doi: 10.1093/ageing/afw189

Gleerup, H. S., Hasselbalch, S. G., and Simonsen, A. H. (2019). Biomarkers for Alzheimer's disease in saliva: A systematic review. *Dis. Markers* 2019:4761054. doi: 10.1155/2019/4761054

Goetzl, E. J., Boxer, A., Schwartz, J. B., Abner, E. L., Petersen, R. C., Miller, B. L., et al. (2015a). Low neural exosomal levels of cellular survival factors in Alzheimer's disease. *Ann. Clin. Transl. Neurol.* 2, 769–773. doi: 10.1002/acn3.211

Goetzl, E. J., Boxer, A., Schwartz, J. B., Abner, E. L., Petersen, R. C., Miller, B. L., et al. (2015b). Altered lysosomal proteins in neural-derived plasma exosomes in preclinical Alzheimer disease. *Neurology* 85, 40–47. doi: 10.1212/WNL.0000000000001702

Goetzl, E. J., Kapogiannis, D., Schwartz, J. B., Lobach, I. V., Goetzl, L., Abner, E. L., et al. (2016). Decreased synaptic proteins in neuronal exosomes of frontotemporal dementia and Alzheimer's disease. *FASEB J.* 30, 4141–4148. doi: 10.1096/fj.201600816R

Goetzl, E. J., Nogueras-Ortiz, C., Mustapic, M., Mullins, R. J., Abner, E. L., Schwartz, J. B., et al. (2019). Deficient neurotrophic factors of CSPG4-type neural cell exosomes in Alzheimer disease. *FASEB J.* 33, 231–238. doi: 10.1096/fj.201801001

Goldoni, R., Dolci, C., Boccalari, E., Inchingolo, F., Paghi, A., Strambini, L., et al. (2022). Salivary biomarkers of neurodegenerative and demyelinating diseases and biosensors for their detection. *Ageing Res. Rev.* 76:101587. doi: 10.1016/j.arr.2022.101587

Gonzalez-Sanchez, M., Bartolome, F., Antequera, D., Puertas-Martin, V., Gonzalez, P., Gomez-Grande, A., et al. (2020). Decreased salivary lactoferrin levels are specific to Alzheimer's disease. *EBioMedicine* 57:102834.doi: 10.1016/j.ebiom.2020.102834

Goto, M., Chamoto, K., Higuchi, K., Yamashita, S., Noda, K., Iino, T., et al. (2019). Analytical performance of a new automated chemiluminescent magnetic immunoassays for soluble PD-1, PD-L1, and CTLA-4 in human plasma. *Sci. Rep.* 9:10144. doi: 10.1038/s41598-019-46548-3

Gouras, G. K., Olsson, T. T., and Hansson, O. (2015). beta-Amyloid peptides and amyloid plaques in Alzheimer's disease. *Neurotherapeutics* 12, 3–11. doi: 10.1007/s13311-014-0313-y

Greening, D. W., Xu, R., Ji, H., Tauro, B. J., and Simpson, R. J. (2015). A protocol for exosome isolation and characterization: Evaluation of ultracentrifugation, density-gradient separation, and immunoaffinity capture methods. *Methods Mol. Biol.* 1295, 179–209. doi: 10.1007/978-1-4939-2550-6_15

Guard, S. E., Ebmeier, C. C., and Old, W. M. (2019). Label-free immunoprecipitation mass spectrometry workflow for large-scale nuclear interactome profiling. *J. Vis. Exp.* e60432. doi: 10.3791/60432

Guo, M., Hao, Y., Feng, Y., Li, H., Mao, Y., Dong, Q., et al. (2021). Microglial exosomes in neurodegenerative disease. *Front. Mol. Neurosci.* 14:630808. doi: 10.3389/fnmol.2021.630808

Gustafson, D. R., Skoog, I., Rosengren, L., Zetterberg, H., Blennow, K. J. J. O. N., Neurosurgery, et al. (2007). Cerebrospinal fluid β-amyloid 1–42 concentration may predict cognitive decline in older women. *J. Neurol. Neurosurg. Psychiatry* 78, 461–464. doi: 10.1136/jnnp.2006.100529

Hampel, H., Lista, S., and Vergallo, A. (2019). Commentary: Development of the blood-based Alzheimer's disease liquid biopsy. *J. Prev. Alzheimers Dis.* 6, 182–184. doi: 10.14283/jpad.2019.22

Hampel, H., O'Bryant, S. E., Durrleman, S., Younesi, E., Rojkova, K., Escott-Price, V., et al. (2017). A precision medicine initiative for Alzheimer's disease: The road ahead to biomarker-guided integrative disease modeling. *Climacteric* 20, 107–118. doi: 10.1080/13697137.2017.1287866

Hampel, H., Vergallo, A., Caraci, F., Cuello, A. C., Lemercier, P., Vellas, B., et al. (2021). Future avenues for Alzheimer's disease detection and therapy: Liquid biopsy, intracellular signaling modulation, systems pharmacology drug discovery. *Neuropharmacology* 185:108081. doi: 10.1016/j.neuropharm.2020.108081

Hane, F. T., Robinson, M., Lee, B. Y., Bai, O., Leonenko, Z., and Albert, M. S. (2017). Recent progress in Alzheimer's disease research, Part 3: Diagnosis and treatment. *J. Alzheimers Dis.* 57, 645–665.doi: 10.3233/JAD-160907

Hansson, O., Seibyl, J., Stomrud, E., Zetterberg, H., Trojanowski, J. Q., Bittner, T., et al. (2018). CSF biomarkers of Alzheimer's disease concord with amyloid−β PET and predict clinical progression: A study of fully automated immunoassays in BioFINDER and ADNI cohorts. *Alzheimers Dement.* 14, 1470–1481. doi: 10.1016/j.jalz.2018.01.010

Hansson, O., Zetterberg, H., Buchhave, P., Londos, E., Blennow, K., and Minthon, L. (2006). Association between CSF biomarkers and incipient Alzheimer's disease in patients with mild cognitive impairment: A follow-up study. *Lancet Neurol.* 5, 228–234. doi: 10.1016/S1474-4422(06)70355-6

Hara, N., Kikuchi, M., Miyashita, A., Hatsuta, H., Saito, Y., Kasuga, K., et al. (2017). Serum microRNA miR-501-3p as a potential biomarker related to the progression of Alzheimer's disease. *Acta Neuropathol. Commun.* 5:10. doi: 10.1186/s40478-017-0414-z

Hartmann, S., and Kist, T. B. L. (2018). A review of biomarkers of Alzheimer's disease in noninvasive samples. *Biomark. Med.* 12, 677–690. doi: 10.2217/bmm-2017-0388

Hemler, M. E. (2003). Tetraspanin proteins mediate cellular penetration, invasion, and fusion events and define a novel type of membrane microdomain. *Annu. Rev. Cell Dev. Biol.* 19, 397–422. doi: 10.1146/annurev.cellbio.19.111301.153609

Hendricks, R., Baker, D., Brumm, J., Davancaze, T., Harp, C., Herman, A., et al. (2019). Establishment of neurofilament light chain Simoa assay in cerebrospinal fluid and blood. *Bioanalysis* 11, 1405–1418. doi: 10.4155/bio-2019-0163

Hersi, M., Irvine, B., Gupta, P., Gomes, J., Birkett, N., and Krewski, D. (2017). Risk factors associated with the onset and progression of Alzheimer's disease: A systematic review of the evidence. *Neurotoxicology* 61, 143–187. doi: 10.1016/j.neuro.2017.03.006

Hesse, C., Rosengren, L., Andreasen, N., Davidsson, P., Vanderstichele, H., Vanmechelen, E., et al. (2001). Transient increase in total tau but not phospho-tau in human cerebrospinal fluid after acute stroke. *Neurosci. Lett.* 297, 187–190. doi: 10.1016/S0304-3940(00)01697-9

Hodson, R. (2018). Alzheimer's disease. *Nature* 559:S1. doi: 10.1038/d41586-018-05717-6

Hu, W. T., Chen-Plotkin, A., Arnold, S. E., Grossman, M., Clark, C. M., Shaw, L. M., et al. (2010). Novel CSF biomarkers for Alzheimer's disease and mild cognitive impairment. *Acta Neuropathol.* 119, 669–678. doi: 10.1007/s00401-010-0667-0

Hu, Y. Y., He, S. S., Wang, X., Duan, Q. H., Grundke-Iqbal, I., Iqbal, K., et al. (2002). Levels of nonphosphorylated and phosphorylated tau in cerebrospinal fluid of Alzheimer's disease patients: An ultrasensitive bienzyme-substrate-recycle enzyme-linked immunosorbent assay. *Am. J. Pathol.* 160, 1269–1278. doi: 10.1016/S0002-9440(10)62554-0

Huang, S., Wang, Y. J., and Guo, J. (2022). Biofluid biomarkers of Alzheimer's disease: Progress, problems, and perspectives. *Neurosci. Bull.* 38, 677–691. doi: 10.1007/s12264-022-00836-7

Illan-Gala, I., Lleo, A., Karydas, A., Staffaroni, A. M., Zetterberg, H., Sivasankaran, R., et al. (2021). Plasma tau and neurofilament light in frontotemporal lobar degeneration and Alzheimer disease. *Neurology* 96, e671–e683. doi: 10.1212/WNL.0000000000011226

Ishiguro, K., Ohno, H., Arai, H., Yamaguchi, H., Urakami, K., Park, J.-M., et al. (1999). Phosphorylated tau in human cerebrospinal fluid is a diagnostic marker for Alzheimer's disease. *Neurosci. Lett.* 270, 91–94. doi: 10.1016/S0304-3940(99)00476-0

Jack, C. R. Jr., Bennett, D. A., Blennow, K., Carrillo, M. C., Dunn, B., et al. (2018). NIA-AA research framework: Toward a biological definition of Alzheimer's disease. *Alzheimers Dement.* 14, 535–562. doi: 10.1016/j.jalz.2018.02.018

Jafari, A., Babajani, A., Abdollahpour-Alitappeh, M., Ahmadi, N., and Rezaei-Tavirani, M. (2021). Exosomes and cancer: From molecular mechanisms to clinical applications. *Med. Oncol.* 38:45. doi: 10.1007/s12032-021-01491-0

Janelidze, S., Berron, D., Smith, R., Strandberg, O., Proctor, N. K., Dage, J. L., et al. (2021). Associations of Plasma Phospho-Tau217 levels with tau positron emission tomography in early Alzheimer disease. *JAMA Neurol.* 78, 149–156. doi: 10.1001/jamaneurol.2020.4201

Janelidze, S., Mattsson, N., Palmqvist, S., Smith, R., Beach, T. G., Serrano, G. E., et al. (2020a). Plasma P-tau181 in Alzheimer's disease: Relationship to other biomarkers, differential diagnosis, neuropathology and longitudinal progression to Alzheimer's dementia. *Nat. Med.* 26, 379–386. doi: 10.1038/s41591-020-0755-1

Janelidze, S., Stomrud, E., Smith, R., Palmqvist, S., Mattsson, N., Airey, D. C., et al. (2020b). Cerebrospinal fluid p-tau217 performs better than p-tau181 as a biomarker of Alzheimer's disease. *Nat. Commun.* 11:1683.doi: 10.1038/s41467-020-15436-0

Janelidze, S., Zetterberg, H., Mattsson, N., Palmqvist, S., Vanderstichele, H., Lindberg, O., et al. (2016). CSF Aβ42/Aβ40 and Aβ42/Aβ38 ratios: Better diagnostic markers of Alzheimer disease. *Ann. Clin. Transl. Neurol.* 3, 154–165. doi: 10.1002/acn3.274

Jann, M. W. (2000). Rivastigmine, a new-generation cholinesterase inhibitor for the treatment of Alzheimer's disease. *Pharmacotherapy* 20, 1–12. doi: 10.1592/phco.20.1.1.34664

Jia, L., Qiu, Q., Zhang, H., Chu, L., Du, Y., Zhang, J., et al. (2019). Concordance between the assessment of Abeta42, T-tau, and P-T181-tau in peripheral blood neuronal-derived exosomes and cerebrospinal fluid. *Alzheimers Dement.* 15, 1071–1080. doi: 10.1016/j.jalz.2019.05.002

Jia, L. H., and Liu, Y. N. (2016). Downregulated serum miR-223 servers as biomarker in Alzheimer's disease. *Cell Biochem. Funct.* 34, 233–237. doi: 10.1002/cbf.3184

Jiang, L., Dong, H., Cao, H., Ji, X., Luan, S., and Liu, J. (2019). Exosomes in pathogenesis, diagnosis, and treatment of Alzheimer's disease. *Med. Sci. Monit.* 25, 3329–3335. doi: 10.12659/MSM.914027

Johnstone, R. M., Adam, M., Hammond, J. R., Orr, L., and Turbide, C. (1987). Vesicle formation during reticulocyte maturation. Association of plasma membrane activities with released vesicles (exosomes). *J. Biol. Chem.* 262, 9412–9420. doi: 10.1016/S0021-9258(18)48095-7

Jack C. R. jr., Bennett, D. A., Blennow, K., Carrillo, M. C., Feldman, H. H., Frisoni, G. B., et al. (2016). A/T/N- An unbiased descriptive classification scheme for Alzheimer disease biomarkers. *Neurology* 87, 539–547. doi: 10.1212/WNL.0000000000002923

Kahlert, C., Melo, S. A., Protopopov, A., Tang, J., Seth, S., Koch, M., et al. (2014). Identification of double-stranded genomic DNA spanning all chromosomes with mutated KRAS and p53 DNA in the serum exosomes of patients with pancreatic cancer. *J. Biol. Chem.* 289, 3869–3875. doi: 10.1074/jbc.C113.532267

Kalluri, R., and LeBleu, V. S. (2020). The biology, function, and biomedical applications of exosomes. *Science* 367:eaau6977. doi: 10.1126/science.aau6977

Kanninen, K. M., Bister, N., Koistinaho, J., and Malm, T. (2016). Exosomes as new diagnostic tools in CNS diseases. *Biochim. Biophys. Acta* 1862, 403–410. doi: 10.1016/j.bbadis.2015.09.020

Karikari, T. K., Benedet, A. L., Ashton, N. J., Lantero Rodriguez, J., Snellman, A., Suarez-Calvet, M., et al. (2021a). Diagnostic performance and prediction of clinical progression of plasma phospho-tau181 in the Alzheimer's Disease Neuroimaging Initiative. *Mol. Psychiatry* 26, 429–442. doi: 10.1038/s41380-020-00923-z

Karikari, T. K., Emersic, A., Vrillon, A., Lantero-Rodriguez, J., Ashton, N. J., Kramberger, M. G., et al. (2021b). Head-to-head comparison of clinical performance of CSF phospho-tau T181 and T217 biomarkers for Alzheimer's disease diagnosis. *Alzheimers Dement.* 17, 755–767. doi: 10.1002/alz.12236

Karikari, T. K., Pascoal, T. A., Ashton, N. J., Janelidze, S., Benedet, A. L., Rodriguez, J. L., et al. (2020). Blood phosphorylated tau 181 as a biomarker for Alzheimer's disease: A diagnostic performance and prediction modelling study using data from four prospective cohorts. *Lancet Neurol.* 19, 422–433. doi: 10.1016/S1474-4422(20)30071-5

Katsipis, G., Tzekaki, E. E., Tsolaki, M., and Pantazaki, A. A. (2021). Salivary GFAP as a potential biomarker for diagnosis of mild cognitive impairment and Alzheimer's disease and its correlation with neuroinflammation and apoptosis. *J. Neuroimmunol.* 361:577744. doi: 10.1016/j.jneuroim.2021.577744

Kenny, A., Mcardle, H., Calero, M., Rabano, A., Madden, S. F., Adamson, K., et al. (2019). Elevated plasma microRNA-206 levels predict cognitive decline and progression to dementia from mild cognitive impairment. *Biomolecules* 9:734.doi: 10.3390/biom9110734

Keshavan, A., Pannee, J., Karikari, T. K., Rodriguez, J. L., Ashton, N. J., Nicholas, J. M., et al. (2021). Population-based blood screening for preclinical Alzheimer's disease in a British birth cohort at age 70. *Brain* 144, 434–449.

Kester, M. I., Teunissen, C. E., Sutphen, C., Herries, E. M., Ladenson, J. H., Xiong, C., et al. (2015). Cerebrospinal fluid VILIP-1 and YKL-40, candidate biomarkers to diagnose, predict and monitor Alzheimer's disease in a memory clinic cohort. *Alzheimers Res. Ther.* 7:59. doi: 10.1186/s13195-015-0142-1

Khan, S. S., and Bloom, G. S. (2016). Tau: The center of a signaling nexus in Alzheimer's disease. *Front. Neurosci.* 10:31. doi: 10.3389/fnins.2016.00031

Kim, C. B., Choi, Y. Y., Song, W. K., and Song, K. B. (2014). Antibody-based magnetic nanoparticle immunoassay for quantification of Alzheimer's disease pathogenic factor. *J. Biomed. Opt.* 19:051205. doi: 10.1117/1.JBO.19.5.051205

Kloten, V., Lampignano, R., Krahn, T., and Schlange, T. (2019). Circulating tumor cell PD-L1 expression as biomarker for therapeutic efficacy of immune checkpoint inhibition in NSCLC. *Cells* 8:809. doi: 10.3390/cells8080809

Knapskog, A. B., Henjum, K., Idland, A. V., Eldholm, R. S., Persson, K., Saltvedt, I., et al. (2020). Cerebrospinal fluid sTREM2 in Alzheimer's disease: Comparisons between clinical presentation and AT classification. *Sci. Rep.* 10:15886. doi: 10.1038/s41598-020-72878-8

Kohnken, R., Buerger, K., Zinkowski, R., Miller, C., Kerkman, D., Debernardis, J., et al. (2000). Detection of tau phosphorylated at threonine 231 in cerebrospinal fluid of Alzheimer's disease patients. *Neurosci. Lett.* 287, 187–190. doi: 10.1016/S0304-3940(00)01178-2

Kugeratski, F. G., and Kalluri, R. (2021). Exosomes as mediators of immune regulation and immunotherapy in cancer. *FEBS J.* 288, 10–35. doi: 10.1111/febs.15558

Kulichikhin, K. Y., Fedotov, S. A., Rubel, M. S., Zalutskaya, N. M., Zobnina, A. E., Malikova, O. A., et al. (2021). Development of molecular tools for diagnosis of Alzheimer's disease that are based on detection of amyloidogenic proteins. *Prion* 15, 56–69. doi: 10.1080/19336896.2021.1917289

Kumar, S., and Reddy, P. H. (2018). MicroRNA-455-3p as a potential biomarker for Alzheimer's disease: An update. *Front. Aging Neurosci.* 10:41. doi: 10.3389/fnagi.2018.00041

Lakshmi, S., Hughes, T. A., and Priya, S. (2021). Exosomes and exosomal RNAs in breast cancer: A status update. *Eur. J. Cancer* 144, 252–268.doi: 10.1016/j.ejca.2020.11.033

Lane, C. A., Hardy, J., and Schott, J. M. (2018). Alzheimer's disease. *Eur. J. Neurol.* 25, 59–70. doi: 10.1111/ene.13439

Lantero-Rodriguez, J., Snellman, A., Benedet, A. L., Mila-Aloma, M., Camporesi, E., Montoliu-Gaya, L., et al. (2021). P-tau235: A novel biomarker for staging preclinical Alzheimer's disease. *EMBO Mol. Med.* 13:e15098. doi: 10.15252/emmm.202115098

Lashley, T., Schott, J. M., Weston, P., Murray, C. E., Wellington, H., Keshavan, A., et al. (2018). Molecular biomarkers of Alzheimer's disease: Progress and prospects. *Dis. Model. Mech.* 11:dmm031781. doi: 10.1242/dmm.031781

Lau, H. C., Lee, I. K., Ko, P. W., Lee, H. W., Huh, J. S., Cho, W. J., et al. (2015). Non-invasive screening for Alzheimer's disease by sensing salivary sugar using *Drosophila* cells expressing gustatory receptor (Gr5a) immobilized on an extended gate ion-sensitive field-effect transistor (EG-ISFET) biosensor. *PLoS One* 10:e0117810. doi: 10.1371/journal.pone.0117810

Lee, H., Ugay, D., Hong, S., and Kim, Y. (2020). Alzheimer's disease diagnosis using misfolding proteins in Blood. *Dement. Neurocogn. Disord.* 19, 1–18. doi: 10.12779/dnd.2020.19.1.1

Lee, J. C., Kim, S. J., Hong, S., and Kim, Y. (2019). Diagnosis of Alzheimer's disease utilizing amyloid and tau as fluid biomarkers. *Exp. Mol. Med.* 51, 1–10. doi: 10.1038/s12276-019-0299-y

Lee, J. H., Yang, D. S., Goulbourne, C. N., Im, E., Stavrides, P., Pensalfini, A., et al. (2022). Faulty autolysosome acidification in Alzheimer's disease mouse models induces autophagic build-up of Abeta in neurons, yielding senile plaques. *Nat. Neurosci.* 25, 688–701. doi: 10.1038/s41593-022-01084-8

Lee, M., Guo, J. P., Kennedy, K., Mcgeer, E. G., and Mcgeer, P. L. (2017). A method for diagnosing Alzheimer's disease based on salivary amyloid-β protein 42 levels. *J. Alzheimers Dis.* 55, 1175–1182. doi: 10.3233/JAD-160748

Leuzy, A., Ashton, N. J., Mattsson-Carlgren, N., Dodich, A., Boccardi, M., Corre, J., et al. (2021). 2020 update on the clinical validity of cerebrospinal fluid amyloid, tau, and phospho-tau as biomarkers for Alzheimer's disease in the context of a structured 5-phase development framework. *Eur. J. Nucl. Med. Mol. Imaging* 48, 2121–2139. doi: 10.1007/s00259-021-05258-7

Lewczuk, P., Matzen, A., Blennow, K., Parnetti, L., Molinuevo, J. L., Eusebi, P., et al. (2017). Cerebrospinal Fluid Aβ 42/40 Corresponds Better than Aβ 42 to Amyloid PET in Alzheimer's Disease. *J. Alzheimers Dis.* 55, 813–822. doi: 10.3233/JAD-160722

Li, Y., Guan, S., Jin, H., Liu, H., Kang, M., Wang, X., et al. (2020). The relationship between urinary Alzheimer-associated neuronal thread protein and blood biochemical indicators in the general population. *Aging* 12, 15260–15280. doi: 10.18632/aging.103356

Li, W., Kui, L., Demetrios, T., Gong, X., and Tang, M. (2020). A glimmer of hope: Maintain mitochondrial homeostasis to mitigate Alzheimer's disease. *Aging Dis.* 11, 1260–1275. doi: 10.14336/AD.2020.0105

Li, Y., Lim, E., Fields, T., Wu, H., Xu, Y., Wang, Y. A., et al. (2019). Improving sensitivity and specificity of amyloid-beta peptides and tau protein detection with antibiofouling magnetic nanoparticles for liquid biopsy of Alzheimer's disease. *ACS Biomater. Sci. Eng.* 5, 3595–3605. doi: 10.1021/acsbiomaterials.9b00086

Li, Y., Xiong, C., Aschenbrenner, A. J., Chang, C. H., Weiner, M. W., Nosheny, R. L., et al. (2021). Item response theory analysis of the Clinical Dementia Rating. *Alzheimers Dement.* 17, 534–542. doi: 10.1002/alz.12210

Liang, D., and Lu, H. (2019). Salivary biological biomarkers for Alzheimer's disease. *Arch. Oral Biol.* 105, 5–12. doi: 10.1016/j.archoralbio.2019.06.004

Liang, Y., Eng, W. S., Colquhoun, D. R., Dinglasan, R. R., Graham, D. R., and Mahal, L. K. (2014). Complex N-linked glycans serve as a determinant for exosome/microvesicle cargo recruitment. *J. Biol. Chem.* 289, 32526–32537.doi: 10.1074/jbc.M114.606269

Lim, K., Kim, S. Y., Lee, B., Segarra, C., Kang, S., Ju, Y., et al. (2015). Magnetic microparticle-based multimer detection system for the detection of prion oligomers in sheep. *Int. J. Nanomedicine* 10, 241–250. doi: 10.2147/IJN.S88377

Lindwall, G., and Cole, R. D. (1984). Phosphorylation affects the ability of tau protein to promote microtubule assembly. *J. Biol. Chem.* 259, 5301–5305. doi: 10.1016/S0021-9258(17)42989-9

Lista, S., Faltraco, F., Prvulovic, D., and Hampel, H. (2013). Blood and plasma-based proteomic biomarker research in Alzheimer's disease. *Prog. Neurobiol.* 101-102, 1–17. doi: 10.1016/j.pneurobio.2012.06.007

Liu, C. G., Song, J., Zhang, Y. Q., and Wang, P. C. (2014). MicroRNA-193b is a regulator of amyloid precursor protein in the blood and cerebrospinal fluid derived exosomal microRNA-193b is a biomarker of Alzheimer's disease. *Mol. Med. Rep.* 10, 2395–2400.doi: 10.3892/mmr.2014.2484

Liu, J., Chen, Y., Pei, F., Zeng, C., Yao, Y., Liao, W., et al. (2021). Extracellular vesicles in liquid biopsies: Potential for disease diagnosis. *Biomed Res. Int.* 2021:6611244. doi: 10.1155/2021/6611244

Liu, L., Liu, L., Lu, Y., Zhang, T., and Zhao, W. (2021). Serum aberrant expression of miR-24-3p and its diagnostic value in Alzheimer's disease. *Biomark. Med.* 15, 1499–1507. doi: 10.2217/bmm-2021-0098

Liu, T., Hooda, J., Atkinson, J. M., Whiteside, T. L., Oesterreich, S., and Lee, A. V. (2021). Exosomes in breast cancer - mechanisms of action and clinical potential. *Mol. Cancer Res.* 19, 935–945. doi: 10.1158/1541-7786.MCR-20-0952

Liu, L., Chen, X., Chen, Y. H., and Zhang, K. (2020). Identification of Circular RNA hsa_Circ_0003391 in peripheral blood is potentially associated with Alzheimer's disease. *Front. Aging Neurosci.* 12:601965. doi: 10.3389/fnagi.2020.601965

Lue, L. F., Kuo, Y. M., and Sabbagh, M. (2019). Advance in plasma AD core biomarker development: Current findings from immunomagnetic reduction-based SQUID technology. *Neurol. Ther.* 8, 95–111. doi: 10.1007/s40120-019-00167-2

Lugli, G., Cohen, A. M., Bennett, D. A., Shah, R. C., Fields, C. J., Hernandez, A. G., et al. (2015). Plasma Exosomal miRNAs in persons with and without Alzheimer disease: Altered expression and prospects for biomarkers. *PLoS One* 10:e0139233. doi: 10.1371/journal.pone.0139233

Lukiw, W. J. (2007). Micro-RNA speciation in fetal, adult and Alzheimer's disease hippocampus. *Neuroreport* 18, 297–300. doi: 10.1097/WNR.0b013e3280148e8b

Lukiw, W. J., Alexandrov, P. N., Zhao, Y., Hill, J. M., and Bhattacharjee, S. (2012a). Spreading of Alzheimer's disease inflammatory signaling through soluble micro-RNA. *Neuroreport* 23, 621–626.doi: 10.1097/00001756-201207110-00009

Lukiw, W. J., Andreeva, T. V., Grigorenko, A. P., and Rogaev, E. I. (2012b). Studying micro RNA function and dysfunction in Alzheimer's disease. *Front. Genet.* 3:327. doi: 10.3389/fgene.2012.00327

Mader, S., and Pantel, K. (2017). Liquid biopsy: Current status and future perspectives. *Oncol. Res. Treat.* 40, 404–408. doi: 10.1159/000478018

Manouchehrinia, A., Piehl, F., Hillert, J., Kuhle, J., Alfredsson, L., Olsson, T., et al. (2020). Confounding effect of blood volume and body mass index on blood neurofilament light chain levels. *Ann. Clin. Transl. Neurol.* 7, 139–143.doi: 10.1002/acn3.50972

Markesbery, W. R., Schmitt, F. A., Kryscio, R. J., Davis, D. G., Smith, C. D., and Wekstein, D. R. (2006). Neuropathologic substrate of mild cognitive impairment. *Arch. Neurol.* 63, 38–46. doi: 10.1001/archneur.63.1.38

Mattsson, N., Andreasson, U., Zetterberg, H., Blennow, K., Alzheimer's Disease, and Neuroimaging, I. (2017). Association of plasma neurofilament light with neurodegeneration in patients with Alzheimer disease. *JAMA Neurol.* 74, 557–566.doi: 10.1001/jamaneurol.2016.6117

Mattsson, N., Cullen, N. C., Andreasson, U., Zetterberg, H., and Blennow, K. (2019). Association between longitudinal plasma neurofilament light and neurodegeneration in patients with Alzheimer disease. *JAMA Neurol.* 76, 791–799. doi: 10.1001/jamaneurol.2019.0765

Mawuenyega, K. G., Kasten, T., Sigurdson, W., and Bateman, R. J. (2013). Amyloid-beta isoform metabolism quantitation by stable isotope-labeled kinetics. *Anal. Biochem.* 440, 56–62. doi: 10.1016/j.ab.2013.04.031

Mayeux, R., Honig, L. S., Tang, M.-X., Manly, J., Stern, Y., Schupf, N., et al. (2003). Plasma Aβ40 and Aβ42 and Alzheimer's disease: Relation to age, mortality, and risk. *Neurology* 61, 1185–1190. doi: 10.1212/01.WNL.0000091890.32140.8F

McGeer, P. L., Guo, J. P., Lee, M., Kennedy, K., and Mcgeer, E. G. (2018). Alzheimer's disease can be spared by nonsteroidal anti-inflammatory drugs. *J. Alzheimers Dis.* 62, 1219–1222. doi: 10.3233/JAD-170706

McGowan, E., Pickford, F., Kim, J., Onstead, L., Eriksen, J., Yu, C., et al. (2005). Aβ42 is essential for parenchymal and vascular amyloid deposition in mice. *Neuron* 47, 191–199. doi: 10.1016/j.neuron.2005.06.030

Meng, X., Li, T., Wang, X., Lv, X., Sun, Z., Zhang, J., et al. (2019). Association between increased levels of amyloid-beta oligomers in plasma and episodic memory loss in Alzheimer's disease. *Alzheimers Res. Ther.* 11:89. doi: 10.1186/s13195-019-0535-7

Miura, M., Fujinami, N., Shimizu, Y., Mizuno, S., Saito, K., Suzuki, T., et al. (2020). Usefulness of plasma full-length glypican-3 as a predictive marker of hepatocellular carcinoma recurrence after radial surgery. *Oncol. Lett.* 19, 2657–2666. doi: 10.3892/ol.2020.11371

Molinuevo, J. L., Ayton, S., Batrla, R., Bednar, M. M., Bittner, T., Cummings, J., et al. (2018). Current state of Alzheimer's fluid biomarkers. *Acta Neuropathol.* 136, 821–853. doi: 10.1007/s00401-018-1932-x

Molinuevo, J. L., Blennow, K., Dubois, B., Engelborghs, S., Lewczuk, P., Perret-Liaudet, A., et al. (2014). The clinical use of cerebrospinal fluid biomarker testing for Alzheimer's disease diagnosis: A consensus paper from the Alzheimer's Biomarkers Standardization Initiative. *Alzheimers Dement.* 10, 808–817.doi: 10.1016/j.jalz.2014.03.003

Monte, S. M. D. L., and Wands, J. R. (2001). Alzheimer-associated neuronal thread protein-induced apoptosis and impaired mitochondrial function in human central nervous system-derived neuronal cells. *J. Neuropathol. Exp. Neurol.* 60, 195–207. doi: 10.1093/jnen/60.2.195

Moscoso, A., Grothe, M. J., Ashton, N. J., Karikari, T. K., Rodriguez, J. L., Snellman, A., et al. (2021). Time course of phosphorylated-tau181 in blood across the Alzheimer's disease spectrum. *Brain* 144, 325–339. doi: 10.1093/brain/awaa399

Mullins, R. J., Mustapic, M., Goetzl, E. J., and Kapogiannis, D. (2017). Exosomal biomarkers of brain insulin resistance associated with regional atrophy in Alzheimer's disease. *Hum. Brain Mapp.* 38, 1933–1940. doi: 10.1002/hbm.23494

Muraoka, S., Jedrychowski, M. P., Yanamandra, K., Ikezu, S., Gygi, S. P., and Ikezu, T. (2020).). Proteomic profiling of extracellular vesicles derived from cerebrospinal fluid of Alzheimer's disease patients: A pilot study. *Cells* 9:1959. doi: 10.3390/cells9091959

Mustapic, M., Eitan, E., Werner, J. K. Jr., Berkowitz, S. T., Lazaropoulos, M. P., et al. (2017). Plasma extracellular vesicles enriched for neuronal origin: A potential window into brain pathologic processes. *Front. Neurosci.* 11:278. doi: 10.3389/fnins.2017.00278

Naseri, N. N., Wang, H., Guo, J., Sharma, M., and Luo, W. (2019). The complexity of tau in Alzheimer's disease. *Neurosci. Lett.* 705, 183–194. doi: 10.1016/j.neulet.2019.04.022

Nitsch, R. M., Blusztajn, J. K., Pittas, A. G., Slack, B. E., Growdon, J. H., and Wurtman, R. J. (1992). Evidence for a membrane defect in Alzheimer disease brain. *Proc. Natl. Acad. Sci. U.S.A.* 89, 1671–1675.doi: 10.1073/pnas.89.5.1671

Noda, K., Matsuda, K., Yagishita, S., Maeda, K., Akiyama, Y., Terada-Hirashima, J., et al. (2021). A novel highly quantitative and reproducible assay for the detection of anti-SARS-CoV-2 IgG and IgM antibodies. *Sci. Rep.* 11:5198. doi: 10.1038/s41598-021-84387-3

Nutu, M., Zetterberg, H., Londos, E., Minthon, L., Nägga, K., Blennow, K., et al. (2013). Evaluation of the cerebrospinal fluid amyloid-β1-42/amyloid-β1-40 ratio measured by alpha-LISA to distinguish Alzheimer's disease from other dementia disorders. *Dement. Geriatr. Cogn. Disord.* 36, 99–110. doi: 10.1159/000353442

O'Brien, R. J., and Wong, P. C. (2011). Amyloid precursor protein processing and Alzheimer's disease. *Annu. Rev. Neurosci.* 34, 185–204. doi: 10.1146/annurev-neuro-061010-113613

O'Bryant, S. E., Gupta, V., Henriksen, K., Edwards, M., Jeromin, A., Lista, S., et al. (2015). Guidelines for the standardization of preanalytic variables for blood-based biomarker studies in Alzheimer's disease research. *Alzheimers Dement.* 11, 549–560. doi: 10.1016/j.jalz.2014.08.099

O'Bryant, S. E., Mielke, M. M., Rissman, R. A., Lista, S., Vanderstichele, H., Zetterberg, H., et al. (2017). Blood-based biomarkers in Alzheimer disease: Current state of the science and a novel collaborative paradigm for advancing from discovery to clinic. *Alzheimers Dement.* 13, 45–58. doi: 10.1016/j.jalz.2016.09.014

Olsson, B., Lautner, R., Andreasson, U., Öhrfelt, A., Portelius, E., Bjerke, M., et al. (2016). CSF and blood biomarkers for the diagnosis of Alzheimer's disease: A systematic review and meta-analysis. *Lancet Neurol.* 15, 673–684.doi: 10.1016/S1474-4422(16)00070-3

Ovod, V., Ramsey, K. N., Mawuenyega, K. G., Bollinger, J. G., Hicks, T., Schneider, T., et al. (2017). Amyloid beta concentrations and stable isotope labeling kinetics of human plasma specific to central nervous system amyloidosis. *Alzheimers Dement.* 13, 841–849. doi: 10.1016/j.jalz.2017.06.2266

Palmqvist, S., Janelidze, S., Quiroz, Y. T., Zetterberg, H., Lopera, F., Stomrud, E., et al. (2020). Discriminative accuracy of plasma phospho-tau217 for Alzheimer disease vs other neurodegenerative disorders. *JAMA* 324, 772–781. doi: 10.1001/jama.2020.12134

Palmqvist, S., Janelidze, S., Stomrud, E., Zetterberg, H., Karl, J., Zink, K., et al. (2019). Performance of fully automated plasma assays as screening tests for Alzheimer disease-related beta-amyloid status. *JAMA Neurol.* 76, 1060–1069. doi: 10.1001/jamaneurol.2019.1632

Pannee, J., Portelius, E., Minthon, L., Gobom, J., Andreasson, U., Zetterberg, H., et al. (2016). Reference measurement procedure for CSF amyloid beta (Aβ) 1–42 and the CSF Aβ1–42/Aβ1–40 ratio–a cross-validation study against amyloid PET. *J. Neurochem.* 139, 651–658. doi: 10.1111/jnc.13838

Paraskevaidi, M., Allsop, D., Karim, S., Martin, F. L., and Crean, S. (2020). Diagnostic biomarkers for Alzheimer's disease using non-invasive specimens. *J. Clin. Med.* 9:1673. doi: 10.3390/jcm9061673

Park, S. A., Han, S. M., and Kim, C. E. (2020). New fluid biomarkers tracking non-amyloid-beta and non-tau pathology in Alzheimer's disease. *Exp. Mol. Med.* 52, 556–568. doi: 10.1038/s12276-020-0418-9

Paterson, R. W., Gabelle, A., Lucey, B. P., Barthelemy, N. R., Leckey, C. A., Hirtz, C., et al. (2019). SILK studies - capturing the turnover of proteins linked to neurodegenerative diseases. *Nat. Rev. Neurol.* 15, 419–427. doi: 10.1038/s41582-019-0222-0

Patterson, V., Humphreys, J., Chua, R. J. J. O. N., Neurosurgery, and Psychiatry. (2004). Email triage of new neurological outpatient referrals from general practice. *J. Neurol. Neurosurg. Psychiatry*<refvol>75, 617–620. doi: 10.1136/jnnp.2003.024489

Pawlik, P., and Blochowiak, K. (2021). The role of salivary biomarkers in the early diagnosis of Alzheimer's disease and Parkinson's disease. *Diagnostics* 11:371. doi: 10.3390/diagnostics11020371

Pegtel, D. M., Cosmopoulos, K., Thorley-Lawson, D. A., Van Eijndhoven, M. A., Hopmans, E. S., Lindenberg, J. L., et al. (2010). Functional delivery of viral miRNAs via exosomes. *Proc. Natl. Acad. Sci. U.S.A.* 107, 6328–6333. doi: 10.1073/pnas.0914843107

Pegtel, D. M., and Gould, S. J. (2019). Exosomes. *Annu. Rev. Biochem.* 88, 487–514. doi: 10.1146/annurev-biochem-013118-111902

Pena-Bautista, C., Tirle, T., Lopez-Nogueroles, M., Vento, M., Baquero, M., and Chafer-Pericas, C. (2019). Oxidative damage of DNA as early marker of Alzheimer's disease. *Int. J. Mol. Sci.* 20:6136. doi: 10.3390/ijms20246136

Pereira, J. B., Janelidze, S., Stomrud, E., Palmqvist, S., Van Westen, D., Dage, J. L., et al. (2021). Plasma markers predict changes in amyloid, tau, atrophy and cognition in non-demented subjects. *Brain* 144, 2826–2836. doi: 10.1093/brain/awab163

Pessoa, L. S., Heringer, M., and Ferrer, V. P. (2020). ctDNA as a cancer biomarker: A broad overview. *Crit. Rev. Oncol. Hematol.* 155:103109. doi: 10.1016/j.critrevonc.2020.103109

Pinnell, J. R., Cui, M., and Tieu, K. (2021). Exosomes in Parkinson disease. *J. Neurochem.* 157, 413–428. doi: 10.1111/jnc.15288

Platenik, J., Fisar, Z., Buchal, R., Jirak, R., Kitzlerova, E., Zverova, M., et al. (2014). GSK3beta, CREB, and BDNF in peripheral blood of patients with Alzheimer's disease and depression. *Prog. Neuropsychopharmacol. Biol. Psychiatry* 50, 83–93. doi: 10.1016/j.pnpbp.2013.12.001

Portelius, E., Lashley, T., Westerlund, A., Persson, R., Fox, N. C., Blennow, K., et al. (2015). Brain amyloid-beta fragment signatures in pathological ageing and Alzheimer's disease by hybrid immunoprecipitation mass spectrometry. *Neurodegener. Dis.* 15, 50–57. doi: 10.1159/000369465

Portelius, E., Westman-Brinkmalm, A., Zetterberg, H., and Blennow, K. (2006). Determination of beta-amyloid peptide signatures in cerebrospinal fluid using immunoprecipitation-mass spectrometry. *J. Proteome Res.* 5, 1010–1016. doi: 10.1021/pr050475v

Potter, R., Patterson, B. W., Elbert, D. L., Ovod, V., Kasten, T., Sigurdson, W., et al. (2013). Increased in vivo amyloid-β42 production, exchange, and loss in presenilin mutation carriers. *Sci. Transl. Med.* 5:189ra177.doi: 10.1126/scitranslmed.3005615

Poulet, G., Massias, J., and Taly, V. (2019). Liquid biopsy: General concepts. *Acta Cytol.* 63, 449–455. doi: 10.1159/000499337

Preische, O., Schultz, S. A., Apel, A., Kuhle, J., Kaeser, S. A., Barro, C., et al. (2019). Serum neurofilament dynamics predicts neurodegeneration and clinical progression in presymptomatic Alzheimer's disease. *Nat. Med.* 25, 277–283. doi: 10.1038/s41591-018-0304-3

Pu, Z., Tang, X., Fei, Y., Hou, Q., Lin, Y., and Zha, X. (2020). Bone metabolic biomarkers and bone mineral density in male patients with early-stage Alzheimer's disease. *Eur. Geriatr. Med.* 11, 403–408.doi: 10.1007/s41999-020-00289-z

Pyun, J. M., Ryu, J. S., Lee, R., Shim, K. H., Youn, Y. C., Ryoo, N., et al. (2021). Plasma amyloid-beta oligomerization tendency predicts amyloid PET positivity. *Clin. Interv. Aging* 16, 749–755. doi: 10.2147/CIA.S312473

Racine, A. M., Koscik, R. L., Nicholas, C. R., Clark, L. R., Okonkwo, O. C., Oh, J. M., et al. (2016). Cerebrospinal fluid ratios with Aβ42 predict preclinical brain β−amyloid accumulation. *Alzheimers Dement.* 2, 27–38. doi: 10.1016/j.dadm.2015.11.006

Rani, A., O'Shea, A., Ianov, L., Cohen, R. A., Woods, A. J., and Foster, T. C. (2017). miRNA in circulating microvesicles as biomarkers for age-related cognitive decline. *Front. Aging Neurosci.* 9:323. doi: 10.3389/fnagi.2017.00323

Raposo, G., Nijman, H. W., Stoorvogel, W., Liejendekker, R., Harding, C. V., Melief, C. J., et al. (1996). B lymphocytes secrete antigen-presenting vesicles. *J. Exp. Med.* 183, 1161–1172. doi: 10.1084/jem.183.3.1161

Rastogi, S., Sharma, V., Bharti, P. S., Rani, K., Modi, G. P., Nikolajeff, F., et al. (2021). The evolving landscape of exosomes in neurodegenerative diseases: Exosomes characteristics and a promising role in early diagnosis. *Int. J. Mol. Sci.* 22:440. doi: 10.3390/ijms22010440

Ratajczak, J., Miekus, K., Kucia, M., Zhang, J., Reca, R., Dvorak, P., et al. (2006). Embryonic stem cell-derived microvesicles reprogram hematopoietic progenitors: Evidence for horizontal transfer of mRNA and protein delivery. *Leukemia* 20, 847–856. doi: 10.1038/sj.leu.2404132

Rauchmann, B. S., Schneider-Axmann, T., Perneczky, R., Alzheimer's Disease Neuroimaging Initiative (2021). Associations of longitudinal plasma p-tau181 and NfL with tau-PET, Abeta-PET and cognition. *J. Neurol. Neurosurg. Psychiatry* 92, 1289–1295. doi: 10.1136/jnnp-2020-325537

Reale, M., Gonzales-Portillo, I., and Borlongan, C. V. (2020). Saliva, an easily accessible fluid as diagnostic tool and potent stem cell source for Alzheimer's Disease: Present and future applications. *Brain Res.* 1727:146535. doi: 10.1016/j.brainres.2019.146535

Reiss, A. B., Arain, H. A., Stecker, M. M., Siegart, N. M., and Kasselman, L. J. (2018). Amyloid toxicity in Alzheimer's disease. *Rev. Neurosci.* 29, 613–627. doi: 10.1515/revneuro-2017-0063

Richard, B. C., Bayer, T. A., Lind, S. B., Shevchenko, G., and Bergquist, J. (2019). A simplified and sensitive immunoprecipitation mass spectrometry protocol for the analysis of amyloid-beta peptides in brain tissue. *Clin. Mass Spectrom.* (14 Pt B), 83–88.doi: 10.1016/j.clinms.2019.07.001

Rohanizadegan, M., and Kulkarni, S. (2018). Transformational role of liquid biopsy in diagnosis and treatment of cancer. *Cancer Genet.* 228-229, 129–130. doi: 10.1016/j.cancergen.2018.11.006

Sabbagh, M. N., Shi, J., Lee, M., Arnold, L., Al-Hasan, Y., Heim, J., et al. (2018). Salivary beta amyloid protein levels are detectable and differentiate patients with Alzheimer's disease dementia from normal controls: Preliminary findings. *BMC Neurol.* 18:155. doi: 10.1186/s12883-018-1160-y

Sancesario, G., and Bernardini, S. (2019). AD biomarker discovery in CSF and in alternative matrices. *Clin. Biochem.* 72, 52–57. doi: 10.1016/j.clinbiochem.2019.08.008

Sandua, A., Alegre, E., and Gonzalez, A. (2021). Exosomes in lung cancer: Actors and heralds of tumor development. *Cancers* 13:4330. doi: 10.3390/cancers13174330

Sansone, P., Savini, C., Kurelac, I., Chang, Q., Amato, L. B., Strillacci, A., et al. (2017). Packaging and transfer of mitochondrial DNA via exosomes regulate escape from dormancy in hormonal therapy-resistant breast cancer. *Proc. Natl. Acad. Sci. U.S.A.* 114, E9066–E9075. doi: 10.1073/pnas.1704862114

Santos Seckler, H. D., Park, H. M., Lloyd-Jones, C. M., Melani, R. D., Camarillo, J. M., Wilkins, J. T., et al. (2021). New interface for faster proteoform analysis: Immunoprecipitation coupled with samplestream-mass spectrometry. *J. Am. Soc. Mass Spectrom.* 32, 1659–1670. doi: 10.1021/jasms.1c00026

Sato, C., Barthelemy, N. R., Mawuenyega, K. G., Patterson, B. W., Gordon, B. A., Jockel-Balsarotti, J., et al. (2018). Tau kinetics in neurons and the human central nervous system. *Neuron* 97, 1284–1298.e7. doi: 10.1016/j.neuron.2018.02.015

Schepici, G., Silvestro, S., Trubiani, O., Bramanti, P., and Mazzon, E. (2020). Salivary biomarkers: Future approaches for early diagnosis of neurodegenerative diseases. *Brain Sci.* 10:245. doi: 10.3390/brainsci10040245

Segura, E., Nicco, C., Lombard, B., Veron, P., Raposo, G., Batteux, F., et al. (2005). ICAM-1 on exosomes from mature dendritic cells is critical for efficient naive T-cell priming. *Blood* 106, 216–223. doi: 10.1182/blood-2005-01-0220

Seol, W., Kim, H., and Son, I. (2020). Urinary biomarkers for neurodegenerative diseases. *Exp. Neurobiol.* 29, 325–333. doi: 10.5607/en20042

Shi, M., Sui, Y. T., Peskind, E. R., Li, G., Hwang, H., Devic, I., et al. (2011). Salivary tau species are potential biomarkers of Alzheimer's disease. *J. Alzheimers Dis.* 27, 299–305. doi: 10.3233/JAD-2011-110731

Shioya, M., Obayashi, S., Tabunoki, H., Arima, K., Saito, Y., Ishida, T., et al. (2010). Aberrant microRNA expression in the brains of neurodegenerative diseases: miR-29a decreased in Alzheimer disease brains targets neurone navigator 3. *Neuropathol. Appl. Neurobiol.* 36, 320–330. doi: 10.1111/j.1365-2990.2010.01076.x

Silva, M. V. F., Loures, C. M. G., Alves, L. C. V., De Souza, L. C., Borges, K. B. G., and Carvalho, M. D. G. (2019). Alzheimer's disease: Risk factors and potentially protective measures. *J. Biomed. Sci.* 26:33.doi: 10.1186/s12929-019-0524-y

Simrén, J., Leuzy, A., Karikari, T. K., Hye, A., Benedet, A. L., Lantero-Rodriguez, J., et al. (2021). The diagnostic and prognostic capabilities of plasma biomarkers in Alzheimer's disease. *Alzheimers Dement.* 17, 1145–1156. doi: 10.1002/alz.12283

Skog, J., Wurdinger, T., Van Rijn, S., Meijer, D. H., Gainche, L., Sena-Esteves, M., et al. (2008). Glioblastoma microvesicles transport RNA and proteins that promote tumour growth and provide diagnostic biomarkers. *Nat. Cell Biol.* 10, 1470–1476. doi: 10.1038/ncb1800

Smania, M. A. (2020). Liquid biopsy for cancer screening, diagnosis, and treatment. *J. Am. Assoc. Nurse Pract.* 32, 5–7. doi: 10.1097/JXX.0000000000000359

Sokolova, V., Ludwig, A. K., Hornung, S., Rotan, O., Horn, P. A., Epple, M., et al. (2011). Characterisation of exosomes derived from human cells by nanoparticle tracking analysis and scanning electron microscopy. *Colloids Surf. B Biointerfaces* 87, 146–150. doi: 10.1016/j.colsurfb.2011.05.013

Song, Z., Xu, Y., Zhang, L., Zhou, L., Zhang, Y., Han, Y., et al. (2020). Comprehensive proteomic profiling of urinary exosomes and identification of potential non-invasive early biomarkers of Alzheimer's disease in 5XFAD mouse model. *Front. Genet.* 11:565479. doi: 10.3389/fgene.2020.565479

Sorensen, S. S., Nygaard, A. B., and Christensen, T. (2016). miRNA expression profiles in cerebrospinal fluid and blood of patients with Alzheimer's disease and other types of dementia - an exploratory study. *Transl. Neurodegener.* 5:6. doi: 10.1186/s40035-016-0053-5

Soria Lopez, J. A., Gonzalez, H. M., and Leger, G. C. (2019). Alzheimer's disease. *Handb. Clin. Neurol.* 167, 231–255. doi: 10.1016/B978-0-12-804766-8.00013-3

Stomrud, E., Hansson, O., Blennow, K., Minthon, L., Londos, E. J. D., and Disorders, G. C. (2007). Cerebrospinal fluid biomarkers predict decline in subjective cognitive function over 3 years in healthy elderly. *Dement. Geriatr. Cogn. Disord.* 24, 118–124. doi: 10.1159/000105017

Strozyk, D., Blennow, K., White, L., and Launer, L. J. N. (2003). CSF Aβ 42 levels correlate with amyloid-neuropathology in a population-based autopsy study. *Neurology* 60, 652–656.doi: 10.1212/01.WNL.0000046581.81650.D0

Suarez-Calvet, M., Karikari, T. K., Ashton, N. J., Lantero Rodriguez, J., Mila-Aloma, M., Gispert, J. D., et al. (2020). Novel tau biomarkers phosphorylated at T181, T217 or T231 rise in the initial stages of the preclinical Alzheimer's continuum when only subtle changes in Abeta pathology are detected. *EMBO Mol. Med.* 12:e12921.

Suarez-Calvet, M., Kleinberger, G., Araque Caballero, M. A., Brendel, M., Rominger, A., Alcolea, D., et al. (2016). sTREM2 cerebrospinal fluid levels are a potential biomarker for microglia activity in early-stage Alzheimer's disease and associate with neuronal injury markers. *EMBO Mol. Med.* 8, 466–476. doi: 10.15252/emmm.201506123

Sun, R., Wang, H., Shi, Y., Gao, D., Sun, Z., Chen, Z., et al. (2019). A pilot study of urinary exosomes in Alzheimer's disease. *Neurodegener. Dis.* 19, 184–191. doi: 10.1159/000505851

Suzuki, N., Iwatsubo, T., Odaka, A., Ishibashi, Y., Kitada, C., and Ihara, Y. (1994). High tissue content of soluble beta 1-40 is linked to cerebral amyloid angiopathy. *Am. J. Pathol.* 145, 452–460.

Tan, C. C., Yu, J. T., and Tan, L. (2014). Biomarkers for preclinical Alzheimer's disease. *J. Alzheimers Dis.* 42, 1051–1069. doi: 10.3233/JAD-140843

Tapiola, T., Alafuzoff, I., Herukka, S.-K., Parkkinen, L., Hartikainen, P., Soininen, H., et al. (2009). Cerebrospinal fluid β-amyloid 42 and tau proteins as biomarkers of Alzheimer-type pathologic changes in the brain. *Arch. Neurol.* 66, 382–389. doi: 10.1001/archneurol.2008.596

Tariciotti, L., Casadei, M., Honig, L. S., Teich, A. F., Mckhann, Ii, G. M., et al. (2018). Clinical experience with cerebrospinal fluid Abeta42, total and phosphorylated Tau in the evaluation of 1,016 individuals for suspected dementia. *J. Alzheimers Dis.* 65, 1417–1425. doi: 10.3233/JAD-180548

Thakur, B. K., Zhang, H., Becker, A., Matei, I., Huang, Y., Costa-Silva, B., et al. (2014). Double-stranded DNA in exosomes: A novel biomarker in cancer detection. *Cell Res.* 24, 766–769. doi: 10.1038/cr.2014.44

Thambisetty, M., and Lovestone, S. J. B. I. M. (2010). Blood-based biomarkers of Alzheimer's disease: Challenging but feasible. *Biomark. Med.* 4, 65–79. doi: 10.2217/bmm.09.84

Thebault, S., Booth, R. A., and Freedman, M. S. (2020). Blood neurofilament light chain: The Neurologist's troponin? *Biomedicines* 8:523. doi: 10.3390/biomedicines8110523

Thijssen, E. H., La Joie, R., Wolf, A., Strom, A., Wang, P., Iaccarino, L., et al. (2020). Diagnostic value of plasma phosphorylated tau181 in Alzheimer's disease and frontotemporal lobar degeneration. *Nat. Med.* 26, 387–397. doi: 10.1038/s41591-020-0762-2

Tiwari, S., Atluri, V., Kaushik, A., Yndart, A., and Nair, M. (2019). Alzheimer's disease: Pathogenesis, diagnostics, and therapeutics. *Int. J. Nanomedicine* 14, 5541–5554. doi: 10.2147/IJN.S200490

Trams, E. G., Lauter, C. J., Salem, N. Jr., and Heine, U. (1981). Exfoliation of membrane ecto-enzymes in the form of micro-vesicles. *Biochim. Biophys. Acta* 645, 63–70. doi: 10.1016/0005-2736(81)90512-5

Tvarijonaviciute, A., Zamora, C., Ceron, J. J., Bravo-Cantero, A. F., Pardo-Marin, L., Valverde, S., et al. (2020). Salivary biomarkers in Alzheimer's disease. *Clin. Oral Investig.* 24, 3437–3444. doi: 10.1007/s00784-020-03214-7

Uljon, S. N., Mazzarelli, L., Chait, B. T., and Wang, R. (2000). Analysis of proteins and peptides directly from biological fluids by immunoprecipitation/mass spectrometry. *Methods Mol. Biol.* 146, 439–452. doi: 10.1385/1-59259-045-4:439

Underwood, J. J., Quadri, R. S., Kalva, S. P., Shah, H., Sanjeevaiah, A. R., Beg, M. S., et al. (2020). Liquid biopsy for cancer: Review and implications for the radiologist. *Radiology* 294, 5–17. doi: 10.1148/radiol.2019182584

Vaidyanathan, R., Soon, R. H., Zhang, P., Jiang, K., and Lim, C. T. (2018). Cancer diagnosis: From tumor to liquid biopsy and beyond. *Lab Chip* 19, 11–34. doi: 10.1039/C8LC00684A

Valadi, H., Ekstrom, K., Bossios, A., Sjostrand, M., Lee, J. J., and Lotvall, J. O. (2007). Exosome-mediated transfer of mRNAs and microRNAs is a novel mechanism of genetic exchange between cells. *Nat. Cell Biol.* 9, 654–659. doi: 10.1038/ncb1596

van der Pol, E., Coumans, F. A., Grootemaat, A. E., Gardiner, C., Sargent, I. L., Harrison, P., et al. (2014). Particle size distribution of exosomes and microvesicles determined by transmission electron microscopy, flow cytometry, nanoparticle tracking analysis, and resistive pulse sensing. *J. Thromb. Haemost.* 12, 1182–1192. doi: 10.1111/jth.12602

van Oijen, M., Hofman, A., Soares, H. D., Koudstaal, P. J., and Breteler, M. M. (2006). Plasma Aβ1–40 and Aβ1–42 and the risk of dementia: A prospective case-cohort study. *Lancet Neurol.* 5, 655–660. doi: 10.1016/S1474-4422(06)70501-4

Vandendriessche, C., Bruggeman, A., Van Cauwenberghe, C., and Vandenbroucke, R. E. (2020). Extracellular vesicles in Alzheimer's and Parkinson's disease: Small entities with large consequences. *Cells* 9:2485. doi: 10.3390/cells9112485

Vandermeeren, M., Mercken, M., Vanmechelen, E., Six, J., Van De Voorde, A., Martin, J. J., et al. (1993). Detection of proteins in normal and Alzheimer's disease cerebrospinal fluid with a sensitive sandwich enzyme-linked immunosorbent assay. *J. Neurochem.* 61, 1828–1834. doi: 10.1111/j.1471-4159.1993.tb09823.x

Vanmechelen, E., Vanderstichele, H., Davidsson, P., Van Kerschaver, E., Van Der Perre, B., Sjögren, M., et al. (2000). Quantification of tau phosphorylated at threonine 181 in human cerebrospinal fluid: A sandwich ELISA with a synthetic phosphopeptide for standardization. *Neurosci. Lett.* 285, 49–52. doi: 10.1016/S0304-3940(00)01036-3

Veerabhadrappa, B., Delaby, C., Hirtz, C., Vialaret, J., Alcolea, D., Lleo, A., et al. (2020). Detection of amyloid beta peptides in body fluids for the diagnosis of Alzheimer's disease: Where do we stand? *Crit. Rev. Clin. Lab. Sci.* 57, 99–113. doi: 10.1080/10408363.2019.1678011

Wang, M. J., Yi, S., Han, J. Y., Park, S. Y., Jang, J. W., Chun, I. K., et al. (2017). Oligomeric forms of amyloid-beta protein in plasma as a potential blood-based biomarker for Alzheimer's disease. *Alzheimers Res. Ther.* 9:98. doi: 10.1186/s13195-017-0324-0

Wang, N., Chen, J., Xiao, H., Wu, L., Jiang, H., and Zhou, Y. (2019). Application of artificial neural network model in diagnosis of Alzheimer's disease. *BMC Neurol.* 19:154. doi: 10.1186/s12883-019-1377-4

Wang, Y., Pan, F., Xie, F., He, R., and Guo, Q. (2022). Correlation between urine formaldehyde and cognitive abilities in the clinical spectrum of Alzheimer's disease. *Front. Aging Neurosci.* 14:820385. doi: 10.3389/fnagi.2022.820385

Watanabe, Y., Hirao, Y., Kasuga, K., Tokutake, T., Kitamura, K., Niida, S., et al. (2020). Urinary apolipoprotein C3 is a potential biomarker for Alzheimer's disease. *Dement. Geriatr. Cogn. Dis. Extra* 10, 94–104. doi: 10.1159/000509561

Wei, H., Xu, Y., Xu, W., Zhou, Q., Chen, Q., Yang, M., et al. (2018). Serum Exosomal miR-223 Serves as a potential diagnostic and prognostic biomarker for dementia. *Neuroscience* 379, 167–176. doi: 10.1016/j.neuroscience.2018.03.016

Weller, J., and Budson, A. (2018). Current understanding of Alzheimer's disease diagnosis and treatment. *F1000Res.* 7:F1000 Faculty Rev-1161. doi: 10.12688/f1000research.14506.1

Wildburger, N. C., Gyngard, F., Guillermier, C., Patterson, B. W., Elbert, D., Mawuenyega, K. G., et al. (2018). Amyloid-beta plaques in clinical Alzheimer's disease brain incorporate stable isotope tracer *in vivo* and exhibit nanoscale heterogeneity. *Front. Neurol.* 9:169. doi: 10.3389/fneur.2018.00169

Winston, C. N., Goetzl, E. J., Akers, J. C., Carter, B. S., Rockenstein, E. M., Galasko, D., et al. (2016). Prediction of conversion from mild cognitive impairment to dementia with neuronally derived blood exosome protein profile. *Alzheimers Dement.* 3, 63–72. doi: 10.1016/j.dadm.2016.04.001

Winston, C. N., Goetzl, E. J., Schwartz, J. B., Elahi, F. M., and Rissman, R. A. (2019). Complement protein levels in plasma astrocyte-derived exosomes are abnormal in conversion from mild cognitive impairment to Alzheimer's disease dementia. *Alzheimers Dement.* 11, 61–66. doi: 10.1016/j.dadm.2018.11.002

Wolozin, B., and Davies, P. J. A. O. N. (1987). Alzheimer-related neuronal protein A68: Specificity and distribution. *Ann. Neurol.* 22, 521–526.

Wu, L., and Qu, X. (2015). Cancer biomarker detection: Recent achievements and challenges. *Chem. Soc. Rev.* 44, 2963–2997. doi: 10.1039/C4CS00370E

Wu, Y., Xu, J., Xu, J., Cheng, J., Jiao, D., Zhou, C., et al. (2017). Lower serum levels of miR-29c-3p and miR-19b-3p as biomarkers for Alzheimer's disease. *Tohoku J. Exp. Med.* 242, 129–136. doi: 10.1620/tjem.242.129

Xu, K., Zhang, C., Du, T., Gabriel, A. N. A., Wang, X., Li, X., et al. (2021). Progress of exosomes in the diagnosis and treatment of lung cancer. *Biomed. Pharmacother.* 134:111111. doi: 10.1016/j.biopha.2020.111111

Xu, Y., Shen, Y. Y., Zhang, X. P., Gui, L., Cai, M., Peng, G. P., et al. (2020). Diagnostic potential of urinary monocyte chemoattractant protein-1 for Alzheimer's disease and amnestic mild cognitive impairment. *Eur. J. Neurol.* 27, 1429–1435. doi: 10.1111/ene.14254

Yamashita, K., Watanabe, S., Ishiki, K., Miura, M., Irino, Y., Kubo, T., et al. (2021). Fully automated chemiluminescence enzyme immunoassays showing high correlation with immunoprecipitation mass spectrometry assays for β-amyloid (1–40) and (1–42) in plasma samples. Biochem. Biophys. Res. Commun. 576, 22–26. doi: 10.1016/j.bbrc.2021.08.066

Yan, Z., Zhou, Z., Wu, Q., Chen, Z. B., Koo, E. H., and Zhong, S. (2020). Presymptomatic increase of an extracellular RNA in blood plasma associates with the development of Alzheimer's disease. *Curr. Biol.* 30, 1771–1782.e3. doi: 10.1016/j.cub.2020.02.084

Yang, S. Y., Chiu, M. J., Chen, T. F., and Horng, H. E. (2017). Detection of plasma biomarkers using immunomagnetic reduction: A promising method for the early diagnosis of Alzheimer's disease. *Neurol. Ther.* 6, 37–56. doi: 10.1007/s40120-017-0075-7

Yang, S. Y., Liu, H. C., and Chen, W. P. (2020). Immunomagnetic reduction detects plasma Abeta1-42 levels as a potential dominant indicator predicting cognitive decline. *Neurol. Ther.* 9, 435–442. doi: 10.1007/s40120-020-00215-2

Yang, T. T., Liu, C. G., Gao, S. C., Zhang, Y., and Wang, P. C. (2018). The serum exosome derived microRNA-135a, -193b, and -384 Were potential Alzheimer's disease biomarkers. *Biomed. Environ. Sci.* 31, 87–96.

Yang, Z., and Wang, K. K. (2015). Glial fibrillary acidic protein: From intermediate filament assembly and gliosis to neurobiomarker. *Trends Neurosci.* 38, 364–374.doi: 10.1016/j.tins.2015.04.003

Yao, F., Hong, X., Li, S., Zhang, Y., Zhao, Q., Du, W., et al. (2018). Urine-based biomarkers for Alzheimer's disease identified through coupling computational and experimental methods. *J. Alzheimers Dis.* 65, 421–431. doi: 10.3233/JAD-180261

Yin, Q., Ji, X., Lv, R., Pei, J. J., Du, Y., Shen, C., et al. (2020). Targetting exosomes as a new biomarker and therapeutic approach for Alzheimer's disease. *Clin. Interv. Aging* 15, 195–205. doi: 10.2147/CIA.S240400

Yoo, Y. K., Lee, J., Kim, H., Hwang, K. S., Yoon, D. S., and Lee, J. H. (2018). Toward exosome-based neuronal diagnostic devices. *Micromachines* 9:634. doi: 10.3390/mi9120634

Youn, Y. C., Kang, S., Suh, J., Park, Y. H., Kang, M. J., Pyun, J. M., et al. (2019). Blood amyloid-beta oligomerization associated with neurodegeneration of Alzheimer's disease. *Alzheimers Res. Ther.* 11:40.doi: 10.1186/s13195-019-0499-7

Zetterberg, H., and Blennow, K. (2021). Moving fluid biomarkers for Alzheimer's disease from research tools to routine clinical diagnostics. *Mol. Neurodegener.* 16:10. doi: 10.1186/s13024-021-00430-x

Zetterberg, H., Hietala, M. A., Jonsson, M., Andreasen, N., Styrud, E., Karlsson, I., et al. (2006). Neurochemical aftermath of amateur boxing. *Arch. Neurol.* 63, 1277–1280. doi: 10.1001/archneur.63.9.1277

Zetterberg, H., Skillback, T., Mattsson, N., Trojanowski, J. Q., Portelius, E., Shaw, L. M., et al. (2016). Association of cerebrospinal fluid neurofilament light concentration with Alzheimer disease progression. *JAMA Neurol.* 73, 60–67. doi: 10.1001/jamaneurol.2015.3037

Zhang, A. H., Sharma, G., Undheim, E. A., Jia, X., and Mobli, M. J. N. L. (2018). A complicated complex: Ion channels, voltage sensing, cell membranes and peptide inhibitors. *Neurosci. Lett.* 679, 35–47. doi: 10.1016/j.neulet.2018.04.030

Zhang, Y., Li, Q., Liu, C., Gao, S., Ping, H., Wang, J., et al. (2016). MiR-214-3p attenuates cognition defects via the inhibition of autophagy in SAMP8 mouse model of sporadic Alzheimer's disease. *Neurotoxicology* 56, 139–149. doi: 10.1016/j.neuro.2016.07.004

Zhang, Y., Lu, C., and Zhang, J. (2021). Lactoferrin and its detection methods: A review. *Nutrients* 13:2492. doi: 10.3390/nu13082492

Zhou, Y., Zhang, Y., Gong, H., Luo, S., and Cui, Y. (2021). The role of exosomes and their applications in cancer. *Int. J. Mol. Sci.* 22:12204. doi: 10.3390/ijms222212204

Zhuang, J., Cai, P., Chen, Z., Yang, Q., Chen, X., Wang, X., et al. (2020). Long noncoding RNA MALAT1 and its target microRNA-125b are potential biomarkers for Alzheimer's disease management via interactions with FOXQ1, PTGS2 and CDK5. *Am. J. Transl. Res.* 12, 5940–5954.

Zou, K., Liu, J., Watanabe, A., Hiraga, S., Liu, S., Tanabe, C., et al. (2013). Aβ43 is the earliest-depositing Aβ species in APP transgenic mouse brain and is converted to Aβ41 by two active domains of ACE. *Am. J. Pathol.* 182, 2322–2331. doi: 10.1016/j.ajpath.2013.01.053

frontiers | Frontiers in Aging Neuroscience

TYPE Review
PUBLISHED 09 August 2022
DOI 10.3389/fnagi.2022.975248

Check for updates

OPEN ACCESS

EDITED BY
Shenfeng Qiu,
University of Arizona, United States

REVIEWED BY
Weinan Zhou,
University of Illinois at
Urbana-Champaign, United States
Jinyuan Ma,
Henry Ford Health System,
United States

*CORRESPONDENCE
Gang Li
ligang111666@163.com
Min Tang
mt3138@ujs.edu.cn

SPECIALTY SECTION
This article was submitted to
Cellular and Molecular Mechanisms of
Brain-aging,
a section of the journal
Frontiers in Aging Neuroscience

RECEIVED 22 June 2022
ACCEPTED 11 July 2022
PUBLISHED 09 August 2022

CITATION
Zhang H, Liu X, Liu Y, Liu J, Gong X, Li G and Tang M (2022) Crosstalk between regulatory non-coding RNAs and oxidative stress in Parkinson's disease. Front. Aging Neurosci. 14:975248. doi: 10.3389/fnagi.2022.975248

COPYRIGHT
© 2022 Zhang, Liu, Liu, Liu, Gong, Li and Tang. This is an open-access article distributed under the terms of the Creative Commons Attribution License (CC BY). The use, distribution or reproduction in other forums is permitted, provided the original author(s) and the copyright owner(s) are credited and that the original publication in this journal is cited, in accordance with accepted academic practice. No use, distribution or reproduction is permitted which does not comply with these terms.

Crosstalk between regulatory non-coding RNAs and oxidative stress in Parkinson's disease

Hantao Zhang[1], Xiaoyan Liu[1], Yi Liu[1,2], Junlin Liu[1], Xun Gong[3], Gang Li[4]* and Min Tang[1]*

[1]School of Life Sciences, Jiangsu University, Zhenjiang, China, [2]Institute of Animal Husbandry, Jiangsu Academy of Agricultural Sciences, Nanjing, China, [3]Department of Rheumatology & Immunology, Affiliated Hospital of Jiangsu University, Zhenjiang, China, [4]Department of Vascular Surgery, The Second Affiliated Hospital of Shandong First Medical University, Taian, China

Parkinson's disease is the second most common neurodegenerative disease after Alzheimer's disease, which imposes an ever-increasing burden on society. Many studies have indicated that oxidative stress may play an important role in Parkinson's disease through multiple processes related to dysfunction or loss of neurons. Besides, several subtypes of non-coding RNAs are found to be involved in this neurodegenerative disorder. However, the interplay between oxidative stress and regulatory non-coding RNAs in Parkinson's disease remains to be clarified. In this article, we comprehensively survey and overview the role of regulatory ncRNAs in combination with oxidative stress in Parkinson's disease. The interaction between them is also summarized. We aim to provide readers with a relatively novel insight into the pathogenesis of Parkinson's disease, which would contribute to the development of pre-clinical diagnosis and treatment.

KEYWORDS

Parkinson's disease, microRNAs, long non-coding RNAs, circular RNAs, oxidative stress

Introduction

Parkinson's disease (PD) is a common neurologic disease, which affected about 6.1 million people around the world in 2016 (Bloem et al., 2021). The elderly are more likely to suffer from this disease, with most cases occurring after the age of 50 (Opara et al., 2017). PD is mainly characterized by the loss of dopaminergic neurons and the presence of Lewy bodies in surviving neurons, while its exact cause is unknown (Antony et al., 2013; Raza et al., 2019; Li W. et al., 2020). The disease can be intolerable because it is a progressive disease and can severely damage the somatic motor system, making it difficult for PD patients to use their hands or walk normally (Schneider et al., 2017; Cerri et al.,

2019; Hayes, 2019). They may also exhibit multiple non-motor symptoms, including cognitive decline, depression, anxiety, and sleep disorders (Reich and Savitt, 2019). A number of studies illustrated that many types of RNA have been deeply involved in the whole disease progression even after onset, including but not limited to long non-coding RNAs (lncRNAs), microRNAs (miRNAs), and circularRNAs (circRNAs; Choi et al., 2018, Liu N. et al., 2020; Liu et al., 2021; Wu and Kuo, 2020; Wang W. et al., 2021). All of the three most well-known and most commonly studied RNAs belong to the regulatory non-coding RNAs (ncRNAs), a category of ncRNAs that are transcribed from DNA and not involved in coding proteins (Szymański and Barciszewski, 2002).

lncRNAs are a collective term for a group of highly heterogeneous regulatory ncRNAs (Hombach and Kretz, 2016). The common characteristics of lncRNA mainly include transcripts longer than 200 and a lack of ability to encode proteins (Yang et al., 2021). Given their wide variety, their biological roles can be quite diverse. An important function of lncRNA is to regulate gene expression at the transcriptional, post-transcriptional, and epigenetic levels (Panni et al., 2020). lncRNAs can bind certain RNAs and proteins to prevent them from interacting with other molecules (Wang, 2018). They can also affect epigenetic modifications of genes and histones. In addition, several lncRNAs have been found to have a role in the maintenance of chromosome stability and the regulation of the cell cycle (Lee et al., 2016; Munschauer et al., 2018; Wang R. et al., 2018; Zhang et al., 2018).

miRNAs, small RNA molecules with an average length of 22 nt, must be the most extensively studied and best understood small non-coding RNAs (sncRNAs; Zhang P. et al., 2019). The major function of miRNAs is to control mRNA translation, which is usually based on the complementary base pairing between seed regions of miRNAs and 3' untranslated regions of mRNAs (Wei J. W. et al., 2017). The miRNA first incorporates Argonaute proteins to form an RNA-induced silencing complex (RISC; Scott and Ono, 2011). Then, if miRNAs show imperfect complementarity to their target mRNAs, which is usually the case in animals, deadenylation of the mRNA will occur, leading to translation inhibition (Carvalho Barbosa et al., 2020). Furthermore, a small number of miRNAs can upregulate gene expression, though this process is fairly rare (Gerin et al., 2010).

circRNAs, a unique group of regulatory ncRNAs, are characterized by their covalently closed structures (Zhou W. Y. et al., 2020). Due to a lack of capping and polyadenylation, circRNAs are resistant to RNA exonucleases and more stable than linear RNAs (Huang et al., 2020). The size of circRNA range from 100 nt to over 4 kb, so it might belong to lncRNA and sncRNA at the same time (Zhang P. et al., 2019). Increasing evidence has demonstrated that a subset of circRNAs exerts their functions by functioning as competing endogenous RNA (ceRNA) or miRNA sponges (Cao et al., 2020; Jiang Q. et al., 2020; Li L. et al., 2020; Peng et al., 2021). miRNAs captured by circRNAsare unable to regulate gene expression (Jin et al., 2020). In addition, several circRNAs can act as protein decoys. Through the interaction with these circRNAs, the biological functions of a variety of proteins can be changed (Altesha et al., 2019).

In addition to the aforementioned regulatory ncRNAs, oxidative stress is believed to have a notable effect on the pathological progression of PD (Wang X. et al., 2020). It results from an imbalance between oxidant production and antioxidative defenses (Forman and Zhang, 2021). The oxidant refers to reactive oxygen species (ROS) and reactive nitrogen species (RNS), which are mainly produced in mitochondria (Turrens, 2003). ROS includes superoxide ($O_2^{\bullet -}$), hydrogen peroxide (H_2O_2), hydroxyl radical (•OH), ozone, and singlet oxygen. These small molecules are all derived from the reaction of oxygen with electrons (Brieger et al., 2012). The primary intermediate in the biosynthesis of RNS is nitric oxide (NO; Lushchak and Lushchak, 2021). NO reacts with ROS, thereby giving rise to other forms of RNS such as peroxynitrite and peroxynitrous acid (ONOOH; Tharmalingam et al., 2017). Disruption of the ATP production function of mitochondria as well as inflammation may cause an increase in oxidant production (Brand and Nicholls, 2011; Islam, 2017). In response to ROS and RON, organisms have evolved antioxidant defense systems. Such antioxidant defenses are largely provided by antioxidant enzymes, including superoxide dismutase (SOD), catalase (CAT), and glutathione peroxidase (GPx; Prasad et al., 2017). By catalyzing specific reactions, these enzymes can scavenge oxidants and repair oxidative damage. Excessive oxidant production combined with decreased expression and activity of antioxidant enzymes will induce oxidative stress, which can greatly impair cell viability (Nunomura et al., 2012; Chen and Zhong, 2014).

It is undeniable that a lot of research has been conducted on the role of regulatory ncRNAs or oxidative stress in PD (Lu et al., 2017, 2019; Pavlou and Outeiro, 2017; Cao et al., 2019; Nies et al., 2021; Zhu et al., 2021). However, the interaction between the minPD has not been well studied. It is worth noting that both regulatory ncRNAs and oxidative stress are closely involved in neurodegenerative disorders (Nunomura and Perry, 2020). On the one hand, oxidative stress can cause damage to nucleic acids and affect the expression levels of varieties of regulatory ncRNAs (Radi et al., 2014). On the other hand, several regulatory ncRNAs have the potential to regulate oxidative stress-related pathways, which represent promising therapeutic targets (Geng et al., 2017; Song et al., 2019; Li Y. et al., 2020; Li et al., 2021). Hence, further research on this molecular mechanism in PD may be beneficial to our understanding of the neurodegenerative disorder in conjunction with the development of novel strategies for pre-clinical diagnosis and therapeutic intervention.

How do the ncRNAs regulate Parkinson's disease?

Once it was thought that ncRNAs did not have any biological function. Only recently has it been discovered that the roles of RNAs are not limited to bridging genes and proteins (Carvalho Barbosa et al., 2020). The last decade has witnessed the discovery and annotation of thousands of both housekeeping and regulatory ncRNAs, which are emerging as key regulators of gene expression at the transcriptional or post-transcriptional level (Li et al., 2015; Merry et al., 2015; Yildirim et al., 2020; Rezaei et al., 2021). Several subtypes of regulatory ncRNAs, including miRNAs, lncRNAs, and circRNAs, are involved in the pathogenesis of PD (Majidinia et al., 2016). The PD models used and the regulatory ncRNAs identified are shown in **Table 1**.

Effects of miRNAs in Parkinson's disease

PD is characterized by the loss of dopaminergic neurons (DAs) in the substantia nigra (Goh et al., 2019). Convincing evidence indicated that neuroinflammation was involved in DA death (Gordon et al., 2018; Rodriguez-Perez et al., 2018). Activated microglia may initiate the inflammatory process in the central nervous system (CNS). The upregulation of microRNA-132-3p (miR-132-3p) and microRNA-873 (miR-873) in PD led to the deficiency of ATP-binding cassette transporter A1 (ABCA1) and GLRX, which may give rise to the activation of microglial cells and subsequent neuronal death (Wu et al., 2020; Gong et al., 2022). microRNA-29b2/c (miR-29b2/c) and microRNA-124 (miR-124) played contrasting roles in microglia activation. Knockout of miR-29b2/c would inhibit microglia activation, whereas decreased expression of miR-124 correlated with the progression of microglia activation (Yao et al., 2018; Bai et al., 2021). Feng et al. found that activated microglia can be transformed into two different phenotypes, i.e., M1 polarization and M2 polarization. M1 microglia could produce proinflammatory cytokines to maintain the homeostasis of the central nervous system. However, this process may be prolonged by microRNA-330 (miR-330), which in turn caused inflammatory damage to neuronal cells (Feng et al., 2021). TNF-α was a proinflammatory factor released by M1 polarization, whose production was downregulated by micro-RNA-7116-5p (miR-7116-5p; He et al., 2017). Nod-like receptor protein 3 (Nlrp3) functioned in regulating proinflammatory cytokines. Both microRNA-30e (miR-30e) and microRNA-190 (miR-190) targeted the 3' UTR of Nlrp3 mRNA and thus inhibited neuroinflammation (Li D. et al., 2018; Sun et al., 2019). Furthermore, Specific protein-1 (SP1), nuclear factor of activated T cells 5 (NFAT5), Rho-associated kinase 1 (ROCK1), and transcriptional activator 3 (STAT3) participated in regulating neuroinflammation. By suppressing the expression of SP1, NFAT5, ROCK1, and STAT3, microRNA-29c (miR-29c), microRNA-195 (miR-195), microRNA-93 (miR-93), and microRNA-let-7a (miR-let-7a) may reduce neuronal damage caused by inflammatory responses (Ren et al., 2019; Zhang J. et al., 2019; Wang et al., 2020a,b; Wang X. et al., 2021).

Another hallmark of PD is the formation of Lewy bodies in neurons (Singh and Sen, 2017). The main component of Lewy bodies was α-synuclein fibrils (α-syn) toxic to DA neurons. Apoptosis was induced when the formation of α-syn aggregates exceeded the limit of what the cell can tolerate, suggesting α-syn is an essential player in the PD neurodegenerative process (Rocha et al., 2018). miRNA-7 (miR-7) was found to not only inhibit α-syn expression by interacting with its messenger RNA (mRNA) but also help remove α-syn by promoting autophagy (Choi et al., 2018). As McMillan et al. stated in their study, miR-7 may promote autophagy by suppressing the expression of epidermal growth factor receptor (EGFR), since the activated EGFR was able to inhibit autophagy. Then, α-syn can be degraded by autophagy (McMillan et al., 2017). In addition to promoting α-syn degradation, researchers found that two RNAs affected the toxicity of α-syn. Both phosphorylation and acetylation were essential mechanisms regulating the neurotoxicity of α-syn. Su et al. discovered that miRNA-26a (miR-26a) directly downregulated the expression level of death-associated protein kinase 1 (DAPK1), and DAPK1 was capable of promoting the phosphorylation of α-syn (Su et al., 2019). Also, sirtuin 2 (SIRT2) was identified to catalyze the deacetylation reaction of α-syn, and miRNA-486-3p (miR-486-3p) may affect the toxicity of α-syn by regulating the expression of SIRT2 (Wang Y. et al., 2018).

Accumulating evidence suggested that autophagy participated in the pathogenesis of PD. Autophagy dysregulation can impair many subcellular functions, including α-syn degradation (Lu J. et al., 2020). Based on the findings of Zhao et al., UNC51-like kinase (ULK1), a serine/threonine kinase responsible for promoting cell autophagy, was positively regulated by miRNA-132-5p (miR-132-5p; Zhao et al., 2020a). In addition, both miRNA-181b and miRNA-199a were able to mediate autophagy by targeting the PTEN/Akt/mTOR pathway. The downregulation of miRNA-181b in PD inhibited the Akt/mTOR signaling pathway, thereby improving autophagy (Li W. et al., 2018). Similarly, the downregulation of miRNA-199a in PD enhanced autophagy by regulating the activity of mTOR (Ba et al., 2020). Mitophagy is a form of autophagy in which cells remove damaged mitochondria to maintain cellular homeostasis. It has been reported that the accumulation of dysfunctional mitochondria would lead to the death of DA neurons (John et al., 2020). According to the research conducted by Zhou et al., miRNA-103a-3p (miR-103a-3p) was able to regulate mitophagy by mediating Parkin at the post-transcriptional level. Since Parkin is an E3 ubiquitin ligase that function in promoting the removal of damaged mitochondria *via* mitophagy, the upregulated level of miR-

TABLE 1 Summary of regulatory non-coding RNAs that regulate Parkinson's disease.

Model/ Cell Type	Name	Target	Potential Role	References
Human pluripotent H9 cells and neural progenitor ReNcell VM cells, HEK293T cells, C57BL/6J mice	miRNA-7 ↓	SNCA	Suppressed α-synuclein expression	(McMillan et al., 2017; Choi et al., 2018; Adusumilli et al., 2020)
C57BL/6 mice	miRNA-26a ↓	DAPK1	Alleviated DA neuron loss	(Su et al., 2019)
A mouse model of PD	miRNA-29b2/c ↓	AMPK	Promoted neuroinflammation	(Bai et al., 2021)
SH-SY5Y cells, C57BL/6 mice	miRNA-29c ↓	SP1, NFAT5	Attenuated the neuroinflammation and apoptosis of PD	(Wang X. et al., 2020)
C57BL/6 mice	miRNA-30a-5p ↑	PKCα	Downregulated GLT-1 and caused glutamate excitotoxicity	(Meng X. et al., 2021)
Human neuroblastoma SH-SY5Y cells	miRNA-30b ↓	SNCA	Inhibited MPP+-induced neuronal apoptosis	(Shen et al., 2020)
C57BL/6 mice	miRNA-30e ↓	Nlrp3	Attenuated neuroinflammation	(Li D. et al., 2018)
BV-2 and HEK-293T cells, C57BL/6J mice	miRNA-93 ↓	STAT3	Reduced neuronal injuries and suppressed inflammatory reaction	(Wang X. et al., 2021)
C57BL/6J mice	miRNA-103a-3p ↑	Parkin	Prevented mitophagy	(Zhou J. et al., 2020)
C57BL/6 mice	miRNA-124 ↓	MEKK3, EDN2	Inhibited neuroinflammation and suppressed neuronal apoptosis	(Yao et al., 2018; Wang J. et al., 2019)
C57BL/6 mice	miRNA-128 ↓	AXIN1	Reduced DA neuron apoptosis	(Zhou et al., 2018)
Human SH-SY5Y cells, a mouse model of PD	miRNA-132 ↑	SIRT1	Induced apoptosis	(Qazi et al., 2021)
PD patients, C57BL/6J mice, BV-2 microglial cells	miRNA-132-3p ↑	GLRX	Aggravated neuroinflammation	(Gong et al., 2022)
C57BL/6 mice	miRNA-132-5p ↑	ULK1	Induced autophagy	(Zhao et al., 2020a)
PC-12 rat adrenal pheochromocytoma cells	miRNA-133a ↓	RAC1	Inhibited cell apoptosis and autophagy	(Lu W. et al., 2020)
PC-12 cells	miRNA-133b ↓	ERK1/2	Inhibited nerve cell apoptosis	(Dong et al., 2020)
Human neuroblastoma SK-N-SH cells	miRNA-181a ↓	p38, JNK	Inhibited apoptosis and autophagy	(Liu Y. et al., 2017)
PC-12 cells	miRNA-181b ↓	PTEN	Inhibited autophagy and promoted cell viability	(Li W. et al., 2018)
PC-12 cells	miRNA-181c ↓	BCL2L11	Inhibited cell apoptosis and promoted cell viability	(Wei M. et al., 2017)
C57BL/6 mice	miRNA-183 ↑	OSMR	Promoted the apoptosis of substantia nigra neurons	(Gao et al., 2019)

(Continued)

10.3389/fnagi.2022.975248

TABLE 1 Continued

Model/ Cell Type	Name	Target	Potential Role	References
Human neuroblastoma SH-SY5Y cells	miRNA-185 ↓	AMPK, mTOR	Inhibited autophagy and apoptosis of dopaminergic cells	(Wen et al., 2018)
BV2, HEK293, and SH-SY5Y cells, C57BL/6J mice	miRNA-190 ↓	Nlrp3	Alleviated neuronal damage and inhibited inflammation	(Sun et al., 2019)
BV2 microglial cells	miRNA-195 ↓	ROCK1	Inhibited neuroinflammation	(Ren et al., 2019)
MPP+-induced mouse model of PD	miRNA-199a ↓	GSK3β	Reduced autophagy and alleviated PD-related phenotypes	(Ba et al., 2020)
Humandopaminergic neuroblastoma SH-SY5Y cells	miRNA-216a ↑	Bax	Reduced MPP+-induced neuronal apoptosis	(Yang et al., 2020)
Ratadrenal pheochromocytoma PC-12cells	miRNA-221 ↓	PTEN	Promoted cell proliferation and inhibited cell apoptosis	(Li L. et al., 2018)
C57BL/6 mice	miRNA-330 ↑	SHIP1	Suppressed chronic neuroinflammation	(Feng et al., 2021)
SH-SY5Y cells, C57BL/6 mice	miRNA-384-5p ↑	SIRT1	Promoted the progression of PD	(Tao et al., 2020)
Mouse embryonic substantial nigra–derived SN4741 cells	miRNA-421 ↑	MEF2D	Promoted DA neuron death	(Dong et al., 2021)
HEK293T, SH-SY5Y, and U87 cells	miRNA-486-3p ↓	SIRT2	Reduced α-Syn aggregation and suppressed α-Syn	(Wang Y. et al., 2018)
C57BL/6 mice	miRNA-543-3p ↑	Slc1a2	Down-regulated GLT-1 and caused glutamate excitotoxicity	(Wu X. et al., 2019)
C57BL/6 mice	miRNA-599 ↓	LRRK2	Suppressed cell apoptosis	(Wu Q. et al., 2019)
A mouse model of PD	miRNA-873 ↑	A20	Aggravated neuroinflammation	(Wu et al., 2020)
C57BL/6 mice	miRNA-7116-5p ↓	TNF-α	Prevented loss of DA neurons	(He et al., 2017)
BV2 microglial cells, C57BL/ 6 mice	miRNA-let-7a ↓	STAT3	Inhibited microglial activation and inflammation	(Zhang J. et al., 2019)
MN9D cells	miRNA-let-7d ↓	Caspase-3	Enhanced cell viability and inhibited cell apoptosis	(Li et al., 2017)
Human dopaminergic neuronal SH-SY5Y cells, a mouse model of PD	BDNF-AS ↑	miRNA-125b-5p	Inhibited cell apoptosis and autophagy	(Fan Y. et al., 2020)
BV2 microglia cells, C57BL/ 6 mice	GAS5 ↑	miRNA-223-3p, miRNA-150	Promoted the release of inflammatory cytokines and contributed to the neuron loss	(Xu et al., 2020; Ma et al., 2022)
N27 dopaminergic neurons, C57BL/6 mice	H19 ↓	miRNA-301b-3p, miRNA-585-3p	Protected against dopaminergic neuron loss	(Jiang J. et al., 2020)

(Continued)

10.3389/fnagi.2022.975248

TABLE 1 Continued

Model/ Cell Type	Name	Target	Potential Role	References
Human neuroblastoma SH-SY5Y cells, C57BL/6 mice	HOTAIR ↑	miRNA-126-5p	Induced cell apoptosis	(Wang et al., 2017; Lin et al., 2019)
Dopaminergic neuron SH-SY5Ycells and BV2 microglial cells, C57BL/6 mice	HOXA11-AS ↑	miRNA-124-3p	Induced neuroinflammation	(Cao et al., 2021)
Human neuroblastoma SK-N-SH cells, C57BL/6 mice	LINC-00943 ↑	miRNA-7-5p	Regulated the apoptosis and inflammation of nerve cells	(Meng C. et al., 2021; Sun et al., 2022)
Human neuroblastoma SH-SY5Y cells, C57BL/6 mice	LincRNA-p21 ↑	miRNA-1277-5p	Inhibited viability and promoted apoptosis of cells	(Xu et al., 2018)
Human neuroblastoma SK-N-SH, SK-N-BE, and SH-SY5Y cells, human embryonic kidneyHEK293 cells, MN9D dopaminergic neuronal cells, C57BL/6 mice	MALAT1 ↑	miRNA-135b-5p, miRNA-124, miRNA-205-5p	Promoted cell apoptosis	(Liu W. et al., 2017; Chen Q. et al., 2018; Lv et al., 2021)
BALB/c mice	MIAT ↓	miRNA-34-5p	Exerted neuroprotective effects in PD	(Shen et al., 2021a)
Human neuroblastoma SH-SY5Y, SK-N-SH, and SK-N-AS cells, embryonic kidney epithelialHEK293T cells, C57BL/6 mice	NEAT1 ↑	miRNA-124, miRNA-212-5p, miRNA-1301-3p, miRNA-519a-3p, miRNA-213-3p	Promoted inflammatory response and neuronal apoptosis	(Yan et al., 2018; Xie S. P. et al., 2019; Liu R. et al., 2020, Liu et al., 2021; Chen M. Y. et al., 2021)
SH-SY5Y cells	OIP5-AS1 ↓	miRNA-137	Promoted mitochondrial autophagy, reduced the level and toxicity of α-syn	(Song and Xie, 2021; Zhao et al., 2022)
Human neuroblastoma SK-N-SH, SK-N-AS cells, SH-SY5Y cells, MN9Ddopaminergic neurons, C57BL/6 mice	SNHG1 ↑	miRNA-7, miRNA-15b-5p, miRNA-181a-5p, miRNA-221/222, miRNA-216-3p	Affected neuroinflammation, autophagy, and apoptosis in PD	(Cao et al., 2018; Chen Y. et al., 2018; Qian et al., 2019; Wang C. et al., 2021; Wang et al., 2021a,b)
C57BL/6 mice	SNHG14 ↑	miRNA-214-3p	Exacerbated damage to DA neurons, accelerated the progression of PD	(Zhang L. M. et al., 2019; Zhou S. et al., 2020)
SH-SY5Ycells, C57BL/6 mice	UCA1 ↑	miRNA-423-5p	Promoted α-Syn accumulation	(Lu et al., 2018)
Human neuroblastoma SH-SY5Y cells and rat adrenal pheochromocytoma PC-12 cells	XIST ↑	miRNA-199a-3p	Contributed to the apoptosis of DA neurons	(Zhou Q. et al., 2021)
Human neuroblastomaSH-SY5Y cellsand mice dopaminergic neuronal MN9D cells, C57BL/6 mice	circDLGAP4 ↓	miRNA-134-5p	Induced apoptosis and enhanced autophagy	(Feng et al., 2020)
SH-SY5Yneuroblastoma cells and BV-2 microglial cells, C57BL/6 mice	circSAMD4A ↑	miRNA-29c-3p	Affected the apoptosis and autophagy of DAs	(Wang W. et al., 2021)

The upward arrows indicate that the levels of non-coding RNAs are significantly higher in PD patients than in [illegible] iduals and vice versa.

10.3389/fnagi.2022.975248

103a-3p in PD may harm the nervous system (Zhou J. et al., 2020).

In addition to autophagy dysregulation, dysregulated apoptosis had a crucial role in the pathogenesis of PD (Li D. et al., 2020). Although apoptosis was necessary for building neural networks, excessive apoptosis would accelerate the progression of PD (Liu et al., 2019). Three miRNAs were found to downregulate neuroprotective factors, including miRNA-183 (miR-183), miRNA-384-5p (miR-384-5p), and miRNA-421 (miR-421; Gao et al., 2019; Tao et al., 2020; Dong et al., 2021). Conversely, several miRNAs were able to inhibit neuronal apoptosis and therefore played a protective role in PD. Increasing evidence has shown that SNCA, Bcl-2-like protein 11 (BCL2L11), Ras-related C3 botulinum toxin substrate 1 (RAC1), Bax, caspase-3, and p53 were apoptotic activators. Their overexpression can be attenuated by microRNA-30b (miR-30b), microRNA-181c (miR-181c), microRNA-133a (miR-133a), microRNA-216a (miR-216a), let-7d, and microRNA-132 (miR-132), respectively (Li et al., 2017; Wei M. et al., 2017; Lu W. et al., 2020; Shen et al., 2020; Yang et al., 2020; Qazi et al., 2021). However, this effect may be diminished due to the downregulation of these six miRNAs in PD. p38 MAPK pathway has been proven to be important in regulating cell apoptosis. microRNA-599 (miR-599) and microRNA-181a (miR-181a) functioned in inactivating the p38 MAPK pathway, thereby protecting neurons (Liu Y. et al., 2017; Wu Q. et al., 2019). In addition, the activation of ERK1/2 and AMPK/mTOR pathways were essential to cell proliferation, which could be suppressed by microRNA-133b (miR-133b) and microRNA-185 (miR-185; Wen et al., 2018; Dong et al., 2020). miR-7 and microRNA-128 (miR-128) regulated the Wnt/beta-catenin signaling pathway differently. miR-7 suppressed the proliferation of DAs by inhibiting Wnt/beta-catenin pathway, whereas microRNA-128 (miR-128) alleviated the inhibiting effect of axis inhibition protein 1 (AXIN1) on this pathway and blocked DA apoptosis (Zhou et al., 2018; Adusumilli et al., 2020). microRNA-221 (miR-221) and miR-124 could extend cell lifespan *via* indirect regulation of PI3K/Akt and Hedgehog pathways (Li L. et al., 2018; Wang J. et al., 2019).

In recent years, the neuropathological consequences of dysregulated glutamate homeostasis have been recognized, and glutamate excitotoxicity has been associated with PD. Glutamate is an essential neurotransmitter in the mammalian central nervous system, responsible for transmitting excitatory signals between neurons. The amount of glutamate at the synapse above the physiological range was toxic and could have a detrimental effect on neuron cells, which was termed glutamate excitotoxicity (Iovino et al., 2020). Glutamate transporter-1 (GLT-1) was responsible for clearing excess glutamate from the synaptic gap to maintain glutamate homeostasis. It was found that GLT-1 mRNA was directly targeted by miRNA-543-3p (miR-543-3p). The overexpression of miR-543-3p in PD was able to suppress the expression and function of GLT-1 protein (Wu X. et al., 2019). miRNA-30a-5p (miR-30a-5p) was also upregulated in a mouse model of PD, while the regulatory mechanism of PKCα by miR-30a-5p needs further research. Meng et al. revealed that once PKCα was activated, it could induce ubiquitination and subsequent degradation of GLT-1 (Meng X. et al., 2021). Hence, both miR-543-3p and miR-30a-5p contributed to the pathology of PD by reducing the level of GLT-1, making them promising targets for treatment.

Briefly, numerous studies have validated those miRNAs were capable of regulating recognized causative factors of PD such as neuronal cell damage, microglia activation, and α-syn production, and chemical modifications by repressing the expression of target genes. The lncRNA can also influence the progress of this disease, however, it does not do so in the same way as the miRNA.

Effects of lncRNAs in Parkinson's disease

The progression of PD is normally accompanied by apoptosis and inflammation of nerve cells (Bhattacharyya et al., 2021). Two lncRNAs, namely nuclear-enriched abundant transcript 1 (NEAT1) and SNHG gene 14 (SNHG14), were identified to accelerate this progression (Zhou S. et al., 2020; Liu et al., 2021). The main hallmark of PD is the loss of dopaminergic neurons (DAs) in the substantia nigra, which correlates with typical PD symptoms including resting tremors and bradykinesia (Xin and Liu, 2021). SNHG14 reduced the number of DAsby sponging miR-133b, whereas H19 exerted a protective role against DAneuron damage (Zhang L. M. et al., 2019; Jiang J. et al., 2020). This protection was based on the overexpression of hypoxanthine-guanine phosphoribosyltransferase (HPRT), which was prompted by H19 sponging microRNA-301b-3p (miR-301b-3p; Jiang J. et al., 2020).

In PD, the main form of DA neuron death is apoptosis. Abnormalities in apoptosis are a sign of the loss of DAs in the substantia nigra, which have a notable effect on the development of PD. Zhang et al. found that microRNA-583-3p (miR-583-3p) downregulated the expression of PIK3R3. lncRNA H19 could attenuate the apoptosis of neurons by interacting with miR-583-3p (Zhang Y. et al., 2020). lncRNA myocardial infarction-associated transcript (MIAT) also exerted a neuroprotective role in PD. Shen et al. revealed that MIAT regulated synaptotagmin-1 (SYT1) by binding to microRNA-34-5p (miR-34-5p), which enhanced cell viability and inhibited apoptosis (Shen et al., 2021a). In contrast, growth arrest-specific 5 (GAS5) may cause loss of neuronal cells. The underlying mechanism was that GAS5 negatively regulated microRNA-150 (miR-150) and positively regulated fos-like antigen-1 (Fosl1), which resulted in cell apoptosis (Ma et al., 2022). In addition, a number of evidence indicated that LINC00943, long intergenic noncoding RNA-p21 (lincRNA-

p21), NEAT1, and small molecule RNA host gene 1 (SNHG1) acted as molecular sponges of microRNA-338-3p (miR-338-3p), microRNA-1277-5p (miR-1277-5p), miR-124, microRNA-1301-3p (miR-1301-3p), and microRNA-216-3p (miR-216-3p), thereby inhibiting cell viability (Xu et al., 2018, Liu J. et al., 2020; Meng C. et al., 2021; Wang et al., 2021b). LRRK2 gene has been acknowledged to be associated with PD. Researchers found that Hox transcript antisense intergenic RNA (HOTAIR), X-inactive specific transcript (XIST), and metastasis-associated lung adenocarcinoma transcript 1 (MALAT1) indirectly enhanced the expression of LRRK2, which would increase the rate of apoptosis (Wang et al., 2017; Chen Q. et al., 2018; Zhou Q. et al., 2021). HOTAIR may also promote apoptosis of neuronal cells through microRNA-126-5p (miR-126-5p)/RAB3A-interacting protein (RAB3IP) axis (Lin et al., 2019). Furthermore, MALAT1 contributed to the apoptosis of DAs by combining with miR-124 and microRNA-135-5p (miR-135-5p; Liu W. et al., 2017; Lv et al., 2021).

Neuroinflammation is believed to play important role in the development of PD. Multiple proinflammatory cytokines released by activated microglia are involved in neuroinflammatory responses, which would eventually induce apoptosis of DA neurons (Xin and Liu, 2021). Cao et al. revealed that lncRNA HOXA11-AS activated microglia and promoted neuroinflammation *via* regulating miR-124-3p/NF-κB axis (Cao et al., 2021). Besides, lncRNA nuclear enriched abundant transcript 1 (NEAT1) acted as sponges of miR-124, microRNA-212-5p (miR-212-5p), and microRNA-519a-3p, thereby increasing the expression of phosphodiesterase 4B (PDE4B), RAB3A-interacting protein (RAB3IP), and specific protein 1 (SP1; Xie S. P. et al., 2019; Liu R. et al., 2020; Chen M. Y. et al., 2021). Since PDE4B, RAB3IP, and SP1were shown to facilitate cell inflammation, the knockdown of NEAT1 could be a potential strategy for treating PD patients. Based on the study of Sun et al., LINC00943 also positively regulated SP1 expression, making it a possible therapeutic target in PD (Sun et al., 2022). Small molecule RNA host gene 1 (SNHG1) was found to prevent microRNA-181a-5p (miR-181a-5p) from suppressing C-X-C motif chemokine 12 (CXCL12). This may trigger inflammatory responses (Wang et al., 2021a). In addition, SNHG1 as well as growth arrest-specific 5 (GAS5) had a promotion effect on the expression of an inflammasome named nod-like receptor protein 3 (NLRP3), which would stimulate the secretion of inflammatory factors (Cao et al., 2018; Xu et al., 2020).

Abnormal aggregation of α-syn also causes damage to DA neurons. Liu et al. discovered that the expression of nuclear-enriched abundant transcript (NEAT) was positively correlated with the α-syn expression, suggesting that the knockdown of NEAT may protect neurons (Liu and Lu, 2018). Both UCA1 and small nucleolar RNA host gene 1 (SNHG1) were able to promote the accumulation of α-syn. Based on the study of Lu et al., UCA1 could upregulate the expression of SCNA (Lu et al., 2018). In addition, Chen et al. found that the inhibitory effect of microRNA-15b-5p (miR-15b-5p) on the expression of seven in absentia homolog 1 (SIAH1) could be reversed by SNHG1. The overexpression of SIAH1 would induce the aggregation of α-syn and elevate its toxicity (Chen Y. et al., 2018).

Autophagy is responsible for the degradation of α-syn. The dysregulation of this process is an important contributor to the development of PD (Xin and Liu, 2021). Yan et al. revealed that lncRNA nuclear paraspeckle assembly transcript 1 (NEAT1) might promote autophagy in PD by stabilizing PTEN-induced kinase 1 (PINK1; Yan et al., 2018). Brain-derived neurotrophic factor anti-sense (BDNF-AS) was also able to promote autophagy. According to the study by Fan et al., BDNF-AS enhanced the number of autophagosomes by regulating microRNA-125b-5p (miR-125b-5p) negatively (Fan Y. et al., 2020). In contrast, SNHG1 was found to increase the expression level of p27 *via* sponging microRNA-221/222 (miR-221/222). Since p27 was believed to have a role in inhibiting autophagy, the downregulation of SNHG1 may promote autophagic activation (Qian et al., 2019). PLK2 was associated with a pathway that induced α-syn degradation *via* autophagy. microRNA-126 (miR-126) suppressed the expression of p27, which could be blocked by Opa interacting protein five antisense RNA 1 (OIP5-AS1). Hence, OIP5-AS1 exerted a protective role in PD by accelerating the clearance of α-syn (Song and Xie, 2021). Based on the findings of Zhao et al., OIP5-AS1 also had a role in promoting mitochondrial autophagy, a process that selectively removes unwanted or damaged mitochondria. Specifically, the expression of NIX was down-regulated by microRNA-137 (miR-137), which was reversed by OIP5-AS1. Overexpression of NIX was proved to promote mitochondrial autophagy, which would prevent neuronal death (Zhao et al., 2022). For further review on targeting α-syn as a therapy for PD, please refer to Taylor et al. (2002), Wong and Cuervo (2010), Vidal et al. (2014), Martire et al. (2015), Pickrell and Youle (2015), Dunn et al. (2019), and Fields et al. (2019).

To sum up, lncRNAs have been shown to affect apoptosis and autophagy of neurons, the accumulation and degradation of α-syn, and neuronal inflammation. The regulatory roles they play in PD are largely accomplished by sponging miRNAs.

The *in vitro* and *in vivo* experiments have indicated the feasibility of treating PD by targeting miRNAs and lncRNAs. These regulatory ncRNAs may serve as targets in PD treatment, while the effectiveness and safety of this therapy have yet to be tested in human trials. Other regulatory ncRNAs, such as circRNAs, may sponge specific miRNAs, thus contributing to the development of PD (Lu et al., 2019; Feng et al., 2020; Wang W. et al., 2021). Further research is needed to unravel the role of a wider class of regulatory ncRNAs in PD progression, which would not only further our understanding but also lead to the development of novel and effective therapeutic strategies (Acharya et al., 2020).

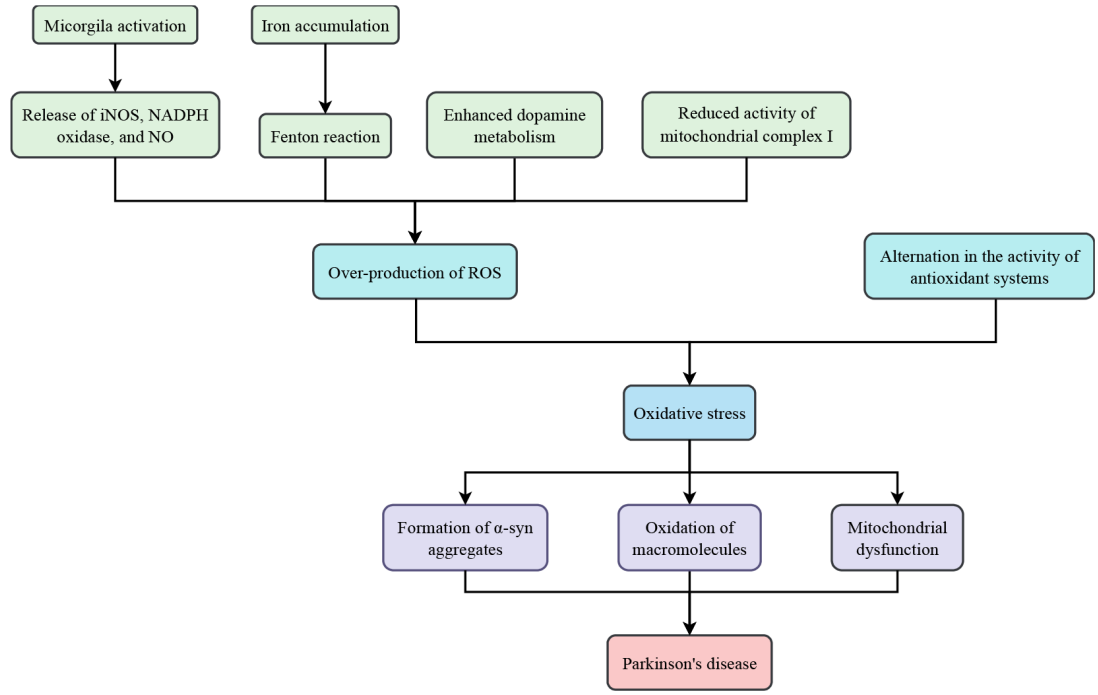

FIGURE 1
Oxidative stress in Parkinson's disease.

Toxicological effects of oxidative stress in Parkinson's disease

ROS generated in the body perform physiologic functions such as stimulating growth factors, promoting inflammatory responses, and regulating cell production. However, when their levels far exceed that of antioxidants, human cells will be subjected to devastating effects (Surendran and Rajasankar, 2010; Zuo and Motherwell, 2013; Hemmati-Dinarvand et al., 2019). Neurons are likely to be attacked by oxidative stress since they consume large amounts of oxygen and possess relatively modest levels of antioxidant enzymes. Accumulating evidence has demonstrated that oxidative stress is an important factor in the etiology and progression of PD (**Figure 1**; Percario et al., 2020).

Oxidative stress

Mitochondrial dysfunction was found in the substantia nigra (SN) in some patients with PD. Although the mechanism by which mitochondrial depletion causes oxidative stress and bioenergetic deficiency is not fully understood, researchers have correlated the impairment or inhibition of mitochondrial complex I with elevated levels of ROS (Schapira et al., 1990a,b,c). Complex I (NADH-ubiquinone oxidoreductase) is a major component of the oxidative phosphorylation system responsible for converting molecular oxygen into water and driving energy synthesis (Hauser and Hastings, 2013). Reduced activity of complex I may lead to disruption of electron transfer, which would result in excessive ROS production (**Figure 2**; Sarkar et al., 2016).

Mitochondrial-related energy failure may also disrupt the vesicular storage of DA (Puspita et al., 2017). Under normal circumstances, dopamine was preserved in synaptic vesicles, which were an acidic and stable environment that protected dopamine from oxidation (Jin et al., 2014). In the SN of PD patients, however, a rise in the amount of free dopamine in the cytoplasm has been observed (Sackner-Bernstein, 2021). Monoamine oxidases (MAO) functioned in catalyzing the transition from cytosolic dopamine to $H_2O_2$and 3,4-dihydroxyphenylacetaldehyde (DOPAL; Raza et al., 2019; Zaman et al., 2021). In addition, dopamine may undergo auto-oxidation to form DA quinones (Janda et al., 2012; Smeyne and Smeyne, 2013). H_2O_2 was a by-product of both of these reactions, which could be further transformed into •OH *via* the Fenton reaction (Vallee et al., 2020). This reaction was largely dependent on the presence of iron, which was also identified to be elevated in the PD SN (Vallée et al., 2021a). Therefore, enhanced dopamine metabolism in combination with iron accumulation may contribute to cellular ROS in dopaminergic neurons.

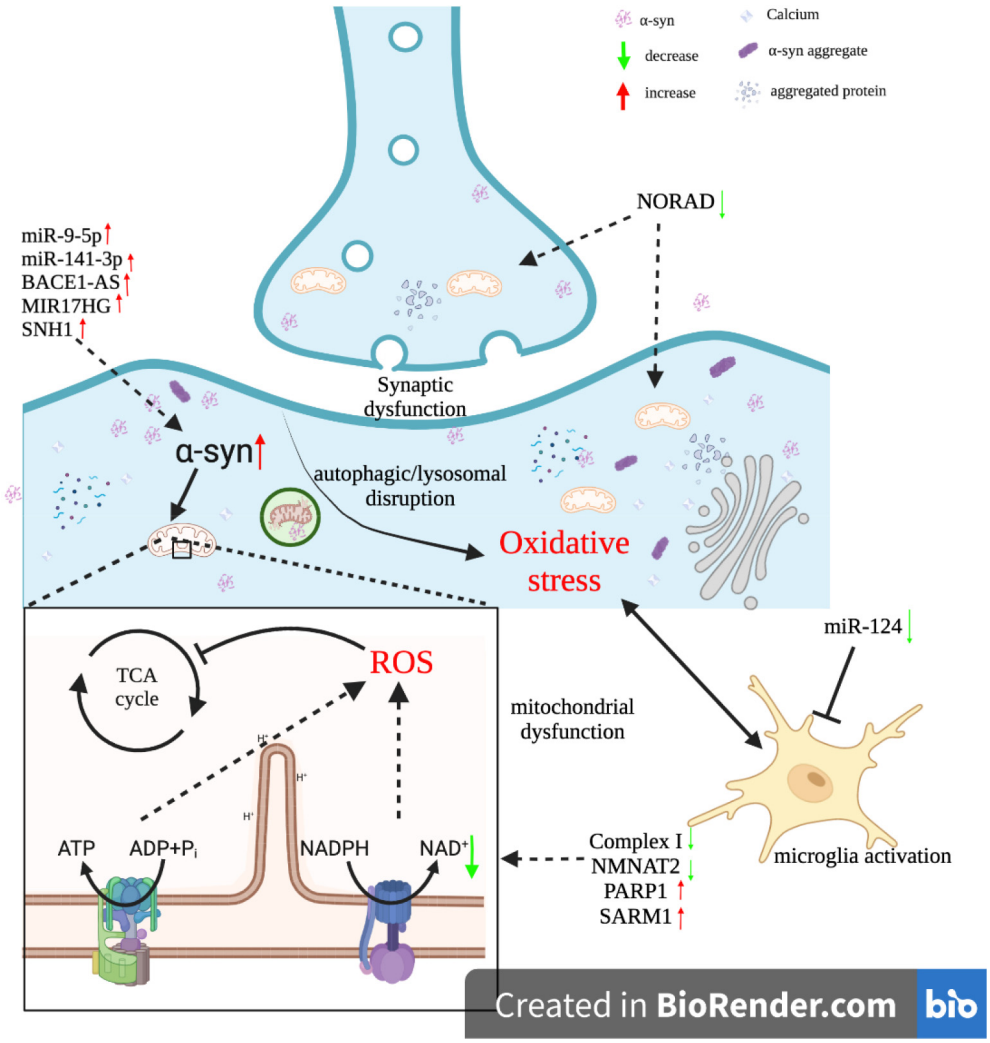

FIGURE 2
Interactions between ncRNAs and oxidative stress in Parkinson's disease.

In addition to the alternations occurring within neuronal cells, microglia activation has been regarded as an essential contributor to ROS production (Hassanzadeh and Rahimmi, 2018). Usually, microglia cells, the main immune cells in the brain, remained quiescent. Once activated, microglia released ROS and RNS such as H_2O_2, $O_2^{\bullet-}$, and NO (Onyango, 2008). The reaction of the latter two free radicals produced peroxynitrite ($ONOO^-$), a highly reactive molecule that may induce apoptosis of DA neurons (Varcin et al., 2012). Furthermore, the capacity of activated microglia to produce ROS and RNS was enhanced due to the increased release of inducible nitric oxide synthase (iNOS) and NADPH oxidase. These two enzymes promoted the generation of $O_2^{\bullet-}$ and NO, respectively (Drechsel and Patel, 2008; Koppula et al., 2012). Excessive intracellular and intercellular free radicals would lead to oxidative stress (Hald and Lotharius, 2005).

To deal with high contents of ROS and protect themselves from oxidative damage, neuronal cells utilized an antioxidant system consisting of antioxidant enzymes in conjunction with low molecular compounds (Manoharan et al., 2016). The enzymes included catalase (CAT), superoxide dismutase (SOD), and glutathione peroxidase (GPx), whereas glutathione (GSH) was a major non-enzymatic antioxidant (Redensek et al., 2019; Robea et al., 2020). CAT and GPx were believed to be responsible for scavenging H_2O_2 (Foley and Riederer, 2000). In the substantia nigra pars compacta (SNc) of PD patients, however, a dramatic decrease in the activity of antioxidative enzymes and the levels of non-enzymatic antioxidants has been observed (Damier et al., 1993; Mythri et al., 2011). Such an imbalance may induce oxidative stress and accelerate PD progression (Hauser and Hastings, 2013).

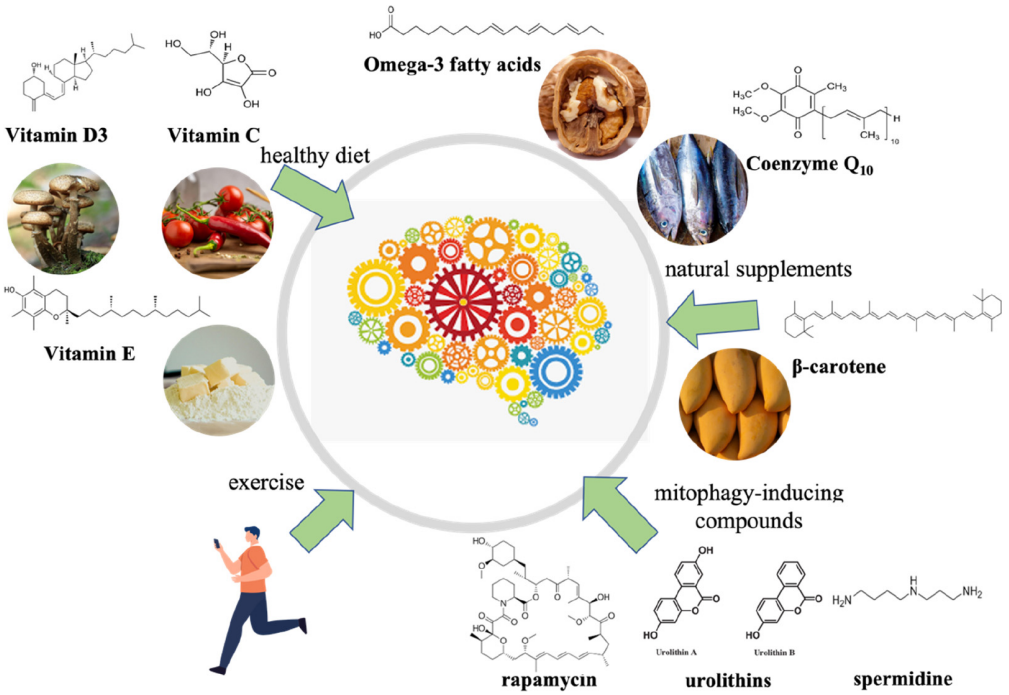

FIGURE 3
Multiple antioxidant strategies to prevent and cure Parkinson's disease.

Oxidative stress accelerates the progression of Parkinson's disease

Oxidative stress correlates with increased oxidation of macromolecules, including lipid, nucleic acid, and protein (Vallée et al., 2021a). Lipids are components of cell membranes, maintaining membrane fluidity and permeability. Hence, lipid oxidation would directly cause structural damage to cell membranes, which may lead to neuronal damage or even death (Dalle and Mabandla, 2018). Elevated oxidative damage to nucleic acids was also revealed in the PD SN (Hegde et al., 2006). The conformation and stability of DNA were altered because of oxidative stress, which could result in cell death (Guo et al., 2018). Protein oxidation is believed to be a feature of oxidative damage in the PD SN (Taylor et al., 2013). Oxidative stress caused nitration or carbonylation of proteins, which may lead to loss of function or aggregation (Maguire-Zeiss et al., 2005). The cellular systems responsible for the removal of misfolded or aggregated proteins were impaired by oxidative stress, which also contributed to the formation of protein aggregates (Hassanzadeh and Rahimmi, 2018).

Mitochondria are the main source of ROS in cells and are highly vulnerable to oxidative damage (Yuan et al., 2007). A dramatic outbreak of free radicals impaired the capability of the ETC to transfer electrons, which would result in a steady decline in mitochondrial activity and increased ROS production (Subramaniam and Chesselet, 2013). Significant elevation of ROS levels in neurons was found to be responsible for GSH leakage, mitochondrial DNA (mtDNA) mutation, and DA oxidation, which further promoted the production of free radicals (Janda et al., 2012; Yan et al., 2013; Vallée et al., 2021a,b). The damage to neurons caused by the positive feedback loop consisting of these PD elements will eventually lead to apoptosis (Trist et al., 2019).

Oxidative stress was also found to induce the formation of α-syn aggregates. Under normal physiological conditions, the α-syn existed as monomers or tetramers (**Figure 2**). Due to sensitivity to the excessive accumulation of ROS, the α-syn was induced to misfold by oxidative stress (Tsang and Chung, 2009). Misfolded α-syn proteins formed oligomers or fibrils and eventually insoluble aggregates (Jiang et al., 2016). The degradation of α-syn aggregates within Das is dependent mainly on the ubiquitin-proteasomal system (UPS) or chaperone-mediated autophagy (CMA). However, in a highly oxidized environment, these two pathways became ineffective in mediating the degradation of α-syn aggregates (Ganguly et al., 2017). This is because oxidative stress along with α-syn proteins subjected to oxidative modifications impaired the UPS and CMA (Jimenez-Moreno and Lane, 2020). α-syn accumulation and aggregation were found to inhibit the synthesis of ATP by mitochondria and induce microglia activation, which led to chronic effects of oxidative stress on the SN (Maguire-Zeiss

et al., 2005). Hence, the interaction between oxidative stress and α-syn proteins can be regarded as a positive feedback loop that drives pathological conditions, which ultimately leads to the development of PD (Puspita et al., 2017).

PD remains an incurable neurodegenerative disease, and the etiologies of it is not completely understood (Jiang et al., 2016; Raza et al., 2019). However, since researchers have found that oxidative stress can trigger PD or accelerate its progression, there is a consensus that combating oxidative stress is a promising medicinal strategy (Janda et al., 2012). Many molecules and natural compounds exert antioxidant properties, including carvacrol, coenzyme Q10 (CoQ10), creatine, curcumin, melatonin, lipoic acid (LA), lycopene, N-acetyl-cysteine (NAC), vitamin B_3, vitamin C, vitamin D_3, and urate (Chen et al., 2012; Crotty et al., 2017; Ciulla et al., 2019; **Figure 3**). These antioxidants may serve as neuroprotective agents, while they need to be proven safe and effective in clinical trials (Henchcliffe and Beal, 2008; Hassanzadeh and Rahimmi, 2018). In addition, regular physical exercise has been identified to have a positive impact on PD *via* reducing oxidative stress (Fan B. et al., 2020; Robea et al., 2020).

Interaction between oxidative stress and regulatory ncRNAs in Parkinson's disease

As mentioned above, both regulatory non-coding RNAs, as well as oxidative stress, are closely associated with PD. Furthermore, oxidative stress can cause oxidative damage to RNA. In contrast, regulatory ncRNAs such as miRNAs and lncRNAs play a role in regulating ROS production (**Figure 2**). Their interactions have been confirmed to be involved in the pathophysiology of PD (Konovalova et al., 2019).

RNA oxidation

RNA is susceptible to oxidative stress due to its single-stranded structure and dense distribution near the mitochondria, where most intracellular ROS are generated (Nunomura et al., 2009; Liu Z. et al., 2020). Excessive amounts of ROS may lead to RNA strand breaks and chemical modification and excision of RNA bases (Song et al., 2011; Zhao et al., 2017). Due to the lack of advanced repair mechanisms, oxidatively damaged RNA would accumulate in cells, resulting in reduced protein synthesis, erroneous protein generation, and eventual cell death (Zhang et al., 1999; Nunomura et al., 2006). RNA oxidation is not only a common feature of PD but also an early event in the progression of this disease (Nunomura et al., 2007; Cervinkova et al., 2017). Among oxidative marks on RNA, 8-oxo-7, 8-dihydroguanosine (8-oxoG) might be the most abundant and most extensively studied one (Gonzalez-Rivera et al., 2020). This base adduct can be produced by the exposure of guanine to free radicals and may cause incorrect base pairing (Zhang and Li, 2020). Researchers have found that 8-OHG levels in cerebrospinal fluid (CSF) and serum are significantly higher in PD patients than in healthy controls, indicating that 8-OHG may serve as a biomarker for PD (Alam et al., 1997; Kikuchi et al., 2002; Abe et al., 2003).

Non-coding RNAs, which are not responsible for encoding proteins, make up the majority of RNAs in human cells (Moreira et al., 2008). As a category of ncRNAs, regulatory ncRNAs, including miRNAs, lncRNAs, and circRNAs, are involved in the regulation of gene expression (Kong and Lin, 2010). Compared to mRNAs, these regulatory ncRNAs live relatively longer. Hence, oxidative damage that impairs their function would have a detrimental effect on cellular homeostasis (Yan and Zaher, 2019). For example, miRNAs attacked by free radicals may fail to correctly recognize their target mRNAs, which may lead to increased expression of certain proteins (Nunomura and Perry, 2020). In the experiment conducted by Je and Kim, miR-7 and miR-153 were identified to suppress the expression of α-SYN. Their mediated translational inhibition was abolished by oxidative stress, resulting in increased α-SYN levels and subsequent development of PD (Je and Kim, 2017). Furthermore, the study of Chen et al. showed that oxidative stress induced N6-methyladenosine (m^6A) modification of circRNAs. m^6Amodified circRNAs influenced the expression of stress response genes, which could be a potential mechanism for oxidative stress-induced neurodegenerative diseases (Chen N. et al., 2021).

miRNAs regulate oxidative stress

α-syn is responsible for inducing oxidative stress. Both microRNA-141-3p (miR-141-3p) and microRNA-9-5p (miR-9-5p) were found to target the 3' UTR of SIRT1 mRNA. Since SIRT1 inhibited the formation of α-syn aggregates, knockdown of miR-141-3p and miR-9-5p may alleviate oxidative stress and boost the viability of Das (Wang Z. et al., 2019; Zheng et al., 2020). In addition, microglia are thought to have a role in the pathophysiology of PD, since cytotoxic substances released from activated microglia can exacerbate oxidative stress. miR-124 inhibited microglia activation, thereby representing a neuroprotective factor (Lushchak and Lushchak, 2021). Recently, researchers found that dysregulation of Fe^{2+} homeostasis may lead to the accumulation of ROS in cells. This homeostasis was maintained by ferritin heavy chain 1 (FTH1) since FTH1 converted Fe^{2+} ions into soluble, non-toxic Fe^{3+} ions. microRNA-335 (miR-335) suppressed the expression of FTH1, thereby promoting the release of Fe^{2+} ions and the generation of free radicals (Li et al., 2021). Furthermore, downregulation of microRNA-410 (miR-410) expression in PD was identified to be associated with elevated ROS production,

although the underlying mechanism by which miR-410 exerted its neuroprotective role needs further study (Ge et al., 2019).

SOD, CAT, and GPx are responsible for detoxifying oxidants and repairing oxidative damage. Based on some research, microRNA-375 (miR-375), microRNA-218-5p (miR-218-5p), and miR-185 attenuated oxidative stress, as evidenced by elevated SOD and GPx activity in PD rats treated with these miRNAs (Cai et al., 2020; Ma et al., 2021b; Qin et al., 2021). In contrast, miR-137 and microRNA-494-3p (miR-494-3p) aggravated oxidative stress by reducing the level of SOD (Geng et al., 2018; Jiang et al., 2019). The activity of SOD was down-regulated by microRNA-155-5p (miR-155-5p; Lv et al., 2020).

lncRNAs regulate oxidative stress

Mitochondrial dysfunction, a common feature of PD, is directly related to the excessive production of ROS. This process can be inhibited by upregulated NORAD (Song et al., 2019). In addition, the formation of α-syn aggregates is capable of exacerbating oxidative stress *via* downregulating complex I activity or activating microglia. Li et al. found that the upregulation of lncRNA beta-amyloid cleaving enzyme-antisense (BACE1-AS) in PD wasassociatedwithrisingα-syn levels (Li Y. et al., 2020). Besides, Zhang et al. discovered that the lncRNA miR-17-92a-1 cluster host gene (MIR17HG) played a role in promoting the expression of α-syn. MIR17HG sponged microRNA-153-5p (miR-153-5p), thereby preventing miR-153-5p from downregulating α-syn expression (Zhang et al., 2022). GSK3β was revealed to promote α-syn accumulation *via* inhibiting autophagy. The expression of GSK3β was suppressed by miR-15b-5p, which was reversed by SNHG1 binding to miR-15b-5p (Xie N. et al., 2019).

Among the 17 newly studied lncRNAs, 13 were identified to aggravate oxidative stress and inflammatory responses in neurons, namely AL049437, HOTAIR, LINC00943, lncRNA-p21 (lnc-p21), MIAT, NEAT1, rhabdomyosarcoma 2-associate transcript (RMST), SNHG1, SNHG7, SOS1 intronic transcript 1 (SOS1-IT1), SRY-box transcription factor 2 overlapping transcript (SOX2-OT), taurine upregulated gene 1 (TUG1), and UCA1 (Cai et al., 2019; Ding et al., 2019; Zhai et al., 2020; Zhang L. et al., 2020; Zhao et al., 2020b; Guo et al., 2021; Lian et al., 2021; Ma et al., 2021a; Zhang et al., 2021; Zhou S. et al., 2021; Fan et al., 2022; Lang et al., 2022). The other four lncRNAs, namely JHDM1D antisense 1 (JHDM1D-AS1), myocardial infarction associated transcript 2 (Mirt2), small nucleolar RNA host gene 12 (SNHG12), and PART1, exhibited anti-oxidant and anti-inflammatory roles in models of PD, as evidenced by the decline in proinflammatory cytokines and increase in SOD contents (Han et al., 2019; Shen et al., 2021b; Wang C. et al., 2021; Yan et al., 2021). Nevertheless, the precise mechanism by which these 17 RNAs affect oxidative stress and thereby regulate PD progression remains unclear.

At present, we are in the early stage of investigating the cellular consequences of oxidatively damaged RNA and the mechanism by which regulatory ncRNAs affect oxidative stress (Kong et al., 2008; Xu et al., 2021). Further investigations are needed to explore the association between regulatory ncRNA oxidation and PD, which is beneficial to the development of early diagnosis and treatment for this disease (Nunomura et al., 2017).

Conclusion

We described the role of regulatory ncRNAs, oxidative stress, and their interactions in the regulation of PD. In recent years, the intrinsic correlation between regulatory ncRNAs and oxidative stress in PD has been increasingly studied. It is worth pointing out that some regulatory ncRNAs have been found to influence the progression of PD *via* regulating oxidative stress, which makes them potential therapeutic targets. However, there is fairly limited research that uncovers the precise mechanisms. In addition, because of the differences between the brains of laboratory animals and the human brain in combination with the inability of experimental models to accurately recapitulate the various features of PD, translating the results from PD models to humans may face considerable difficulties (Chia et al., 2020). There are still many hurdles to be overcome in the study of the interplay between regulatory ncRNAs and oxidative stress in PD. With the continuous innovation of experimental methods and techniques, the application of safe and effective targeted drugs for PD treatment is foreseeable.

Author contributions

The outline of this review was conceived by MT and XG. The draft manuscript was accomplished by HZ and polished by XL and GL. The tables were provided by JL and the figures were constructed by YL. All authors made a direct and intellectual contribution to this topic. All authors contributed to the article and approved the submitted version.

Funding

This work was financially supported by grants from the National Natural Science Foundation of China (32002235).

Acknowledgments

We thank all the individuals who have helped us in this study. We acknowledge the valuable work of the many investigators

whose published articles we were unable to cite owing to space limitations.

Conflict of interest

The authors declare that the research was conducted in the absence of any commercial or financial relationships that could be construed as a potential conflict of interest.

Publisher's note

All claims expressed in this article are solely those of the authors and do not necessarily represent those of their affiliated organizations, or those of the publisher, the editors and the reviewers. Any product that may be evaluated in this article, or claim that may be made by its manufacturer, is not guaranteed or endorsed by the publisher.

References

Abe, T., Isobe, C., Murata, T., Sato, C., and Tohgi, H. (2003). Alteration of 8-hydroxyguanosine concentrations in the cerebrospinal fluid and serum from patients with Parkinson's disease. *Neurosci. Lett.* 336, 105–108. doi: 10.1016/s0304-3940(02)01259-4

Acharya, S., Salgado-Somoza, A., Stefanizzi, F. M., Lumley, A. I., Zhang, L., Glaab, E., et al. (2020). Non-coding RNAs in the brain-heart axis: the case of Parkinson's disease. *Int. J. Mol. Sci.* 21:6513. doi: 10.3390/ijms21186513

Adusumilli, L., Facchinello, N., Teh, C., Busolin, G., Le, M. T., Yang, H., et al. (2020). miR-7 controls the dopaminergic/oligodendroglial fate through Wnt/β-catenin signaling regulation. *Cells* 9:711. doi: 10.3390/cells9030711

Alam, Z. I., Jenner, A., Daniel, S. E., Lees, A. J., Cairns, N., Marsden, C. D., et al. (1997). Oxidative DNA damage in the parkinsonian brain: an apparent selective increase in 8-hydroxyguanine levels in substantia nigra. *J. Neurochem.* 69, 1196–1203. doi: 10.1046/j.1471-4159.1997.69031196.x

Altesha, M. A., Ni, T., Khan, A., Liu, K., and Zheng, X. (2019). Circular RNA in cardiovascular disease. *J. Cell Physiol.* 234, 5588–5600. doi: 10.1002/jcp.27384

Antony, P. M., Diederich, N. J., Kruger, R., and Balling, R. (2013). The hallmarks of Parkinson's disease. *FEBS J.* 280, 5981–5993. doi: 10.1111/febs.12335

Ba, R. Q., Liu, J., Fan, X. J., Jin, G. L., Huang, B. G., Liu, M. W., et al. (2020). Effects of miR-199a on autophagy by targeting glycogen synthase kinase 3β to activate PTEN/AKT/mTOR signaling in an MPP^+ *in vitro* model of Parkinson's disease. *Neurol. Res.* 42, 308–318. doi: 10.1080/01616412.2020.1726584

Bai, X., Zhang, X., Fang, R., Wang, J., Ma, Y., Liu, Z., et al. (2021). Deficiency of miR-29b2/c leads to accelerated aging and neuroprotection in MPTP-induced Parkinson's disease mice. *Aging (Albany NY)* 13, 22390–22411. doi: 10.18632/aging.203545

Bhattacharyya, N., Pandey, V., Bhattacharyya, M., and Dey, A. (2021). Regulatory role of long non coding RNAs (lncRNAs) in neurological disorders: from novel biomarkers to promising therapeutic strategies. *Asian J. Pharm. Sci.* 16, 533–550. doi: 10.1016/j.ajps.2021.02.006

Bloem, B. R., Okun, M. S., and Klein, C. (2021). Parkinson's disease. *Lancet* 397, 2284–2303. doi: 10.1016/S0140-6736(21)00218-X

Brand, M. D., and Nicholls, D. G. (2011). Assessing mitochondrial dysfunction in cells. *Biochem. J.* 435, 297–312. doi: 10.1042/BJ20110162

Brieger, K., Schiavone, S., Miller, F. J., Jr., and Krause, K. H. (2012). Reactive oxygen species: from health to disease. *Swiss Med. Wkly* 142:w13659. doi: 10.4414/smw.2012.13659

Cai, L., Tu, L., Li, T., Yang, X., Ren, Y., Gu, R., et al. (2019). Downregulation of lncRNA UCA1 ameliorates the damage of dopaminergic neurons, reduces oxidative stress and inflammation in Parkinson's disease through the inhibition of the PI3K/Akt signaling pathway. *Int. Immunopharmacol.* 75:105734. doi: 10.1016/j.intimp.2019.105734

Cai, L. J., Tu, L., Li, T., Yang, X. L., Ren, Y. P., Gu, R., et al. (2020). Up-regulation of microRNA-375 ameliorates the damage of dopaminergic neurons, reduces oxidative stress and inflammation in Parkinson's disease by inhibiting SP1. *Aging (Albany NY)* 12, 672–689. doi: 10.18632/aging.102649

Cao, Q., Guo, Z., Yan, Y., Wu, J., and Song, C. (2019). Exosomal long noncoding RNAs in aging and age-related diseases. *IUBMB Life* 71, 1846–1856. doi: 10.1002/iub.2141

Cao, H., Han, X., Jia, Y., and Zhang, B. (2021). Inhibition of long non-coding RNA HOXA11-AS against neuroinflammation in Parkinson's disease model via targeting miR-124-3p mediated FSTL1/NF-κB axis. *Aging (Albany NY)* 13, 11455–11469. doi: 10.18632/aging.202837

Cao, L., Wang, M., Dong, Y., Xu, B., Chen, J., Ding, Y., et al. (2020). Circular RNA circRNF20 promotes breast cancer tumorigenesis and Warburg effect through miR-487a/HIF-1α/HK2. *Cell Death Dis.* 11:145. doi: 10.1038/s41419-020-2336-0

Cao, B., Wang, T., Qu, Q., Kang, T., and Yang, Q. (2018). Long noncoding RNA SNHG1 promotes neuroinflammation in Parkinson's disease via regulating miR-7/NLRP3 pathway. *Neuroscience* 388, 118–127. doi: 10.1016/j.neuroscience.2018.07.019

Carvalho Barbosa, C., Calhoun, S. H., and Wieden, H. J. (2020). Non-coding RNAs: what are we missing. *Biochem. Cell Biol.* 98, 23–30. doi: 10.1139/bcb-2019-0037

Cerri, S., Mus, L., and Blandini, F. (2019). Parkinson's disease in women and men: what's the difference. *J. Parkinsons Dis.* 9, 501–515. doi: 10.3233/JPD-191683

Cervinkova, B., Krcmova, L. K., Sestakova, V., Solichova, D., and Solich, P. (2017). A fully validated bioanalytical method using an UHPLC-MS/MS system for quantification of DNA and RNA oxidative stress biomarkers. *Anal. Bioanal. Chem.* 409, 3611–3621. doi: 10.1007/s00216-017-0301-2

Chen, M. Y., Fan, K., Zhao, L. J., Wei, J. M., Gao, J. X., and Li, Z. F. (2021). Long non-coding RNA nuclear enriched abundant transcript 1 (NEAT1) sponges microRNA-124-3p to up-regulate phosphodiesterase 4B (PDE4B) to accelerate the progression of Parkinson's disease. *Bioengineered* 12, 708–719. doi: 10.1080/21655979.2021.1883279

Chen, Q., Huang, X., and Li, R. (2018). lncRNA MALAT1/miR-205-5p axis regulates MPP^+-induced cell apoptosis in MN9D cells by directly targeting LRRK2. *Am. J. Transl. Res.* 10, 563–572.

Chen, Y., Lian, Y. J., Ma, Y. Q., Wu, C. J., Zheng, Y. K., and Xie, N. C. (2018). LncRNA SNHG1 promotes alpha-synuclein aggregation and toxicity by targeting miR-15b-5p to activate SIAH1 in human neuroblastoma SH-SY5Y cells. *Neurotoxicology* 68, 212–221. doi: 10.1016/j.neuro.2017.12.001

Chen, N., Tang, J., Su, Q., Chou, W. C., Zheng, F., Guo, Z., et al. (2021). Paraquat-induced oxidative stress regulates N6-methyladenosine (m(6)A) modification of circular RNAs. *Environ. Pollut.* 290:117816. doi: 10.1016/j.envpol.2021.117816

Chen, X., Wu, G., and Schwarzschild, M. A. (2012). Urate in Parkinson's disease: more than a biomarker. *Curr. Neurol. Neurosci. Rep.* 12, 367–375. doi: 10.1007/s11910-012-0282-7

Chen, Z., and Zhong, C. (2014). Oxidative stress in Alzheimer's disease. *Neurosci. Bull.* 30, 271–281. doi: 10.1007/s12264-013-1423-y

Chia, S. J., Tan, E. K., and Chao, Y. X. (2020). Historical perspective: models of Parkinson's disease. *Int. J. Mol. Sci.* 21:2464. doi: 10.3390/ijms21072464

Choi, D. C., Yoo, M., Kabaria, S., and Junn, E. (2018). MicroRNA-7 facilitates the degradation of alpha-synuclein and its aggregates by promoting autophagy. *Neurosci. Lett.* 678, 118–123. doi: 10.1016/j.neulet.2018.05.009

Ciulla, M., Marinelli, L., Cacciatore, I., and Stefano, A. D. (2019). Role of dietary supplements in the management of Parkinson's disease. *Biomolecules* 9:271. doi: 10.3390/biom9070271

Crotty, G. F., Ascherio, A., and Schwarzschild, M. A. (2017). Targeting urate to reduce oxidative stress in Parkinson disease. *Exp. Neurol.* 298, 210–224. doi: 10.1016/j.expneurol.2017.06.017

Dalle, E., and Mabandla, M. V. (2018). Early life stress, depression and Parkinson's disease: a new approach. *Mol. Brain* 11:18. doi: 10.1186/s13041-018-0356-9

Damier, P., Hirsch, E. C., Zhang, P., Agid, Y., and Javoy-Agid, F. (1993). Glutathione peroxidase, glial cells and Parkinson's disease. *Neuroscience* 52, 1–6. doi: 10.1016/0306-4522(93)90175-f

Ding, X. M., Zhao, L. J., Qiao, H. Y., Wu, S. L., and Wang, X. H. (2019). Long non-coding RNA-p21 regulates MPP^+-induced neuronal injury by targeting miR-625 and derepressing TRPM2 in SH-SY5Y cells. *Chem. Biol. Interact.* 307, 73–81. doi: 10.1016/j.cbi.2019.04.017

Dong, L. G., Lu, F. F., Zu, J., Zhang, W., Xu, C. Y., Jin, G. L., et al. (2020). MiR-133b inhibits MPP^+-induced apoptosis in Parkinson's disease model by inhibiting the ERK1/2 signaling pathway. *Eur. Rev. Med. Pharmacol. Sci.* 24, 11192–11198. doi: 10.26355/eurrev_202011_23607

Dong, Y., Xiong, J., Ji, L., and Xue, X. (2021). MiR-421 aggravates neurotoxicity and promotes cell death in Parkinson's disease models by directly targeting MEF2D. *Neurochem. Res.* 46, 299–308. doi: 10.1007/s11064-020-03166-0

Drechsel, D. A., and Patel, M. (2008). Role of reactive oxygen species in the neurotoxicity of environmental agents implicated in Parkinson's disease. *Free Radic. Biol. Med.* 44, 1873–1886. doi: 10.1016/j.freeradbiomed.2008.02.008

Dunn, A. R., O'connell, K. M. S., and Kaczorowski, C. C. (2019). Gene-by-environment interactions in Alzheimer's disease and Parkinson's disease. *Neurosci. Biobehav. Rev.* 103, 73–80. doi: 10.1016/j.neubiorev.2019.06.018

Fan, B., Jabeen, R., Bo, B., Guo, C., Han, M., Zhang, H., et al. (2020). What and how can physical activity prevention function on Parkinson's disease. *Oxid. Med. Cell Longev.* 2020:4293071. doi: 10.1155/2020/4293071

Fan, J., Wu, D., Guo, Y., and Yang, Z. (2022). SOS1-IT1 silencing alleviates MPP^+-induced neuronal cell injury through regulating the miR-124-3p/PTEN/AKT/mTOR pathway. *J. Clin. Neurosci.* 99, 137–146. doi: 10.1016/j.jocn.2022.01.003

Fan, Y., Zhao, X., Lu, K., and Cheng, G. (2020). LncRNA BDNF-AS promotes autophagy and apoptosis in MPTP-induced Parkinson's disease via ablating microRNA-125b-5p. *Brain Res. Bull.* 157, 119–127. doi: 10.1016/j.brainresbull.2020.02.003

Feng, Y., Li, T., Xing, C., Wang, C., Duan, Y., Yuan, L., et al. (2021). Effective inhibition of miR-330/SHIP1/NF-κB signaling pathway via miR-330 sponge repolarizes microglia differentiation. *Cell Biol. Int.* 45, 785–794. doi: 10.1002/cbin.11523

Feng, Z., Zhang, L., Wang, S., and Hong, Q. (2020). Circular RNA circDLGAP4 exerts neuroprotective effects via modulating miR-134-5p/CREB pathway in Parkinson's disease. *Biochem. Biophys. Res. Commun.* 522, 388–394. doi: 10.1016/j.bbrc.2019.11.102

Fields, C. R., Bengoa-Vergniory, N., and Wade-Martins, R. (2019). Targeting alpha-synuclein as a therapy for Parkinson's disease. *Front. Mol. Neurosci.* 12:299. doi: 10.1016/j.bbrc.2019.11.102

Foley, P., and Riederer, P. (2000). Influence of neurotoxins and oxidative stress on the onset and progression of Parkinson's disease. *J. Neurol.* 247, II82–II94. doi: 10.1007/pl00007766

Forman, H. J., and Zhang, H. (2021). Targeting oxidative stress in disease: promise and limitations of antioxidant therapy. *Nat. Rev. Drug Discov.* 20, 689–709. doi: 10.1038/s41573-021-00233-1

Ganguly, G., Chakrabarti, S., Chatterjee, U., and Saso, L. (2017). Proteinopathy, oxidative stress and mitochondrial dysfunction: cross talk in Alzheimer's disease and Parkinson's disease. *Drug Des. Dev. Ther.* 11, 797–810. doi: 10.2147/DDDT.S130514

Gao, J. X., Li, Y., Wang, S. N., Chen, X. C., Lin, L. L., and Zhang, H. (2019). Overexpression of microRNA-183 promotes apoptosis of substantia nigra neurons via the inhibition of OSMR in a mouse model of Parkinson's disease. *Int. J. Mol. Med.* 43, 209–220. doi: 10.3892/ijmm.2018.3982

Ge, H., Yan, Z., Zhu, H., and Zhao, H. (2019). MiR-410 exerts neuroprotective effects in a cellular model of Parkinson's disease induced by 6-hydroxydopamine via inhibiting the PTEN/AKT/mTOR signaling pathway. *Exp. Mol. Pathol.* 109, 16–24. doi: 10.1016/j.yexmp.2019.05.002

Geng, L., Liu, W., and Chen, Y. (2017). miR-124-3p attenuates MPP^+-induced neuronal injury by targeting STAT3 in SH-SY5Y cells. *Exp. Biol. Med. (Maywood)* 242, 1757–1764. doi: 10.1177/1535370217734492

Geng, L., Zhang, T., Liu, W., and Chen, Y. (2018). miR-494-3p modulates the progression of *in vitro* and *in vivo* Parkinson's disease models by targeting SIRT3. *Neurosci. Lett.* 675, 23–30. doi: 10.1128/JVI.00955-15

Gerin, I., Bommer, G. T., Mccoin, C. S., Sousa, K. M., Krishnan, V., and Macdougald, O. A. (2010). Roles for miRNA-378/378* in adipocyte gene expression and lipogenesis. *Am. J. Physiol. Endocrinol. Metab.* 299, E198–E206. doi: 10.1152/ajpendo.00179.2010

Goh, S. Y., Chao, Y. X., Dheen, S. T., Tan, E. K., and Tay, S. S. (2019). Role of MicroRNAs in Parkinson's disease. *Int. J. Mol. Sci.* 20:5649. doi: 10.3390/ijms20225649

Gong, X., Huang, M., and Chen, L. (2022). Mechanism of miR-132-3p promoting neuroinflammation and dopaminergic neurodegeneration in Parkinson's disease. *eNeuro* 9:ENEURO.0393-21.2021. doi: 10.1101/lm.039578.115

Gonzalez-Rivera, J. C., Sherman, M. W., Wang, D. S., Chuvalo-Abraham, J. C. L., Hildebrandt Ruiz, L., and Contreras, L. M. (2020). RNA oxidation in chromatin modification and DNA-damage response following exposure to formaldehyde. *Sci. Rep.* 10:16545. doi: 10.1038/s41598-020-73376-7

Gordon, R., Albornoz, E. A., Christie, D. C., Langley, M. R., Kumar, V., Mantovani, S., et al. (2018). Inflammasome inhibition prevents α-synuclein pathology and dopaminergic neurodegeneration in mice. *Sci. Transl. Med.* 10:eaah4066. doi: 10.1126/scitranslmed.aah4066

Guo, Y., Liu, Y., Wang, H., and Liu, P. (2021). Long noncoding RNA SRY-box transcription factor 2 overlapping transcript participates in Parkinson's disease by regulating the microRNA-942-5p/nuclear apoptosis-inducing factor 1 axis. *Bioengineered* 12, 8570–8582. doi: 10.1080/21655979.2021.1987126

Guo, J. D., Zhao, X., Li, Y., Li, G. R., and Liu, X. L. (2018). Damage to dopaminergic neurons by oxidative stress in Parkinson's disease (Review). *Int. J. Mol. Med.* 41, 1817–1825. doi: 10.3892/ijmm.2018.3406

Hald, A., and Lotharius, J. (2005). Oxidative stress and inflammation in Parkinson's disease: is there a causal link. *Exp. Neurol.* 193, 279–290. doi: 10.1016/j.expneurol.2005.01.013

Han, Y., Kang, C., Kang, M., Quan, W., Gao, H., and Zhong, Z. (2019). Long non-coding RNA Mirt2 prevents TNF-alpha-triggered inflammation via the repression of microRNA-101. *Int. Immunopharmacol.* 76:105878. doi: 10.1016/j.intimp.2019.105878

Hassanzadeh, K., and Rahimmi, A. (2018). Oxidative stress and neuroinflammation in the story of Parkinson's disease: could targeting these pathways write a good ending. *J. Cell Physiol.* 234, 23–32. doi: 10.1002/jcp.26865

Hauser, D. N., and Hastings, T. G. (2013). Mitochondrial dysfunction and oxidative stress in Parkinson's disease and monogenic parkinsonism. *Neurobiol. Dis.* 51, 35–42. doi: 10.1016/j.nbd.2012.10.011

Hayes, M. T. (2019). Parkinson's disease and Parkinsonism. *Am. J. Med.* 132, 802–807. doi: 10.1016/j.amjmed.2019.03.001

He, Q., Wang, Q., Yuan, C., and Wang, Y. (2017). Downregulation of miR-7116-5p in microglia by MPP^+ sensitizes TNF-alpha production to induce dopaminergic neuron damage. *Glia* 65, 1251–1263. doi: 10.1002/glia.23153

Hegde, M. L., Gupta, V. B., Anitha, M., Harikrishna, T., Shankar, S. K., Muthane, U., et al. (2006). Studies on genomic DNA topology and stability in brain regions of Parkinson's disease. *Arch. Biochem. Biophys.* 449, 143–156. doi: 10.1016/j.abb.2006.02.018

Hemmati-Dinarvand, M., Saedi, S., Valilo, M., Kalantary-Charvadeh, A., Alizadeh Sani, M., Kargar, R., et al. (2019). Oxidative stress and Parkinson's disease: conflict of oxidant-antioxidant systems. *Neurosci. Lett.* 709:134296. doi: 10.1016/j.neulet.2019.134296

Henchcliffe, C., and Beal, M. F. (2008). Mitochondrial biology and oxidative stress in Parkinson disease pathogenesis. *Nat. Clin. Pract. Neurol.* 4, 600–609. doi: 10.1038/ncpneuro0924

Hombach, S., and Kretz, M. (2016). Non-coding RNAs: classification, biology and functioning. *Adv. Exp. Med. Biol.* 937, 3–17. doi: 10.1007/978-3-319-42059-2_1

Huang, A., Zheng, H., Wu, Z., Chen, M., and Huang, Y. (2020). Circular RNA-protein interactions: functions, mechanisms and identification. *Theranostics* 10, 3503–3517. doi: 10.7150/thno.42174

Iovino, L., Tremblay, M. E., and Civiero, L. (2020). Glutamate-induced excitotoxicity in Parkinson's disease: the role of glial cells. *J. Pharmacol. Sci.* 144, 151–164. doi: 10.1016/j.jphs.2020.07.011

Islam, M. T. (2017). Oxidative stress and mitochondrial dysfunction-linked neurodegenerative disorders. *Neurol. Res.* 39, 73–82. doi: 10.1080/01616412.2016.1251711

Janda, E., Isidoro, C., Carresi, C., and Mollace, V. (2012). Defective autophagy in Parkinson's disease: role of oxidative stress. *Mol. Neurobiol.* 46, 639–661. doi: 10.1007/s12035-012-8318-1

Je, G., and Kim, Y. S. (2017). Mitochondrial ROS-mediated post-transcriptional regulation of alpha-synuclein through miR-7 and miR-153. *Neurosci. Lett.* 661, 132–136. doi: 10.1016/j.neulet.2017.09.065

Jiang, Y., Liu, J., Chen, L., Jin, Y., Zhang, G., Lin, Z., et al. (2019). Serum secreted miR-137-containing exosomes affects oxidative stress of neurons by regulating OXR1 in Parkinson's disease. *Brain Res.* 1722:146331. doi: 10.1016/j.brainres.2019.146331

Jiang, Q., Liu, C., Li, C. P., Xu, S. S., Yao, M. D., Ge, H. M., et al. (2020). Circular RNA-ZNF532 regulates diabetes-induced retinal pericyte degeneration and vascular dysfunction. *J. Clin. Invest.* 130, 3833–3847. doi: 10.1172/JCI123353

Jiang, J., Piao, X., Hu, S., Gao, J., and Bao, M. (2020). LncRNA H19 diminishes dopaminergic neuron loss by mediating microRNA-301b-3p in Parkinson's disease via the HPRT1-mediated Wnt/β-catenin signaling pathway. *Aging (Albany NY)* 12, 8820–8836. doi: 10.18632/aging.102877

Jiang, T., Sun, Q., and Chen, S. (2016). Oxidative stress: a major pathogenesis and potential therapeutic target of antioxidative agents in Parkinson's disease and Alzheimer's disease. *Prog. Neurobiol.* 147, 1–19. doi: 10.1016/j.pneurobio.2016.07.005

Jimenez-Moreno, N., and Lane, J. D. (2020). Autophagy and redox homeostasis in Parkinson's: a crucial balancing act. *Oxid. Med. Cell Longev.* 2020:8865611. doi: 10.1155/2020/8865611

Jin, H., Kanthasamy, A., Ghosh, A., Anantharam, V., Kalyanaraman, B., and Kanthasamy, A. G. (2014). Mitochondria-targeted antioxidants for treatment of Parkinson's disease: preclinical and clinical outcomes. *Biochim. Biophys. Acta* 1842, 1282–1294. doi: 10.1016/j.bbadis.2013.09.007

Jin, J., Sun, H., Shi, C., Yang, H., Wu, Y., Li, W., et al. (2020). Circular RNA in renal diseases. *J. Cell Mol. Med.* 24, 6523–6533. doi: 10.1111/jcmm.15295

John, A., Kubosumi, A., and Reddy, P. H. (2020). Mitochondrial MicroRNAs in aging and neurodegenerative diseases. *Cells* 9:1345. doi: 10.3390/cells9061345

Kikuchi, A., Takeda, A., Onodera, H., Kimpara, T., Hisanaga, K., Sato, N., et al. (2002). Systemic increase of oxidative nucleic acid damage in Parkinson's disease and multiple system atrophy. *Neurobiol. Dis.* 9, 244–248. doi: 10.1006/nbdi.2002.0466

Kong, Q., and Lin, C. L. (2010). Oxidative damage to RNA: mechanisms, consequences and diseases. *Cell Mol. Life Sci.* 67, 1817–1829. doi: 10.1007/s00018-010-0277-y

Kong, Q., Shan, X., Chang, Y., Tashiro, H., and Lin, C. L. (2008). RNA oxidation: a contributing factor or an epiphenomenon in the process of neurodegeneration. *Free Radic Res.* 42, 773–777. doi: 10.1080/10715760802311187

Konovalova, J., Gerasymchuk, D., Parkkinen, I., Chmielarz, P., and Domanskyi, A. (2019). Interplay between MicroRNAs and oxidative stress in neurodegenerative diseases. *Int. J. Mol. Sci.* 20:6055. doi: 10.3390/ijms20236055

Koppula, S., Kumar, H., Kim, I. S., and Choi, D. K. (2012). Reactive oxygen species and inhibitors of inflammatory enzymes, NADPH oxidase and iNOS in experimental models of Parkinson's disease. *Mediators Inflamm.* 2012:823902. doi: 10.1155/2012/823902

Lang, Y., Zhang, H., Yu, H., Li, Y., Liu, X., and Li, M. (2022). Long non-coding RNA myocardial infarction-associated transcript promotes 1-Methyl-4-phenylpyridinium ion-induced neuronal inflammation and oxidative stress in Parkinson's disease through regulating microRNA-221-3p/ transforming growth factor /nuclear factor E2-related factor 2 axis. *Bioengineered* 13, 930–940. doi: 10.1080/21655979.2021.2015527

Lee, S., Kopp, F., Chang, T. C., Sataluri, A., Chen, B., Sivakumar, S., et al. (2016). Noncoding RNA NORAD regulates genomic stability by sequestering PUMILIO proteins. *Cell* 164, 69–80. doi: 10.1016/j.cell.2015.12.017

Li, Y., Fang, J., Zhou, Z., Zhou, Q., Sun, S., Jin, Z., et al. (2020). Downregulation of lncRNA BACE1-AS improves dopamine-dependent oxidative stress in rats with Parkinson's disease by upregulating microRNA-34b-5p and downregulating BACE1. *Cell Cycle* 19, 1158–1171. doi: 10.1080/15384101.2020.1749447

Li, L., Liu, H., Song, H., Qin, Y., Wang, Y., Xu, M., et al. (2017). Let-7d microRNA attenuates 6-OHDA-induced injury by targeting Caspase-3 in MN9D cells. *J. Mol. Neurosci.* 63, 403–411. doi: 10.1007/s12031-017-0994-x

Li, W., Jiang, Y., Wang, Y., Yang, S., Bi, X., Pan, X., et al. (2018). MiR-181b regulates autophagy in a model of Parkinson's disease by targeting the PTEN/Akt/mTOR signaling pathway. *Neurosci. Lett.* 675, 83–88. doi: 10.1016/j.neulet.2018.03.041

Li, W., Kui, L., Demetrios, T., Gong, X., and Tang, M. (2020). A glimmer of hope: maintain mitochondrial homeostasis to mitigate Alzheimer's disease. *Aging Dis.* 11, 1260–1275. doi: 10.14336/AD.2020.0105

Li, D., Mastaglia, F. L., Fletcher, S., and Wilton, S. D. (2020). Progress in the molecular pathogenesis and nucleic acid therapeutics for Parkinson's disease in the precision medicine era. *Med. Res. Rev.* 40, 2650–2681. doi: 10.1002/med.21718

Li, X., Si, W., Li, Z., Tian, Y., Liu, X., Ye, S., et al. (2021). miR-335 promotes ferroptosis by targeting ferritin heavy chain 1 in *in vivo* and *in vitro* models of Parkinson's disease. *Int. J. Mol. Med.* 47:61. doi: 10.3892/ijmm.2021.4894

Li, H., Xu, J. D., Fang, X. H., Zhu, J. N., Yang, J., Pan, R., et al. (2020). Circular RNA circRNA_000203 aggravates cardiac hypertrophy via suppressing miR-26b-5p and miR-140-3p binding to Gata4. *Cardiovasc. Res.* 116, 1323–1334. doi: 10.1093/cvr/cvz215

Li, L., Xu, J., Wu, M., and Hu, J. M. (2018). Protective role of microRNA-221 in Parkinson's disease. *Bratisl Lek Listy* 119, 22–27. doi: 10.4149/BLL_2018_005

Li, D., Yang, H., Ma, J., Luo, S., Chen, S., and Gu, Q. (2018). MicroRNA-30e regulates neuroinflammation in MPTP model of Parkinson's disease by targeting Nlrp3. *Hum. Cell* 31, 106-115. doi: 10.1007/s13577-017-0187-5

Li, J., Zhang, Y., Li, D., Liu, Y., Chu, D., Jiang, X., et al. (2015). Small non-coding RNAs transfer through mammalian placenta and directly regulate fetal gene expression. *Protein Cell* 6, 391–396. doi: 10.1007/s13238-015-0156-2

Lian, H., Wang, B., Lu, Q., Chen, B., and Yang, H. (2021). LINC00943 knockdown exerts neuroprotective effects in Parkinson's disease through regulates CXCL12 expression by sponging miR-7-5p. *Genes Genomics* 43, 797–805. doi: 10.1007/s13258-021-01084-1

Lin, Q., Hou, S., Dai, Y., Jiang, N., and Lin, Y. (2019). LncRNA HOTAIR targets miR-126-5p to promote the progression of Parkinson's disease through RAB3IP. *Biol. Chem* 400, 1217–1228. doi: 10.1515/hsz-2018-0431

Liu, Z., Chen, X., Li, Z., Ye, W., Ding, H., Li, P., et al. (2020). Role of RNA oxidation in neurodegenerative diseases. *Int. J. Mol. Sci.* 21:5022. doi: 10.3390/ijms21145022

Liu, R., Li, F., and Zhao, W. (2020). Long noncoding RNA NEAT1 knockdown inhibits MPP^+-induced apoptosis, inflammation and cytotoxicity in SK-N-SH cells by regulating miR-212-5p/RAB3IP axis. *Neurosci. Lett.* 731:135060. doi: 10.1016/j.neulet.2020.135060

Liu, J., Liu, W., and Yang, H. (2019). Balancing apoptosis and autophagy for Parkinson's disease therapy: targeting BCL-2. *ACS Chem. Neurosci.* 10, 792–802. doi: 10.1021/acschemneuro.8b00356

Liu, J., Liu, D., Zhao, B., Jia, C., Lv, Y., Liao, J., et al. (2020). Long non-coding RNA NEAT1 mediates MPTP/MPP^+-induced apoptosis via regulating the miR-124/KLF4 axis in Parkinson's disease. *Open Life Sci.* 15, 665–676. doi: 10.1515/biol-2020-0069

Liu, Y., and Lu, Z. (2018). Long non-coding RNA NEAT1 mediates the toxic of Parkinson's disease induced by MPTP/MPP^+ via regulation of gene expression. *Clin. Exp. Pharmacol. Physiol.* 45, 841–848. doi: 10.1111/1440-1681.12932

Liu, N., Wang, Z. Z., Zhao, M., Zhang, Y., and Chen, N. H. (2020). Role of non-coding RNA in the pathogenesis of depression. *Gene* 735:144276. doi: 10.1016/j.gene.2019.144276

Liu, T., Zhang, Y., Liu, W., and Zhao, J. (2021). LncRNA NEAT1 regulates the development of Parkinson's disease by targeting AXIN1 via sponging miR-212-3p. *Neurochem. Res.* 46, 230–240. doi: 10.1007/s11064-020-03157-1

Liu, W., Zhang, Q., Zhang, J., Pan, W., Zhao, J., and Xu, Y. (2017). Long non-coding RNA MALAT1 contributes to cell apoptosis by sponging miR-124 in Parkinson disease. *Cell Biosci.* 7:19. doi: 10.1186/s13578-017-0147-5

Liu, Y., Song, Y., and Zhu, X. (2017). MicroRNA-181a regulates apoptosis and autophagy process in Parkinson's disease by inhibiting p38 mitogen-activated protein kinase (MAPK)/c-Jun N-Terminal kinases (JNK) signaling pathways. *Med. Sci. Monit.* 23, 1597–1606. doi: 10.12659/msm.900218

Lu, W., Lin, J., Zheng, D., Hong, C., Ke, L., Wu, X., et al. (2020). Overexpression of MicroRNA-133a inhibits apoptosis and autophagy in a cell model of Parkinson's disease by downregulating ras-related C3 botulinum toxin substrate 1 (RAC1). *Med. Sci. Monit.* 26:e922032. doi: 10.12659/MSM.922032

Lu, M., Sun, W. L., Shen, J., Wei, M., Chen, B., Qi, Y. J., et al. (2018). LncRNA-UCA1 promotes PD development by upregulating SNCA. *Eur. Rev. Med. Pharmacol. Sci.* 22, 7908–7915. doi: 10.26355/eurrev_201811_16417

Lu, J., Wu, M., and Yue, Z. (2020). Autophagy and Parkinson's disease. *Adv. Exp. Med. Biol.* 1207, 21–51. doi: 10.1007/978-981-15-4272-5_2

Lu, J., Xu, Y., Quan, Z., Chen, Z., Sun, Z., and Qing, H. (2017). Dysregulated microRNAs in neural system: implication in pathogenesis and biomarker development in Parkinson's disease. *Neuroscience* 365, 70–82. doi: 10.1016/j.neuroscience.2017.09.033

Lu, S., Yang, X., Wang, C., Chen, S., Lu, S., Yan, W., et al. (2019). Current status and potential role of circular RNAs in neurological disorders. *J. Neurochem.* 150, 237–248. doi: 10.1111/jnc.14724

Lushchak, V. I., and Lushchak, O. (2021). Interplay between reactive oxygen and nitrogen species in living organisms. *Chem. Biol. Interact.* 349:109680. doi: 10.1016/j.cbi.2021.109680

Lv, R., Du, L., Zhou, F., Yuan, X., Liu, X., and Zhang, L. (2020). Rosmarinic acid alleviates inflammation, apoptosis and oxidative stress through regulating miR-155-5p in a mice model of Parkinson's disease. *ACS Chem. Neurosci.* 11, 3259–3266. doi: 10.1021/acschemneuro.0c00375

Lv, K., Liu, Y., Zheng, Y., Dai, S., Yin, P., and Miao, H. (2021). Long non-coding RNA MALAT1 regulates cell proliferation and apoptosis via miR-135b-5p/GPNMB axis in Parkinson's disease cell model. *Biol. Res.* 54:10. doi: 10.1186/s40659-021-00332-8

Ma, J., Sun, W., Chen, S., Wang, Z., Zheng, J., Shi, X., et al. (2022). The long noncoding RNA GAS5 potentiates neuronal injury in Parkinson's disease by binding to microRNA-150 to regulate Fosl1 expression. *Exp. Neurol.* 347:113904. doi: 10.1016/j.expneurol.2021.113904

Ma, X., Wang, Y., Yin, H., Hua, L., Zhang, X., Xiao, J., et al. (2021a). Down-regulated long non-coding RNA RMST ameliorates dopaminergic neuron damage in Parkinson's disease rats via regulation of TLR/NF-kappaB signaling pathway. *Brain Res. Bull.* 174, 22–30. doi: 10.1016/j.brainresbull.2021.04.026

Ma, X., Zhang, H., Yin, H., Geng, S., Liu, Y., Liu, C., et al. (2021b). Up-regulated microRNA-218-5p ameliorates the damage of dopaminergic neurons in rats with Parkinson's disease via suppression of LASP1. *Brain Res. Bull.* 166, 92–101. doi: 10.1016/j.brainresbull.2020.10.019

Maguire-Zeiss, K. A., Short, D. W., and Federoff, H. J. (2005). Synuclein, dopamine and oxidative stress: co-conspirators in Parkinson's disease. *Brain Res. Mol. Brain Res.* 134, 18–23. doi: 10.1016/j.molbrainres.2004.09.014

Majidinia, M., Mihanfar, A., Rahbarghazi, R., Nourazarian, A., Bagca, B., and Avci, C. B. (2016). The roles of non-coding RNAs in Parkinson's disease. *Mol. Biol. Rep.* 43, 1193–1204. doi: 10.1007/s11033-016-4054-3

Manoharan, S., Guillemin, G. J., Abiramasundari, R. S., Essa, M. M., Akbar, M., and Akbar, M. D. (2016). The role of reactive oxygen species in the pathogenesis of Alzheimer's disease, Parkinson's disease and Huntington's disease: a mini review. *Oxid. Med. Cell Longev.* 2016:8590578. doi: 10.1155/2016/8590578

Martire, S., Mosca, L., and D'erme, M. (2015). PARP-1 involvement in neurodegeneration: a focus on Alzheimer's and Parkinson's diseases. *Mech. Ageing Dev.* 146–148, 53–64. doi: 10.1016/j.mad.2015.04.001

McMillan, K. J., Murray, T. K., Bengoa-Vergniory, N., Cordero-Llana, O., Cooper, J., Buckley, A., et al. (2017). Loss of MicroRNA-7 regulation leads to alpha-synuclein accumulation and dopaminergic neuronal loss *in vivo*. *Mol. Ther.* 25, 2404–2414. doi: 10.1016/j.ymthe.2017.08.017

Meng, C., Gao, J., Ma, Q., Sun, Q., and Qiao, T. (2021). LINC00943 knockdown attenuates MPP^+-induced neuronal damage via miR-15b-5p/RAB3IP axis in SK-N-SH cells. *Neurol. Res.* 43, 181–190. doi: 10.1080/01616412.2020.1834290

Meng, X., Zhong, J., Zeng, C., Yung, K. K. L., Zhang, X., Wu, X., et al. (2021). MiR-30a-5p regulates GLT-1 function via a PKCα-mediated ubiquitin degradation pathway in a mouse model of Parkinson's disease. *ACS Chem. Neurosci.* 12, 1578–1592. doi: 10.1021/acschemneuro.1c00076

Merry, C. R., Forrest, M. E., Sabers, J. N., Beard, L., Gao, X. H., Hatzoglou, M., et al. (2015). DNMT1-associated long non-coding RNAs regulate global gene expression and DNA methylation in colon cancer. *Hum. Mol. Genet.* 24, 6240–6253. doi: 10.1093/hmg/ddv343

Moreira, P. I., Nunomura, A., Nakamura, M., Takeda, A., Shenk, J. C., Aliev, G., et al. (2008). Nucleic acid oxidation in Alzheimer disease. *Free Radic. Biol. Med.* 44, 1493–1505. doi: 10.1016/j.freeradbiomed.2008.01.002

Munschauer, M., Nguyen, C. T., Sirokman, K., Hartigan, C. R., Hogstrom, L., Engreitz, J. M., et al. (2018). The NORAD lncRNA assembles a topoisomerase complex critical for genome stability. *Nature* 561, 132–136. doi: 10.1038/s41586-018-0453-z

Mythri, R. B., Venkateshappa, C., Harish, G., Mahadevan, A., Muthane, U. B., Yasha, T. C., et al. (2011). Evaluation of markers of oxidative stress, antioxidant function and astrocytic proliferation in the striatum and frontal cortex of Parkinson's disease brains. *Neurochem. Res.* 36, 1452–1463. doi: 10.1007/s11064-011-0471-9

Nies, Y. H., Mohamad Najib, N. H., Lim, W. L., Kamaruzzaman, M. A., Yahaya, M. F., and Teoh, S. L. (2021). MicroRNA dysregulation in Parkinson's disease: a narrative review. *Front. Neurosci.* 15:660379. doi: 10.3389/fnins.2021.660379

Nunomura, A., Hofer, T., Moreira, P. I., Castellani, R. J., Smith, M. A., and Perry, G. (2009). RNA oxidation in Alzheimer disease and related neurodegenerative disorders. *Acta Neuropathol.* 118, 151–166. doi: 10.1007/s00401-009-0508-1

Nunomura, A., Honda, K., Takeda, A., Hirai, K., Zhu, X., Smith, M. A., et al. (2006). Oxidative damage to RNA in neurodegenerative diseases. *J. Biomed. Biotechnol.* 2006:82323. doi: 10.1155/JBB/2006/82323

Nunomura, A., Lee, H. G., Zhu, X., and Perry, G. (2017). Consequences of RNA oxidation on protein synthesis rate and fidelity: implications for the pathophysiology of neuropsychiatric disorders. *Biochem. Soc. Trans.* 45, 1053–1066. doi: 10.1042/BST20160433

Nunomura, A., Moreira, P. I., Castellani, R. J., Lee, H. G., Zhu, X., Smith, M. A., et al. (2012). Oxidative damage to RNA in aging and neurodegenerative disorders. *Neurotox. Res.* 22, 231–248. doi: 10.1007/s12640-012-9331-x

Nunomura, A., Moreira, P. I., Takeda, A., Smith, M. A., and Perry, G. (2007). Oxidative RNA damage and neurodegeneration. *Curr. Med. Chem.* 14, 2968–2975. doi: 10.2174/092986707782794078

Nunomura, A., and Perry, G. (2020). RNA and oxidative stress in Alzheimer's disease: focus on microRNAs. *Oxid. Med. Cell Longev.* 2020:2638130. doi: 10.1155/2020/2638130

Onyango, I. G. (2008). Mitochondrial dysfunction and oxidative stress in Parkinson's disease. *Neurochem. Res.* 33, 589–597. doi: 10.1007/s11064-007-9482-y

Opara, J., Malecki, A., Malecka, E., and Socha, T. (2017). Motor assessment in Parkinson's disease. *Ann. Agric. Environ. Med.* 24, 411–415. doi: 10.5604/12321966.1232774

Panni, S., Lovering, R. C., Porras, P., and Orchard, S. (2020). Non-coding RNA regulatory networks. *Biochim. Biophys. Acta Gene Regul. Mech.* 1863:194417. doi: 10.1016/j.bbagrm.2019.194417

Pavlou, M. a. S., and Outeiro, T. F. (2017). Epigenetics in Parkinson's disease. *Adv. Exp. Med. Biol.* 978, 363–390. doi: 10.1007/978-3-319-53889-1_19

Peng, F., Gong, W., Li, S., Yin, B., Zhao, C., Liu, W., et al. (2021). circRNA_010383 acts as a sponge for miR-135a and its downregulated expression contributes to renal fibrosis in diabetic nephropathy. *Diabetes* 70, 603–615. doi: 10.2337/db20-0203

Percario, S., Da Silva Barbosa, A., Varela, E. L. P., Gomes, A. R. Q., Ferreira, M. E. S., De Nazare Araujo Moreira, T., et al. (2020). Oxidative stress in Parkinson's disease: potential benefits of antioxidant supplementation. *Oxid. Med. Cell Longev.* 2020:2360872. doi: 10.1155/2020/2360872

Pickrell, A. m., and Youle, R. j. (2015). The roles of PINK1, parkin and mitochondrial fidelity in Parkinson's disease. *Neuron* 85, 257–273. doi: 10.1016/j.neuron.2014.12.007

Prasad, S., Gupta, S. C., and Tyagi, A. K. (2017). Reactive oxygen species (ROS) and cancer: role of antioxidative nutraceuticals. *Cancer Lett.* 387, 95–105. doi: 10.1016/j.canlet.2016.03.042

Puspita, L., Chung, S. Y., and Shim, J. W. (2017). Oxidative stress and cellular pathologies in Parkinson's disease. *Mol. Brain* 10:53. doi: 10.1186/s13041-017-0340-9

Qazi, T. J., Lu, J., Duru, L., Zhao, J., and Qing, H. (2021). Upregulation of mir-132 induces dopaminergic neuronal death via activating SIRT1/P53 pathway. *Neurosci. Lett.* 740:135465. doi: 10.1016/j.neulet.2020.135465

Qian, C., Ye, Y., Mao, H., Yao, L., Sun, X., Wang, B., et al. (2019). Downregulated lncRNA-SNHG1 enhances autophagy and prevents cell death through the miR-221/222 /p27/mTOR pathway in Parkinson's disease. *Exp. Cell Res.* 384:111614. doi: 10.1016/j.yexcr.2019.111614

Qin, X., Zhang, X., Li, P., Wang, M., Yan, L., Pan, P., et al. (2021). MicroRNA-185 activates PI3K/AKT signalling pathway to alleviate dopaminergic neuron damage via targeting IGF1 in Parkinson's disease. *J. Drug Target.* 29, 875–883. doi: 10.1080/1061186X.2021.1886300

Radi, E., Formichi, P., Battisti, C., and Federico, A. (2014). Apoptosis and oxidative stress in neurodegenerative diseases. *J. Alzheimers Dis.* 42, S125–S152. doi: 10.3233/JAD-132738

Raza, C., Anjum, R., and Shakeel, N. U. A. (2019). Parkinson's disease: mechanisms, translational models and management strategies. *Life Sci.* 226, 77–90. doi: 10.1016/j.lfs.2019.03.057

Redensek, S., Flisar, D., Kojovic, M., Kramberger, M. G., Georgiev, D., Pirtosek, Z., et al. (2019). Genetic variability of inflammation and oxidative stress genes does not play a major role in the occurrence of adverse events of dopaminergic treatment in Parkinson's disease. *J. Neuroinflammation* 16:50. doi: 10.1186/s12974-019-1439-y

Reich, S. G., and Savitt, J. M. (2019). Parkinson's disease. *Med. Clin. North Am.* 103, 337–350. doi: 10.1016/j.mcna.2018.10.014

Ren, Y., Li, H., Xie, W., Wei, N., and Liu, M. (2019). MicroRNA195 triggers neuroinflammation in Parkinson's disease in a Rho-associated kinase

1-dependent manner. *Mol. Med. Rep.* 19, 5153–5161. doi: 10.3892/mmr.2019.10176

Rezaei, O., Nateghinia, S., Estiar, M. A., Taheri, M., and Ghafouri-Fard, S. (2021). Assessment of the role of non-coding RNAs in the pathophysiology of Parkinson's disease. *Eur. J. Pharmacol.* 896:173914. doi: 10.1016/j.ejphar.2021.173914

Robea, M. A., Balmus, I. M., Ciobica, A., Strungaru, S., Plavan, G., Gorgan, L. D., et al. (2020). Parkinson's disease-induced zebrafish models: focussing on oxidative stress implications and sleep processes. *Oxid. Med. Cell. Longev.* 2020:1370837. doi: 10.1155/2020/1370837

Rocha, E. M., De Miranda, B., and Sanders, L. H. (2018). Alpha-synuclein: pathology, mitochondrial dysfunction and neuroinflammation in Parkinson's disease. *Neurobiol. Dis.* 109, 249–257. doi: 10.1016/j.nbd.2017.04.004

Rodriguez-Perez, A. I., Sucunza, D., Pedrosa, M. A., Garrido-Gil, P., Kulisevsky, J., Lanciego, J. L., et al. (2018). Angiotensin type 1 receptor antagonists protect against alpha-synuclein-induced neuroinflammation and dopaminergic neuron death. *Neurotherapeutics* 15, 1063–1081. doi: 10.1007/s13311-018-0646-z

Sackner-Bernstein, J. (2021). Estimates of intracellular dopamine in parkinson's disease: a systematic review and meta-analysis. *J. Parkinsons Dis.* 11, 1011–1018. doi: 10.3233/JPD-212715

Sarkar, S., Raymick, J., and Imam, S. (2016). Neuroprotective and therapeutic strategies against Parkinson's disease: recent perspectives. *Int. J. Mol. Sci.* 17:904. doi: 10.3390/ijms17060904

Schapira, A. H., Cooper, J. M., Dexter, D., Clark, J. B., Jenner, P., and Marsden, C. D. (1990a). Mitochondrial complex I deficiency in Parkinson's disease. *J. Neurochem.* 54, 823–827. doi: 10.1111/j.1471-4159.1990.tb02325.x

Schapira, A. H., Holt, I. J., Sweeney, M., Harding, A. E., Jenner, P., and Marsden, C. D. (1990b). Mitochondrial DNA analysis in Parkinson's disease. *Mov. Disord.* 5, 294–297. doi: 10.1002/mds.870050406

Schapira, A. H., Mann, V. M., Cooper, J. M., Dexter, D., Daniel, S. E., Jenner, P., et al. (1990c). Anatomic and disease specificity of NADH CoQ1 reductase (complex I) deficiency in Parkinson's disease. *J. Neurochem.* 55, 2142–2145. doi: 10.1111/j.1471-4159.1990.tb05809.x

Schneider, R. B., Iourinets, J., and Richard, I. H. (2017). Parkinson's disease psychosis: presentation, diagnosis and management. *Neurodegener. Dis. Manage.* 7, 365–376. doi: 10.2217/nmt-2017-0028

Scott, M. S., and Ono, M. (2011). From snoRNA to miRNA: dual function regulatory non-coding RNAs. *Biochimie* 93, 1987–1992. doi: 10.1016/j.biochi.2011.05.026

Shen, Y., Cui, X., Hu, Y., Zhang, Z., and Zhang, Z. (2021a). LncRNA-MIAT regulates the growth of SHSY5Y cells by regulating the miR-34-5p-SYT1 axis and exerts a neuroprotective effect in a mouse model of Parkinson's disease. *Am. J. Transl. Res.* 13, 9993–10013.

Shen, Y., Cui, X., Xu, N., Hu, Y., and Zhang, Z. (2021b). lncRNA PART1 mitigates MPP^+-induced neuronal injury in SH-SY5Y cells via micRNA-106b-5p/MCL1 axis. *Am. J. Transl. Res.* 13, 8897–8908.

Shen, Y. F., Zhu, Z. Y., Qian, S. X., Xu, C. Y., and Wang, Y. P. (2020). miR-30b protects nigrostriatal dopaminergic neurons from MPP^+-induced neurotoxicity via SNCA. *Brain Behav.* 10:e01567. doi: 10.1002/brb3.1567

Singh, A., and Sen, D. (2017). MicroRNAs in Parkinson's disease. *Exp. Brain Res.* 235, 2359–2374. doi: 10.1007/s00221-017-4989-1

Smeyne, M., and Smeyne, R. J. (2013). Glutathione metabolism and Parkinson's disease. *Free Radic. Biol. Med.* 62, 13–25. doi: 10.1016/j.freeradbiomed.2013.05.001

Song, Q., Geng, Y., Li, Y., Wang, L., and Qin, J. (2019). Long noncoding RNA NORAD regulates MPP+-induced Parkinson's disease model cells. *J. Chem. Neuroanat.* 101:101668. doi: 10.1016/j.jchemneu.2019.101668

Song, Z., and Xie, B. (2021). LncRNA OIP5-AS1 reduces alpha-synuclein aggregation and toxicity by targeting miR-126 to activate PLK2 in human neuroblastoma SH-SY5Y cells. *Neurosci. Lett.* 740:135482. doi: 10.1016/j.neulet.2020.135482

Song, X. N., Zhang, L. Q., Liu, D. G., Lin, J., Zheng, J. D., Dai, D. P., et al. (2011). Oxidative damage to RNA and expression patterns of MTH1 in the hippocampi of senescence-accelerated SAMP8 mice and Alzheimer's disease patients. *Neurochem. Res.* 36, 1558–1565. doi: 10.1007/s11064-011-0484-4

Su, Y., Deng, M. F., Xiong, W., Xie, A. J., Guo, J., Liang, Z. H., et al. (2019). MicroRNA-26a/death-associated protein kinase 1 signaling induces synucleinopathy and dopaminergic neuron degeneration in Parkinson's disease. *Biol. Psychiatry* 85, 769–781. doi: 10.1016/j.biopsych.2018.12.008

Subramaniam, S. R., and Chesselet, M. F. (2013). Mitochondrial dysfunction and oxidative stress in Parkinson's disease. *Prog. Neurobiol.* 106–107, 17–32. doi: 10.1016/j.pneurobio.2013.04.004

Sun, Q., Wang, S., Chen, J., Cai, H., Huang, W., Zhang, Y., et al. (2019). MicroRNA-190 alleviates neuronal damage and inhibits neuroinflammation via Nlrp3 in MPTP-induced Parkinson's disease mouse model. *J. Cell. Physiol.* 234, 23379–23387. doi: 10.1002/jcp.28907

Sun, X., Zhang, C., Tao, H., Yao, S., and Wu, X. (2022). LINC00943 acts as miR-338-3p sponge to promote MPP^+-induced SK-N-SH cell injury by directly targeting SP1 in Parkinson's disease. *Brain Res.* 1782:147814. doi: 10.1016/j.brainres.2022.147814

Surendran, S., and Rajasankar, S. (2010). Parkinson's disease: oxidative stress and therapeutic approaches. *Neurol. Sci.* 31, 531–540. doi: 10.1007/s10072-010-0245-1

Szymański, M., and Barciszewski, J. (2002). Beyond the proteome: non-coding regulatory RNAs. *Genome Biol.* 3:reviews0005. doi: 10.1186/gb-2002-3-5-reviews0005

Tao, H., Liu, Y., and Hou, Y. (2020). miRNA-384-5p regulates the progression of Parkinson's disease by targeting SIRT1 in mice and SH-SY5Y cell. *Int. J. Mol. Med.* 45, 441–450. doi: 10.3892/ijmm.2019.4426

Taylor, J. P., Hardy, J., and Fischbeck, K. H. (2002). Toxic proteins in neurodegenerative disease. *Science* 296, 1991–1995. doi: 10.1126/science.1067122

Taylor, J. M., Main, B. S., and Crack, P. J. (2013). Neuroinflammation and oxidative stress: co-conspirators in the pathology of Parkinson's disease. *Neurochem. Int.* 62, 803–819. doi: 10.1016/j.neuint.2012.12.016

Tharmalingam, S., Alhasawi, A., Appanna, V. P., Lemire, J., and Appanna, V. D. (2017). Reactive nitrogen species (RNS)-resistant microbes: adaptation and medical implications. *Biol. Chem.* 398, 1193–1208. doi: 10.1515/hsz-2017-0152

Trist, B. G., Hare, D. J., and Double, K. L. (2019). Oxidative stress in the aging substantia nigra and the etiology of Parkinson's disease. *Aging Cell* 18:e13031. doi: 10.1111/acel.13031

Tsang, A. H., and Chung, K. K. (2009). Oxidative and nitrosative stress in Parkinson's disease. *Biochim. Biophys. Acta* 1792, 643–650. doi: 10.1016/j.bbadis.2008.12.006

Turrens, J. F. (2003). Mitochondrial formation of reactive oxygen species. *J. Physiol.* 552, 335–344. doi: 10.1113/jphysiol.2003.049478

Vallee, A., Lecarpentier, Y., Guillevin, R., and Vallee, J. N. (2020). Circadian rhythms, neuroinflammation and oxidative stress in the story of Parkinson's disease. *Cells* 9:314. doi: 10.3390/cells9020314

Vallée, A., Vallée, J. N., and Lecarpentier, Y. (2021a). Parkinson's disease: potential actions of lithium by targeting the WNT/β-catenin pathway, oxidative stress, inflammation and glutamatergic pathway. *Cells* 10:230. doi: 10.3390/cells10020230

Vallée, A., Vallée, J. N., and Lecarpentier, Y. (2021b). Potential role of cannabidiol in Parkinson's disease by targeting the WNT/β-catenin pathway, oxidative stress and inflammation. *Aging (Albany NY)* 13, 10796–10813. doi: 10.18632/aging.202951

Varcin, M., Bentea, E., Michotte, Y., and Sarre, S. (2012). Oxidative stress in genetic mouse models of Parkinson's disease. *Oxid. Med. Cell. Longev.* 2012:624925. doi: 10.1155/2012/624925

Vidal, R. L., Matus, S., Bargsted, L., and Hetz, C. (2014). Targeting autophagy in neurodegenerative diseases. *Trends Pharmacol. Sci.* 35, 583–591. doi: 10.1016/j.tips.2014.09.002

Wang, Z. (2018). Diverse roles of regulatory non-coding RNAs. *J. Mol. Cell. Biol.* 10, 91–92. doi: 10.1093/jmcb/mjy026

Wang, Y., Cai, Y., Huang, H., Chen, X., Chen, X., Chen, X., et al. (2018). miR-486-3p influences the neurotoxicity of a-synuclein by targeting the SIRT2 gene and the polymorphisms at target sites contributing to Parkinson's disease. *Cell. Physiol. Biochem.* 51, 2732–2745. doi: 10.1159/000495963

Wang, R., Li, Q., He, Y., Yang, Y., Ma, Q., and Li, C. (2020a). miR-29c-3p inhibits microglial NLRP3 inflammasome activation by targeting NFAT5 in Parkinson's disease. *Genes Cells* 25, 364–374. doi: 10.1111/gtc.12764

Wang, R., Yang, Y., Wang, H., He, Y., and Li, C. (2020b). MiR-29c protects against inflammation and apoptosis in Parkinson's disease model *in vivo* and *in vitro* by targeting SP1. *Clin. Exp. Pharmacol. Physiol.* 47, 372–382. doi: 10.1111/1440-1681.13212

Wang, X., Liu, Z., and Wang, F. (2021). MicroRNA-93 blocks signal transducers and activator of transcription 3 to reduce neuronal damage in Parkinson's disease. *Neurochem. Res.* 46, 1859–1868. doi: 10.1007/s11064-021-03333-x

Wang, W., Lv, R., Zhang, J., and Liu, Y. (2021). circSAMD4A participates in the apoptosis and autophagy of dopaminergic neurons via the miR-29c-3p-mediated

AMPK/mTOR pathway in Parkinson's disease. *Mol. Med. Rep.* 24:540. doi: 10.3892/mmr.2021.12179

Wang, R., Ma, Z., Feng, L., Yang, Y., Tan, C., Shi, Q., et al. (2018). LncRNA MIR31HG targets HIF1A and P21 to facilitate head and neck cancer cell proliferation and tumorigenesis by promoting cell-cycle progression. *Mol. Cancer* 17:162. doi: 10.1186/s12943-018-0916-8

Wang, Z., Sun, L., Jia, K., Wang, H., and Wang, X. (2019). miR-9-5p modulates the progression of Parkinson's disease by targeting SIRT1. *Neurosci. Lett.* 701, 226–233. doi: 10.1016/j.neulet.2019.02.038

Wang, J., Wang, W., and Zhai, H. (2019). MicroRNA-124 enhances dopamine receptor expression and neuronal proliferation in mouse models of Parkinson's disease via the hedgehog signaling pathway by targeting EDN2. *Neuroimmunomodulation* 26, 174–187. doi: 10.1159/000501339

Wang, H., Wang, X., Zhang, Y., and Zhao, J. (2021a). LncRNA SNHG1 promotes neuronal injury in Parkinson's disease cell model by miR-181a-5p/CXCL12 axis. *J. Mol. Histol.* 52, 153–163. doi: 10.1007/s10735-020-09931-3

Wang, H., Zhang, M., Wei, T., Zhou, J., Zhang, Y., and Guo, D. (2021b). Long non-coding RNA SNHG1 mediates neuronal damage in Parkinson's disease model cells by regulating miR-216a-3p/Bcl-2-associated X protein. *Ann. Transl. Med.* 9:851. doi: 10.21037/atm-21-1613

Wang, S., Zhang, X., Guo, Y., Rong, H., and Liu, T. (2017). The long noncoding RNA HOTAIR promotes Parkinson's disease by upregulating LRRK2 expression. *Oncotarget* 8, 24449–24456. doi: 10.18632/oncotarget.15511

Wang, C., Zhang, H., and Li, J. (2021). LncRNA JHDM1D-AS1 suppresses MPP^+-induced neuronal injury in Parkinson's disease via miR-134-5p/PIK3R3 axis. *Neurotox. Res.* 39, 1771–1781. doi: 10.1007/s12640-021-00437-8

Wang, X., Zhou, Y., Gao, Q., Ping, D., Wang, Y., Wu, W., et al. (2020). The role of exosomal microRNAs and oxidative stress in neurodegenerative diseases. *Oxid. Med. Cell. Longev.* 2020:3232869. doi: 10.1155/2020/3232869

Wei, M., Cao, L. J., Zheng, J. L., Xue, L. J., Chen, B., Xiao, F., et al. (2017). MicroRNA-181c functions as a protective factor in a 1-methyl-4-phenylpyridinium iodide-induced cellular Parkinson's disease model via BCL2L11. *Eur. Rev. Med. Pharmacol. Sci.* 21, 3296–3304.

Wei, J. W., Huang, K., Yang, C., and Kang, C. S. (2017). Non-coding RNAs as regulators in epigenetics (review). *Oncol. Rep.* 37, 3–9. doi: 10.3892/or.2016.5236

Wen, Z., Zhang, J., Tang, P., Tu, N., Wang, K., and Wu, G. (2018). Overexpression of miR185 inhibits autophagy and apoptosis of dopaminergic neurons by regulating the AMPK/mTOR signaling pathway in Parkinson's disease. *Mol. Med. Rep.* 17, 131–137. doi: 10.3892/mmr.2017.7897

Wong, E., and Cuervo, A. M. (2010). Autophagy gone awry in neurodegenerative diseases. *Nat. Neurosci.* 13, 805–811. doi: 10.1038/nn.2575

Wu, Y. Y., and Kuo, H. C. (2020). Functional roles and networks of non-coding RNAs in the pathogenesis of neurodegenerative diseases. *J. Biomed. Sci.* 27:49. doi: 10.1186/s12929-020-00636-z

Wu, X., Meng, X., Tan, F., Jiao, Z., Zhang, X., Tong, H., et al. (2019). Regulatory mechanism of miR-543-3p on GLT-1 in a mouse model of Parkinson's disease. *ACS Chem. Neurosci.* 10, 1791–1800. doi: 10.1021/acschemneuro.8b00683

Wu, Q., Xi, D. Z., and Wang, Y. H. (2019). MicroRNA-599 regulates the development of Parkinson's disease through mediating LRRK2 expression. *Eur. Rev. Med. Pharmacol. Sci.* 23, 724–731. doi: 10.26355/eurrev_201901_16886

Wu, J., Yu, X., Xue, K., Wu, J., Wang, R., Xie, X., et al. (2020). The inhibition of miR-873 provides therapeutic benefit in a lipopolysaccharide-induced neuroinflammatory model of Parkinson's disease. *Oxid. Med. Cell. Longev.* 2020:8735249. doi: 10.1155/2020/8735249

Xie, N., Qi, J., Li, S., Deng, J., Chen, Y., and Lian, Y. (2019). Upregulated lncRNA small nucleolar RNA host gene 1 promotes 1-methyl-4-phenylpyridinium ion-induced cytotoxicity and reactive oxygen species production through miR-15b-5p/GSK3beta axis in human dopaminergic SH-SY5Y cells. *J. Cell. Biochem.* 120, 5790–5801. doi: 10.1002/jcb.27865

Xie, S. P., Zhou, F., Li, J., and Duan, S. J. (2019). NEAT1 regulates MPP^+-induced neuronal injury by targeting miR-124 in neuroblastoma cells. *Neurosci. Lett.* 708:134340. doi: 10.1016/j.neulet.2019.134340

Xin, C., and Liu, J. (2021). Long Non-coding RNAs in Parkinson's disease. *Neurochem. Res.* 46, 1031–1042. doi: 10.1007/s11064-021-03230-3

Xu, Z., Huang, J., Gao, M., Guo, G., Zeng, S., Chen, X., et al. (2021). Current perspectives on the clinical implications of oxidative RNA damage in aging research: challenges and opportunities. *Geroscience* 43, 487–505. doi: 10.1007/s11357-020-00209-w

Xu, W., Zhang, L., Geng, Y., Liu, Y., and Zhang, N. (2020). Long noncoding RNA GAS5 promotes microglial inflammatory response in Parkinson's disease by regulating NLRP3 pathway through sponging miR-223-3p. *Int. Immunopharmacol.* 85:106614. doi: 10.1016/j.intimp.2020.106614

Xu, X., Zhuang, C., Wu, Z., Qiu, H., Feng, H., and Wu, J. (2018). LincRNA-p21 inhibits cell viability and promotes cell apoptosis in Parkinson's disease through activating alpha-synuclein expression. *Biomed. Res. Int.* 2018:8181374. doi: 10.1155/2018/8181374

Yan, W., Chen, Z. Y., Chen, J. Q., and Chen, H. M. (2018). LncRNA NEAT1 promotes autophagy in MPTP-induced Parkinson's disease through stabilizing PINK1 protein. *Biochem. Biophys. Res. Commun.* 496, 1019–1024. doi: 10.1016/j.bbrc.2017.12.149

Yan, L., Li, L., and Lei, J. (2021). Long noncoding RNA small nucleolar RNA host gene 12/microRNA-138-5p/nuclear factor I/B regulates neuronal apoptosis, inflammatory response and oxidative stress in Parkinson's disease. *Bioengineered* 12, 12867–12879. doi: 10.1080/21655979.2021.2005928

Yan, M. H., Wang, X., and Zhu, X. (2013). Mitochondrial defects and oxidative stress in Alzheimer disease and Parkinson disease. *Free Radic. Biol. Med.* 62, 90–101. doi: 10.1016/j.freeradbiomed.2012.11.014

Yan, L. L., and Zaher, H. S. (2019). How do cells cope with RNA damage and its consequences? *J. Biol. Chem.* 294, 15158–15171. doi: 10.1074/jbc.REV119.006513

Yang, S., Yang, H., Luo, Y., Deng, X., Zhou, Y., and Hu, B. (2021). Long non-coding RNAs in neurodegenerative diseases. *Neurochem. Int.* 148:105096. doi: 10.1016/j.neuint.2021.105096

Yang, X., Zhang, M., Wei, M., Wang, A., Deng, Y., and Cao, H. (2020). MicroRNA-216a inhibits neuronal apoptosis in a cellular Parkinson's disease model by targeting Bax. *Metab. Brain Dis.* 35, 627–635. doi: 10.1007/s11011-020-00546-x

Yao, L., Ye, Y., Mao, H., Lu, F., He, X., Lu, G., et al. (2018). MicroRNA-124 regulates the expression of MEKK3 in the inflammatory pathogenesis of Parkinson's disease. *J. Neuroinflammation* 15:13. doi: 10.1186/s12974-018-1053-4

Yildirim, O., Izgu, E. C., Damle, M., Chalei, V., Ji, F., Sadreyev, R. I., et al. (2020). S-phase enriched non-coding RNAs regulate gene expression and cell cycle progression. *Cell Rep.* 31:107629. doi: 10.1016/j.celrep.2020.107629

Yuan, H., Zheng, J. C., Liu, P., Zhang, S. F., Xu, J. Y., and Bai, L. M. (2007). Pathogenesis of Parkinson's disease: oxidative stress, environmental impact factors and inflammatory processes. *Neurosci. Bull.* 23, 125–130. doi: 10.1007/s12264-007-0018-x

Zaman, V., Shields, D. C., Shams, R., Drasites, K. P., Matzelle, D., Haque, A., et al. (2021). Cellular and molecular pathophysiology in the progression of Parkinson's disease. *Metab. Brain Dis.* 36, 815–827. doi: 10.1007/s11011-021-00689-5

Zhai, K., Liu, B., and Gao, L. (2020). Long-noncoding RNA TUG1 promotes Parkinson's disease via modulating MiR-152-3p/PTEN pathway. *Hum. Gene Ther.* 31, 1274–1287. doi: 10.1089/hum.2020.106

Zhang, J., Dongwei, Z., Zhang, Z., Xinhui, Q., Kunwang, B., Guohui, L., et al. (2019). miR-let-7a suppresses alpha-Synuclein-induced microglia inflammation through targeting STAT3 in Parkinson's disease. *Biochem. Biophys. Res. Commun.* 519, 740–746. doi: 10.1016/j.bbrc.2019.08.140

Zhang, X., and Li, L. (2020). The significance of 8-oxoGsn in aging-related diseases. *Aging Dis.* 11, 1329–1338. doi: 10.14336/AD.2019.1021

Zhang, L., Kang, W., Lu, X., Ma, S., Dong, L., and Zou, B. (2018). LncRNA CASC11 promoted gastric cancer cell proliferation, migration and invasion *in vitro* by regulating cell cycle pathway. *Cell Cycle* 17, 1886–1900. doi: 10.1080/15384101.2018.1502574

Zhang, J., Perry, G., Smith, M. A., Robertson, D., Olson, S. J., Graham, D. G., et al. (1999). Parkinson's disease is associated with oxidative damage to cytoplasmic DNA and RNA in substantia nigra neurons. *Am. J. Pathol.* 154, 1423–1429. doi: 10.1016/S0002-9440(10)65396-5

Zhang, H., Wang, Z., Hu, K., and Liu, H. (2021). Downregulation of long noncoding RNA SNHG7 protects against inflammation and apoptosis in Parkinson's disease model by targeting the miR-425-5p/TRAF5/NF-κB axis. *J. Biochem. Mol. Toxicol.* 35:e22867. doi: 10.1002/jbt.22867

Zhang, L., Wang, J., Liu, Q., Xiao, Z., and Dai, Q. (2020). Knockdown of long non-coding RNA AL049437 mitigates MPP^+-induced neuronal injury in SH-SY5Y cells via the microRNA-205-5p/MAPK1 axis. *Neurotoxicology* 78, 29–35. doi: 10.1016/j.neuro.2020.02.004

Zhang, L. M., Wang, M. H., Yang, H. C., Tian, T., Sun, G. F., Ji, Y. F., et al. (2019). Dopaminergic neuron injury in Parkinson's disease is mitigated by interfering lncRNA SNHG14 expression to regulate the miR-133b/ α-synuclein pathway. *Aging (Albany NY)* 11, 9264–9279. doi: 10.18632/aging.102330

Zhang, P., Wu, W., Chen, Q., and Chen, M. (2019). Non-coding RNAs and their integrated networks. *J. Integr. Bioinform.* 16:20190027. doi: 10.1515/jib-2019-0027

Zhang, Y., Xia, Q., and Lin, J. (2020). LncRNA H19 attenuates apoptosis in MPTP-induced Parkinson's disease through regulating miR-585-

3p/PIK3R3. *Neurochem. Res.* 45, 1700–1710. doi: 10.1007/s11064-020-03035-w

Zhang, J., Yang, Y., Zhou, C., Zhu, R., Xiao, X., Zhou, B., et al. (2022). LncRNA miR-17-92a-1 cluster host gene (MIR17HG) promotes neuronal damage and microglial activation by targeting the microRNA-153-3p/alpha-synuclein axis in Parkinson's disease. *Bioengineered* 13, 4493–4516. doi: 10.1080/21655979.2022.2033409

Zhao, Y., Xie, Y., Yao, W. Y., Wang, Y. Y., and Song, N. (2022). Long non-coding RNA Opa interacting protein 5-antisense RNA 1 promotes mitochondrial autophagy and protects SH-SY5Y cells from 1-methyl-4-phenylpyridine-induced damage by binding to microRNA-137 and upregulating NIX. *Kaohsiung J. Med. Sci.* 38, 207–217. doi: 10.1002/kjm2.12485

Zhao, J., Yang, M., Li, Q., Pei, X., and Zhu, X. (2020a). miR-132-5p regulates apoptosis and autophagy in MPTP model of Parkinson's disease by targeting ULK1. *Neuroreport* 31, 959–965. doi: 10.1097/WNR.0000000000001494

Zhao, J., Li, H., and Chang, N. (2020b). LncRNA HOTAIR promotes MPP^+-induced neuronal injury in Parkinson's disease by regulating the miR-874-5p/ATG10 axis. *EXCLI J.* 19, 1141–1153. doi: 10.17179/excli2020-2286

Zhao, J., Yu, S., Zheng, Y., Yang, H., and Zhang, J. (2017). Oxidative modification and its implications for the neurodegeneration of Parkinson's disease. *Mol. Neurobiol.* 54, 1404–1418. doi: 10.1007/s12035-016-9743-3

Zheng, Y., Dong, L., Liu, N., Luo, X., and He, Z. (2020). Mir-141-3p regulates apoptosis and mitochondrial membrane potential via targeting sirtuin1 in a 1-methyl-4-phenylpyridinium *in vitro* model of Parkinson's disease. *Biomed. Res. Int.* 2020:7239895. doi: 10.1002/kjm2.12485

Zhou, W. Y., Cai, Z. R., Liu, J., Wang, D. S., Ju, H. Q., and Xu, R. H. (2020). Circular RNA: metabolism, functions and interactions with proteins. *Mol. Cancer* 19:172. doi: 10.1186/s12943-020-01286-3

Zhou, L., Yang, L., Li, Y. J., Mei, R., Yu, H. L., Gong, Y., et al. (2018). MicroRNA-128 protects dopamine neurons from apoptosis and upregulates the expression of excitatory amino acid transporter 4 in Parkinson's disease by binding to AXIN1. *Cell. Physiol. Biochem.* 51, 2275–2289. doi: 10.1159/000495872

Zhou, J., Zhao, Y., Li, Z., Zhu, M., Wang, Z., Li, Y., et al. (2020). miR-103a-3p regulates mitophagy in Parkinson's disease through Parkin/Ambra1 signaling. *Pharmacol. Res.* 160:105197. doi: 10.1016/j.phrs.2020.105197

Zhou, S., Zhang, D., Guo, J., Chen, Z., Chen, Y., and Zhang, J. (2021). Deficiency of NEAT1 prevented MPP^+-induced inflammatory response, oxidative stress and apoptosis in dopaminergic SK-N-SH neuroblastoma cells via miR-1277-5p/ARHGAP26 axis. *Brain Res.* 1750:147156. doi: 10.1016/j.brainres.2020.147156

Zhou, S., Zhang, D., Guo, J., Zhang, J., and Chen, Y. (2020). Knockdown of SNHG14 alleviates MPP^+-induced injury in the cell model of Parkinson's disease by targeting the miR-214-3p/KLF4 axis. *Front. Neurosci.* 14:930. doi: 10.3389/fnins.2020.00930

Zhou, Q., Zhang, M. M., Liu, M., Tan, Z. G., Qin, Q. L., and Jiang, Y. G. (2021). LncRNA XIST sponges miR-199a-3p to modulate the Sp1/LRRK2 signal pathway to accelerate Parkinson's disease progression. *Aging (Albany NY)* 13, 4115–4137. doi: 10.18632/aging.202378

Zhu, W., Zhang, H., Gao, J., and Xu, Y. (2021). Silencing of miR-497-5p inhibits cell apoptosis and promotes autophagy in Parkinson's disease by upregulation of FGF2. *Environ. Toxicol.* 36, 2302–2312. doi: 10.1002/tox.23344

Zuo, L., and Motherwell, M. S. (2013). The impact of reactive oxygen species and genetic mitochondrial mutations in Parkinson's disease. *Gene* 532, 18–23. doi: 10.1016/j.gene.2013.07.085

frontiers | Frontiers in Aging Neuroscience

TYPE Original Research
PUBLISHED 01 September 2022
DOI 10.3389/fnagi.2022.979183

Check for updates

OPEN ACCESS

EDITED BY
Yuzhen Xu,
The Second Affiliated Hospital of Shandong First Medical University, China

REVIEWED BY
Xize Jia,
Hangzhou Normal University, China
Francesco Amenta,
University of Camerino, Italy

*CORRESPONDENCE
Fengjiao Sun
bydxsfj@126.com
Gaohua Wang
wgh6402@163.com
Yi Zhong
zhongyisq@gmail.com

†These authors have contributed equally to this work and share first authorship

SPECIALTY SECTION
This article was submitted to Cellular and Molecular Mechanisms of Brain-aging, a section of the journal Frontiers in Aging Neuroscience

RECEIVED 27 June 2022
ACCEPTED 12 August 2022
PUBLISHED 01 September 2022

CITATION
Gao Y, Zhao X, Huang J, Wang S, Chen X, Li M, Sun F, Wang G and Zhong Y (2022) Abnormal regional homogeneity in right caudate as a potential neuroimaging biomarker for mild cognitive impairment: A resting-state fMRI study and support vector machine analysis. *Front. Aging Neurosci.* 14:979183. doi: 10.3389/fnagi.2022.979183

COPYRIGHT
© 2022 Gao, Zhao, Huang, Wang, Chen, Li, Sun, Wang and Zhong. This is an open-access article distributed under the terms of the Creative Commons Attribution License (CC BY). The use, distribution or reproduction in other forums is permitted, provided the original author(s) and the copyright owner(s) are credited and that the original publication in this journal is cited, in accordance with accepted academic practice. No use, distribution or reproduction is permitted which does not comply with these terms.

Abnormal regional homogeneity in right caudate as a potential neuroimaging biomarker for mild cognitive impairment: A resting-state fMRI study and support vector machine analysis

Yujun Gao[1†], Xinfu Zhao[2†], JiChao Huang[3†], Sanwang Wang[1], Xuan Chen[4], Mingzhe Li[5], Fengjiao Sun[6*], Gaohua Wang[1*] and Yi Zhong[7,8*]

[1]Department of Psychiatry, Renmin Hospital of Wuhan University, Wuhan, China, [2]Wuxi Mental Health Center, Nanjing Medical University, Wuxi, China, [3]Affiliated Shuyang Hospital, Nanjing University of Chinese Medicine, Suqian, China, [4]Department of Psychiatry, The First Affiliated Hospital of Xinxiang Medical University, Xinxiang, China, [5]Peking-Tsinghua Center for Life Sciences and PKU-IDG/McGovern Institute for Brain Research, Peking University, Beijing, China, [6]Medical Research Center, Binzhou Medical University Hospital, Binzhou, China, [7]Department of Neuroscience, City University of Hong Kong, Kowloon, Hong Kong SAR, China, [8]NHC Key Laboratory of Mental Health, Peking University Sixth Hospital, Peking University Institute of Mental Health, Peking University, Beijing, China

Objective: Mild cognitive impairment (MCI) is a heterogeneous syndrome characterized by cognitive impairment on neurocognitive tests but accompanied by relatively intact daily activities. Due to high variation and no objective methods for diagnosing and treating MCI, guidance on neuroimaging is needed. The study has explored the neuroimaging biomarkers using the support vector machine (SVM) method to predict MCI.

Methods: In total, 53 patients with MCI and 68 healthy controls were involved in scanning resting-state functional magnetic resonance imaging (rs-fMRI). Neurocognitive testing and Structured Clinical Interview, such as Alzheimer's Disease Assessment Scale-Cognitive Subscale (ADAS-Cog) test, Activity of Daily Living (ADL) Scale, Hachinski Ischemic Score (HIS), Clinical Dementia Rating (CDR), Montreal Cognitive Assessment (MoCA), and Hamilton Rating Scale for Depression (HRSD), were utilized to assess participants' cognitive state. Neuroimaging data were analyzed with the regional homogeneity (ReHo) and SVM methods.

Results: Compared with healthy comparisons (HCs), ReHo of patients with MCI was decreased in the right caudate. In addition, the SVM classification achieved an overall accuracy of 68.6%, sensitivity of 62.26%, and specificity of 58.82%.

Conclusion: The results suggest that abnormal neural activity in the right cerebrum may play a vital role in the pathophysiological process of MCI. Moreover, the ReHo in the right caudate may serve as a neuroimaging biomarker for MCI, which can provide objective guidance on diagnosing and managing MCI in the future.

KEYWORDS

mild cognitive impairment, neuroimaging, fMRI, regional homogeneity, support vector machine, machine learning, biomarker

Introduction

Mild cognitive impairment (MCI) is a heterogeneous syndrome defined as deficits on neurocognitive testing but without significant damage to activities of daily living (ADLs) (Winblad et al., 2004). Objective evidence cognitive or functional decline, labeled "subjective cognitive decline," does not always accompany subjective awareness of cognitive impairment (Tao et al., 2021). MCI reflects that cognitive function deteriorates in neuropsychological testing, but ADL is intact relatively (Petersen, 2006).

One characteristic of MCI is heterogeneous, which means that about 5–15% of the patients are at the risk of getting dementia every year. At the same time, about half of the patients keep stable at 5 years, and symptoms sort out over time in the minority (Dunne et al., 2021). The collaboration of Cohort Studies of Memory in an International Consortium (COSMIC), which spread standard diagnostic criteria to estimate the prevalence of MCI more reliably across different regions, confirmed the prevalence of MCI in adults over 60 years up to 6% across 11 studies (Sachdev et al., 2015).

The guideline date updated by the American Academy of Neurology estimated a prevalence of 6.7% in 65–69-year-olds and 25% for 80–84-year-olds (Livingston et al., 2017). Jia et al. estimated that overall MCI prevalence was 15.5% in China, representing 38.77 million people (Jia et al., 2020). Consistently, 10 million new instances of dementia are enlisted, and it is assessed that 13,500,000 individuals are associated with the risk of dementia by 2050 (WHO., 2022). It presents an opportunity for reducing vascular risk and altering behavioral patterns when a diagnosis of MCI is made. Given diagnostic and therapeutic practice variation, things could change if a more definitive diagnosis is available. Therefore, standard national guidance is eagerly needed for using neuroimaging in MCI (Gillis et al., 2019; McWhirter et al., 2020). There is a need for precise prognosis methods to ensure that the diagnosis of MCI is a possibility for people to prevent the risk of Alzheimer's disease (AD). To improve the specificity and sensitivity of MCI diagnosis, we need cognitive testing and neuroimaging with more evidence.

Resting-state functional magnetic resonance imaging (rs-fMRI) is a non-invasive imaging tool to detect brain activity (Biswal et al., 1995; Smitha et al., 2017). As shown in previous research, rs-fMRI has been confirmed as a reliable instrument to explore the brain's mechanism, reflecting the signature of the brain's neural network (van den Heuvel and Hulshoff Pol, 2010; Pan et al., 2021). Regional homogeneity (ReHo) is a test-retest method to detect the characteristic of brain connectome (Biswal, 2012; Cheng et al., 2019; Geng et al., 2019; Hou et al., 2021). The support vector machine (SVM) is among the most popular methods in the machine learning (ML) that has exceeded practical neuroimage analysis in the past 20 years (Orru et al., 2012; Pisner and Schnyer, 2020). SVM has been applied in different fields and addresses various classification problems because of its relative simplicity and flexibility (Gori et al., 2015; Cheng et al., 2021; Shan et al., 2021; Gao et al., 2022). There have been hundreds of studies using ML to accurately classify patients with heterogeneous mental and neurodegenerative disorders, which make improvements in the early diagnosis.

In brain disorders research, SVMs are deployed by multivoxel pattern analysis (MVPA) and solve plenty of clinical problems because of their relative simplicity. Even if data are high dimensional, there is a lower risk of overfitting in SVMs (Zhang et al., 2020). Recently, SVMs have been applied in precision medicine. SVM analysis can predict the diagnosis and prognosis, particularly for patients with brain diseases, such as Alzheimer's (Franzmeier et al., 2020; Xie et al., 2022), schizophrenia's (Chand et al., 2022; Lei et al., 2022), and depression's (Al-Hakeim et al., 2019; Bone et al., 2021). The results would make improvement in the diagnostic accuracy.

More research participation is required to increase the investment in neuroimaging biomarkers to achieve this goal. To determine whether there are distinct or specific alterations in MCI that can be used to differentiate MCI from healthy controls, we examined specific or distinctive alterations in MCI. The study hypothesized that patients with MCI have abnormal ReHo in the brain region and the abnormal region serves as a biomarker to aid in diagnosing and prediction of MCI.

Methods

Participants and procedures

In total, 140 subjects were consecutively recruited from Wuxi Mental Health Center in China between June 2018 and May 2022.

In total, 70 patients with MCI and 70 age-, education-, and gender-matched healthy subjects, which were right-handed, were recruited. The patients were diagnosed by two psychiatrists with criteria in the Structured Clinical Interview of the fifth version of the Diagnostic and Statistical Manual of Mental Disorders (DSM-V) independently. All participants were assessed by Alzheimer's Disease Assessment Scale-Cognitive Subscale (ADAS-Cog) test (Kueper et al., 2018), ADL Scale, Hachinski Ischemic Score (HIS), Hamilton Rating Scale for Depression-17 (HRSD), Clinical Dementia Rating (CDR), and Montreal Cognitive Assessment (MoCA). The patients who met the criteria (CDR $\geq$ 0.5, MoCA $<$ 26) were included. Exclusion criteria were as follows: history of brain damage, other neurological disorders, other mental disorders, such as acute illness, substance abuse, schizophrenia, dementia, bipolar disorder, and other severe limb or head tremor. All healthy comparisons (HCs) were recruited from the community as volunteers without a history of neurologic disorders. In control comparisons, neuropsychology evaluations were also performed the same as patients with MCI. The study was approved by the Medical Ethics Committee of Wuxi Mental Health Center. Each participant had written informed consent and submitted it before enrollment.

Materials

ADAS-Cog test

The ADAS-Cog helps to evaluate cognition and differentiation between normal and impaired cognitive functioning. The administrator accumulates points for the errors in the test task for a total score. The score ranges from 0 to 70 and a score of 70 epitomizes the most severe impairment (Cano et al., 2010).

The ADL scale

The ADL is used to describe fundamental skills in taking care of oneself independently (Edemekong et al., 2022). ADL is used as an indicator of a person's functional status and to assess older adults' functional status (Árnadóttir, 2016).

Hachinski ischemic score

The vascular burden is considered a risk factor for cognitive dysfunction. HIS is a clinical tool used to identify vascular dementia (Johnson et al., 2014). The scores were related to cognitive functioning, such as global cognition, executive functioning, immediate memory, and attention. HIS can significantly predict the diagnosis of MCI (Paul et al., 2003).

Hamilton rating scale for depression

A 17-item HRSD was used to assess the symptom of depression (Hamilton, 1967).

Clinical dementia rating

Clinical Dementia Rating is a global rating device calculated on six behavioral and cognitive fields, such as memory, orientation, problem solving, judgment, personal care, and home and hobbies performance. The CDR is based on a scale ranging from 0 to 3: no dementia (CDR = 0), questionable dementia (CDR = 0.5), MCI (CDR = 1), moderate cognitive impairment (CDR = 2), and severe cognitive impairment (CDR = 3) (Khan, 2016).

Montreal cognitive assessment

Montreal Cognitive Assessment score ranges from 0 to 30 points, and a cut score of 26 represents excellent specificity and sensitivity separating MCI from healthy subjects (De Reuck, 2020).

Image acquisition

All the rs-MRI data were obtained by an Achieva 3.0T Scanner (Philips, Amsterdam, the Netherlands) at the Wuxi Mental Health Center on the first day. Participants were instructed to remain still, close their eyes, and avoid falling asleep during the scan. Echo-planar imaging of resting-state functional images was performed using the following parameters: repetition time/echo time (TR/TE) 2,000/30 ms, 31 slices, 90° flip angles, 22 cm $\times$ 22 cm field of view (FOV), 5 mm slice thickness, and 1 mm pitch.

Data preprocessing

Imaging data were preprocessed with Data Processing Assistant for Resting-State (DPARSF) software in MATLAB (Yan et al., 2016). It was necessary to exclude the first five time points to minimize the error caused by the initial signal instability and participants' adaptation times. Following this, time-slice correction and head movement correction were completed. Maximum displacements in x-, y-, or z-axes and maximum rotations in angular direction were no more than 2 mm and 2°,

TABLE 1 Demographics of the study population.

	MCI ($n = 53$)	Control ($n = 68$)	P
Age(years)	69.07 ± 4.932	68.80 ± 4.951	$P > 0.05$
Sex(M/F)	40/30	34/34	$P > 0.05$
Education (years)	10.04 ± 3.321	9.75 ± 3.414	$P > 0.05$
ADL	14.243 ± 0.824	14.059 ± 0.237	$P > 0.05$
HRSD	2.114 ± 2.446	1.441 ± 2.153	$P > 0.05$
ADAS-Cog	9.527 ± 3.480	7.066 ± 2.760	$P < 0.05$
HIS	1.371 ± 0.819	1.044 ± 0.818	$P < 0.05$
CDR	0.814 ± 0.889	0.316 ± 0.487	$P < 0.05$
MoCA	22.814 ± 4.150	26.265 ± 1.671	$P < 0.05$

ADAS-Cog, Alzheimer's Disease Assessment Scale-Cognitive Subscale test; ADL, Activity of Daily Living Scale; HIS, Hachinski ischemic Score; CDR, Clinical Dementia Rating; MoCA, Montreal Cognitive Assessment; HRSD, Hamilton Rating Scale for Depression. The p-value was obtained by t-tests and gender was compared by Chi-square test.

TABLE 2 ReHo difference among MCI and healthy subjects.

Brain areas (AAL)	Peak MNI coordinates			Cluster size	Peak T value
	X	Y	Z		
MCI vs. CONTROL Right caudate	6	−3	21	43	−4.0112

ReHo, regional homogeneity; MCI, mild cognitive impairment; MNI, Montreal Neurological Institute.

respectively. Image data were corrected for spatial normalization to the standard Montreal Neurological Institute (MNI) space. Samples were resampled to 3 × 3 × 3 mm. Filter was used along with linear detrending (0.01–0.08 Hz) and linearly detrended. A series of covariates were removed that included the signal from a region centered in the white matter, and six head-motion parameters were calculated from rigid bodies (Gao et al., 2022).

ReHo analyses

Using the Kendall coefficient of concordance (KCC) between the time series of a given voxel and the 26 nearest voxels, we generated the ReHo map for each participant. The non-brain tissues were then removed using a whole-brain mask. As part of the standardization process, we divided each ReHo map by its global mean KCC within the whole-brain mask. Spatial smoothing of the ReHo maps was performed with a Gaussian kernel of 4.5 mm full-width at half-maximum (FWHM).

Statistical analysis

With the help of two-sample t-tests, age, education, and whole-brain voxel-based maps were compared. The gender was compared by the chi-square test. By controlling topological family-wise errors (FWEs) computed using Gaussian Random Field theory, all significant clusters were corrected at the cluster level. The threshold was $p < 0.01$ for cluster-forming voxel-level heights, and the threshold was $p < 0.05$ for cluster-wise FWEs. Gray matter (GM) masks were generated group wise, i.e., voxels.

Classification analysis

For each participant, we calculated the Pearson correlation between the time series of all pairs of brain voxels. In MATLAB, LIBSVM was used to run the SVM method. With ReHo values extracted from different brain regions, SVM was applied to test the ability to distinguish patients from healthy controls.

Results

Demographics

From June 2018 to May 2022, 140 participants were enrolled. Among all participants, 17 patients and 2 HCs were excluded because of the head motion parameters. The remaining 53 patients with MCI and 68 age-, education-, and sex-matched control volunteers were recruited. The subjects were divided into 2 groups: patients with MCI (n = 53) and HCs (n = 68). Demographic information and clinical assessment scores are shown in Table 1. There were no significant differences in age, gender, and year of education between the two groups ($p > 0.05$). Compared with the HCs, MCI patients has poorer scores in all cognition tests, including ADAS-Cog test ($p < 0.05$), HIS ($p < 0.05$), CDR ($p < 0.05$), and MoCA ($p < 0.05$). There was no significance in the ADL Scale and HRSD between groups ($p > 0.05$, Table 1).

ReHO: Patients vs. HCs

Compared with HCs, patients with MCI displayed a significantly decreased ReHo in the right caudate (Table 2 and Figure 1).

The results of the SVM

A combination of decreased ReHo in right caudate was a potential biomarker to diagnose MCI by SVM. The SVM classification achieved an overall accuracy (68.6%), sensitivity (62.26%), and specificity (58.82%) (Figure 2).

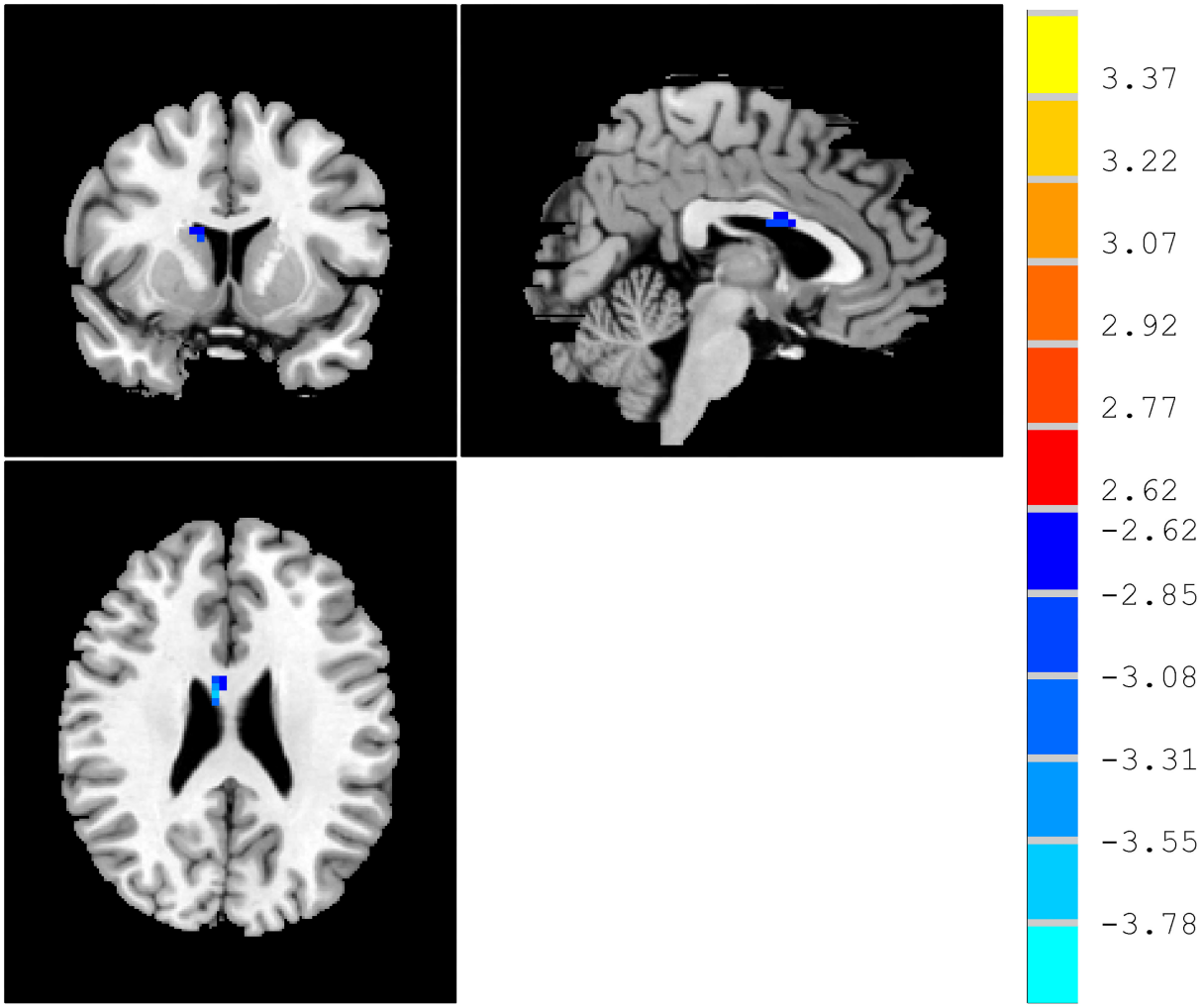

FIGURE 1
ReHo differences between patients with MCI and HCs. Red and blue denote higher and lower ReHo, respectively, and the color bars represent the *t*-values from the *t*-test of the group analysis. ReHo, regional homogeneity; MCI, mild cognitive impairment; HCs, healthy comparisons.

Discussion

Mild cognitive impairment could be a prodromal stage of dementia. Over the past decade, neuroimaging has gained increasing attention as a predictor of mental disorders (Grueso and Viejo-Sobera, 2021). The association between MCI and right caudate was assessed in fMRI comprising 53 MCI patients with a range of demographic characteristics, and HCs were matched to patients. As shown in the results, when compared with the HCs, patients with MCI had poorer scores in all cognition tests, such as ADAS-Cog test ($p < 0.05$), HIS ($p < 0.05$), CDR ($p < 0.05$), and MoCA ($p < 0.05$). There was no significance in the ADL Scale and HRSD between the two groups ($p > 0.05$). Patients with MCI at times will ultimately advance to dementia, yet the cognitive symptoms have not ultimately shown.

Compared with HCs, the ReHo of patients with MCI in the right caudate is lower than HCs. The caudate nucleus plays a critical role in various higher neurological functions. It is a region that is not only in executive functioning but also related to learning, memory, motivation, and emotion (Fisher et al., 2006; Grahn et al., 2008). One can consider the head of the caudate nucleus as the cognitive and emotional portion (Seger and Cincotta, 2005; Graff-Radford et al., 2017). It is possible that the caudate was restricted from overactivity due to its significant involvement in the working memory task. Ekman et al. found in patients with Parkinson's disease and MCI, blood-oxygen-level-dependent (BOLD) signals are reduced in the right caudate and frontal cortex, as well as impaired presynaptic function in the caudate (Ekman et al., 2012). Working memory is updated by the caudate and anterior cingulate cortex and their functional changes are associated with Parkinson's disease with

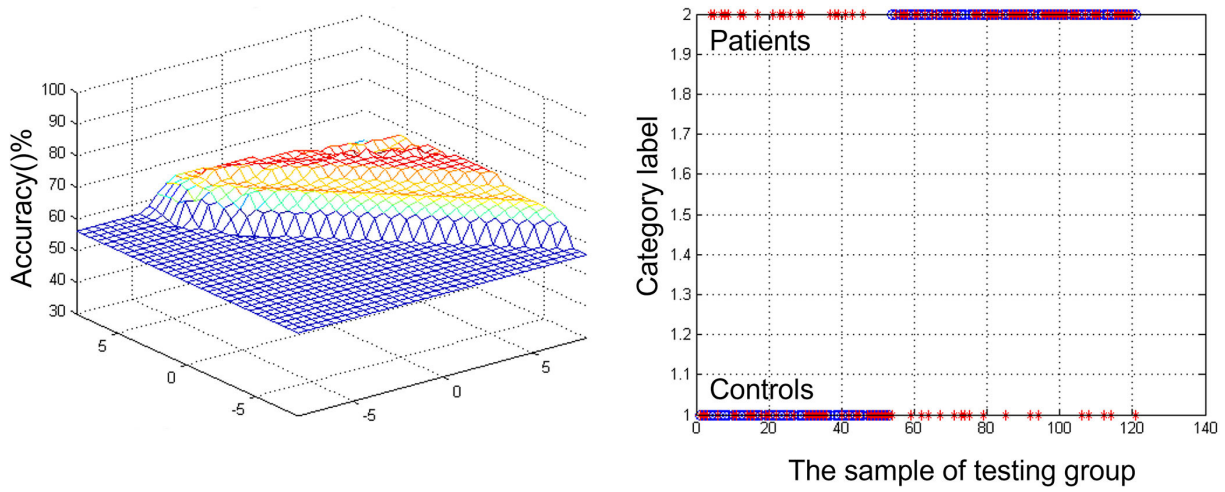

FIGURE 2
Visualizing classifications based on support vector machine (SVM) by the decreased regional homogeneity (ReHo) values in the right caudate to discriminate patients with mild cognitive impairment (MCI) from healthy comparisons. **(Left)** SVM parameters' result of 3D view. **(Right)** Classified map of the ReHo values in the right caudate.

MCI. Specifically, Qiu et al. found that MCI smokers showed decreased functional connectivity of right caudate to left inferior parietal lobule (Qiu et al., 2022). Compared to controls, caudate volumes were lower in MCI (4.43% right) (Madsen et al., 2010).

Nevertheless, in the early stages, although biomarkers might be found in the result of fMRI, it stays trying for the location of MCI to dementia progression in clinical practice (Zhang et al., 2012). For this reason, finding the contrast between those patients with MCI and healthy subjects is significant. To tackle this issue, researchers established neuroimaging datasets from patients with MCI, HCs, and different variables, such as demographic, genetic, and cognitive measurements (Pellegrini et al., 2018). SVM can characterize non-linear choice limits in high-layered variable space by tackling a quadratic improvement issue (Grueso and Viejo-Sobera, 2021). This technique can provide a valuable insight into a disease that occurs with neural patterns, such as autism (Gori et al., 2015), attention deficit hyperactivity disorder (Park et al., 2016), and schizophrenia (Cheng et al., 2015; Pina-Camacho et al., 2015; Arbabshirani et al., 2017). In the study, the decreased ReHo of right caudate was a potential biomarker to diagnose MCI by SVM. The SVM results showed a diagnostic accuracy of 68.6% (83/121). The ReHo was decreased in the right caudate, with a sensitivity of 62.26% (33/53) and a specificity of 58.82% (40/68). The level of prediction may seem modest, but it must be viewed in the context of other risk factors that patients may have for progression over the next 20–30 years. Since these patients usually coexist, it is crucial to understand how they interact. The results suggest that future therapy studies should directly verify the ability to deliver compounds to the caudate nucleus as the cognitive and emotional portion.

In summary, this study is the first to demonstrate the relation between the right cerebrum and MCI using ML based on fMRI imaging data. The right cerebrum may play an important role in early intervention in patients with MCI. It would be interesting to combine ReHo value and MCI to fully investigate its diagnostic accuracy.

They can serve as an objective and reliable complementary tool to improve diagnosis accuracy and ultimately predict the MCI. In addition, by classifying biomarkers, it is possible to revise clinical diagnosis in cases of uncertain diagnosis. The results add to a superior comprehension of the mechanism in the cognitive decline of patients with MCI.

Limitation

With regard to the research methods, some limitations need to be acknowledged. First, cross-sectional design limits our ability to interpret causal relationships between patients with MCI and HCs. This study needs to be confirmed in the future to increase the likelihood of generalizing its results to MCI patients with different clinical characteristics. Second, several factors confound our study, such as illness duration, medication, lifestyle, and diet. In the future, we will explore potential variations. Third, there was no information available about whether changes occurred in the caudate before the development of MCI. Understanding the cause and effect may be possible through long-term follow-up observations. Fourth, we do not make the use of the medial temporal lobe atrophy (MTA) score (Scheltens' scale) in distinguishing patients with MCI and AD from those without impairment.

Conclusion

In conclusion, the results suggest that abnormal neural activity in the right cerebrum plays a vital role in the process of MCI. Moreover, the ReHo in right caudate may serve as a neuroimaging biomarker for MCI, which can provide objective guidance on diagnosing and managing MCI in the future.

Data availability statement

The raw data supporting the conclusions of this article will be made available by the authors, without undue reservation.

Ethics statement

The studies involving human participants were reviewed and approved by Medical Ethics Committee of Wuxi Mental Health Center. The patients/participants provided their written informed consent to participate in this study. Written informed consent was obtained from the individual(s) for the publication of any potentially identifiable images or data included in this article.

Author contributions

GW, YZ, and FS: conception and design. YG: statistical analysis. YZ: drafting of the manuscript. XZ, JH, and SW: conduction. XC and ML: critical revision of the manuscript. All authors read and approved the final paper.

Conflict of interest

The authors declare that the research was conducted in the absence of any commercial or financial relationships that could be construed as a potential conflict of interest.

Publisher's note

All claims expressed in this article are solely those of the authors and do not necessarily represent those of their affiliated organizations, or those of the publisher, the editors and the reviewers. Any product that may be evaluated in this article, or claim that may be made by its manufacturer, is not guaranteed or endorsed by the publisher.

References

Al-Hakeim, H. K., Al-Fadhel, S. Z., Al-Dujaili, A. H., Carvalho, A., Sriswasdi, S., Maes, M., et al. (2019). Development of a novel neuro-immune and opioid-associated fingerprint with a cross-validated ability to identify and authenticate unknown patients with major depression: far beyond differentiation, discrimination, and classification. *Mol. Neurobiol.* 56, 7822–7835. doi: 10.1007/s12035-019-01647-0

Arbabshirani, M. R., Plis, S., Sui, J., and Calhoun, V. D. (2017). Single subject prediction of brain disorders in neuroimaging: Promises and pitfalls. *Neuroimage* 145, 137–165. doi: 10.1016/j.neuroimage.2016.02.079

Árnadóttir, G. (2016). "Chapter 26 - Impact of neurobehavioral deficits on activities of daily living," in: G. Gillen, (Ed.), *Stroke Rehabilitation* (Fourth Edition), Mosby. p. 573–611. doi: 10.1016/B978-0-323-17281-3.00026-5

Biswal, B., Yetkin, F. Z., Haughton, V. M., and Hyde, J. S. (1995). Functional connectivity in the motor cortex of resting human brain using echo-planar MRI. *Magn. Reson. Med.* 34, 537–541. doi: 10.1002/mrm.1910340409

Biswal, B. B. (2012). Resting state fMRI: a personal history. *Neuroimage* 62, 938–944. doi: 10.1016/j.neuroimage.2012.01.090

Bone, C., Simmonds-Buckley, M., Thwaites, R., Sandford, D., Merzhvynska, M., Rubel, J., et al. (2021). Dynamic prediction of psychological treatment outcomes: development and validation of a prediction model using routinely collected symptom data. *Lancet Digit Health* 3, e231–e240. doi: 10.1016/S2589-7500(21)00018-2

Cano, S. J., Posner, H. B., Moline, M. L., Hurt, S. W., Swartz, J., Hsu, T., et al. (2010). The ADAS-cog in Alzheimer's disease clinical trials: psychometric evaluation of the sum and its parts. *J. Neurol. Neurosurg. Psychiat.* 81, 1363–1368. doi: 10.1136/jnnp.2009.204008

Chand, G. B., Singhal, P., Dwyer, D. B., Wen, J., Erus, G., Doshi, J., et al. (2022). Schizophrenia imaging signatures and their associations with cognition, psychopathology, and genetics in the general population. *Am. J. Psychiatry*. doi: 10.1176/appi.ajp.21070686. [Epub ahead of print].

Cheng, H., Newman, S., Goni, J., Kent, J. S., Howell, J., Bolbecker, A., et al. (2015). Nodal centrality of functional network in the differentiation of schizophrenia. *Schizophr. Res.* 168, 345–352. doi: 10.1016/j.schres.2015.08.011

Cheng, J., Liu, Z., Guan, H., Wu, Z., Zhu, H., Jiang, J., et al. (2021). Brain age estimation from MRI using cascade networks with ranking loss. *IEEE Trans. Med. Imaging* 40, 3400–3412. doi: 10.1109/TMI.2021.3085948

Cheng, J., Yang, H., and Zhang, J. (2019). Donepezil's effects on brain functions of patients with Alzheimer disease: a regional homogeneity study based on resting-state functional magnetic resonance imaging. *Clin. Neuropharmacol.* 42, 42–48. doi: 10.1097/WNF.0000000000000324

De Reuck, J. (2020). "Chapter 1 - Mixed dementia: a neuropathological overview," in *Diagnosis and Management in Dementia*, eds C. R. Martin, and V. R. Preedy (Lille: Academic Press), 3–15. doi: 10.1016/B978-0-12-815854-8.00001-X

Dunne, R. A., Aarsland, D., O'Brien, J. T., Ballard, C., Banerjee, S., Fox, N. C., et al. (2021). Mild cognitive impairment: the Manchester consensus. *Age Ageing* 50, 72–80. doi: 10.1093/ageing/afaa228

Edemekong, P. F., Bomgaars, D. L., Sukumaran, S., and Levy, S. B. (2022). *Activities of Daily Living*. Treasure Island, FL: StatPearls.

Ekman, U., Eriksson, J., Forsgren, L., Mo, S. J., Riklund, K., Nyberg, L., et al. (2012). Functional brain activity and presynaptic dopamine uptake in patients with Parkinson's disease and mild cognitive impairment: a cross-sectional study. *Lancet Neurol.* 11, 679–687. doi: 10.1016/S1474-4422(12)70138-2

Fisher, H. E., Aron, A., and Brown, L. L. (2006). Romantic love: a mammalian brain system for mate choice. *Philos. Trans. R Soc. Lond. B Biol. Sci.* 361, 2173–2186. doi: 10.1098/rstb.2006.1938

Franzmeier, N., Koutsouleris, N., Benzinger, T., Goate, A., Karch, C. M., Fagan, A. M., et al. (2020). Predicting sporadic Alzheimer's disease progression via inherited Alzheimer's disease-informed machine-learning. *Alzheimers Dement* 16, 501–511. doi: 10.1002/alz.12032

Gao, Y., Xiong, Z., Wang, X., Ren, H., Liu, R., Bai, B., et al. (2022). Abnormal degree centrality as a potential imaging biomarker for right

temporal lobe epilepsy: a resting-state functional magnetic resonance imaging study and support vector machine analysis. *Neuroscience* 487, 198–206. doi: 10.1016/j.neuroscience.2022.02.004

Geng, J., Yan, R., Shi, J., Chen, Y., Mo, Z., Shao, J., et al. (2019). Altered regional homogeneity in patients with somatic depression: A resting-state fMRI study. *J. Affect Disord.* 246, 498–505. doi: 10.1016/j.jad.2018.12.066

Gillis, C., Mirzaei, F., Potashman, M., Ikram, M. A., and Maserejian, N. (2019). The incidence of mild cognitive impairment: A systematic review and data synthesis. *Alzheimers Dement (Amst)* 11, 248–256. doi: 10.1016/j.dadm.2019.01.004

Gori, I., Giuliano, A., Muratori, F., Saviozzi, I., Oliva, P., Tancredi, R., et al. (2015). Gray matter alterations in young children with autism spectrum disorders: comparing morphometry at the voxel and regional level. *J. Neuroimaging* 25, 866–874. doi: 10.1111/jon.12280

Graff-Radford, J., Williams, L., Jones, D. T., and Benarroch, E. E. (2017). Caudate nucleus as a component of networks controlling behavior. *Neurology* 89, 2192–2197. doi: 10.1212/WNL.0000000000004680

Grahn, J. A., Parkinson, J. A., and Owen, A. M. (2008). The cognitive functions of the caudate nucleus. *Prog. Neurobiol.* 86, 141–155. doi: 10.1016/j.pneurobio.2008.09.004

Grueso, S., and Viejo-Sobera, R. (2021). Machine learning methods for predicting progression from mild cognitive impairment to Alzheimer's disease dementia: a systematic review. *Alzheimers Res. Ther.* 13, 162. doi: 10.1186/s13195-021-00900-w

Hamilton, M. (1967). Development of a rating scale for primary depressive illness. *Br. J. Soc. Clin. Psychol.* 6, 278–296. doi: 10.1111/j.2044-8260.1967.tb00530.x

Hou, Z., Kong, Y., Yin, Y., Zhang, Y., and Yuan, Y. (2021). Identification of first-episode unmedicated major depressive disorder using pretreatment features of dominant coactivation patterns. *Prog. Neuropsychopharmacol. Biol. Psychiat.* 104, 110038. doi: 10.1016/j.pnpbp.2020.110038

Jia, L., Du, Y., Chu, L., Zhang, Z., Li, F., Lyu, D., et al. (2020). Prevalence, risk factors, and management of dementia and mild cognitive impairment in adults aged 60 years or older in China: a cross-sectional study. *Lancet Public Health* 5, e661–e671. doi: 10.1016/S2468-2667(20)30185-7

Johnson, L. A., Cushing, B., Rohlfing, G., Edwards, M., Davenloo, H., D'Agostino, D., et al. (2014). The Hachinski ischemic scale and cognition: the influence of ethnicity. *Age Ageing* 43, 364–369. doi: 10.1093/ageing/aft189

Khan, T. K. (2016). "Chapter 2 - Clinical Diagnosis of Alzheimer's Disease," in *Biomarkers in Alzheimer's Disease*, ed T. K. Khan (Morgantown, WV: Academic Press), 27–48. doi: 10.1016/B978-0-12-804832-0.00002-X

Kueper, J. K., Speechley, M., and Montero-Odasso, M. (2018). The Alzheimer's disease assessment scale-cognitive subscale (ADAS-Cog): modifications and responsiveness in pre-dementia populations. a narrative review. *J. Alzheimers Dis.* 63, 423–444. doi: 10.3233/JAD-170991

Lei, D., Qin, K., Pinaya, W. H. L., Young, J., Van Amelsvoort, T., Marcelis, M., et al. (2022). Graph convolutional networks reveal network-level functional dysconnectivity in schizophrenia. *Schizophrenia Bull.* doi: 10.1093/schbul/sbac047. [Epub ahead of print].

Livingston, G., Sommerlad, A., Orgeta, V., Costafreda, S. G., Huntley, J., Ames, D., et al. (2017). Dementia prevention, intervention, and care. *Lancet* 390, 2673–2734. doi: 10.1016/S0140-6736(17)31363-6

Madsen, S. K., Ho, A. J., Hua, X., Saharan, P. S., Toga, A. W., Jack, C. R., et al. (2010). 3D maps localize caudate nucleus atrophy in 400 Alzheimer's disease, mild cognitive impairment, and healthy elderly subjects. *Neurobiol. Aging* 31, 1312–1325. doi: 10.1016/j.neurobiolaging.2010.05.002

McWhirter, L., Ritchie, C., Stone, J., and Carson, A. (2020). Functional cognitive disorders: a systematic review. *Lancet Psychiat.* 7, 191–207. doi: 10.1016/S2215-0366(19)30405-5

Orru, G., Pettersson-Yeo, W., Marquand, A. F., Sartori, G., and Mechelli, A. (2012). Using Support Vector Machine to identify imaging biomarkers of neurological and psychiatric disease: a critical review. *Neurosci. Biobehav. Rev.* 36, 1140–1152. doi: 10.1016/j.neubiorev.2012.01.004

Pan, Y., Liu, Z., Xue, Z., Sheng, Y., Cai, Y., Cheng, Y., et al. (2021). Abnormal network properties and fiber connections of DMN across major mental disorders: a probability tracing and graph theory study. *Cereb Cortex*. 32, 3127–3136. doi: 10.1093/cercor/bhab405

Park, B. Y., Kim, M., Seo, J., Lee, J. M., and Park, H. (2016). Connectivity analysis and feature classification in attention deficit hyperactivity disorder sub-types: a task functional magnetic resonance imaging study. *Brain Topogr.* 29, 429–439. doi: 10.1007/s10548-015-0463-1

Paul, R. H., Cohen, R. A., Moser, D. J., Ott, B. R., Sethi, M., Sweet, L., et al. (2003). Clinical correlates of cognitive decline in vascular dementia. *Cogn. Behav. Neurol.* 16, 40–46. doi: 10.1097/00146965-200303000-00005

Pellegrini, E., Ballerini, L., Hernandez, M., Chappell, F. M., Gonzalez-Castro, V., Anblagan, D., et al. (2018). Machine learning of neuroimaging for assisted diagnosis of cognitive impairment and dementia: A systematic review. *Alzheimers Dement (Amst)* 10, 519–535. doi: 10.1016/j.dadm.2018.07.004

Petersen, R. C. (2006). Mild cognitive impairment. *Lancet* 367, 1979. doi: 10.1016/S0140-6736(06)68881-8

Pina-Camacho, L., Garcia-Prieto, J., Parellada, M., Castro-Fornieles, J., Gonzalez-Pinto, A. M., Bombin, I., et al. (2015). Predictors of schizophrenia spectrum disorders in early-onset first episodes of psychosis: a support vector machine model. *Eur. Child Adolesc. Psychiatry* 24, 427–440. doi: 10.1007/s00787-014-0593-0

Pisner, D. A., and Schnyer, D. M. (2020). "Chapter 6 - Support vector machine," in *Machine Learning*, eds A. Mechelli and S. Vieira (Austin, TX: Academic Press), 101–121. doi: 10.1016/B978-0-12-815739-8.00006-7

Qiu, T., Xie, F., Zeng, Q., Shen, Z., Du, G., Xu, X., et al. (2022). Interactions between cigarette smoking and cognitive status on functional connectivity of the cortico-striatal circuits in individuals without dementia: A resting-state functional MRI study. *CNS Neurosci Ther*. doi: 10.1111/cns.13852. [Epub ahead of print].

Sachdev, P. S., Lipnicki, D. M., Kochan, N. A., Crawford, J. D., Thalamuthu, A., Andrews, G., et al. (2015). The prevalence of Memory in an International, The Prevalence of Mild Cognitive Impairment in Diverse Geographical and Ethnocultural Regions: The COSMIC Collaboration. *PLoS ONE* 10, e0142388. doi: 10.1371/journal.pone.0142388

Seger, C. A., and Cincotta, C. M. (2005). The roles of the caudate nucleus in human classification learning. *J. Neurosci.* 25, 2941–2951. doi: 10.1523/JNEUROSCI.3401-04.2005

Shan, X., Cui, X., Liu, F., Li, H., Huang, R., Tang, Y., et al. (2021). Shared and distinct homotopic connectivity changes in melancholic and non-melancholic depression. *J. Affect. Disord.* 287, 268–275. doi: 10.1016/j.jad.2021.03.038

Smitha, K. A., Akhil Raja, K., Arun, K. M., Rajesh, P. G., Thomas, B., Kapilamoorthy, T. R., et al. (2017). Resting state fMRI: A review on methods in resting state connectivity analysis and resting state networks. *Neuroradiol. J.* 30, 305–317. doi: 10.1177/1971400917697342

Tao, W., Li, H., Li, X., Huang, R., Shao, W., Guan, Q., et al. (2021). Progressive brain degeneration from subjective cognitive decline to amnestic mild cognitive impairment: evidence from large-scale anatomical connection classification analysis. *Front. Aging Neurosci.* 13, 687530. doi: 10.3389/fnagi.2021.687530

van den Heuvel, M. P., and Hulshoff Pol, H. E. (2010). Exploring the brain network: a review on resting-state fMRI functional connectivity. *Eur. Neuropsychopharmacol.* 20, 519–534. doi: 10.1016/j.euroneuro.2010.03.008

WHO. (2022). *Dementia*. Available online at: https://www.who.int/health-topics/dementia (accessed June 26, 2022).

Winblad, B., Palmer, K., Kivipelto, M., Jelic, V., Fratiglioni, L., Wahlund, L. O., et al. (2004). Mild cognitive impairment–beyond controversies, towards a consensus: report of the International Working Group on Mild Cognitive Impairment. *J. Intern. Med.* 256, 240–246. doi: 10.1111/j.1365-2796.2004.01380.x

Xie, C., Zhuang, X. X., Niu, Z., Ai, R., Lautrup, S., Zheng, S., et al. (2022). Amelioration of Alzheimer's disease pathology by mitophagy inducers identified via machine learning and a cross-species workflow. *Nat. Biomed. Eng.* 6, 76–93. doi: 10.1038/s41551-021-00819-5

Yan, C. G., Wang, X. D., Zuo, X. N., and Zang, Y. F. (2016). DPABI: data processing and analysis for (Resting-State) brain imaging. *Neuroinformatics* 14, 339–351. doi: 10.1007/s12021-016-9299-4

Zhang, D., Shen, D., and Alzheimer's Disease Neuroimaging, I. (2012). Multi-modal multi-task learning for joint prediction of multiple regression and classification variables in Alzheimer's disease. *Neuroimage* 59, 895–907. doi: 10.1016/j.neuroimage.2011.09.069

Zhang, L., Chao, B., and Zhang, X. (2020). Modeling and optimization of microbial lipid fermentation from cellulosic ethanol wastewater by Rhodotorula glutinis based on the support vector machine. *Bioresour. Technol.* 301, 122781. doi: 10.1016/j.biortech.2020.122781

frontiers | Frontiers in Neuroscience

TYPE Review
PUBLISHED 07 September 2022
DOI 10.3389/fnins.2022.998275

Check for updates

OPEN ACCESS

EDITED BY
Yuzhen Xu,
The Second Affiliated Hospital of Shandong First Medical University, China

REVIEWED BY
Qihua Chen,
Central South University, China
Zhiqin Liu,
Xi'an Jiaotong University School of Medicine, China

*CORRESPONDENCE
Manxia Wang
wmx322@aliyun.com

SPECIALTY SECTION
This article was submitted to Neurodegeneration, a section of the journal Frontiers in Neuroscience

RECEIVED 19 July 2022
ACCEPTED 18 August 2022
PUBLISHED 07 September 2022

CITATION
Wu G, Li Z, Li J, Li X, Wang M, Zhang J, Liu G and Zhang P (2022) A neglected neurodegenerative disease: Adult-onset globoid cell leukodystrophy.
Front. Neurosci. 16:998275.
doi: 10.3389/fnins.2022.998275

COPYRIGHT
© 2022 Wu, Li, Li, Li, Wang, Zhang, Liu and Zhang. This is an open-access article distributed under the terms of the Creative Commons Attribution License (CC BY). The use, distribution or reproduction in other forums is permitted, provided the original author(s) and the copyright owner(s) are credited and that the original publication in this journal is cited, in accordance with accepted academic practice. No use, distribution or reproduction is permitted which does not comply with these terms.

A neglected neurodegenerative disease: Adult-onset globoid cell leukodystrophy

Guode Wu[1], Zhenhua Li[1], Jing Li[1], Xin Li[1], Manxia Wang[1]*, Jing Zhang[2], Guangyao Liu[2] and Pengfei Zhang[2]

[1]Department of Neurology, Lanzhou University Second Hospital, Lanzhou, China, [2]Department of Magnetic Resonance, Lanzhou University Second Hospital, Lanzhou, China

Globoid cell leukodystrophy (GLD), or Krabbe disease (KD) is a rare neurodegenerative disease, and adult-onset GLD is more even neglected by clinicians. This review provides detailed discussions of the serum enzymes, genes, clinical manifestations, neuroimaging features, and therapies of GLD, with particular emphasis on the characteristics of adult-onset GLD, in an attempt to provide clinicians with in-depth insights into this disease.

KEYWORDS

globoid cell leukodystrophy, Krabbe disease, adult-onset GLD, galactosylceramidase, GALC, psychosine

Introduction

Globoid cell leukodystrophy (GLD), or Krabbe disease (KD), is a rare neurodegenerative disorder of the nervous system caused by autosomal-recessive lysosomal dysfunction. Specifically, the mutation in the gene encoding galactosylceramidase (GALC) leads to the deficiency of β-galactosidase activity, which induces the accumulation of neurotoxic galactosylsphingosine [psychosine (PSY)] in oligodendrocytes and Schwann cells, thereby eventually causing progressive demyelination and secondary axonal degeneration in the central (CNS) and peripheral nervous systems (PNS) (Graziano and Cardile, 2015). According to the age of onset, GLD can be clinically classified into early infantile onset, late infantile onset, late childhood onset, adolescent onset, and adult onset, with early infantile phenotype accounting for about 90% of GLD (Duffner et al., 2009a, 2012), while late adult onset GLD is rarely reported. Thus, clinicians are less diagnostically sensitive to adult phenotype, especially the late adult onset, which causes frequent misdiagnoses and mistreatment.

History of research on globoid cell leukodystrophy pathogenesis

There are three milestones in the research history of globoid cell leukodystrophy

The first milestone includes the early 19th century, when the Danish neurologist Knud Haraldsen Krabbe first described the pathological features of five infant patients with injured white matter and cerebellum as "diffuse sclerosis of the brain". In 1924, Collier (Wenger et al., 2016) provided a full description of the globular swelling of multinucleated bodies (multinucleated macrophages) and astrocytic hyperplasia in infant patients, which may be the histopathological features of this disease.

Second, in the early 1970s, Malone and Suzuki demonstrated an extremely low or lost activity for a lysosomal enzyme used for degrading galactosylceramide (GalCer) in GLD, the kind of lysosomal enzyme known as galactocerebrosidase or galactosylceramide β-galactosidase (GALC). In the settings of the lack of GALC, PSY, with a neurotoxic effect, would accumulate in macrophages and nerve cells, especially oligodendrocytes and Schwann cells, eventually causing hypomyelination, known as the "Psychosine hypothesis" (Suzuki and Suzuki, 1970). Therefore, enzymatic determination of GALC activity is a fundamental method for the early diagnosis and screening of GLD in newborns worldwide, especially in Europe and the United States (Macarov et al., 2011; Schrier Vergano et al., 2022).

Third, in the 1990s, Chen (Chen et al., 1993) first cloned human GALC complementary DNA (cDNA) from the urine of a GLD patient. Specifically, the entire length of GALC cDNA consisted of 3,795 bp, the coding region was 2,007 bp in size, the 5' untranslated sequence was 47 bp in size, and the 3' untranslated sequence was 1,741 bp in size. Thus, the researcher mapped the gene to human chromosome 14 by an *in situ* hybridization with a cDNA probe, specifically chromosome 14q13 region (Cannizzaro et al., 1994).

Research on *GALC* genes and protein

Undoubtedly, significant efforts have been made throughout the research history of GLD because it is challenging to obtain protein sequencing with sufficient purity from human tissues, including the liver, brain, and even placenta. In the past two decades, a small amount of pure GALC has been purified from urine (Chen and Wenger, 1993). After the amino acid sequence has been obtained, human GALC cDNA has been successfully revealed (Luzi et al., 1995), consisting of 17 exons and 16 introns. Additionally, compared with lesser exons, the introns range in size from 247 bp for intron 2 to about 12 kb for intron 10. Based on the above-mentioned studies, Cannizzaro (Cannizzaro et al., 1994) confirmed that *GALC* gene is located on human chromosome 14 by linkage analysis, and mapped it to chromosome 14q13 region by an *in situ* hybridization with a cDNA probe. The *GALC* gene may encode the precursor protein of GALC, which was processed into a mature form by being cut into 50-kDa N-terminal fragments and 30-kDa C-terminal fragments by proteases in lysosomes (Nagano et al., 1998). Deane (Deane et al., 2011) has discovered the crystal structures of GALC enzyme and revealed three distinctive domain architectures contributing to substrate binding. Besides, some researchers cloned GALC cDNA from other species, including dogs (Victoria et al., 1996), mice (Sakai et al., 1996), and rhesus monkeys (Luzi et al., 1997), which laid a foundation for establishing animal models of GLD for the future.

Early studies preliminarily revealed that the deletion of 30 kb subunits encoding non-functional proteins is the most common pathogenic mutation of GLD, accounting for about 35%–50% of cases (Rafi et al., 1995). This deletion occurs in the C > T transition polymorphism at position 502 of cDNA, inducing the elimination of the coding regions of seven exons, including all 30-kDa subunits and about 15% of 50-kDa subunits. An increasing number of pathogenic gene mutations has been reported in the past three decades (Wenger et al., 2021). Until now, a total of 296 *GALC* gene mutations related to GLD have been cataloged in the Human Gene Mutation Database (HGMD), including missense mutations, non-sense mutations, deletion, and insertion (**Figure 1**), and the sites and types of gene mutations have regional and racial variation (Rafi et al., 1996; Kleijer et al., 1997; Xu et al., 2006; Zayed, 2015). Unlike infantile GLD with mutations in the central domain of the coding region, adult GLD has GALC mutations at the N or C terminals, and most mutations are located in GALC gene region encoding 50-kDa subunits (Furuya et al., 1997; Wenger et al., 1997). There is a certain correlation between the clinical manifestations and genotypes of GLD in terms of theory: the type and location of gene mutations would affect GALC protein and its activity; hence, it is ideal to be able to classify a disease-causing variant as "severe" or "mild" to predict as the possible type and severity of GLD a patient will have. For instance, c.857G > A (809G > A) mutation and 30-kb deletion are more common in adult onset (De Gasperi et al., 1996), and p.G286D is common in patients with late childhood GLD (De Gasperi et al., 1999; Tappino et al., 2010). c.169G > A (121G > A) mutation is associated with the late-infantile KD form, especially in Japan (Hossain et al., 2014). and Furthermore, the activity of residual β-galactosidase can be detected in these patients. The exploration into the correlation between the clinical manifestations and genotypes of GLD contributes to predicting patients with GLD during screening, but high variability of polymorphic changes on allelic genes complicates the relationship between genotype and clinical phenotype.

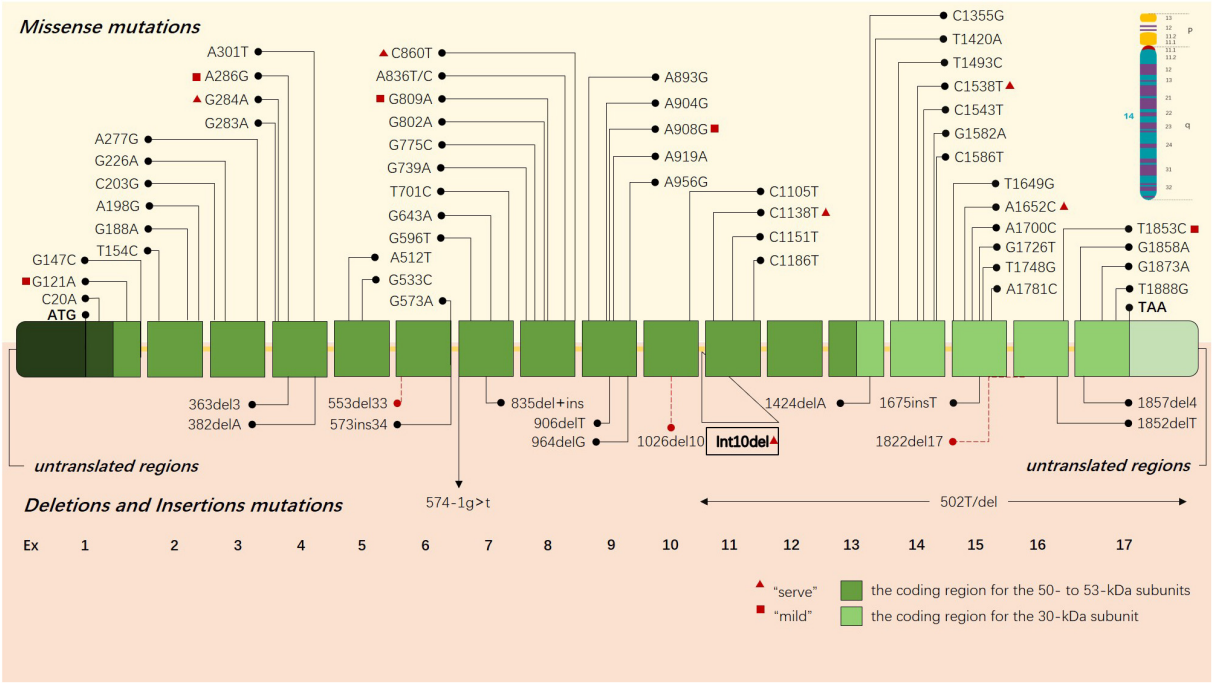

FIGURE 1
GLD-causing common sites and types of gene mutations are presented in the schematic drawing of GALC gene. Missense mutations are above the gene, and deletions and insertions are shown below the gene. Each box represents an exon, the dark green boxes contain the coding region for the 50- to 53-kDa subunits, and the light green boxes contain the coding region for the 30-kDa subunit. The red triangle indicates that this gene may cause a severe clinical phenotype, and the red square indicates that the gene may lead to a mild clinical phenotype.

We summarized some pathogenic heterozygous mutations associated with adult-onset GLD by gathering and analyzing previously published literature (**Table 1**).

Pathogenesis

Normal physiological metabolism of galactocerebrosides and psychosine

Normally, PSY is a cytotoxic lysolipid that can be generated either by the galactosylation of sphingosine by UDP-galactose ceramide galactosyl transferase (CGT) (UDP-galactose-CGT), or by the deacylation of GalCer by *N*-deacylase (Lgisu, 1989; Kanazawa et al., 2000). Having a critical role in the normal physiological mechanism, UDP-galactose-CGT in oligodendrocytes and Schwann cells participates in the synthesis of myelin lipids and myelin formation (Schulte and Stoffel, 1993; Marcus et al., 2006) and plays a vital role in maintaining the function and structure of membranes of other cells (Dupree et al., 1999). The expression of CGT is high in oligodendrocytes and Schwann cells, but lower in neurons and astrocytes (Schaeren-Wiemers et al., 1995; Pernber et al., 2002). Under In GALC-deficient conditions, PSY would accumulate to high levels in tissues, especially in the brain (Suzuki, 1998). Notably, the primary substrate of GALC is hydrolyzed by GM1 ganglioside β-galactosidase in this situation. Therefore, the level of GalCer in tissues would not be high. Additionally, the number of cells expressing UDP-galactose-CGT may be reduced due to the susceptibility to the toxic effect of PSY, which would further increase the accumulation of PSY (Nagara et al., 1986; Ida et al., 1990; **Figure 2**).

The correlation between the myelination stage and globoid cell leukodystrophy

The correlation between the myelination stage and the onset of diseases demonstrates that GLD-induced myelin sheath injuries often occur at the most active myelination stage. The spinal cord is one of the first CNS regions to obtain myelin, and myelination occurs from the gestational age of 20 weeks to 2 years in the spinal cord (Tanaka et al., 1995). Myelination in the pyramidal tract occurs from the gestational age of 25 weeks to 2–3 years (Kinney et al., 1988). Myelination in the posterior corpus callosum occurs

TABLE 1 The pathogenic genes associated with adult onset GLD.

Gene genotype (Heterozygous mutations)	Age of onset	Comments
p.T96A; (c.286A > G) **p.D171V**; (c.512A > T) (Luzi et al., 1996)	45	Mild
G286D; (c.809G > A)**K343AfsX3**; (1027_1036delAAGACAGTTG) (De Stefano et al., 2000)	42	Mild
p.T633Tfs*2; (c.1899delG) **p.T529M**; (c.1586C > T) (Zhong et al., 2020)	27	Severe
p.L634S; (c.1901T > C) **p.L95fs**; (c.283_284del) (Zhang et al., 2021)	22	Mild
30kbdel; (IVS10del30kb) **p.G286D**; (c.809G > A) (Harzer et al., 2002)	50	Mild
p.G496S; (c.1486G > A) **p.G569S**; (c.1705G > A) (Tokushige et al., 2013)	60	Mild
30kbdel; (IVS10del30kb) **G622S**; (c.1864G > A) (Debs et al., 2013)	24	Mild
p.V681M; (c.2041G > A) **c.1911 + 1_1911 + 5delGTAAG** (Yang et al., 2013)	29	Mild
p.G43R; (c.127G > C) **p.I66M** (c.198A > G) + I289V (Lim et al., 2016)	35	Mild
p.N228_S232delTP (c683_694delinsCTC) **p.G286D**; (c.857G > A) (Hossain et al., 2014)	30	Mild
p.L634S; (c.1901T > C) **p.L634X**; (c.1901delT) (Zhang et al., 2018)	20	Mild
p.L634S (c.1901T > C) **p.Y335X**; (c.1005C > G) (Meng et al., 2020)	40	Mild
p.G286D; (c.857G > A) **p.Y490N**; (c1468T > A) (Iacono et al., 2022)	45	Mild

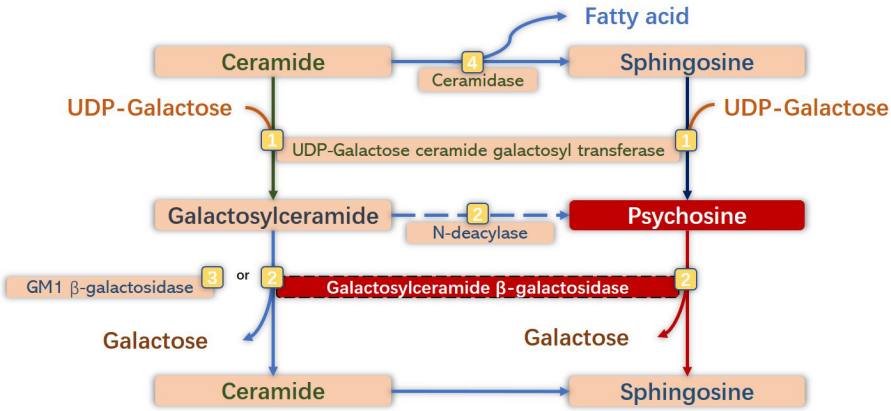

FIGURE 2
Anabolic and catabolic pathways of galactosylsphingosine [psychosine (PSY)] and galactosylceramide. Galactosylceramide is one of the significant glycosphingolipids of oligodendrocytes (OLs) and Schwann cells, which is synthesized by galactosylation of ceramide by UDP-galactose ceramide galactosyl transferase (UDP-galactose CGT) (Graziano and Cardile, 2015), and is degraded to ceramide by degalactosylation by both galactosylceramide β-galactosidase (GALC) (Duffner et al., 2009a) and GM1 β-galactosidase (Duffner et al., 2012). Sphingosine is synthesized by hydrolysis of ceramide by ceramidase (Wenger et al., 2016). PSY is synthesized by galactosylation of sphingosine by UDP-galactose CGT, and from galactosylceramide by *N*-deacylase (Suzuki and Suzuki, 1970), and degraded to sphingosine by degalactosylation by GALC. Under GALC-deficient conditions, neurotoxic PSY accumulates to high levels in macrophages (globoid cells) and neural cells, especially in OLs and Schwann cells.

from 3 to 8 months after birth to adolescence and adulthood (Barkovich et al., 1988; Courchesne et al., 2000). Myelination in the parieto-occipital white matter begins from at 4–6 months after delivery and reaches 50% at 11–14 months after birth (Bartzokis et al., 2001; Deoni et al., 2011). The most significant changes in myelination occur between midgestation and the end of the second postnatal year. The temporal and spatial pattern of myelination seems to explain the temporal features of myelin sheath abnormalities in GLD. According to studies based on magnetic resonance imaging (MRI), spinal cord involvement precedes intracranial abnormalities in infantile GLD (Vasconcellos and Smith, 1998). In infantile GLD (within 2 years of birth), MR signal abnormalities appear at the active myelination stage, including corticospinal projection fibers (pyramidal tract), posterior corpus callosum, and parietal white matter. Besides, it can also be used to explain that the abnormalities of the cerebellar white matter are only observed in early GLD (including early infantile and late infantile types) but not in adult GLD. We suggest that the myelination of cerebellar white matter begins during pregnancy and reaches the adult level at the age of 3–18 months. The myelination of the cerebellar white matter reaches the adult level before the onset of adult GLD. Hence, adult GLD will not be accompanied by

cerebellar lesions or related clinical signs, especially in patients with late adult GLD.

Mechanism of psychosine toxicity in the central and peripheral nervous systems

Psychosine is a metabolic by-product of the precursor of GALC causing membrane structure changes due to its detergent-like properties, inducing oligodendrocyte death and myelin sheath loss. However, it has been proved that PSY could induce abnormal membrane structure by changing the structure and function of lipid rafts in animal experiments (White et al., 2011; Hawkins-Salsbury et al., 2013). As has been revealed in many studies, the mechanisms of PSY toxicity in the CNS and PNS also include PSY-induced stress and proapoptosis signaling pathways, PSY-induced immune and inflammatory responses, PSY-induced mitochondrial energy disorder, peripheral nerve injury, and cerebral microvascular dysfunction (neurovascular unit damage) (Won et al., 2016). Multiple signaling pathways are involved in oxidative stress (OS) and apoptosis of oligodendrocytes induced by PSY (Jatana et al., 2002; Hamanoue et al., 2004; Pannuzzo et al., 2010). PSY plays a vital role in the apoptosis of oligodendrocytes by activating stress-activated protein kinases (SAPKs) (Jurewicz et al., 2006). In addition, it can induce the activity and expression of cell death signals and simultaneously inhibit cell survival signals, such as phosphoinositide 3-kinase (PI3K) (Arai and Lo, 2010; Won et al., 2013; Graziano et al., 2016). Multinucleated activated microglia or macrophages can be observed in the brain of patients with GLD and animal models from previous studies, especially the activation and proliferation of astrocytes and the proliferation of glial fibrillary acidic protein (GFAP) in the demyelination area of the white matter, implying that immune and inflammatory reactions mediated by microglia and peripheral immune cells are involved in GLD pathogenesis (Kobayashi et al., 1986; Ransohoff and Brown, 2012). Some researchers have thought that the immune and inflammatory responses of GLD are secondary performance. However, it has been confirmed that PSY-induced infiltration of immune cells and overexpression of cytokines, such as tumor necrosis factor-α, interleukins, and chemokine, can further activate transcription factors, making the up-regulation of inflammatory response appear at an early stage of this disease (Wu et al., 2001; Borda et al., 2008; Ripoll et al., 2011; Hawkins-Salsbury et al., 2012; SSnook et al., 2014). The accumulation of PSY would induce mitochondrial dysfunction and adenosine triphosphate (ATP) consumption (Haq et al., 2003; Giri et al., 2006; Voccoli et al., 2014). Currently, the increased activity of secretory phospholipase A2 (sPLA2) induced by PSY is considered the critical pathological mechanism, and its products can inhibit mitochondrial enzyme activity and destroy mitochondrial integrity (Kalous et al., 1992; Hollie et al., 2014; Wu et al., 2021). AMP-activated protein kinases (AMPKs) can be activated during energy deficiency to produce and preserve ATP (Hardie, 2004; Carling, 2005). The accumulation of PSY down-regulates or even inactivates the activity of AMPKs, accelerating the consumption of ATP in oligodendrocytes, causes mitochondrial dysfunction in oligodendrocytes and their inactivation, which has been confirmed to be irreversible (Giri et al., 2008). According to previous studies, the excessive accumulation of PSY can also inhibit the function of peroxisomes, which would disturb metabolism and energy homeostasis (Khan et al., 2005; Haq et al., 2006). Lower motor neuron disease induced by peripheral nerve demyelination is the most common non-central nervous system disorder in GLD, such as peripheral neuropathy and muscle diseases. As has been revealed in current studies, the toxic effects of PSY might directly mediate injuries in neuron, axon, and neuromuscular junctions (Castelvetri et al., 2011). PSY induces the production of α-synuclein, a neuronal inclusion, leading to abnormalities of neurofilaments by relieving the regulation of PP1 and PP2A phosphatases (Cantuti-Castelvetri et al., 2012) and inducing an axon transport imbalance by activating glycogen synthase kinase 3β (GSK3β) (Cantuti Castelvetri et al., 2013). This results in axon damage and neuron death in the PNS. PSY can reduce peripheral nerve conduction by activating caspase and inhibiting Akt activities, aggravating the damage to neuromuscular junctions.

In this article, we propose that GLD can involve neurovascular units, which may be the ultimate pathological mechanism contributing to the commonalities of CNS degeneration. Abnormalities of microvasculature and disruption of the blood-brain barrier (BBB) in patients with GLD, mainly including perivascular space enlargement, cerebrovascular permeability increases, endothelial morphology changes, macrophage infiltration, and microvascular structure changes, would develop (Giacomini et al., 2015; Belleri and Presta, 2016). It has been confirmed in some studies that the decreased proliferation and migration of endothelial cells induced by PSY and the declined response to angiogenic factors may hinder angiogenesis. The destroyed actin cytoskeleton and the down-regulated expression of tight junction proteins induced by PSY might lead to changes in microvascular ultrastructure and permeability (Belleri et al., 2013). The damage of PSY to oligodendrocytes would cause secondary damage to astrocytes and neurons, accompanied by microvascular injury (Cantuti Castelvetri et al., 2015).

Clinical features

According to the age of onset, GLD can be clinically classified into five types: early infantile type (onset at

0–6 months), late infantile type (onset at 7–12 months), late childhood type (onset at 13 months-10 years), adolescent type (onset at 11–20 years), and adult type (onset at > 21 years) (Hagberg, 1984). There is a close correlation between clinical symptoms and the age of onset in GLD patients. Patients with the early infantile type account for about 85–95% of cases, and the early infantile type has the worst prognosis, and the general median survival time is 8–36 months (Duffner et al., 2011). The clinical course is usually divided into three clinical stages: non-specific symptom stage, symptom progression stage, and end burnt-out stage. At the non-specific symptom stage, infants often present with crying, irritability, poor feeding, vomiting, and myoclonic seizures (Duffner et al., 2009b), accompanied by peripheral neuropathy (Siddiqi et al., 2006). At the symptom progression stage, infants often present with optic atrophy, aggravated epileptic seizures, and the rapid progression of psychomotor degeneration. At the end burnt-out stage, infants completely lose autonomous movement, require nasal feeding, and eventually die of infection and respiratory failure (Chabali et al., 1997). The late infantile type is characterized by progressive deterioration of motor function, spastic paraplegia, cerebellar ataxia, hemiplegia (Fiumara et al., 2011). About 12.5% of patients with late infantile GLD have a visual impairment or even blindness (Lyon et al., 1991). Compared with the early-infantile onset, the late-infantile onset type has a significantly extended lifetime of 2∼14 years (Barone et al., 1996). The late childhood type is a transitional clinical phenotype from late infantile type to adolescent type. The symptoms related to motor functions of the adolescent type are not as significant as those in the early infantile or late infantile types. However, spastic paralysis or cerebellar ataxia can still occur in the adolescent type, and visual dysfunction is the most common clinical symptom in the adolescent type (Phelps et al., 1991). With aging, symptoms would become alleviated in these patients (Arvidsson et al., 1995).

The adult type has the lowest incidence, with chronic progressive pyramidal tract injuries as the main manifestation. Additionally, patients with this type present with chronic progressive spastic paralysis and gait disorders, with or without peripheral nerve injuries, mental disorders, cognitive disorders, bulbar paralysis, and tremor (Henderson et al., 2003; Tokushige et al., 2013). Almost all patients with adult GLD present with chronic progressive spastic paraplegia or walking difficulties, and sometimes the symptoms may be mild (Paiva et al., 2022), but a patient can also present with acute hemiparesis (Mamada et al., 2016). Most patients also develop peripheral nerve injuries (Sabatelli et al., 2002), and isolated peripheral nerve injury occur in some patients (Marks et al., 1997; Adachi et al., 2016). In these patients, asymmetric peripheral nerve conduction abnormalities have been revealed in some electrophysiological studies. Specifically, prolonged F wave incubation period, reduced motor nerve conduction velocity homogeneity, and prolonged distal incubation period are the most common abnormal manifestations, which are consistent with peripheral nerve demyelination (Matsumoto et al., 1996). When the patient is complicated by pes cavus, differential diagnosis with respect to complicated forms of Charcot-Marie-Tooth disease or hereditary spastic paraplegia is necessary (Malandrini et al., 2013). However, a study conducted by Adachi has demonstrates demonstrated that there are many obvious thin thin-myelinated nerve fibers in sural nerves of patients with GLD, and the density of myelinated nerve fibers decreases (Madsen et al., 2019). However, there is no characteristic "onion ball" structure of peronial peroneal myoatrophy, which may be one of the key points for the differential diagnosis between demyelination and dysmyelination. Mild cognitive impairment (MCI) and psychiatric symptoms often occur in patients with adult GLD (Xia et al., 2020). Compared with adolescent GLD, optic atrophy is less likely to occur in adult GLD (Madsen et al., 2019). Notably, cerebellar ataxia would not occur in patients with adult GLD, and this temporal and spatial pattern correlates with the pathological mechanism of this disease. The majority of patients have slow or insidious progress of dyskinesia, and sometimes cognitive impairment, but such patients have survived up to 10–15 years after the initial onset of symptoms, according to the literature (Liao et al., 2014).

It is difficult to evaluate the clinical manifestations of adult GLD in real-world clinical practice, it is impossible to assess whether these patients are completely normal before the age of 20 years or have some mild clinical symptoms that are difficult to observe, hindering the further exploration into adult GLD.

Imaging features

Features of white matter lesions

Bilateral symmetrical white matter lesions are a mark of most hereditary white matter lesions and a few secondary white matter lesions. Patchy white matter lesions are common in inflammatory demyelination of the CNS, such as multiple sclerosis, and scattered multiple punctate lesions are common in ischemic white matter lesions (Schiffmann and van der Knaap, 2009). MRI features of the brain have been correlated with the age of onset of GLD patients (Abdelhalim et al., 2014; Muthusamy et al., 2019; Andriescu et al., 2020). For example, white matter hyperintensities (WMHs) mainly involve the cerebellar white matter and the dentate nucleus at the early and late stages of infantile GLD. The cerebellum of adolescent GLD patients is basically normal, but WMHs involve the parietal white matter.

Bilateral WMHs usually occur in adult GLD patients and are limited to the parietal white matter (temporo-parietal junction), corona radiata, optic radiation, proximal corticospinal tract,

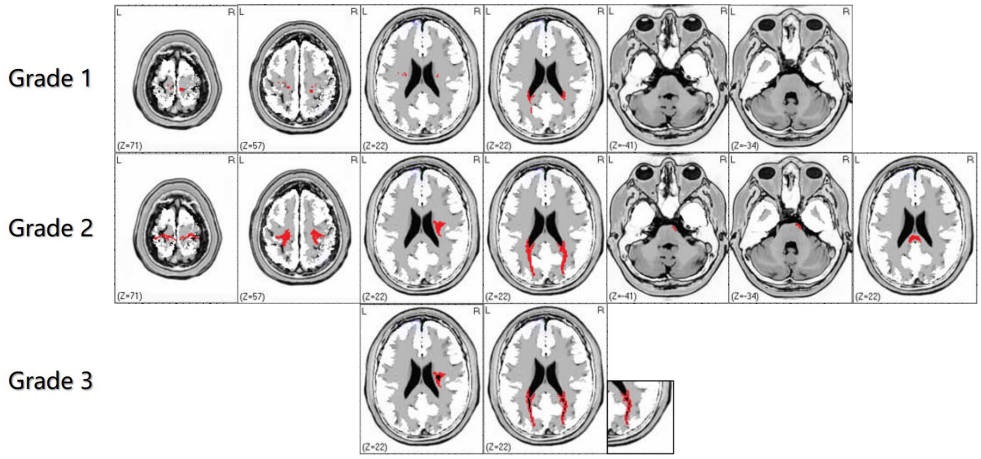

FIGURE 3
The characteristics of white matter lesions should be graded by imaging, including grade 1: sporadic punctate white matter lesions; grade 2: patchy or continuous linear white matter lesions; grade 3: obvious cavity-like changes in the lesion site. In the supratentorial and infratentorial structures, the damage degree of the corticospinal tract and medial lemniscus should shall be highlighted in the transverse and coronal sections of brain magnetic resonance imaging (MRI). Grade 1 is defined as discontinuous white matter lesions, and grade 2 is defined as continuous white matter lesions. The red area refers to WMHs, and the black part of the red area refers to necrosis or cavity formation in WMHs.

posterior lateral periventricular white matter, and corpus callosum (Wang et al., 2007; Tokushige et al., 2013), with or without brain and spinal cord atrophy (Bajaj et al., 2002). Noteworthy, cerebellar white matter lesions seldom occur in adult GLD patients. Due to the undefined correlation between gene mutation types and clinical phenotypes, the focus of recent studies has been placed on the classification and scoring of intracranial white matter abnormalities, to identify the correlation of the site and severity of white matter lesions with clinical phenotypes (Cousyn et al., 2019). Based on the analysis and summary of the MRI features of adult GLD patients in our clinical center, we simplified the imaging scoring criteria for GLD to better define the pattern of leukodystrophy and provide treatment opportunities earlier (**Figure 3**). In the revised scoring criteria, we still highlighted the significance of "continuity of lesions" in the site and severity of white matter lesions, which correlated with the scoring of the lesion site. Discontinuous supratentorial white matter lesions are mainly involved in four parts in the transverse section of brain MRI, including pre- and postcentral gyrus, corona radiate, posterior lateral periventricular white matter, and optic radiations. The degree of white matter lesions of the corpus callosum should be highlighted in the median sagittal section. In theory, the higher the score, the more serious the clinical symptoms. The sensitivity and specificity of the grading scale should still be verified by numerous clinical data.

Adult GLD patients usually have a relatively slow progression of white matter lesions. Therefore, the clinical process from an acute attack to rapid aggravation may be misdiagnosed as acute cerebral infarction or inflammatory demyelination of the CNS, such as multiple sclerosis (Debs et al., 2013; Mamada et al., 2016). Therefore, dynamic and longitudinal image follow-up shall be regularly performed to systematically evaluate the accuracy of diagnosis.

Other imaging features

Other imaging features include unilateral white matter involvement, advanced brain atrophy with different degrees (Lemmens et al., 2011). Optic neuropathy, optic chiasma lesions, and enhanced oculomotor nerves and trigeminal nerves are common findings in infantile patients (Beslow et al., 2008; Patel et al., 2008; Ganesan et al., 2010; Garcia et al., 2010; Quintas-Neves et al., 2020), which have rarely been reported in adult-onset GLD. Compared with often reported thickened cauda equina nerves in early-infantile and late-infantile Krabbe disease patients (Hwang et al., 2016), brachial plexus enlargement is a more common MRI finding in adult-onset Krabbe disease (Hiyama et al., 2016).

As the study of white matter lesions at an early stage by magnetic resonance spectroscopy (MRS) confirmed, the pattern of metabolic alterations as detected by MRS in infantile-onset, juvenile-onset, and adult-onset has been related to age (Brockmann et al., 2003; Romano et al., 2009), and the concentration of white matter metabolites in adult GLD patients is close to the normal level. Furthermore, the concentration of *N*-acetylaspartate and *N*-acetylaspartylglutamate decreases; while, that of choline-containing compounds, creatine, and phosphocreatine increases. There is a slight change in the concentration of myoinositol. The spectra of the gray matter show a slight decrease in the concentration of all metabolites

(Udow et al., 2012). Diffusion tensor imaging (DTI) is the most valuable neuroimaging method for CNS demyelination, assess the severity of white matter damage in infantile GLD (Provenzale et al., 2005; Escolar et al., 2009; Wang et al., 2011; Poretti et al., 2014). It may detect early white matter injury in asymptomatic neonates, predict motor functions and prognosis after stem cell transplantation (Poretti et al., 2016).

Therapies

Enzyme replacement therapy (ERT) has been emphasized in the preliminary studies on GLD treatment. This therapy has been adopted from the treatment of lysosomal storage diseases (Desnick and Schuchman, 2012). However, it is difficult to achieve efficacy owing to the blocking effect of the BBB, especially clinical symptoms exist at diagnosis (Escolar et al., 2005). Currently, hematopoietic stem cell transplantation (HSCT) is the optimal viable therapy for GLD treatment, and these cells are mainly derived from the bone marrow (BM) or umbilical cord blood (UCB) (Wright et al., 2017). Moreover, virus-mediated gene therapy, anti-inflammatory and antioxidant therapy, oligodendrocyte transplantation, and substrate reduction therapy have been subjected to drug tests based on animal models (Mikulka and Sands, 2016). However, a single therapy cannot achieve satisfactory efficacy. GalCer deficiency in GLD can trigger various pathogenic mechanisms, suggesting that there may be multiple targets during the treatment of this disease. Therefore, the focus of recent studies has been placed on different combined therapies based on these therapeutic regimens. Additionally, treatment strategies emphasize symptomatic and supportive treatment from multidisciplinary collaboration for patients (Escolar et al., 2016).

Enzyme replacement therapies

Lysosomal storage diseases, such as Fabry disease, are usually treated with ERT (Griffiths, 1989). The core of treatment lies in providing active GALC for dysfunctional cells and tissues in the CNS and PNS. In 2005, Lee (Lee et al., 2005) prolonged the life span of twitcher mice to 47 days by an intraperitoneal injection of recombinant GALC. However, this ERT based on intraperitoneal injection could not provide a long-term effect due to the existence of the BBB. In 2007, Lee (Lee et al., 2007) improved the activity of GALC in the CNS of twitcher mice by injecting recombinant GALC into the ventricle. However, there are two defects in this therapy. First, repeated invasive injections are required to maintain high GALC concentration. Second, multiple injections may be required because GLD widely influences the CNS and PNS. These defects hinder the application of ERTs in clinical practice.

Hematopoietic stem cell transplantation

Currently, HSCT is the standard therapy for GLD treatment. GALC-positive donor cells from BM or UCB are transplanted to the CNS to continuously provide GALC and reduce the degree of neuroinflammation (Reddy et al., 2011). Bone marrow transplantation (BMT) is widely used in the early treatment of this disease. At present, umbilical cord blood transplantation can be used for the treatment of patients with early infantile GLD. However, early screening should be performed on newborns (Kwon et al., 2018). The process of hematopoietic stem cells performing a therapeutic role is called cross-correction. Functional GALC secreted by hematopoietic stem cells is ingested and combined with mannose receptors on the surface of defective cells in the CNS through mannose-6-phosphate (M6P), and then transported to lysosomes through endocytosis (Neufeld and Fratantoni, 1970). Both the animal experiment results and the evidence of GLD treatment demonstrate the effectiveness of HSCT, especially for infantile GLD patients before the appearance of symptoms (Krivit et al., 1998). Further, HSCT has been reported to exert immune regulation by reducing the degree of neuroinflammation (Caniglia et al., 2002). Notably, patients receiving HSCT are at risk of severe graft-versus-host disease (GVHD), and this therapy can improve clinical symptoms only to a certain extent.

Virus-mediated gene therapy

It has been confirmed in previous animal experiments that virus-mediated gene therapies mediated by adeno-associated virus (AAV) orienting the CNS can improve enzyme activity and enhance behavior and cognitive function in mouse models with lysosomal storage diseases (Passini et al., 2005, 2006). Adenovirus capsid proteins (AAV1, 5, 9, rh10) are currently widely used in GLD treatment (Asokan et al., 2012), and several types of capsid proteins have presented favorable outcomes. After GALC cDNA is delivered by adenovirus to twitcher mice, GALC activity increases several times in the CNS, and the survival time is significantly prolonged compared with untreated mice, by 40–50% (Rafi et al., 2005). Recently, Rafi et al. treated twitcher mice by intravenously injecting AAV2/rh10-mGALC into the tail vein. The results showed that the survival time of treated mice was significantly longer than that of untreated mice, and the GALC activity in the brain, spinal cord, and sciatic nerve reached or exceeded the recombinant wild-type (WT) level (Rafi et al., 2012, 2015a). This implies that multiple injections are not required in virus-mediated gene therapy, which is different from ERT. The efficacy of virus-mediated gene therapy correlates with the improvement of adenovirus vectors, and this therapy is one of the most

promising therapies for treating GLD (Rafi, 2016; Nasir et al., 2021; Hordeaux et al., 2022).

Anti-inflammatory and antioxidant therapy

PSY-related hyperoxidative stress and inflammatory reactions are also the targets for treating GLD. It has been confirmed through animal experiments that ibudilast, a phosphodiesterase inhibitor, can reduce the degree of tremor and demyelination in twitcher mice, but cannot prolong their life span (Kagitani-Shimono et al., 2005). Luzi (Luzi et al., 2009) used indomethacin, ibuprofen, and minocycline to prolong the life of twi-trs mice (an animal model of GLD). The result has shown that indomethacin could significantly reduce pro-inflammatory cytokines, including interleukin (IL)-6 and tumor necrosis factor (TNF)-α. Paintlia (Paintlia et al., 2015) significantly prolonged the average life span of twitcher mice *via* a diet therapy with a high level of vitamin D, leading to a decreased accumulation velocity of PSY in the body, and a mitigated degree of demyelination.

Oligodendrocyte transplantation

Oligodendrocytes in the CNS are one of the targets in treating GLD. Hence, the ultimate goal of treatment is to stabilize the normal function of oligodendrocytes and other myelin sheath cells. Kuai (Kuai et al., 2015) injected oligodendrocyte precursor cells differentiated from normal mouse embryonic stem cells into twitcher mice. However, the researchers obtained unsatisfactory results. Both the motor function and life span could not be improved through this therapy.

Substrate reduction therapy

Substrate reduction therapy has shown some prospects in the treatment of lysosomal storage diseases. Although this therapy can only alleviate clinical severity and prolong the life span, GLD can still not be eliminated (Parenti et al., 2015). Galactose ceramide galactosyl transferase (CGT) is the enzyme directly responsible for synthesizing PSY in GLD. However, there is no effective inhibitor for this enzyme. Thus, it is necessary to identify the target enzyme upstream of PSY synthesis for achieving effective treatment (LeVine et al., 2000). However, many downstream metabolites related to these upstream enzymes may be affected.

Combined therapies

Currently, there are many synergistic regimens based on HSCT, including BMT + endothelial growth factors (Young et al., 2004), BMT + substrate reduction therapy (LeVine et al., 2000), BMT + enzyme replacement therapy (Qin et al., 2012), BMT + virus-mediated gene therapy (Lin et al., 2007; Galbiati et al., 2009; Rafi et al., 2015b), and BMT + gene therapy therapies + substrate reduction therapy (Hawkins-Salsbury et al., 2015). These synergistic regimens outperform single-drug regimens in multiple aspects, including alleviating pathological demyelination, prolonging the life span of twitcher mice, and improving motor function (Bradbury et al., 2021). However, these synergistic regimens are still in the stage of animal experiments, and a long-term research may be required for the real-world application of these regimens for GLD patients.

Among the treatments for globoid cell leukodystrophy, hematopoietic stem cells are used clinically, especially in infants, except for other treatment options, which are basically in the animal experimental stage. There are currently few reports on the treatment of GLD in adults due to the low incidence in this population and the limitations of clinical therapies. According to some case reports, HSCT may be effective in treating adult-onset GLD patients (Sharp et al., 2013). Moreover, the intravenous injection of gamma globulin has been effective in treating adult-onset GLD patients (Fukazawa et al., 2021). Symptomatic and supportive therapies are still the main clinical regimens for treating adult-onset GLD patients.

Step.1	The core clinical symptom, as "chronic progressive symmetrical spasmodic paralysis"	1	
	Electrophysiological examination	1	
	Plexus root imaging	1	
Step.2	Neuroimaging features, as "mild white matter demyelination of anterior or posterior central gyrus, coronal radiography, posterior horn of lateral ventricle, and visual radiation"	1	
Step.3	GLCA enzyme/gene test	4	

FIGURE 4
Feasible diagnostic ideas and criteria. If the total score is > 4, it is a confirmed diagnosis; If the total score equals 4 points (without enzyme or gene testing), it is strongly recommended to perform GALC enzyme or genetic testing. If the total score is < 4, differential diagnosis should be focused on, and GALC enzyme or genetic testing should be performed when necessary.

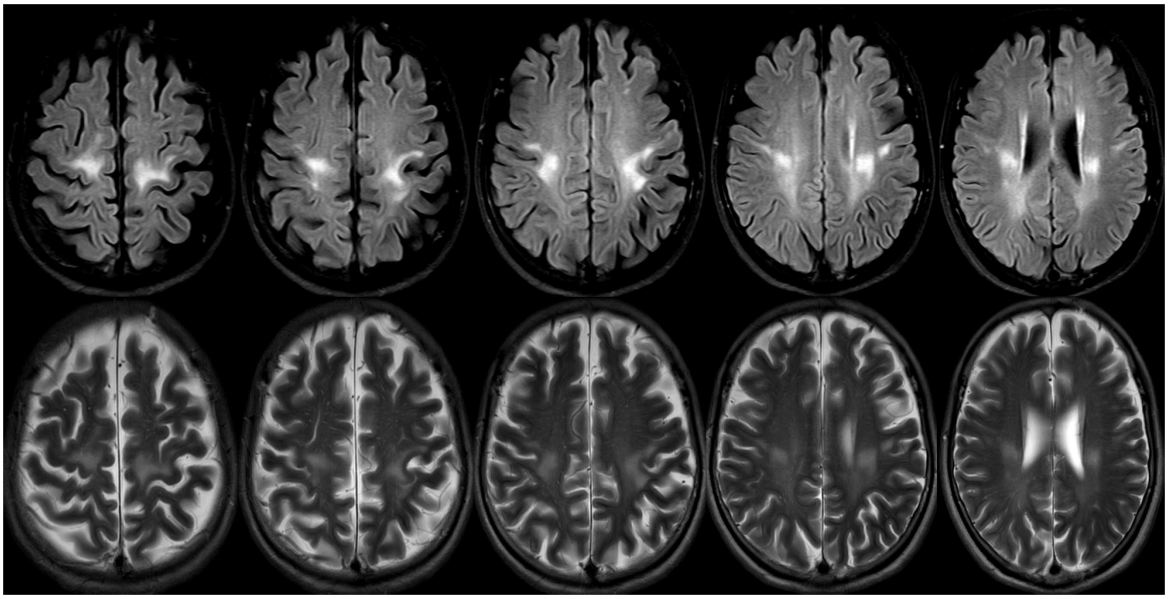

FIGURE 5
A 69-years-old female presented with a 2-year history of progressive weakness of the lower limbs. A brain magnetic resonance imaging (MRI) revealed abnormal T2 and flair hyperintensities in the periventricular and deep cerebral white matter, and the bilateral subcortical areas of parietal white matter (the lesions were continuous and symmetrically distributed). Reduced galactocerebrosidase activity and GALC gene confirmed the diagnosis of adult late-onset GLD.

A feasible diagnostic idea and criteria

Despite a systematic review of the pathogenesis, clinical manifestations, and neuroimaging features of globoid cell leukodystrophy, the actual clinical diagnosis of this type of CNS degeneration is mains a challenge. Based on our experience, we tried to provide feasible diagnostic ideas and criteria (**Figure 4**).

Step 1 is to: assess the patient whether they meet the core clinical symptom of the vast majority of adult-onset GLD, which is "chronic progressive symmetrical spasmodic paralysis", If the conditions are met, one point is added. Further, an electrophysiological examination should be performed to identify whether it is peripheral neuropathy or evaluate whether it is accompanied by peripheral nerve damage; if the conditions are met, one point is added. If the electrophysiological examination results are abnormal, further brachial plexus root imaging is required (it adds the evidence of diagnosis, but is not used as the diagnostic criteria); if the conditions are met, one point is added.

Step 2 is to: assess patient whether the patient meets the imaging core symptoms of most adult-onset globoid cell leukodystrophy are "mild white matter demyelination of anterior or posterior central gyrus, coronal radiography, posterior horn of the lateral ventricle, and visual radiation" (it adds the evidence of diagnosis, but is not used as the diagnostic criteria); if the conditions are met, one point is added.

Step 3: is to determine the affected GLCA enzyme, or perform genetic testing; if the conditions are met, four points are added.

Through this diagnostic process and strategy, a 67-year-old patient was diagnosed with late adult onset GLD in our clinical center. This patient presented with chronic progressive spastic gait, mild cognitive impairment, and anxiety, and there was no clinical symptom of peripheral nerve involvement. However, the electrophysiological examination results suggested decreased nerve conduction velocity and demyelination. The clinical symptoms of this patient were consistent with the typical clinical manifestations of late adult onset GLD, and this patient has been the oldest case reported in China (**Figure 5**).

Conclusion

Adult-onset GLD is a rare degenerative disease of the CNS caused by abnormal lysosomal storage. This disease is characterized by chronic progressive spastic paralysis and gait disorders, with or without peripheral nerve injury, cognitive impairment, and mental disorders. Although there is no effective therapy for adult-onset GLD, this disease is expected to be eliminated by pharmacological chaperones based on animal models to improve the activity GALC enzyme, viral vectors for gene therapy, and neural progenitor cells injected into the CNS. To treat GLD, clinicians should accurately differentiate it from other acquired white matter demyelination diseases of the

CNS based on the clinical and MRI features of this disease, to avoid misdiagnoses.

Author contributions

ZL and JL contributed to the study design and drafted the manuscript. GW and XL edited the manuscript. JZ, PZ, and GL contributed to MRI of the data in the literature. MW supervised the writing of the manuscript and critically reviewed the manuscript. All authors contributed to the article and approved the submitted version.

Funding

This work was supported by grants from the Natural Science Foundation of Gansu Province, China (grant no. 21JR1RA121), the Natural Science Foundation of Gansu Province, China (grant no. 21JR1RA132), and Scientific research topics of Traditional Chinese Medicine and Health Commission of Gansu Province, China (grant no. GZKZ-2021-9).

Acknowledgments

We thank all the subjects who participated in our study.

Conflict of interest

The authors declare that the research was conducted in the absence of any commercial or financial relationships that could be construed as a potential conflict of interest.

Publisher's note

All claims expressed in this article are solely those of the authors and do not necessarily represent those of their affiliated organizations, or those of the publisher, the editors and the reviewers. Any product that may be evaluated in this article, or claim that may be made by its manufacturer, is not guaranteed or endorsed by the publisher.

References

Abdelhalim, A. N., Alberico, R. A., Barczykowski, A. L., and Duffner, P. K. (2014). Patterns of magnetic resonance imaging abnormalities in symptomatic patients with Krabbe disease correspond to phenotype. *Pediatr. Neurol.* 50, 127–134. doi: 10.1016/j.pediatrneurol.2013.10.001

Adachi, H., Ishihara, K., Tachibana, H., Oka, N., Higuchi, Y., Takashima, H., et al. (2016). Adult-onset Krabbe disease presenting with an isolated form of peripheral neuropathy. *Muscle Nerve* 54, 152–157. doi: 10.1002/mus.25067

Andriescu, E. C., Russo, S. N., and Pérez, C. A. (2020). Teaching neuroImages: Infantile-onset Krabbe disease with tigroid appearance of the white matter. *Neurology* 94, e1964–e1965. doi: 10.1212/WNL.0000000000009380

Arai, K., and Lo, E. H. (2010). Astrocytes protect oligodendrocyte precursor cells via MEK/ERK and PI3K/Akt signaling. *J. Neurosci. Res.* 88, 758–763. doi: 10.1002/jnr.22256

Arvidsson, J., Hagberg, B., Månsson, J. E., and Svennerholm, L. (1995). Late onset globoid cell leukodystrophy (Krabbe's disease)–Swedish case with 15 years of follow-up. *Acta Paediatr.* 84, 218–221. doi: 10.1111/j.1651-2227.1995.tb13616.x

Asokan, A., Schaffer, D. V., and Samulski, R. J. (2012). The AAV vector toolkit: Poised at the clinical crossroads. *Mol. Ther.* 20, 699–708. doi: 10.1038/mt.2011.287

Bajaj, N. P., Waldman, A., Orrell, R., Wood, N. W., and Bhatia, K. P. (2002). Familial adult onset of Krabbe's disease resembling hereditary spastic paraplegia with normal neuroimaging. *J. Neurol. Neurosurg. Psychiatry* 72, 635–638. doi: 10.1136/jnnp.72.5.635

Barkovich, A. J., Kjos, B. O., Jackson, D. E. Jr., and Norman, D. (1988). Normal maturation of the neonatal and infant brain: MR imaging at 1.5 T. *Radiology* 166(1 Pt 1), 173–180. doi: 10.1148/radiology.166.1.3336675

Barone, R., Brühl, K., Stoeter, P., Fiumara, A., Pavone, L., and Beck, M. (1996). Clinical and neuroradiological findings in classic infantile and late-onset globoid-cell leukodystrophy (Krabbe disease). *Am. J. Med. Genet.* 63, 209–217. doi: 10.1002/(SICI)1096-8628(19960503)63:1<209::AID-AJMG37>3.0.CO;2-Q

Bartzokis, G., Beckson, M., Lu, P. H., Nuechterlein, K. H., Edwards, N., and Mintz, J. (2001). Age-related changes in frontal and temporal lobe volumes in men: A magnetic resonance imaging study [published correction appears in Arch Gen Psychiatry 2001 Aug;58(8):774]. *Arch. Gen. Psychiatry* 58, 461–465. doi: 10.1001/archpsyc.58.5.461

Belleri, M., and Presta, M. (2016). Endothelial cell dysfunction in globoid cell leukodystrophy. *J. Neurosci. Res.* 94, 1359–1367. doi: 10.1002/jnr.23744

Belleri, M., Ronca, R., Coltrini, D., Nico, B., Ribatti, D., Poliani, P. L., et al. (2013). Inhibition of angiogenesis by β-galactosylceramidase deficiency in globoid cell leukodystrophy. *Brain* 136(Pt 9), 2859–2875. doi: 10.1093/brain/awt215

Beslow, L. A., Schwartz, E. S., and Bönnemann, C. G. (2008). Thickening and enhancement of multiple cranial nerves in conjunction with cystic white matter lesions in early infantile Krabbe disease. *Pediatr. Radiol.* 38, 694–696. doi: 10.1007/s00247-008-0763-7

Borda, J. T., Alvarez, X., Mohan, M., Ratterree, M. S., Phillippi-Falkenstein, K., Lackner, A. A., et al. (2008). Clinical and immunopathologic alterations in rhesus macaques affected with globoid cell leukodystrophy. *Am. J. Pathol.* 172, 98–111. doi: 10.2353/ajpath.2008.070404

Bradbury, A. M., Bongarzone, E. R., and Sands, M. S. (2021). Krabbe disease: New hope for an old disease. *Neurosci. Lett.* 752:135841. doi: 10.1016/j.neulet.2021.135841

Brockmann, K., Dechent, P., Wilken, B., Rusch, O., Frahm, J., and Hanefeld, F. (2003). Proton MRS profile of cerebral metabolic abnormalities in Krabbe disease. *Neurology* 60, 819–825. doi: 10.1212/01.wnl.0000049469.29011.e9

Caniglia, M., Rana, I., Pinto, R. M., Fariello, G., Caruso, R., Angioni, A., et al. (2002). Allogeneic bone marrow transplantation for infantile globoid-cell leukodystrophy (Krabbe's disease). *Pediatr. Transplant.* 6, 427–431. doi: 10.1034/j.1399-3046.2002.02026.x

Cannizzaro, L. A., Chen, Y. Q., Rafi, M. A., and Wenger, D. A. (1994). Regional mapping of the human galactocerebrosidase gene (GALC) to 14q31 by in situ hybridization. *Cytogenet. Cell Genet.* 66, 244–245. doi: 10.1159/000133703

Cantuti Castelvetri, L., Givogri, M. I., Hebert, A., Smith, B., Song, Y., Kaminska, A., et al. (2013). The sphingolipid psychosine inhibits fast axonal transport in Krabbe disease by activation of GSK3β and deregulation of molecular motors. *J. Neurosci.* 33, 10048–10056. doi: 10.1523/JNEUROSCI.0217-13.2013

Cantuti Castelvetri, L., Maravilla, E., Marshall, M., Tamayo, T., D'auria, L., Monge, J., et al. (2015). Mechanism of neuromuscular dysfunction in Krabbe disease. *J. Neurosci.* 35, 1606–1616. doi: 10.1523/JNEUROSCI.2431-14.2015

Cantuti-Castelvetri, L., Zhu, H., Givogri, M. I., Chidavaenzi, R. L., Lopez-Rosas, A., and Bongarzone, E. R. (2012). Psychosine induces the dephosphorylation of neurofilaments by deregulation of PP1 and PP2A phosphatases. *Neurobiol. Dis.* 46, 325–335. doi: 10.1016/j.nbd.2012.01.013

Carling, D. (2005). AMP-activated protein kinase: Balancing the scales. *Biochimie* 87, 87–91. doi: 10.1016/j.biochi.2004.10.017

Castelvetri, L. C., Givogri, M. I., Zhu, H., Smith, B., Lopez-Rosas, A., Qiu, X., et al. (2011). Axonopathy is a compounding factor in the pathogenesis of Krabbe disease. *Acta Neuropathol.* 122, 35–48. doi: 10.1007/s00401-011-0814-2

Chabali, R., Matre, W. M., and Greene, M. K. (1997). Infant with irritability, feeding problems, and progressive developmental abnormalities presenting repeatedly to a pediatric emergency department. *Pediatr. Emerg. Care* 13, 123–126. doi: 10.1097/00006565-199704000-00011

Chen, Y. Q., Rafi, M. A., de Gala, G., and Wenger, D. A. (1993). Cloning and expression of cDNA encoding human galactocerebrosidase, the enzyme deficient in globoid cell leukodystrophy. *Hum. Mol. Genet.* 2, 1841–1845. doi: 10.1093/hmg/2.11.1841

Chen, Y. Q., and Wenger, D. A. (1993). Galactocerebrosidase from human urine: Purification and partial characterization. *Biochim. Biophys. Acta* 1170, 53–61. doi: 10.1016/0005-2760(93)90175-9

Courchesne, E., Chisum, H. J., Townsend, J., Cowles, A., Covington, J., Egaas, B., et al. (2000). Normal brain development and aging: Quantitative analysis at in vivo MR imaging in healthy volunteers. *Radiology* 216, 672–682. doi: 10.1148/radiology.216.3.r00au37672

Cousyn, L., Law-Ye, B., Pyatigorskaya, N., Debs, R., Froissart, R., Piraud, M., et al. (2019). Brain MRI features and scoring of leukodystrophy in adult-onset Krabbe disease. *Neurology* 93, e647–e652. doi: 10.1212/WNL.0000000000007943

De Gasperi, R., Gama Sosa, M. A., Sartorato, E., Battistini, S., Raghavan, S., and Kolodny, E. H. (1999). Molecular basis of late-life globoid cell leukodystrophy. *Hum. Mutat.* 14, 256–262. doi: 10.1002/(SICI)1098-1004(1999)14:3<256::AID-HUMU9>3.0.CO;2-6

De Gasperi, R., Gama Sosa, M. A., Sartorato, E. L., Battistini, S., MacFarlane, H., Gusella, J. F., et al. (1996). Molecular heterogeneity of late-onset forms of globoid-cell leukodystrophy [published correction appears in Am J Hum Genet 1997 May;60(5):1264]. *Am. J. Hum. Genet.* 59, 1233–1242.

De Stefano, N., Dotti, M. T., Mortilla, M., Pappagallo, E., Luzi, P., Rafi, M. A., et al. (2000). Evidence of diffuse brain pathology and unspecific genetic characterization in a patient with an atypical form of adult-onset Krabbe disease. *J. Neurol.* 247, 226–228. doi: 10.1007/s004150050571

Deane, J. E., Graham, S. C., Kim, N. N., Stein, P. E., McNair, R., Cachón-González, M. B., et al. (2011). Insights into Krabbe disease from structures of galactocerebrosidase. *Proc. Natl. Acad. Sci. U.S.A.* 108, 15169–15173. doi: 10.1073/pnas.1105639108

Debs, R., Froissart, R., Aubourg, P., Papeix, C., Douillard, C., Degos, B., et al. (2013). Krabbe disease in adults: Phenotypic and genotypic update from a series of 11 cases and a review. *J. Inherit. Metab. Dis.* 36, 859–868. doi: 10.1007/s10545-012-9560-4

Deoni, S. C., Mercure, E., Blasi, A., Gasston, D., Thomson, A., Johnson, M., et al. (2011). Mapping infant brain myelination with magnetic resonance imaging. *J. Neurosci.* 31, 784–791. doi: 10.1523/JNEUROSCI.2106-10.2011

Desnick, R. J., and Schuchman, E. H. (2012). Enzyme replacement therapy for lysosomal diseases: Lessons from 20 years of experience and remaining challenges. *Annu. Rev. Genomics Hum. Genet.* 13, 307–335. doi: 10.1146/annurev-genom-090711-163739

Duffner, P. K., Barczykowski, A., Jalal, K., Yan, L., Kay, D. M., and Carter, R. L. (2011). Early infantile Krabbe disease: Results of the World-Wide Krabbe Registry. *Pediatr. Neurol.* 45, 141–148. doi: 10.1016/j.pediatrneurol.2011.05.007

Duffner, P. K., Barczykowski, A., Kay, D. M., Jalal, K., Yan, L., Abdelhalim, A., et al. (2012). Later onset phenotypes of Krabbe disease: Results of the world-wide registry. *Pediatr. Neurol.* 46, 298–306. doi: 10.1016/j.pediatrneurol.2012.02.023

Duffner, P. K., Caggana, M., Orsini, J. J., Wenger, D. A., Patterson, M. C., Crosley, C. J., et al. (2009a). Newborn screening for Krabbe disease: The New York State model. *Pediatr. Neurol.* 40, 245–255. doi: 10.1016/j.pediatrneurol.2008.11.010

Duffner, P. K., Jalal, K., and Carter, R. L. (2009b). The hunter's hope Krabbe family database. *Pediatr. Neurol.* 40, 13–18. doi: 10.1016/j.pediatrneurol.2008.08.011

Dupree, J. L., Girault, J. A., and Popko, B. (1999). Axo-glial interactions regulate the localization of axonal paranodal proteins. *J. Cell Biol.* 147, 1145–1152. doi: 10.1083/jcb.147.6.1145

Escolar, M. L., Poe, M. D., Provenzale, J. M., Richards, K. C., Allison, J., Wood, S., et al. (2005). Transplantation of umbilical-cord blood in babies with infantile Krabbe's disease. *N. Engl. J. Med.* 352, 2069–2081. doi: 10.1056/NEJMoa042604

Escolar, M. L., Poe, M. D., Smith, J. K., Gilmore, J. H., Kurtzberg, J., Lin, W., et al. (2009). Diffusion tensor imaging detects abnormalities in the corticospinal tracts of neonates with infantile Krabbe disease. *AJNR Am. J. Neuroradiol.* 30, 1017–1021. doi: 10.3174/ajnr.A1476

Escolar, M. L., West, T., Dallavecchia, A., Poe, M. D., and LaPoint, K. (2016). Clinical management of Krabbe disease. *J. Neurosci. Res.* 94, 1118–1125. doi: 10.1002/jnr.23891

Fiumara, A., Barone, R., Arena, A., Filocamo, M., Lissens, W., Pavone, L., et al. (2011). Krabbe leukodystrophy in a selected population with high rate of late onset forms: Longer survival linked to c.121G>A (p.Gly41Ser) mutation. *Clin. Genet.* 80, 452–458. doi: 10.1111/j.1399-0004.2010.01572.x

Fukazawa, R., Takeuchi, H., Oka, N., Shibuya, T., Sakai, N., and Fujii, A. (2021). Adult Krabbe disease that was successfully treated with intravenous immunoglobulin. *Intern. Med.* 60, 1283–1286. doi: 10.2169/internalmedicine.6094-20

Furuya, H., Kukita, Y., Nagano, S., Sakai, Y., Yamashita, Y., Fukuyama, H., et al. (1997). Adult onset globoid cell leukodystrophy (Krabbe disease): Analysis of galactosylceramidase cDNA from four Japanese patients. *Hum. Genet.* 100, 450–456. doi: 10.1007/s004390050532

Galbiati, F., Givogri, M. I., Cantuti, L., Rosas, A. L., Cao, H., van Breemen, R., et al. (2009). Combined hematopoietic and lentiviral gene-transfer therapies in newborn Twitcher mice reveal contemporaneous neurodegeneration and demyelination in Krabbe disease. *J. Neurosci. Res.* 87, 1748–1759. doi: 10.1002/jnr.22006

Ganesan, K., Desai, S., and Hegde, A. (2010). Multiple cranial nerve enhancement: Uncommon imaging finding in early infantile Krabbe's disease. *J. Neuroimaging* 20, 195–197. doi: 10.1111/j.1552-6569.2008.00308.x

Garcia, A. M., Morais, N. M., Ohlweiler, L., Winckler, M. I., Ranzan, J., Artigalás, O. A., et al. (2010). Optic nerve enlargement and leukodystrophy: An unusual finding of the infantile form of Krabbe disease. *Arq. Neuropsiquiatr.* 68, 816–818. doi: 10.1590/s0004-282x2010000500029

Giacomini, A., Ackermann, M., Belleri, M., Coltrini, D., Nico, B., Ribatti, D., et al. (2015). Brain angioarchitecture and intussusceptive microvascular growth in a murine model of Krabbe disease. *Angiogenesis* 18, 499–510. doi: 10.1007/s10456-015-9481-6

Giri, S., Khan, M., Nath, N., Singh, I., and Singh, A. K. (2008). The role of AMPK in psychosine mediated effects on oligodendrocytes and astrocytes: Implication for Krabbe disease. *J. Neurochem.* 105, 1820–1833. doi: 10.1111/j.1471-4159.2008\vspace*{1pt}.05279.x

Giri, S., Khan, M., Rattan, R., Singh, I., and Singh, A. K. (2006). Krabbe disease: Psychosine-mediated activation of phospholipase A2 in oligodendrocyte cell death. *J. Lipid Res.* 47, 1478–1492. doi: 10.1194/jlr.M600084-JLR200

Graziano, A. C., and Cardile, V. (2015). History, genetic, and recent advances on Krabbe disease. *Gene* 555, 2–13. doi: 10.1016/j.gene.2014.09.046

Graziano, A. C., Parenti, R., Avola, R., and Cardile, V. (2016). Krabbe disease: Involvement of connexin43 in the apoptotic effects of sphingolipid psychosine on mouse oligodendrocyte precursors. *Apoptosis* 21, 25–35. doi: 10.1007/s10495-015-1183-4

Griffiths, G. (1989). The structure and function of a mannose 6-phosphate receptor-enriched, pre-lysosomal compartment in animal cells. *J. Cell Sci. Suppl.* 11, 139–147. doi: 10.1242/jcs.1989.supplement_11.11

Hagberg, B. (1984). Krabbe's disease: Clinical presentation of neurological variants. *Neuropediatrics* 15(Suppl.), 11–15. doi: 10.1055/s-2008-1052374

Hamanoue, M., Yoshioka, A., Ohashi, T., Eto, Y., and Takamatsu, K. (2004). NF-kappaB prevents TNF-alpha-induced apoptosis in an oligodendrocyte cell line. *Neurochem. Res.* 29, 1571–1576. doi: 10.1023/b:nere.0000029571.39497.56

Haq, E., Contreras, M. A., Giri, S., Singh, I., and Singh, A. K. (2006). Dysfunction of peroxisomes in twitcher mice brain: A possible mechanism of psychosine-induced disease. *Biochem. Biophys. Res. Commun.* 343, 229–238. doi: 10.1016/j.bbrc.2006.02.131

Haq, E., Giri, S., Singh, I., and Singh, A. K. (2003). Molecular mechanism of psychosine-induced cell death in human oligodendrocyte cell line. *J. Neurochem.* 86, 1428–1440. doi: 10.1046/j.1471-4159.2003.01941.x

Hardie, D. G. (2004). The AMP-activated protein kinase pathway–new players upstream and downstream. *J. Cell Sci.* 117(Pt 23), 5479–5487. doi: 10.1242/jcs.01540

Harzer, K., Knoblich, R., Rolfs, A., Bauer, P., and Eggers, J. (2002). Residual galactosylsphingosine (psychosine) beta-galactosidase activities and associated

GALC mutations in late and very late onset Krabbe disease. *Clin. Chim. Acta* 317, 77–84. doi: 10.1016/s0009-8981(01)00791-4

Hawkins-Salsbury, J. A., Parameswar, A. R., Jiang, X., Schlesinger, P. H., Bongarzone, E., Ory, D. S., et al. (2013). Psychosine, the cytotoxic sphingolipid that accumulates in globoid cell leukodystrophy, alters membrane architecture. *J. Lipid Res.* 54, 3303–3311. doi: 10.1194/jlr.M039610

Hawkins-Salsbury, J. A., Qin, E. Y., Reddy, A. S., Vogler, C. A., and Sands, M. S. (2012). Oxidative stress as a therapeutic target in globoid cell leukodystrophy. *Exp. Neurol.* 237, 444–452. doi: 10.1016/j.expneurol.2012.07.013

Hawkins-Salsbury, J. A., Shea, L., Jiang, X., Hunter, D. A., Guzman, A. M., Reddy, A. S., et al. (2015). Mechanism-based combination treatment dramatically increases therapeutic efficacy in murine globoid cell leukodystrophy. *J. Neurosci.* 35, 6495–6505. doi: 10.1523/JNEUROSCI.4199-14.2015

Henderson, R. D., MacMillan, J. C., and Bradfield, J. M. (2003). Adult onset Krabbe disease may mimic motor neurone disease. *J. Clin. Neurosci.* 10, 638–639. doi: 10.1016/s0967-5868(02)00302-8

Hiyama, T., Masumoto, T., Hara, T., Kunimatsu, A., Mamada, N., Kiyotaka, N., et al. (2016). Enlargement of the brachial plexus on magnetic resonance imaging: A novel finding in adult-onset Krabbe disease. *BJR Case Rep.* 2:20150213. doi: 10.1259/bjrcr.20150213

Hollie, N. I., Cash, J. G., Matlib, M. A., Wortman, M., Basford, J. E., Abplanalp, W., et al. (2014). Micromolar changes in lysophosphatidylcholine concentration cause minor effects on mitochondrial permeability but major alterations in function. *Biochim. Biophys. Acta* 1841, 888–895. doi: 10.1016/j.bbalip.2013.11.013

Hordeaux, J., Jeffrey, B. A., Jian, J., Choudhury, G. R., Michalson, K., Mitchell, T. W., et al. (2022). Efficacy and safety of a Krabbe disease gene therapy. *Hum. Gene Ther.* 33, 499–517. doi: 10.1089/hum.2021.245

Hossain, M. A., Otomo, T., Saito, S., Ohno, K., Sakuraba, H., Hamada, Y., et al. (2014). Late-onset Krabbe disease is predominant in Japan and its mutant precursor protein undergoes more effective processing than the infantile-onset form. *Gene* 534, 144–154. doi: 10.1016/j.gene.2013.11.003

Hwang, M., Zuccoli, G., Panigrahy, A., Rodriguez, D., Poe, M. D., and Escolar, M. L. (2016). Thickening of the cauda equina roots: A common finding in Krabbe disease. *Eur. Radiol.* 26, 3377–3382. doi: 10.1007/s00330-016-4233-6

Iacono, S., Del Giudice, E., Leon, A., La Bella, V., and Spataro, R. (2022). A novel compound heterozygous mutation in GALC associated with adult-onset Krabbe disease: Case report and literature review. *Neurogenetics* 23, 157–165. doi: 10.1007/s10048-021-00682-1

Ida, H., Eto, Y., and Maekawa, K. (1990). Biochemical pathogenesis of demyelination in globoid cell leukodystrophy (Krabbe's disease): The effects of psychosine upon oligodendroglial cell culture. *Acta Paediatr. Jpn.* 32, 20–26. doi: 10.1111/j.1442-200x.1990.tb00779.x

Jatana, M., Giri, S., and Singh, A. K. (2002). Apoptotic positive cells in Krabbe brain and induction of apoptosis in rat C6 glial cells by psychosine. *Neurosci. Lett.* 330, 183–187. doi: 10.1016/s0304-3940(02)00655-9

Jurewicz, A., Matysiak, M., Andrzejak, S., and Selmaj, K. (2006). TRAIL-induced death of human adult oligodendrocytes is mediated by JNK pathway. *Glia* 53, 158–166. doi: 10.1002/glia.20249

Kagitani-Shimono, K., Mohri, I., Fujitani, Y., Suzuki, K., Ozono, K., Urade, Y., et al. (2005). Anti-inflammatory therapy by ibudilast, a phosphodiesterase inhibitor, in demyelination of twitcher, a genetic demyelination model. *J. Neuroinflammation* 2:10. doi: 10.1186/1742-2094-2-10

Kalous, M., Rauchová, H., and Drahota, Z. (1992). The effect of lysophosphatidylcholine on the activity of various mitochondrial enzymes. *Biochim. Biophys. Acta* 1098, 167–171. doi: 10.1016/s0005-2728(05)80332-9

Kanazawa, T., Nakamura, S., Momoi, M., Yamaji, T., Takematsu, H., Yano, H., et al. (2000). Inhibition of cytokinesis by a lipid metabolite, psychosine. *J. Cell Biol.* 149, 943–950. doi: 10.1083/jcb.149.4.943

Khan, M., Haq, E., Giri, S., Singh, I., and Singh, A. K. (2005). Peroxisomal participation in psychosine-mediated toxicity: Implications for Krabbe's disease. *J. Neurosci. Res.* 80, 845–854. doi: 10.1002/jnr.20529

Kinney, H. C., Brody, B. A., Kloman, A. S., and Gilles, F. H. (1988). Sequence of central nervous system myelination in human infancy. II. Patterns of myelination in autopsied infants. *J. Neuropathol. Exp. Neurol.* 47, 217–234. doi: 10.1097/00005072-198805000-00003

Kleijer, W. J., Keulemans, J. L., van der Kraan, M., Geilen, G. G., van der Helm, R. M., Rafi, M. A., et al. (1997). Prevalent mutations in the GALC gene of patients with Krabbe disease of Dutch and other European origin. *J. Inherit. Metab. Dis.* 20, 587–594. doi: 10.1023/a:1005315311165

Kobayashi, S., Chiu, F. C., Katayama, M., Sacchi, R. S., Suzuki, K., and Suzuki, K. (1986). Expression of glial fibrillary acidic protein in the CNS and PNS of murine globoid cell leukodystrophy, the twitcher. *Am. J. Pathol.* 125, 227–243.

Krivit, W., Shapiro, E. G., Peters, C., Wagner, J. E., Cornu, G., Kurtzberg, J., et al. (1998). Hematopoietic stem-cell transplantation in globoid-cell leukodystrophy. *N. Engl. J. Med.* 338, 1119–1126. doi: 10.1056/NEJM199804163381605

Kuai, X. L., Ni, R. Z., Zhou, G. X., Mao, Z. B., Zhang, J. F., Yi, N., et al. (2015). Transplantation of mouse embryonic stem cell-derived oligodendrocytes in the murine model of globoid cell leukodystrophy. *Stem Cell Res. Ther.* 6:30. doi: 10.1186/s13287-015-0024-2

Kwon, J. M., Matern, D., Kurtzberg, J., Wrabetz, L., Gelb, M. H., Wenger, D. A., et al. (2018). Consensus guidelines for newborn screening, diagnosis and treatment of infantile Krabbe disease. *Orphanet. J. Rare Dis.* 13:30. doi: 10.1186/s13023-018-0766-x

Lee, W. C., Courtenay, A., Troendle, F. J., Stallings-Mann, M. L., Dickey, C. A., DeLucia, M. W., et al. (2005). Enzyme replacement therapy results in substantial improvements in early clinical phenotype in a mouse model of globoid cell leukodystrophy. *FASEB J.* 19, 1549–1551. doi: 10.1096/fj.05-3826fje

Lee, W. C., Tsoi, Y. K., Troendle, F. J., DeLucia, M. W., Ahmed, Z., Dicky, C. A., et al. (2007). Single-dose intracerebroventricular administration of galactocerebrosidase improves survival in a mouse model of globoid cell leukodystrophy. *FASEB J.* 21, 2520–2527. doi: 10.1096/fj.06-6169com

Lemmens, R., Piessens, F., Demaerel, P., and Robberecht, W. (2011). Unilateral white matter involvement in Krabbe disease. *Arch. Neurol.* 68, 130–131. doi: 10.1001/archneurol.2010.331

LeVine, S. M., Pedchenko, T. V., Bronshteyn, I. G., and Pinson, D. M. (2000). L-cycloserine slows the clinical and pathological course in mice with globoid cell leukodystrophy (twitcher mice). *J. Neurosci. Res.* 60, 231–236. doi: 10.1002/(SICI)1097-4547(20000415)60:2<231::AID-JNR12>3.0.CO;2-E

Lgisu, H. (1989). Psychosine: A "toxin" produced in the brain–its mechanism of action. *J. UOEH* 11, 487–493. doi: 10.7888/juoeh.11.487

Liao, P., Gelinas, J., and Sirrs, S. (2014). Phenotypic variability of Krabbe disease across the lifespan. *Can. J. Neurol. Sci.* 41, 5–12. doi: 10.1017/s0317167100016188

Lim, S. M., Choi, B. O., Oh, S. I., Choi, W. J., Oh, K. W., Nahm, M., et al. (2016). Patient fibroblasts-derived induced neurons demonstrate autonomous neuronal defects in adult-onset Krabbe disease. *Oncotarget* 7, 74496–74509. doi: 10.18632/oncotarget.12812

Lin, D., Donsante, A., Macauley, S., Levy, B., Vogler, C., and Sands, M. S. (2007). Central nervous system-directed AAV2/5-mediated gene therapy synergizes with bone marrow transplantation in the murine model of globoid-cell leukodystrophy. *Mol. Ther.* 15, 44–52. doi: 10.1038/sj.mt.6300026

Luzi, P., Abraham, R. M., Rafi, M. A., Curtis, M., Hooper, D. C., and Wenger, D. A. (2009). Effects of treatments on inflammatory and apoptotic markers in the CNS of mice with globoid cell leukodystrophy. *Brain Res.* 1300, 146–158. doi: 10.1016/j.brainres.2009.09.017

Luzi, P., Rafi, M. A., Victoria, T., Baskin, G. B., and Wenger, D. A. (1997). Characterization of the rhesus monkey galactocerebrosidase (GALC) cDNA and gene and identification of the mutation causing globoid cell leukodystrophy (Krabbe disease) in this primate. *Genomics* 42, 319–324. doi: 10.1006/geno.1997.4744

Luzi, P., Rafi, M. A., and Wenger, D. A. (1995). Structure and organization of the human galactocerebrosidase (GALC) gene. *Genomics* 26, 407–409. doi: 10.1016/0888-7543(95)80230-j

Luzi, P., Rafi, M. A., and Wenger, D. A. (1996). Multiple mutations in the GALC gene in a patient with adult-onset Krabbe disease. *Ann. Neurol.* 40, 116–119. doi: 10.1002/ana.410400119

Lyon, G., Hagberg, B., Evrard, P., Allaire, C., Pavone, L., and Vanier, M. (1991). Symptomatology of late onset Krabbe's leukodystrophy: The European experience. *Dev. Neurosci.* 13, 240–244. doi: 10.1159/000112167

Macarov, M., Zlotogora, J., Meiner, V., Khatib, Z., Sury, V., Mengistu, G., et al. (2011). Genetic screening for Krabbe disease: Learning from the past and looking to the future. *Am. J. Med. Genet. Part A* 155A, 574–576. doi: 10.1002/ajmg.a.33815

Madsen, A. M. H., Wibrand, F., Lund, A. M., Ek, J., Dunø, M., and Østergaard, E. (2019). Genotype and phenotype classification of 29 patients affected by Krabbe disease. *JIMD Rep.* 46, 35–45. doi: 10.1002/jmd2.12007

Malandrini, A., D'Eramo, C., Palmeri, S., Gaudiano, C., Gambelli, S., Sicurelli, F., et al. (2013). Peripheral neuropathy in late-onset Krabbe disease: Report of three cases. *Neurol. Sci.* 34, 79–83. doi: 10.1007/s10072-012-0956-6

Mamada, N., Nakamagoe, K., Shioya, A., Furuta, J., Sakai, N., Ishii, A., et al. (2016). Adult-onset Krabbe disease presenting as acute hemiparesis and progressive demyelination detected by diffusion-weighted imaging. *J. Neurol. Sci.* 367, 326–328. doi: 10.1016/j.jns.2016.06.026

Marcus, J., Honigbaum, S., Shroff, S., Honke, K., Rosenbluth, J., and Dupree, J. L. (2006). Sulfatide is essential for the maintenance of CNS myelin and axon structure. *Glia* 53, 372–381. doi: 10.1002/glia.20292

Marks, H. G., Scavina, M. T., Kolodny, E. H., Palmieri, M., and Childs, J. (1997). Krabbe's disease presenting as a peripheral neuropathy. *Muscle Nerve* 20, 1024–1028.

Matsumoto, R., Oka, N., Nagahama, Y., Akiguchi, I., and Kimura, J. (1996). Peripheral neuropathy in late-onset Krabbe's disease: Histochemical and ultrastructural findings. *Acta Neuropathol.* 92, 635–639. doi: 10.1007/s004010050573

Meng, X., Li, Y., Lian, Y., Li, Y., Du, L., Xie, N., et al. (2020). A new compound heterozygous mutation in adult-onset Krabbe disease. *Int. J. Neurosci.* 130, 1267–1271. doi: 10.1080/00207454.2020.1731504

Mikulka, C. R., and Sands, M. S. (2016). Treatment for Krabbe's disease: Finding the combination. *J. Neurosci. Res.* 94, 1126–1137. doi: 10.1002/jnr.23822

Muthusamy, K., Sudhakar, S. V., Thomas, M., Yoganathan, S., Christudass, C. S., Chandran, M., et al. (2019). Revisiting magnetic resonance imaging pattern of Krabbe disease - Lessons from an Indian cohort. *J. Clin. Imaging Sci.* 9:25. doi: 10.25259/JCIS-18-2019

Nagano, S., Yamada, T., Shinnoh, N., Furuya, H., Taniwaki, T., and Kira, J. (1998). Expression and processing of recombinant human galactosylceramidase. *Clin. Chim. Acta* 276, 53–61. doi: 10.1016/s0009-8981(98)00095-3

Nagara, H., Ogawa, H., Sato, Y., Kobayashi, T., and Suzuki, K. (1986). The twitcher mouse: Degeneration of oligodendrocytes in vitro. *Brain Res.* 391, 79–84. doi: 10.1016/0165-3806(86)90009-x

Nasir, G., Chopra, R., Elwood, F., and Ahmed, S. S. (2021). Krabbe disease: Prospects of finding a cure using AAV gene therapy. *Front. Med.* 8:760236. doi: 10.3389/fmed.2021.760236

Neufeld, E. F., and Fratantoni, J. C. (1970). Inborn errors of mucopolysaccharide metabolism. *Science* 169, 141–146. doi: 10.1126/science.169.3941.141

Paintlia, M. K., Singh, I., and Singh, A. K. (2015). Effect of vitamin D3 intake on the onset of disease in a murine model of human Krabbe disease. *J. Neurosci. Res.* 93, 28–42. doi: 10.1002/jnr.23476

Paiva, A. R. B., Fonseca Neto, R. E., Afonso, C. L., Freua, F., Nóbrega, P. R., and Kok, F. (2022). Incidental magnetic resonance imaging findings leading to an unusual diagnosis: Adult onset Krabbe disease. *Eur. J. Neurol.* 29, 1859–1862. doi: 10.1111/ene.15298

Pannuzzo, G., Cardile, V., Costantino-Ceccarini, E., Alvares, E., Mazzone, D., and Perciavalle, V. (2010). A galactose-free diet enriched in soy isoflavones and antioxidants results in delayed onset of symptoms of Krabbe disease in twitcher mice. *Mol. Genet. Metab.* 100, 234–240. doi: 10.1016/j.ymgme.2010.03.021

Parenti, G., Andria, G., and Ballabio, A. (2015). Lysosomal storage diseases: From pathophysiology to therapy. *Annu. Rev. Med.* 66, 471–486. doi: 10.1146/annurev-med-122313-085916

Passini, M. A., Dodge, J. C., Bu, J., Yang, W., Zhao, Q., Sondhi, D., et al. (2006). Intracranial delivery of CLN2 reduces brain pathology in a mouse model of classical late infantile neuronal ceroid lipofuscinosis. *J. Neurosci.* 26, 1334–1342. doi: 10.1523/JNEUROSCI.2676-05.2006

Passini, M. A., Macauley, S. L., Huff, M. R., Taksir, T. V., Bu, J., Wu, I. H., et al. (2005). AAV vector-mediated correction of brain pathology in a mouse model of Niemann-Pick A disease. *Mol. Ther.* 11, 754–762. doi: 10.1016/j.ymthe.2005.01.011

Patel, B., Gimi, B., Vachha, B., Agadi, S., and Koral, K. (2008). Optic nerve and chiasm enlargement in a case of infantile Krabbe disease: Quantitative comparison with 26 age-matched controls. *Pediatr. Radiol.* 38, 697–699. doi: 10.1007/s00247-008-0849-2

Pernber, Z., Molander-Melin, M., Berthold, C. H., Hansson, E., and Fredman, P. (2002). Expression of the myelin and oligodendrocyte progenitor marker sulfatide in neurons and astrocytes of adult rat brain. *J. Neurosci. Res.* 69, 86–93. doi: 10.1002/jnr.10264

Phelps, M., Aicardi, J., and Vanier, M. T. (1991). Late onset Krabbe's leukodystrophy: A report of four cases. *J. Neurol. Neurosurg. Psychiatry* 54, 293–296. doi: 10.1136/jnnp.54.4.293

Poretti, A., Meoded, A., Bunge, M., Fatemi, A., Barrette, P., Huisman, T. A., et al. (2014). Novel diffusion tensor imaging findings in Krabbe disease. *Eur. J. Paediatr. Neurol.* 18, 150–156. doi: 10.1016/j.ejpn.2013.09.008

Poretti, A., Meoded, A., and Fatemi, A. (2016). Diffusion tensor imaging: A biomarker of outcome in Krabbe's disease. *J. Neurosci. Res.* 94, 1108–1115. doi: 10.1002/jnr.23769

Provenzale, J. M., Escolar, M., and Kurtzberg, J. (2005). Quantitative analysis of diffusion tensor imaging data in serial assessment of Krabbe disease. *Ann. N. Y. Acad. Sci.* 1064, 220–229. doi: 10.1196/annals.1340.040

Qin, E. Y., Hawkins-Salsbury, J. A., Jiang, X., Reddy, A. S., Farber, N. B., Ory, D. S., et al. (2012). Bone marrow transplantation increases efficacy of central nervous system-directed enzyme replacement therapy in the murine model of globoid cell leukodystrophy. *Mol. Genet. Metab.* 107, 186–196. doi: 10.1016/j.ymgme.2012.05.021

Quintas-Neves, M., Xavier, S. A., and Soares-Fernandes, J. P. (2020). Sixth cranial nerve involvement in early onset Krabbe disease. *Neuropediatrics* 51, 307–308. doi: 10.1055/s-0040-1701661

Rafi, M. A. (2016). Gene therapy for CNS diseases - Krabbe disease. *Bioimpacts* 6, 69–70. doi: 10.15171/bi.2016.09

Rafi, M. A., Luzi, P., Chen, Y. Q., and Wenger, D. A. (1995). A large deletion together with a point mutation in the GALC gene is a common mutant allele in patients with infantile Krabbe disease. *Hum. Mol. Genet.* 4, 1285–1289. doi: 10.1093/hmg/4.8.1285

Rafi, M. A., Luzi, P., Zlotogora, J., and Wenger, D. A. (1996). Two different mutations are responsible for Krabbe disease in the Druze and Moslem Arab populations in Israel. *Hum. Genet.* 97, 304–308. doi: 10.1007/BF02185759

Rafi, M. A., Rao, H. Z., Luzi, P., Curtis, M. T., and Wenger, D. A. (2012). Extended normal life after AAVrh10-mediated gene therapy in the mouse model of Krabbe disease. *Mol. Ther.* 20, 2031–2042. doi: 10.1038/mt.2012.153

Rafi, M. A., Rao, H. Z., Luzi, P., Luddi, A., Curtis, M. T., and Wenger, D. A. (2015a). Intravenous injection of AAVrh10-GALC after the neonatal period in twitcher mice results in significant expression in the central and peripheral nervous systems and improvement of clinical features. *Mol. Genet. Metab.* 114, 459–466. doi: 10.1016/j.ymgme.2014.12.300

Rafi, M. A., Rao, H. Z., Luzi, P., and Wenger, D. A. (2015b). Long-term improvements in lifespan and pathology in CNS and PNS after BMT plus one intravenous injection of AAVrh10-GALC in twitcher mice. *Mol. Ther.* 23, 1681–1690. doi: 10.1038/mt.2015.145

Rafi, M. A., Zhi Rao, H., Passini, M. A., Curtis, M., Vanier, M. T., Zaka, M., et al. (2005). AAV-mediated expression of galactocerebrosidase in brain results in attenuated symptoms and extended life span in murine models of globoid cell leukodystrophy. *Mol. Ther.* 11, 734–744. doi: 10.1016/j.ymthe.2004.12.020

Ransohoff, R. M., and Brown, M. A. (2012). Innate immunity in the central nervous system. *J. Clin. Invest.* 122, 1164–1171. doi: 10.1172/JCI58644

Reddy, A. S., Kim, J. H., Hawkins-Salsbury, J. A., Macauley, S. L., Tracy, E. T., Vogler, C. A., et al. (2011). Bone marrow transplantation augments the effect of brain- and spinal cord-directed adeno-associated virus 2/5 gene therapy by altering inflammation in the murine model of globoid-cell leukodystrophy. *J. Neurosci.* 31, 9945–9957. doi: 10.1523/JNEUROSCI.1802-11.2011

Ripoll, C. B., Flaat, M., Klopf-Eiermann, J., Fisher-Perkins, J. M., Trygg, C. B., Scruggs, B. A., et al. (2011). Mesenchymal lineage stem cells have pronounced anti-inflammatory effects in the twitcher mouse model of Krabbe's disease. *Stem Cells* 29, 67–77. doi: 10.1002/stem.555

Romano, A., De Simone, R., Fasoli, F., Ferrante, M., Cipriani, V., Fantozzi, L. M., et al. (2009). Selective white matter involvement in a patient with late onset Krabbe disease: MR, MR spectroscopy, and diffusion tensor study. *J. Neuroimaging* 19, 191–193. doi: 10.1111/j.1552-6569.2008.00258.x

Sabatelli, M., Quaranta, L., Madia, F., Lippi, G., Conte, A., Lo Monaco, M., et al. (2002). Peripheral neuropathy with hypomyelinating features in adult-onset Krabbe's disease. *Neuromuscul. Disord.* 12, 386–391. doi: 10.1016/s0960-8966(01)00285-1

Sakai, N., Inui, K., Tatsumi, N., Fukushima, H., Nishigaki, T., Taniike, M., et al. (1996). Molecular cloning and expression of cDNA for murine galactocerebrosidase and mutation analysis of the twitcher mouse, a model of Krabbe's disease. *J. Neurochem.* 66, 1118–1124. doi: 10.1046/j.1471-4159.1996.66031118.x

Schaeren-Wiemers, N., van der Bijl, P., and Schwab, M. E. (1995). The UDP-galactose:ceramide galactosyltransferase: Expression pattern in oligodendrocytes and Schwann cells during myelination and substrate preference for hydroxyceramide. *J. Neurochem.* 65, 2267–2278. doi: 10.1046/j.1471-4159.1995.65052267.x

Schiffmann, R., and van der Knaap, M. S. (2009). Invited article: An MRI-based approach to the diagnosis of white matter disorders. *Neurology* 72, 750–759. doi: 10.1212/01.wnl.0000343049.00540.c8

Schrier Vergano, S. A., Kanungo, S., and Arnold, G. (2022). Making decisions about Krabbe disease newborn screening. *Pediatrics* 149:e2021053175. doi: 10.1542/peds.2021-053175

Schulte, S., and Stoffel, W. (1993). Ceramide UDPgalactosyltransferase from myelinating rat brain: Purification, cloning, and expression. *Proc. Natl. Acad. Sci. U.S.A.* 90, 10265–10269. doi: 10.1073/pnas.90.21.10265

Sharp, M. E., Laule, C., Nantel, S., Mädler, B., Aul, R. B., Yip, S., et al. (2013). Stem cell transplantation for adult-onset Krabbe disease: Report of a case. *JIMD Rep.* 10, 57–59. doi: 10.1007/8904_2012_203

Siddiqi, Z. A., Sanders, D. B., and Massey, J. M. (2006). Peripheral neuropathy in Krabbe disease: Electrodiagnostic findings. *Neurology* 67, 263–267. doi: 10.1212/01.wnl.0000230153.34613.84

SSnook, E. R., Fisher-Perkins, J. M., Sansing, H. A., Lee, K. M., Alvarez, X., MacLean, A. G., et al. (2014). Innate immune activation in the pathogenesis of a murine model of globoid cell leukodystrophy. *Am. J. Pathol.* 184, 382–396. doi: 10.1016/j.ajpath.2013.10.011

Suzuki, K. (1998). Twenty five years of the "psychosine hypothesis": A personal perspective of its history and present status. *Neurochem. Res.* 23, 251–259. doi: 10.1023/a:1022436928925

Suzuki, K., and Suzuki, Y. (1970). Globoid cell leucodystrophy (Krabbe's disease): Deficiency of galactocerebroside beta-galactosidase. *Proc. Natl. Acad. Sci. U.S.A.* 66, 302–309. doi: 10.1073/pnas.66.2.302

Tanaka, S., Mito, T., and Takashima, S. (1995). Progress of myelination in the human fetal spinal nerve roots, spinal cord and brainstem with myelin basic protein immunohistochemistry. *Early Hum. Dev.* 41, 49–59. doi: 10.1016/0378-3782(94)01608-r

Tappino, B., Biancheri, R., Mort, M., Regis, S., Corsolini, F., Rossi, A., et al. (2010). Identification and characterization of 15 novel GALC gene mutations causing Krabbe disease. *Hum. Mutat.* 31, E1894–E1914. doi: 10.1002/humu.21367

Tokushige, S., Sonoo, T., Maekawa, R., Shirota, Y., Hanajima, R., Terao, Y., et al. (2013). Isolated pyramidal tract impairment in the central nervous system of adult-onset Krabbe disease with novel mutations in the GALC gene. *Brain Dev.* 35, 579–581. doi: 10.1016/j.braindev.2012.08.004

Udow, S., Bunge, M., Ryner, L., Mhanni, A. A., and Salman, M. S. (2012). Prolonged survival and serial magnetic resonance imaging/magnetic resonance spectroscopy changes in infantile Krabbe disease. *Pediatr. Neurol.* 47, 299–302. doi: 10.1016/j.pediatrneurol.2012.06.015

Vasconcellos, E., and Smith, M. (1998). MRI nerve root enhancement in Krabbe disease. *Pediatr. Neurol.* 19, 151–152. doi: 10.1016/s0887-8994(98)00033-2

Victoria, T., Rafi, M. A., and Wenger, D. A. (1996). Cloning of the canine GALC cDNA and identification of the mutation causing globoid cell leukodystrophy in West Highland White and Cairn terriers. *Genomics* 33, 457–462. doi: 10.1006/geno.1996.0220

Voccoli, V., Tonazzini, I., Signore, G., Caleo, M., and Cecchini, M. (2014). Role of extracellular calcium and mitochondrial oxygen species in psychosine-induced oligodendrocyte cell death. *Cell Death Dis.* 5:e1529. doi: 10.1038/cddis.2014.483

Wang, C., Melberg, A., Weis, J., Månsson, J. E., and Raininko, R. (2007). The earliest MR imaging and proton MR spectroscopy abnormalities in adult-onset Krabbe disease. *Acta Neurol. Scand.* 116, 268–272. doi: 10.1111/j.1600-0404.2007.00867.x

Wang, Y., Gupta, A., Liu, Z., Zhang, H., Escolar, M. L., Gilmore, J. H., et al. (2011). DTI registration in atlas based fiber analysis of infantile Krabbe disease. *Neuroimage* 55, 1577–1586. doi: 10.1016/j.neuroimage.2011.01.038

Wenger, D. A., Luzi, P., and Rafi, M. A. (2021). Advances in the diagnosis and treatment of Krabbe disease. *Int. J. Neonatal Screen.* 7:57. doi: 10.3390/ijns7030057

Wenger, D. A., Rafi, M. A., and Luzi, P. (1997). Molecular genetics of Krabbe disease (globoid cell leukodystrophy): Diagnostic and clinical implications. *Hum. Mutat.* 10, 268–279. doi: 10.1002/(SICI)1098-1004(1997)10:4<268::AID-HUMU2>3.0.CO;2-D

Wenger, D. A., Rafi, M. A., and Luzi, P. (2016). Krabbe disease: One Hundred years from the bedside to the bench to the bedside. *J. Neurosci. Res.* 94, 982–989. doi: 10.1002/jnr.23743

White, A. B., Galbiati, F., Givogri, M. I., Lopez Rosas, A., Qiu, X., van Breemen, R., et al. (2011). Persistence of psychosine in brain lipid rafts is a limiting factor in the therapeutic recovery of a mouse model for Krabbe disease. *J. Neurosci. Res.* 89, 352–364. doi: 10.1002/jnr.22564

Won, J. S., Kim, J., Paintlia, M. K., Singh, I., and Singh, A. K. (2013). Role of endogenous psychosine accumulation in oligodendrocyte differentiation and survival: Implication for Krabbe disease. *Brain Res.* 1508, 44–52. doi: 10.1016/j.brainres.2013.02.024

Won, J. S., Singh, A. K., and Singh, I. (2016). Biochemical, cell biological, pathological, and therapeutic aspects of Krabbe's disease. *J. Neurosci. Res.* 94, 990–1006. doi: 10.1002/jnr.23873

Wright, M. D., Poe, M. D., DeRenzo, A., Haldal, S., and Escolar, M. L. (2017). Developmental outcomes of cord blood transplantation for Krabbe disease: A 15-year study. *Neurology* 89, 1365–1372. doi: 10.1212/WNL.0000000000004418

Wu, L., Liao, X., Yang, S., and Gan, S. (2021). Krabbe disease associated with mitochondrial dysfunction in a Chinese family. *Front. Neurol.* 12:750095. doi: 10.3389/fneur.2021.750095

Wu, Y. P., McMahon, E. J., Matsuda, J., Suzuki, K., Matsushima, G. K., and Suzuki, K. (2001). Expression of immune-related molecules is downregulated in twitcher mice following bone marrow transplantation. *J. Neuropathol. Exp. Neurol.* 60, 1062–1074. doi: 10.1093/jnen/60.11.1062

Xia, Z., Wenwen, Y., Xianfeng, Y., Panpan, H., Xiaoqun, Z., and Zhongwu, S. (2020). Adult-onset Krabbe disease due to a homozygous GALC mutation without abnormal signals on an MRI in a consanguineous family: A case report. *Mol. Genet. Genomic Med.* 8:e1407. doi: 10.1002/mgg3.1407

Xu, C., Sakai, N., Taniike, M., Inui, K., and Ozono, K. (2006). Six novel mutations detected in the GALC gene in 17 Japanese patients with Krabbe disease, and new genotype-phenotype correlation. *J. Hum. Genet.* 51, 548–554. doi: 10.1007/s10038-006-0396-3

Yang, Y., Ren, X., Xu, Q., Wang, C., Liu, H., and He, X. (2013). Four novel GALC gene mutations in two Chinese patients with Krabbe disease. *Gene* 519, 381–384. doi: 10.1016/j.gene.2013.02.010

Young, P. P., Fantz, C. R., and Sands, M. S. (2004). VEGF disrupts the neonatal blood-brain barrier and increases life span after non-ablative BMT in a murine model of congenital neurodegeneration caused by a lysosomal enzyme deficiency. *Exp. Neurol.* 188, 104–114. doi: 10.1016/j.expneurol.2004.03.007

Zayed, H. (2015). Krabbe disease in the arab world. *J. Pediatr. Genet.* 4, 1–8. doi: 10.1055/s-0035-1554981

Zhang, C., Liu, Z., and Dong, H. (2021). Two cases of female Chinese adult-onset krabbe disease with one novel mutation and a review of literature. *J. Mol. Neurosci.* 71, 1185–1192. doi: 10.1007/s12031-020-01742-1

Zhang, T., Yan, C., Ji, K., Lin, P., Chi, L., Zhao, X., et al. (2018). Adult-onset Krabbe disease in two generations of a Chinese family. *Ann. Transl. Med.* 6:174. doi: 10.21037/atm.2018.04.30

Zhong, J., Jiang, F., Yang, H., Li, J., Cheng, J., Zeng, Q., et al. (2020). Novel GALC mutations cause adult-onset Krabbe disease with myelopathy in two Chinese families: Case reports and literature review. *Front. Neurol.* 11:830. doi: 10.3389/fneur.2020.00830

frontiers | Frontiers in Neuroscience

TYPE Original Research
PUBLISHED 28 September 2022
DOI 10.3389/fnins.2022.1019989

Check for updates

OPEN ACCESS

EDITED BY
Yuzhen Xu,
Tongji University, China

REVIEWED BY
Shangkun Ou,
Xiamen University, China
Xuzhou Li,
Yunnan Normal University, China
Ce Shi,
Zhejiang University, China

*CORRESPONDENCE
Yu-Lin He
173386424@qq.com

†These authors have contributed equally to this work

SPECIALTY SECTION
This article was submitted to Neurodegeneration, a section of the journal Frontiers in Neuroscience

RECEIVED 15 August 2022
ACCEPTED 05 September 2022
PUBLISHED 28 September 2022

CITATION
Yang J, Shao Y, Li B, Yu Q-Y, Ge Q-M, Li B, Pan Y-C, Liang R-B, Wu S-N, Li Q-Y and He Y-L (2022) Altered regional homogeneity of spontaneous brain activity in patients with toothache: A resting-state functional magnetic resonance imaging study. *Front. Neurosci.* 16:1019989. doi: 10.3389/fnins.2022.1019989

COPYRIGHT
© 2022 Yang, Shao, Li, Yu, Ge, Li, Pan, Liang, Wu, Li and He. This is an open-access article distributed under the terms of the Creative Commons Attribution License (CC BY). The use, distribution or reproduction in other forums is permitted, provided the original author(s) and the copyright owner(s) are credited and that the original publication in this journal is cited, in accordance with accepted academic practice. No use, distribution or reproduction is permitted which does not comply with these terms.

Altered regional homogeneity of spontaneous brain activity in patients with toothache: A resting-state functional magnetic resonance imaging study

Jun Yang[1†], Yi Shao[2†], Bin Li[3], Qiu-Yue Yu[3], Qian-Min Ge[2], Biao Li[2], Yi-Cong Pan[2], Rong-Bin Liang[2], Shi-Nan Wu[2], Qiu-Yu Li[2] and Yu-Lin He[3]*

[1]The Key Laboratory of Oral Biomedicine, The Affiliated Stomatological Hospital of Nanchang University, Nanchang, China, [2]Department of Ophthalmology, The First Affiliated Hospital of Nanchang University, Nanchang, China, [3]Department of Radiology, The First Affiliated Hospital of Nanchang University, Nanchang, China

Toothache (TA) is a common and severe pain, but its effects on the brain are somewhat unclear. In this study, functional magnetic resonance imaging (fMRI) was used to compare regional homogeneity (ReHo) between TA patients and a normal control group and to explore the brain activity changes during TA, establishing the theoretical basis for the mechanism of neuropathic pain. In total, 20 TA patients and 20 healthy controls (HCs) were recruited and underwent assessment of pain, and then resting-state fMRI (rs-fMRI). The ReHo method was used to analyze the original whole-brain images. Pearson's correlation analysis was used to assess the relationship between mean ReHo values in each brain region and clinical symptoms, and the receiver operating characteristic (ROC) curve was used to conduct correlation analysis on the brain regions studied. The ReHo values of the right lingual gyrus (RLG), right superior occipital gyrus (RSOG), left middle occipital gyrus (LMOG) and right postcentral gyrus (RPG) in the TA group were significantly higher than in HCs. The mean ReHo values in the RLG were positively correlated with the anxiety score (AS) (r = 0.723, $p < 0.001$), depression score (DS) (r = 0.850, $p < 0.001$) and visual analogue score (VAS) (r = 0.837, $p < 0.001$). The mean ReHo values of RSOG were also positively correlated with AS (r = 0.687, p = 0.001), DS (r = 0.661, p = 0.002) and VAS (r = 0.712, $p < 0.001$). The areas under the ROC curve of specific brain area ReHo values were as follows: RLG, 0.975; RSOG,

0.959; LMOG, 0.975; RPG, 1.000. Various degrees of brain activity changes reflected by ReHo values in different areas of the brain indicate the impact of TA on brain function. These findings may reveal related neural mechanisms underlying TA.

KEYWORDS

toothache, regional homogeneity, rs-fMRI, neuroimaging, disease markers

Introduction

Toothache (TA) is the most common and severe pain in the field of stomatology. The oral area is distinct from other parts of the body due to its special anatomical characteristics and receptors. Medical images of typical TA show that it is often accompanied by swollen gums and severe alveolar bone resorption. TA is a symptom of potential damage, such as pulp infection. Clinical treatment to alleviate pain mainly targets pathological changes and is based on the assumption: the pain sensation of peripheral innervation can often be accurate positioning. Studies have shown that the treatment of tooth lesions does not achieve the purpose of pain relief. The reason was that the root cause of TA in some TA patients was not the teeth themselves, but the pain in this area caused by trigeminal neuropathy and bone afferent pain (Nixdorf et al., 2012). In addition, the degree of TA and the severity of lesions do not show a linear relationship, and the pain experienced is instead closely related to personal characteristics, psychological factors, and other factors (Wiech et al., 2008). Therefore, it is important to understand the cognitive regulation of the pain system to explore brain function in TA.

Resting-state functional magnetic resonance imaging (rs-fMRI) is a functional brain imaging technique that records signals reflecting metabolic changes related to neural activity in specific brain regions. The consistency of blood oxygen level-dependent (BOLD) signals between adjacent voxels in the brain is measured to evaluate the brain activity of subjects at rest (Zang et al., 2004; Biswal, 2012; Lin et al., 2013a). At each location in the brain, neighboring voxel BOLD signals show similar modulation over time. The ReHo is calculated using the REST toolkit using Kendall's coefficient of consistency (KCC) (Kippenhan et al., 1992). The ReHo (rs-ReHo) diagram of an individual's resting state is generated by combining the KCC value of each voxel and its 26 nearest neighboring voxels (Zang et al., 2004). Individual rs-ReHo diagrams are standardized with their own average KCC. Based on this concept, the regional homogeneity (ReHo) method can be used to measure the degree of similarity of different voxel time series in brain regions, to obtain information about brain activity, and determine the spontaneous fMRI signal partial synchronization (Brügger et al., 2011, 2012). As one of the data-driven methods for the study of fMRI, ReHo can collect more regional functional activity information than the model-driven method without any prior assumptions about the hemodynamic model, to further analyze the functional activity changes of temporary specific brain regions performing corresponding tasks (Zang et al., 2004). One of the advantages of ReHo is that it does not require random seed assignment and can be used to detect changes in any region of the cerebral (Tononi et al., 1998). In addition, compared with other traditional ALFF sequences, ReHo sequences can observe synchronous signals of neural functional activity in cerebral regions with similar functional activity changes. Therefore, the sequence can be used to analyze the corresponding cerebral regions as a whole and expand the wholeness of observation (Yue et al., 2020). Up to now, ReHo has also been used by some researchers in the study of pathology in psychiatric, neurological, and ophthalmic diseases such as the pathogenesis of epilepsy (Tang et al., 2014), optic neuritis (Shao et al., 2015), and comitant strabismus (Huang et al., 2016b).

Neuro-electrophysiology and neuro-orbital procedures have shown that structural networks involved in the multidimensional aspects of pain perception mainly included the primary and secondary somatosensory cortex, insula cortex, the anterior cingulate, prefrontal cortex, the thalamus, and cerebellar cortex (Apkarian et al., 2005; Farrell et al., 2005). Studies have found that the influence of TA on brain-associated networks is strikingly similar to that reported for spinal pain (Iannetti and Mouraux, 2010). A previous study reported the changes in brain functional connections in TA and found that the functional activities of the right lingual gyrus, right precentral gyrus, and left middle temporal gyrus were significantly higher than those of healthy subjects (Wu et al., 2020). The study also first confirmed that the degree centrality (DC) value of the right gyrus was positively correlated with the anxiety and depression scores of the subjects, and the DC value of the left middle temporal gyrus was positively correlated with the pain score. Our other previous study using ALFF sequence to study the changes in brain functional activities in TA patients also showed similar

results (Yang et al., 2019). Studies on the changes in functional activities in the corresponding brain regions of TA showed that different levels of TA stimulation were closely related to specific subregions in the cerebral cortex pain network, including the bilateral anterior insula and cingulate gyrus (Brügger et al., 2012). However, these pain-related brain changes which had been confirmed maybe not be caused by pain entirely, even if the location of the lesions and the nature of the stimulus are the same. The study of the changes in cerebral functional activity in patients with TA provides conditions for further study of the neuropathological mechanism of TA. To a certain extent, the severity of the disease and the exposure to clinical symptoms can be evaluated by monitoring the changes in cerebral function and activity, to provide personalized treatment for patients with TA. The purpose of this study was to analyze the relationship between changes in ReHo values alternations in specific brain regions and clinical outcomes in TA patients by processing fMRI data using the ReHo method.

Materials and methods

Participants

A total of 20 patients with TA and 20 healthy controls (HCs) were recruited at the first affiliated Hospital of Nanchang University. The inclusion criteria of TA patients were: (1) pulp and/or periodontal pain due to dental or non-dental disease; (2) acute and/or chronic TA (including trigeminal nerve pain); (3) no other comorbid pain diseases; (4) no contraindications to MRI examination; (5) no obvious abnormal signals showed in Routine MRI T1WI and T2WI sequences. Exclusion criteria included: (1) structural brain abnormalities, (2) systemic disease, recent intake of analgesic drugs, anti-inflammatory or narcotic drug allergy history, (3) long-term anxiety, depression, and other mental health abnormalities, (4) heart pacemakers and other metals in the body, contraindicating an MRI scan. A visual analog scale (VAS) was used to evaluate subjects' pain (Bijur et al., 2001). A score of 0 represented painlessness, and a score of 10 denoted excruciating pain. In addition, all subjects completed the Hospital Anxiety and fepression Scale (HADS) (Bjelland et al., 2002). Subjects were instructed to take no alcohol for 12 h before testing and MRI measurements were performed between 1 PM and 9 PM.

This study met the requirements of the Medical Ethics Committee of the first affiliated Hospital of Nanchang University. The approval number is cdyfy2017021. Subjects participating in this study expressed their willingness to participate and signed a declaration of informed consent after learning about the purpose, methods, and potential risks of the study.

Magnetic resonance imaging parameters

The Trio 3T MR scanner (Siemens Healthcare, Erlangen, Germany) was used for MRI scans Whole-brain T1 images were weighted using prepared magnetic gradient-echo images (MPRAGE). The corresponding metamorphic gradient echo sequence was conducted using the following parameters: repetition time (TR) 1,900 ms, echo time TE 2.26 ms, thickness 1.0 mm, gap 0.5 mm, acquisition matrix 256 × 256, the field of view (FOV) 250 mm × 250 mm and turning angle 9°. Functional images were then obtained using the gradient echo plane image sequence in the static scanning session with parameters TR 2,000 ms, TE 30 ms, thickness 4.0 mm, gap 1.2 mm, acquisition matrix 64 × 64, FOV 220 mm × 220 mm, turning angle 90° and 29 axial slices. In addition, all TA patients did not use other analgesic drugs during the rS-FMRI examination.

Functional magnetic resonance imaging data processing

To analyze the functional images we first used MRIcro software to filter unusable data and then used fMRI data processing assistant and Statistical Parameter Mapping (SPM8) for data processing (Huang et al., 2016a). To ensure that the measurement signals from each individual were balanced, the first ten volumes recorded from each individual were deleted. A series of recent studies have shown that head movement can significantly affect the results of rs-fMRI. In this study, we used the Friston 24-head motion parameter model to reduce the potential impact of head movement on the results (Van Dijk et al., 2012; Zeng et al., 2014). In addition, we used linear regression to eliminate the effects of respiration, local small motion, and low-frequency drift on the variables from variation or movement effects. After the correction of head movement, the functional magnetic resonance image was normalized to Montreal Neurological Institute space (Tate et al., 2014). Then the images were de-trended by bandpass filtering (0.01–0.08 Hz) to reduce the influence of factors such as physiological high-frequency breathing, low-frequency drift, and cardiac noise. Through the above data preprocessing methods, we ensure the image quality included in the experiment. Voxel calculations were then made in 27 individual clusters using the KCC. Based on the ReHo method, KCC was used to calculate the similarity between the time series of a given voxel and its nearest time series at the voxel level, to judge the functional activity changes of the corresponding cerebral regions. The details of the KCC calculation can be found in the references (Zang et al., 2004). The remaining data were smoothed using a full width half maximum Gaussian of 6 mm × 6 mm × 6 mm.

Regional homogeneity statistical analysis

ReHo computations were conducted using REST software. ReHo analysis was calculated for a given time series and its neighboring voxel time series using KCC to assess the consistency and comparability of each voxel, assuming similarity with its neighbors.

Statistical analysis

In this study, SPSS version 16.0 (IBM Corp., USA) was used to analyze clinical variables and demographics. Comparisons were made using an independent samples *t*-test, with *p* values less than 0.05 indicating statistical significance. The SPM8 toolkit was then used for general linear model analysis. To compare ReHo between the TA and HC groups, the two-sample *t*-test was used and Gaussian random field theory was applied to adjust for multiple comparisons ($P = 0.01$, 40 voxels, AlphaSim correction).

The receiver operating characteristic (ROC) curve was used to analyze the correlation between the mean ReHo values of different brain regions in each group. After obtaining the corresponding results, Pearson's correlation analysis was used to evaluate relationships between behavioral characteristics and ReHo values in the corresponding brain regions in the TA group, with $P < 0.05$ indicating a significant difference.

Results

Demographics

No significant difference in age was found between the two groups ($P = 0.692$). Demographic information and pain assessment of subjects are shown in Table 1. The mean ± standard deviation of TA duration was 0.19 ± 0.07 years.

TABLE 1 Demographics and behavioral results of TA and HC groups.

	TA	HC	*t*-value	*P*-value
Male/female	8/12	8/12	N/A	>0.99
Age (years)	41.18 ± 11.65	42.73 ± 12.66	0.094	0.692
Handedness	18 R	18 R	N/A	>0.99
Duration (years)	0.19 ± 0.07	N/A	N/A	N/A
VAS	6.41 ± 1.69	N/A	N/A	N/A

Independent *t*-tests comparing the two groups ($p < 0.05$ represented statistically significant differences). Data shown as mean standard deviation or *n*. TA, toothache; HC, healthy control; N/A, not applicable; VAS, Visual Analogue Scale.

Regional homogeneity differences

ReHo values were significantly higher in patients with TA than in HCs in the following brain regions: right lingual gyrus (RLG), right postcentral gyrus (RPG), left middle occipital gyrus (LMOG), and right superior occipital gyrus (RSOG) (Figures 1A,B, yellow and Table 2). Figure 1C shows differences in mean ReHo between TA and HC groups.

Correlation analysis

In the TA group, the mean ReHo values in the RLG were positively correlated with the anxiety score (AS) ($r = 0.723$, $p < 0.001$), depression score (DS) ($r = 0.850$, $p < 0.001$) and VAS ($r = 0.837$, $p < 0.001$). ReHo values at the RSOG were also positively correlated with the AS ($r = 0.687$, $p = 0.001$), DS ($r = 0.661$, $p = 0.002$) and VAS ($r = 0.712$, $p < 0.001$) (Figure 2).

Receiver operating characteristic curve

We adopted the ROC curve for differential diagnosis analysis, where the area under the curve (AUC) ranges from 0.5 to 0.7, indicating that the differential diagnosis accuracy of this indicator is low; when the AUC value ranges from 0.7 to 0.9, indicating that this indicator has moderate accuracy; when the AUC value is greater than 0.9, it means excellent precision in differential diagnosis (Chen et al., 2021). Areas under the curve (AUCs) for each region were as follows: RLG, 0.975; RSOG, 0.959 (Figure 3A); LMOG, 0.975; RPG, 1.000 (Figure 3B).

Discussion

Analysis of central nervous system activity has been an area of intense interest for many years. Since the invention of the electroencephalogram (EEG), brain function has been explored using a range of tools under various conditions. In recent decades, the characteristics of brain activity in the resting state have become a subject of great interest to various medical departments (Raichle and Snyder, 2007; Buckner et al., 2008), providing a new perspective for related studies on brain functional organization. Resting-state analysis has been used to assess ReHo values alternations relating to, movement, language, vision, processing, and other functions (Moussa et al., 2012; Lee et al., 2014). The stimuli produced by TA generate activity that may be analyzed in the resting state.

Studies have shown the importance of treating and diagnosing TA. To some extent, controlling pain is as important as treating the injury, the latter being challenging due to the difficulty in locating the damage. Even when pain-associated lesions are identified, TA is an emotional cognition-related

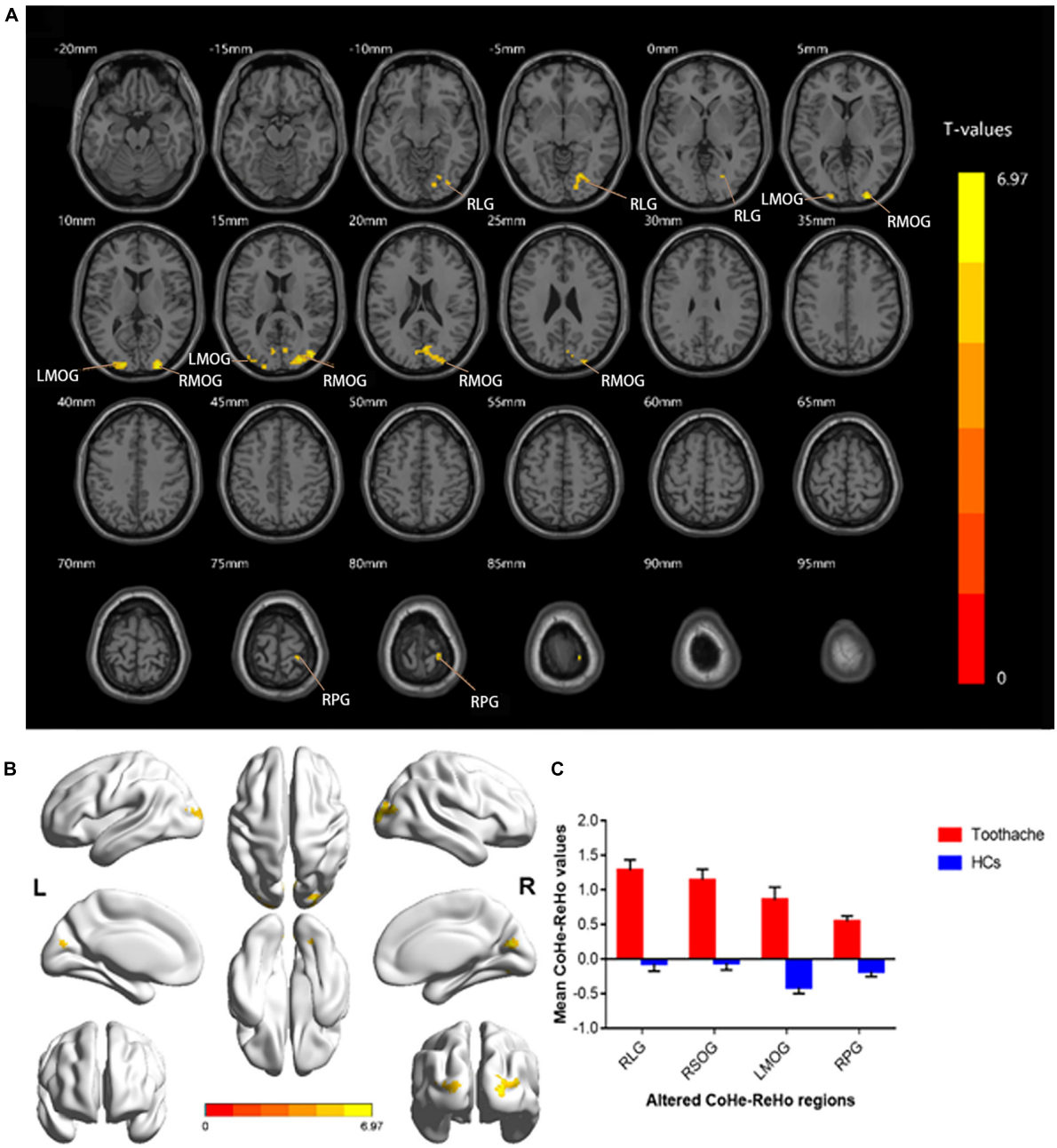

FIGURE 1
Spontaneous brain activity in the TA and HC groups. RLG, RSOG, LMOG, and RPG showed significant between-group differences in activity. Higher ReHo values are shown in red or yellow; lower values in blue [$P < 0.01$ for multiple comparisons using Gaussian random field theory (cluster 40 > voxels, AlphaSim corrected; $z > 2.3$, $P < 0.01$)] **(A,B)**. The mean differences in ReHo values between the HC and TA groups **(C)**. ReHo, regional homogeneity; RLG, right lingual gyrus; RSOG, right superior occipital gyrus; LMOG, left middle occipital gyrus; RPG, right postcentral gyrus; HCs, healthy controls.

experience. The brain affects the memory of the pain input, and related factors such as emotion and cognition can affect the patient's experience (Tracey and Mantyh, 2007). It is difficult to study the ability of the brain to respond to non-specific memory and pain, which is largely reflected in pain caused by noxious stimuli (Mouraux et al., 2011). However, through functional methods such as fMRI, relevant information about brain pain can be obtained (Apkarian et al., 2005; Dunckley et al., 2005; Iannetti et al., 2005); many studies have used ReHo methods to explore pain-related diseases and this approach has a broad scope for further development (**Table 3**; Yu et al., 2012; Xie et al., 2013; Wang et al., 2014, 2015; Zhang et al., 2014; Ke et al., 2015;

TABLE 2 Brain regions with significant differences in CoHe-ReHo between TA patients and HC.

TA patients and HCs				MNI coordinates		
Brain areas	**BA**	***T*-values**	**Peak voxels**	***x***	***y***	***z***
The right lingual gyrus	19	6.6032	43	24	−72	−3
The right superior occipital gyrus	18	6.7611	180	24	−99	6
The left middle occipital gyrus	19	6.4052	50	−18	−96	12
The right postcentral gyrus	2	6.9664	20	24	−33	81

The statistical threshold was set at voxel with $P < 0.01$ for multiple comparisons using false discovery rate. CoHe-ReHo, Coherence-based regional homogeneity; HCs, healthy controls; MNI, Montreal Neurological Institute; BA, Brodmann area.

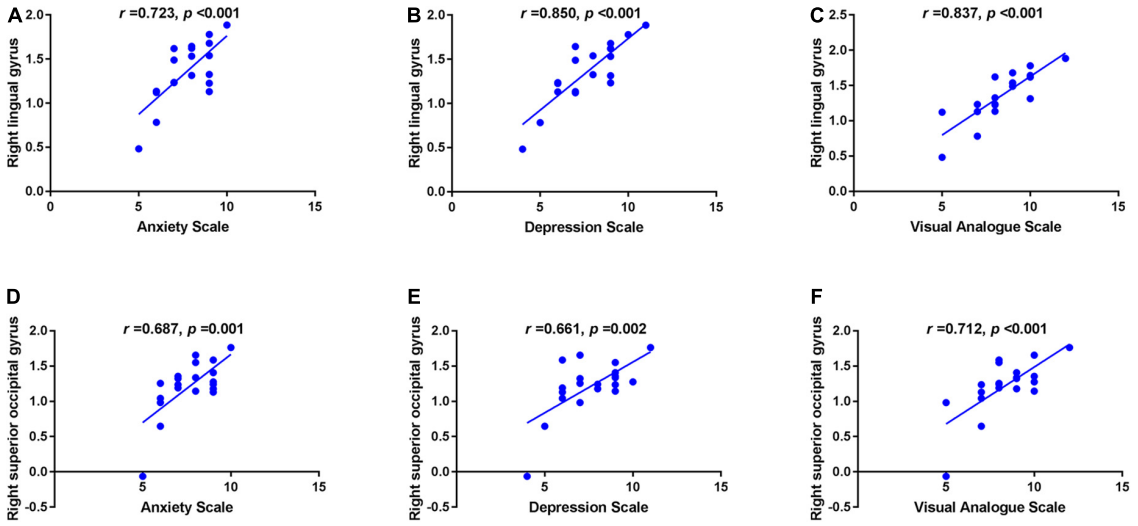

FIGURE 2
Correlations between the mean ReHo values in different brain regions and the clinical behaviors in the TA group. The mean ReHo value in the right lingual gyrus was positively correlated with the anxiety score ($r = 0.723$, $p < 0.001$) **(A)**, depression score ($r = 0.850$, $p < 0.001$) **(B)** and visual analogue score ($r = 0.837$, $p < 0.001$) **(C)**; and the right superior occipital gyrus value was positively correlated with the anxiety score ($r = 0.687$, $p = 0.001$) **(D)**, depression score ($r = 0.661$, $p = 0.002$) **(E)**, and visual analogue score ($r = 0.712$, $p < 0.001$) **(F)**. ReHo, regional homogeneity; TA, toothache; RLG, right lingual gyrus; RSOG, right superior occipital gyrus.

Wu et al., 2016; Tang et al., 2018). In addition, a study of rs-fMRI in patients with chronic cervical spondylosis showed that ReHo values in the left sensorimotor cortex and temporal lobe were significantly higher than those in normal subjects (Chen et al., 2018). This study also plays a background role in our research. ReHo has the advantage of determining the "global changes" in brain activity during pain and changes in neural activity in areas of the brain associated with pain. The pain experience is regulated by psychological, social, and other factors, with extensive inter-individual variations. Understanding how TA affects related brain mechanisms is crucial to customizing pain control for individual patients with dental disease.

The results of this study showed significant increases in ReHo values in the RLG, RSOG, LMOG, and RPG (**Figure 4**), indicating that the stimulation caused by TA affects the above four cerebral areas.

The RLG is associated with emotional control and cognitive function. One study showed that the normal functioning of the lingual gyrus (LG) helped fight anxiety and depression and maintain normal cognitive function (Jung et al., 2014). Related studies further showed that in Alzheimer's disease and depression, functional connectivity between LG and other cortical regions was decreased (Liu et al., 2017). Our study did not measure functional connectivity but we found that LG activity was increased in TA. Previous reports have indicated that TA experiences are associated with aversion emotions. Activation of the patient's brain in disgust might mean that the individual was positively responding to painful stimuli, constantly reassessing the pain (Borsook et al., 2013; Baliki and Vania Apkarian, 2015). When the TA experience was related to aversion, activated brain areas included the frontal lobe, amygdala, hippocampus, and others (Duerden and Albanese, 2013; Lin et al., 2013b). These areas associated with TA have been described as the "cognitive-emotional" network, indicating that cognition and emotion play significant roles in the development of TA (Wiech et al., 2008). The main function of the occipital lobe is to process visual information. Furthermore, the RSOG responds preferentially to visual

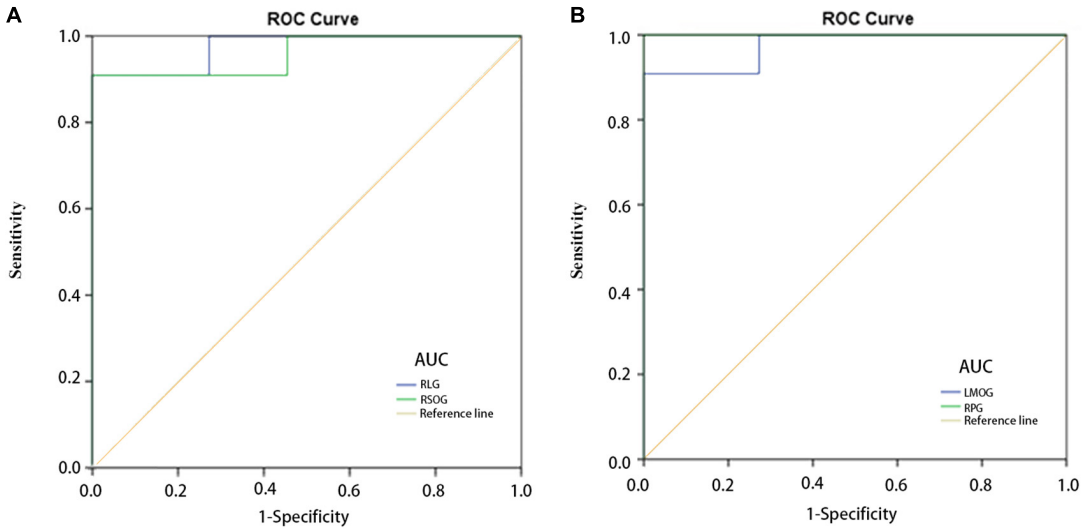

FIGURE 3
ROC curve analysis of the mean regional homogeneity values for altered brain regions. **(A)** The AUCs were 0.975 ($P < 0.001$; 95% CI: 0.918–1.000) for the RLG, and 0.959 ($P < 0.001$; 95% CI: 0.873–1.000) for the RSOG. **(B)** The AUCs were 0.975 ($P < 0.001$; 95% CI: 0.918–1.000) for the LMOG, and 1.000 ($P < 0.001$; 95% CI: 1.000–1.000) for the RPG. AUC, area under the curve; CI, confidence interval; HC, healthy control; RLG, right lingual gyrus; RSOG, right superior occipital gyrus; LMOG, left middle occipital gyrus; RPG, right postcentral gyrus; ROC, receiver operating characteristic.

TABLE 3 ReHo method applied in pain-related diseases.

Author	Disease	Brain regions	
		TAs > HCs	TAs < HCs
Bjelland et al. (2002)	Migraine	N/A	rACC, PFC, OFC, SMA
Huang et al. (2016a)	Idiopathic trigeminal neuralgia	ITG, thalamus, IPL, PCG	Amygdala, PHCG and cerebellum
Van Dijk et al. (2012)	Tension-type headache	N/A	CN, precuneus, putamen, MFG and SFG
Zeng et al. (2014)	Acute eye pain	SFG, IPL, precuneus	Pre/PostCG, MFG
Tate et al. (2014)	Low back pain	MPFC, precuneus, insula, PHCG, CPL	PSC, ACC, PHCG, IPL
Chen et al. (2021)	Knee osteoarthritis	Thalamus, EN, PL	Cerebrum, FL
Buckner et al. (2008)	Visceral pain	PostCG, thalamus	ACC, PFC
Raichle and Snyder (2007)	Dysmenorrhea	Declive, OFC	aIPS/SPL

ReHo, regional homogeneity; TA, toothache; HC, healthy control; N/A, not applicable; rACC, rostral anterior cingulate cortex; PFC, prefrontal cortex; OFC, orbitofrontal cortex; SMA, supplementary motor area; ITG, inferior temporal gyrus; IPL, inferior parietal lobule; PCG, postcentral gyrus; PHCG, parahippocampal gyrus; CN, caudate nucleus; MFG, middle frontal gyrus; SFG, superior frontal gyrus; Pre/PostCG, precentral/postcentral gyrus; MPFC, medial prefrontal cortex; CPL, cerebellum (posterior lobe); PSC, primary somatosensory cortex; ACC, anterior cingulate cortex; EN, extra-nucleus; PL, parietal lobe; FL, frontal lobe; PostCG, postcentral gyrus; aIPS, anterior part of the left intraparietal sulcus; SPL, superior parietal lobe.

information about spatial characteristics (Renier et al., 2010). In addition, epidemiological studies have confirmed that patients with visual impairment have relatively poor periodontal health, and the incidence of gingival bleeding and dental calculus is higher than that of normal subjects, which increases the risk of toothache (Liu et al., 2019). However, the effect of toothache on visual dysfunction needs further study. On the other hand, other studies found a potential link between the lingual region of the occipital lobe and the hippocampus and amygdala, with a major change in mood due to TA associated with occipital gyrus activation (Isenberg et al., 1999; Cho et al., 2012). A related study in children also suggested that the SOG played a role in pediatric bipolar disorder (Wei et al., 2018). In addition, a resting-state imaging study showed that the functional state of the LMOG was associated with major depressive disorder in females (Teng et al., 2018). The alterations in RLG, RSOG, and LMOG activity in the present study can partially confirm these findings. The functional state of ReHo values in these three cerebral cortex regions was related to the body's emotional and cognitive functions, and changes in their ReHo values may affect their functions.

Patients with TA often experience unbearable pain. It has been found that pain activates the primary (S1) and secondary (S2) somatosensory cortex, insular cortex, cingulate cortex, and

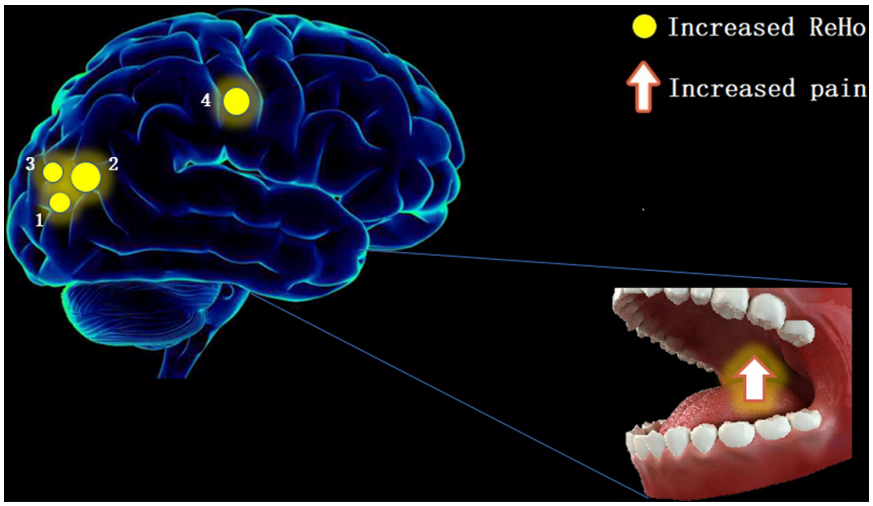

FIGURE 4
The ReHo results of brain activity in the TA group. Compared with the HCs, the ReHo value was increased in the following regions: 1—right lingual gyrus (BA19, t = 6.603), 2—right superior occipital gyrus (BA18, t = 6.7611), 3—left middle occipital gyrus (BA19, t = 6.4052), and 4—right postcentral gyrus (BA2, t = 6.9664). Spot size denotes the degree of quantitative changes. ReHo, regional homogeneity; TA, toothache; HC, healthy control.

TABLE 4 Brain regions alternation and its potential impact.

Brain regions	Experimental result	Brain function	Anticipated results
Right lingual gyrus	TA > HCs	Emotional control and cognitive function	Anxiety and depression
Right superior occipital gyrus	TA > HCs	Processing language, motion perception, abstract concepts, and visual information	Motor perception and visual impairment
Left middle occipital gyrus	TA > HCs	Visual information processing of spatial characteristics	Visual impairment, depression and anxiety
Right postcentral gyrus	TA > HCs	Body somatosensory	Left somatosensory disorder

HCs, healthy controls; TA, toothache.

parietal and thalamus regions. Some previous studies have suggested that many pain-related diseases activate the S1 region (Peyron et al., 2000; Apkarian et al., 2005; Frot et al., 2013). Gerstner et al. (2013) found by comparing harmful stimulation with a resting baseline that the somatosensory cortex, parietal lobe, and cingulate gyrus played key roles in oral pain. The right postcentral gyrus is part of the somatosensory cortex. Integrated stimulation of the somatosensory cortex, insula, and anterior central cingulate cortex may regulate the development of TA, and our experimental results can to some extent confirm this. We, therefore, consider that change in activity at the right postcentral gyrus was due to the stimulation of the brain caused by the TA itself. **Table 4** shows the functions of the above cerebral regions and the diseases associated with dysfunction.

ROC curves can be used to distinguish between healthy and diseased states and higher AUC values (above 0.7) indicate higher diagnostic accuracy. In our research, the AUC values of each cortical region were all greater than 0.9, indicating good accuracy and suggesting that ReHo at the brain regions discussed above may be a practical method for the diagnosis of TA in the future. The present study had some limitations. First, the sample is small, limiting the reliability of the experimental results (Button et al., 2013). Second, there is a lack of standardized noxious stimulation in the field of pain research, so while many clinical factors can cause TA in patients, we could not evaluate these in a standardized manner. Third, the psychological characteristics of patients with TA vary,

and we could not determine the connection between these characteristics and those related to brain activity.

In summary, using ReHo to study fMRI data was an effective way to study brain regional changes in a neural functional state in TA patients. Our results showed that areas of the brain in TA patients, including the somatosensory area, exhibited altered synchronous neural activity. These results provide a basis for further understanding of TA and relevant brain mechanisms and the development of customized pain control for individual dental patients.

Data availability statement

The original data can be obtained by contacting the corresponding author. Requests to access these datasets should be directed to Y-LH, 173386424@qq.com.

Ethics statement

This study was reviewed and approved by the Medical Ethics Committee of the first affiliated Hospital of Nanchang University (cdyfy2017021). All procedures performed in studies involving human participants were following the 1964 Helsinki declaration and its later amendments or comparable ethical standards.

Author contributions

JY and Y-LH contributed to the study inception and design. JY and YS equally contributed to the literature search, analysis, and writing of the manuscript. BiaL, BinL, Q-MG, Q-YL, Q-YY, R-BL, S-NW, and Y-CP contributed to the study design and study supervision. All authors approved the final version of the manuscript.

Funding

Key Research Foundation of Jiangxi Province (Nos: 20203BBG73059 and 20181BBG70004), Excellent Talents Development Project of Jiangxi Province (20192BCBL23020), Natural Science Foundation of Jiangxi Province (20181BAB205034), Grassroots Health Appropriate Technology "Spark Promotion Plan" Project of Jiangxi Province (No: 20188003), Health Development Planning Commission Science Foundation of Jiangxi Province (No: 20201032), and Health Development Planning Commission Science TCM Foundation of Jiangxi Province (No: 2018A060).

Conflict of interest

The authors declare that the research was conducted in the absence of any commercial or financial relationships that could be construed as a potential conflict of interest.

Publisher's note

All claims expressed in this article are solely those of the authors and do not necessarily represent those of their affiliated organizations, or those of the publisher, the editors and the reviewers. Any product that may be evaluated in this article, or claim that may be made by its manufacturer, is not guaranteed or endorsed by the publisher.

References

Apkarian, A. V., Bushnell, M. C., Treede, R. D., and Zubieta, J. K. (2005). Human brain mechanisms of pain perception and regulation in health and disease. *Eur. J. Pain* 9, 463–463. doi: 10.1016/j.ejpain.2004.11.001

Baliki, M., and Vania Apkarian, A. (2015). Nociception, pain, negative moods, and behavior selection. *Neuron* 87, 474–491. doi: 10.1016/j.neuron.2015.06.005

Bijur, P. E., Silver, W., and Gallagher, E. J. (2001). Reliability of the visual analog scale for measurement of acute pain. *Acad. Emerg. Med.* 8, 1153–1157. doi: 10.1111/j.1553-2712.2001.tb01132.x

Biswal, B. B. (2012). Resting state fMRI: A personal history. *Neuroimage* 62, 938–944. doi: 10.1016/j.neuroimage.2012.01.090

Bjelland, I., Dahl, A. A., Haug, T. T., and Neckelmann, D. (2002). The validity of the hospital anxiety and depression scale. An updated literature review. *J. Psychosom. Res.* 52, 69–77. doi: 10.1016/S0022-3999(01)00296-3

Borsook, D., Edwards, R., Elman, I., Becerra, L., and Levine, J. (2013). Pain and analgesia: The value of salience circuits. *Prog. Neurobiol.* 104, 93–105. doi: 10.1016/j.pneurobio.2013.02.003

Brügger, M., Ettlin, D. A., Meier, M., Keller, T., Luechinger, R., Barlow, A., et al. (2011). Taking sides with pain–lateralization aspects related to cerebral processing of dental pain. *Front. Hum. Neurosci.* 5:12. doi: 10.3389/fnhum.2011.00012

Brügger, M., Lutz, K., Brönnimann, B., Meier, M., Luechinger, R., Barlow, A., et al. (2012). Tracing toothache intensity in the brain. *J. Dent. Res.* 91, 156–160. doi: 10.1177/0022034511431253

Buckner, R. L., Andrews-Hanna, J. R., and Schacter, D. L. (2008). The brain's default network: Anatomy, function, and relevance to disease. *Ann. N. Y. Acad. Sci.* 1124, 1–38. doi: 10.1196/annals.1440.011

Button, K. S., Ioannidis, J. P., Mokrysz, C., Nosek, B. A., Flint, J., Robinson, E. S., et al. (2013). Power failure: Why small sample size undermines the reliability of neuroscience. *Nat. Rev. Neurosci.* 14, 365–376. doi: 10.1038/nrn3475

Chen, J., Wang, Z., Tu, Y., Liu, X., Jorgenson, K., Ye, G., et al. (2018). Regional homogeneity and multivariate pattern analysis of cervical spondylosis neck pain and the modulation effect of treatment. *Front. Neurosci.* 12:900. doi: 10.3389/fnins.2018.00900

Chen, S. Y., Cai, G. Q., Liang, R. B., Yang, Q. C., Min, Y. L., Ge, Q. M., et al. (2021). Regional brain changes in patients with diabetic optic neuropathy: A

resting-state functional magnetic resonance imaging study. *Quant. Imaging Med. Surg.* 11, 2125–2137. doi: 10.21037/qims-20-453

Cho, S., Metcalfe, A. W., Young, C. B., Ryali, S., Geary, D. C., and Menon, V. (2012). Hippocampal–prefrontal engagement and dynamic causal interactions in the maturation of children's fact retrieval. *J. Cogn. Neurosci.* 24, 1849–1866. doi: 10.1162/jocn_a_00246

Duerden, E. G., and Albanese, M. C. (2013). Localization of pain-related brain activation: A meta-analysis of neuroimaging data. *Hum. Brain Mapp.* 34, 109–149. doi: 10.1002/hbm.21416

Dunckley, P., Wise, R. G., Fairhurst, M., Hobden, P., Aziz, Q., Chang, L., et al. (2005). A comparison of visceral and somatic pain processing in the human brainstem using functional magnetic resonance imaging. *J. Neurosci.* 25, 7333–7341. doi: 10.1523/JNEUROSCI.1100-05.2005

Farrell, M. J., Laird, A. R., and Egan, G. F. (2005). Brain activity associated with painfully hot stimuli applied to the upper limb: A meta-analysis. *Hum. Brain Mapp.* 25, 129–139. doi: 10.1002/hbm.20125

Frot, M., Magnin, M., Mauguière, F., and Garcia-Larrea, L. (2013). Cortical representation of pain in primary sensory-motor areas (S1/M1)—a study using intracortical recordings in humans. *Hum. Brain Mapp.* 34, 2655–2668. doi: 10.1002/hbm.22097

Gerstner, G., Ichesco, E., and Schmidt-Wilcke, T. (2013). "Brain imaging of pain phenomena," in *Treatment of temporomandibular disorders: bridging the gap between advances in basic research and clinical pain management*, eds S. G. Charles and D. M. Laskin (Milton Park: Taylor & Francis Ltd), 141–154.

Huang, X., Li, H.-J., Ye, L., Zhang, Y., Wei, R., Zhong, Y.-L., et al. (2016a). Altered regional homogeneity in patients with unilateral acute open-globe injury: a resting-state functional MRI study. *Neuropsychiatr. Dis. Treat.* 12:1901. doi: 10.2147/NDT.S110541

Huang, X., Li, S. H., Zhou, F. Q., Zhang, Y., Zhong, Y. L., Cai, F. Q., et al. (2016b). Altered intrinsic regional brain spontaneous activity in patients with comitant strabismus: A resting-state functional MRI study. *Neuropsychiatr. Dis. Treat.* 12, 1303–1308. doi: 10.2147/NDT.S105478

Iannetti, G. D., and Mouraux, A. (2010). From the neuromatrix to the pain matrix (and back). *Exp. Brain Res.* 205, 1–12. doi: 10.1007/s00221-010-2340-1

Iannetti, G., Zambreanu, L., Wise, R. G., Buchanan, T., Huggins, J., Smart, T., et al. (2005). Pharmacological modulation of pain-related brain activity during normal and central sensitization states in humans. *Proc. Natl. Acad. Sci. U.S.A.* 102, 18195–18200. doi: 10.1073/pnas.0506624102

Isenberg, N., Silbersweig, D., Engelien, A., Emmerich, S., Malavade, K., Beattie, B. A., et al. (1999). Linguistic threat activates the human amygdala. *Proc. Natl. Acad. Sci. U.S.A.* 96, 10456–10459. doi: 10.1073/pnas.96.18.10456

Jung, J., Kang, J., Won, E., Nam, K., Lee, M.-S., Tae, W. S., et al. (2014). Impact of lingual gyrus volume on antidepressant response and neurocognitive functions in major depressive disorder: A voxel-based morphometry study. *J. Affect. Disord.* 169, 179–187. doi: 10.1016/j.jad.2014.08.018

Ke, J., Qi, R., Liu, C., Xu, Q., Wang, F., Zhang, L., et al. (2015). Abnormal regional homogeneity in patients with irritable bowel syndrome: A resting-state functional MRI study. *Neurogastroenterol. Motil.* 27, 1796–1803. doi: 10.1111/nmo.12692

Kippenhan, J. S., Barker, W. W., Pascal, S., Nagel, J., and Duara, R. (1992). Evaluation of a neural-network classifier for PET scans of normal and Alzheimer's disease subjects. *J. Nucl. Med.* 33, 1459–1467.

Lee, T.-W., Northoff, G., and Wu, Y.-T. (2014). Resting network is composed of more than one neural pattern: An fMRI study. *Neuroscience* 274, 198–208. doi: 10.1016/j.neuroscience.2014.05.035

Lin, C.-S., Hsieh, J.-C., Yeh, T.-C., Lee, S.-Y., and Niddam, D. M. (2013a). Functional dissociation within insular cortex: The effect of pre-stimulus anxiety on pain. *Brain Res.* 1493, 40–47. doi: 10.1016/j.brainres.2012.11.035

Lin, C.-S., Niddam, D., Hsu, M.-L., and Hsieh, J.-C. (2013b). Pain catastrophizing is associated with dental pain in a stressful context. *J. Dent. Res.* 92, 130–135. doi: 10.1177/0022034512467804

Liu, L., Zhang, Y., Wu, W., He, M., Lu, Z., Zhang, K., et al. (2019). Oral health status among visually impaired schoolchildren in Northeast China. *BMC Oral Health* 19:63. doi: 10.1186/s12903-019-0752-2

Liu, X., Chen, W., Hou, H., Chen, X., Zhang, J., Liu, J., et al. (2017). Decreased functional connectivity between the dorsal anterior cingulate cortex and lingual gyrus in Alzheimer's disease patients with depression. *Behav. Brain Res.* 326, 132–138. doi: 10.1016/j.bbr.2017.01.037

Mouraux, A., Diukova, A., Lee, M. C., Wise, R. G., and Iannetti, G. D. (2011). A multisensory investigation of the functional significance of the "pain matrix". *Neuroimage* 54, 2237–2249. doi: 10.1016/j.neuroimage.2010.09.084

Moussa, M. N., Steen, M. R., Laurienti, P. J., and Hayasaka, S. (2012). Consistency of network modules in resting-state FMRI connectome data. *PLoS One* 7:e44428. doi: 10.1371/journal.pone.0044428

Nixdorf, D. R., Drangsholt, M., Ettlin, D. A., Gaul, C., De Leeuw, R., Svensson, P., et al. (2012). Classifying orofacial pains: A new proposal of taxonomy based on ontology. *J. Oral Rehabil.* 39, 161–169. doi: 10.1111/j.1365-2842.2011.02247.x

Peyron, R., Laurent, B., and Garcia-Larrea, L. (2000). Functional imaging of brain responses to pain. A review and meta-analysis (2000). *Neurophysiol. Clin.* 30, 263–288. doi: 10.1016/S0987-7053(00)00227-6

Raichle, M. E., and Snyder, A. Z. (2007). A default mode of brain function: A brief history of an evolving idea. *Neuroimage* 37, 1083–1090. doi: 10.1016/j.neuroimage.2007.02.041

Renier, L. A., Anurova, I., De Volder, A. G., Carlson, S., VanMeter, J., and Rauschecker, J. P. (2010). Preserved functional specialization for spatial processing in the middle occipital gyrus of the early blind. *Neuron* 68, 138–148. doi: 10.1016/j.neuron.2010.09.021

Shao, Y., Cai, F. Q., Zhong, Y. L., Huang, X., Zhang, Y., Hu, P. H., et al. (2015). Altered intrinsic regional spontaneous brain activity in patients with optic neuritis: A resting-state functional magnetic resonance imaging study. *Neuropsychiatr. Dis. Treat.* 11, 3065–3073. doi: 10.2147/NDT.S92968

Tang, L.-Y., Li, H.-J., Huang, X., Bao, J., Sethi, Z., Ye, L., et al. (2018). Assessment of synchronous neural activities revealed by regional homogeneity in individuals with acute eye pain: A resting-state functional magnetic resonance imaging study. *J. Pain Res.* 11:843. doi: 10.2147/JPR.S156634

Tang, Y. L., Ji, G. J., Yu, Y., Wang, J., Wang, Z. J., Zang, Y. F., et al. (2014). Altered regional homogeneity in rolandic epilepsy: A resting-state FMRI study. *Biomed. Res. Int.* 2014:960395. doi: 10.1155/2014/960395

Tate, M. C., Herbet, G., Moritz-Gasser, S., Tate, J. E., and Duffau, H. (2014). Probabilistic map of critical functional regions of the human cerebral cortex: Broca's area revisited. *Brain* 137(Pt 10), 2773–2782. doi: 10.1093/brain/awu168

Teng, C., Zhou, J., Ma, H., Tan, Y., Wu, X., Guan, C., et al. (2018). Abnormal resting state activity of left middle occipital gyrus and its functional connectivity in female patients with major depressive disorder. *BMC Psychiatry* 18:370. doi: 10.1186/s12888-018-1955-9

Tononi, G., McIntosh, A. R., Russell, D. P., and Edelman, G. M. (1998). Functional clustering: Identifying strongly interactive brain regions in neuroimaging data. *Neuroimage* 7, 133–149. doi: 10.1006/nimg.1997.0313

Tracey, I., and Mantyh, P. W. (2007). The cerebral signature for pain perception and its modulation. *Neuron* 55, 377–391. doi: 10.1016/j.neuron.2007.07.012

Van Dijk, K. R., Sabuncu, M. R., and Buckner, R. L. (2012). The influence of head motion on intrinsic functional connectivity MRI. *Neuroimage* 59, 431–438. doi: 10.1016/j.neuroimage.2011.07.044

Wang, P., Du, H., Chen, N., Guo, J., Gong, Q., Zhang, J., et al. (2014). Regional homogeneity abnormalities in patients with tensiontype headache: A resting-state fMRI study. *Neurosci. Bull.* 30, 949–955. doi: 10.1007/s12264-013-1468-6

Wang, Y., Zhang, X., Guan, Q., Wan, L., Yi, Y., and Liu, C.-F. (2015). Altered regional homogeneity of spontaneous brain activity in idiopathic trigeminal neuralgia. *Neuropsychiatr. Dis. Treat.* 11:2659. doi: 10.2147/NDT.S94877

Wei, M., Gao, W., Jiao, Q., Cui, D., Cao, W., Xu, Q., et al. (2018). Resting-state functional connectivity of occipital cortex in euthymic pediatric bipolar disorder patients. *J. Med. Imaging Health Inform.* 8, 28–32. doi: 10.1166/jmihi.2018.2227

Wiech, K., Ploner, M., and Tracey, I. (2008). Neurocognitive aspects of pain perception. *Trends Cogn. Sci.* 12, 306–313. doi: 10.1016/j.tics.2008.05.005

Wu, S. N., Zhang, M. Y., Shu, H. Y., Liang, R. B., Ge, Q. M., Pan, Y. C., et al. (2020). Changes in functional connectivity of specific cerebral regions in patients with toothache: A resting-state functional magnetic resonance imaging study. *Dis. Markers* 2020:6683161. doi: 10.1155/2020/6683161

Wu, T.-H., Tu, C.-H., Chao, H.-T., Li, W.-C., Low, I., Chuang, C.-Y., et al. (2016). Dynamic changes of functional pain connectome in women with primary dysmenorrhea. *Sci. Rep.* 6:24543. doi: 10.1038/srep24543

Xie, H., Xu, F., Chen, R., Luo, T., Chen, M., Fang, W., et al. (2013). Image formation of brain function in patients suffering from knee osteoarthritis treated with moxibustion. *J. Trad. Chine. Med.* 33, 181–186. doi: 10.1016/S0254-6272(13)60122-3

Yang, J., Li, B., Yu, Q. Y., Ye, L., Zhu, P. W., Shi, W. Q., et al. (2019). Altered intrinsic brain activity in patients with toothaches using the amplitude of low-frequency fluctuations: a resting-state fMRI study. *Neuropsychiatr. Dis. Treat.* 15, 283–291. doi: 10.2147/NDT.S189962

Yu, D., Yuan, K., Zhao, L., Zhao, L., Dong, M., Liu, P., et al. (2012). Regional homogeneity abnormalities in patients with interictal migraine without aura: A resting-state study. *NMR Biomed.* 25, 806–812. doi: 10.1002/nbm.1796

Yue, Y., Jiang, Y., Shen, T., Pu, J., Lai, H. Y., and Zhang, B. (2020). ALFF and ReHo mapping reveals different functional patterns in early- and late-onset Parkinson's disease. *Front. Neurosci.* 14:141. doi: 10.3389/fnins.2020.00141

Zang, Y., Jiang, T., Lu, Y., He, Y., and Tian, L. (2004). Regional homogeneity approach to fMRI data analysis. *Neuroimage* 22, 394–400. doi: 10.1016/j.neuroimage.2003.12.030

Zeng, L. L., Wang, D., Fox, M. D., Sabuncu, M., Hu, D., Ge, M., et al. (2014). Neurobiological basis of head motion in brain imaging. *Proc. Natl. Acad. Sci. U.S.A.* 111, 6058–6062. doi: 10.1073/pnas.1317424111

Zhang, S.-S., Wu, W., Liu, Z.-P., Huang, G.-Z., Guo, S.-G., and Yang, J.-M. (2014). Altered regional homogeneity in experimentally induced low back pain: A resting-state fMRI study. *J. Neuroeng. Rehabil.* 11:115. doi: 10.1186/1743-0003-11-115

frontiers | Frontiers in Aging Neuroscience

TYPE Original Research
PUBLISHED 18 October 2022
DOI 10.3389/fnagi.2022.1001447

Check for updates

OPEN ACCESS

EDITED BY
Yuzhen Xu,
Tongji University, China

REVIEWED BY
Bao-liang Sun,
Shandong First Medical University, China
Yueran Zhao,
Shandong University, China

*CORRESPONDENCE
Lin Lu
linlu@bjmu.edu.cn
Xinyu Sun
sunxinyu@bjmu.edu.cn
Jiahui Deng
jiahuideng2012@bjmu.edu.cn

†These authors have contributed equally to this work

SPECIALTY SECTION
This article was submitted to Cellular and Molecular Mechanisms of Brain-aging, a section of the journal Frontiers in Aging Neuroscience

RECEIVED 23 July 2022
ACCEPTED 13 September 2022
PUBLISHED 18 October 2022

CITATION
Liu W, Li H, Lin X, Li P, Zhu X, Su S, Shi J, Lu L, Deng J and Sun X (2022) Blunted superior temporal gyrus activity to negative emotional expression after mindfulness-based cognitive therapy for late-life depression.
Front. Aging Neurosci. 14:1001447.
doi: 10.3389/fnagi.2022.1001447

COPYRIGHT
© 2022 Liu, Li, Lin, Li, Zhu, Su, Shi, Lu, Deng and Sun. This is an open-access article distributed under the terms of the Creative Commons Attribution License (CC BY). The use, distribution or reproduction in other forums is permitted, provided the original author(s) and the copyright owner(s) are credited and that the original publication in this journal is cited, in accordance with accepted academic practice. No use, distribution or reproduction is permitted which does not comply with these terms.

Blunted superior temporal gyrus activity to negative emotional expression after mindfulness-based cognitive therapy for late-life depression

Weijian Liu[1†], Hui Li[1†], Xiao Lin[1†], Peng Li[1], Ximei Zhu[1], Sizhen Su[1], Jie Shi[2], Lin Lu[1,2,3]*, Jiahui Deng[1]* and Xinyu Sun[1]*

[1]Peking University Sixth Hospital, Peking University Institute of Mental Health, NHC Key Laboratory of Mental Health (Peking University), National Clinical Research Center for Mental Disorders (Peking University Sixth Hospital), Beijing, China, [2]National Institute on Drug Dependence and Beijing Key Laboratory of Drug Dependence, Peking University, Beijing, China, [3]Peking-Tsinghua Center for Life Sciences and PKU-IDG/McGovern Institute for Brain Research, Peking University, Beijing, China

Facial emotion recognition plays an important role in social functioning. Patients with late-life depression (LLD) often have abnormal facial emotion recognition. Mindfulness-based cognitive therapy (MBCT) is beneficial in treating depression. This study examined whether MBCT can act as an effective augmentation of antidepressants and improve facial emotion recognition in patients with LLD and its underlying neural mechanism. Patients with LLD were randomized into two groups (n = 30 per group). The MBCT group received an eight-week MBCT in conjunction with stable medication treatment. The other group was treated as usual (TAU group) with stable medication treatment. The positive affect (PA) scale, negative affect (NA) scale, and facial emotion recognition task with an fMRI scan were performed before and after the trial. After eight weeks of treatment, the repeated ANOVA showed that the PA score in the MBCT group significantly increased [$F_{(1,54)}$ = 13.31, p = 0.001], but did not change significantly [$F_{(1,54)}$ = 0.58, p = 0.449] in the TAU group. The NA scores decreased significantly in both the MBCT group [$F_{(1,54)}$ = 19.01, $p < 0.001$] and the TAU group [$F_{(1,54)}$ = 16.16, $p < 0.001$]. Patients showed an increase in recognition accuracy and speed of angry and sad faces after 8 weeks of MBCT. No improvement was detected in the TAU group after treatment. A significant interaction effect was found in the change of activation of the left superior temporal gyrus (L-STG) to negative emotional expression between time and groups. Furthermore, a decrease in activation of L-STG to negative emotional expression was positively correlated with the increase in PA score. The MBCT is beneficial for improving affect status and facial emotion recognition in patients with LLD, and the L-STG is involved in this process.

KEYWORDS

mindfulness-based cognitive therapy (MBCT), facial emotion recognition, superior temporal gyrus (STG), late-life depression (LLD), neural mechanism

Introduction

Late-life depression (LLD) is one of the most common mental disorders in aged individuals. The prevalence of major depressive disorder (MDD) is approximately 10% in people aged 60 and over (Blazer, 2003; Sjoberg et al., 2017). The recurrence rate and disability rate are high in LLD, which places a heavy burden on families and society (Alexopoulos, 2005). LLD is characterized by depression, anxiety, restless symptoms, a sense of somatic discomfort (Korten et al., 2014), and a deficit in maintaining social interactions (Washburn et al., 2016; Bomfim et al., 2019). Recognition of facial expressions is an essential part of social interactions. The interpretation of expressions and feelings of others is associated with the capacity to recognize facial expressions of emotions (Bomfim et al., 2019). Regulation of emotion is related to facial expression recognition, enabling individuals to use emotion adaptively (Celeghin et al., 2017). An inverse correlation was found between the severity of depressive symptoms and accuracy in the perception of neutral expression (Mah and Pollock, 2010). Moreover, a previous study showed that the accuracy of the recognition of angry and fearful faces decreased in elderly individuals with depressive symptoms (Orgeta, 2014). If the function of emotion recognition is damaged, the social function of depressed patients will be significantly affected, which is likely to aggravate depression and social isolation, resulting in a vicious circle. In conclusion, facial emotion recognition plays an essential role in LLD. However, it is often neglected in antidepressant therapy.

Treating LLD has always been an open question. Drug therapy has been the principal treatment measure for LLD (Flint, 1998; Chang et al., 2018). Nevertheless, traditional antidepressants have insufficient efficacy in nearly 60% of older adults due to their complex somatic situations and susceptibility to adverse events (Alexopoulos et al., 2002; Kessler et al., 2010; Nyer et al., 2013). Furthermore, evidence indicates that pure medication therapy does not modify the cognitive pattern. Thus, a non-pharmacological intervention named mindfulness-based cognitive therapy (MBCT) based on meditation and cognitive therapy is of interest (Ionson et al., 2019; Torres-Platas et al., 2019). MBCT was proven effective for depression and could improve the response rate in pharmacotherapy (Eisendrath et al., 2016). Furthermore, a randomized controlled trial showed that affective processes in remitted depressed patients improved after mindfulness training (Timm et al., 2018). Although the MBCT has been proven effective in depressive symptoms, few studies have focused on the efficacy of the MBCT for emotion recognition in depressed aged.

As MBCT, a non-drug therapy has attracted much attention in treating depression, its neuroimaging mechanism is also a subject of interest. The anterior cingulate cortex, multiple prefrontal regions, medial prefrontal cortex, striatum, and amygdala are the most frequently reported brain regions involved in the mindfulness meditation (Tang et al., 2015). Several studies also consider the temporal lobe as a critical brain region associated with mindfulness meditation, including the left inferior temporal gyrus (Zeidan et al., 2011), left middle temporal gyrus (Holzel et al., 2011), and left inferior temporal lobe (Pickut et al., 2013). However, to date, the findings regarding the neuro-mechanism of regulating facial emotion recognition with MBCT in LLD patients have been inconsistent.

Thus, we conducted an 8-week MBCT on LLD patients in the present study to investigate the change in facial emotion recognition and the related neuroimaging mechanism.

Materials and methods

Study design

This study was registered at http://www.chictr.org.cn (registration No. ChiCTR1800017725) and was undertaken from June 1, 2018 to February 1, 2020. Participants were randomized into the MBCT and the treatment as usual (TAU) group. The MBCT group accepted MBCT based on medication therapy for eight weeks. The TAU group merely accepted pure medication treatment for 8 weeks. All patients were asked to maintain stable medication intake throughout the trial. Clinical scales and facial emotion recognition tasks in the MRI scanner were conducted to measure the severity of symptoms and brain activity changes regarding facial emotion recognition in LLD patients before and after the treatment. The execution of the trial was approved by the Ethics Committee of the Peking University Sixth Hospital (Institute of Mental Health). The agreement number concerning human research ethics is No. 2018 (15). Informed consent was signed by all participants.

Participants

A sample size of 48 was calculated using GPower 3.0.10 software for a power of statistical 80% with an alpha of 5% ($p \leq 0.05$). Considering the correction for a dropout rate of one in five (20.0%), six additional participants per group should be enrolled, resulting in a total sample size of 60 subjects (30 subjects per group). During the trial, four patients in the TAU group were lost in follow-ups. Clinical data were analyzed in 56 patients (30 in the MBCT group and 26 in the TAU group). Moreover, ten MRI data were excluded in the MBCT group and 13 fMRI data were excluded in the TAU group because of excessive head movement or poor data quality. Finally, 20 patients in the MBCT group and 13 in the TAU group were included in the final fMRI analyses (details in the flow chart, **Figure 1**).

Patients aged over 60 years who fulfilled the diagnostic criteria for MDD (single episode or recurrent) listed in the Diagnostic and Statistical Manual of Mental Disorders-4th

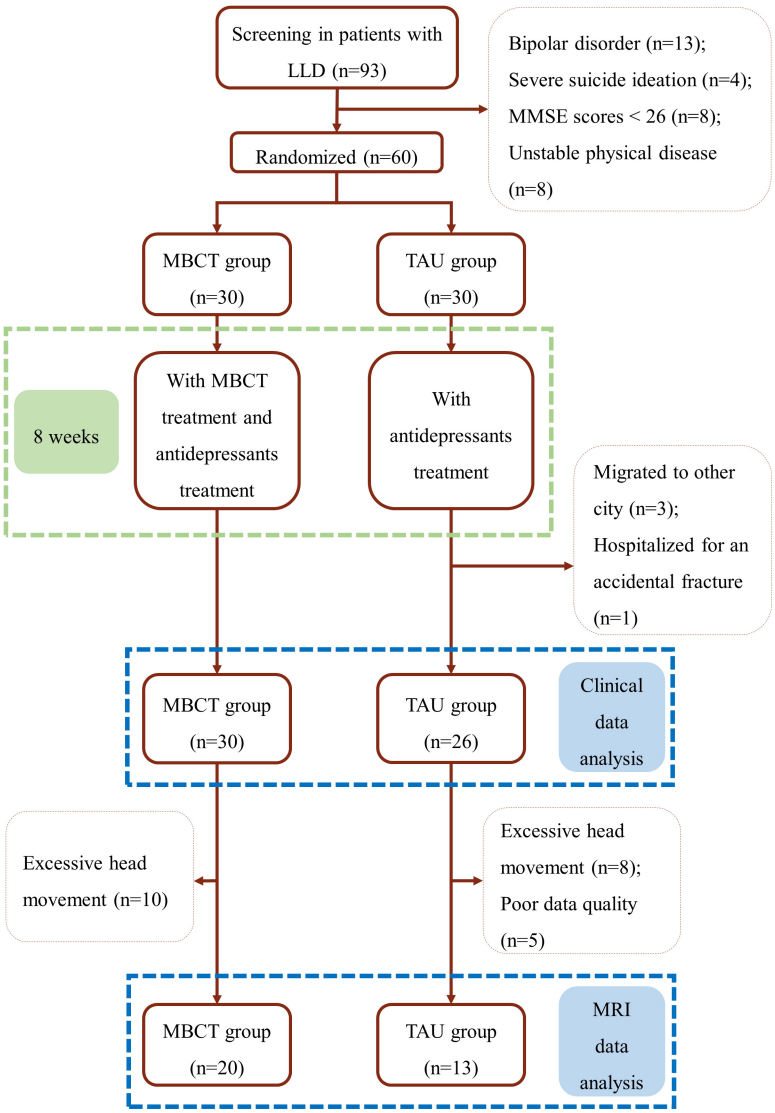

FIGURE 1
Flow chart. LLD, late-life depression; MBCT, mindfulness-based cognitive therapy; TAU, treatment as usual; MMSE, the Mini-Mental State Examination.

edition (DSM-IV) (American Psychological Association [APA], 2000) were enrolled. The Structured Clinical Interview for DSM-IV (SCID) was used to screen participants. The diagnosis of MDD was confirmed by two experienced doctors with at least five years of clinical experience. In addition, all participants had normal visual acuity, either naked or corrected, and were right-handed. All participants took medications stably for more than two weeks before enrollment. The exclusion criteria were as follows: (1) at a high risk of suicide; (2) once or currently diagnosed with other psychiatric disorders such as schizophrenia, bipolar disorder, and substance abuse; (3) a history of neurological disorders such as epilepsy, Parkinson's disease, and dementia; (4) current unstable severe physical diseases; (5) with a Mini-Mental State Examination (MMSE) scores less than 26; (6) taking part in psychotherapy concurrently; and (7) contraindications to MRI scans.

Intervention

The TAU group maintained stable medications without any psychotherapies for eight weeks. Regular visits were conducted once a week in the TAU group.

The MBCT group accepted additional MBCT based on stable medication therapy. The MBCT intervention consists of eight weekly face-to-face group-practice sessions of 1–1.5 h each. Furthermore, participants performed 45 min of self-practice each day. The MBCT was led by two

TABLE 1 Demographic and clinical characteristics of the MBCT and TAU groups at baseline.

Participants	MBCT (n = 30)	TAU (n = 30)	t/χ^2	P
	Mean ± SD/n (%)	Mean ± SD/n (%)		
Age (years)	67.66 ± 5.93	67.22 ± 5.78	0.29	0.776
Gender (male)	6 (20.00%)	8 (26.67%)	0.37	0.761
Education (years)	13.73 ± 2.66	12.5 ± 3.08	1.66	0.103
BMI (kg/m^2)	22.64 ± 2.42	23.63 ± 1.83	−1.77	0.082
Married	25 (83.33%)	25 (83.33%)	0.00	1.000
Duration of Illness (months)	48.23 ± 43.36	50.23 ± 35.41	−0.20	0.846
Age of onset (years)	62.33 ± 7.26	61.96 ± 5.56	0.22	0.827
Comorbidity				
Hypertension	11 (36.67%)	10 (33.33%)	0.07	0.787
Diabetes mellitus	1 (3.33%)	2 (6.67%)	0.35	0.554
HAMD-17	17.67 ± 6.69	18.56 ± 7.00	−0.50	0.617
PA score	24.23 ± 6.94	23.27 ± 6.19	0.57	0.571
NA score	20.43 ± 6.24	22.53 ± 6.46	−1.28	0.205
Type of antidepressant				
SSRI	22 (73.33%)	23 (76.67%)	0.09	0.766
SNRI	8 (26.67%)	7 (23.33%)	0.09	0.766

BMI, body mass index; PA, positive affect; NA, negative affect; MBCT, mindfulness-based cognitive therapy; TAU, treatment as usual; SSRI, selective serotonin reuptake inhibitor; SNRI, selective noradrenalin reuptake inhibitors; HAMD-17, hamilton depression scale-17.

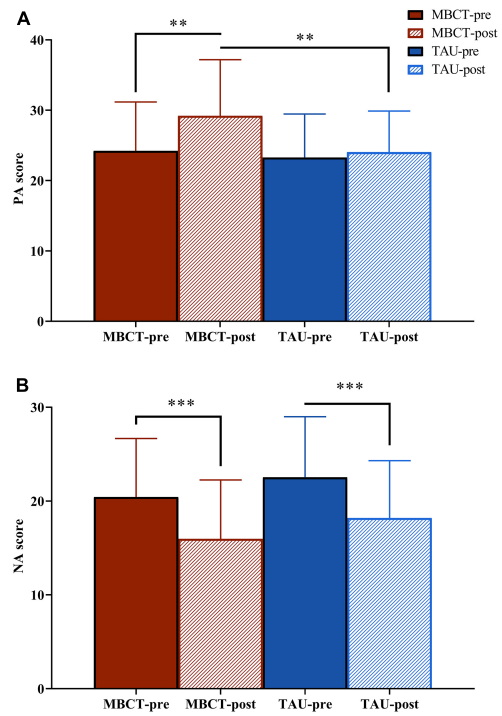

FIGURE 2
The PA and NA scores of the two groups before and after the intervention. Repeated analysis of variance. **(A)** PA score; **(B)** NA score. The red bar is the MBCT group (n = 30) and the blue bar is the TAU group (n = 26). PA, positive affect; NA, negative affect; MBCT, mindfulness-based cognitive therapy; TAU, treatment as usual. $^{**}p < 0.01$; $^{***}p < 0.001$.

experienced therapists trained in mindfulness, and two other psychiatrists assisted in the face-to-face group practice session. An online communication group was established through WeChat software. All subjects were required to punch in online after daily practice and report their time and feelings regarding self-practice at home. Self-practice manuals were distributed before the treatment, and the subjects had to make a paper record after each self-practice session, including but not limited to their practice time, practice items, and any problems encountered. Participants who had two or more absences from face-to-face group practice were considered lost in follow-ups. The intervention framework and content of MBCT are shown in Supplementary Table 1.

Clinical outcomes

The positive and negative affect scale (PANAS) and its subscales [positive affect (PA) scale and negative affect (NA) scale] were performed before and after the trial to examine the affective change in LLD patients. Hamilton depression scale-17 (HAMD-17) was preformed at baseline.

Facial emotion recognition task

Our study administered a facial emotion recognition task during fMRI scanning with E-Prime software (Psychology Software Tools, Pittsburgh, PA, USA). The facial emotion

pictures are derived from the Chinese Affective Face Picture System (CAFPS) (Xu et al., 2011). Thirty pictures with happy, sad, angry, fearful, and neutral faces were randomly presented. The pictures were shown to subjects through a visual system with the magnetic resonance machine. Two faces, one male and one female, were presented for each facial emotion image. All pictures were consistent in size, brightness, and emotional intensity.

Clear instruction and a block of practice were performed outside the magnetic resonance room before the formal task to ensure that all the participants understood the content and procedures of the experiment. Subjects were asked to identify the genders of the pictures and press the reaction box button as fast as possible. Correctness was defined as the subjects selecting the right gender for the picture. The formal task could only be carried out when the correct rate reached more than 70%. The task used the implicit paradigm of facial emotion processing. Facial emotion pictures were presented as target stimuli for 2,000 ms. Then, a "+" appears in the center of the screen for 300–700 ms. The task had two sessions, each of which had 30 trials and lasted approximately 3 min (**Supplementary Figure 1**). A short rest time between sessions was designed to prevent the effects of fatigue on the subjects. Each subject's average accuracy and response time in different facial emotion type trials were calculated.

Imaging acquisition and data processing

Participants were scanned using a 3.0 Tesla General Electric scanner (GE MR750 3.0T). High-resolution T1-weighted structural images were acquired using the following parameters: field of view (FOV) = 25.6 cm^1, flip angle = 12°. The fMRI images were acquired with the following parameters: FOV = 22.0 cm^3, TR = 2,000 ms, TE = 30 ms, flip angle = 90°, number of slices = 43, total scans = 240).

Image data processing was based on MATLAB 2013.[2] Statistical parametric mapping 12 (SPM12)[3] was used to preprocess image data. The preprocessing of the images included slice timing and realignment. Then the realigned image volumes were used to construct a mean functional image volume for each subject. The T1-weighted anatomical images were coregistered to the mean functional image and normalized to the Montreal Neurological Institute (MNI) coordinate system. After normalization, functional images were resliced into 3 mm × 3 mm × 3 mm voxels and smoothed with a 6 mm Gaussian kernel.

First- and second-level analyses were performed in NeuroElf.[3] General linear model (GLM) analyses were conducted to identify the blood oxygen level-dependent (BOLD) signal related to facial emotion types (happy, sad, angry, fearful, and neutral faces). Six standard motion parameters from realignment, onsets, and durations of events convolved with the hemodynamic response function (HRF) were included in subject-level models. A high-pass temporal filtering method (with a cutoff of 128 s) was conducted to remove low-frequency artifacts.

As only recognition of negative facial emotions (angry, fearful, and sad) significantly changed in behavioral data analyses, one contract (negative > neutral) was constructed. A two-way analysis of variance (ANOVA) was used to examine the interaction effects of the group (MBCT and TAU groups) and time (pre- and posttreatment) on neural activation (negative > neutral), with the accuracy and reaction time of five emotional faces at baseline as covariates. After a voxel-level correction at $p < 0.001$ and a cluster-level at p-FWE < 0.05. The cluster extent threshold was 23 voxels (smoothness: 8 mm kernel).

Data analysis

Clinical and behavioral data were described as the means ± standard deviations (SD) or percentages (%), and data analyses were conducted using SPSS 20.0 statistical software (SPSS Inc., Chicago, IL, United States). Comparisons of differences between the MBCT group and the TAU group were performed using the independent samples *t*-test and the chi-squared test. For the clinical accuracy and response time, repeated ANOVA was performed to compare whether there were significant differences between baseline and endpoint in the two groups. Facial emotional type and time point were regarded as intragroup factors, and the group was regarded as an intergroup factor, followed by a simple effect analysis.

Activation of a significant interactive brain region was extracted (β value). Independent samples t-test was used to detect whether changes in activation of the interactive brain region were significantly different between the two groups. Partial correlation analysis was conducted to detect the relationship between the deviation of the β value and change in clinical scales in each group with the accuracy and reaction time of five facial emotions at baseline as covariates.

Results

Demographic and clinical features

In our study, 60 LLD patients were enrolled (30 per group). The participants in the MBCT group were 67.66 ± 5.93 years

1 http://www.neuroelf.net
2 https://www.mathworks.com/products/matlab.html
3 https://www.fil.ion.ucl.ac.uk/spm/software/spm12/

TABLE 2 The accuracy rate of facial emotion pre- and post-treatment in the MBCT and TAU groups.

Facial emotion types	MBCT group (n = 30)		TAU group (n = 26)	
	Pre-treatment (%)	Post-treatment (%)	Pre-treatment (%)	Post-treatment (%)
Angry	70.44 ± 12.62	77.36 ± 11.35	71.43 ± 17.04	69.08 ± 17.90
Fearful	78.48 ± 11.16	86.67 ± 11.12	72.22 ± 12.25	70.88 ± 12.40
Sad	80.14 ± 10.98	87.08 ± 9.49	78.93 ± 9.54	74.10 ± 14.51
Happy	89.27 ± 9.69	89.30 ± 9.88	90.05 ± 6.58	88.77 ± 9.46
Neutral	92.25 ± 11.20	94.19 ± 5.89	91.84 ± 6.08	94.19 ± 5.89

MBCT, mindfulness-based cognitive therapy; TAU, treatment as usual.

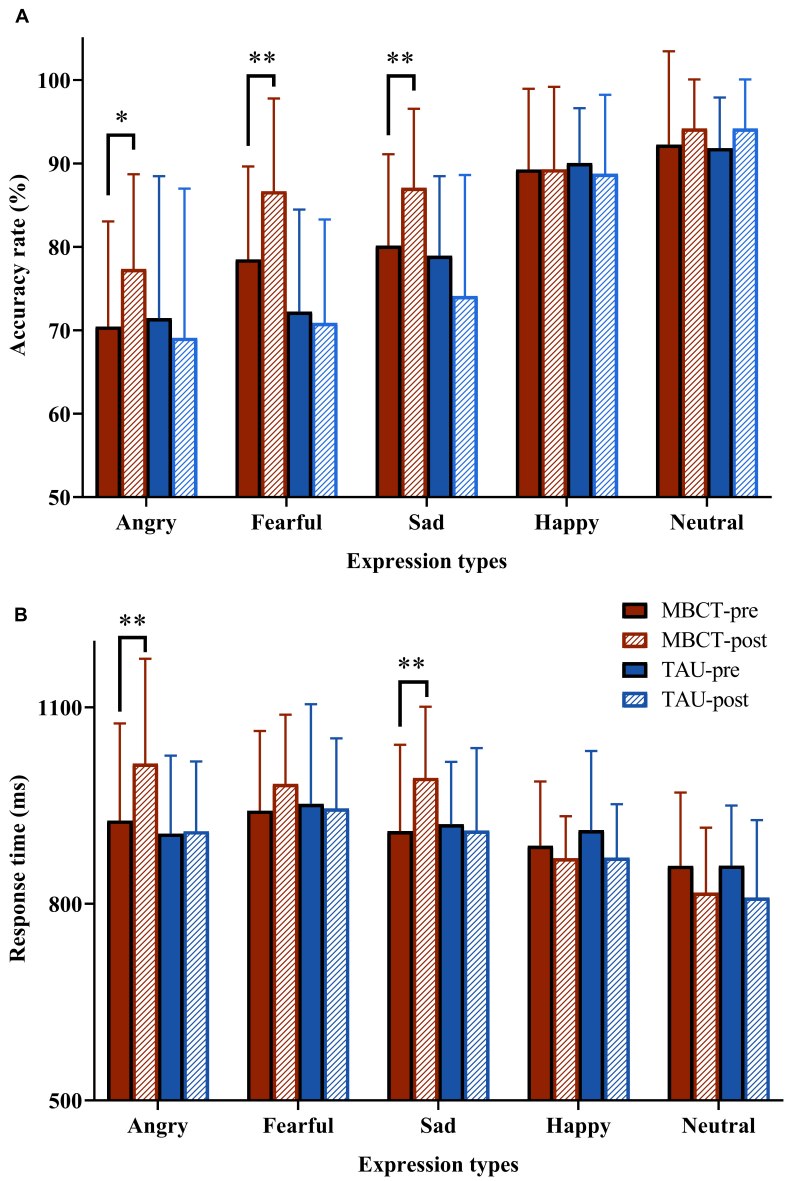

FIGURE 3
The accuracy and response time to facial emotion pictures in the two groups before and after the intervention. **(A)** PA score; **(B)** NA score. Repeated analysis of variance. The red bar is the MBCT group (n = 30) and the blue bar is the TAU group (n = 26). MBCT, mindfulness-based cognitive therapy; TAU, treatment as usual. *$p < 0.05$, **$p < 0.01$, compared with MBCT-pre group.

TABLE 3 The response time to facial emotion pre- and post-treatment in the MBCT and TAU groups.

Faci al emotion types	MBCT group (n = 30)		TAU group (n = 26)	
	Pre-treatment (ms)	Post-treatment (ms)	Pre-treatment (ms)	Pre-treatment (ms)
Angry	926.77 ± 148.69	1014.17 ± 159.80	907.19 ± 119.06	910.50 ± 106.76
Fearful	941.94 ± 121.97	982.78 ± 106.00	952.28 ± 152.42	945.61 ± 106.81
Sad	910.97 ± 131.83	991.96 ± 109.03	921.15 ± 95.65	911.78 ± 125.82
Happy	888.48 ± 98.19	869.45 ± 64.18	912.49 ± 120.81	870.36 ± 81.59
Neutral	857.91 ± 111.96	817.05 ± 99.28	858.18 ± 91.96	809.60 ± 118.26

MBCT, mindfulness-based cognitive therapy; TAU, treatment as usual.

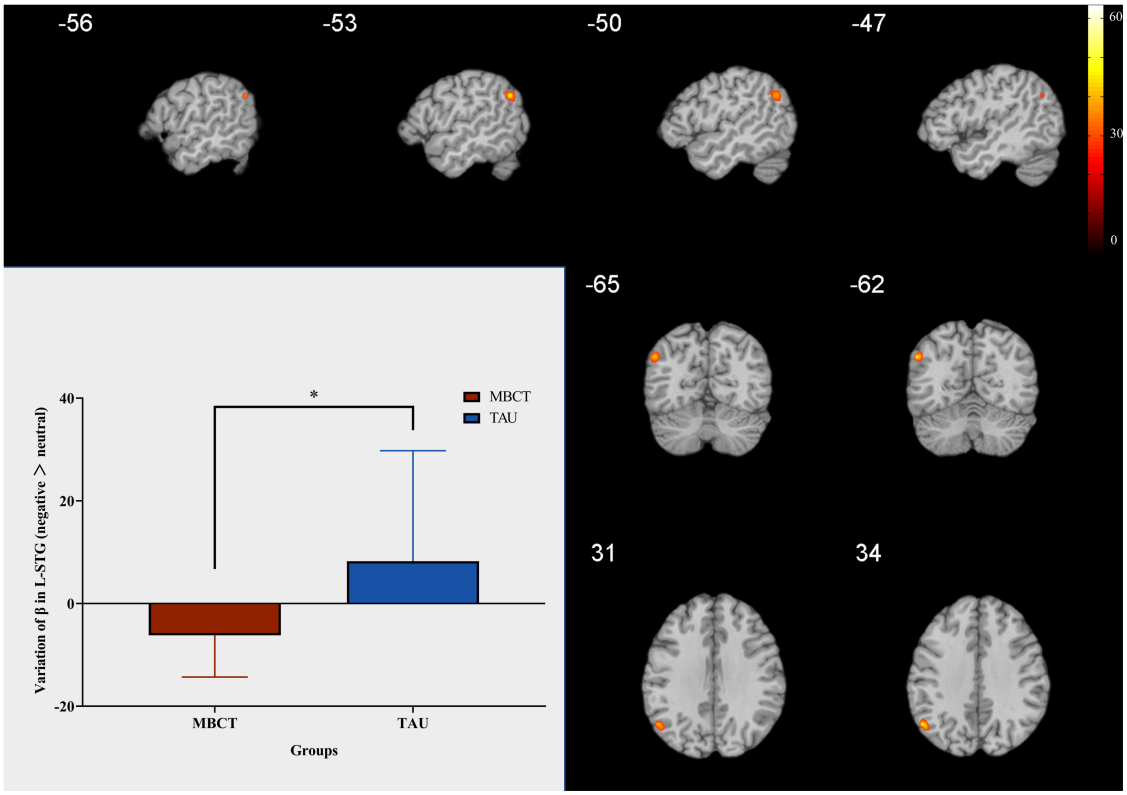

FIGURE 4
Change in L-STG response to negative facial emotion. Independent samples t-test. The red bar is the MBCT group (n = 20) and the blue bar is the TAU group (n = 13). The region marked in the figure is the brain region with significant interaction between the time point and the group. L-STG = left superior temporal gyrus; MBCT, mindfulness-based cognitive therapy; TAU, treatment as usual. *$p < 0.05$.

old and 67.22 ± 5.78 years old in the TAU group. Six (20.00%) males were in the MBCT group, and 8 (26.67%) males were in the TAU group. The HAMD-17 scores were 17.67 ± 6.69 and 18.56 ± 7.00 in the MBCT and TAU groups, respectively. There were no significant differences in demographic characteristics, age of onset, duration of MDD, comorbidity, or medication use between the two groups (Table 1, all $p > 0.05$). The demographic and clinical characteristics of the MRI analysis are shown in Supplementary Table 2, and no significant differences were found.

Mindfulness-based cognitive therapy improved the positive affect score in patients with late-life depression

All participants in the MBCT group finished the study. In contrast, four participants were lost in follow-ups with the TAU group (three participants traveled to other cities, and one was hospitalized for an accidental fracture). Finally, 30 participants in the MBCT group and 26 in the TAU group were included in

the clinical outcomes and behavioral data analyses. The HAMD-17 scores decreased significantly in the two groups mentioned in our previous study (Li et al., 2022). Moreover, the results of PA and NA are shown in Figures 2A,B.

For PA, the repeated ANOVA indicated a significant time effect [$F_{(1,54)} = 9.26$, $p = 0.004$]. The effect of time × group was on the threshold of significance [$F_{(1,54)} = 3.71$, $p = 0.059$]. After treatment, the PA score in the MBCT group was significantly higher than that in the TAU group [$F_{(1,54)} = 7.43$, $p = 0.009$]. In the MBCT group, the PA score significantly increased [$F_{(1,54)} = 13.31$, $p = 0.001$) after treatment. In the TAU group, the PA score did not change significantly [$F_{(1,54)} = 0.58$, $p = 0.449$] after treatment.

For the NA, the repeated ANOVA showed no time × group effect [$F_{(1,54)} = 0.01$, $p = 0.977$] but a significant time effect [$F_{(1,54)} = 34.97$, $p < 0.001$]. The NA scores decreased significantly in both the MBCT group [$F_{(1,54)} = 19.01$, $p < 0.001$] and the TAU group [$F_{(1,54)} = 16.16$, $p < 0.001$].

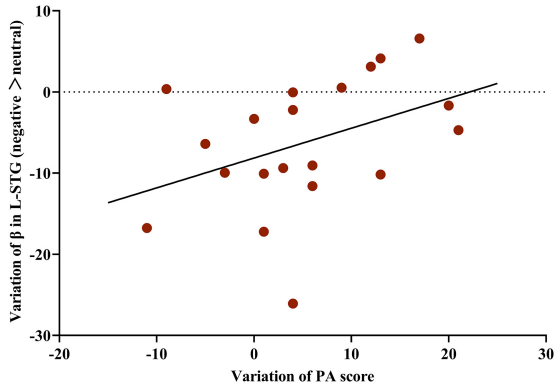

FIGURE 5
Correlation between the change in activation of the L-STG and variation in PA score in the MBCT group. Partial correlation analysis ($n = 20$) with the accuracy and reaction time of five facial emotions at baseline as covariates.L-STG, left superior temporal gyrus; MBCT, mindfulness-based cognitive therapy; PA, positive affect.

Mindfulness-based cognitive therapy improved the recognition accuracy and response time of negative facial emotions

For the accuracy of facial emotion, the repeated ANOVA showed a significant emotion types main effect [$F_{(4,216)} = 87.34$, $p < 0.001$], a non-significant time main effect [$F_{(1,54)} = 1.97$, $p = 0.166$], a significant time × group interaction effect [$F_{(1,54)} = 7.25$, $p = 0.009$], a significant emotion types × group interaction effect [$F_{(4,216)} = 6.63$, $p < 0.001$], a non-significant emotion types × time interaction effect [$F_{(4,216)} = 1.21$, $p = 0.306$], a significant emotion types × time × group interaction effect [$F_{(4,216)} = 4.15$, $p = 0.003$] and a significant group main effect [$F_{(1,54)} = 5.50$, $p = 0.023$]. Simple effect analysis revealed that in the TAU group, the accuracy of facial emotions was not significantly different between baseline and endpoint. However, the accuracy of angry ($p = 0.011$), fearful ($p = 0.002$), and sad ($p = 0.005$) expressions in the MBCT group increased significantly after the intervention (Table 2 and Figure 3A).

For the response time of facial emotion, the repeated ANOVA showed a significant emotion types main effect [$F_{(4,216)} = 27.50$, $p < 0.001$], a non-significant time main effect [$F_{(1,54)} = 0.17$, $p = 0.681$], a significant time × group interaction effect [$F_{(1,54)} = 5.18$, $p = 0.027$], a non-significant emotion types × group interaction effect [$F_{(4,216)} = 2.36$, $p = 0.054$], a significant emotion types × time interaction effect [$F_{(4,216)} = 7.36$, $p < 0.001$], a non-significant emotion types × time × group interaction effect [$F_{(4,216)} = 1.56$, $p = 0.185$] and non-significant group main effect [$F_{(1,54)} = 1.06$, $p = 0.307$]. Simple effect analysis revealed that in the TAU group, the response time of facial emotions was not significantly different between baseline and endpoint. However, the response time of angry ($p = 0.001$) and sad ($p = 0.002$) expressions in the MBCT group increased significantly after the intervention. Furthermore, the response time to fearful expressions showed a marginally significant increase in the MBCT group at the end of the study ($p = 0.056$) (Table 3 and Figure 3B).

Mindfulness-based cognitive therapy reduced left superior temporal gyrus response to negative emotion

As we discovered the behavioral indicators of negative facial emotions changed significantly after MBCT, the angry, fearful, and sad conditions were combined as negative facial emotion conditions.

In the whole-brain analysis, the interaction between the time point and the group was found in only one brain region (L-STG, voxel size = 23, coordinate = −53; −62; 29). The change in activation in the L-STG in the MBCT group was significantly lower than that in the TAU group ($t = -2{,}74$, $p = 0.01$). The results are shown in Figure 4.

Positive correlation between activation of the left superior temporal gyrus and the changes in the positive affect score

In the MBCT group, the change in activation of the L-STG was positively associated with the changes in the PA score ($r = 0.76$, $p = 0.011$, Figure 5). However, neither change in PA

nor NA score was significantly associated with the change in L-STG activation in the TAU group.

Discussion

To our knowledge, this is the first study to investigate whether MBCT would change the recognition accuracy and speed of facial emotion in LLD patients, and the underlying neuroimaging mechanism. The significant findings of this study were as follows: (1) the PA score was increased and the NA score decreased after MBCT; (2) the accuracy of angry, fearful, and sad faces were increased, and the response time of angry and sad faces increased after MBCT; (3) an interaction effect was found in the change of activation of L-STG between MBCT group and TAU group; and (4) reduction of activation of L-STG was positively associated with the increase of PA score.

In the present study, the NA score decreased in both the MBCT and TAU groups, which means that both pure medication treatment and MBCT effectively regulated emotion recognition. Nevertheless, the PA score increased only in the MBCT group but not in the TAU group. This means that MBCT showed an advantage in improving PA in LLD patients. A previous study found that reports of increased experience of positive emotions were related to MBCT (van der Velden et al., 2015). In contrast to progressive muscle relaxation, PA increased and NA decreased after four weeks of mindfulness training (Timm et al., 2018). MBCT has been shown to have emotion regulation effects in many studies, including boosting the positive mood (Hofmann et al., 2010; Goyal et al., 2014) and decreasing the negative mood (Jha et al., 2010). Consistent with prior evidence, the addition of MBCT to conventional medication therapy has an advantage in emotion regulation compared to medication alone.

In this study, the accuracy of angry, fearful, and sad faces increased, and the response time of angry and sad faces increased after MBCT. A recent meta-analysis showed that depressed patients have impaired facial emotion recognition (Dalili et al., 2015). A negative response bias toward sadness in individuals with major depression was proven by consistent evidence (Bourke et al., 2010). A previous study found that older people without depression are more accurate in recognizing anger and sad faces than depressed older people (Bomfim et al., 2019). In our study, the accuracy and response time of negative facial emotion were increased after MBCT, indicating that adding MBCT to conventional medication treatment improves facial emotion bias in elderly patients with depression. Non-judgemental acceptance and present-moment awareness during mindfulness meditation make people more sensitive to facial and emotional stimuli, which is probably the vital reason for promoting the cognitive control (Teper et al., 2013).

In neuroimaging mechanisms, we found that the reduction in activation of L-STG was positively associated with an increase in PA score. Previous research has shown that the STG plays an important role in the social cognitive functions (Allison et al., 2000; Jou et al., 2010), perception of social information (Allison et al., 2000), and emotion processing and encoding changes in facial emotion (Tseng et al., 2016). Right STG is also associated with the social anhedonia (Germine et al., 2011). In people with familial risk for psychosis, the STG relates to the facial emotion recognition (Pulkkinen et al., 2015). In children with subclinical anxiety, the STG was concerned with the facial emotional recognition (Kennedy et al., 2021). In patients with schizophrenia, the STG volume plays a role in social functions (Jung et al., 2020). In ischemic stroke patients, the ability to recognize angry expressions was only related to the STG (van den Berg et al., 2021). Moreover, after mindfulness practice, altered temporal nodal efficiency of the STG was found in aging adults (Fam et al., 2020). The above evidence supports our finding that STG plays an essential role in MBCT for patients with LLD.

Several limitations must be pointed out in this study. First, the sample size was small. Further study with a larger sample size should be performed. Second, a relative amount of MRI data was excluded after preprocessing. Given that it is not easy for older adults to remain still throughout the entire scan, it is not surprising that some of the participants were excluded for excessive head movement and poor data quality. Third, the only additional condition conducted in the control group was regular visits. A previous study regarded antidepressant medications and non-structured supportive therapy as their control condition (Ionson et al., 2019). A more convincing control condition should be performed in future studies.

Conclusion

In conclusion, this study showed that MBCT is beneficial to older adults with LLD in improving affect and facial emotion recognition, and the L-STG plays a significant role in this process.

Data availability statement

The raw data supporting the conclusions of this article will be made available by the authors, without undue reservation, after permission of all authors.

Ethics statement

The studies involving human participants were reviewed and approved by Ethics Committee of the Peking University Sixth Hospital (Institute of Mental Health). The

patients/participants provided their written informed consent to participate in this study.

Author contributions

HL, LL, JD, and XS contributed to the study design. HL, XZ, SS, and XS performed the research and collected the data. WL, HL, XL, and PL performed the data analysis. WL, XL, HL, and JD drafted the manuscript. All authors reviewed the results and approved the final version of the manuscript.

Funding

This work was partly supported by the National Natural Science Foundation of China (nos. 82171524, 81821092, and 81761128036) and National Key Research and Development Program of China (no. 2019YFA0706200).

Acknowledgments

We thank all the participants in this study.

Conflict of interest

The authors declare that the research was conducted in the absence of any commercial or financial relationships that could be construed as a potential conflict of interest.

Publisher's note

All claims expressed in this article are solely those of the authors and do not necessarily represent those of their affiliated organizations, or those of the publisher, the editors and the reviewers. Any product that may be evaluated in this article, or claim that may be made by its manufacturer, is not guaranteed or endorsed by the publisher.

Supplementary material

The Supplementary Material for this article can be found online at: https://www.frontiersin.org/articles/10.3389/fnagi.2022.1001447/full#supplementary-material

References

Alexopoulos, G. S. (2005). Depression in the elderly. *Lancet* 365, 1961–1970. doi: 10.1016/s0140-6736(05)66665-2

Alexopoulos, G. S., Buckwalter, K., Olin, J., Martinez, R., Wainscott, C., and Krishnan, K. R. (2002). Comorbidity of late life depression: An opportunity for research on mechanisms and treatment. *Biol. Psychiatry* 52, 543–558. doi: 10.1016/s0006-3223(02)01468-3

Allison, T., Puce, A., and McCarthy, G. (2000). Social perception from visual cues: Role of the STS region. *Trends Cogn. Sci.* 4, 267–278. doi: 10.1016/s1364-6613(00)01501-1

American Psychological Association [APA] (2000). *Diagnostic and statistical manual of mental disorders: DSM-IV-TR*. Washington, DC: American Psychiatric Press.

Blazer, D. G. (2003). Depression in late life: Review and commentary. *J. Gerontol. A Biol. Sci. Med. Sci.* 58, 249–265. doi: 10.1093/gerona/58.3.m249

Bomfim, A. J. L., Ribeiro, R., and Chagas, M. H. N. (2019). Recognition of dynamic and static facial expressions of emotion among older adults with major depression. *Trends Psychiatry Psychother.* 41, 159–166. doi: 10.1590/2237-6089-2018-0054

Bourke, C., Douglas, K., and Porter, R. (2010). Processing of facial emotion expression in major depression: A review. *Aust. N. Z. J. Psychiatry* 44, 681–696. doi: 10.3109/00048674.2010.496359

Celeghin, A., Diano, M., Bagnis, A., Viola, M., and Tamietto, M. (2017). Basic emotions in human neuroscience: Neuroimaging and beyond. *Front. Psychol.* 8:1432. doi: 10.3389/fpsyg.2017.01432

Chang, D. D., Eyreeuro, H. A., Abbott, R., Coudreaut, M., Baune, B. T., Shaman, J. A., et al. (2018). Pharmacogenetic guidelines and decision support tools for depression treatment: Application to late-life. *Pharmacogenomics* 19, 1269–1284. doi: 10.2217/pgs-2018-0099

Dalili, M. N., Penton-Voak, I. S., Harmer, C. J., and Munafo, M. R. (2015). Meta-analysis of emotion recognition deficits in major depressive disorder. *Psychol. Med.* 45, 1135–1144. doi: 10.1017/S0033291714002591

Eisendrath, S. J., Gillung, E., Delucchi, K. L., Segal, Z. V., Nelson, J. C., McInnes, L. A., et al. (2016). A randomized controlled trial of mindfulness-based cognitive therapy for treatment-resistant depression. *Psychother. Psychosom.* 85, 99–110. doi: 10.1159/000442260

Fam, J., Sun, Y., Qi, P., Lau, R. C., Feng, L., Kua, E. H., et al. (2020). Mindfulness practice alters brain connectivity in community-living elders with mild cognitive impairment. *Psychiatry Clin. Neurosci.* 74, 257–262. doi: 10.1111/pcn.12972

Flint, A. J. (1998). Choosing appropriate antidepressant therapy in the elderly. A risk-benefit assessment of available agents. *Drugs Aging* 13, 269–280. doi: 10.2165/00002512-199813040-00003

Germine, L. T., Garrido, L., Bruce, L., and Hooker, C. (2011). Social anhedonia is associated with neural abnormalities during face emotion processing. *Neuroimage* 58, 935–945. doi: 10.1016/j.neuroimage.2011.06.059

Goyal, M., Singh, S., Sibinga, E. M., Gould, N. F., Rowland-Seymour, A., Sharma, R., et al. (2014). Meditation programs for psychological stress and well-being: A systematic review and meta-analysis. *JAMA Intern. Med.* 174, 357–368. doi: 10.1001/jamainternmed.2013.13018

Hofmann, S. G., Sawyer, A. T., Witt, A. A., and Oh, D. (2010). The effect of mindfulness-based therapy on anxiety and depression: A meta-analytic review. *J. Consult. Clin. Psychol.* 78, 169–183. doi: 10.1037/a0018555

Holzel, B. K., Carmody, J., Vangel, M., Congleton, C., Yerramsetti, S. M., Gard, T., et al. (2011). Mindfulness practice leads to increases in regional brain gray matter density. *Psychiatry Res.* 191, 36–43. doi: 10.1016/j.pscychresns.2010.08.006

Ionson, E., Limbachia, J., Rej, S., Puka, K., Newman, R. I., Wetmore, S., et al. (2019). Effects of sahaj samadhi meditation on heart rate variability and depressive symptoms in patients with late-life depression. *Br. J. Psychiatry* 214, 218–224. doi: 10.1192/bjp.2018.265

Jha, A. P., Stanley, E. A., Kiyonaga, A., Wong, L., and Gelfand, L. (2010). Examining the protective effects of mindfulness training on working memory capacity and affective experience. *Emotion* 10, 54–64. doi: 10.1037/a0018438

Jou, R. J., Minshew, N. J., Keshavan, M. S., Vitale, M. P., and Hardan, A. Y. (2010). Enlarged right superior temporal gyrus in children and adolescents with autism. *Brain Res.* 1360, 205–212. doi: 10.1016/j.brainres.2010.09.005

Jung, M., Baik, S. Y., Kim, Y., Kim, S., Min, D., Kim, J. Y., et al. (2020). Empathy and social attribution skills moderate the relationship between temporal lobe volume and facial expression recognition ability in schizophrenia. *Clin. Psychopharmacol. Neurosci.* 18, 362–374. doi: 10.9758/cpn.2020.18.3.362

Kennedy, M., Simcock, G., Jamieson, D., Hermens, D. F., Lagopoulos, J., and Shan, Z. (2021). Elucidating the neural correlates of emotion recognition in children with sub-clinical anxiety. *J. Psychiatr. Res.* 143, 75–83. doi: 10.1016/j.jpsychires.2021.08.024

Kessler, R. C., Birnbaum, H., Bromet, E., Hwang, I., Sampson, N., and Shahly, V. (2010). Age differences in major depression: Results from the national comorbidity survey replication (NCS-R). *Psychol. Med.* 40, 225–237. doi: 10.1017/S0033291709990213

Korten, N. C., Penninx, B. W., Kok, R. M., Stek, M. L., Oude Voshaar, R. C., Deeg, D. J., et al. (2014). Heterogeneity of late-life depression: Relationship with cognitive functioning. *Int. Psychogeriatr.* 26, 953–963. doi: 10.1017/S1041610214000155

Li, H., Yan, W., Wang, Q., Liu, L., Lin, X., Zhu, X., et al. (2022). Mindfulness-based cognitive therapy regulates brain connectivity in patients with late-life depression. *Front. Psychiatry* 13:841461. doi: 10.3389/fpsyt.2022.841461

Mah, L., and Pollock, B. G. (2010). Emotional processing deficits in late-life depression. *Am. J. Geriatr. Psychiatry* 18, 652–656. doi: 10.1097/jgp.0b013e3181d6b762

Nyer, M., Doorley, J., Durham, K., Yeung, A. S., Freeman, M. P., and Mischoulon, D. (2013). What is the role of alternative treatments in late-life depression? *Psychiatr. Clin. North Am.* 36, 577–596. doi: 10.1016/j.psc.2013.08.012

Orgeta, V. (2014). Emotion recognition ability and mild depressive symptoms in late adulthood. *Exp. Aging Res.* 40, 1–12. doi: 10.1080/0361073X.2014.857535

Pickut, B. A., Van Hecke, W., Kerckhofs, E., Marien, P., Vanneste, S., Cras, P., et al. (2013). Mindfulness based intervention in parkinson's disease leads to structural brain changes on MRI: A randomized controlled longitudinal trial. *Clin. Neurol. Neurosurg.* 115, 2419–2425. doi: 10.1016/j.clineuro.2013.10.002

Pulkkinen, J., Nikkinen, J., Kiviniemi, V., Maki, P., Miettunen, J., Koivukangas, J., et al. (2015). Functional mapping of dynamic happy and fearful facial expressions in young adults with familial risk for psychosis – Oulu brain and mind study. *Schizophr. Res.* 164, 242–249. doi: 10.1016/j.schres.2015.01.039

Sjoberg, L., Karlsson, B., Atti, A. R., Skoog, I., Fratiglioni, L., and Wang, H. X. (2017). Prevalence of depression: Comparisons of different depression definitions in population-based samples of older adults. *J. Affect. Disord.* 221, 123–131. doi: 10.1016/j.jad.2017.06.011

Tang, Y. Y., Holzel, B. K., and Posner, M. I. (2015). The neuroscience of mindfulness meditation. *Nat. Rev. Neurosci.* 16, 213–225. doi: 10.1038/nrn3916

Teper, R., Segal, Z. V., and Inzlicht, M. (2013). Inside the mindful mind: How mindfulness enhances emotion regulation through improvements in executive control. *Curr. Dir. Psychol. Sci.* 22, 449–454. doi: 10.1177/0963721413495869

Timm, C., Rachota-Ubl, B., Beddig, T., Zamoscik, V. E., Ebner-Priemer, U., Reinhard, I., et al. (2018). Mindfulness-based attention training improves cognitive and affective processes in daily life in remitted patients with recurrent depression: A randomized controlled trial. *Psychother. Psychosom.* 87, 184–186. doi: 10.1159/000488862

Torres-Platas, S. G., Escobar, S., Belliveau, C., Wu, J., Sasi, N., Fotso, J., et al. (2019). Mindfulness-based cognitive therapy intervention for the treatment of late-life depression and anxiety symptoms in primary care: A randomized controlled trial. *Psychother. Psychosom.* 88, 254–256. doi: 10.1159/000501214

Tseng, W. L., Thomas, L. A., Harkins, E., Pine, D. S., Leibenluft, E., and Brotman, M. A. (2016). Neural correlates of masked and unmasked face emotion processing in youth with severe mood dysregulation. *Soc. Cogn. Affect. Neurosci.* 11, 78–88. doi: 10.1093/scan/nsv087

van den Berg, N. S., de Haan, E. H. F., Huitema, R. B., Spikman, J. M., and visual brain group (2021). The neural underpinnings of facial emotion recognition in ischemic stroke patients. *J. Neuropsychol.* 15, 516–532. doi: 10.1111/jnp.12240

van der Velden, A. M., Kuyken, W., Wattar, U., Crane, C., Pallesen, K. J., Dahlgaard, J., et al. (2015). A systematic review of mechanisms of change in mindfulness-based cognitive therapy in the treatment of recurrent major depressive disorder. *Clin. Psychol. Rev.* 37, 26–39. doi: 10.1016/j.cpr.2015.02.001

Washburn, D., Wilson, G., Roes, M., Rnic, K., and Harkness, K. L. (2016). Theory of mind in social anxiety disorder, depression, and comorbid conditions. *J. Anxiety Disord.* 37, 71–77. doi: 10.1016/j.janxdis.2015.11.004

Xu, G., Yuxia, H., Yan, W., and Yuejia, L. (2011). Revision of the Chinese facial affective picture system [Chinese version]. *Chin. Ment. Health J.* 25, 40–46.

Zeidan, F., Martucci, K. T., Kraft, R. A., Gordon, N. S., McHaffie, J. G., and Coghill, R. C. (2011). Brain mechanisms supporting the modulation of pain by mindfulness meditation. *J. Neurosci.* 31, 5540–5548. doi: 10.1523/JNEUROSCI.5791-10.2011

frontiers | Frontiers in Aging Neuroscience

TYPE Original Research
PUBLISHED 24 October 2022
DOI 10.3389/fnagi.2022.1014472

Check for updates

OPEN ACCESS

EDITED BY
Yuzhen Xu,
Tongji University, China

REVIEWED BY
Shoujiang You,
Second Affiliated Hospital of Soochow University, China
Simin Li,
Southern Medical University, China

*CORRESPONDENCE
Yan-Wen Xu
xyw890930@163.com

SPECIALTY SECTION
This article was submitted to Cellular and Molecular Mechanisms of Brain-aging, a section of the journal Frontiers in Aging Neuroscience

RECEIVED 08 August 2022
ACCEPTED 05 October 2022
PUBLISHED 24 October 2022

CITATION
Wang C-L, Yan X-J, Zhang C-L and Xu Y-W (2022) Elevated serum nuclear factor erythroid 2-related factor 2 levels contribute to a poor prognosis after acute supratentorial intracerebral hemorrhage: A prospective cohort study. *Front. Aging Neurosci.* 14:1014472. doi: 10.3389/fnagi.2022.1014472

COPYRIGHT
© 2022 Wang, Yan, Zhang and Xu. This is an open-access article distributed under the terms of the Creative Commons Attribution License (CC BY). The use, distribution or reproduction in other forums is permitted, provided the original author(s) and the copyright owner(s) are credited and that the original publication in this journal is cited, in accordance with accepted academic practice. No use, distribution or reproduction is permitted which does not comply with these terms.

Elevated serum nuclear factor erythroid 2-related factor 2 levels contribute to a poor prognosis after acute supratentorial intracerebral hemorrhage: A prospective cohort study

Chuan-Liu Wang[1], Xin-Jiang Yan[2], Cheng-Liang Zhang[1] and Yan-Wen Xu[1]*

[1]Department of Neurology, The Quzhou Affiliated Hospital of Wenzhou Medical University, Quzhou People's Hospital, Quzhou, Zhejiang, China, [2]Department of Neurosurgery, The Quzhou Affiliated Hospital of Wenzhou Medical University, Quzhou People's Hospital, Quzhou, Zhejiang, China

Objective: Nuclear factor erythroid 2-related factor 2 (Nrf2) is a key transcriptional factor for antioxidant response element-regulated genes. The purpose of this study was to assess the prognostic role of serum Nrf2 in intracerebral hemorrhage (ICH).

Materials and methods: In this prospective observational study, serum Nrf2 levels of 115 acute supratentorial ICH patients and 115 controls were gaged. Early neurologic deterioration (END) was defined as an increase of four or greater points in National Institutes of Health Stroke Scale (NIHSS) score or death at post-stroke 24 h. A poor outcome was referred to as the post-stroke 90-day modified Rankin scale (mRS) score of 3–6. END and a poor outcome were considered as the two prognostic parameters.

Results: As compared to controls, serum Nrf2 levels of patients were substantially elevated ($P < 0.001$), with its levels increasing during the 6-h period immediately, peaking in 12–18 h, plateauing at 18–24 h, and decreasing gradually thereafter ($P < 0.05$). Serum Nrf2 levels of patients were independently correlated with NIHSS score ($t = 3.033$; $P = 0.003$) and hematoma volume ($t = 3.210$; $P = 0.002$), independently predicted END (odds ratio 1.125; 95% confidence interval 1.027–1.232; $P = 0.011$) and poor outcome (odds ratio 1.217; 95% confidence interval 1.067–1.387; $P = 0.013$), as well as efficiently distinguished END (area under curve 0.771; 95% confidence interval 0.666–0.877; $P < 0.001$) and poor outcome (area under curve 0.803; 95% confidence interval 0.725–0.882; $P < 0.001$). Its predictive ability was equivalent to those of NIHSS score and hematoma volume (both $P > 0.05$), and it also significantly improved their

predictive abilities under receiver operating characteristic (ROC) curve (all $P < 0.05$).

Conclusion: Elevated serum Nrf2 levels are closely correlated with severity, END, and 90-day poor outcome following ICH. Hence, Nrf2 may play an important role in acute brain injury after ICH, and serum Nrf2 may have the potential to serve as a prognostic biomarker of ICH.

KEYWORDS

nuclear factor-erythroid 2-related factor 2, intracerebral hemorrhage, early neurologic deterioration, outcome, severity, mechanism

Introduction

Spontaneous intracerebral hemorrhage (ICH) is an acute life-threatening cerebrovascular disease that features neurologic deficits and even a decline in consciousness (Hemphill et al., 2015). National Institutes of Health Stroke Scale (NIHSS) is a conventional indicator of neurologic function (Kwah and Diong, 2014), and hematoma volume is a common variable for assessing ICH radiological severity (LoPresti et al., 2014). Early neurologic deterioration (END) is a frequently encountered adverse event, which has potentially serious consequences on patient outcome (Leira et al., 2004). Hence, early distinguishing ICH patients at risk of END and a poor outcome can have considerable clinical significance.

Oxidative stress arising from intraparenchymal blood deposited during ICH is extensively accepted as the important pathophysiology of secondary brain injury after ICH (Masomi-Bornwasser et al., 2021). During recent decades, biomarkers have obtained researchers' interests with respect to ICH severity assessment and prognosis prediction (Cai et al., 2021; Wu et al., 2021). Clearly, some oxidative stress-related biomarkers such as malondialdehyde, myeloperoxidase, lipid hydroperoxide, 8-iso-prostaglandin F2α, and thioredoxin have been demonstrated to be highly associated with ICH severity and clinical outcomes (Alexandrova and Danovska, 2011; Du et al., 2014; Qian et al., 2016; Lorente et al., 2018; Zheng et al., 2018). Nevertheless, those biomarkers in the peripheral blood have not been routinely determined for clinical service. Consequently, a clinical investigation of biochemical markers is still underway for ICH severity and prognosis analysis.

Nuclear factor erythroid 2-related factor 2 (Nrf2) has been extensively investigated as a very important cytoprotective transcription factor that can regulate the expression of genes coding antioxidant, anti-inflammatory, and detoxifying proteins (Pi et al., 2019). Nrf2 by neurons can be highly expressed under brain oxidative stress and inflammation injury (Sandberg et al., 2014). Compelling experimental evidence has confirmed that Nrf2 may confer brain-protective function *via* attenuating free radical oxidative damage in ICH (Wang et al., 2007; Zhao et al., 2007, 2015a,b). Taken together, circulating Nrf2 is hypothesized to represent a potential biomarker of ICH. Recently, in autism children, serum Nrf2 levels were found to be significantly elevated, as compared to healthy children (Ayaydin et al., 2020). However, to the best of our knowledge, there is a paucity of data available regarding Nrf2 levels in the peripheral blood of humans with acute brain injury, including ICH. In this study, we determined serum Nrf2 levels in a cohort of patients with spontaneous supratentorial ICH and compared them with those of controls. In addition, we investigated the role of serum Nrf2 as a potential biomarker for severity assessment and prognosis prediction of ICH.

Materials and methods

Study design ad participant selection

Patients with first-ever spontaneous supratentorial ICH were consecutively recruited into this prospective observational study performed at our hospital from February 2018 to July 2021. Next, we excluded those patients with (1) time from the onset of stroke symptom to hospital admission >24 h; (2) age <18 years; (3) ICH resulting from secondary causes (such as congenital or acquired coagulation abnormalities, hemorrhagic transformation of cerebral infarction, moyamoya disease, cerebral aneurysm, cerebral arteriovenous malformation, and intracranial tumors); (4) primary intraventricular hemorrhage; (5) a surgical procedure for hematoma evacuation; or (6) a history of some specific diseases or conditions (e.g., ischemic stroke, aneurysmal subarachnoid hemorrhage, intracranial tumors, severe traumatic brain injury, malignancies, immune

Abbreviations: END, early neurologic deterioration; CT, computerized tomography; ICH, intracerebral hemorrhage; NIHSS, National Institutes of Health Stroke Scale; ROC, receiver operating characteristic; mRS, modified Rankin scale; Nrf2, nuclear factor erythroid 2-related factor 2; SD, standard deviation; ROS, reactive oxygen species.

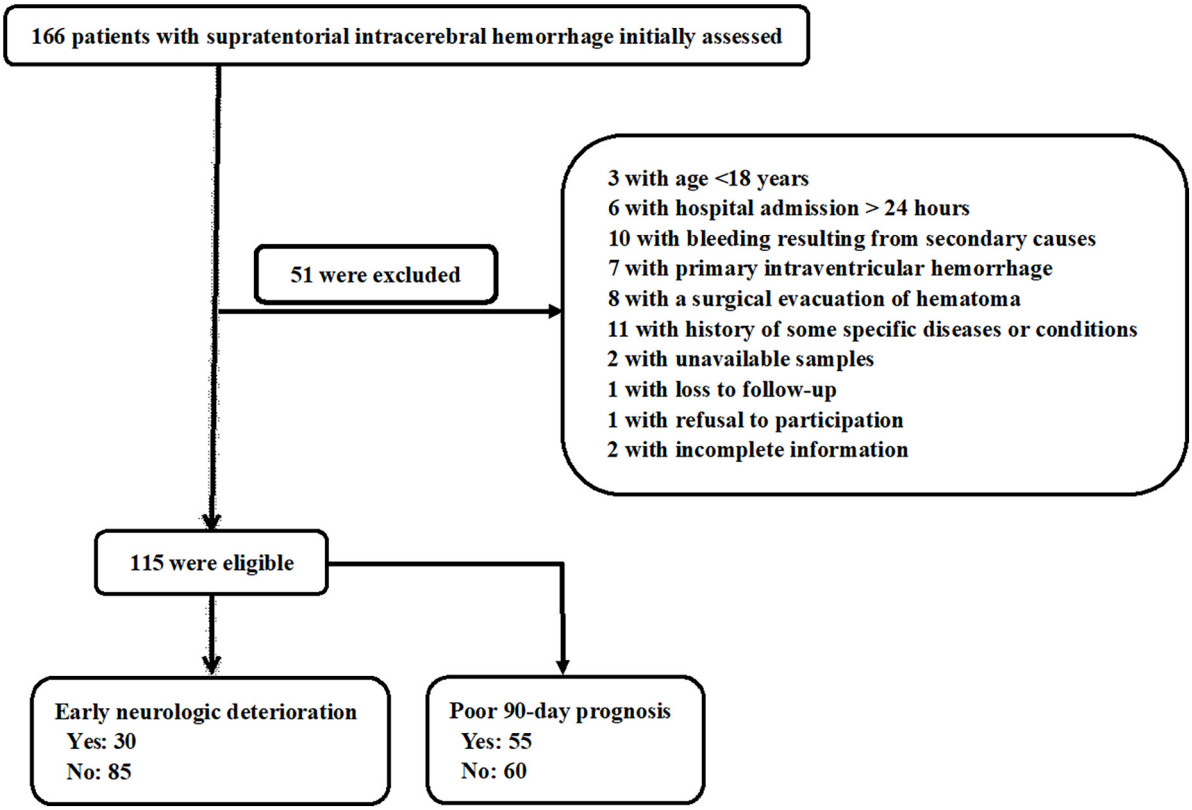

FIGURE 1
Flowchart for selecting eligible patients with acute supratentorial intracerebral hemorrhage (ICH). After 51 were excluded from 166 patients, a total of 115 patients were retained for final analysis.

TABLE 1 Comparison of the baseline characteristics between healthy controls and patients with intracerebral hemorrhage (ICH).

	Patients	Controls	*P*-value
Age (years)	62.9 ± 12.0	63.3 ± 13.7	0.770
Gender (male/female)	65/50	60/55	0.508
Hypertension	73 (63.5%)	–	
Diabetes mellitus	18 (15.7%)	–	
Hyperlipidemia	33 (28.7%)	–	
Cigarette smoking	39 (33.9%)	35 (30.4%)	0.572
Alcohol drinking	44 (38.3%)	42 (36.5%)	0.785

Variables were presented as count (percentage) or mean ± standard deviation as appropriate, and statistical methods included the Chi-square test, Fisher's exact test, and Student's *t*-test.

deficiency syndromes, pregnancies, and severe heart, liver, lung, or kidney dysfunction). During the same period, a group of healthy subjects were recruited as controls. This study was performed according to the tenets of the Declaration of Helsinki, and the approval for the protocol of this study was acquired from the ethics committee at our hospital. Informed consent to participate in this study was signed by next of kin to patients or controls themselves.

Data collection and outcome assessment

We collected some relevant information such as demographics (age and gender), adverse life habits (cigarette smoking and alcohol drinking), previous usage of some specific drugs (statins, anticoagulation drugs, and antiplatelet drugs), vascular risk factors (hypertension, diabetes mellitus, and hyperlipidemia), and vital signs (systolic and diastolic arterial blood pressures). Admission NIHSS scores were recorded to assess neurologic function. Hematoma volume was calculated based on the formula $0.5 \times a \times b \times c$ (Kothari et al., 1996). The ICH topography was classified as lobar, including parietal, frontal, temporal, and occipital, when it affected predominantly the cortical or subcortical white matter of the cerebral lobes or as deep, including putamen, caudate, internal capsule, and thalamus, when it was limited to the internal capsule, the basal ganglia, or the thalamus. Extension of hematoma into subarachnoid or intraventricular cavity was observed. The severity of intraventricular hematoma was estimated utilizing the Graeb scale (Graeb et al., 1982). END was defined as an increase of ≥4 in the NIHSS score or death within 24 h after

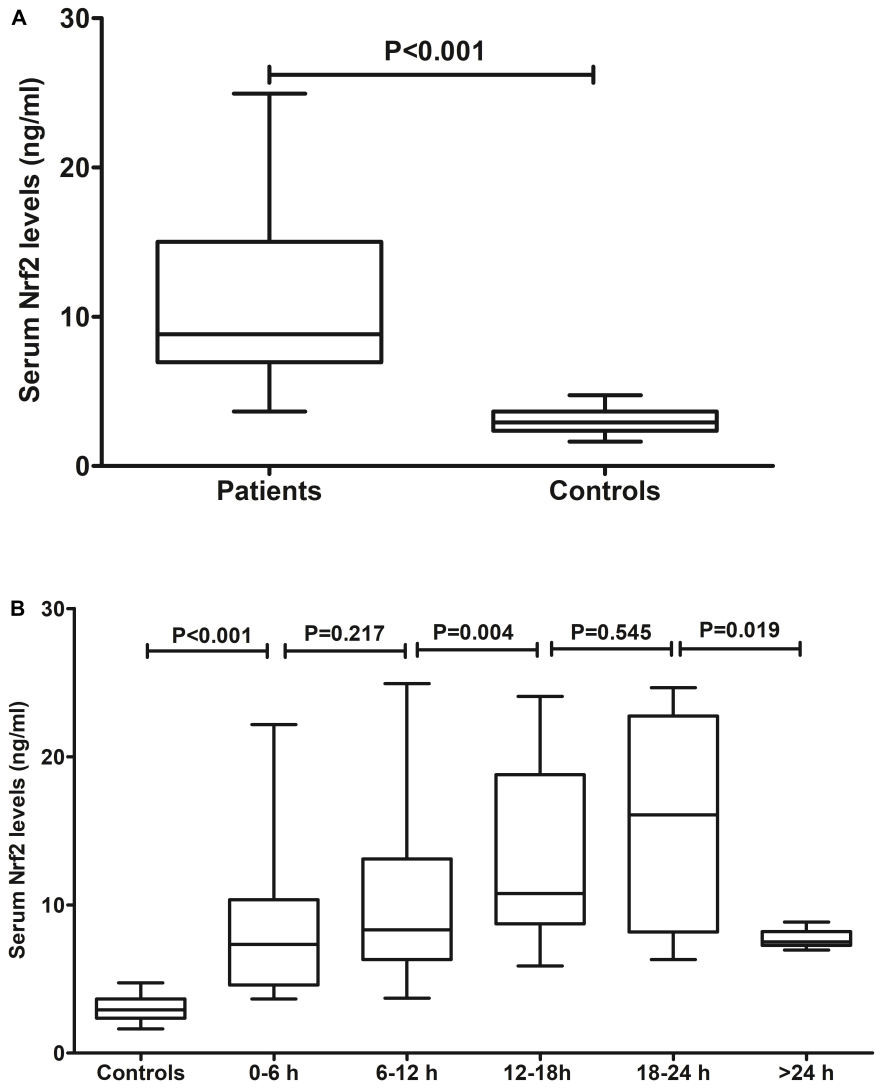

FIGURE 2
Serum nuclear factor erythroid 2-related factor 2 (Nrf2) levels after acute intracerebral hemorrhage (ICH). **(A)** Difference in serum Nrf2 levels between controls and patients. **(B)** Dynamic change in serum Nrf2 levels after acute ICH. After stroke, serum Nrf2 levels of patients increased during the 6-h period immediately, peaked at 12–18 h, plateaued at 18–24 h, decreased gradually thereafter, and were significantly higher than those in healthy controls (all $P < 0.05$). Nrf2 indicates nuclear factor erythroid 2-related factor 2.

admission (Du et al., 2013). A poor outcome was defined as post-stroke 90-day modified Rankin scale (mRS) scores of 3–6 (Dong et al., 2015).

Immune analysis

Five milliliters of venous blood was drawn *via* the antecubital vein from ICH patients and healthy controls and promptly placed into gel-containing biochemistry tubes. The blood samples were immediately centrifuged at 3,500 *g* for 10 min. Serum was preserved at −80°C in Eppendorf tubes until assayed. Serum Nrf2 levels were quantified in the biochemistry laboratory using the enzyme-linked immunosorbent assay (Active Motif, Carlsbad, CA, USA) and read at 450 nm on a microplate reader (Multiskan GO, Thermo Fisher Scientific, Waltham, MA, USA). Each sample was in duplicate measured by the same technician blinded to clinical data, the results were reported as ng/ml, and two measures were averaged for final analysis.

Statistical analysis

Statistical analysis was performed using the Statistical Package for Social Sciences (SPSS) 23.0 software (SPSS Inc.,

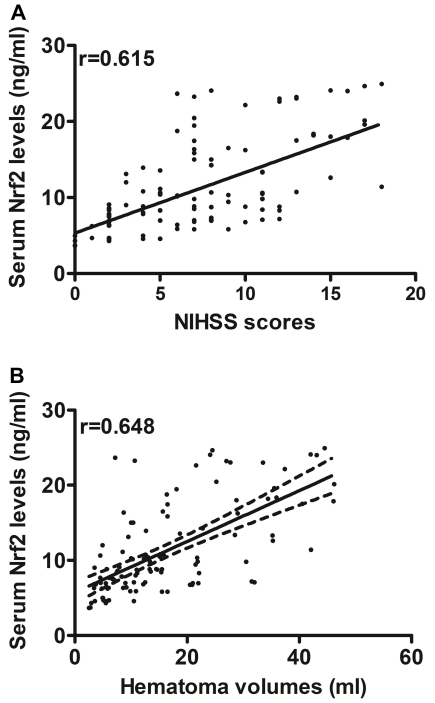

FIGURE 3
Relationship between serum nuclear factor erythroid 2-related factor 2 (Nrf2) levels and stroke severity after acute supratentorial ICH. **(A)** Correlation of serum Nrf2 levels with National Institutes of Health Stroke Scale (NIHSS) score. **(B)** Correlation of serum Nrf2 levels with hematoma volume. Serum Nrf2 levels were closely and positively correlated with NIHSS score and hematoma volume (both $P < 0.001$). Nrf2 indicates nuclear factor erythroid 2-related factor 2; NIHSS, National Institutes of Health Stroke Scale.

TABLE 2 Factors correlated with serum nuclear factor erythroid 2-related factor 2 (Nrf2) levels after acute intracerebral hemorrhage (ICH).

Variables	*r*	*P*-value
Age >60 years	0.092	0.327
Gender (male/female)	−0.059	0.532
Hypertension	0.082	0.381
Diabetes mellitus	0.162	0.084
Hyperlipidemia	0.058	0.539
Cigarette smoking	0.165	0.077
Alcohol drinking	0.099	0.293
Pretreatment of statins	0.097	0.305
Pretreatment of anticoagulation drugs	−0.168	0.073
Pretreatment of antiplatelet drugs	0.114	0.224
Admission time (h)	0.211	0.024
Blood collection time (h)	0.220	0.018
Systolic arterial pressure (mmHg)	0.068	0.469
Diastolic arterial pressure (mmHg)	0.092	0.330
Hemorrhage locations (lobar/deep)	0.035	0.712
Intraventricular hemorrhage	0.477	<0.001
Graeb scores	0.430	<0.001
Subarachnoid hemorrhage	0.279	0.003
NIHSS scores	0.615	<0.001
Hematoma volume (ml)	0.648	<0.001
Blood leukocyte count ($\times 10^9$/l)	0.439	<0.001
Blood glucose levels (mmol/l)	0.279	0.003

Correlations were analyzed using Spearman's correlation coefficient test, and the results were reported as *r* values. NIHSS indicates National Institutes of Health Stroke Scale.

Chicago, IL, USA). The Pearson Chi-square test was applied to compare the proportions of categorical variables, which were herein reported as frequencies (percentages). The Shapiro–Wilk normality test was used to assess normal distribution of continuous variables, which were therein summarized as medians (upper–lower quartiles) if non-normally distributed and as means (standard deviation, SD) if normally distributed. If the continuous data were not normally distributed, we used non-parametric tests, including the Mann–Whitney U test for two-group comparisons and the Kruskal–Wallis test for multiple-group comparisons. If the continuous data were under normal distribution, the independent sample *t*-tests were utilized for two-group comparisons. Spearman's correlation coefficient was applied to evaluate the relationships between serum Nrf2 levels and other variables, and afterward, linear regression analysis was performed. The binary logistic regression model was established to discern predictors, which were independently associated with END and 90-day poor outcome after ICH. Associations were reported as odds ratio (OR) with the corresponding 95% confidence interval (CI). In this study, those variables, which were significant using univariate analysis, were forced into the multivariate model. Under the receiver operating characteristic (ROC) curve, we observed predictive efficiency. The area under ROC curve (AUC) was shown to reflect prognostic ability. The two-sided significance level was set at $P < 0.05$.

Results

Participant selection

In this study, a total of 166 patients with first-ever supratentorial ICH were assessed for eligibility, of whom 51 patients were excluded from this study because of the reasons outlined in Figure 1 and 115 patients were finally analyzed. Also, 115 healthy subjects constituted controls. Patients were aged from 37 to 86 years (mean 62.9 years; SD 12.0 years), of whom 65 were men and 50 were women. Controls, 60 being men and 55 being women, were aged from 30 to 93 years (mean 63.3 years; SD 13.7 years). There were no substantial differences in age and gender percentage between controls and patients (both $P > 0.05$). Other baseline characteristics are provided in Table 1 for comparison between ICH patients and healthy

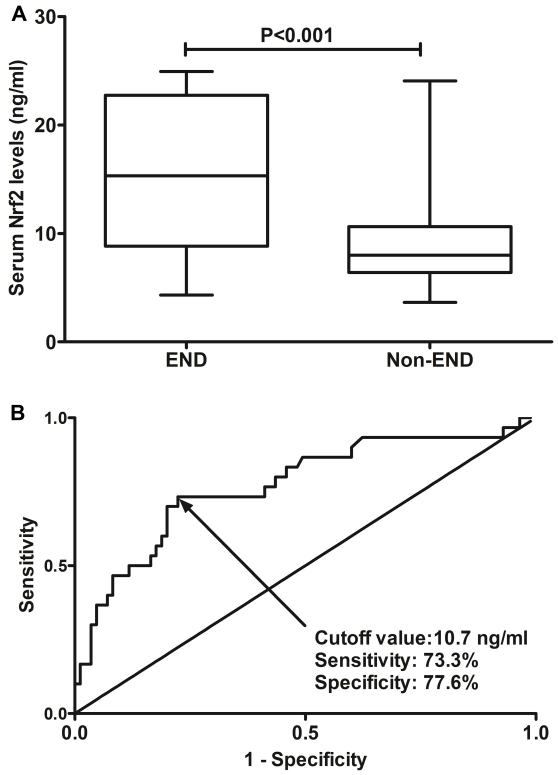

FIGURE 4
Predictive ability with respect to serum nuclear factor erythroid 2-related factor 2 (Nrf2) levels for risk of early neurologic deterioration (END) after acute supratentorial intracerebral hemorrhage (ICH). **(A)** Comparison of serum Nrf2 levels between patients with END and those who did not present with END. **(B)** Discriminatory capability of serum Nrf2 levels for END under the receiver operating characteristic (ROC) curve. Serum Nrf2 levels were markedly higher in patients suffering from END than in those without development of END ($P < 0.001$). Serum Nrf2 levels statistically significantly predicted END after acute stroke ($P < 0.001$). Nrf2 indicates nuclear factor erythroid 2-related factor 2; END, early neurologic deterioration.

controls. Also, alcohol drinking and cigarette smoking did not significantly differ between ICH patients and healthy controls (both $P > 0.05$).

Patient characteristics

Among this cohort of patients, 73 (63.5%) presented with hypertension, 18 (15.7%) had diabetes mellitus, 33 (28.7%) suffered from hyperlipidemia, 39 (33.9%) were cigarette smokers, and 44 (38.3%) were alcohol consumers. In total, prior to hospital admission, 25 (21.7%), 6 (5.2%), and 16 (13.9%) patients orally took statins, anticoagulation drugs, and antiplatelet drugs, respectively. Patients were admitted from 0.5 to 24.0 h (median 10.0 h; lower–upper quartiles 6.9–14.8 h) following ICH. Systolic arterial pressure and diastolic arterial pressure ranged from 98 to 214 mmHg (mean 150.2 mmHg; SD 23.8 mmHg) and from 65 to 114 mmHg (mean 87.1 mmHg; SD 10.9 mmHg), respectively. Lobar hematomas and deep hematomas were revealed in 26 and 89 patients, respectively. Hematomas were extended into intraventricular cavity in 38 patients (33.0%) and into subarachnoid space in 12 patients (10.4%). NIHSS scores, Graeb scores, and bleeding size ranged from 0 to 18 ml (median 7 ml; lower–upper quartiles 4–11 ml), from 0 to 9 ml (median 0 ml; lower–upper quartiles 0–1 ml), and from 3 to 46 ml (median 13 ml; lower–upper quartiles 7–22 ml), respectively.

Serum nuclear factor erythroid 2-related factor 2 levels after intracerebral hemorrhage

Blood samples of patients were collected from 1.0 to 26.0 h (median 11.5 h; lower–upper quartiles 7.8–16.4 h) after ICH. In Figure 2A, serum Nrf2 levels were substantially higher in patients than those in controls ($P < 0.001$). In addition, blood collection time was divided into five time points, namely, 0–6 h, 6–12 h, 12–18 h, 18–24 h, and >24 h. After ICH, serum Nrf2 levels of patients increased during the 6-h period immediately, peaked at 12–18 h, plateaued at 18–24 h, decreased gradually thereafter, and were significantly higher than those in healthy controls (all $P < 0.05$; Figure 2B).

Serum nuclear factor erythroid 2-related factor 2 levels and illness severity after intracerebral hemorrhage

Serum Nrf2 levels of patients were intimately correlated with NIHSS scores ($P < 0.001$; Figure 3A), hematoma volume ($P < 0.001$; Figure 3B), and other variables, including admission time, blood collection time, intraventricular hemorrhage, Graeb scores, subarachnoid hemorrhage, blood glucose levels, and blood leukocyte count (all $P < 0.05$; Table 2). Using the multivariate linear regression model, which contained significant variables in the Spearman test, it was shown that serum Nrf2 levels were independently related to NIHSS scores ($t = 3.033$; $P = 0.003$) and hematoma volume ($t = 3.210$; $P = 0.002$).

Serum nuclear factor erythroid 2-related factor 2 levels and early neurologic deterioration risk

A total of 30 ICH patients experienced END. In Figure 4A, patients at risk of END had significantly higher serum Nrf2

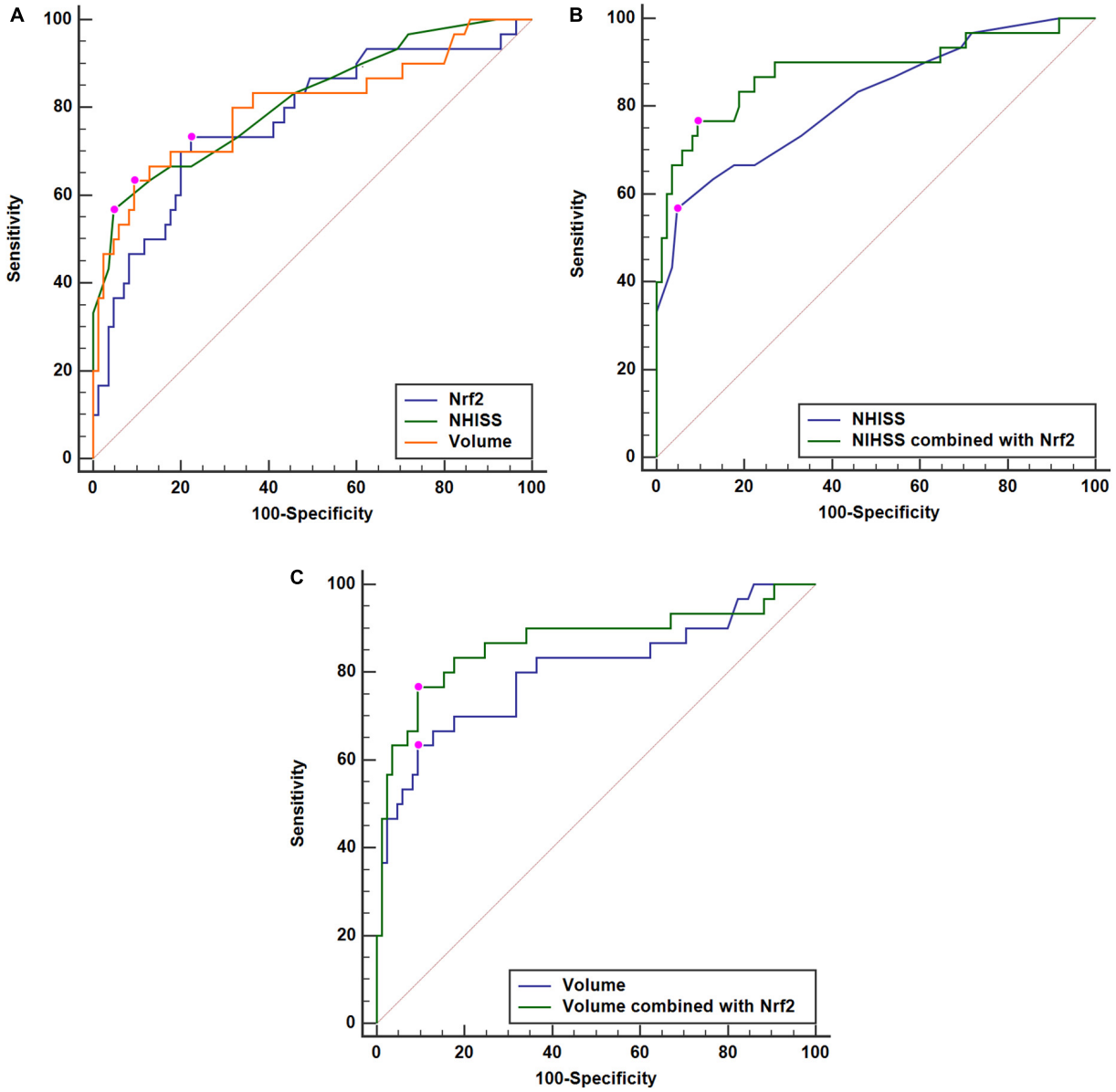

FIGURE 5
Comparisons of discriminatory capabilities for early neurologic deterioration (END) among serum nuclear factor erythroid 2-related factor 2 (Nrf2) levels, National Institutes of Health Stroke Scale (NIHSS) scores, and hematoma volume after acute supratentorial intracerebral hemorrhage (ICH). **(A)** Comparisons of areas under curve for END among serum Nrf2 levels, NIHSS scores, and hematoma volume after acute supratentorial ICH. **(B)** Comparison of areas under curve for END between serum Nrf2 levels combined with NIHSS scores and NIHSS scores after acute supratentorial ICH. **(C)** Comparison of areas under curve for END between serum Nrf2 levels combined with hematoma volume and hematoma volume after acute supratentorial ICH. Serum Nrf2 levels had similar area under curve, as compared to NIHSS scores and hematoma volume (both $P > 0.05$). Moreover, serum Nrf2 levels profoundly improved areas under curve of NIHSS scores and hematoma volume (both $P < 0.05$). Nrf2 indicates nuclear factor erythroid 2-related factor 2; NIHSS, National Institutes of Health Stroke Scale.

levels than those without development of END ($P < 0.001$). Using Youden's method, serum Nrf2 levels >10.7 ng/ml discriminated patients at risk of END with medium–high sensitivity and specificity values (Figure 4B). In Figure 5A, using the ROC curve, the predictive ability of serum Nrf2 levels was in the range of NIHSS scores and hematoma volume (both $P > 0.05$). Moreover, serum Nrf2 levels significantly improved the predictive values of NIHSS scores ($P = 0.030$; Figure 5B) and hematoma volume ($P = 0.019$; Figure 5C).

In Table 3, as compared to patients who did not suffer from END, those at risk of END had significantly elevated percentages of intraventricular hemorrhage ($P < 0.01$) and subarachnoid hemorrhage ($P < 0.05$) and displayed substantially raised Graeb

TABLE 3 Factors associated with early neurologic deterioration (END) after acute intracerebral hemorrhage (ICH).

	Early neurologic deterioration		*P*-value
	Presence	Absence	
Number	30	85	
Age >60 years	21 (70.0%)	47 (55.3%)	0.159
Gender (male/female)	15/15	50/35	0.402
Hypertension	20 (66.7%)	53 (62.4%)	0.673
Diabetes mellitus	7 (23.3%)	11 (12.9%)	0.241
Hyperlipidemia	10 (33.3%)	23 (27.1%)	0.514
Cigarette smoking	12 (40.0%)	27 (31.8%)	0.413
Alcohol drinking	14 (46.7%)	30 (35.3%)	0.271
Pretreatment of statins	9 (30.0%)	16 (18.8%)	0.202
Pretreatment of anticoagulation drugs	1 (3.3%)	5 (5.9%)	1.000
Pretreatment of antiplatelet drugs	6 (20.0%)	10 (11.8%)	0.356
Admission time (h)	11.2 (7.3–15.0)	9.8 (6.2–14.6)	0.586
Blood collection time (h)	12.2 (9.2–16.7)	11.2 (7.5–16.0)	0.649
Systolic arterial pressure (mmHg)	147.4 ± 23.2	151.2 ± 24.0	0.463
Diastolic arterial pressure (mmHg)	85.0 ± 9.3	87.9 ± 11.4	0.207
Hemorrhage locations (lobar/deep)	9/21	17/68	0.260
Intraventricular hemorrhage	17 (56.7%)	21 (24.7%)	0.001
Graeb scores	1 (0–7)	0 (0–0)	<0.001
Subarachnoid hemorrhage	7 (23.3%)	5 (5.9%)	0.013
NIHSS scores	12 (7–15)	6 (2–8)	<0.001
Hematoma volume (ml)	28 (15–36)	11 (7–16)	<0.001
Blood leukocyte count ($\times 10^9$/l)	7.8 ± 2.8	7. 3 ± 2.9	0.364
Blood glucose levels (mmol/l)	12.9 ± 3.7	10.4 ± 3.8	0.003
Serum Nrf2 levels (ng/ml)	15.3 (8.8–22.7)	8.0 (6.4–10.6)	<0.001

Variables were presented as count (percentage), mean ± standard deviation, or median (upper-lower quartile) as appropriate, and statistical methods included the Chi-square test, Fisher's exact test, Student's *t*-test, and the Mann–Whitney test. NIHSS indicates National Institutes of Health Stroke Scale; Nrf2, nuclear factor erythroid 2-related factor 2.

scores ($P < 0.01$), NIHSS scores ($P < 0.001$), hematoma volume ($P < 0.001$), blood glucose levels ($P < 0.001$), and serum Nrf2 levels ($P < 0.001$). Using the binary logistic regression model, which contained the preceding significant variables in univariate analysis, we found that NIHSS score, hematoma volume, and serum Nrf2 levels independently predicted END (Table 4).

TABLE 4 Results of multivariate analysis for prognostic prediction after acute intracerebral hemorrhage (ICH).

	Odds ratio (95% confidence interval)	*P*-value
Early neurologic deterioration		
NIHSS score	1.276 (1.070–1.522)	0.007
Hematoma volume	1.095 (1.016–1.181)	0.018
Serum Nrf2 levels	1.125 (1.027–1.232)	0.011
90-day poor prognosis		
NIHSS score	1.601 (1.239–2.067)	0.001
Hematoma volume	1.094 (1.036–1.156)	0.001
Serum Nrf2 levels	1.217 (1.067–1.387)	0.013

NIHSS indicates National Institutes of Health Stroke Scale; Nrf2, nuclear factor erythroid 2-related factor 2.

Serum nuclear factor erythroid 2-related factor 2 levels and development of poor 90-day prognosis

At 90 days after ICH, mRS scores ranged from 0 to 6, with a median value of 2 (lower–upper quartiles 1–3). Among them, 10 patients had mRS score 0; 21, mRS score 1; 29, mRS score 2; 33, mRS score 3; 7, mRS score 4; 10, mRS score 5; and 5, mRS score 6. In total, 55 patients experienced a poor 90-day prognosis. In Figure 6A, serum Nrf2 levels were substantially different among subgroups divided by mRS scores, with higher levels in mRS score 6 subgroup and lowest levels in mRS score 0 subgroup ($P < 0.001$). In Figure 6B, serum Nrf2 levels were significantly correlated with mRS scores ($P < 0.001$). In addition, poor prognosis patients had markedly higher serum Nrf2 levels than other remainders ($P < 0.001$; Figure 6C). Under the ROC curve, serum Nrf2 levels >10.5 ng/ml differentiated between poor prognosis patients and good prognosis ones with medium–high sensitivity and specificity values (Figure 6D). In Figure 7A, under the ROC curve, the discriminatory capability of serum Nrf2 levels was similar to those of NIHSS scores and hematoma volume (both $P > 0.05$). Moreover, serum Nrf2 levels substantially enhanced the predictive abilities of NIHSS scores ($P = 0.034$; Figure 7B) and hematoma volume ($P = 0.024$; Figure 7C).

Just as displayed in Table 5, as compared to patients without risk of poor prognosis, those, who were likely to experience poor prognosis, had significantly raised percentages of intraventricular bleedings and subarachnoid bleedings (both $P < 0.01$) and were more prone to exhibit significantly increased

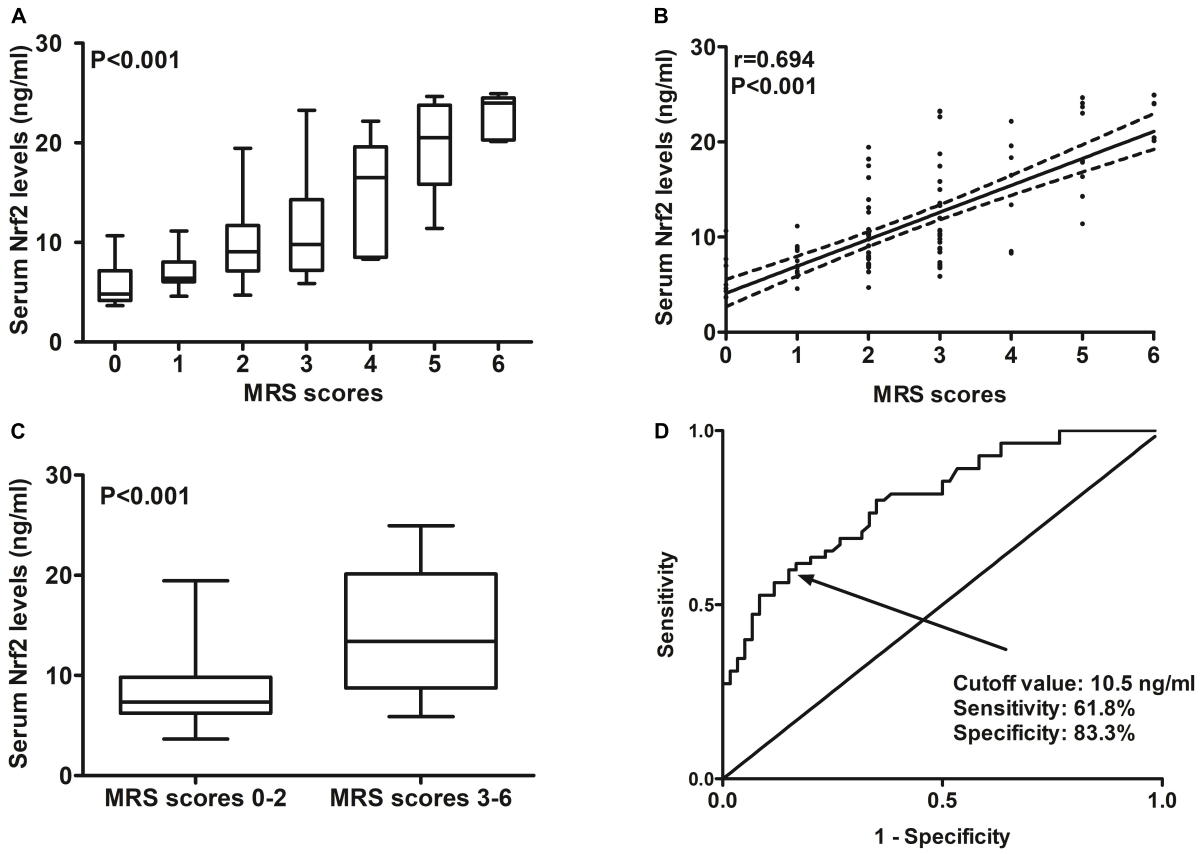

FIGURE 6
Predictive ability with respect to serum nuclear factor erythroid 2-related factor 2 (Nrf2) levels for post-stroke 90-day poor prognosis after acute supratentorial intracerebral hemorrhage (ICH). **(A)** Comparisons of serum Nrf2 levels among subgroups based on modified Rankin scale (mRS) scores. **(B)** Relationship between serum Nrf2 levels and mRS scores. **(C)** Comparison of serum Nrf2 levels between patients with mRS scores 3–6 and those with scores 0–2. **(D)** Discriminatory capability of serum Nrf2 levels for post-stroke 90-day poor prognosis under the receiver operating characteristic (ROC) curve. Serum Nrf2 levels were intimately correlated with mRS scores and were markedly higher in patients with mRS scores 3–6 than in those with scores 0–2 (all $P < 0.001$). Serum Nrf2 levels statistically significantly predicted 90-day poor prognosis after acute stroke ($P < 0.001$). Nrf2 indicates nuclear factor erythroid 2-related factor 2; mRS, modified Rankin scale.

NIHSS scores ($P < 0.001$), hematoma volume ($P < 0.001$), blood glucose levels ($P < 0.05$), and serum Nrf2 levels ($P < 0.001$). The above significant variables were forced into the binary logistic regression model, and as a subsequence, NIHSS scores, hematoma volume, and serum Nrf2 levels were retained as the independent predictors of post-stroke 90-day poor prognosis (Table 4).

Discussion

To the best of our knowledge, no data are available regarding the relationship between circulating Nrf2 levels and severity in addition to the prognosis of patients with acute brain injury. Our study mainly found such results: (1) Serum Nrf2 levels were profoundly higher in ICH patients than those in healthy controls; (2) there was a dynamic change in serum Nrf2 levels of ICH patients, showing that its levels increased within 6 h, peaked at 24 h, and decreased gradually; (3) serum Nrf2 levels not only were closely correlated with NIHSS scores and hematoma volume using the Spearman test, but also were independently related to NIHSS scores and hematoma volume using multivariable linear regression analysis; (4) serum Nrf2 levels, which were considered as whether the categorical or continuous variable, were highly correlated with 90-day mRS scores after ICH; (5) serum Nrf2 emerged as an independent predictor of END and 90-day poor prognosis; (6) serum Nrf2 levels had similar prognostic predictive ability for END and 90-day poor prognosis after hemorrhagic stroke, as compared to NIHSS scores and hematoma volume; and (7) serum Nrf2 levels substantially improved the predictive efficiency of NIHSS scores and hematoma volume. In a word, serum Nrf2 levels, in close correlation with hemorrhagic severity, independently predicted END and 90-day poor prognosis after ICH, indicating serum Nrf2 may be a promising biochemical marker for facilitating severity assessment and prognosis prediction after acute ICH.

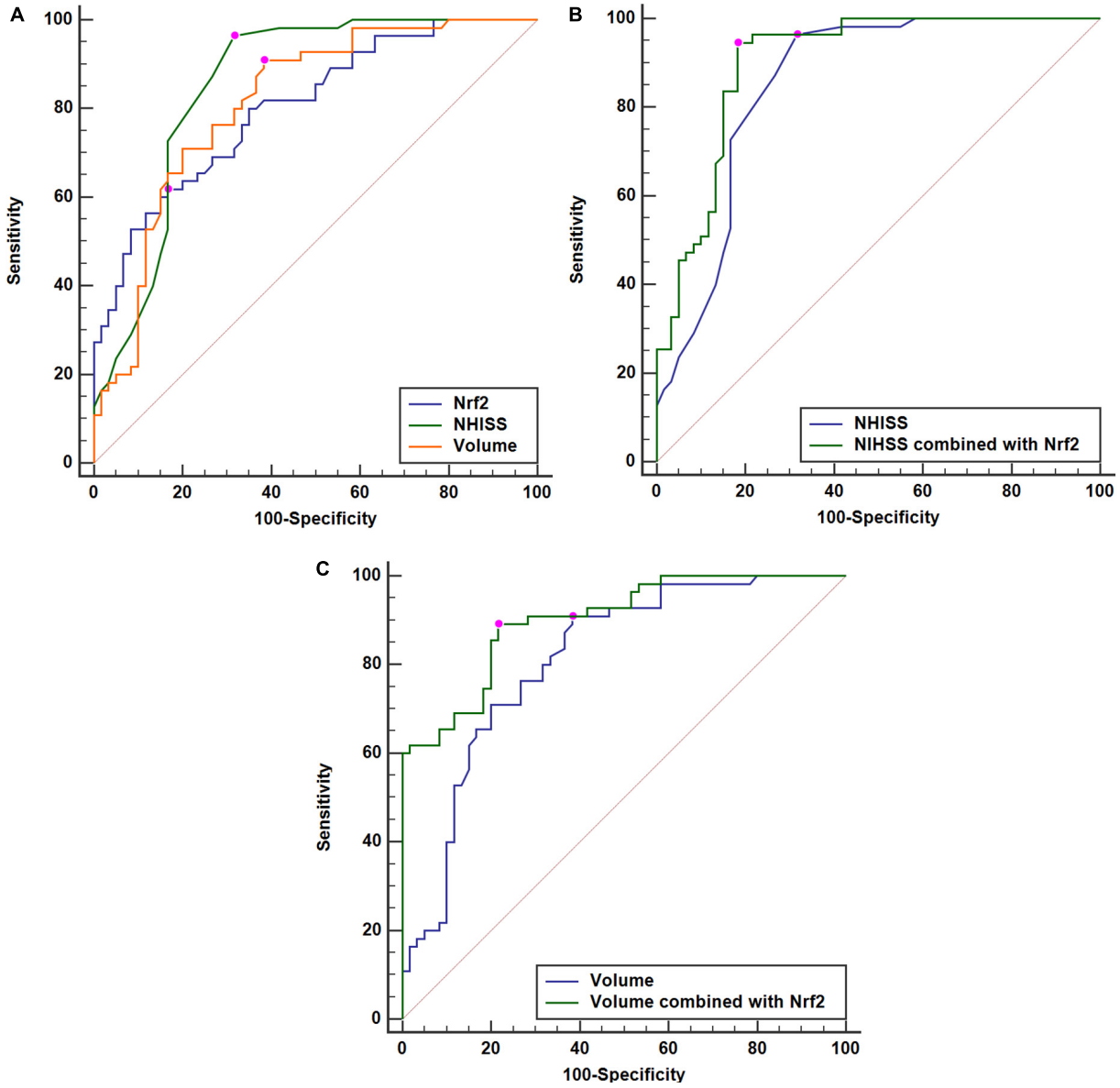

FIGURE 7
Comparisons of discriminatory capabilities for post-stroke 90-day poor prognosis among serum nuclear factor erythroid 2-related factor 2 (Nrf2) levels, National Institutes of Health Stroke Scale (NIHSS) scores, and hematoma volume after acute supratentorial intracerebral hemorrhage (ICH). **(A)** Comparisons of areas under curve for post-stroke 90-day poor prognosis among serum Nrf2 levels, NIHSS scores, and hematoma volume after acute supratentorial intracerebral hemorrhage (ICH). **(B)** Comparison of areas under curve for post-stroke 90-day poor prognosis between serum Nrf2 levels combined with NIHSS scores and NIHSS scores after acute supratentorial ICH. **(C)** Comparison of areas under curve for post-stroke 90-day poor prognosis between serum Nrf2 levels combined with hematoma volume and hematoma volume after acute supratentorial ICH. Serum Nrf2 levels had similar area under curve, as compared to NIHSS scores and hematoma volume (both $P > 0.05$). Moreover, serum Nrf2 levels profoundly improved areas under curve of NIHSS scores and hematoma volume (both $P < 0.05$). Poor prognosis was defined as modified Rankin Scale (mRS) scores 3–6. Nrf2 indicates nuclear factor erythroid 2-related factor 2; NIHSS, National Institutes of Health Stroke Scale.

Accumulating evidence has shown that inflammation and oxidative stress participate in the progression of acute brain injury following ICH (Wilkinson et al., 2018). Nrf2, which is identified as a key transcriptional factor, can modulate antioxidant response element-regulated genes (Tonelli et al., 2018). Reportedly, increasing Nrf2 activity could protect against cerebral ischemia *in vivo* (Son et al., 2010). Several animal studies have identified a protective role of Nrf2 in ICH (Wang et al., 2007; Zhao et al., 2007, 2015a,b). Specifically, as compared to wild-type mice, Nrf2-knockout mice had significantly increased injury volume, leukocyte infiltration, production of reactive oxygen species (ROS), DNA damage, and

TABLE 5 Factors associated with 90-day functional outcome after acute intracerebral hemorrhage (ICH).

Variables	MRS scores 3–6	MRS scores 0–2	*P*-value
Number	55	60	
Age >60 years	37 (67.3%)	31 (51.7%)	0.089
Gender (male/female)	27/28	38/22	0.124
Hypertension	36 (65.5%)	37 (61.7%)	0.673
Diabetes mellitus	8 (14.5%)	10 (16.7%)	0.754
Hyperlipidemia	15 (27.3%)	18 (30.0%)	0.747
Cigarette smoking	17 (30.9%)	22 (36.7%)	0.515
Alcohol drinking	22 (40.0%)	22 (36.7%)	0.713
Pretreatment of statins	13 (23.6%)	12 (20.0%)	0.637
Pretreatment of anticoagulation drugs	2 (3.6%)	4 (6.7%)	0.681
Pretreatment of antiplatelet drugs	8 (14.5%)	8 (13.3%)	0.851
Admission time (h)	10.5 (7.4–15.2)	9.3 (6.2–14.2)	0.258
Blood collection time (h)	12.2 (9.3–17.0)	10.8 (7.3–15.7)	0.214
Systolic arterial pressure (mmHg)	150.1 ± 24.4	150.3 ± 23.3	0.956
Diastolic arterial pressure (mmHg)	87.0 ± 10.6	87.3 ± 11.2	0.903
Hemorrhage locations (lobar/deep)	15/40	11/49	0.252
Intraventricular hemorrhage	25 (45.5%)	13 (21.7%)	0.007
Graeb scores	0 (0–5)	0 (0–0)	0.086
Subarachnoid hemorrhage	10 (18.2%)	2 (3.3%)	0.009
NIHSS scores	9 (7–12)	4 (2–7)	<0.001
Hematoma volume (ml)	21 (13–28)	9 (5–13)	<0.001
Blood leukocyte count ($\times 10^9$/l)	7.9 ± 3.0	7.0 ± 2.7	0.094
Blood glucose levels (mmol/l)	11.8 ± 3.9	10.3 ± 3.8	0.042
Serum Nrf2 levels (ng/ml)	13.4 (8.8–19.9)	7.4 (6.2–9.8)	<0.001

Variables were presented as count (percentage), mean ± standard deviation, or median (upper-lower quartile) as appropriate, and statistical methods included the Chi-square test, Fisher's exact test, Student's *t*-test, and the Mann–Whitney test. NIHSS indicates National Institutes of Health Stroke Scale; Nrf2, nuclear factor erythroid 2-related factor 2; mRS, modified Rankin scale.

cytochrome c release after intracerebral injection of collagenase (Wang et al., 2007). Also, a study of Nrf2-knockout mice has demonstrated that Nrf2 may play an important role in modulating microglia function and hematoma clearance (Zhao et al., 2015a). In a pre-clinical study investigating dimethyl fumarate, a substance for the treatment of multiple sclerosis, as therapy for ICH, Nrf2 was considered as a key factor involved in the protective effects of dimethyl fumarate on ICH (Zhao et al., 2015b). Sulforaphane-activated Nrf2 could obviously reduce neutrophil count, oxidative damage, and behavioral deficits in rats with ICH, and Nrf2-deficient mice had more severe neurologic deficits after ICH (Zhao et al., 2007). Overall, Nrf2 may be a protective factor in acute brain injury after ICH, and recruitment of the antioxidative defense system may be one of its important mechanisms.

Nuclear factor erythroid 2-related factor 2 can be chiefly expressed in neuronal cells. Brain Nrf2 expressions were significantly increased at 2 h and peaked at 8 h of reperfusion in mice after transient middle cerebral artery occlusion (Tanaka et al., 2011). In ICH rat brain, Nrf2 expressions were substantially elevated at 2 h with a peak at 24 h (Shang et al., 2013). Also, there was a significant elevation of expression of Nrf2 in brain tissues after human cerebral cortex contusion (Guo et al., 2019). In the current study, there was a significant enhancement in serum Nrf2 levels after ICH, as compared to healthy controls, and serum Nrf2 levels increased within 6 h, peaked at 24 h, and decreased gradually. Presumably, Nrf2 in the peripheral blood may be at least partially derived from injured brain tissues after ICH. In consideration of its cytoprotective effects, Nrf2 released from brain tissues may be a compensatory response to brain inflammatory and oxidative damage after ICH. Hence, Nrf2 may play an important role in acute brain injury after ICH.

Experimentally, Nrf2 expressions in brain tissues had close correlation with brain edema and neurologic deficit after ICH (Shang et al., 2013). In our study, serum Nrf2 levels, in independent correlation with hemorrhagic severity indicated by NIHSS scores and hematoma volume, were independently predictive of END and poor neurologic function prognosis after ICH. Interestingly, serum Nrf2 levels were of significant efficiency in predicting END and poor prognosis after ICH under the ROC curve. Of note, the predictive ability of its combination with NIHSS scores or hematoma volume substantially exceeded that of NIHSS scores or hematoma volume alone. Taken together, our data are supportive of the hypothesis that serum Nrf2, as a potential prognostic biomarker, may be of clinical value in the treatment of ICH.

In the current study, it was confirmed that increased serum Nrf2 levels were independently associated with hemorrhagic severity and poor clinical outcome after acute ICH. However, the average turnaround time for laboratory results in the emergency departments is between 30 and 40 min currently. Nevertheless, it holds great potential, as it were, to become more time efficient and, more importantly, to have another way to predict outcome will not only help the clinicians but also the family to make decisions as well as necessary adjustments to care for the recovering patient.

There are several limitations in the current study. First, the sample size is small in this study, so this is a pilot study and makes a preliminary conclusion that serum Nrf2 levels

may be associated with severity and prognosis after acute ICH. A larger cohort study is warranted to validate the conclusions. Second, we do not do routine work to complete two times head computed tomography scans within 24 h after ICH. Subsequently, there is a paucity of data available regarding early hematoma growth. So, the results may be biased and the conclusions should be explained cautiously. Third, we performed a clinical epidemiological investigation regarding the relationship between serum Nrf2 levels and severity plus poor prognosis after acute ICH. Nevertheless, a further study using some bioinformatics analyses, computational biological analyses, PCR, and western blotting assay may provide some information to identify which oxidative stress-related signaling pathways Nrf2 may regulate in the pathogenesis of acute ICH. Last, our study did not use the ROS detection assay for determining ROS, so there is not enough evidence supportive of the notion that Nrf2 may regulate ROS in ICH. Hence, the role of Nrf2 in pathophysiological processes of ICH remains to be confirmed.

Conclusion

To the best of our knowledge, our study, for the first time, measured circulating Nrf2 levels of humans with acute brain injury and further investigated the relation of serum Nrf2 levels to illness severity and prognosis after ICH. Independent correlation is ascertained between serum Nrf2 levels and NIHSS scores in addition to hematoma volume, and also, independent association is discerned between serum Nrf2 levels and END plus 90-day poor prognosis in this cohort of ICH patients. Hypothetically, Nrf2 may participate in pathophysiological processes of acute brain injury after ICH, and serum Nrf2 may be a promising biomarker, which could be of clinical significance in severity assessment and prognosis prediction of ICH.

Data availability statement

The raw data supporting the conclusions of this article will be made available by the authors, without undue reservation.

Ethics statement

The studies involving human participants were reviewed and approved by The Quzhou Affiliated Hospital of Wenzhou Medical University. The patients/participants provided their written informed consent to participate in this study.

Author contributions

All authors listed have made a substantial, direct, and intellectual contribution to the work, and approved it for publication.

Acknowledgments

We gratefully thank all study participants, their relatives, and the staffs at the recruitment centers for their invaluable contributions.

Conflict of interest

The authors declare that the research was conducted in the absence of any commercial or financial relationships that could be construed as a potential conflict of interest.

Publisher's note

All claims expressed in this article are solely those of the authors and do not necessarily represent those of their affiliated organizations, or those of the publisher, the editors and the reviewers. Any product that may be evaluated in this article, or claim that may be made by its manufacturer, is not guaranteed or endorsed by the publisher.

References

Alexandrova, M. L., and Danovska, M. P. (2011). Serum C-reactive protein and lipid hydroperoxides in predicting short-term clinical outcome after spontaneous intracerebral hemorrhage. *J. Clin. Neurosci.* 18, 247–252. doi: 10.1016/j.jocn.2010.07.125

Ayaydin, H., Akaltun, I., Koyuncu, I., ÇelÝk, H., KÝrmÝt, A., and Takatak, H. (2020). High KEAP1, NRF2 and low HO-1 serum levels in children with autism. *Noro Psikiyatr. Ars.* 57, 274–279. doi: 10.29399/npa.24862

Cai, Y., Zhuang, Y. K., Wu, X. Y., Dong, X. Q., Du, Q., Yu, W. H., et al. (2021). Serum hypoxia-inducible factor 1alpha levels correlate with outcomes after intracerebral hemorrhage. *Ther. Clin. Risk Manag.* 17, 717–726. doi: 10.2147/TCRM.S313433

Dong, X. Q., Yu, W. H., Zhu, Q., Cheng, Z. Y., Chen, Y. H., Lin, X. F., et al. (2015). Changes in plasma thrombospondin-1 concentrations following acute intracerebral hemorrhage. *Clin. Chim. Acta* 450, 349–355. doi: 10.1016/j.cca.2015.09.013

Du, Q., Yang, D. B., Shen, Y. F., Yu, W. H., Zhang, Z. Y., Zhu, Q., et al. (2013). Plasma leptin level predicts hematoma growth and early neurological deterioration after acute intracerebral hemorrhage. *Peptides* 45, 35–39. doi: 10.1016/j.peptides.2013.04.017

Du, Q., Yu, W. H., Dong, X. Q., Yang, D. B., Shen, Y. F., Wang, H., et al. (2014). Plasma 8-iso-prostaglandin F2α concentrations and outcomes after acute intracerebral hemorrhage. *Clin. Chim. Acta* 437, 141–146. doi: 10.1016/j.cca.2014.07.014

Graeb, D. A., Robertson, W. D., Lapointe, J. S., Nugent, R. A., and Harrison, P. B. (1982). Computed tomographic diagnosis of intraventricular hemorrhage. Etiology and prognosis. *Radiology* 143, 91–96.

Guo, X. S., Wen, S. H., Dong, W. W., Li, B. X., Chen, Z. Y., Wang, L. L., et al. (2019). Expression of Nrf2 in different cells after human cerebral cortex contusion. *Fa Yi Xue Za Zhi* 35, 273–279. doi: 10.12116/j.issn.1004-5619.2019.03.002

Hemphill, J. C. III, Greenberg, S. M., Anderson, C. S., Becker, K., Bendok, B. R., Cushman, M., et al. (2015). Guidelines for the management of spontaneous intracerebral hemorrhage: A guideline for healthcare professionals from the American Heart Association/American Stroke Association. *Stroke* 46, 2032–2060.

Kothari, R. U., Brott, T., Broderick, J. P., Barsan, W. G., Sauerbeck, L. R., Zuccarello, M., et al. (1996). The ABCs of measuring intracerebral hemorrhage volumes. *Stroke* 27, 1304–1305.

Kwah, L. K., and Diong, J. (2014). National Institutes of Health Stroke Scale (NIHSS). *J. Physiother.* 60:61.

Leira, R., Dávalos, A., Silva, Y., Gil-Peralta, A., Tejada, J., Garcia, M., et al. (2004). Early neurologic deterioration in intracerebral hemorrhage: Predictors and associated factors. *Neurology* 63, 461–467.

LoPresti, M. A., Bruce, S. S., Camacho, E., Kunchala, S., Dubois, B. G., Bruce, E., et al. (2014). Hematoma volume as the major determinant of outcomes after intracerebral hemorrhage. *J. Neurol. Sci.* 345, 3–7.

Lorente, L., Martín, M. M., Abreu-González, P., Sabatel, R., Ramos, L., Argueso, M., et al. (2018). Serum malondialdehyde levels and mortality in patients with spontaneous intracerebral hemorrhage. *World Neurosurg.* 113, e542–e547.

Masomi-Bornwasser, J., Kurz, E., Frenz, C., Schmitt, J., Wesp, D. M. A., König, J., et al. (2021). The influence of oxidative stress on neurological outcomes in spontaneous intracerebral hemorrhage. *Biomolecules* 11:1615.

Pi, J., Hayes, J. D., and Yamamoto, M. (2019). New insights into nuclear factor erythroid 2-related factors in toxicology and pharmacology. *Toxicol. Appl. Pharmacol.* 367, 33–35. doi: 10.1016/j.taap.2019.01.014

Qian, S. Q., Hu, X. C., He, S. R., Li, B. B., Zheng, X. D., and Pan, G. H. (2016). Prognostic value of serum thioredoxin concentrations after intracerebral hemorrhage. *Clin. Chim. Acta* 455, 15–19. doi: 10.1016/j.cca.2016.01.010

Sandberg, M., Patil, J., D'Angelo, B., Weber, S. G., and Mallard, C. (2014). NRF2-regulation in brain health and disease: Implication of cerebral inflammation. *Neuropharmacology* 79, 298–306. doi: 10.1016/j.neuropharm.2013.11.004

Shang, H., Yang, D., Zhang, W., Li, T., Ren, X., Wang, X., et al. (2013). Time course of Keap1-Nrf2 pathway expression after experimental intracerebral haemorrhage: Correlation with brain oedema and neurological deficit. *Free Radic. Res.* 47, 368–375. doi: 10.3109/10715762.2013.778403

Son, T. G., Camandola, S., Arumugam, T. V., Cutler, R. G., Telljohann, R. S., Mughal, M. R., et al. (2010). Plumbagin, a novel Nrf2/ARE activator, protects against cerebral ischemia. *J. Neurochem.* 112, 1316–1326. doi: 10.1111/j.1471-4159.2009.06552.x

Tanaka, N., Ikeda, Y., Ohta, Y., Deguchi, K., Tian, F., Shang, J., et al. (2011). Expression of Keap1-Nrf2 system and antioxidative proteins in mouse brain after transient middle cerebral artery occlusion. *Brain Res.* 1370, 246–253. doi: 10.1016/j.brainres.2010.11.010

Tonelli, C., Chio, I. I. C., and Tuveson, D. A. (2018). Transcriptional regulation by Nrf2. *Antioxid. Redox Signal.* 29, 1727–1745.

Wang, J., Fields, J., Zhao, C., Langer, J., Thimmulappa, R. K., Kensler, T. W., et al. (2007). Role of Nrf2 in protection against intracerebral hemorrhage injury in mice. *Free Radic. Biol. Med.* 43, 408–414.

Wilkinson, D. A., Pandey, A. S., Thompson, B. G., Keep, R. F., Hua, Y., and Xi, G. (2018). Injury mechanisms in acute intracerebral hemorrhage. *Neuropharmacology* 134(Pt B), 240–248.

Wu, X. Y., Zhuang, Y. K., Cai, Y., Dong, X. Q., Wang, K. Y., Du, Q., et al. (2021). Serum glucose and potassium ratio as a predictive factor for prognosis of acute intracerebral hemorrhage. *J. Int. Med. Res.* 49:3000605211009689. doi: 10.1177/03000605211009689

Zhao, X., Sun, G., Ting, S. M., Song, S., Zhang, J., Edwards, N. J., et al. (2015a). Cleaning up after ICH: The role of Nrf2 in modulating microglia function and hematoma clearance. *J. Neurochem.* 133, 144–152. doi: 10.1111/jnc.12974

Zhao, X., Sun, G., Zhang, J., Ting, S. M., Gonzales, N., and Aronowski, J. (2015b). Dimethyl fumarate protects brain from damage produced by intracerebral hemorrhage by mechanism involving Nrf2. *Stroke* 46, 1923–1928. doi: 10.1161/STROKEAHA.115.009398

Zhao, X., Sun, G., Zhang, J., Strong, R., Dash, P. K., Kan, Y. W., et al. (2007). Transcription factor Nrf2 protects the brain from damage produced by intracerebral hemorrhage. *Stroke* 38, 3280–3286.

Zheng, G. R., Chen, B., Shen, J., Qiu, S. Z., Yin, H. M., Mao, W., et al. (2018). Serum myeloperoxidase concentrations for outcome prediction in acute intracerebral hemorrhage. *Clin. Chim. Acta* 487, 330–336. doi: 10.1016/j.cca.2018.10.026

frontiers | Frontiers in Aging Neuroscience

TYPE Original Research
PUBLISHED 24 October 2022
DOI 10.3389/fnagi.2022.1033434

Check for updates

OPEN ACCESS

EDITED BY
Yuzhen Xu,
Tongji University,
China

REVIEWED BY
Lanhai Lu,
Neucyte, United States
Kagaku Azuma,
University of Occupational and
Environmental Health Japan, Japan

*CORRESPONDENCE
Chunming Jiang
jiangsy1112@zju.edu.cn
Marong Fang
fangmaro@zju.edu.cn

SPECIALTY SECTION
This article was submitted to
Cellular and Molecular Mechanisms of
Brain-aging,
a section of the journal
Frontiers in Aging Neuroscience

RECEIVED 31 August 2022
ACCEPTED 03 October 2022
PUBLISHED 24 October 2022

CITATION
Luo Y, Chen S, Wu F, Jiang C and
Fang M (2022) The identification of the key
residues E829 and R845 involved in
transient receptor potential melastatin 2
channel gating.
Front. Aging Neurosci. 14:1033434.
doi: 10.3389/fnagi.2022.1033434

COPYRIGHT
© 2022 Luo, Chen, Wu, Jiang and Fang.
This is an open-access article distributed
under the terms of the Creative Commons
Attribution License (CC BY). The use,
distribution or reproduction in other
forums is permitted, provided the original
author(s) and the copyright owner(s) are
credited and that the original publication in
this journal is cited, in accordance with
accepted academic practice. No use,
distribution or reproduction is permitted
which does not comply with these terms.

The identification of the key residues E829 and R845 involved in transient receptor potential melastatin 2 channel gating

Yuhuan Luo[1], Shijia Chen[2], Fei Wu[3], Chunming Jiang[1]* and Marong Fang[4]*

[1]Department of Pediatrics, Affiliated Hangzhou First People's Hospital, Zhejiang University School of Medicine, Hangzhou, China, [2]National Clinical Research Center for Child Health, Children's Hospital of Zhejiang University School of Medicine, Hangzhou, China, [3]Institute of Systemic Medicine, Zhejiang University School of Medicine, Hangzhou, China, [4]Institute of Neuroscience, Zhejiang University School of Medicine, Hangzhou, China

Transient receptor potential melastatin 2 (TRPM2), a non-selective cation channel, is involved in many physiological and pathological processes, including temperature sensing, synaptic plasticity regulation, and neurodegenerative diseases. However, the gating mechanism of TRPM2 channel is complex, which hinders its functional research. With the discovery of the Ca^{2+} binding site in the S2–S3 domain of TRPM2 channel, more and more attention has been drawn to the role of the transmembrane segments in channel gating. In this study, we focused on the D820-F867 segment around the S2 domain, and identified the key residues on it. Functional assays of the deletion mutants displayed that the deletions of D820-W835 and L836-P851 destroyed channel function totally, indicating the importance of these two segments. Sequence alignments on them found three polar and charged residues with high conservation (D820, E829, and R845). D820A, E829A, and R845A which removed the charge and the side chain of the residues were tested by 500μM adenosine diphosphate-ribose (ADPR) or 50mM Ca^{2+}. E829A and R845A affected the characteristic of channel currents, while D820A behaved similarly to WT, indicating the participations of E829 and R845 in channel gating. The charge reversing mutants, E829K and R845D were then constructed and the electrophysiological tests showed that E829A and E829K made the channel lose function. Interestingly, R845A and R845D exhibited an inactivation process when using 500μM ADPR, but activated normally by 50mM Ca^{2+}. Our data suggested that the negative charge at E829 took a vital part in channel activation, and R845 increased the stability of the Ca^{2+} combination in S2-S3 domain, thus guaranteeing the opening of TRPM2 channel. In summary, our identification of the key residues E829 and R845 in the transmembrane segments of TRPM2. By exploring the gating process of TRPM2 channel, our work helps us better understand the mechanism of TRPM2 as a potential biomarker in neurodegenerative diseases, and provides a new approach for the prediction, diagnosis, and prognosis of neurodegenerative diseases.

KEYWORDS

TRPM2, key residues, gating mechanism, activation, inactivation, transmembrane segments

Introduction

As an important non-selective cation channel, transient receptor potential melastatin 2 (TRPM2), has an endogenous expression in many organs, such as brain (Li and Jiao, 2020; Zong et al., 2022), heart (Ji et al., 2021), liver (Feng et al., 2019), kidney (Wang et al., 2019), and lung (Wang et al., 2020), and participates in various physiological and pathological processes. For example, TRPM2 channel is involved in temperature sensing (Song et al., 2016; Kamm et al., 2021), synaptic plasticity regulation (Wang et al., 2016), and insulin secretion (Ito et al., 2017). Based on its response to oxidative stress, the activation of TRPM2 channel mediates several neurodegenerative diseases, including Alzheimer's disease (Aminzadeh et al., 2018), Parkinson's disease (Ferreira et al., 2022), multiple sclerosis (Shao et al., 2021), and stroke (Zong et al., 2022). It is also regarded as a therapeutic target for the treatments of neurological diseases (Belrose and Jackson, 2018). However, the mechanism of TRPM2 gating is still unclear, which hinders the researches about its pathological role. Recent years have seen lots of work about TRPM2 channel structural resolution, key residues identification and gating mechanism exploration, especially its opening and closing processes (Luo et al., 2018; Wang et al., 2018; Yu et al., 2021).

Transient receptor potential melastatin 2 channel can be opened mainly by adenosine diphosphate-ribose (ADPR), Ca^{2+}, and reactive oxygen species (Hu et al., 2021; Yu et al., 2021). As an efficient agonist, ADPR activates the channel through its binding in the TRPM homology region 1/2 (MHR1/2) at N-terminal of the channel, and the NUDT9 homology (NUDT9-H) domain at C-terminal (Huang et al., 2019). Although there are two binding sites for ADPR, ADPR only opens the channel in the existence of Ca^{2+} (Starkus et al., 2007), indicating a vital role of Ca^{2+} in TRPM2 activation. By the using of cryo-electron microscopy, a Ca^{2+} binding site was identified in the domain of the second and third transmembrane segment (S2-S3) of human TRPM2, composed by E843, Q846, N869, D872, and E1073 (Wang et al., 2018). What is more, this highly conserved Ca^{2+} binding site exists in various species, including human, Nematostella vectensis and zebrafish (Huang et al., 2018; Wang et al., 2018; Zhang et al., 2018), and the five residues involved also exhibit a high conservation among the TRPM family (Zhang et al., 2018). During the channel gating, Ca^{2+} can open the channel by itself (Du et al., 2009), or display a synergistic effect with ADPR, which promotes channel activation (Lange et al., 2008).

Inhibition and inactivation are the two methods for closing the channel. Former studies have discovered several compounds that can inhibit TRPM2 channel, such as N-(p-amycinnamoyl) anthranilic acid (ACA), and 2-aminoethoxydiphenyl borate (2-APB; Jiang et al., 2010; Malko and Jiang, 2020). On the other hand, some metal ions (Zn^{2+} and Cu^{2+}) inactivate the channel in a concentration-dependent way. Zn^{2+} inactivates TRPM2 channel through residues K952 and D1002 (Yang et al., 2011), and Cu^{2+} inactivates TRPM2 channel through its interaction with H995 (Yu et al., 2014). Apart from all these exogenous substances, the mutations at the key residue of TRPM2 channel, also lead to inactivation. For example, the alanine and glutamate mutations at Q846, and aspartate mutation at N869 inactivated TRPM2 channel significantly (Luo et al., 2019).

Although the gating mechanism for TRPM2 channel is complex, the key amino acid residues and regions take an important part during the opening and closing of the channel. The discovery of the Ca^{2+} binding site in S2-S3 domain of TRPM2 channel drew attention to exploring the role of transmembrane segments in the channel gating process (Wang et al., 2018). Here, we focused on the S2 domain, and chose the D820-F867 segment that contains residues from the end of S1 domain to the start of S3 domain as the target segment. Apart from its close location to the Ca^{2+} binding site, D820-F867 segment is also located in the voltage-sensing-like domain (Wang et al., 2018), which increases the probability of its participation in channel gating.

In this study, we aimed to identify the key residues that involved in TRPM2 channel gating within the D820-F867 segment. Electrophysiological examination of three deletion mutants displayed the importance of D820-W835 and L836-P851 for TRPM2 gating. Sequence alignment were used to find the polar and charged residues with high conservation in these two segments. Alanine mutations and mutations reversing the charge of the residue were constructed, and their channel currents were recorded by the activation of intracellular solution containing 500 μM ADPR or 50 mM Ca^{2+}. Our work identified E829 and R845 as the key residues closely related with channel gating, and expanded the understandings of the gating mechanism of the transmembrane region in TRPM2 channel.

Materials and methods

Cell culture and molecular biology

Human Embryonic Kidney 293 T (HEK293T) cells are widely used in the function tests of the target ion channels and its mutants because of the high transfection ability and rare expression of endogenous receptors (Wang and Wang, 2017; Glazer et al., 2020; El Ghaleb et al., 2021). In this study, HEK293T cells (purchased from ATCC) were cultured using Dulbecco's modified Eagle medium (DMEM, Thermo Fisher Scientific, United States) with 10% fetal bovine serum (FBS; Thermo Fisher Scientific, United States) in a humidity-controlled incubator (5% CO_2, 37°C). The cDNA encoding full-length human TRPM2 (protein accession number: NP_003298.2) was kindly provided by Dr. A. M. Scharenberg (University of Washington, Seattle, WA, United States), and was subcloned into pcDNA3.1 vector as it was reported previously (Yu et al., 2017, 2019, 2021). Mutant constructions were done through site-directed or deletional mutagenesis followed by full coding sequence sequencing (Yang and Jiang, 2013). Briefly, for each mutation: 5 μl of 10× reaction buffer, 2 μl (50–100 ng) of cDNA template, 2 μl of 10 μM sense mutagenic primer, 2 μl of

10 μM antisense mutagenic primer, and 4 μl of 2.5 mM dNTP mix were added into the PCR reaction system. The sterile DNAase-free H_2O was then added to a final volume of 49 μl, and 1 μl of 2.5 U/μl Pfu DNA polymerase was added finally. The reaction program for the PCR: 95°C for 5 min; 20 cycles of 95°C for 30s, 58°C for 60s, and 68°C for 12 min; 68°C for 10 min. After the PCR process, 1 μl of DpnI enzyme (10 U/μl) was added to each PCR sample, and was mixed gently and thoroughly before incubated at 37°C for 1 h to remove the cDNA templates. The mutations verified by full coding sequence sequencing were used in the experiments.

Transfection

The transfections were done following the instruction of the Lipofectamine 2000 reagent (Thermo Fisher Scientific, United States). HEK293T cells were grown in 35-mm petri dishes and transfected with 1 μg TRPM2 plasmid and 0.1 μg green fluorescent protein (GFP) plasmid (Mei et al., 2006). Briefly, 2 μl lipo2000 was added into 100 μl Opti-MEM™ I (OPTI, Thermo Fisher Scientific, United States). The solution was then mixed and stood for about 5 min. Meanwhile, 1 μg WT TRPM2 or its mutants, together with 0.1 μg GFP, were added into 100 μl OPTI, and these two solutions were mixed well and stood for 20 min. After that, the DMEM in the dishes was replaced with 800 μl fresh DMEM and the mixed solution was added into the dishes for cell culture. 24 h after the transfection, the transfected cells were seeded on glass coverslips and the electrophysiological recording were carried out 12 h later.

Electrophysiology

Whole-cell recordings were carried out at room temperature using an Axopatch 200B amplifier. Patch electrodes with a resistance of 3–5 MΩ were fabricated from borosilicate glass (Sutter Instrument). The protocols for electrophysiological recordings were described in our previous studies (Luo et al., 2018, 2019). Briefly, voltage ramps with 500 ms duration from-100 mV to +100 mV were applied every 5 s. The currents at-80 mV were denoted by circles in figures. The intracellular solution (ICS) of 500 μM ADPR contained: 147 mM NaCl, 1 mM $MgCl_2$, 0.05 mM EGTA, 10 mM Hepes, and 500 μM ADPR (pH 7.4, adjusted with NaOH). The ICS of 50 mM Ca^{2+} contained: 50 mM $CaCl_2$, 75 mM NaCl, 1 mM $MgCl_2$, and 10 mM Hepes (pH 7.4, adjusted with NaOH). For all experiments, the standard extracellular solution (ECS) contained: 147 mM NaCl, 2 mM KCl, 1 mM $MgCl_2$, 2 mM $CaCl_2$, 10 mM Hepes, and 13 mM glucose (pH 7.4, adjusted with NaOH). To confirm the TRPM2 channel currents, 20 mM N-(pamylcinnamoyl) anthranilic acid (ACA; Sigma) was applied at the end of each recording, and only the cells whose currents were completely inhibited by ACA were used for analysis.

Statistical analysis

The electrophysiological data were analyzed using pCLAMP9 software (Axon Instruments), and presented as Mean ± SEM. Origin software was used for curve fitting. Statistical analysis was performed using Student's *t*-test ($p < 0.05$ designated as significant).

Results

The deletion of D820-W835 and L836-P851 segments resulted in the loss of function of TRPM2 channel

In order to check whether D820-F867 segment participates in TRPM2 channel gating, and also to detect the possible regions where the key residues are located, we constructed three deletion mutants, that is △D820-W835 (deletion of D820-W835 residues), △L836-P851 (deletion of L836-P851 residues), △D852-F867(deletion of D852-F867 residues), and activated these three mutants by ICS of 500 μM ADPR. The inhibitor of TRPM2 channel, 20 μM ACA, was applied at the end of the experiments, to confirm the currents of TRPM2 channel.

Our data showed that, △D820-W835, △L836-P851 mutants made the channel currents disappeared totally (Figures 1B,C), suggesting the existence of the key residues within them. In contrast, despite the loss of 16 residues, △D852-F867 mutant still retained part of currents of TRPM2 channel (Figure 1D), suggesting its minor role in channel gating. Based on this result, sequence alignment and electrophysiological examination were carried out for D820-W835 and L836-P851 segments in the following research.

Sequence alignment

The high conservation is one of the characteristics of the key residues in the course of the evolution, so the sequence alignment was done to find the residues highly conserved. The D820-F867 segment of hTRPM2 (NP_003298.2) was compared with its corresponding segment in mouse TRPM2 (mTRPM2, NP_001398829.1) and mouse TRPM8 (mTRPM8, NP_599013.1), and the analysis of conservation was carried out for D820-W835 and L836-P851.

As Figure 2 shows, there are 11 residues of high conservation, that is: D820, F821, P825, E829, Y833, F837, L839, C841, E843, R845, and Q846. Among them, E843 and Q846 have been reported to constitute the Ca^{2+} binding site in S2-S3 domain. According to the polarity and charge, the other nine residues were divided into three types: polar and charged residues (D820, E829, and R845; Qiao et al., 2021), polar and uncharged residues (Y833, C841), and non-polar residues (F821, F837, P825, and L839). During the channel gating, polarity and charge are two important ways for residues to interact with their surrounding residues or channel ligands. Therefore, the highly conserved residues: D820,

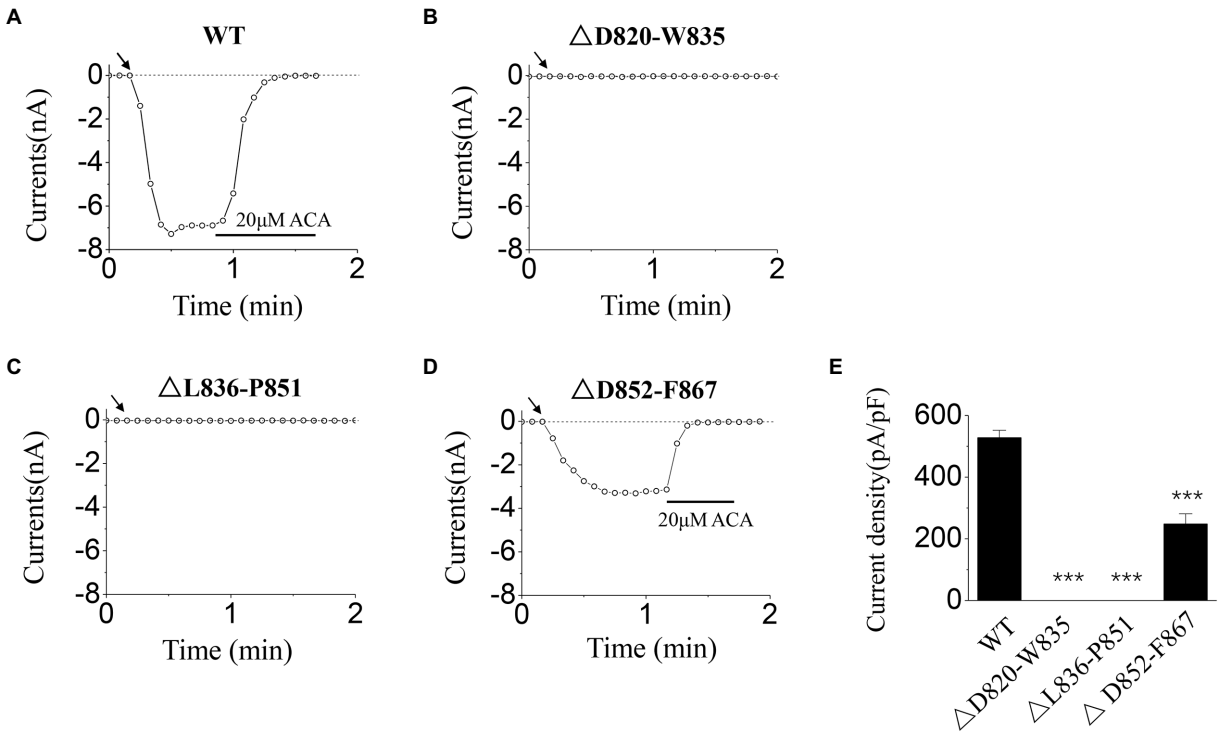

FIGURE 1
Functional assay of WT transient receptor potential melastatin 2 (TRPM2) and three deletion mutants. **(A–D)** Representative whole-cell recordings of TRPM2 channel currents induced by intracellular solution (ICS) of 500μM adenosine diphosphate-ribose (ADPR) from Human Embryonic Kidney 293 T (HEK293T) cells expressing **(A)** WT, **(B)** △D820-W835, **(C)** △L836-P851, and **(D)** △D852-F867. The arrow in each panel indicates the time point at which whole cell configuration was established. **(E)** Summary of the current density induced in cells expressing WT and deletion mutants. In each case, six cells were tested. ***p<0.001 compared with WT.

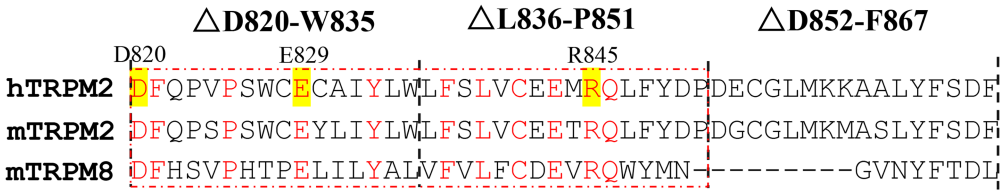

FIGURE 2
Sequence alignments between hTRPM2, mTRPM2, and mTRPM8. The sequence alignments were done for the residues in the red dashed box. Apart from the residues constitute the Ca^{2+} binding site (E843 and Q846), residues with high conservation were marked in red, and the polar and charged ones among them were highlighted in yellow (D820, E829, and R845).

E829, and R845, which also possess both of the polarity and charge, were most likely to participate in TRPM2 gating. In order to confirm their effects and explore the mechanism, electrophysiology of the site-directed mutants at these three residues was carried out in this study.

Alanine mutations at E829, R845 altered TRPM2 channel currents

Here, we substituted the D820, E829, and R845 residues with alanine, which has no charge or side chain. According to our former studies (Luo et al., 2018, 2019), ICS of 500 μM ADPR and 50 mM Ca^{2+} were used in the activation tests for these mutants.

When using ICS of 500 μM ADPR, D820A behaved similarly with WT (Figures 3A,B,E): the currents of D820A were induced rapidly after the whole-cell configuration was established, and were inhibited completely by the channel inhibitor (20 μM ACA). However, E829A could not be activated by 500 μM ADPR (Figure 3C,E), and R845A exhibited inactivation which did not exist in WT TRPM2 (Figure 3D): After the peak value, the currents of R845A dropped rapidly until it entirely disappeared.

In the activation tests by ICS of 50 mM Ca^{2+}, our results showed there was no significant difference between D820A,

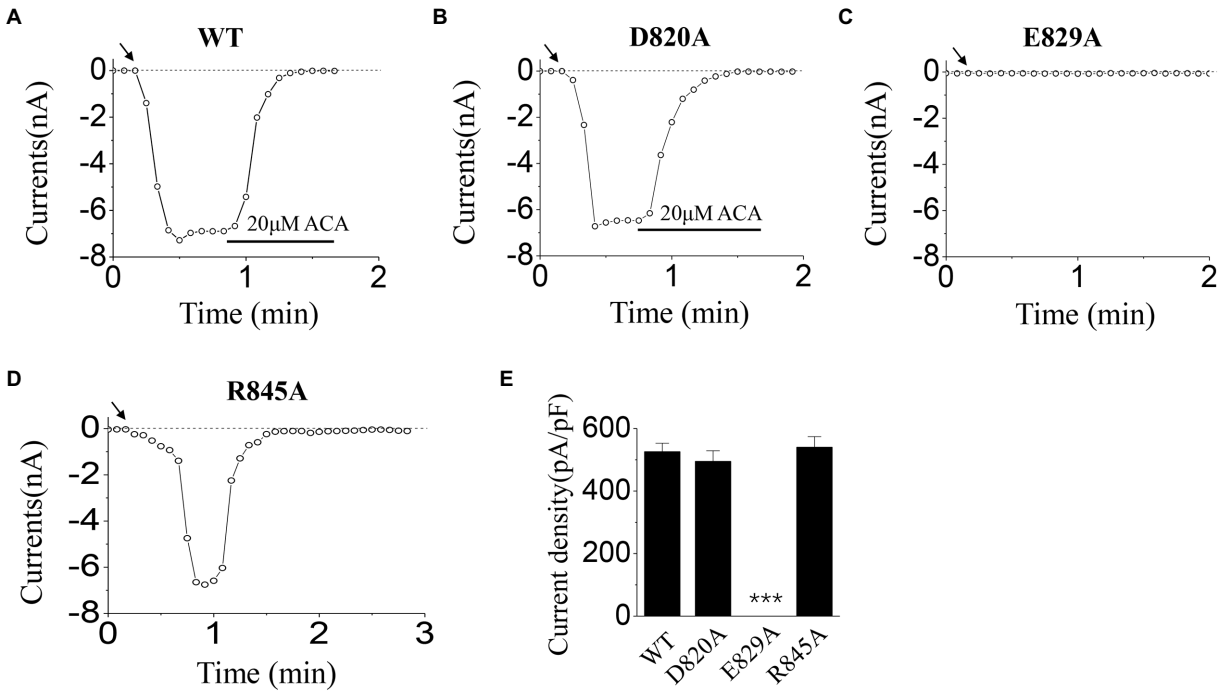

FIGURE 3
Functional assay of WT TRPM2 and its alanine mutants. **(A–D)** Representative whole-cell recordings of TRPM2 channel currents induced by ICS of 500μM ADPR from HEK293T cells expressing **(A)** WT, **(B)** D820A, **(C)** E829A, and **(D)** R845A. The arrow in each panel indicates the time point at which whole cell configuration was established. **(E)** Summary of the current density induced in cells expressing WT and the mutants. In each case, six cells were tested. ***p<0.001 compared with WT.

R845A, and WT (Figures 4A,B,D,E). However, no current was evoked for E829A by 50 mM Ca^{2+} (Figure 4C,E). All these data displayed the interesting phenomenon in the gating processes of mutants at E829 and R845, which needed our further exploration.

The alternations of channel gating by mutations of E829K and R845D

To explore the gating mechanism of E829, the positively charged mutant, E829K, which reserved the charge was designed, and the activation tests were done using ICS of 500 μM ADPR (Figures 5A–D) and 50 mM Ca^{2+} (Figures 5E–H). Together with the data of E829A, our whole-cell recordings presented the loss of function resulted from the mutations at E829: any alternation in charge at this residue (charge deletion mutant: E829A, or charge reversion mutant: E829K) led the channel failed to open.

As for R845, we constructed the negatively charged mutant, R845D, which also reversed the charge at this residue. During the activation tests by ICS of 500 μM ADPR, R845D behaved the characteristic of rapid inactivation as well as R845A (Figures 6A–D). On the contrary, no difference was seen between these two mutants and WT when activated by ICS of 50 mM Ca^{2+} (Figures 6E–H).

Discussion

As a Ca^{2+}-permeable channel that can be activated by Ca^{2+}, Ca^{2+} binding at the S2-S3 domain of TRPM2 channel is a vital step for channel activation. After the channel opens, the Ca^{2+} influx facilitates the channel opening with positive feedback, and causes intracellular Ca^{2+} overload, which leads to cell death and neuronal loss (Jiang et al., 2010; Malko and Jiang, 2020). In this way, TRPM2 channel plays an important part in neurodegenerative diseases. Moreover, the upregulation of the TRPM2 channel was reported in human or animal with neurodegenerative diseases (For example, patients or mouse with Parkinson's disease; Sun et al., 2018; Ferreira et al., 2022). All of these provide the foundations for TRPM2 channel as a potential biomarker in neurodegenerative diseases. Through the identification of the key residues in the D820-F867 segment around the S2 domain, our work promoted the understanding and development of TRPM2 channel. The results of electrophysiology showed that the residues E829 and R845 played an important part in channel gating. Mutations of E829A and E829K prevented the channel from being activated by 500 μM ADPR or 50 mM Ca^{2+}, while R845A and R845D showed rapid inactivation when using ICS of 500 μM ADPR, but could be opened by 50 mM Ca^{2+}.

Firstly, the activation tests were carried out for the three deletion mutants (△D820-W835, △L836-P851, and △D852-F867), using ICS of 500 μM ADPR. After the stability of the channel currents, 20 μM ACA was applied in the extracellular

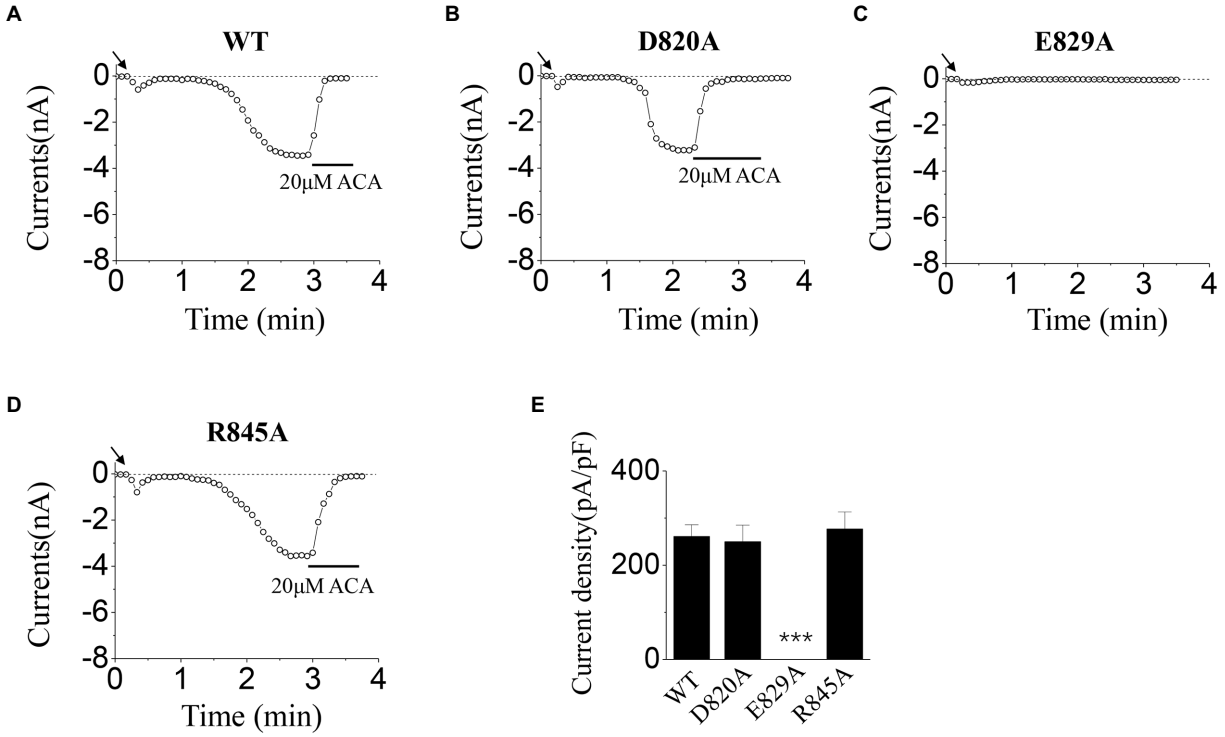

FIGURE 4
Functional assay of WT TRPM2 and its alanine mutants. **(A–D)** Representative whole-cell recordings of TRPM2 channel currents induced by ICS of 50mM Ca^{2+} from HEK293T cells expressing **(A)** WT, **(B)** D820A, **(C)** E829A, and **(D)** R845A. The arrow in each panel indicates the time point at which whole cell configuration was established. **(E)** Summary of the current density induced in cells expressing WT and the mutants. In each case, six cells were tested. ***p<0.001 compared with WT.

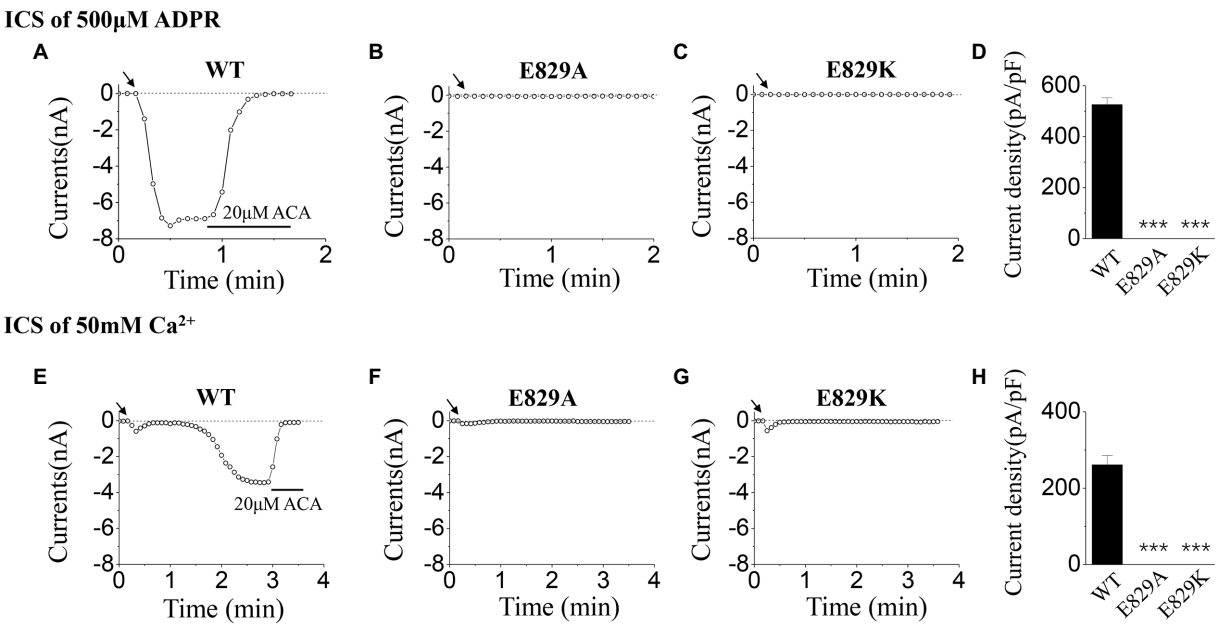

FIGURE 5
Functional assay of WT TRPM2 and mutants at E829. **(A–C)** Representative whole-cell recordings of TRPM2 channel currents induced by ICS of 500μM ADPR from HEK293T cells expressing **(A)** WT, **(B)** E829A, **(C)** E829K, and **(D)** Summary of the current density induced in cells expressing WT and mutants. In each case, six cells were tested. **(E–H)** Representative whole-cell recordings of TRPM2 channel currents induced by ICS of 50mM Ca^{2+} from HEK293T cells expressing **(E)** WT, **(F)** E829A, **(G)** E829K, and **(H)** Summary of the current density induced in cells expressing WT and mutants. The arrow in each panel indicates the time point at which whole cell configuration was established. In each case, six cells were tested. ***p<0.001 compared with WT.

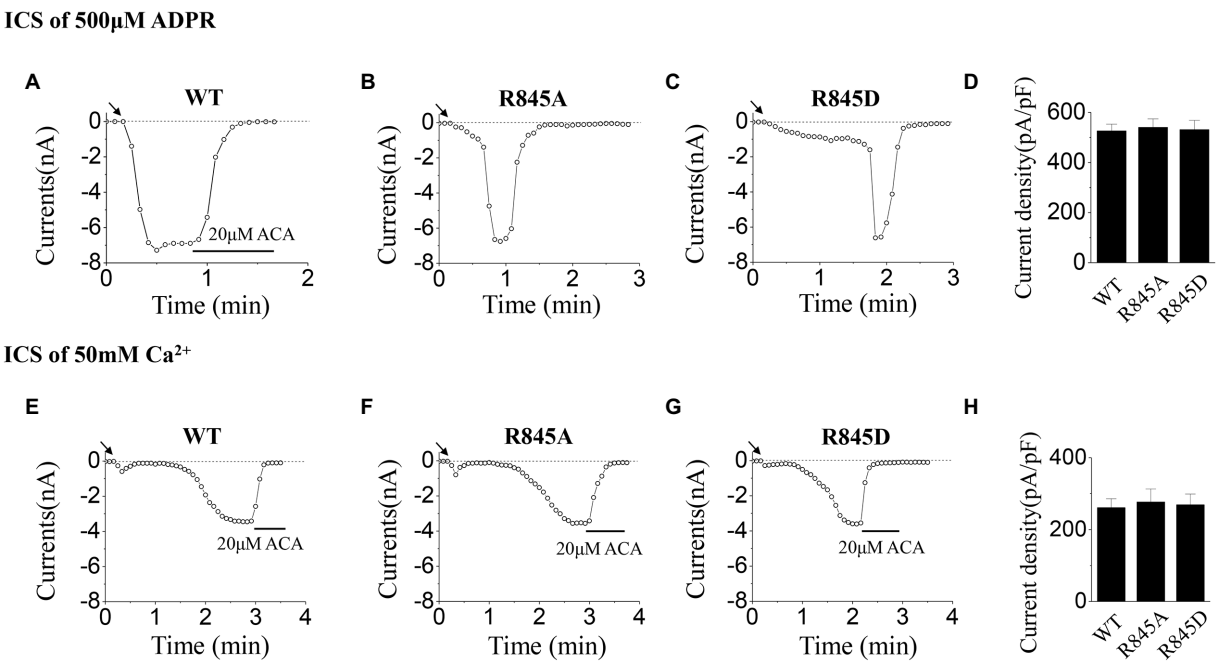

FIGURE 6
Functional assay of WT TRPM2 and mutants at R845. **(A–C)** Representative whole-cell recordings of TRPM2 channel currents induced by ICS of 500μM ADPR from HEK293T cells expressing **(A)** WT, **(B)** R845A, **(C)** R845D, and **(D)** Summary of the current density induced in cells expressing WT and mutants. In each case, six cells were tested. **(E–H)** Representative whole-cell recordings of TRPM2 channel currents induced by ICS of 50mM Ca^{2+} from HEK293T cells expressing **(E)** WT, **(F)** R845A, **(G)** R845D, and **(H)** Summary of the current density induced in cells expressing WT and mutants. The arrow in each panel indicates the time point at which whole cell configuration was established. In each case, six cells were tested.

solution to exclude the data deviation caused by leakage currents. As our data showed, all of the currents induced could be inhibited totally (Figures 1A,D), suggesting that the currents we recorded resulted from the opening of TRPM2 channel. Considering the influence of cell size on the amplitude of the whole-cell currents, current density was used in statistical analysis. Among the three deletion mutants, △D852-F867 was the only one that reserved part of the currents with the deletion of 16 residues, indicating that the residues within D852-F867 segment have a relatively milder influence on channel gating (Figures 1D,E). On the contrary, deletion mutants of △D820-W835 and △L836-P851 resulted in a complete loss of channel function, indicating the existence of key residues in these two sequences (Figures 1B,C,E).

Based on the residue conservation and its polarity and charge, we focused on D820, E829, and R845 residues in △D820-W835 and △L836-P851 segments (Figure 2). The alanine mutants were constructed at these three residues with the eliminations of charge and side chain, and the activation tests by ICS of 500 μM ADPR or 50 mM Ca^{2+} were done to analyze the function of the mutants.

Our data displayed that the D820A mutant could be activated normally, and the characteristic of its currents was similar to WT TRPM2 (for example, the magnitude and stability), demonstrating the relatively small contribution of D820 during TRPM2 gating (Figures 3B, 4B). However, E829A made the channel lose function (Figures 3C, 4C), and R845A exhibited rapid inactivation in the activation test by ICS of 500 μM ADPR (Figure 3D), suggesting the involvement of these two residues in channel gating. To further explore the mechanism, we designed the charge-reversing mutants E829K and R845D, and detected their currents by electrophysiology.

As for mutants at E829, no current was induced by 500 μM ADPR or 50 mM Ca^{2+}, neither E829A nor E829K (Figure 5). Former studies have illustrated that single site mutation did not affect TRPM2 channel expression, so the influences of channel gating by the mutations were focused (Luo et al., 2018, 2019). As a residue within the voltage-sensing-like domain of TRPM2 (Wang et al., 2018), the negative charge at E829 was involved in the series of conformational changes during channel opening. In this case, the alanine or lysine substitution which deleted or reversed its negative charge destroyed the linkage effect at this residue, thus resulting in the loss of function of the channel. Apart from mutation, the molecule combination at the channel voltage-sensing-like domain can also alter channel gating. For example, the structural changes caused by the inhibitor binding at the voltage-sensing-like domain of TRPC4 channel is the primary cause for channel closing (Vinayagam et al., 2020).

As for mutants at R845, the currents activated by ICS of 500 μM ADPR, exhibited fast inactivation after the peak currents, while the currents activated by ICS of 50 mM Ca^{2+} behaved similarly to WT (Figure 6). However, according to the structure of the TRPM2 channel, R845 is not within the ADPR binding site: MHR1/2 nor NUDT9-H domain, so the mutations here had little effect on the activation process by ADPR (Wang et al., 2018; Huang et al., 2019).

Interestingly, R845 is located in the Ca^{2+} binding site of S2-S3 domain, just between E843 and Q846 (Wang et al., 2018). Considering the fact that Ca^{2+} binding in S2-S3 domain is the basis for the activation effect of ADPR, we proposed that R845 plays an important role in keeping the right construction of E843 and Q846 for Ca^{2+} binding, which guarantees the stability of Ca^{2+} binding here and also the opening of the channel. Any alternation of the charge at R845 will reduce the stability of Ca^{2+} binding, thus leading to inactivation. In the experiments using ICS of 500 μM ADPR, the concentration of Ca^{2+} is limited, during the opening of R845A or R845D, the change of the channel structure resulted in the dropping of Ca^{2+} from S2-S3 domain. However, there was not enough Ca^{2+} to fill this site, so the channel inactivated (Figures 6B,C). Only the WT TRPM2 channel, which bound Ca^{2+} tightly, displayed stable currents without any inactivation (Figure 6A). A similar phenomenon was also occurred in our former research about the effects of mutations at Q846 and N869 in TRPM2 gating process (Luo et al., 2019). Compared with R845A, the mutation of R845D made more changes to the charge at this residue, so it took R845D a much longer time to open (Figures 6B,C). On the other hand, in the experiments using ICS of 50 mM Ca^{2+}, the high concentration of Ca^{2+} promised the binding of Ca^{2+} here, so R845A and R845D could be activated similarly to WT (Figures 6E–H).

In summary, our study identified two key residues: E829 and R845, in the D820-F867 segment around S2 domain of TRPM2. E829 participates in channel gating through its negative charge, and R845 affects channel gating through its influence on the stability of Ca^{2+} binding in the S2-S3 domain. Our work expanded the research about the mechanisms of the transmembrane region of TRPM2 in channel gating process, and provided a solid foundation for the study of the physiological and pathological functions of TRPM2 channel. The exploration of the mechanism of TRPM2 as a potential biomarker in neurodegenerative diseases also provides a new approach for the prediction, diagnosis, and prognosis of neurodegenerative diseases.

Data availability statement

The datasets presented in this study can be found in online repositories. The names of the repository/repositories and accession number(s) can be found in the article/supplementary material.

Author contributions

YL, CJ, and MF designed and performed the experiments and analyzed the data. YL conceived the study and wrote the manuscript. SC and FW revised the manuscript. All authors contributed to the article and approved the submitted version.

Funding

This work was supported by the National Natural Science Foundation of China (No. 82272163 to MF) and the Joint-research Fund for Clinical Research of Affiliated Hangzhou First People's Hospital (YYJJ2019Q08 to YL).

Acknowledgments

We thank Wei Yang for great support and helpful discussions for improving this manuscript.

Conflict of interest

The authors declare that the research was conducted in the absence of any commercial or financial relationships that could be construed as a potential conflict of interest.

Publisher's note

All claims expressed in this article are solely those of the authors and do not necessarily represent those of their affiliated organizations, or those of the publisher, the editors and the reviewers. Any product that may be evaluated in this article, or claim that may be made by its manufacturer, is not guaranteed or endorsed by the publisher.

References

Aminzadeh, M., Roghani, M., Sarfallah, A., and Riazi, G. H. (2018). TRPM2 dependence of ROS-induced NLRP3 activation in Alzheimer's disease. *Int. Immunopharmacol.* 54, 78–85. doi: 10.1016/j.intimp.2017.10.024

Belrose, J. C., and Jackson, M. F. (2018). TRPM2: a candidate therapeutic target for treating neurological diseases. *Acta Pharmacol. Sin.* 39, 722–732. doi: 10.1038/aps.2018.31

Du, J., Xie, J., and Yue, L. (2009). Intracellular calcium activates TRPM2 and its alternative spliced isoforms. *Proc. Natl. Acad. Sci. U. S. A.* 106, 7239–7244. doi: 10.1073/pnas.0811725106

El Ghaleb, Y., Schneeberger, P. E., Fernandez-Quintero, M. L., Geisler, S. M., Pelizzari, S., Polstra, A. M., et al. (2021). CACNA1I gain-of-function mutations differentially affect channel gating and cause neurodevelopmental disorders. *Brain* 144, 2092–2106. doi: 10.1093/brain/awab101

Feng, Q., Liu, C., Gao, W., Geng, X. L., and Dai, N. (2019). Salidroside-mitigated inflammatory injury of hepatocytes with non-alcoholic fatty liver disease via inhibition TRPM2 Ion Channel activation. *Diabetes Metab. Syndr. Obes.* 12, 2755–2763. doi: 10.2147/DMSO.S210764

Ferreira, A. F. F., Singulani, M. P., Ulrich, H., Feng, Z. P., Sun, H. S., and Britto, L. R. (2022). Inhibition of TRPM2 by AG490 is neuroprotective in a Parkinson's disease animal model. *Mol. Neurobiol.* 59, 1543–1559. doi: 10.1007/s12035-022-02723-8

Glazer, A. M., Kroncke, B. M., Matreyek, K. A., Yang, T., Wada, Y., Shields, T., et al. (2020). Deep mutational scan of an SCN5A voltage sensor. *Circ. Genom. Precis. Med.* 13:e002786. doi: 10.1161/CIRCGEN.119.002786

Hu, X., Wu, L., Liu, X., Zhang, Y., Xu, M., Fang, Q., et al. (2021). Deficiency of ROS-activated TRPM2 channel protects neurons from cerebral ischemia-

reperfusion injury through upregulating autophagy. *Oxidative Med. Cell. Longev.* 2021:7356266. doi: 10.1155/2021/7356266

Huang, Y., Roth, B., Lu, W., and Du, J. (2019). Ligand recognition and gating mechanism through three ligand-binding sites of human TRPM2 channel. *elife* 8:50175. doi: 10.7554/eLife.50175

Huang, Y., Winkler, P. A., Sun, W., Lu, W., and Du, J. (2018). Architecture of the TRPM2 channel and its activation mechanism by ADP-ribose and calcium. *Nature* 562, 145–149. doi: 10.1038/s41586-018-0558-4

Ito, K., Dezaki, K., Yoshida, M., Yamada, H., Miura, R., Rita, R. S., et al. (2017). Endogenous alpha2A-adrenoceptor-operated Sympathoadrenergic tones attenuate insulin secretion via cAMP/TRPM2 signaling. *Diabetes* 66, 699–709. doi: 10.2337/db16-1166

Ji, M., Kim, H. J., Ahn, C. B., Son, K. H., and Hong, J. H. (2021). Cellular channelopathy mediated by hypergravity: IL-6-mediated Nkcc1 activation and enhanced Trpm2 expression in rat atrium. *Cell Tissue Res.* 383, 1017–1024. doi: 10.1007/s00441-020-03299-2

Jiang, L. H., Yang, W., Zou, J., and Beech, D. J. (2010). TRPM2 channel properties, functions and therapeutic potentials. *Expert Opin. Ther. Targets* 14, 973–988. doi: 10.1517/14728222.2010.510135

Kamm, G. B., Boffi, J. C., Zuza, K., Nencini, S., Campos, J., Schrenk-Siemens, K., et al. (2021). A synaptic temperature sensor for body cooling. *Neuron* 109, 3283.e11–3297.e11. doi: 10.1016/j.neuron.2021.10.001

Lange, I., Penner, R., Fleig, A., and Beck, A. (2008). Synergistic regulation of endogenous TRPM2 channels by adenine dinucleotides in primary human neutrophils. *Cell Calcium* 44, 604–615. doi: 10.1016/j.ceca.2008.05.001

Li, Y., and Jiao, J. (2020). Deficiency of TRPM2 leads to embryonic neurogenesis defects in hyperthermia. *Sci. Adv.* 6:eaay6350. doi: 10.1126/sciadv.aay6350

Luo, Y., Yu, X., Ma, C., Luo, J., and Yang, W. (2018). Identification of a novel EF-loop in the N-terminus of TRPM2 channel involved in calcium sensitivity. *Front. Pharmacol.* 9:581. doi: 10.3389/fphar.2018.00581

Luo, Y. H., Yu, X. F., Ma, C., Yang, F., and Yang, W. (2019). Effects of calcium-binding sites in the S2-S3 loop on human and Nematostella vectensis TRPM2 channel gating processes. *J Zhejiang Univ Sci B* 20, 972–982. doi: 10.1631/jzus.B1900477

Malko, P., and Jiang, L. H. (2020). TRPM2 channel-mediated cell death: an important mechanism linking oxidative stress-inducing pathological factors to associated pathological conditions. *Redox Biol.* 37:101755. doi: 10.1016/j.redox.2020.101755

Mei, Z. Z., Mao, H. J., and Jiang, L. H. (2006). Conserved cysteine residues in the pore region are obligatory for human TRPM2 channel function. *Am. J. Phys. Cell Physiol.* 291, C1022–C1028. doi: 10.1152/ajpcell.00606.2005

Qiao, X., Qu, L., Guo, Y., and Hoshino, T. (2021). Secondary structure and conformational stability of the antigen residues making contact with antibodies. *J. Phys. Chem. B* 125, 11374–11385. doi: 10.1021/acs.jpcb.1c05997

Shao, Y., Chen, C., Zhu, T., Sun, Z., Li, S., Gong, L., et al. (2021). TRPM2 contributes to neuroinflammation and cognitive deficits in a cuprizone-induced multiple sclerosis model via NLRP3 inflammasome. *Neurobiol. Dis.* 160:105534. doi: 10.1016/j.nbd.2021.105534

Song, K., Wang, H., Kamm, G. B., Pohle, J., Reis, F. C., Heppenstall, P., et al. (2016). The TRPM2 channel is a hypothalamic heat sensor that limits fever and can drive hypothermia. *Science* 353, 1393–1398. doi: 10.1126/science.aaf7537

Starkus, J., Beck, A., Fleig, A., and Penner, R. (2007). Regulation of TRPM2 by extra-and intracellular calcium. *J. Gen. Physiol.* 130, 427–440. doi: 10.1085/jgp.200709836

Sun, Y. Y., Sukumaran, P., Selvaraj, S., Cilz, N. I., Schaar, A., Lei, S. B., et al. (2018). TRPM2 promotes neurotoxin MPP+/MPTP-induced cell death. *Mol. Neurobiol.* 55, 409–420. doi: 10.1007/s12035-016-0338-9

Vinayagam, D., Quentin, D., Yu-Strzelczyk, J., Sitsel, O., Merino, F., Stabrin, M., et al. (2020). Structural basis of TRPC4 regulation by calmodulin and pharmacological agents. *elife* 9:60603. doi: 10.7554/eLife.60603

Wang, Y., Chen, L., Wang, K., Da, Y., Zhou, M., Yan, H., et al. (2019). Suppression of TRPM2 reduces renal fibrosis and inflammation through blocking TGF-beta1-regulated JNK activation. *Biomed. Pharmacother.* 120:109556. doi: 10.1016/j.biopha.2019.109556

Wang, L., Fu, T. M., Zhou, Y., Xia, S., Greka, A., and Wu, H. (2018). Structures and gating mechanism of human TRPM2. *Science* 362:aav4809. doi: 10.1126/science.aav4809

Wang, J., Jackson, M. F., and Xie, Y. F. (2016). Glia and TRPM2 channels in plasticity of central nervous system and Alzheimer's diseases. *Neural Plast.* 2016:1680905. doi: 10.1155/2016/1680905

Wang, C., Meng, X., Meng, M., Shi, M., Sun, W., Li, X., et al. (2020). Oxidative stress activates the TRPM2-ca(2+)-NLRP3 axis to promote PM2.5-induced lung injury of mice. *Biomed. Pharmacother.* 130:110481. doi: 10.1016/j.biopha.2020.110481

Wang, S. Y., and Wang, G. K. (2017). Single rat muscle Na(+) channel mutation confers batrachotoxin autoresistance found in poison-dart frog Phyllobates terribilis. *Proc. Natl. Acad. Sci. U. S. A.* 114, 10491–10496. doi: 10.1073/pnas.1707873114

Yang, W., and Jiang, L. H. (2013). Site-directed mutagenesis to study the structure-function relationships of ion channels. *Methods Mol. Biol.* 998, 257–266. doi: 10.1007/978-1-62703-351-0_20

Yang, W., Manna, P. T., Zou, J., Luo, J., Beech, D. J., Sivaprasadarao, A., et al. (2011). Zinc inactivates melastatin transient receptor potential 2 channels via the outer pore. *J. Biol. Chem.* 286, 23789–23798. doi: 10.1074/jbc.M111.247478

Yu, W., Jiang, L. H., Zheng, Y., Hu, X., Luo, J., and Yang, W. (2014). Inactivation of TRPM2 channels by extracellular divalent copper. *PLoS One* 9:e112071. doi: 10.1371/journal.pone.0112071

Yu, P., Liu, Z., Yu, X., Ye, P., Liu, H., Xue, X., et al. (2019). Direct gating of the TRPM2 channel by cADPR via specific interactions with the ADPR binding pocket. *Cell Rep.* 27, 3684.e4–3695.e4. doi: 10.1016/j.celrep.2019.05.067

Yu, X., Xie, Y., Zhang, X., Ma, C., Liu, L., Zhen, W., et al. (2021). Structural and functional basis of the selectivity filter as a gate in human TRPM2 channel. *Cell Rep.* 37:110025. doi: 10.1016/j.celrep.2021.110025

Yu, P., Xue, X., Zhang, J., Hu, X., Wu, Y., Jiang, L. H., et al. (2017). Identification of the ADPR binding pocket in the NUDT9 homology domain of TRPM2. *J. Gen. Physiol.* 149, 219–235. doi: 10.1085/jgp.201611675

Zhang, Z., Toth, B., Szollosi, A., Chen, J., and Csanady, L. (2018). Structure of a TRPM2 channel in complex with ca(2+) explains unique gating regulation. *elife* 7:36409. doi: 10.7554/eLife.36409

Zong, P., Feng, J., Yue, Z., Li, Y., Wu, G., Sun, B., et al. (2022). Functional coupling of TRPM2 and extrasynaptic NMDARs exacerbates excitotoxicity in ischemic brain injury. *Neuron* 110, 1944.e8–1958.e8. doi: 10.1016/j.neuron.2022.03.021

frontiers | Frontiers in Aging Neuroscience

TYPE Original Research
PUBLISHED 03 November 2022
DOI 10.3389/fnagi.2022.1027705

Check for updates

OPEN ACCESS

EDITED BY
Jun Xu,
Capital Medical University,
China

REVIEWED BY
Wangcai Gao,
Allina Health,
United States
Na Wu,
Shanghai Jiao Tong University, China
Xiaokuang Ma,
The University of Arizona College of Medicine – Phoenix, United States

*CORRESPONDENCE
Hong Xu
xuhong@sjtu.edu.cn
Qing Peng
pengqing@tongji.edu.cn

†These authors have contributed equally to this work

SPECIALTY SECTION
This article was submitted to Cellular and Molecular Mechanisms of Brain-aging, a section of the journal Frontiers in Aging Neuroscience

RECEIVED 25 August 2022
ACCEPTED 11 October 2022
PUBLISHED 03 November 2022

CITATION
Bai J, Wan Z, Wang M, Wu X, Wang T, Zhang Y, Xue Y, Xu H and Peng Q (2022) Association of cognitive function with Neurofilament light chain in the aqueous humor of human eye.
Front. Aging Neurosci. 14:1027705.
doi: 10.3389/fnagi.2022.1027705

COPYRIGHT
© 2022 Bai, Wan, Wang, Wu, Wang, Zhang, Xue, Xu and Peng. This is an open-access article distributed under the terms of the Creative Commons Attribution License (CC BY). The use, distribution or reproduction in other forums is permitted, provided the original author(s) and the copyright owner(s) are credited and that the original publication in this journal is cited, in accordance with accepted academic practice. No use, distribution or reproduction is permitted which does not comply with these terms.

Association of cognitive function with Neurofilament light chain in the aqueous humor of human eye

Jianhao Bai[1†], Zhongqi Wan[1†], Minli Wang[1], Xue Wu[2], Tianyu Wang[1], Yuanyuan Zhang[1], Yawen Xue[1], Hong Xu[2]* and Qing Peng[1]*

[1]Department of Ophthalmology, Shanghai Tenth People's Hospital of Tongji University, Tongji University School of Medicine, Shanghai, China, [2]School of Biomedical Engineering, Shanghai Jiao Tong University, Shanghai, China

Objectives: To evaluate the predictive clinical role of neurofilament light chain (NfL), amyloid-β (Aβ), glial fibrillary acidic protein (GFAP), and phosphorylated tau at threonine 181 (p-tau181) proteins in human aqueous humor (AH) and quantify the retinal macular microvascular parameters by optical coherence tomography angiography (OCTA) as early diagnostic markers of Alzheimer's disease (AD).

Methods: This prospective, single-site, cross-sectional, cohort study enrolled 55 participants, including 38 patients with neovascular age-related macular degeneration (nAMD) and 17 individuals with senile cataracts. The single-molecule array platform was used to quantitatively measure the levels of AH NfL, Aβ40, Aβ42, GFAP, and p-tau181 proteins in AH. The mini-mental state examination (MMSE) score was used to assess the global cognitive function. OCTA scan with 6×6mm macular area was used to quantify the retinal thickness and microvascular densities of superficial retinal capillary plexuses and deep retinal capillary plexuses.

Results: NfL, Aβ40, Aβ42, GFAP, and p-tau181 were detected in all AH samples by Simoa platform. Individuals with cataract had higher concentrations of NfL and p-tau181 but lower Aβ40 and Aβ42 and similar GFAP compared to those with nAMD. Lower MMSE scores showed a negative correlation with NfL concentration of AH not only in the nAMD group (p=0.043), but also in the cataract group (p=0.032). However, the MMSE scores were not associated with the levels of Aβ40, Aβ42, GFAP, or p-Tau181. Further analysis found that the Aβ40 and Aβ42 concentrations showed a strong positive correlation (p<0.0001). In addition, the NfL concentration showed a mild positive correlation with that of GFAP in the cataract group (p=0.021). Although it has not reached statistical significance, there was a correlation between the levels of NfL and Aβ42 in the nAMD group (p=0.051). Moreover, the macular superficial vessel density values had a negative correlation with the concentration of NfL (p=0.004) but a positive correlation with MMSE scores (p=0.045). The macular deep vessel density values were negatively correlated with the concentration of p-tau181 (p=0.031) and positively correlated with MMSE scores (p=0.020).

Conclusion: The examination of AD-related biomarkers in human AH and OCTA may improve the ocular-based AD detection methods and contribute to forestalling the progression of preclinical AD.

KEYWORDS

age-related macular degeneration, cataract, Alzheimer's disease, aqueous humor, neurofilament light chain

Introduction

In the past few decades, the increase in life expectancy and the growing aging population have increased the global prevalence of neurodegenerative diseases, including Alzheimer's disease (AD) and Parkinson's disease (PD; Hou et al., 2019). Globally, >35 million people are estimated to be suffering from dementia, and the number is expected to rise to 131.5 million by 2050 (Reilly et al., 2015). Accounting for 60–70% of dementia cases worldwide, AD is the most common type, and the prevalence is estimated to rise to 13.8 million by 2060 (Alzheimer's disease facts and figures, 2022). The etiology of AD is multifactorial, in addition to genetic factors, the risk of developing AD can also be attributed to acquired factors including cerebrovascular diseases, hypertension, diabetes, dyslipidemia, diet and nutrition(Silva et al., 2019; Hou et al., 2022). Since only a few treatments are effective, these neurodegenerative diseases often develop in an irreversible manner.

Therefore, early diagnosis of AD is essential. However, the disease can be diagnosed definitely only by histopathological examination (Javaid et al., 2016). The clinicians make the diagnosis based on the medical history, observing the clinical manifestations, and using expensive imaging or invasive tests, such as magnetic resonance imaging (MRI), positron emission tomography (PET), and evaluation of cerebrospinal fluid (CSF) biomarkers (O'Bryhim et al., 2018). Although assessed by experienced doctors, 10–15% of cases with prenatal diagnosis tend to be inaccurate (Thal et al., 2006). Due to the difficulties and delay in clinical diagnosis, patients often have irreversible pathological damage before starting the treatment. The classic symptoms of decreased memory, learning, calculation, and thinking are apparent only in the late stages of AD when an irreversible neuronal loss has already occurred (Salobrar-García et al., 2019). Thus, early detection is essential to prevent the disease progression. However, finding reliable, low-cost, and widely available screening methods remains a challenge (Blennow and Zetterberg, 2018).

Interestingly, AD is a heterogeneous disease with various cognitive subtypes. Visual symptoms are prominent due to local pathology of the parietal-occipital region in the visual variant AD (VVAD; Kaeser et al., 2015). The eye is a transparent medium to the brain. In anatomy and development, the retina is considered a part of the central nervous system (CNS). The retina and the internal visual membrane of the eye are derived from a neural tube and share a common neuro-ectodermal embryological origin and vasculature with the brain and transfer the visual stimuli to the brain (Sernagor et al., 2001; Javaid et al., 2016). The vital connection between the eyes and the brain suggests that the eyes could be regarded as an extension of the CNS (Marchesi et al., 2021), and the early manifestations of neurodegenerative diseases could be identified through the eyes. In addition, the immune response of the eye is similar to that of the brain and spinal cord, although it has unique anatomical structures and a local array of surface molecules and cytokines. Furthermore, various eye-specific pathologies are similar to the other CNS pathologies. These anatomical similarities permit common manifestations of the disease among the eye and brain, and the eye provides a direct window to neuroretinal diseases (London et al., 2013). Several neurodegenerative diseases, such as AD and PD, have manifestations in the eye, and eye symptoms usually precede the clinical symptoms and traditional diagnosis of such disorders (Javaid et al., 2016; Levin et al., 2016; Colligris et al., 2018; Guo et al., 2021). Accumulating evidence of the genetic, epidemiological, molecular, and clinical links between AD and various disorders of the eye, such as cataracts, neovascular age-related macular degeneration (nAMD), glaucoma, and diabetic retinopathy, indicate that these eye diseases and AD might share common risk factors and pathological mechanisms at the molecular level (Hersi et al., 2017; Zhang et al., 2017; Mancino et al., 2018; Lee et al., 2019). For example, some researches demonstrated that individuals with these eye diseases are at an increased risk of AD (Lee et al., 2019). These studies suggest that eye examination could serve as a non-invasive method for the early diagnosis of AD.

Previous studies on the early detection of AD have been focused on the diagnostic utility of protein markers in the CSF and blood, and levels of NfL, amyloid-β (Aβ), and total tau (T-tau) are correlated with the cognitive function in individuals with AD (Agarwal and Tripathi, 2011; Haapalinna et al., 2018; Hampel et al., 2018). Several recent clinical studies have shown that elevated phosphorylated tau 181 (p-Tau181) contribute to diagnostically relevant and accurate information in the early AD stages (Janelidze et al., 2020). However, previous studies on these AD biomarkers were only focused on CSF or blood of AD patients but rarely reported in aqueous humor (AH). Herein, we postulated that analysis of AH may have a clinical utility in early AD detection. Therefore, the present study aimed to investigate the correlation among AD protein biomarkers including NfL, Aβ40,

Aβ42, GFAP, and p-tau181 in human AH, macular microvascular parameters and neurocognition in the nAMD and cataract patients.

Materials and methods

Standard protocol approvals

This prospective, single-site, cross-sectional, cohort study was approved by the Research Ethics Committee of Shanghai Tenth People's Hospital and registered in the China Clinical Trials Registration Center (ClinicalTrials.gov: ChiCTR2100051795). This study conducted in the Department of Ophthalmology of Shanghai Tenth People's Hospital Affiliated to the School of Medicine of Tongji University, according to the principles of Helsinki Declaration. All patients signed informed consent before enrolling in the study.

Study design

A total of 55 patients, including 38 with neovascular age-related macular degeneration (nAMD group) and 17 individuals with senile cataract (cataract group), were included in this study. All patients underwent magnetic resonance imaging (MRI) and comprehensive ophthalmic examination, including intraocular pressure examination, visual acuity test, optometry, slit lamp biomicroscope, digital fundus photography, and optical coherence tomography angiography (OCTA). In addition, the mini-mental state examination (MMSE) was performed to evaluate the neurocognitive function and status of the subjects before the operation. Moreover, all nAMD patients were diagnosed by three retinal experts and examined by fundus fluorescein angiography (FFA) and indocyanine green angiography (ICGA).

Inclusion and exclusion criteria

The inclusion criteria of the nAMD group were as follows: (1) age 55–85 years; (2) newly diagnosed nAMD patients who have not received any anti-vascular endothelial growth factor (VEGF) treatment before; (3) willing to provide AH samples; (4) without cataract or other retinal diseases. The inclusion criteria of the cataract group were as follows: (1) age 55–85 years; (2) senile cataract patients who need phacoemulsification; 3) willing to provide AH samples; 4) patients without any retinal diseases.

The exclusion criteria for the patients were as follows: (1) received any intraocular or photocoagulation therapy; (2) history of pre-existing other ocular diseases, such as glaucoma, uveitis, retinal degeneration, and optic neuropathy; (3) diagnosed with any type of dementia, including AD; (4) systemic immune diseases; (5) history of head injuries or craniocerebral surgery; (6) family history of cognitive disorders or any genetic history; (7) allergic to sodium fluorescein and indocyanine green; (8) those the researchers believe that they should be excluded.

Sample collection and processing

All patients with nAMD received the intravitreal anti-VEGF drugs injection. Limbal puncture was performed before vitreous injection. An equivalent of 50–100 μl AH was collected through the limbus with an insulin syringe. Subsequently, 0.05 ml of Lucentis (Novartis Pharma Schweiz, AG) was injected into the vitreous cavity to restore the intraocular pressure balance. 17 AH samples of the cataract group were collected from 17 patients with senile cataracts. At the beginning of phacoemulsification, the surgeon used insulin syringes to obtain 50–100 μl of undiluted AH samples through the corneoscleral margin incision that was then transported to the laboratory for analysis.

Biomarker measurement

All the AH samples were clarified by centrifugation at 1000 rpm, 4°C for 15 min. The concentration of NfL, Aβ 1–40, Aβ 1–42, GFAP, and p-tau181 were measured using kits in each AH sample on the Simoa HD-X platform using a supersensitive Single molecule array (SIMOA) technology (Quantrick, MA, United States), according to the manufacturer's instructions, by technicians involved in the test blinded to the clinical data. The NF-light assay (Cat. No. 103186), multiplex Neurology 4-Plex A kits (Cat. No. 101995), and p-tau181 assay kit V2 (Cat. No.103714) were purchased from Quanterix.

OCTA measurements

OCTA was performed using an angioscope with a $6 \times 6\,mm^2$ area (Optovue RTVue XR Avanti, Optovue, Inc.) to scan the patients' macular area, and the flow density map software AngioAnalytics in-built version 2016.1.0.26 was used to quantify the retinal thickness and microvascular densities of superficial retinal capillary plexuses and deep retinal capillary plexuses automatically. All measurements are repeated twice with sufficient image quality (signal strength index >7).

Neurocognitive function test

MMSE test was administered to all subjects within 1 week before collecting AH samples, and the scores were used to assess the global cognitive function of each patient. All the tests were performed by the same well-trained, blinded certified psychometrist. The changes in the neurocognitive function of the

TABLE 1 The levels of AD-related biomarkers in AH in two groups (pg/ml).

	nAMD group			Cataract group		
	Mean	Median	*SD*	Mean	Median	*SD*
NfL	8.08	3.61	9.89	18.80	8.08	27.37
Aβ40	246.21	240.74	68.85	202.13	191.80	66.71
Aβ42	11.32	10.79	3.60	8.63	8.35	3.25
GFAP	586.38	385.79	481.84	772.91	368.28	822.95
p-tau181	2.38	2.15	1.18	3.47	3.07	1.25

NfL, neurofilament light chain; Aβ, amyloid-β; GFAP, glial fibrillary acidic protein; p-tau181, phosphorylated tau at threonine 181.

TABLE 2 General condition of the nAMD and cataract groups.

	nAMD group ($n=38$)	Cataract group ($n=17$)
Age	67.11 ± 8.16	68.82 ± 8.69
Gender (Female/Male)	20/18	8/9
MMSE scores	27.63 ± 1.70	20.12 ± 3.50
Eye (OD/OS)	17/21	9/8
Intraocular pressure	16.17 ± 1.32	15.86 ± 1.74
BCVA (Log MAR)	0.86 ± 0.11	0.88 ± 0.11
Highest level of education	10.29 ± 2.50	10.65 ± 2.15
Cerebrovascular diseases (*n*, %)	9(23.7%)	4(23.5%)
Hypertension (*n*, %)	13(34.2%)	7(41.2%)
Diabetes (*n*, %)	9(23.7%)	5(29.4%)
Dyslipidemia (*n*, %)	6(15.8%)	3(17.6%)

MMSE, The mini-mental state examination; BCVA, Best corrected visual acuity.

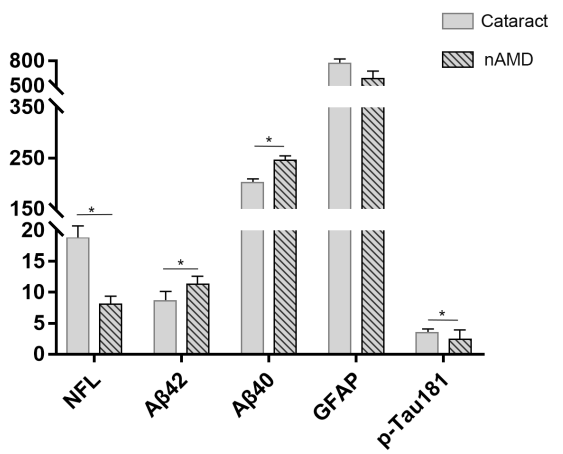

FIGURE 1
The difference evaluation of AD-related biomarkers in the two groups. Higher concentrations of NfL and p-tau181 but lower concentrations of Aβ40 and Aβ42, while similar concentrations of GFAP in AH of cataract group compared to those in nAMD group. *$p<0.05$.

subjects were analyzed according to the MMSE score, and the correlation between MMSE and AD-related biomarkers was explored in AH.

Statistical analysis

Linear regression was used to test the correlations among AD biomarker levels, MMSE scores, macular superficial and deep vessel density values and retinal thickness. The AD biomarker levels >0 were used after log transformation to fit the skewed distributions for regression. The associations of AD biomarker levels with MMSE scores and between AD biomarker levels and the vascular density, retinal thickness of the superficial and deep retina were assessed. *p*-values <0.05 indicated statistical significance.

Results

The introduction of supersensitive immunoassay (Simoa) used in this study allows a more accurate quantification of the low NfL and p-tau181 concentrations in AH, even at very low concentrations (down to a few pg./ml). This study determined the concentrations of NfL, Aβ40, and Aβ42, GFAP, and p-tau181 proteins in all AH samples from nAMD and cataract subjects. The summary statistics of AD biomarker levels in AH samples of the two groups are shown in Table 1. Due to the skewed distribution of the original data, the AD-related proteins in the two groups of AH samples showed normal distribution after the values were checked *via* quality control and converted by $\log_2$ transformation. In addition, about 52.9% of the cataract patients were males with an average age of 68.82 years, and the mean MMSE score was 20.12. Similarly, 47.4% of nAMD patients were males with an average age of 67.11 years, and the mean MMSE score was 27.63. The data showed no structural bias between age, gender, and education level of the two groups, but lower mean MMSE score in the cataract group was observed compared to that in the nAMD group (Table 2). Notably, the difference evaluation of AD biomarkers in the two groups found that individuals with cataracts had higher concentrations of NfL ($p=0.039$) and p-tau181 ($p=0.029$) but lower concentrations of Aβ40 ($p=0.031$) and Aβ42 ($p=0.011$), while the GFAP ($p=0.296$) concentrations were similar in the AH compared to those with nAMD (Figure 1).

The correlation analysis of the AD biomarkers in the nAMD group showed lower MMSE scores, indicating poorer cognitive function, had a negative correlation with the concentration of NfL ($r=-0.334$, $p=0.043$) in AH (Figure 2A). However, MMSE scores was not associated with the level of Aβ40, Aβ42, GFAP, or p-Tau181. Further analysis found there was a correlation between the levels of NfL and Aβ42, although it has not reached statistical significance ($r=0.323$, $p=0.051$) (Figure 2B). In addition, higher levels of Aβ40 in AH were associated with higher levels of Aβ42 ($r=0.795$, $p<0.0001$) (Figure 2C). Although it has not reached statistical significance, there was a positive correlation between the concentrations of p-tau181 and GFAP ($r=0.300$, $p=0.071$) (Figure 2D).

In the cataract group, the concentration of NfL in AH also showed a negative correlation with MMSE scores ($r=-0.415$,

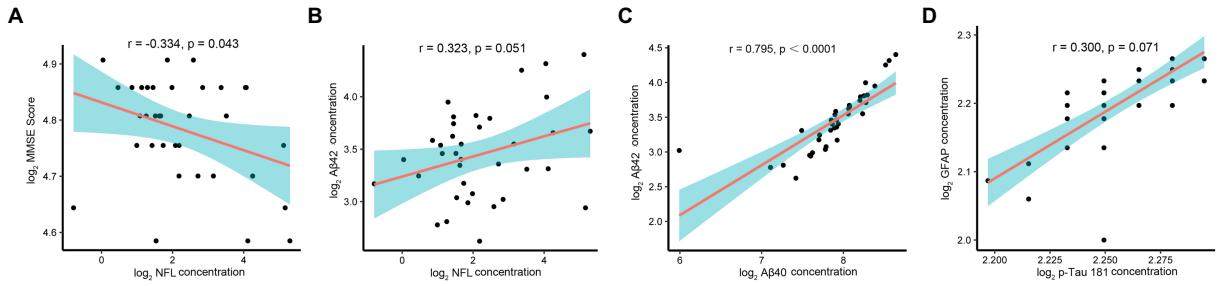

FIGURE 2
Correlation analysis, AD-related biomarkers and MMSE scores in nAMD group. Note: The AD-related biomarkers concentrations and MMSE scores were log-transformed. p<0.05 was considered statistically significant. The blue area represented the 95% confidence interval. **(A)** Lower MMSE scores correlated with higher AH levels of NfL (r=−0.334, p=0.043). **(B)** Although it has not reached statistical significance, there was a correlation between the levels of NfL and Aβ42 (r=0.323, p=0.051). **(C)** Higher levels of Aβ40 in AH were associated with higher levels of Aβ42 (r=0.795, p<0.0001). **(D)** Although it has not reached statistical significance, there was a positive correlation between the concentrations of p-tau181 and GFAP (r=0.300, p=0.071).

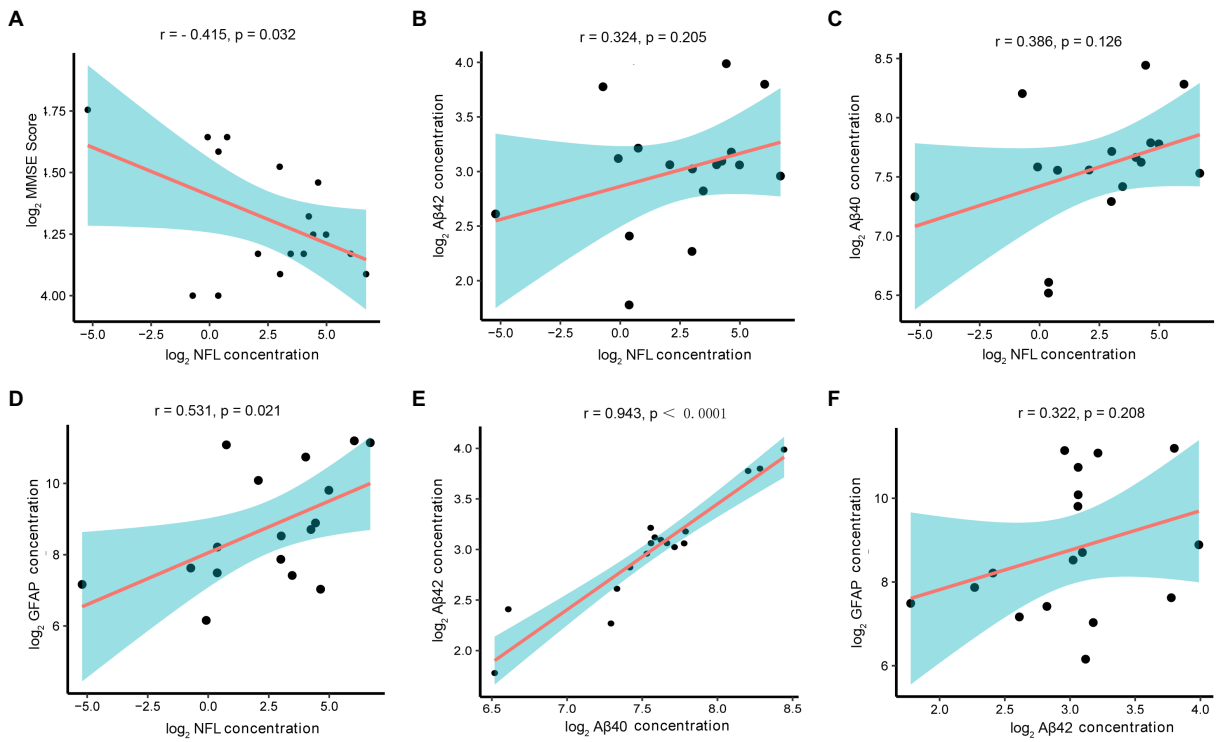

FIGURE 3
Correlation of AD-related biomarkers concentrations with MMSE scores in the cataract group. Note: The AD-related biomarkers concentrations and MMSE scores were log-transformed. p<0.05 was considered statistically significant. The blue area represented the 95% confidence interval. **(A)** Lower MMSE scores correlated with higher AH levels of NfL(r=−0.415, p=0.032). **(B–D)** The NfL concentration showed a mild positively correlation with the concentrations of Aβ42 (r=0.324, p=0.205), Aβ40 (r=0.386, p=0.126), and GFAP (r=0.531, p=0.021). **(E)** The Aβ40 and Aβ42 concentrations showed a strong positive correlation (r=0.943, p<0.0001). **(F)** Although it has not reached statistical significance, there was a correlation between the concentrations of Aβ42 and GFAP (r=0.322, p=0.208).

p=0.032) (Figure 3A). In the association analysis among the AD biomarkers, the NfL concentration showed a mild positively correlation with the concentrations of Aβ42 (r=0.324, p=0.205), Aβ40 (r=0.386, p=0.126), and GFAP (r=0.531, p=0.021) (Figures 3B–D). Moreover, the Aβ40 and Aβ42 concentrations showed a strong positive correlation (r=0.943, p<0.0001) (Figure 3E). Interestingly, although it has not reached statistical significance, there was a mild positive correlation between the concentrations of Aβ42 and GFAP (r=0.322, p=0.208) (Figure 3F).

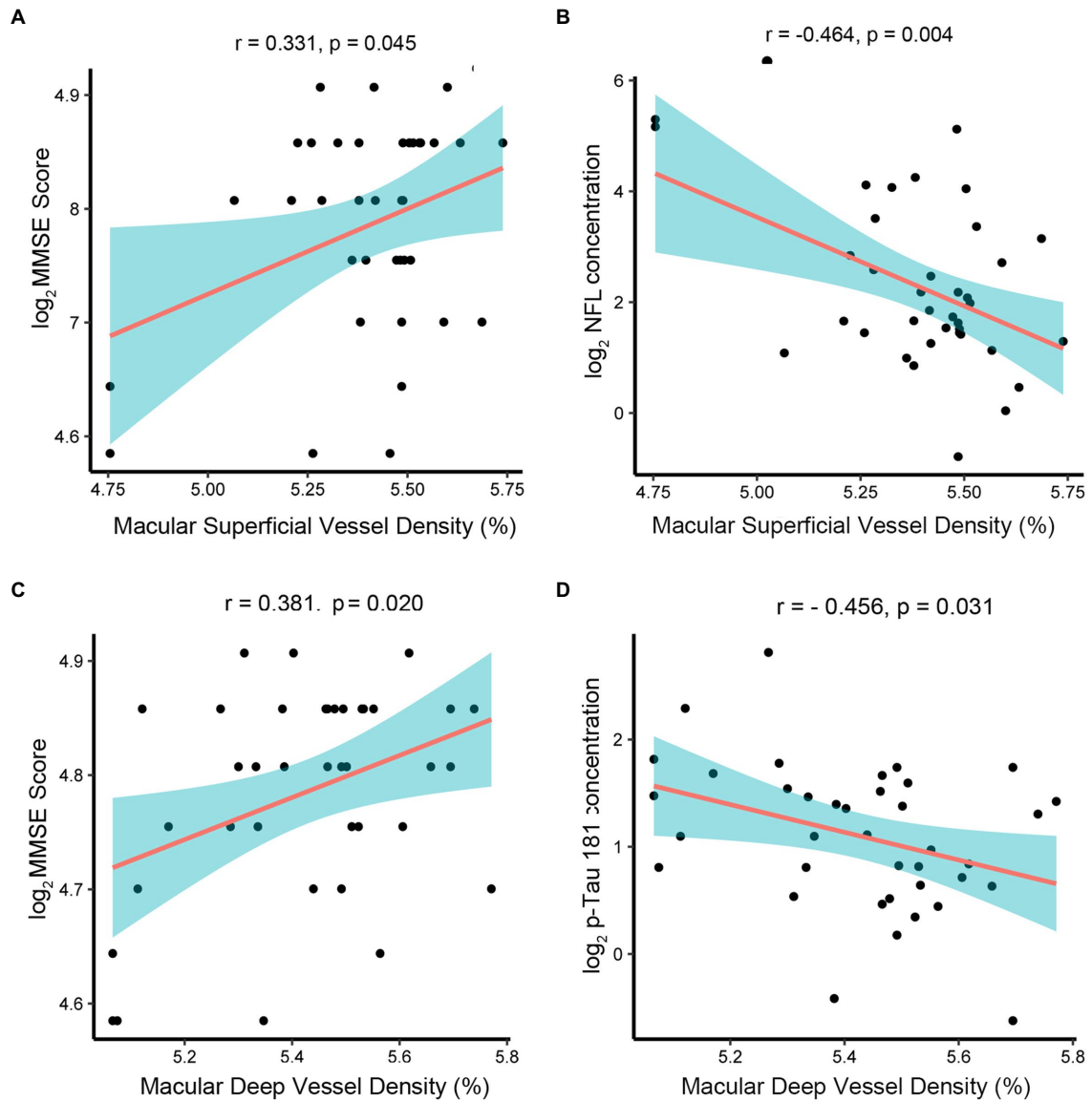

FIGURE 4
Associations between retinal thickness, retinal vessel density, and AD-related proteins in AMD group. The AD-related biomarkers concentrations and MMSE scores were log-transformed. $p<0.05$ was considered statistically significant. The blue area represented the 95% confidence interval. **(A,B)** The macular whole enface superficial vessel density values had a positive correlation with MMSE scores ($r=0.331$, $p=0.045$) but a negative correlation with the concentration of NfL ($r=-0.464$, $p=0.004$). **(C,D)** The macular whole enface deep vessel density values were positively correlated with MMSE scores ($r=0.381$, $p=0.020$) and negatively correlated with the concentration of p-tau181 ($r=-0.456$, $p=0.031$).

In order to explore the feasibility and effectiveness of retinal biomarkers measured by OCTA images as a diagnostic tool for early AD, we analyzed the correlation between retinal-specific markers of neurodegeneration obtained by OCTA, including superficial retinal thickness, retinal deep thickness, superficial retinal vessel density, deep retinal vessel density, and AD-related proteins in AH. We found that the macular whole enface superficial vessel density values measured by OCTA had a positive correlation with MMSE scores ($r=0.331$, $p=0.045$) (Figure 4A) but a negative correlation with the concentration of NfL ($r=-0.464$, $p=0.004$) (Figure 4B). The macular whole enface deep vessel density values were positively correlated with MMSE scores ($r=0.381$, $p=0.020$) (Figure 4C) and negatively correlated with the concentration of p-tau181 ($r=-0.456$, $p=0.031$) (Figure 4D). However, the current data showed that superficial retinal thickness was not associated with AD biomarker levels in the AH of nAMD patients or MMSE scores. Additionally, no significant correlation was established between deep retinal thickness and AD biomarker levels or MMSE scores.

Discussion

The eye is the medium of brain pathology. The eye biomarkers may exist in the early stage of AD and predate the occurrence of cognitive impairment or dementia symptoms observed in the clinic. The detection of eye biomarkers may be valuable to the early diagnosis of AD to minimize the physical damage and expensive assessment caused by invasive examination or multiple imaging scans of the brain. Prior investigations on the role of the eye in AD have focused primarily on retinal markers of neurodegeneration obtained through optical coherence tomography (OCT) scans or OCTA, including choroidal thickness, nerve fiber layer and ganglion cell layer thickness. However, retinal biomarkers measured by OCT imaging alone may not be sufficient as a diagnostic tool in early AD, a approach that involves both protein biomarkers in AH and OCT images might be more comprehensive.

More and more animal experiments and clinical evidence have shown an epidemiological, genetic, molecular, and clinical link between AD, nAMD, and cataracts (Baker et al., 2009; Tsai et al., 2015; Hwang et al., 2021). AD is the most common dementia of the elderly, wherein visual abnormalities occur before cognitive impairment. nAMD is a retinal degenerative disease and a leading cause of irreversible blindness worldwide.AD and nAMD, both being diseases of the elderly, have several epidemiological, etiological and histological overlaps in pathogenesis. The neuroinflammatory response and cell loss were considered of crucial importance in AD, such inflammatory response in the brain can occur in the retina of nAMD patients as the eye represents an extension of the brain. A cataract is a lens disease that is highly related to age. These three diseases have similar pathophysiological mechanisms (Melov et al., 2005; Liu and Zhu, 2017; Ashok et al., 2020). A large number of clinical studies have consistently shown that NfL, Aβ40, Aβ42, and p-tau181 in CSF and plasma are the key factors with predictive value for early AD detection (Agarwal and Tripathi, 2011; Schoonenboom et al., 2012; Olsson et al., 2016; Hampel et al., 2018; Paquet et al., 2018). However, there is still a lack of research on the early diagnosis and treatment of AD by detecting the concentration of AD-related proteins in human AH. AH is a specific biological sample. The total protein content in AH is only 0.2 mg/ml, which is 1/400–1/300 of that in the plasma. Consequently, the expression of AD-related proteins in AH has been rarely reported. Simoa assay has shown 126- fold higher sensitivity than the ELISA(Kuhle et al., 2016), and it facilitates automatic analysis of these biomarkers in AH with high precision and stability.

The current study determined and quantified the concentrations of NfL, Aβ40, Aβ42, GFAP, and p-tau181 proteins in the AH samples from all nAMD and cataract subjects. To the best of our knowledge, this is the first study reported in AH and correlating these AD-related proteins with neurocognition measured by MMSE and macular microvascular parameters in nAMD and age-rerated cataract patients. Notably, except for GFAP, the concentrations of all the AD-related proteins were significantly different in AH samples from nAMD and cataract patients. These proteins are related to cognitive function scores, indicating that AD-related proteins in AH of non-AD patients are related to eye conditions and changes in cognitive function. A recent study (Tsai et al., 2014) detected the vitreous levels of the same proteins in patients with epiretinal membrane, macular hole, diabetic retinopathy, and retinal detachment. However, one of the limitations of that study was the variance in co-existing ocular and systemic morbidities among the participants. However, our results demonstrated that individuals with nAMD had lower concentrations of NfL and p-tau181 but higher concentrations of Aβ40 and Aβ42, and similar GFAP concentrations in AH compared to those with cataracts. A previous study (Zhu et al., 2021) confirmed that the Aβ42 expression was significantly lower in the cataract group compared to the nAMD group, which is consistent with our finding.

It is worth noting that most of the previous clinical studies conducted by testing human AH samples took the AH samples of age-related cataract patients as the control group and AH of other non-cataract patients as the experimental group, because in the real clinical situation, it is very difficult for researchers to obtain AH samples of completely normal subjects (this is not in line with ethical principles). AH samples of senile cataract patients would be considered to be the closest to normal physiological conditions. However, in this study, AH of senile cataract patients cannot serve as the control group, because there might be a potentially important link between cataract and AD as mentioned above. For example, a population-based prospective study of 5,888 adults, aged ≥65 years, found that cataracts were associated with both AD and VAD/mixed dementia, whereas nAMD was associated with AD only (Hwang et al., 2021). Based on our data, it could be speculated that cataracts and nAMD are risk factors for AD, and cataracts may be more likely to develop various types of dementia than patients with nAMD. For verifying this conjecture, data on AD biomarkers in AH from healthy elderly are crucial, but difficult to achieve.

The basic pathological features of AD are an extracellular accumulation of Aβ and the intracellular deposition of p-tau, which in turn leads to neurodegeneration and glial activation. nAMD and cataracts exhibit similar pathological damage. Notably, Aβ protein is not only the main component of senile plaque but also a critical component of drusen. Many studies have shown Aβ deposition in retinal pigment epithelium (Ohno-Matsui, 2011; Guo et al., 2014; Ong et al., 2019). Additionally, the increased level of amyloid in the retina and AH may be involved in the apoptosis of retinal ganglion cells, resulting in AD before early symptoms (Prakasam et al., 2010; More and Vince, 2015). The overexpression and accumulation of Aβ lead to early pathological changes in nAMD (Prasad et al., 2017). Some clinical studies also have detected Aβ in the human lens (Shah et al., 2017; van Wijngaarden et al., 2017). Kerbage et al. (2015) utilized a fluorescent ligand eye scanning (FLES) technique to detect the fluorescence signature specific to an exogenous ligand bound to Aβ in the lens of the eye; the

technique could be used to predict AD with 85% sensitivity and 95% specificity [48]. Together, the above studies suggested that the pathological mechanism of AD may be related to the development of age-related cataracts. In this study, Aβ40 and Aβ42 were quantitatively detected in all AH samples of patients with nAMD and cataracts. Thus, we speculated that the Aβ protein in AH samples might be due to the accumulation of Aβ in the retinal pigment epithelium and its entry in the anterior chamber through the scleral venous sinus or vitreous humor. Another possible approach is from the aging lens. Additionally, in our study, the Aβ40 and Aβ42 concentrations showed a strong positive correlation in the AH of both groups, which was consistent with that in CSF and plasma. However, the mechanism of AD-related biomarkers entering AH and protein concentration difference in patients with different ophthalmopathy needs to be further elucidated with animal experiments and clinical studies.

NfL is a subunit of the neurofilament (NF) protein, which provides structural stability and maintains the integrity and pulse velocity of neurons. Some clinical studies found that patients with neurodegeneration have high levels of NfL in CSF; elevated levels of NfL in CSF and plasma could accurately distinguish healthy individuals from AD patients (Mattsson et al., 2017; Gaetani et al., 2019; Olsson et al., 2019). Modvig et al. (2016) reported that the NfL level in CSF predicts the visual outcomes after optic neuritis. In the event of degenerative changes in the retina of patients with nAMD, NfL will be released locally from the axons that degrade the retinal nerve fiber layer and spread to the vitreous fluid and AH, resulting in an increase in the concentration of NfL in AH, which was consistent with the findings of Subramanian et al. (2020). However, due to many diseases in the particular subject, the correlation between NfL levels and ophthalmopathy cannot be proved. Some other studies demonstrated that the decreased level of NfL in the ganglion cell layer of the retina and optic nerve is a response to induced injury or ischemia (Taniguchi et al., 2004; Sasaoka et al., 2006; Kamalden et al., 2011). The release of NfL in AH of cataract patients may be another mechanism. Therefore, the pathophysiological mechanism of AD biomarkers in AH needs to be explored further by neurologists, ophthalmologists, and basic researchers.

p-tau181 is also a known biomarker of neurodegeneration in CSF and blood (Hampel et al., 2018). Although both NfL and tau prote p-tau181 in AH ins are released from axons due to axonal degeneration, no correlation has been detected between NfL and, which is not consistent with the phenomenon in the brain and CSF. In addition, p-tau181 was not associated with Aβ in either nAMD or cataract patients' AH, which might be due to the replacement of local sources of NfL and Aβ proteins in the eyes, such as the release of NfL from the retinal nerve fiber layer or amyloid plaques found in the retina independent of those found in the brain (Jin et al., 2019). The development of supersensitive immunoassay and new mass spectrometry technology has provided clinical data showing that p-tau181 can be used as a biomarker for early diagnosis of AD; however, additional studies are required to verify the diagnostic value of p-tau181 in AH.

Furthermore, lower MMSE scores indicated poor cognitive function, showing a negative correlation with the concentration of NfL in the AH of patients with nAMD. However, our data showed that the level of Aβ40, Aβ42, GFAP, or p-Tau181 was not associated with MMSE scores. In addition, the commercial spectral-domain OCTA was used to obtain the retina images of all patients, The correlation analysis between macular vessel density, retinal thickness, and AD biomarkers in the nAMD group explored the feasibility and effectiveness of retinal biomarkers measured by OCTA images as a diagnostic tool for early AD. However, OCTA images of the cataract group were not included in the analysis due to that phacoscotasmus caused poor retinal image quality and affected retinal stratification analysis. To the best of our knowledge, the association of AD biomarkers in AH and retinal specific markers of neurodegeneration obtained by OCTA or MMSE scores has not yet been elaborated. The current results lay a foundation for a large sample size cohort study in the future.

The highest advantage of this study is that the AH samples were obtained from patients with nAMD and cataracts. Unlike previous studies on the correlation between AD and ophthalmopathy, none of our subjects were diagnosed with any type of dementia, nor had any history of head injury or family history of cognitive disorders. This is helpful while exploring the potential of NfL, Aβ, and p-tau181 proteins as early diagnostic tools for AD using biological samples other than CSF and plasma. On the other hand, AH is a crucial component of the intraocular fluid and communicates with vitreous fluid. The expression of cytokines in AH reflects the physiological and pathological changes in lens and retina, while eyes and brain have a common embryological source and retina is the extension of cortical nerves; thus, intraocular fluid may be closer to the pathophysiological state of CSF than plasma and less affected by systemic diseases. Compared to the non-renewable vitreous fluid, AH is an ideal detection material. Because acquiring AH samples is more convenient and less traumatic to eyes, an appropriate amount can be obtained by anterior chamber puncture in the outpatient treatment or operating room. In this study, all AH samples of nAMD patients were collected by intravitreal injection treatment (Xing et al., 2014), and those from cataracts by phacoemulsification. These sampling procedures do not cause additional harm to the patient and can also prevent the increase in intraocular pressure caused by the injection of the drug into the eye (Saxena et al., 2019). Moreover, many eye diseases, such as nAMD and DR, were related to AD and routinely required multiple intravitreal injections (anti-VEGF treatment), facilitating multiple AH samples to observe the change rate of AD biomarkers.

Nevertheless, the present study has several limitations. Firstly, we could not obtain aqueous humor samples from healthy elderly

because it is not in accordance with ethical conduct. Secondly, our sample size, limited by the scarcity of aqueous humor specimens, needs to be expanded to verify the correlation between AD biomarkers in AH and cognitive function in non-dementia patients. In addition, cataract patients had poor OCTA images due to lens opacity, which affected the accuracy of fundus retinal thickness and blood flow density measurement, so hence were not included in the statistical analysis. Finally, MMSE tests that are approximate assessments of cognitive function are less specific and effective than PET or MRI in detecting moderate dementia especially in mild dementia, and while it is highly specific and valid in detection of moderate dementia. Therefore, more sensitive way to assess cognitive function, including neurologist evaluation, detailed neuropsychological testing, and brain imaging would be needed to further verify the relationship between the AH biomarkers and development of dementia. Furthermore, future multicenter clinical studies with larger sample size and/or longitudinal study would be helpful to verify the correlation between AD biomarkers in AH and CSF and their correlation with brain imaging markers. Despite the above limitations, the current study provided an early AD diagnosis method that is less invasive, easy to obtain, less affected by systemic conditions, and can is widely applicable. Future directions include investigation to determine if tear secretions, which are easier to access and less invasive, contain biomarker levels that are associated with cognition, and a more comprehensive and sensitive way, including neurologist evaluation, detailed neuropsychological test, protein biomarkers in AH and OCTA images might be needed to further explore the clinical value of AD biomarkers in AH for early diagnosis of AD.

Conclusion

NfL, Aβ40, Aβ42, GFAP, and p-tau181 can be detected in the aqueous humor and may play a role in early dementia detection in individuals at risk for AD. We observed that NfL, Aβ40, Aβ42, and p-tau181 levels in aqueous humor were influenced by the patients' clinical eye conditions. Thus, this study served as a foundation for further investigation of the above AD-related biomarkers in ocular fluids. To the best of our knowledge, this is the first study that correlates neurocognition with AD-related proteins in the aqueous humor and macular microvascular parameters. The results suggested that the examination of AD-related biomarker content in human aqueous humor and OCTA may improve the ocular-based AD detection methods and forestall the progression of preclinical AD.

Data availability statement

The original contributions presented in the study are included in the article/Supplementary material, further inquiries can be directed to the corresponding authors.

Ethics statement

The studies involving human participants were reviewed and approved by the Medical Ethics Committee of The Shanghai Tenth People's Hospital of Tongji University. All of the participants provided their written informed consent to participate in this study.

Author contributions

JB participated in the data analysis and writing of the paper. ZW, MW, TW, YZ, and YX participated in data collection and revising the paper. QP and HX designed the study and wrote and revised the paper. All authors contributed to the article and approved the submitted version.

Funding

This work was supported by the National Natural Science Foundation of China [grant number 81470025); the Shanghai Municipal Health Bureau [grant number ZY (2018–2020)-ZWB-1001-CPJS10); and the Three-Year Action Plan for Promoting Clinical Skills and Clinical Innovation in Municipal Hospitals (grant number SHDC2020CR5014).

Conflict of interest

The authors declare that the research was conducted in the absence of any commercial or financial relationships that could be construed as a potential conflict of interest.

The reviewer NW declared a shared affiliation with the author HX to the handling editor at the time of review.

Publisher's note

All claims expressed in this article are solely those of the authors and do not necessarily represent those of their affiliated organizations, or those of the publisher, the editors and the reviewers. Any product that may be evaluated in this article, or claim that may be made by its manufacturer, is not guaranteed or endorsed by the publisher.

Supplementary material

The Supplementary material for this article can be found online at: https://www.frontiersin.org/articles/10.3389/fnagi.2022.1027705/full#supplementary-material

References

Alzheimer's disease facts and figures (2022). Alzheimers Dement. doi: 10.1002/alz.12638

Agarwal, R., and Tripathi, C. B. (2011). Diagnostic utility of CSF tau and Aβ(42) in dementia: a meta-analysis. *Int. J. Alzheimers Dis.* 2011:503293. doi: 10.4061/2011/503293

Ashok, A., Singh, N., Chaudhary, S., Bellamkonda, V., Kritikos, A. E., Wise, A. S., et al. (2020). Retinal degeneration and Alzheimer's disease: an evolving link. *Int. J. Mol. Sci.* 21: 7290. doi: 10.3390/ijms21197290

Baker, M. L., Wang, J. J., Rogers, S., Klein, R., Kuller, L. H., Larsen, E. K., et al. (2009). Early age-related macular degeneration, cognitive function, and dementia: the cardiovascular health study. *Arch. Ophthalmol.* 127, 667–673. doi: 10.1001/archophthalmol.2009.30

Blennow, K., and Zetterberg, H. (2018). Biomarkers for Alzheimer's disease: current status and prospects for the future. *J. Intern. Med.* 284, 643–663. doi: 10.1111/joim.12816

Colligris, P., Perez de Lara, M. J., Colligris, B., and Pintor, J. (2018). Ocular manifestations of Alzheimer's and other neurodegenerative diseases: the Prospect of the eye as a tool for the early diagnosis of Alzheimer's disease. *J. Ophthalmol.* 2018:8538573. doi: 10.1155/2018/8538573

Gaetani, L., Blennow, K., Calabresi, P., Di Filippo, M., Parnetti, L., and Zetterberg, H. (2019). Neurofilament light chain as a biomarker in neurological disorders. *J. Neurol. Neurosurg. Psychiatry* 90, 870–881. doi: 10.1136/jnnp-2018-320106

Guo, L., Ravindran, N., Shamsher, E., Hill, D., and Cordeiro, M. F. (2021). Retinal changes in transgenic mouse models of Alzheimer's disease. *Curr. Alzheimer Res.* 18, 89–102. doi: 10.2174/1567205018666210414113634

Guo, L. Y., Alekseev, O., Li, Y., Song, Y., and Dunaief, J. L. (2014). Iron increases APP translation and amyloid-beta production in the retina. *Exp. Eye Res.* 129, 31–37. doi: 10.1016/j.exer.2014.10.012

Haapalinna, F., Kokki, M., Jääskeläinen, O., Hallikainen, M., Helisalmi, S., Koivisto, A., et al. (2018). Subtle cognitive impairment and Alzheimer's disease-type pathological changes in cerebrospinal fluid are common among neurologically healthy subjects. *J. Alzheimers Dis.* 62, 165–174. doi: 10.3233/jad-170534

Hampel, H., Toschi, N., Baldacci, F., Zetterberg, H., Blennow, K., Kilimann, I., et al. (2018). Alzheimer's disease biomarker-guided diagnostic workflow using the added value of six combined cerebrospinal fluid candidates: Aβ(1-42), total-tau, phosphorylated-tau, NFL, neurogranin, and YKL-40. *Alzheimers Dement.* 14, 492–501. doi: 10.1016/j.jalz.2017.11.015

Hersi, M., Irvine, B., Gupta, P., Gomes, J., Birkett, N., and Krewski, D. (2017). Risk factors associated with the onset and progression of Alzheimer's disease: a systematic review of the evidence. *Neurotoxicology* 61, 143–187. doi: 10.1016/j.neuro.2017.03.006

Hou, K., Wu, Z. X., Chen, X. Y., Wang, J. Q., Zhang, D., Xiao, C., et al. (2022). Microbiota in health and diseases. *Signal Transduct. Target. Ther.* 7:135. doi: 10.1038/s41392-022-00974-4

Hou, Y., Dan, X., Babbar, M., Wei, Y., Hasselbalch, S. G., Croteau, D. L., et al. (2019). Ageing as a risk factor for neurodegenerative disease. *Nat. Rev. Neurol.* 15, 565–581. doi: 10.1038/s41582-019-0244-7

Hwang, P. H., Longstreth, W. T., Thielke, S. M., Francis, C. E., Carone, M., Kuller, L. H., et al. (2021). Ophthalmic conditions associated with dementia risk: the cardiovascular health study. *Alzheimers Dement.* 17, 1442–1451. doi: 10.1002/alz.12313

Janelidze, S., Mattsson, N., Palmqvist, S., Smith, R., Beach, T. G., Serrano, G. E., et al. (2020). Plasma P-tau181 in Alzheimer's disease: relationship to other biomarkers, differential diagnosis, neuropathology and longitudinal progression to Alzheimer's dementia. *Nat. Med.* 26, 379–386. doi: 10.1038/s41591-020-0755-1

Javaid, F. Z., Brenton, J., Guo, L., and Cordeiro, M. F. (2016). Visual and ocular manifestations of Alzheimer's disease and their use as biomarkers for diagnosis and progression. *Front. Neurol.* 7:55. doi: 10.3389/fneur.2016.00055

Jin, M., Cao, L., and Dai, Y. P. (2019). Role of Neurofilament light chain as a potential biomarker for Alzheimer's Di e: a correlative meta-analysis. *Front. Aging Neurosci.* 11:254. doi: 10.3389/fnagi.20seas19.00254

Kaeser, P. F., Ghika, J., and Borruat, F. X. (2015). Visual signs and symptoms in patients with the visual variant of Alzheimer disease. *BMC Ophthalmol.* 15:65. doi: 10.1186/s12886-015-0060-9

Kamalden, T. A., Ji, D., Fawcett, R. J., and Osborne, N. N. (2011). Genistein blunts the negative effect of ischaemia to the retina caused by an elevation of intraocular pressure. *Ophthalmic Res.* 45, 65–72. doi: 10.1159/000313985

Kerbage, C., Sadowsky, C. H., Tariot, P. N., Agronin, M., Alva, G., Turner, F. D., et al. (2015). Detection of amyloid β signature in the lens and its correlation in the brain to aid in the diagnosis of Alzheimer's disease. *Am. J. Alzheimers Dis. Other Dement.* 30, 738–745. doi: 10.1177/1533317513520214

Kuhle, J., Barro, C., Andreasson, U., Derfuss, T., Lindberg, R., Sandelius, Å., et al. (2016). Comparison of three analytical platforms for quantification of the neurofilament light chain in blood samples: ELISA, electrochemiluminescence immunoassay and Simoa. *Clin. Chem. Lab. Med.* 54, 1655–1661. doi: 10.1515/cclm-2015-1195

Lee, C. S., Larson, E. B., Gibbons, L. E., Lee, A. Y., McCurry, S. M., Bowen, J. D., et al. (2019). Associations between recent and established ophthalmic conditions and risk of Alzheimer's disease. *Alzheimers Dement.* 15, 34–41. doi: 10.1016/j.jalz.2018.06.2856

Levin, J., Kurz, A., Arzberger, T., Giese, A., and Höglinger, G. U. (2016). The differential diagnosis and treatment of atypical parkinsonism. *Dtsch. Arztebl. Int.* 113, 61–69. doi: 10.3238/arztebl.2016.0061

Liu, S. S., and Zhu, S. Q. (2017). Correlation between Alzheimer disease and cataract. *Zhonghua Yan Ke Za Zhi* 53, 314–316. doi: 10.3760/cma.j.issn.0412-4081.2017.04.016

London, A., Benhar, I., and Schwartz, M. (2013). The retina as a window to the brain-from eye research to CNS disorders. *Nat. Rev. Neurol.* 9, 44–53. doi: 10.1038/nrneurol.2012.227

Mancino, R., Martucci, A., Cesareo, M., Giannini, C., Corasaniti, M. T., Bagetta, G., et al. (2018). Glaucoma and Alzheimer disease: one age-related neurodegenerative disease of the brain. *Curr. Neuropharmacol.* 16, 971–977. doi: 10.2174/1570159x16666171206144045

Marchesi, N., Fahmideh, F., Boschi, F., Pascale, A., and Barbieri, A. (2021). Ocular neurodegenerative diseases: interconnection between retina and cortical areas. *Cells* 10: 2394. doi: 10.3390/cells10092394

Mattsson, N., Andreasson, U., Zetterberg, H., and Blennow, K. (2017). Association of Plasma Neurofilament Light with Neurodegeneration in patients with Alzheimer disease. *JAMA Neurol.* 74, 557–566. doi: 10.1001/jamaneurol.2016.6117

Melov, S., Wolf, N., Strozyk, D., Doctrow, S. R., and Bush, A. I. (2005). Mice transgenic for Alzheimer disease beta-amyloid develop lens cataracts that are rescued by antioxidant treatment. *Free Radic. Biol. Med.* 38, 258–261. doi: 10.1016/j.freeradbiomed.2004.10.023

Modvig, S., Degn, M., Sander, B., Horwitz, H., Wanscher, B., Sellebjerg, F., et al. (2016). Cerebrospinal fluid neurofilament light chain levels predict visual outcome after optic neuritis. *Mult. Scler.* 22, 590–598. doi: 10.1177/1352458515599074

More, S. S., and Vince, R. (2015). Hyperspectral imaging signatures detect amyloidopathy in Alzheimer's mouse retina well before onset of cognitive decline. *ACS Chem. Neurosci.* 6, 306–315. doi: 10.1021/cn500242z

O'Bryhim, B. E., Apte, R. S., Kung, N., Coble, D., and Van Stavern, G. P. (2018). Association of Preclinical Alzheimer disease with optical coherence tomographic angiography findings. *JAMA Ophthalmol* 136, 1242–1248. doi: 10.1001/jamaophthalmol.2018.3556

Ohno-Matsui, K. (2011). Parallel findings in age-related macular degeneration and Alzheimer's disease. *Prog. Retin. Eye Res.* 30, 217–238. doi: 10.1016/j.preteyeres.2011.02.004

Olsson, B., Lautner, R., Andreasson, U., Öhrfelt, A., Portelius, E., Bjerke, M., et al. (2016). CSF and blood biomarkers for the diagnosis of Alzheimer's disease: a systematic review and meta-analysis. *Lancet Neurol.* 15, 673–684. doi: 10.1016/s1474-4422(16)00070-3

Olsson, B., Portelius, E., Cullen, N. C., Sandelius, Å., Zetterberg, H., Andreasson, U., et al. (2019). Association of Cerebrospinal Fluid Neurofilament Light Protein Levels with Cognition in patients with dementia, motor neuron disease, and movement disorders. *JAMA Neurol.* 76, 318–325. doi: 10.1001/jamaneurol.2018.3746

Ong, S. S., Proia, A. D., Whitson, H. E., Farsiu, S., Doraiswamy, P. M., and Lad, E. M. (2019). Ocular amyloid imaging at the crossroad of Alzheimer's disease and age-related macular degeneration: implications for diagnosis and therapy. *J. Neurol.* 266, 1566–1577. doi: 10.1007/s00415-018-9028-z

Paquet, C., Bouaziz-Amar, E., Cognat, E., Volpe-Gillot, L., Haddad, V., Mahieux, F., et al. (2018). Distribution of cerebrospinal fluid biomarker profiles in patients explored for cognitive disorders. *J. Alzheimers Dis.* 64, 889–897. doi: 10.3233/jad-180240

Prakasam, A., Muthuswamy, A., Ablonczy, Z., Greig, N. H., Fauq, A., Rao, K. J., et al. (2010). Differential accumulation of secreted AbetaPP metabolites in ocular fluids. *J. Alzheimers Dis.* 20, 1243–1253. doi: 10.3233/jad-2010-100210

Prasad, T., Zhu, P., Verma, A., Chakrabarty, P., Rosario, A. M., Golde, T. E., et al. (2017). Amyloid β peptides overexpression in retinal pigment epithelial cells via AAV-mediated gene transfer mimics AMD-like pathology in mice. *Sci. Rep.* 7:3222. doi: 10.1038/s41598-017-03397-2

Reilly, S., Miranda-Castillo, C., Malouf, R., Hoe, J., Toot, S., Challis, D., et al. (2015). Case management approaches to home support for people with dementia. *Cochrane Database Syst. Rev.* 1:Cd008345. doi: 10.1002/14651858.CD008345.pub2

Salobrar-García, E., de Hoz, R., Ramírez, A. I., López-Cuenca, I., Rojas, P., Vazirani, R., et al. (2019). Changes in visual function and retinal structure in the progression of Alzheimer's disease. *PLoS One* 14:e0220535. doi: 10.1371/journal.pone.0220535

Sasaoka, M., Taniguchi, T., Shimazawa, M., Ishida, N., Shimazaki, A., and Hara, H. (2006). Intravitreal injection of endothelin-1 caused optic nerve damage following to ocular hypoperfusion in rabbits. *Exp. Eye Res.* 83, 629–637. doi: 10.1016/j.exer.2006.03.007

Saxena, S., Lai, T. Y., Koizumi, H., Farah, M. E., Ferrara, D., Pelayes, D., et al. (2019). Anterior chamber paracentesis during intravitreal injections in observational trials: effectiveness and safety and effects. *Int. J. Retina Vitreous* 5:8. doi: 10.1186/s40942-019-0157-z

Schoonenboom, N. S., Reesink, F. E., Verwey, N. A., Kester, M. I., Teunissen, C. E., et al. (2012). Cerebrospinal fluid markers for differential dementia diagnosis in a large memory clinic cohort. *Neurology* 78, 47–54. doi: 10.1212/WNL.0b013e31823ed0f0

Sernagor, E., Eglen, S. J., and Wong, R. O. (2001). Development of retinal ganglion cell structure and function. *Prog. Retin. Eye Res.* 20, 139–174. doi: 10.1016/s1350-9462(00)00024-0

Shah, T. M., Gupta, S. M., Chatterjee, P., Campbell, M., and Martins, R. N. (2017). Beta-amyloid sequelae in the eye: a critical review on its diagnostic significance and clinical relevance in Alzheimer's disease. *Mol. Psychiatry* 22, 353–363. doi: 10.1038/mp.2016.251

Silva, M. V. F., Loures, C. M. G., Alves, L. C. V., de Souza, L. C., Borges, K. B. G., and Carvalho, M. D. G. (2019). Alzheimer's disease: risk factors and potentially protective measures. *J. Biomed. Sci.* 26:33. doi: 10.1186/s12929-019-0524-y

Subramanian, M. L., Vig, V., Chung, J., Fiorello, M. G., Xia, W., Zetterberg, H., et al. (2020). Neurofilament light chain in the vitreous humor of the eye. *Alzheimers Res. Ther.* 12:111. doi: 10.1186/s13195-020-00677-4

Taniguchi, T., Shimazawa, M., and Hara, H. (2004). Alterations in neurofilament light in optic nerve in rat kainate and monkey ocular hypertension models. *Brain Res.* 1013, 241–248. doi: 10.1016/j.brainres.2004.04.023

Thal, L. J., Kantarci, K., Reiman, E. M., Klunk, W. E., Weiner, M. W., Zetterberg, H., et al. (2006). The role of biomarkers in clinical trials for Alzheimer disease. *Alzheimer Dis. Assoc. Disord.* 20, 6–15. doi: 10.1097/01.wad.0000191420.61260.a8

Tsai, D. C., Chen, S. J., Huang, C. C., Yuan, M. K., and Leu, H. B. (2015). Age-related macular degeneration and risk of degenerative dementia among the elderly in Taiwan: a population-based cohort study. *Ophthalmology* 122, 2327–2335.e2. doi: 10.1016/j.ophtha.2015.07.033

Tsai, Y., Lu, B., Ljubimov, A. V., Girman, S., Ross-Cisneros, F. N., Sadun, A. A., et al. (2014). Ocular changes in TgF344-AD rat model of Alzheimer's disease. *Invest. Ophthalmol. Vis. Sci.* 55, 523–534. doi: 10.1167/iovs.13-12888

van Wijngaarden, P., Hadoux, X., Alwan, M., Keel, S., and Dirani, M. (2017). Emerging ocular biomarkers of Alzheimer disease. *Clin. Exp. Ophthalmol.* 45, 54–61. doi: 10.1111/ceo.12872

Xing, L., Dorrepaal, S. J., and Gale, J. (2014). Survey of intravitreal injection techniques and treatment protocols among retina specialists in Canada. *Can. J. Ophthalmol.* 49, 261–266. doi: 10.1016/j.jcjo.2014.03.009

Zhang, J., Chen, C., Hua, S., Liao, H., Wang, M., Xiong, Y., et al. (2017). An updated meta-analysis of cohort studies: diabetes and risk of Alzheimer's disease. *Diabetes Res. Clin. Pract.* 124, 41–47. doi: 10.1016/j.diabres.2016.10.024

Zhu, J., Su, T., Wang, M., Li, M., Liu, L., and Wang, F. (2021). Highly expressed amyloid Beta-42 of aqueous humor in patients with Neovascular macular degeneration. *Semin. Ophthalmol.* 36, 9–13. doi: 10.1080/08820538.2021.1883679

frontiers | Frontiers in Aging Neuroscience

TYPE Original Research
PUBLISHED 07 November 2022
DOI 10.3389/fnagi.2022.1052765

Check for updates

OPEN ACCESS

EDITED BY
Yuzhen Xu,
Tongji University, China

REVIEWED BY
Liang Wang,
Tangdu Hospital, China
Tian Weidong,
Shihezi University, China

*CORRESPONDENCE
Ping Lei
leiping1974@163.com

†These authors have contributed equally to this work and share first authorship

SPECIALTY SECTION
This article was submitted to Cellular and Molecular Mechanisms of Brain-aging, a section of the journal Frontiers in Aging Neuroscience

RECEIVED 24 September 2022
ACCEPTED 18 October 2022
PUBLISHED 07 November 2022

CITATION
Ge X, Guo M, Li M, Zhang S, Qiang J, Zhu L, Cheng L, Li W, Wang Y, Yu J, Yin Z, Chen F, Tong W and Lei P (2022) Potential blood biomarkers for chronic traumatic encephalopathy: The multi-omics landscape of an observational cohort. *Front. Aging Neurosci.* 14:1052765. doi: 10.3389/fnagi.2022.1052765

COPYRIGHT
© 2022 Ge, Guo, Li, Zhang, Qiang, Zhu, Cheng, Li, Wang, Yu, Yin, Chen, Tong and Lei. This is an open-access article distributed under the terms of the Creative Commons Attribution License (CC BY). The use, distribution or reproduction in other forums is permitted, provided the original author(s) and the copyright owner(s) are credited and that the original publication in this journal is cited, in accordance with accepted academic practice. No use, distribution or reproduction is permitted which does not comply with these terms.

Potential blood biomarkers for chronic traumatic encephalopathy: The multi-omics landscape of an observational cohort

Xintong Ge[1,2,4†], Mengtian Guo[1,2†], Meimei Li[1,2†], Shishuang Zhang[1,2], Junlian Qiang[1], Luoyun Zhu[3], Lu Cheng[1,2], Wenzhu Li[1,2], Yan Wang[1,2], Jinwen Yu[1,2], Zhenyu Yin[1,2], Fanglian Chen[4], Wen Tong[5] and Ping Lei[1,2,4]*

[1]Haihe Laboratory of Cell Ecosystem, Department of Geriatrics, Tianjin Medical University General Hospital, Tianjin, China, [2]Tianjin Geriatrics Institute, Tianjin, China, [3]Department of Medical Examination, Tianjin Medical University General Hospital, Tianjin, China, [4]Key Laboratory of Injuries, Key Laboratory of Post-trauma Neuro-repair and Regeneration in Central Nervous System, Variations and Regeneration of Nervous System, Tianjin Neurological Institute, Tianjin, China, [5]Weightlifting, Wrestling, Judo, Boxing and Taekwondo Sports Management Center of Tianjin Sports Bureau, Tianjin, China

Chronic traumatic encephalopathy (CTE) is a neurodegenerative disease associated with exposure to repetitive head impacts, which is susceptible in elderly people with declined mobility, athletes of full contact sports, military personnel and victims of domestic violence. It has been pathologically diagnosed in brain donors with a history of repetitive mild traumatic brain injury (rmTBI), but cannot be clinically diagnosed for a long time. By the continuous efforts by neuropathologists, neurologists and neuroscientists in recent 10 years, an expert consensus for the diagnostic framework of CTE was proposed in 2021 funded by the National Institute of Neurological Disorders and Stroke. The new consensus contributes to facilitating research in the field. However, it still needs to incorporate *in vivo* biomarkers to further refine and validate the clinical diagnostic criteria. From this, a single-center, observational cohort study has been being conducted by Tianjin Medical University General Hospital since 2021. As a pilot study of this clinical trial, the present research recruited 12 pairs of gender- and age-matched rmTBI patients with healthy subjects. Their blood samples were collected for exosome isolation, and multi-omics screening to explore potential diagnostic biomarkers in blood and its exosomes. The expression level of CHL1 protein, KIF2A mRNA, LIN7C mRNA, miR-297, and miR-1183 in serum and exosomes were found to be differentially expressed between groups. Besides, serum and exosomal CHL1, KIF2A, and miR-1183, as well as exosomal miR-297 were further verified as potential biomarkers for CTE by low-throughput assays.

They are expected to contribute to establishing a novel set of CTE diagnostic signatures with classic neurodegenerative indicators in our future study, thereby updating the consensus diagnostic criteria for CTE by incorporating new evidence of the *in vivo* biomarkers.

KEYWORDS

chronic traumatic encephalopathy, traumatic encephalopathy syndrome, traumatic brain injury, biomarker, exosomes, multi-omics, transcriptomics, proteomics

Introduction

Chronic traumatic encephalopathy (CTE) is a neurodegenerative disease associated with exposure to repetitive head impacts, typically brain concussion and subconcussive trauma (Reams et al., 2016). Elderly people with declined mobility, athletes of full contact sports, military personnel and domestic violence victims are at high risk of CTE (Thompson et al., 2006; McKee, 2020). Different from single mild head trauma which always makes full recovery within a few days, patients with CTE have a chronic disease course, characterized by progressive neurological disorders due to cumulative brain injury, named traumatic encephalopathy syndrome (TES) (Montenigro et al., 2014).

The diagnosis of CTE can be confirmed only by post-mortem neuropathologic examination demonstrating a unique pattern of perivascular hyperphosphorylated tau deposition in neurons and astrocytes at the depths of cerebral sulci (McKee et al., 2013). In order to promote clinical evaluation, diagnosis and future research for CTE, an evidence-informed, expert consensus for the diagnostic framework of CTE was developed recently by the Diagnostics, Imaging, and Genetics Network for the Objective Study and Evaluation of CTE (DIAGNOSE CTE) Research Project (Katz et al., 2021). The consensus facilitates investigations into the clinical features of TES associated with CTE pathology, and closes significant knowledge gaps, including the development of diagnostic biomarkers for CTE. However, it is still limited by the lack of objective biomarkers, resulting in a complicated and time-consuming diagnosis course based on clinical manifestations, which can only be conducted by experienced clinicians.

Although there have been several studies on fluid biomarkers for CTE pathology (Pierre et al., 2021; Bergauer et al., 2022), most of them have the disadvantage of focusing on former professional football players, but not using age-matched control groups. In addition, the research did not perform high-throughput screening, but only tested for identified indicators of other neurodegenerative diseases (e.g., neurofilament light chain protein, total tau and phosphorylated tau-181), which have been found to be lack of specificity for CTE diagnosis. Besides, many investigations collected cerebrospinal fluid samples for biomarker exploration. This is understandable, but in clinical practice, obtaining cerebrospinal fluid requires an invasive lumbar puncture, which may cause additional pain to the patient. In addition, several potential neuroimaging biomarkers with high specificity and sensitivity have been reported (Alosco et al., 2021; Bergauer et al., 2022), including Tau-PET imaging, functional MRI measures of network connectivity, MRS (magnetic resonance spectroscopy) measures of neurochemical metabolism, and structural MRI measures of volumetric and white matter injury. However, the complex technical requirements and relatively expensive medical expenditure limit the application of the above neuroimaging methods in clinical practice. Consequently, there is an urgent need to explore reliable blood biomarkers to assist clinical diagnosis for CTE.

Recently, with the development of bioinformatics, the potential value of transcriptomic and proteomics information as disease biomarkers has aroused wide attention. Exosomes are small vesicles secreted by living cells into the extracellular space that function as important carriers of information transferred among cells. They contain a large number of specific proteins and functional nucleic acids, participate in pathophysiological processes, and correlated with the occurrence and progression of various diseases. Because the membrane structure of exosomes can protect their internal ribonucleic acid (RNA) from RNase degradation, exosomal RNA is more stable and has higher concentration than free RNA in serum or plasma. Besides, in view of the maturity of the isolation and purification technique for exosomes, exosomal RNAs and proteins have been regarded as an important source of clinical biomarkers. Therefore, exploring exosomal diagnostic biomarkers for CTE would be a breakthrough point to solve the problem of early and efficient diagnosis of the disease.

In the present study, we developed a population-based matched CTE cohort, and performed multi-omics screening to explore potential diagnostic biomarkers (RNAs and proteins)

Abbreviations: CTE, chronic traumatic encephalopathy; ELISA, Enzyme Linked Immunosorbent Assay; GO, Gene Ontology; KEGG, Kyoto Encyclopedia of Genes and Genomes; PPI, protein-protein Interaction; RT-PCR, Reverse Transcription—Polymerase Chain Reaction; TES, traumatic encephalopathy syndrome.

in blood and its exosomes. The verified biomarkers are expected to contribute to establishing a novel set of CTE diagnostic signatures with classic neurodegenerative indicators, thereby updating the consensus diagnostic criteria for CTE by incorporating new evidence of the *in vivo* biomarkers.

Materials and methods

Study population and experimental design

The present research was conducted as a pilot study of the clinical trial (ClinicalTrials Identifier: NCT04928534) we hosted, named observational cohort study of blood transcriptomics and proteomics information as biomarkers of TES, which is aimed at exploring a novel set of diagnostic signatures for CTE or TES by recruiting 120 subjects with the history of rmTBI. The inclusion of human subjects was approved by the Ethics Committees of Tianjin Medical University General Hospital (Grant No. IRB2021-YX-056-01). The work began in June, 2021, and is still open to the public till now.

In this research, blood samples were collected from 12 patients with rmTBI (6 female, 6 male) who visited Cadre Physical Examination Center or Department of Neurosurgery in Tianjin Medical University General Hospital from August, 2021 to July, 2022. Blood samples from 12 gender- and age-matched healthy subjects were used as controls. Inclusion criteria for patients with rmTBI are as follows: (1) Age $\geq$ 18 and $\leq$ 80 years old with independent behavior ability. (2) Have a clear history of rmTBI. (3) The most recent head injury occurred 3 months ago. Inclusion criteria for healthy controls are as follows: (1) Age $\geq$ 18 and $\leq$ 80 years old with independent behavior ability. (2) No history of repetitive mild TBI. (3) Generally healthy with normal basic laboratory tests. Exclusion criteria include pregnant or lactating women, past history of cancer, moderate to severe traumatic brain injury, other neurological or psychiatric disorders, complications of hematological diseases, severe cardiopulmonary diseases, hepatic failure, or renal failure. More detailed information of the trial protocol is specified in the trial registration.

All patients underwent an evaluation for determining the certainty of CTE pathology according to the expert consensus, in which 1 of them were diagnosed with probable CTE (high certainty), 3 of them were diagnosed with possible CTE (medium certainty), and other 8 patients were diagnosed with suggestive of CTE (low certainty). The 4 patients with probable or possible CTE and their matched healthy individuals were selected for multi-omics high-throughput assays (RNA microarray and proteomics sequencing). Their baseline characteristics are shown in **Supplementary Table 1**. All subjects underwent low-throughput verification experiments [reverse transcription—polymerase chain (RT-PCR) and enzyme linked immunosorbent assay (ELISA)] for the selected candidate biomarkers, including RNAs and proteins.

Collection of the blood and serum exosomes

Twenty milliliter blood samples were collected from all enrolled individuals in the morning after a 12-h fast and were kept in polypropylene tubes containing coagulant. They were centrifuged at 3,000 × g for 5 min at 4°C to obtain the serum (8–12 ml), and then stored at −80°C.

Six to eight milliliter serum samples were proceeded to collect exosomes using a TiO_2 magnet protocol (Gao et al., 2019). Briefly, the serum was incubated with TiO_2 microspheres (Q-0092910; QiYue Biology, Xi'an, China) at the concentration of 50 mg/ml for 5 min at 4°C on a thermos-shaker to allow sufficient enrichment. Exosomes were lysed from the surface of microspheres by washing three times with PBS, and were identified using electron microscopy, nanoparticle tracking analysis and surface biomarker (CD81; 1:1000, ab79559, Abcam, Cambridge, UK) detection by Western Blotting.

Extraction of free and exosomal ribonucleic acid/protein from serum

Free RNA from the serum sample (1–1.5 ml) was extracted using TRIzol reagent (15596026; Invitrogen, Carlsbad, CA, USA) and purified with a RNeasy mini kit (74104; Qiagen, Valencia, CA, USA). Free protein from another 1–1.5 ml serum sample was extracted by a serum protein extraction kit (EX1180; Solarbio, Beijing, China). Exosomal RNA and protein from the serum sample (6–9 ml) was extracted using the Total Exosome RNA and Protein Isolation Kit (Invitrogen) following the manufacturer's protocol.

RNA concentration of each sample was determined by NanoDrop ND-2000 Spectrophotometer (NanoDrop Technologies, Wilmington, DE, USA), and the quality was assessed with electrophoresis on 2% agarose gels. Protein concentration of each sample was quantified using spectrophotometry and the BCA (PC0020, Solarbio) method.

Ribonucleic acid microarray

Before microarray assay, total RNA was first amplified using the GeneChip^{TM} WT PLUS Piko Reagent Kit (902281; ThermoFisher Scientific, MA, USA). Biotinylated cDNA was then prepared from 250 ng total RNA according to the standard GeneChip^{TM} protocol (Affymetrix, CA, USA). Following labeling, fragmented cDNA was hybridized for 16 h at 45°C on Clariom^{TM} D Array and GeneChip^{TM} miRNA 4.0 Array. GeneChips were then washed and stained in the

GeneChip™ Fluidics Station 450. All arrays were scanned with GeneChip™ Scanner 3000 7G. The raw data was normalized by Transcriptome Analysis Console Software Version 4.0.1 with Robust Multichip Analysis algorithm using Affymetrix default analysis settings, and global scaling as a normalization method. Values presented are log2 RMA signal intensity. The threshold set for up- and down-regulated RNAs was more than 1.2-fold change with a *p*-value of less than 0.05. Hierarchical clustering was performed based on differentially expressed lncRNAs (DElncRNAs), circRNAs (DEcircRNAs), miRNAs (DEmiRNAs), and mRNAs (DEmRNAs) using R package Pheatmap Version 1.0.12 (OE biotech, Shanghai, China).

Proteomic sequencing

The protein sample was digested, prepared for transition library construction, and scanned by mass spectrometry using the data-independent acquisition (DIA) mode by Orbitrap mass spectrometer (Q Exactive HF-X, Thermo Fisher Scientific). The MS data of the single-shot subject samples were used to generate a hybrid library for protein identification and quantitation using Spectronaut software Version 15.7 (Biognosys AG, Switzerland). All searches were performed against the human UniProt reference proteome of canonical and isoform sequences with 20,373 entries downloaded in March 2022. Searches used carbamidomethylation as fixed modification, and acetylation of the protein N-terminus as well as oxidation of methionines as variable modifications. The trypsin/P proteolytic cleavage rule was applied, permitting a maximum of two miscleavages and a peptide length of 7–52 amino acids. Protein intensities were normalized using the Local Normalization algorithm based on a local regression model (Callister et al., 2006). Spectral library generation stipulated a minimum of three fragments per peptide, and maximally, the six best fragments were included. A *Q*-value of 1% for the precursor and protein were used, and protein quantities were reported only in samples that passed the filter. The significantly differentially expressed proteins (DEPs) were screened out if their absolute ratio of fold change > 1.20 with *Q*-value < 0.05 (OE biotech).

Gene ontology and Kyoto Encyclopedia of Genes and Genomes enrichment analyses for co-DEmRNAs and target genes of co-DEmiRNAs

Genes that were simultaneously differentially expressed in serum and its exosomes with the same trend (both up-regulated or down-regulated) were obtained for subsequent analysis. They were named as co-DEmRNAs, co-DEmiRNAs, co-DElncRNAs, and co-DEcircRNAs.

The Gene Ontology (GO) is a structured and controlled vocabulary of terms, which are subdivided into 3 non-overlapping ontologies, Molecular Function, Biological Process and Cellular Component. GO enrichment analysis was performed to analyze the primary function of a list of genes using the GO database.[1] Kyoto Encyclopedia of Genes and Genomes (KEGG) is a knowledge base for systematic analysis of gene functions, linking the genomic information with higher order functional information. The pathway enrichment analysis was used to find out the significant pathway of a list of genes using the KEGG database.[2] According to the obtained miRNA-mRNA interaction, GO and KEGG enrichment analyses for co-DEmRNAs and target genes of co-DEmiRNAs were carried out using the enrichment analysis tool of Metascape.[3]

Prediction of miRNA-mRNA, lncRNA-miRNA, and circRNA-miRNA regulation relationship

The interaction of miRNA-mRNA was predicted using the miRWalk 3.0,[4] an integrated public miRNA-target prediction database that includes the data from PITA, miRmap, miRanda, PicTar, and TargetScan. The predicted miRNA-mRNA pairs were then integrated with the data of co-DEmiRNAs and co-DEmRNAs to obtain their regulatory relationships.

The lncRNA-miRNA and circRNA-miRNA interaction prediction was performed using the ENCORI,[5] a website identified 1.5 million of RNA-RNA interactions through analyzing thousands of CLIP-seq and various high-throughput sequencing data. The screening criteria were number of supporting experiments low stringency R1, and the predicted lncRNA-miRNA and circRNA-miRNA pairs were integrated with the data of co-DElncRNAs and co-DEcircRNAs to obtain their regulatory relationships.

Co-expression analysis of co-DElncRNAs, co-DEcircRNAs, and co-DEmRNAs

Using the matrix data of co-DElncRNAs, co-DEcircRNAs, and co-DEmRNAs, the Pearson correlation coefficients was calculated for each lncRNA-mRNA and circRNA-mRNA pair. A correlated test was then performed to find significant pairs with the threshold of $|r| > 0.9$ and $p < 0.05$.

1 http://geneontology.org/
2 https://www.genome.jp/kegg/
3 https://metascape.org
4 http://mirwalk.umm.uni-heidelberg.de/
5 https://starbase.sysu.edu.cn/index.php

Construction of competing endogenous RNAs network

The ceRNA network was constructed to discover the ceRNA mechanism based on co-DERNAs, including co-DElncRNAs, co-DEcircRNAs, co-DEmiRNAs, and co-DEmRNAs. Briefly, the Pearson Correlation Coefficient between matched miRNA-mRNA, lncRNA-miRNA, circRNA-miRNA, lncRNA-Mrna, and circRNA-mRNA was computed using R function cor.test (Hmisc and corplot) based on their expression data. The significant correlation pair was defined with a correlation value of more than 0.99. For a given lncRNA-mRNA or circRNA-mRNA pair, both of them were targeted by a common miRNA, and co-expressed negatively with it. Such a lncRNA-miRNA-mRNA or circRNA-miRNA-mRNA pair was identified as competing ceRNA triplets. The two complex networks were finally integrated, and the visualization of the ceRNA network was built by software Cytoscape Version 3.6.0.

Construction of protein-protein interaction network

Based on the interactions of proteins in the KEGG database, global signal transduction network was generated to demonstrate the interaction among the DEPs, in order to select the key proteins with powerful ability to modulate others in the network. The visualization of PPI network was built by software Cytoscape Version 3.6.0. Briefly, to get the most closely related interaction pairs, the PPI score was set to 0.99 (high confidence). The CytoHubba plug-in Version 0.1 was used to analyze the network topology properties of the nodes, and obtain the significant ones by score ranking. The MCODE plug-in Version 2.0.2 was then used to analyze the most important clustering modules in the PPI network with a score threshold of more than 10.

Multi-omics analysis strategy

The results of high-throughput assays on blood samples from the 8 subjects include 4 datasets: serum free RNAs, serum free proteins, exosomal RNAs and exosomal proteins. Multi-omics analysis was performed following the steps as below: (1) Obtained serum and exosomal differentially expressed indicators on both mRNA and protein level. They were analyzed as the first part of candidate CTE biomarkers (KIF2A, FCER1G, GNAZ, RAP1B, and RSU1). (2) Obtained the intersection of serum free DEPs and exosomal DEPs. The indicators in the two intersections were analyzed as the second part of candidate CTE biomarkers (CHL1 and CFB). (3) Screened out hub genes with the highest connectivity in the ceRNA network as the third part of candidate CTE biomarkers (LIN7C, hsa-miR-297, hsa-miR-1183, NON-HSAT081066.2, AND NON-HSAT205595.1). (4) Screened out hub genes with the highest degree of link in the PPI network as the fourth part of candidate CTE biomarkers (APOA1, CFB, C1QA, C1QB, C1QC, and CD9). (5) Manually search the function of above candidate biomarkers using the GeneCards database[6] and the RNAdisease database,[7] and selected the genes (CHL1, KIF2A, LIN7C, hsa-miR-297, and hsa-miR-1183) that associated with neuropathology to ensure the diagnostic specificity. Their expression levels were further determined by low-throughput assays for blood samples from all 24 subjects in the cohort.

Enzyme linked immunosorbent assay

Low-throughput verification for potential protein biomarkers of CTE were performed using ELISA. The CHL1 concentration was determined by the ELISA kit (ABIN5510733; antibodies-online, Aachen, Germany) following the manufacturer's instructions.

Reverse transcription—polymerase chain reaction

Low-throughput verification for potential RNA biomarkers of CTE were performed using RT-PCR. Briefly, reverse transcription and PCR were performed using the Hairpin-it miRNA/mRNA RT-PCR Quantitation kit (GenePharma, Shanghai, China) with corresponding primers. GAPDH and U6 were used as the internal control for mRNA and miRNA quantification, respectively. All PCR reactions were performed using standard PCR conditions. The Ct value was detected by CFX Connect™ RT-PCR system (Bio-Rad, Hercules, CA USA), and the data were analyzed by means of $2^{-\Delta\Delta Ct}$ method on each group. The primers used were as follows: GAPDH, GCCAAGGCTGTGGGCAAGGT (forward) and TCTCCAGGCGGCACGTCAGA (reverse); U6, CTCGCTT CGGCAGCACA (forward) and AACGCTTCACGAATTT GCGT (reverse); KIF2A, ATTTTCTCTCATTGACCTGGCTG (forward) and ACTCCTTGAGTGCTAAAAGGC (reverse); LIN7C, TGCCGCCACAGAAACTTCAG (forward) and TGATGTCCACCGTCTCATAAACA (reverse); hsa-miR-297, GCAGATGTATGTGTGCATGTG (forward) and AGGTCCAGTTTTTTTTTTTTTTTCAT (reverse); hsa-miR-1183, CACTGTAGGTGATGGTGAGA (forward) and AGTTTTTTTTTTTTTTTGCCCACT (reverse).

6 https://www.genecards.org/
7 http://www.rnadisease.org/

Statistical analysis

The continuous variables were expressed as mean ± standard deviation, and compared using the Student's *t*-test or Wilcoxon rank sum test as appropriate. Categorical data were expressed as number (percentage) and compared using the chi-square test. Statistical analyses for GO and KEGG enrichment analysis were performed using Fisher's exact test. Pearson's correlation test was utilized to calculate the correlation coefficients between hub genes in the PPI network. All statistical analyses were performed using SPSS Statistics Version 27.0 (IBM, Armonk, NY, USA). A two-tailed *p*-value of less than 0.05 was considered to be statistically significant.

Results

Baseline characteristics of enrolled subjects

Twelve pairs of gender- and age-matched rmTBI patients with healthy subjects were enrolled in this research, and their demographic characteristics are presented in **Table 1**. First, no difference of age and gender was observed between groups. Second, we evaluated the degree of CTE diagnosis for the enrolled subjects using a grading method as follows: (1) Probable CTE. (2) Possible CTE. (3) Suggestive of CTE or only with rmTBI history. (4) Healthy control. Therefore, a lower score represents a higher possibility of clinical diagnosis, as patients with rmTBI history had a lower score than healthy subjects. Third, cognitive and neurobehavioral tests, including Mini-Mental State Examination (MMSE) (Folstein et al., 1975), Montreal Cognitive Assessment (MoCA) (Nasreddine et al., 2005) and Rivermead Post-Concussion Symptoms Questionnaire (RPQ) (King et al., 1995) as the consensus suggested. We found that rmTBI patients performed poorly on the tests compared with the healthy subjects, which suggested greater cognitive impairment and neurobehavioral dysregulation.

TABLE 1 Baseline characteristics of enrolled patients with rmTBI and control subjects.

Variables	rmTBI (n = 12)	Healthy (n = 12)	P-value
Age, Years	50.00 ± 3.11	49.08 ± 2.71	0.826
Male, n (%)	6 (50.0)	6 (50.0)	1.000
CTE degree	2.58 ± 0.19	4.00 ± 0.00	<0.001***
Cognitive and neurobehavioral tests			
MoCA	25.08 ± 0.72	29.33 ± 0.36	<0.001***
MMSE	27.66 ± 0.82	29.83 ± 0.17	0.020*
RPQ-3	1.75 ± 0.46	0.08 ± 0.08	<0.001***
RPQ-16	7.00 ± 1.75	1.17 ± 0.48	0.001**

The data were expressed as mean ± SD or n (%). *P < 0.05, **P < 0.01, ***P < 0.001. CTE, chronic traumatic encephalopathy; MMSE, Mini-Mental State Examination; MoCA, Montreal Cognitive Assessment; RPQ, Rivermead Post-Concussion Symptoms Questionnaire.

Acquisition of DERNAs and differentially expressed proteins in serum and exosomes

The results of RNA microarray and proteomic sequencing for 4 pairs of gender- and age-matched CTE patients with healthy subjects were comprehensively analyzed, and the original data were uploaded as **Supplementary Data Sheets**. As shown in **Figure 1**, the distribution of DERNAs and DEPs were nearly identical after normalization within a group. According to the screening criterion, 1,189 DEmRNAs (1,049 up-regulated and 140 down-regulated), 249 DEmiRNAs (39 up-regulated and 210 down-regulated), 4,235 DElncRNAs (1,412 up-regulated and 2,823 down-regulated), 77 DEcircRNAs (32 up-regulated and 45 down-regulated), and 24 DEPs (17 up-regulated and 7 down-regulated) were found in serum. In addition, 1,359 DEmRNAs (335 up-regulated and 1,024 down-regulated), 251 DEmiRNAs (101 up-regulated and 140 down-regulated), 3,759 DElncRNAs (1,189 up-regulated and 2,570 down-regulated), 94 DEcircRNAs (21 up-regulated and 73 down-regulated), and 190 DEPs (154 up-regulated and 36 down-regulated) were identified in serum exosomes.

Gene ontology and Kyoto Encyclopedia of Genes and Genomes enrichment analyses for co-DEmRNAs and target genes of co-DEmiRNAs

The co-DEmRNAs and co-DEmiRNAs were defined as mRNAs and miRNAs that were both up-regulated or down-regulated in serum and its exosomes of the 4 CTE patients, compared with healthy subjects. A functional enrichment analysis was performed for co-DEmRNAs and target genes of co-DEmiRNAs, and the top 10 GO and all KEGG pathway terms are shown in **Figure 2**.

In terms of biological progress of GO analysis, the genes were significantly enriched in synaptic vesicle uncoating, protein localized to basolateral plasma membrane, protein depolymerization, synaptic vesicle endocytosis, presynaptic endocytosis, cellular protein complex disassembly, protein-containing complex disassembly, neurotransmitter secretion, cellular component disassembly, and positive regulation of hydrolase activity, most of which are associated with synaptic function. Regarding cellular component of GO analysis, the enriched terms included bicellular tight junction, postsynaptic density, asymmetric synapse, postsynaptic specialization, neuron to neuron synapse, presynapse, anchoring junction, adherens junction, postsynapse, and synapse part. The

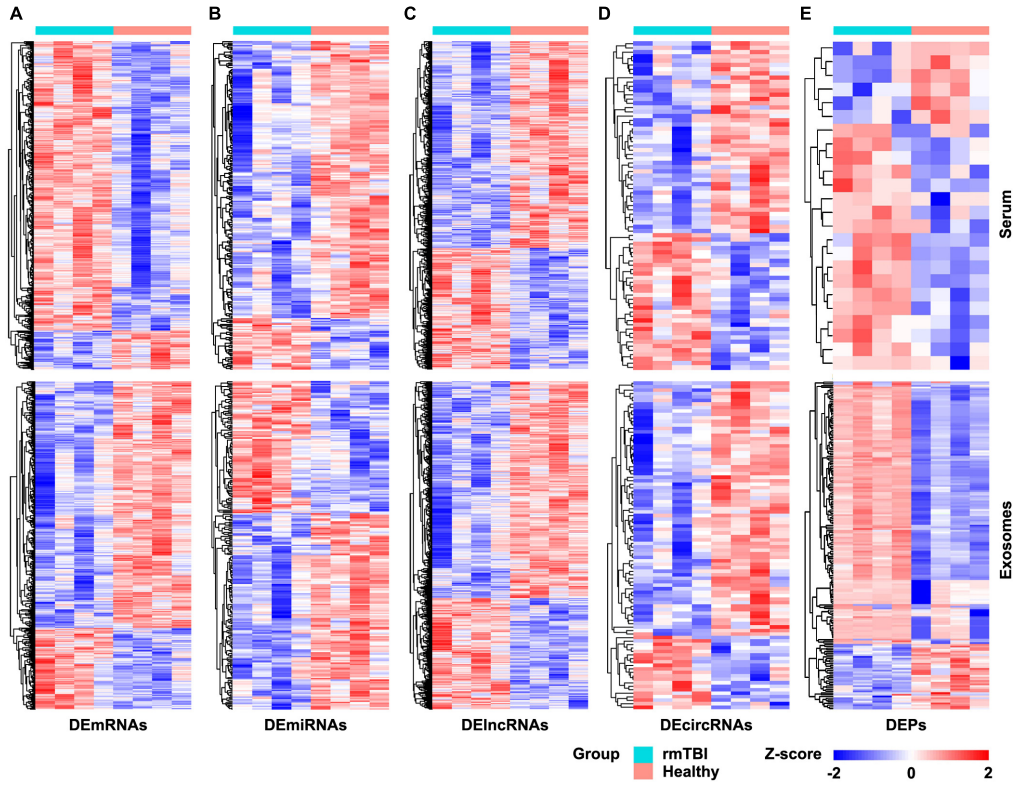

FIGURE 1
Heatmap of DERNAs and DEPs in serum and exosomes between patients with rmTBI and healthy subjects. **(A)** DEmRNAs in serum and exosomes. **(B)** DEmiRNAs in serum and exosomes. **(C)** DElncRNAs in serum and exosomes. **(D)** DEcircRNAs in serum and exosomes. **(E)** DEPs in serum and exosomes. Up-regulated genes are shown in red, and down-regulated genes are shown in blue. DE, differentially expressed; DEPs, differentially expressed proteins.

function of them are related to tight junction (important component of blood-brain barrier) and neurotransmitter. As to molecular function of GO analysis, peptide-aspartate beta-dioxygenase activity, L27 domain binding, structural constituent of muscle, oxidoreductase activity, clathrin binding, PDZ domain binding, dioxygenase activity, protein tyrosine phosphatase activity, electron transfer activity, and protein domain specific binding were enriched. For KEGG analysis, the most significantly enriched pathways were cardiac muscle contraction, transcriptional misregulation in cancer, calcium signaling pathway and endocytosis. Consequently, changes in the expression levels of co-DEmRNAs and target genes of co-DEmiRNAs in serum and exosomes may reflect altered function on synapse-mediated neurotransmitter transmission and blood-brain barrier permeability after rmTBI.

Competing endogenous RNA network of co-DERNAs

Using the matrix data of co-DERNAs and online tools to predict their regulation relationship, 4 DElncRNAs were found to target 2 DEmiRNAs, which are able to bind 3 DEmRNAs. A ceRNA network was thus constructed according to the lncRNA-miRNA-mRNA triplets (Figure 3A). Then, the hub genes with the highest connectivity in the network were acquired as candidate CTE biomarkers (LIN7C, hsa-miR-297, hsa-miR-1183, NON-HSAT081066.2, AND NON-HSAT205595.1) for further analysis.

Protein-protein interaction network and correlations of differentially expressed proteins in serum and exosomes

The PPI network of DEPs in serum and exosomes were constructed individually based on their interaction relationship in the KEGG database. As shown in Figure 3B, we found 17 hub genes in the PPI network of serum DEPs, which included APOA1, C1QA, C1QB, C1QC, CETP, CFB, CFHR3, CHL1, ECM1, EFEMP1, LCAT, LRG1, LYVE1, ORM1, PFN1, TPM4, and YWHAZ. In addition, 10 hub genes were screened out from the PPI network of exosomes DEPs. They were ADAM10,

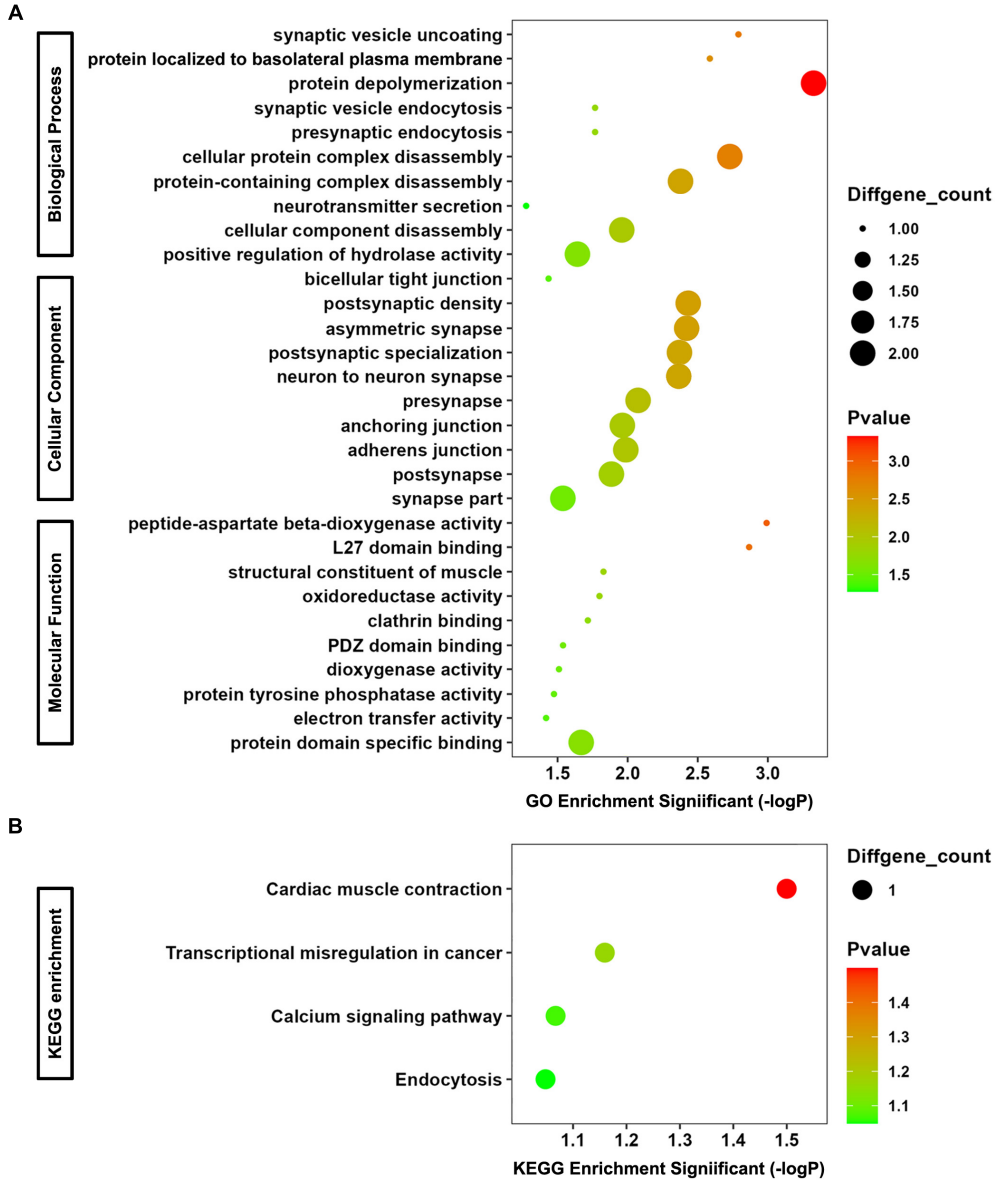

FIGURE 2
GO and KEGG Enrichment Analyses for co-DEmRNAs and target genes of co-DEmiRNAs. **(A)** Bubble chart of GO analysis. **(B)** Bubble chart of KEGG analysis.

ANXA3, BRK1, CD151, CD9, COL1A1, CYFIP1, SLC44A1, TPM1, and VIM.

Hub genes with more than 3 links in the PPI network of DEPs in serum, and those with more than 2 links in the PPI network of DEPs in exosomes were selected for the Pearson correlation analysis (Figure 3C). We found that no DEP showed a $|r|$ value of more than 0.8 (or p-values of less than 0.01) with all the other DEPs. In addition, GO and KEGG Enrichment Analyses were performed, which indicated that the genes were enriched in synapse pruning, cell junction disassembly, integrin binding complement activation, immune effector process, regulation of immune system process, and complement/coagulation cascades.

Potential diagnostic biomarkers for chronic traumatic encephalopathy confirmed by low-throughput assays

The candidate CTE biomarkers (CHL1 protein, KIF2A mRNA, LIN7C mRNA, hsa-miR-297, and hsa-miR-1183) were screened out through multi-omics analysis using Venn map

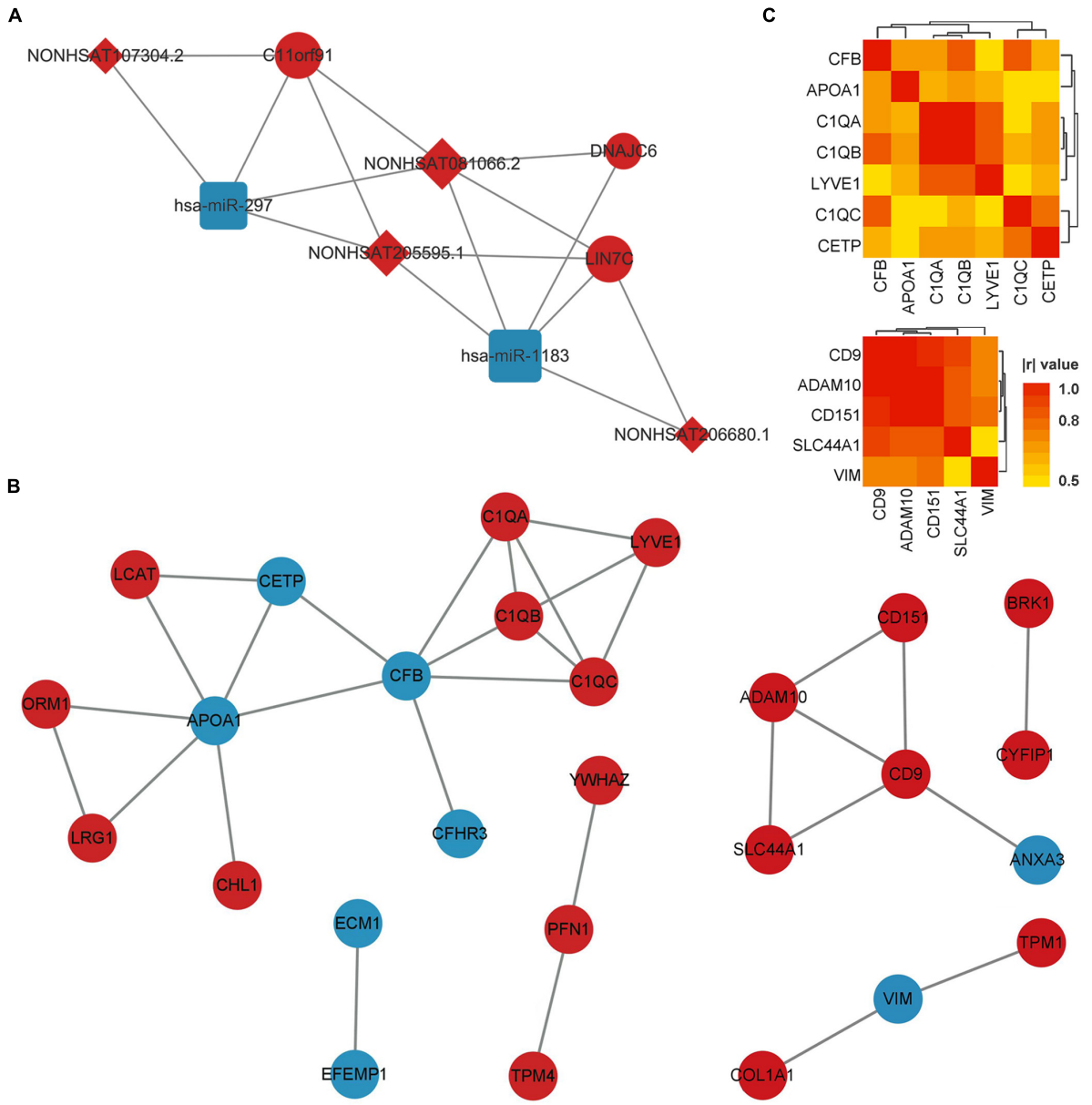

FIGURE 3
ceRNA network of co-DERNAs and PPI network of DEPs in serum and exosomes. **(A)** ceRNA network of co-DERNAs. A circle represents a mRNA, a square represents a miRNA, a rhombus represents a lncRNA, and relationships between them are represented by edges. **(B)** PPI network of DEPs in serum and exosomes. Nodes represent the proteins, and edges represent relationships. Up-regulated genes and proteins are shown in red, and down-regulated genes and proteins are shown in blue. **(C)** Heatmap of correlations among the hub genes in the PPI network of DEPs in serum and exosomes. PPI, protein-protein interaction; DEPs, differentially expressed proteins; DERNAs, differentially expressed RNAs.

(Figure 4) and functional investigation by online database. Their expression levels were further determined by ELISA and RT-PCR for blood samples from all 24 subjects in the cohort. We found that serum and exosomal CHL1 protein level was decreased in rmTBI patients compared with the healthy controls, which are consistent with the results of proteomic sequencing (Figure 5A). Besides, the mRNA level of KIF2A in serum and exosomes were both up-regulated in patients with rmTBI (Figure 5B). However, no difference was observed on serum and exosomal LIN7C mRNA level, as well as serum miR-297 level between patients with rmTBI and healthy subjects, suggesting that they are not suitable biomarkers for CTE (Figures 5C,D). In addition, exosomal miR-297, serum miR-1183, and exosomal miR-1183 levels were all down-regulated in rmTBI patients (Figures 5D,E). These findings indicated that serum and exosomal CHL1, KIF2A and miR-1183, as well

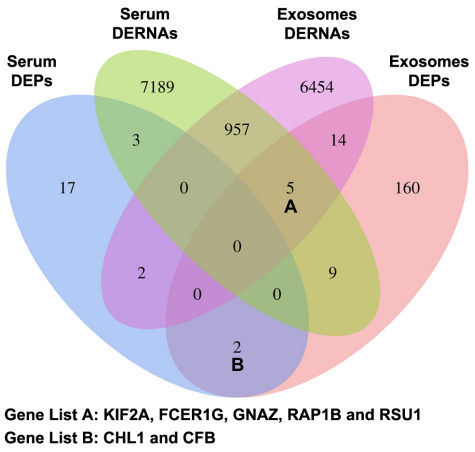

FIGURE 4
Venn map of DERNAs and DEPs in serum and exosomes between patients with rmTBI and healthy subjects. DERNAs, differentially expressed RNAs; DEPs, differentially expressed proteins.

as exosomal miR-297 are the potential diagnostic signatures for CTE.

Discussion

Patients with CTE are characterized by progressive neurological disorders. Their clinical symptoms mainly include cognitive decline, behavioral change, emotional dysregulation and motor disturbance (Reams et al., 2016). The cognitive decline typically affects more than one domain of neurological deficits including executive, visuospatial, memory, and language. Patients with mainly behavioral change may exhibit violence, poor impulse control, socially inappropriate behavior, avolition, apathy, change in personality, and comorbid substance abuse. The emotional dysregulation includes depression, anxiety, agitation, aggression, paranoid ideation, deterioration of interpersonal relationships, and suicidality, while the motor disturbance contains bradykinesia, tremor, rigidity, gait instability, dysarthria, dysphagia, ataxia, and gaze disturbance. Consequently, the clinical symptoms of CTE could be very difficult to identify, which leads to a complicated and time-consuming diagnosis course in accordance with the current expert consensus.

In order to explore novel blood signatures to improve the diagnostic framework of CTE, we started the observational cohort study of blood transcriptomics and proteomics information as biomarkers of TES in 2021. In the present research, we collected blood samples from the first 12 pairs of rmTBI patients with healthy volunteers that had been recruited for the cohort. By high-throughput multi-omics screening, we found that co-DEmRNAs, target genes of co-DEmiRNAs and hub genes of the PPI network in serum and exosomes were significantly enriched in synapse-mediated neurotransmitter transmission and blood-brain barrier permeability. It is worth noting that chronic synaptic adaptation and reorganization, as well as blood-brain barrier breakdown and repair are indeed important neuropathological changes in CTE, and associated with the cognitive dysfunction (Sweeney et al., 2018; Kim et al., 2021; Sloley et al., 2021). On this basis, serum and exosomal CHL1, KIF2A, and miR-1183, as well as exosomal miR-297 were further identified to be potential diagnostic biomarkers for CTE using low-throughput verification experiments.

CHL1 protein is a member of the L1 gene family of neural cell adhesion molecules. It is a neural recognition molecule that involves in L1CAM interactions, nervous system development and synaptic plasticity. Specifically, it could promote neurite outgrowth of hippocampal neurons, suppress neuronal cell death, and regulate cell migration in nerve regeneration and cortical development. CHL1 also plays a role in positioning of pyramidal neurons, regulating the number of interneurons and the efficacy of GABAergic synapses, and potentiating integrin-dependent cell migration toward extracellular matrix proteins (Schmid and Maness, 2008; Irintchev and Schachner, 2012). These functions are consistent with our findings on GO and KEGG enrichment analysis, in which synapse, tight junction and related biological progress were significantly enriched. Therefore, the observed decreased CHL1 protein level suggested the neural and synaptic damage following rmTBI. KIF2A, named Kinesin Family Member 2A, encodes protein that is required for normal spindle activity during mitosis and brain development. Its dysfunction is associated with cortical dysplasia and brain malformations. KIF2A may also regulate synaptic transmission and axonal transport coupled with neuroinflammation, as well as microtubule dynamics during axonal growth (Chung et al., 2009; Niwa, 2015). As neural inflammation is the most crucial neuropathology that leads to neural death, neurodegeneration and subsequent cognitive impairment (Morganti-Kossmann et al., 2019), it's up-regulation in serum and exosomes observed in rmTBI patients may be a manifestation of the neuroprotective compensatory mechanism. miR-297 and miR-1183 are potential biomarkers for a series of neurological diseases, including ischemic stroke, intracerebral hemorrhage, intracranial aneurysm, Moyamoya disease, Parkinson's disease, and glioma manifested by the RNAdisease database. From this, it could be inferred that their decrease following rmTBI may be an indicator of both acute and chronic brain injury.

The verified biomarkers are expected to contribute to CTE diagnosis. However, several limitations, especially the small cohort size should be taken into account when interpreting the results. First, according to the provisional levels of certainty for CTE pathology proposed by the expert consensus, the patients we recruited were classified as 1 probable CTE, 3 possible CTE and 8 suggested of CTE or only with rmTBI history. Due to the low incidence of the disease, we failed to follow the

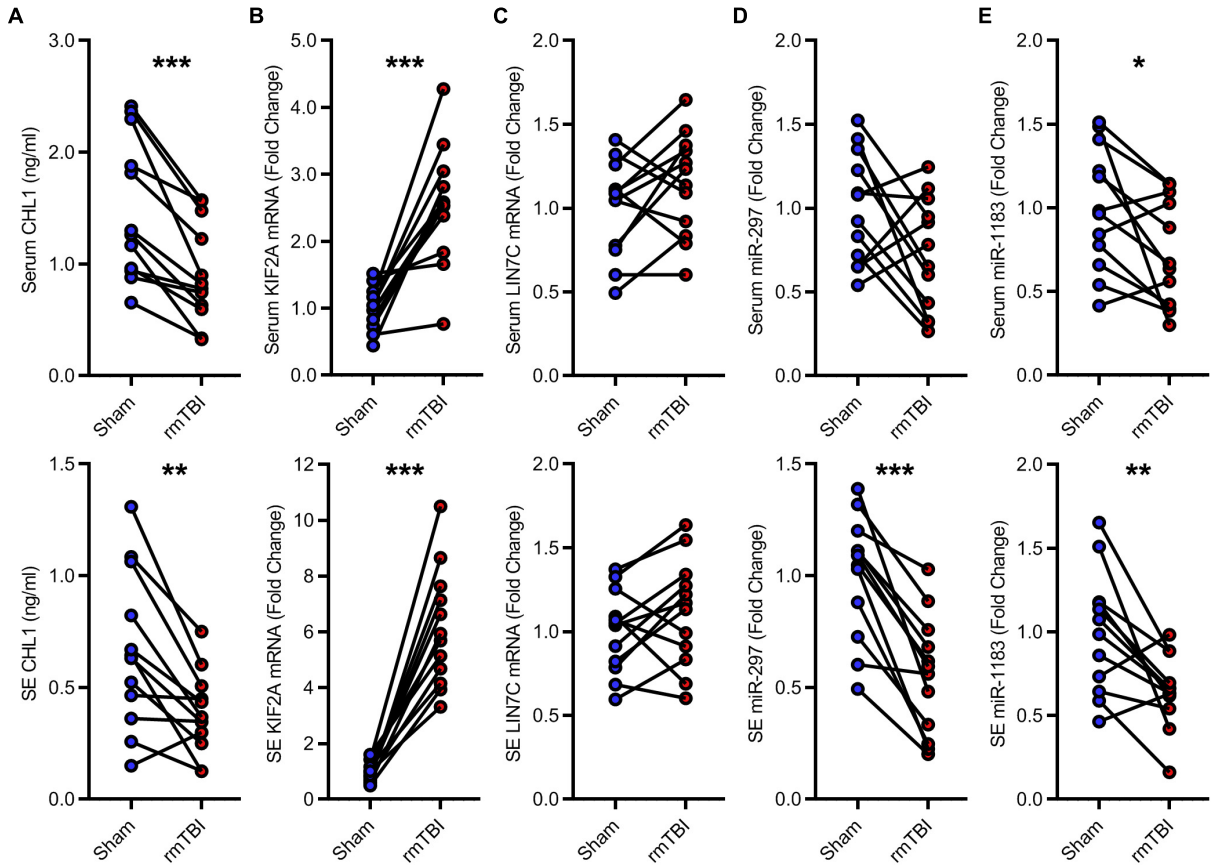

FIGURE 5
Low-throughput assays for candidate diagnostic biomarkers for CTE. **(A)** Quantitative data of ELISA for serum and exosomal CHL1 level in indicated groups. **(B–E)** Quantitative data of RT-PCR for serum and exosomal KIF2A, LIN7C, hsa-miR-297, hsa-miR-1183. $n = 12$ per group. Mean ± SD. $^{*}P < 0.05$, $^{**}P < 0.01$, $^{***}P < 0.001$. Statistical analyses were performed using two-tailed paired Student's t-test. SE, serum exosomes.

opinions of expert consensus, in which cohorts of patients with probable CTE as primary subjects are recommended for the biomarker study. It may lead to a decrease in the specificity of the biomarkers we found. Second, the small sample size for high-throughput sequencing and low-throughput verification assays may result in the screened differentially expressed RNAs and proteins cannot well reveal characteristics of the whole CTE population due to individual differences. Therefore, we did not depict Receiver-Operating Characteristic curve to show the outcome prediction performance of each potential biomarker, or compare with that of classic neurodegenerative biomarkers, in order to avoid their misuse in future research and clinical diagnosis.

Conclusion

In conclusion, this research is a pilot study of our ongoing cohort study (ClinicalTrials.gov Identifier: NCT04928534). It provides effective methodologies for managing subsequent large-scale cohort study and analyzing the multi-omics big data. Although the potential biomarkers for CTE we found are not recommended to be directly applied to clinical use, they contribute to further studies on establishing a novel set of CTE diagnostic signatures with classic neurodegenerative indicators. As specified in the trial registration, our research team will continue to develop a CTE cohort including 120 strictly matched rmTBI patients and healthy subjects, aiming to update the consensus diagnostic criteria by incorporating solid evidence of the *in vivo* biomarkers.

Data availability statement

The RNA microarray and proteomic sequencing datasets for this study can be found in the ArrayExpress database (Accession numbers: E-MATB-12328, E-MATB-12329, E-MATB-12330, and E-MATB-12331) and the ProteomeXchange database (Project ID: PXD037637). The processed matrix data of high-throughput assays can be found in the **Supplementary material**.

Ethics statement

The studies involving human participants were reviewed and approved by the Ethics Committees of Tianjin Medical University General Hospital (Grant No. IRB2021-YX-056-01). The patients/participants provided their written informed consent to participate in this study.

Author contributions

XG and PL were responsible to conception and design of the study. XG developed the method, performed data visualization, statistical analysis, and wrote the manuscript. ML, MG, and LZ conducted laboratory examinations. SZ, JQ, LC, WL, YW, JY, ZY, and WT contributed to cohort recruitment. FC provided methodological supports. PL reviewed the manuscript. All authors contributed to manuscript revision, read, and approved the submitted version.

Funding

This research was supported by the Haihe Laboratory of Cell Ecosystem Innovation Fund (HH22KYZX0048), the National Natural Science Foundation of China (82071394, 82271401, and 82072166), the Science and Technology Foundation of Tianjin (21JCYBJC01180), and the Science and Technology Project of Tianjin Municipal Health Commission (TJWJ2021QN005).

Acknowledgments

We express acknowledgments to Dongdong Jia from Sheweisi Biotechnology Co., Ltd., for the technical support.

Conflict of interest

The authors declare that the research was conducted in the absence of any commercial or financial relationships that could be construed as a potential conflict of interest.

Publisher's note

All claims expressed in this article are solely those of the authors and do not necessarily represent those of their affiliated organizations, or those of the publisher, the editors and the reviewers. Any product that may be evaluated in this article, or claim that may be made by its manufacturer, is not guaranteed or endorsed by the publisher.

Supplementary material

The Supplementary Material for this article can be found online at: https://www.frontiersin.org/articles/10.3389/fnagi.2022.1052765/full#supplementary-material

References

Alosco, M., Culhane, J., and Mez, J. (2021). Neuroimaging biomarkers of chronic traumatic encephalopathy: Targets for the academic memory disorders clinic. *Neurotherapeutics* 18, 772–791. doi: 10.1007/s13311-021-01028-3

Bergauer, A., van Osch, R., van Elferen, S., Gyllvik, S., Venkatesh, H., and Schreiber, R. (2022). The diagnostic potential of fluid and imaging biomarkers in chronic traumatic encephalopathy (CTE). *Biomed. Pharmacother.* 146:112602. doi: 10.1016/j.biopha.2021.112602

Callister, S., Dominguez, M., Nicora, C., Zeng, X., Tavano, C., Kaplan, S., et al. (2006). Application of the accurate mass and time tag approach to the proteome analysis of sub-cellular fractions obtained from *Rhodobacter sphaeroides* 2.4.1. Aerobic and photosynthetic cell cultures. *J. Proteome Res.* 5, 1940–1947. doi: 10.1021/pr060050o

Chung, C., Koprich, J., Siddiqi, H., and Isacson, O. (2009). Dynamic changes in presynaptic and axonal transport proteins combined with striatal neuroinflammation precede dopaminergic neuronal loss in a rat model of AAV alpha-synucleinopathy. *J. Neurosci.* 29, 3365–3373. doi: 10.1523/jneurosci.5427-08.2009

Folstein, M., Folstein, S., and McHugh, P. (1975). Mini-mental state". A practical method for grading the cognitive state of patients for the clinician. *J. Psychiatr. Res.* 12, 189–198. doi: 10.1016/0022-3956(75)90026-6

Gao, F., Jiao, F., Xia, C., Zhao, Y., Ying, W., Xie, Y., et al. (2019). A novel strategy for facile serum exosome isolation based on specific interactions between phospholipid bilayers and TiO. *Chem. Sci.* 10, 1579–1588. doi: 10.1039/c8sc04197k

Irintchev, A., and Schachner, M. (2012). The injured and regenerating nervous system: Immunoglobulin superfamily members as key players. *Neuroscientist* 18, 452–466. doi: 10.1177/1073858411419047

Katz, D., Bernick, C., Dodick, D., Mez, J., Mariani, M., Adler, C., et al. (2021). National institute of neurological disorders and stroke consensus diagnostic criteria for traumatic encephalopathy syndrome. *Neurology* 96, 848–863. doi: 10.1212/wnl.0000000000011850

Kim, J., Jung, H., Kim, A., Shim, H., Hyeon, S., Lee, Y., et al. (2021). Hevin-calcyon interaction promotes synaptic reorganization after brain injury. *Cell Death Differ.* 28, 2571–2588. doi: 10.1038/s41418-021-00772-5

King, N. S., Crawford, S., Wenden, F. J., Moss, N. E., and Wade, D. T. (1995). The Rivermead Post Concussion Symptoms Questionnaire: A measure of symptoms commonly experienced after head injury and its reliability. *J. Neurol.* 242, 587–592. doi: 10.1007/BF00868811

McKee, A. (2020). The neuropathology of chronic traumatic encephalopathy: The status of the literature. *Semin. Neurol.* 40, 359–369. doi: 10.1055/s-0040-1713632

McKee, A., Stern, R., Nowinski, C., Stein, T., Alvarez, V., Daneshvar, D., et al. (2013). The spectrum of disease in chronic traumatic encephalopathy. *Brain* 136, 43–64. doi: 10.1093/brain/aws307

Montenigro, P. H., Baugh, C. M., Daneshvar, D. H., Mez, J., Budson, A. E., Au, R., et al. (2014). Clinical subtypes of chronic traumatic encephalopathy: Literature review and proposed research diagnostic criteria for traumatic

encephalopathy syndrome. *Alzheimers Res. Ther.* 6:68. doi: 10.1186/s13195-014-0068-z

Morganti-Kossmann, M., Semple, B., Hellewell, S., Bye, N., and Ziebell, J. (2019). The complexity of neuroinflammation consequent to traumatic brain injury: From research evidence to potential treatments. *Acta Neuropathol.* 137, 731–755. doi: 10.1007/s00401-018-1944-6

Nasreddine, Z., Phillips, N., Bédirian, V., Charbonneau, S., Whitehead, V., Collin, I., et al. (2005). The montreal cognitive assessment, MoCA: A brief screening tool for mild cognitive impairment. *J. Am. Geriatr. Soc.* 53, 695–699. doi: 10.1111/j.1532-5415.2005.53221.x

Niwa, S. (2015). Kinesin superfamily proteins and the regulation of microtubule dynamics in morphogenesis. *Anatom. Sci. Int.* 90, 1–6. doi: 10.1007/s12565-014-0259-5

Pierre, K., Dyson, K., Dagra, A., Williams, E., Porche, K., and Lucke-Wold, B. (2021). Chronic traumatic encephalopathy: Update on current clinical diagnosis and management. *Biomedicines* 9:415. doi: 10.3390/biomedicines9040415

Reams, N., Eckner, J. T., Almeida, A. A., Aagesen, A. L., Giordani, B., Paulson, H., et al. (2016). A clinical approach to the diagnosis of traumatic encephalopathy syndrome: A review. *JAMA Neurol.* 73, 743–749. doi: 10.1001/jamaneurol.2015.5015

Schmid, R., and Maness, P. (2008). L1 and NCAM adhesion molecules as signaling coreceptors in neuronal migration and process outgrowth. *Curr. Opin. Neurobiol.* 18, 245–250. doi: 10.1016/j.conb.2008.07.015

Sloley, S., Main, B., Winston, C., Harvey, A., Kaganovich, A., Korthas, H., et al. (2021). High-frequency head impact causes chronic synaptic adaptation and long-term cognitive impairment in mice. *Nat. Commun.* 12:2613. doi: 10.1038/s41467-021-22744-6

Sweeney, M., Sagare, A., and Zlokovic, B. (2018). Blood-brain barrier breakdown in Alzheimer disease and other neurodegenerative disorders. *Nat. Rev. Neurol.* 14, 133–150. doi: 10.1038/nrneurol.2017.188

Thompson, H. J., McCormick, W. C., and Kagan, S. H. (2006). Traumatic brain injury in older adults: Epidemiology, outcomes, and future implications. *J. Am. Geriatr. Soc.* 54, 1590–1595. doi: 10.1111/j.1532-5415.2006.00894.x

frontiers | Frontiers in Aging Neuroscience

TYPE Original Research
PUBLISHED 05 December 2022
DOI 10.3389/fnagi.2022.1032401

Check for updates

OPEN ACCESS

EDITED BY
Jun Xu,
Capital Medical University,
China

REVIEWED BY
Sakhawat Ali,
Beijing Institute of Technology,
China
Muqaddas Masood,
Shanghai Institutes for Biological
Sciences (CAS), China

*CORRESPONDENCE
Shaonan Hu
shaonan_hu@smu.edu.cn
Shaohong Huang
hsh.china@tom.com

†These authors have contributed equally to this work and share first authorship

‡Senior author

SPECIALTY SECTION
This article was submitted to
Cellular and Molecular Mechanisms
of Brain-aging,
a section of the journal
Frontiers in Aging Neuroscience

RECEIVED 30 August 2022
ACCEPTED 16 November 2022
PUBLISHED 05 December 2022

CITATION
Hu S, Li S, Ning W, Huang X, Liu X, Deng Y, Franceschi D, Ogbuehi AC, Lethaus B, Savkovic V, Li H, Gaus S, Zimmerer R, Ziebolz D, Schmalz G and Huang S (2022) Identifying crosstalk genetic biomarkers linking a neurodegenerative disease, Parkinson's disease, and periodontitis using integrated bioinformatics analyses. *Front. Aging Neurosci.* 14:1032401. doi: 10.3389/fnagi.2022.1032401

COPYRIGHT
© 2022 Hu, Li, Ning, Huang, Liu, Deng, Franceschi, Ogbuehi, Lethaus, Savkovic, Li, Gaus, Zimmerer, Ziebolz, Schmalz and Huang. This is an open-access article distributed under the terms of the Creative Commons Attribution License (CC BY). The use, distribution or reproduction in other forums is permitted, provided the original author(s) and the copyright owner(s) are credited and that the original publication in this journal is cited, in accordance with accepted academic practice. No use, distribution or reproduction is permitted which does not comply with these terms.

Identifying crosstalk genetic biomarkers linking a neurodegenerative disease, Parkinson's disease, and periodontitis using integrated bioinformatics analyses

Shaonan Hu[1*†], Simin Li[1†], Wanchen Ning[1], Xiuhong Huang[1], Xiangqiong Liu[2], Yupei Deng[2], Debora Franceschi[3], Anthony Chukwunonso Ogbuehi[4], Bernd Lethaus[5], Vuk Savkovic[5], Hanluo Li[5], Sebastian Gaus[5], Rüdiger Zimmerer[5], Dirk Ziebolz[6], Gerhard Schmalz[6‡] and Shaohong Huang[1*]

[1]Stomatological Hospital, Southern Medical University, Guangzhou, China, [2]Laboratory of Molecular Cell Biology, Beijing Tibetan Hospital, China Tibetology Research Center, Beijing, China, [3]Department of Experimental and Clinical Medicine, University of Florence, Florence, Italy, [4]Faculty of Physics, University of Münster, Münster, Germany, [5]Department of Cranio Maxillofacial Surgery, University Clinic Leipzig, Leipzig, Germany, [6]Department of Cariology, Endodontology and Periodontology, University of Leipzig, Leipzig, Germany

Objective: To identify the genetic linkage mechanisms underlying Parkinson's disease (PD) and periodontitis, and explore the role of immunology in the crosstalk between both these diseases.

Methods: The gene expression omnibus (GEO) datasets associated with whole blood tissue of PD patients and gingival tissue of periodontitis patients were obtained. Then, differential expression analysis was performed to identify the differentially expressed genes (DEGs) deregulated in both diseases, which were defined as crosstalk genes. Inflammatory response-related genes (IRRGs) were downloaded from the MSigDB database and used for dividing case samples of both diseases into different clusters using k-means cluster analysis. Feature selection was performed using the LASSO model. Thus, the hub crosstalk genes were identified. Next, the crosstalk IRRGs were selected and Pearson correlation coefficient analysis was applied to investigate the correlation between hub crosstalk genes and hub IRRGs. Additionally, immune infiltration analysis was performed to examine the enrichment of immune cells in both diseases. The correlation between hub crosstalk genes and highly enriched immune cells was also investigated.

Results: Overall, 37 crosstalk genes were found to be overlapping between the PD-associated DEGs and periodontitis-associated DEGs. Using clustering analysis, the most optimal clustering effects were obtained for periodontitis and PD when k=2 and k=3, respectively. Using the LASSO feature selection, five hub crosstalk genes, namely, FMNL1, MANSC1, PLAUR, RNASE6, and TCIRG1,

were identified. In periodontitis, MANSC1 was negatively correlated and the other four hub crosstalk genes (FMNL1, PLAUR, RNASE6, and TCIRG1) were positively correlated with five hub IRRGs, namely, AQP9, C5AR1, CD14, CSF3R, and PLAUR. In PD, all five hub crosstalk genes were positively correlated with all five hub IRRGs. Additionally, RNASE6 was highly correlated with myeloid-derived suppressor cells (MDSCs) in periodontitis, and MANSC1 was highly correlated with plasmacytoid dendritic cells in PD.

Conclusion: Five genes (i.e., FMNL1, MANSC1, PLAUR, RNASE6, and TCIRG1) were identified as crosstalk biomarkers linking PD and periodontitis. The significant correlation between these crosstalk genes and immune cells strongly suggests the involvement of immunology in linking both diseases.

KEYWORDS

neurodegenerative disease, Parkinson's disease, periodontitis, crosstalk genes, bioinformatics

Introduction

Parkinson's disease (PD) is a chronic, debilitating, neurodegenerative disorder with both motor and nonmotor symptoms that gradually worsen over time (Blaszczyk, 2016). Systemic inflammatory response plays a critical role in the progression of PD by activating microglial cells and initiating the cascade of neurodegeneration (Kaur et al., 2016). Periodontitis is a highly prevalent, multifactorial, chronic inflammatory disease of the periodontium, which causes destruction of the supportive tissues of the teeth and, eventually, tooth loss (Kaur et al., 2018). Several previous epidemiological studies have indicated a possible link between periodontal disease and PD. Some studies have reported that PD patients have a higher prevalence and risk of developing periodontal disease compared to a person without PD (Schwarz et al., 2006; Hanaoka and Kashihara, 2009). The cognitive dysfunction of PD patients prevented them from effectively performing routine daily oral hygiene activities (Al-Omari et al., 2014). Additionally, one of the side effects of multiple medications was altered salivary flow rates, thereby affecting self-cleaning oral mechanisms (Auffret et al., 2021). In other studies, periodontitis was found to be associated with an increased risk of developing PD (Chen et al., 2017). The ulcerations in the periodontal pocket lining provided easy access for periodontal pathogens (e.g., *Aggregatibacter actinomycetemcomitans* (Aa), *Porphyromonas gingivalis* (Pg), *Tannerella forsythia* (Tf), *Treponema denticola* (Td), and *Fusobacterium nucleatum* (Fn)) and inflammatory mediators (e.g., pro-inflammatory cytokines) to infiltrate the systemic peripheral blood circulation (Scannapieco, 2004). Lipopolysaccharide (LPS), an endotoxin and component of the Gram-negative bacterial cell wall, caused the breakdown of the blood brain barrier (BBB) and activated the microglial cells, which led to the necrosis and apoptosis of dopaminergic neurons in the substantia nigra (SN) of the midbrain (Bohatschek et al., 2001; Olsen et al., 2020).

Apart from inflammatory response, systemic immune activation may be another link connecting periodontitis and PD. It is suggested that periodontitis triggers the systemic immune response, following which the activated immune cells from the peripheral blood overcome the BBB and promote central nervous system (CNS) inflammation in PD patients (Zhang et al., 2021). Further, certain genetic susceptibility factors have been demonstrated to increase the risk of both periodontitis and PD (Tettamanti et al., 2017; Karimi-Moghadam et al., 2018). A previous study conducted by João Botelho and colleagues analyzed the Genome-Wide Association Studies (GWAS) data and identified the protein variants strongly associated with PD and periodontitis onset (Botelho et al., 2020). However, it may be worthy to note that a potential limitation of this research is that its study design was not from an inflammatory or immunological perspective. Thus, to fill this gap, our current study aimed to explore the missing genetic links between PD and periodontitis, particularly focusing on inflammatory response-associated genes and immune cells.

Many previous studies used computational biology approaches to explore the shared genetic linkages between two pathogenesis-related diseases (Li et al., 2018; Chen et al., 2021, 2022; He et al., 2021; Alves et al., 2022; Pan et al., 2022; Yan et al., 2022; Liu et al., 2022a,b). In order to investigate the shared genetic links between PD and periodontitis, integrated bioinformatics analyses were also utilized. First, differentially expressed genes (DEGs) deregulated in both diseases were obtained, and crosstalk genes were identified. The hub crosstalk genes were selected by performing k-means cluster analysis based on inflammatory response-related genes (IRRGs). Then, the correlation between hub crosstalk genes and IRRGs as well as the correlation between hub crosstalk genes and immune cells were investigated.

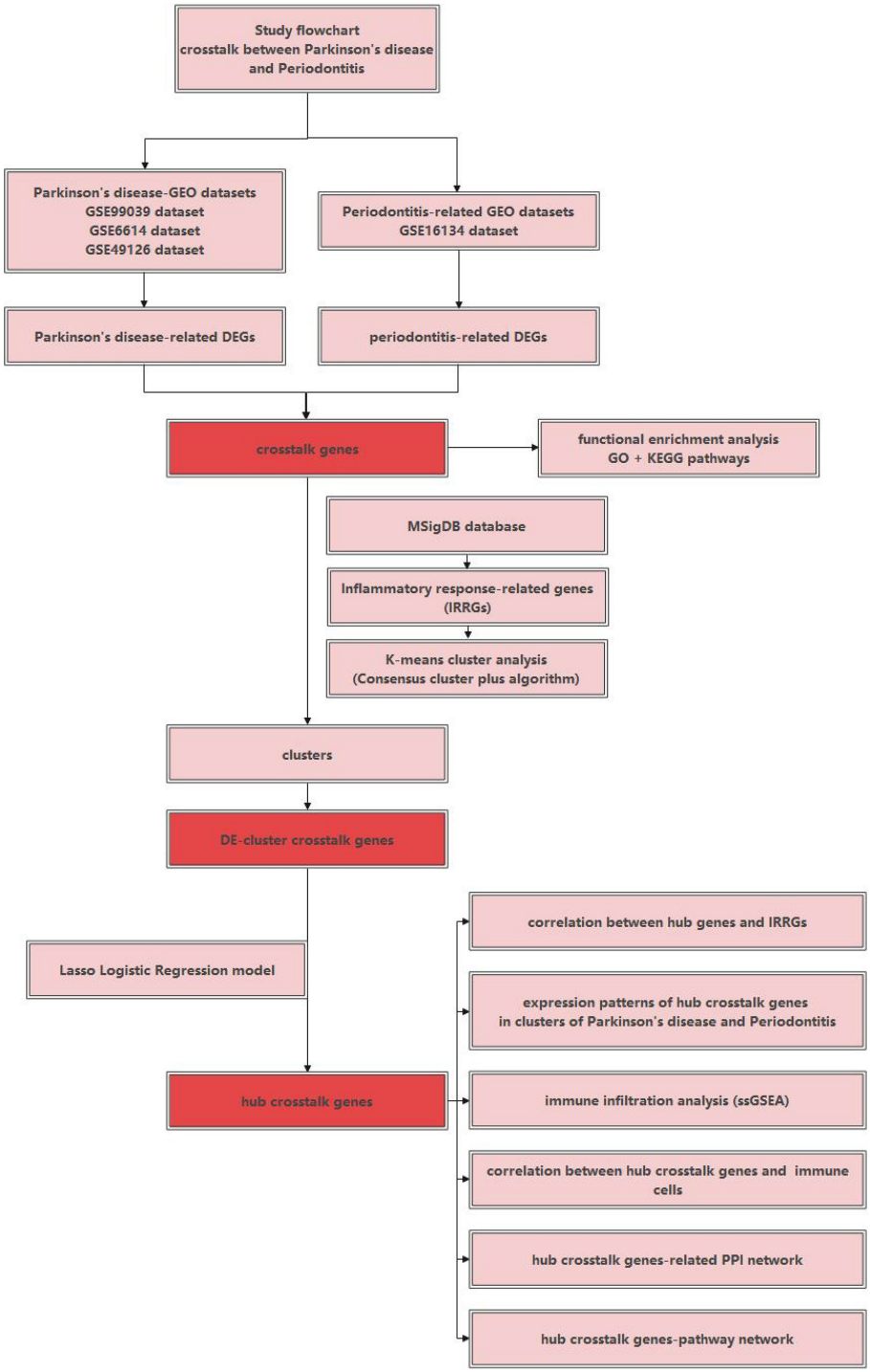

FIGURE 1
The study flowchart of the current research.

Materials and methods

Study design of the current research

Figure 1 used a schematic diagram to show the study flowchart of the current research. Firstly, differential expression analysis was performed to identify the DEGs belonging to PD and periodontitis respectively, and thus crosstalk genes were identified. Secondly, IRRGs were obtained and used for performing the K-means cluster analysis, and then differentially expressed (DE)- cluster crosstalk genes were identified. Thirdly, hub crosstalk genes were identified by building the Lasso logistic regression model. Lastly,

TABLE 1 Datasets of periodontitis and Parkinson's disease.

	Periodontitis		Parkinson's	
Series	GSE16134	GSE99039	GSE6613	GSE49126
Platform	GPL570	GPL570	GPL96	GPL4133
Tissue	**Gingival**		**Whole blood**	
Case	241	205	50	30
Control	69	233	22	20
Total sample	310	438	72	50

hub crosstalk genes as the investigation focus were researched from many aspects, for example, correlation with IRRGs; expression patterns of hub crosstalk genes in clusters of both diseases; correlation with immune cells; related PPI network; related pathway network.

Datasets

The datasets related to periodontitis and PD were, respectively, downloaded from the gene expression omnibus (GEO)[1] database (Edgar et al., 2002). The inclusion criteria for the periodontitis-related GEO datasets are as below: (1) The study design should be set as: established periodontitis samples as the experimental group and healthy gingival samples as the control group. (2) Periodontitis was defined in accordance with the case definition presented in the 2017 World Workshop: ① interdental CAL detectable at ≥2 nonadjacent teeth or ② buccal or oral with CAL ≥3 mm with pocketing >3 mm detectable at ≥2 teeth (Tonetti et al., 2018). (3) The sample size of the disease samples should be more than 20. The inclusion criteria for the PD-related GEO datasets are as below: (1) The study design should aim to compare the transcriptomic profiling of the blood samples (e.g., whole blood, peripheral blood mononuclear cells) between PD patients and healthy control subjects. (2) The sample size of the disease samples should be more than 20. Following such inclusion criteria, the GSE16134 dataset (Papapanou et al., 2009; Kebschull et al., 2014) was selected to be a periodontitis-related GEO dataset, and three datasets [GSE6613 (Scherzer et al., 2007, 2008), GSE49126 (Mutez et al., 2014), and GSE99039 (Shamir et al., 2017)] were selected to be PD-related datasets. Table 1 shows detailed information about these four included datasets.

By downloading the human gene set "HALLMARK_INFLAMMATORY_RESPONSE"[2] from the MSigDB database[3] (Lopez et al., 2018), 200 IRRGs were obtained. In addition, the gene signatures of 28 tumor-infiltrating lymphocytes were downloaded from the TISIDB database[4] (Zhang et al., 2013).

1 http://www.ncbi.nlm.nih.gov/

2 https://www.gsea-msigdb.org/gsea/msigdb/human/geneset/HALLMARK_INFLAMMATORY_RESPONSE.html

3 https://www.gsea-msigdb.org/gsea/msigdb/

4 http://cis.hku.hk/TISIDB/download.php

Data preprocessing

The Probe ID in the expression matrix was converted to the gene symbol based on the respective platform information for the downloaded data. If one Probe ID corresponds to multiple gene symbols, the gene symbols were de-duplicated based on the average of the sample expression values. When the number of samples with a gene of 0 in the expression matrix exceeds half of the total number of samples, the gene was removed from the expression matrix. In addition, Log2 was calculated for the dataset with large sample expression values, in order to achieve data standardization.

For PD, three datasets related to PD (i.e., GSE6613, GSE49126, GSE99039) were combined based on a common Gene Symbol. These three datasets were designed under different experimental platforms: GSE6613—GPL96 [HG-U133A] Affymetrix Human Genome U133A Array; GSE49126—GPL4133 Agilent-014850 Whole Human Genome Microarray 4x44K G4112F (Feature Number version); GSE99039—GPL570 [HG-U133_Plus_2] Affymetrix Human Genome U133 Plus 2.0 Array. After merging, the ComBat funtion in the "sva" package (version 4.1.3) (Leek et al., 2019) was used to eliminate the batch effect of the merged data. The PCA analysis was carried out, respectively, on the combined expression matrix and the expression matrix after ComBat correction, in order to examine the effects after ComBat correction.

Differential expression analysis

The "limma" package (version 3.15) (Ritchie et al., 2015) was used to analyze the differential expression between Case-sample and Normal-sample and identify the DEGs. DEGs were identified according to different thresholds of P.adjust and log2FC (log2 fold change) for periodontitis dataset and PD dataset, respectively. The P.adjust<0.05 and | log2FC | > 0.5 were selected as the threshold for selecting DEGs in periodontitis dataset. The P.adjust<0.05 and | log2FC | > 0.15 was selected as the threshold when selecting DEGs in PD datasets.

Cross-talk gene between periodontitis disease and PD

To explore potential relationships between Periodontitis disease and PD, DEGs deregulated in periodontitis and DEGs deregulated in PD were obtained respectively, and their intersection genes were labelled as cross-talk genes. These intersection genes could be considered as the bridge genes connecting the relationship between periodontitis and PD. The "pheatmap" package (version 1.0.12) (Kolde and Kolde, 2018) was used to analyze the expression level of these cross-talk genes. The "ClusterProfiler" package (version 3.15) (Yu et al., 2012; Wu et al., 2021) in R was utilized to analyze the cross-talk gene for Gene Ontology (GO) term-biological processes (BPs) and KEGG pathways to observe the biological functions affected by these cross-talk genes.

Consensus cluster plus analysis of periodontitis and Parkinson's based on the IRRG dataset

The differentially expressed IRRGs were obtained from periodontitis and PD, respectively. Then the expression values of the differentially expressed IRRGs in case samples were obtained for periodontitis and PD, respectively. The Consensus Cluster Plus algorithm (Wilkerson and Hayes, 2010) was utilized to carry out k-means cluster analysis based on the expression matrix of case samples.

Before using the Consensus Cluster Plus algorithm, it is important to determine the number of clusters. To determine the optimal number of samples, the interval silhouette width and elbow method were used to analyze the IRRGs expression matrix of periodontitis and PD, respectively. The fviz_nbclust method of "factoextra" package (version 1.0.7) (Kassambara and Mundt, 2017) was used for the analysis. The average silhouette width automatically calculated the number of the optimum clusters. The elbow method was used to observe the slope change of the vertical within sum of square (WSS). When the WSS decreases very slowly, increasing the number of clusters can no longer increase the clustering effect, and the existence of this "elbow point" is the optimal number of clusters. The optimal number of clusters was determined by considering the results of the two methods together. The "ConsensusClusterPlus" algorithm was used, and optimum cluster value was defined as the value of the parameter maxK. The case samples in periodontitis and PD were divided into different clusters based on IRRGs. Afterward, the expression levels of IRRG in different clusters were analyzed.

Identification of hub cross-talk genes based on cluster

The expression values of cross-talk gene in the case sample of the two diseases were obtained, and then "limma" package (version 3.15) (Ritchie et al., 2015) was used to analyze the cross-talk gene differentially expressed in different clusters according to the respective cluster categories. The cross-talk genes of p.adjust <0.01 were labeled as DE-cluster cross-talk genes. The least absolute shrinkage and selection operator (LASSO) Logistic Regression approach was used to further filter the DE-cluster cross-talk gene.

The expression values of the DE-cluster cross-talk gene in the respective disease's case samples were obtained, and then LASSO model was used for feature screening according to the respective cluster. According to the lambda.min value in the analysis results, the feature genes of both diseases were obtained. Finally, the intersection of the feature genes of the two diseases were obtained, and these intersection genes were regarded as the final hub cross-talk genes. These hub cross-talk genes were not only differentially expressed in periodontitis and PD, but also had a potential relationship with IRRG.

The correlation between hub cross-talk genes and IRRGs

To observe the relationship between hub cross-talk genes and IRRGs, the overlapping between IRRGs and cross-talk genes were obtained and considered as the IRR cross-talk genes. The expression values of hub cross-talk genes and IRR cross-talk genes in the case sample of two diseases were obtained. The Pearson correlation coefficient analysis was used to analyze the relationship among hub cross-talk genes, as well as the correlation between hub cross-talk genes and hub IRRGs.

Hub cross-talk gene expression analysis

The expression matrix of hub cross-talk genes in periodontitis and PD were obtained, and the Wilcoxon test was performed to examine the significance of hub cross-talk genes. Meanwhile, the expression matrix of the hub cross-talk genes under different clusters were obtained. Periodontitis data set has two clusters, and Wilcoxon test was used to examine the significance of hub cross-talk genes. PD-related data set had three clusters, and Kruskal test was used to examine the significance of hub cross-talk genes. ROC analysis was carried out to investigate the predictive effects of hub cross-talk genes, based on the expression matrices of these genes in case-samples and control-samples.

Immune infiltrates

After downloading the immune cell-related data from TISDB database, we performed ssGSEA quantitative analysis was performed to calculate the abundance of immune cells in both diseases. The "GSVA" package (version 3.15) (Hänzelmann et al., 2013) was used in this analysis. The enriched and abundant immune cells were obtained through hierarchical clustering. The correlation between the abundant immune cells and other immune cells was analyzed by using Pearson correlation coefficient analysis. The Wilcoxon test was performed to analyze the differences of the abundance levels of these immune cells between case samples and control samples.

Correlation between immune cells and hub cross-talk genes

The fractions of abundant immune cells in the case samples and the expression of hub cross-talk gene in the case samples were obtained. The correlation between immune cells and the hub cross-talk genes were analyzed by using the Pearson correlation coefficient analysis.

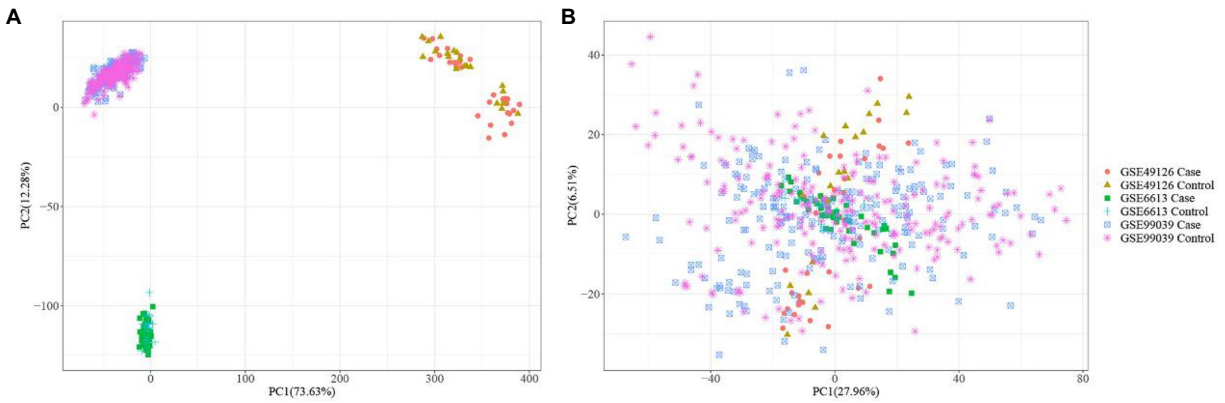

FIGURE 2
PCA analysis plots before **(A)** and after batch correction **(B)** of Parkinson's disease related dataset.

Hub cross-talk gene PPI network and pathway network

The protein–protein interaction (PPI) relationship pair between the Hub cross-talk gene and other genes were extracted from the human protein reference database (HPRD)[5] (Peri et al., 2004) and the biological general repository for interaction datasets (BIOGRID)[6] (Oughtred et al., 2021). These interaction pairs were regarded as the hub cross-talk genes-target interaction pairs. The relevant genes under all pathways were procured from the Kyoto Encyclopedia of Genes and Genomes (KEGG) database[7] (Kanehisa and Goto, 2000). The hub cross-talk gene-pathway relationship pair was firstly obtained. Afterward, the pathway-target relationship pair was obtained according to the pathways in the hub cross-talk gene-pathway interaction pairs. Therefore the hub cross-talk gene-pathway-target interaction pairs were identified, based on which the complex network of Hub cross-talk gene-Target and Hub cross-talk gene-Pathway-Target were constructed by using Cytoscape software (version 3.8) (Shannon et al., 2003).

Results

Data preprocessing

The three datasets related to PD (i.e., GSE6613, GSE49126, GSE99039) were merged, and then the PCA analysis was performed (Figure 2A). Figure 2A shows that the 3 datasets differed significantly. Figure 2B shows that the batch effect generated by merging datasets was significantly eliminated. By comparing Figures 2A,B, it was found that the differences between the three datasets were significantly reduced.

Differentially expressed genes

Differential expression analysis was conducted for the periodontitis and PD-related datasets. For periodontitis-related dataset (GSE16134), the genes of P.adjust < 0.05 and |log2FC| > 0.5 were selected as DEGs, where log2FC >0.5 was the upregulated DEGs and log2FC < −0.5 was the downregulated DEGs. For PD-related datasets (GSE6613, GSE49126, GSE99039), the genes of P.adjust < 0.05 and | log2FC| > 0.15 were selected as DEGs, where log2FC > 0.15 were upregulated DEGs and log2FC < −0.15 were down-regulated DEGs. Table 2 shows the number of upregulated and downregulated DEGs deregulated in periodontitis and PD.

A volcano map was utilized to show the distribution of DEGs in Periodontitis- (Figure 3A) and PD-related data (Figure 3B). The top5 up-regulated and down-regulated DEGs with the most significant P.adjust values were labeled.

Cross-talk gene

The common DEGs of Periodontitis disease and PD were extracted, and thus 37 Cross-talk genes were obtained (Figure 4A). Then the expression values of 37 cross-talk genes in periodontitis and PD were extracted, base on which heatmaps were plotted for periodontitis (Figure 4B) and PD (Figure 4C).

The "ClusterProfiler" package in R was used to identify the BPs and KEGG pathways enriched by 37 cross-talk genes. The $p < 0.05$ was established as statistical significance and the top 20 terms were visualized (Figures 5A,B; Tables 3, 4).

5 http://www.hprd.org/
6 http://thebiogrid.org/
7 https://www.kegg.jp/

TABLE 2 DEG statistical results.

Datasets	Periodontitis		Parkinson's	
	GSE16134	GSE6613	GSE49126	GSE99039
P.adjust	P.adj < 0.05		P.adj < 0.05	
|Log2(FC)|	|Log2(FC)| > 0.5		|Log2(FC)| > 0.15	
DEG up	795		199	
DEG down	546		12	
Total DEG	1,341		211	

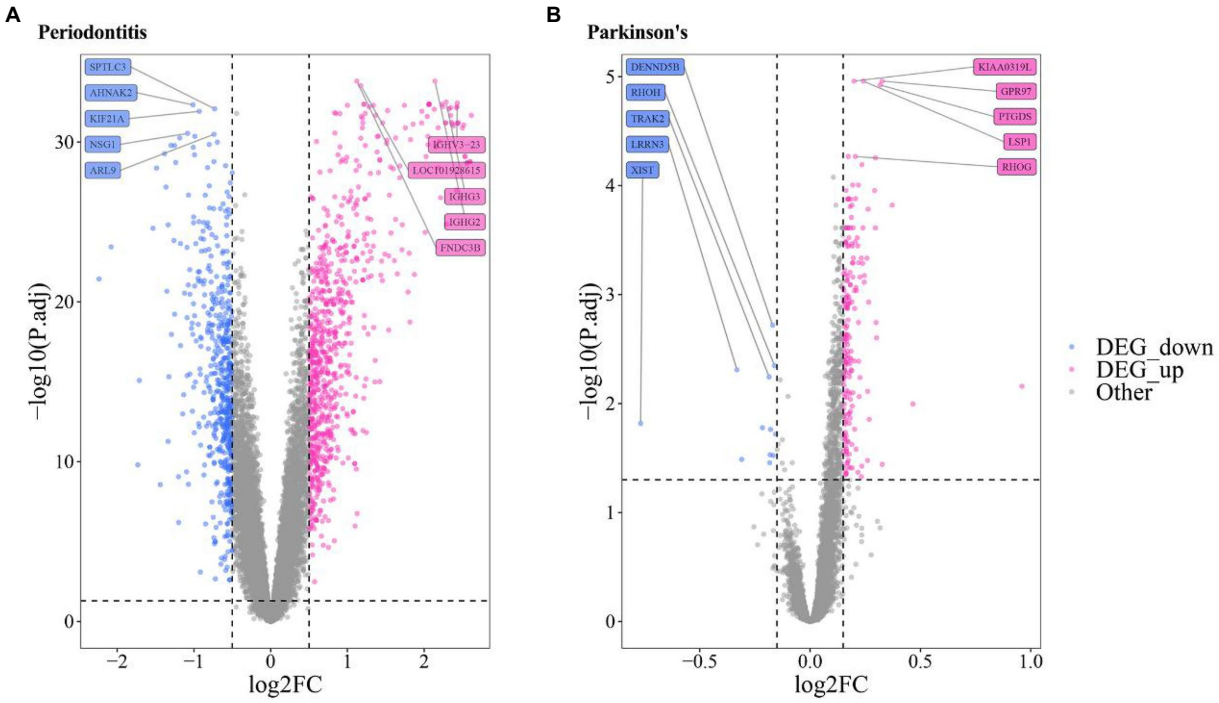

FIGURE 3
Volcanic map of the differentially expressed gene of **(A)** Periodontitis disease **(A)** and **(B)** Parkinson's disease.

The cross-talk genes were mainly involved in several BPs, for example, cellular defense response, leukocyte degranulation, neutrophil migration, and neutrophil activation involved in immune response (Figure 5A; Table 3). In addition, cross-talk genes regulate several KEGG pathways, for instance, phagotsome, leukocyte transendothelial migration, neutrophil extracellular trap formation, staphylococcus aureus infection, cell adhesion molecules, and Fc epsilon RI Signaling pathways (Figure 5B; Table 4).

Consensus cluster plus analysis results

The differentially expressed IRRGs in periodontitis and PD were extracted; thereby 47 periodontitis-related IRRGs and 9 PD-related IRRGs were identified. The expression values of periodontitis-related IRRGs and PD-related IRRGs were obtained, respectively. Afterward, the IRRG-related expression profiles were analyzed by using the average silhouette width and elbow method (Figures 6A–D).

The clusters' numbers of Periodontitis disease were determined as 2 (Figure 6A) and 5 (Figure 6C) respectively. Based on this, the maxK parameter was set as 5 when periodontitis dataset was calculated by using "Consensus Cluster Plus" function. The clusters' numbers of PD are 2 (Figure 6B) and 3 (Figure 6D). Based on this, the maxK parameter was set as 3 when PD-related data set was calculated by using "Consensus Cluster Plus" function.

By using "Consensus Cluster Plus" function, two diseases' clustering results were obtained (Figures 7A–D). Figures 7A,C

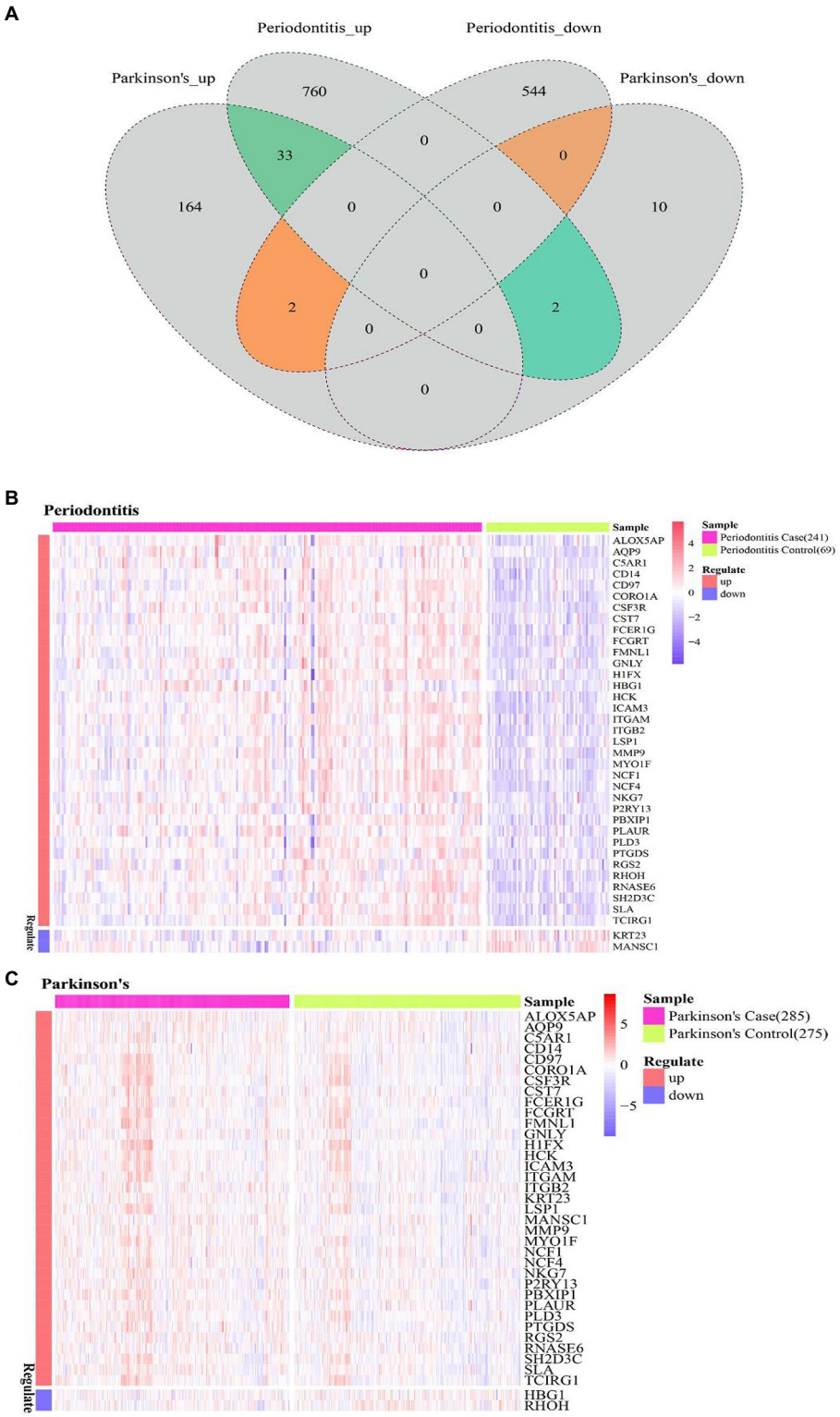

FIGURE 4
Cross-talk gene expression level. **(A)** Venn diagram of periodontitis disease and Parkinson's disease differentially expressed genes; **(B,C)** cross-talk gene at the level of expression of Periodontitis disease and Parkinson's disease.

show that the periodontitis-related data achieved the best clustering effects when k = 2. Figures 7B,D show that the PD-related data achieved the best clustering effects when k = 3. Figures 7E,F shows the sample correlation results when k = 2 being selected for periodontitis data (Figure 7E) and when k = 3 being selected for PD data (Figure 7F).

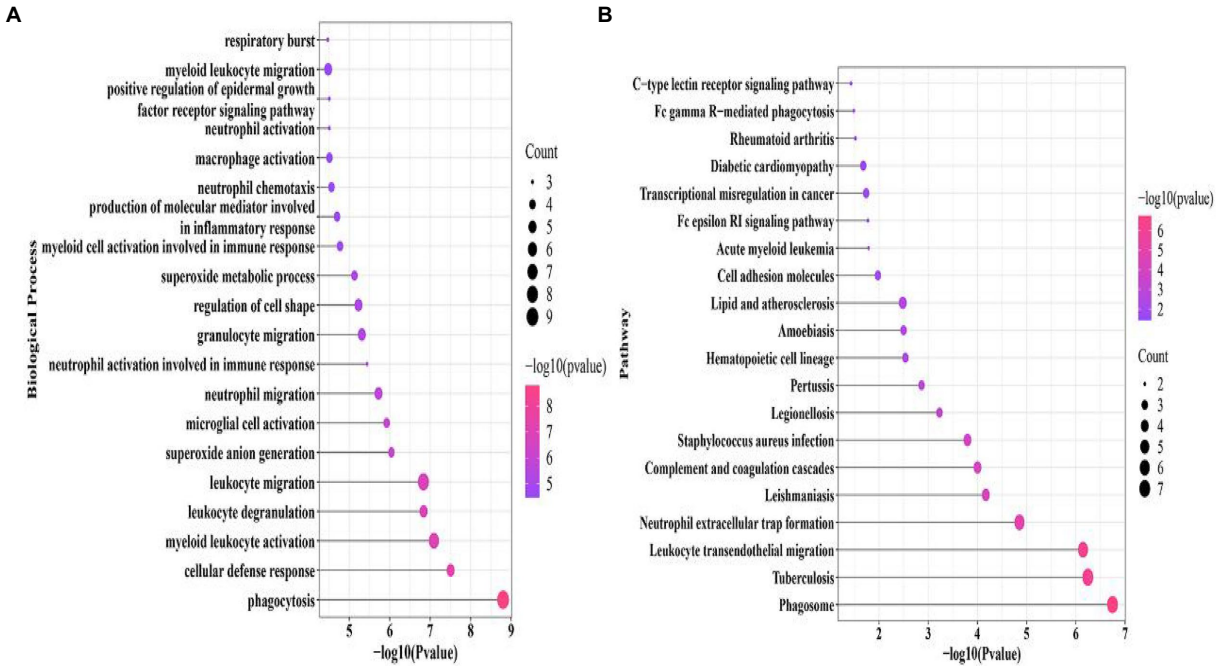

FIGURE 5
Cross-talk gene significant enrichment of biological processes **(A)** and pathway **(B)**.

TABLE 3 The top 20 biological processes enriched by the crosstalk genes.

ID	Description	GeneRatio	BgRatio	*p*-value	P.adjust	*q*-value	geneID	Count
GO:0006909	Phagocytosis	9/32	308/18723	1.58E-09	1.46E-06	9.79E-07	929/11151/2207/3055/3385/3684/3689/4689/399	9
GO:0006968	Cellular defense response	5/32	54/18723	3.13E-08	1.45E-05	9.71E-06	728/10578/4046/653361/10312	5
GO:0002274	Myeloid leukocyte activation	7/32	223/18723	8.09E-08	2.49E-05	1.67E-05	728/8530/2207/3684/3689/5730/399	7
GO:0043299	Leukocyte degranulation	5/32	73/18723	1.45E-07	2.71E-05	1.82E-05	11,151/3055/3684/3689/5730	5
GO:0050900	Leukocyte migration	8/32	369/18723	1.47E-07	2.71E-05	1.82E-05	728/11151/1441/2207/3055/3689/4318/399	8
GO:0042554	Superoxide anion generation	4/32	44/18723	9.09E-07	0.000140002	9.39E-05	3684/3689/653361/4689	4
GO:0001774	Microglial cell activation	4/32	47/18723	1.19E-06	0.000157107	0.000105418	728/8530/3684/3689	4
GO:1990266	Neutrophil migration	5/32	122/18723	1.89E-06	0.000218547	0.000146644	728/1441/2207/3689/399	5
GO:0002283	Neutrophil activation involved in immune response	3/32	18/18723	3.64E-06	0.000373357	0.000250521	2207/3684/3689	3
GO:0097530	Granulocyte migration	5/32	148/18723	4.89E-06	0.000451796	0.000303153	728/1441/2207/3689/399	5
GO:0008360	Regulation of cell shape	5/32	154/18723	5.94E-06	0.000498738	0.000334651	11,151/752/3055/3689/399	5
GO:0006801	Superoxide metabolic process	4/32	74/18723	7.43E-06	0.000572401	0.000384078	3684/3689/653361/4689	4
GO:0002275	Myeloid cell activation involved in immune response	4/32	91/18723	1.69E-05	0.001202578	0.000806925	2207/3684/3689/5730	4
GO:0002532	Production of molecular mediator involved in inflammatory response	4/32	95/18723	2.01E-05	0.001323779	0.00088825	241/653361/57326/23646	4
GO:0030593	Neutrophil chemotaxis	4/32	103/18723	2.76E-05	0.001475695	0.000990185	728/1441/2207/3689	4
GO:0042116	Macrophage activation	4/32	106/18723	3.09E-05	0.001475695	0.000990185	728/8530/3684/3689	4
GO:0042119	Neutrophil activation	3/32	36/18723	3.12E-05	0.001475695	0.000990185	2207/3684/3689	3
GO:0045742	Positive regulation of epidermal growth factor receptor signaling pathway	3/32	36/18723	3.12E-05	0.001475695	0.000990185	4318/653361/5329	3
GO:0097529	Myeloid leukocyte migration	5/32	220/18723	3.33E-05	0.001475695	0.000990185	728/1441/2207/3689/399	5
GO:0045730	Respiratory burst	3/32	37/18723	3.39E-05	0.001475695	0.000990185	3055/653361/4689	3

TABLE 4 The top 20 signaling pathways enriched by the crosstalk genes.

ID	Description	GeneRatio	BgRatio	*p*-value	p.adjust	*q*-value	geneID	Count
hsa04145	Phagosome	7/24	152/8160	1.80E-07	1.31E-05	1.00E-05	929/11151/3684/3689/653361/4689/10312	7
hsa05152	Tuberculosis	7/24	180/8160	5.70E-07	1.74E-05	1.33E-05	929/11151/2207/3684/3689/4046/10312	7
hsa04670	Leukocyte transendothelial migration	6/24	114/8160	7.14E-07	1.74E-05	1.33E-05	3684/3689/4318/653361/4689/399	6
hsa04613	Neutrophil extracellular trap formation	6/24	190/8160	1.40E-05	0.000255023	0.000194899	366/728/3684/3689/653361/4689	6
hsa05140	Leishmaniasis	4/24	77/8160	6.75E-05	0.000985329	0.000753027	3684/3689/653361/4689	4
hsa04610	Complement and coagulation cascades	4/24	85/8160	9.94E-05	0.001209374	0.000924251	728/3684/3689/5329	4
hsa05150	Staphylococcus aureus infection	4/24	96/8160	0.000159591	0.00166431	0.001271931	728/3684/3689/25984	4
hsa05134	Legionellosis	3/24	57/8160	0.000589439	0.005378627	0.004110558	929/3684/3689	3
hsa05133	Pertussis	3/24	76/8160	0.00136523	0.01107353	0.008462828	929/3684/3689	3
hsa04640	Hematopoietic cell lineage	3/24	99/8160	0.002913961	0.020016567	0.015297448	929/1441/3684	3
hsa05146	Amoebiasis	3/24	102/8160	0.003171487	0.020016567	0.015297448	929/3684/3689	3
hsa05417	Lipid and atherosclerosis	4/24	215/8160	0.003290395	0.020016567	0.015297448	929/4318/653361/4689	4
hsa04514	Cell adhesion molecules	3/24	157/8160	0.010513557	0.059037667	0.045118909	3385/3684/3689	3
hsa05221	Acute myeloid leukemia	2/24	67/8160	0.016316475	0.081667353	0.062413406	929/3684	2
hsa04664	Fc epsilon RI signaling pathway	2/24	68/8160	0.016780963	0.081667353	0.062413406	241/2207	2
hsa05202	Transcriptional misregulation in cancer	3/24	193/8160	0.018292556	0.083459789	0.063783256	929/3684/4318	3
hsa05415	Diabetic cardiomyopathy	3/24	203/8160	0.020897732	0.089737318	0.068580791	4318/653361/4689	3
hsa05323	Rheumatoid arthritis	2/24	93/8160	0.030142526	0.12224469	0.093424204	3689/10312	2
hsa04666	Fc gamma R-mediated phagocytosis	2/24	97/8160	0.032573664	0.125151447	0.095645662	3055/653361	2
hsa04625	C-type lectin receptor signaling pathway	2/24	104/8160	0.037008335	0.135080423	0.103233777	2207/4046	2

Hub cross-talk genes screening

A multi-group differential expression analysis of cross-talk genes were carried out based on the clusters of two diseases, and genes with P.adjust < 0.01 were selected to be the DE-cluster cross-talk genes. The DE-cluster cross-talk genes for both diseases were overlapped and thereby 26 common DE-cluster cross-talk genes were obtained (Figure 8A). Based on the clusters of both diseases, LASSO regression analysis was used to further screen the DE-cluster cross-talk genes (Figures 8B–E). After further screening for DE-cluster cross-talk genes common to both diseases, 5 Hub cross-talk genes (i.e., FMNL1, MANSC1, PLAUR, RNASE6, TCIRG1) were obtained (Figure 8F).

Correlation between hub cross-talk genes and hub IRRGs

The inflammatory response-related cross-talk genes were obtained and 5 genes (i.e., AQP9, C5AR1, CD14, CSF3R, PLAUR) were labeled as hub IRRGs. The expression values of 5 hub IRRGs and 5 hub cross-talk genes in the case sample of periodontitis and PD were obtained. Afterward, the relationship among the hub cross-talk genes, as well as the relationship between the hub cross-talk genes and the hub IRRGs were analyzed by using the Pearson correlation coefficient analysis (Figures 9A,B; Tables 5–6). MANSC1 was significantly negatively correlated with 4 hub cross-talk genes in periodontitis, and MANSC1 was significantly negatively correlated with 5 hub IRRGs. There was a significant positive correlation among the remaining 4 hub cross-talk genes, and the remaining 4 Hub cross-talk genes were also significantly positively correlated with 5 Hub IRRGs (Figure 9A). Five hub cross-talk genes were significantly positively correlated with five hub IRRGs in PD. Among these correlation, the correlation between CD14 and five hub cross-talk genes showed comparatively higher correlation (Figure 9B).

Hub cross-talk genes' expression level analysis

The expression values of five hub cross-talk genes in periodontitis and PD were obtained. The Wilcoxon test results showed that five hub cross-talk genes had significant differences between disease samples and normal samples (Figures 10A,B). Afterward, the expression matrix of the five hub cross-talk genes in different clusters were obtained. The Wilcoxon test and Kruskal test results showed that the five hub cross-talk genes had significant differences between different cluster samples (Figures 10C,D). Furthermore, ROC analysis results showed that the AUC values of all five hub cross-talk gene in periodontitis were greater than 70% (Figure 10E). The AUC values of the five hub cross-talk gene in PD were greater than 58%. The AUC values of FMNL1 and PLAUR in PD were comparatively higher compared to the remaining three hub cross-talk genes (Figure 10F).

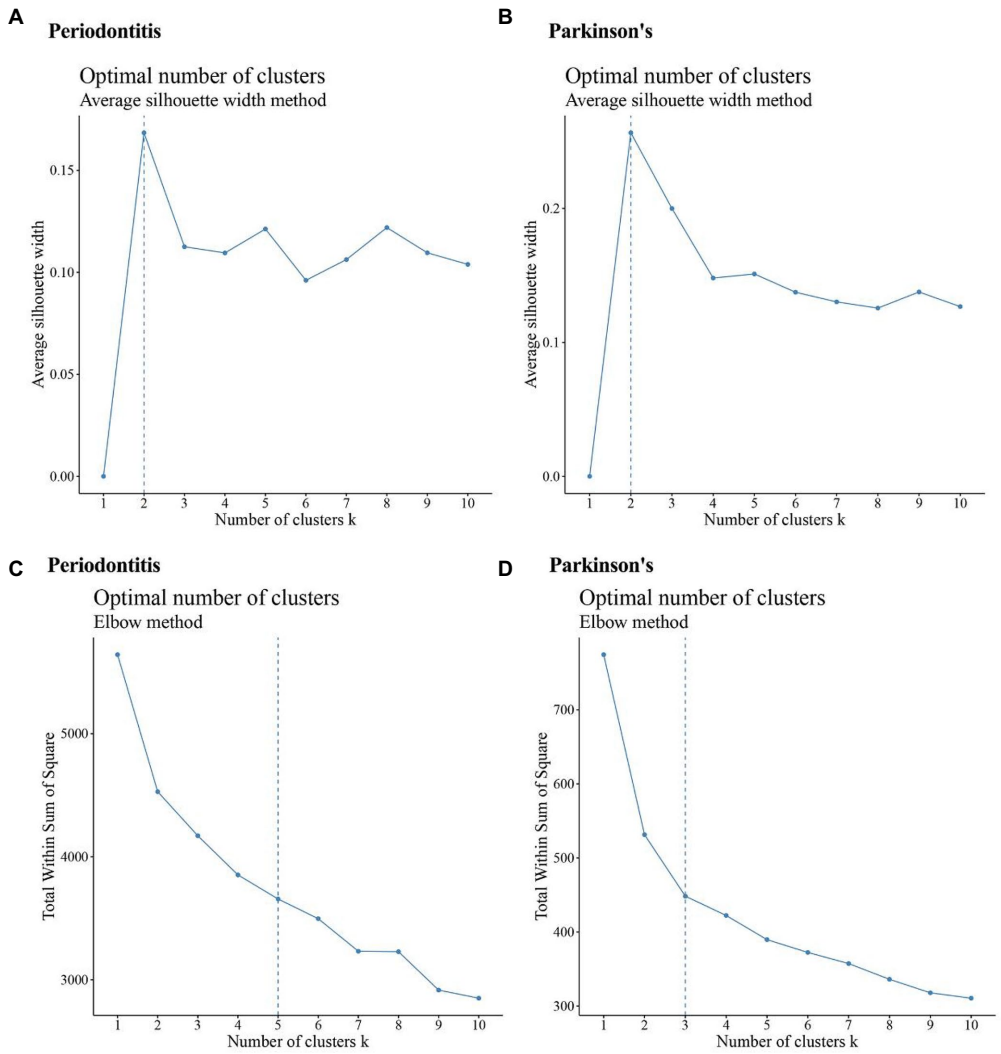

FIGURE 6
Results of a cluster analysis of periodontitis and Parkinson's disease. **(A,B)** Results of a silhouette width analysis of the IRRGs associated with periodontitis and the average of IRRGs associated with Parkinson's disease; **(C,D)** Results of an elbow method analysis of Periodontitis disease-related IRRGs and Parkinson's disease-related IRRGs.

Immune infiltration analysis of periodontitis and PD

The immune cell-related dataset were obtained from TISDB database, which included 782 genes and 28 types of immune cells. The immune infiltration quantification analysis was performed by using the ssGSEA algorithm, and the enrichment fractions of immune cells in periodontitis and PD were obtained. The "pheamap" package of R was used to demonstrate immune-infiltrating cell scores for case samples in periodontitis and PD. The results showed that central memory CD4 T cell, MDSC, Effector memory CD8 T cell, plasmacytoid dendritic cell, activated CD8 T cell, activated dendritic cell and monocyte were highly expressed in periodontitis and PD (Figures 11A,B).

The correlation between these high-abundance immune cells and other immune cells were analyzed by using the Pearson correlation coefficient, and the immune cells with value of $p < 0.05$ were visualized (Table 7). The results showed that MDSC was highly positively related with active B cell, type 1 T helper cell, regulatory T cell, and immature B cell in periodontitis (cor > 0.8; Figure 11C). Activated CD4 T cell and Activated CD8 T cell were positively correlated in PD (cor = 0.6; Figure 11D). The active CD4 T cell was positively correlated with activated CD8 T cell in periodontitis.

The violin plots were used to show the fractional distribution of high-abundance immune cells in periodontitis and PD, and the Wilcoxon test was applied to observe the significance of samples. The results showed that the high abundance of immune cells varied greatly between case samples and normal samples in periodontitis (Figure 11D). The high-abundance immune cells differed less between case samples and normal samples in PD (Figure 11E). The effector

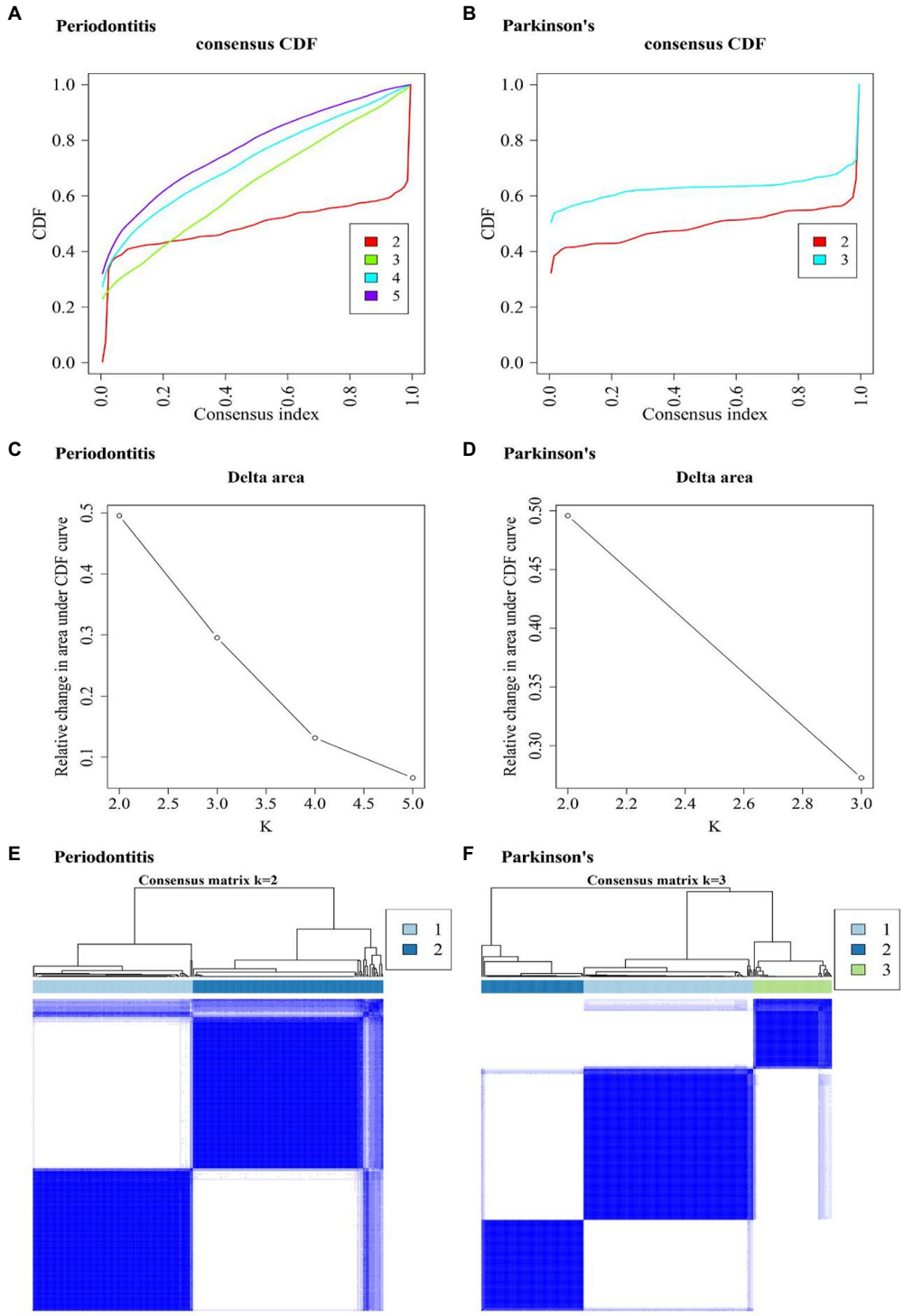

FIGURE 7
Consensus Cluster Plus analysis results. **(A,B)** Consistent cumulative distribution function (CDF) plot of periodontitis and Parkinson's disease. This plot shows the cumulative distribution function of the score when k takes different values, which is used to determine when k is taken, CDF reaches an approximate maximum, and the cluster analysis results are the most reliable. That is, consider the k-value of the CDF descent slope is small. **(C,D)** The k and k-1 relative changes in area under the CDF curve in periodontitis and Parkinson's disease. The total area under the CDF curve at k=2 (the area below the line in **(A,B)** rather than the relative change in area). To select the final k-value, we should consider that the descending slope of the midline of **(A,B)** is as small as possible, and also consider that the relative change in the area under k and k-1 in **(C,D)** compared to the CDF curve is as small as possible. **(E,F)** Consistent cluster diagram of periodontitis and Parkinson's disease.

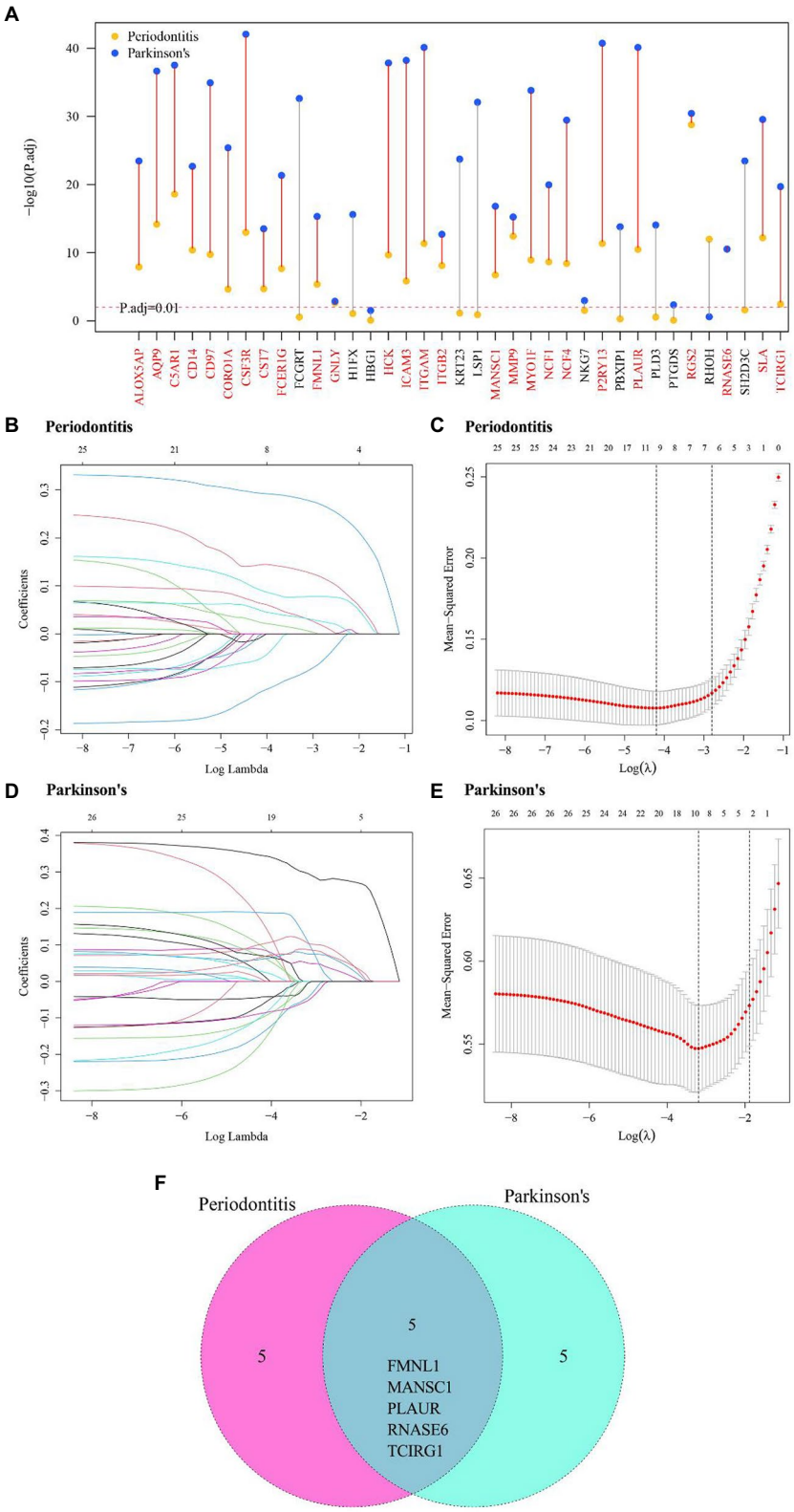

FIGURE 8
Hub cross-talk gene screening. **(A)** DE-cluster cross-talk gene of periodontitis and Parkinson's disease's. **(B–D)** Results of LASSO analysis for periodontitis and Parkinson's disease. Each line in the graph represents a gene, and a larger value of the log lambda as the gene tends to 0 indicates that the gene is more critical. **(C–E)** cross-validation results of Periodontitis disease and Parkinson's disease model. **(F)** Periodontitis disease and Parkinson's disease's hub cross-talk genes.

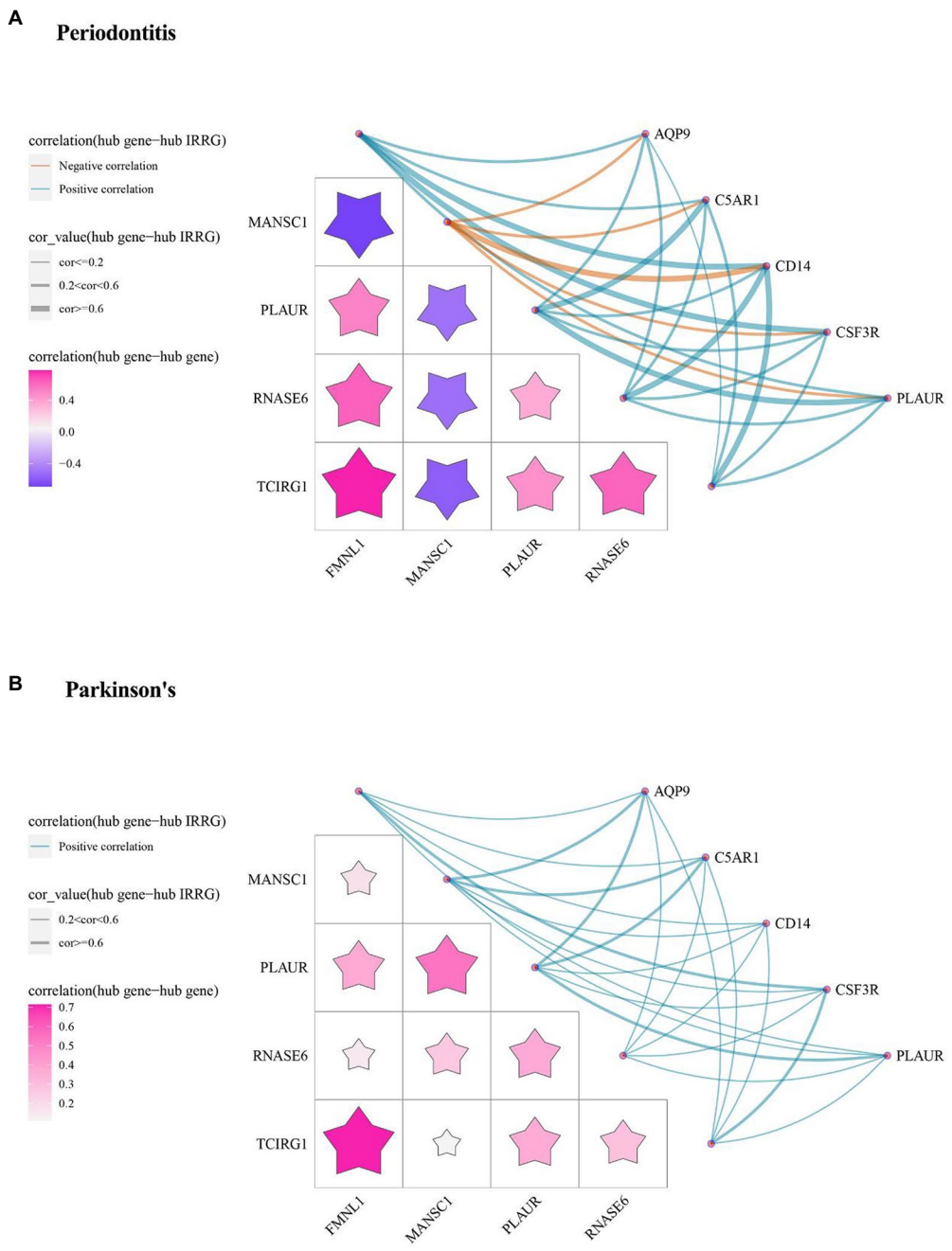

FIGURE 9
The relationships among Hub cross-talk genes and Hub IRRG in **(A)** Periodontitis disease and **(B)** Parkinson's disease. The matrix graph in the lower left part of the figure shows the correlation coefficient between the hub cross-talk gene and the hub cross-talk gene, and the upper right part of the network diagram shows the correlation coefficient between the hub cross-talk gene and the hub IRRG.

memory CD8 T cell was highly enriched in both periodontitis and PD.

Relationship between high-abundance immune cells and hub cross-talk genes

The case sample scores for 7 high-abundance immune cells and 5 hub cross-talk genes were obtained. The correlation analysis was carried out to invesitgate the correlation between immune cells and hub cross-talk genes. The relationship pairs with value of $p < 0.05$ was defined to be significant. The absolute value of correlation coefficient was calculated and the results of the top12 were visualized. The results shwoed that RNASE6 gene was highly correlated with MDSC in periodontitis (Figure 12). MANSC1 was highly correlated with plasmacytoid dendritic cell in PD (Figure 13; Table 8).

TABLE 5 The correlation among hub crosstalk genes in periodontitis and Parkinson's disease, respectively.

Hub gene	Hub gene	Cor.	*p*-value	Sig.
Periodontitis				
FMNL1	TCIRG1	0.776680579	8.72E-64	***
TCIRG1	FMNL1	0.776680579	8.72E-64	***
FMNL1	RNASE6	0.630304404	9.84E-36	***
RNASE6	FMNL1	0.630304404	9.84E-36	***
RNASE6	TCIRG1	0.623645546	8.28E-35	***
TCIRG1	RNASE6	0.623645546	8.28E-35	***
FMNL1	PLAUR	0.519504303	7.95E-23	***
PLAUR	FMNL1	0.519504303	7.95E-23	***
PLAUR	TCIRG1	0.463852082	6.06E-18	***
TCIRG1	PLAUR	0.463852082	6.06E-18	***
PLAUR	RNASE6	0.356920531	9.59E-11	***
RNASE6	PLAUR	0.356920531	9.59E-11	***
MANSC1	PLAUR	−0.501651214	3.67E-21	***
PLAUR	MANSC1	−0.501651214	3.67E-21	***
MANSC1	RNASE6	−0.508910042	7.94E-22	***
RNASE6	MANSC1	−0.508910042	7.94E-22	***
MANSC1	TCIRG1	−0.583097828	1.25E-29	***
TCIRG1	MANSC1	−0.583097828	1.25E-29	***
FMNL1	MANSC1	−0.687320353	1.13E-44	***
MANSC1	FMNL1	−0.687320353	1.13E-44	***
Parkinson's disease				
FMNL1	TCIRG1	0.714413971	1.39E-88	***
TCIRG1	FMNL1	0.714413971	1.39E-88	***
MANSC1	PLAUR	0.542333646	3.87E-44	***
PLAUR	MANSC1	0.542333646	3.87E-44	***
FMNL1	PLAUR	0.375957267	3.05E-20	***
PLAUR	FMNL1	0.375957267	3.05E-20	***
PLAUR	RNASE6	0.373867758	5.10E-20	***
RNASE6	PLAUR	0.373867758	5.10E-20	***
PLAUR	TCIRG1	0.369494651	1.48E-19	***
TCIRG1	PLAUR	0.369494651	1.48E-19	***
RNASE6	TCIRG1	0.294141212	1.22E-12	***
TCIRG1	RNASE6	0.294141212	1.22E-12	***
MANSC1	RNASE6	0.268167983	1.12E-10	***
RNASE6	MANSC1	0.268167983	1.12E-10	***
FMNL1	MANSC1	0.181137877	1.61E-05	***
MANSC1	FMNL1	0.181137877	1.61E-05	***
FMNL1	RNASE6	0.151556057	0.000319114	***
RNASE6	FMNL1	0.151556057	0.000319114	***
MANSC1	TCIRG1	0.110844015	0.008657743	**
TCIRG1	MANSC1	0.110844015	0.008657743	**

**$p <= 0.01$, ***$p <= 0.001$.

Hub cross-talk gene PPI-pathway network

The 192 hub cross-talk gene-target interaction pairs were obtained from the HPRD and BIOGRID database. Based on the KEGG database, 105 hub cross-talk gene-pathway-target

TABLE 6 The correlation between hub crosstalk genes and hub IRRGs in periodontitis and Parkinson's disease.

Hub gene	Hub IRRG	Cor.	*p*-value	Sig.
Periodontitis				
RNASE6	CD14	0.764628729	1.02E-60	***
PLAUR	C5AR1	0.671344512	5.74E-42	***
TCIRG1	CD14	0.664226041	8.15E-41	***
FMNL1	CSF3R	0.645560153	6.13E-38	***
FMNL1	CD14	0.643618516	1.19E-37	***
FMNL1	C5AR1	0.590656767	1.54E-30	***
RNASE6	C5AR1	0.569100882	5.29E-28	***
TCIRG1	CSF3R	0.568078374	6.90E-28	***
RNASE6	CSF3R	0.550156788	6.35E-26	***
PLAUR	CSF3R	0.542527119	4.02E-25	***
FMNL1	PLAUR	0.519504303	7.95E-23	***
PLAUR	CD14	0.509187187	7.48E-22	***
TCIRG1	C5AR1	0.479173686	3.36E-19	***
TCIRG1	PLAUR	0.463852082	6.06E-18	***
PLAUR	AQP9	0.424911367	5.07E-15	***
RNASE6	AQP9	0.4075901	7.75E-14	***
RNASE6	PLAUR	0.356920531	9.59E-11	***
FMNL1	AQP9	0.263403908	2.57E-06	***
TCIRG1	AQP9	0.179628798	0.001494316	**
MANSC1	AQP9	−0.245665691	1.21E-05	***
MANSC1	C5AR1	−0.407813463	7.49E-14	***
MANSC1	PLAUR	−0.501651214	3.67E-21	***
MANSC1	CSF3R	−0.533100941	3.68E-24	***
MANSC1	CD14	−0.620737902	2.06E-34	***
Parkinson's disease				
TCIRG1	CSF3R	0.739465803	5.77E-98	***
FMNL1	CSF3R	0.730984072	1.14E-94	***
MANSC1	C5AR1	0.723131244	9.90E-92	***
PLAUR	C5AR1	0.69290086	2.67E-81	***
MANSC1	AQP9	0.631283537	1.35E-63	***
PLAUR	AQP9	0.630607165	2.01E-63	***
MANSC1	PLAUR	0.542333646	3.87E-44	***
PLAUR	CSF3R	0.505325432	1.25E-37	***
PLAUR	CD14	0.440176835	6.11E-28	***
FMNL1	C5AR1	0.422459064	1.20E-25	***
RNASE6	AQP9	0.41039563	3.66E-24	***
FMNL1	PLAUR	0.375957267	3.05E-20	***
RNASE6	PLAUR	0.373867758	5.10E-20	***
TCIRG1	C5AR1	0.372498455	7.13E-20	***
TCIRG1	PLAUR	0.369494651	1.48E-19	***
TCIRG1	CD14	0.363230267	6.59E-19	***
RNASE6	C5AR1	0.359788021	1.48E-18	***
FMNL1	CD14	0.358011298	2.24E-18	***
RNASE6	CD14	0.355084478	4.39E-18	***
MANSC1	CSF3R	0.347787555	2.29E-17	***
MANSC1	CD14	0.324463762	3.40E-15	***
RNASE6	CSF3R	0.282898522	9.14E-12	***
TCIRG1	AQP9	0.231098723	3.17E-08	***
FMNL1	AQP9	0.205778472	9.04E-07	***

**$p <= 0.01$, ***$p <= 0.001$.

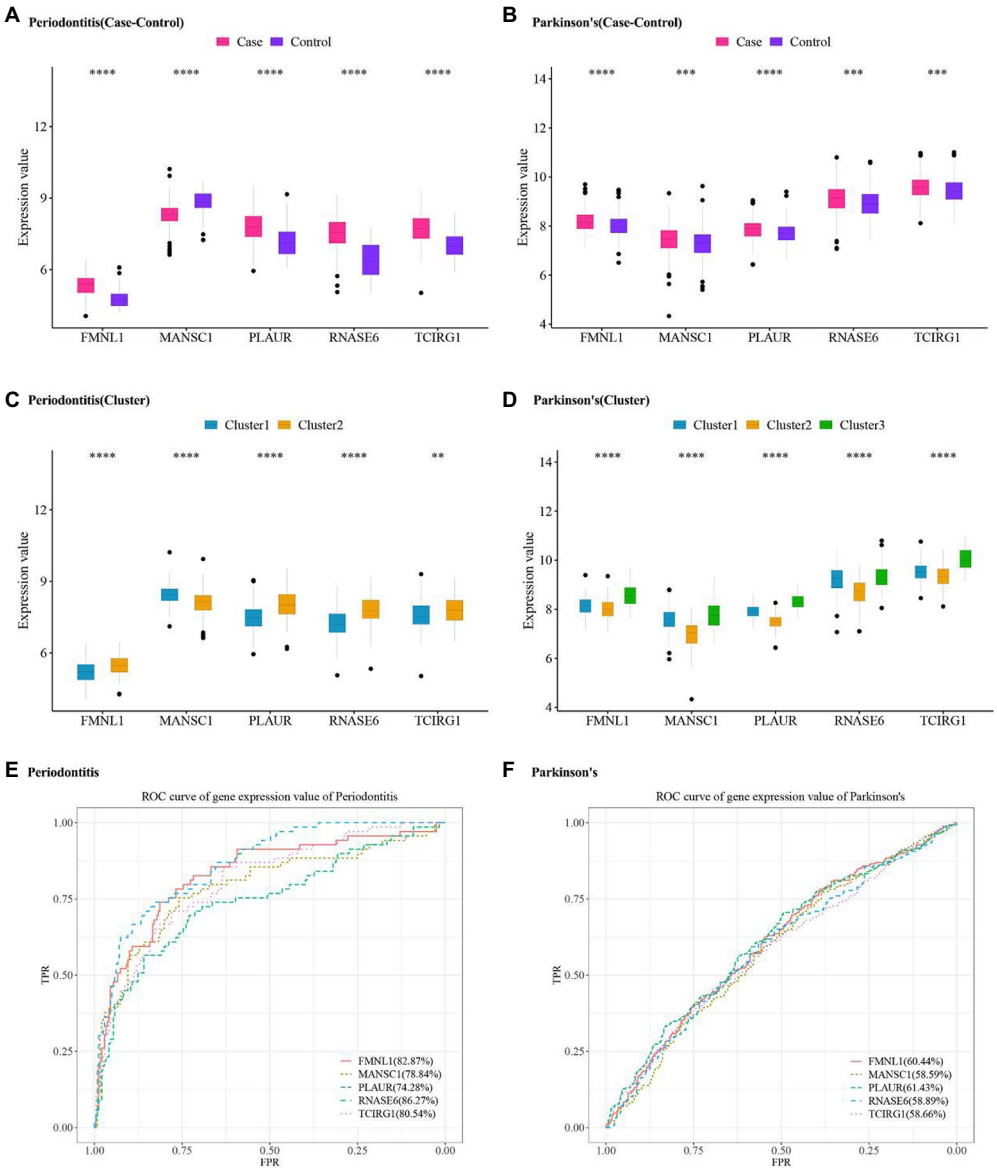

FIGURE 10
Hub cross-talk gene expression level and ROC analysis in periodontitis and Parkinson's disease. **(A,B)** Hub cross-talk gene expression levels and differences between disease samples and normal samples in periodontitis and Parkinson's disease, respectively. **(C,D)** Hub cross-talk gene expresses levels and differences in different clusters of periodontitis and Parkinson's disease. The smaller the test result, the more "*" on the plot, and the correspondence between the *p* value and the "*" sign is ns: $p>0.05$, *: $p\leq0.05$, **: $p\leq0.01$, ***: $p\leq0.001$, ****: $p\leq0.0001$. **(E,F)** ROC analysis results regarding the diagnostic accuracy of hub cross-talk genes in periodontitis and Parkinson's disease.

interaction pairs were obtained. The Cytoscape software was used to integrate the hub cross-talk gene-target pairs with the hub cross-talk gene-pathway-target interaction pairs; thereby a hub cross-talk gene related complex network was constructed (Figure 14). Figure 14 shows that PLAUR interacted with other genes and regulated the composite and coagulation cascades pathway. TCIRG1 interacted with other hub cross-talk genes and was involved in regulating oxidative phosphorylation pathway and phagosome pathway.

Discussion

The main findings of the current study identified five hub crosstalk genes (i.e., FMNL1, MANSC1, PLAUR, RNASE6, and TCIRG1) to be the linking mechanisms between periodontitis and PD. In addition, this study also identified several signaling pathways enriched by the crosstalk genes, for example, complement and coagulation cascades, neutrophil extracellular trap formation, transendothelial leukocyte migration, and

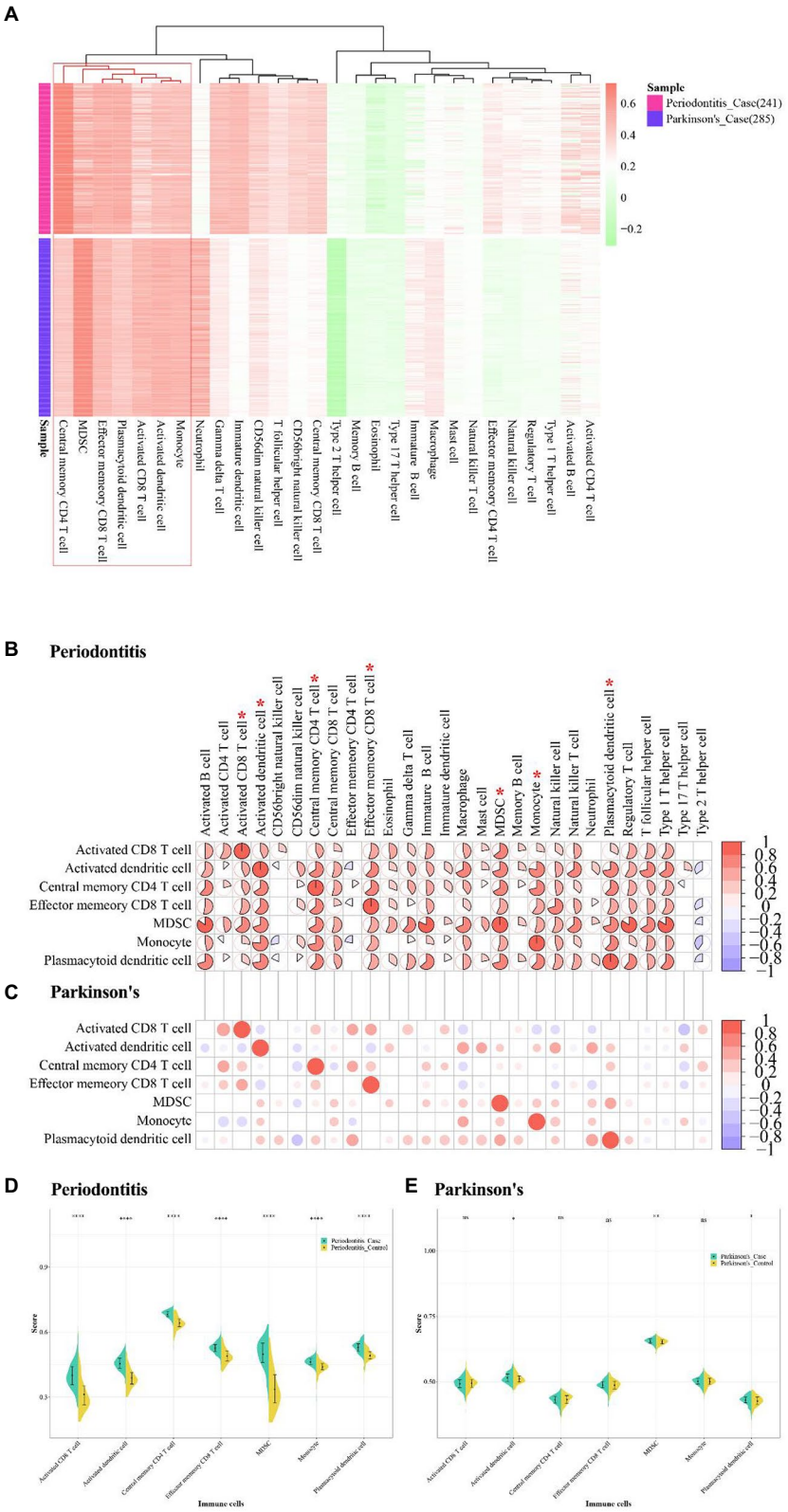

FIGURE 11
Immune infiltrative analysis of Periodontitis disease and Parkinson's disease. **(A)** The abundance fraction of immune cells in disease samples of Periodontitis disease and Parkinson's disease. **(B,C)** Correlation of higher abundance immune cells and other immune cells in Periodontitis disease and Parkinson's disease. **(D,E)** Immune cell enrichment fractions in different sample types of Periodontitis and Parkinson's disease.

TABLE 7 The correlation between immune cells in periodontitis and Parkinson's disease.

Immune cell Type 1	Immune cell Type 2	*r*-value	*p*-value	Significance
Periodontitis				
Activated B cell	MDSC	0.84697554	1.60E-67	***
Type 1 T helper cell	MDSC	0.840122561	1.95E-65	***
Regulatory T cell	MDSC	0.837361374	1.26E-64	***
Immature B cell	MDSC	0.816824025	5.01E-59	***
Activated dendritic cell	Monocyte	0.764481625	1.80E-47	***
Monocyte	Activated dendritic cell	0.764481625	1.80E-47	***
Activated dendritic cell	Plasmacytoid dendritic cell	0.722465839	3.53E-40	***
Plasmacytoid dendritic cell	Activated dendritic cell	0.722465839	3.53E-40	***
Central memory CD4 T cell	Monocyte	0.714514793	6.01E-39	***
Monocyte	Central memory CD4 T cell	0.714514793	6.01E-39	***
T follicular helper cell	Activated dendritic cell	0.711295204	1.84E-38	***
MDSC	Plasmacytoid dendritic cell	0.707824783	6.05E-38	***
Plasmacytoid dendritic cell	MDSC	0.707824783	6.05E-38	***
Natural killer cell	Effector memory CD8 T cell	0.706920024	8.23E-38	***
Activated B cell	Plasmacytoid dendritic cell	0.705392312	1.38E-37	***
Activated dendritic cell	MDSC	0.697836471	1.69E-36	***
MDSC	Activated dendritic cell	0.697836471	1.69E-36	***
Macrophage	MDSC	0.686624343	6.05E-35	***
Macrophage	Activated dendritic cell	0.67722499	1.08E-33	***
Central memory CD4 T cell	MDSC	0.66604896	2.87E-32	***
MDSC	Central memory CD4 T cell	0.66604896	2.87E-32	***
T follicular helper cell	MDSC	0.664832249	4.07E-32	***
Activated dendritic cell	Central memory CD4 T cell	0.657279808	3.43E-31	***
Central memory CD4 T cell	Activated dendritic cell	0.657279808	3.43E-31	***
Natural killer T cell	Activated dendritic cell	0.653593529	9.49E-31	***
Type 1 T helper cell	Activated dendritic cell	0.65032303	2.31E-30	***
Activated CD8 T cell	MDSC	0.644174127	1.20E-29	***
MDSC	Activated CD8 T cell	0.644174127	1.20E-29	***
Natural killer T cell	MDSC	0.64259343	1.82E-29	***
Immature B cell	Plasmacytoid dendritic cell	0.637325431	7.19E-29	***
Central memory CD4 T cell	Effector memory CD8 T cell	0.636332538	9.29E-29	***
Effector memory CD8 T cell	Central memory CD4 T cell	0.636332538	9.29E-29	***
Monocyte	Plasmacytoid dendritic cell	0.618419171	8.02E-27	***
Plasmacytoid dendritic cell	Monocyte	0.618419171	8.02E-27	***
Central memory CD4 T cell	Plasmacytoid dendritic cell	0.61554209	1.60E-26	***
Plasmacytoid dendritic cell	Central memory CD4 T cell	0.61554209	1.60E-26	***
Activated dendritic cell	Effector memory CD8 T cell	0.612911102	2.98E-26	***
Effector memory CD8 T cell	Activated dendritic cell	0.612911102	2.98E-26	***
Activated B cell	Central memory CD4 T cell	0.609622487	6.46E-26	***
Gamma delta T cell	MDSC	0.609155618	7.20E-26	***
Type 1 T helper cell	Plasmacytoid dendritic cell	0.606999798	1.19E-25	***
Regulatory T cell	Plasmacytoid dendritic cell	0.602434095	3.39E-25	***
Effector memory CD8 T cell	Monocyte	0.595426389	1.64E-24	***
Monocyte	Effector memory CD8 T cell	0.595426389	1.64E-24	***
Activated B cell	Activated dendritic cell	0.582637192	2.64E-23	***
Type 1 T helper cell	Activated CD8 T cell	0.582132066	2.93E-23	***
Type 1 T helper cell	Central memory CD4 T cell	0.58162473	3.27E-23	***
Regulatory T cell	Activated dendritic cell	0.58144374	3.39E-23	***
Type 1 T helper cell	Effector memory CD8 T cell	0.574544534	1.44E-22	***

(Continued)

TABLE 7 (Continued)

Immune cell Type 1	Immune cell Type 2	*r*-value	*p*-value	Significance
Eosinophil	MDSC	0.572134369	2.36E-22	***
Activated CD4 T cell	Activated CD8 T cell	0.569621164	3.94E-22	***
Effector memory CD8 T cell	MDSC	0.569618568	3.94E-22	***
MDSC	Effector memory CD8 T cell	0.569618568	3.94E-22	***
Effector memory CD8 T cell	Plasmacytoid dendritic cell	0.563135876	1.45E-21	***
Plasmacytoid dendritic cell	Effector memory CD8 T cell	0.563135876	1.45E-21	***
Natural killer cell	MDSC	0.561420539	2.04E-21	***
Natural killer cell	Plasmacytoid dendritic cell	0.552501589	1.16E-20	***
Regulatory T cell	Activated CD8 T cell	0.549123737	2.21E-20	***
T follicular helper cell	Activated CD8 T cell	0.54876323	2.36E-20	***
Activated CD8 T cell	Effector memory CD8 T cell	0.545321557	4.52E-20	***
Effector memory CD8 T cell	Activated CD8 T cell	0.545321557	4.52E-20	***
Central memory CD8 T cell	MDSC	0.54186573	8.60E-20	***
Natural killer T cell	Plasmacytoid dendritic cell	0.541209893	9.71E-20	***
MDSC	Monocyte	0.54120915	9.71E-20	***
Monocyte	MDSC	0.54120915	9.71E-20	***
Central memory CD8 T cell	Activated dendritic cell	0.541083811	9.93E-20	***
Central memory CD8 T cell	Central memory CD4 T cell	0.540839323	1.04E-19	***
Gamma delta T cell	Plasmacytoid dendritic cell	0.531789461	5.38E-19	***
T follicular helper cell	Monocyte	0.531104362	6.09E-19	***
Immature B cell	Activated CD8 T cell	0.529705171	7.81E-19	***
Regulatory T cell	Central memory CD4 T cell	0.528671052	9.38E-19	***
Activated B cell	Effector memory CD8 T cell	0.528579509	9.54E-19	***
Type 1 T helper cell	Monocyte	0.504458027	5.80E-17	***
Macrophage	Plasmacytoid dendritic cell	0.500397599	1.12E-16	***
Activated B cell	Activated CD8 T cell	0.499708365	1.25E-16	***
T follicular helper cell	Effector memory CD8 T cell	0.497187741	1.88E-16	***
Eosinophil	Activated CD8 T cell	0.485978771	1.09E-15	***
Immature B cell	Central memory CD4 T cell	0.485824724	1.12E-15	***
T follicular helper cell	Plasmacytoid dendritic cell	0.485378278	1.20E-15	***
Natural killer cell	Activated dendritic cell	0.48420841	1.43E-15	***
Natural killer T cell	Activated CD8 T cell	0.475167393	5.60E-15	***
Natural killer cell	Central memory CD4 T cell	0.472655726	8.13E-15	***
Central memory CD8 T cell	Monocyte	0.471236629	1.00E-14	***
Activated CD4 T cell	MDSC	0.463909411	2.90E-14	***
Immature B cell	Effector memory CD8 T cell	0.46250849	3.54E-14	***
Activated B cell	Monocyte	0.460718763	4.57E-14	***
Macrophage	Activated CD8 T cell	0.457572029	7.13E-14	***
Natural killer T cell	Effector memory CD8 T cell	0.456250217	8.58E-14	***
Natural killer cell	Monocyte	0.451913064	1.57E-13	***
Macrophage	Monocyte	0.447029978	3.05E-13	***
Regulatory T cell	Effector memory CD8 T cell	0.444491073	4.30E-13	***
T follicular helper cell	Central memory CD4 T cell	0.441533585	6.40E-13	***
Central memory CD8 T cell	Plasmacytoid dendritic cell	0.439049415	8.89E-13	***
Activated CD8 T cell	Activated dendritic cell	0.436269671	1.28E-12	***
Activated dendritic cell	Activated CD8 T cell	0.436269671	1.28E-12	***
CD56dim natural killer cell	Activated dendritic cell	0.433192287	1.91E-12	***
Activated CD8 T cell	Central memory CD4 T cell	0.43163635	2.34E-12	***
Central memory CD4 T cell	Activated CD8 T cell	0.43163635	2.34E-12	***
Immature B cell	Activated dendritic cell	0.426458372	4.54E-12	***

(Continued)

TABLE 7 (Continued)

Immune cell Type 1	Immune cell Type 2	*r*-value	*p*-value	Significance
Gamma delta T cell	Activated dendritic cell	0.420832272	9.21E-12	***
Mast cell	MDSC	0.414996797	1.89E-11	***
Gamma delta T cell	Central memory CD4 T cell	0.407666833	4.58E-11	***
Macrophage	Central memory CD4 T cell	0.400362875	1.08E-10	***
Neutrophil	Activated dendritic cell	0.367303528	4.12E-09	***
Gamma delta T cell	Activated CD8 T cell	0.366367009	4.54E-09	***
Natural killer T cell	Central memory CD4 T cell	0.363634497	6.02E-09	***
CD56dim natural killer cell	Monocyte	0.363021235	6.41E-09	***
Macrophage	Effector memory CD8 T cell	0.353705384	1.64E-08	***
Immature dendritic cell	Central memory CD4 T cell	0.353607436	1.66E-08	***
Immature dendritic cell	Activated dendritic cell	0.349212099	2.56E-08	***
Natural killer T cell	Monocyte	0.345840064	3.55E-08	***
Eosinophil	Plasmacytoid dendritic cell	0.34454255	4.02E-08	***
Natural killer cell	Activated CD8 T cell	0.344293922	4.12E-08	***
CD56dim natural killer cell	Effector memory CD8 T cell	0.338007281	7.48E-08	***
Neutrophil	Plasmacytoid dendritic cell	0.336720129	8.44E-08	***
Regulatory T cell	Monocyte	0.327379534	1.99E-07	***
Activated CD8 T cell	Plasmacytoid dendritic cell	0.323496414	2.83E-07	***
Plasmacytoid dendritic cell	Activated CD8 T cell	0.323496414	2.83E-07	***
Eosinophil	Effector memory CD8 T cell	0.320532888	3.68E-07	***
Eosinophil	Central memory CD4 T cell	0.302555673	1.71E-06	***
Parkinson's disease				
Activated CD4 T cell	Activated CD8 T cell	0.599074977	3.77E-29	***
Neutrophil	Plasmacytoid dendritic cell	0.500181503	1.90E-19	***
Effector memory CD4 T cell	Plasmacytoid dendritic cell	0.484410676	3.56E-18	***
Activated CD4 T cell	Central memory CD4 T cell	0.476766534	1.40E-17	***
Macrophage	Activated dendritic cell	0.473049766	2.68E-17	***
Activated CD8 T cell	Effector memory CD8 T cell	0.456873144	4.20E-16	***
Effector memory CD8 T cell	Activated CD8 T cell	0.456873144	4.20E-16	***
Effector memory CD4 T cell	Activated CD8 T cell	0.443595434	3.61E-15	***
MDSC	Plasmacytoid dendritic cell	0.435338298	1.31E-14	***
Plasmacytoid dendritic cell	MDSC	0.435338298	1.31E-14	***
Neutrophil	Activated dendritic cell	0.433717488	1.68E-14	***
Natural killer cell	Activated dendritic cell	0.4192127	1.48E-13	***
Effector memory CD4 T cell	Central memory CD4 T cell	0.416668771	2.14E-13	***
Macrophage	Monocyte	0.405530203	1.04E-12	***
Mast cell	Activated dendritic cell	0.400738176	2.03E-12	***
Mast cell	Plasmacytoid dendritic cell	0.388706161	1.03E-11	***
Gamma delta T cell	Activated CD8 T cell	0.384135928	1.87E-11	***
Type 2 T helper cell	Central memory CD4 T cell	0.363258068	2.57E-10	***
Immature dendritic cell	Plasmacytoid dendritic cell	0.351256754	1.07E-09	***
Activated CD8 T cell	Central memory CD4 T cell	0.349402777	1.32E-09	***
Central memory CD4 T cell	Activated CD8 T cell	0.349402777	1.32E-09	***
Central memory CD4 T cell	Effector memory CD8 T cell	0.340048326	3.82E-09	***
Effector memory CD8 T cell	Central memory CD4 T cell	0.340048326	3.82E-09	***
Macrophage	Plasmacytoid dendritic cell	0.333212561	8.11E-09	***
Gamma delta T cell	Plasmacytoid dendritic cell	0.330016388	1.15E-08	***
Natural killer cell	Monocyte	0.326552107	1.66E-08	***
Immature dendritic cell	Activated CD8 T cell	0.310533819	8.69E-08	***
Type 2 T helper cell	Activated CD8 T cell	0.309078509	1.00E-07	***

***$p <= 0.001$.

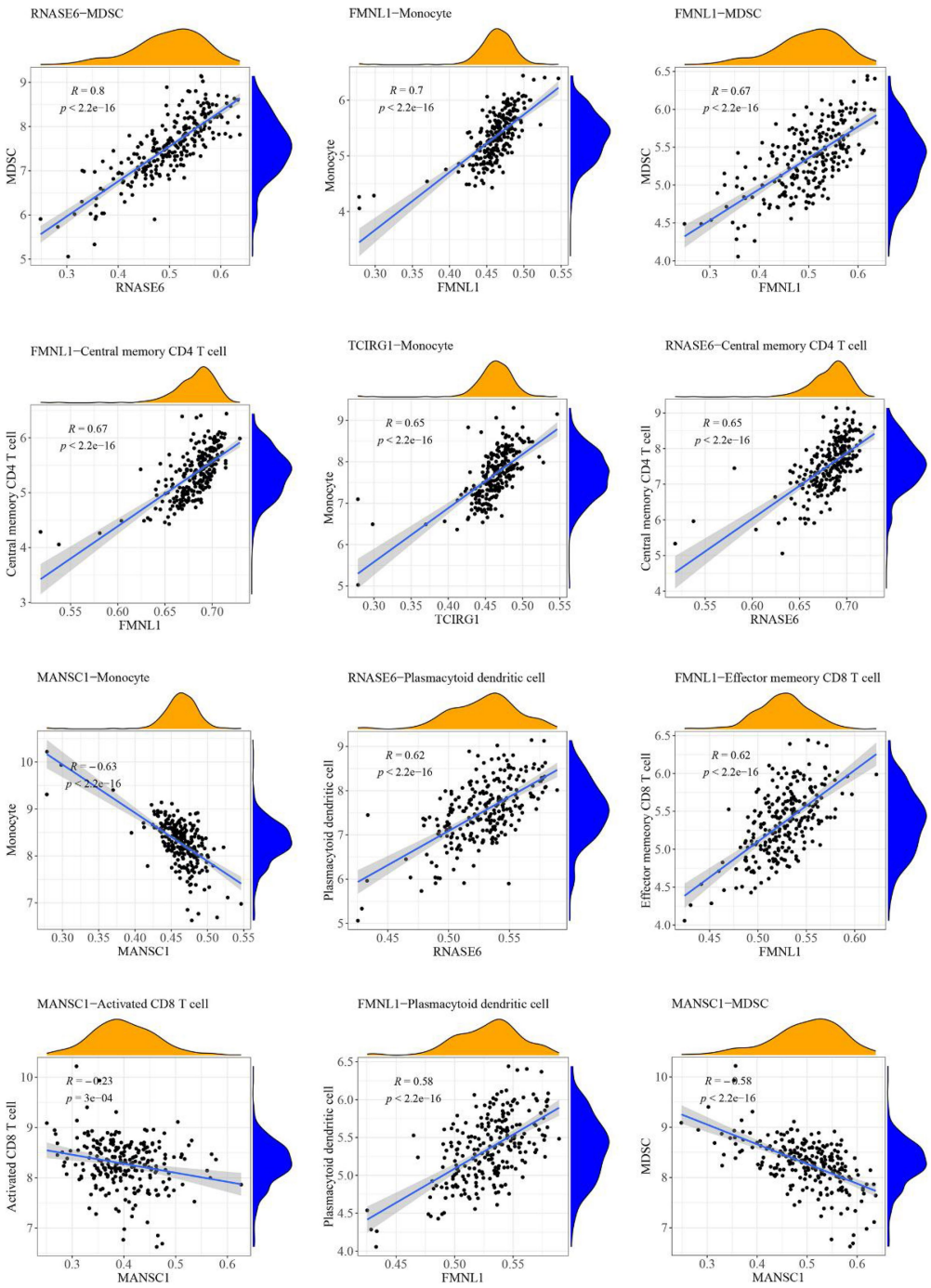

FIGURE 12
Relationship between high-abundance immune cells and hub cross-talk genes in periodontitis.

phagosome formation. In this section, previous literature were reviewed to explain the linking role of these genetic factors in the pathogenesis of both diseases.

The formin FRL1 (FMNL1) resides in the actin-rich cores of primary macrophage podosomes. During adhesion and migration of macrophages, FMNL1 is responsible for modifiying actin at the podosome in macrophages (Mersich et al., 2010). By stabilizing podosome lifespans without interacting with fast-growing actin termini, FMNL1 promotes migration and recruitment activity of macrophages (Miller et al., 2017). Additionally, FMNL1 is upregulated in the course of monocyte differentiation to macrophages (Mersich et al., 2010), which might be used for explaining the significant correlation between FMNL1 and monocytes in periodontitis (Table 8: $r = 0.701080924$;

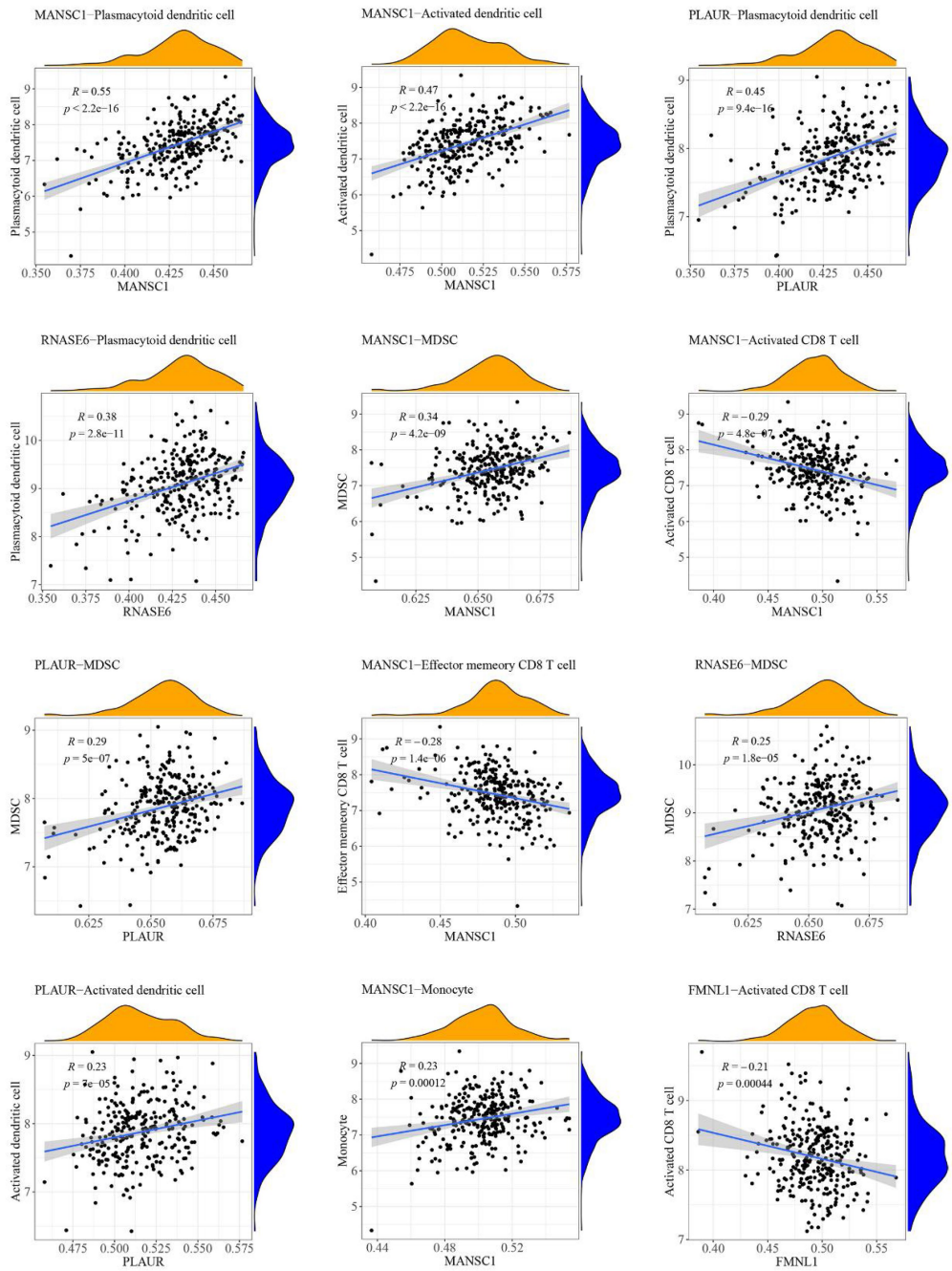

FIGURE 13
Relationship between high-abundance immune cells and hub cross-talk gene in Parkinson's disease.

$p = 5.82E-37$) and PD (Table 8: $r = 0.143364384$; $p = 0.015428656$). The potential role of FMNL1 in enhancing macrophage activity might be involved in the mechanism of periodontitis inducing PD progression. In periodontitis, overgrowth of Gram-negative bacteria and LPS access to the blood circulation may enhance the activation of macrophages in peripheral blood (Pussinen et al., 2004). One of the hallmarks of PD is the impairment of BBB integrity and function (Al-Bachari et al., 2020), due to which immune cells, including macrophage clusters, can infiltrate from the peripheral blood into the CNS (Su and Zhou, 2021). The periodontal pathogen, *Escherichia coli (E. coli)*, can also penetrate the impaired BBB of a PD patient. In a study, the LPS extracted from the cell wall of *E. coli* was found to induce rapid and intense activation of microglia and macrophages (Blaylock, 2017). The macrophages stimulated by LPS caused robust neurotoxicity and immunoexcitotoxicity, which may play a central role in PD-associated neurodegeneration progression (Blaylock, 2017). Based on these studies, it may be suggested that the crosstalk gene FMNL1 is a common link between periodontitis and PD *via* macrophage activation. However, there is no published research

TABLE 8 The correlation between hub crosstalk genes and immune cells in periodontitis and Parkinson's disease, respectively.

Hub crosstalk genes	Immune cells	*r*-value	abs_r value	*p*-value	Significance
Periodontitis					
RNASE6	MDSC	0.804313666	8.04E-01	5.98E-56	***
FMNL1	Monocyte	0.701080924	7.01E-01	5.82E-37	***
FMNL1	MDSC	0.674505139	6.75E-01	2.42E-33	***
FMNL1	Central memory CD4 T cell	0.668905401	6.69E-01	1.26E-32	***
TCIRG1	Monocyte	0.651103432	6.51E-01	1.87E-30	***
RNASE6	Central memory CD4 T cell	0.647773522	6.48E-01	4.60E-30	***
RNASE6	Plasmacytoid dendritic cell	0.620123162	6.20E-01	5.31E-27	***
FMNL1	Effector memory CD8 T cell	0.618680488	6.19E-01	7.53E-27	***
FMNL1	Plasmacytoid dendritic cell	0.582572461	5.83E-01	2.67E-23	***
TCIRG1	Central memory CD4 T cell	0.555225112	5.55E-01	6.85E-21	***
FMNL1	Activated dendritic cell	0.55205012	5.52E-01	1.26E-20	***
PLAUR	Activated dendritic cell	0.532123801	5.32E-01	5.07E-19	***
TCIRG1	MDSC	0.506582068	5.07E-01	4.09E-17	***
RNASE6	Activated dendritic cell	0.468481658	4.68E-01	1.50E-14	***
RNASE6	Activated CD8 T cell	0.446647646	4.47E-01	3.22E-13	***
PLAUR	Monocyte	0.443562776	4.44E-01	4.88E-13	***
RNASE6	Monocyte	0.437623294	4.38E-01	1.07E-12	***
TCIRG1	Activated dendritic cell	0.427129687	4.27E-01	4.17E-12	***
TCIRG1	Plasmacytoid dendritic cell	0.420248526	4.20E-01	9.90E-12	***
TCIRG1	Effector memory CD8 T cell	0.40759104	4.08E-01	4.62E-11	***
PLAUR	Effector memory CD8 T cell	0.383329366	3.83E-01	7.43E-10	***
RNASE6	Effector memory CD8 T cell	0.376706992	3.77E-01	1.53E-09	***
FMNL1	Activated CD8 T cell	0.346157886	3.46E-01	3.44E-08	***
PLAUR	Plasmacytoid dendritic cell	0.345852593	3.46E-01	3.54E-08	***
PLAUR	Central memory CD4 T cell	0.342304629	3.42E-01	4.98E-08	***
PLAUR	MDSC	0.318805279	3.19E-01	4.28E-07	***
TCIRG1	Activated CD8 T cell	0.234786142	0.234786142	0.000235579	***
MANSC1	Activated CD8 T cell	−0.231175404	0.231175404	0.000295404	***
MANSC1	Central memory CD4 T cell	−0.529187133	5.29E-01	8.56E-19	***
MANSC1	Effector memory CD8 T cell	−0.532649636	5.33E-01	4.61E-19	***
MANSC1	Plasmacytoid dendritic cell	−0.539617258	5.40E-01	1.30E-19	***
MANSC1	MDSC	−0.576288835	5.76E-01	1.00E-22	***
MANSC1	Activated dendritic cell	−0.60804292	6.08E-01	9.33E-26	***
MANSC1	Monocyte	−0.625435826	6.25E-01	1.45E-27	***
Parkinson's disease					
MANSC1	Plasmacytoid dendritic cell	0.551790642	0.551790642	4.15E-24	***
MANSC1	Activated dendritic cell	0.467804822	0.467804822	6.65E-17	***
PLAUR	Plasmacytoid dendritic cell	0.451944976	0.451944976	9.43E-16	***
RNASE6	Plasmacytoid dendritic cell	0.381089523	0.381089523	2.77E-11	***
MANSC1	MDSC	0.33920803	0.33920803	4.19E-09	***
PLAUR	MDSC	0.292493364	0.292493364	4.99E-07	***
RNASE6	MDSC	0.251153249	0.251153249	1.78E-05	***
PLAUR	Activated dendritic cell	0.233308169	0.233308169	7.00E-05	***
MANSC1	Monocyte	0.226357563	0.226357563	0.000115866	***
PLAUR	Monocyte	0.183419906	0.183419906	0.001875335	**
TCIRG1	Effector memory CD8 T cell	0.169561529	0.169561529	0.004094811	**
RNASE6	Activated CD8 T cell	0.167950803	0.167950803	0.004467738	**
FMNL1	Monocyte	0.143364384	0.143364384	0.015428656	*
TCIRG1	Monocyte	0.143009576	0.143009576	0.015687724	*

(Continued)

TABLE 8 (Continued)

Hub crosstalk genes	Immune cells	*r*-value	abs_r value	*p*-value	Significance
RNASE6	Monocyte	0.131393959	0.131393959	0.026550632	*
TCIRG1	Activated dendritic cell	−0.120360896	0.120360896	0.042317655	*
FMNL1	Central memory CD4 T cell	−0.12064161	0.12064161	0.041835486	*
PLAUR	Activated CD8 T cell	−0.123935985	0.123935985	0.036514285	*
FMNL1	MDSC	−0.143148162	0.143148162	0.015586084	*
FMNL1	Activated CD8 T cell	−0.206836013	0.206836013	0.000440536	***
MANSC1	Effector memory CD8 T cell	−0.281186359	0.281186359	1.41E-06	***
MANSC1	Activated CD8 T cell	−0.292814914	0.292814914	4.85E-07	***

*p <= 0.05, **p <= 0.01, ***p <= 0.001.

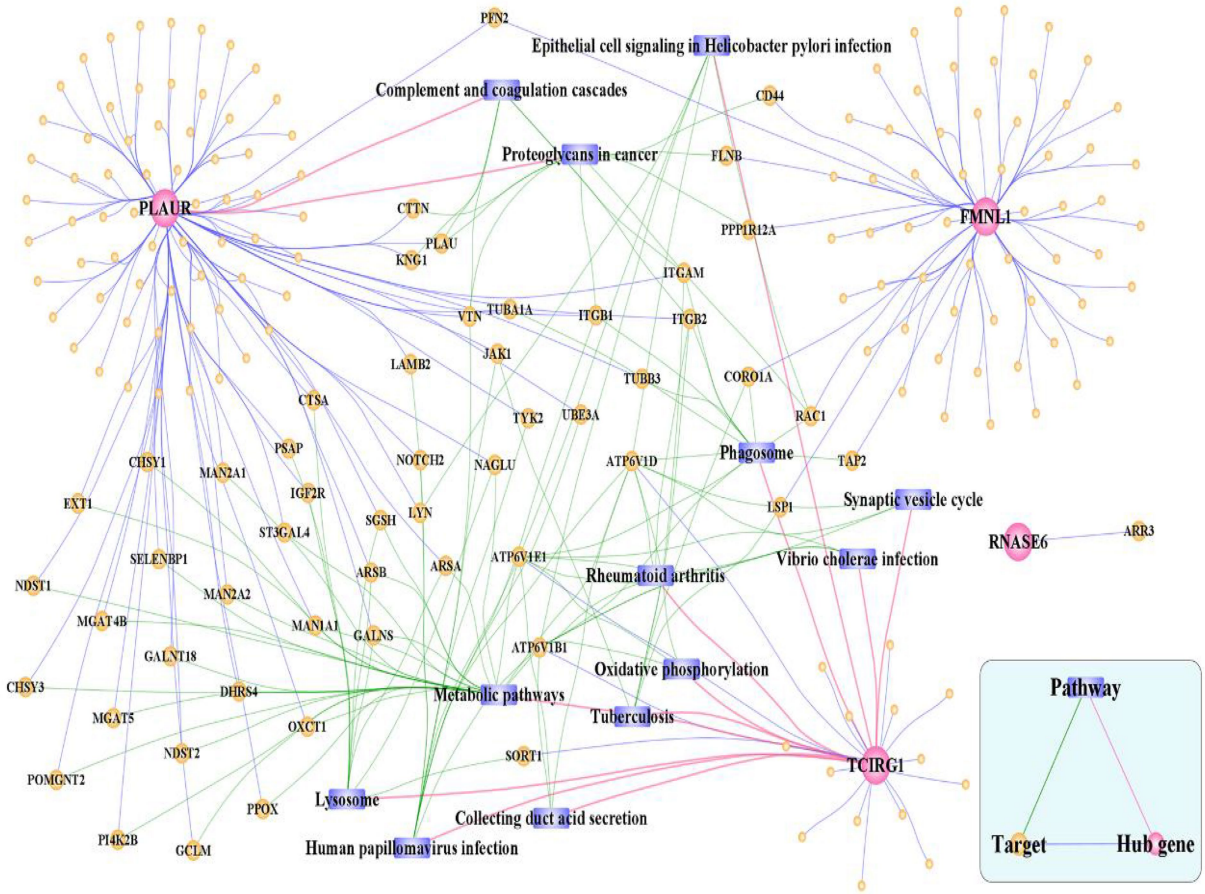

FIGURE 14
Hub cross-talk gene related complex network. The network consists of 210 nodes and 303 edges.

investigating the deregulation and function of FMNL1 in linking periodontitis and PD to date.

The Plasminogen Activator Urokinase (PLAU) gene encodes the receptor for Urokinase-type Plasminogen Activator (uPA). uPA has a role in localizing and promoting plasmin formation and was found to be implicated in the pathological processes associated with cell-surface plasminogen activation and localized degradation of the extracellular matrix. In periodontitis, uPA converts plasminogen to plasmin, leading to the uPA proteolytic cascade activated by *P. gingivalis* and inducing tissue destruction, particularly, alveolar bone loss (Fleetwood et al., 2015). Additionally, uPA was found to be a marker of macrophage activation based on its role in regulating macrophage motility and macrophage-mediated matrix degradation in periodontitis (Fleetwood et al., 2014). In PD, uPA was found to act as an activator protease in the process of plasminogen activation and upregulate the expression of the serine protease inhibitor (serpin) plasminogen activator inhibitor-1 (PAI-1), leading to

neuroinflammation (Reuland and Church, 2020). Further, an increased expression of Urokinase Plasminogen-activator Receptor (uPAR) was observed in activated microglia in the brain of a patient with another neurodegenerative disease (Alzheimer's disease), and uPAR expression was found to be mediated by oxidative stress-related mechanisms (Walker et al., 2002).

TCIRG1 (T Cell Immune Regulator 1, ATPase H+ Transporting V0) encodes the a3 isoform of V-ATPase a subunit, which is essential for osteoclastic bone resorption. The promoter activity of serial-deletion fragments of the TCIRG1 gene promoter was observed to be enhanced throughout the osteoclastic differentiation process of osteoclast RAW264.7 cells, and such alteration was found to be induced by the receptor activator of nuclear factor kB ligand (RANKL) (Beranger et al., 2007). TCIRG1 expression was found to induce the bone resorption activity of osteoclasts in periodontal disease (Heo et al., 2022). TCIRG1 was highly expressed in myeloid cells and involved in myeloid cell activation and microglial neuroinflammation (Funatsu et al., 2022). The mRNA expression of TCIRG1 gene was recently examined in human alloactivated T lymphocytes, which indicates that TCIRG1 was essential in T cell activation (Heinemann et al., 1999). Our present study found that the TCIRG1 expression level was positively correlated with effector memory cluster of differentiation (CD)8+ T cells ($r = 0.41$; $p = 4.62E-11$) in periodontitis. Similarly, a positive and significant correlation was found between the TCIRG1 expression level and effector memory CD8+ T cells ($r = 0.17$; $p = 0.004$) in PD. In periodontitis, the CD8+ T cells with an effector memory phenotype were shown to release anti-inflammatory cytokines (interleukin [IL]-10 and transforming growth factor [TGF]-β) and suppress bone-destructive cytokines (interferon [IFN]-γ and IL-17), and thus play a protective role for the alveolar bone (Cardoso and Arosa, 2017). In PD, the cytotoxic attack of a robust CD8+ T cell infiltration might initiate and propagate neuronal death and synucleinopathy by secreting cytolytic enzymes (granzymes A, B, and K) and/or pro-inflammatory cytokines (IFN-γ) (Galiano-Landeira et al., 2020). These studies validated the possibility of our findings that the hub crosstalk gene TCIRG1 links periodontitis and PD *via* regulating effector memory CD8+ T cells.

The complement and coagulation cascade pathway was found to be enriched by the crosstalk genes linking periodontitis and PD. The complement system plays a vital role in immune surveillance, homeostasis, and bridges the innate and adaptive immune systems (Ricklin et al., 2010). A study showed that suppressing component 3 (C3) in the complement cascade directly inhibits periodontal inflammation and indirectly counteracts dysbiosis, thus showing promising clinical potential for treating periodontitis (Hajishengallis et al., 2019). The complement C3-positive astrocytes were increased in the ventral midbrain of the intrastriatal α-synuclein preformed fibril (PFF)-injected mice, and C3 secreted from astrocytes could induce the degeneration of dopaminergic neurons, suggesting the potential involvement of complement and coagulation cascades in dopaminergic neurodegeneration in PD (Ma et al., 2021). Considering the involvement of complement system activation in both periodontitis and PD, this pathway might link both diseases by means of neuroimmune interaction. The complement system activation triggered by periodontitis may regulate the migration and invasion function of the peripheral immune cells (Merle et al., 2015), which may penetrate the damaged BBB and induce neuroinflammation and neurodegeneration in PD patients (Chao et al., 2014). Apart from the complement and coagulation cascade pathway, oxidative phosphorylation was identified to be an important pathogenic pathway contributing the linkages between both diseases. It is through oxygen oxidative phosphorylation that oxygen inhaled by the body is used to produce energy (Cole, 2016). Mutations in mitochondrial DNA result in reduced efficiency of oxidative phosphorylation and ATP production, overproduction of ROS, and a significant reduction in mitochondrial membrane potential (MMP) levels in pathophysiological conditions (Xu et al., 2021). The downregulation of PD-related gene-complex I was found to be involved in oxidative phosphorylation by leading to reduced ATP formation in neurons and further inducing neuronal apoptosis (Ali and Dholaniya, 2022). In addition, *P. gingivalis* infection was found to promote mitochondrial fragmentation and dysfunction, increase the levels of mitochondrial reactive oxygen species (mtROS), and upregulate the phosphorylation of Drp1 gene (Xu et al., 2021).

The current study found that several immune cells (e.g., central memory CD4 T cells, effector memory CD8 T cells, activated CD8 T cells, myeloid-derived suppressor cells (MDSCs), plasmacytoid dendritic cells, activated dendritic cells, and Monocytes) were highly expressed in periodontitis disease and PD. Among these immune cells, MDSCs and dendritic cells obtained our particular interest. It is believed that MDSCs have the most potential for restoring homeostasis after inflammation, as well as being able to suppress adaptive immunity by suppressing T cell response (Kauppinen et al., 2020). The MDSCs was detected to be significantly increased in peripheral blood of patients with PD compared with healthy control individuals, which led to the increased production of immunosuppression-related genes [arginase 1 (ARG1), interleukin-10 (IL-10), and cyclooxygenase 2 (COX-2)] (Yang et al., 2018). MDSCs were also found to be expanded, activated, and recruited as the result of the inflammatory response induced by *P. gingivalis* infection in periodontitis (Valero-Monroy et al., 2016; Su et al., 2017). As professional antigen-presenting cells, dendritic cells link innate and adaptive immunity and are vital to the induction of protective immune responses against pathogens (Liu et al., 2021). Peripheral blood dendritic cells in chronic periodontitis was found to carry *P. gingivalis*. Such microbial carriage state not only enhanced the differentiation of monocytes into immature myeloid dendritic cells, but also promoted the production of matrix metalloproteinase-9 and upregulated C1q, heat shock protein 60, heat shock protein 70, CCR2, and CXCL16 (Carrion et al., 2012). The recruitment of activated subsets of dendritic cells in the brain was found to increase the production of pro-inflammatory cytokines (e.g., TNFα, IL1β, and IL6) and aggregate alpha synuclein (Agg α-syn) fuels neuroinflammation in PD (Magnusen et al., 2018).

It is noteworthy to highlight the limitation of the current study. The genetic factors identified in the current study are obtained solely using computational prediction based on the periodontitis-and PD-associated datasets; however, these factors were not validated by performing related experiments. The representative periodontal pathogen *P. gingivalis* or its derived LPS could be used for infecting the microglia and its activated immune and inflammation-related signaling pathways could be examined. The transcriptomic alterations of microglial cells under such stimulation can be examined by performing next generation sequencing approach. The animal model with PD could be established to identify the influence of *P. gingivalis* or its derived LPS on the immune cells in the brain. Another limitation is regarding the GEO datasets analyzed in the current research. Although four datasets were included and analyzed in the current research, the sample size included in each dataset restricted the prediction accuracy of the results. In addition, there is no public dataset integrating both diseases and investigating the alteration in mRNA expression of the peripheral blood tissue in PD with/without periodontitis. Nevertheless, this study has potential for clinical application by suggesting putative genetic mechanisms underlying the increased risk of periodontitis in PD progression. The five hub crosstalk genes discussed in this study hold promise to be developed as a chair-side kit for predicting the risk of PD in elderly periodontitis patients. Further investigation is needed to validate the prediction accuracy of these genetic findings.

Conclusion

Five genes (i.e., FMNL1, MANSC1, PLAUR, RNASE6, and TCIRG1) were identified as crosstalk biomarkers linking PD and periodontitis. The significant correlation between these crosstalk genes and immune cells strongly suggests the involvement of immunology in linking both diseases.

Data availability statement

The original contributions presented in the study are included in the article/Supplementary material, further inquiries can be directed to the corresponding author.

Author contributions

SHu and SL: conceptualization, funding acquisition, methodology, formal analysis, and writing—original draft. WN, XH, XL, YD, DF, AO, BL, VS, HL, SG, RZ, and DZ: methodology, formal analysis, review, and editing. GS, SHu, and SHuang: project administration and supervision. All authors contributed to the article and approved the submitted version.

Funding

We appreciate the funding by the Science Research Cultivation Program of Stomatological Hospital, Southern Medical University (Grant No.: PY2022001 for supporting the postdoc research of Dr. Shaonan Hu (Email: shaonan_hu@smu.edu.cn) and Grant No.: PY2020004 for supporting the postdoc research of Dr. Simin Li (Email: simin.li.dentist@ gmail.com)).

Conflict of interest

The authors declare that the research was conducted in the absence of any commercial or financial relationships that could be construed as a potential conflict of interest.

Publisher's note

All claims expressed in this article are solely those of the authors and do not necessarily represent those of their affiliated organizations, or those of the publisher, the editors and the reviewers. Any product that may be evaluated in this article, or claim that may be made by its manufacturer, is not guaranteed or endorsed by the publisher.

Supplementary material

The Supplementary material for this article can be found online at: https://www.frontiersin.org/articles/10.3389/fnagi.2022.1032401/full#supplementary-material

References

Al-Bachari, S., Naish, J. H., Parker, G. J. M., Emsley, H. C. A., and Parkes, L. M. (2020). Blood–brain barrier leakage is increased in Parkinson's disease. *Front. Physiol.* 11:593026. doi: 10.3389/fphys.2020.593026

Ali, M. Z., and Dholaniya, P. S. (2022). Oxidative phosphorylation mediated pathogenesis of Parkinson's disease and its implication via Akt signaling. *Neurochem. Int.* 157:105344. doi: 10.1016/j.neuint.2022.105344

Al-Omari, F. A., Al Moaleem, A. M., Al-Qahtani, S. S., Al Garni, A. S., Sadatullah, S., Luqman, M., et al. (2014). Oral rehabilitation of Parkinson's disease patient: a review and case report. *Case Rep. Dent.* 2014, 1–4. doi: 10.1155/2014/432475

Alves, S. R., Silva, C., Rosa, I. M., Henriques, A. G., and Silva, O. A. B. (2022). A bioinformatics approach toward unravelling the synaptic molecular crosstalk between Alzheimer's disease and diabetes. *J. Alzheimers Dis.* 86, 1917–1933. doi: 10.3233/JAD-215059

Auffret, M., Meuric, V., Boyer, E., Bonnaure-Mallet, M., and Vérin, M. (2021). Oral health disorders in Parkinson's disease: more than meets the eye. *J. Parkinsons Dis.* 11, 1507–1535. doi: 10.3233/JPD-212605

Beranger, G. E., Momier, D., Guigonis, J. M., Samson, M., Carle, G. F., and Scimeca, J. C. (2007). Differential binding of poly (ADP-ribose) polymerase-1 and JunD/Fra2 accounts for RANKL-induced Tcirg1 gene expression during osteoclastogenesis. *J. Bone Miner. Res.* 22, 975–983. doi: 10.1359/jbmr.070406

Blaszczyk, J. W. (2016). Parkinson's disease and Neurodegeneration: GABA-collapse hypothesis. *Front. Neurosci.* 10:269. doi: 10.3389/fnins.2016.00269

Blaylock, R. L. (2017). Parkinson's disease: microglial/macrophage-induced immunoexcitotoxicity as a central mechanism of neurodegeneration. *Surg. Neurol. Int.* 8:65. doi: 10.4103/sni.sni_441_16

Bohatschek, M., Werner, A., and Raivich, G. (2001). Systemic LPS injection leads to granulocyte influx into normal and injured brain: effects of ICAM-1 deficiency. *Exp. Neurol.* 172, 137–152. doi: 10.1006/exnr.2001.7764

Botelho, J., Mascarenhas, P., Mendes, J. J., and Machado, V. (2020). Network protein interaction in Parkinson's disease and periodontitis interplay: a preliminary Bioinformatic analysis. *Genes (Basel)* 11:1385. doi: 10.3390/genes11111385

Cardoso, E. M., and Arosa, F. A. (2017). CD8+ T cells in chronic periodontitis: roles and rules. *Front. Immunol.* 8:145. doi: 10.3389/fimmu.2017.00145

Carrion, J., Scisci, E., Miles, B., Sabino, G. J., Zeituni, A. E., Gu, Y., et al. (2012). Microbial carriage state of peripheral blood dendritic cells (DCs) in chronic periodontitis influences DC differentiation, atherogenic potential. *J. Immunol.* 189, 3178–3187. doi: 10.4049/jimmunol.1201053

Chao, Y., Wong, S. C., and Tan, E. K. (2014). Evidence of inflammatory system involvement in Parkinson's disease. *Biomed. Res. Int.* 2014, 1–9. doi: 10.1155/2014/308654

Chen, H., Peng, L., Wang, Z., He, Y., Tang, S., and Zhang, X. (2022). Exploration of cross-talk and pyroptosis-related gene signatures and molecular mechanisms between periodontitis and diabetes mellitus via peripheral blood mononuclear cell microarray data analysis. *Cytokine* 159:156014. doi: 10.1016/j.cyto.2022.156014

Chen, C. K., Wu, Y. T., and Chang, Y. C. (2017). Periodontal inflammatory disease is associated with the risk of Parkinson's disease: a population-based retrospective matched-cohort study. *PeerJ* 5:e3647. doi: 10.7717/peerj.3647

Chen, Y., Yu, X., and Kong, J. (2021). Identification of neuropeptides as potential cross talks linking down syndrome and periodontitis revealed by transcriptomic analyses. *Dis. Markers* 2021, 1–18. doi: 10.1155/2021/7331821

Cole, L. A. (2016). "Chapter 10 - Adenosine triphosphate energetics" in *Biology of Life*. ed. L. A. Cole (Elsevier Academic Press), 65–77.

Edgar, R., Domrachev, M., and Lash, A. E. (2002). Gene expression omnibus: NCBI gene expression and hybridization array data repository. *Nucleic Acids Res.* 30, 207–210. doi: 10.1093/nar/30.1.207

Fleetwood, A. J., Achuthan, A., Schultz, H., Nansen, A., Almholt, K., Usher, P., et al. (2014). Urokinase plasminogen activator is a central regulator of macrophage three-dimensional invasion, matrix degradation, and adhesion. *J. Immunol.* 192, 3540–3547. doi: 10.4049/jimmunol.1302864

Fleetwood, A. J., O'Brien-Simpson, N. M., Veith, P. D., Lam, R. S., Achuthan, A., Cook, A. D., et al. (2015). *Porphyromonas gingivalis*-derived RgpA-Kgp complex activates the macrophage urokinase plasminogen activator system: implications for periodontitis. *J. Biol. Chem.* 290, 16031–16042. doi: 10.1074/jbc.M115.645572

Funatsu, J., Murakami, Y., Shimokawa, , Nakatake, S., Fujiwara, K., Okita, A., et al. (2022). Circulating inflammatory monocytes oppose microglia and contribute to cone cell death in retinitis pigmentosa. *PNAS Nexus* 1:pgac003. doi: 10.1093/pnasnexus/pgac003

Galiano-Landeira, J., Torra, A., Vila, M., and Bové, J. (2020). CD8 T cell nigral infiltration precedes synucleinopathy in early stages of Parkinson's disease. *Brain* 143, 3717–3733. doi: 10.1093/brain/awaa269

Hajishengallis, G., Kajikawa, T., Hajishengallis, E., Maekawa, T., Reis, E. S., Mastellos, D. C., et al. (2019). Complement-dependent mechanisms and interventions in periodontal disease. *Front. Immunol.* 10:406. doi: 10.3389/fimmu.2019.00406

Hanaoka, A., and Kashihara, K. (2009). Increased frequencies of caries, periodontal disease and tooth loss in patients with Parkinson's disease. *J. Clin. Neurosci.* 16, 1279–1282. doi: 10.1016/j.jocn.2008.12.027

Hänzelmann, S., Castelo, R., and Guinney, J. (2013). GSVA: gene set variation analysis for microarray and RNA-seq data. *BMC Bioinformatics* 14, 1–15. doi: 10.1186/1471-2105-14-7

He, Z., Jiang, Q., Li, F., and Chen, M. (2021). Crosstalk between venous thromboembolism and periodontal diseases: a bioinformatics analysis. *Dis. Markers* 2021, 1–16. doi: 10.1155/2021/1776567

Heinemann, T., Bulwin, G. C., Randall, J., Schnieders, B., Sandhoff, K., Volk, H. D., et al. (1999). Genomic organization of the gene coding for TIRC7, a novel membrane protein essential for T cell activation. *Genomics* 57, 398–406. doi: 10.1006/geno.1999.5751

Heo, S. C., You, J. C., Jung, S., Kim, Y. N., Shin, S. H., Lee, J. Y., et al. (2022). Pim-2 regulates bone resorptive activity of osteoclasts via V-ATPase a3 isoform expression in periodontal disease. *J. Cell. Physiol.* 237, 3381–3393. doi: 10.1002/jcp.30814

Kanehisa, M., and Goto, S. (2000). KEGG: Kyoto encyclopedia of genes and genomes. *Nucleic Acids Res.* 28, 27–30. doi: 10.1093/nar/28.1.27

Karimi-Moghadam, A., Charsouei, S., Bell, B., and Jabalameli, M. R. (2018). Parkinson disease from Mendelian forms to genetic susceptibility: new molecular insights into the Neurodegeneration process. *Cell. Mol. Neurobiol.* 38, 1153–1178. doi: 10.1007/s10571-018-0587-4

Kassambara, A., and Mundt, F. (2017). Package 'factoextra'. Extract and visualize the results of multivariate data analyses. 1–74. Available at: http://www.sthda.com/english/rpkgs/factoextra

Kauppinen, A., Kaarniranta, K., and Salminen, A. (2020). Potential role of myeloid-derived suppressor cells (MDSCs) in age-related macular degeneration (AMD). *Front. Immunol.* 11:384. doi: 10.3389/fimmu.2020.00384

Kaur, G., Grover, V., Bhaskar, N., Kaur, R. K., and Jain, A. (2018). Periodontal infectogenomics. *Inflamm. Regen.* 38:8. doi: 10.1186/s41232-018-0065-x

Kaur, T., Uppoor, A., and Naik, D. (2016). Parkinson's disease and periodontitis - the missing link? A review. *Gerodontology* 33, 434–438. doi: 10.1111/ger.12188

Kebschull, M., Demmer, R. T., Grün, B., Guarnieri, P., Pavlidis, P., and Papapanou, P. N. (2014). Gingival tissue transcriptomes identify distinct periodontitis phenotypes. *J. Dent. Res.* 93, 459–468. doi: 10.1177/0022034514527288

Kolde, R., and Kolde, M. R. (2018). Package 'pheatmap'. *R Package* 1, 1–8.

Leek, J. T., Johnson, W. E., Parker, H. S., Fertig, E. J., Jaffe, A. E., Storey, J. D., et al. (2019). Sva: surrogate variable analysis. *R Package Version* 3, 882–883.

Li, S., Liu, X., Zhou, Y., Acharya, A., Savkovic, V., Xu, C., et al. (2018). Shared genetic and epigenetic mechanisms between chronic periodontitis and oral squamous cell carcinoma. *Oral Oncol.* 86, 216–224. doi: 10.1016/j.oraloncology.2018.09.029

Liu, S., Fu, Y., Ziebolz, D., Li, S., Schmalz, G., and Li, F. (2022a). Transcriptomic analysis reveals pathophysiological relationship between chronic obstructive pulmonary disease (COPD) and periodontitis. *BMC Med. Genet.* 15, 1–16. doi: 10.1186/s12920-022-01278-w

Liu, J., Zhang, D., Cao, Y., Zhang, H., Li, J., Xu, J., et al. (2022b). Screening of crosstalk and pyroptosis-related genes linking periodontitis and osteoporosis based on bioinformatics and machine learning. *Front. Immunol.* 13:955441. doi: 10.3389/fimmu.2022.955441

Liu, J., Zhang, X., Cheng, Y., and Cao, X. (2021). Dendritic cell migration in inflammation and immunity. *Cell. Mol. Immunol.* 18, 2461–2471. doi: 10.1038/s41423-021-00726-4

Lopez, R., Regier, J., Cole, M. B., Jordan, M. I., and Yosef, N. (2018). Deep generative modeling for single-cell transcriptomics. *Nat. Methods* 15, 1053–1058. doi: 10.1038/s41592-018-0229-2

Ma, S.-X., Seo, B. A., Kim, D., Xiong, Y., Kwon, S. H., Brahmachari, S., et al. (2021). Complement and coagulation cascades are potentially involved in dopaminergic neurodegeneration in α-synuclein-based mouse models of Parkinson's disease. *J. Proteome Res.* 20, 3428–3443. doi: 10.1021/acs.jproteome.0c01002

Magnusen, D., Nyamajenjere, T., Rapien, J., Mckay, M., Magnusen, A., and Pandey, M. (2018). Dendritic cells, CD4+ T cells, and α synuclein triangle fuels neuroinflammation in Parkinson's disease (P3. 053). *Neurology* 90.

Merle, N. S., Noe, R., Halbwachs-Mecarelli, L., Fremeaux-Bacchi, V., and Roumenina, L. T. (2015). Complement system part II: role in immunity. *Front. Immunol.* 6:257. doi: 10.3389/fimmu.2015.00257

Mersich, A. T., Miller, M. R., Chkourko, H., and Blystone, S. D. (2010). The formin FRL1 (FMNL1) is an essential component of macrophage podosomes. *Cytoskeleton* 67, 573–585. doi: 10.1002/cm.20468

Miller, M. R., Miller, E. W., and Blystone, S. D. (2017). Non-canonical activity of the podosomal formin FMNL1γ supports immune cell migration. *J. Cell Sci.* 130, 1730–1739. doi: 10.1242/jcs.195099

Mutez, E., Nkiliza, A., Belarbi, K., de Broucker, A., Vanbesien-Mailliot, C., Bleuse, S., et al. (2014). Involvement of the immune system, endocytosis and EIF2 signaling in both genetically determined and sporadic forms of Parkinson's disease. *Neurobiol. Dis.* 63, 165–170. doi: 10.1016/j.nbd.2013.11.007

Olsen, I., Kell, D. B., and Pretorius, E. (2020). Is *Porphyromonas gingivalis* involved in Parkinson's disease? *Eur. J. Clin. Microbiol. Infect. Dis.* 39, 2013–2018. doi: 10.1007/s10096-020-03944-2

Oughtred, R., Rust, J., Chang, C., Breitkreutz, B. J., Stark, C., Willems, A., et al. (2021). The BioGRID database: a comprehensive biomedical resource of curated protein, genetic, and chemical interactions. *Protein Sci.* 30, 187–200. doi: 10.1002/pro.3978

Pan, S., Hu, B., Sun, J., Yang, Z., Yu, W., He, Z., et al. (2022). Identification of cross-talk pathways and ferroptosis-related genes in periodontitis and type 2 diabetes mellitus by bioinformatics analysis and experimental validation. *Front. Immunol.* 13:1015491. doi: 10.3389/fimmu.2022.1015491

Papapanou, P. N., Behle, J. H., Kebschull, M., Celenti, R., Wolf, D. L., Handfield, M., et al. (2009). Subgingival bacterial colonization profiles correlate with gingival tissue gene expression. *BMC Microbiol.* 9:221. doi: 10.1186/1471-2180-9-221

Peri, S., Navarro, J. D., Kristiansen, T. Z., Amanchy, R., Surendranath, V., Muthusamy, B., et al. (2004). Human protein reference database as a discovery

resource for proteomics. *Nucleic Acids Res.* 32, 497D–4501D. doi: 10.1093/nar/gkh070

Pussinen, P. J., Vilkuna-Rautiainen, T., Alfthan, G., Palosuo, T., Jauhiainen, M., Sundvall, J., et al. (2004). Severe periodontitis enhances macrophage activation via increased serum lipopolysaccharide. *Arterioscler. Thromb. Vasc. Biol.* 24, 2174–2180. doi: 10.1161/01.ATV.0000145979.82184.9f

Reuland, C. J., and Church, F. C. (2020). Synergy between plasminogen activator inhibitor-1, α-synuclein, and neuroinflammation in Parkinson's disease. *Med. Hypotheses* 138:109602. doi: 10.1016/j.mehy.2020.109602

Ricklin, D., Hajishengallis, G., Yang, K., and Lambris, J. D. (2010). Complement: a key system for immune surveillance and homeostasis. *Nat. Immunol.* 11, 785–797. doi: 10.1038/ni.1923

Ritchie, M. E., Phipson, B., Wu, D., Hu, Y., Law, C. W., Shi, W., et al. (2015). Limma powers differential expression analyses for RNA-sequencing and microarray studies. *Nucleic Acids Res.* 43:e47. doi: 10.1093/nar/gkv007

Scannapieco, F. A. (2004). Periodontal inflammation: from gingivitis to systemic disease? *Compend. Contin. Educ. Dent.* 25, 16–25.

Scherzer, C. R., Eklund, A. C., Morse, L. J., Liao, Z., Locascio, J. J., Fefer, D., et al. (2007). Molecular markers of early Parkinson's disease based on gene expression in blood. *Proc. Natl. Acad. Sci.* 104, 955–960. doi: 10.1073/pnas.0610204104

Scherzer, C. R., Grass, J. A., Liao, Z., Pepivani, I., Zheng, B., Eklund, A. C., et al. (2008). GATA transcription factors directly regulate the Parkinson's disease-linked gene alpha-synuclein. *Proc. Natl. Acad. Sci. U. S. A.* 105, 10907–10912. doi: 10.1073/pnas.0802437105

Schwarz, J., Heimhilger, E., and Storch, A. (2006). Increased periodontal pathology in Parkinson's disease. *J. Neurol.* 253, 608–611. doi: 10.1007/s00415-006-0068-4

Shamir, R., Klein, C., Amar, D., Vollstedt, E. J., Bonin, M., Usenovic, M., et al. (2017). Analysis of blood-based gene expression in idiopathic Parkinson disease. *Neurology* 89, 1676–1683. doi: 10.1212/WNL.0000000000004516

Shannon, P., Markiel, A., Ozier, O., Baliga, N. S., Wang, J. T., Ramage, D., et al. (2003). Cytoscape: a software environment for integrated models of biomolecular interaction networks. *Genome Res.* 13, 2498–2504. doi: 10.1101/gr.1239303

Su, L., Xu, Q., Zhang, P., Michalek, S. M., and Katz, J. (2017). Phenotype and function of myeloid-derived suppressor cells induced by *Porphyromonas gingivalis* infection. *Infect. Immun.* 85:e00213-17. doi: 10.1128/IAI.00213-17

Su, R., and Zhou, T. (2021). Alpha-synuclein induced immune cells activation and associated therapy in Parkinson's disease. Frontiers in aging. *Neuroscience* 13. doi: 10.3389/fnagi.2021.769506

Tettamanti, L., Gaudio, R. M., Iapichino, A., Mucchi, D., and Tagliabue, A. (2017). Genetic susceptibility and periodontal disease: a retrospective study on a large Italian sample. *Oral Implantol. (Rome)* 10, 20–27. doi: 10.11138/orl/2017.10.1.020

Tonetti, M. S., Greenwell, H., and Kornman, K. S. (2018). Staging and grading of periodontitis: framework and proposal of a new classification and case definition. *J. Periodontol.* 89, S159–S172. doi: 10.1002/JPER.18-0006

Valero-Monroy, O., Garcia-Cervantes, G., Marquez-Corrales, L. F., Leija-Montoya, A. G., Sandoval-Basilio, J., Martinez-Coronilla, G., et al. (2016). Myeloid derived suppressor cell: a new player in periodontal disease? *Med. Hypotheses* 95, 35–38. doi: 10.1016/j.mehy.2016.08.010

Walker, D. G., Lue, L. F., and Beach, T. G. (2002). Increased expression of the urokinase plasminogen-activator receptor in amyloid beta peptide-treated human brain microglia and in AD brains. *Brain Res.* 926, 69–79. doi: 10.1016/S0006-8993(01)03298-X

Wilkerson, M. D., and Hayes, D. N. (2010). ConsensusClusterPlus: a class discovery tool with confidence assessments and item tracking. *Bioinformatics* 26, 1572–1573. doi: 10.1093/bioinformatics/btq170

Wu, T., Hu, E., Xu, S., Chen, M., Guo, P., Dai, Z., et al. (2021). clusterProfiler 4.0: a universal enrichment tool for interpreting omics data. The. *Innovations* 2:100141. doi: 10.1016/j.xinn.2021.100141

Xu, T., Dong, Q., Luo, Y., Liu, Y., Gao, L., Pan, Y., et al. (2021). *Porphyromonas gingivalis* infection promotes mitochondrial dysfunction through Drp1-dependent mitochondrial fission in endothelial cells. *Int. J. Oral Sci.* 13, 1–11. doi: 10.1038/s41368-021-00134-4

Yan, B., Ren, F., Shang, W., and Gong, X. (2022). Transcriptomic analysis reveals genetic cross-talk between periodontitis and hypothyroidism. *Dis. Markers* 2022, 1–12. doi: 10.1155/2022/5736394

Yang, Y., Zhang, X. L., Guan, Q. B., Guo, L., Zhang, H., Han, C. Y., et al. (2018). Detection and clinical significance of myeloid-derived suppressor cells in peripheral blood of patients with Parkinson disease. *Chin. J. Pathophysiol.* 12, 107–111.

Yu, G., Wang, L. G., Han, Y., and He, Q. Y. (2012). clusterProfiler: an R package for comparing biological themes among gene clusters. *Omics J. Integr. Biol.* 16, 284–287. doi: 10.1089/omi.2011.0118

Zhang, X., Shao, Z., Xu, S., Liu, Q., Liu, C., Luo, Y., et al. (2021). Immune profiling of Parkinson's disease revealed its association with a subset of infiltrating cells and signature genes. *Front. Aging Neurosci.* 13:605970. doi: 10.3389/fnagi.2021.605970

Zhang, L., Zhang, J., Yang, J., Ying, D., Lau, Y., and Yang, W. (2013). PriVar: a toolkit for prioritizing SNVs and indels from next-generation sequencing data. *Bioinformatics* 29, 124–125. doi: 10.1093/bioinformatics/bts627

frontiers | Frontiers in Neuroscience

TYPE Original Research
PUBLISHED 25 January 2023
DOI 10.3389/fnins.2022.1035444

Check for updates

OPEN ACCESS

EDITED BY
Yuzhen Xu,
Tongji University, China

REVIEWED BY
Zhen Wang,
Quzhou City People's Hospital, China
Mandi Gandelman,
The University of Utah, United States
Meijie Qu,
The Affiliated Hospital of Qingdao University, China
Shaoxing Dai,
Kunming University of Science and Technology, China
Yuhu Zhang,
Guangdong Provincial People's Hospital, China

*CORRESPONDENCE
Qinyong Ye
✉ unionqyye@163.com
Haiqiang Zou
✉ dr_zou@163.com

†These authors have contributed equally to this work and share first authorship

SPECIALTY SECTION
This article was submitted to Neurodegeneration, a section of the journal Frontiers in Neuroscience

RECEIVED 02 September 2022
ACCEPTED 06 December 2022
PUBLISHED 25 January 2023

CITATION
Weng H, Song W, Fu K, Guan Y, Cai G, Huang E, Chen X, Zou H and Ye Q (2023) Proteomic profiling reveals the potential mechanisms and regulatory targets of sirtuin 4 in 1-methyl-4-phenyl-1,2,3,6-tetrahydropyridine-induced Parkinson's mouse model. *Front. Neurosci.* 16:1035444. doi: 10.3389/fnins.2022.1035444

COPYRIGHT
© 2023 Weng, Song, Fu, Guan, Cai, Huang, Chen, Zou and Ye. This is an open-access article distributed under the terms of the Creative Commons Attribution License (CC BY). The use, distribution or reproduction in other forums is permitted, provided the original author(s) and the copyright owner(s) are credited and that the original publication in this journal is cited, in accordance with accepted academic practice. No use, distribution or reproduction is permitted which does not comply with these terms.

Proteomic profiling reveals the potential mechanisms and regulatory targets of sirtuin 4 in 1-methyl-4-phenyl-1,2,3,6-tetrahydropyridine-induced Parkinson's mouse model

Huidan Weng[1,2†], Wenjing Song[1,2†], Kangyue Fu[1], Yunqian Guan[3], Guoen Cai[1,2], En Huang[4], Xiaochun Chen[1,2], Haiqiang Zou[5]* and Qinyong Ye[1,2]*

[1]Department of Neurology, Fujian Medical University Union Hospital, Fuzhou, China, [2]Fujian Key Laboratory of Molecular Neurology, Institute of Neuroscience, Fujian Medical University, Fuzhou, China, [3]Cell Therapy Center, Xuanwu Hospital, Capital Medical University, Beijing, China, [4]The School of Basic Medical Sciences, Fujian Key Laboratory of Brain Aging and Neurodegenerative Diseases, Fujian Medical University, Fuzhou, China, [5]Department of Neurosurgery, General Hospital of Southern Theatre Command, PLA, Guangzhou, Guangdong, China

Introduction: Parkinson's disease (PD), as a common neurodegenerative disease, currently has no effective therapeutic approaches to delay or stop its progression. There is an urgent need to further define its pathogenesis and develop new therapeutic targets. An increasing number of studies have shown that members of the sirtuin (SIRT) family are differentially involved in neurodegenerative diseases, indicating their potential to serve as targets in therapeutic strategies. Mitochondrial SIRT4 possesses multiple enzymatic activities, such as deacetylase, ADP ribosyltransferase, lipoamidase, and deacylase activities, and exhibits different enzymatic activities and target substrates in different tissues and cells; thus, mitochondrial SIRT4 plays an integral role in regulating metabolism. However, the role and mechanism of SIRT4 in PD are not fully understood. This study aimed to investigate the potential mechanism and possible regulatory targets of SIRT4 in 1-methyl-4-phenyl-1,2,3,6-tetrahydropyridine (MPTP)-induced PD mice.

Methods: The expression of the SIRT4 protein in the MPTP-induced PD mouse mice or key familial Parkinson disease protein 7 knockout (DJ-1 KO) rat was compared against the control group by western blot assay. Afterwards, quantitative proteomics and bioinformatics analyses were performed to identify altered proteins in the vitro model and reveal the possible functional role of SIRT4. The most promising molecular target of SIRT4 were screened and validated by viral transfection, western blot assay and reverse transcription quantitative PCR (RT-qPCR) assays.

Results: The expression of the SIRT4 protein was found to be altered both in the MPTP-induced PD mouse mice and DJ-1KO rats. Following the viral transfection of SIRT4, a quantitative proteomics analysis identified 5,094

altered proteins in the vitro model, including 213 significantly upregulated proteins and 222 significantly downregulated proteins. The results from bioinformatics analyses indicated that SIRT4 mainly affected the ribosomal pathway, propionate metabolism pathway, peroxisome proliferator-activated receptor (PPAR) signaling pathway and peroxisome pathway in cells, and we screened 25 potential molecular targets. Finally, only fatty acid binding protein 4 (FABP4) in the PPAR signaling pathway was regulated by SIRT4 among the 25 molecules. Importantly, the alterations in FABP4 and PPARγ were verified in the MPTP-induced PD mouse model.

Discussion: Our results indicated that FABP4 in the PPAR signaling pathway is the most promising molecular target of SIRT4 in an MPTP-induced mouse model and revealed the possible functional role of SIRT4.This study provides a reference for future drug development and mechanism research with SIRT4 as a target or biomarker.

KEYWORDS

Parkinson's disease, SIRT4, quantitative proteomic analysis, bioinformatics, biomarkers, FABP4, PPAR signaling pathway

1. Introduction

Neurological diseases are the leading cause of disability/paralysis worldwide; notably, among these diseases, Parkinson's disease (PD) has the fastest rate of increase in incidence and an increasingly younger onset, and it is closely related to damage to substantia nigra dopaminergic neurons (Dorsey and Bloem, 2018). The current studies examining the pathogenesis of PD focus on the misfolding and aggregation of α-synuclein, mitochondrial dysfunction, impaired protein clearance, neuroinflammation, and oxidative stress, which interact and lead to cascading and irreversible cellular damage (Michel et al., 2016; Jankovic and Tan, 2020). However, current therapeutic approaches are unable to stop the progression of the underlying neurodegenerative disease. Furthermore, the lack of reliable and sensitive biomarkers for the disease limits the development of neuroprotective therapies (Poewe et al., 2017). Therefore, a better understanding of the pathophysiology of neurodegenerative diseases such as PD and the identification of new therapeutic targets are crucial.

The SIRT family consists of seven proteins (SIRT1-SIRT7) with distinct nicotinamide adenine dinucleotide (NAD^+)-dependent deacetylase and ADP ribosyltransferase activities. These proteins interact with a variety of signaling proteins and transcription factors and exhibit different enzymatic activities, targets, and subcellular localizations, resulting in powerful epigenetic regulation and posttranslational modifications (Tang, 2017). SIRT is expressed at high levels in the brain and is involved in a variety of cellular processes, including cell survival, chromatin remodeling, energy metabolism, neuroprotection, and tumor development; it is also an important regulator of biological processes (Lavu et al., 2008; Rose et al., 2017; Xu et al., 2020). An increasing number of studies have confirmed that mitochondrial sirtuins (SIRT3-SIRT5) stabilize respiratory chain function, increase the activity of mitochondrial respiratory chain complexes, increase energy metabolism, promote autophagy, inhibit oxidative stress and inflammatory responses. Consequently, these proteins have become important targets in PD research (He et al., 2022). Furthermore, activators or inhibitors of SIRT proteins in PD models also exert neuroprotective effects (Gomes et al., 2019). For example, resveratrol, a SIRT1 activator, reduces cell death in animal models of neurotoxin-induced PD (Lofrumento et al., 2014); SIRT2 inhibitors rescue α-syn-mediated PD toxicity in cell models (Outeiro et al., 2007; Singh et al., 2019). SIRT3 interacts with α-synuclein to exert a protective effect in a mouse model of MPTP-induced PD (Liu et al., 2015; Park et al., 2020). In summary, SIRT family proteins may affect the development of PD through diverse mechanisms.

Notably, SIRT4-7, which are currently less studied, play a key role in brain health (Yeong et al., 2020). SIRT4 expression and activity are mainly associated with susceptibility to endocrine diseases, tumors, and neurodegenerative diseases (Betsinger and Cristea, 2019). Related studies suggested that SIRT4 is a major regulator of mitochondrial metabolism and is widely involved in energy metabolism in mammalian cells, such as inhibiting insulin secretion, regulating mitochondrial ATP homeostasis, and modulating redox reactions (Li and Zheng, 2018). In addition, it affects leucine metabolism (Csibi et al., 2013; Komlos et al., 2013; Anderson et al., 2017). SIRT4

also increases ADP or AMP levels by inhibiting glutamine metabolism and blocking the mTOR signaling pathway, thus exerting its tumor-suppressive effects in hepatocellular carcinoma (Wang et al., 2019). In the central nervous system, SIRT4 overexpression prevents the differentiation of radial glial cells into astrocytes (Komlos et al., 2013). The recovery of olfactory function is associated with increased expression of medullary SIRT1 and SIRT4 (Marin et al., 2019). In addition, a neurotoxin (erythropoietin) induces increases in SIRT4 expression (Shih et al., 2014). Most importantly, SIRT4 overexpression increases the expression levels of GLT-1 and glutamate dehydrogenase (GDH), which results in avoiding the uptake of excess glutamate while preventing the conversion of glutamine to glutamate by inhibiting glutamine synthetase, thereby maintaining the levels of glutamate in the brain (Csibi et al., 2013; Yalçın and Colak, 2020). Although mitochondrial SIRT4 exhibits some therapeutic potential, SIRT4 remains the least studied SIRT, and its role in neurodegenerative diseases such as PD is largely unknown. This lack of evidence may be related to its low *in vitro* enzyme activity and the identification of fewer acting substrates. Members of the SIRT family share some protein substrates and physiological activities (Haigis and Sinclair, 2010), and different isoforms may compete for the same substrates to alter their acetylation status and activity (Luo et al., 2017). This complexity necessitates a better understanding of the mechanism of action and potential targets of SIRT4.

Fatty acid binding proteins (FABPs) have a central role in coordinating lipid transport, metabolism, and reactions in different tissues and organs, and different members are expressed in a tissue-specific manner to optimize local fatty acid utilization (Frizzell et al., 2020). FABP4 is one of these isoforms (Li et al., 2020). Increased concentrations of B-FABP are associated with human brain tumors (e.g., glioblastoma and astrocytoma), neurodegenerative diseases (Alzheimer's disease and PD), and other cognitive dysfunctions (Choromańska et al., 2011). A series of studies suggest that FABP3, FABP5, and FABP7 play important roles in α-synuclein oligomerization and migration, trigger the loss of neuronal mitochondrial function, and even interact with VDAC-1 to modulate the formation of channel pores in the mitochondrial membrane (Kawahata et al., 2019; Matsuo et al., 2019; Cheng et al., 2021; Kawahata and Fukunaga, 2022). Thus, FABP is considered a promising therapeutic target for α-synucleinopathies (Kawahata and Fukunaga, 2022). Although FABP4 has been less studied in PD, previous studies suggest that FABP4 is a powerful and novel biomarker for acute stroke (Bacigaluppi and Martino, 2020), an effective target for diabetes treatment (Cao et al., 2013), a predictor of adverse cardiovascular events (Peeters et al., 2011), a key determinant of the metastatic potential of ovarian cancer (Gharpure et al., 2018) and a regulator of neuroinflammation and cognitive decline in obese mice (So et al., 2022), which indicates that further studies of SIRT4 in the field of PD are warranted. In human hepatocellular carcinoma cells (HepG2/HuH7), SIRT1-FOXO1 signaling promotes the increased secretion of FABP4 protein and neutral lipid accumulation (Attal et al., 2022). Although this study was not conducted using PD models, it also reveals the relevance of SIRT to FABP4.

Peroxisome proliferator-activated receptor (PPAR) is a key sensor and major regulator of cellular metabolism and a potential therapeutic target for Alzheimer's disease, PD, Huntington's disease and other degenerative diseases (Zolezzi et al., 2017). A significant reduction in the levels of PPARγ and FABP4 transcripts (key genes in the adipose network) has been observed in bone marrow stem cells from patients with atypical PD (Angelova et al., 2018). Based on this finding, FABP4 in the PPAR signaling pathway may play a role in PD-related disorders. In addition, a close link between the SIRT family and PPAR signaling has been identified. For example, SIRT binds to PPARα and protects the heart from hypertrophy, metabolic dysregulation, and inflammation (Planavila et al., 2011). SIRT6 promotes hepatic β-oxidation by activating PPARα (Naiman et al., 2019). In conclusion, the SIRT family, FABP4, and PPAR are more or less inextricably linked.

Tandem mass tag (TMT)-labeled quantitative proteomics and liquid chromatography-tandem mass spectrometry (LC–MS/MS) have been used to analyse various biological processes and screen for promising molecular targets, which are useful for understanding molecular biological mechanisms (Moulder et al., 2018). As shown in **Figure 1**, we found that SIRT4 played a role in PD models (MPTP-induced Parkinson's mouse model and DJ-1 KO rat model) and subsequently revealed the possible mechanism of action of SIRT4 and potential molecular targets using quantitative proteomics and bioinformatics analyses in this study. Then our study further screened and validated that FABP4 in the PPAR signaling pathway is the most promising target of SIRT4 in the PD model based on the results from biochemical assays. Our results provide a therapeutic strategy targeting SIRT4 for the diagnosis and management of PD.

2. Materials and methods

2.1. Cell culture and cell transfection

The SH-SY5Y cell was purchased from Shanghai Zhong Qiao Xin Zhou Biotechnology Corp., Ltd. The cells were inoculated into DMEM/F12 (Sigma-HyClone, MO, USA, Cat#sh30023.01) containing 10% fetal bovine serum (Sigma-Gibco, MO, USA, Cat#16140089), 100 IU/ml penicillin, and 100 μg/ml streptomycin (Sigma-Gibco, MO, USA, Cat#15140148) after STR identification and mycoplasma detection and then incubated at 37°C with 5% CO_2. Subculture was performed when the cells reached 80–90% confluence.

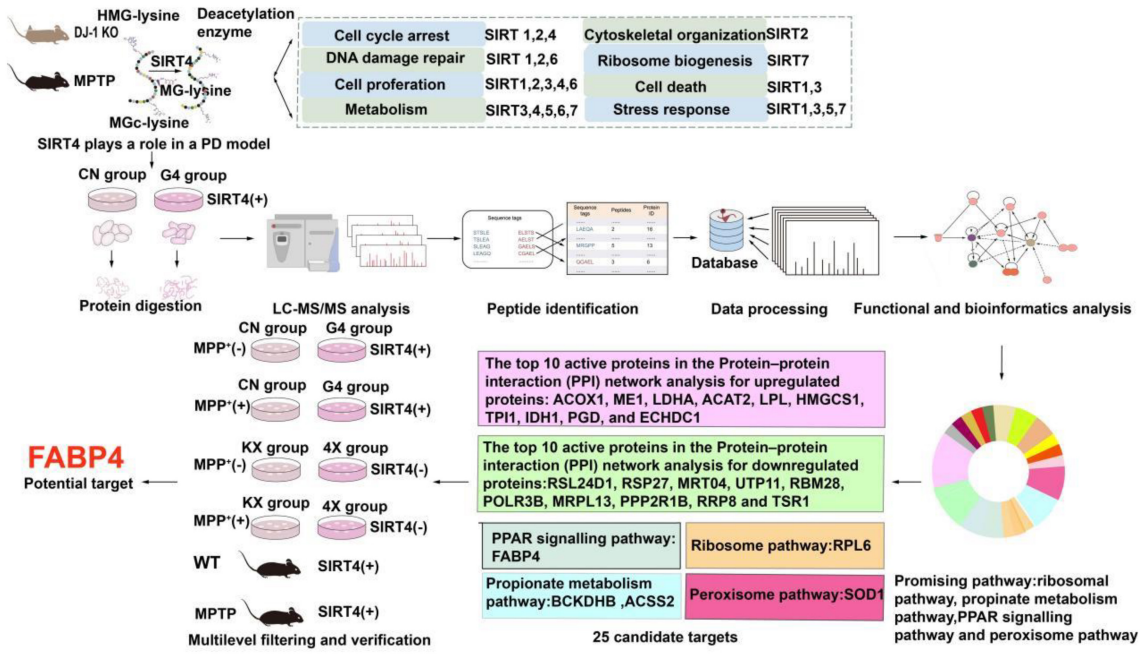

FIGURE 1
Workflow of the study. The summary of the main functions of SIRT family proteins come from reference (Imai and Guarente, 2014; Li et al., 2018).

Human SIRT4 lentivirus to knock down (PLKD-CMV-EGFP-2A-PURO-U6-ShRNA) or overexpress (PRLENTI-EF1-EGFP-P2A-PURO-CMV-SIRT4-3xFLAG-WPRE) SIRT4 and mouse SIRT4-AAV virus to overexpress SIRT4 (pAAV-CMV-Sirt4-HA-EF1a-EGFP-tWPA) were purchased from Obio Technology (Shanghai) Corp., Ltd. Cells were plated in six-well plates at a density of 5×10^4 cells per well and transfected with the SIRT4 lentivirus at an MOI of 80. The transfection rate was calculated by determining the fluorescence ratio after 72 h. Subsequently, SH-SY5Y cells were treated with 1500 μmol/L MPP^+ (Sigma–Aldrich, MO, USA, Cat#D048) for 24 h, and then a PD cytotoxicity model was established. Cells were collected after 5 days to determine whether SIRT4 was overexpressed or knocked down. SH-SY5Y cells were divided into four groups: overexpression lentivirus control group (CN group), lentivirus-mediated SIRT4 overexpression group (G4 group), knockdown lentivirus control group (KX group), and lentivirus-mediated SIRT4 knockdown group (4X group).

2.2. Animals

Male C57BL/6 mice weighing 24–27 g and aged 10–12 weeks were chosen for the experiment, and were provided by the Fujian Medical University's Experimental Animal Center. Two sgRNAs were designed to generate a 3.5 kb chromosomal deletion (exon 3∼5) at the Park7 locus in the rat genome. DJ-1 KO rats were purchased from Beijing Biositu Gene Biotechnology Co., Ltd. The animals used in the experiment were maintained in a standard breeding facility under pathogen-free conditions, with an ambient temperature of (22 ± 2)°C, relative humidity of 50–60%, a 12 h dark/light cycle, and access to water and food at all times. The experiment was approved by the Fujian Medical University Institutional Committee for Animal Care and Use with the ethics approval numbers FJMUIACUC 2021-0369 for mice and FJMUIACUC 2020-0016 for rats. All animal experiments were carried out in accordance with international animal biomedical research guidelines. The gene identification scheme for key familial Parkinson disease protein 7 knockout (DJ-1 KO) rats can be found in Supplementary Table 2.

2.3. Establishment of the MPTP-induced mouse model

The mice used in the experiment were randomly assigned to receive either an intraperitoneal injection of normal saline (Fns group) or MPTP (Fmptp group). The mice were administered 30 mg/kg MPTP (Sigma–Aldrich, MO, USA, Cat#M0896) intraperitoneally once a day for five days to establish an MPTP-induced mouse model. The substantia nigra was removed from mice, and lysates were detected by western blotting and RT–qPCR on the first day after the last intraperitoneal injection. The specific operation process is depicted in Figure 2A.

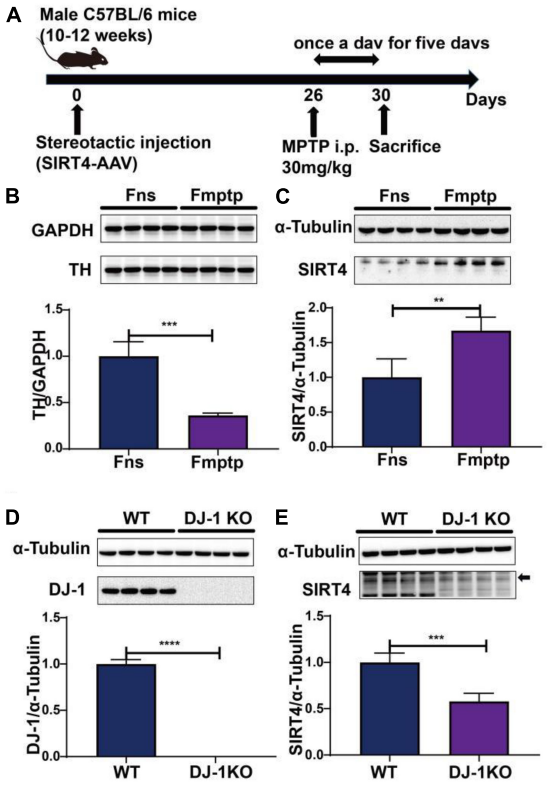

FIGURE 2
SIRT4 plays a role in a PD model. **(A)** Flow chart of stereotactic injection of SIRT4-AAV virus and the establishment of a mouse model of PD induced by MPTP. **(B)** Representative western blots and densitometric analysis for TH protein between groups. TH protein extracts from substantia nigra after mice were intraperitoneally injected with saline and MPTP for 5 days. GAPDH was used as a loading control (n = 4 mice per group). **(C)** Representative western blots and densitometric analysis for SIRT4 protein between groups. SIRT4 protein extracts from substantia nigra after mice were intraperitoneally injected with saline or MPTP for 5 days. Tubulin was used as a loading control (n = 4 mice per group). **(D,E)** Representative western blots and densitometric analysis for DJ-1 or SIRT4 protein between groups, respectively. DJ-1 or SIRT4 protein extracts from substantia nigra of WT rats or DJ-1 KO rats. Tubulin was used as a loading control (n = 4 mice per group). All results are depicted as means ± SEM. The comparison across groups was analyzed by t-test. $^{**}P < 0.01$, $^{***}P < 0.001$, and $^{****}P < 0.0001$ compared with the control group. TH, tyrosine hydroxylase; SIRT4, NAD-dependent protein lipoamidase sirtuin-4, mitochondrial.

2.4. Stereotactic injection

Male C57BL/6 mice aged 10–12 weeks underwent stereotactic injections. These animals were placed in a stereotactic frame and sedated with 2% isoflurane administered through a mask (oxygen flow rate of 2 L/min). Eye ointment was applied to the cornea and surrounding areas to ensure that they did not dry out during surgery. SIRT4-AAV and control-AAV were injected into the right striatum and right substantia nigra using a 2.5 L Hamilton syringe (32 G needle) in a stereotactic manner using the following coordinates of the right striatum and right substantia nigra: AP = +0.8 mm, ML = +2 mm and DV = −3.5 mm and AP = −2.6 mm, ML = +1.4 mm and DV = −4.5 mm from the bregma, respectively. Antibiotics and pain relievers were applied to the surface of the wound in each mouse. We waited for 10 min for virus infusion after the injection was done. One month after stereotactic injection of the virus, samples were collected for RT–qPCR and western blotting. Male C57BL/6 mice were divided into two groups: stereotactic injection of control AAV virus without intraperitoneal injection of MPTP group (KS group) and stereotactic injection of SIRT4-AAV virus without intraperitoneal injection of MPTP group (4S group). MPTP-induced Parkinson's mouse model was divided into three groups: non-stereotactic injection group (Fmptp group), stereotactic injection of the control AAV group (kFmptp group), and stereotactic injection of the SIRT4-AAV group (4Fmptp group).

2.5. Western blot assay

After protein extraction, the protein concentration in the sample was determined by using the BCA method (Beyotime Biotechnology, Shanghai, China, Cat# P0012). Cell or tissue lysates were mixed with protein buffer and boiled for 10 min. Then, 30 μg from each group of samples was loaded in each lane and subjected to 10% sodium dodecyl sulfate–polyacrylamide gel electrophoresis (SDS-PAGE) (Beyotime Biotechnology, Shanghai, China, Cat# P0012A). Proteins with different molecular weights were separated at a voltage of 120 V and transferred to activated polyvinylidene difluoride (PVDF) membranes. After blocking with 5% skim milk powder for 2 h at room temperature, PVDF membranes were mixed with primary antibodies [SIRT4 (Proteintech, Wuhan, China, Cat#66543-1-IG), FABP4 (Proteintech, Wuhan, China, Cat#12802-1-AP), PPARγ (Proteintech, Wuhan, China, Cat#16643-1-AP), glyceraldehyde-3-phosphate dehydrogenase (GAPDH) (Abcam, Cambridge, UK, Cat#ab8245), α-tubulin (Abcam, Cambridge, UK, Cat# ab7291, DJ-1 (Abcam, Cambridge, UK, Cat#ab18257), β-actin (Abcam, Cambridge, UK, Cat#ab8227) and tyrosine hydroxylase (TH; Abcam, Cambridge, UK, Cat#ab112)]. After washing the membrane, it was soaked in ECL solution (solution A: solution B = 1:1) and reacted for 1–2 min. The membrane was then automatically exposed in a chemiluminescence instrument (PROTEIN SIMPLE, FluorChem M), and the gray value of the band was analysed using ImageJ software ($n = 4$).

2.6. RT-qPCR

RNA was extracted from each group of samples using TRIzol reagent (Invitrogen, Carlsbad, CA, Cat#15596018) for RT–qPCR analysis ($n = 6$). For reverse transcription, the

EvoScript Universal Master one-step reverse transcription kit (Roche, Basel, Switzerland, Cat#7912439001) was used. Primers were designed based on the human/mouse gene sequence in NCBI GenBank, and their specificity was confirmed in advance using NCBI Blast. **Supplementary Table 1** summarizes all primers used in this study. Fuzhou Shangya Biotechnology Co., Ltd. synthesized the primers and tested their quality. FastStart Universal SYBR Green Master Mix (ROX) (Roche, Basel, Switzerland, Cat# 04913914001) and a 7,500 PCR instrument (Applied Biosystems) were used for relative quantification with the following thermal cycling program: 55°C for 2 min; 95°C for 10 min; 40 cycles of 95°C for 15 s and 60°C for 60 s; 95°C for 15 s; 60°C for 60 s, and 95°C for 15 s. The expression of the target mRNAs in all the samples was normalized to that of β-actin using the $2^{-\Delta\Delta Ct}$ method.

2.7. Quantitative proteomics: Sample preparation, protein digestion, TMT labeling, and LC–MS/MS analysis

SH-SY5Y cells transfected with empty virus (CN group) and SIRT4 overexpression lentivirus (G4 group) were used in this study. An equal number of samples from each group were chosen for enzymolysis and the appropriate amount of standard protein was added. Dithiothreitol (DTT) was added to the samples to a final concentration of 5 mM, and then the concentration was reduced by incubating the samples at 56°C for 30 min. Subsequently, iodoacetamide (IAA) was added to a final concentration of 11 mM, and the mixture was incubated at room temperature in the dark for 15 min. In addition, triethylamine-carbonic acid buffer solution (TEAB) was added to dilute the urea to a concentration lower 2 M. Finally, trypsin was added at a 1:50 (protease:protein, m/m) ratio, and enzymolysis was performed overnight. Trypsin was then added at a ratio of 1:100 (protease:protein, m/m), and the enzymolysis reaction was continued for 4 h.

The trypsin-digested peptides were desalted with Strata X (Phenomenex) and lyophilized under a vacuum. Peptides were dissolved in 0.5 M TEAB and labeled according to the instructions provided with the labeling kit. The peptides were separated using an ultrahigh-performance liquid system, injected into nanospray ionization source, and analysed by mass spectrometry. The ion source voltage was set to 2.0 kV, and the parent ion of the peptide as well as its secondary fragments were detected and analysed with a high-resolution Orbitrap system.

2.8. Database analysis

WoLF PSORT software was used in this study to predict the protein structure and subcellular localization. For protein domain annotations, InterProScan, a software package that searches the InterPro database based on sequence alignment was used. Protein GO annotation data were primarily derived from the UniProt-GOA database. The ID of the protein was first converted into the ID of the UniProtKB database, and then the relevant GO annotation information was retrieved from the UniProt-GOA based on the UniProtKB ID. If some identified proteins were not annotated in the database, their GO classification was annotated using the InterProScan homology alignment method. Protein metabolic pathways were annotated in the Kyoto Encyclopedia of Genes and Genomes (KEGG) database. KAAS, a KEGG online service tool, was used to annotate the proteins and obtain the KO number of the proteins corresponding to the KEGG database. The KO number was then mapped to a specific biological route using KEGG Mapper, a KEGG online service tool. Fisher's exact test was utilized for the enrichment analysis of differentially expressed proteins identified from the different comparisons based on GO terms, KEGG pathways, and protein domains, and the corresponding *P*-values were calculated. The related functions of differentially expressed proteins identified from the different comparisons were clustered by hierarchical clustering analysis. The protein–protein interactions (PPIs) of differentially expressed proteins were extracted based on a confidence score greater than 0.7 after comparing the database numbers or protein sequences of the differentially expressed proteins selected from the sets identified from the different comparisons with the STRING (v.10) database. The interactive network of differentially expressed genes and proteins was then visualized using the R package "networkD3" tool. The gene set enrichment analysis (GSEA) algorithm was created by the Broad Institute. The enrichment results for differentially expressed proteins were filtered based on a P-value < 0.05.

2.9. Statistical analysis

The parameters used for the GO enrichment analysis were as follows: background, the number of identified proteins in the GO classification; mapping, the number of differentially expressed proteins in the GO classification; all Mapping, the number of all differentially expressed proteins annotated by GO; all Background: the number of all identified proteins annotated by GO; fold enrichment, the ratio of the number of expressed proteins in the specific GO classification to the number of identified proteins in the classification. If mapping = a, background = b, all mapping = c, and all background = d, fold enrichment = (a/c)/(b/d). The KEGG pathway and protein domain enrichment analyses were performed using similar methods. GraphPad Prism 7.0 software (San Diego, CA, USA) was used

for the statistical analyses. Student's *t*-test was used to analyse the differences between two groups, ANOVA was used to analyse the differences among multiple groups, and $P < 0.05$ was considered to indicate a significant difference.

3. Results

3.1. SIRT4 plays a role in a PD model

Figure 2A depicts the establishment of the MPTP-induced mouse model. TH protein expression was significantly lower in the MPTP-induced mouse model than in the control group ($P < 0.05$), indicating that the MPTP-induced mouse model was successfully established (Figure 2B). In this model, decreases in TH protein expression were accompanied by increases in the expression of SIRT4 protein, and the correlation was significant (Figure 2C).Compared with the WT group, DJ-1 was completely knocked out in the DJ-1KO rat model (Figure 2D) and SIRT4 protein expression was decreased ($P < 0.05$) (Figure 2E). PD is caused by the interaction of genes and the environment. These results imply that both the PD model induced by environmental toxins and the early-onset PD model induced by DJ-1 gene deletion are accompanied by obvious changes in SIRT4 protein expression. Furthermore, a GSEA of differentially expressed proteins in SH-SY5Y cells transfected with the empty virus (CN group) compared with cells transfected with SIRT4 overexpression lentivirus (G4 group) revealed the number of functional sets enriched by upregulated/downregulated proteins and the number of functional sets enriched at different significance thresholds. A positive enrichment score (ES) indicates that the functional set is enriched at the top of the list, namely, an upregulated protein is enriched in the functional set, and a negative value indicates that a downregulated protein is enriched in the functional set. NES is the abbreviation for the normalized enrichment score. The main results for the NES values (G4/CN) are summarized in Supplementary Table 3. In the table, the NES value of the PD pathway was 3.666, indicating that this pathway ranked fourth among all the pathways (Supplementary Table 3). Figure 3 also shows the protein's position in the ordered list, the corresponding expression level, and the ratio from the comparison. Furthermore, Figure 3C displays a heatmap of the related proteins enriched in the PD pathway. SIRT4 overexpression increases the expression of related proteins in the PD pathway, which play a protective role in PD. In summary, a GSEA of the proteomics results from the *in vitro* model supports the notion that SIRT4 significantly participates in PD by exerting protective effects.

3.2. Identification of differentially expressed proteins between the SIRT4 group and control group in SH-SY5Y cells

The quantitative proteomics results revealed that the G4 group had 207 upregulated proteins and 211 downregulated proteins compared with the CN group based on a fold change in protein expression higher than 1.2. The G4 group had 84 upregulated proteins and 108 downregulated proteins compared with the CN group based on a fold change in protein expression greater than 1.3. In addition, the G4 group had 25 upregulated proteins and 46 downregulated proteins compared with the CN group with fold change in protein expression higher than 1.5 (Figure 4A). Furthermore, our findings revealed that 30 upregulated and 30 downregulated proteins exhibited the most notable changes (Supplementary Figures 4, 5).

3.3. Functional annotation of differentially expressed proteins between the SIRT4 group and control group in SH-SY5Y cells

Gene Ontology (GO) annotation, biological pathways, protein domains, subcellular structure localization, and Clusters of Orthologous Groups/EuKaryotic Orthologous Groups (COG/KOG) categories are all aspects of protein functional annotation. GO annotation is a major bioinformatics analysis method and is classified into three categories: biological processes (BPs), cellular components (CCs), and molecular functions (MFs). Compared with the levels in the CN group, the proteins whose expression changed after SIRT4 overexpression were mainly involved in the following BPs: cellular processes, biological regulation and single biological processes, metabolic processes, and responses to stimulation. In terms of CCs, the majority of the differentially expressed proteins were located in cells (27%), organelles (24%), and membrane closed cavities (12.78%). In terms of MFs, differentially expressed proteins were mainly enriched in binding (50%) and catalytic activity (25.38%) (Figure 4C).

The analysis of the subcellular localization of the differentially expressed proteins revealed that they were mainly located in the cytoplasm (34.53%), nucleus (32.61%), and extracellular space (10.79%) (Figure 4B).

COG/KOG categories indicated that the differentially expressed proteins following SIRT4 overexpression primarily affected biological processes such as ribosome structure and biogenesis, lipid transport and metabolism, signal transduction mechanism, translation process and

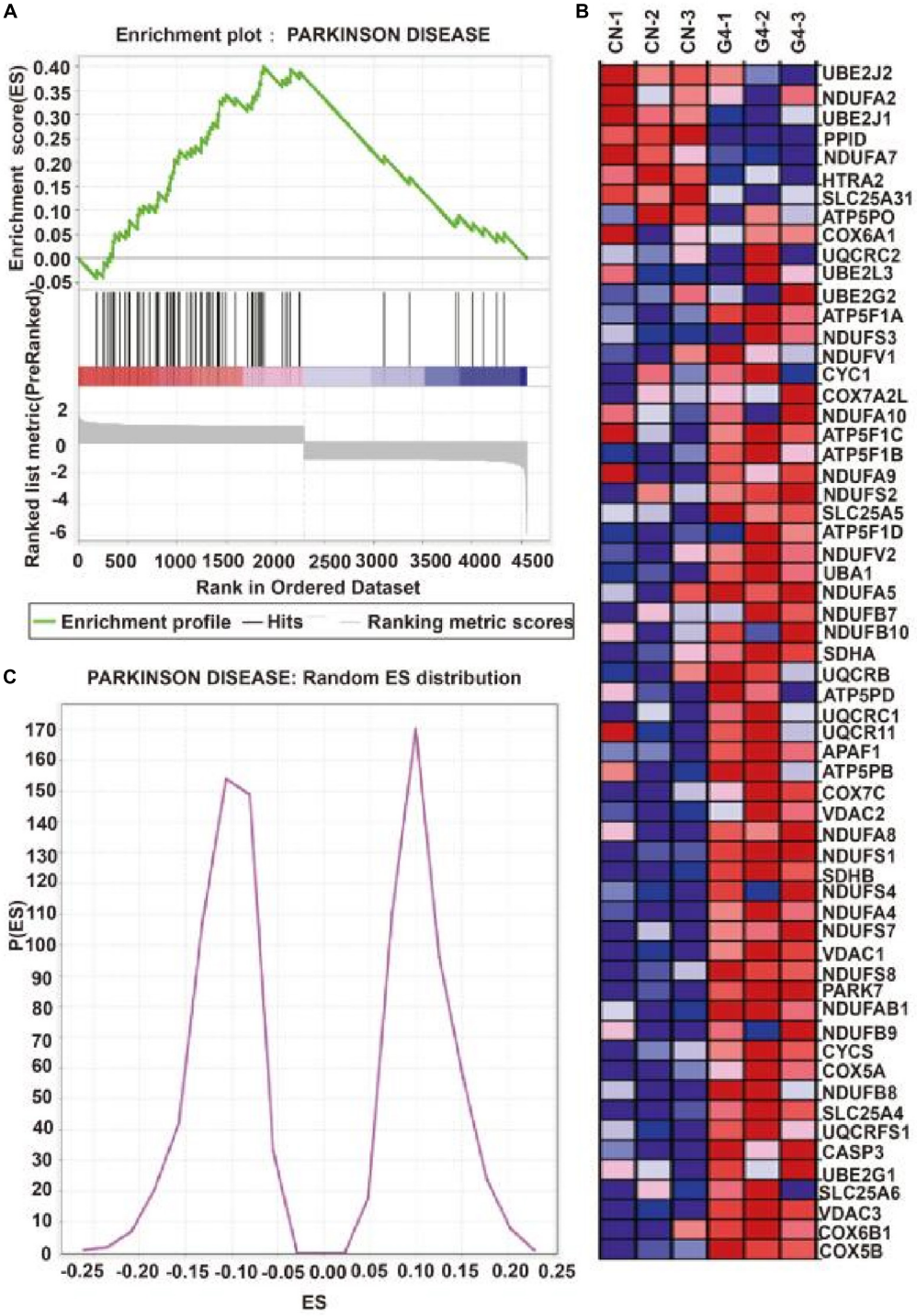

FIGURE 3
Gene set enrichment analysis of differentially expressed proteins after SIRT4 overexpression in SH-SY5Y cells. **(A)** Gene set enrichment analysis of differentially expressed protein after overexpression of SIRT4 in Parkinson's disease pathway. The graph is divided into three parts. The first part is the line graph of Enrichment Score (ES). The horizontal axis is all proteins (arranged from high to low according to the protein expression). The vertical axis is the running ES corresponding to the proteins under the functional set. The second part is hit information. Whether the proteins in the sorted list exist in the functional set is marked by lines. The lower color bar indicates the corresponding expression of proteins. The third part is the distribution map of ratios of all proteins. **(B)** Random ES distribution in Parkinson's disease pathway. **(C)** The heat map of differentially expressed proteins in Parkinson's disease pathway after gene set enrichment analysis.

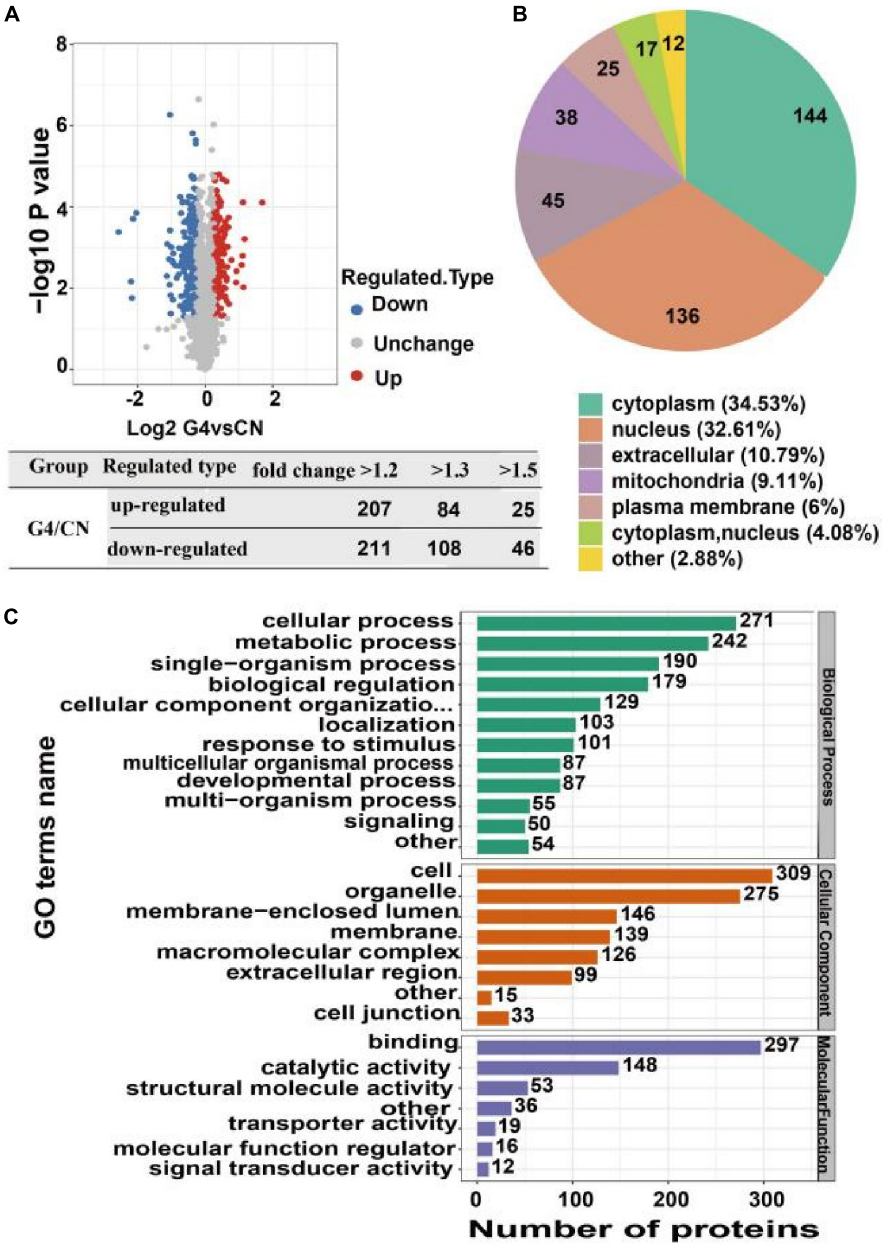

Group	Regulated type	fold change >1.2	>1.3	>1.5
G4/CN	up-regulated	207	84	25
	down-regulated	211	108	46

FIGURE 4
Identification, subcellular distribution and Gene Ontology annotation of differentially expressed proteins in SH-SY5Y cells after SIRT4 overexpression. **(A)** Volcanic map of differentially expressed proteins identified from the comparisons. Each dot in the figure represents a protein. The red dots represent upregulated proteins, the blue dots represent downregulated proteins, and the gray dots represent upregulated proteins with no significant difference. The horizontal axis shows the protein expression ratio after log2 conversion. The vertical axis shows the *P*-value of the difference determined by the statistical analysis after conversion by −log10. The number of differentially expressed proteins based on different fold changes is also summarized. **(B)** Pie chart of the subcellular distribution of differentially expressed proteins. Different colors indicate different subcellular locations. The legend indicates the name and proportion of the subcellular localization corresponding to the color. **(C)** Bar graph of Gene Ontology annotation. The vertical axis represents the secondary classification of GO terms. The horizontal axis represents the number of differentially expressed proteins. The color of the bar graph represents three different first-level GO classifications: biological process (green), molecular function (purple), and cellular component (orange).

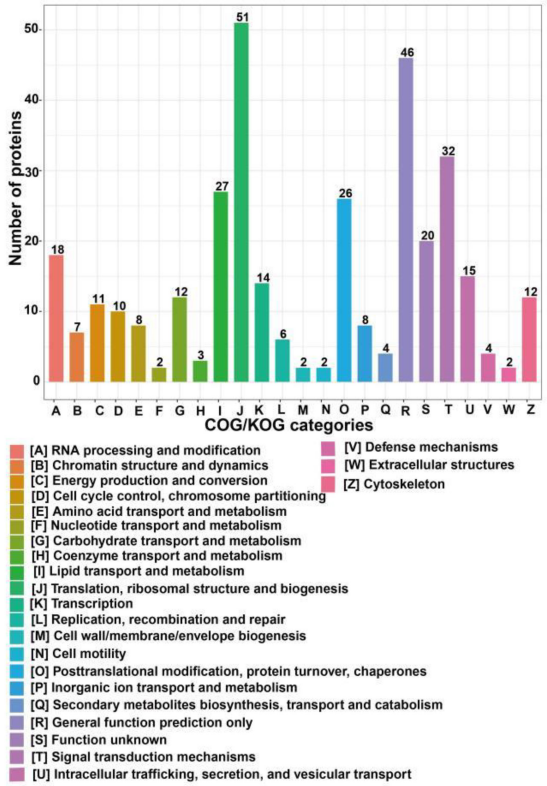

FIGURE 5
COG/KOG categories of differentially expressed proteins after SIRT4 overexpression in SH-SY5Y cells. The vertical axis of the bar graph is the COG classification, and the horizontal axis is the number of differential proteins.

posttranslational modification, protein turnover, molecular chaperone, RNA processing, modification, chromosome allocation, cellular endocrine and vesicle transport, and carbohydrates involved in amino acid transport and metabolism (Figure 5).

3.4. Functional enrichment analysis of differentially expressed proteins between the SIRT4 group and control group in SH-SY5Y cells

The functional enrichment analyses of differentially expressed proteins included GO, KEGG pathway and protein domain enrichment analyses. AMP-dependent synthetase/ligase, acyl-CoA dehydrogenase/oxidase, N-terminal, acyl-CoA dehydrogenase/oxidase, and intermediate domains were the most commonly upregulated protein domains (Figure 6A). The translation protein SH3-like domain, ribosomal protein L2 domain 2, and zinc-binding ribosomal protein were the most commonly downregulated protein domains (Figure 6B). All the enriched protein domains mainly included the translation protein SH3-like domain, AMP-dependent synthetase/ligase and lipocalin/cytoplasmic fatty acid binding domain (Figure 6C). In summary, SIRT4 primarily affects the translation protein SH3-like domain.

The GO enrichment analysis of upregulated proteins included carboxylic acid metabolism, oxyacid metabolism, and cellular lipid catabolism (Figure 7A). The GO enrichment analysis of downregulated proteins included viral gene expression, peptide biosynthesis, and amide biosynthesis (Figure 7B). The GO enrichment analysis of all differentially expressed proteins included protein localization to the endoplasmic reticulum, viral gene expression, and peptide metabolism (Figure 7C). In summary, the GO terms enriched in the altered proteins were primarily associated with protein localization to the endoplasmic reticulum and viral gene expression. The KEGG enrichment analysis of upregulated proteins mainly included propionic acid metabolism, the PPAR signalling pathway, peroxisome, valine, leucine, and isoleucine degradation, and fatty acid degradation (Figure 7D). The KEGG enrichment analysis of downregulated proteins mainly included the ribosome, haematopoietic lineage, ribosome biogenesis in eukaryotes, and lipoic acid metabolism (Figure 7E). The KEGG enrichment analysis of all differentially expressed proteins included ribosome, propionic acid metabolism, PPAR signaling pathway, fatty acid degradation and peroxisome, valine, leucine, and isoleucine degradation (Figure 7F). Figure 8 depicts the main enriched KEGG pathways and the corresponding altered proteins.

3.5. Protein-protein interaction (PPI) network analysis of differentially expressed proteins between the SIRT4 group and control group in SH-SY5Y cells

We extracted the interactions of different proteins with a confidence score >0.7 after comparing all differentially up/downregulated proteins with the STRING (v.10) database. Betweenness centrality is a parameter reflecting the activity and importance of proteins in the protein–protein interaction network. The ACOX1, ME1, LDHA, ACAT2, LPL, HMGCS1, TPI1, IDH1, PGD, and ECHDC1 proteins were identified in the PPI analysis for upregulated proteins sorted by the ratio of betweenness centrality (Figure 9A). The RSL24D1, RSP27, MRT04, UTP11, RBM28, POLR3B, MRPL13, PPP2R1B, RRP8, and TSR1 proteins were identified in the PPI analysis for downregulated proteins sorted by the ratio of betweenness centrality (Figure 9B).

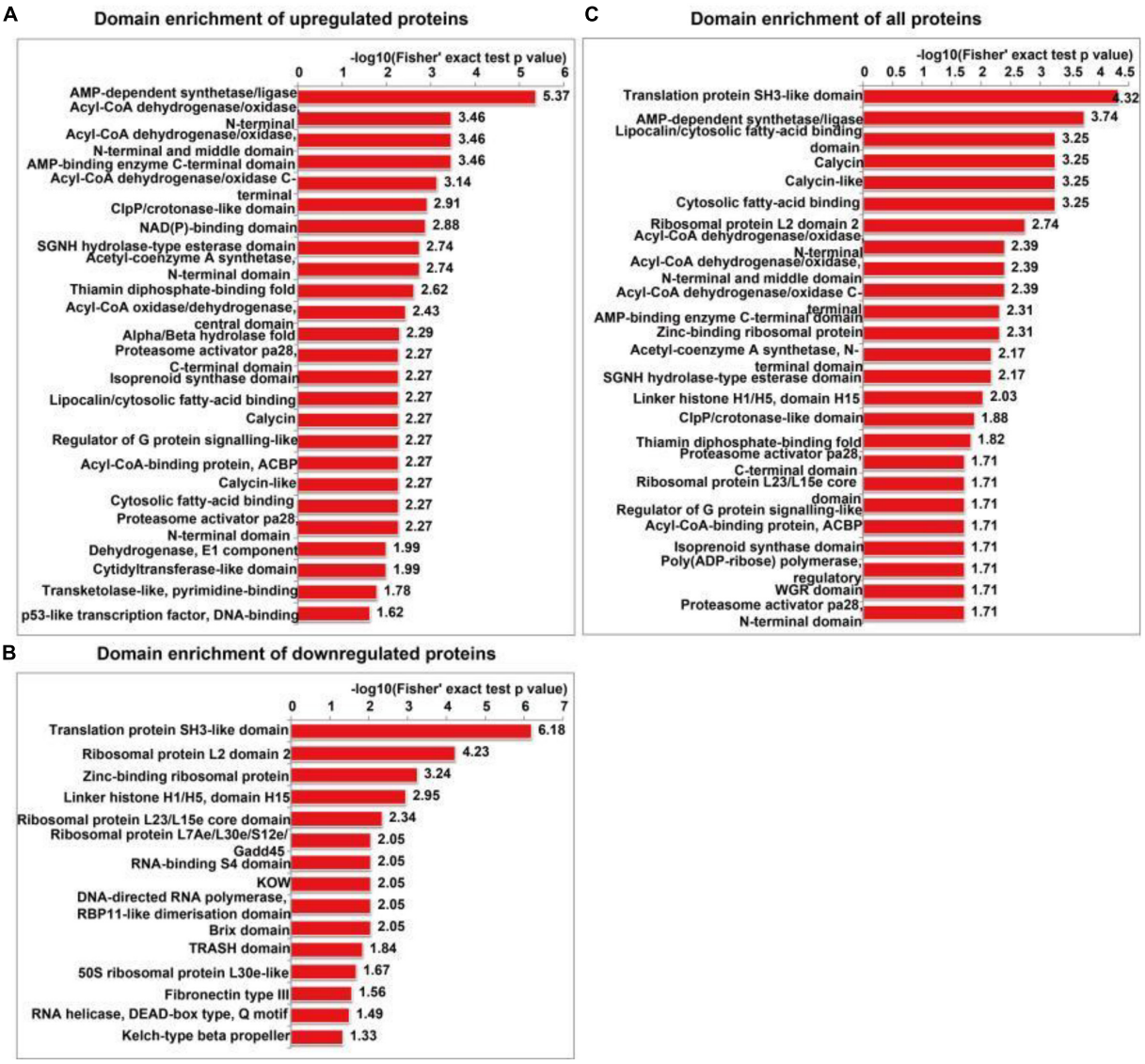

FIGURE 6
Protein domain enrichment analysis of differentially expressed proteins in SH-SY5Y cells after SIRT4 overexpression. **(A–C)** Represents the visual results from the protein domain enrichment analysis of upregulated proteins, downregulated proteins and differentially expressed proteins (including upregulated and downregulated proteins). The vertical axis shows the GO classification, and the horizontal axis shows Fisher's exact *P*-value after logarithmic conversion. The longer the bar graph is, the more significantly the differentially expressed proteins are enriched in the corresponding classification or function.

Following the change in SIRT4 expression, the activity of these molecules changes and are regarded as promising potential targets for SIRT4 to play a role in the PD model, which merits further investigation in follow-up studies. Furthermore, we conducted a KEGG enrichment analysis of these active proteins and discovered that they were primarily enriched in the ribosome, the PPAR signaling pathway, propionic acid metabolism, inositol phosphate metabolism, lipid metabolism, and glutathione metabolism. Figure 10 depicts the main enriched KEGG pathways of these active proteins and the corresponding altered proteins.

3.6. Among the 25 candidate targets, only the transcription of FABP4 can be regulated by SIRT4 in SH-SY5Y cells or SH-SY5Y cells with MPP^+ intervention

Regardless of whether the results were obtained from the enrichment analysis of differentially expressed proteins or related proteins following the PPI network analysis, the mechanism of action of SIRT4 is primarily anchored in the ribosome pathway, the PPAR signaling pathway, the propionic

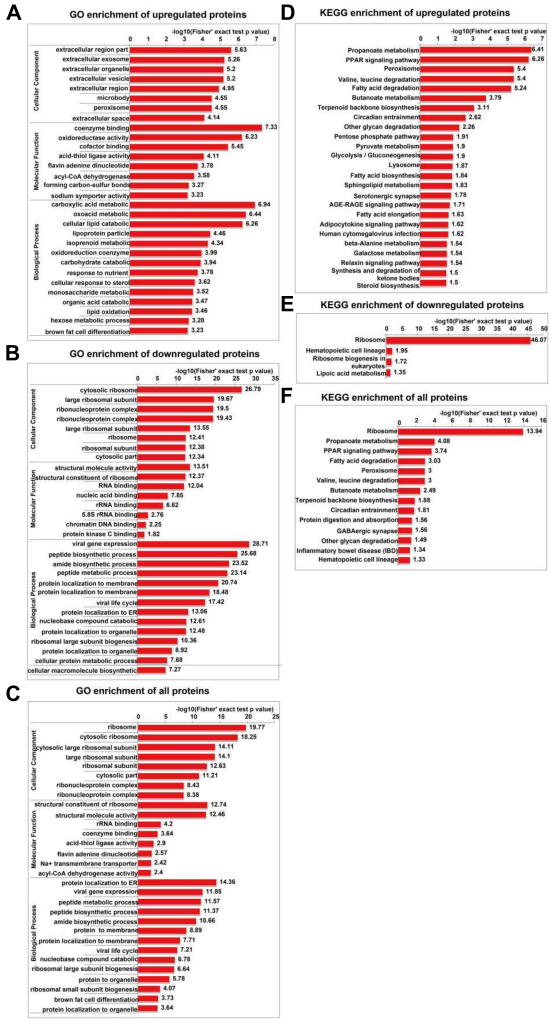

FIGURE 7
GO and KEGG enrichment analyses of differentially expressed proteins in SH-SY5Y cells after SIRT4 overexpression. The data used for the GO and KEGG enrichment analyses were derived from all the identified proteins. **(A–C)** Represents the visual results from the GO enrichment analysis of upregulated proteins, downregulated proteins and differentially expressed proteins (including both upregulated and downregulated proteins). **(D–F)** Show the visual results from the KEGG enrichment analysis of upregulated proteins, downregulated proteins and differentially expressed proteins (including both upregulated and downregulated proteins). The vertical axis is the GO classification, and the horizontal axis is the Fisher's exact *P*-value after logarithmic conversion. The longer the bar graph is, the more significantly the differentially expressed proteins are enriched in the corresponding classification or function.

acid metabolism pathway and the peroxisome pathway. RPL6 is the protein in the ribosome pathway exhibiting the most significant change. FABP4 is the protein in the PPAR pathway exhibiting the most significant change. BCKDHB and ACSS2 are the most significantly altered proteins in the propionic acid metabolism pathway. SOD1 is the protein in the peroxisome pathway displaying the most significant change. We identified the above proteins, the top 10 active proteins in the PPI network analysis for upregulated proteins as well as the top 10 active proteins in the PPI network analysis for downregulated proteins as potential targets for SIRT4 regulation.

We transfected SH-SY5Y cells or SH-SY5Y cells with MPP^+ intervention by lentiviruses that overexpressed or knocked down SIRT4 to observe the expression of these proteins and further assessed the most promising regulatory targets (Figures 11, 12). Table 1 summarizes the related results and clearly shows that only FABP4 transcription increased after SIRT4 overexpression and decreased after the knockdown of SIRT4 expression, indicating that it is regulated by SIRT4 in both SH-SY5Y cells or SH-SY5Y cells intervented with MPP^+.

3.7. FABP4 in the PPAR signaling pathway is a potential target in the MPTP-induced PD mouse model

We selected male C57BL/6 mice for the stereotactic injection of SIRT4-AAV to observe the changes in the mRNA expression of 25 potential molecules in mice (4S group), and the results are shown in Figure 13 and Table 1. Compared with the control empty virus group (KS group), we discovered that the mRNA level of FABP4 decreased after SIRT4 overexpression, and the difference was significant ($P < 0.05$). We administered stereotactic injection of SIRT4-AAV into the substantia nigra and striatum of the MPTP mouse model (4Fmptp group). After SIRT4 overexpression, FABP4 expression decreased significantly at the mRNA level ($P < 0.05$) compared with that in the control empty virus group (kFmptp group). At the protein level, the expression of FABP4 and PPARγ increased compared with that in the control empty virus group (kFmptp group) ($P < 0.05$) (Figure 14). Our results support the hypothesis that FABP4 in the PPAR signalling pathway is a potential target in the mouse model of MPTP-induced PD.

4. Discussion

NAD^+ is a key metabolite involved in cellular bioenergetics, genomic stability, mitochondrial homeostasis, adaptive stress responses, and cell survival (Montaigne et al., 2021). The SIRT family is a group of NAD^+-dependent deacetylases that have become a focus of interest in recent years due to their multiple regulatory functions, especially in aging and metabolism. Sirtuins act in different cellular substructures: they deacetylate histones and several transcriptional regulators in the nucleus as well as specific proteins in the cytoplasm, mitochondria, and other organelles, thus acting as key regulators of energy homeostatic networks (Houtkooper et al., 2012). Interactions have also been observed between different SIRTs, and thus

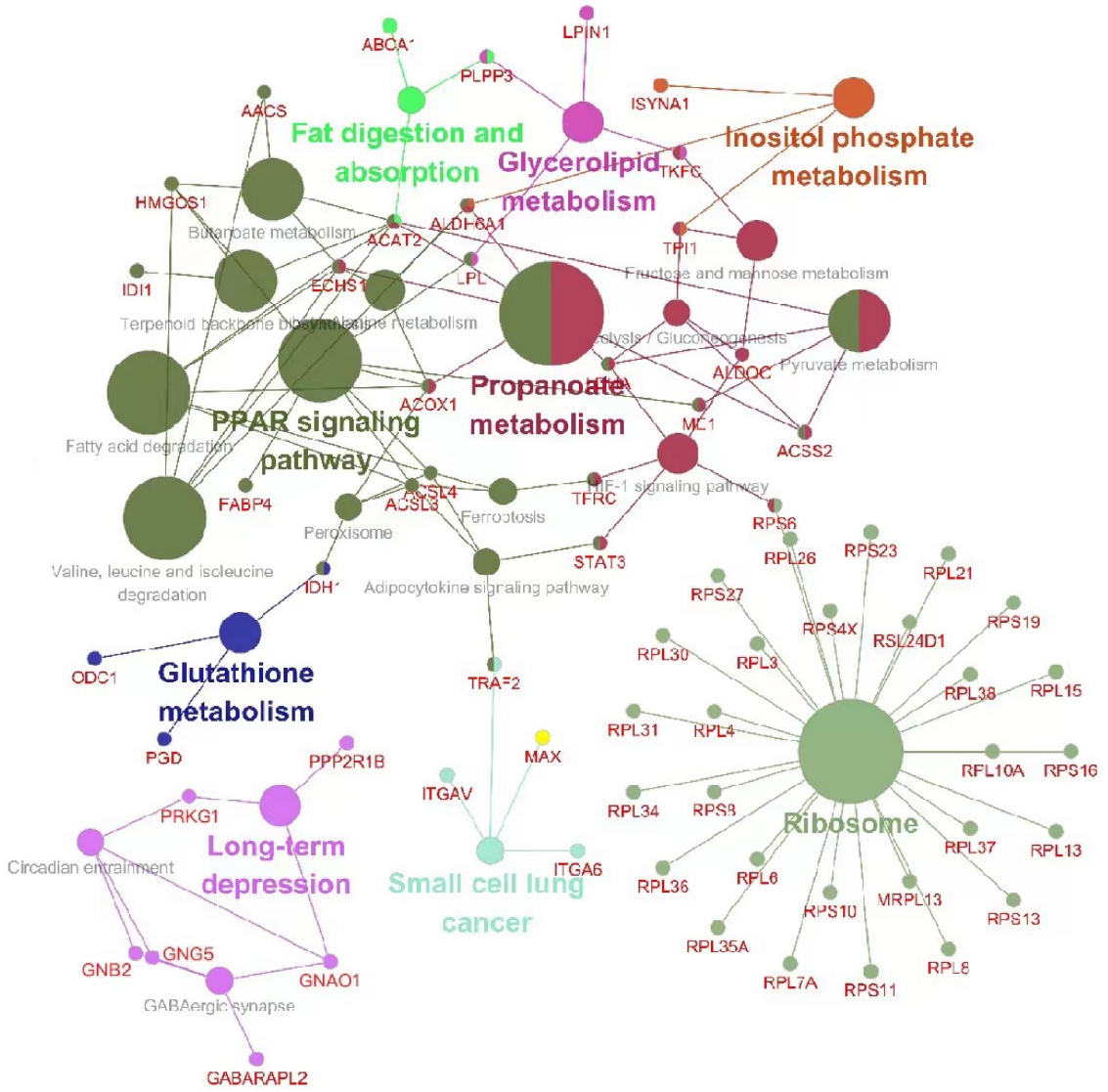

FIGURE 8
Data visualizations of the results from the KEGG enrichment analysis of differentially expressed genes and proteins in SH-SY5Y cells after SIRT4 overexpression with ClueGO. A KEGG enrichment analysis of differentially expressed proteins in SH-SY5Y cells after SIRT4 overexpression was performed using ClueGO. The figure clearly shows the main proteins in the enriched pathways and the connection between A protein and different pathways. The size of the circle represents the number of different proteins.

a comprehensive understanding of the function of the SIRT family in several pathways is thus crucial (Singh et al., 2018). The function of mitochondria in the pathogenesis/aetiology of PD is specifically prominent, which includes damage to the mitochondrial respiratory chain complex as an important feature of PD, the extensive involvement of the mitochondrial genome in its progression, the interactions between α-syn and mitochondrial function, the disruption of mitochondrial homeostasis by Parkinson's disease-associated pathogenic genes, and the drugs targeting mitochondrial mechanisms to improve its prognosis (Grünewald et al., 2019). Mitochondrial SIRTs are anchored in the mitochondria and show the advantages of influencing neurodegenerative diseases through posttranslational modifications of substrate proteins to regulate the activity and biological functions of mitochondrial proteins, making them of great interest to us (He et al., 2022). SIRT4 is the least studied SIRT, thus necessitating its exploration as a new potential target and the determination of its role in PD. This study focused on whether SIRT4 was involved in PD models, and we innovatively investigated possible pathways and molecular targets of SIRT4 by performing quantitative proteomics with TMT Labeling. PD is considered to result

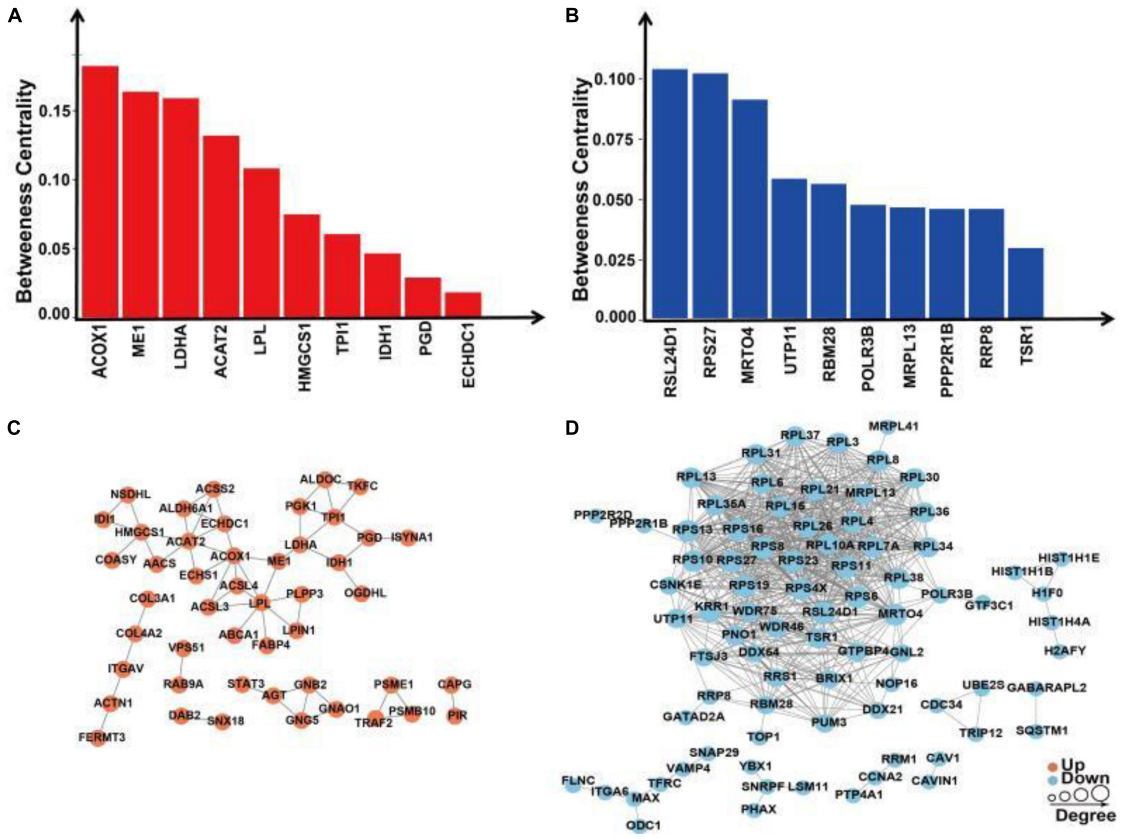

FIGURE 9
Protein–protein interaction network analysis of differentially expressed proteins in SH-SY5Y cells after SIRT4 overexpression. **(A)** Histogram of the top 10 active proteins in the PPI network analysis of upregulated proteins according to the betweenness centrality. **(B)** Histogram of the top 10 active proteins in the PPI network analysis of downregulated proteins according to the betweenness centrality. **(C)** Visual display of the PPI network analysis of upregulated proteins. **(D)** Visual display of the PPI network analysis of downregulated proteins. A network of interactions from the STRING database with a confidence score >0.7 (high confidence) was visualized in Cytoscape. The betweenness centrality was calculated based on the Cytoscape plug-in CytoNCA. The size of the circle represents the number of proteins interacting with the corresponding differentially expressed proteins.

from genes, environment, and gene-environment interactions. The MPTP mouse model is a typical drug toxicity model of PD, and the DJ-1KO rat is a PD model with deletion of the DJ-1 gene associated with oxidative stress (Díaz-Casado et al., 2016). In our study, SIRT4 levels were altered in both the MPTP-induced PD mouse model and the DJ-1KO rat model, reflecting that SIRT4 may be involved in the progression of PD. In addition, we selected SH-SY5Y cell as the cell model, which exhibits various properties of dopaminergic neurons, such as tyrosine hydroxylase, dopamine 2B2 hydroxylase, and dopamine transporter expression, for *in vitro* study of PD. GSEA of differentially expressed proteins after overexpression of SIRT4 also supports the possible involvement of SIRT4 in the onset and development of PD. This result is consistent with previous studies of mitochondrial SIRT in neurodegenerative disease (van de Ven et al., 2017).

However, what kind of mechanisms about SIRT4 involved in the onset and development of PD? Previous studies on SIRT4 mainly identified that SIRT4 is an early regulator of branched-chain amino acid catabolism and promotes adipogenesis (Laurent et al., 2013). In non-alcoholic fatty liver disease (NAFLD), SIRT4 deacetylates and destabilizes mitochondrial trifunctional protein-alpha (MTPα), thereby affecting fatty acid β-oxidation (van Maarschalkerweerd et al., 2015). The mTORC1 pathway inhibits cell differentiation and glutamate metabolism by affecting SIRT4 transcription (Csibi et al., 2021). SIRT4 promotes cardiac dysfunction caused by myocardial fibrosis and hypertrophy by increasing ROS levels in response to pathological stimuli (Luo et al., 2017). Our comprehensive analysis of the functional mechanisms of SIRT4 by quantitative proteomic identification and bioinformatics has provided some new perspectives in addition to confirming the changes in the discovered mechanisms. The biological processes identified from an enrichment analysis of differentially expressed proteins after SIRT4 overexpression compared with the CN group included the ribosomal pathway, propionate

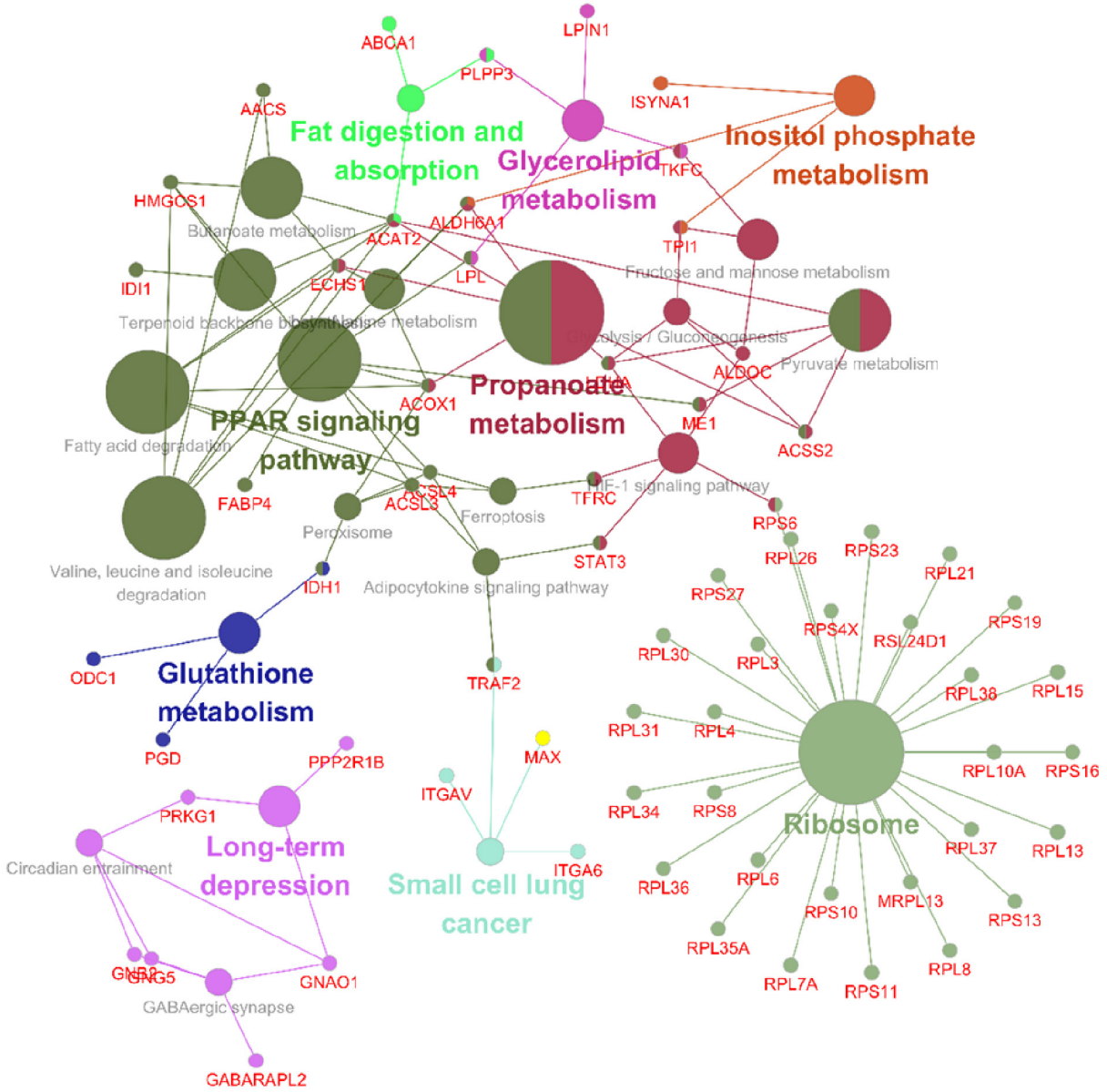

FIGURE 10
KEGG enrichment analysis of all interacting proteins after SIRT4 overexpression in SH-SY5Y cells with ClueGO. The figure clearly shows the main proteins in the enrichment pathway and the connection between the same protein and different pathways. The size of the circle represents the number of different proteins.

metabolic pathway, PPAR signalling pathway, fatty acid degradation pathway, and peroxisome pathway. Besides, some other pathways with lower levels of enrichment that deserve attention include circadian rhythm pathway, 5-hydroxytryptaminergic synapses pathway, relaxation signaling pathway, and lipoic acid metabolism pathway. Moreover, the PPI network analysis of differentially expressed proteins mainly enriched in the ribosomal pathway, the PPAR signaling pathway, lipid metabolism pathway, propionate metabolism pathway, phosphatidylinositol metabolism pathway, and glutathione metabolism pathway. What is more important, the most active protein in the PPI network analysis of upregulated proteins was ACOX1, while the most active protein in the PPI network analysis of downregulated proteins was RSL24D1. ACOX1 is associated with the peroxisomal pathway and PPAR signaling pathway, while RSL24D1 is closely related to the ribosomal pathway. Finally, The COG/KOG categories indicated that SIRT4 is most closely associated with translation, ribosome structure, and biogenesis. The multi-level analysis of the above situations shows that SIRT4 functions in dopaminergic neurons

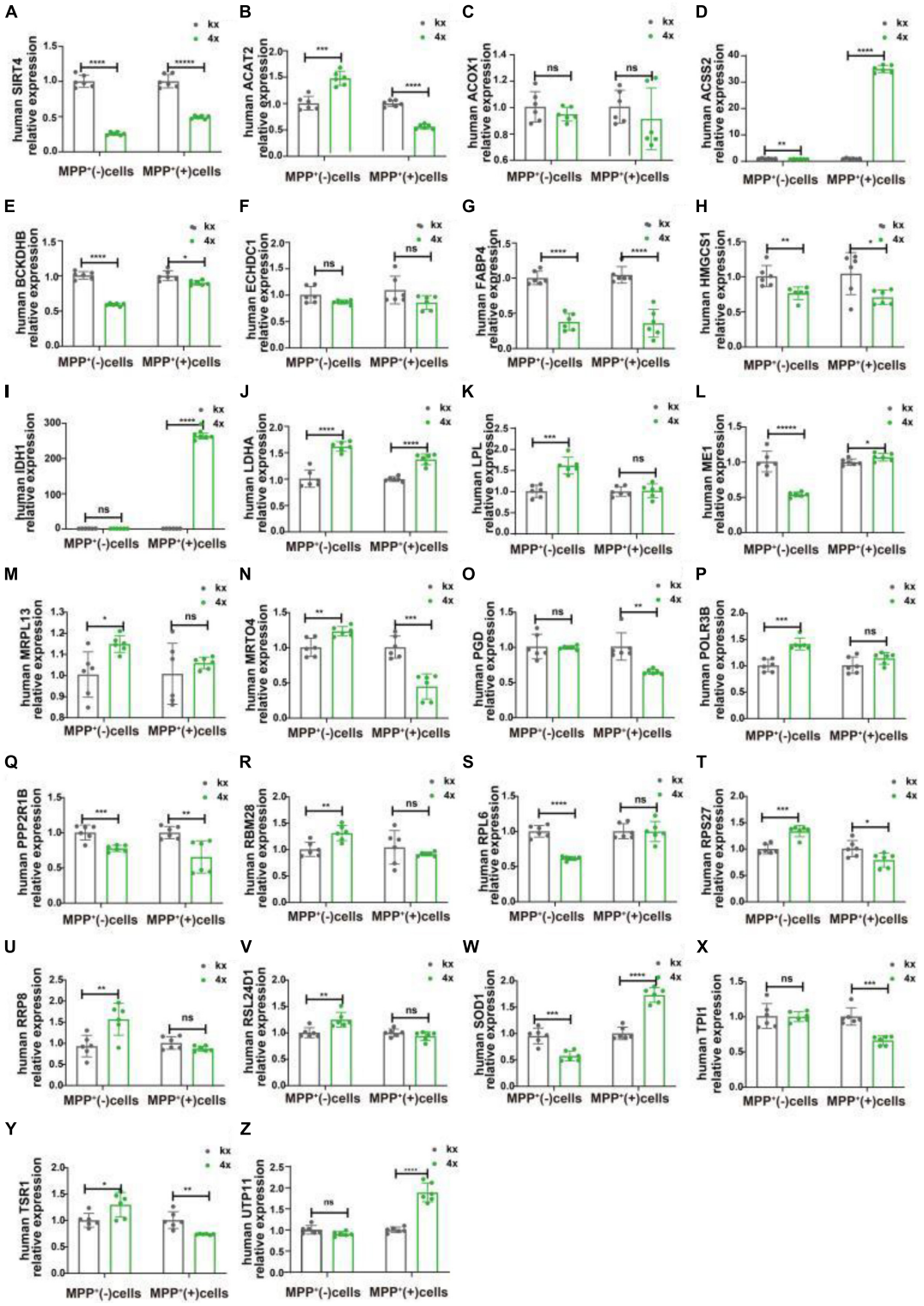

FIGURE 11

The mRNA expression of 25 potential targets in SH-SY5Y cells or MPP + -treated SH-SY5Y cells after knocking down SIRT4. **(A)** The mRNA expression of SIRT4 in SH-SY5Y cells or MPP^+-treated SH-SY5Y cells after knocking down SIRT4. **(B–Z)** Compared with the control group, the mRNA expression of 25 potential targets in SH-SY5Y cells or MPP^+-treated SH-SY5Y cells after knocking down SIRT4, respectively. The different mRNA expressions were normalized by β-ACTIN (n = 6 per group). Results are depicted as means ± SEM. *P < 0.05, **P < 0.01, ***P < 0.001, and ****P < 0.0001 compared with the control group.

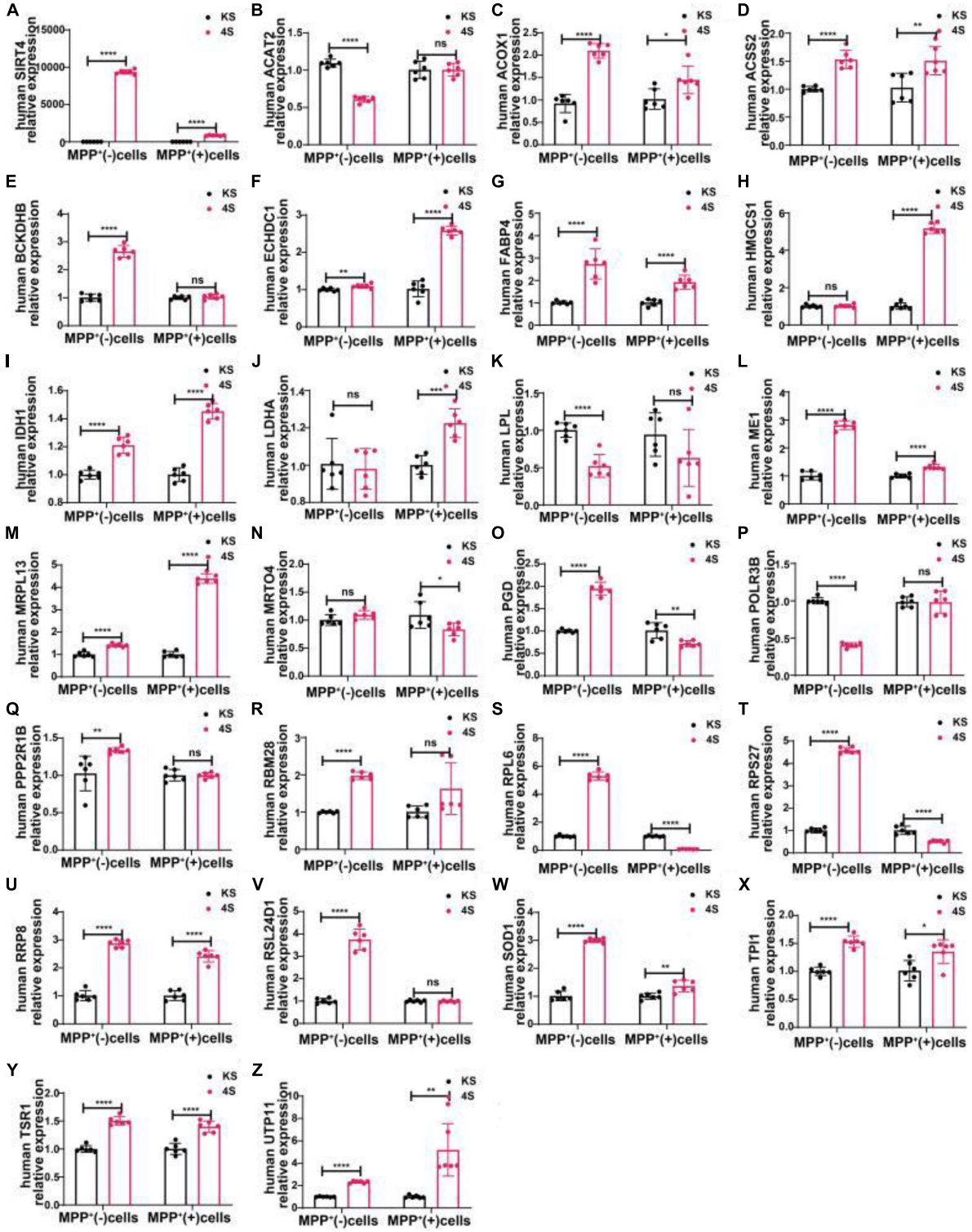

FIGURE 12

The mRNA expression of 25 potential targets in SH-SY5Y cells or MPP^+-treated SH-SY5Y cells after SIRT4 overexpression. **(A)** The mRNA expression of SIRT4 in SH-SY5Y cells or MPP^+-treated SH-SY5Y cells after SIRT4 overexpression. **(B–Z)** Compared with the control group, the mRNA expression of 25 potential targets in SH-SY5Y cells or MPP^+-treated SH-SY5Y cells after SIRT4 overexpression, respectively. The different mRNA expressions were normalized by β-ACTIN (n = 6 per group). Results are depicted as means ± SEM. *P < 0.05, **P < 0.01, ***P < 0.001, and ****P < 0.0001 compared with the control group.

TABLE 1 The changes of 25 potential targets in mRNA expression under different intervention conditions in SH-SY5Y cells and wild-type (C57) mice.

Gene	Gene description	Compared with the corresponding group				
		SIRT4 overexpression in SH-SY5Y	Knock-down of SIRT4 in SH-SY5Y	SIRT4 overexpression in MPP+ intervention SH-SY5Y cell	Knock-down of SIRT4 in MPP+ intervention SH-SY5Y cell	SIRT4 overexpression in normal mice
		G4 group	KX group	G4+M group	KX+M group	4S
SIRT4	NAD-dependent protein lipoamidase sirtuin-4	↑	↓	↑	↓	↑
RPL6	60S ribosomal protein L6	↑	↓	↓	ns	ns
LPL	Lipoprotein lipase	↓	↑	↓	ns	↓
PGD	6-phosphogluconate dehydrogenase, decarboxylating	↑	**ns**	↓	↓	↑
HMGCS1	Hydroxymethylglutaryl-CoA synthase, cytoplasmic	**ns**	↓	↑	↓	↑
TPI1	Triosephosphate isomerase	↑	ns	↑	↓	ns
BCKDHB	2-oxoisovalerate dehydrogenase subunit beta	↑	↓	**ns**	↓	↓
ECHDC1	Ethylmalonyl-CoA decarboxylase	**ns**	ns	↑	ns	↓
UTP11	Probable U3 small nucleolar RNA-associated protein 11	↑	**ns**	↑	↑	↑
POLR3B	DNA-directed RNA polymerase III subunit RPC2	↓	↑	**ns**	ns	ns
ACSS2	Acetyl-coenzyme A synthetase, cytoplasmic	↑	↓	↑	↑	↑
RSL24D1	Probable ribosome biogenesis protein RLP24	↑	↑	**ns**	ns	ns
RBM28	RNA-binding protein 28	↑	↑	**ns**	ns	↓
MRPL13	39S ribosomal protein L13, mitochondrial	↑	↑	↑	ns	ns
MRT04	mRNA turnover protein 4 homolog	**ns**	↑	↓	↓	↑
PPP2R1B	Serine/threonine-protein phosphatase 2A 65 kDa regulatory subunit A beta isoform	↑	↓	ns	↓	↓
AC0X1	Peroxisomal acyl-coenzyme A oxidase 1	↑	**ns**	↑	ns	↓
S0D1	Superoxide dismutase [Cu-Zn]	↑	↓	↑	↑	↓
ME1	NADP-dependent malic enzyme	↑	↓	↑	↑	ns
RPS27	40S ribosomal protein S27	↑	↑	↓	↓	↓
ACAT2	Acetyl-CoA acetyltransferase, cytosolic	↓	↑	**ns**	↓	ns
LDHA	L-Lactate dehydrogenase A chain	**ns**	↑	↑	↑	ns
FABP4	Fatty acid-binding protein, adipocyte	↑	↓	↑	↓	↓
IDH1	Isocitrate dehydrogenase [NADP] cytoplasmic	↑	**ns**	↑	↑	↓
RRP8	Ribosomal RNA-processing protein 8	↑	↑	↑	ns	ns
TSR1	Pre-rRNA-processinq protein TSR1 homolog	↑	↑	↑	↓	↓

Red font represents among the 25 molecules, FABP4 as the most potential target.

mainly by modulating the ribosomal pathway, propionate metabolic pathway, PPAR signaling pathway, and peroxisomal pathway, which compensates to some extent for the lack of previous studies on the mechanisms of SIRT4. Although few studies have examined the roles of SIRT4 in the ribosomal pathway and propionate metabolic pathway, these mechanisms are more or less associated with PD. For example, ribosomal protein s15 is a substrate for LRRK2, a key pathogenic protein in *Drosophila* and human PD models (Martin et al., 2014). Antibodies against ribosomal proteins have been used as predictive markers for age-related neurodegenerative diseases (Yin et al., 2021). In the propionate metabolic pathway, the combined concentrations of acetate and propionate may be a potential biomarker to distinguish MSA patients from

PD patients (He et al., 2021). Increasing the level of gut microbiota-derived propionate effectively ameliorated the loss of dopaminergic neurons and motor deficits in a mouse 6-hydroxydopa-induced PD model (Hou et al., 2021). Reduced propionate levels in fecal samples might exert beneficial effects on intestinal epithelial barrier function and motor behavior *via* the AKT signaling pathway in a mouse model of MPTP-induced PD (Huang et al., 2021). In summary, these mechanisms provide new insights into our studies on the function of SIRT4 in PD.

Further confirmation of the regulatory targets of SIRT4 in PD models was achieved by selecting differentially expressed proteins exhibiting higher activity in protein-protein interaction networks as well as differentially expressed proteins with significant changes in major enriched pathways as candidate targets for multilevel screening and validation. Our study revealed only the expression of FABP4 in the PPAR signaling pathway was significantly altered accordingly with increased or decreased SIRT4 expression in SH-SY5Y cells/MPP^+-treated SH-SY5Y cells and normal mice/MPTP-induced PD mice. Similar to other members of the nuclear receptor superfamily, PPAR is proposed to be a ligand-activated transcription factor involved in lipid, glucose, and amino acid metabolism that simultaneously reprograms immune responses, stimulates metabolic and mitochondrial functions, promotes axonal growth, induces progenitor cell differentiation into myelinated oligodendrocytes, and increases brain clearance of toxic molecules such as β-amyloid (Lautrup et al., 2019). The PPARg agonist pioglitazone has been shown to attenuate MPTP-induced dopamine depletion in a mouse model of PD (Quinn et al., 2008). The beneficial effects of regular treadmill exercise on reducing α-synuclein levels in the brain have been suggested to be mediated by PPARα (Dutta et al., 2022). All of these findings suggest the clinical importance of the PPAR signaling pathway in the field of PD. Maintenance of neuronal metabolic integrity requires moderate lipid transfer between neurons and glial cells via lipid transport proteins. Lipid accumulation in glial cells due to reactive oxygen species production and mitochondrial damage leads to further neuronal damage and degeneration (Ioannou et al., 2019). Moderate cholesterol homeostasis maintains the structure of α-synuclein; however, excess cholesterol promotes the local deposition of α-synuclein and the formation of Lewy vesicles with aggregated α-synuclein, which in turn affects the function of DATs and dopaminergic neurons (van Maarschalkerweerd et al., 2015; Zhuge et al., 2019). Furthermore, the cholesterol metabolite 27-OHC decreases TH activity and causes oxidative stress and apoptosis (Dai et al., 2021). Thus, dyslipidemia is closely associated with PD and LBD, and lipids and small molecules in sebum have even been suggested as potential biomarkers of PD (Klemann et al., 2017; Sinclair et al., 2021). That is to say, abnormal lipid metabolism is clearly an important mechanism in PD. FABP4 is a lipid carrier that is considered a key mediator of systemic metabolic and inflammatory processes (Ron et al., 2021) and is closely associated with the development of metabolic syndrome, inflammation, and atherosclerosis. Importantly, it regulates the onset and development of inflammation and metabolism, resists the progression of atherosclerosis, and improves insulin sensitivity (Furuhashi et al., 2007; Prentice et al., 2021). In other words, FABP4 is a signaling molecule for metabolic abnormalities, and its effects on metabolism, particularly blood glucose and lipid metabolism, will inevitably affect the incidence of PD. Recent studies have also shown that FABP3, belonging to the FABP family, is expressed at high levels in the brain and accelerates α-Syn oligomerization upon cellular exposure to MPTP (Cheng et al., 2019). This finding more or less supports the relevance of FABP4 to PD. SIRT4 plays an important role in lipid metabolism. In skeletal muscle and white adipose tissue, SIRT4 deacetylates and inhibits malonyl coenzyme A decarboxylase (MCD) to regulate lipid metabolism (Laurent et al., 2013). This finding supports the association of SIRT4 with FABP4 to some extent. Although the relationship between the SIRT family and FABP4 has not been explored in PD, upregulation of FABP4 expression in the macrophages of wounds may promote inflammation by decreasing SIRT3 expression in diabetic mice (Boniakowski et al., 2019). FABP4-Cre-mediated SIRT6 deficiency impairs adipose tissue function and metabolic homeostasis in mice (Xiong et al., 2017). These results also confirm that SIRT4, a member of the SIRT family, may be associated with FABP4.

Fatty acid binding proteins are cytoplasmic lipid chaperones that promote fatty acid solubilization, transport, and metabolism and interact with various membrane and intracellular proteins [for example, PPAR, hormone-sensitive lipase (HSL), etc.] (Li et al., 2020). A bidirectional interaction between the FABP4 and PPARγ pathways has been identified to potentially drive the aggressive behavior of tumor cells in bone (Herroon et al., 2013). FABP4 also triggers the ubiquitination and subsequent proteasomal degradation of PPARγ (Herroon et al., 2013). Furthermore, FABP4 induces IL-4-stimulated adipogenesis in human skeletal muscle cells through the activation of the PPARγ signaling pathway (Wang et al., 2022). The correlation between FABP4 and PPARγ is also supported by our findings. However, in the MPTP-induced PD mouse model, SIRT4 overexpression inhibited FABP4 transcription but promoted FABP4 protein expression. This inconsistency between the results obtained at the mRNA and protein levels involves complex mechanisms. Protein abundance depends on the following factors: the transcription rate, mRNA half-life, translation rate [the composition of mRNA sequence codon, upstream open reading frame, internal ribosome entry site (IRES), proteins binding to regulatory elements on transcripts, relative availability of transcript and ribosomes], protein half-life (complex ubiquitin–proteasome pathways or autophagy may affect the protein concentration independent of the transcript concentration), delays in protein synthesis, and protein transport (the protein spatial output separates

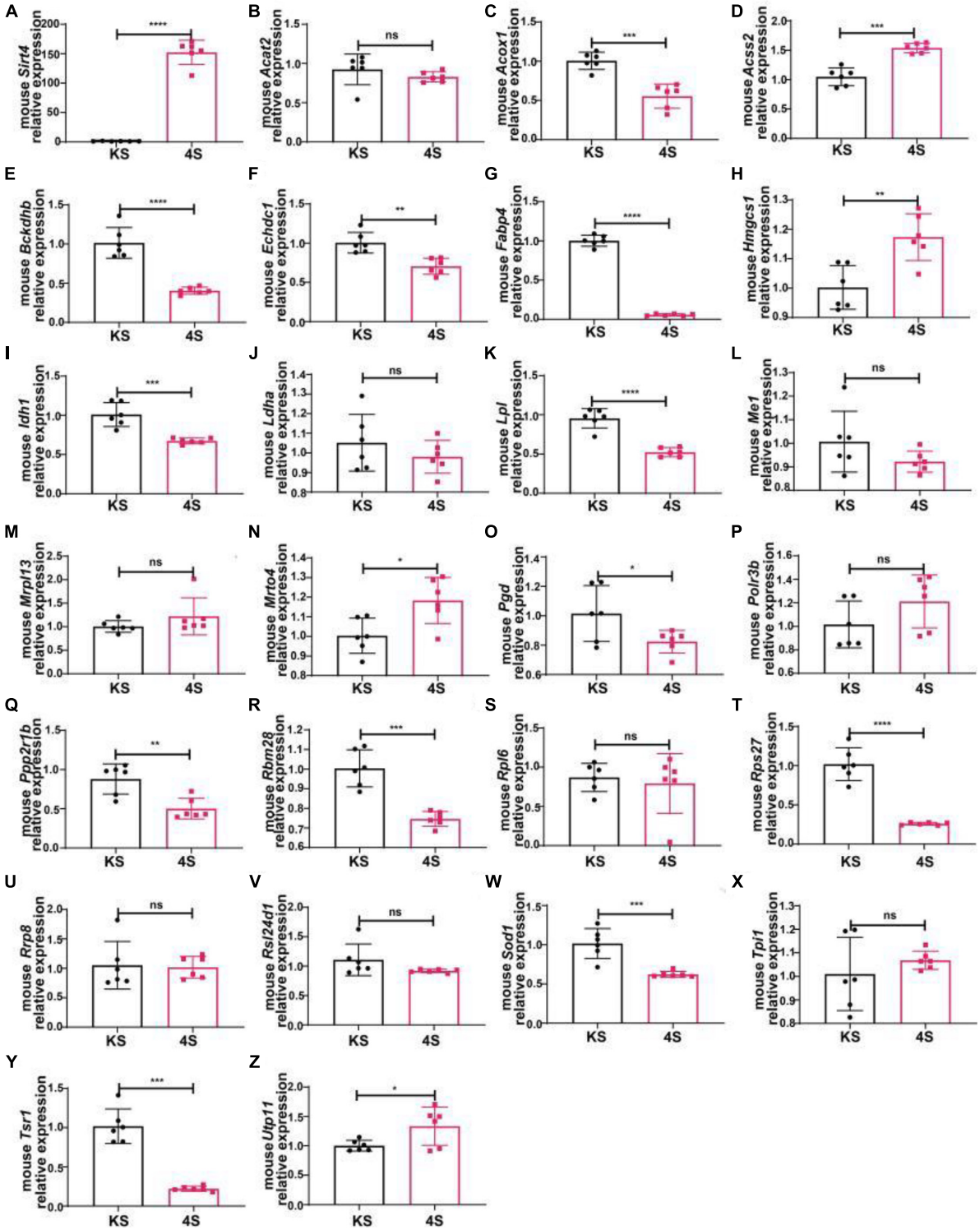

FIGURE 13

The mRNA expression of 25 potential targets in wild-type (C57) mice after SIRT4 overexpression. **(A)** The mRNA expression of SIRT4 in the substantia nigra of wild-type (C57) mice after stereotactic injection of SIRT4-AAV. **(B–Z)** The mRNA expression of 25 potential targets in the substantia nigra of wild-type (C57) mice after stereotactic injection of SIRT4-AAV, respectively. The different mRNA expression levels were normalized to that of β-actin (n = 6 per group). The results are depicted as the means ± SEMs. *$P < 0.05$, **$P < 0.01$, ***$P < 0.001$, and ****$P < 0.0001$ compared with the control group.

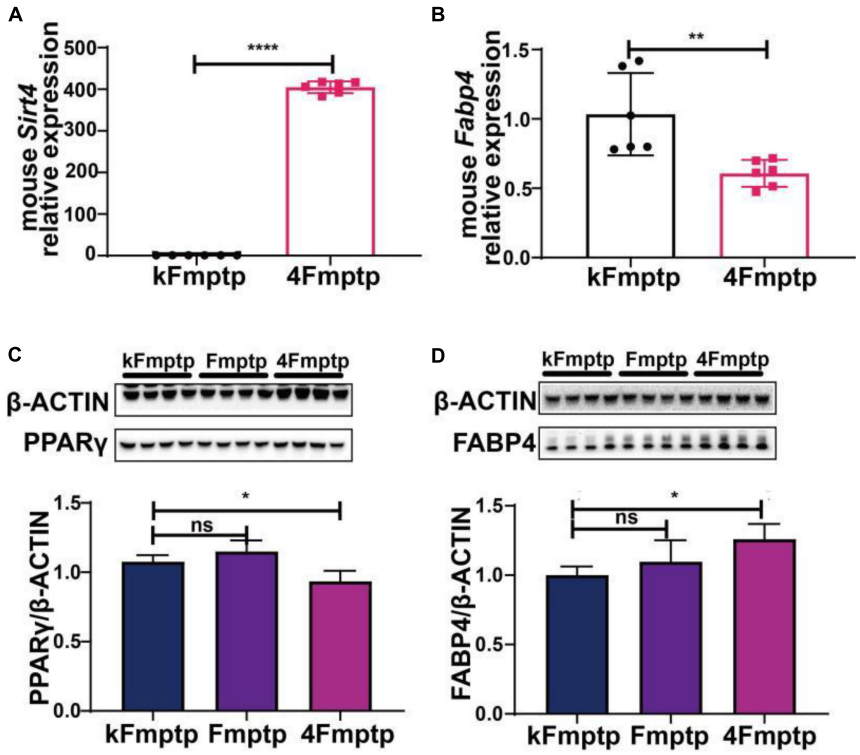

FIGURE 14
SIRT4 overexpression in the substantia nigra of MPTP-induced Parkinson's mouse model can induce the changes of FABP4 and PPARγ. **(A)** The mRNA expression of SIRT4 in the substantia nigra of MPTP-induced Parkinson's mouse model after stereotactic injection of SIRT4-AAV. **(B)** The mRNA expression of FABP4 in the substantia nigra of MPTP-induced Parkinson's mouse model after stereotactic injection of SIRT4-AAV. **(C,D)** Representative western blots and densitometric analysis for FABP4 γ PPAR protein between groups, respectively. FABP4 γ PPAR protein extracts from the substantia nigra of MPTP-induced Parkinson's mouse model after stereotactic injection of SIRT4-AAV or the control group. The different protein expressions were normalized by β-Actin (n = 6 per group). Results are depicted as means ± SEM. *P < 0.05, **P < 0.01, and ****P < 0.0001 compared with the control group. FABP4, Fatty acid binding protein 4; PPARγ, Peroxisome proliferator-activated receptor gamma.

proteins from synthesized transcripts) (Liu et al., 2016). Among them, the transcription rate and mRNA half-life determine the level of mRNA. Posttranscriptional and posttranslational regulation induce important functional changes in protein abundance, which are not observed at the mRNA level (Schwanhäusser et al., 2011; Kristensen et al., 2013; Baum et al., 2019; Buccitelli and Selbach, 2020). In summary, translation itself is a complex multistep process, and post-translational modifications and protein interactions with other biomolecules together contribute to a phenotype that is more functionally stable than mRNA (Mann and Jensen, 2003; Ryan et al., 2013; Buccitelli and Selbach, 2020). There is no doubt that our results are not contradictory, providing a deeper understanding of the mechanism of SIRT4; however, the exact molecular mechanism requires further elucidation.

Our study, of course, has some limitations. Firstly, although *in vitro* studies exclude the effects of other cell types of the brain on dopaminergic neuronal mechanisms *in vivo*, artificial interference with SIRT4 expression through viral transfection makes the findings different from the real physiological and pathological state, and thus models closer to the disease state are required for verification and confirmation. Secondly, although SH-SY5Y cells with MPP^+ intervention and MPTP-induced PD mouse model are classical models used in the study of PD, they mainly reflect Parkinson's disease induced by drug toxicity and do not fully mimic the pathogenic mechanisms of PD. Finally, as the changes in protein are related to differences in transcription, translation, and post-translational modifications, the results of which may vary substantially. Moreover, because changes in protein are related to differences in transcription, translation, and posttranslational modifications, the results may vary substantially. Therefore, multiomics analyses are needed in the future. In conclusion, this study confirms that SIRT4 plays a role in PD models, provides a relatively comprehensive understanding of the possible mechanisms of SIRT4, and identifies the most promising regulatory targets. Although most of the data obtained in this study are still descriptive, our findings provide powerful evidence to support the study of SIRT4-centred biomarkers in PD.

Data availability statement

The original contributions presented in this study are included in the article/**Supplementary material**, further inquiries can be directed to the corresponding authors.

Ethics statement

The animal study was reviewed and approved by the Institutional Committee for Animal Care and Use of Fujian Medical University.

Author contributions

HW, WS, and KF performed the experiments and wrote the manuscript. GC and YG revised the manuscript. XC, HZ, and QY guided the process and interpreted the results. All authors acquired the data, analyzed the results, read, and approved the final manuscript.

Funding

This work was supported by the National Natural Science Foundation of China to QY (grant numbers: 82171402 and 81870995) and the Startup Fund for scientific research of Fujian Medical University, China (grant numbers: 2020QH2017 to HW and 2021QH2016 to WS).

Acknowledgments

We thank Jingjie PTM BioLab (Hangzhou) for technical support and Bullet Edits Limited for the linguistic editing and proofreading of the manuscript.

Conflict of interest

The authors declare that the research was conducted in the absence of any commercial or financial relationships that could be construed as a potential conflict of interest.

Publisher's note

All claims expressed in this article are solely those of the authors and do not necessarily represent those of their affiliated organizations, or those of the publisher, the editors and the reviewers. Any product that may be evaluated in this article, or claim that may be made by its manufacturer, is not guaranteed or endorsed by the publisher.

Supplementary material

The Supplementary Material for this article can be found online at: https://www.frontiersin.org/articles/10.3389/fnins.2022.1035444/full#supplementary-material

SUPPLEMENTARY FIGURE 1
The first 30 upregulated proteins with significant difference after sirtuin 4 (SIRT4) overexpression in SH-SY5Y cells. The table clearly shows the protein name, molecular weight and G4/CN ratio of the first 30 upregulated proteins. The heat map visually shows the changes of the first 30 upregulated proteins compaired with the control group.

SUPPLEMENTARY FIGURE 2
The first 30 downregulated proteins with significant difference after sirtuin 4 (SIRT4) overexpression in SH-SY5Y cells. The table clearly shows the protein name, molecular weight and G4/CN ratio of the first 30 downregulated proteins. The heat map visually shows the changes of the first 30 downregulated proteins compaired with the control group.

SUPPLEMENTARY TABLE 1
Primer sequences for human or mouse RT-PCR experiments.

SUPPLEMENTARY TABLE 2
Primer sequence and PCR conditions for identification of DJ-1 KO rats.

SUPPLEMENTARY TABLE 3
The main normalized enrichment score (NES) of differentially expressed proteins after SIRT4 overexpression in SH-SY5Y cells with gene set enrichment analysis.

References

Anderson, K. A., Huynh, F. K., Fisher-Wellman, K., Stuart, J. D., Peterson, B. S., Douros, J. D., et al. (2017). SIRT4 Is a lysine deacylase that controls leucine metabolism and insulin secretion. *Cell Metab.* 25, 838–855.e15. doi: 10.1016/j.cmet.2017.03.003

Angelova, P. R., Barilani, M., Lovejoy, C., Dossena, M., Viganò, M., Seresini, A., et al. (2018). Mitochondrial dysfunction in Parkinsonian mesenchymal stem cells impairs differentiation. *Redox Biol.* 14, 474–484. doi: 10.1016/j.redox.2017.10.016

Attal, N., Marrero, E., Thompson, K. J., and McKillop, I. H. (2022). Cytochrome P450 2E1-dependent hepatic ethanol metabolism induces fatty acid-binding protein 4 and steatosis. *Alcohol. Clin. Exp. Res.* 46, 928–940. doi: 10.1111/acer.14828

Bacigaluppi, M., and Martino, G. (2020). FABP4 a novel therapeutic target in ischaemic stroke. *Eur. Heart J.* 41, 3181–3183. doi: 10.1093/eurheartj/ehaa230

Baum, K., Schuchhardt, J., Wolf, J., and Busse, D. (2019). Of gene expression and cell division time: A mathematical framework for advanced differential gene expression and data analysis. *Cell Syst.* 9, 569–579.e7. doi: 10.1016/j.cels.2019.07.009

Betsinger, C. N., and Cristea, I. M. (2019). Mitochondrial function, metabolic regulation, and human disease viewed through the prism of sirtuin 4 (SIRT4) functions. *J. Proteome Res.* 18, 1929–1938. doi: 10.1021/acs.jproteome.9b00086

Boniakowski, A. M., denDekker, A. D., Davis, F. M., Joshi, A., Kimball, A. S., Schaller, M., et al. (2019). SIRT3 regulates macrophage-mediated inflammation in

diabetic wound repair. *J. Invest. Dermatol.* 139, 2528–2537.e2. doi: 10.1016/j.jid.2019.05.017

Buccitelli, C., and Selbach, M. (2020). mRNAs, proteins and the emerging principles of gene expression control. *Nat. Rev. Genet.* 21, 630–644. doi: 10.1038/s41576-020-0258-4

Cao, H., Sekiya, M., Ertunc, M. E., Burak, M. F., Mayers, J. R., White, A., et al. (2013). Adipocyte lipid chaperone AP2 is a secreted adipokine regulating hepatic glucose production. *Cell Metab.* 17, 768–778. doi: 10.1016/j.cmet.2013.04.012

Cheng, A., Jia, W., Kawahata, I., and Fukunaga, K. (2021). Impact of fatty acid-binding proteins in α-synuclein-induced mitochondrial injury in synucleinopathy. *Biomedicines* 9:560. doi: 10.3390/biomedicines9050560

Cheng, A., Shinoda, Y., Yamamoto, T., Miyachi, H., and Fukunaga, K. (2019). Development of FABP3 ligands that inhibit arachidonic acid-induced α-synuclein oligomerization. *Brain Res.* 1707, 190–197. doi: 10.1016/j.brainres.2018.11.036

Choromańska, B., Myśliwiec, P., Dadan, J., Hady, H. R., and Chabowski, A. (2011). [The clinical significance of fatty acid binding proteins]. *Postepy Hig. Med. Dosw. (Online)* 65, 759–763. doi: 10.5604/17322693.966983

Csibi, A., Fendt, S. M., Li, C., Poulogiannis, G., Choo, A. Y., Chapski, D. J., et al. (2013). The mTORC1 pathway stimulates glutamine metabolism and cell proliferation by repressing SIRT4. *Cell* 153, 840–854. doi: 10.1016/j.cell.2013.04.023

Csibi, A., Fendt, S. M., Li, C., Poulogiannis, G., Choo, A. Y., Chapski, D. J., et al. (2021). The mTORC1 pathway stimulates glutamine metabolism and cell proliferation by repressing SIRT4. *Cell* 184:2256. doi: 10.1016/j.cell.2021.03.059

Dai, L., Zou, L., Meng, L., Qiang, G., Yan, M., and Zhang, Z. (2021). Cholesterol metabolism in neurodegenerative diseases: Molecular mechanisms and therapeutic targets. *Mol. Neurobiol.* 58, 2183–2201. doi: 10.1007/s12035-020-02232-6

Díaz-Casado, M. E., Lima, E., García, J. A., Doerrier, C., Aranda, P., Sayed, R. K., et al. (2016). Melatonin rescues zebrafish embryos from the parkinsonian phenotype restoring the parkin/PINK1/DJ-1/MUL1 network. *J. Pineal Res.* 61, 96–107. doi: 10.1111/jpi.12332

Dorsey, E. R., and Bloem, B. R. (2018). The Parkinson Pandemic-A Call to Action. *JAMA Neurol.* 75, 9–10. doi: 10.1001/jamaneurol.2017.3299

Dutta, D., Paidi, R. K., Raha, S., Roy, A., Chandra, S., and Pahan, K. (2022). Treadmill exercise reduces α-synuclein spreading via PPARα. *Cell Rep.* 40:111058. doi: 10.1016/j.celrep.2022.111058

Frizzell, H., Fonseca, R., Christo, S. N., Evrard, M., Cruz-Gomez, S., Zanluqui, N. G., et al. (2020). Organ-specific isoform selection of fatty acid-binding proteins in tissue-resident lymphocytes. *Sci. Immunol.* 5:eaay9283. doi: 10.1126/sciimmunol.aay9283

Furuhashi, M., Tuncman, G., Görgün, C. Z., Makowski, L., Atsumi, G., Vaillancourt, E., et al. (2007). Treatment of diabetes and atherosclerosis by inhibiting fatty-acid-binding protein aP2. *Nature* 447, 959–965. doi: 10.1038/nature05844

Gharpure, K. M., Pradeep, S., Sans, M., Rupaimoole, R., Ivan, C., Wu, S. Y., et al. (2018). FABP4 as a key determinant of metastatic potential of ovarian cancer. *Nat. Commun.* 9:2923. doi: 10.1038/s41467-018-04987-y

Gomes, P., Leal, H., Mendes, A. F., Reis, F., and Cavadas, C. (2019). Dichotomous sirtuins: Implications for drug discovery in neurodegenerative and cardiometabolic diseases. *Trends Pharmacol. Sci.* 40, 1021–1039. doi: 10.1016/j.tips.2019.09.003

Grünewald, A., Kumar, K. R., and Sue, C. M. (2019). New insights into the complex role of mitochondria in Parkinson's disease. *Prog. Neurobiol.* 177, 73–93. doi: 10.1016/j.pneurobio.2018.09.003

Haigis, M. C., and Sinclair, D. A. (2010). Mammalian sirtuins: Biological insights and disease relevance. *Annu. Rev. Pathol.* 5, 253–295. doi: 10.1146/annurev.pathol.4.110807.092250

He, L., Wang, J., Yang, Y., Li, J., and Tu, H. (2022). Mitochondrial sirtuins in Parkinson's disease. *Neurochem. Res.* 47, 1491–1502. doi: 10.1007/s11064-022-03560-w

He, X., Qian, Y., Xu, S., Zhang, Y., Mo, C., Guo, W., et al. (2021). Plasma short-chain fatty acids differences in multiple system atrophy from Parkinson's disease. *J. Parkinsons Dis.* 11, 1167–1176. doi: 10.3233/jpd-212604

Herroon, M. K., Rajagurubandara, E., Hardaway, A. L., Powell, K., Turchick, A., Feldmann, D., et al. (2013). Bone marrow adipocytes promote tumor growth in bone via FABP4-dependent mechanisms. *Oncotarget* 4, 2108–2123. doi: 10.18632/oncotarget.1482

Hou, Y. F., Shan, C., Zhuang, S. Y., Zhuang, Q. Q., Ghosh, A., Zhu, K. C., et al. (2021). Gut microbiota-derived propionate mediates the neuroprotective effect of osteocalcin in a mouse model of Parkinson's disease. *Microbiome* 9:34. doi: 10.1186/s40168-020-00988-6

Houtkooper, R. H., Pirinen, E., and Auwerx, J. (2012). Sirtuins as regulators of metabolism and healthspan. *Nat. Rev. Mol. Cell Biol.* 13, 225–238. doi: 10.1038/nrm3293

Huang, T., Shi, H., Xu, Y., and Ji, L. (2021). The gut microbiota metabolite propionate ameliorates intestinal epithelial barrier dysfunction-mediated Parkinson's disease via the AKT signaling pathway. *Neuroreport* 32, 244–251. doi: 10.1097/wnr.0000000000001585

Imai, S., and Guarente, L. (2014). NAD+ and sirtuins in aging and disease. *Trends Cell Biol.* 24, 464–471. doi: 10.1016/j.tcb.2014.04.002

Ioannou, M. S., Jackson, J., Sheu, S. H., Chang, C. L., Weigel, A. V., Liu, H., et al. (2019). Neuron-astrocyte metabolic coupling protects against activity-induced fatty acid toxicity. *Cell* 177, 1522–1535.e14. doi: 10.1016/j.cell.2019.04.001

Jankovic, J., and Tan, E. K. (2020). Parkinson's disease: Etiopathogenesis and treatment. *J. Neurol. Neurosurg. Psychiatry* 91, 795–808. doi: 10.1136/jnnp-2019-322338

Kawahata, I., and Fukunaga, K. (2022). Impact of fatty acid-binding proteins and dopamine receptors on α-synucleinopathy. *J. Pharmacol. Sci.* 148, 248–254. doi: 10.1016/j.jphs.2021.12.003

Kawahata, I., Bousset, L., Melki, R., and Fukunaga, K. (2019). Fatty acid-binding protein 3 is critical for α-synuclein uptake and MPP(+)-induced mitochondrial dysfunction in cultured dopaminergic neurons. *Int. J. Mol. Sci.* 20:5358. doi: 10.3390/ijms20215358

Klemann, C., Martens, G. J. M., Sharma, M., Martens, M. B., Isacson, O., Gasser, T., et al. (2017). Integrated molecular landscape of Parkinson's disease. *NPJ Parkinsons Dis.* 3:14. doi: 10.1038/s41531-017-0015-3

Komlos, D., Mann, K. D., Zhuo, Y., Ricupero, C. L., Hart, R. P., Liu, A. Y., et al. (2013). Glutamate dehydrogenase 1 and SIRT4 regulate glial development. *Glia* 61, 394–408. doi: 10.1002/glia.22442

Kristensen, A. R., Gsponer, J., and Foster, L. J. (2013). Protein synthesis rate is the predominant regulator of protein expression during differentiation. *Mol. Syst. Biol.* 9:689. doi: 10.1038/msb.2013.47

Laurent, G., German, N. J., Saha, A. K., de Boer, V. C., Davies, M., Koves, T. R., et al. (2013). SIRT4 coordinates the balance between lipid synthesis and catabolism by repressing malonyl CoA decarboxylase. *Mol. Cell* 50, 686–698. doi: 10.1016/j.molcel.2013.05.012

Lautrup, S., Sinclair, D. A., Mattson, M. P., and Fang, E. F. (2019). NAD(+) in brain aging and neurodegenerative disorders. *Cell Metab.* 30, 630–655. doi: 10.1016/j.cmet.2019.09.001

Lavu, S., Boss, O., Elliott, P. J., and Lambert, P. D. (2008). Sirtuins–novel therapeutic targets to treat age-associated diseases. *Nat. Rev. Drug Discov.* 7, 841–853. doi: 10.1038/nrd2665

Li, B., Hao, J., Zeng, J., and Sauter, E. R. (2020). SnapShot: FABP functions. *Cell* 182, 1066–1066.e1. doi: 10.1016/j.cell.2020.07.027

Li, S., and Zheng, W. (2018). Mammalian sirtuins SIRT4 and SIRT7. *Prog. Mol. Biol. Transl. Sci.* 154, 147–168. doi: 10.1016/bs.pmbts.2017.11.001

Li, Y., Zhou, Y., Wang, F., Chen, X., Wang, C., Wang, J., et al. (2018). SIRT4 is the last puzzle of mitochondrial sirtuins. *Bioorg. Med. Chem.* 26, 3861–3865. doi: 10.1016/j.bmc.2018.07.031

Liu, L., Peritore, C., Ginsberg, J., Kayhan, M., and Donmez, G. (2015). SIRT3 attenuates MPTP-induced nigrostriatal degeneration via enhancing mitochondrial antioxidant capacity. *Neurochem. Res.* 40, 600–608. doi: 10.1007/s11064-014-1507-8

Liu, Y., Beyer, A., and Aebersold, R. (2016). On the Dependency of cellular protein levels on mRNA abundance. *Cell* 165, 535–550. doi: 10.1016/j.cell.2016.03.014

Lofrumento, D. D., Nicolardi, G., Cianciulli, A., De Nuccio, F., La Pesa, V., Carofiglio, V., et al. (2014). Neuroprotective effects of resveratrol in an MPTP mouse model of Parkinson's-like disease: Possible role of SOCS-1 in reducing pro-inflammatory responses. *Innate Immun.* 20, 249–260. doi: 10.1177/1753425913488429

Luo, Y. X., Tang, X., An, X. Z., Xie, X. M., Chen, X. F., Zhao, X., et al. (2017). SIRT4 accelerates Ang II-induced pathological cardiac hypertrophy by inhibiting manganese superoxide dismutase activity. *Eur. Heart J.* 38, 1389–1398. doi: 10.1093/eurheartj/ehw138

Mann, M., and Jensen, O. N. (2003). Proteomic analysis of post-translational modifications. *Nat. Biotechnol.* 21, 255–261. doi: 10.1038/nbt0303-255

Marin, C., Langdon, C., Alobid, I., Fuentes, M., Bonastre, M., and Mullol, J. (2019). Recovery of olfactory function after excitotoxic lesion of the olfactory

bulbs is associated with increases in bulbar SIRT1 and SIRT4 expressions. *Mol. Neurobiol.* 56, 5643–5653. doi: 10.1007/s12035-019-1472-y

Martin, I., Kim, J. W., Lee, B. D., Kang, H. C., Xu, J. C., Jia, H., et al. (2014). Ribosomal protein s15 phosphorylation mediates LRRK2 neurodegeneration in Parkinson's disease. *Cell* 157, 472–485. doi: 10.1016/j.cell.2014.01.064

Matsuo, K., Cheng, A., Yabuki, Y., Takahata, I., Miyachi, H., and Fukunaga, K. (2019). Inhibition of MPTP-induced α-synuclein oligomerization by fatty acid-binding protein 3 ligand in MPTP-treated mice. *Neuropharmacology* 150, 164–174. doi: 10.1016/j.neuropharm.2019.03.029

Michel, P. P., Hirsch, E. C., and Hunot, S. (2016). Understanding dopaminergic cell death pathways in Parkinson disease. *Neuron* 90, 675–691. doi: 10.1016/j.neuron.2016.03.038

Montaigne, D., Butruille, L., and Staels, B. (2021). PPAR control of metabolism and cardiovascular functions. *Nat. Rev. Cardiol.* 18, 809–823. doi: 10.1038/s41569-021-00569-6

Moulder, R., Bhosale, S. D., Goodlett, D. R., and Lahesmaa, R. (2018). Analysis of the plasma proteome using iTRAQ and TMT-based Isobaric labeling. *Mass Spectrom. Rev.* 37, 583–606. doi: 10.1002/mas.21550

Naiman, S., Huynh, F. K., Gil, R., Glick, Y., Shahar, Y., Touitou, N., et al. (2019). SIRT6 Promotes Hepatic Beta-Oxidation via Activation of PPARα. *Cell Rep.* 29, 4127–4143.e8. doi: 10.1016/j.celrep.2019.11.067

Outeiro, T. F., Kontopoulos, E., Altmann, S. M., Kufareva, I., Strathearn, K. E., Amore, A. M., et al. (2007). Sirtuin 2 inhibitors rescue alpha-synuclein-mediated toxicity in models of Parkinson's disease. *Science* 317, 516–519. doi: 10.1126/science.1143780

Park, J. H., Burgess, J. D., Faroqi, A. H., DeMeo, N. N., Fiesel, F. C., Springer, W., et al. (2020). Alpha-synuclein-induced mitochondrial dysfunction is mediated via a sirtuin 3-dependent pathway. *Mol. Neurodegener.* 15:5. doi: 10.1186/s13024-019-0349-x

Peeters, W., de Kleijn, D. P., Vink, A., van de Weg, S., Schoneveld, A. H., Sze, S. K., et al. (2011). Adipocyte fatty acid binding protein in atherosclerotic plaques is associated with local vulnerability and is predictive for the occurrence of adverse cardiovascular events. *Eur. Heart J.* 32, 1758–1768. doi: 10.1093/eurheartj/ehq387

Planavila, A., Iglesias, R., Giralt, M., and Villarroya, F. (2011). Sirt1 acts in association with PPARα to protect the heart from hypertrophy, metabolic dysregulation, and inflammation. *Cardiovasc. Res.* 90, 276–284. doi: 10.1093/cvr/cvq376

Poewe, W., Seppi, K., Tanner, C. M., Halliday, G. M., Brundin, P., Volkmann, J., et al. (2017). Parkinson disease. *Nat. Rev. Dis. Primers* 3:17013. doi: 10.1038/nrdp.2017.13

Prentice, K. J., Saksi, J., Robertson, L. T., Lee, G. Y., Inouye, K. E., Eguchi, K., et al. (2021). A hormone complex of FABP4 and nucleoside kinases regulates islet function. *Nature* 600, 720–726. doi: 10.1038/s41586-021-04137-3

Quinn, L. P., Crook, B., Hows, M. E., Vidgeon-Hart, M., Chapman, H., Upton, N., et al. (2008). The PPARgamma agonist pioglitazone is effective in the MPTP mouse model of Parkinson's disease through inhibition of monoamine oxidase B. *Br. J. Pharmacol.* 154, 226–233. doi: 10.1038/bjp.2008.78

Ron, I., Lerner, R. K., Rathaus, M., Livne, R., Ron, S., Barhod, E., et al. (2021). The adipokine FABP4 is a key regulator of neonatal glucose homeostasis. *JCI Insight* 6:e138288. doi: 10.1172/jci.insight.138288

Rose, G., Santoro, A., and Salvioli, S. (2017). Mitochondria and mitochondria-induced signalling molecules as longevity determinants. *Mech. Ageing Dev.* 165(Pt B), 115–128. doi: 10.1016/j.mad.2016.12.002

Ryan, C. J., Cimermančič, P., Szpiech, Z. A., Sali, A., Hernandez, R. D., and Krogan, N. J. (2013). High-resolution network biology: Connecting sequence with function. *Nat. Rev. Genet.* 14, 865–879. doi: 10.1038/nrg3574

Schwanhäusser, B., Busse, D., Li, N., Dittmar, G., Schuchhardt, J., Wolf, J., et al. (2011). Global quantification of mammalian gene expression control. *Nature* 473, 337–342. doi: 10.1038/nature10098

Shih, J., Liu, L., Mason, A., Higashimori, H., and Donmez, G. (2014). Loss of SIRT4 decreases GLT-1-dependent glutamate uptake and increases sensitivity to kainic acid. *J. Neurochem.* 131, 573–581. doi: 10.1111/jnc.12942

Sinclair, E., Trivedi, D. K., Sarkar, D., Walton-Doyle, C., Milne, J., Kunath, T., et al. (2021). Metabolomics of sebum reveals lipid dysregulation in Parkinson's disease. *Nat. Commun.* 12:1592. doi: 10.1038/s41467-021-21669-4

Singh, A. P., Ramana, G., Bajaj, T., Singh, V., Dwivedi, S., Behari, M., et al. (2019). Elevated serum SIRT 2 may differentiate Parkinson's disease from atypical parkinsonian syndromes. *Front. Mol. Neurosci.* 12:129. doi: 10.3389/fnmol.2019.00129

Singh, C. K., Chhabra, G., Ndiaye, M. A., Garcia-Peterson, L. M., Mack, N. J., and Ahmad, N. (2018). The role of sirtuins in antioxidant and redox signaling. *Antioxid. Redox Signal.* 28, 643–661. doi: 10.1089/ars.2017.7290

So, S. W., Fleming, K. M., Duffy, C. M., Nixon, J. P., Bernlohr, D. A., and Butterick, T. A. (2022). Microglial FABP4-UCP2 axis modulates neuroinflammation and cognitive decline in obese mice. *Int. J. Mol. Sci.* 23:4354. doi: 10.3390/ijms23084354

Tang, B. L. (2017). Sirtuins as modifiers of Parkinson's disease pathology. *J. Neurosci. Res.* 95, 930–942. doi: 10.1002/jnr.23806

van de Ven, R. A. H., Santos, D., and Haigis, M. C. (2017). Mitochondrial sirtuins and molecular mechanisms of aging. *Trends Mol. Med.* 23, 320–331. doi: 10.1016/j.molmed.2017.02.005

van Maarschalkerweerd, A., Vetri, V., and Vestergaard, B. (2015). Cholesterol facilitates interactions between α-synuclein oligomers and charge-neutral membranes. *FEBS Lett.* 589(19 Pt B), 2661–2667. doi: 10.1016/j.febslet.2015.08.013

Wang, X. W., Sun, Y. J., Chen, X., and Zhang, W. Z. (2022). Interleukin-4-induced FABP4 promotes lipogenesis in human skeletal muscle cells by activating the PPAR γ signaling pathway. *Cell Biochem. Biophys.* 80, 355–366. doi: 10.1007/s12013-022-01063-7

Wang, Y. S., Du, L., Liang, X., Meng, P., Bi, L., Wang, Y. L., et al. (2019). Sirtuin 4 depletion promotes hepatocellular carcinoma tumorigenesis through regulating adenosine-monophosphate-activated protein kinase alpha/mammalian target of rapamycin axis in mice. *Hepatology* 69, 1614–1631. doi: 10.1002/hep.30421

Xiong, X., Zhang, C., Zhang, Y., Fan, R., Qian, X., and Dong, X. C. (2017). Fabp4-Cre-mediated Sirt6 deletion impairs adipose tissue function and metabolic homeostasis in mice. *J. Endocrinol.* 233, 307–314. doi: 10.1530/joe-17-0033

Xu, Y., Wang, Q., Chen, J., Ma, Y., and Liu, X. (2020). Updating a strategy for histone deacetylases and its inhibitors in the potential treatment of cerebral ischemic stroke. *Dis Markers* 2020:8820803. doi: 10.1155/2020/8820803

Yalçın, G. D., and Colak, M. (2020). SIRT4 prevents excitotoxicity via modulating glutamate metabolism in glioma cells. *Hum. Exp. Toxicol.* 39, 938–947. doi: 10.1177/0960327120907142

Yeong, K. Y., Berdigaliyev, N., and Chang, Y. (2020). Sirtuins and their implications in neurodegenerative diseases from a drug discovery perspective. *ACS Chem. Neurosci.* 11, 4073–4091. doi: 10.1021/acschemneuro.0c00696

Yin, J., Ibrahim, S., Petersen, F., and Yu, X. (2021). Autoimmunomic signatures of aging and age-related neurodegenerative diseases are associated with brain function and ribosomal proteins. *Front. Aging Neurosci.* 13:679688. doi: 10.3389/fnagi.2021.679688

Zhuge, W., Wen, F., Ni, Z., Zheng, Z., Zhu, X., Lin, J., et al. (2019). Dopamine burden triggers cholesterol overload following disruption of synaptogenesis in minimal hepatic encephalopathy. *Neuroscience* 410, 1–15. doi: 10.1016/j.neuroscience.2019.04.056

Zolezzi, J. M., Santos, M. J., Bastías-Candia, S., Pinto, C., Godoy, J. A., and Inestrosa, N. C. (2017). PPARs in the central nervous system: Roles in neurodegeneration and neuroinflammation. *Biol. Rev. Camb. Philos. Soc.* 92, 2046–2069. doi: 10.1111/brv.12320

frontiers | Frontiers in Aging Neuroscience

TYPE Original Research
PUBLISHED 10 February 2023
DOI 10.3389/fnagi.2023.1106497

Check for updates

OPEN ACCESS

EDITED BY
Shenfeng Qiu,
University of Arizona, United States

REVIEWED BY
Paul Roy Heath,
The University of Sheffield, United Kingdom
Hongwei Yang,
UMass Chan Medical School, United States
Dejun Yang,
Xuzhou Medical University, China

*CORRESPONDENCE
Hui-Fang Shang
✉ hfshang2002@126.com
Yong-Ping Chen
✉ yongping.chen@wchscu.cn

SPECIALTY SECTION
This article was submitted to
Cellular and Molecular Mechanisms
of Brain-aging,
a section of the journal
Frontiers in Aging Neuroscience

RECEIVED 23 November 2022
ACCEPTED 09 January 2023
PUBLISHED 10 February 2023

CITATION
Cheng Y-F, Gu X-J, Yang T-M, Wei Q-Q, Cao B, Zhang Y, Shang H-F and Chen Y-P (2023) Signature of miRNAs derived from the circulating exosomes of patients with amyotrophic lateral sclerosis.
Front. Aging Neurosci. 15:1106497.
doi: 10.3389/fnagi.2023.1106497

COPYRIGHT
© 2023 Cheng, Gu, Yang, Wei, Cao, Zhang, Shang and Chen. This is an open-access article distributed under the terms of the Creative Commons Attribution License (CC BY). The use, distribution or reproduction in other forums is permitted, provided the original author(s) and the copyright owner(s) are credited and that the original publication in this journal is cited, in accordance with accepted academic practice. No use, distribution or reproduction is permitted which does not comply with these terms.

Signature of miRNAs derived from the circulating exosomes of patients with amyotrophic lateral sclerosis

Yang-Fan Cheng[1,2], Xiao-Jing Gu[1,2], Tian-Mi Yang[1], Qian-Qian Wei[1], Bei Cao[1], Yang Zhang[3], Hui-Fang Shang[1,2]* and Yong-Ping Chen[1,2]*

[1]Department of Neurology, Laboratory of Neurodegenerative Disorders, Rare Disease Center, West China Hospital, Sichuan University, Chengdu, China, [2]Laboratory of Neurodegenerative Disorders, National Clinical Research Center for Geriatric, West China Hospital, Sichuan University, Chengdu, China, [3]West China School of Medicine, West China Hospital, Sichuan University, Chengdu, China

Background: Amyotrophic lateral sclerosis (ALS) is a progressive, fatal neurodegenerative disorder (NDS) with unclear pathophysiology and few therapeutic options. Mutations in *SOD1* and *C9orf72* are the most common in Asian and Caucasian patients with ALS, respectively. Aberrant (microRNAs) miRNAs found in patients with gene-mutated ALS may be involved in the pathogenesis of gene-specific ALS and sporadic ALS (SALS). The aim of this study was to screen for differentially expressed miRNAs from exosomes in patients with ALS and healthy controls (HCs) and to construct a miRNA-based diagnostic model to classify patients and HCs.

Methods: We compared circulating exosome-derived miRNAs of patients with ALS and HCs using the following two cohorts: a discovery cohort (three patients with *SOD1*-mutated ALS, three patients with *C9orf72*-mutated ALS, and three HCs) analyzed by microarray and a validation cohort (16 patients with gene-mutated ALS, 65 patients with SALS, and 61 HCs) confirmed by RT-qPCR. The support vector machine (SVM) model was used to help diagnose ALS using five differentially expressed miRNAs between SALS and HCs.

Results: A total of 64 differentially expressed miRNAs in patients with *SOD1*-mutated ALS and 128 differentially expressed miRNAs in patients with *C9orf72*-mutated ALS were obtained by microarray compared to HCs. Of these, 11 overlapping dysregulated miRNAs were identified in both groups. Among the 14 top-hit candidate miRNAs validated by RT-qPCR, hsa-miR-34a-3p was specifically downregulated in patients with *SOD1*-mutated ALS, while hsa-miR-1306-3p was downregulated in ALS patients with both *SOD1* and *C9orf72* mutations. In addition, hsa-miR-199a-3p and hsa-miR-30b-5p were upregulated significantly in patients with SALS, while hsa-miR-501-3p, hsa-miR-103a-2-5p, and hsa-miR-181d-5p had a trend to be upregulated. The SVM diagnostic model used five miRNAs as features to distinguish ALS from HCs in our cohort with an area under receiver operating characteristic curve (AUC) of 0.80.

Conclusion: Our study identified aberrant miRNAs from exosomes of SALS and ALS patients with *SOD1*/*C9orf72* mutations and provided additional evidence that aberrant miRNAs were involved in the pathogenesis of ALS regardless of the presence or absence of the gene mutation. The machine learning algorithm had high accuracy

in predicting the diagnosis of ALS, shedding light on the foundation for the clinical application of blood tests in the diagnosis of ALS, and revealing the pathological mechanisms of the disease.

KEYWORDS

amyotrophic lateral sclerosis, microRNAs, exosomes, gene mutation, diagnostic model

Introduction

Amyotrophic lateral sclerosis (ALS) is a fatal, neurodegenerative disease (NDS) characterized by selective loss of upper and lower motor neurons (Cleveland and Rothstein, 2001). This degeneration of neurons manifests clinically with insidious focal weakness that spreads to most skeletal muscles, eventually to the diaphragm, leading to death in most of those diagnosed 2–5 years after the onset of symptoms due to respiratory dysfunction (Kiernan et al., 2011). The cause of most patients with ALS is unknown, although 5–10% of them have familial forms and some of them are associated with mutated genes, such as *C9orf72*, *SOD1*, *TARDBP*, and *FUS* (Brown and Al-Chalabi, 2017). Pathologically, a specific mechanism for neurodegeneration in patients with gene mutation might differ from that in those with sporadic ALS (SALS) mainly in the initial stage, but the shared pathological alteration might also be seen, especially in the advanced stage. Clinically, the dilemma for clinical doctors is the delay from the onset to diagnosis owing to the huge heterogeneous clinical presentation (Paganoni et al., 2014). Thus, identification of clinically and mechanically relevant different or shared biomarkers, hidden in patients with or without gene mutation, will benefit unearthing the pathogenesis of ALS, and early and efficiently diagnosing the various forms of ALS.

Exosomes, also known as intraluminal vesicles, are a subpopulation of extracellular vesicles with a 30–150-nm diameter derived from multi-vesicular bodies that transmit cellular molecular constituents to promote intercellular communication (Cheng et al., 2014). It could be secreted by nearly all types of cells that cross the blood–brain barrier and enter the circulatory system. Transactive response DNA-binding protein 43 kD (*TDP-43*), a major disease-associated component in the brain of patients with ALS, was reported in the presence of cellular exosomes (Feiler et al., 2015). Basso et al. (2013) found that superoxide dismutase 1, encoded by *SOD1*, which is the most common causative gene in the Chinese patients (Chen et al., 2021), could be transferred from astrocyte-derived exosomes to spinal neurons, inducing selective motor neuron death (Basso et al., 2013). Moreover, Westergard et al. (2016) found evidence for cell-to-cell spreading of dipeptide repeat proteins (DRPs) produced by pathologic *C9orf72* hexanucleotide repeat expansions (HREs) *via* exosome-dependent in the spinal motor neurons derived from induced pluripotent stem cells from patients with ALS. These studies supported a prion-like cell-to-cell diffusion mechanism in ALS that was possibly mediated by exosomes.

More importantly, non-coding RNAs (ncRNAs) are among the most abundant contents in exosomes, which exist stably and can be tested easily (Valadi et al., 2007; Tang et al., 2021). Among them, microRNAs (miRNAs) are small single-stranded RNA genes (18–25 nucleotides) that are involved in the host cells by targeting mRNAs for cleavage or post-transcriptional gene regulation (Bartel, 2004). Many studies found that miRNA participated in nervous system development (Åkerblom et al., 2012; Zhu et al., 2013) and dysregulation of miRNA had been shown to influence the pathogenesis of neurological diseases (Feng et al., 2018; Pan et al., 2021). Our previous studies have also reported aberrant miRNAs in leukocytes from SALS (Chen et al., 2016), among which miR-183-5p (Li C. et al., 2020) and miR-193b-3p (Li et al., 2017) were involved in the neurodegeneration by functional investigations. Although the identified miRNAs in leukocytes or from plasma/serum practical significance for ALS diagnosis, it is difficult to explain the degeneration of the selected motor neuron due to the lack of the targeted from exosomes membrane receptors (Gonda et al., 2019). Thus, whether miRNAs derived from exosomes of patients with ALS are aberrant and how they might participate in the pathogenesis of ALS is yet unclear.

In this study, we sought to: (1) identify aberrant miRNAs from circulating exosomes of *SOD1*-ALS, *C9orf72*-ALS, and SALS by microarray screening and RT-qPCR validation; (2) construct a support vector machine (SVM) model by using differentially expressed miRNAs between SALS and HCs to help diagnose ALS; and (3) perform functional analysis of predicted gene targets of aberrant miRNAs to find potential pathophysiological pathways.

Materials and methods

Subject

The recruitment of patients and healthy controls (HCs) was conducted at the Department of Neurology, West China Hospital of Sichuan University, from August 2017 to August 2019. All the patients with ALS were diagnosed based on the revised El Escorial criteria for definite or probable ALS (Brooks et al., 2000) by board-certified neurologists. HCs were typically spouses and friends. They were also evaluated by experienced neurologists, and routine blood tests were carried out to eliminate neurological conditions. Demographic characteristics, clinical information, and blood samples were collected from all participants at baseline. Disease severity was

Abbreviations: AD, Alzheimer's disease; ALS, amyotrophic lateral sclerosis; ALSFRS-R, amyotrophic lateral sclerosis functional rating scale-revised; AUC, areas under receiver operating characteristic curve; DE, differential expressed; EDTA, ethylene diamine tetra acetic acid; fALS, familial amyotrophic lateral sclerosis; GO, Gene Ontology; KEGG, Kyoto Encyclopedia of Genes and Genomes; HCs, healthy controls; HF, heart failure; miRNA, microRNA; NDS, neurodegenerative disease; RT-qPCR, quantitative reverse transcription polymerase chain reaction; SALS, sporadic amyotrophic lateral sclerosis; SD, standard deviation; SVM, support vector machine; SEM, standard error of mean; TDP-43, transactive response DNA-binding protein 43 kD; UTR, untranslated region.

assessed with the Revised ALS Functional Rating Scale (ALSFRS-R), and disease progression was calculated as (48-ALSFRSR)/disease duration (months) (Kimura et al., 2006). Besides, all the patients with ALS received a genetic test (Chen et al., 2021). Written and signed informed consent was obtained from all the participants. Approval was obtained from the Ethics Committee of the West China Hospital of Sichuan University (approval number 2016-097).

Sample collection, study design, and microarray

Whole human peripheral blood, collected in sterile vacutainer tubes containing the anticoagulant ethylenediaminetetraacetic acid (EDTA), was centrifuged at 2,000 rpm for 10 min at 4°C within 2 h after collection. Plasma fractions were subsequently collected, aliquoted, and stored at −80°C. To avoid the interference of hemolysis, plasma samples were examined for hemolysis based on a two-step method. First, absorbance was measured at 414 nm by using a spectrophotometer (Thermo Fisher Scientific Nanodrop), and samples with results lower than 0.3 were selected for the next step. Second, plasma samples were further tested for expression levels of two miRNAs, namely, miR-451 and miR-23a. A ratio between two miRNAs calculated as delta Ct (miRNA-23a-3p–miRNA-451) was used as a hemolysis indicator. A ratio of more than seven indicates a high risk of hemolysis. For both $\text{absorbance}_{414nm} < 0.3$ and delta Ct < 7, the plasma sample could be extracted from the exosomes (Blondal et al., 2013).

The schematic diagram of the study design is shown in **Figure 1**. In the initial screening phase, we selected three patients with *SOD1*-mutated ALS, three patients with *C9orf72*-mutated ALS (HREs > 30 in *C9orf72*, Dekker et al., 2016; Chen et al., 2021), and three HCs. Although microarray was based on a small number of samples, it also allowed us to explore the miRNAs of patients with ALS, compare them to HCs, then select an interesting subset of miRNAs for further study, and perform real-time PCR validation. Total RNA extracted from exosomes originating from plasma (1 ml) was labeled with the Flashtag™ Biotin HSR RNA labeling kit (Thermo Fisher Scientific) following the manufacturer's instructions. Labeled RNA was hybridized at 48°C for 16 h at 60 rpm on an Affymetrix GeneChip™ human miRNA 4.0 array (Thermo Fisher Scientific), which contains 2,578 human mature miRNA probe sets and 2,025 human pre-miRNA (stem-loop) probe sets. GeneChips were scanned using the Affymetrix GeneChip scanner G3000 7G with the standard setting to capture signal intensities for the miRNAs. The raw intensity data were imported into the Affymetrix Expression Console software (version 1.4.1.46) for signal pre-processing, including background correction utilizing the robust multi-array average algorithm, median polish summarization from probe-to-probe set level of signal values, and the quantile method to normalize across multiple arrays. A detection call on the strength of miRNA signal was made using the Affymetrix "Detection Above Background" algorithm, which generates a *p*-value for the signal above background probability (Zheng et al., 2021). The normalized $\log_2$ intensity values were analyzed for differential expression between different time points using the R software "limma" package, which uses a moderated *t*-test with linear modeling and empirical Bayes statistics (Ritchie et al., 2015). The significance for differential expression was set at (absolute $\log_2$ fold-change) ≥ 1.2 and adjusted $p < 0.05$. In the validation phase, the selected miRNAs were further validated with 8 patients with *SOD1*-mutated ALS, 8 patients with *C9orf72*-mutated ALS, and 61 HCs. Meanwhile, 65 patients with SALS were also recruited to validate whether miRNAs, which were differentially expressed between ALS patients with *SOD1*/*C9orf72* mutations and HCs, had alteration in SALS. The selected differential expression of miRNA was based on the following conditions: (1) highly expressed in brain tissue relative to other tissues; (2) predicted target genes of miRNA included *TARDBP*, *SOD1*, *C9orf72*, *FUS*, *SQSTM1* (p62), *UBQLN2*, or neurofilament protein; (3) combined with bioinformatics functional prediction, online miRNA database, and pathophysiological characteristics of ALS; and (4) differentially expressed in the ALS group with absolute $\log_2$ fold-change ≥ 1.2 and adjusted *p*-value of < 0.05.

miRNA isolation from exosomes, reverse transcription to cDNA, and quantitative RT-qPCR validation

Exosomes from frozen plasma (1 ml) were extracted by the exoRNeasy Midi Kit (Qiagen) according to the manufacturer's instructions after thawing on ice and centrifuging at 13,000 rpm for 1 min to get rid of cellular debris. *Caenorhabditis elegans* miR-39 (cel-miR-39) synthetic oligonucleotide RNA (miRNeasy Serum/Plasma Spike-In Control) was used as an exogenous control (Aday et al., 2021), which was added to the plasma after the addition of a denaturing solution. The concentration of miRNA was measured using NanoDrop One (Thermo Fisher Scientific). For cDNA synthesis, 10 ng of total RNA was reverse-calculated from the concentration and was reverse-transcribed in a 10-μl reaction using the miRCURY LNA miRNA PCR Starter Kit (Qiagen). A miRCURY LNA SYBR® Green PCR Kit (Qiagen) and miScript Primer Assays (Qiagen) were used on the Applied Biosystems® StepOnePlus RT-qPCR system to quantify the miRNAs in exosomes. According to the abovementioned selected condition, 14 candidate miRNAs (**Figure 1**), including two *SOD1*-ALS exclusively (hsa-miR-3928-3p and hsa-miR-340-5p), three *C9Orf72*-ALS exclusively (hsa-miR-199a-3p, hsa-miR-30b-5p, and hsa-miR-485-5p), and nine overlapped in *SOD1* and *C9orf72*-ALS (hsa-miR-1915-3p, hsa-miR-181d-5p, hsa-miR-4729, hsa-miR-4455, hsa-miR-34a-3p, hsa-miR-1306-3p, hsa-miR-6824-5p, hsa-miR-501-3p, and hsa-miR-103a-2-5p), were amplificated using Qiagen miScript primers. Hsa-miR-16-5p was used as an endogenous control because it showed minimum variance and approximation value between patients and HCs according to miRNA microarray analysis and previous studies (Lange et al., 2017; Bohatá et al., 2021). Run in triplicate and comparative quantification was used to determine the relative quantities of miRNA from hsa-miR-16-5p and cel-miR-39-3p.

Prediction of miRNA target genes, functional analysis, and preliminary validation

The prediction of miRNA target genes/sites was carried out by three different miRNA online databases, including

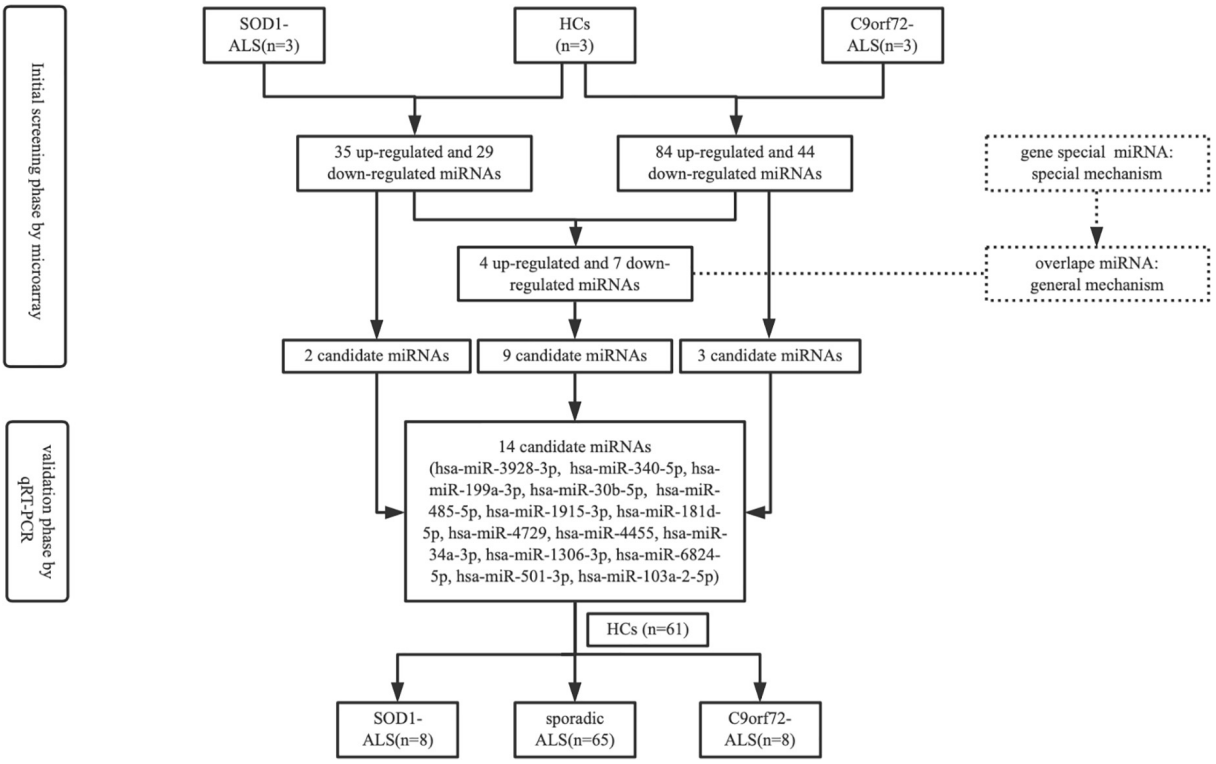

FIGURE 1
Schematic diagram illustrating the study design.

TargetScanHuman 7.2[1] (Agarwal et al., 2015), Diana Tools[2], (Vlachos et al., 2015), and miRND[3] (Chen and Wang, 2020). The expression of miRNA in human tissue refers to the YM500v2 database[4] (Cheng W. C. et al., 2015). Venn diagrams were calculated and drawn by an online website[5]. Gene ontology (GO) analyses, which consisted of cellular components, molecular function, biological process, and Kyoto Encyclopedia of Genes and Genomes (KEGG) analyses, were conducted by DAVID Bioinformatics Resources version 6.8[6] (Huang da et al., 2009a,b). Dot plots were drawn by the online tool bioinformatics[7]. A double fluorescent enzyme reporter assay was used to verify the binding between miRNA and the 3′UTR of the targeted gene.

Statistical analysis and modeling

Statistical analysis for RT-qPCR was conducted on $2^{-\Delta\Delta Ct}$ values ($\Delta Ct = Ct_{miRNA} - 0.5 * [Ct_{miR-16} + Ct_{cel-miR-39}]$) for each sample with GraphPad Prism version 6.0 and SPSS version 24. The continuous variable was presented as mean ± standard error of the mean (SEM). Outliers were identified using the ROUT method in GraphPad Prism version 6.0 (Q1/41%). The distribution of the data was determined using the D'Agostino–Pearson test and the Kolmogorov–Smirnov test. To compare the two groups of continuous variables, a two-sample *t*-test or Welch's *t*-test was used when the data were in accordance with normal distribution, while the Mann–Whitney *U*-test was used. Correlations were analyzed using Pearson's and Spearman's rank correlation tests if the data were parametric and non-parametric, respectively. All statistics were two-tailed, and significance was set at $p < 0.05$.

The prediction model of ALS diagnosis was carried out by R environment (version 3.6.3). Standardized data were established for the machine learning-based SVM model by using the R package e1071. Patients were classified into a training cohort and a validation cohort in a ratio of 4:1. Approximately, 20% of the datasets were used to validate the predictive model created by the other 80% of the datasets. To obtain the average diagnostic performance, 5-fold cross-validation was used. Then, we created a confusion matrix that showed the results of the prediction of models to get the mean sensitivity, specificity, accuracy, and areas under the receiver operating characteristic curve (AUCs) of each model, which could be used to evaluate the efficacy of the diagnostic model.

1 www.targetscan.org/vert_72/
2 https://dianalab.e-ce.uth.gr/html/diana/web/index.php?r=tarbasev8
3 www.mirdb.org
4 ngs.ym.edu.tw/ym500v2/index.php
5 bioinformatics.psb.ugent.be/webtools/Venn/
6 https://david.ncifcrf.gov/home.jsp
7 www.bioinformatics.com.cn

Results

Clinical characteristics

A total of 65 patients with SALS, 22 ALS patients with *SOD1/C9orf72* mutations, and 64 HCs participated in this study, of

which 3 patients with *SOD1*-mutated ALS, 3 patients with *C9orf72*-mutated ALS, and 3 HCs were in the initial screening phase and 8 patients with *SOD1*-mutated ALS, 8 patients with *C9orf72*-mutated ALS, 65 patients with SALS, and 61 HCs were in the validation stage. Demographic characteristics and clinical information are shown in Table 1. Genetic data for ALS patients with *SOD1/C9orf72* mutations are detailed in Supplementary Table 1.

In the validation group, gender and age were not statistically significant in patients with SALS and *SOD1*-mutated ALS compared to HCs. Regarding disease duration, no statistical significance was shown in patients with SALS, *SOD1*-mutated ALS, and *C9orf72*-mutated ALS. However, the mean age of onset was much higher in the *C9orf72*-mutated group than in the *SOD1*-mutated group ($p = 0.027$).

Differential expression of miRNAs from exosomes by using microarray

Exosomes were isolated from hemolysis-free plasma and characterized by transmission electron microscopy (TEM), Nanosight Tracking Analysis (NTA), and expression of the exosome surface markers (Supplementary Figure 1). Compared to HCs, we found 64 miRNAs differentially expressed in *SOD1*-mutated ALS, of which 35 were upregulated and 29 were downregulated. Meanwhile, 128 miRNAs were dysregulated in patients with *C9orf72*-mutated ALS, including 84 upregulated and 44 downregulated miRNAs, based on our cutoff values for differential expression (fold change ≥ 1.2; adjusted p-value < 0.05) (Figures 2A, B). Interestingly, 11 miRNAs, including 4 upregulated and 7 downregulated miRNAs, were differentially expressed in patients with *SOD1*-mutated ALS and *C9orf72*-mutated ALS with overlapping (Supplementary Figure 2 and Supplementary Table 2), which might indicate a common pathology involved in ALS.

Among the differentially expressed miRNAs screened by microarray, the online miRNA databases were used to predict the potential target genes and their binding sites. We focused more on those miRNAs that were predicted to bind to ALS-related genes, including *TARDBP*, *SOD1*, *C9orf72*, *FUS*, *SQSTM1 (p62)*, and *UBQLN2*. For example, hsa-miR-340-5p (*SOD1*-ALS exclusively) was combined with UTR of *SOD1* potentially as a 7mer-A1 type [an exact match to positions 2–7 of the mature miRNA (the seed) followed by an "A"], while hsa-miR-199a-3p and hsa-miR-30b-5p (two of them were *C9orf72*-ALS exclusively) were predicted to combine with the UTR of *C9orf72* as 7mer-m8 type (an exact match to positions 2–8 of the mature miRNA). In addition, hsa-miR-181d-5p (overlapped in *SOD1&C9orf72* groups) was also predicted to combine with the UTR of *TARDBP* as 7mer-m8 type. More details can be seen in Supplementary Table 3. According to the criteria of candidate miRNAs selection mentioned in the Section "Materials and methods," a total of 14 miRNAs, including two *SOD1*-ALS exclusively (hsa-miR-3928-3p and hsa-miR-340-5p), three *C9orf72*-ALS exclusively (hsa-miR-199a-3p, hsa-miR-30b-5p, and hsa-miR-485-5p), and nine overlapped both in *SOD1* and *C9orf72*-ALS (hsa-miR-1915-3p, hsa-miR-181d-5p, hsa-miR-4729, hsa-miR-4455, hsa-miR-34a-3p, hsa-miR-1306-3p, hsa-miR-6824-5p, hsa-miR-501-3p, and hsa-miR-103a-2-5p), were found to be highly expressed in the brain tissue[8] and were selected to be validated by RT-qPCR.

8 http://ngs.ym.edu.tw/ym500v2/sample.php

Differential expression of miRNAs from exosomes validated by RT-qPCR

To confirm the above-dysregulated candidate miRNAs, 8 patients with *SOD1*-mutated ALS, 8 patients with *C9orf72*-mutated ALS, and 61 HCs were recruited for validation by RT-qPCR. In addition, 65 patients with SALS were also included to verify whether these candidate miRNAs were also differentially expressed, particularly miRNAs that overlapped between *SOD1*-ALS and *C9orf72*-ALS. Only the samples that passed the hemolysis test were used (refer to Supplementary Table 4). The external and internal controls had a good stability and quality control (the mean Ct and SD of hsa-miR-16-5p: 19.85 ± 1.53; cel-miR-39-3p: 14.90 ± 1.33) (refer to Supplementary Table 4).

Hsa-miR-34a-3p was found to be specifically downregulated in patients with *SOD1*-ALS compared to patients with *C9orf72*-ALS ($p = 0.0175$), patients with SALS ($p = 0.032$), and HCs ($p = 0.0022$), while no statistical significance was found between SALS and HCs ($p = 0.151$). Interestingly, hsa-miR-1306-3p showed significant downregulation in patients with *SOD1* and *C9orf72* gene mutations, compared to patients with SALS and HCs (SALS vs. *SOD1*-ALS: $p = 0.0021$, SALS vs. *C9orf72*-ALS: $p = 0.0032$, *SOD1*-ALS vs. HCs: $p = 0.002$, *C9orf72*-ALS vs. HCs: $p = 0.0032$) and no statistical significance was found between patients with SALS and HCs ($p = 0.807$) (Figure 3A). Compared to HCs, hsa-miR-199a-3p ($p = 0.0003$) and hsa-miR-30b-5p ($p = 0.0474$) were significantly upregulated in patients with SALS (Figure 3B). Interestingly, these differences were found mainly in the male subgroup (male group: hsa-miR-199a-3p: $p = 0.0014$; hsa-miRNA-30b-5p: $p = 0.0309$) but not in the female subgroup (female group: hsa-miR-199a-3p: $p = 0.1639$; hsa-miRNA-30b-5p: $p = 0.7760$; Figure 3C). In addition, hsa-miR-501-3p ($p = 0.0533$), hsa-miR-103a-2-5p ($p = 0.0603$), and hsa-miR-181d-5p ($p = 0.0782$) were also potentially upregulated ($0.05 < p < 0.10$) in patients with SALS (Supplementary Figure 3). The comparison of these 14 candidate miRNAs by microarray and RT-qPCR can be found in Supplementary Table 5.

The correlation between miRNAs and clinical phenotype

Then, we conducted a correlation analysis of miRNA expression with the demographic and clinical characteristics of patients with ALS. We found that hsa-miR-501-3p was increased in patients with initial symptoms presenting at bulbar-onset ($p = 0.0098$) compared to the spinal cord-onset group. In more detail, compared to the lower limb-onset group, hsa-miR-501-3p was significantly increased in bulbar-onset patients with ALS ($p = 0.0027$), with no significance between the upper and lower limb-onset groups (Figure 4A). Interestingly, if we grouped patients with ALS according to the new clinical phenotype classification (Chiò et al., 2011), the expression of hsa-miR-501-3p was also increased in the bulbar phenotype in comparison with the classic (Charcot's) phenotype ($p = 0.0178$, Figure 4B). Furthermore, we found a positive correlation between the expression of hsa-miR-501-3p and the age of patients with ALS at the last assessment ($r = 0.3245$, $p = 0.0384$, simple linear regression: $Y = 18.88*X + 48.89$) and a potentially positive correlation between the expression of hsa-miR-501-3p and the age of onset in patients with ALS ($r = 0.3012$, $p = 0.0557$, simple

10.3389/fnagi.2023.1106497

TABLE 1 The demographic characteristics and clinical information of participants in this study.

Variables	Initial screening group			Validation group			
	SOD1-ALS	*C9orf72*-ALS	HCs	SALS	*SOD1*-ALS	*C9orf72*-ALS	HCs
Num.	3	3	3	65	8	8	61
Male (%)	1 (33.3%)	2 (66.7%)	1 (33.3%)	39 (60.0%)	2 (25.0%)	5 (62.5%)	34 (55.7)
Mean age (SD), years	51.0 (4.6)	51.3 (4.1)	51.6 (3.5)	51.3 (8.5)	51.8 (8.2)	59.8 (7.5)	51.4 (7.3)
Mean disease duration (SD), months	19.8 (14.2)	11.2 (7.3)	/	11.9 (6.8)	17.8 (13.9)	12.5 (5.3)	/
Mean age at onset (SD), years	49.3 (4.6)	50.4 (4.0)	/	50.3 (5.8)	50.3 (7.9)	58.8 (7.4)	/
ALSFRS-R	38.7 (4.8)	31 (7.1)	/	38.6 (7.1)	38.9 (7.5)	42.6 (3.6)	/

ALS, amyotrophic lateral sclerosis; ALSFRS-R, ALS functional rating scale revised; *C9orf72*-fALS, C9orf72-mutant familial ALS; HC, healthy control; SALS, sporadic ALS; SD, standard deviation; *SOD1*-fALS, *SOD1*-mutant familial ALS. ALSFRS-R score at the time of sample collection.

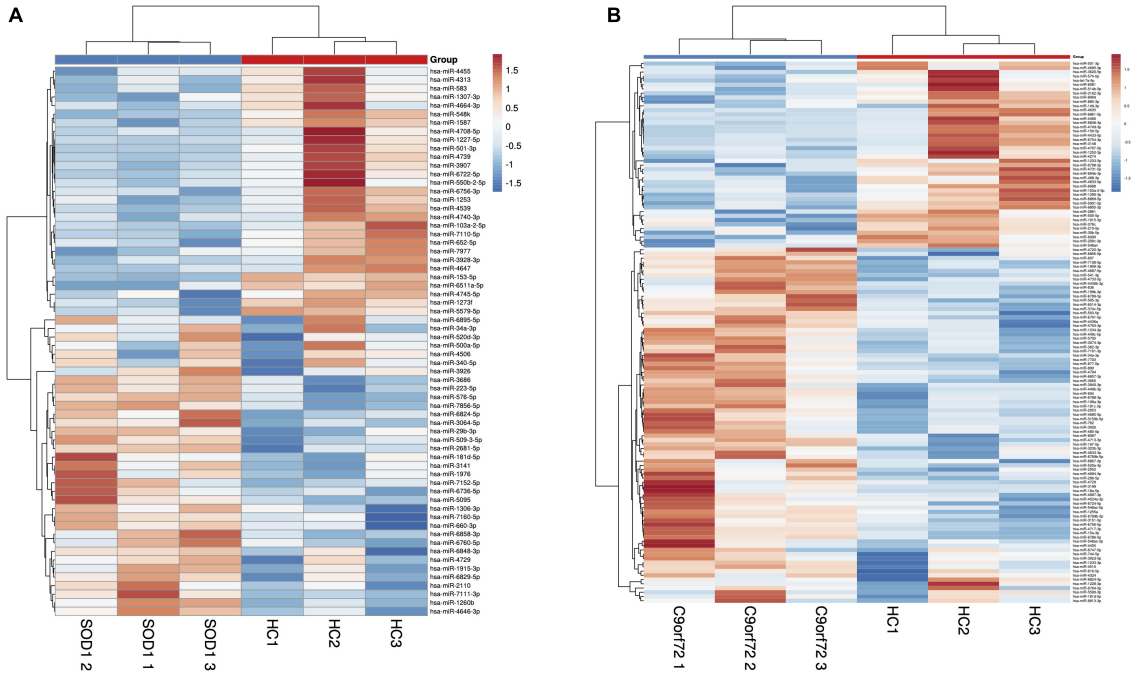

FIGURE 2
The heatmap of differentially expressed miRNAs by means of microarray. **(A)** The comparison of patients with *SOD1*-mutated amyotrophic lateral sclerosis (ALS) and healthy controls; **(B)** The comparison of patients with *C9orf72*-mutated ALS and healthy controls. Compared with HCs, we found 64 miRNAs differentially expressed in *SOD1*-mutant ALS where 35 of them were upregulated, and 29 of them were downregulated, and 128 miRNAs dysregulated including 84 upregulation and 44 downregulation in patients with *C9orf72*-mutated ALS.

linear regression: Y = 19.85*X + 47.80) (Supplementary Figure 4A). Moreover, we found the expression of hsa-miR-30b-5p, and the disease progression in patients with ALS showed a potentially positive correlation ($r = 0.2499$, $p = 0.0521$, simple linear regression: Y = 0.5408*X + 0.9906) and a potentially negative correlation between the expression of hsa-miR-30b-5p and ALSFRS scores ($r = -0.2169$,95% CI: −0.4524 to 0.04684, $p = 0.096$), although they did not reach statistical significance (Supplementary Figure 4B).

Prediction of miRNA target genes and functional analyses

To speculate on how hsa-miR-34a-3p, hsa-miR-1306-3p, hsa-miR-199a-3p, hsa-miR-30b-5p, and three potentially statistically significant miRNAs (hsa-miR-501-3p, hsa-miR-103a-2-5p, and hsa-miR-181d-5p) participate in the pathogenesis of ALS through downstream genes, we used three different online miRNA databases, namely, TargetScan, miRBD, and Tarbase, to perform the prediction and took the predicted target genes, which were the subset of at least two databases to conduct functional analysis. The predicted target genes and Venn diagrams of these seven miRNAs (hsa-miR-34a-3p, hsa-miR-1306-3p, hsa-miR-199a-3p, hsa-miR-30b-5p, hsa-miR-501-3p, hsa-miR-103a-2-5p, and hsa-miR-181d-5p) can be found in Supplementary Figure 5 and Supplementary Texts 1–7. Functional analysis, including GO and KEGG analyses of hsa-miR-34a-3p, is shown in Figure 5A. GO and KEGG analyses of six other differentially expressed miRNAs (hsa-miR-1306-3p, hsa-miR-199a-3p, hsa-miR-30b-5p, hsa-miR-501-3p, hsa-miR-103a-2-5p, and hsa-miR-181d-5p) between patients with ALS and HCs are

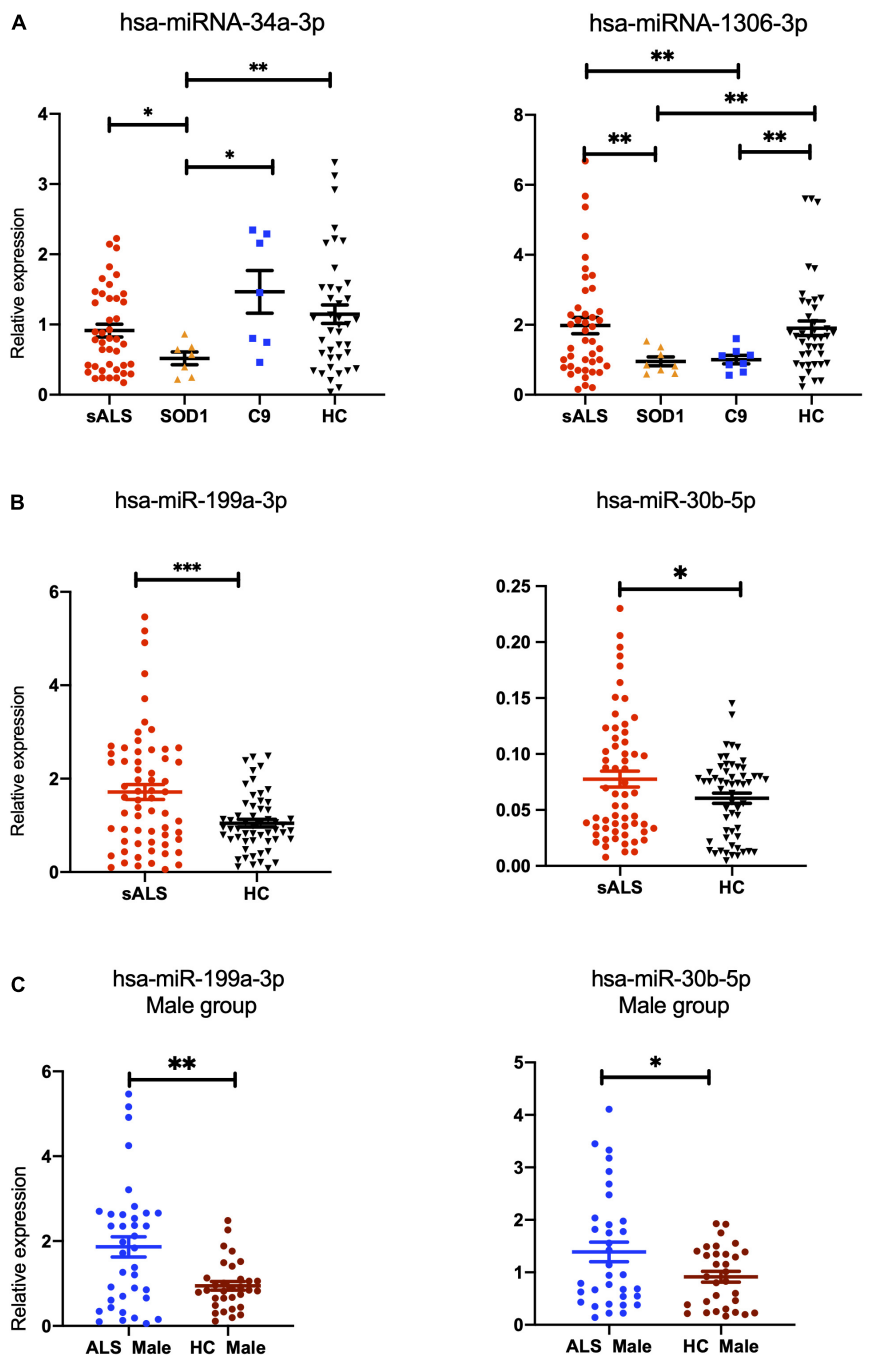

FIGURE 3
The differentially expressed miRNAs found in patients with gene-mutant and sporadic ALS compared with healthy controls validated by RT-qPCR. **(A)** hsa-miR-34a-3p was found to be specifically downregulated in patients with *SOD1*-ALS compared to patients with *C9orf72*-ALS ($p = 0.0175$), sporadic amyotrophic lateral sclerosis (SALS) ($p = 0.032$), and HCs ($p = 0.0022$), while no statistical significance was found between SALS and HCs ($p = 0.151$). Interestingly, hsa-miR-1306-3p showed significant downregulation in ALS patients with *SOD1* and *C9orf72* gene mutations, compared to SALS and HCs (SALS vs. *SOD1*-ALS: $p = 0.0021$, SALS vs. *C9orf72*-ALS: $p = 0.0032$, *SOD1*-ALS vs. HCs: $p = 0.002$, *C9orf72*-ALS vs. HCs: $p = 0.0032$) and no statistical significance was found between SALS and HCs ($p = 0.807$). **(B)** Compared to HC, hsa-miR-199a-3p ($p = 0.0003$) and hsa-miR-30b-5p ($p = 0.0474$) were found to be upregulated in patients with SALS ($p = 0.0474$). **(C)** In the subgroup analysis on gender, compared to male HCs, hsa-miR-199a-3p ($p = 0.0014$) and hsa-miR-30b-5p ($p = 0.0309$) were confirmed to be upregulated significantly in the male SALS group. HCs, health controls. $^{***}p < 0.001$, $^{**}p < 0.01$, $^{*}p < 0.05$.

shown in Supplementary Figures 6–11. Of these, GO analysis of the biological process showed that apoptotic process and RNA transport were at the top for hsa-miR-34a-3p and hsa-miR-1306-3p, respectively. We also provided a graphical summary of five differentially expressed miRNAs' KEGG network (Supplementary Figure 12). The predominant pathways, i.e., MAPK signaling pathway for hsa-miR-181d-5p, hsa-miR-30b-5p, hsa-miR-199a-3p, and hsa-miR-103a-2-5p; PI3K-Akt signaling pathway for hsa-miR-34a-3p, hsa-miR-181d-5p, and hsa-miR-199a-3p; and axon guidance for hsa-miR-30b-5p and hsa-miR-103a-2-5p, were also reported in an *in vitro* hSOD1-mutant model (Peviani et al., 2014) and participated in the aggregation of TDP43 (Aaron et al., 2016).

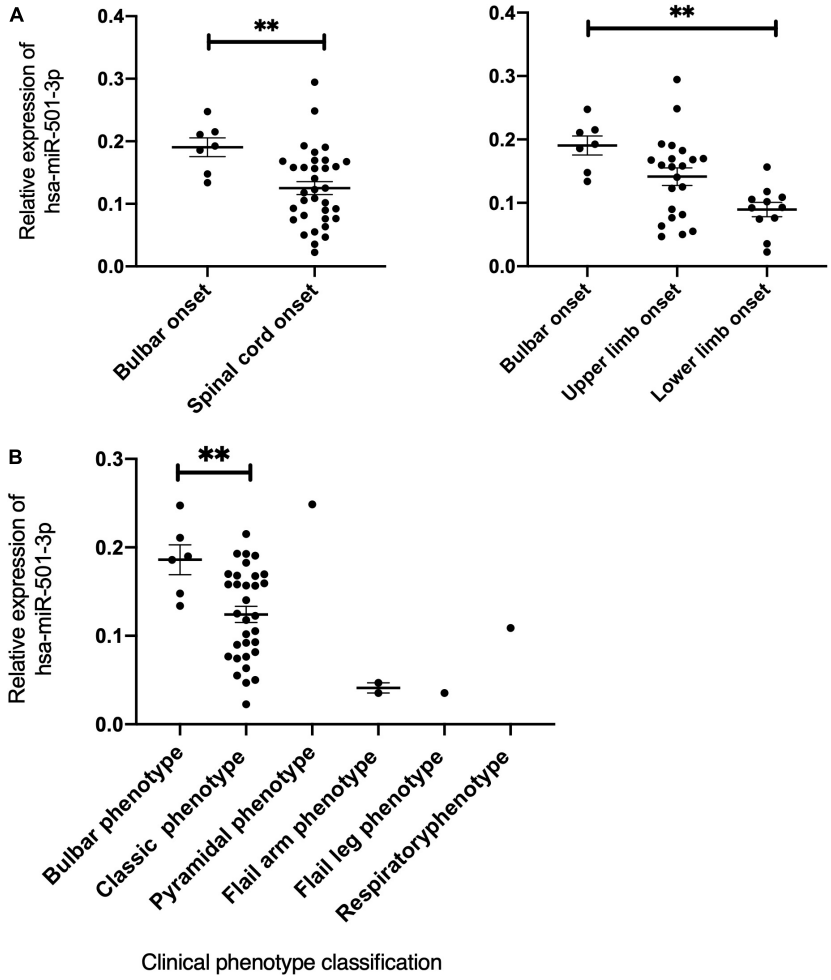

FIGURE 4
The expression of has-miR-501-3p and the correlation with clinical characteristics in patients with ALS. **(A)** The relationship of the relative expression of hsa-miR-501-3p and the onset site. Hsa-miR-501-3p was found to be specifically increased in patients whose initial symptoms presenting at bulbar-onset (p = 0.0098). Compared to lower limb onset, hsa-miR-501-3p was increased significantly in bulbar-onset of patients with ALS (p = 0.0027) and there was no significance between upper limb onset and lower limb onset groups. **(B)** The relationship of the relative expression of hsa-miR-501-3p and the clinical phenotype classification. $^{**}p < 0.01$.

Preliminary validation of putative target of hsa-miR-34a-3p

We conducted experimental validation of the putative target gene of hsa-miR-34a-3p. Enoyl-CoA Hydratase, Short Chain 1 (*ECHS1*) was predicted as a target gene of hsa-miR-34a-3p by three databases mentioned earlier. The predicted binding site of hsa-miR-34a-3p to ECHS1 was located in the 355-362 region of the *ECHS1* 3′ UTR from the TargetScan online database and the site binding type was 8mer. The dual-Luciferase reporter assay validated that hsa-miR-34a-3p could bind to *ECHS1* at both 24 h (p = 0.0001) and 48 h ($p < 0.0001$) and cause a statistically significant decrease in fluorometric intensity (**Figure 5B**).

SVM model to aid in the diagnosis of ALS

In the SVM model, we selected five miRNAs, including hsa-miR-199a-3p, hsa-miR-30b-5p, hsa-miR-501-3p, hsa-miR-103a-2-5p, and hsa-miR-181d-5p, as differentially expressed or potentially differentially expressed in patients with SALS and characterized to distinguish patients with SALS from HCs. Patients were classified into a training cohort and a validation cohort in a ratio of 4:1. The 5-fold cross-validated SVM model separating patients with ALS from non-ALS participants in the test cohort had an AUC of 0.80 and an accuracy of 78.67% (**Figure 6**). The sensitivity and specificity of the model for the diagnosis of ALS were 0.72 and 0.86, respectively. The detailed data of this model's performance are shown in **Supplementary Table 5**.

Discussion

Here, we presented a study showing the differentially expressed miRNAs in SALS and ALS patients with *SOD1*/*C9orf72* mutations and potential disease biomarkers for miRNAs derived from circulating exosomes in ALS. In this study, hsa-miR-34a-3p was exclusively downregulated in patients with *SOD1*-mutated ALS and hsa-miR-1306-3p was downregulated in ALS patients with *SOD1* and *C9orf72* mutations. Alternatively, hsa-miR-199a-3p and

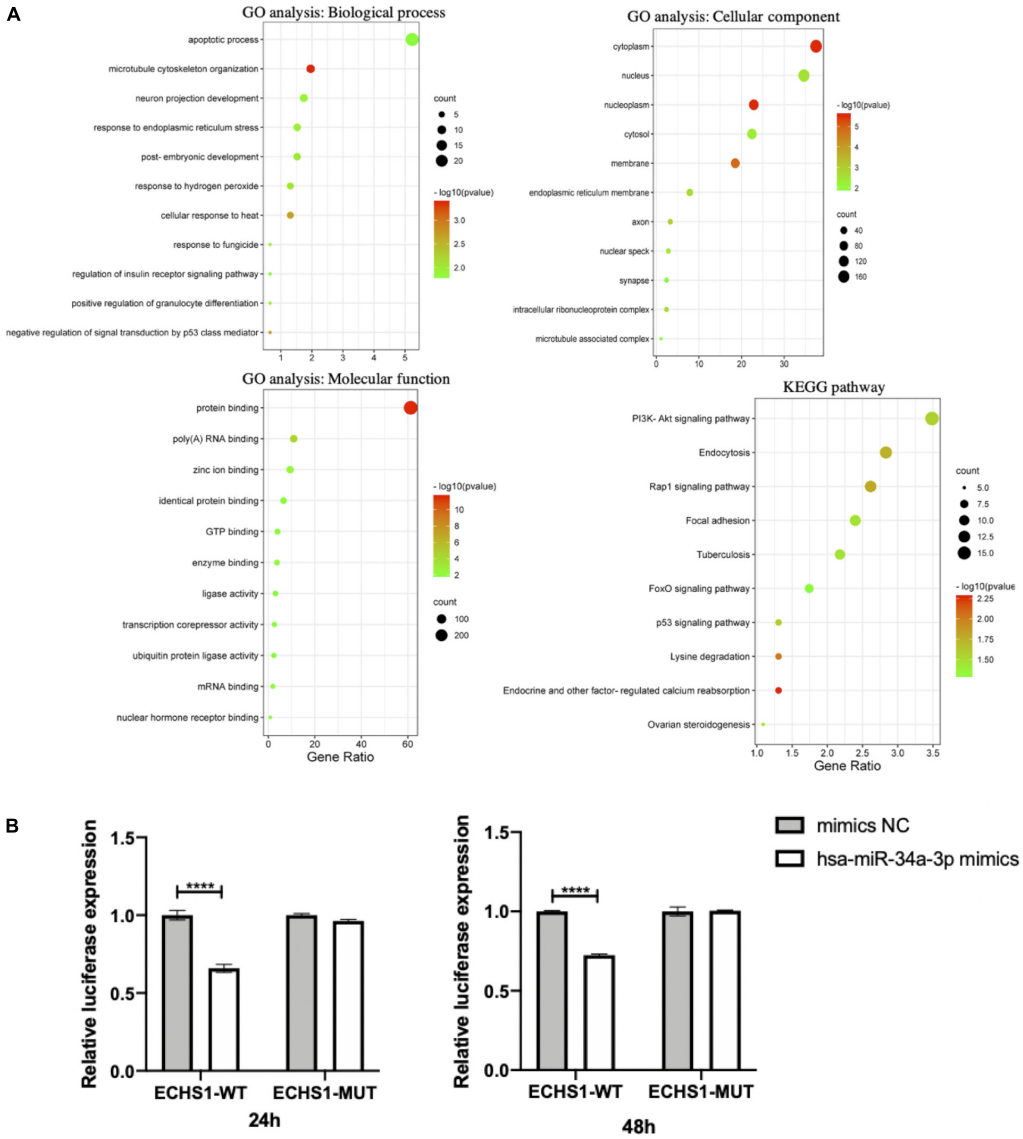

FIGURE 5
The downstream prediction and validation of hsa-miR-34a-3p. **(A)** The functional analysis including GO and KEGG analyses of target genes predicted hsa-miR-34a-3p. **(B)** Preliminary validation of putative target gene *ECHS1* of hsa-miR-34a-3p by Dual-Luciferase reporter assay. The result showed that hsa-miR-34a-3p bound to ECHS1 at both 24 h ($p = 0.0001$) and 48 h ($p < 0.0001$) and caused a statistically significant decrease in fluorometric intensity. ****$p < 0.0001$.

hsa-miR-30b-5p were confirmed to be significantly upregulated in patients with SALS. Furthermore, hsa-miR-501-3p was particularly significantly increased in ALS patients with the bulbar-onset group and the bulbar phenotype. The expression of hsa-miR-501-3p showed a potentially positive correlation with the age at onset, and the expression of hsa-miR-30b-5p showed a potentially positive correlation with disease progression and a potentially negative correlation with ALSFRS scores. In practice, the SVM model provided us with differential diagnostic performance between patients with ALS and HCs with an accuracy of 78.67% and an AUC of 0.80.

Exosomes, a subtype of EVs, are membrane-enclosed vehicles containing abundant proteins, lipids, and nucleic acids, which can participate in the bidirectional brain-periphery cross-talk. Owing to the ability of cell targeting to transfer materials (Sluijter et al., 2014), exosomes and their cargos were investigated in cancer, immune, and neurodegenerative diseases (Holm et al., 2018). Previously, efforts have been made to confirm exosomes may contribute to the spreading of toxic protein aggregates, such as TARDBP (Nonaka et al., 2013; Feneberg et al., 2014), SOD1 (Gomes et al., 2007), as well as the clearance of the toxic protein aggregates (Thompson et al., 2016). *TDP-43* has been reported to cooperate with other microprocessors such as Drosha and Dicer to promote miRNA biogenesis (Kawahara and Mieda-Sato, 2012). ALS pathogenesis may be a cause or consequence of the disrupted biological processes of miRNA, including synthesis, maturation, and degradation. Hence, detecting potential miRNA biomarkers in ALS could open up a whole new area of knowledge to help gain a better understanding of disease pathophysiology. The present study characterized the miRNA signature identified from exosomes which was collected from SALS

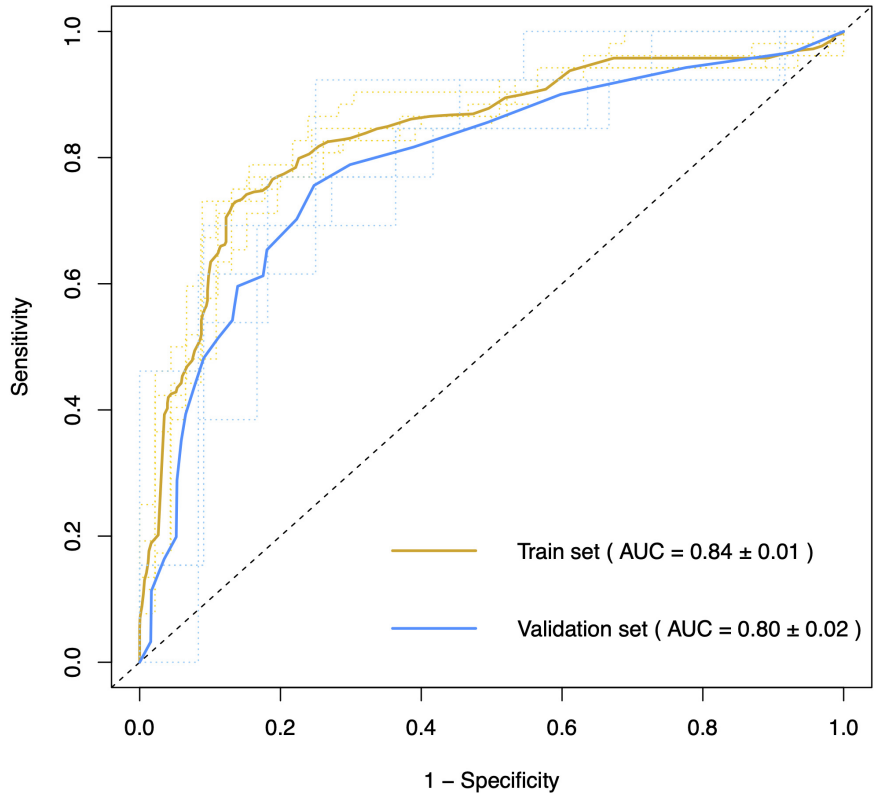

FIGURE 6
Area under curve of support vector machine model for differentiating patients with and without ALS. The 5-fold cross-validation support vector machine model classified patients with ALS and non-ALS participants in the test cohort with an accuracy of 78.67% (AUC = 0.80).

and gene-mutated ALS. It is known that it is difficult and challenging to isolate low-concentration miRNAs from exosomes/biofluids efficiently. The isolation method used in our study was a commercial kit called exoRNeasy Serum/Plasma Midi Kit (EXR) from Qiagen (Germany). Ding et al. (2018) compared four commonly used commercial kits for exosomal miRNA profile and reported that EXR performed better in the specific exosomal miRNAs recovery; among four commercial kits for miRNA extraction from exosomes, EXR achieved a better correlation of the results obtained from serum and plasma samples. In addition, exoRNeasy is a spin column-based method for the isolation of total RNA from EVs in serum and plasma. This method isolates highly pure RNA of equal or higher quantity compared to the traditional method of ultracentrifugation, with high specificity for vesicular over non-vesicular RNA. This method has been an improvement over traditional methods in providing a faster, more standardized way to achieve reliable high-quality RNA preparations from EVs in biofluids such as serum and plasma (Enderle et al., 2015).

In this study, hsa-miR-34a-3p was found to be downregulated in patients with *SOD1*-mutated ALS, whereas it was found to be increased in patients with *C9orf72*-mutated ALS despite not achieving the statistical significance. Pioneering work on hsa-miR-34a was consistent with our findings. Zhou et al. (2018) found that miR-34a was decreased at three different stages of disease in the spinal cord and the hypoglossal, facial, and red nuclei of $SOD1^{G93A}$ mice compared with $SOD1^{WT}$ mice. Moreover, Rizzuti et al. (2018) reported that hsa-miR-34a was downregulated in motor neuron progenitors differentiated from human ALS-induced pluripotent stem cells. Inversely, miR-34a-5p was overexpressed in patients with *C9orf72* mutation and pre-symptomatic carriers compared with HCs, suggesting that miR-34a-5p expression was dysregulated in cases with *C9orf72* mutation (Kmetzsch et al., 2021). All of the above indicated the differential pathogenesis caused by *SOD1* and *C9orf72* mutations, although further studies are needed. Mechanically, miR-34a was also reported to be involved in the apoptotic signaling pathway, including the downregulation of BCL-2 expression in a double transgenic mouse model of Alzheimer's disease (AD) (Wang et al., 2009) and in other neurological diseases (Mollinari et al., 2015; Modi et al., 2016), all of which being consistent with the GO analysis in this study showed that hsa-miR-34a-3p was linked with the apoptotic process and neuron projection development. Thus, miR-34a, an apoptosis-related miRNA, also regarded as a tumor suppressor or senescence inducer, was thought to involve in the p53 pathway (Raver-Shapira et al., 2007), synaptic vesicle regulation, and oxidative stress pathway, which might participate in the pathological mechanism of ALS. Hsa-miR-34a-3p was a specific differentially expressed miRNA found in ALS patients with *SOD1* mutation, suggesting that there might be a different pathogenesis between ALS with gene mutation and SALS, even underly ALS patients with *SOD1* and *C9orf72* mutations. Interestingly, hsa-miR-1306-3p showed downregulation significantly in patients with gene mutation, both in *SOD1* and *C9orf72* groups, but not in the SALS group. To date, hsa-miR-1306-3p has been reported in AD and cerebral ischemia/reperfusion injury in neurological diseases. Significant downregulation of hsa-miR-1306-5p was found in EVs (Li F. et al., 2020) and serum (Cheng L. et al., 2015) from patients with AD compared to HCs. The regulation

of ADAM10 by hsa-miR-1306 was demonstrated in SH-SY5Y cells expressing the 3'UTR of ADAM10 under a luciferase reporting vector (Augustin et al., 2012). ADAM10, an essential AD gene, controls the proteolytic processing of amyloid-beta precursor protein and the formation of the amyloid plaques (Pereira Vatanabe et al., 2021). In addition, miR-1306-5p expression was significantly downregulated in the oxygen-glucose deprivation/reoxygenation-induced SH-SY5Y cell model, and the upregulation of miR-1306-5p could decrease cerebral ischemia/reperfusion injury (Chen et al., 2019), suggesting miR-1306-5p involves in the cell survival rate and inhibits the cell injury. GO analysis revealed that the top group of target genes for hsa-miR-1306-3p has process networks for RNA transport and mRNA export from the nucleus, which was also consistent with the theory that *C9orf72* is involved in ALS (Vatsavayai et al., 2019). In addition, RNA processing, including transportation and clear, especially proteins belonging to hnRNP classes, were reported to participate in the pathological biological processes or pathways of gene-associated ALS (*TARDBP* and *FUS*) (Guerreiro et al., 2015). Hsa-miR-199a-3p was confirmed to be upregulated significantly in patients with SALS by the microarray and RT-qPCR. In a previous study, miR-199a-3p expression was reported to be downregulated in Parkinson's disease (PD) (Zhou et al., 2021); more exactly, it was specifically downregulated in stage II of PD and miR-199a-3p overexpression inhibited the cell apoptosis induced by MPP+ treatment and promoted cell proliferation (He et al., 2021). Moreover, miR-199a-3p has also been regarded as a tumor suppressor in various human cancers (Shatseva et al., 2011). The functional analysis showed that the potentially predicted genes of miR-199a-3p were involved in the transcription of DNA-template, signal transduction, and positive regulation of transcription from RNA polymerase II promoter, suggesting that they might be of importance in cell proliferation and migration. Therefore, we speculated that the elevation of miR-199a-3p found in patients with SALS might be a secondary compensatory response to alleviate the cell damage caused by the disease. Compared with HCs, hsa-miR-30b-5p was found to be upregulated in SALS. Interestingly, Brennan et al. (2019). reported that hsa-miR-30b-5p was the single miRNA that overlapped between all four NDS, including AD, PD, multiple sclerosis, and ALS, which suggested hsa-miR-30b-5p may involve in the same pathogenesis of these four NDS. Remarkably, KEGG analysis showed that hsa-miR-30b-5p was represented in the axon guidance, ubiquitin-mediated proteolysis, and ALS. Thus, we should pay more attention to hsa-miR-30b-5p and try to dig into the pathogenesis underlying the dysfunction of hsa-miR-30b-5p. Except for miRNAs discussed earlier, some other miRNAs were also reported to be differentially expressed in patients with ALS compared with HCs, such as miR-27a-3p, which was found as a downregulation miRNA in serum exosomes from patients with ALS (Xu et al., 2018). The reason for the diverse findings might be the sample size and the patients with different disease durations.

Regarding the clinical features, patients who were at bulbar-onset showed a higher expression in hsa-miR-501-3p. Similarly, patients with ALS classified with bulbar phenotype had a higher expression in hsa-miR-501-3p than those with classic phenotype. The result suggests that hsa-miR-501-3p could be a biomarker of disease classification, which will benefit early identification, improve the quality of life, and avoid complications for the bulbar-onset subgroup. In addition, miR-501-3p was reported to be dysregulated in the serum of patients with AD and positively correlated with the Mini-Mental State Examination, suggesting it might be a biomarker related to the progression of AD (Hara et al., 2017). Interestingly, we also found a positive correlation between this miRNA and the onset age in patients with ALS, suggesting miR-501-3p might be associated with aging and degeneration.

The support vector machine is a powerful tool that can analyze data whose number of predictors is approximately equal to or greater than the number of observations (Suh et al., 2018), commonly used in radiomics. SVM constructs hyperplanes of the covariates' space that separate the observations according to their category (Huang et al., 2018). The current study highlighted the diagnostic relevance of selected miRNAs, which could be used for the clinical diagnosis of patients with ALS. Using five differentially expressed miRNA biomarkers in combination as a signature to classify the disease state of our samples, we observed an almost 0.80 classification accuracy between ALS and non-ALS samples and an AUC of 0.80 after 5-fold cross-validation in the test cohort. This is significant as it demonstrates that these biomarkers may prove useful in diagnosing the disease, but still, challenges are needed to be met. Patients with other NDS are needed to be as disease controls to verify whether these diagnostic tool work. And more detailed classification might enhance the predictive accuracy and increase miRNAs concentration from exosomes are needed.

Although our study provided valuable results, it did have some drawbacks. First, miRNA expression in exosomes was only collected at baseline, so we were unable to obtain the dynamics of miRNA expression in exosomes over time. Moreover, we do not know if these miRNAs varied before the onset of symptoms. Thus, more follow-up data, even in asymptomatic individuals with pathogenic mutations, and a functional study of selected miRNAs in the ALS model are the next steps that are envisioned. Second, the miRNA profile in exosomes might be altered by the isolation method, and the protocol used in our study was a spin column-based method for the isolation of miRNAs from the plasma. Further study is needed to validate the expression of the miRNAs reported in the current study from exosomes purified with a different protocol. While recent years have seen unparalleled advances in the isolation and analysis of miRNAs from exosomes, challenges such as how efficiently low-concentration miRNAs can be isolated from exosomes and the heterogeneity of miRNAs derived from exosomes still remain unresolved. Third, we noticed that all differentially expressed miRNAs identified in the study were also reported in other NDS, which might reflect an underlying change that occurs as a result of neuron breakdown. This might be the reason that the predictive accuracy of the comparison between patients with ALS and HCs was only 78.67%, which was a little low as a diagnostic tool. The pathological mechanisms underlying these aberrant miRNAs need to be further studied. In addition, we have only conducted the internal validation of five miRNA biomarkers by the SVM model. Exploring these dysregulated miRNAs in another external validation cohort of ALS will be considered to enhance their diagnostic potential for this disease.

Conclusion

Overall, our results confirmed a key role in the unique signature of miRNAs from circulating exosomes in patients with ALS. By combining microarray and RT-qPCR results, we reported the dysregulation of hsa-miR-34a-3p and hsa-miR-1306-3p in ALS patients with *SOD1*/*C9orf72* mutations, and hsa-miR-199a-3p and hsa-miR-30b-5p in patients with SALS, suggesting the different

mechanisms underlying the gene-mutant ALS and SALS. The machine-learning algorithms have high accuracy in the prediction of ALS diagnosis and, if replicated in further studies, will provide the basis for the clinical application of blood tests in ALS diagnosis and ALS classification diagnosis. Identification of the downstream genetic pathways predicted by candidate miRNAs might lead to the discovery of pathological mechanisms and the development of therapeutic strategies.

Data availability statement

The datasets presented in this article are not readily available because of the ethical restrictions of West China hospital. Requests to access the datasets should be directed to the authors/corresponding authors.

Ethics statement

The studies involving human participants were reviewed and approved by the Ethics Committee of West China Hospital of Sichuan University (approval number 2016-097). The patients/participants provided their written informed consent to participate in this study.

Author contributions

H-FS and Y-PC contributed to the conceptualization, carried out the funding acquisition, wrote, reviewed, and edited the manuscript, and supervised the data. X-JG, T-MY, Q-QW, BC, and YZ performed the methodology, carried out the software, and validated and investigated the data. Y-FC carried out the formal analysis and data curation, wrote the original draft, and investigated the data. All authors read and approved the final manuscript.

Funding

This study was supported by the National Natural Science Foundation of China (Grant No. 81971188), the Science and Technology Bureau Fund of Sichuan Province (Grant No. 2019YFS0216), and the 1.3.5 project for disciplines of excellence, West China Hospital, Sichuan University (Grant No. 2019HXFH046).

Acknowledgments

We thank all the participants and their families who supported them. We are grateful to Yujiao Yu, Chunyu Li, and Dejiang Pang from the National Clinical Research Center for Geriatric, Laboratory of Neurodegenerative Disorders, West China Hospital, Sichuan University, for the valuable comments on the manuscript.

Conflict of interest

The authors declare that the research was conducted in the absence of any commercial or financial relationships that could be construed as a potential conflict of interest.

Publisher's note

All claims expressed in this article are solely those of the authors and do not necessarily represent those of their affiliated organizations, or those of the publisher, the editors and the reviewers. Any product that may be evaluated in this article, or claim that may be made by its manufacturer, is not guaranteed or endorsed by the publisher.

Supplementary material

The Supplementary Material for this article can be found online at: https://www.frontiersin.org/articles/10.3389/fnagi.2023.1106497/full#supplementary-material

References

Aaron, C., Beaudry, G., Parker, J. A., and Therrien, M. (2016). Maple syrup decreases TDP-43 proteotoxicity in a *Caenorhabditis elegans* model of amyotrophic lateral sclerosis (ALS). *J. Agric. Food Chem.* 64, 3338–3344. doi: 10.1021/acs.jafc.5b05432

Aday, S., Hazan-Halevy, I., Chamorro-Jorganes, A., Anwar, M., Goldsmith, M., Beazley-Long, N., et al. (2021). Bioinspired artificial exosomes based on lipid nanoparticles carrying let-7b-5p promote angiogenesis in vitro and in vivo. *Mol. Ther.* 29, 2239–2252. doi: 10.1016/j.ymthe.2021.03.015

Agarwal, V., Bell, G. W., Nam, J. W., and Bartel, D. P. (2015). Predicting effective microRNA target sites in mammalian mRNAs. *Elife* 4:e05005. doi: 10.7554/eLife.05005

Åkerblom, M., Sachdeva, R., Barde, I., Verp, S., Gentner, B., Trono, D., et al. (2012). MicroRNA-124 is a subventricular zone neuronal fate determinant. *J. Neurosci.* 32, 8879–8889. doi: 10.1523/jneurosci.0558-12.2012

Augustin, R., Endres, K., Reinhardt, S., Kuhn, P., Lichtenthaler, S., Hansen, J., et al. (2012). Computational identification and experimental validation of microRNAs binding to the Alzheimer-related gene ADAM10. *BMC Med. Genet.* 13:35.

Bartel, D. P. (2004). MicroRNAs: Genomics, biogenesis, mechanism, and function. *Cell* 116, 281–297. doi: 10.1016/s0092-8674(04)00045-5

Basso, M., Pozzi, S., Tortarolo, M., Fiordaliso, F., Bisighini, C., Pasetto, L., et al. (2013). Mutant copper-zinc superoxide dismutase (SOD1) induces protein secretion pathway alterations and exosome release in astrocytes: Implications for disease spreading and motor neuron pathology in amyotrophic lateral sclerosis. *J. Biol. Chem.* 288, 15699–15711. doi: 10.1074/jbc.M112.425066

Blondal, T., Jensby Nielsen, S., Baker, A., Andreasen, D., Mouritzen, P., Wrang Teilum, M., et al. (2013). Assessing sample and miRNA profile quality in serum and plasma or other biofluids. *Methods* 59, S1–S6.

Bohatá, J., Horváthová, V., Pavlíková, M., and Stibùrková, B. (2021). Circulating microRNA alternations in primary hyperuricemia and gout. *Arthritis Res. Ther.* 23:186. doi: 10.1186/s13075-021-02569-w

Brennan, S., Keon, M., Liu, B., Su, Z., and Saksena, N. K. (2019). Panoramic visualization of circulating MicroRNAs across neurodegenerative diseases in humans. *Mol. Neurobiol.* 56, 7380–7407. doi: 10.1007/s12035-019-1615-1

Brooks, B. R., Miller, R. G., Swash, M., and Munsat, T. L. (2000). El Escorial revisited: Revised criteria for the diagnosis of amyotrophic lateral sclerosis. *Amyotroph. Lateral Scler. Other Motor Neuron Disord* 1, 293–299. doi: 10.1080/146608200300079536

Brown, R. H., and Al-Chalabi, A. (2017). Amyotrophic lateral sclerosis. *N. Engl. J. Med.* 377, 162–172. doi: 10.1056/NEJMra1603471

Chen, X., Li, C., Li, J., Sheng, L., and Liu, X. (2019). Upregulation of miR-1306-5p decreases cerebral ischemia/reperfusion injury in vitro by targeting BIK. *Biosci. Biotechnol. Biochem.* 83, 2230–2237. doi: 10.1080/09168451.2019.1654846

Chen, Y. P., Yu, S., Wei, Q., Cao, B., Gu, X., Chen, X., et al. (2021). Role of genetics in amyotrophic lateral sclerosis: A large cohort study in Chinese mainland population. *J. Med. Genet.* 59, 840–849. doi: 10.1136/jmedgenet-2021-107965

Chen, Y., and Wang, X. (2020). miRDB: An online database for prediction of functional microRNA targets. *Nucleic Acids Res.* 48, D127–D131. doi: 10.1093/nar/gkz757

Chen, Y., Wei, Q., Chen, X., Li, C., Cao, B., Ou, R., et al. (2016). Aberration of miRNAs expression in leukocytes from sporadic amyotrophic lateral sclerosis. *Front. Mol. Neurosci.* 9:69. doi: 10.3389/fnmol.2016.00069

Cheng, L., Doecke, J., Sharples, R., Villemagne, V., Fowler, C., Rembach, A., et al. (2015). Prognostic serum miRNA biomarkers associated with Alzheimer's disease shows concordance with neuropsychological and neuroimaging assessment. *Mol. Psychiatry* 20, 1188–1196. doi: 10.1038/mp.2014.127

Cheng, L., Sharples, R. A., Scicluna, B. J., and Hill, A. F. (2014).@@ Exosomes provide a@ protective and enriched source of miRNA for biomarker profiling compared to intracellular and cell-free blood. *J. Extracell. Vesicles* 3. doi: 10.3402/jev.v3.23743

Cheng, W. C., Chung, I., Tsai, C., Huang, T., Chen, C., Wang, S., et al. (2015). YM500v2: A small RNA sequencing (smRNA-seq) database for human cancer miRNome research. *Nucleic Acids Res.* 43, D862–D867. doi: 10.1093/nar/gku1156

Chiò, A., Calvo, A., Moglia, C., Mazzini, L., and Mora, G. (2011). Phenotypic heterogeneity of amyotrophic lateral sclerosis: A population based study. *J. Neurol. Neurosurg. Psychiatry* 82, 740–746. doi: 10.1136/jnnp.2010.235952

Cleveland, D. W., and Rothstein, J. D. (2001). From Charcot to Lou Gehrig: Deciphering selective motor neuron death in ALS. *Nat. Rev. Neurosci.* 2, 806–819. doi: 10.1038/35097565

Dekker, A. M., Seelen, M., van Doormaal, P., van Rheenen, W., Bothof, R., van Riessen, T., et al. (2016). Large-scale screening in sporadic amyotrophic lateral sclerosis identifies genetic modifiers in C9orf72 repeat carriers. *Neurobiol. Aging* 39, 220.e9–15. doi: 10.1016/j.neurobiolaging.2015.12.012

Ding, M., Wang, C., Lu, X., Zhang, C., Zhou, Z., Chen, X., et al. (2018). Comparison of commercial exosome isolation kits for circulating exosomal microRNA profiling. *Anal. Bioanal. Chem.* 410, 3805–3814.

Enderle, D., Spiel, A., Coticchia, C. M., Berghoff, E., Mueller, R., Schlumpberger, M., et al. (2015). Characterization of RNA from exosomes and other extracellular vesicles isolated by a novel spin column-based method. *PLoS one* 10:e0136133. doi: 10.1371/journal.pone.0136133

Feiler, M. S., Strobel, B., Freischmidt, A., Helferich, A., Kappel, J., Brewer, B., et al. (2015). TDP-43 is intercellularly transmitted across axon terminals. *J. Cell Biol.* 211, 897–911. doi: 10.1083/jcb.201504057

Feneberg, E., Steinacker, P., Lehnert, S., Schneider, A., Walther, P., Thal, D., et al. (2014). Limited role of free TDP-43 as a diagnostic tool in neurodegenerative diseases. *Amyotroph. Lateral Scler. Frontotemporal Degener.* 15, 351–356. doi: 10.3109/21678421.2014.905606

Feng, M. G., Liu, C., Chen, L., Feng, W., Liu, M., Hai, H., et al. (2018). MiR-21 attenuates apoptosis-triggered by amyloid-β via modulating PDCD4/ PI3K/AKT/GSK-3β pathway in SH-SY5Y cells. *Biomed. Pharmacother.* 101, 1003–1007. doi: 10.1016/j.biopha.2018.02.043

Gomes, C., Keller, S., Altevogt, P., and Costa, J. (2007). Evidence for secretion of Cu,Zn superoxide dismutase via exosomes from a cell model of amyotrophic lateral sclerosis. *Neurosci. Lett.* 428, 43–46. doi: 10.1016/j.neulet.2007.09.024

Gonda, A., Kabagwira, J., Senthil, G. N., and Wall, N. R. (2019). Internalization of Exosomes through receptor-mediated endocytosis. *Mol. Cancer Res.* 17, 337–347. doi: 10.1158/1541-7786.Mcr-18-0891

Guerreiro, R., Brás, J., and Hardy, J. (2015). SnapShot: Genetics of ALS and FTD. *Cell* 160, 798–798.e1. doi: 10.1016/j.cell.2015.01.052

Hara, N., Kikuchi, M., Miyashita, A., Hatsuta, H., Saito, Y., Kasuga, K., et al. (2017). Serum microRNA miR-501-3p as a potential biomarker related to the progression of Alzheimer's disease. *Acta Neuropathol. Commun.* 5:10. doi: 10.1186/s40478-017-0414-z

He, S., Huang, L., Shao, C., Nie, T., Xia, L., Cui, B., et al. (2021). Several miRNAs derived from serum extracellular vesicles are potential biomarkers for early diagnosis and progression of Parkinson's disease. *Transl. Neurodegener.* 10:25. doi: 10.1186/s40035-021-00249-y

Holm, M. M., Kaiser, J., and Schwab, M. E. (2018). Extracellular vesicles: Multimodal envoys in neural maintenance and repair. *Trends Neurosci.* 41, 360–372. doi: 10.1016/j.tins.2018.03.006

Huang da, W., Sherman, B. T., and Lempicki, R. A. (2009a). Systematic and integrative analysis of large gene lists using DAVID bioinformatics resources. *Nat. Protoc.* 4, 44–57. doi: 10.1038/nprot.2008.211

Huang da, W., Sherman, B. T., and Lempicki, R. A. (2009b). Bioinformatics enrichment tools: Paths toward the comprehensive functional analysis of large gene lists. *Nucleic Acids Res.* 37, 1–13. doi: 10.1093/nar/gkn923

Huang, S., Cai, N., Pacheco, P., Narrandes, S., Wang, Y., and Xu, W. (2018). Applications of support vector machine (SVM) learning in cancer genomics. *Cancer Genomics Proteomics* 15, 41–51. doi: 10.21873/cgp.20063

Kawahara, Y., and Mieda-Sato, A. (2012). TDP-43 promotes microRNA biogenesis as a component of the Drosha and Dicer complexes. *Proc. Natl. Acad. Sci. U.S.A.* 109, 3347–3352. doi: 10.1073/pnas.1112427109

Kiernan, M. C., Vucic, S., Cheah, B., Turner, M., Eisen, A., Hardiman, O., et al. (2011). Amyotrophic lateral sclerosis. *Lancet* 377, 942–955. doi: 10.1016/s0140-6736(10)61156-7

Kimura, F., Fujimura, C., Ishida, S., Nakajima, H., Furutama, D., Uehara, H., et al. (2006). Progression rate of ALSFRS-R at time of diagnosis predicts survival time in ALS. *Neurology* 66, 265–267. doi: 10.1212/01.wnl.0000194316.91908.8a

Kmetzsch, V., Anquetil, V., Saracino, D., Rinaldi, D., Camuzat, A., Gareau, T., et al. (2021). Plasma microRNA signature in presymptomatic and symptomatic subjects with C9orf72-associated frontotemporal dementia and amyotrophic lateral sclerosis. *J. Neurol. Neurosurg. Psychiatry* 92, 485–493. doi: 10.1136/jnnp-2020-324647

Lange, T., Stracke, S., Rettig, R., Lendeckel, U., Kuhn, J., Schlüter, R., et al. (2017). Identification of miR-16 as an endogenous reference gene for the normalization of urinary exosomal miRNA expression data from CKD patients. *PLoS One* 12:e0183435. doi: 10.1371/journal.pone.0183435

Li, C., Chen, Y., Chen, X., Wei, Q., Cao, B., Shang, H., et al. (2017). Downregulation of MicroRNA-193b-3p promotes autophagy and cell survival by targeting TSC1/mTOR signaling in NSC-34 cells. *Front. Mol. Neurosci.* 10:160. doi: 10.3389/fnmol.2017.00160

Li, C., Chen, Y., Chen, X., Wei, Q., Ou, R., Gu, X., et al. (2020). MicroRNA-183-5p is stress-inducible and protects neurons against cell death in amyotrophic lateral sclerosis. *J. Cell. Mol. Med.* 24, 8614–8622. doi: 10.1111/jcmm.15490

Li, F., Xie, X., Sui, X., Wang, P., Chen, Z., and Zhang, J. (2020). Profile of pathogenic proteins and MicroRNAs in plasma-derived extracellular vesicles in Alzheimer's disease: A pilot study. *Neuroscience* 432, 240–246. doi: 10.1016/j.neuroscience.2020.02.044

Modi, P. K., Jaiswal, S., and Sharma, P. (2016). Regulation of neuronal cell cycle and apoptosis by MicroRNA 34a. *Mol. Cell Biol.* 36, 84–94. doi: 10.1128/mcb.00589-15

Mollinari, C., Racaniello, M., Berry, A., Pieri, M., de Stefano, M., Cardinale, A., et al. (2015). miR-34a regulates cell proliferation, morphology and function of newborn neurons resulting in improved behavioural outcomes. *Cell Death Dis.* 6:e1622. doi: 10.1038/cddis.2014.589

Nonaka, T., Masuda-Suzukake, M., Arai, T., Hasegawa, Y., Akatsu, H., Obi, T., et al. (2013). Prion-like properties of pathological TDP-43 aggregates from diseased brains. *Cell Rep.* 4, 124–134. doi: 10.1016/j.celrep.2013.06.007

Paganoni, S., Macklin, E., Lee, A., Murphy, A., Chang, J., Zipf, A., et al. (2014). Diagnostic timelines and delays in diagnosing amyotrophic lateral sclerosis (ALS). *Amyotroph. Lateral Scler. Frontotemporal Degener.* 15, 453–456. doi: 10.3109/21678421.2014.903974

Pan, W., Xu, X., Zhang, M., and Song, X. (2021). Human urine-derived stem cell-derived exosomal miR-21-5p promotes neurogenesis to attenuate Rett syndrome via the EPha4/TEK axis. *Lab. Invest.* 101, 824–836. doi: 10.1038/s41374-021-00574-w

Pereira Vatanabe, I., Peron, R., Mantellatto Grigoli, M., Pelucchi, S., De Cesare, G., Magalhães, T., et al. (2021). ADAM10 plasma and CSF levels are increased in mild Alzheimer's disease. *Int. J. Mol. Sci.* 22:2416. doi: 10.3390/ijms22052416

Peviani, M., Tortarolo, M., Battaglia, E., Piva, R., and Bendotti, C. (2014). Specific induction of Akt3 in spinal cord motor neurons is neuroprotective in a mouse model of familial amyotrophic lateral sclerosis. *Mol. Neurobiol.* 49, 136–148. doi: 10.1007/s12035-013-8507-6

Raver-Shapira, N., Marciano, E., Meiri, E., Spector, Y., Rosenfeld, N., Moskovits, N., et al. (2007). Transcriptional activation of miR-34a contributes to p53-mediated apoptosis. *Mol. Cell* 26, 731–743. doi: 10.1016/j.molcel.2007.05.017

Ritchie, M. E., Phipson, B., Wu, D., Hu, Y., Law, C., Shi, W., et al. (2015). limma powers differential expression analyses for RNA-sequencing and microarray studies. *Nucleic Acids Res.* 43:e47. doi: 10.1093/nar/gkv007

Rizzuti, M., Filosa, G., Melzi, V., Calandriello, L., Dioni, L., Bollati, V., et al. (2018). MicroRNA expression analysis identifies a subset of downregulated miRNAs in ALS motor neuron progenitors. *Sci. Rep.* 8:10105. doi: 10.1038/s41598-018-28366-1

Shatseva, T., Lee, D. Y., Deng, Z., and Yang, B. B. (2011). MicroRNA miR-199a-3p regulates cell proliferation and survival by targeting caveolin-2. *J. Cell Sci.* 124, 2826–2836. doi: 10.1242/jcs.077529

Sluijter, J. P., Verhage, V., Deddens, J. C., van den Akker, F., and Doevendans, P. A. (2014). Microvesicles and exosomes for intracardiac communication. *Cardiovasc. Res.* 102, 302–311. doi: 10.1093/cvr/cvu022

Suh, H. B., Choi, Y., Bae, S., Ahn, S., Chang, J., Kang, S., et al. (2018). Primary central nervous system lymphoma and atypical glioblastoma: Differentiation using radiomics approach. *Eur. Radiol.* 28, 3832–3839. doi: 10.1007/s00330-018-5368-4

Tang, X. H., Guo, T., Gao, X., Wu, X., Xing, X., Ji, J., et al. (2021). Exosome-derived noncoding RNAs in gastric cancer: Functions and clinical applications. *Mol. Cancer* 20:99. doi: 10.1186/s12943-021-01396-6

Thompson, A. G., Gray, E., Heman-Ackah, S., Mäger, I., Talbot, K., Andaloussi, S., et al. (2016). Extracellular vesicles in neurodegenerative disease - pathogenesis to biomarkers. *Nat. Rev. Neurol.* 12, 346–357. doi: 10.1038/nrneurol.2016.68

Valadi, H., Ekström, K., Bossios, A., Sjöstrand, M., Lee, J., Lötvall, J., et al. (2007). Exosome-mediated transfer of mRNAs and microRNAs is a novel mechanism of genetic exchange between cells. *Nat. Cell Biol.* 9, 654–659. doi: 10.1038/ncb1596

Vatsavayai, S. C., Nana, A. L., Yokoyama, J. S., and Seeley, W. W. (2019). C9orf72-FTD/ALS pathogenesis: Evidence from human neuropathological studies. *Acta Neuropathol.* 137, 1–26. doi: 10.1007/s00401-018-1921-0

Vlachos, I. S., Paraskevopoulou, M., Karagkouni, D., Georgakilas, G., Vergoulis, T., Kanellos, I., et al. (2015). DIANA-TarBase v7.0: Indexing more than half a million experimentally supported miRNA:mRNA interactions. *Nucleic Acids Res.* 43, D153–D159. doi: 10.1093/nar/gku1215

Wang, X., Liu, P., Zhu, H., Xu, Y., Ma, C., Dai, X., et al. (2009). miR-34a, a microRNA up-regulated in a double transgenic mouse model of Alzheimer's disease, inhibits bcl2 translation. *Brain Res. Bull.* 80, 268–273. doi: 10.1016/j.brainresbull.2009.08.006

Westergard, T., Jensen, B., Wen, X., Cai, J., Kropf, E., Iacovitti, L., et al. (2016). Cell-to-cell transmission of dipeptide repeat proteins linked to C9orf72-ALS/FTD. *Cell Rep.* 17, 645–652. doi: 10.1016/j.celrep.2016.09.032

Xu, Q., Zhao, Y., Zhou, X., Luan, J., Cui, Y., and Han, J. (2018). Comparison of the extraction and determination of serum exosome and miRNA in serum and the detection of miR-27a-3p in serum exosome of ALS patients. *Intractable Rare Dis. Res.* 7, 13–18. doi: 10.5582/irdr.2017.01091

Zheng, H., Liu, J., Yu, J., and McAlinden, A. (2021). Expression profiling of mitochondria-associated microRNAs during osteogenic differentiation of human MSCs. *Bone* 151:116058. doi: 10.1016/j.bone.2021.116058

Zhou, F., Zhang, C., Guan, Y., Chen, Y., Lu, Q., Jie, L., et al. (2018). Screening the expression characteristics of several miRNAs in G93A-SOD1 transgenic mouse: Altered expression of miRNA-124 is associated with astrocyte differentiation by targeting Sox2 and Sox9. *J. Neurochem.* 145, 51–67. doi: 10.1111/jnc.14229

Zhou, Q., Zhang, M., Liu, M., Tan, Z., Qin, Q., Jiang, Y., et al. (2021). LncRNA XIST sponges miR-199a-3p to modulate the Sp1/LRRK2 signal pathway to accelerate Parkinson's disease progression. *Aging (Albany NY)* 13, 4115–4137.

Zhu, H., Bhattacharyya, B., Lin, H., and Gomez, C. M. (2013). Skeletal muscle calpain acts through nitric oxide and neural miRNAs to regulate acetylcholine release in motor nerve terminals. *J. Neurosci.* 33, 7308–7324. doi: 10.1523/jneurosci.0224-13.2013

frontiers | Frontiers in Neuroscience

TYPE Original Research
PUBLISHED 14 February 2023
DOI 10.3389/fnins.2023.1122235

Check for updates

OPEN ACCESS

EDITED BY
Jun Xu,
Beijing Tiantan Hospital, Capital Medical University, China

REVIEWED BY
Zhen Yuan,
University of Macau, Macao SAR, China
Hassan Soleimanpour,
Tabriz University of Medical Sciences, Iran

*CORRESPONDENCE
Juebao Li
✉ lijuebao@hmc.edu.cn
Kai Wang
✉ wk1982405@163.com

†These authors have contributed equally to this work and share first authorship

SPECIALTY SECTION
This article was submitted to Neurodegeneration, a section of the journal Frontiers in Neuroscience

RECEIVED 12 December 2022
ACCEPTED 31 January 2023
PUBLISHED 14 February 2023

CITATION
Zhao K, Wang R, Chen R, Liu J, Ye Q, Wang K and Li J (2023) Association between bilirubin levels with incidence and prognosis of stroke: A meta-analysis.
Front. Neurosci. 17:1122235.
doi: 10.3389/fnins.2023.1122235

COPYRIGHT
© 2023 Zhao, Wang, Chen, Liu, Ye, Wang and Li. This is an open-access article distributed under the terms of the Creative Commons Attribution License (CC BY). The use, distribution or reproduction in other forums is permitted, provided the original author(s) and the copyright owner(s) are credited and that the original publication in this journal is cited, in accordance with accepted academic practice. No use, distribution or reproduction is permitted which does not comply with these terms.

Association between bilirubin levels with incidence and prognosis of stroke: A meta-analysis

Kun Zhao[1,2†], Rui Wang[1,3†], Rongrong Chen[2], Jialei Liu[2], Qing Ye[1], Kai Wang[4*] and Juebao Li[1*]

[1]Department of Rehabilitation Medicine, Center for Rehabilitation Medicine, Rehabilitation & Sports Medicine Research Institute of Zhejiang Province, Zhejiang Provincial People's Hospital, Affiliated People's Hospital, Hangzhou Medical College, Hangzhou, Zhejiang, China, [2]Zhejiang University School of Medicine, Hangzhou, Zhejiang, China, [3]Bengbu Medical College, Bengbu, Anhui, China, [4]Department of Neurology, The Second Affiliated Hospital of Xuzhou Medical University, Xuzhou, Jiangsu, China

Objective: Bilirubin has anti-inflammatory, antioxidant, and neuroprotective properties, but the association between bilirubin and stroke remains contentious. A meta-analysis of extensive observational studies on the relationship was conducted.

Methods: Studies published before August 2022 were searched in PubMed, EMBASE, and Cochrane Library. Cohort, cross-sectional and case-control studies that examined the association between circulating bilirubin and stroke were included. The primary outcome included the incidence of stroke and bilirubin quantitative expression level between stroke and control, and the secondary outcome was stroke severity. All pooled outcome measures were determined using random-effects models. The meta-analysis, subgroup analysis, and sensitivity analysis were performed using Stata 17.

Results: A total of 17 studies were included. Patients with stroke had a lower total bilirubin level (mean difference = −1.33 μmol/L, 95% CI: −2.12 to −0.53, $P < 0.001$). Compared with the lowest bilirubin level, total odds ratio (OR) of the highest bilirubin for the occurrence of stroke was 0.71 (95% CI: 0.61–0.82) and ischemic stroke was 0.72 (95% CI: 0.57–0.91), especially in cohort studies with accepted heterogeneity ($I^2 = 0$). Serum total and direct bilirubin levels were significantly and positively associated with stroke severity. A stratified analysis based on gender showed that the total bilirubin level in males correlated with ischemic stroke or stroke, which was not noted in females.

Conclusion: While our findings suggest associations between bilirubin levels and stroke risk, existing evidence is insufficient to establish a definitive association. Better-designed prospective cohort studies should further clarify pertinent questions (PROSPERO registration number: CRD42022374893).

KEYWORDS

direct bilirubin, total bilirubin, ischemic stroke, stroke, meta-analysis

Introduction

Stroke is a clinical syndrome of brain injury due to blood vessel blockage or blood vessel rupture and bleeding classified as ischemic and hemorrhagic stroke (Campbell and Khatri, 2020). Intravenous plasminogen activator is currently the gold standard treatment for patients with acute ischemic stroke. However, it is prone to cause adverse reactions such as cerebral hemorrhage, and most patients arriving at the stroke center exceed the optimal treatment window of 4.5 h (Thakkar et al., 2019). Therefore, early prediction of stroke occurrence and identification of stroke prognostic factors are important for stroke management.

Bilirubin, an end-product of heme catabolic pathway, has long been regarded as a potentially toxic substance whose elevated levels can cause irreversible damage to the brain and nervous system. However, there is strong evidence that bilirubin has anti-inflammatory, antioxidant, and neuroprotective properties (Thakkar et al., 2019). Previous meta-analyses suggested that a higher total level of bilirubin was related to a lower stroke prevalence and had a significant association with stroke severity, indicating that bilirubin might be involved in the progression of stroke (Zhong et al., 2019; Song et al., 2022). Recently, however, there has been no definitive consensus on the relationship of bilirubin levels with stroke risk (Page et al., 2021). In addition, few studies have concentrated on direct or indirect bilirubin, limiting the explanation of the relation between stroke and bilirubin of various types. Therefore, this study aimed to systematically update the meta-analysis to investigate the connection between the different bilirubin subtypes and the risk as well as the prognostic outcome of stroke.

Materials and methods

This study was registered on the PROSPERO (register number: CRD42022374893) and was conducted following the Preferred Reporting Items for Systematic review and Meta-analyses (PRISMA) guidelines (Page et al., 2021).

Search strategy

The electronic databases of PubMed, EMBASE, and Cochrane Central were searched till 25 August 2022, using a string of keywords that are related to bilirubin (such as "bilirubin" or "BIL") and stroke (such as "stroke," "cerebral infarction"). No language restrictions have been established within the research strategy. The search strategy in detail was shown in **Supplementary Table 1**. To avoid the absence of documentation, manual searches were also carried out from the reference lists of all included articles and previous meta-analyses.

Selection criteria

Inclusion criteria for included studies are as follow: (1) observational studies, including cohort studies, case-control studies, and cross-sectional studies; (2) the relationship between circulating total bilirubin level, direct bilirubin level, or indirect bilirubin level and stroke risk was investigated; and (3) reporting hazard ratio (HR), relative risk (RR), or odds ratio (OR) with the corresponding confidence intervals (CI) for stroke risk or other poor clinical outcomes, or reporting mean differences of concentrations for various bilirubin subtype between stroke patients and control group at discharge or follow-up. Exclusion criteria are as follows: (1) the study did not provide complete effect estimates or data were not available, including conference abstract, data cannot be transformed to standard format or blending stroke data with other cardiovascular diseases, and (2) articles not published in English. Screening of relevant articles to identify eligible studies for inclusion was performed separately by two investigators, and disagreements were resolved through discussion.

Data extraction

The primary outcome was the occurrence risk of ischemic stroke or all stroke subtypes. The secondary outcome was the occurrence of poor outcomes [modified Rankin score (mRS) >2, National Institutes of Health Stroke Scale (NIHSS) ≥ 8] and the mean difference in bilirubin levels between patients with or without stroke. Two researchers independently reviewed the full text of potential included studies to extract pertinent information as follow: first author, location, age, gender, sample size, cases size and definition criteria, study design, sample nature, source, category of exposure (total, direct, or indirect bilirubin) and determination method, adjusted confounding factors, and outcome with summary statistics. The disagreements in this process were reviewed by discussion.

Quality assessment

The Newcastle-Ottawa Scale (NOS) criteria was used to perform quality assessment for cohort studies and case-control studies (Wells et al., 2022). For cross-sectional studies, quality assessment using the Agency for Healthcare Research and Quality (AHRQ) criteria (Rostom et al., 2004). Disagreements about methodological quality were addressed through discussion and mutual consultation. Overall, scores of six or more were rated as being of good quality.

Statistical analysis

The impact of bilirubin subtypes levels on all stroke or ischemic stroke risk was assessed using OR with corresponding 95% CI, and HR or RR was directly converted into OR. Because statistical results were reported in distinct ways among different studies (OR per quartile, per quintile or per 1-unit increment in the continuous bilirubin traits), the results were first transformed into the OR between the highest and lowest levels (reference group) for each study. Individual adjusted OR and 95% CI were preferentially estimated for pooling. For studies that investigated the difference in bilirubin subtype levels between stroke patients and the control group, we pooled the mean differences by meta-analysis. All units

were converted to μmol/L and 1 mg/L total bilirubin equal to 17.1 μmol/L if not consistent.

Heterogeneity between the studies was estimated using the Cochran Q test and statistical method I^2, and low, moderate and high levels of heterogeneity were cut-off with the values of 25, 50, and 75%, respectively (Higgins et al., 2003). Due to the variation in study characteristics, we assumed that the actual effect size may vary from study to study as the existence of clinical heterogeneity, random-effects model of DerSimonian and Laird method were determined to perform meta-analysis (DerSimonian and Laird, 1986). Pre-established subgroup analyses of study design, gender, and bilirubin subtypes were conducted. Sensitivity analysis was conducted by omitting one study by turns to examine the robustness of pooled risk estimates. If the number of studies included for the outcome indicators exceeds 10, the funnel plot and egger test are used for qualitative and quantitative testing of publication bias. Statistical analyses were performed using STATA version 17.0. Two-sided P-values below 0.05 were considered statistically significant.

Certainty of evidence assessment

The Grading of Recommendations Assessment, Development and Evaluation (GRADE) approach which graded the evidence as "high," "moderate," "low," or "very low" was used to assess the certainty of the evidence (Guyatt et al., 2011).

Results

Study identification and selection

The searching and screening process of the included studies are shown in **Figure 1**. The initial search included 5,030 potential studies from databases (PubMed, EMBASE, and Cochrane Library). After the exclusion of duplicates and irrelevant studies, 33 reports were left for retrieval. After the full-text search, 17 studies were included in the final meta-analysis (Perlstein et al., 2008; Pineda et al., 2008; Kimm et al., 2009; Ekblom et al., 2010; Luo et al., 2012; Oda and Kawai, 2012; Xu et al., 2013; Jørgensen et al., 2014; Li et al., 2014, 2020; Mahabadi et al., 2014; Zhou et al., 2014; Kunutsor et al., 2015; Lee et al., 2017; Marconi et al., 2018; Liu et al., 2020; Peng et al., 2022; **Figure 1**).

Study characteristics

Table 1 lists study-level characteristics and shows the quality assessment score of included studies. Seventeen studies between 2008 and 2022 were included, including 7 prospective cohort studies (Kimm et al., 2009; Ekblom et al., 2010; Luo et al., 2012; Mahabadi et al., 2014; Kunutsor et al., 2015; Lee et al., 2017; Marconi et al., 2018), and 10 cross-sectional studies (Perlstein et al., 2008; Pineda et al., 2008; Oda and Kawai, 2012; Xu et al., 2013; Jørgensen et al., 2014; Li et al., 2014, 2020; Zhou et al., 2014; Liu et al., 2020; Peng et al., 2022). The sample size varied between 316 and 96,381, involving a total of 12,081 stroke patients. Three studies presented their respective findings for men and women (Kimm et al., 2009; Ekblom et al., 2010; Oda and Kawai, 2012). Based on the NOS criteria, all studies are of good quality.

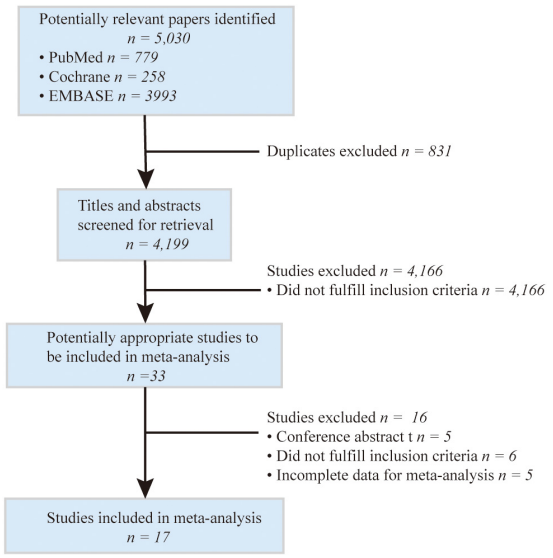

FIGURE 1
PRISMA Flow chart of the study collection for the present review and meta-analysis.

Primary outcome

Twelve included studies examined the association of total bilirubin level with stroke, **Figure 2** shows the adjusted ORs for each study and the pooled OR with the highest vs. lowest bilirubin level groups. Heterogeneity ($I^2 = 80.56\%$, $P < 0.01$) was observed and compared to the group at the lowest bilirubin level group, the risk of stroke was significantly lower among participants at the highest bilirubin level (OR = 0.71, 95% CI: 0.61–0.82, $P < 0.01$). Similarly, the random-effect model analysis comparing ischemic risk and total bilirubin level quartiles showed a significant inverse association, with a pooled effect OR of 0.72 (95% CI: 0.57–0.91, $P = 0.01$, **Figure 3**) and a high degree of heterogeneity ($I^2 = 87.17\%$, $P < 0.01$). Sensitivity analysis revealed no apparent influence of an individual study on the results of meta-analysis for all types of stroke (**Supplementary Figure 1**). However, when the Marconi et al. (2018) study was excluded, the findings did not reveal any significant association with the risk of ischemic stroke (OR = 0.73, 95% CI: 0.51–1.03, $P = 0.07$), implying that the pooled risk estimates were not robust (**Supplementary Figure 2**). No studies were conducted on the relationship between direct or indirect bilirubin levels and the risk of stroke or ischemic stroke.

Secondary outcome

Nine studies reported the differences in different bilirubin types level between stroke patients and the control group. Six studies showed that the group of stroke patients had a significantly

TABLE 1 The characteristic of included studies.

References	Country	Design	Sample size	Age (years)	Male (%)	Cases	Category of exposure	Exposure level	Adjustment	Outcome	Study quality (NOS/AHRQ)
Perlstein et al., 2008	USA	Cross-sectional	13,214	≥20	48.1	453, AS	Total bilirubin	Highest: 0.8–12.9 Lowest: 0.1–0.5	Age, sex, race/ethnicity, smoking, hypertension, total to HDL cholesterol ratio, and diabetes	Stroke prevalence and adverse stroke outcomes	7
Pineda et al., 2008	USA	Cross-sectional	743	67.5 ± 16.6	47.60	743	Direct (Dbil) bilirubin	Highest: ≤0.1 mg/dl Lowest: ≥0.4 mg/dl	Sex, serum glucose, prior antithrombotic use, hypertension, atrial fibrillation, and mRS scores	Adverse stroke outcomes (NIHSS > 12)	9
Kimm et al., 2009	Korea	Prospective cohort	78,724	30–89	52.15	1,964 1,189 473	Total bilirubin	Highest: 22.2–34.2 Lowest: 0–10.2	Age, smoking (nonsmoker, ex-smoker, and current smoker), alcohol (yes or no), exercise (yes or no), ALT, GGT, total cholesterol, type 2 diabetes, and hypertension	Stroke prevalence	9
Ekblom et al., 2010	Sweden	Prospective cohort	693	25–74	55	231	Total bilirubin	Unclear	Age, BMI, systolic blood pressure, smoking, apolipoprotein B/A1, diabetes and hsCRP	Stroke prevalence	7
Luo et al., 2012	China	Prospective cohort	531	67.00 ± 12.9	63.5	531	Total bilirubin Direct (Dbil) bilirubin	Highest: ≥22.2 Lowest: 0–10.2 Highest: ≥6.84 Lowest: 0–3.42	BG, TC, HDL-C, hypertension, AF, sex, and age	Adverse stroke outcomes (NIHSS ≥8)	9
Oda and Kawai, 2012	Japan	Cross-sectional	5,444	> 18	62	92	Total bilirubin	Highest: 17.9–71.8 Lowest: 2.6–9.3	Age, aspartate aminotransferase, alanine aminotransferase, γ-glutamyl transferase, current smoking, physical activity, and everyday drinking	Stroke prevalence	6
Xu et al., 2013	China	Cross-sectional	2,361	NS	63.2	2,361	Total bilirubin Direct bilirubin	Highest: 18.0–88.0 Lowest: 1.0–10.0 Highest: 4.2–37 Lowest: 0.4–2.0	Age, sex, alcohol consumption, cigarette smoking, blood levels of glucose and lipids, admission SBP and DBP, blood urea nitrogen, serum creatinine, sodium, hematocrit, history of stroke, hypertension, diabetes, coronary heart disease, rheumatic heart disease, and atrial fibrillation, family history of stroke, hypertension, and diabetes	Adverse stroke outcomes (NIHSS ≥10)	8
Jørgensen et al., 2014	16 countries	Cross-sectional	9,742	≥55	57.4	221	Total bilirubin	Highest: > 13 Lowest: ≤8	Sex, age, and sibutramine/placebo	Stroke prevalence	8
Li et al., 2014	China	Cross-sectional	2,856	30–69	63.9	343	Total bilirubin	Highest: > 13.9 Lowest: ≤7.8	Sex, BMI, smoking status, DBP, LDL-C, FPG, eGFR, TB, DM, and baPWV	Stroke prevalence	8
Mahabadi et al., 2014	Germany	Prospective cohort	3,553	45–75	44	95	Total bilirubin	/	Age, gender, BMI, systolic blood pressure, LDL, HDL, antihypertensive medication, lipid-lowering medication, diabetes, smoking status, and CAC score	Stroke prevalence	9

(Continued)

10.3389/fnins.2023.1122235

TABLE 1 (Continued)

References	Country	Design	Sample size	Age (years)	Male (%)	Cases	Category of exposure	Exposure level	Adjustment	Outcome	Study quality (NOS/AHRQ)
Zhou et al., 2014	China	Cross-sectional	1,098	>18	45.7	733	Total bilirubin	Highest: >12.99 Lowest: ≤9.58	Age, sex, and vascular risk factors	Stroke prevalence	8
Kunutsor et al., 2015	Netherlands	Prospective cohort	7,222	28–75	48.5	159	Total bilirubin	Per 1-SD higher	Age and sex, smoking status, history of diabetes, systolic blood pressure, total cholesterol, high-density lipoprotein cholesterol, and BMI, alcohol consumption, glucose, and triglycerides, γ-glutamyl transferase, and alanine aminotransferase	Stroke prevalence	9
Lee et al., 2017	Korea	Prospective cohort	5,599	>18	66.9	806	Total bilirubin		Age, sex, systolic blood pressure, fasting serum glucose, total cholesterol, high-density lipoprotein-cholesterol, and smoking status	Stroke prevalence	9
Marconi et al., 2018	USA	Prospective cohort	96,381	48 (mean)	97	2,112	Total bilirubin	Highest: ≥15.39 Lowest: ≤6.84	Age, sex, race-ethnicity, systolic blood pressure, smoking, diabetes mellitus, total cholesterol, high-density lipoprotein cholesterol, HIV, hepatitis C, liver fibrosis measured by FIB-4, alcohol abuse/dependence, cocaine, and obesity	Stroke prevalence	9
Li et al., 2020	China	Cross-sectional	610	66.7 (mean)	63.11	610	Total bilirubin	/	High density lipoprotein cholesterol, and triglyceride	Adverse stroke outcomes	9
Liu et al., 2020	China	Cross-sectional	316	70.36 ± 10.06	42.72	42	Total bilirubin	Highest: 34.15 ± 9.78 Lowest: ≤8.04 ± 2.03	Age, sex, body mass index, systolic blood pressure, the congestive heart failure, hypertension, age >75 years, diabetes, and previous stroke/transient ischemic attack score, left ventricular ejection fraction, left atrial diameter, alanine aminotransferase, aspartate aminotransferase, uric acid, total cholesterol, low-density lipoprotein cholesterol, high-density lipoprotein cholesterol, triglycerides, estimated glomerular filtration rate, heart failure, coronary artery disease, hypertension, diabetes, drinking, smoking, international standardized ratio value, and taking oral anticoagulant and antiplatelet drugs	Stroke prevalence	9
Peng et al., 2022	China	Cross-sectional	585	64.9 ± 12.2	66.5	585	Total bilirubin Direct bilirubin Indirect bilirubin		Age, sex, onset-time to treatment, admission glucose, admission ALT, admission AST, current smoking, alcohol drinking, history of stroke, cerebral hemorrhage, hypertension, diabetes mellitus, and hyperlipidemia, admission NIHSS score	Adverse stroke outcomes	8

10.3389/fnins.2023.1122235

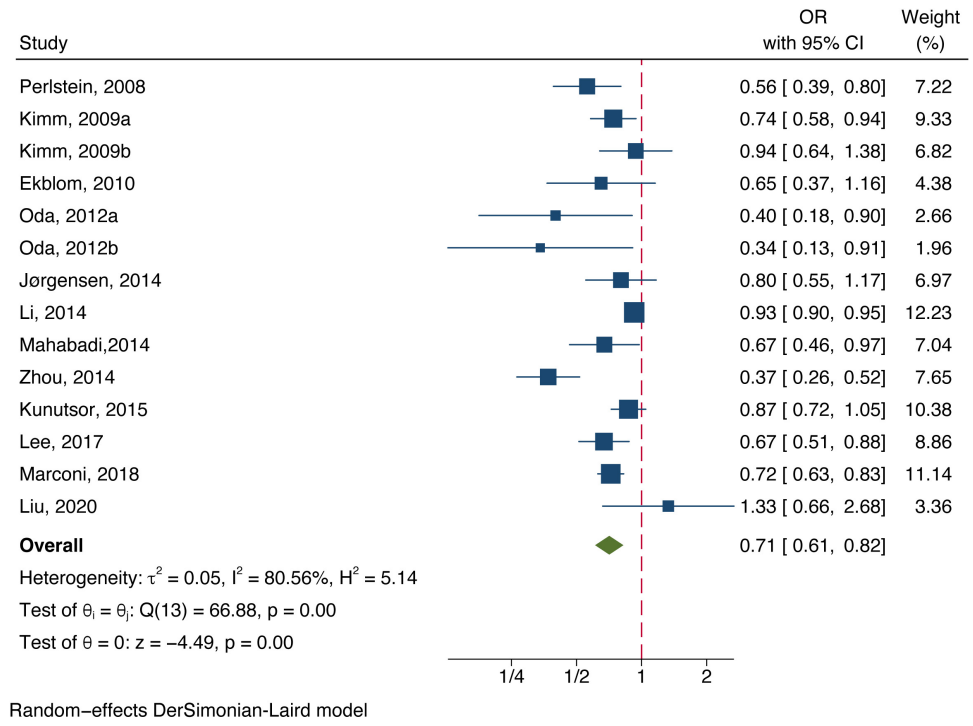

FIGURE 2
Forest plot of the association between total bilirubin level and stroke prevalence.

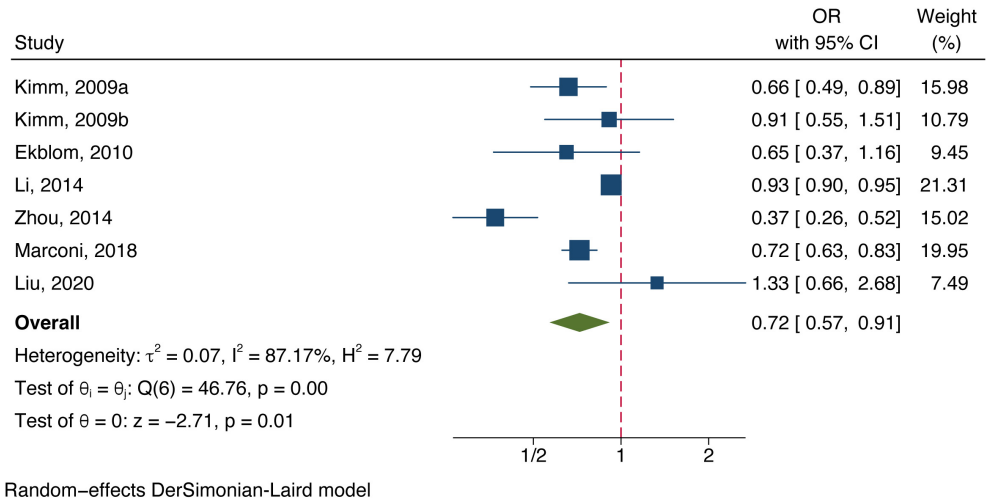

FIGURE 3
Forest plot of the association between total bilirubin level and ischemic stroke prevalence.

lower total bilirubin level (mean difference = −1.33 μmol/L, 95% CI: −2.12 to −0.53, $P < 0.01$, **Supplementary Figure 3**). Sensitivity analysis by omitting one study each time also revealed no evident influence on the pooled results (**Supplementary Figure 4**). Direct bilirubin and indirect bilirubin level did not show a significant difference due to the limited included studies (**Supplementary Figure 3**).

All included studies concentrated on associating bilirubin subtypes with ischemic stroke severity. Five data groups were obtained from four studies examining total bilirubin levels and the severity of ischemic stroke. [Three studies (Luo et al., 2012; Xu et al., 2013; Li et al., 2020) defined severe strokes as NIHSS score ≥8 and one study defined them as 3–6 in mRS (Peng et al., 2022).] The meta-analysis results showed a positive correlation between total bilirubin level and stroke poor outcome (OR: 1.13, 95% CI: 1.03–1.24) with a high degree of heterogeneity (I^2 = 86.45%) (shown in **Figure 4**). Six datasets of direct bilirubin from five studies were pooled, and the findings indicated that direct bilirubin level was also positively associated with the poor outcome of ischemic stroke (OR: 1.93, 95% CI: 1.43–2.61, and I^2 = 88.59%)

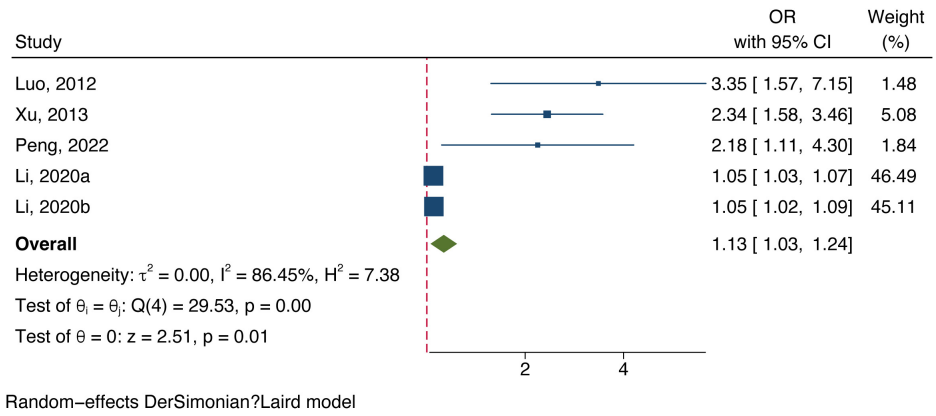

FIGURE 4
Forest plot of the association between total bilirubin level and ischemic stroke severity.

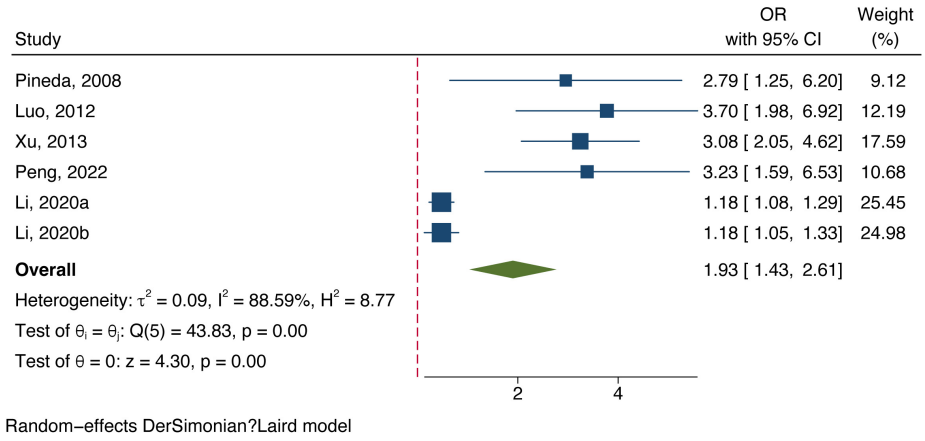

FIGURE 5
Forest plot of the association between direct bilirubin level and ischemic stroke severity.

(shown in Figure 5). Additionally, when we performed sensitivity analyses, the meta-analyses results were robust (Supplementary Figures 5, 6). Not enough data was collected because we could not pool the correlation between indirect bilirubin level and ischemic stroke severity.

Subgroup analysis

For the primary outcome, prespecified subgroup analyses by study design, gender, and location were performed (Table 2). The results showed less heterogeneity after being grouped by study design. No substantial heterogeneity was found among prospective cohorts ($I^2 = 0.00\%$) and pooled results for a significant relationship between stroke (OR: 0.75, 95% CI: 0.69–0.82) and ischemic stroke patients (OR: 0.72, 95% CI: 0.64–0.81). Three studies separately reviewed the relationship between total bilirubin level and stroke risk in males and females, respectively. Two of them examined the correlation between total bilirubin level and the risk of ischemic stroke. Interestingly, we observed a statistical association between a low risk of stroke or ischemic stroke with higher total bilirubin levels in the male population, but this statistical difference disappeared in females.

Publication bias

We tested the publication bias for the outcome of the correlation between total bilirubin level and stroke risk, and the *P*-values of the egger test were 0.08, indicating no inflation of effect sizes due to selective publication. The funnel plot was performed in Supplementary Figure 7.

GRADE assessment

The Supplementary Table 2 shows that the level of the evidence was graded as "low" owing to upgrade for dose-response and downgrades for inconsistency.

Discussion

To more comprehensively and accurately assess the influence of bilirubin subtype levels on stroke outcomes, we performed this comprehensive updated meta-analysis. The pooled results showed that bilirubin level was negatively associated with ischemic stroke

TABLE 2 Subgroup analysis of the correlation between bilirubin level and all stroke or ischemic stroke risk.

Subgroups	Stroke risk			Ischemic stroke risk		
	Number of groups of data	Pooled OR [95% CI]	Heterogeneity	Number of groups of data	Pooled OR [95% CI]	Heterogeneity
Study design						
Cohort	7	0.75 [0.69, 0.82]	$I^2 = 0\%, P = 0.49$	4	0.72 [0.64, 0.81]	$I^2 = 0\%, P = 0.74$
Cross-sectional	7	0.63 [0.43, 0.91]	$I^2 = 86.74\%, P < 0.01$	3	0.74 [0.37, 1.49]	$I^2 = 93.27\%, P < 0.01$
Gender						
Male	3	0.71 [0.55, 0.91]	$I^2 = 6.34\%, P = 0.34$	2	0.68 [0.52, 0.90]	$I^2 = 0\%, P = 0.61$
Female	3	0.55 [0.25, 1.18]	$I^2 = 65.87\%, P = 0.05$	2	0.64 [0.26, 1.54]	$I^2 = 61.61\%, P = 0.11$

OR, odds ratio; CI, confidence intervals.

and stroke risk after adjustment. Furthermore, a highly significant relationship was detected between total bilirubin levels or direct bilirubin levels and ischemic stroke severity. The sensitivity analysis provided additional insight into the robustness of the pooled risk estimates. Moreover, subgroup analyses by gender showed a statistical association between a low risk of stroke or ischemic stroke with higher total bilirubin levels in the male population, but this statistical difference disappeared in females. As a result, this meta-analysis confirms that bilirubin levels at the onset are a biomarker for improved diagnosis and prognosis in stroke patients.

The relationship between total bilirubin level and all types of stroke or ischemic stroke risk was consistent with previous studies (Zhong et al., 2019). Unlike it, we excluded Ren et al.'s (2016) study, because its outcome was cardiovascular disease, including prior coronary heart disease or peripheral arterial disease with stroke. However, it did not provide data on stroke separately, which will lead to biased results. In addition, we have added two new studies (Marconi et al., 2018; Liu et al., 2020) to confirm the link between bilirubin levels and stroke more comprehensively and accurately. It was worth mentioning that Liu's study reported that each 1 mmol/L increase in total bilirubin would increase the risk of first ischemic stroke in patients with non-valvular atrial fibrillation. The sensitivity analysis showed that this did not affect the robustness of the conclusion. Our meta-analysis observed a negative statistical association between ischemic stroke/stroke and total bilirubin level in the male population, but this statistical difference disappeared in females. These results were consistent with the study of Zhong and his colleagues (Zhong et al., 2019). The difference in bilirubin levels between gender might be attributed to differences in heme oxygenase, serum oestrogen, iron storage, and the influence of lifestyle (Zhong et al., 2019). Our subgroup analysis of prospective cohort studies indicated that total bilirubin level was inversely associated with the incidence of all stroke or ischemic stroke with low heterogeneity. This result again emphasized that bilirubin level was essential in developing stroke risk. However, the causal relationship needs to be confirmed by further cohort studies, as genetic evidence according to Mendelian randomization approaches did not suggest any causal effect of bilirubin levels on developing stroke in Koreans (Lee et al., 2017). Therefore, Mendelian randomization studies based on different races should also be carried out in the future to avoid ignoring some important information or leading to erroneous conclusions. In addition to diagnostic value, we investigated the prognostic value of bilirubin subtypes in ischemic stroke. Our results determined that the direct and total bilirubin levels were positively correlated with the ischemic stroke severity, consistent with the systematic review of Ghojazadeh et al.'s (2020) study and Song et al.'s (2022) study. Song et al. also established that bilirubin is linear with ischemic stroke severity and trial sequential analysis found that the sample size for this study is sufficient. A cross-sectional descriptive analysis conducted by Sagheb Asl et al. (2018) also showed that total, direct and indirect bilirubin levels was significantly associated with mortality in ischemic stroke patients. Total bilirubin and direct bilirubin may be critical endogenous antioxidants and their levels can reflect the stroke severity and can be used as an auxiliary indicator. Because of the limited number of studies, future investigations may explore the association between indirect bilirubin levels and stroke severity.

Ischemic stroke is characterized by a sudden loss of blood circulation in a focal area of the brain, preventing the proper delivery of glucose, oxygen, and nutrients, causing chemokines, cytokines, and reactive oxygen species (ROS) trigger inflammatory responses (Maida et al., 2020). ROS can stimulate many signal transduction pathways important for maintaining neuronal homeostasis, but the overproduction of ROS can induce structural and functional damage of neurons throughout the whole process of acute ischemic stroke, leading to brain injury (Niizuma et al., 2009). Bilirubin is an endogenous antioxidant that protects against the oxidation of low-density lipoprotein cholesterol, scavenging oxygen-free radicals boosting heme oxygenase activity and helping serum cholesterol to dissolve (Schwertner et al., 1994). Bilirubin contains an extended conjugated double bond system and a reactive hydrogen atom, which has strong antioxidant properties, thus preventing the generation of cellular ROS and the formation of atherosclerotic plaques (Vogel et al., 2017), thereby avoiding the onset of stroke; at the same time bilirubin can affect the inflammatory pathways by preventing the connection between C1q and immunoglobulins, significantly reduces the ability of complement to initiate through the traditional pathway, controlling the proliferation of T-regulatory cells (Tregs), modifies the activity of cytotoxic T-lymphocytes, blocking the production of pro-inflammatory cytokines, as the recruitment of pro-inflammatory cytokines is one of important factors in the formation of stroke (Thakkar et al., 2019); it can also resist myeloperoxidase-induced protein or lipid oxidation, scavenges hypochlorous acid, and prevents stroke (Boon et al., 2015). The exact mechanism linking direct bilirubin level to the high incidence of ischemic stroke remains unclear, and some possible explanations can be suggested. Direct bilirubin is more soluble in serum than the lipophilic indirect bilirubin, thus making direct bilirubin an active form

that is more readily available than indirect bilirubin (Hansen et al., 2020). Additionally, as a systemic disease, an elevated level of direct bilirubin may indicate the injury of hepatocytes (Sharma et al., 2021); therefore, the positive association of direct bilirubin levels with poor clinical outcomes might be due to the hepatic dysfunction. Future studies are required to demonstrate the specific differences in various bilirubin subtypes concerning their molecular mechanisms of action.

In summary, the relationship between bilirubin levels and stroke is complex. On the one hand, the production of bilirubin was physiologically enhanced in response to oxidative stress. When bilirubin level was upregulated through the stroke, we suppose it would play an important role. Additionally, strokes with higher severity are accompanied by higher levels of oxidative stress, which may also induce elevated anti-oxidative power reflected by the level of bilirubin (Domínguez et al., 2010). On the other hand, upregulated bilirubin can protect neurons against oxidation between a specific concentration range. At pathologic levels, bilirubin has been considered as a neurotoxic agent. Therefore, future studies can explore the impact of high-concentration bilirubin levels on the nervous system of stroke, so as to provide more decision-making suggestions for drug use.

This study is a meta-analysis of observational studies investigating the association between bilirubin levels of various subtypes and strokes from the most comprehensive literature research for now. The enrolled studies were analyzed according to the adjusted results. The limitations of this study also need to be recognized. Firstly, the substantial heterogeneity of included studies suggests that applicability of the results should be interpreted with caution. Secondly, the sample nature and the laboratory measurement method of bilirubin level were inconsistent, which may lead to some bias into the results. Thirdly, only a few studies in this meta-analysis have taken gender into consideration. As previous studies have revealed, the association between the bilirubin level and stroke risk was only confirmed in the males population using a gender stratified analysis, there is a lot of space remained to be explored in these results (Zhong et al., 2019). Fourthly, due to the limited number of studies, some outcomes have not enough power to be addressed in the clinical practice. More research is needed to investigate this relationship in the future. Lastly, hemorrhagic stroke is also a subtype of stroke, but only one showed that total bilirubin levels were not significantly associated with hemorrhagic stroke risk (Kimm et al., 2009). The relationship between bilirubin level and hemorrhagic stroke needs further investigation.

Conclusion

Although our findings suggested a negative association between total bilirubin levels and all stroke or ischemic stroke risk and a highly significant relationship between total/direct bilirubin levels and the severity of ischemic stroke, the existing evidence is inadequate to establish a definitive conclusion. More sophisticated prospective cohort studies and further analyses are required to further explain relevant issues.

Data availability statement

The original contributions presented in this study are included in this article/**Supplementary material**, further inquiries can be directed to the corresponding authors.

Author contributions

KZ and JBL contributed to the study design and data research. RW, RC, and JLL contributed to study selection and quality evaluation. KZ, RW, and KW contributed to statistical analysis. KZ, RC, JLL, QY, KW, and JBL contributed to drafting of the manuscript and language modification. All authors contributed to the article and approved the submitted version.

Funding

This work was supported by the Natural Science Foundation of Zhejiang Province, China (No. LGF20H170012), Scientific Research Project of Jiangsu Health Committee (No. H2019054), and the Xuzhou Science and Technology Planning Project (No. KC21220).

Acknowledgments

We thank Dr. Lu Zhang for the language polish.

Conflict of interest

The authors declare that the research was conducted in the absence of any commercial or financial relationships that could be construed as a potential conflict of interest.

Publisher's note

All claims expressed in this article are solely those of the authors and do not necessarily represent those of their affiliated organizations, or those of the publisher, the editors and the reviewers. Any product that may be evaluated in this article, or claim that may be made by its manufacturer, is not guaranteed or endorsed by the publisher.

Supplementary material

The Supplementary Material for this article can be found online at: https://www.frontiersin.org/articles/10.3389/fnins.2023.1122235/full#supplementary-material

References

Boon, A., Hawkins, C., Coombes, J., Wagner, K., and Bulmer, A. (2015). Bilirubin scavenges chloramines and inhibits myeloperoxidase-induced protein/lipid oxidation in physiologically relevant hyperbilirubinemic serum. *Free Radic. Biol. Med.* 86, 259–268. doi: 10.1016/j.freeradbiomed.2015.05.031

Campbell, B., and Khatri, P. (2020). Stroke. *Lancet* 396, 129–142. doi: 10.1016/S0140-6736(20)31179-X

DerSimonian, R., and Laird, N. (1986). Meta-analysis in clinical trials. *Control Clin. Trials* 7, 177–188. doi: 10.1016/0197-2456(86)90046-2

Domínguez, C., Delgado, P., Vilches, A., Martín-Gallán, P., Ribó, M., Santamarina, E., et al. (2010). Oxidative stress after thrombolysis-induced reperfusion in human stroke. *Stroke* 41, 653–660. doi: 10.1161/STROKEAHA.109.571935

Ekblom, K., Marklund, S., Johansson, L., Osterman, P., Hallmans, G., Weinehall, L., et al. (2010). Bilirubin and UGT1A1*28 are not associated with lower risk for ischemic stroke in a prospective nested case-referent setting. *Cerebrovasc. Dis.* 30, 590–596. doi: 10.1159/000319778

Ghojazadeh, M., Asl, E., Vahed, N., Hassanpour, R., Sanaie, S., Mahmoodpoor, A., et al. (2020). Determination of the predictive value of serum bilirubin in patients with ischemic stroke: A systematic review. *Arch. Neurosci.* 7, e99302. doi: 10.1186/s13054-016-1208-6

Guyatt, G., Oxman, A., Akl, E., Kunz, R., Vist, G., Brozek, J., et al. (2011). GRADE guidelines: 1. Introduction-GRADE evidence profiles and summary of findings tables. *J. Clin. Epidemiol.* 64, 383–394. doi: 10.1016/j.jclinepi.2010.04.026

Hansen, T., Wong, R., and Stevenson, D. (2020). molecular physiology and pathophysiology of bilirubin handling by the blood, liver, intestine, and brain in the Newborn. *Physiol. Rev.* 100, 1291–1346. doi: 10.1152/physrev.00004.2019

Higgins, J., Thompson, S., Deeks, J., and Altman, D. (2003). Measuring inconsistency in meta-analyses. *BMJ* 327, 557–560. doi: 10.1136/bmj.327.7414.557

Jørgensen, M., Torp-Pedersen, C., Finer, N., Caterson, I., James, W., Legler, U., et al. (2014). Association between serum bilirubin and cardiovascular disease in an overweight high risk population from the SCOUT trial. *Nutr. Metab. Cardiovasc. Dis.* 24, 656–662. doi: 10.1016/j.numecd.2013.12.009

Kimm, H., Yun, J., Jo, J., and Jee, S. (2009). Low serum bilirubin level as an independent predictor of stroke incidence: A prospective study in Korean men and women. *Stroke* 40, 3422–3427. doi: 10.1161/STROKEAHA.109.560649

Kunutsor, S., Bakker, S., Gansevoort, R., Chowdhury, R., and Dullaart, R. (2015). Circulating total bilirubin and risk of incident cardiovascular disease in the general population. *Arterioscler. Thromb. Vasc. Biol.* 35, 716–724. doi: 10.1161/ATVBAHA.114.304929

Lee, S., Jee, Y., Jung, K., Hong, S., Shin, E., and Jee, S. (2017). Bilirubin and stroke risk using a mendelian randomization design. *Stroke* 48, 1154–1160. doi: 10.1161/STROKEAHA.116.015083

Li, R., Cao, Z., Zhang, J., Li, Y., and Wang, R. (2014). Decreased serum bilirubin is associated with silent cerebral infarction. *Arterioscler. Thromb. Vasc. Biol.* 34, 946–951. doi: 10.1161/ATVBAHA.113.303003

Li, Z., Zhang, J., and Luo, Y. (2020). Impact of triglyceride playing on stroke severity correlated to bilirubin. *Medicine* 99, e21792. doi: 10.1097/MD.0000000000021792

Liu, Y., Wang, J., Zeng, W., and Lyu, Q. (2020). Nonlinear relationship between serum total bilirubin levels and initial ischemic stroke in patients with non-valvular atrial fibrillation. *J. Int. Med. Res.* 48:300060520962347. doi: 10.1177/0300060520962347

Luo, Y., Li, J., Lu, Z., Wang, C., Guan, D., and Xu, Y. (2012). Serum bilirubin after acute ischemic stroke is associated with stroke severity. *Curr. Neurovasc. Res.* 9, 128–132. doi: 10.2174/156720212800410876

Mahabadi, A., Lehmann, N., Möhlenkamp, S., Kälsch, H., Bauer, M., Schulz, R., et al. (2014). Association of bilirubin with coronary artery calcification and cardiovascular events in the general population without known liver disease: The Heinz Nixdorf Recall study. *Clin. Res. Cardiol.* 103, 647–653. doi: 10.1007/s00392-014-0697-z

Maida, C., Norrito, R., Daidone, M., Tuttolomondo, A., and Pinto, A. (2020). Neuroinflammatory mechanisms in ischemic stroke: Focus on cardioembolic stroke, background, and therapeutic approaches. *Int. J. Mol. Sci.* 21:6454. doi: 10.3390/ijms21186454

Marconi, V., Duncan, M., So-Armah, K., Re, V. III, Lim, J., Butt, A., et al. (2018). Bilirubin is inversely associated with cardiovascular disease among HIV-positive and HIV-negative individuals in VACS (Veterans Aging Cohort Study). *J. Am. Heart Assoc.* 7, e007792. doi: 10.1161/JAHA.117.007792

Niizuma, K., Endo, H., and Chan, P. (2009). Oxidative stress and mitochondrial dysfunction as determinants of ischemic neuronal death and survival. *J. Neurochem.* 109(Suppl. 1), 133–138.

Oda, E., and Kawai, R. (2012). A possible cross-sectional association of serum total bilirubin with coronary heart disease and stroke in a Japanese health screening population. *Heart Vessels* 27, 29–36. doi: 10.1007/s00380-011-0123-7

Page, M., McKenzie, J., Bossuyt, P., Boutron, I., Hoffmann, T., Mulrow, C., et al. (2021). The PRISMA 2020 statement: An updated guideline for reporting systematic reviews. *BMJ* 372, n71.

Peng, Q., Bi, R., Chen, S., Chen, J., Li, Z., Li, J., et al. (2022). Predictive value of different bilirubin subtypes for clinical outcomes in patients with acute ischemic stroke receiving thrombolysis therapy. *CNS Neurosci. Ther.* 28, 226–236. doi: 10.1111/cns.13759

Perlstein, T., Pande, R., Creager, M., Weuve, J., and Beckman, J. (2008). Serum total bilirubin level, prevalent stroke, and stroke outcomes: NHANES 1999-2004. *Am. J. Med.* 121, 781.e–788.e. doi: 10.1016/j.amjmed.2008.03.045

Pineda, S., Bang, O., Saver, J., Starkman, S., Yun, S., Liebeskind, D., et al. (2008). Association of serum bilirubin with ischemic stroke outcomes. *J. Stroke Cerebrovasc. Dis.* 17, 147–152. doi: 10.1016/j.jstrokecerebrovasdis.2008.01.009

Ren, Y., Jin, N., Hong, T., Mu, Y., Guo, L., Ji, Q., et al. (2016). Interactive effect of serum uric acid and total bilirubin for cardiovascular disease in Chinese patients with type 2 diabetes. *Sci. Rep.* 6:36437.

Rostom, A., Dubé, C., Cranney, A., Saloojee, N., Sy, R., Garritty, C., et al. (2004). *Celiac Disease*. Rockville, MD: Agency for Healthcare Research and Quality (US).

Sagheb Asl, E., Taheraghdam, A., Rahmani, F., Javadrashid, R., Golzari, S., Ghaemian, N., et al. (2018). Determination of the predictive value of serum bilirubin in patients with ischemic stroke: A prospective descriptive analytical study. *Adv. Pharm. Bull.* 8, 715–719. doi: 10.15171/apb.2018.080

Schwertner, H., Jackson, W., and Tolan, G. (1994). Association of low serum concentration of bilirubin with increased risk of coronary artery disease. *Clin. Chem.* 40, 18–23.

Sharma, K., Zajc, I., and Žiberna, L. (2021). Dietary vitamin D equilibrium in serum ameliorates direct bilirubin associated diabetes mellitus. *Chem. Biol. Interact.* 337:109399. doi: 10.1016/j.cbi.2021.109399

Song, Y., Zhang, X., Li, C., Xu, S., Zhou, B., and Wu, X. (2022). Is bilirubin associated with the severity of ischemic stroke? A dose response meta-analysis. *J. Clin. Med.* 11:3262.

Thakkar, M., Edelenbos, J., and Doré, S. (2019). Bilirubin and ischemic stroke: Rendering the current paradigm to better understand the protective effects of bilirubin. *Mol. Neurobiol.* 56, 5483–5496. doi: 10.1007/s12035-018-1440-y

Vogel, M., Idelman, G., Konaniah, E., and Zucker, S. (2017). Bilirubin prevents atherosclerotic lesion formation in low-density lipoprotein receptor-deficient mice by inhibiting endothelial VCAM-1 and ICAM-1 signaling. *J. Am. Heart Assoc.* 6:e004820. doi: 10.1161/JAHA.116.004820

Wells, G., Shea, B., O'Connell, D., Peterson, J., Welch, V., Losos, M., et al. (2022). *The Newcastle-Ottawa Scale (NOS) for Assessing the Quality of Nonrandomised Studies in Meta-Analyses*. Available online at: https://www.ohri.ca/programs/clinical_epidemiology/oxford.asp (accessed October 13, 2022).

Xu, T., Zhang, J., Xu, T., Liu, W., Kong, Y., and Zhang, Y. (2013). Association of serum bilirubin with stroke severity and clinical outcomes. *Can. J. Neurol. Sci.* 40, 80–84.

Zhong, P., Wu, D., Ye, X., Wang, X., Zhou, Y., Zhu, X., et al. (2019). Association of circulating total bilirubin level with ischemic stroke: A systemic review and meta-analysis of observational evidence. *Ann. Transl. Med.* 7:335. doi: 10.21037/atm.2019.06.71

Zhou, X., Wang, L., Liu, H., Zhang, C., Zhu, M., Zhu, X., et al. (2014). Serum antioxidant levels associated with subcortical ischemic vascular disease. *Can. J. Neurol. Sci.* 41, 375–381. doi: 10.1017/S0317167100017339

frontiers | Frontiers in Neuroscience

TYPE Review
PUBLISHED 15 February 2023
DOI 10.3389/fnins.2023.1125376

Check for updates

OPEN ACCESS

EDITED BY
Wen-Jun Tu,
Chinese Academy of Medical Sciences
and Peking Union Medical College, China

REVIEWED BY
Ekaterina Alexandrovna Rudnitskaya,
Institute of Cytology and Genetics (RAS), Russia
Zhen Yuan,
University of Macau, Macao SAR, China

*CORRESPONDENCE
Renjun Gu
✉ renjungu@hotmail.com
Geng Zhang
✉ zhg9355@126.com
Qing Lin
✉ linqing522@126.com

†These authors have contributed equally to this work and share first authorship

SPECIALTY SECTION
This article was submitted to
Neurodegeneration,
a section of the journal
Frontiers in Neuroscience

RECEIVED 16 December 2022
ACCEPTED 31 January 2023
PUBLISHED 15 February 2023

CITATION
Zhou Y, Wang X, Liu Y, Gu Y, Gu R, Zhang G and Lin Q (2023) Mechanisms of abnormal adult hippocampal neurogenesis in Alzheimer's disease.
Front. Neurosci. 17:1125376.
doi: 10.3389/fnins.2023.1125376

COPYRIGHT
© 2023 Zhou, Wang, Liu, Gu, Gu, Zhang and Lin. This is an open-access article distributed under the terms of the Creative Commons Attribution License (CC BY). The use, distribution or reproduction in other forums is permitted, provided the original author(s) and the copyright owner(s) are credited and that the original publication in this journal is cited, in accordance with accepted academic practice. No use, distribution or reproduction is permitted which does not comply with these terms.

Mechanisms of abnormal adult hippocampal neurogenesis in Alzheimer's disease

Yujuan Zhou[1†], Xu Wang[1†], Yingying Liu[2], Yulu Gu[1], Renjun Gu[3*], Geng Zhang[1,4*] and Qing Lin[1,4*]

[1]Key Laboratory of Brain Aging and Neurodegenerative Diseases, Fujian Medical University, Fuzhou, China, [2]Department of Physiology and Pathophysiology, Health Science Center, Peking University, Beijing, China, [3]School of Chinese Medicine and School of Integrated Chinese and Western Medicine, Nanjing University of Chinese Medicine, Nanjing, China, [4]Laboratory of Clinical Applied Anatomy, School of Basic Medical Sciences, Fujian Medical University, Fuzhou, China

Alzheimer's disease (AD) is a degenerative disease of the central nervous system, the most common type of dementia in old age, which causes progressive loss of cognitive functions such as thoughts, memory, reasoning, behavioral abilities and social skills, affecting the daily life of patients. The dentate gyrus of the hippocampus is a key area for learning and memory functions, and an important site of adult hippocampal neurogenesis (AHN) in normal mammals. AHN mainly consists of the proliferation, differentiation, survival and maturation of newborn neurons and occurs throughout adulthood, but the level of AHN decreases with age. In AD, the AHN will be affected to different degrees at different times, and its exact molecular mechanisms are increasingly elucidated. In this review, we summarize the changes of AHN in AD and its alteration mechanism, which will help lay the foundation for further research on the pathogenesis and diagnostic and therapeutic approaches of AD.

KEYWORDS

adult hippocampal neurogenesis, Alzheimer's disease, energy metabolism, epigenetics, neuroinflammation

1. Introduction

Alzheimer's disease (AD), also known as senile dementia, is a degenerative disease of the central nervous system with age-related cognitive and functional decline that can eventually lead to death, with an insidious onset and a chronic progressive course, and is the most common type of dementia in old age (Alzheimer's Association, 2019). The main pathological manifestations of AD are amyloid β-protein (Aβ) deposition, neurogenic fiber tangles due to Tau protein hyperphosphorylation, and neuronal loss (Lei et al., 2021). The clinical manifestations of AD patients are characterized by comprehensive dementia, such as memory impairment, aphasia, loss of use, loss of recognition, impairment of visuospatial skills, executive dysfunction, and personality and behavioral changes. Mild cognitive impairment is the precursor stage of dementia, characterized by subjective cognitive deficits and objective memory impairment in daily life (Xie et al., 2021). Patients have difficulties in reasoning, abstract concepts, and even language difficulties. And, patients may also experience increased manifestations of depression, sleep difficulties and anxiety. According to the Alzheimer's Disease International assessment, 75% of people with dementia worldwide are undiagnosed, and it can be as high as 90% in

some low- and middle-income countries. Based on the latest data from the World Health Organization, the number of people suffering from dementia is estimated to be 55 million in 2019 and expected to increase to 139 million in 2050 (Gauthier et al., 2022). Therefore, it is crucial to study the pathogenesis of AD to find diagnostic methods and the treatment strategies.

In-depth studies of postmortem AD patient brains or transgenic AD mouse models have shown that the neuropathology of AD brain is mainly characterized by neuronal cell death, aggregation of neurogenic fiber tangles and formation of neural plaques (Kou et al., 2020; Rahman et al., 2020). Of these, the aggregation of plaques and fiber tangles in the hippocampus are closely associated with cognitive decline. Unlike other brain regions, the adult mammalian hippocampus contains Neural Stem Cells (NSCs), which can generate new neurons, a process known as Adult Hippocampal Neurogenesis (AHN) (Babcock et al., 2021).

For decades, it was widely believed that the death and loss of neurons was permanent and irrecoverable. However, thanks to continuous efforts in the field of neuroscience, it is now generally accepted that certain areas of adult human brain do undergo neurogenesis during a long lifetime (Kumar et al., 2019), which can produce new functional neurons. The Subgranular Zone (SGZ) in the dentate gyrus (DG) portion of the hippocampus is one of the sites where neurogenesis exists in adult human brain, a process known as AHN. Most NSCs in the adult brain are quiescent and are not active in proliferating, whereas NSCs in the SGZ and the Subependymal Ventricular Zone (SVZ) have the ability to self-renew, divide and differentiate into mature granule neurons (Imayoshi et al., 2008).

AHN is a complex process with multiple steps (**Figure 1**), including (1) Neural Precursor Cells (NPCs) in the SGZ, origin of neurons, divide to be new NSCs or neural progenitor cells; (2) Both NSCs and neural progenitor cells have the ability to proliferate and differentiate into new neurons; (3) Newborn neurons go into the granule cell layer to grow axons and dendrites, eventually connecting with the internal olfactory cortex and hippocampus and integrating into the hippocampal network (Kempermann et al., 2003, 2015; Babcock et al., 2021; Gillotin et al., 2021).

Long-term studies in rodents show that the proportion of NSCs dividing actively in DG region becomes less with age, indicating that neural regeneration declines significantly with age. Like rodents, hippocampal neurogenesis in humans persists with age, but the amount of neurons decreases significantly (Boldrini et al., 2018).

Sustained hippocampal neurogenesis in adults is important for neuronal plasticity, learning and memoring, and emotion regulation, and therefore the importance and relevance of AHN in AD cannot be overstated (Kempermann et al., 2018). In this review, we will summarize the changes of AHN in AD and its alteration mechanisms, laying the groundwork for further investigation into the pathogenesis and diagnostic approaches of AD.

2. Altered adult hippocampal neurogenesis in Alzheimer's disease

Although AHN still exists, its regeneration will decrease with age (Boldrini et al., 2018). As for AD patients, "what is the status of the AHN?" During a long period of research, different voices appeared.

2.1. The increase of AHN

More than a decade ago, studies on the effects of AHN in AD mostly based on the brains of deceased AD patients and AD mice model. These findings showed an increase of AHN in the older AD patients, based mainly on the upregulation of the expression of the neuronal markers DCX, neurogenic differentiation factor TUC4 and PSA-NCAM (Jin et al., 2004b). Scientists believe that such an increase of AHN is a compensatory mechanism overcoming neuronal damage due to neurodegeneration (Boekhoorn et al., 2006). To study the occurrence and development of AD, hundreds of AD animal models are available for scientific research. Studies have shown that an increase of AHN in $APP_{Sw,Ind}$ AD model mice (Jin et al., 2004a). In addition, increased neurogenesis has been observed in PS-1 overexpressing and APP/PS1 double transgenic AD mice with disease progression (Zeng et al., 2016).

2.2. The decrease of AHN

However, with our deep understanding of the pathogenesis of AD disease and brain networks, different research results have been presented. Comparison between NSCs in brain tissue of AD deaths and that of the control group found that the AD group's cell survived less, or failed prematurely (Lovell et al., 2006). Even at early stages of Braak staging, when the levels of Aβ and neurogenic fiber tangles accumulation were low, the expression of DCX, SOX2, and MAP2A in the hippocampus were decreased dramatically in AD patients compared with the control group, indicating downregulation of hippocampal neurogenesis (Li et al., 2008; Crews et al., 2010). Mushashi is an evolutionarily conserved RNA-binding protein and stem cell marker that regulates neurogenesis by altering the balance of self-renewal and differentiation (Velasco et al., 2019). When Mushashi and Ki-67 were used as markers in the AD patients, it is found that the number and viability of neural progenitor cells in SVZ were reduced significantly (Ziabreva et al., 2006; Velasco et al., 2019). And a cross-sectional study of several AD patients aged 52–97 found that a relative decline in the number of immature neurons at all stages, compared to healthy older adults. In particular, although DCX-positive cells decreased with age, the decline in AD patients was more severe (Moreno-Jiménez et al., 2019; Tobin et al., 2019). In the study of AD animal models, the SGZ and SVZ regions of 3xTg mice showed significantly impaired neurogenesis, with a 63% decrease in hippocampal neural stem cell proliferation at the age of 4 months and almost no new neurons at the age of 12 months (Rodríguez et al., 2008, 2009; Hamilton et al., 2015). For 5xFAD mice, DCX positive expression in the hippocampal region began to decline at the age of 2 months, and was almost undetectable by the age of 7 months, indicating reduced hippocampal neurogenesis in the mice (Moon et al., 2014).

The differences in findings for AD patients may be due to limitations in sample size or individualized differences that may be accompanied by other diseases. The contradiction between different genotypes of mice may also be the result of the way in which the model mice are induced leading to their different effects on AHN. However, some studies show that for the early stages of AD pathological development, the immune system in the brain still plays a role in improving the microenvironment of the brain by removing cellular debris, which favors AHN. Whereas, as AD

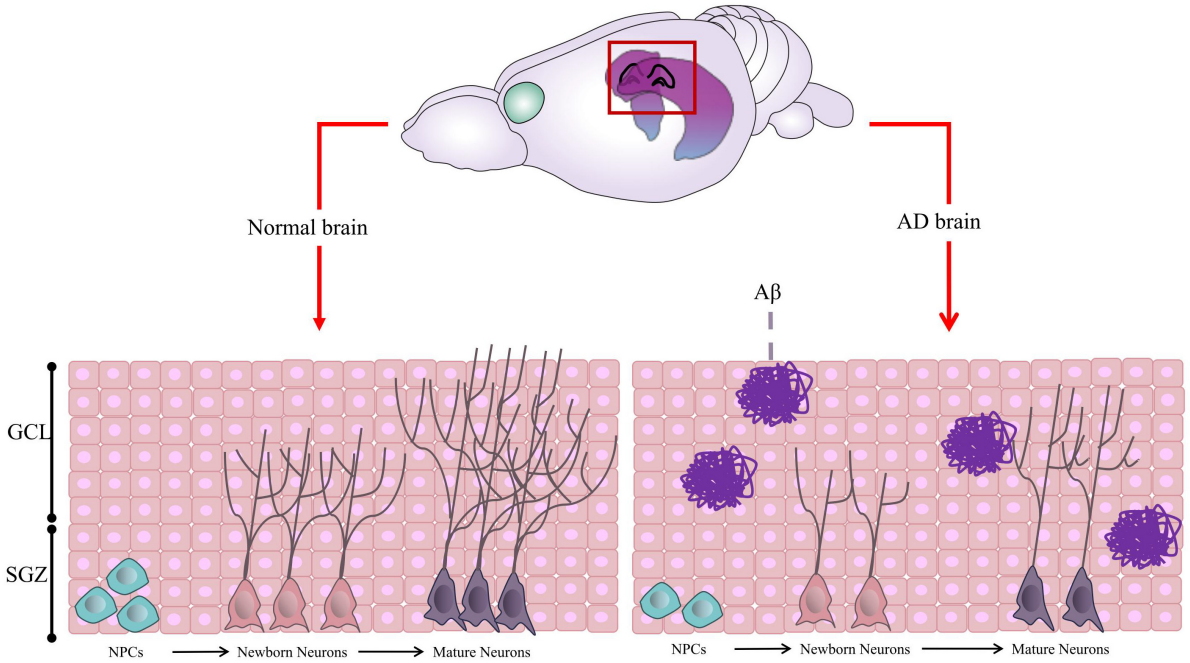

FIGURE 1
Graphic illustration of Adult Hippocampal Neurogenesis (AHN). In normal brain, the neural precursor cells (NPCs) located in the Subgranular Zone (SGZ) proliferate and differentiate to form neural progenitor cells or neuroblasts, which further differentiate into new neurons. The newborn neurons continue to migrate, proliferate, develop axons and dendrites, become mature neurons, and integrate into the hippocampal network. However, in AD brain, the proliferation and differentiation of neurons are inhibited due to Aβ aggregation and other factors in most cases. Some of this illustration was started from a Scidraw Template.

TABLE 1 Summary of adult hippocampal neurogenesis in AD patients and model mice.

Sample		Group	Changes in AD hippocampal structure	Neurogenesis marker expression	References
AD patients		Control (n = 11),AD (n = 14)	The number of new neurons in CA1 region increased	DCX↑,PSA-NCAM↑	Jin et al., 2004b
		Control (n = 10),AD (n = 9)	The cross-sectional area of CA1 and CA2 zones decreased	Ki67↑,GFAP↑	Boekhoorn et al., 2006
		Control (n = 15),AD (n = 14)	—	MAP2a/b↑,	Li et al., 2008
		Control (n = 5),AD (n = 14)	—	DCX↓,SOX2↓	Crews et al., 2010
		Control (n = 7),AD (n = 7)	Neural progenitor cells in SVZ region were significantly reduced	Musashi1↓,Nestin↑	Ziabreva et al., 2006
AD models	APPTg mice	n = 4	Dense amyloid deposits	BrdU↓,DCX↓,SOX2↓	Crews et al., 2010
	Tg2576 mice	—	—	BrdU↓,DCX↓	Krezymon et al., 2013
		—	—	BrdU↓,DCX↓,NeuN↓	Li et al., 2015
	$APP_{Sw,Ind}$ mice	—	—	BrdU↑,DCX↑	Jin et al., 2004a
	PS1 mice	—	—	BrdU↓,NeuN↓	Wang et al., 2004
		—	—	BrdU↓,Calretinin↓	Wen et al., 2004
	3xTg mice	n = 3∼7	New neurons appear in the dentate gyrus	HH3↓	Rodríguez et al., 2008
		—	—	DCX↓,Ki67↓,GFAP↓	Hamilton et al., 2015
	5xFAD mice	—	—	DCX↓,HH3↓,Calretinin↓	Moon et al., 2014
		Tg (n = 12),non-Tg (n = 12)	—	Ki67 (—),DCX↓	Zaletel et al., 2018
		—	—	DCX↑,Ki67↑	Ziegler-Waldkirch et al., 2018
	APP/PS1 mice	—	—	BrdU↓,DCX↓	Demars et al., 2010
		—	—	BrdU↓,Nestin↓	Zeng et al., 2016
		—	—	BrdU↓,DCX↓	Demars et al., 2010

DCX, doublecortin; PSA-NCAM, polysialated form of neural cell adhesion molecule; Ki67, proliferative marker; GFAP, glial fibrillary acidic protein; SOX2, SRY (sex determining region Y)-box 2; BrdU, 5-Bromodeoxyuridine; HH3, Histone H3.

disease progresses, the inflammatory response in the brain increases, exacerbating neurotoxicity and decreasing AHN levels (Song et al., 2012; Gray et al., 2020).

In summary, the AHN shows different degrees of changes during the development of AD disease (**Table 1**). The underlying mechanisms of AHN alteration have also been studied more extensively.

3. Key mechanisms of altered AHN in Alzheimer's disease

Among the major pathogenesis of AD, one of the important hypotheses is the amyloid hypothesis, which states that there is an abnormal accumulation of Aβ in the brain tissue. These peptides are neurotoxic and eventually lead to neuronal death and degeneration, with the hippocampus being the "hardest hit" area (Santin et al., 2011). The hippocampus is the main area where adults continue to produce new neurons. This AHN is closely related to memory, learning, and cognitive abilities in AD patients. With the increasing number of studies on the mechanisms of hippocampal neurogenesis, more is known about how ANH plays its role during the development of AD disease.

3.1. Energy metabolism

3.1.1. Glycolysis

Glucose is the only source of energy in the brain. When the utilization of glucose in the brain is impaired, the function of brain will be affected to a large extent (Vercruysse et al., 2018). In a healthy brain, glucose metabolism is an important source of energy for neurons. And when glucose utilization in the brain decreases, so does human cognitive ability (Tingley et al., 2021). In total, 30% of glucose used by the human brain is aerobic glycolysis (Magistretti and Allaman, 2015). Astrocytes are the most abundant cell type and major consumer of glucose in the central nervous system (CNS). Glycolysis and lactate production are metabolic features of astrocytes, while neurons meet their energy requirements mainly through oxidative phosphorylation (Bélanger et al., 2011; Magistretti and Allaman, 2015). Aerobic glycolysis of astrocytes provides important nutritional support for CNS neurons. It has been shown that SNX27^{R196W} (equivalent to human R198W) attenuates glucose uptake by astrocytes *via* Glucose Transporter 1 (GLUT) in mice, and causes a decrease in lactate production and deficits in synaptic function and learning behavior (Zhang et al., 2022).

NSCs in the SVZ and SGZ regions undergo various stages in the process of differentiation into mature neurons. In this process, stem cells rely on glycolytic metabolism rather than mitochondrial oxidative phosphorylation (Folmes et al., 2011). Mitochondria manage metabolites and the epigenetic state of NSCs, regulating the differentiation process of NSCs during AHN (Khacho et al., 2019). In AD, excessive aggregation of Aβin the brain induces mitochondrial dysfunction in neural progenitor cells and inhibits the differentiation of newborn neurons by reducing glucose utilization, leading to AHN dysregulation (Kim et al., 2022). In addition, abnormal insulin metabolism is another essential feature of AD, and insulin resistance mainly affects glucose metabolism of the brain in the hippocampus (Watson and Craft, 2003). The reduction of glucose transport and uptake may be caused by GLUT deficiencies. The GLUTs distributed in the brain are mainly GLUT1 and GLUT3, with GLUT1 involved in glucose transport to brain glial cells and GLUT3 transporting glucose to neurons. It has been demonstrated that metformin can normalize glucose transport and uptake in the brain by inhibiting the activity of GSK-3βand increasing the expression of GLUT1 and GLUT3 to promote neuronal regeneration and prevent neuronal damage (Pilipenko et al., 2020).

3.1.2. Lactate metabolism

In addition to important substrates of energy metabolism such as glucose and ketone bodies that provide energy to the brain, lactate metabolism also plays a crucial role in memory. Under high energy demand, lactate is involved in regulating neurogenesis-related processes such as angiogenesis, neuronal excitability and plasticity. Moreover, lactate is also involved in regulating the metabolism and signaling pathways of non-neural cells in the neurogenic microenvironment, such as endothelial cells, oligodendrocytes, microglia and astrocytes (Matsui et al., 2017; Lev-Vachnish et al., 2019). Among the large number of metabolites consumed by oligodendrocytes, in addition to glucose, there is also important lactate, which is used for myelin formation or myelin repair after demyelination injury to promote axonal integrity. Furthermore, the addition of lactate under low glucose conditions can rescue oligodendrocyte lineage cells and promote their myelin formation. It has been suggested that oligodendrocyte dysfunction and early demyelination in APP/PS1 mice may accelerate the progression of AD disease (Ichihara et al., 2017). And lactate treatment produces more myelin compared to glucose, suggesting that oligodendrocytes may be more dependent on lactate as a substrate for myelin production (Rinholm et al., 2011). Some studies have shown that when demyelinating lesions occur in mice, the expression of p-CREB and BDNF will be significantly reduced, further affecting the development of mature neurons in mice, and damaging AHN (Hahn et al., 2022).

Lactate metabolism in the CNS is categorically inseparable from the process of exploring lactate transport, and there are 1–14 isoforms of Monocarboxylate Transporter (MCT), which are distributed in different cells and play different roles. In the central nervous system, MCT1, MCT2, and MCT4 facilitate lactate transport between nerve cells (Pierre et al., 2000). Lactate transport is required for memory formation and synaptic transmission in the hippocampus. When MCT transport is dysfunctional, it may lead to impaired lactate transport, which in turn hinders energy metabolism and causes memory impairment (Nagase et al., 2014). In endothelial cells, the PI3K/AKT pathway regulates MCT-1 expression and subsequent lactate transport, and the transported lactate activates HCAR1 on astrocytes to regulate vascular endothelial growth factor (VEGF) levels, thereby enhancing angiogenesis and promoting AHN. Thus, abnormal lactate accumulation in the hippocampus disrupts AHN and impairs learning and memory functions (Scandella and Knobloch, 2019). According to the astrocyte-neuron lactate shuttle hypothesis, astrocytes promote glucose consumption or glycogen breakdown to enhance lactate production, which is then transported to neurons *via* MCT to support neuronal activity. In AD, the astrocyte's ability to take up glucose is diminished and lactate production is reduced, which affects the subsequent neuronal regeneration process (Nicola and Okun, 2021). In the course of neuroinflammation, MCT1 dysfunction and changes in lactate levels affect the pro-inflammatory response of microglia. Microglia

can phagocytose and remove apoptotic cells, including neoplastic neurons through phagocytosis to further balance the proliferation and survival of neoplastic neurons (Kong L. et al., 2019).

A growing body of research suggests that voluntary physical exercise can upregulate specific neurotransmitters levels in the brain, including the brain-derived neurotrophic factors (BDNF) and VEGF, and increase adult hippocampal neurogenesis, in which lactate plays an important role (Vivar and van Praag, 2017). During physical exercise, lactate concentration in the blood increases, which facilitates neuronal differentiation and survival of newborn neurons (Lev-Vachnish et al., 2019). But how this relationship develops in AD requires further research.

3.1.3. Lipids metabolism

Extracellular aggregation of neuritic plaques and intracellular aggregation of neurofibrillary tangles are histopathological hallmarks of AD and are closely associated with synaptic defects and neurodegeneration (Yamaguchi et al., 1991). Amyloid Precursor Protein (APP) is sheared by β-secretase and γ-secretase to form Aβ fragments, which form neuritic plaques in the brains of AD patients. Both β-secretase and γ-secretase are intact lipoproteins, and their action depends mainly on the level of lipids present in the membrane (Campos-Peña et al., 2022). Evidence suggests that AHN disorders caused by lipid metabolism disorders make patients more susceptible to AD. Monoacylglycerol lipase (Mgll), a hydrolase that breaks down endogenous fats, is now considered a potential target for AD. It was demonstrated that in postmortem AD patients and 3xTgAD mouse models, there is an age-dependent induction of Mgll due to diminished aPKC-CBP signaling, thereby reducing neuronal production in the brains of AD patients and impairing their cognitive function (Syal et al., 2020).

It is well known that cholesterol is the main protein required to maintain the dynamic homeostasis of cell membranes, and the brain is the organ with the highest cholesterol content. It has been demonstrated that cholesterol homeostasis affects the production of amyloid protein. In addition, there are many lipids present in the cell membrane, such as sphingomyelin and cardiolipin, which may alter the function of a variety of transmembrane proteins (Fabiani and Antollini, 2019). In the adult brain, 70–80% of cholesterol is found mainly in the myelin sheath, with the rest in the plasma membrane of astrocytes and neurons, protecting their morphologies and synaptic transmission processes (Dietschy and Turley, 2004; Zhang and Liu, 2015). High levels of cholesterol in the cell membrane also cause significant changes in the dynamic homeostasis of neurons, which affects the proteolytic activity of γ-secretase (a transmembrane protein), including promoting amyloidogenesis, increasing APP processing, producing amyloid, and affecting the microenvironment of AHN (Kao et al., 2020). ApoE is a glycoprotein mainly secreted by astrocytes, which is involved in regulating lipid transport, synaptogenesis and amyloid clearance, and also plays an important role in hippocampal neurogenesis. There are three common isoforms of ApoE in humans, including ApoE2, ApoE3, and ApoE4. The study indicated that overexpression of ApoE4 decreased adult neurogenesis in mice comparing with wild-type controls, while ApoE3 and ApoE2 expression promoted the proliferation and genesis of neural progenitor cells in the DG region (Koutseff et al., 2014). Moreover, ApoE4 can negatively affect adult hippocampal neurogenesis by modulating γ-aminobutyric acid interneurons and decreasing levels of neurosteroids (e.g., allopregnanolone). In contrast, ApoE3 can counteract chemokine-induced neuroinflammation and improve AHN (Suidan and Ramaswamy, 2019). Therefore, ApoE is expected to be a therapeutic target for AD (Chen et al., 2021).

In addition, by studying the "senile plaques" in the brain of AD patients, it was found that in addition to Aβ aggregation, there are many kinds of lipids in the senile plaques, such as ganglioside. Specific accumulation of monosialic acid gangliosides was found in the hippocampal subgranular region of a 12-month-old 5xFAD-AD mouse model, suggesting a potential relationship between the accumulation of plaque-associated gangliosides and damaged neural regeneration (Kaya et al., 2020).

3.2. Epigenetics

As technology improves, more and more studies show that epigenetic mechanisms, such as DNA methylation, histone post-translational modifications and microRNA-mediated post-transcriptional gene regulation, are involved in the pathogenesis of AD and thus influence the onset and progression of AD (Hernaiz et al., 2022; van Zundert and Montecino, 2022).

3.2.1. DNA methylation

DNA methylation is an epigenetic mechanism that occurs by the covalent transfer of a methyl group to the C-5 position of the nuclear base cytosine to form 5-methylcytosine, which is involved in the regulation of gene expression (Moore et al., 2013). In order to investigate whether epigenetic alterations lead to late-onset AD, some researches focused on the DNA methylation status of the risk genes. The results showed that there is a decrease in CpG methylation at the APP gene promoter in neurons and glial cells, accompanied by an increase in APP gene expression, which in turn leads to an overproduction of Aβ (Tohgi et al., 1999). In addition, changes in DNA methylation also occur in other related genes, such as MCF2L, MAP2, ANK1, HOX3A, etc. (Gasparoni et al., 2018).

Among the pathological features of AD, impairments in epigenetic mechanisms also lead to the generation of damaged neurons by neural stem cells, which will aggravate the loss of neurons and the defects of learning and memory (Li et al., 2016). DNA methylation of promoters can result in transcriptional repression through DNA methyltransferases (DNMTs) in neurodevelopment, while the deletion of DNMT1 in neural progenitors impairs the maturation and survival state of neurons, causing precocious astrocyte differentiation (Hutnick et al., 2009). And it was shown that the IL-6/JAK2/STAT3 pathway can regulate neurogenesis by improving DNMT1 in NSCs, promote DNA demethylation to regulate NSCs status at the epigenetic level, and further regulate AHN (Kong X. et al., 2019; **Figure 2**). The development of neural progenitor cells is an important node in the process of AHN, and mitochondria in neural progenitor cells play a crucial role in AHN (Gage, 2019). Whether in AD model mice or in Aβ-induced *in vitro* cell lines, the aggregation of Aβ can induce mitochondrial damage in neural progenitor cells and lead to the defect of AHN and cognitive function. In-depth mechanistic studies revealed that damage to mitochondria causes degradation of lysine demethylase 5A (KDM5A) in neural progenitor cells, which in turn result in AHN deficits. It may be because the genetic reduction of KDM5A expression reduces the transcription of BDNF in the brain, inhibits neural differentiation and leads to memory deficits (Bath et al., 2012; Kim et al., 2022). Additionally, the human neural progenitor

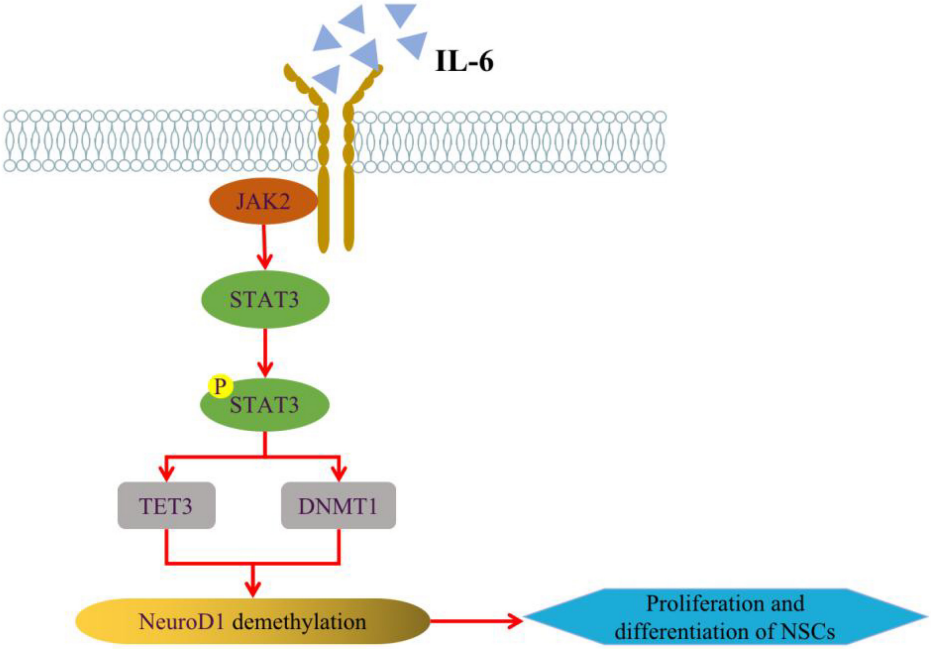

FIGURE 2
Regulation of IL-6/JAK2/STAT3 pathway on AHN. IL-6 can alter the expression of TET3 and DNMT1 in NSCs through JAK2/STAT3 signaling pathway, thus enhancing the expression of NeuroD1 (Neurogenic differentiation 1) gene through active or passive DNA demethylation, and regulating NSCs neurogenesis at the epigenetic level. Some of this illustration was started from a Scidraw Template.

cells induced from pluripotent stem cells were used to establish a simple *in vitro* adult neurogenesis model to study DNA methylation in the context of AD disease. And it found that the methylation levels of NXN genes were elevated and differential DNA methylation were observed in immature neurons by quantifying genes related to neurogenesis in the hippocampal region in the context of simulated AD (Blanco-Luquin et al., 2022).

3.2.2. Histone modification

The appearance of neurofibrillary tangles and the aggregation of neural plaques in AD patients are some markers of abnormal histone post-translational modifications during the development of AD, and these abnormal modifications are closely related to the cognitive impairment of AD patients in the later stage. Histones are structural proteins that form DNA nucleosomes. Their N-terminal sequences protrude beyond the boundaries of nucleosomes and provide a surface for the recognition and subsequent interaction of proteins that regulate transcription. They usually participate in the expression and repression of target genes through chromatin modification. At present, histone modifications that have been studied extensively include acetylation, methylation and phosphorylation (Voigt and Reinberg, 2013; Audia and Campbell, 2016). Phosphorylation is one of the most common modifications in proteome biology, and approximately 30% of proteins undergo this modification by adding phosphate groups to serine, tyrosine and threonine residues. There is also growing evidence that phosphorylation modifications in many diseases alter the basic function of proteins and drive cell death signals (Humphrey et al., 2015). Tau protein, a microtubule-associated protein, has been proved to promote the formation of neurogenic fiber tangles by hyperphosphorylation in the brains of AD patients. The phosphorylated Tau protein accumulates excessively in GABAergic interneurons in the DG region of AD patients and mice, which impair the AHN by suppressing GABAergic transmission (Zheng et al., 2020). And this hyperphosphorylated Tau protein accumulation occurs mainly in the early and middle stages of AD. In the late stage of AD, the phosphorylated Tau protein gradually disappears from the nuclei of the granule cell of the DG region (Gil et al., 2022). Heme oxygenase was found to be neuroprotective in AD mice by modulating the levels of p–Ser9-GSKβ and p–Tyr216-GSKβ to improve the survival and proliferation capacity of NSCs and promote AHN in AD disease model (Si et al., 2020). In a mouse model of fragile X-chromosome syndrome, scientists found that neurogenesis could be improved by improving the level of histone acetylation modification to rescue cognitive deficits in mice (Li et al., 2018). In addition, H3K9me3, the ninth lysine on histone H3 is methylated and is a common inhibitory histone modification. Scientists have demonstrated that the expression and distribution of H3K9me3 changes dynamically in dentate gyrus of adult mouse and cultured adult hippocampal neurons, exhibiting high levels of expression early in neurogenesis. And silencing of H3K9 transferase mediated by retrovirus significantly impairs neural progenitor cell differentiation (Guerra et al., 2021). To understand the specific role of histone modifications in AD, more future studies are needed to be carried out.

3.2.3. miRNAs

MiRNAs are a class of single stranded non-coding RNAs with about 19–23 nucleotides, which are important epigenetic and post-transcriptional regulators of mRNA complexity. Due to their small molecular weight, amphiphilic and high solubility, they have strong mobility and are ubiquitous in the central nervous system. They are the minimum information of nucleic acid signal molecules in eukaryotes described so far (Zhao et al., 2020). In recent years, a growing number of studies have shown that miRNAs play a

key role in the development of many neurodegenerative diseases, and their role in the pathogenesis of AD involves the regulation of amyloid precursor protein (APP), BACE1, neuronal apoptosis and other factors (Deng et al., 2014). With the development of scientific technology, miRNA dysregulation has also been found to be associated with the development of AD (Rahman et al., 2020). The network analysis of brain miRNAs in AD patients at Braak stage III revealed that a large number of miRNAs were related with the immune system, cell cycle, gene expression, cellular stress response, nerve growth factor signal, Wnt signal and cellular senescence, such as miR-107, 26b, 30e, 34a, 485, 200c, 210, 146a, 34c, 125a. Among them, miR-200c, 146a, 34c, 125 expression is increased in the brains of AD patients, while miR-210, 485, 107 expression is decreased, and the remaining ones are dynamically changed with disease progression (Swarbrick et al., 2019).

As increasing studies have observed the dysregulation of microRNA expressions in AD, more researches have been conducted on their effect on AHN. MiR-9 is one of the most abundant microRNAs in mammalian central nervous system. It can promote neural differentiation of NSCs by targeting related genes to induce neurogenesis (Landgraf et al., 2007; Yoo et al., 2009). And it can inhibit Notch signal pathway (participating in the regulation of nervous system development and stem cell biological activity) in AD and promote NSCs to differentiate into neurons, thus promoting AHN (Li et al., 2017). The expression levels of miR-206 were increased in Tg2576 AD mice and AD patients. Inhibition of miR-206 expression in AD mice could improve Aβ deposition as well as BDNF expression levels, enhance hippocampal synaptic density and neurogenesis, and further improve memory function (Lee et al., 2012). MiR-351-5p is a pathogenic factor of hippocampal neural progenitor cells, which is widely expressed in AD patients. Inhibition of its downstream gene Miro 2 can induce a large number of mitochondrial divisions and lead to bad mitosis, which result in the loss of a large number of normal mitochondria and the death of hippocampal neural progenitor cells (Woo et al., 2020). MiR-132 is one of the consistently downregulated microRNAs in the development of AD. And it is an effective regulator of AHN. When miR-132 levels were restored in the hippocampus, the hippocampal AHN and associated memory deficits can be improved in AD mice (Walgrave et al., 2021). MiR-188-5p expression is also reduced in AD samples, while increasing its expression levels in primary hippocampal neurons and 5xFAD mouse neurons was found to further improve cognitive deficits by improving neuronal survival (Lee et al., 2016).

3.3. Neuroinflammation

In the brain of AD patients, neuroinflammation is one of the key pathological features. Microglia are the major inflammatory cells of the central nervous system, and under normal physiological conditions, their main functions are to support the integrity and survival of neuronal networks and to maintain brain homeostasis, development, etc. More and more studies have found that many AD-associated risk locus are unique or highly expressed in microglia, which suggests that microglia play an important role in the development of disease under the pathological conditions of AD (Pintado et al., 2017; Eshraghi et al., 2021; Lopes et al., 2022). The activation time of microglia is earlier than that of Aβ and Tau protein pathology in both brains of AD patients and AD mouse models (Tarkowski et al., 2003; Wright et al., 2013). And previous study also proved that Aβ can induce lysosomal damage and activate inflammatory corpuscles in microglia to mediate inflammatory reaction in central nervous system (Halle et al., 2008).

For AHN, only a small number of newborn cells in SGZ of DG are able to survive after phagocytosis by microglia and eventually integrate into local circuits, suggesting that microglia are critical for the homeostatic formation of the regenerative microenvironment within the brain for hippocampal neuroregeneration. More and more researches revealed that alterations in microglia status are critical for AHN. Interleukin-6 (IL-6), a pro-inflammatory cytokine known to regulate neurogenesis, has been reported to inhibit neurogenesis in neural stem cells *via* the JAK2/STAT3 signaling pathway (Kong X. et al., 2019). It was also demonstrated that photobiomodulation therapy can upregulate IFN-γand IL-10 expression levels in the brain of APP/PS1 and 3xTg AD model through JAK2-mediated signaling and STAT4/STAT5 signaling pathways, and induce improved microenvironmental conditions in the brain, which promotes AHN and reverse cognitive deficits (Wu et al., 2022). These findings are critical for potential therapeutic approaches in AD. In the early stage of AD, microglia can inhibit the progression of inflammation and assist in the clearance of Aβ to improve the intracerebral microenvironment, which is beneficial to AHN. However, with the development of AD disease, microglia will be affected by inflammatory factors that exacerbate the inflammatory reaction, and the interaction with astrocytes will further aggravate the neurotoxicity (Song et al., 2012; Gray et al., 2020). As a part of the innate immune system, the complement system plays an important role in the clearance of pathogens and cellular debris. In the healthy brain, complement affects neurodevelopment, neurogenesis, synapse formation and phagocyte recruitment, and protects the body from pathogens (Schartz and Tenner, 2020). However, in the process of AD disease, excessive activation of downstream complement will lead to the production of C5a, which can bind with the receptor and cause a series of negative reactions such as inflammation, injury and neuronal death (Ager et al., 2010). It has been shown that in AD, the C5a-C5aR1 signaling pathway can accelerate disease progression by enhancing the activation of microglia and exacerbating neuroinflammation (Carvalho et al., 2022). In the process of finding an effective treatment for AD, people found that sigma1 receptors (S1Rs) may regulate AHN, prevent Aβ-induced neurotoxicity and modulate the pathophysiology of AD, and have great potential as new targets for treatment (Penke et al., 2018; Ma et al., 2021). In an early AD model induced by Aβ 1–42, it was found that the use of two agonists of S1Rs–DMT and PRE084 not only significantly reduce the proliferation of highly reactive astrocytes, but also affect neurogenesis and the survival of mature neurons. Furthermore, as a presynaptic self-receptor, the histamine H3 receptor is highly expressed not only in neurons but also in microglia, and regulates the inflammatory response together with microglia (Naddafi and Mirshafiey, 2013). Inhibition of H3R decreases the activity of microglia, promotes a phenotypic shift from pro-inflammatory M1 to anti-inflammatory M2, and attenuates neuroinflammation. In addition, hippocampal neurogenesis was improved by enhancing histamine release, which in turn improved cognitive dysfunction (Wang et al., 2022).

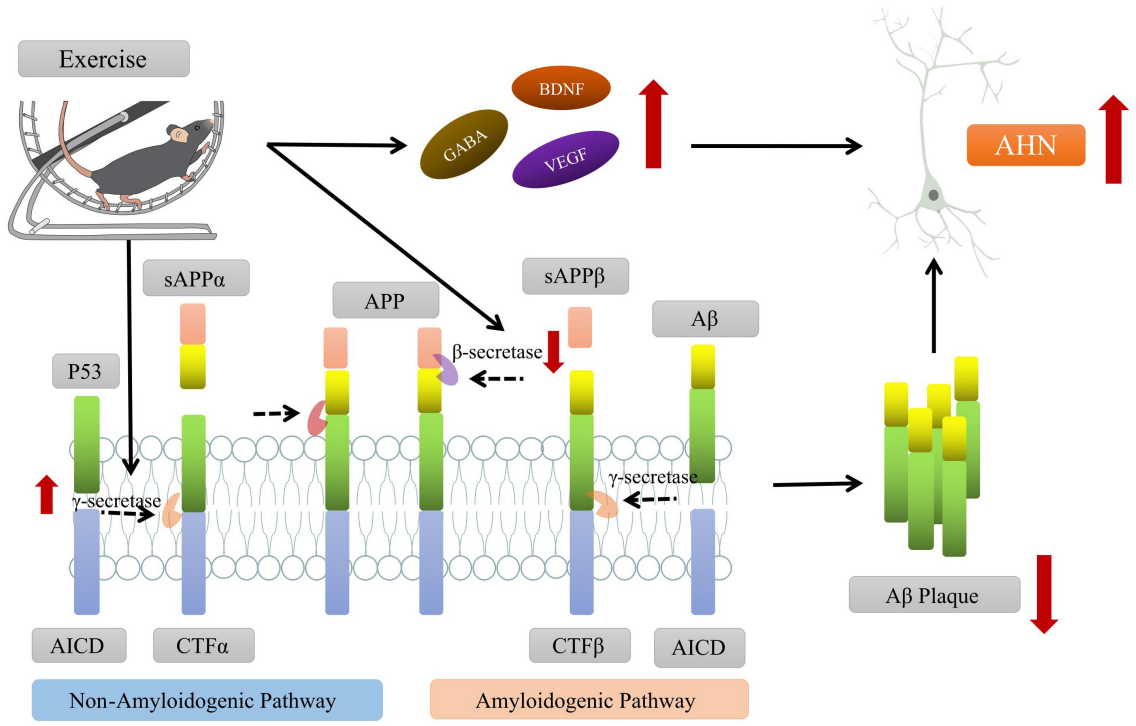

FIGURE 3
Exercise promoting the adult hippocampal neurogenesis (AHN) and improving the cognitive function of AD mice. On one hand, exercise intervention can promote the cleavage of amyloid precursor protein (APP) by affecting the levels of key secretory enzymes (such as β-secretase, γ-secretase, etc.) and reduce the aggregation of Aβ in brain. On the other hand, exercise can regulate the levels of neurotrophic factors (such as BDNF, VEGF, etc.), create a microenvironment conducive to AHN, and promote the survival and differentiation of new neurons. Some of this illustration was started from a Scidraw Template.

4. Therapeutic potential of AHN in AD

As more and more researches demonstrate that AHN declines in AD patients, promoting nerve regeneration has emerged as a new target for AD treatment. It has been found that nerve regeneration can be promoted by reducing neuroinflammation. For example, the use of the anti-inflammatory drug minocycline can reduce neuroinflammation in the hippocampus by inhibiting microglia activation, which further promotes AHN (Lue et al., 2001). In addition, many studies support Chinese Herbal Medicine can be used for the routine treatment of AD (Cui et al., 2008; Mao et al., 2015; Chen et al., 2016; Yang et al., 2017). Stem cell transplantation can also reduce the effect of nerve inflammation on nerve regeneration and promote the emergence of new neurons, which is a promising method to change the pathology of diseases. However, due to some "side effects," this type of treatment has not been widely used (Levenstein et al., 2006). Today, stem cell therapy using mesenchymal stem cells (MSCs) has emerged as a promising strategy for regulating the adult hippocampal niche. MSCs can migrate across the blood-brain barrier with the help of stimulants, generate and differentiate new neurons, and enhance memory function by secreting cytokines and trophic factors important for promoting and anti-inflammatory regulation (Noureddini and Bagheri-Mohammadi, 2021). Other studies have shown that enhancing neural progenitor cell differentiation can improve AHN. For example, fluoxetine can increase the proliferation of progenitor cells, while phosphodiesterase inhibitors can promote the differentiation of cells. Both of them can improve AHN to rescue cognitive dysfunction in mice with AD (Bartolome et al., 2018; Ou et al., 2018). Furthermore, lentivirus-mediated gene therapy for Wnt3 (upstream activator of the β-catenin pathway) overexpression can also promote AHN in the brains of AD patients (Lie et al., 2005). While NeuroD1 was shown to be an important target for repairing neuronal differentiation defects in the brains of AD patients, its overexpression promotes the transcription of genes related to neuronal differentiation, facilitating neuronal maturation and effectively improving spatial memory deficits in AD mice (Richetin et al., 2015; Pataskar et al., 2016). In recent years, studies at the molecular level have become increasingly advanced, and it has been found that miR-132 level changes are closely related to NSCs proliferation and differentiation besides Aβ pathology in AD mice. The overexpression of miR-132 can effectively regulate AHN, but whether it can be effectively applied to clinical needs more relevant researches (Walgrave et al., 2021).

In addition to drugs, a growing body of research suggests that physical exercise may be an effective method for prevention or rehabilitation, which can improve the AHN and cognitive dysfunction in AD animal models through upregulating synaptic signaling pathways, downregulating inflammation-related genes and promoting neurogenesis (Maliszewska-Cyna et al., 2016; Santiago et al., 2022). To investigate the potential mechanisms between physical exercise and AHN, the scientists assessed the effects of treadmill exercise on the cognitive ability of AD mouse model. They found that exercise could modulate various neurotrophic factors (e.g., BDNF) and secretory enzymes (e.g., γ-secretase) that cleave APP through the non-β-amyloid pathway to reduce Aβ aggregation and improve the hippocampal microenvironment, which further

promotes the survival, proliferation and differentiation of newborn neuron to enhance AHN and improve cognitive function of AD mouse (Vaynman et al., 2004; Inoue et al., 2015; Yu et al., 2021; **Figure 3**).

In a word, lots of studies have demonstrated the effectiveness of enhancing AHN to improve learning and memory cognitive performance in AD mice. However, more research is needed to improve the clinical use of this treatment.

5. Summary

In conclusion, the impairment of AHN during the development of AD is closely associated with learning memory and cognitive dysfunction in AD patients or animal models, which is widely confirmed. However, there are still some unknown factors that affect the consistency of the findings, which will require more research to verify its characteristic manifestations at different stages of AD development. In addition, as the pathogenesis of AD is increasingly elucidated and the mechanisms of AHN become clearer and clearer, the exact mechanisms of altered AHN in AD are gradually gaining more attention. Impaired energy metabolism, epigenetic mechanisms and neuroinflammation are important pathological features in the development of AD. And a growing number of studies have demonstrated that these pathological alterations have potential important link with the impairment of AHN. Overall, these findings provide strong evidence for our understanding of the interaction between the development of AD and AHN, which will help us to further identify targets that regulate neurogenesis as a potential approach to treat AD-related deficits. Although many studies have shown that promoting AHN can effectively improve cognitive deficits in AD, animal models, it is still challenging to put it into the clinical practice. Therefore, we need to improve our research to make it more applicable to AD patients, and provide new and effective therapeutic approaches.

Author contributions

YZ, XW, and YL drafted the manuscript. YG assisted in data collection. RG, GZ, and QL helped to frame up and revised the manuscript. All authors have read and approved the final manuscript.

Funding

This work was supported by Fujian Provincial Natural Science Foundation of China (Grant number: 2022J01664).

Conflict of interest

The authors declare that the research was conducted in the absence of any commercial or financial relationships that could be construed as a potential conflict of interest.

Publisher's note

All claims expressed in this article are solely those of the authors and do not necessarily represent those of their affiliated organizations, or those of the publisher, the editors and the reviewers. Any product that may be evaluated in this article, or claim that may be made by its manufacturer, is not guaranteed or endorsed by the publisher.

References

Ager, R., Fonseca, M., Chu, S., Sanderson, S., Taylor, S., Woodruff, T., et al. (2010). Microglial C5aR (CD88) expression correlates with amyloid-beta deposition in murine models of Alzheimer's disease. *J. Neurochem.* 113, 389–401. doi: 10.1111/j.1471-4159.2010.06595.x

Alzheimer's Association (2019). Alzheimer's disease facts and figures. *Alzheimers Dem.* 15:66.

Audia, J., and Campbell, R. (2016). Histone modifications and cancer. *Cold Spring Harb. Perspect. Biol.* 8:a019521. doi: 10.1101/cshperspect.a019521

Babcock, K., Page, J., Fallon, J., and Webb, A. (2021). Adult hippocampal neurogenesis in aging and Alzheimer's disease. *Stem Cell Rep.* 16, 681–693. doi: 10.1016/j.stemcr.2021.01.019

Bartolome, F., de la Cueva, M., Pascual, C., Antequera, D., Fernandez, T., Gil, C., et al. (2018). Amyloid β-induced impairments on mitochondrial dynamics, hippocampal neurogenesis, and memory are restored by phosphodiesterase 7 inhibition. *Alzheimers Res Ther.* 10:24. doi: 10.1186/s13195-018-0352-4

Bath, K., Akins, M., and Lee, F. S. (2012). BDNF control of adult SVZ neurogenesis. *Dev. Psychobiol.* 54, 578–589. doi: 10.1002/dev.20546

Bélanger, M., Allaman, I., and Magistretti, P. (2011). Brain energy metabolism: Focus on astrocyte-neuron metabolic cooperation. *Cell Metab.* 14, 724–738. doi: 10.1016/j.cmet.2011.08.016

Blanco-Luquin, I., Acha, B., Urdánoz-Casado, A., Gómez-Orte, E., Roldan, M., Pérez-Rodríguez, D., et al. (2022). NXN gene epigenetic changes in an adult neurogenesis model of Alzheimer's disease. *Cells* 11:1069. doi: 10.3390/cells11071069

Boekhoorn, K., Joels, M., and Lucassen, P. (2006). Increased proliferation reflects glial and vascular-associated changes, but not neurogenesis in the presenile Alzheimer hippocampus. *Neurobiol. Dis.* 24, 1–14. doi: 10.1016/j.nbd.2006.04.017

Boldrini, M., Fulmore, C., Tartt, A., Simeon, L., Pavlova, I., Poposka, V., et al. (2018). Human hippocampal neurogenesis persists throughout aging. *Cell Stem Cell* 22, 589.e5–599.e5. doi: 10.1016/j.stem.2018.03.015

Campos-Peña, V., Pichardo-Rojas, P., Sánchez-Barbosa, T., Ortíz-Islas, E., Rodríguez-Pérez, C., Montes, P., et al. (2022). Amyloid β, lipid metabolism, basal cholinergic system, and therapeutics in Alzheimer's disease. *Int. J. Mol. Sci.* 23:12092. doi: 10.3390/ijms232012092

Carvalho, K., Schartz, N., Balderrama-Gutierrez, G., Liang, H., Chu, S., Selvan, P., et al. (2022). Modulation of C5a-C5aR1 signaling alters the dynamics of AD progression. *J. Neuroinflammation* 19:178. doi: 10.1186/s12974-022-02539-2

Chen, B. H., Park, J. H., Cho, J. H., Kim, I. H., Lee, J. C., Lee, T. K., et al. (2016). Tanshinone I enhances neurogenesis in the mouse hippocampal dentate gyrus via increasing Wnt-3, Phosphorylated glycogen synthase kinase-3beta and beta-catenin immunoreactivities. *Neurochem. Res.* 41, 1958–1968.

Chen, Y., Strickland, M., Soranno, A., and Holtzman, D. (2021). Apolipoprotein E: Structural insights and links to Alzheimer disease pathogenesis. *Neuron* 109, 205–221. doi: 10.1016/j.neuron.2020.10.008

Crews, L., Adame, A., Patrick, C., Delaney, A., Pham, E., Rockenstein, E., et al. (2010). Increased BMP6 levels in the brains of Alzheimer's disease patients and APP transgenic mice are accompanied by impaired neurogenesis. *J. Neurosci.* 30, 12252–12262. doi: 10.1523/JNEUROSCI.1305-10.2010

Cui, Y. M., Ao, M. Z., Li, W., and Yu, L. J. (2008). Effect of glabridin from *Glycyrrhiza glabra* on learning and memory in mice. *Planta Med.* 74, 377–380.

Demars, M., Hu, Y., Gadadhar, A., and Lazarov, O. (2010). Impaired neurogenesis is an early event in the etiology of familial Alzheimer's disease in transgenic mice. *J. Neurosci. Res.* 88, 2103–2117. doi: 10.1002/jnr.22387

Deng, Y., Ding, Y., and Hou, D. (2014). Research status of the regulation of miRNA on BACE1. *Int. J. Neurosci.* 124, 474–477. doi: 10.3109/00207454.2013.858249

Dietschy, J., and Turley, S. (2004). Thematic review series: Brain lipids. Cholesterol metabolism in the central nervous system during early development and in the mature animal. *J. Lipid Res.* 45, 1375–1397. doi: 10.1194/jlr.R400004-JLR200

Eshraghi, M., Adlimoghaddam, A., Mahmoodzadeh, A., Sharifzad, F., Yasavoli-Sharahi, H., Lorzadeh, S., et al. (2021). Alzheimer's disease pathogenesis: Role of autophagy and mitophagy focusing in *Microglia*. *Int. J. Mol. Sci.* 22:3330. doi: 10.3390/ijms22073330

Fabiani, C., and Antollini, S. (2019). Alzheimer's disease as a membrane disorder: Spatial cross-talk among beta-amyloid peptides, nicotinic acetylcholine receptors and lipid rafts. *Front. Cell Neurosci.* 13:309. doi: 10.3389/fncel.2019.00309

Folmes, C., Nelson, T., Martinez-Fernandez, A., Arrell, D., Lindor, J., Dzeja, P., et al. (2011). Somatic oxidative bioenergetics transitions into pluripotency-dependent glycolysis to facilitate nuclear reprogramming. *Cell Metab.* 14, 264–271. doi: 10.1016/j.cmet.2011.06.011

Gage, F. (2019). Adult neurogenesis in mammals. *Science* 364, 827–828. doi: 10.1126/science.aav6885

Gasparoni, G., Bultmann, S., Lutsik, P., Kraus, T., Sordon, S., Vlcek, J., et al. (2018). DNA methylation analysis on purified neurons and glia dissects age and Alzheimer's disease-specific changes in the human cortex. *Epigenetics Chromatin* 11:41. doi: 10.1186/s13072-018-0211-3

Gauthier, S., Webster, C., Servaes, S., Morais, J. A., and Rosa-Neto, P. (2022). *World Alzheimer report 2022: Life after diagnosis: Navigating treatment, care and support*. London: Alzheimer's Disease International.

Gil, L., Chi-Ahumada, E., Niño, S., Capdeville, G., Méndez-Torres, A., Guerrero, C., et al. (2022). Pathological nuclear hallmarks in dentate granule cells of Alzheimer's patients: A biphasic regulation of neurogenesis. *Int. J. Mol. Sci.* 23:12873. doi: 10.3390/ijms232112873

Gillotin, S., Sahni, V., Lepko, T., Hanspal, M., Swartz, J., Alexopoulou, Z., et al. (2021). Targeting impaired adult hippocampal neurogenesis in ageing by leveraging intrinsic mechanisms regulating neural stem cell activity. *Ageing Res. Rev.* 71:101447. doi: 10.1016/j.arr.2021.101447

Gray, S., Kinghorn, K., and Woodling, N. (2020). Shifting equilibriums in Alzheimer's disease: The complex roles of microglia in neuroinflammation, neuronal survival and neurogenesis. *Neural. Regen. Res.* 15, 1208–1219. doi: 10.4103/1673-5374.272571

Guerra, M. V., Cáceres, M. I., Herrera-Soto, A., Arredondo, S. B., Varas-Godoy, M., van Zundert, B., et al. (2021). H3K9 Methyltransferases Suv39h1 and Suv39h2 control the differentiation of neural progenitor cells in the adult hippocampus. *Front. Cell Dev. Biol.* 9:778345. doi: 10.3389/fcell.2021.778345

Hahn, K. R., Kim, W., Jung, H. Y., Kwon, H. J., Kim, D. W., Hwang, I. K., et al. (2022). Comparison of the effects of cuprizone on demyelination in the corpus callosum and hippocampal progenitors in young adult and aged mice. *Neurochem. Res.* 47, 1073–1082.

Halle, A., Hornung, V., Petzold, G., Stewart, C., Monks, B., Reinheckel, T., et al. (2008). The NALP3 inflammasome is involved in the innate immune response to amyloid-beta. *Nat. Immunol.* 9, 857–865. doi: 10.1038/ni.1636

Hamilton, L., Dufresne, M., Joppé, S., Petryszyn, S., Aumont, A., Calon, F., et al. (2015). Aberrant lipid metabolism in the forebrain niche suppresses adult neural stem cell proliferation in an animal model of Alzheimer's disease. *Cell Stem Cell* 17, 397–411. doi: 10.1016/j.stem.2015.08.001

Hernaiz, A., Toivonen, J., Bolea, R., and Martín-Burriel, I. (2022). Epigenetic changes in prion and prion-like neurodegenerative diseases: Recent advances, potential as biomarkers, and future perspectives. *Int. J. Mol. Sci.* 23:12609. doi: 10.3390/ijms232012609

Humphrey, S., James, D., and Mann, M. (2015). Protein phosphorylation: A major switch mechanism for metabolic regulation. *Trends Endocrinol. Metab.* 26, 676–687. doi: 10.1016/j.tem.2015.09.013

Hutnick, L., Golshani, P., Namihira, M., Xue, Z., Matynia, A., Yang, X., et al. (2009). DNA hypomethylation restricted to the murine forebrain induces cortical degeneration and impairs postnatal neuronal maturation. *Hum. Mol. Genet.* 18, 2875–2888. doi: 10.1093/hmg/ddp222

Ichihara, Y., Doi, T., Ryu, Y., Nagao, M., Sawada, Y., and Ogata, T. (2017). Oligodendrocyte progenitor cells directly utilize lactate for promoting cell cycling and differentiation. *J. Cell Physiol.* 232, 986–995. doi: 10.1002/jcp.25690

Imayoshi, I., Sakamoto, M., Ohtsuka, T., Takao, K., Miyakawa, T., Yamaguchi, M., et al. (2008). Roles of continuous neurogenesis in the structural and functional integrity of the adult forebrain. *Nat. Neurosci.* 11, 1153–1161. doi: 10.1038/nn.2185

Inoue, K., Okamoto, M., Shibato, J., Lee, M., Matsui, T., Rakwal, R., et al. (2015). Correction: Long-term mild, rather than intense, exercise enhances adult hippocampal neurogenesis and greatly changes the transcriptomic profile of the hippocampus. *PLoS One* 10:e0133089. doi: 10.1371/journal.pone.0133089

Jin, K., Peel, A., Mao, X., Xie, L., Cottrell, B., Henshall, D., et al. (2004b). Increased hippocampal neurogenesis in Alzheimer's disease. *Proc. Natl. Acad. Sci. U.S.A.* 101, 343–347. doi: 10.1073/pnas.2634794100

Jin, K., Galvan, V., Xie, L., Mao, X., Gorostiza, O., Bredesen, D., et al. (2004a). Enhanced neurogenesis in Alzheimer's disease transgenic (PDGF-APPSw,Ind) mice. *Proc. Natl. Acad. Sci. U.S.A.* 101, 13363–13367. doi: 10.1073/pnas.0403678101

Kao, Y., Ho, P., Tu, Y., Jou, I., and Tsai, K. (2020). Lipids and Alzheimer's disease. *Int. J. Mol. Sci.* 21:1505. doi: 10.3390/ijms21041505

Kaya, I., Jennische, E., Dunevall, J., Lange, S., Ewing, A., Malmberg, P., et al. (2020). Spatial lipidomics reveals region and long chain base specific accumulations of monosialogangliosides in amyloid plaques in familial Alzheimer's disease mice (5xFAD) brain. *ACS Chem. Neurosci.* 11, 14–24. doi: 10.1021/acschemneuro.9b00532

Kempermann, G., Gage, F., Aigner, L., Song, H., Curtis, M., Thuret, S., et al. (2018). Human adult neurogenesis: Evidence and remaining questions. *Cell Stem Cell* 23, 25–30. doi: 10.1016/j.stem.2018.04.004

Kempermann, G., Gast, D., Kronenberg, G., Yamaguchi, M., and Gage, F. (2003). Early determination and long-term persistence of adult-generated new neurons in the hippocampus of mice. *Development* 130, 391–399. doi: 10.1242/dev.00203

Kempermann, G., Song, H., and Gage, F. (2015). Neurogenesis in the adult hippocampus. *Cold Spring Harb. Perspect. Biol.* 7:a018812. doi: 10.1101/cshperspect.a018812

Khacho, M., Harris, R., and Slack, R. (2019). Mitochondria as central regulators of neural stem cell fate and cognitive function. *Nat. Rev. Neurosci.* 20, 34–48. doi: 10.1038/s41583-018-0091-3

Kim, D., Jeong, H., Bae, J., Cha, M., Kang, M., Shin, D., et al. (2022). Aβ-induced mitochondrial dysfunction in neural progenitors controls KDM5A to influence neuronal differentiation. *Exp. Mol. Med.* 54, 1461–1471. doi: 10.1038/s12276-022-00841-w

Kong, L., Wang, Z., Liang, X., Wang, Y., Gao, L., and Ma, C. (2019). Monocarboxylate transporter 1 promotes classical microglial activation and pro-inflammatory effect via 6-phosphofructo-2-kinase/fructose-2, 6-biphosphatase 3. *J. Neuroinflammation* 16:240. doi: 10.1186/s12974-019-1648-4

Kong, X., Gong, Z., Zhang, L., Sun, X., Ou, Z., Xu, B., et al. (2019). JAK2/STAT3 signaling mediates IL-6-inhibited neurogenesis of neural stem cells through DNA demethylation/methylation. *Brain Behav. Immun.* 79, 159–173. doi: 10.1016/j.bbi.2019.01.027

Kou, X., Chen, D., and Chen, N. (2020). The regulation of microRNAs in Alzheimer's disease. *Front. Neurol.* 11:288. doi: 10.3389/fneur.2020.00288

Koutseff, A., Mittelhaeuser, C., Essabri, K., Auwerx, J., and Meziane, H. (2014). Impact of the apolipoprotein E polymorphism, age and sex on neurogenesis in mice: Pathophysiological relevance for Alzheimer's disease? *Brain Res.* 1542, 32–40. doi: 10.1016/j.brainres.2013.10.003

Krezymon, A., Richetin, K., Halley, H., Roybon, L., Lassalle, J., Francès, B., et al. (2013). Modifications of hippocampal circuits and early disruption of adult neurogenesis in the tg2576 mouse model of Alzheimer's disease. *PLoS One* 8:e76497. doi: 10.1371/journal.pone.0076497

Kumar, A., Pareek, V., Faiq, M., Ghosh, S., and Kumari, C. (2019). Adult neurogenesis in humans: A review of basic concepts, history, current research, and clinical implications. *Innov. Clin. Neurosci.* 16, 30–37.

Landgraf, P., Rusu, M., Sheridan, R., Sewer, A., Iovino, N., Aravin, A., et al. (2007). A mammalian microRNA expression atlas based on small RNA library sequencing. *Cell* 129, 1401–1414. doi: 10.1016/j.cell.2007.04.040

Lee, K., Kim, H., An, K., Kwon, O., Park, S., Cha, J., et al. (2016). Replenishment of microRNA-188-5p restores the synaptic and cognitive deficits in 5XFAD mouse model of Alzheimer's disease. *Sci. Rep.* 6:34433. doi: 10.1038/srep34433

Lee, S., Chu, K., Jung, K., Kim, J., Huh, J., Yoon, H., et al. (2012). MiR-206 regulates brain-derived neurotrophic factor in Alzheimer disease model. *Ann. Neurol.* 72, 269–277. doi: 10.1002/ana.23588

Lei, P., Ayton, S., and Bush, A. I. (2021). The essential elements of Alzheimer's disease. *J. Biol. Chem.* 296:100105.

Levenstein, M., Ludwig, T., Xu, R., Llanas, R., VanDenHeuvel-Kramer, K., Manning, D., et al. (2006). Basic fibroblast growth factor support of human embryonic stem cell self-renewal. *Stem Cells* 24, 568–574. doi: 10.1634/stemcells.2005-0247

Lev-Vachnish, Y., Cadury, S., Rotter-Maskowitz, A., Feldman, N., Roichman, A., Illouz, T., et al. (2019). L-Lactate promotes adult hippocampal neurogenesis. *Front. Neurosci.* 13:403. doi: 10.3389/fnins.2019.00403

Li, B., Yamamori, H., Tatebayashi, Y., Shafit-Zagardo, B., Tanimukai, H., Chen, S., et al. (2008). Failure of neuronal maturation in Alzheimer disease dentate gyrus. *J. Neuropathol. Exp. Neurol.* 67, 78–84. doi: 10.1097/nen.0b013e318160c5db

Li, F., Dong, H., Gong, Q., Wu, Q., Jin, F., and Shi, J. (2015). Icariin decreases both APP and Aβ levels and increases neurogenesis in the brain of Tg2576 mice. *Neuroscience.* 304, 29–35. doi: 10.1016/j.neuroscience.2015.06.010

Li, S., Gao, P., Wang, L., Yan, Y., Xia, Y., Song, J., et al. (2017). Osthole stimulated neural stem cells differentiation into neurons in an Alzheimer's disease cell model via upregulation of MicroRNA-9 and rescued the functional impairment of hippocampal neurons in APP/PS1 transgenic mice. *Front. Neurosci.* 11:340. doi: 10.3389/fnins.2017.00340

Li, X., Bao, X., and Wang, R. (2016). Neurogenesis-based epigenetic therapeutics for Alzheimer's disease (Review). *Mol. Med. Rep.* 14, 1043–1053. doi: 10.3892/mmr.2016.5390

Li, Y., Stockton, M. E., Eisinger, B. E., Zhao, Y., Mill-er, J. L., Bhuiyan, I., et al. (2018). Reducing histone acetylation rescues cognitive deficits in a mouse model of Fragile X syndrome. *Nat. Commun.* 9:2494.

Lie, D., Colamarino, S., Song, H., Désiré, L., Mira, H., Consiglio, A., et al. (2005). Wnt signalling regulates adult hippocampal neurogenesis. *Nature* 437, 1370–1375. doi: 10.1038/nature04108

Lopes, K., Snijders, G., Humphrey, J., Allan, A., Sneeboer, M., Navarro, E., et al. (2022). Genetic analysis of the human microglial transcriptome across brain regions, aging and disease pathologies. *Nat. Genet.* 54, 4–17. doi: 10.1038/s41588-021-00976-y

Lovell, M., Geiger, H., Van Zant, G., Lynn, B., and Markesbery, W. (2006). Isolation of neural precursor cells from Alzheimer's disease and aged control postmortem brain. *Neurobiol. Aging* 27, 909–917. doi: 10.1016/j.neurobiolaging.2005.05.004

Lue, L., Walker, D., and Rogers, J. (2001). Modeling microglial activation in Alzheimer's disease with human postmortem microglial cultures. *Neurobiol. Aging* 22, 945–956. doi: 10.1016/s0197-4580(01)00311-6

Ma, W., Chen, A., Xie, X., and Huang, Y. (2021). Sigma ligands as potent inhibitors of Aβ and AβOs in neurons and promising therapeutic agents of Alzheimer's disease. *Neuropharmacology* 190:108342. doi: 10.1016/j.neuropharm.2020.108342

Magistretti, P., and Allaman, I. (2015). A cellular perspective on brain energy metabolism and functional imaging. *Neuron* 86, 883–901. doi: 10.1016/j.neuron.2015.03.035

Maliszewska-Cyna, E., Xhima, K., and Aubert, I. A. (2016). Comparative study evaluating the impact of physical exercise on disease progression in a mouse model of Alzheimer's disease. *J. Alzheimers Dis.* 53, 243–257. doi: 10.3233/JAD-150660

Mao, J., Huang, S., Liu, S., Feng, X. L., Yu, M., Liu, J., et al. (2015). A herbal medicine for Alzheimer's disease and its active constituents promote neural progenitor proliferation. *Aging Cell* 14, 784–796.

Matsui, T., Omuro, H., Liu, Y., Soya, M., Shima, T., McEwen, B., et al. (2017). Astrocytic glycogen-derived lactate fuels the brain during exhaustive exercise to maintain endurance capacity. *Proc. Natl. Acad. Sci. U.S.A.* 114, 6358–6363. doi: 10.1073/pnas.1702739114

Moon, M., Cha, M., and Mook-Jung, I. (2014). Impaired hippocampal neurogenesis and its enhancement with ghrelin in 5XFAD mice. *J. Alzheimers Dis.* 41, 233–241. doi: 10.3233/JAD-132417

Moore, L., Le, T., and Fan, G. (2013). DNA methylation and its basic function. *Neuropsychopharmacology* 38, 23–38. doi: 10.1038/npp.2012.112

Moreno-Jiménez, E., Flor-García, M., Terreros-Roncal, J., Rábano, A., Cafini, F., Pallas-Bazarra, N., et al. (2019). Adult hippocampal neurogenesis is abundant in neurologically healthy subjects and drops sharply in patients with Alzheime's disease. *Nat. Med.* 25, 554–560. doi: 10.1038/s41591-019-0375-9

Naddafi, F., and Mirshafiey, A. (2013). The neglected role of histamine in Alzheimer's disease. *Am. J. Alzheimers Dis.* 28, 327–336. doi: 10.1177/1533317513488925

Nagase, M., Takahashi, Y., Watabe, A., Kubo, Y., and Kato, F. (2014). On-site energy supply at synapses through monocarboxylate transporters maintains excitatory synaptic transmission. *J. Neurosci.* 34, 2605–2617. doi: 10.1523/JNEUROSCI.4687-12.2014

Nicola, R., and Okun, E. (2021). Adult hippocampal neurogenesis: One lactate to rule them all. *Neuromol. Med.* 23, 445–448. doi: 10.1007/s12017-021-08658-y

Noureddini, M., and Bagheri-Mohammadi, S. (2021). Adult hippocampal neurogenesis and Alzheimer's disease: Novel application of mesenchymal stem cells and their role in hippocampal neurogenesis. *Int. J. Mol. Cell Med.* 10, 1–10.

Ou, Z., Kong, X., Sun, X., He, X., Zhang, L., Gong, Z., et al. (2018). Metformin treatment prevents amyloid plaque deposition and memory impairment in APP/PS1 mice. *Brain Behav. Immun.* 69, 351–363. doi: 10.1016/j.bbi.2017.12.009

Pataskar, A., Jung, J., Smialowski, P., Noack, F., Calegari, F., Straub, T., et al. (2016). NeuroD1 reprograms chromatin and transcription factor landscapes to induce the neuronal program. *EMBO J.* 35, 24–45. doi: 10.15252/embj.201591206

Penke, B., Fulop, L., Szucs, M., and Frecska, E. (2018). The role of sigma-1 receptor, an intracellular chaperone in neurodegenerative diseases. *Curr. Neuropharmacol.* 16, 97–116. doi: 10.2174/1570159X15666170529104323

Pierre, K., Pellerin, L., Debernardi, R., Riederer, B., and Magistretti, P. (2000). Cell-specific localization of monocarboxylate transporters, MCT1 and MCT2, in the adult mouse brain revealed by double immunohistochemical labeling and confocal microscopy. *Neuroscience* 100, 617–627. doi: 10.1016/s0306-4522(00)00294-3

Pilipenko, V., Narbute, K., Pupure, J., Langrate, I., Muceniece, R., and Kluša, V. (2020). Neuroprotective potential of antihyperglycemic drug metformin in streptozocin-induced rat model of sporadic Alzheimer's disease. *Eur. J. Pharmacol.* 881:173290. doi: 10.1016/j.ejphar.2020.173290

Pintado, C., Macías, S., Domínguez-Martín, H., Castaño, A., and Ruano, D. (2017). Neuroinflammation alters cellular proteostasis by producing endoplasmic reticulum stress, autophagy activation and disrupting ERAD activation. *Sci. Rep.* 7:8100. doi: 10.1038/s41598-017-08722-3

Rahman, M., Islam, T., Zaman, T., Shahjaman, M., Karim, M., Huq, F., et al. (2020). Identification of molecular signatures and pathways to identify novel therapeutic targets in Alzheimer's disease: Insights from a systems biomedicine perspective. *Genomics* 112, 1290–1299. doi: 10.1016/j.ygeno.2019.07.018

Richetin, K., Leclerc, C., Toni, N., Gallopin, T., Pech, S., Roybon, L., et al. (2015). Genetic manipulation of adult-born hippocampal neurons rescues memory in a mouse model of Alzheimer's disease. *Brain* 138, 440–455. doi: 10.1093/brain/awu354

Rinholm, J., Hamilton, N., Kessaris, N., Richardson, W., Bergersen, L., and Attwell, D. (2011). Regulation of oligodendrocyte development and myelination by glucose and lactate. *J. Neurosci.* 31, 538–548. doi: 10.1523/JNEUROSCI.3516-10.2011

Rodríguez, J., Jones, V., and Verkhratsky, A. (2009). Impaired cell proliferation in the subventricular zone in an Alzheimer's disease model. *Neuroreport* 20, 907–912. doi: 10.1097/WNR.0b013e32832be77d

Rodríguez, J., Jones, V., Tabuchi, M., Allan, S., Knight, E., LaFerla, F., et al. (2008). Impaired adult neurogenesis in the dentate gyrus of a triple transgenic mouse model of Alzheimer's disease. *PLoS One* 3:e2935. doi: 10.1371/journal.pone.0002935

Santiago, J., Quinn, J., and Potashkin, J. (2022). Physical activity rewires the human brain against neurodegeneration. *Int. J. Mol. Sci.* 23:6223. doi: 10.3390/ijms23116223

Santin, I., Moore, F., Colli, M. L., Gurzov, E. N., Marselli, L., Marchetti, P., et al. (2011). PTPN2, a candidate gene for type 1 diabetes modulates pancreatic β-cell apoptosis via regulation of the BH3-onlyprotein Bim. *Diabetes* 12, 3279–3288.

Scandella, V., and Knobloch, M. (2019). Sensing the environment: Extracellular lactate levels control adult neurogenesis. *Cell Stem Cell* 25, 729–731. doi: 10.1016/j.stem.2019.11.008

Schartz, N., and Tenner, A. (2020). The good, the bad, and the opportunities of the complement system in neurodegenerative disease. *J. Neuroinflammation* 17:354. doi: 10.1186/s12974-020-02024-8

Si, Z., Wang, X., Kang, Y., Wang, X., Sun, C., Li, Y., et al. (2020). Heme oxygenase 1 inhibits adult neural stem cells proliferation and survival via modulation of Wnt/β-catenin signaling. *J. Alzheimers Dis.* 76, 623–641. doi: 10.3233/JAD-200114

Song, S., Zhou, F., and Chen, W. (2012). Low-level laser therapy regulates microglial function through Src-mediated signaling pathways: Implications for neurodegenerative diseases. *J. Neuroinflammation* 9:219. doi: 10.1186/1742-2094-9-219

Suidan, G., and Ramaswamy, G. (2019). Targeting apolipoprotein E for Alzheimer's disease: An industry perspective. *Int. J. Mol. Sci.* 20:2161. doi: 10.3390/ijms20092161

Swarbrick, S., Wragg, N., Ghosh, S., and Stolzing, A. (2019). Systematic review of miRNA as biomarkers in Alzheimer's disease. *Mol. Neurobiol.* 56, 6156–6167. doi: 10.1007/s12035-019-1500-y

Syal, C., Kosaraju, J., Hamilton, L., Aumont, A., Chu, A., Sarma, S., et al. (2020). Dysregulated expression of monoacylglycerol lipase is a marker for anti-diabetic drug metformin-targeted therapy to correct impaired neurogenesis and spatial memory in Alzheimer's disease. *Theranostics* 10, 6337–6360. doi: 10.7150/thno.44962

Tarkowski, E., Andreasen, N., Tarkowski, A., and Blennow, K. (2003). Intrathecal inflammation precedes development of Alzheimer's disease. *J. Neurol. Neurosurg. Psychiatry* 74, 1200–1205. doi: 10.1136/jnnp.74.9.1200

Tingley, D., McClain, K., Kaya, E., Carpenter, J., and Buzsáki, G. (2021). A metabolic function of the hippocampal sharp wave-ripple. *Nature* 597, 82–86. doi: 10.1038/s41586-021-03811-w

Tobin, M., Musaraca, K., Disouky, A., Shetti, A., Bheri, A., Honer, W., et al. (2019). Human hippocampal neurogenesis persists in aged adults and Alzheimer's disease patients. *Cell Stem Cell* 24, 974.e3–982.e3. doi: 10.1016/j.stem.2019.05.003

Tohgi, H., Utsugisawa, K., Nagane, Y., Yoshimura, M., Genda, Y., and Ukitsu, M. (1999). Reduction with age in methylcytosine in the promoter region -224 approximately -101 of the amyloid precursor protein gene in autopsy human cortex. *Brain Res. Mol. Brain Res.* 70, 288–292. doi: 10.1016/s0169-328x(99)00163-1

van Zundert, B., and Montecino, M. (2022). Epigenetic changes and chromatin reorganization in brain function: Lessons from fear memory ensemble and Alzheimer's disease. *Int. J. Mol. Sci.* 23:12081. doi: 10.3390/ijms232012081

Vaynman, S., Ying, Z., and Gómez-Pinilla, F. (2004). Exercise induces BDNF and synapsin I to specific hippocampal subfields. *J. Neurosci. Res.* 76, 356–362. doi: 10.1002/jnr.20077

Velasco, M., Kosti, A., Guardia, G., Santos, M., Tegge, A., Qiao, M., et al. (2019). Antagonism between the RNA-binding protein Musashi1 and miR-137 and its potential impact on neurogenesis and glioblastoma development. *RNA* 25, 768–782. doi: 10.1261/rna.069211.118

Vercruysse, P., Vieau, D., Blum, D., Petersén, Å, and Dupuis, L. (2018). Hypothalamic alterations in neurodegenerative diseases and their relation to abnormal energy metabolism. *Front. Mol. Neurosci.* 11:2. doi: 10.3389/fnmol.2018.00002

Vivar, C., and van Praag, H. (2017). Running changes the brain: The long and the short of it. *Physiology.* 32, 410–424. doi: 10.1152/physiol.00017.2017

Voigt, P., and Reinberg, D. (2013). Epigenome editing. *Nat. Biotechnol.* 31, 1097–1099. doi: 10.1038/nbt.2756

Walgrave, H., Balusu, S., Snoeck, S., Vanden Eynden, E., Craessaerts, K., Thrupp, N., et al. (2021). Restoring miR-132 expression rescues adult hippocampal neurogenesis and memory deficits in Alzheimer's disease. *Cell Stem Cell* 28, 1805–1821. doi: 10.1016/j.stem.2021.05.001

Wang, J., Liu, B., Sun, F., Xu, Y., Luan, H., Yang, M., et al. (2022). Histamine H3R antagonist counteracts the impaired hippocampal neurogenesis in lipopolysaccharide-induced neuroinflammation. *Int. Immunopharmacol.* 110:109045. doi: 10.1016/j.intimp.2022.109045

Wang, R., Dineley, K., Sweatt, J., and Zheng, H. (2004). Presenilin 1 familial Alzheimer's disease mutation leads to defective associative learning and impaired adult neurogenesis. *Neuroscience* 126, 305–312. doi: 10.1016/j.neuroscience.2004.03.048

Watson, G., and Craft, S. (2003). The role of insulin resistance in the pathogenesis of Alzheimer's disease: Implications for treatment. *CNS Drugs* 17, 27–45. doi: 10.2165/00023210-200317010-00003

Wen, P., Hof, P., Chen, X., Gluck, K., Austin, G., Younkin, S., et al. (2004). The presenilin-1 familial Alzheimer disease mutant P117L impairs neurogenesis in the hippocampus of adult mice. *Exp. Neurol.* 188, 224–237. doi: 10.1016/j.expneurol.2004.04.002

Woo, H., Park, S., Kim, H., Jung, M., Pack, C., Park, J., et al. (2020). MiR-351-5p/Miro2 axis contributes to hippocampal neural progenitor cell death via unbalanced mitochondrial fission. *Mol. Ther. Nucleic Acids* 23, 643–656. doi: 10.1016/j.omtn.2020.12.014

Wright, A., Zinn, R., Hohensinn, B., Konen, L., Beynon, S., Tan, R., et al. (2013). Neuroinflammation and neuronal loss precede Aβ plaque deposition in the hAPP-J20 mouse model of Alzheimer's disease. *PLoS One* 8:e59586. doi: 10.1371/journal.pone.0059586

Wu, X., Shen, Q., Chang, H., Li, J., and Xing, D. (2022). Promoted CD4+ T cell-derived IFN-γ/IL-10 by photobiomodulation therapy modulates neurogenesis to ameliorate cognitive deficits in APP/PS1 and 3xTg-AD mice. *J. Neuroinflammation* 19:253. doi: 10.1186/s12974-022-02617-5

Xie, Y., Li, Y., Nie, L., Zhang, W., Ke, Z., Ku, Y., et al. (2021). Cognitive enhancement of repetitive transcranial magnetic stimulation in patients with mild cognitive impairment and early Alzheimer's disease: A systematic review and meta-analysis. *Front. Cell Dev. Biol.* 9:734046. doi: 10.3389/fcell.2021.734046

Yamaguchi, H., Nakazato, Y., Kawarabayashi, T., Ishiguro, K., Ihara, Y., Morimatsu, M., et al. (1991). Extracellular neurofibrillary tangles associated with degenerating neurites and neuropil threads in Alzheimer-type dementia. *Acta Neuropathol.* 81, 603–609. doi: 10.1007/BF00296369

Yang, W. T., Zheng, X. W., Chen, S., Shan, C. S., Xu, Q. Q., Zhu, J. Z., et al. (2017). Chinese herbal medicine for Alzheimer's disease: Clinical evidence and possible mechanism of neurogenesis. *Biochem. Pharmacol.* 141, 143–155.

Yoo, A., Staahl, B., Chen, L., and Crabtree, G. (2009). MicroRNA-mediated switching of chromatin-remodelling complexes in neural development. *Nature* 460, 642–646. doi: 10.1038/nature08139

Yu, H., Zhang, C., Xia, J., and Xu, B. (2021). Treadmill exercise ameliorates adult hippocampal neurogenesis possibly by adjusting the APP proteolytic pathway in APP/PS1 transgenic mice. *Int. J. Mol. Sci.* 22:9570. doi: 10.3390/ijms22179570

Zaletel, I., Schwirtlich, M., Perović, M., Jovanović, M., Stevanović, M., Kanazir, S., et al. (2018). Early impairments of hippocampal neurogenesis in 5xFAD mouse model of Alzheimer's disease are associated with altered expression of SOXB transcription factors. *J. Alzheimers Dis.* 65, 963–976. doi: 10.3233/JAD-180277

Zeng, Q., Zheng, M., Zhang, T., and He, G. (2016). Hippocampal neurogenesis in the APP/PS1/nestin-GFP triple transgenic mouse model of Alzheimer's disease. *Neuroscience* 314, 64–74. doi: 10.1016/j.neuroscience.2015.11.054

Zhang, H., Zheng, Q., Guo, T., Zhang, S., Zheng, S., Wang, R., et al. (2022). Metabolic reprogramming in astrocytes results in neuronal dysfunction in intellectual disability. *Mol. Psychiatry* doi: 10.1038/s41380-022-01521-x [Epub ahead of print].

Zhang, J., and Liu, Q. (2015). Cholesterol metabolism and homeostasis in the brain. *Protein Cell.* 6, 254–264. doi: 10.1007/s13238-014-0131-3

Zhao, Y., Jaber, V., Alexandrov, P., Vergallo, A., Lista, S., Hampel, H., et al. (2020). MicroRNA-based biomarkers in Alzheimer's disease (AD). *Front. Neurosci.* 14:585432. doi: 10.3389/fnins.2020.585432

Zheng, J., Li, H., Tian, N., Liu, F., Wang, L., Yin, Y., et al. (2020). Interneuron accumulation of phosphorylated tau impairs adult hippocampal neurogenesis by suppressing GABAergic transmission. *Cell Stem Cell.* 26, 462–466. doi: 10.1016/j.stem.2020.01.021

Ziabreva, I., Perry, E., Perry, R., Minger, S., Ekonomou, A., Przyborski, S., et al. (2006). Altered neurogenesis in Alzheimer's disease. *J. Psychosom. Res.* 61, 311–316. doi: 10.1016/j.jpsychores.2006.07.017

Ziegler-Waldkirch, S., d'Errico, P., Sauer, J., Erny, D., Savanthrapadian, S., Loreth, D., et al. (2018). Seed-induced Aβ deposition is modulated by microglia under environmental enrichment in a mouse model of Alzheimer's disease. *EMBO J.* 37, 167–182. doi: 10.15252/embj.201797021

frontiers | Frontiers in Neuroscience

TYPE Original Research
PUBLISHED 23 February 2023
DOI 10.3389/fnins.2023.1136499

Check for updates

OPEN ACCESS

EDITED BY
Jun Xu,
Beijing Tiantan Hospital, Capital Medical University, China

REVIEWED BY
Yi Qu,
Huazhong University of Science and Technology, China
Leonardo Sacco,
Neurocenter of Southern Switzerland, Switzerland

*CORRESPONDENCE
Chao Ren
✉ renchaotg@126.com
Dian-Shuai Gao
✉ gds@xzhmu.edu.cn

†These authors have contributed equally to this work

SPECIALTY SECTION
This article was submitted to Neurodegeneration, a section of the journal Frontiers in Neuroscience

RECEIVED 03 January 2023
ACCEPTED 10 February 2023
PUBLISHED 23 February 2023

CITATION
Tong S-Y, Wang R-W, Li Q, Liu Y, Yao X-Y, Geng D-Q, Gao D-S and Ren C (2023) Serum glial cell line-derived neurotrophic factor (GDNF) a potential biomarker of executive function in Parkinson's disease. *Front. Neurosci.* 17:1136499. doi: 10.3389/fnins.2023.1136499

COPYRIGHT
© 2023 Tong, Wang, Li, Liu, Yao, Geng, Gao and Ren. This is an open-access article distributed under the terms of the Creative Commons Attribution License (CC BY). The use, distribution or reproduction in other forums is permitted, provided the original author(s) and the copyright owner(s) are credited and that the original publication in this journal is cited, in accordance with accepted academic practice. No use, distribution or reproduction is permitted which does not comply with these terms.

Serum glial cell line-derived neurotrophic factor (GDNF) a potential biomarker of executive function in Parkinson's disease

Shu-Yan Tong[1†], Rui-Wen Wang[2†], Qian Li[3†], Yi Liu[4], Xiao-Yan Yao[5], De-Qin Geng[6], Dian-Shuai Gao[4*] and Chao Ren[5,7,8*]

[1]Department of Neurology, The Second Affiliated Hospital of Xuzhou Medical University, General Hospital of Xuzhou Mining Group, Xuzhou, Jiangsu, China, [2]Department of Anesthesiology, Yantai Yuhuangding Hospital, Qingdao University, Yantai, Shandong, China, [3]Department of Scientific Research, Yantai Yuhuangding Hospital, Qingdao University, Yantai, Shandong, China, [4]Department of Cell Biology and Neurobiology, Xuzhou Key Laboratory of Neurobiology, Xuzhou Medical University, Xuzhou, Jiangsu, China, [5]Department of Neurology, Yantai Yuhuangding Hospital, Qingdao University, Yantai, Shandong, China, [6]Department of Neurology, Affiliated Hospital of Xuzhou Medical University, Xuzhou, Jiangsu, China, [7]Shandong Provincial Innovation and Practice Base for Postdoctors, Yantai Yuhuangding Hospital, Yantai, Shandong, China, [8]Department of Otorhinolaryngology, Head and Neck Surgery, Yantai Yuhuangding Hospital, Qingdao University, Yantai, Shandong, China

Objective: Evidence shows that the impairment of executive function (EF) is mainly attributed to the degeneration of frontal-striatal dopamine pathway. Glial cell line-derived neurotrophic factor (GDNF), as the strongest protective neurotrophic factor for dopaminergic neurons (DANs), may play a role in EF to some extent. This study mainly explored the correlation between serum GDNF concentration and EF performance in Parkinson's disease (PD).

Methods: This study recruited 45 healthy volunteers (health control, HC) and 105 PD patients, including 44 with mild cognitive impairment (PD-MCI), 20 with dementia (PD-D), and 20 with normal cognitive function (PD-N). Neuropsychological tests were performed to evaluate EF (working memory, inhibitory control, and cognitive flexibility), attention, language, memory, and visuospatial function. All subjects were tested for serum GDNF and homovanillic acid (HVA) levels by ELISA and LC-ESI-MS/MS, respectively.

Results: PD-MCI patients showed impairments in the trail making test (TMT) A (TMT-A), TMT-B, clock drawing test (CDT) and semantic fluency test (SFT), whereas PD-D patients performed worse in most EF tests. With the deterioration of cognitive function, the concentration of serum GDNF and HVA in PD patients decreased. In the PD group, the serum GDNF and HVA levels were negatively correlated with TMT-A ($r_{GDNF} = -0.304$, $P < 0.01$; $r_{HVA} = -0.334$, $P < 0.01$) and TMT-B ($r_{GDNF} = -0.329$, $P < 0.01$; $r_{HVA} = -0.323$, $P < 0.01$) scores. Serum GDNF levels were positively correlated with auditory verbal learning test (AVLT-H) ($r = 0.252$, $P < 0.05$) and SFT ($r = 0.275$, $P < 0.05$) scores. Serum HVA levels showed a positively correlation with digit span test (DST) ($r = 0.277$, $P < 0.01$) scores. Stepwise linear regression analysis suggested that serum GDNF and HVA concentrations and UPDRS-III were the influence factors of TMT-A and TMT-B performances in PD patients.

Conclusion: The decrease of serum GDNF concentration in PD patients was associated with impaired inhibitory control, cognitive flexibility, and attention performances. The changes of GDNF and HVA might synergistically participate in the occurrence and development of executive dysfunction in PD patients.

KEYWORDS

Parkinson's disease, executive function, glial cell line-derived neurotrophic factor, homovanillic acid, neuropsychological test

Introduction

Mild cognitive impairment (MCI) is a transitional stage between normal aging and senile dementia, with a high risk of developing dementia (Svenningsson et al., 2012; Gonzalez-Redondo et al., 2014; Brennan et al., 2017). In patients with Parkinson's disease (PD), the incidence of MCI can reach 40% even in the early stage of the disease course (Litvan et al., 2012; Gonzalez-Redondo et al., 2014). Executive dysfunction (EDF) is the most prominent feature of PD with cognitive dysfunction, affecting about 30% of all PD patients. This deficit can occur in the early course of PD, and includes impairments in the coordination of a range of cognitive process required to achieve complex, goal-oriented and new cognitive operations (Parker et al., 2013), manifesting as impairments in the three core executive functions (EFs) (working memory, cognitive flexibility, and inhibitory control), as well as in higher-level EFs such as reasoning, problem solving, and planning (Diamond, 2013).

In PD patients, the degeneration of frontal-striatal dopamine pathway contributes to EDF, manifesting as deficits in cognitive flexibility, planning, inhibitory control and working memory, usually relate to MCI in PD; whereas the degeneration of cholinergic systems and Lewy body pathological changes in the posterior brain system result in the visuospatial and memory dysfunction, relate to dementia of PD (Kehagia et al., 2010, 2013). A study suggested that homovanillic acid (HVA), as the main metabolite of dopamine, could be used as an intracerebral marker of dopamine function and metabolism (Saracino et al., 2006).

Glial cell line-derived neurotrophic factor (GDNF) has a strong neurotrophic effect on a variety of neurons, especially on dopaminergic neurons (DANs). GDNF promotes the survival, morphological differentiation, damage repair, and dopamine release of DANs, and regulates their excitability in the midbrain (Grondin et al., 2003; Wang et al., 2011; Brown et al., 2018), and play important role in motor symptoms of animal models of PD. So we wonder if serum GDNF may be involved in the EDF of PD patients, by acting alone or in conjunction with HVA (Liu et al., 2020).

To this end, we studied the correlation of the levels of GDNF and HVA in the peripheral blood serum of PD patients with EF and its components (working memory, cognitive flexibility, and inhibitory control), in order to explore the possible mechanism of GDNF participating in the occurrence and development of EDF, and to provide a theoretical basis for early identification of cognitive dysfunction in PD.

Materials and methods

Subjects

We enrolled a total of 105 PD outpatients and inpatients from the Neurology Department of the Affiliated Hospital of Xuzhou Medical University between May 2016 and October 2017. Inclusion criteria: (1) aged between 40 and 80 years old; (2) able to complete all cognitive tests under doctor's instructions, and had no difficulties in listening, understanding and writing; (3) the diagnosis of PD was made independently by two experienced neurologists based on the UK PD Society Brain Bank Clinical Diagnostic Criteria (Hughes et al., 1993); (4) written informed consents were signed by the patients or their legal representatives. Exclusion criteria: (1) with neurological histories other than PD, e.g., moderate or serious brain injury, stroke, and vascular dementia confirmed by CT/MRI; (2) secondary parkinsonism induced by drugs, vascular lesions, tumors, trauma, and other insults, Parkinsonism-plus syndrome such as the progressive supranuclear palsy and multiple system atrophy; (3) major psychological diseases such as anxiety, depression and schizophrenia (Stuart et al., 2020); (4) systemic disease affecting the heart, liver or kidney, and other diseases that might affect cognitive function (Gonzalez-Redondo et al., 2014).

We also recruited 45 healthy normally aging volunteers with comparable age, sex, and education level with the PD patients as the healthy control (HC) group. Detailed materials and methods were as described in our previous research (Liu et al., 2020).

This study was approved by the ethics committee of the Affiliated Hospital of Xuzhou Medical University (approval no: XYFY2017-KL047-01). Written informed consents were signed by all subjects for enrollment.

Neuropsychological assessment

We assessed the global cognitive function and the five cognitive domains (attention, executive function, language, memory, and visuospatial function) of all subjects. The global cognitive function was assessed using the mini-mental state examination (MMSE). Attention was tested by forward digit span test (DST). Language was assessed by Boston naming test (BNT). Memory was examined

by auditory verbal learning test-HuaShan version (AVLT-H). Visuospatial function was evaluated by clock copying test (CCT).

Executive function was evaluated by trail making test (TMT) (inhibitory control), backward DST (working memory), clock drawing test (CDT) (planning and inhibitory control), semantic fluency test (SFT) (cognitive flexibility).

All patients were evaluated in the "ON" state, and those with scores 1.5 SD lower than the HC group were considered to have neuropsychological impairment. PD patients were classified using the diagnostic criteria recommended by Movement Disorder Society (MDS) of literature support as PD-MCI (Litvan et al., 2012) (n = 41) and PD-D (Emre et al., 2007) (n = 20). Those who did not fulfill criteria for PD-MCI or PD-D were classified as PD-N (n = 44).

Blood sampling

We took the blood sample from overnight fasting subjects between 8:00 a.m. and 9:00 a.m., including both the PD group and HC group. Blood samples were centrifuged at 1,500 × g for 15 min, aliquoted, and stored at −80°C until further examination.

Determination of serum GDNF and HVA concentrations

Serum GDNF and HVA concentrations were determined by enzyme linked immunosorbent assay (ELISA) and liquid chromatography tandem mass spectrometry (LC-ESI-MS/MS analysis), respectively.

Statistical analysis

SPSS 16.0 software was used for statistical analysis. Normality test was performed and normally distributed data were shown as mean ± standard deviation (X ± SD), whereas the non-normal data were expressed as median (interquartile range). T-test was used for comparison between two groups. For multi-group comparison, parametric data were analyzed by analysis of variance (ANOVA), and non-parametric data were compared by Kruskal–Wallis test, with LSD method (or Bonferroni method) for multiple comparison between groups. Correlation analysis was carried out using Pearson or Spearman correlation coefficient according to the distribution of variables. Stepwise linear regression analysis was used to identify the influence factors of cognitive test performance. Chi-square test was performed on binary variables. A two-sided $P < 0.05$ was considered statistical significance.

Results

Comparison of the general demographic data between the PD and HC groups

A total of 105 PD patients (PD group) were included in the study and classified into three groups: PD patients with normal cognitive function (PD-N, n = 44), PD patients with MCI (PD-MCI, n = 41), PD patients with dementia (PD-D, n = 20), and were compared with healthy controls (HC, n = 45) for general demographic data as well as MMSE and GDS-30 scores (Table 1). There was no significant difference in the age, sex ratio and education level among all four groups ($P > 0.05$). Compared with the HC group, PD patients had worse MMSE scores and more severely depressive symptoms (MMSE: H = 81.192, $P < 0.001$; GDS-30 $F_{3,150}$ = 9.958, $P < 0.001$).

We also compared the clinical symptoms (UPDRS-III and Hoehn-Yahr grades), course of disease and equivalent levodopa dose (LED) among PD-N, PD-MCI and PD-D groups (Table 1), and found a decrease of cognitive function with the increase of UPDRS-III score (H = 21.852, $P < 0.001$), Hoehn-Yahr grade (H = 30.868, $P < 0.001$) and the progress of disease course (H = 8.655, P = 0.013) in PD patients. There was a significant difference in LED among the three PD groups ($F_{2,105}$ = 9.386, $P < 0.001$). LED of the PD-D group was higher than that in the PD-N group and PD-MCI group ($P < 0.05$).

Different degrees of EF impairment among the PD groups

For all the cognitive tests that we performed, there were statistically significant differences among groups ($P < 0.001$). The scores of the PD-D group were lower than those of the PD-N, PD-MCI and HC groups ($P < 0.001$), except for CDT (PD-MCI vs. PD-D, P = 0.008). The performances of the PD-MCI group were lower than those of the HC group ($P < 0.001$) and PD-N group ($P < 0.001$) in four EF tests TMT-A, TMT-B, CDT, and CFT. For backward DST: HC vs. PD-MCI, P = 0.011, PD-N vs. PD-MCI, P = 0.197. There was no significant difference in the rest of the tests among the PD groups or in all test between the PD-N and HC groups ($P > 0.05$) (Table 2).

The serum GDNF and HVA concentrations of the PD group were lower than the HC group

There was a significant difference in serum GDNF level between the PD group (475.65 ± 139.43 pg/mL) and the HC group (572.96 ± 210.55 pg/mL) (t = 2.706, P = 0.008). The serum GDNF concentration of the PD-N group (532.13 ± 138.30 pg/mL) was significantly higher than that of the PD-MCI group (439.87 ± 139.59 pg/mL, $P < 0.01$) and the PD-D group (424.73 ± 101.96 pg/mL, $P < 0.01$). There was no statistically significant difference in the serum GDNF level between the PD-MCI group and the PD-D group (P = 0.899).

The serum HVA level in PD groups (65.55 ± 33.88 ng/mL) was significantly lower than the HC group (82.27 ± 32.98 ng/mL) (t = 2.972, P = 0.006). The serum HVA concentration of the PD-D group (44.88 ± 19.28 ng/mL) was lower than that of the PD-N group (76.24 ± 36.79 ng/mL, P = 0.001) and the PD-MCI

TABLE 1 Comparison of the general demographic data between the PD and HC groups.

	PD-N (*n* = 44)	PD-MCI (*n* = 41)	PD-D (*n* = 20)	HC (*n* = 45)	*P*-value
Age (years)	61.66 ± 8.31	65.02 ± 8.61	67.75 ± 6.16	64.56 ± 8.08	0.056
Education (years)	10.82 ± 2.36	9.93 ± 2.30	9.35 ± 2.23	10.58 ± 2.96	0.090
Male *n* (%)	27 (61.4%)	23 (56.1%)	6 (30.0%)	27 (55.3%)	0.100
MMSE score	28.5 (27–29)	27 (27–28)	22 (20–23)	29 (28–29.5)	< 0.001
GDS-30 score	9.48 ± 6.16	7.76 ± 4.6	15.15 ± 6.48	6.62 ± 3.97	< 0.001
UPDRS-III score	20.24 ± 8.03	28.24 ± 8.88	34.08 ± 7.28	–	< 0.001
Hoehn-Yahr grade	1.75 (1–2)	2.5 (2–2.75)	3 (2.5–3)	–	< 0.001
Disease course (months)	24 (9–57)	24 (12–66)	54 (24–93)	–	0.013
LED (mg/d)	297.16 ± 27.48	354.57 ± 31.37	534.38 ± 56.19	–	< 0.001

PD-N, PD with normal cognitive function; PD-MCI, PD with mild cognitive impairment; PD-D, PD with dementia; HC, normal control; MMSE, mini-mental state examination; GDS-30, Geriatric Depression Scale-30; UPDRS-III, unified PD rating scale part III exercise evaluation; LED, equivalent levodopa dose. Data were represented as X ± SD or median (interquartile range).

TABLE 2 Comparison of neuropsychological test results between the PD groups and the HC group.

	PD-N (*n* = 44)	PD-MCI (*n* = 41)	PD-D (*n* = 20)	HC (*n* = 45)	*P*-value
Forward DST (n)	6 (6–8)	6 (5–7)	4 (3.5–4)	6 (6–7.5)	< 0.001
Backward DST (*n*)	4 (3–5)	4 (3–4)	2 (2–3)	4 (4–5)	< 0.001
Total digit span (*n*)	11 (9.5–12)	10 (9–11)	6 (6–7)	4 (4–5)	< 0.001
TMT-A (s)	60.80 ± 16.31	89.07 ± 36.46	120.95 ± 41.09	55.42 ± 27.22	< 0.001
TMT-B (s)	134.18 ± 29.09	205.29 ± 50.67	270.25 ± 29.08	132.84 ± 48.61	< 0.001
CDT	4 (4–4)	3 (2–4)	1 (1–1.5)	4 (4–4)	< 0.001
SFT (*n*)	15.36 ± 2.87	12.37 ± 2.87	10.75 ± 3.14	15.76 ± 2.87	< 0.001
BNT (*n*)	22.55 ± 2.71	20.46 ± 3.39	18.60 ± 3.28	23.51 ± 3.56	< 0.001
AVLT-H free recall (n)	17.95 ± 4.64	12.49 ± 4.67	8.10 ± 4.14	17.82 ± 5.32	< 0.001
CCT	4 (4–4)	4 (3–4)	1 (1–4)	4 (4–4)	< 0.001

PD-N, PD with normal cognitive function; PD-MCI, PD with mild cognitive impairment; PD-D, PD with dementia; HC, normal control; DST, digit span test; TMT, trail making test; CDT, clock drawing test; SFT, semantic fluency test; BNT, Boston naming test; AVLT-H, auditory verbal learning test-HuaShan version; CCT, clock copying test. Data were represented as X ± SD or median (interquartile range).

group (64.16 ± 31.81 ng/mL, $P = 0.035$). There was no significant difference in serum HVA level between the PD-D group and the PD-MCI group ($P = 0.087$) (Figure 1).

Serum GDNF level was related to TMT and SFT, and serum HVA level was related to TMT and DST in PD groups

The comparison of the correlation between GDNF serum concentration and neuropsychological test showed that in PD group, serum GDNF level was negatively correlated with TMT-A and TMT-B scores, and positively correlated with AVLT-H and SFT performances. There was no correlation with the HC groups.

Through correlation analysis of serum HVA concentration and cognition function, we found that in the PD groups, HVA serum level was negatively correlated with TMT-A and TMT-B scores, and positively correlated with backward DST and total DST scores. There was no correlation with the HC group (Table 3 and Figure 2).

Serum GDNF and HVA concentrations and UPDRS-III were the influence factors of TMT-A and TMT-B performances in PD patients

The neuropsychological tests performed in this study were taken as dependent variables, and the GDNF, HVA, sex, age, course of disease, medication, UPDRS-III, Hoehn-Yahr grade were taken as independent variables for stepwise linear regression analysis, in order to identify the influence factors that predict the performance of neuropsychological tests. The results were as follows: When using TMT-A as the dependent variable ($F_{3,105} = 25.756$, $P < 0.001$, $R^2 = 0.665$, adjusted $R^2 = 0.639$), among the included variables GDNF, HVA and UPDRS-III had statistically significant impacts on the test results ($P < 0.05$) (Table 4). When using TMT-B as the dependent variable ($F_{4,105} = 25.756$, $P < 0.001$, $R^2 = 0.700$, adjusted $R^2 = 0.668$), among the included variables, GDNF, HVA, UPDRS-III, and age had statistically significant impacts on the test results ($P < 0.05$) (Table 5). The performances of TMT-A and TMT-B improved with the increase of GDNF and HVA concentrations,

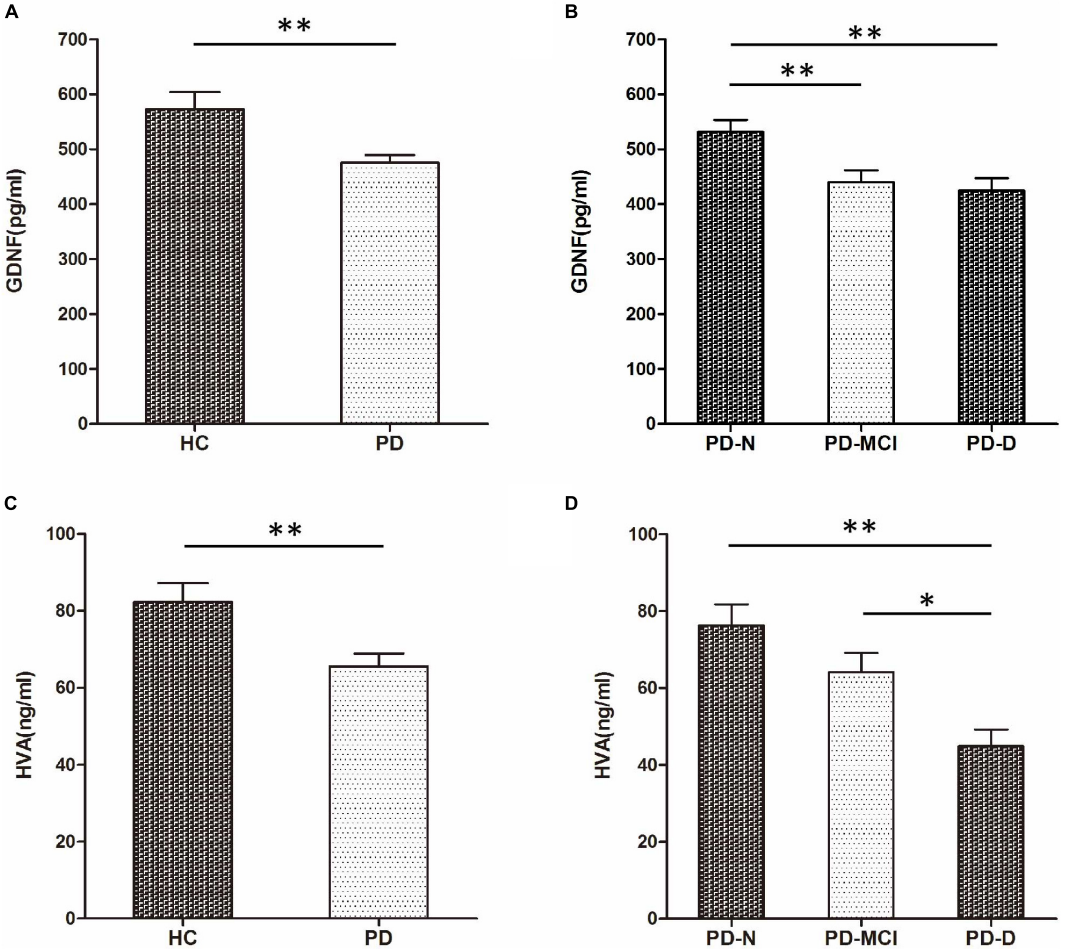

FIGURE 1
Comparison of serum glial cell line-derived neurotrophic factor (GDNF) and homovanillic acid (HVA) concentrations among groups. **(A)** Comparison of serum GDNF concentration between HC and PD groups. **(B)** Comparison of serum GDNF concentrations among PD-N, PD-MCI, and PD-D groups. **(C)** Comparison of serum HVA concentration between HC and PD groups. **(D)** Comparison of serum HVA concentration among PD-N, PD-MCI, and PD-D groups. $^{*}P < 0.05$ and $^{**}P < 0.01$.

TABLE 3 Relationship between serum glial cell line-derived neurotrophic factor (GDNF) or high vanillic acid (HVA) concentration and neuropsychological tests (correlation coefficient *r*).

	GDNF (pg/mL)		HVA (ng/mL)	
	PD (*n* = 105)	HC (*n* = 45)	PD (*n* = 105)	HC (*n* = 45)
Backward DST[a]	0.143	0.238	0.277**	0.246
Forward DST[a]	0.175	−0.015	0.185	0.049
Total DST[a]	0.186	0.132	0.25*	0.15
TMT-A (s)[b]	−0.304**	0.006	−0.334**	−0.165
TMT-B (s)[b]	−0.329**	−0.083	−0.323**	−0.165
SFT[b]	0.275*	0.164	0.104	0.213
CDT[a]	0.177	0.005	0.166	0.046
BNT[b]	0.061	0.014	0.006	0.256
AVLT-H[b]	0.252*	−0.153	0.147	0.051
CCT[a]	0.092	0.035	0.152	0.046

DST, digit span test; TMT, trail making test; SFT, semantic fluency test; CDT, clock drawing test; CCT, clock copying test; AVLT-H, auditory verbal learning test-HuaShan version.
[a]Spearman correlation coefficient.
[b]Pearson's correlation coefficient.
$^{*}P < 0.05$ and $^{**}P < 0.01$.

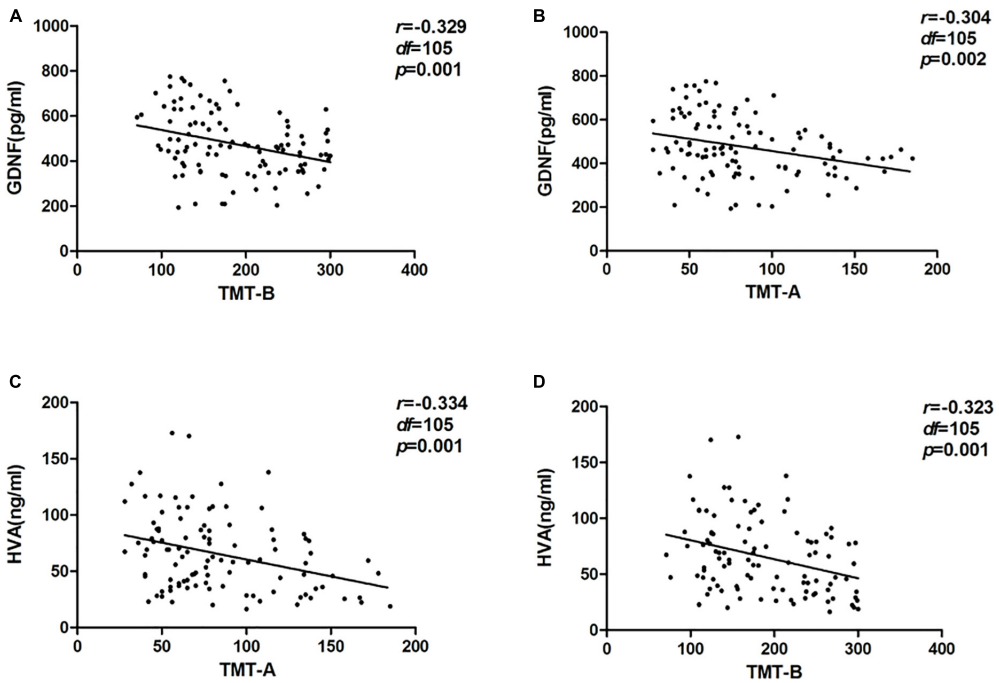

FIGURE 2
Correlation between serum glial cell line-derived neurotrophic factor (GDNF) and homovanillic acid (HVA) concentrations and trail making test (TMT) in the PD group. **(A)** Correlation between serum GDNF concentration and TMT-A. **(B)** Correlation between serum GDNF concentration and TMT-B. **(C)** Correlation between serum HVA concentration and TMT-A. **(D)** Correlation between serum HVA concentration and TMT-B.

TABLE 4 Stepwise linear regression analysis result of TMT-A as the dependent variable.

Independent variable	Unstandardized coefficients (B)	Standard error (SE)	Standardized regression coefficient (β)	*T*-value	*P*-value
Constant term	172.262	18.699	–	9.201	< 0.001
GDNF	−0.107	0.030	−0.356	−3.582	0.001
HVA	−0.387	0.101	−0.415	−3.846	< 0.001
UPDRS-III	1.203	0.378	0.325	3.185	0.003

GDNF, glial cell line-derived neurotrophic factor; HVA, homovanillic acid; UPDRS-III, unified PD rating scale part III-motor function.

and deteriorated with the aggravation of motor symptoms. The performance of TMT-B also deteriorated with the increase of age.

When using SFT was taken as the dependent variable, the influences of UPDRS-III and education level on the test performance were statistically significant. The SFT performance worsened with the aggravation of motor symptoms and progression of disease, and improved with the increase of education level. Hoehn-Yahr grade was an independent influence factor of CDT, AVLT, backward DST, and total DST, which increased with the severity of the disease. The influence factor of BNT performance was UPDRS-III, which the test performance deteriorated with the aggravation of motor symptoms.

Discussion

The cognitive progress of PD patients can develop from the normal cognitive function stage (PD with normal cognition, PD-N) to the transition stage of PD with MCI (PD-MCI), and finally deteriorates to dementia (PD with dementia, PD-D) (Litvan et al., 2012). There is a high risk of MCI developing dementia (Svenningsson et al., 2012). Cognitive impairment in PD affects patient's EF, attention, memory, language and visuospatial function, among which the EDF seems to be the most serious (Kehagia et al., 2013). In PD patients, the depletion of dopamine may lead to the disruption of the frontal-striatal circuit, which contributes to EDF (Uekermann et al., 2004; Kudlicka et al., 2011; Zhang et al., 2020).

In this study, the PD-N patients did not show obvious EDF. PD-MCI patients mainly suffered from impairment of attention, planning, inhibitory control, attention switching, and cognitive flexibility, which largely accorded with the results of Kudlicka et al. (2011), that is, impairment of EFs including the cognitive flexibility, reaction inhibition, inhibitory distraction of attention, and attention maintenance can occur in the early stage of PD. Unsurprisingly, PD-D patients performed worse in extensive EF tests. At present, the exact development pattern of EDF in PD is still controversial (Diamond, 2013), which may be attributed to the complex pathoanatomical mechanism of PD. The dual syndrome hypothesis holds that degeneration of frontal-striatal dopamine

TABLE 5 Stepwise linear regression analysis results of TMT-B test as dependent variable.

Independent variable	Unstandardized coefficients (B)	Standard error (SE)	Standardized regression coefficient (β)	*T*-value	*P*-value
Constant term	162.492	32.873	–	4.943	< 0.001
GDNF	−0.119	0.036	−0.272	−3.284	0.002
HVA	−0.454	0.129	−0.321	−3.506	0.001
UPDRS-III	1.829	0.448	0.395	4.088	< 0.001
Age	1.431	0.439	0.294	3.259	0.002

GDNF, glial cell line-derived neurotrophic factor; HVA, homovanillic acid; UPDRS-III, unified PD rating scale part III-motor function.

pathway contributes to executive dysfunction, manifesting as deficits in cognitive flexibility, planning, inhibitory control and working memory, usually relate to MCI in PD; whereas the degeneration of cholinergic systems and Lewy body pathological changes in the posterior brain system result in the visuospatial and memory dysfunction, relate to dementia of PD (Kehagia et al., 2010, 2013). The dopamine overdose hypothesis holds that dopamine deficiency first appears in the dorsal striatum at the early stage of PD, whereas dopamine is relatively better preserved in the ventral striatum, and the dorsolateral frontal striatal pathway is more likely to degenerate in the early stage of PD than the ventral frontal striatal pathway. Therefore, impairment of attention switching mainly occurs in the early stage, whereas the reverse learning ability (cognitive flexibility) is better preserved in the dorsal side (Vaillancourt et al., 2013). The results of this study found that the impaired performance of attention switching and cognitive flexibility in early PD patients might be related to the overdose effect of dopamine medication on the ventral striatum. On the other hand, it might also be association with the complex and vague features of EF *per se* (Zhang et al., 2020).

This study also found lower peripheral serum GDNF level in the PD patients than the health controls, which was consistent with the results of previous clinical studies. One study found that the GDNF concentration in cerebrospinal fluid of PD patients was lower than that of normal controls, and was lower in early PD patients than late PD patients (Vaillancourt et al., 2013). Nagatsu and Sawada (2007) reported that the concentration of neurotrophic factors including GDNF decreased in the substantia nigra of PD patients. A large number of trials had used GDNF as a potential therapy to treat motor symptoms of PD. At present, gene and cell therapies are widely applied in preclinical and clinical researches, and have achieved certain success (Garbayo et al., 2016). However, the research of GDNF application in the field of cognition in PD patients was mostly limited to animal experiments. Some studies found that after intracerebroventricular injection of lentiviral vector carrying the human *GDNF* coding sequence in PD rats, the expression of GDNF increased and the spatial learning and memory ability improved (Lu-Nguyen et al., 2014). Another study described reduced GDNF concentration in the brain of rats with induced nerve infection, and their cognitive function, especially learning and memory, also deteriorated (Gui et al., 2017). It was also found that after amantadine treatment, the expression of GDNF in the hippocampus of PD rats increased, and their learning and memory abilities also improved (Zhang et al., 2014).

Through further exploration of the correlation between serum GDNF and neuropsychological test performance, this study found that the increase of GDNF concentration was correlated with better working memory, attention, inhibitory control, cognitive flexibility and memory. The correlation between serum GDNF concentration and EF tests has been reported previously, and it was found that the serum GDNF concentration of schizophrenic patients who were initially untreated was negatively correlated with the performance of TMT-B (Xiao et al., 2017). Niitsu et al. (2014) found that the GDNF concentration in the peripheral serum was positively correlated with DST performance in the healthy normal population. The research of Wang et al. (2011) showed that the plasma GDNF concentration of late-onset depression patients was positively correlated with the performance of backward DST and negatively correlated with that of TMT-B. These results show that with the increase of GDNF concentration, the test performance of attention and working memory improves, which is consistent with our results. We also found that GDNF is correlated with the performance of AVLT (memory), TMT-A (attention) and SFT (cognitive flexibility). We believed that the improvement of cognition induced by GDNF might be related to its strong neurotrophic and neuroprotective effects not only on DANs, but also on the serotonin neurons, norepinephrine neurons, cholinergic neurons. Studies have found that the complex neurotransmitter circuits are involved in various cognitive processes (Murley and Rowe, 2018; Hirano, 2021). For example, the dopamine system is involved in the regulation of EF by the frontal system (Halliday et al., 2014), the serotonin system is closely related to cognitive flexibility (Clarke et al., 2004), the norepinephrine system can affect set-switching, attention, response inhibition and reverse learning (Logue and Gould, 2014), and episodic memory coding and spatial memory processing are thought to rely on the acetylcholine system to maintain normal functions (Newman et al., 2012). GDNF might synergistically participate in the process of cognitive function through its neuroprotective effects by regulating the survival of these neurons and synaptic plasticity. Another theory believes that GDNF can antagonize the degeneration of neurons and thus delay the occurrence of cognitive decline. The specific mechanism is not completely clear, which may involve the antagonism of GDNF against oxidative stress, inhibition of microglial excitability and neuroinflammation (Gill et al., 2003; Tome et al., 2017).

In addition, this study also found that the serum HVA concentration in PD patients was lower than that in normal controls. HVA is the main metabolite of dopamine, and the measurement of HVA concentration in body fluid may be the most direct method to reflect the function and activity changes of human central DANs (Pickar et al., 1988). Through further analysis of the correlations between HVA concentration and the performances of EF tests in PD patients, we found that serum HVA level was closely related to the performance of backward DST, total DST and

TWT in PD patient, suggesting the correlation between serum HVA level with the EF components such as working memory, inhibitory control, cognitive flexibility, and attention. This was consistent with the results of a previous study that the dopamine system is involved in the regulation of EF by the prefrontal cortex (Martinez et al., 2016).

The levels of GDNF and HVA in peripheral serum were negatively correlated with the performance of TMT-A and TMT-B in PD patients. Regression analysis showed that both GDNF and HVA were influence factors for TMT performance. A meta-analysis by Yuan and Raz (2014) showed that the prefrontal cortex (especially the lateral prefrontal cortex) was involved in the regulation of functional tests such as trial making tests. In this study, we proposed that there were two possible causes of EF impairment in PD patients. On one hand, primary PD is usually accompanied by EDF similar to that in patients with frontal lobe injury (Christopher and Strafella, 2013; Mak et al., 2014), especially the degeneration of the dorsolateral prefrontal cortex and its closely related dorsal striatum dopamine system (O'Callaghan et al., 2014; Koshimori et al., 2015). On the other hand, we suspected that GDNF might be involved in the development of EDF possibly through the following mechanisms: (1) GDNF indirectly affect EF through its protective and repair effects on DANs. GDNF has a protective effect on midbrain DANs. GDNF prevents the loss of DANs and the degeneration of dopaminergic nerve terminals, and increase the level of dopamine in the striatum (Olanow et al., 2015). (2) GDNF antagonizes aging-related cognitive decline through an unknown mechanism. It antagonizes neuronal degeneration through antioxidant stress, inhibition of microglial excitability, and neuroinflammation (Pertusa et al., 2008; Budni et al., 2015). (3) More consistent evidence proved that brain-derived neurotrophic factor and GDNF participate in the pathophysiological process of PD (Nagatsu and Sawada, 2007). Therefore, GDNF might affect the cognitive process of PD patients through a yet unknown mechanism.

Conclusion and expectation

Under our experimental conditions, this study found that the decrease of serum GDNF concentration in PD patients was associated with inhibitory control, cognitive flexibility, and attention performances. The changes of GDNF and HVA might synergistically participate in the occurrence and development of executive dysfunction in PD patients. Of course, due to the limitation of funds and other conditions, our research also has some shortcomings. We did not use objective cognitive assessment tools, such as functional MRI or PET scanning, to evaluate EF. Our study was a cross-sectional study rather than a cohort study and without follow-up study. All subjects were limited to the affiliated hospital of Xuzhou Medical University, and no other multicenter study data. In the future, more in-depth studies will be carried out combining animal models, cell experiments, functional imaging methodologies and multicenter prospective cohort study to explore its possible mechanism. Although there are a few limitations in this study, we have solved some problems in this field. All in all, GDNF might be used as a biomarker to identify early cognitive decline in PD, and might serve in clinical practice.

Data availability statement

The original contributions presented in this study are included in the article/supplementary material, further inquiries can be directed to the corresponding authors.

Ethics statement

This study was approved by the Ethics Committee of the Affiliated Hospital of Xuzhou Medical University (approval no: XYFY2017-KL047-01). Written informed consents were signed by all subjects for enrollment. The patients/participants provided their written informed consent to participate in this study.

Author contributions

CR and D-SG: conception, design, and administrative support. S-YT, R-WW, and QL: provision of study materials. S-YT, R-WW, QL, YL, X-YY, and D-QG: collection and assembly of data. S-YT, D-SG, and CR: data analysis and interpretation. All authors manuscript writing and final approval of manuscript.

Funding

This work was supported by the Key Project of Shandong Provincial Natural Science Foundation (ZR2020KH024), the National Natural Science Foundation of China (81971006), the Yantai Science and Technology Innovation Development Plan (2022YD004), and the Outstanding Young Talents Project in Health of Qilu.

Acknowledgments

We thank to all the staffs and subjects who participated in the investigation.

Conflict of interest

The authors declare that the research was conducted in the absence of any commercial or financial relationships that could be construed as a potential conflict of interest.

Publisher's note

All claims expressed in this article are solely those of the authors and do not necessarily represent those of their affiliated organizations, or those of the publisher, the editors and the reviewers. Any product that may be evaluated in this article, or claim that may be made by its manufacturer, is not guaranteed or endorsed by the publisher.

References

Brennan, L., Devlin, K. M., Xie, S. X., Mechanic-Hamilton, D., Tran, B., Hurtig, H. H., et al. (2017). Neuropsychological subgroups in non-demented parkinson's disease: a latent class analysis. *J. Parkinsons. Dis.* 7, 385–395. doi: 10.3233/JPD-171081

Brown, R. W., Schlitt, M. A., Owens, A. S., DePreter, C. C., Cummins, E. D., Kirby, S. L., et al. (2018). Effects of environmental enrichment on nicotine sensitization in rats neonatally treated with quinpirole: analyses of glial cell line-derived neurotrophic factor and implications towards schizophrenia. *Dev. Neurosci.* 40, 64–72. doi: 10.1159/000486391

Budni, J., Bellettini-Santos, T., Mina, F., Garcez, M. L., and Zugno, A. I. (2015). The involvement of BDNF, NGF and GDNF in aging and Alzheimer's disease. *Aging Dis.* 6, 331–341. doi: 10.14336/AD.2015.0825

Christopher, L., and Strafella, A. P. (2013). Neuroimaging of brain changes associated with cognitive impairment in Parkinson's disease. *J. Neuropsychol.* 7, 225–240.

Clarke, H. F., Dalley, J. W., Crofts, H. S., Robbins, T. W., and Roberts, A. C. (2004). Cognitive inflexibility after prefrontal serotonin depletion. *Science* 304, 878–880.

Diamond, A. (2013). Executive functions. *Annu. Rev. Psychol.* 64, 135–168.

Emre, M., Aarsland, D., Brown, R., Burn, D. J., Duyckaerts, C., Mizuno, Y., et al. (2007). Clinical diagnostic criteria for dementia associated with Parkinson's disease. *Mov. Disord.* 22, 1689–1707.

Garbayo, E., Ansorena, E., Lana, H., Carmona-Abellan, M. D., Marcilla, I., Lanciego, J. L., et al. (2016). Brain delivery of microencapsulated GDNF induces functional and structural recovery in parkinsonian monkeys. *Biomaterials* 110, 11–23. doi: 10.1016/j.biomaterials.2016.09.015

Gill, S. S., Patel, N. K., Hotton, G. R., O'Sullivan, K., McCarter, R., Bunnage, M., et al. (2003). Direct brain infusion of glial cell line-derived neurotrophic factor in Parkinson disease. *Nat. Med.* 9, 589–595.

Gonzalez-Redondo, R., García-García, D., Clavero, P., Gasca-Salas, C., García-Eulate, R., Zubieta, J. L., et al. (2014). Grey matter hypometabolism and atrophy in Parkinson's disease with cognitive impairment: a two-step process. *Brain* 137(Pt 8), 2356–2367.

Grondin, R., Cass, W. A., Zhang, Z., Stanford, J. A., Gash, D. M., and Gerhardt, G. A. (2003). Glial cell line-derived neurotrophic factor increases stimulus-evoked dopamine release and motor speed in aged rhesus monkeys. *J. Neurosci.* 23, 1974–1980. doi: 10.1523/JNEUROSCI.23-05-01974.2003

Gui, L., Lei, X., and Zuo, Z. (2017). Decrease of glial cell-derived neurotrophic factor contributes to anesthesia- and surgery-induced learning and memory dysfunction in neonatal rats. *J. Mol. Med.* 95, 369–379. doi: 10.1007/s00109-017-1521-9

Halliday, G. M., Leverenz, J. B., Schneider, J. S., and Adler, C. H. (2014). The neurobiological basis of cognitive impairment in Parkinson's disease. *Mov. Disord.* 29, 634–650.

Hirano, S. (2021). Clinical implications for dopaminergic and functional neuroimage research in cognitive symptoms of Parkinson's disease. *Mol. Med.* 27:40.

Hughes, A. J., Daniel, S. E., Blankson, S., and Lees, A. J. (1993). A clinicopathologic study of 100 cases of Parkinson's disease. *Arch. Neurol.* 50, 140–148.

Kehagia, A. A., Barker, R. A., and Robbins, T. W. (2010). Neuropsychological and clinical heterogeneity of cognitive impairment and dementia in patients with Parkinson's disease. *Lancet Neurol.* 9, 1200–1213.

Kehagia, A. A., Barker, R. A., and Robbins, T. W. (2013). Cognitive impairment in Parkinson's disease: the dual syndrome hypothesis. *Neurodegener. Dis.* 11, 79–92.

Koshimori, Y., Segura, B., Christopher, L., Lobaugh, N., Duff-Canning, S., Mizrahi, R., et al. (2015). Imaging changes associated with cognitive abnormalities in Parkinson's disease. *Brain Struct. Funct.* 220, 2249–2261.

Kudlicka, A., Clare, L., and Hindle, J. V. (2011). Executive functions in Parkinson's disease: systematic review and meta-analysis. *Mov. Disord.* 26, 2305–2315.

Litvan, I., Goldman, J. G., Tröster, A. I., Schmand, B. A., Weintraub, D., Petersen, R. C., et al. (2012). Diagnostic criteria for mild cognitive impairment in Parkinson's disease: movement Disorder Society Task Force guidelines. *Mov. Disord.* 27, 349–356.

Liu, Y., Tong, S., Ding, L., Liu, N., and Gao, D. (2020). Serum levels of glial cell line-derived neurotrophic factor and multiple neurotransmitters: in relation to cognitive performance in Parkinson's disease with mild cognitive impairment. *Int. J. Geriatr. Psychiatry* 35, 153–162. doi: 10.1002/gps.5222

Logue, S. F., and Gould, T. J. (2014). The neural and genetic basis of executive function: attention, cognitive flexibility, and response inhibition. *Pharmacol. Biochem. Behav.* 123, 45–54. doi: 10.1016/j.pbb.2013.08.007

Lu-Nguyen, N. B., Broadstock, M., Schliesser, M. G., Bartholomae, C. C., von Kalle, C., Schmidt, M., et al. (2014). Transgenic expression of human glial cell line-derived neurotrophic factor from integration-deficient lentiviral vectors is neuroprotective in a rodent model of Parkinson's disease. *Hum. Gene Ther.* 25, 631–641. doi: 10.1089/hum.2014.003

Mak, E., Zhou, J., Tan, L. C., Au, W. L., Sitoh, Y. Y., and Kandiah, N. (2014). Cognitive deficits in mild Parkinson's disease are associated with distinct areas of grey matter atrophy. *J. Neurol. Neurosurg. Psychiatry* 85, 576–580.

Martinez, L., Prada, E., Satler, C., Tavares, M. C. H., and Tomaz, C. (2016). Executive dysfunctions: the role in attention deficit hyperactivity and post-traumatic stress neuropsychiatric disorders. *Front. Psychol.* 7:1230. doi: 10.3389/fpsyg.2016.01230

Murley, A. G., and Rowe, J. B. (2018). Neurotransmitter deficits from frontotemporal lobar degeneration. *Brain* 141, 1263–1285.

Nagatsu, T., and Sawada, M. (2007). Biochemistry of postmortem brains in Parkinson's disease: historical overview and future prospects. *J. Neural Transm. Suppl.* 72, 113–120. doi: 10.1007/978-3-211-73574-9_14

Newman, E. L., Gupta, K., Climer, J. R., Monaghan, C. K., and Hasselmo, M. E. (2012). Cholinergic modulation of cognitive processing: insights drawn from computational models. *Front. Behav. Neurosci.* 6:24. doi: 10.3389/fnbeh.2012.00024

Niitsu, T., Shirayama, Y., Matsuzawa, D., Shimizu, E., Hashimoto, K., and Iyo, M. (2014). Association between serum levels of glial cell-line derived neurotrophic factor and attention deficits in schizophrenia. *Neurosci. Lett.* 575, 37–41. doi: 10.1016/j.neulet.2014.05.034

O'Callaghan, C., Bertoux, M., and Hornberger, M. (2014). Beyond and below the cortex: the contribution of striatal dysfunction to cognition and behaviour in neurodegeneration. *J. Neurol. Neurosurg. Psychiatry* 85, 371–378. doi: 10.1136/jnnp-2012-304558

Olanow, C. W., Bartus, R. T., Volpicelli-Daley, L. A., and Kordower, J. H. (2015). Trophic factors for Parkinson's disease: to live or let die. *Mov. Disord.* 30, 1715–1724.

Parker, K. L., Lamichhane, D., Caetano, M. S., and Narayanan, N. S. (2013). Executive dysfunction in Parkinson's disease and timing deficits. *Front. Integr. Neurosci.* 7:75. doi: 10.3389/fnint.2013.00075

Pertusa, M., García-Matas, S., Mammeri, H., Adell, A., Rodrigo, T., Mallet, J., et al. (2008). Expression of GDNF transgene in astrocytes improves cognitive deficits in aged rats. *Neurobiol. Aging* 29, 1366–1379. doi: 10.1016/j.neurobiolaging.2007.02.026

Pickar, D., Breier, A., and Kelsoe, J. (1988). Plasma homovanillic acid as an index of central dopaminergic activity: studies in schizophrenic patients. *Ann. N.Y. Acad. Sci.* 537, 339–346.

Saracino, M. A., Mandrioli, R., Mercolini, L., Ferranti, A., Zaimovic, A., Leonardi, C., et al. (2006). Determination of homovanillic acid (HVA) in human plasma by HPLC with coulometric detection and a new SPE procedure. *J. Pharm. Biomed. Anal.* 42, 107–112. doi: 10.1016/j.jpba.2005.11.030

Stuart, S., Morris, R., Giritharan, A., Quinn, J., Nutt, J. G., and Mancini, M. (2020). Prefrontal cortex activity and gait in parkinson's disease with cholinergic and dopaminergic therapy. *Mov. Disord.* 35, 2019–2027. doi: 10.1002/mds.28214

Svenningsson, P., Westman, E., Ballard, C., and Aarsland, D. (2012). Cognitive impairment in patients with Parkinson's disease: diagnosis, biomarkers, and treatment. *Lancet Neurol.* 11, 697–707.

Tome, D., Fonseca, C. P., Campos, F. L., and Baltazar, G. (2017). Role of neurotrophic factors in Parkinson's disease. *Curr. Pharm. Des.* 23, 809–838.

Uekermann, J., Daum, I., Bielawski, M., Muhlack, S., Peters, S., Przuntek, H., et al. (2004). Differential executive control impairments in early Parkinson's disease. *J. Neural. Transm. Suppl.* 68, 39–51.

Vaillancourt, D. E., Schonfeld, D., Kwak, Y., Bohnen, N. I., and Seidler, R. (2013). Dopamine overdose hypothesis: evidence and clinical implications. *Mov. Disord.* 28, 1920–1929. doi: 10.1002/mds.25687

Wang, X., Hou, Z., Yuan, Y., Hou, G., Liu, Y., Li, H., et al. (2011). Association study between plasma GDNF and cognitive function in late-onset depression. *J. Affect. Disord.* 132, 418–421. doi: 10.1016/j.jad.2011.03.043

Xiao, W., Ye, F., Liu, C., Tang, X., Li, J., Dong, H., et al. (2017). Cognitive impairment in first-episode drug-naive patients with schizophrenia: relationships with serum concentrations of brain-derived neurotrophic factor and glial cell line-derived neurotrophic factor. *Prog. Neuropsychopharmacol. Biol. Psychiatry* 76, 163–168. doi: 10.1016/j.pnpbp.2017.03.013

Yuan, P., and Raz, N. (2014). Prefrontal cortex and executive functions in healthy adults: a meta-analysis of structural neuroimaging studies. *Neurosci. Biobehav. Rev.* 42, 180–192.

Zhang, J., Tan, H., Jiang, W., and Zuo, Z. (2014). Amantadine alleviates postoperative cognitive dysfunction possibly by increasing glial cell line-derived neurotrophic factor in rats. *Anesthesiology* 121, 773–785. doi: 10.1097/ALN.0000000000000352

Zhang, Q., Aldridge, G. M., Narayanan, N. S., Anderson, S. W., and Uc, E. Y. (2020). Approach to cognitive impairment in Parkinson's disease. *Neurotherapeutics* 17, 1495–1510.

frontiers | Frontiers in Aging Neuroscience

TYPE Original Research
PUBLISHED 23 February 2023
DOI 10.3389/fnagi.2023.1072184

Check for updates

OPEN ACCESS

EDITED BY
Shenfeng Qiu,
University of Arizona,
United States

REVIEWED BY
Zhixiang Yu,
Fourth Military Medical University,
China
Yaozeng Xu,
The First Affiliated Hospital of Soochow University,
China

*CORRESPONDENCE
Fang Ye
✉ yfxh00@163.com

SPECIALTY SECTION
This article was submitted to
Cellular and Molecular Mechanisms of Brain-aging,
a section of the journal
Frontiers in Aging Neuroscience

RECEIVED 17 October 2022
ACCEPTED 30 January 2023
PUBLISHED 23 February 2023

CITATION
Zhang J, Li X, Xiao J, Xiang Y and Ye F (2023) Analysis of gene expression profiles in Alzheimer's disease patients with different lifespan: A bioinformatics study focusing on the disease heterogeneity.
Front. Aging Neurosci. 15:1072184.
doi: 10.3389/fnagi.2023.1072184

COPYRIGHT
© 2023 Zhang, Li, Xiao, Xiang and Ye. This is an open-access article distributed under the terms of the Creative Commons Attribution License (CC BY). The use, distribution or reproduction in other forums is permitted, provided the original author(s) and the copyright owner(s) are credited and that the original publication in this journal is cited, in accordance with accepted academic practice. No use, distribution or reproduction is permitted which does not comply with these terms.

Analysis of gene expression profiles in Alzheimer's disease patients with different lifespan: A bioinformatics study focusing on the disease heterogeneity

Ji Zhang[1], Xiaojia Li[2,3], Jun Xiao[2,3], Yang Xiang[2,3] and Fang Ye[2,3]*

[1]Department of Neurology, West China Hospital of Sichuan University, Chengdu, China, [2]Department of Neurology, Sichuan Academy of Medical Sciences & Sichuan Provincial People's Hospital, Chengdu, China, [3]Department of Neurology, Chinese Academy of Sciences Sichuan Translational Medicine Research Hospital, Chengdu, China

Objective: Alzheimer's disease (AD) as the most frequent neurodegenerative disease is featured by gradual decline of cognition and social function in the elderly. However, there have been few studies focusing on AD heterogeneity which exists both genetically and clinically, leading to the difficulties of AD researches. As one major kind of clinical heterogeneity, the lifespan of AD patients varies significantly. Aiming to investigate the potential driving factors, the current research identified the differentially expressed genes (DEGs) between longer-lived AD patients and shorter-lived ones *via* bioinformatics analyses.

Methods: Qualified datasets of gene expression profiles were identified in National Center of Biotechnology Information Gene Expression Omnibus (NCBI-GEO). The data of the temporal lobes of patients above 60years old were used. Two groups were divided according to the lifespan: the group ≥85years old and the group <85years old. Then GEO2R online software and R package of Robust Rank Aggregation (RRA) were used to screen DEGs. Bioinformatic tools were adopted to identify possible pathways and construct protein–protein interaction network.

Result: Sixty-seven AD cases from four qualified datasets (GSE28146, GSE5281, GSE48350, and GSE36980) were included in this study. 740 DEGs were identified with 361 upregulated and 379 downregulated when compared longer-lived AD patients with shorter-lived ones. These DEGs were primarily involved in the pathways directly or indirectly associated with the regulation of neuroinflammation and cancer pathogenesis, as shown by pathway enrichment analysis. Among the DEGs, the top 15 hub genes were identified from the PPI network. Notably, the same bioinformatic procedures were conducted in 62 non-AD individuals (serving as controls of AD patients in the four included studies) with distinctly different findings from AD patients, indicating different regulatory mechanisms of lifespan between non-AD controls and AD, reconfirming the necessity of the present study.

Conclusion: These results shed some lights on lifespan-related regulatory mechanisms in AD patients, which also indicated that AD heterogeneity should be more taken into account in future investigations.

KEYWORDS

Alzheimer's disease, lifespan, differentially expressed genes, functional enrichment analysis, hub gene

1. Introduction

Alzheimer's disease (AD), featured by progressive decline of cognition and individual social functioning, is the most prevalent neurodegenerative disease in older people (Scheltens et al., 2016). AD accounts for more than half of all dementia cases, leading to serious burdens on the patients, the families and the society as a whole (Jia et al., 2018). The typical pathological characteristics of AD were recognized to be hyper-phosphorylated tau aggregations and amyloid-β (Aβ) plaques in the brain (Bakota and Brandt, 2016). However, it has been well aware that Aβ pathology and tau pathology could not represent the whole picture of the pathogenesis of AD. Thus, researchers have developed more hypotheses hoping to clarify its pathogenesis, such as neuroinflammation, oxidative stress and mitochondrial dysfunction, protein oxidation, lipid peroxidation, etc. (Serrano-Pozo et al., 2011). However, the exact mechanisms leading to the beginning and development of AD still need to be further clarified.

One major reason might be the huge heterogeneity of AD, both genetically and clinically (Devi and Scheltens, 2018). It has long been acknowledged that the clinical manifestations of AD patients vary significantly in many aspects including but not limited to the onset age, progressive rate, the lifespan, the affected cognitive domains, and so on(Lam et al., 2013). Thanks to the uncovering of many AD risk genes using high-throughput biochips in recent decades, AD has been recognized to be the dysregulation of a substantial number of genes resulting in the alteration of their complex interactions, which finally leads to the varieties of disease manifestations (Zhu et al., 2017). Some previous studies have focused on the link between its genetic and clinical heterogeneity with results suggesting that using more genetically or clinically homogeneous patients may be helpful to identify additional risk genes. Lo et al.'s (2019) study performed stratified gene-based genome-wide association studies (GWAS) and polygenic variation analyses in the younger and older age-at-onset groups in order to explore genetic heterogeneity of AD related to age and locate risk genes showing different effects across age. Belloy et al. (2020) probe the link between longevity gene KLOTHO and the APOE4-AD risk and found that KL-VS (a functional variant of KLOTHO) heterozygosity was significantly associated with decreased risk for AD and conversion to AD, and also reduced Aβ biomarkers in individuals who carry APOE4 but not in those who do not carry APOE4. These results suggest that there might be different regulatory mechanisms in different AD subgroups, which are of great significance to be further investigated. However, AD was studied as a monolithic disease in most studies and compared with non-AD controls, which might cause considerable confounding when exploring its pathogenesis.

Notably, the lifespan of AD patients also exhibits considerable heterogeneity. Some AD patients present with later onset and/or slower progression leading to longer lifespan, while some others might have significantly shorter lifespan. Although one of the major targets of AD intervention is to prolong patients' lifespan, the heterogeneity in AD lifespan has not been much explored. Aoyagi et al.'s (2019) study quantically measures the intracellular self-propagating conformers in postmortem brain samples from AD patients and shows that the longevity-dependent reduction in self-propagating tau conformers were identified in spite of increasing levels of total insoluble tau, demonstrating an inverse correlation between longevity and the amounts of pathological tau conformers in AD patients. The underlying mechanisms have not been clarified so far. In this case, analyzing lifespan-related gene expression profiles in AD patients might be a promising strategy to provide information about the genetic regulatory mechanisms underlying the phenotype of different lifespans. To date, there has been no such study published before.

This study acquired qualified gene profiles of AD patients from GEO database and the differentially expressed genes (DEGs) between AD patients with longer lifespan and shorter lifespan were meta-analyzed using the R package of Robust Rank Aggregation (RRA). Then, the functional pathway annotations and protein–protein interaction (PPI) networks of DEGs were performed *via* bioinformatics approaches. We investigate the lifespan-related regulatory mechanisms in AD patients at a molecular level and help uncovering potential candidate genes for AD intervention.

2. Methods

2.1. Dataset selection and data preprocessing

The Gene Expression Omnibus (GEO)[1] is a public repository for researchers worldwide to submit high-throughput microarray and next-generation sequence functional genomic datasets. All data are available for download without charge (Barrett et al., 2013). The datasets of gene expression profiles used in the present study were obtained from GEO with the search strategy as follows: (((Expression profiling by high throughput sequencing [DataSet Type]) OR Expression profiling by array [DataSet Type]) AND homo sapiens[Organism]) AND Alzheimer's disease[Title] (Figure 1). The inclusion criteria of qualified datasets were as follows: investigating the expression profiles by arrays or high throughput sequencing in GEO; using brain samples of AD cases and non-AD controls; containing complete information of age at death. Since the brain samples were donated by volunteers and collected postmortem, the ages displayed in these studies were in fact the ages at death, serving as a qualified indicator of lifespan.

Through literature reviewing, it was found that several datasets (for example GSE48350, GSE5281, GSE36980) are designed to obtain samples from multiple brain regions of one donor. However, one previous study(Moradifard et al., 2018) has proved that the gene expression profiles vary across different brain regions. Thus, it might cause substantial confounding if all the samples were included in the meta-analysis. Thus, only the samples of temporal lobe were chosen for the analysis in order to minimize the heterogenicity of samples. If one dataset included samples of different regions in the temporal lobe, the region with the largest sample size was chosen. With regard to the cut-off age, it was firstly set to be above 80 years old which has been reported to be the average life expectancy of Chinese elderly (Huang et al., 2021). After several grouping attempts, the cut-off age of 85 years old was selected which would include more datasets and make the grouping more balanced. Then, according to the lifespan: the group with longer lifespan (>=85 years old) and the group with shorter

1 http://www.ncbi.nlm.nih.gov/geo/

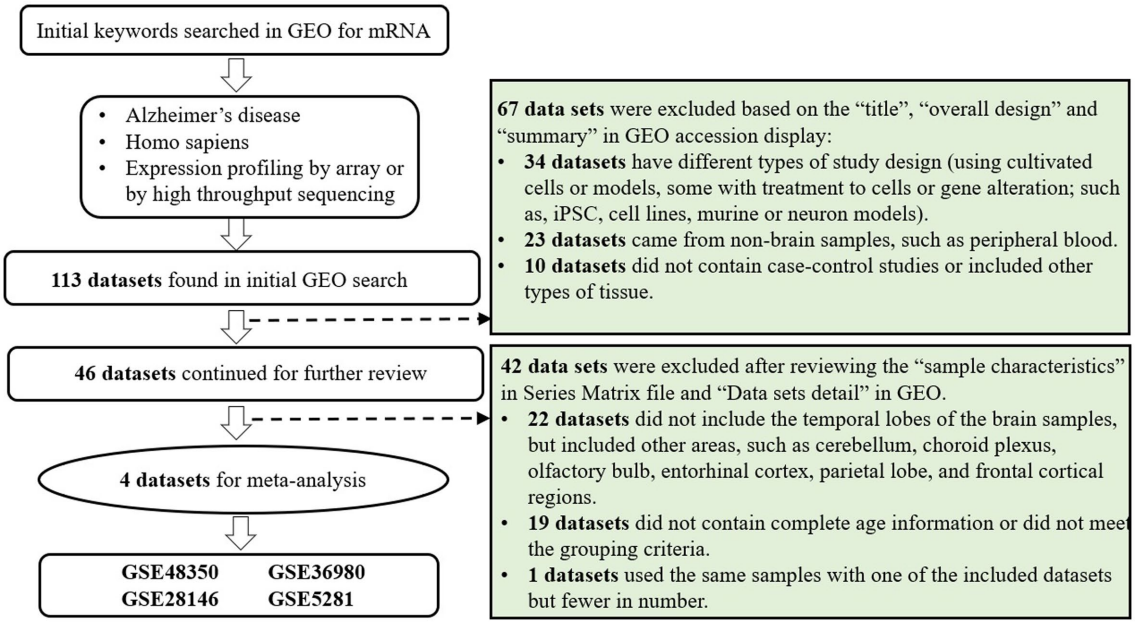

FIGURE 1
Data set selection flowchart.

lifespan (<85 years old), the samples of each dataset were divided into two groups. In addition, the samples with age over 60 years old were chosen to lower the possible influences of unnatural deaths.

2.2. DEGs identification

The R tools GEOquery and limma from the Bioconductor project were used to export and analyze the gene expression data of the comparisons between AD patients (AD patients with longer lifespan vs. those with shorter lifespan). Bioconductor, an open-source software project built on the R programming language, offers tools for the study of high-throughput genetic data. The R package GEOquery transforms GEO data into R data structures for usage by other R tools (Davis and Meltzer, 2007). Differentially expressed genes (DEGs) between the two groups of each dataset with p values <0.05 were selected to be further analyzed. Then the values of fold changes (FC) were log2 transformed and represented as log FC in short. Log FCs which were below zero indicated the DEGs were down regulated, and vice versa. The meta p values of the DEGs were calculated using the R package of Robust Rank Aggregation (RRA) and the results were represented as meta-analysis scores (Kolde et al., 2012). The RRA technique, which can manage fluctuating gene content from various microarray platforms in the presence of noise or with partial rankings, is based on a comparison of real data with a null model that assumes random order of input lists. Besides, the mean values of log FCs were also calculated. Genes with meta p values less than 0.05 and average $|\log FC| \geq 1$ were considered as final DEGs. Data processing was performed using Python Jupyter Notebook (Edition 5.0.0).

Notably, data of non-AD controls were also analyzed using the same methodology to serve as comparisons. The non-AD data came from the included datasets and were used to be controls of AD patients in the original studies.

2.3. Gene functional enrichment analysis

The DEGs were uploaded to Metascape[2] (Zhou et al., 2019). Pathway and process enrichment analyses were carried out with ontology sources of KEGG pathway, GO Biological Processes, Reactome Gene Sets, Canonical Pathways, and WikiPathways. Genes of the whole genome were adopted as the enrichment background. Terms with p value <0.01, count of genes ≥3, and an enrichment factor > 1.5 were collected and grouped into clusters based on their membership similarities. The top 20 clusters were collected using the most statistically significant term in each cluster as the representative.

Protein–protein interaction (PPI) enrichment analysis was conducted based on the following databases: STRING, BioGrid, OmniPath, InWeb_IM. If the network contains 3 to 500 proteins, the Molecular Complex Detection (MCODE) algorithm would be applied to identify densely connected network components. Pathway and process enrichment analysis was applied to each MCODE component independently, and the three best-scoring terms by value of p were retained as the functional description of the corresponding components.

2.4. Hub genes identification and association enrichment analysis

To screen hub genes, CytoHubba plug-in of Cytoscape was utilized to analyze PPI networks exported from the corresponding Metascape results in the present study (Jeong et al., 2001). The top 15

2 http://metascape.org

hub genes ranked by the method of Maximal Clique Centrality (MCC) were calculated. Enrichment analysis were also performed in ontology categories of DisGeNET *via* Metascape (Piñero et al., 2017). DisGeNET integrates data from expert curated repositories, GWAS catalogs, animal models and the scientific literature to provide information about the genetic basis of human diseases. Genes of the whole genome were adopted as the enrichment background. Terms with p value <0.01, count of genes ≥3, and an enrichment factor > 1.5 were collected and grouped into clusters based on their membership similarities.

2.5. Analysis of immune infiltration and hub genes

The gene sets of 28 immune cells and four classes of immune factors were downloaded from TISIDB database.[3] The following 28 types of immune cells were obtained: central memory CD4+ T cells (CD4+ Tcm), central memory CD8+ T cells (CD8+ Tcm), type-2 T helper cells (Th2), CD56dim natural killer cells (CD56− NK), activated CD8+ T cells (CD8+ Ta), activated CD4+ T cells (CD4+ Ta), activated B cells (Ba), effector memory CD8+ T cells (CD8+ Tem), effector memory CD4+ T cells (CD4+ Tem), macrophages, eosinophils, memory B cells (Bm), immature dendritic cells (DCi), gamma delta T cells (γδT), CD56bright natural killer cells (CD56+ NK), monocytes, mast cells, natural killer cells (NK), immature B cells (Bi), type-1 T helper cells (Th1), neutrophils, plasmacytoid dendritic cells (DCp), natural killer T cells (NK T), type-17 T helper cells (Th17), follicular helper T cells (Tfh), regulatory T cells (Tregs), myeloid-derived suppressor cells (MDSC), and activated dendritic cells (DCa). The four classes of immune factors include 41 chemokines, 24 immunosuppressive factors, 46 immunostimulatory factors, and 18 immune receptors.

The ssGSEA algorithm, which classifies gene sets with common biological functions, physiological regulation, and chromosomal localization, was employed *via* R packages (GSVA 1.42.0) to comprehensively assess the immunologic characteristics of each sample included in the analyses (Hänzelmann et al., 2013). Normalized data of gene expression profiles were compared with the gene sets to demonstrate the enrichment of immune cells in each AD brain samples. Then, ANOVA was adopted to identify immune cell types with significant differences between the groups with longer lifespan and shorter lifespan. Pearson correlations between the gene expression level of each hub gene and the concentrations of immune cells were carried out using cor.test in R software (version: 4.0.3). The hub genes were identified in 2.4.

The correlations between the gene expression levels of each hub gene and the gene sets of immune factors were also calculated, respectively. Then, the pairs of hub genes and immune-related molecules with |cor| > 0.6 & p value<0.05 were selected to generate a circos plot *via* Cytoscape.

3 http://cis.hku.hk/TISIDB/download.php

3. Result

3.1. Identification of DEGs

The flowchart of dataset selection was shown in Figure 1. Four qualified microarray datasets (GSE48350, GSE5281, GSE28146, GSE36980) and one dataset of high throughput sequencing (GSE173955) were identified according to the inclusion and grouping criteria. Thereinto, the samples used in GSE173955 were also used in GSE36980 as stated in the abstract of the article (Mizuno et al., 2021). In order to include more samples and reduce batch effect and other confounding, GSE36980 were included in the analysis rather than including both or GSE173955 alone.

In total, 129 samples (62 non-AD controls and 67 AD cases) were analyzed in this study; the grouping and baseline information were shown in Table 1. After comparing longer-lived AD patients with shorter-lived ones in each dataset, genes with $p < 0.05$ were selected and formed a list, respectively. The Venn diagram showing the overlap of the four gene lists was displayed as Figure 2A. After meta-analysis, a list of 740 DEGs with 361 upregulated and 379 downregulated was identified in the AD group with longer lifespan compared to that with shorter lifespan. The top 15 most significantly upregulated and downregulated genes when comparing longer-lived individuals with shorter-lived ones in AD patients were shown in Table 2.

In addition, the data of non-AD controls were also analyzed using the same methodology to serve as comparison and 888 DEGs were identified with 459 up-regulated and 429 down-regulated. Volcano plots showing DEGs from both comparisons (the groups of AD and non-AD controls) were as Figure 2B. The Venn diagrams showing the overlap of AD and non-AD DEGs were exhibited in Figure 2C.

3.2. Gene functional enrichment analysis of DEGs and hub genes identification

The top 20 clusters with their representative enriched terms (one per cluster) of the up-and downregulated DEGs in the AD and non-AD comparisons were displayed in Figure 3. More details of the top five clusters were shown in Tables 3, 4. The PPI networks and MCODE components identified in the DEGs of the AD comparison were shown in Figures 4A,B. The top clusters (one term per cluster) of enrichment analysis in DisGeNET were shown in Figure 4C.

When comparing AD patients with longer lifespan to those with shorter lifespan, the three best-scoring terms identified *via* pathway and process enrichment analysis to each MCODE component were as follows: cellular response to nitrogen compound (GO: 1901699, Log10(P) = −7.9), cellular response to organonitrogen compound (GO: 0071417, Log10(P) = −7.9) and regulation of intracellular transport (GO:0032386, Log10(P) = −7.3) in the upregulated DEGs; Interferon Signaling (R-HSA-913531, Log10(P) = −7.6), regulation of viral process (GO:0050792, Log10(P) = −7.6), Interferon alpha/beta signaling (R-HSA-909733, Log10(P) = −7.3) in the downregulated DEGs.

The top 15 hub genes identified in the PPI network of the up-regulated DEGs were SRC (MCC score = 44), RPL24 (MCC score = 33), BRD4 (MCC score = 32), RPL10L (MCC score = 30), CSK (MCC score = 22), JAK2 (MCC score = 20), MRPL4 (MCC score = 20), UBD (MCC score = 19), EIF5A (MCC score = 18), WDR61 (MCC

TABLE 1 Characteristics of the individual studies.

GEO ID	Year	Location and array platform	Brain region	AD samples						Non-AD samples					
				Long lifespan (>=85years old)			Short lifespan (<85years old)			Long lifespan >=85years old			Short lifespan <85years old		
				No	Male	Age	No	Male	Age	No	Male	Age	No	Male	Age
GSE48350	2014	USA GPL570	Hippocampus	11	5	88.91 ± 3.18	8	4	75.00 ± 5.98	10	5	91.80 ± 4.60	15	8	75.40 ± 6.17
GSE5281	2006	USA GPL570	Medial temporal gyrus	4	2	87.50 ± 1.80	12	8	76.33 ± 4.29	3	1	91.67 ± 7.41	9	7	76.22 ± 6.23
GSE28146	2011	USA GPL570	CA1 gray matter	13	4	91.15 ± 4.70	9	2	79.22 ± 5.27	5	3	91.20 ± 4.58	3	3	78.33 ± 2.36
GSE36980	2013	Japan GPL6244	Temporal gyrus	8	3	91.38 ± 2.96	2	2	83.50 ± 0.50	4	2	87.75 ± 1.30	13	5	76.77 ± 5.16

score = 16), CLUH (MCC score = 16), EZH2 (MCC score = 15), CAPN1 (MCC score = 13), ACTN2 (MCC score = 13), CLIC2 (MCC score = 12), in order of ranks. The top 15 hub genes identified in the PPI network of the downregulated DEGs were STAT1 (MCC score = 5,079), MX1 (MCC score = 5,066), IFIT3 (MCC score = 5,064), IFIT1 (MCC score = 5,064), OAS3 (MCC score = 5,043), IRF4 (MCC score = 5,043), XAF1 (MCC score = 5,043), IFI6 (MCC score = 5,040), DDX58 (MCC score = 65), HDAC6 (MCC score = 25), RSL1D1 (MCC score = 24), BIRC3 (MCC score = 22), RPS6 (MCC score = 21), BRD7 (MCC score = 14), RRP12 (MCC score = 14), in order of ranks.

3.3. Analysis of immune infiltration and hub genes

The gene expression profiles of GSE48350 samples (Table 1) were used to perform immune infiltration analysis. As shown in Figures 5A,B, the fractions for activated B cell, effector memory CD8 T cell, plasmacytoid dendritic cell and type 1 T helper cell in the longer-lived AD group were remarkably higher than in those of shorter-lived ones.

Since most pathways identified in the downregulated DEGs were inflammation related, the top 10 hub genes identified in the downregulated DEGs and the top 3 hub genes identified in the upregulated DEGs were selected for the association analysis with immune cells and immune factors. As shown in Figure 5C, STAT1 was positively correlated with gamma delta T cell, activated CD4 T cell, immature dendritic cell and activated CD8 T cell. MX1 was positively correlated with immature dendritic cell and gamma delta T cell. IFIT3 was negatively correlated with immature B cell, activated B cell and mast cell. IFIT1 was positively correlated with effector memory CD4 T cell and negatively correlated with neutrophil, type 17 T helper cell, effector memory CD8 T cell, natural killer cell, type 1 T helper cell and central memory CD8 T cell. IRF4 was positively correlated with activated CD4 T cell, eosinophil and type 2 T helper cell. DDX58 was positively correlated with gamma delta T cell. HDAC6 was positively correlated with monocyte. SRC was positively correlated with CD56 bright natural killer cell and negatively correlated with effector memory CD4 T cell. RPL24 was negatively correlated with T follicular helper cell, immature dendritic cell, mast cell and activated CD4 T cell. BRD4 was positively correlated with CD56 bright natural killer cell and negatively correlated with effector memory CD4 T cell, gamma delta T cell and central memory CD8 T cell. There were no significant findings when analyzing the associations between immune cells and the remaining hub genes (OAS3, XAF1, and IFI6). Protein–protein interaction plot of hub genes and immune-related molecules was shown as Figure 5D.

4. Discussion

In the present study, 740 DEGs with 361 upregulated and 379 downregulated were identified comparing AD patients with longer lifespan to those with shorter lifespan. Bioinformatic analyses were performed based on these DEGs, and the significant findings would be discussed as below. Notably, the same bioinformatic procedures and analyses were conducted basing on the data of non-AD controls (Table 1), with distinctly different findings from those identified in the

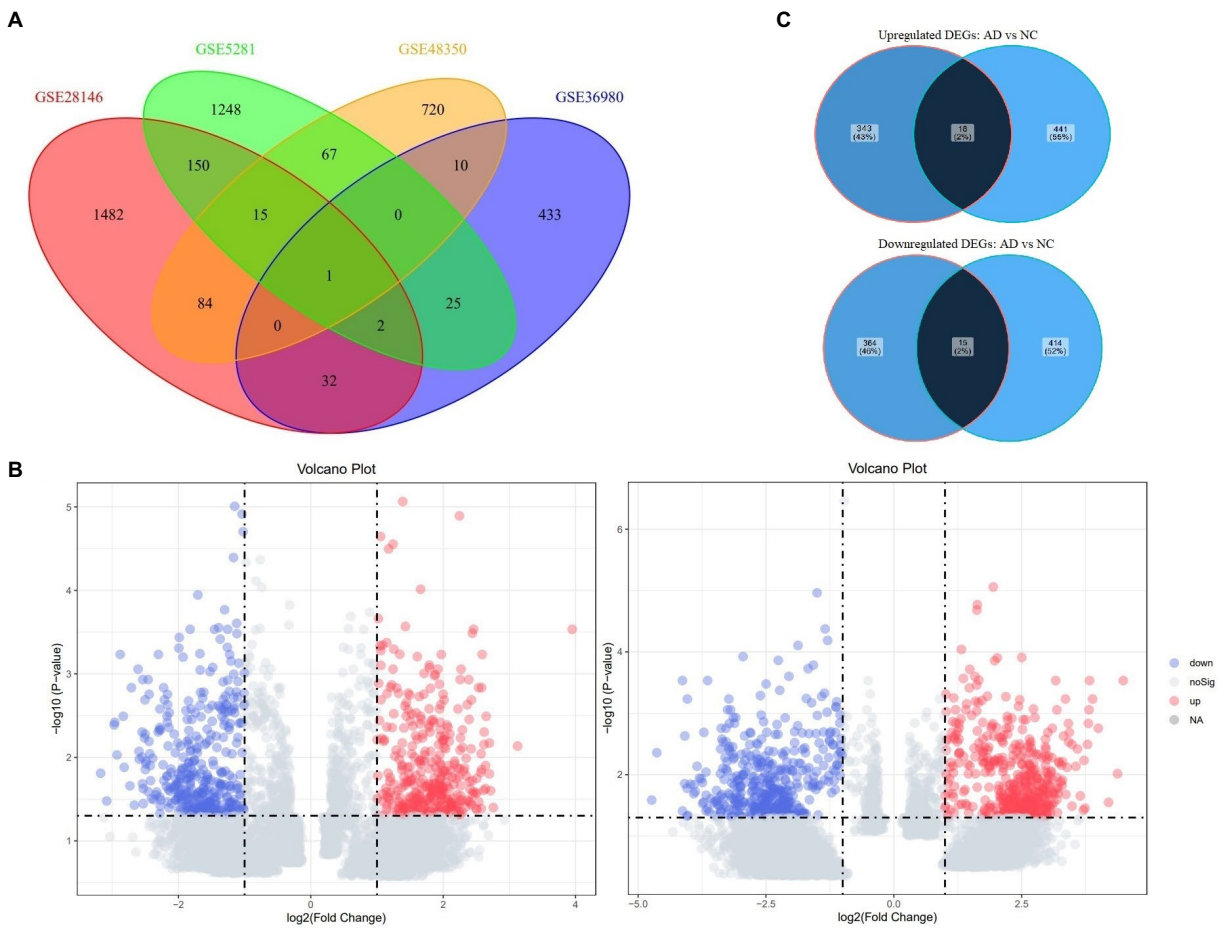

FIGURE 2
Venn diagrams of Four datasets and Volcano plots of DEGs in the groups of AD and non-AD controls. **(A)** Venn diagram of the overlap of genes lists from the Four included datasets. **(B)** Volcano plots of DEGs in the groups of AD (left) and non-AD controls (right). **(C)** Venn diagram of the overlap of DEGs between the groups of AD and non-AD controls. AD, Alzheimer's disease; DEG, differentially expressed genes.

AD comparison (Figures 2C, 3). These results indicated that the underlying regulatory mechanisms of AD lifespan might be quite different from those of non-AD controls, reconfirming the necessity of the present study. Investigating lifespan-related gene expression profiles in AD patients would help to understand the genetic background possibly impacting its clinical course, which has not been published before.

In the lifespan-related pathways identified in the present study, multiple clusters of pathways were directly or indirectly associated to neuroinflammation. The directly associated clusters included those represented by the pathways of interferon Signaling (R-HSA-913531) and regulation of response to cytokine stimulus (GO:0060759) in the downregulated DEGs. The indirectly associated clusters included those about antiviral responses represented by the pathway of regulation of viral process in the downregulated DEGs; those about metabolism processes represented by the pathways of Adipogenesis, glucose metabolic process in the downregulated DEGs; Diseases of metabolism in the upregulated DEGs; and those about autophagy represented by the pathways of apoptotic cell clearance, Phagosome in the upregulated DEGs. These results indicated that neuroinflammation might be closely related to the regulation of AD lifespan.

Amounts of evidence, involving increasing numbers of activated microglial and astroglia in the brains of AD patients, elevated pro-inflammatory cytokine in AD brains, and epidemiological proof that chronic non-steroidal anti-inflammatory drug used before AD associates to a lower incidence, have suggested that neuroinflammation, an early-emerging and continuously existing feature of AD, plays a significant part in the pathogenesis of the disorder (Calsolaro and Edison, 2016). Interferons (IFNs) are a superfamily of cytokine proteins that play a significant part in host immune response to pathogens, infections, and various diseases (de Weerd and Nguyen, 2012). It has been proved that they are critical in the exacerbation of neuroinflammation and actively contribute to AD progression (Taylor et al., 2018). Also, studies have shown that active virus infections in brain may not only accelerate amyloid deposition and the progression of AD (Eimer et al., 2018; Mangold and Szpara, 2019), but also, by inhibiting autophagy, disrupt clearance of the aberrant proteins, resulting in their accumulation and deposition, and finally to AD onset and progression (Itzhaki, 2017). dysregulation of metabolism processes would lead to metabolic changes, induction of obesity and adipose tissue inflammation, resulting in the acceleration of systemic low-grade inflammation and then accumulation of toxic amyloid, eventually the onset of AD (Więckowska-Gacek et al., 2021).

TABLE 2 Top 15 differentially expressed genes (DEGs) identified in the meta-analysis comparing the longer-lived AD group with the shorter-lived one.

Up-regulated			Down-regulated		
Gene symbols	Average Log (FC)	Meta-analysis score	Gene symbols	Average Log (FC)	Meta-analysis score
RNMT	1.388641	8.63E-06	ACAN	−1.14943	9.83E-06
ZBED3-AS1	2.246284	1.28E-05	TNRC6C	−1.03933	1.22E-05
POMZP3	1.242601	2.79E-05	ST3GAL4-AS1	−1.02212	1.98E-05
L3MBTL1	1.175608	3.18E-05	FBXL17	−1.1674	4.05E-05
FBLIM1	1.659288	9.69E-05	KLK8	−1.70629	0.0001
DRICH1	1.021555	0.0002	SUCLG2-AS1	−1.3024	0.0001
SLC44A5	1.429692	0.0002	GAS2L3	−1.11936	0.0002
EZH2	2.459765	0.0002	PKNOX1	−1.39156	0.0003
PLN	3.948696	0.0002	GNRH1	−1.45433	0.0003
PVALB	2.440934	0.0003	NR0B1	−1.8225	0.0003
DYNC1H1	1.146785	0.0004	ZNF366	−1.25511	0.0003
LRRC28	1.081166	0.0005	IL17RB	−1.1153	0.0003
EBP	1.045227	0.0005	RBM33	−1.98674	0.0004
UHRF1BP1L	1.254153	0.0005	PACSIN2	−1.3685	0.0004
ZNF81	1.057144	0.0005	AREG	−1.26	0.0005

Ave log (FC), average log2 fold-change.

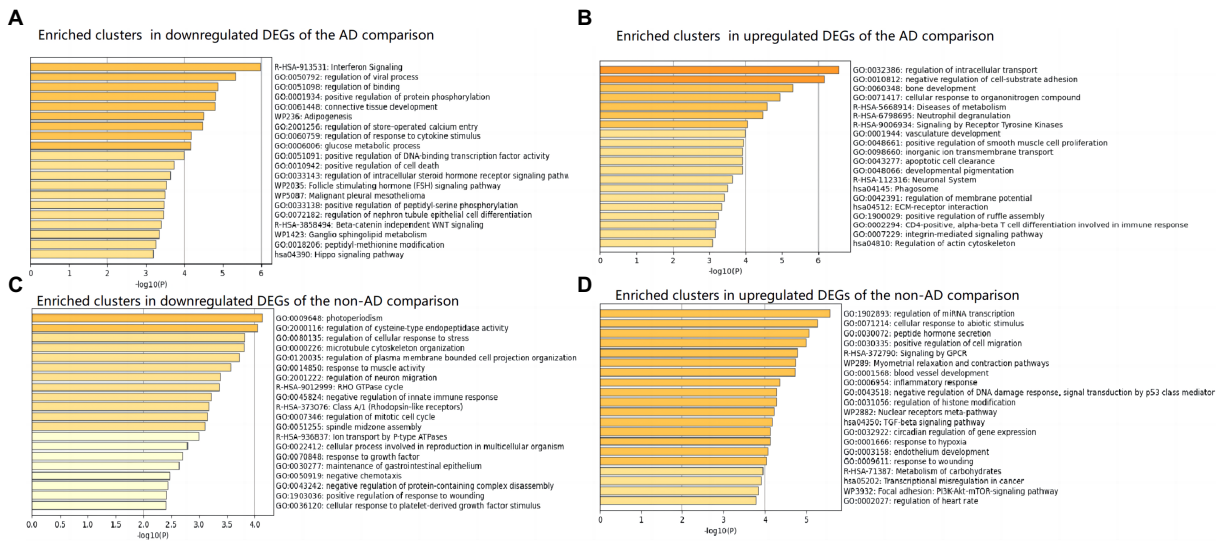

FIGURE 3
Top 20 clusters with their representative enriched terms (one per cluster) in up-and downregulated DEGs of AD and non-AD comparisons, respectively. **(A)** Enriched clusters in downregulated DEGs of the AD comparison. **(B)** Enriched clusters in upregulated DEGs of the AD comparison. **(C)** Enriched clusters in downregulated DEGs of the non-AD comparison. **(D)** Enriched clusters in upregulated DEGs of the non-AD comparison. AD, Alzheimer's disease; DEG, differentially expressed genes.

Regulation of these pathways might result in the mitigation of excessive neuroinflammation in AD brains and thus leading to longer lifespan. In addition, the results of immune infiltration analysis also supported this conclusion, which showed that four kinds of immune cells increased significantly in longer-lifespan AD patients and the hub genes corelated with multiple immune cells and immune factors, indicating that the regulation of AD lifespan might be intertwined with the complex networks of neuroinflammation.

Thus, identifying key mediators regulating the neuroinflammation process might be helpful to develop anti-inflammatory therapies for AD (Taylor et al., 2018). Among the identified hub genes, STAT1, which ranked the first in the hub gene list identified in the downregulated DEGs and corelated with multiple immune cells and immune factors, has already come into notice of researchers. The protein encoded by STAT1 is activated by varieties of ligands including IFN-α, EGF, IFN-γ, PDGF, and IL6.

TABLE 3 The top 5 clusters with their representative enriched terms (one per cluster) of the upregulated DEGs in AD group with longer lifespan.

GO	Category	Description	Count	Log10(P)	Gene Hits
GO:0032386	GO Biological Processes	Regulation of intracellular transport	17	−6.55	ACTN2|CD36|DYNC1H1|STOM|GAS1|JAK2|NF1|PLN|SRC|ITGB
					1BP1|CAPN10|DNAJC13|NRDE2|RIOK2|MAVS|SH3TC2|HPS4
GO:0010812	GO Biological Processes	Negative regulation of cell-substrate adhesion	8	−6.15	ANGPT2|BCL6|COL1A1|EFNA5|NF1|SRC|THBS1|ITGB1BP1
GO:0060348	GO Biological Processes	Bone development	12	−5.29	BGN|COL1A1|RARA|SHOX2|SRC|FGF18|EBP|FOXP1|PDGFC|
					TMEM107|NOTUM|FREM1
GO:0071417	GO Biological Processes	Cellular response to organonitrogen compound	20	−4.93	ACTN2|CD36|CHRM4|COL1A1|COL4A1|CSK|EZH2|HTR2C|JAK
					2|P2RY2|PDE3A|SRC|SOCS1|SOCS2|BCL2L11|RRAGB|CAPN10|
R-HSA-5668914	Reactome Gene Sets	Diseases of metabolism	12	−4.59	BGN|CSF2RA|SLC37A4|HLCS|MGAT2|MUC7|THBS1|CUBN|
					ADAMTS1|ADAMTS9|ALG13|SBSPON

GO, gene ontology; BP, biological process. Count is the number of genes in the user-provided lists with membership in the given ontology term. "Log10(P)" is the *p*-value in log base 10.

TABLE 4 The top 5 clusters with their representative enriched terms (one per cluster) of the downregulated DEGs in AD group with longer lifespan.

GO	Category	Description	Count	Log10(P)	Gene Hits
R-HSA-913531	Reactome Gene Sets	Interferon Signaling	13	−5.98	CD44|IFI6|HLA-DRB4|IFIT1|IFIT3|IRF4|KPNA4|MX1|
					OAS3|STAT1|NUP210|RIGI|XAF1
GO:0050792	GO Biological Processes	Regulation of viral process	11	−5.33	NR5A2|GSN|IFIT1|MX1|OAS3|PPARA|SLPI|
					STAT1|CXCR4|HMGA2|CNOT7
GO:0051098	GO Biological Processes	Regulation of binding	16	−4.87	BDNF|HFE|IFIT1|IRF4|PPARA|SLPI|STK4|HMGA2|SYMPK|
					ADAM15|MBD2|HIPK2|TRIB3|ARHGAP28|PARP9|SPPL3
GO:0001934	GO Biological Processes	Positive regulation of protein phosphorylation	24	−4.80	AREG|BDNF|BMP3|CD44|CKS2|HFE|IL6|ITGB3|LTK|PTGS2|
					STK4|HMGA2|FZD1|TNFRSF10B|GPRC5A|MAP3K13|
					TCL1B|HDAC6|HIPK2|ALS2|CLSPN|PARP9|PROM2|CD24
GO:0061448	GO Biological Processes	Connective tissue development	12	−4.79	BMP1|BMP3|CD44|EVC|HOXA5|LTBP3|MGP|
					HMGA2|TRIP11|RASAL2|CREB3L2|TBL1XR1

GO, gene ontology; BP, biological process. Count is the number of genes in the user-provided lists with membership in the given ontology term. "Log10(P)" is the *p*-value in log base 10.

Zhang et al.'s (2021) study shows that STAT1 knockout suppresses AD typical pathologies. Another study identifies that STAT1 activation abolishes expression of N-methyl-D-aspartate receptors (NMDARs), while the downregulation of STAT1 efficiently mitigates Tau-induced suppression of NMDAR expression and improves the function of synapses and performances in memory tests (Li et al., 2019). He et al.'s (2021) study shows that the overexpression of STAT1 inhibitor represses several AD markers expressions and accelerate the proliferation of mouse hippocampal neuronal cells. These findings might offer some explanations why the downregulated expression of STAT1 is associated with longer lifespan of AD patients in the present study. In addition, the recent study of Zhang et al. (2022) shows that pharmacological degradation and inhibition of BRD4, which affects transcriptional regulation of

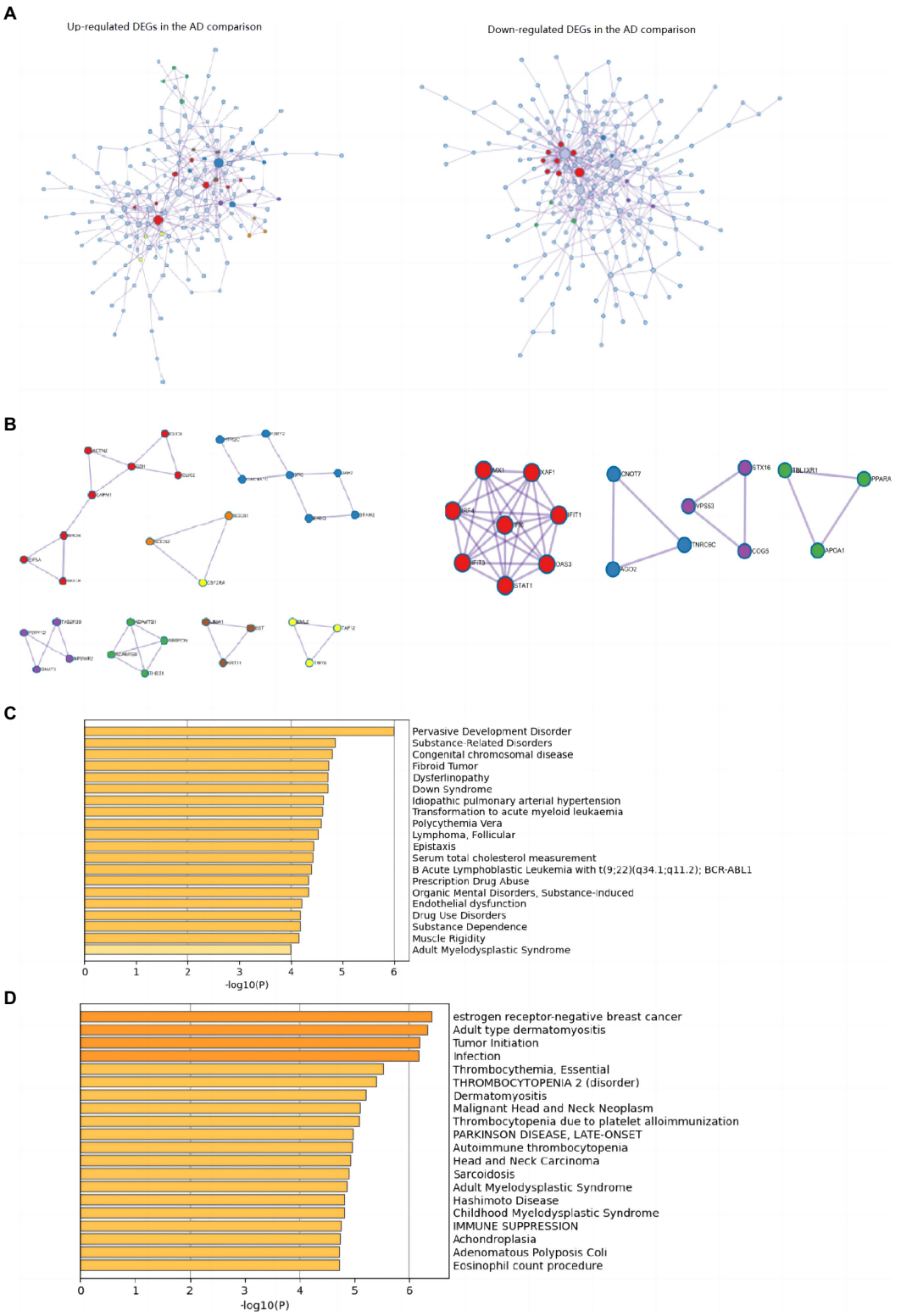

FIGURE 4
PPI networks and top 20 clusters enriched in DisGeNET in up-and downregulated DEGs of AD comparison. **(A)** PPI networks identified in the DEGs of AD comparison (Left: upregulated; right: downregulated). **(B)** MCODE components identified in the DEGs of AD comparison (Left: upregulated; right: downregulated). **(C)** Top 20 clusters enriched in DisGeNET in upregulated DEGs of AD comparison. **(D)** Top 20 clusters enriched in DisGeNET in downregulated DEGs of AD comparison. AD, Alzheimer's disease; DEG, differentially expressed genes.

autophagy and lysosome genes, significantly increase Aβ levels that are related to AD neuropathology in cell models, indicating that the upregulation of BRD4 might be beneficial for AD, consistent with the findings of the present study that BRD4 was upregulated in longer-lived AD patients and corelated with multiple immune cells and factors (Figure 5).

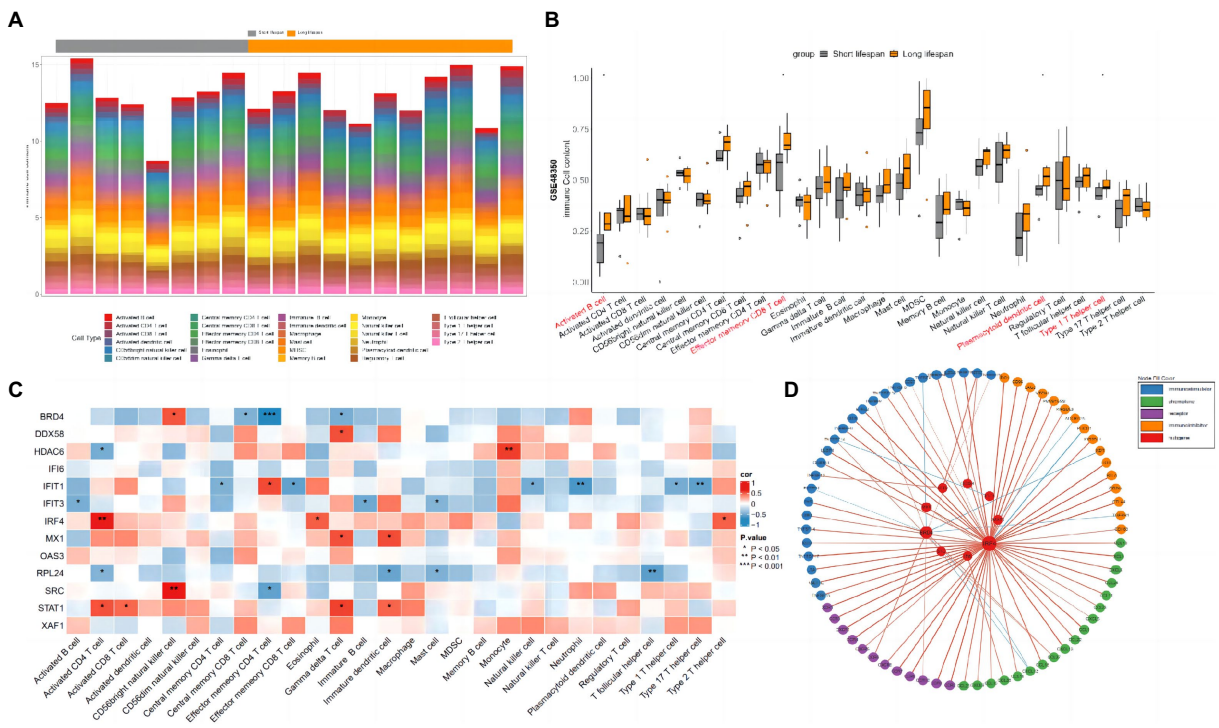

FIGURE 5
Immune infiltration analysis between longer-lived AD and shorter-lived ones. **(A)** The column diagram displaying the relative percentage of the 28 immune cells between in AD samples. **(B)** The difference of immune infiltration between longer-live AD (orange) and shorter-lived ones (gray; * indicates *p*-values<0.05). **(C)** Correlations between hub genes and the infiltration levels of the 28 immune cells. **(D)** Circos plot of the interactions between the hub genes and immune-related molecules.

Interestingly, the enrichment analysis *via* DisGeNET (Figures 4C,D) revealed noteworthy overlaps with neoplastic diseases in both up-and downregulated DEGs of AD comparison. Several AD-lifespan-related pathways identified in the present study were also related to cancer, such as positive regulation of cell death, Malignant pleural mesothelioma, Hippo signaling pathway in the downregulated DEGs and apoptotic cell clearance, Signaling by Receptor Tyrosine Kinases in the upregulated DEGs. These results indicated that the regulation of AD Lifespan and cancer might share common pathways. Nudelman et al. have reviewed about ten hallmark biological alterations which overlap in the pathogenesis of cancer and AD (Nudelman et al., 2019), and proposed that pathways related to inflammation might exhibit similar roles and parallel directions of regulation in the pathogenesis of cancer and AD (Nudelman et al., 2019). It has been assumed that inflammation might accelerate the earliest development of neoplastic progression, especially a chronic state of systemic inflammation. To survive, tumors need to shift the subclasses of immune cells attacking the tumor toward those promoting inflammation and tumor growth (Singh and Singh, 2015; Goswami et al., 2017). As for AD, increasing pro-inflammatory cytokine burden has been proved in AD patients' brains. Epidemiological studies have also shown that long-term use of chronic non-steroidal anti-inflammatory drugs prior to AD onset relates to a lower incidence (Taylor et al., 2018). Thus, regulating the overlapping pathways or genes related to inflammation might be beneficial for the interventions of both cancer and LOAD.

Recent studies have shown that HDAC6 might be of dual function in the regulation of both AD and cancer. Ruzic et al.'s (2022) study discovered two HDAC6 inhibitors with anti-breast cancer activity. As for AD, HDAC6, has shown elevated levels in AD with direct interaction with the tau protein (Qureshi and Chinnathambi, 2022) while Sreenivasmurthy et al.'s (2022) study shows that inhibiting HDAC6 leads to activation of chaperone-mediated autophagy and alleviation of tau pathology in AD models. In the present study, HDAC6 was among the top 10 hub genes identified in the downregulated DEGs of longer-lived AD and corelated with multiple immune cells and factors, indicating that HDAC6 was closely associated with neuroinflammation and its downregulation might be helpful to prolong AD lifespan, concurring with previous studies.

Also, IL6 (meta $p = 0.002$, log FC = −1.01) and CD36 (meta $p = 0.012$, log FC = 1.96) might be potential therapeutic targets, both of which were involved in the pathway related to neuroinflammation in the present study. Escrig et al. study shows that the inhibition of IL-6 trans-signaling partially rescues the AD-induced mortality and reverses AD-induced cognitive and emotional changes in AD animal models, presenting strong potentials as a powerful therapeutic target in AD (Escrig et al., 2019). Interestingly, blocking IL-6 or inhibiting its associated signaling has been proposed to be a potential therapeutic strategy for the treatment of cancers with IL-6-dominated signaling (Kumari et al., 2016). As for CD36, Wang et al.'s study found that upregulating CD36 expression ameliorated hypoxia-induced neuroinflammation, diminished Aβ deposition, and improved spatial memory defects in APP/PS1 mice (Wang et al., 2014). Meanwhile, Fang et al. (2019) report about the tumor-suppressive effects of CD36 and that CD36 inhibits growth and metastasis of colorectal cancer

cells *in vivo*. These findings indicate that IL6 and CD36 might exert parallel function in the regulation of both AD and cancer, serving as promising targets for the two.

To sum up, neuroinflammation might take the center stage in the regulation of AD lifespan and it might be of particular importance to uncover the pathways or genes related to inflammation, especially those exhibiting parallel directions of regulation in the pathogenesis of cancer and AD, which might be promising targets for both diseases.

5. Limitations

The findings of the present study must be interpreted in the light of certain limitations. Firstly, the data used in the present study were obtained from multiple studies, increasing the risk of confounding effects, such as sample size, sample sources and processing, quality and amount of RNA, microarray platform and so on. However, we tried to minimize these effects by selecting samples from the temporal lobe only and including datasets using similar techniques; we also adopted RRA for gene list integration and meta-analysis to reduce batch effects. Secondly, due to the limited number of genes exported from GEO2R when using the standard of adjust value of $p < 0.05$, p value < 0.05 was adopted for the first screening of DEGs, which might cause false positive results. However, after the first screening, we used RRA for value of p meta-analysis, which is designed to integratively select DEGs appearing in multiple datasets with high ranking. RRA has been reported to be robust and accurate in detecting DEGs across datasets. Then the results were screened for the second time using the standards of meta p values less than 0.05 and average $|\log FC|s \geq 1$ in order to further reduce false positive rate. Thirdly, since RNA-Seq technique is more powerful than microarray in evaluating gene expression profiles, thorough search and data digging were performed to locate suitable RNA-seq datasets for the present study. One such dataset was located but not included as previously mentioned. Continuous attention will be paid to newly-published studies or datasets in order to incorporate more data timely.

6. Conclusion

The results of the present study showed that neuroinflammation might take the center stage in the regulation of AD lifespan and it might be of particular importance to uncover the pathways or genes related to inflammation, especially those exhibiting parallel directions of regulation in the pathogenesis of cancer and AD, which might be promising targets for both diseases. The involved pathways and genes identified in the present study might provide information about lifespan-related genetic mechanisms in AD patients and help developing promising strategies in further investigation.

Data availability statement

The data presented in the study are deposited in the Gene Expression Omnibus (GEO, http://www.ncbi.nlm.nih.gov/geo/) repository, accession numbers: GSE48350, GSE5281, GSE28146, GSE36980.

Author contributions

FY was responsible for the rationale and the design of the study and edited and approved the final manuscript. JZ and YX conducted the series of dataset search, data processing, and relevant bioinformatics analyses. JZ wrote the manuscript. XL and JX assisted with the data analyses and manuscript editing, respectively. All authors contributed to the article and approved the submitted version.

Funding

The authors disclosed receipt of the following financial support for the research, authorship, and/or publication of this article: The study was carried out in Chengdu, China, and funded by Clinical Research and Translational Foundation of Sichuan Provincial People's Hospital (2021LY11).

Acknowledgments

The authors would like to thank Jiashun Zhen, who is from the University of California, San Francisco, for technique supporting in data processing.

Conflict of interest

The authors declare that the research was conducted in the absence of any commercial or financial relationships that could be construed as a potential conflict of interest.

Publisher's note

All claims expressed in this article are solely those of the authors and do not necessarily represent those of their affiliated organizations, or those of the publisher, the editors and the reviewers. Any product that may be evaluated in this article, or claim that may be made by its manufacturer, is not guaranteed or endorsed by the publisher.

References

Aoyagi, A., Condello, C., Stöhr, J., Yue, W., Rivera, B. M., Lee, J. C., et al. (2019). Aβ and tau prion-like activities decline with longevity in the Alzheimer's disease human brain. *Sci. Transl. Med.* 11:eaat8462. doi: 10.1126/scitranslmed.aat8462

Bakota, L., and Brandt, R. (2016). Tau biology and tau-directed therapies for Alzheimer's disease. *Drugs* 76, 301–313. doi: 10.1007/s40265-015-0529-0

Barrett, T., Wilhite, S. E., Ledoux, P., Evangelista, C., Kim, I. F., Tomashevsky, M., et al. (2013). NCBI GEO: archive for functional genomics data sets--update. *Nucleic Acids Res.* 41, D991–D995. doi: 10.1093/nar/gks1193

Belloy, M. E., Napolioni, V., Han, S. S., Le Guen, Y., and Greicius, M. D. (2020). Association of Klotho-VS heterozygosity with risk of Alzheimer disease in individuals who carry APOE4. *JAMA Neurol.* 77, 849–862. doi: 10.1001/jamaneurol.2020.0414

Calsolaro, V., and Edison, P. (2016). Neuroinflammation in Alzheimer's disease: current evidence and future directions. *Alzheimers Dement.* 12, 719–732. doi: 10.1016/j.jalz.2016.02.010

Davis, S., and Meltzer, P. S. (2007). GEOquery: a bridge between the gene expression omnibus (GEO) and BioConductor. *Bioinformatics* 23, 1846–1847. doi: 10.1093/bioinformatics/btm254

de Weerd, N. A., and Nguyen, T. (2012). The interferons and their receptors--distribution and regulation. *Immunol. Cell Biol.* 90, 483–491. doi: 10.1038/icb.2012.9

Devi, G., and Scheltens, P. (2018). Heterogeneity of Alzheimer's disease: consequence for drug trials? *Alzheimers Res. Ther.* 10:122. doi: 10.1186/s13195-018-0455-y

Eimer, W. A., Vijaya Kumar, D. K., Navalpur Shanmugam, N. K., Rodriguez, A. S., Mitchell, T., Washicosky, K. J., et al. (2018). Alzheimer's disease-associated β-amyloid is rapidly seeded by herpesviridae to protect against brain infection. *Neuron* 99, 56–63.e3. doi: 10.1016/j.neuron.2018.06.030

Escrig, A., Canal, C., Sanchis, P., Fernández-Gayol, O., Montilla, A., Comes, G., et al. (2019). IL-6 trans-signaling in the brain influences the behavioral and physio-pathological phenotype of the Tg2576 and 3xTgAD mouse models of Alzheimer's disease. *Brain Behav. Immun.* 82, 145–159. doi: 10.1016/j.bbi.2019.08.005

Fang, Y., Shen, Z. Y., Zhan, Y. Z., Feng, X. C., Chen, K. L., Li, Y. S., et al. (2019). CD36 inhibits β-catenin/c-myc-mediated glycolysis through ubiquitination of GPC4 to repress colorectal tumorigenesis. *Nat. Commun.* 10:3981. doi: 10.1038/s41467-019-11662-3

Goswami, K. K., Ghosh, T., Ghosh, S., Sarkar, M., Bose, A., and Baral, R. (2017). Tumor promoting role of anti-tumor macrophages in tumor microenvironment. *Cell. Immunol.* 316, 1–10. doi: 10.1016/j.cellimm.2017.04.005

Hänzelmann, S., Castelo, R., and Guinney, J. (2013). GSVA: gene set variation analysis for microarray and RNA-seq data. *BMC Bioinformatics* 14:7. doi: 10.1186/1471-2105-14-7

He, K., Zhang, J., Liu, J., Cui, Y., Liu, L. G., Ye, S., et al. (2021). Functional genomics study of protein inhibitor of activated STAT1 in mouse hippocampal neuronal cells revealed by RNA sequencing. *Aging* 13, 9011–9027. doi: 10.18632/aging.202749

Huang, G., Guo, F., and Chen, G. (2021). Multidimensional healthy life expectancy of the older population in China. *Popul. Stud.* 75, 421–442. doi: 10.1080/00324728.2021.1914854

Itzhaki, R. F. (2017). Herpes simplex virus type 1 and Alzheimer's disease: possible mechanisms and signposts. *FASEB J.* 31, 3216–3226. doi: 10.1096/fj.201700360

Jeong, H., Mason, S. P., Barabási, A. L., and Oltvai, Z. N. (2001). Lethality and centrality in protein networks. *Nature* 411, 41–42. doi: 10.1038/35075138

Jia, J., Wei, C., Chen, S., Li, F., Tang, Y., Qin, W., et al. (2018). The cost of Alzheimer's disease in China and re-estimation of costs worldwide. *Alzheimers Dement.* 14, 483–491. doi: 10.1016/j.jalz.2017.12.006

Kolde, R., Laur, S., Adler, P., and Vilo, J. (2012). Robust rank aggregation for gene list integration and meta-analysis. *Bioinformatics* 28, 573–580. doi: 10.1093/bioinformatics/btr709

Kumari, N., Dwarakanath, B. S., Das, A., and Bhatt, A. N. (2016). Role of interleukin-6 in cancer progression and therapeutic resistance. *Tumour. Biol.* 37, 11553–11572.

Lam, B., Masellis, M., Freedman, M., Stuss, D. T., and Black, S. E. (2013). Clinical, imaging, and pathological heterogeneity of the Alzheimer's disease syndrome. *Alzheimers Res. Ther.* 5:1. doi: 10.1186/alzrt155

Li, X. G., Hong, X. Y., Wang, Y. L., Zhang, S. J., Zhang, J. F., Li, X. C., et al. (2019). Tau accumulation triggers STAT1-dependent memory deficits by suppressing NMDA receptor expression. *EMBO Rep.* 20:e47202. doi: 10.15252/embr.201847202

Lo, M. T., Kauppi, K., Fan, C. C., Sanyal, N., Reas, E. T., Sundar, V. S., et al. (2019). Identification of genetic heterogeneity of Alzheimer's disease across age. *Neurobiol. Aging* 84, 243.e1–243.e9. doi: 10.1016/j.neurobiolaging.2019.02.022

Mangold, C. A., and Szpara, M. L. (2019). Persistent infection with herpes simplex virus 1 and Alzheimer's disease-a call to study how variability in both virus and host may impact disease. *Viruses* 11:966. doi: 10.3390/v11100966

Mizuno, Y., Abolhassani, N., Mazzei, G., Sakumi, K., Saito, T., Saido, T. C., et al. (2021). MUTYH actively contributes to microglial activation and impaired neurogenesis in the pathogenesis of Alzheimer's disease. *Oxidative Med. Cell. Longev.* 2021, 1–30. doi: 10.1155/2021/8635088

Moradifard, S., Hoseinbeyki, M., Ganji, S. M., and Minuchehr, Z. (2018). Analysis of microRNA and gene expression profiles in Alzheimer's disease: a meta-analysis approach. *Sci. Rep.* 8:4767. doi: 10.1038/s41598-018-20959-0

Nudelman, K. N. H., McDonald, B. C., Lahiri, D. K., and Saykin, A. J. (2019). Biological hallmarks of cancer in Alzheimer's disease. *Mol. Neurobiol.* 56, 7173–7187. doi: 10.1007/s12035-019-1591-5

Piñero, J., Bravo, À., Queralt-Rosinach, N., Gutiérrez-Sacristán, A., Deu-Pons, J., Centeno, E., et al. (2017). DisGeNET: a comprehensive platform integrating information on human disease-associated genes and variants. *Nucleic Acids Res.* 45, D833–D839. doi: 10.1093/nar/gkw943

Qureshi, T., and Chinnathambi, S. (2022). Histone deacetylase-6 modulates Tau function in Alzheimer's disease. *Biochim. Biophys. Acta Rev. Cancer* 1869:119275. doi: 10.1016/j.bbamcr.2022.119275

Ruzic, D., Ellinger, B., Djokovic, N., Santibanez, J. F., Gul, S., Beljkas, M., et al. (2022). Discovery of 1-benzhydryl-piperazine-based HDAC inhibitors with anti-breast cancer activity: synthesis, molecular modeling, in vitro and in vivo biological evaluation. *Pharmaceutics* 14:2600. doi: 10.3390/pharmaceutics14122600

Scheltens, P., Blennow, K., Breteler, M. M., de Strooper, B., Frisoni, G. B., Salloway, S., et al. (2016). Alzheimer's disease. *Lancet* 388, 505–517. doi: 10.1016/s0140-6736(15)01124-1

Serrano-Pozo, A., Frosch, M., Masliah, E., and Hyman, B. (2011). Neuropathological alterations in Alzheimer disease. *Cold Spring Harb. Perspect. Med.* 1:a006189. doi: 10.1101/cshperspect.a006189

Singh, K., and Singh, K. (2015). Carcinogenesis and diabetic wound healing: evidences of parallelism. *Curr. Diabetes Rev.* 11, 32–45. doi: 10.2174/1573399811666150109122205

Sreenivasmurthy, S. G., Iyaswamy, A., Krishnamoorthi, S., Reddi, R. N., Kammala, A. K., Vasudevan, K., et al. (2022). Bromo-protopine, a novel protopine derivative, alleviates tau pathology by activating chaperone-mediated autophagy for Alzheimer's disease therapy. *Front. Mol. Biosci.* 9:1030534. doi: 10.3389/fmolb.2022.1030534

Taylor, J. M., Moore, Z., Minter, M. R., and Crack, P. J. (2018). Type-I interferon pathway in neuroinflammation and neurodegeneration: focus on Alzheimer's disease. *J. Neural Trans.* 125, 797–807. doi: 10.1007/s00702-017-1745-4

Wang, C. Y., Wang, Z. Y., Xie, J. W., Cai, J. H., Wang, T., Xu, Y., et al. (2014). CD36 upregulation mediated by intranasal LV-NRF2 treatment mitigates hypoxia-induced progression of Alzheimer's-like pathogenesis. *Antioxid. Redox Signal.* 21, 2208–2230. doi: 10.1089/ars.2014.5845

Więckowska-Gacek, A., Mietelska-Porowska, A., Wydrych, M., and Wojda, U. (2021). Western diet as a trigger of Alzheimer's disease: from metabolic syndrome and systemic inflammation to neuroinflammation and neurodegeneration. *Ageing Res. Rev.* 70:101397. doi: 10.1016/j.arr.2021.101397

Zhang, S., Bai, P., Lei, D., Liang, Y., Zhen, S., Bakiasi, G., et al. (2022). Degradation and inhibition of epigenetic regulatory protein BRD4 exacerbate Alzheimer's disease-related neuropathology in cell models. *J. Biol. Chem.* 298:101794. doi: 10.1016/j.jbc.2022.101794

Zhang, Z., Li, X. G., Wang, Z. H., Song, M., Yu, S. P., Kang, S. S., et al. (2021). δ-Secretase-cleaved Tau stimulates Aβ production via upregulating STAT1-BACE1 signaling in Alzheimer's disease. *Mol. Psychiatry* 26, 586–603. doi: 10.1038/s41380-018-0286-z

Zhou, Y., Zhou, B., Pache, L., Chang, M., Khodabakhshi, A. H., Tanaseichuk, O., et al. (2019). Metascape provides a biologist-oriented resource for the analysis of systems-level datasets. *Nat. Commun.* 10:1523. doi: 10.1038/s41467-019-09234-6

Zhu, J. B., Tan, C. C., Tan, L., and Yu, J. T. (2017). State of play in Alzheimer's disease genetics. *J. Alzheimer's Dis.* 58, 631–659. doi: 10.3233/jad-170062

frontiers | Frontiers in Neuroscience

TYPE Original Research
PUBLISHED 30 March 2023
DOI 10.3389/fnins.2023.1142741

Check for updates

OPEN ACCESS

EDITED BY
Jun Xu,
Beijing Tiantan Hospital, Capital Medical University, China

REVIEWED BY
Zhen Yuan,
University of Macau, Macao SAR, China
Ekaterina Korshunova,
Research Center of Neurology, Russia

*CORRESPONDENCE
Jing Gan
✉ ganjing@xinhuamed.com.cn
Zhenguo Liu
✉ liuzhenguo@xinhuamed.com.cn

†These authors share first authorship

SPECIALTY SECTION
This article was submitted to Neurodegeneration, a section of the journal Frontiers in Neuroscience

RECEIVED 12 January 2023
ACCEPTED 14 March 2023
PUBLISHED 30 March 2023

CITATION
Hou M, Mao X, Wei Y, Wang J, Zhang Y, Qi C, Song L, Wan Y, Liu Z, Gan J and Liu Z (2023) Pattern of prefrontal cortical activation and network revealed by task-based and resting-state fNIRS in Parkinson's disease's patients with overactive bladder symptoms. *Front. Neurosci.* 17:1142741. doi: 10.3389/fnins.2023.1142741

COPYRIGHT
© 2023 Hou, Mao, Wei, Wang, Zhang, Qi, Song, Wan, Liu, Gan and Liu. This is an open-access article distributed under the terms of the Creative Commons Attribution License (CC BY). The use, distribution or reproduction in other forums is permitted, provided the original author(s) and the copyright owner(s) are credited and that the original publication in this journal is cited, in accordance with accepted academic practice. No use, distribution or reproduction is permitted which does not comply with these terms.

Pattern of prefrontal cortical activation and network revealed by task-based and resting-state fNIRS in Parkinson's disease's patients with overactive bladder symptoms

Miaomiao Hou[1†], Xiaowei Mao[2†], Yarong Wei[1†], Jiali Wang[3], Yu Zhang[1], Chen Qi[1], Lu Song[1], Ying Wan[1], Zhihua Liu[1], Jing Gan[1]* and Zhenguo Liu[1]*

[1]Department of Neurology, Xinhua Hospital Affiliated to Shanghai Jiao Tong University School of Medicine, Shanghai, China, [2]Department of Neurology, The First Affiliated Hospital of Naval Medical University, Shanghai, China, [3]Department of Neurosurgery, The First Affiliated Hospital of Naval Medical University, Shanghai, China

Background: Overactive bladder (OAB) symptoms are common in Parkinson's disease (PD), and negatively contribute to the quality of life (QoL) of patients. To explore the underlying pathophysiological mechanism, we investigated the correlation between the prefrontal cortex (PFC) function and OAB symptoms in PD patients.

Methods: One hundred fifty-five idiopathic PD patients were recruited and classified either as PD-OAB or PD-NOAB candidates based on their corresponding OAB symptom scores (OABSS). A linear regression analysis identified a correlative connection of cognitive domains. Then cortical activation during the performance of the verbal fluency test (VFT) and brain connectivity during resting state were conducted by functional near-infrared spectroscopy (fNIRS) for 10 patients in each group to investigate their frontal cortical activation and network pattern.

Results: In cognitive function analysis, a higher OABS score was significantly correlated with a lower FAB score, MoCA total score, and sub-scores of visuospatial/executive, attention, and orientation as well. In the fNIRS study, the PD-OAB group exhibited significant activations in 5 channels over the left hemisphere, 4 over the right hemisphere, and 1 in the median during the VFT process. In contrast, only 1 channel over the right hemisphere showed significant activation in the PD-NOAB group. The PD-OAB group revealed hyperactivation, particularly in certain channel in the left dorsolateral prefrontal cortex (DLPFC), compared with PD-NOAB (FDR $P < 0.05$). In the resting state, there was a significant increase of the resting state functional connectivity (RSFC) strength between the bilateral Broca area, left frontopolar area (FPA-L) and right Broca's area (Broca-R), between the FPA and Broca's area if merging the bilateral regions of interest (ROI), and also between the two hemispheres in the PD-OAB group. The Spearman's correlation confirmed that the OABS scores were positively

correlated with RSFC strength between the bilateral Broca area, FPA-L and Broca-R, between the FPA and Broca area if merging the bilateral ROI.

Conclusion: In this PD cohort, OAB was related to decreased PFC functions, with particularly hyperactivated left DLPFC during VTF and an enhanced neural connectivity between the two hemispheres in the resting state as observed by fNIRS imaging.

KEYWORDS

Parkinson's disease, overactive bladder, prefrontal cortex, fNIRS, resting state, verbal fluency task

Introduction

Parkinson's disease (PD) is caused by the gradual degeneration of the central nervous system (CNS) in elderly people and is characterized by four main motor symptoms, including resting tremor, rigidity, bradykinesia, and gaiting abnormalities. Recent findings have also recognized remarkable contributions of non-motor symptoms, like neuropsychiatric symptoms, autonomic dysfunctions, sleep disorders, pain, etc. Of these, lower urinary tract (LUT) dysfunction, predominately overactive bladder (OAB) with a prevalence rate of about 62%, becomes one of the most common types of autonomic disorders and seriously impacts the quality of life of PD patients and their caregivers (McDonald et al., 2017; Ogawa et al., 2017).

In addition to playing regulatory roles in micturition reflexes, the prefrontal cortex (PFC) directly modulates goal-directed and executive behaviors (Funahashi, 2001; Sakakibara et al., 2014). Recent investigations have highlighted that alteration of the D1 dopaminergic (DA) neuronal circuitry in the frontal-basal ganglion could be the major inducer of OAB in PD patients (Kitta et al., 2015; Mito et al., 2018). To date, only a few studies have elaborated on the pathological connection between PFC disturbances with OAB onset in PD from the neuropsychiatric perspective (Xu et al., 2019; Tkaczynska et al., 2020). However, there is still a lack of verification from functional neuroimaging examinations.

As the most widely used prefrontal lobe-related cognitive performance assessment method, the verbal (phoneme) fluency test (VFT) is often applied in the clinical evaluation of executive function-associated brain activation patterns, which might give clues to the underlying pathomechanisms in PD (Miller, 1985; Galtier et al., 2017). Functional near-infrared spectroscopy (fNIRS) at a wavelength range of 650∼950 nm is a relatively advanced non-invasive diagnostic modality of tracing changes in cerebral blood oxygen levels as indirect readouts of activities in cerebral cortices. It has the advantages of being capable of real-time monitoring, low-cost, safe and non-invasive, portable, etc. Compared with functional magnetic resonance imaging (fMRI), which is limited by the magnetic field and can only study "imaginary movement," and electroencephalogram (EEG), which is easily interfered with motion artifacts, fNIRS can continuously and qualitatively collect brain function signals in dynamic movements and has been increasingly utilized in diagnosing and treating PD individuals (Zong et al., 2019; Mahmoudzadeh et al., 2021; Schejter-Margalit et al., 2022; Tao et al., 2023). Therefore, we attempted to evaluate the utility and efficacy of fNIRS in delineating the pathological correlation between OAB induction and PFC function in a PD sample to provide potential targets for future interventions.

Materials and methods

Subject selection

Between January 2021 and November 2022, 155 idiopathic PD subjects were enrolled from outpatients of neurology departments of Xinhua Hospital affiliated to Shanghai Jiao Tong University School of Medicine (XH-SJTUSM) and from the outpatients departments of neurology and neurosurgery of the first affiliated hospital of Navy Medical University (NMU) in this study. The Ethics Committee of respective hospitals approved the investigation, provided all participants agreed to give written informed consent. The patients were selected upon meeting the clinical diagnostic criteria of the Movement Disorder Society (MDS) and exhibiting positive responses to the levodopa therapy. If any subject was- (1) diagnosed with any non-PD neurological diseases and/or (2) severe urinary system diseases; (3) taking an anticholinergic drug, and (4) unable to communicate or coordinate with clinicians, he/she was promptly excluded from the study.

Clinical assessments

Socio-demographic characteristics, including gender, age, education level, medical history, and disease duration were collected for the study subjects. The Hoehn-Yahr (H-Y) staging and MDS-Unified PD Rating Scale part III (MDS-UPDRS III) scores were used for evaluating the disease severity, while the Frontal Assessment Battery (FAB) and Montreal Cognitive Assessment (MoCA) scales were employed as cognitive performance evaluation. The psychopathological screening was done by the Hamilton Anxiety Rating Scale of 14 items (HAM-A) and the Hamilton Depression Rating Scale of 24 items (HAM-D). The patients' OAB symptoms were evaluated by OABSS. The non-motor symptoms and QoL were evaluated through the NMSS

and PD questionnaire 39 (PDQ39), respectively. All patients were evaluated in the on-medication states.

The PD patients were classified with or without OAB symptoms (PD-OAB, and PD-NOAB, respectively) based on the OABSS analysis, which has been a simple and effective method for scoring PD-specific symptoms: urgency, nighttime frequency, daytime frequency, and urge incontinence (Homma et al., 2006, 2011; Moussa et al., 2022). A higher OABSS score represents a worse condition. An OAB was diagnosed at OABSS ≥3, including an urgency score of ≥2.

VFT, resting state, and fNIRS examinations

The VFT task was guided by a well-trained instructor. During the 30 s baseline period, subjects were required to sit on a chair and repeatedly go on counting from 1 to 16 until the task began. And throughout the 60 s task period, they were instructed to construct multiple phrases using simple words like big, earth, and sky. In the post-task recovery period, they were further asked to repeat counting from 1 through 32 till the end of the test.

In a resting state, subjects sit on a chair in a quiet room. They were asked to stay awake with their eyes closed, and not thinking about anything as much as possible.

A 53-channel BS-7000 fNIRS system (Wuhan Znion Technology Co., Wuhan, China) was utilized to longitudinally monitor the oxygenation changes (i.e., oxy- to deoxy-hemoglobin proportion) in the cerebral cortices throughout the VFT paradigm. A helmet containing numerous near-infrared light sensors covered both the prefrontal and temporal lobes of the subject. Distribution of near-infrared sensors followed the international standard of 10–20 leads, with the lowest channel positioned at Fp1–Fp2. The region of measurement covered the bilateral DLPFC (Channel 6, 11, 14, 17, 18, 20, 25, 31, 32, 34, 39, 42, 45), FPA (Channel 9, 15, 16, 19, 21, 22, 23, 27, 28, 29, 30, 33, 35, 36, 41, 43, 48), the Pre-Motor and Supplementary Motor Cortex (PreM and SMC) (Channel 1, 4, 10, 40, 47, 52), the Broca's area (Channel 2, 3, 5, 7, 8, 13, 44, 46, 49, 50, 51, 53), and Frontal eye fields (FEF) (Channel 12, 24, 26, 38) according to the Brodmann map of the cortex (**Figure 1**). For VTF, the fNIRS assessment included a 30 s baseline, a 60 s VFT, and a 60 s post-task recovery period at a frequency of 20 Hz. For resting state, the fNIRS data collection lasted for 6 min for each subject.

Statistical analysis

Continuous and categorical variables are, respectively, expressed as mean ± standard deviation (SD) and median (quartiles). A two-sample *t*-test comparing continuous variables while the chi-squared (χ^2) comparing the categorical variables were performed between the PD-OAB and PD-NOAB groups. The Mann–Whitney U (MN-U) test was used to compare the differences in H-Y stages between the groups. A linear regression model was conducted according to OABSS with the enter method. Spearman's analysis was used to discover the correlation between clinical variables and imaging features. *P*-values lesser than 0.05 were statistically significant. SPSS v25.0 was used for all these statistical analyses.

fNIRS data analysis

All fNIRS data of brain networks were analyzed under the environment of Matlab R2014b (The Mathworks, United States) with Homer2_UI (Huppert et al., 2009) and NIRS-SPM software

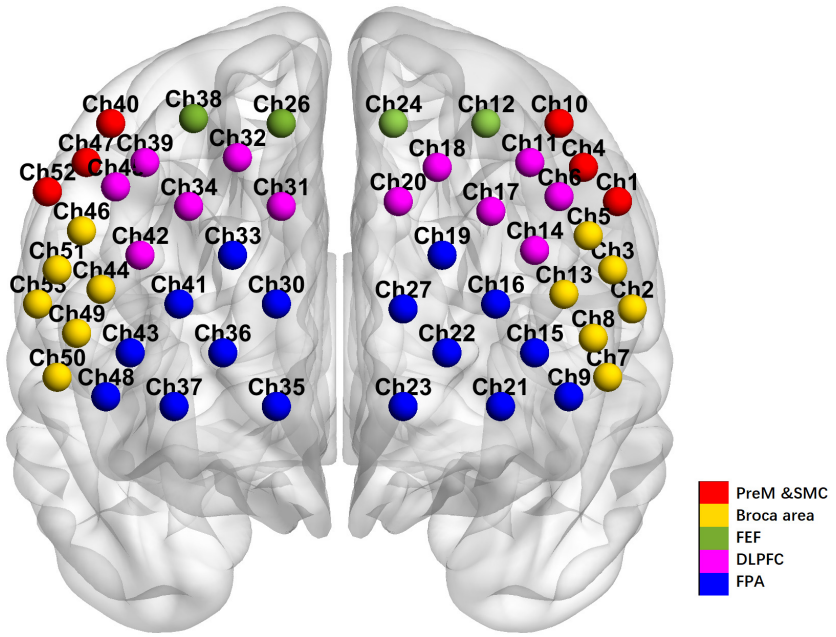

FIGURE 1
The arrangement of channels of the 53-channel near-infrared spectroscopy system according to the Brodmann's map of the cortex.

TABLE 1 Comparisons of demographic and clinical features of PD subjects with or without OAB.

	Total sample ($n = 155$)	PD-OAB ($n = 80$)	PD-NOAB ($n = 75$)	P
Age (years), mean ± SD	63.15 ± 10.05	64.93 ± 9.51	61.49 ± 10.32	<0.05
Gender [n (female) (%)]	64 (41.3%)	36 (45%)	28 (37.3%)	0.333
Education (years), mean ± SD	12.13 ± 3.07	11.92 ± 2.79	12.32 ± 3.31	0.416
Disease duration (years), mean ± SD	7.88 ± 4.75	8.83 ± 4.46	7.00 ± 4.88	<0.05
Hoehn-Yahr staging, median (IQR)	3 (2.5, 3)	3 (3, 4)	3 (2, 3)	<0.05
MDS-UPDRS III	27.35 ± 14.47	30.25 ± 14.12	24.56 ± 14.35	<0.05
LEDD at admission (mg), mean ± SD	645.39 ± 473.15	754.32 ± 431.69	543.27 ± 489.91	<0.05
HAM-D, mean ± SD	12.09 ± 6.19	12.81 ± 5.71	11.41 ± 6.58	0.159
HAM-A, mean ± SD	10.00 ± 5.51	10.83 ± 5.40	9.22 ± 5.52	0.069
MoCA, mean ± SD	24.83 ± 2.93	24.03 ± 3.34	25.59 ± 2.24	<0.05
FAB, mean ± SD	16.14 ± 1.68	15.24 ± 1.48	16.98 ± 1.40	<0.05
PDQ-39, mean ± SD	61.01 ± 22.49	66.36 ± 21.17	56.00 ± 22.66	<0.05
NMSS, mean ± SD	17.35 ± 3.80	19.05 ± 3.41	15.73 ± 3.45	<0.05

MDS-UPDRS III, movement disorder society united Parkinson's disease rating scale part III; LEDD, levodopa equivalent daily dosage; HAM-A, Hamilton Anxiety Rating Scale; HAM-D, Hamilton Depression Rating Scale; MoCA, Montreal Cognitive Assessment; FAB, Frontal Assessment Battery; PDQ39, Parkinson's disease questionnaire 39; NMSS, non-motor symptoms scale; SD, standard deviation; IQR, interquartile range.

TABLE 2 Linear regression analysis of cognitive performance with OABSS.

	PD-OAB	PD-NOAB	Standardized β	95% CI	P
MoCA total score	24.03 ± 3.35	25.59 ± 2.24	−0.25	−0.26∼−0.06	<0.05
Visuospatial/executive	2.94 ± 1.44	3.89 ± 0.96	−0.31	−0.68∼−0.22	<0.05
Naming	2.71 ± 0.49	2.77 ± 0.45	−0.09	−1.00∼0.30	0.29
Attention	5.68 ± 0.67	5.82 ± 0.38	−0.18	−1.20∼−0.08	<0.05
Language	2.51 ± 0.67	2.58 ± 0.63	−0.01	−0.52∼0.43	0.86
Abstraction	1.44 ± 0.60	1.63 ± 0.56	−0.14	−0.98∼0.06	0.08
Delayed recall	2.96 ± 1.52	2.95 ± 1.40	−0.01	−0.23∼0.20	0.89
Orientation	5.69 ± 0.60	5.90 ± 0.30	−0.20	−1.44∼−0.17	<0.05
FAB	15.24 ± 1.48	16.98 ± 1.40	−0.46	−0.68∼−0.36	<0.05

MoCA, Montreal Cognitive Assessment; FAB, frontal assessment battery.

package[1] (Ye et al., 2009) and visualized by NIRS_KIT[2] (Hou et al., 2021) and BrainNet Viewer[3] (Xia et al., 2013).

We mainly focus on oxy-Hb, in that oxy-Hb level reflects more directly cognitive activation and is more closely related to fMRI blood oxygenation level (Cui et al., 2011). For task-based data, the raw data were converted to changes in optical density using hmrIntensity2OD. HmrMotionArtifactByChannel and hmrmotioncorrectspline were applied to correct motion artifacts. HmrBandpassfilt (0.01–0.5 Hz) was applied to eliminate unrelated low- and high-frequency components. The optical density was then converted to changes in oxy-Hb concentration using hmrOD2Conc. The changes in oxy-Hb concentration in each channel on each individual was evaluated using a General Linear Model (GLM). The whole 30 s pre-task period were set as baseline and the task-period conditions were convolved with the standard typical hemodynamic response function (HRF) in the GLM model to form the corresponding regressors. The task-related β-value was determined as the β-value of the VFT minus the β-value of the baseline. The comparisons of β values between the two groups were conducted by a two-sample t-test. The false discovery rate (FDR) was utilized to correct for multiple comparisons (level set at $P < 0.05$) (Singh and Dan, 2006).

For the resting-state data, the first 10 s and the last 30 s of the data were dropped for a stable signal. Motion correction in preprocessing were the same as the above task-based processing. HmrBandpassfilt (0.01–0.1 Hz) was applied to eliminate unrelated components. Then, the functional matrix was obtained by calculating the Pearson correlation coefficient (r-value) of the time series of each channel. Fisher's r-z transformation method was used to convert the obtained r-values to z-scores to create a 52 × 52 correlation matrix. For each group, a one-sample t-test was used to generate a group-specific RSFC map. RSFC strength between the ROI and two hemispheres for the PD-OAB and PD-NOAB groups was conducted by a two-sample t-test.

1 https://www.nitrc.org/projects/nirs_spm/

2 https://doi.org/10.1117/1.NPh.8.1.010802

3 http://www.nitrc.org/projects/bnv/

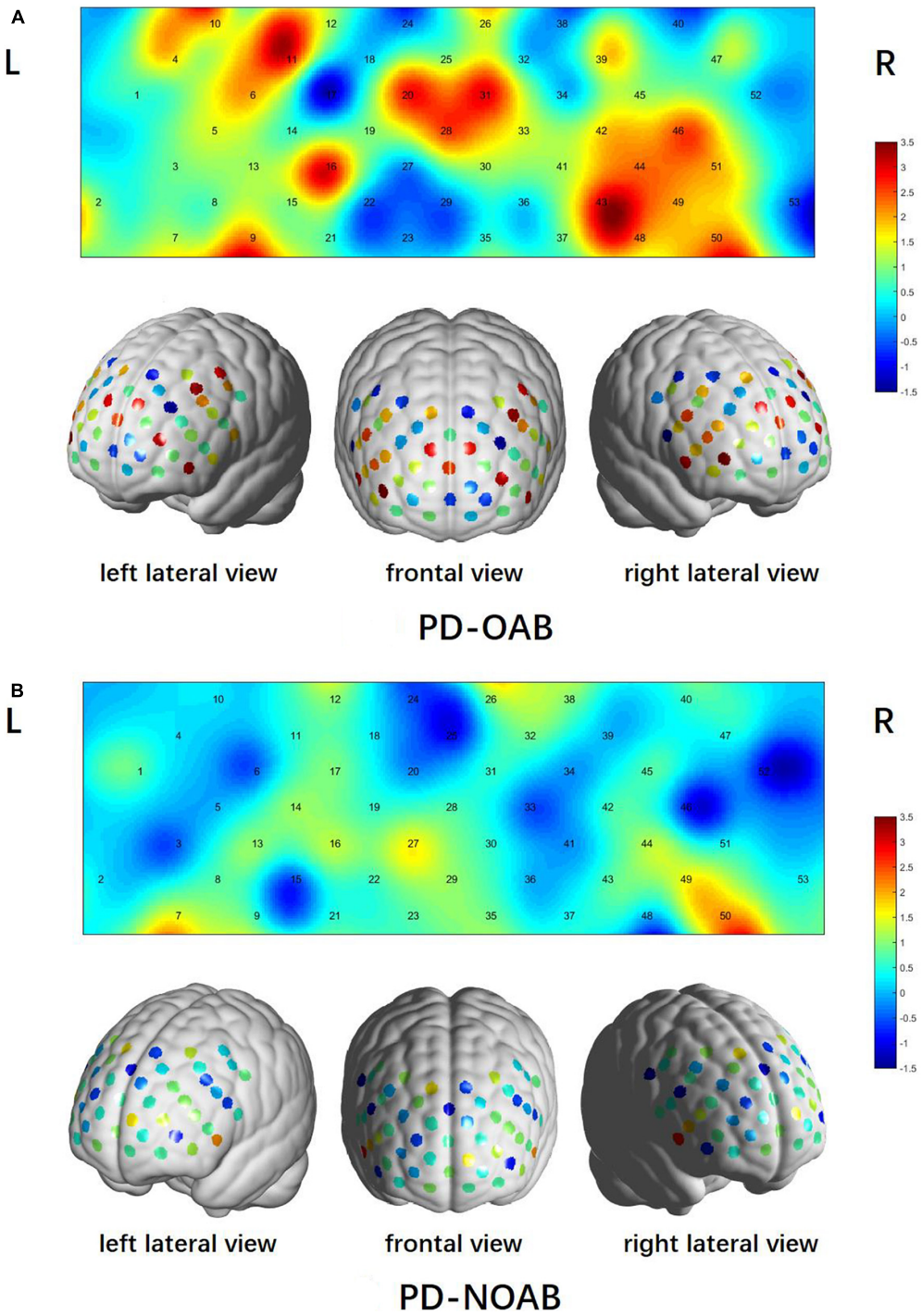

FIGURE 2
Patterns of cortical activations during VFT of PD-OAB **(A)** and PD-NOAB **(B)**.

Results

The mean age of recruited PD patients was 63.15 ± 10.05 years. This cohort had 64 (41.3%) female subjects. The clinical characteristics and comparisons between PD-OAB and PD-NOAB symptoms are shown in Table 1. PD-OAB patients were relatively older in age, had a longer disease duration, a higher LEDD, and advanced scores in H-Y staging, MDS-UPDRS-III, MoCA, FAB, PDQ39, and NMS scores. The gender distribution, years of education, and scores of HAM-A and HAM-D did not statistically differ between the groups.

In cognitive function analysis, the linear regression exhibited that patients with higher OABSS scores presented significantly lower FAB scores, MoCA total scores, and sub-scores of visuospatial/executive, attention and orientation tests (Table 2).

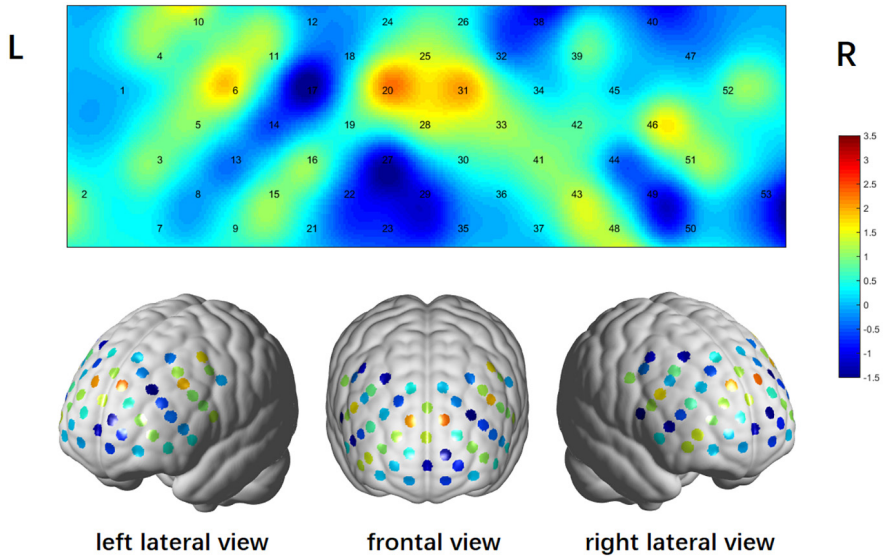

FIGURE 3
Differences in task-related cortical activations between the PD-OAB and PD-NOAB groups.

In the fNIRS study during VTF, the PD-OAB group revealed significant activations in 10 channels (9, 10, 11, 16, 20, 28, 31, 43, 46, and 50, $t = 2.558–3.509$, FDR $P < 0.05$) compared to the baseline condition, including 5 channels over the left hemisphere, 4 over the right hemisphere, and 1 in the median (Figure 2A). In contrast, only 1 channel (50, $t = 2.792$, FDR $P < 0.05$) over the right hemisphere showed significant activation compared to the baseline condition in the PD-NOAB group (Figure 2B). Moreover, compared with PD-NOAB group, the PD-OAB group demonstrated significant hyperactivation at channel 20 ($t = 2.261$, FDR $P < 0.05$) in the left DLPFC (Figure 3).

The results of the RSFC pattern and two-sample t-test for the PD-OAB and PD-NOAB groups are presented in Figures 4, 5 and Supplementary Table 1. A two-sample t-test revealed that there was a significant increase in the RSFC strength between the bilateral Broca's area ($P = 0.027$), FPA-L and Broca -R ($P = 0.006$), between the FPA and Broca's area ($P = 0.032$) if merging the bilateral ROI, and also between the two hemispheres ($P = 0.043$) in the PD-OAB group.

Furthermore, the Spearman's analysis revealed a positive correlation between the OABSS scores and FC strength of Broca R and L ($r = 0.668$, $P = 0.013$), FPA-L and Broca R ($r = 0.779$, $P = 0.002$), as well as Broca's area to FPA if merging the bilateral ROI ($r = 0.604$, $P = 0.029$), but the correlation between OABSS scores and the FC of the two hemispheres or the activation strength (β value) at channel 20 yielded non-significant results.

Discussion

Here, we investigated the association between OAB symptoms and PFC dysfunction in PD patients. The OABSS score was significantly correlated with lower FAB/MoCA total scores and sub-scores of visuospatial/executive, attention and orientation. In the fNIRS study, the PD-OAB group showed a hyperactivation particularly at channel 20 in the left DLPFC during VTF and an enhanced neural connectivity between the two hemispheres in the resting state compared with that in the PD-NOAB, suggesting a possibility of the underlying link between these two symptoms.

Our data showed that PD patients with higher OABSS presented significantly lower FAB scores and MoCA total scores, especially in visuospatial/executive, attention and orientation-related domains, which was well-aligned with previous reports. In a cohort of 189 non-demented PD subjects, urinary urgency was found to be associated with executive dysfunctions, in combination with NMS burden, nocturia, and stigma (Tkaczynska et al., 2020). Xu et al. (2019) have also identified that H-Y staging, FAB scoring, and RBD were accompanying etiological factors for OAB. There could be a multitude of pathological connections underlying the cross-talks between OAB and PFC symptoms, which gradually appear and progress along with the disease severity, probably due to the spread of α-synuclein plaques to the diencephalon and neocortex, corresponding to Braak stages 4–5 in PD (Braak et al., 2003). The urinary tract symptoms of PD patients may also be caused by disruption of the neurotransmitter (e.g., glutamate, dopamine, serotonin, and norepinephrine) signaling networks (Buddhala et al., 2015). A decline in nigrostriatal DAergic function has been linked to urinary tract pathologies in PD, as confirmed by functional neuroimaging studies (Winge et al., 2005; Mito et al., 2018; Wang et al., 2020). Besides, given the older ages of these subjects, the influence of cerebrovascular burden couldn't be eliminated in linking OAB to cognition (Buchman et al., 2011).

Many studies have explored PD with LUT from the perspective of imaging. An MRI study suggests that the thickness and volume of the precuneus (left) and left frontal pole may manifest the severity of LUT symptoms in PD patients (Roh et al., 2021). Kitta et al. (2006) have found significant brain activations in the periaqueductal gray, cerebellar vermis, supplementary motor area,

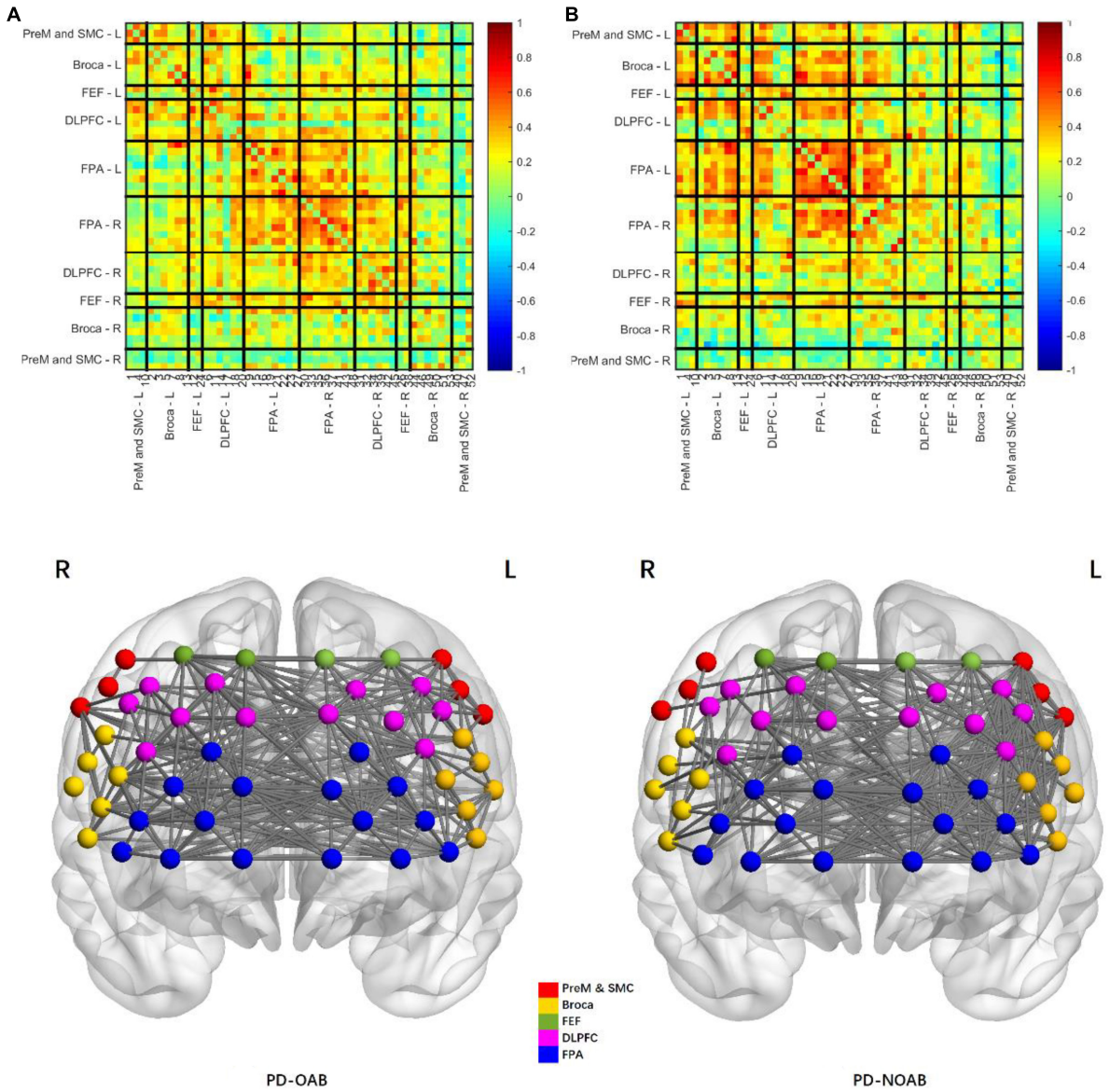

FIGURE 4
Pattern of resting-state functional connectivity strength between the regions of interest of PD-OAB **(A)** and PD-NOAB **(B)** groups.

putamen, insula, and thalamus during detrusor overactivity with positron emission tomography (PET) scanning in nine male PD patients. A ^{123}I-FP-CIT SPECT study involving 31 untreated PD patients indicated PD-OAB individuals had lower striatal DAT availabilities (Mito et al., 2018). An alteration in brain raphe nuclei positioning was reported by Walter et al. (2006) in a cohort of PD-OAB patients using transcranial sonography. Despite the utilization of a variety of research instruments, there is no definite conclusion on the location of the damage and the underlying pathophysiological mechanism of PD with OAB. Hence, strict inclusion criteria, a combination of multiple research methods, relatively large sample sizes, and longitudinal follow-ups may help obtain reliable conclusions in the future.

To our knowledge, no current publications have investigated the cognition function in PD patients with OAB by using fNIRS. Our data revealed that certain PFC regions were activated during VFT and an enhanced neural connectivity between the two hemispheres in the resting state in the PD-OAB group than that in the PD-NOAB group, suggesting this subset of patients may require additional cognitive support to compensate for the damaged bladder control and PFC could be a better target in improving the intervention strategy under this condition. Cortex-specific non-invasive brain stimulation could be a potential approach to evaluate changes in cognition. Our results were in line with several previous findings showing higher brain activation in the PFC of PD patients with a freeze of gait (FoG) than that in PD patients without FoG, indicating a positive correlation between clinical severities and cortical activation strengths (Belluscio et al., 2019; Pu et al., 2022). However, we could not detect any statistical significance in this correlation between the clinical severity with cortical activation, which might be due to some confounding factors between the two that have not been identified and adjusted.

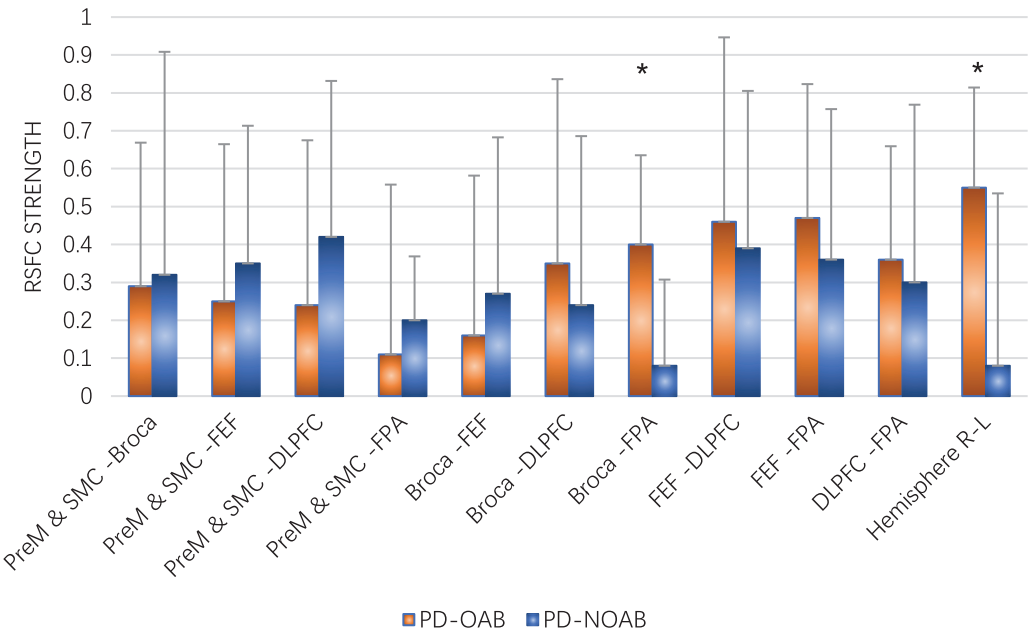

FIGURE 5
Two-sample *t*-test of RSFC strength between the ROI and two hemispheres for the PD-OAB and PD-NOAB groups. $*P < 0.05$.

Or, the correlation between the two may be not linear, by reason of the undurability of the compensatory response of the prefrontal cortex in the advanced stage of the disease. With these results, we plan further to carry out a cohort study with intervention on ROI using a sample size sufficient for stratified analysis.

The major strength of this study was the good generalizability of the conclusion. This study highlighted the outpatient PD subpopulation complicated with OAB symptoms and the possible diagnostic and interventional strategies. Other strengths included the advantages of combining the neuropsychological battery with advanced imaging modalities like fNIRS in the precise evaluation of cortical hemodynamic changes in PD. The crucial limitations of this study were: first, we couldn't explore the causative factors that linked OAB to cognitive impairment because of the cross-sectional nature of this study. Future longitudinal studies will be useful in unveiling the pathological role of neuronal circuitry loss in PFC-inducing OAB symptoms. Second, urodynamic examination reports weren't available for stratifying PD-OAB subjects from PD-NOAB. Despite our strict exclusion criteria, it was difficult to completely avoid false positives and false negatives. Finally, unlike fMRI, fNIRS measurements exhibited a moderate spatial resolution and might not be suitable for investigating the relationship between cortical and subcortical structures. The fNIRS, nevertheless, could provide an overall evaluation of neuronal activities in the PFC.

Conclusion

Non-motor symptoms of OAB, secondary to PD, can seriously impact the quality of life in PD patients and their caregivers. Our study demonstrated that decreased PFC function could be associated with OAB in PD by using neuropsychological examinations and that the pattern of PFC activation and network measured by task-based and resting-state fNIRS altered in PD patients with OAB. The findings of this study are likely to improve our understanding of non-motor complications like OAB in PD patients and highlight a potential alternative intervention target.

Data availability statement

The raw data supporting the conclusions of this article will be made available by the authors, without undue reservation.

Ethics statement

The studies involving human participants were reviewed and approved by the Ethics Committees of the Xinhua Hospital Affiliated to Shanghai Jiao Tong University School of Medicine and the First Affiliated Hospital of Naval Medical University. The patients/participants provided their written informed consent to participate in this study.

Author contributions

JG and ZGL designed the research. XM, JW, YZ, CQ, LS, YiW, and ZHL examined the patients and recruited the data. YaW performed the statistical analysis. MH drafted the manuscript.

All authors made contributions to this study, critically reviewed the content, and approved the final version of this article.

Funding

This study was supported by the Projects of the National Natural Science Foundation of China (81974173, 82271274, and 82171242), the Pilot Project of Clinical Cooperation Between Chinese and Western Medicine in Shanghai (ZXYXZ-201907), the Shanghai Demonstration Project of Cooperative Diagnosis and Treatment for Major Difficult Diseases with Integrated Modern and Traditional Chinese Medicine [ZY(2021-2023)-0207-01-03], the Shanghai Pujiang Program (21PJD046), Innovative Research Team of High-level Local Universities in Shanghai (SHSMU-ZDCX20211901), and the Project of Shanghai Science and Technology Commission (22Y11904100).

Acknowledgments

The authors sincerely thank all the participants for their cooperation.

Conflict of interest

The authors declare that the research was conducted in the absence of any commercial or financial relationships that could be construed as a potential conflict of interest.

Publisher's note

All claims expressed in this article are solely those of the authors and do not necessarily represent those of their affiliated organizations, or those of the publisher, the editors and the reviewers. Any product that may be evaluated in this article, or claim that may be made by its manufacturer, is not guaranteed or endorsed by the publisher.

Supplementary material

The Supplementary Material for this article can be found online at: https://www.frontiersin.org/articles/10.3389/fnins.2023.1142741/full#supplementary-material

References

Belluscio, V., Stuart, S., Bergamini, E., Vannozzi, G., and Mancini, M. (2019). The association between prefrontal cortex activity and turning behavior in people with and without freezing of gait. *Neuroscience* 416, 168–176. doi: 10.1016/j.neuroscience.2019.07.024

Braak, H., Del Tredici, K., Rüb, U., de Vos, R., Jansen Steur, E., and Braak, E. (2003). Staging of brain pathology related to sporadic Parkinson's disease. *Neurobiol. Aging* 24, 197–211. doi: 10.1016/S0197-4580(02)00065-9

Buchman, A., Leurgans, S., Nag, S., Bennett, D., and Schneider, J. (2011). Cerebrovascular disease pathology and parkinsonian signs in old age. *Stroke* 42, 3183–3189. doi: 10.1161/STROKEAHA.111.623462

Buddhala, C., Loftin, S., Kuley, B., Cairns, N., Campbell, M., Perlmutter, J., et al. (2015). Dopaminergic, serotonergic, and noradrenergic deficits in Parkinson disease. *Ann Clin Transl Neurol.* 2, 949–959. doi: 10.1002/acn3.246

Cui, X., Bray, S., Bryant, D., Glover, G., and Reiss, A. (2011). A quantitative comparison of NIRS and fMRI across multiple cognitive tasks. *NeuroImage* 54, 2808–2821. doi: 10.1016/j.neuroimage.2010.10.069

Funahashi, S. (2001). Neuronal mechanisms of executive control by the prefrontal cortex. *Neurosci. Res.* 39, 147–165. doi: 10.1016/S0168-0102(00)00224-8

Galtier, I., Nieto, A., Lorenzo, J., and Barroso, J. (2017). Mild cognitive impairment in Parkinson's Disease: clustering and switching analyses in verbal fluency test. *J. Int. Neuropsychol. Soc.* 23, 511–520. doi: 10.1017/S1355617717000297

Homma, Y., Kakizaki, H., Yamaguchi, O., Yamanishi, T., Nishizawa, O., Yokoyama, O., et al. (2011). Assessment of overactive bladder symptoms: comparison of 3-day bladder diary and the overactive bladder symptoms score. *Urology* 77, 60–64.

Homma, Y., Yoshida, M., Seki, N., Yokoyama, O., Kakizaki, H., Gotoh, M., et al. (2006). Symptom assessment tool for overactive bladder syndrome–overactive bladder symptom score. *Urology* 68, 318–323. doi: 10.1016/j.urology.2006.02.042

Hou, X., Zhang, Z., Zhao, C., Duan, L., Gong, Y., Li, Z., et al. (2021). NIRS-KIT: a MATLAB toolbox for both resting-state and task fNIRS data analysis. *Neurophotonics* 8:010802. doi: 10.1117/1.NPh.8.1.010802

Huppert, T., Diamond, S., Franceschini, M., and Boas, D. (2009). HomER: a review of time-series analysis methods for near-infrared spectroscopy of the brain. *Appl. Optics* 48, D280–D298. doi: 10.1364/ao.48.00d280

Kitta, T., Kakizaki, H., Furuno, T., Moriya, K., Tanaka, H., Shiga, T., et al. (2006). Brain activation during detrusor overactivity in patients with Parkinson's disease: a positron emission tomography study. *J. Urol.* 175(3 Pt 1), 994–998. doi: 10.1016/S0022-5347(05)00324-1

Kitta, T., Mitsui, T., Kanno, Y., Chiba, H., Moriya, K., and Shinohara, N. (2015). Brain-bladder control network: the unsolved 21st century urological mystery. *Int. J. Urol.* 22, 342–348. doi: 10.1111/iju.12721

Mahmoudzadeh, M., Wallois, F., Tir, M., Krystkowiak, P., and Lefranc, M. (2021). Cortical hemodynamic mapping of subthalamic nucleus deep brain stimulation in Parkinsonian patients, using high-density functional near-infrared spectroscopy. *PLoS One* 16:e0245188. doi: 10.1371/journal.pone.0245188

McDonald, C., Winge, K., and Burn, D. (2017). Lower urinary tract symptoms in Parkinson's disease: prevalence, aetiology and management. *Parkinsonism Relat. Disord.* 35, 8–16.

Miller, E. (1985). Possible frontal impairments in Parkinson's disease: a test using a measure of verbal fluency. *Br. J. Clin. Psychol.* 24(Pt 3), 211–212.

Mito, Y., Yabe, I., Yaguchi, H., Takei, T., Terae, S., and Tajima, Y. (2018). Relation of overactive bladder with motor symptoms and dopamine transporter imaging in drug-naïve Parkinson's disease. *Parkinsonism Relat. Disord.* 50, 37–41. doi: 10.1016/j.parkreldis.2018.02.017

Moussa, M., Chakra, M., Dabboucy, B., Fares, Y., Dellis, A., and Papatsoris, A. (2022). The safety and effectiveness of mirabegron in Parkinson's disease patients with overactive bladder: a randomized controlled trial. *Scand. J. Urol.* 56, 66–72.

Ogawa, T., Sakakibara, R., Kuno, S., Ishizuka, O., Kitta, T., and Yoshimura, N. (2017). Prevalence and treatment of LUTS in patients with Parkinson disease or multiple system atrophy. *Nat. Rev. Urol.* 14, 79–89.

Pu, L., Liu, T., Tang, W., Song, C., Jin, M., Ren, L., et al. (2022). Greater prefrontal activation during sitting toe tapping predicts severer freezing of gait in Parkinson's disease: an fNIRS study. *Cereb. Cortex* 33, 959–968. doi: 10.1093/cercor/bhac114

Roh, H., Kang, J., Hwang, S., Koh, S., and Kim, J. (2021). Regional cerebral cortical atrophy is related to urinary tract symptoms in Parkinson's disease. *J. Neuroimaging* 31, 363–371. doi: 10.1111/jon.12829

Sakakibara, R., Tateno, F., Nagao, T., Yamamoto, T., Uchiyama, T., Yamanishi, T., et al. (2014). Bladder function of patients with Parkinson's disease. *Int. J. Urol.* 21, 638–646.

Schejter-Margalit, T., Kizony, R., Ben-Binyamin, N., Hacham, R., Thaler, A., Maidan, I., et al. (2022). Neural activation in the prefrontal cortex during the digital clock drawing test measured with functional near-infrared spectroscopy in early stage Parkinson's disease. *Parkinsonism Relat. Disord.* 105, 9–14. doi: 10.1016/j.parkreldis.2022.10.021

Singh, A., and Dan, I. (2006). Exploring the false discovery rate in multichannel NIRS. *NeuroImage* 33, 542–549. doi: 10.1016/j.neuroimage.2006.06.047

Tao, P., Shao, X., Dong, Y., Adams, R., Preston, E., Liu, Y., et al. (2023). Functional near-infrared spectroscopy measures of frontal hemodynamic responses in Parkinson's patients and controls performing the Timed-Up-and-Go test. *Behav. Brain Res.* 438:114219. doi: 10.1016/j.bbr.2022.114219

Tkaczynska, Z., Becker, S., Maetzler, W., Timmers, M., Van Nueten, L., Sulzer, P., et al. (2020). Executive function is related to the urinary urgency in non-demented patients with Parkinson's Disease. *Front. Aging Neurosci.* 12:55. doi: 10.3389/fnagi.2020.00055

Walter, U., Dressler, D., Wolters, A., Wittstock, M., and Benecke, R. (2006). Overactive bladder in Parkinson's disease: alteration of brainstem raphe detected by transcranial sonography. *Eur. J. Neurol.* 13, 1291–1297. doi: 10.1111/j.1468-1331.2006.01463.x

Wang, J., Cao, R., Huang, T., Liu, C., and Fan, Y. (2020). Urinary dysfunction is associated with nigrostriatal dopaminergic degeneration in early and untreated patients with Parkinson's Disease. *Parkinson's Dis.* 2020:4981647. doi: 10.1155/2020/4981647

Winge, K., Friberg, L., Werdelin, L., Nielsen, K., and Stimpel, H. (2005). Relationship between nigrostriatal dopaminergic degeneration, urinary symptoms, and bladder control in Parkinson's disease. *Eur. J. Neurol.* 12, 842–850. doi: 10.1111/j.1468-1331.2005.01087.x

Xia, M., Wang, J., and He, Y. (2013). BrainNet Viewer: a network visualization tool for human brain connectomics. *PLoS One* 8:e68910. doi: 10.1371/journal.pone.0068910

Xu, D., Han, S., Wang, J., and Feng, J. (2019). Relationship between lower urinary tract dysfunction and clinical features in Chinese Parkinson's Disease patients. *Parkinson's Dis.* 2019:6820937. doi: 10.1155/2019/6820937

Ye, J., Tak, S., Jang, K., Jung, J., and Jang, J. (2009). NIRS-SPM: statistical parametric mapping for near-infrared spectroscopy. *NeuroImage* 44, 428–447. doi: 10.1016/j.neuroimage.2008.08.036

Zong, H., Meng, F., Zhang, Y., Wei, G., and Zhao, H. (2019). Clinical study of the effects of deep brain stimulation on urinary dysfunctions in patients with Parkinson's disease. *Clin. Intervent. Aging* 14, 1159–1166. doi: 10.2147/CIA.S204368

frontiers | Frontiers in Neuroscience

TYPE Original Research
PUBLISHED 18 May 2023
DOI 10.3389/fnins.2023.1125281

Check for updates

OPEN ACCESS

EDITED BY
Shenfeng Qiu,
University of Arizona, United States

REVIEWED BY
Zhen Yuan,
University of Macau, China
Bo Chen,
Suzhou University of Science and Technology, China

*CORRESPONDENCE
Yuanwei Wang
✉ wyweilmn@126.com

RECEIVED 16 December 2022
ACCEPTED 30 March 2023
PUBLISHED 18 May 2023

CITATION
Zhao K, Wu Y, Zhao D, Zhang H, Lin J and Wang Y (2023) Six mitophagy-related hub genes as peripheral blood biomarkers of Alzheimer's disease and their immune cell infiltration correlation.
Front. Neurosci. 17:1125281.
doi: 10.3389/fnins.2023.1125281

COPYRIGHT
© 2023 Zhao, Wu, Zhao, Zhang, Lin and Wang. This is an open-access article distributed under the terms of the Creative Commons Attribution License (CC BY). The use, distribution or reproduction in other forums is permitted, provided the original author(s) and the copyright owner(s) are credited and that the original publication in this journal is cited, in accordance with accepted academic practice. No use, distribution or reproduction is permitted which does not comply with these terms.

Six mitophagy-related hub genes as peripheral blood biomarkers of Alzheimer's disease and their immune cell infiltration correlation

Kun Zhao[1], Yinyan Wu[1], Dongliang Zhao[1], Hui Zhang[2], Jianyang Lin[3] and Yuanwei Wang[4]*

[1]Department of Neurology, Affiliated People's Hospital of Jiangsu University, Zhenjiang, Jiangsu, China, [2]Fujian Center for Safety Evaluation of New Drug, Fujian Medical University, Fuzhou, Fujian, China, [3]Department of General Surgery, Affiliated People's Hospital of Jiangsu University, Zhenjiang, Jiangsu, China, [4]Department of Neurology, Shuyang Hospital Affiliated to Xuzhou Medical University, Shuyang, Jiangsu, China

Background: Alzheimer's disease (AD), a neurodegenerative disorder with progressive symptoms, seriously endangers human health worldwide. AD diagnosis and treatment are challenging, but molecular biomarkers show diagnostic potential. This study aimed to investigate AD biomarkers in the peripheral blood.

Method: Utilizing three microarray datasets, we systematically analyzed the differences in expression and predictive value of mitophagy-related hub genes (MRHGs) in the peripheral blood mononuclear cells of patients with AD to identify potential diagnostic biomarkers. Subsequently, a protein–protein interaction network was constructed to identify hub genes, and functional enrichment analyses were performed. Using consistent clustering analysis, AD subtypes with significant differences were determined. Finally, infiltration patterns of immune cells in AD subtypes and the relationship between MRHGs and immune cells were investigated by two algorithms, CIBERSORT and single-sample gene set enrichment analysis (ssGSEA).

Results: Our study identified 53AD- and mitophagy-related differentially expressed genes and six MRHGs, which may be potential biomarkers for diagnosing AD. Functional analysis revealed that six MRHGs significantly affected biologically relevant functions and signaling pathways such as IL-4 Signaling Pathway, RUNX3 Regulates Notch Signaling Pathway, IL-1 and Megakaryocytes in Obesity Pathway, and Overview of Leukocyteintrinsic Hippo Pathway. Furthermore, CIBERSORT and ssGSEA algorithms were used for all AD samples to analyze the abundance of infiltrating immune cells in the two disease subtypes. The results showed that these subtypes were significantly related to immune cell types such as activated mast cells, regulatory T cells, M0 macrophages, and neutrophils. Moreover, specific MRHGs were significantly correlated with immune cell levels.

Conclusion: Our findings suggest that MRHGs may contribute to the development and prognosis of AD. The six identified MRHGs could be used as valuable diagnostic biomarkers for further research on AD. This study may provide new promising diagnostic and therapeutic targets in the peripheral blood of patients with AD.

KEYWORDS

Alzheimer's disease, hub gene, mitophagy, bioinformatics analysis, blood biomarker, immune infiltration

1. Introduction

Alzheimer's disease (AD) is a common, progressive, and complex neurodegenerative disorder that causes cognitive decline, memory loss, and difficulty performing daily tasks (Heckmann et al., 2020). Globally, AD poses a huge threat to people's health and a significant economic burden to society (Dumitrescu et al., 2020). Thus far, the pathogenesis of AD remains unknown, and there is no definitive treatment. Some molecules correlate with AD progression and cognitive decline; the identification of molecular changes and biological processes connected to AD can increase our understanding of AD pathogenesis and provide biomarkers for AD.

Pathological hallmarks of AD are aggregated amyloid-β (Aβ) protein in senile plaques and aggregated tau protein in neurofibrillary tangles (Liang et al., 2016). However, the molecular mechanisms regulating AD development *via* Aβ, tau, or other factors are poorly understood. Over the past few decades, an increasing number of therapies and immunotherapies, such as vaccines and drugs targeting Aβ protein, tau protein, or AD-related genes, have been developed. The effectiveness of these targeted therapies has been demonstrated in some patient populations and animal models of AD (Town et al., 2008; Sevigny et al., 2016; Congdon and Sigurdsson, 2018; Xiong et al., 2021; Jung et al., 2022); however, it is always challenging to translate these results into humans safely and effectively (Town et al., 2008; Lemere, 2013; Xiong et al., 2021). Thus, it is crucial to identify novel immunological diagnostic and therapeutic AD markers.

Healthy and active mitochondria are essential for neuronal function (Chakravorty et al., 2019; Pradeepkiran and Reddy, 2020). The accumulation of damaged mitochondria and mitochondrial dysfunction are early marker events and core participants in the process of AD (Chakravorty et al., 2019; Fang, 2019). In AD neurons, mitochondrial dysfunction is related to mitochondrial dynamics, biogenesis, and mitophagy (Grimm and Eckert, 2017; Kerr et al., 2017). Mitophagy, also called selective autophagy, is a selective degradation process that gradually accumulates defective mitochondria through autophagy. It is a key mitochondrial quality control system that helps neurons maintain health and function by removing unnecessary and damaged mitochondria. In other words, dysfunctional mitochondria and dysfunctional mitophagy in neurons are closely related to the occurrence of AD. Various proteins related to mitophagy were found to be changed in AD neurons (Rai et al., 2020; Mary et al., 2023). Recent studies (Fang et al., 2019; Morton et al., 2021; Pradeepkiran et al., 2022) from animal and cell models of AD and sporadic late-onset AD showed that impaired mitophagy triggered Aβ and tau protein accumulation by increasing oxidative damage and cell energy deficiency, leading to synaptic dysfunction and cognitive impairment. Moreover, these processes can compromise mitophagy (Fang et al., 2019; Morton et al., 2021; Pradeepkiran et al., 2022). Therefore, interventions that support mitochondrial health or stimulate mitophagy may prevent the neurodegenerative process of AD (Kerr et al., 2017; Fang et al., 2019). Accordingly, by removing defective mitochondria in AD through mitophagy targeting, it might be possible to intervene therapeutically (Wang et al., 2021; Pradeepkiran et al., 2022; Sharma et al., 2022; Xie et al., 2022). Nevertheless, the association of mitophagy with AD pathology and AD-related changes in immune system effectiveness is not fully explained and requires further investigation.

In recent decades, researchers have been interested in finding new biomarkers or models to early identify metabolic risk abnormalities. The progression and prognosis of AD can be affected by many genetic or epigenetic alterations (Karch and Goate, 2015; Efthymiou and Goate, 2017). Familial AD accounts for 5–10% of all AD cases. Pathogenic mutations in genes like *APP*, *PSEN1*, and *PSEN2* are found in approximately 15–20%, 70–80, and 5% of patients with familial AD, respectively (Ryan and Rossor, 2010; Williams, 2011). Apolipoprotein E (*APOE*), as the most important susceptible gene known, may play an important role in the predisposition to sporadic AD; the *APOE4* gene is associated with late-onset AD and contributes to the development of neurofibrillary tangles and Aβ senile plaques (Corder et al., 1993; Poirier et al., 1993). *TREM2* is also a very important gene and encodes the protein, triggering receptor expressed on myeloid cells 2 (TREM2); it is expressed by microglia, the resident immune cells of the brain, and strongly affects the lifelong risk of AD (Roussos et al., 2015; Ulrich et al., 2017). Some other genes such as *CR1*, *SPI1*, *MS4As*, *ABCA7*, *CD33*, and *INPP5D* (Roussos et al., 2015) involved in different biological processes are expressed by microglia as well. *APOE*, *CLU*, and *ABCA7* may be related to lipid metabolism; *ABCA7*, *CD33*, *CR1*, *CLU*, and *EPHA1* may be associated with immune system function (Reitz et al., 2013; Villegas-Llerena et al., 2016); *PICALM*, *BIN1*, *CD33*, and *CD2AP* may be related to cell membrane function including endocytosis (Villegas-Llerena et al., 2016). In addition, polymorphisms of *CLU*, *SORL1*, and *MS4A4A* genes also affect AD-related biomarkers (mainly Aβ, tau, and phosphorylated tau proteins) within the cerebrospinal fluid (Elias-Sonnenschein et al., 2013). However, research on AD is complex, and more experiments are needed to break through the treatment bottleneck of AD. The advances in bioinformatics enable independent studies to identify biomarkers. Numerous genes and loci can be analyzed using bioinformatics to uncover potential biological pathways in AD (Suh et al., 2019).

Abbreviations: AD, Alzheimer's disease; *APOE*, apolipoprotein E; AUROC, area under the receiver operating characteristics curve; Aβ, amyloid-β; BP, biological process; CC, cellular component; CDs, combined datasets; DEG, differentially expressed gene; *DLAT*, dihydrolipoamide S-acetyltransferase; GEO, Gene Expression Omnibus; GO, Gene Ontology; GSEA, gene set enrichment analysis; *ITGAX*, integrin subunit alpha X; KEGG, Kyoto Encyclopedia of Genes and Genomes; LASSO, least absolute shrinkage and selection operator; MDSC, myeloid-derived suppressor cell; MF, molecular function; MRDEG, mitophagy-related differentially expressed gene; MRG, mitophagy-related gene; MRHG, mitophagy-related hub gene; PCA, principal component analysis; *PPARG* (PPAR γ), peroxisome proliferator-activated receptor gamma; PPI, protein–protein interaction; ROC, receiver operating characteristic; ssGSEA, single-sample gene set enrichment analysis; *SUCLA2*, succinate-CoA ligase ADP-forming subunit β; TF, transcription factors; *TREM2*, triggering receptor expressed on myeloid cells 2.

Our study utilized the Gene Expression Omnibus (GEO) database of the National Center for Biotechnology Information to analyze mitophagy-related differential expressed genes (MRDEGs), do functional enrichment analyses, construct a diagnostic model, determine those that play key roles in AD, and identify possible biomarkers in the peripheral blood and their associated immune cell infiltration. Furthermore, we compared the mitophagy-related hub genes (MRHGs) and immune patterns of patients with AD with those of controls. However, the purpose of this research was to investigate AD biomarkers related to mitophagy and their immune cell infiltration correlation in the peripheral blood.

2. Materials and methods

2.1. Data retrieval

The AD-related datasets GSE110226 (Kant et al., 2018; Stopa et al., 2018), GSE1297 (Blalock et al., 2004), and GSE63060 (Sood et al., 2015) were downloaded from the GEO database through the R package GEOquery (Davis and Meltzer, 2007). The control samples of all three datasets were obtained from healthy individuals. In this study, we included 7 AD and 6 control samples from GSE110226, 22 AD and 9 control samples from GSE1297 (Supplementary Table S1), and 145 AD and 104 control samples from GSE63060. The batch effects of the datasets GSE110226 and GSE1297 were removed using the R package *sva* (Leek et al., 2012) to obtain an integrated GEO dataset, i.e., combined datasets (CDs) including 29 AD and 15 control samples. Finally, the CDs and GSE63060 were standardized using the R package *limma*, and the annotation probes were standardized and normalized.

Mitophagy-related genes (MRGs) were collected using the GeneCards database (Stelzer et al., 2016), which provides comprehensive information about human genes. In addition, MRGs in the published literature (Zhuo et al., 2022) were obtained on the PubMed website using the term "mitophagy-related genes." A total of 2,414 MRGs were obtained after combining the results and removing duplicates. A flow diagram of the database search is shown in Figure 1.

2.2. Differentially expressed genes related to AD

According to the sample grouping of the CDs, samples were divided into the AD and control groups. Differential analysis of genes

FIGURE 1
Flow chart for the comprehensive analysis of MRDEGs. MRDEG, mitophagy-related differentially expressed gene.

in different groups was performed using the R package differential gene expression analysis based on the negative binomial distribution (*DESeq2*) (Love et al., 2014). DEGs with logFC>0.5 and $p < 0.05$ were considered statistically significant. Among these, genes with logFC>0.5 and $p < 0.05$ were considered upregulated, and genes with logFC<0.5 and $p < 0.05$ were considered downregulated.

To obtain MRDEGs associated with AD, all DEGs with logFC>0.5 and $p < 0.05$ obtained by differential analysis in the CDs and MRGs were intersected and plotted to obtain MRDEGs. The results of the differential analysis were plotted using the R package *ggplot2*, the heatmap was drawn using the R package *pheatmap*, and chromosome mapping was performed using the R package *RCircos* (Zhang et al., 2013).

2.3. Receiver operating characteristic curve

The ROC curve (Park et al., 2004) is a comprehensive index reflecting continuous variables of sensitivity and specificity. The relationship between sensitivity and specificity is reflected by the composition method. The area under the ROC curve (AUROC) is generally between 0.5 and 1. The closer the AUROC value is to 1, the better the diagnostic effect. The AUC values were considered low, medium, or high accuracy for ranges 0.5–0.7, 0.7–0.9, and > 0.9, respectively. The R package *survivalROC* was used to plot the ROC curves of MRDEGs, as well as the survival times and statuses of patients with AD.

2.4. Construction of the diagnostic model of MRDEGs

In order to obtain a diagnostic model of MRDEGs in the AD datasets, the R package glmnet (Engebretsen and Bohlin, 2019) with set.seed(2) and family = "binary" as parameters was used to perform least absolute shrinkage and selection operator (LASSO) regression analysis based on MRDEGs. To avoid overfitting, the operating cycle is 1,000. LASSO regression is often used to construct a prognostic model, which is based on linear regression and by adding a penalty term (lambda × absolute value of the slope) reduces the overfitting of the model and improves the generalization ability of the model. The results of LASSO regression analysis were visualized utilizing the diagnostic model and variable trajectory diagrams and the molecular expression of each gene in the MRDEG diagnostic model was displayed in a forest plot.

Thereafter, MRDEGs were screened by LASSO regression analysis, and univariate and multivariate Cox regression analyses were performed to construct a multivariate Cox regression model. Nomogram (Wu et al., 2020) is a graph that uses a cluster of disjoint line segments to represent the functional relationship between multiple independent variables in the plane rectangular coordinate system. Based on these results, nomograms were drawn using the R package *rms*. Next, a calibration analysis was performed, and a calibration curve was generated to evaluate the accuracy and resolution of the nomograms. Decision curve analysis (Van Calster et al., 2018) is a simple method to evaluate clinical prediction models, diagnostic tests, and molecular markers. Finally, the accuracy and resolution of the multivariate Cox regression model were evaluated using the R package *ggDCA* to draw the decision curve analysis map.

2.5. Protein–protein interaction network

Protein protein interaction (PPI) network is composed of proteins and proteins through the interaction between them. The STRING database (Szklarczyk et al., 2019) was used to construct the PPI network related to the MRDEGs with a minimum required interaction score of medium confidence (0.400) as the standard, and the Cytoscape software (Shannon et al., 2003) was used to visualize the PPI network model.

In addition, five algorithms in the CytoHubba (Chin et al., 2014) plug-in were applied: maximum neighborhood component, degree, maximal clique centrality, closeness, and edge percolated component (Yang et al., 2019; Liu et al., 2022). In the PPI network, the scores of the MRDEGs were initially calculated, and then the MRDEGs were arranged in the order of their scores. Finally, the genes of the five algorithms were collected and analyzed by drawing the Venn diagram. The intersecting genes of the algorithms were considered hub genes related to mitophagy.

2.6. Construction of transcription factor-mRNA and mRNA-miRNA regulatory networks

Transcription factors (TFs) control gene expression through interaction with a target gene (mRNA) in the post-transcriptional stage. By retrieving TFs from the ChIPBase database (Zhou et al., 2017), the regulatory effects of TFs on MRHGs were analyzed, and the TF-mRNA regulatory network was visualized using the Cytoscape software.

miRNAs play an important regulatory role in the process of biological development and evolution. They are able to regulate multiple target genes; the same target gene can be regulated by multiple miRNAs. To analyze the relationship between MRHGs and miRNAs, miRNAs related to MRHGs were obtained from the StarBase database (Li et al., 2014). Finally, the mRNA-miRNA regulatory network was visualized using the Cytoscape software.

2.7. Gene function enrichment analysis, pathway enrichment analysis, and gene set enrichment analysis

Gene Ontology (GO) analysis (Mi et al., 2019) is a common method for large-scale functional enrichment studies, including biological processes (BPs), molecular functions (MFs) and cell components (CCs). Kyoto Encyclopedia of Genes and Genomes (KEGG) (Kanehisa and Goto, 2000) is a widely used database that stores information about genomes, biological pathways, diseases and drugs. GO and KEGG pathway annotation of MRHGs was analyzed using the R package *clusterProfiler* (Yu et al., 2012). The entry screening criteria were $p < 0.05$ and a false detection rate (q)-value of <0.05, which were considered statistically significant. The value of p was corrected using the Benjamini–Hochberg procedure.

Gene Set Enrichment Analysis (GSEA) (Subramanian et al., 2005) was used to evaluate the distribution trend of genes in a predefined gene set in the gene table sorted by the degree of correlation with phenotype, so as to judge their contribution to phenotype. In this study, genes in the CDs were first divided into two groups with high and low phenotypic correlations according to the phenotypic correlation ranking. Thereafter, all DEGs in the two groups with high and low phenotypic correlations were enriched using the R package *clusterProfiler*. The genes were analyzed by GSEA. We retrieved the c2.cp.v7.2.symbols.gmt gene set from the Molecular Signatures database (Liberzon et al., 2011); the screening criteria for significant enrichment were $p < 0.05$ and q-values of <0.05.

2.8. Molecular subtype construction of MRHGs

Consistency clustering (Lock and Dunson, 2013) refers to multiple iterations of subsamples of a dataset. It provides the index of clustering stability and parameter decision by using subsamples to induce sampling variability. The consensus clustering method using the R package *ConsensusClusterPlus* (Wilkerson and Hayes, 2010) was employed to identify different disease subtypes of AD based on MRHGs.

2.9. Analysis of immune cell infiltration

Using CIBERSORT algorithms (Newman et al., 2015) and the LM22 characteristics gene matrix, the samples with output p-values of <0.05 were filtered to obtain the immune cell infiltration matrix. The data were then filtered for immune cell enrichment scores greater than zero. Finally, the specific results of the immune cell infiltration matrix were obtained. A histogram was drawn using *ggplot2* to show the distribution of 22 types of immune cell infiltrates in different subtypes of AD samples; the correlation heatmap was drawn using *pheatmap* to illustrate the correlation analysis results of the 22 immune cell types with MRHGs in different AD subtypes.

The relative abundance of each infiltrating immune cell type was quantified using single-sample GSEA (ssGSEA) algorithms (Coscia et al., 2018). First, the types of infiltrating immune cells were labeled, such as activated CD8+ T cells, activated dendritic cells, γδ T cells, natural killer cells, regulatory T cells, and other human immune cell subtypes. Second, the enrichment score calculated by ssGSEA was used to express the relative abundance of each immune cell type in each sample. Finally, *ggplot2* was used to display the distributions of infiltrating immune cells in different disease subtypes of AD samples; *pheatmap* was used to draw a correlation heatmap that shows the results of the correlation analysis between immune cells and MRHGs in different AD subtypes.

2.10. Statistical analysis

All data processing and analysis in this article are based on R software version 4.1.2. Continuous variables are presented as mean ± standard deviation. The Wilcoxon rank sum test was used for comparison between two groups; the Kruskal–Wallis test was used for comparisons of three groups or more. The chi-square test or Fisher's exact test was used to compare and analyze statistical significance between two groups of categorical variables. Unless otherwise specified, correlation coefficients between different molecules were calculated using Spearman's correlation analysis, and statistical significance was set at $p < 0.05$.

3. Results

3.1. Analysis of AD-related DEGs

First, the R package *sva* was used to remove batch effects from the AD datasets GSE110226 and GSE1297 and obtain CDs. The datasets before and after batch effect removal were compared using a distribution box diagram and principal component analysis (PCA) (Figures 2A–D). These results showed that the batch effect of the samples in the AD dataset was basically eliminated by this procedure.

Then, the data from the CDs were divided into the control and AD groups. To analyze the intergroup differences in gene expression values in the AD dataset, the R package *DESeq2* was used to perform a differential analysis on the CDs of the two data groups. The CDs contained 436 DEGs that met the threshold of logFC>0.5 and $p < 0.05$. Of these, 212 genes were upregulated (logFC>0.5, $p < 0.05$) and 224 downregulated (logFC<0.5, $p < 0.05$), and a volcano map was drawn accordingly (Figure 3A). To identify MRDEGs, all DEGs with logFC>0.5 and $p < 0.05$ were intersected with MRGs (Supplementary Table S2). A total of 53 MRDEGs were obtained, which are illustrated in the Venn diagram in Figure 3B. Specific gene information is presented in Supplementary Table S3. According to the intersection results, differences in MRDEG expression between different CD sample groups were analyzed and displayed in a heatmap (Figure 3C) by using the R package *pheatmap*. Finally, the positions of the identified 53 MRDEGs on human chromosomes were analyzed using the R package *RCircos*, and their chromosome mappings were displayed (Figure 3D; Supplementary Table S4).

3.2. Correlation analysis of MRDEGs

To further explore the differences in MRDEG expression in the AD dataset, a histogram based on grouping and comparison was generated (Figure 4A). It shows the differential expression of the 53 MRDEGs in the AD and control groups in the CDs. The expression levels of 49 MRDEGs were significantly different (Supplementary Table S4). Of these MRDEGs, *APOO*, *PFN2*, *DHX57*, *PCCB*, *MTX2*, *KIFC3*, and dihydrolipoamide S-acetyltransferase (*DLAT*) were significantly different between the AD and control groups ($p < 0.001$); *ITGA5*, *NDUFS4*, *SLC12A7*, *CHST3*, *GDAP1*, *SLC35E1*, *NNT*, *C1QBP*, *KCNAB1*, *INF2*, *ITGB4*, *EPHA2*, *MON1B*, *TMEM14A*, *SLC1A5*, *RCN2*, *ACTR10*, *NETO2*, *VPS33A*, *TFEB*, *PDE12*, and *MRPS28* were highly significantly different ($p < 0.01$); and *CD44*, *FOXO4*, *MDH1*, *ZNF787*, succinate-CoA ligase ADP-forming subunit β (*SUCLA2*), *NUP93*, *NUPR1*, *FGF13*, *GLRX5*, *MSTN*, *UQCRC1*, *MYC*, *NDE1*, *RAB23*, *PSMA3*, *DAP3*, *DNAJC3*, integrin subunit alpha X CD11c (*ITGAX*), *CPA3*, and *NOS3* were significantly different between the studied groups ($p < 0.05$). The expression levels of the remaining genes, including *PNOC*, *PPARG*, *HILPDA*, and *MRPS15*, were not significantly different (Supplementary Table S4).

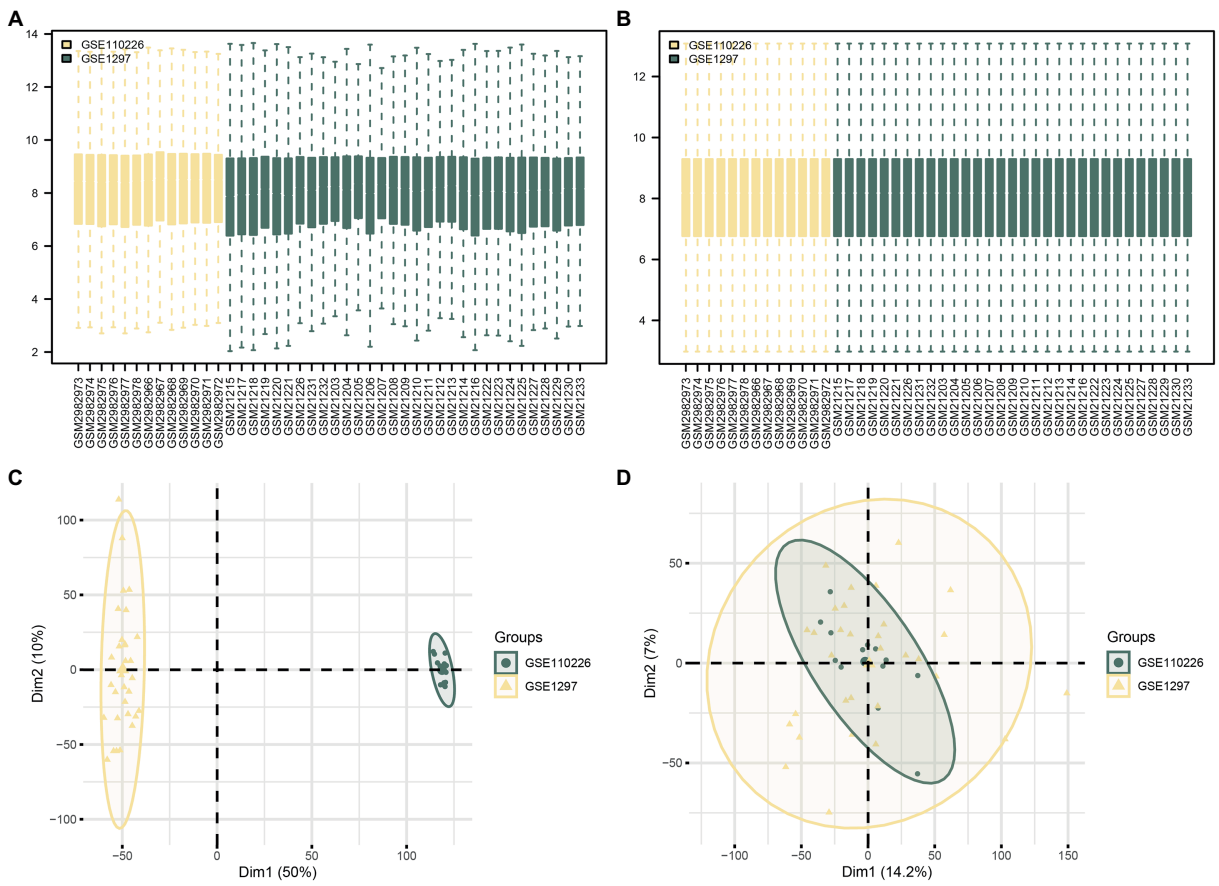

FIGURE 2
Batch effects removal of GSE110226 and GSE1297. **(A)** Distribution boxplot of datasets before batch processing. **(B)** Distribution boxplot of CDs after batch processing. **(C)** PCA diagram of datasets before batch processing. **(D)** PCA diagram of CDs after batch processing. DEG, differentially expressed gene; MRDEG, mitophagy-related differentially expressed gene; CDs, combined datasets; PCA, principal component analysis.

Next, the ROC curves of the abovementioned 49 MRDEGs were drawn (Figures 4B–M). The ROC curves of 45 MRDEGs revealed a medium correlation with different groups (0.7 < AUC < 0.9; Supplementary Table S4), whereas those of the other four MRDEGs, namely *MYC*, *PSMA3*, *ITGAX*, and *CPA3*, showed a low correlation with different groups (0.5 < AUC < 0.7; Supplementary Table S4).

3.3. Construction of the diagnostic model of the MRDEGs

To determine the diagnostic value of the 53 identified MRDEGs in the AD dataset, a diagnostic model of the MRDEGs was constructed by LASSO regression analysis (Figure 5A) and visualized through a LASSO variable trajectory diagram (Figure 5B). The LASSO diagnostic model comprised 17 MRDEGs (Supplementary Table S4), and the expression levels of these genes in the different groups of the LASSO diagnostic model are illustrated by a forest plot (Figure 5C).

In addition, the expression levels of these 17 MRDEGs were used for uni- and multivariate Cox regression analyses, and a Cox regression model was constructed. The prognostic ability of the Cox regression model was evaluated based on a generated nomogram (Figure 5D). The calibration curve was drawn, and the predictive power of the model for the actual results was evaluated based on the fitting of the actual probability. The probability predicted by the model under different conditions is presented in Figure 5E. Finally, the clinical utility of the Cox regression model was evaluated by decision curve analysis (Figure 5F). The range was determined in which the line of the model remained stable and higher than "All positive" and "All negative"; the larger this range, the higher the net benefit, and the better the model effect.

3.4. Construction of the PPI network and screening of the hub genes

Initially, a PPI analysis was carried out, and the PPI network of the 53 MRDEGs was constructed using the STRING database. Interactions were visualized using the Cytoscape software (Supplementary Figure S1A). Among the 53 MRDEGs, 36 were related (Supplementary Table S4), and the scores provided by the STRING database were calculated by applying five algorithms of the CytoHubba plug-in. Then, the MRDEGs were arranged according to their scores. The five algorithms were maximum neighborhood component (Supplementary Figure S1B), degree (Supplementary Figure S1C), maximal clique centrality (Supplementary Figure S1D), closeness (Supplementary Figure S1E), and edge percolated component (Supplementary Figure S1F). The genes identified by the five

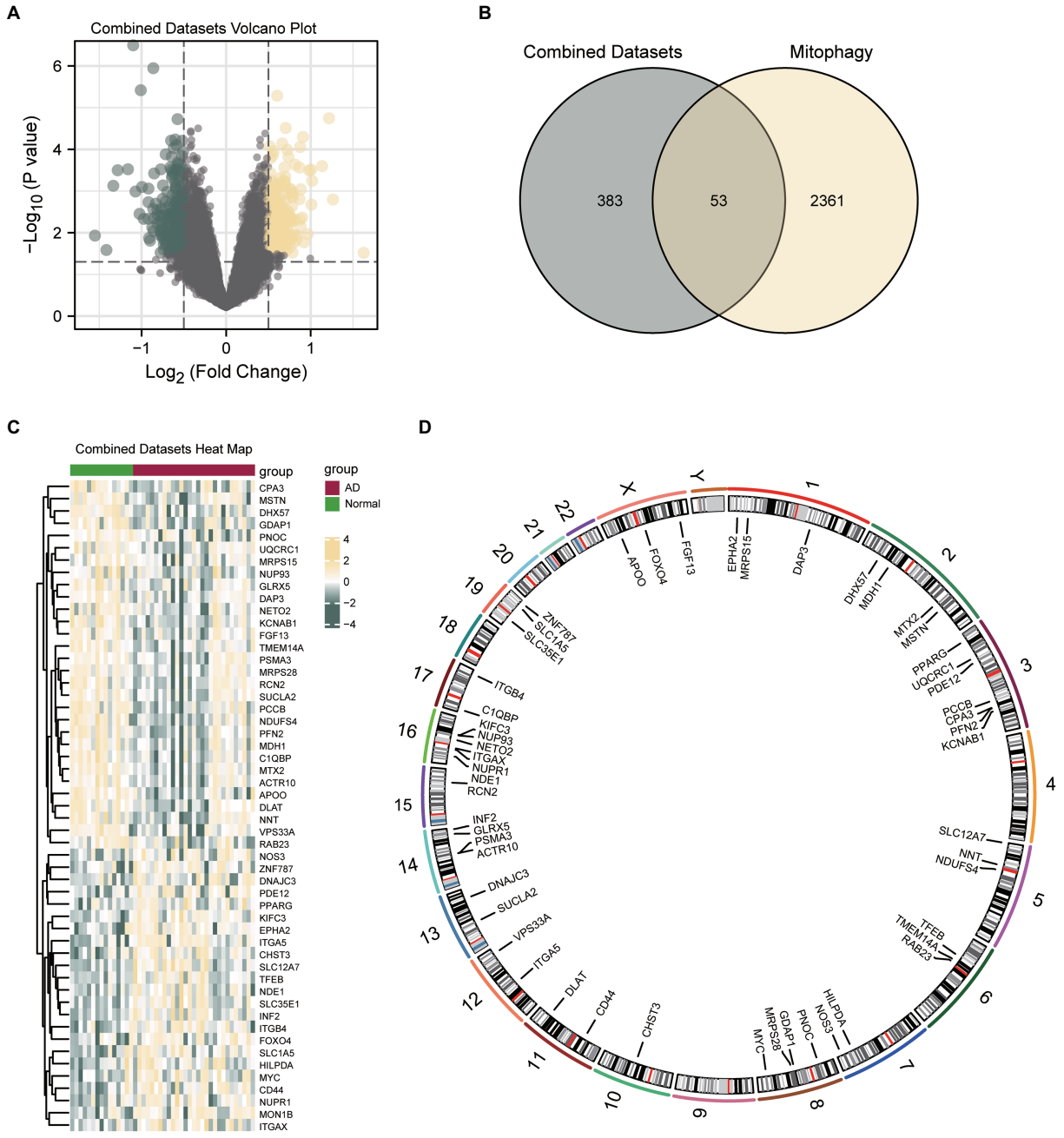

FIGURE 3
Differential gene expression analysis of AD. **(A)** Volcanic map of differential gene analysis between AD and control groups in CDs. **(B)** Venn diagram of DEGs and MRDEGs in CDs. **(C)** Correlation heat map of MRDEGs in CDs. **(D)** Chromosome mapping of MRDEGs. AD, Alzheimer's disease; DEG, differentially expressed gene; MRDEG, mitophagy-related differentially expressed gene; CDs, combined datasets.

algorithms were retrieved, and the Venn diagram was drawn to obtain the MRHGs (Supplementary Figure S1G). The six hub genes were *CD44*, *SUCLA2*, *DLAT*, *ITGAX*, *PPARG*, and *MYC*.

3.5. Construction of TF-mRNA and mRNA-miRNA regulatory networks

TFs associated with the MRHGs were obtained from the ChIPBase database, and the mRNA-TF regulatory network was constructed and visualized using the Cytoscape software (Supplementary Figure S2A). This network contained 6 MRHGs and 59 TFs. Likewise, the miRNAs related to the MRHGs were retrieved from the StarBase database, and the mRNA-miRNA regulatory network was constructed and visualized using Cytoscape (Supplementary Figure S2B). This network contained 6 MRHGs and 61 miRNAs.

3.6. Function enrichment (GO) analysis, pathway enrichment (KEGG) analysis of MRHGs, and GSEA of the AD dataset

Based on GO and KEGG enrichment analyses, the relationships among BPs, MFs, CCs, and biological pathways of the six MRDEGs

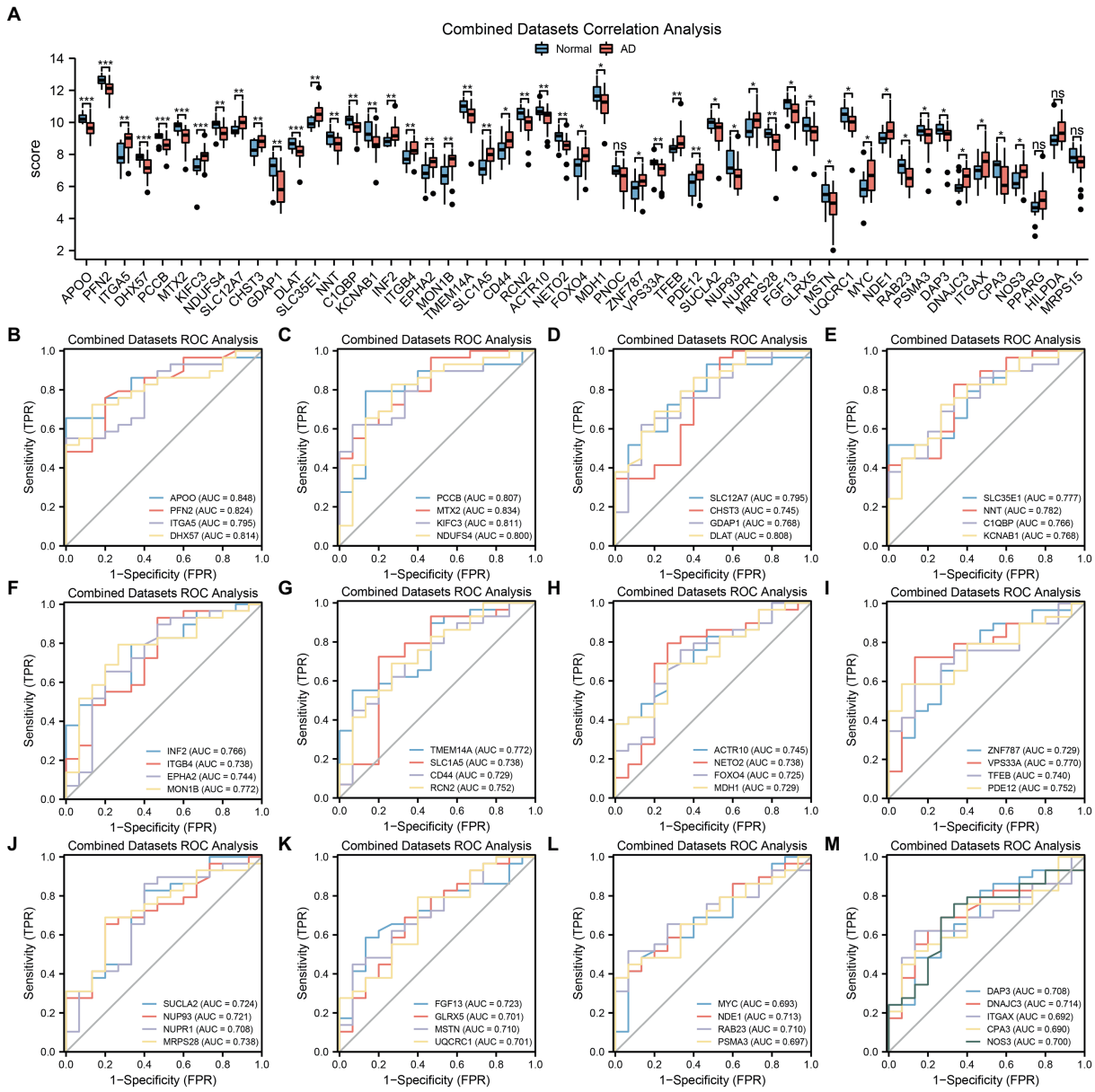

FIGURE 4
MRDEGs correlation and ROC curve analysis. **(A)** Comparison histogram of the results of differential expression analysis of MRDEGs in CDs. **(B–M)** ROC curves of 49 MRDEGs in CDs. ns, p value≥0.05, *p value<0.05, **p value<0.01, ***p value<0.001. AUC at 0.5–0.7 has a low accuracy, while AUC at 0.7–0.9 has a certain accuracy. MRDEG, mitophagy-related differentially expressed gene; ROC, receiver operating characteristic; CDs, combined datasets.

discussed in section 3.5 and AD were further explored. The six MRHGs were applied to GO and KEGG gene function enrichment analysis (Tables 1, 2). The six MRHGs were mainly enriched in the regulation of BPs such as cysteine-type endopeptidase activity involved in apoptosis and negative regulation of fibroblast proliferation, CCs such as secretory granule membrane, tricarboxylic acid cycle enzyme complex, and lamellipodium membrane, and MFs such as E-box binding, repressing TF binding, and activating TF binding. Simultaneously, the MRHGs were also enriched in the tricarboxylic acid cycle, thyroid cancer, and carbon metabolism pathways, among others. The results of these analyses were visualized as a histogram (Supplementary Figure S3A), and GO (Supplementary Figures S3B–D) and KEGG (Supplementary Figure S3E) network maps were drawn. A connecting line indicates a molecule and the annotation of the corresponding entry. The larger the node, the more molecules the entry contains. Finally, GO and KEGG enrichment analyses of the combined logFC were performed for the six MRDEGs (Supplementary Figures S3F,G). Based on the enrichment analysis, the z-score corresponding to each entry was calculated using the molecular logFC. The results of the GO analysis visualized by a circle diagram (Supplementary Figure S3F) and those of the KEGG analysis visualized by a chord diagram (Supplementary Figure S3G) showed that cysteine-type endopeptidase activity involved in apoptosis may be the most important positive regulatory pathway, whereas the tricarboxylic acid cycle enzyme complex pathway may be the most influential negative regulatory

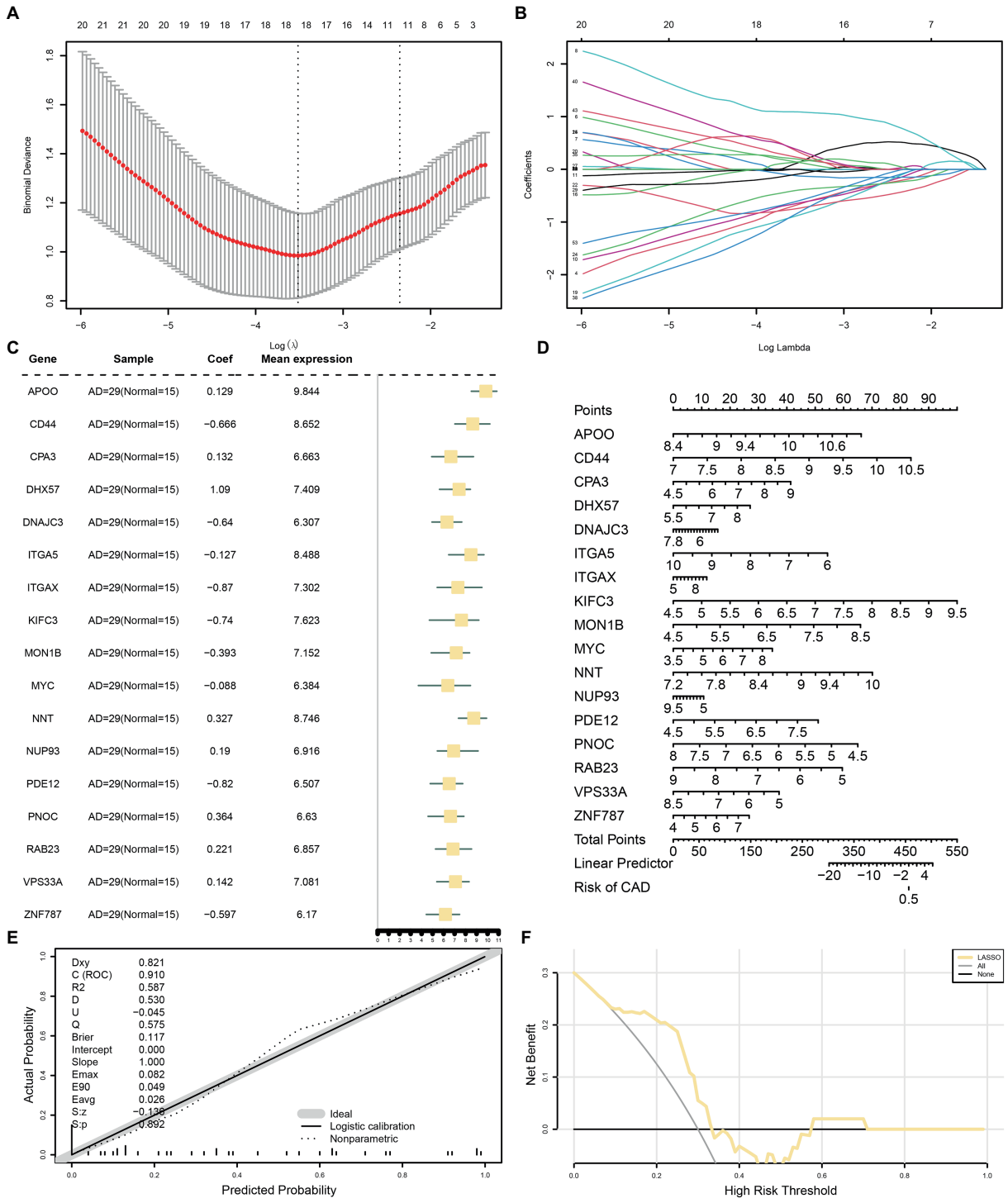

FIGURE 5
LASSO and cox regression analysis for CDs. **(A)** Diagnostic model of MRDEGs in AD datasets. **(B)** Variable trajectories of MRDEGs in the LASSO diagnostic model of AD. **(C)** Forest map of MRDEGs in the LASSO diagnostic model of AD. **(D)** Nomogram diagram of MRDEGs in Cox regression model. **(E)** Calibration curves of MRDEGs in Cox regression model. **(F)** DCA diagram of MRDEGs in Cox regression model. The ordinate is the net income, and the abscissa is the probability threshold or threshold probability. LASSO, least absolute shrinkage and selection operator; CDs, combined datasets; MRDEG, mitophagy-related differentially expressed gene; AD, Alzheimer's disease; DCA, decision curve analysis.

pathway. The connecting line between the left and right parts shows the molecules included in the KEGG pathway entry.

GSEA was used to determine the effects of the DEG expression levels in the AD datasets, specifically the relationships between DEG expression in the CDs and the BPs involved, the CCs affected, and the MFs exerted. As shown in Table 3, DEGs in the CDs significantly affected biologically related functions and signaling pathways (Figures 6A–E) such as IL-4 Signaling Pathway (Figure 6B), RUNX3 Regulates Notch Signaling

TABLE 1 Results of GO enrichment analysis in AD.

Ontology	ID	Description	Gene ratio	Bg ratio	*p* value	*p*. adjust	*q* value
BP	GO:0043281	Regulation of cysteine-type endopeptidase activity involved in apoptotic process	3/6	215/18670	2.94e-05	0.004	0.002
BP	GO:0048147	Negative regulation of fibroblast proliferation	2/6	30/18670	3.73e-05	0.004	0.002
BP	GO:2000116	Regulation of cysteine-type endopeptidase activity	3/6	239/18670	4.03e-05	0.004	0.002
BP	GO:0006099	Tricarboxylic acid cycle	2/6	34/18670	4.81e-05	0.004	0.002
BP	GO:0006101	Citrate metabolic process	2/6	35/18670	5.10e-05	0.004	0.002
CC	GO:0030667	Secretory granule membrane	2/6	298/19717	0.003	0.050	0.031
CC	GO:0045239	Tricarboxylic acid cycle enzyme complex	1/6	14/19717	0.004	0.050	0.031
CC	GO:0031258	Lamellipodium membrane	1/6	22/19717	0.007	0.050	0.031
CC	GO:0005759	Mitochondrial matrix	2/6	469/19717	0.008	0.050	0.031
CC	GO:0008305	Integrin complex	1/6	31/19717	0.009	0.050	0.031
MF	GO:0070888	E-box binding	2/6	50/17697	1.17e-04	0.006	0.002
MF	GO:0070491	Repressing transcription factor binding	2/6	71/17697	2.36e-04	0.006	0.002
MF	GO:0033613	Activating transcription factor binding	2/6	85/17697	3.38e-04	0.006	0.002
MF	GO:0031406	Carboxylic acid binding	2/6	193/17697	0.002	0.020	0.005
MF	GO:0043177	Organic acid binding	2/6	205/17697	0.002	0.020	0.005

GO, Gene Ontology; BP, Biological Process; CC, Cellular Component; MF, Molecular Function, AD, Alzheimer's Disease.

TABLE 2 Results of KEGG enrichment analysis in AD.

Ontology	ID	Description	Gene ratio	Bg ratio	*p* value	*p*. adjust	*q* value
KEGG	hsa00020	Citrate cycle (TCA cycle)	2/6	30/8076	1.98e-04	0.007	0.006
KEGG	hsa05216	Thyroid cancer	2/6	37/8076	3.03e-04	0.007	0.006
KEGG	hsa01200	Carbon metabolism	2/6	118/8076	0.003	0.050	0.039
KEGG	hsa05202	Transcriptional misregulation in cancer	2/6	192/8076	0.008	0.073	0.057
KEGG	hsa05169	Epstein–Barr virus infection	2/6	202/8076	0.009	0.073	0.057
KEGG	hsa05205	Proteoglycans in cancer	2/6	205/8076	0.009	0.073	0.057

KEGG, Kyoto Encyclopedia of Genes and Genomes; AD, Alzheimer's Disease.

(Figure 6C), IL-1 and Megakaryocytes in Obesity Pathway (Figure 6D), and Overview of Leukocyteintrinsic Hippo Pathway (Figure 6E).

3.7. Construction of AD subtypes

To explore the differences in MRG expression in the AD subgroup of the CDs, the R package *ConsensusClusterPlus* was used for consistent clustering analyses to identify different AD subtypes based on the six MRHGs. Two AD subtypes were finally identified: Cluster 1 containing 14 samples represented subtype A, whereas Cluster 2 containing 15 samples represented subtype B (Figures 7A,B). The PCA showed significant differences between these two subtypes (Figure 7C). A heatmap was drawn using the *pheatmap* package to visualize the differences in MRHG expression between the two AD subtypes (Figure 7D).

To further verify the expression differences of the six MRHGs in the AD datasets, the correlation between the expression levels of the six MRHGs in the CDs and the two AD subtypes and the results of the difference analysis were shown in a group comparison histogram (Figure 7E). The differential analysis results of the CDs showed that the two MRHGs were statistically significant ($p < 0.05$): the expression of MYC was statistically significant among different subtypes of AD ($p < 0.001$); the expression of CD44 was highly statistically significant between different subtypes of AD ($p < 0.01$). In addition, the expression levels of DLAT, ITGAX, PPARG and SUCLA2 were not statistically significant between AD subtypes ($p \geq 0.05$).

3.8. Analysis of immune cell infiltration between the two AD subtypes

To explore the differences in immune cell infiltration between the identified AD subtypes, CIBERSORT and ssGSEA algorithms were used to analyze for all samples the abundance of infiltrating immune cells in the two AD subtypes.

Based on the results of the CIBERSORT analysis, a histogram of the proportion of immune cells in the AD samples was drawn (Supplementary Figure S4A). Next, the correlations of immune cell infiltration abundance in leukocyte gene signature matrix (LM22) in

TABLE 3 Results of combined datasets GSEA in AD.

ID	Set size	Enrichment score	NES	*p* value	*p*. adjust	*q* values
REACTOME_INTERLEUKIN_10_SIGNALING	41	0.6888	2.5057	0.0021	0.0724	0.0621
PID_FRA_PATHWAY	34	0.6655	2.3017	0.0021	0.0724	0.0621
WP_TYROBP_CAUSAL_NETWORK	50	0.5603	2.1308	0.0021	0.0724	0.0621
PID_AMB2_NEUTROPHILS_PATHWAY	38	0.5922	2.1238	0.0021	0.0724	0.0621
WP_COMPLEMENT_AND_COAGULATION_CASCADES	54	0.5358	2.0661	0.0021	0.0724	0.0621
WP_IL4_SIGNALING_PATHWAY	53	0.5266	2.0246	0.0021	0.0724	0.0621
KEGG_CYTOKINE_CYTOKINE_RECEPTOR_INTERACTION	221	0.4197	2.0204	0.0021	0.0724	0.0621
PID_P73PATHWAY	74	0.4962	2.0181	0.0021	0.0724	0.0621
REACTOME_RUNX3_ MEDIATED_NOTCH_SIGNALING	12	0.7595	1.9835	0.0040	0.0905	0.0776
KEGG_HEMATOPOIETIC_CELL_LINEAGE	77	0.4812	1.9740	0.0021	0.0724	0.0621
REACTOME_INITIAL_TRIGGERING_OF_COMPLEMENT	20	0.6463	1.9598	0.0041	0.0905	0.0776
REACTOME_TRAF6_MEDIATED_IRF7_ACTIVATION	25	0.6132	1.9565	0.0041	0.0905	0.0776
WP_INTERACTIONS_BETWEEN_IMMUNE_CELLS_AND_MICRORNAS_IN_TUMOR_MICROENVIRONMENT	26	0.6009	1.9514	0.0020	0.0724	0.0621
REACTOME_INTERLEUKIN_4_AND_INTERLEUKIN_13_SIGNALING	103	0.4556	1.9487	0.0021	0.0724	0.0621
REACTOME_SYNTHESIS_OF_LEUKOTRIENES_LT_AND_EOXINS_EX_	16	0.6814	1.9459	0.0041	0.0905	0.0776
REACTOME_YAP1_AND_WWTR1_TAZ_STIMULATED_GENE_EXPRESSION	13	0.7304	1.9355	0.0062	0.1102	0.0945
REACTOME_NOTCH4_INTRACELLULAR_DOMAIN_REGULATES_TRANSCRIPTION	17	0.6647	1.9314	0.0042	0.0905	0.0776
WP_IL1_AND_MEGAKARYOCYTES_IN_OBESITY	24	0.6094	1.9314	0.0040	0.0905	0.0776
REACTOME_REGULATION_OF_GENE_EXPRESSION_IN_LATE_STAGE_BRANCHING_MORPHOGENESIS_ PANCREATIC_BUD_PRECURSOR_CELLS	13	0.7237	1.9179	0.0062	0.1102	0.0945
WP_OVERVIEW_OF_LEUKOCYTEINTRINSIC_HIPPO_PATHWAY_FUNCTIONS	27	0.5898	1.9178	0.0020	0.0724	0.0621

GSEA, Gene Set Enrichment Analysis; AD, Alzheimer's Disease; NES, Normalized Enrichment score.

10.3389/fnins.2023.1125281

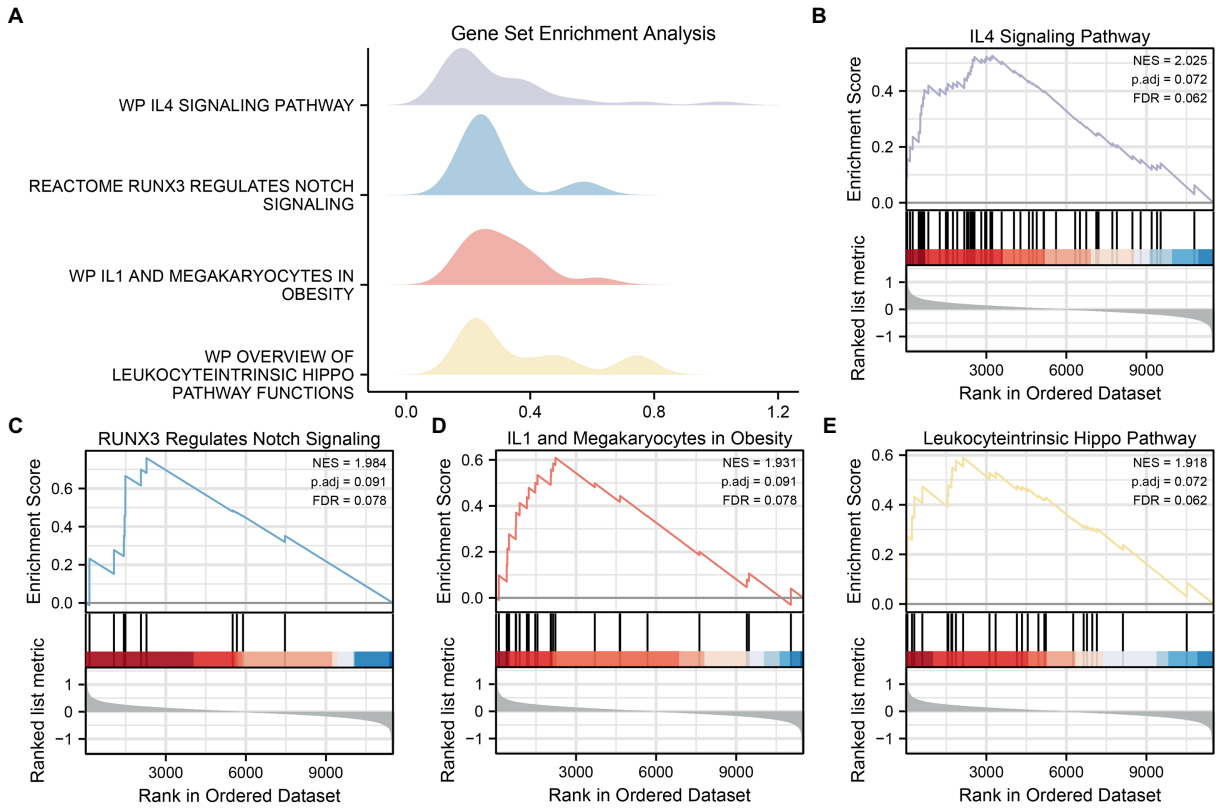

FIGURE 6
GSEA for CDs. **(A)** Mountain map of four biological functions in GSEA for CDs. **(B–E)** AD significantly affecting IL4 Signaling Pathway **(B)**, RUNX3 Regulations Notch Signaling **(C)**, IL1 and Megakaryocells in Obesity **(D)** and Overview of Leukocytric Hippo Pathway Functions **(E)** showed by GSEA. GSEA, gene set enrichment analysis; CDs, combined datasets; AD, Alzheimer's disease.

AD subtype A (Supplementary Figure S4B) and subtype B (Supplementary Figure S4C) were demonstrated by plotting correlation heatmaps. The results showed that the correlation between activated mast cells and regulatory T cells was the highest in subtype A (cor value = 0.90). By contrast, the correlation between M0 macrophages and neutrophils was the highest in subtype B (cor value = 0.84). In addition, the correlation between the abundance of LM22 immune cell infiltration and the expression of the six identified MRHGs in the samples of patients was analyzed by plotting the correlation heatmap of the two subtypes (Supplementary Figures S4D,E). The results showed that in subtype A, *PPARG* expression was significantly positively correlated with follicular helper T cell levels, and *DLAT* expression was significantly negatively correlated with the abundance of activated dendritic cells. In subtype B, *DLAT* expression was significantly negatively correlated with γδ T cell levels.

Similarly, immune cell infiltration was analyzed using ssGSEA. The correlation between the abundance of the 28 types of infiltrating immune cells in subtype A (Supplementary Figure S5A) and subtype B (Supplementary Figure S5B) of AD was demonstrated by plotting the correlation heatmap. The results showed that myeloid-derived suppressor cells (MDSCs) had the highest correlation with neutrophils, mast cells, and central memory CD8+ T cells (cor value = 0.89, 0.77, and 0.82, respectively) in subtype A. In subtype B, the correlation between MDSCs and activated dendritic cells was the highest (cor value = 0.78). Moreover, the correlation between the abundance of these 28 immune cell types and the expression of the six MRHGs in the samples of patients was analyzed by plotting the correlation heatmaps for the two AD subtypes (Supplementary Figures S5C,D). The results showed that in subtype A, *SUCLA2* expression was significantly positively correlated with the levels of effector memory CD4+ T cells and immature dendritic cells, whereas *DLAT* expression was significantly negatively correlated with the level of activated B cells. In subtype B, *SUCLA2* expression was significantly negatively correlated with activated B cell levels.

3.9. Dataset validation and ROC analysis

To further verify differences in MRHG expression in the AD dataset, the results of the differential expression analysis comparing the levels of the six identified MRHGs between the AD and control groups of the GSE63060 dataset were displayed in a group comparison histogram. The differential expression analysis results (Figure 8A) showed that three MRHGs significantly differed between the two groups. Among them, the expression of *ITGAX* and *SUCLA2* in the AD and control groups of the GSE63060 dataset was markedly significantly different ($p < 0.001$), and the expression of *DLAT* was significantly different ($p < 0.05$). The expression levels of the other MRHGs (*CD44*, *MYC*, and *PPARG*) were not significantly different between groups. The ROC curves suggested a low accuracy for *DLAT* (AUC = 0.596, Figure 8B), *ITGAX* (AUC = 0.678, Figure 8C), and *SUCLA2* (AUC = 0.655, Figure 8D) to distinguish AD from control samples in the dataset GSE63060.

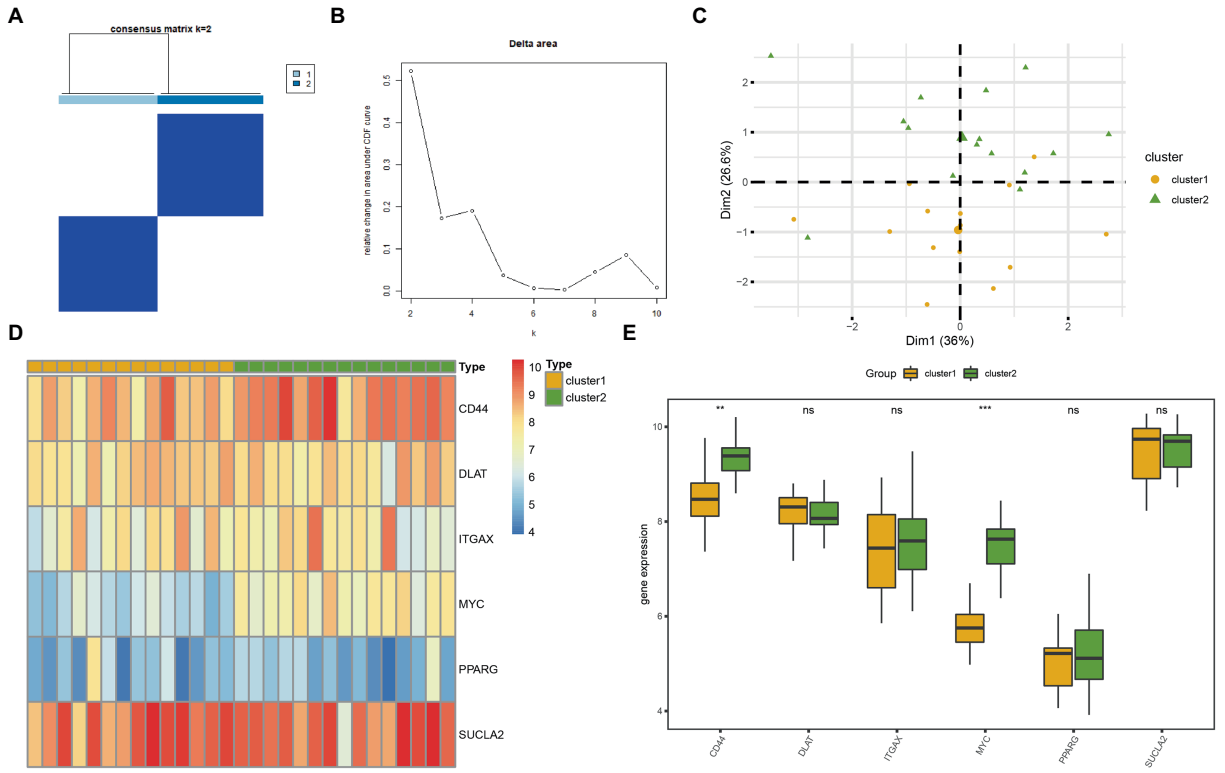

FIGURE 7
Consensus clustering analysis for hub genes. **(A)** Consistency clustering results of AD. **(B)** Delta diagram of different classifications by consistency clustering analysis. **(C)** PCA diagram of two AD subtypes. **(D)** Complex numerical heat map of MRHGs in two AD subtypes. **(E)** Histogram of grouping comparison of MRHGs in two AD subtypes. Orange is Cluster 1, and green is Cluster 2. $^{**}p$ value<0.01, $^{***}p$ value<0.001. AD, Alzheimer's disease; PCA, principal component analysis; MRHG, mitophagy-related hub gene.

4. Discussion

AD is one of the main causes of dementia and death in the elderly, seriously endangering human health, and its course is usually 6–10 years. With the intensification of the global aging society, its incidence rate and prevalence rate are increasing. In March 2019, the Alzheimer's Association of the United States released the impact of AD on public health in the United States. It is expected that by the middle of this century, the number of Americans aged 65 and over suffering from AD may increase to 13.8 million. However, up to now, there is a lack of ideal diagnostic indicators and effective prevention and treatment measures for AD. Therefore, it is of great social significance to strengthen the research on the pathogenesis of AD. Hence, it is crucial for this study to broaden its horizons to search for key molecules that may play a role in the pathogenesis of AD.

Mitophagy as a selective degradation process, is critical to keeping mitochondria healthy, producing ATP, and maintaining neuronal activity and survival by removing impaired mitochondria. MRGs have been previously reported as prognostic or diagnostic markers for various tumors, including pancreatic cancer (Zhuo et al., 2022), breast cancer (Zhao et al., 2022), and liver cancer (Chen et al., 2021; Xu et al., 2022), whereas only a limited number of studies have examined the usefulness of them as AD biomarkers. Pakpian et al. (2020) recently reported that alterations in mitochondrial dynamic-related genes in the peripheral blood may be useful for diagnosing AD. However, MRGs have not yet been evaluated for their diagnostic performance in AD and their role is worth further exploring.

In our study, we investigated the role of MRGs in the diagnosis of AD. Not only did we identify six MRHGs (*CD44*, *SUCLA2*, *DLAT*, *ITGAX*, *PPARG*, and *MYC*) as AD biomarkers, but we also used these MRHGs to create a diagnostic model. Moreover, a validation analysis conducted both internally and externally revealed that this model is effective in discriminating patients with AD from controls. Furthermore, we analyzed the relationships between MRHGs and immune cell infiltration in AD utilizing CIBERSORT and ssGSEA algorithms.

Some diagnostic biomarker signatures have been reported in previous studies. For example, Shigemizu et al. (2020) analyzed the blood samples of cognitively normal adults and patients with AD by RNA sequencing and detected DEGs. A model constructed by the proportion of neutrophils and the most important central genes (*EEF2* and *RPL7*) achieved an AUC of 0.878 in the validation cohort. Based on the results of its application to a prospective cohort, the model achieved an accuracy of 0.727, identifying blood-based biomarkers as early indicators of AD. Using the GEO database, researchers have identified in recent years numerous hub genes that are differentially expressed in AD and control brain samples and have further determined many possible diagnostic biomarkers of AD using the ROC prediction model. Tian et al. (2022) identified three hub genes (*MAFF*, *ADCYAP1*, and *ZFP36L1*; AUC = 0.850) and verified their expression in the AD brain (AUC = 0.935). Wu et al. (2021) found 10

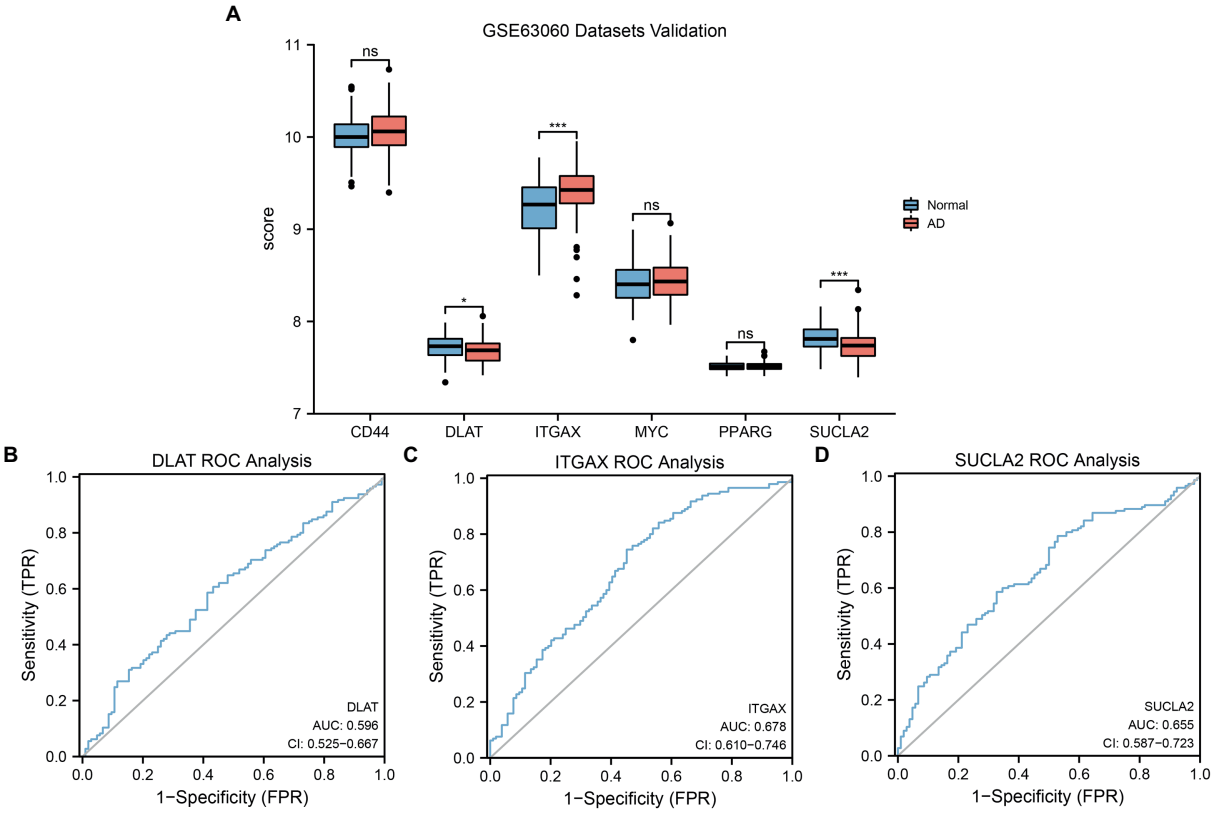

FIGURE 8
GSE63060 datasets validation and ROC analysis. **(A)** Comparison histogram of the results of differential expression analysis of MRHGs in the dataset GSE63060. **(B–D)** ROC curve of the MRHGs *DLAT* **(B)**, *ITGAX* **(C)** and *SUCLA2* **(D)** in dataset GSE63060. ns, *p* value≥0.05, **p* value<0.05, ****p* value<0.001. AUC at 0.5–0.7 has low accuracy. ROC, receiver operating characteristic; MRHG, mitophagy-related hub gene.

hub genes, namely *SERPINE1*, *ZBTB16*, *CD44*, *BCL6*, *HMOX1*, *SLC11A1*, *CEACAM8*, *ITGA5*, *SOCS3*, and *IL4R*, all of which have good diagnostic value (AUC > 0.75). Liu et al. (2021) identified seven genes, including *ABCA2*, *CREBRF*, *CD72*, *CETN2*, *KCNG1*, *NDUFA2*, and *RPL36AL* (AUCs were 0.845 and 0.839 in the test and validation sets, respectively), as hub genes and confirmed them by reverse transcription polymerase chain reaction. Our team (Zhao et al., 2022) found that *AGAP3* is an important hub gene (AUCs in the three studied datasets were 0.878, 0.727, and 0.635), which may be a diagnostic biomarker related to immunity in AD. Among the six MRHGs identified in the current study, the expression levels of *CD44*, *SUCLA2*, *DLAT*, and *PPARG* in the CDs showed a medium correlation with the study groups, whereas *ITGAX* and *MYC* showed a low correlation. Our findings suggest that a combination of a few biomarkers performs fairly well as a diagnostic tool.

Of the six identified MRGs, *CD44*, *ITGAX*, and *PPARG* are clearly correlated with AD according to previous reports (Butovsky et al., 2006; Moreno-Rodriguez et al., 2020; Bottero et al., 2021). The CD44 protein encoded by the *CD44* gene is a cell surface glycoprotein and a receptor for hyaluronic acid. CD44 is involved in cell–cell interaction, as well as cell adhesion and migration (Wang et al., 2018; Moreno-Rodriguez et al., 2020). It is described as a multifaceted molecule involved in several biological and pathological processes. Western blot analyses revealed that CD44 levels of the frontal cortex were increased in sporadic AD and associated with disease progression (Moreno-Rodriguez et al., 2020). This is consistent with our prediction results to some extent. The gene *ITGAX* encodes an integrin α X-chain protein. Integrins are heterodimers composed of α and β chains to integrate membrane proteins, forming αXβ2 integrins (Golinski et al., 2020). *ITGAX* is considered the main driving factor of atherosclerosis (Williams et al., 2020). Using single-cell transcriptome analysis of the brain of AD mice, a recent study on the transcriptional characteristics of plaque-associated microglia found a two-step transition from homeostasis to pathologically related phenotypes, with *Trem2*, to which *Itgax* is related, as the main phenotypic regulator (Mancuso et al., 2019). Ramesha et al. (2021) reported that the inoculation of T cell-based Gramer acetate vaccine against AD-induced dendritic microglia to express *Itgax* and found that the plaque formation and cognitive ability of APP/PS1 mice were reduced (Ramesha et al., 2021). These discoveries are consistent with our predicted changes in the expression of *ITGAX* in AD. The PPAR γ protein encoded by the gene *PPARG*, a member of the peroxisome proliferator-activated receptor subfamily, is a regulator of lipid metabolism and inflammatory response mediators; it may regulate AD switch genes as a TF. It is involved in the pathology of many disorders, such as obesity, atherosclerosis, and AD (Bottero et al., 2021). Activation of platelets and phospholipase D are regarded as its key signal components (Bottero et al., 2021). Like *APOE*, *PPARG* is an important risk gene. CG or GG, which are participant genotypes of rs1805192 in *PPARG*, confer the highest risk for AD (Wang et al., 2017). These research data

above support our prediction results. Overall, these findings may account for the distinct role of these genes in AD.

It has been suggested that the three genes *CD44*, *ITGAX*, and *PPARG* participate in AD pathogenesis mainly through neuroinflammation and immune pathways, making them promising therapeutic targets. Previous studies have shown that *CD44* may be highly involved in biological processes and pathways related to immune inflammatory response, apoptosis, and mitogen-activated protein kinase pathways in AD (Shim et al., 2022; Xu et al., 2022). A systematic review found that *CD44* is related to the complexity of reactive astrocytosis in AD (Viejo et al., 2022). As a microglia-related gene, *ITGAX* was found to be differentially expressed in AD and possibly involved in neuroinflammation, oxidative stress, and Aβ autophagy and transport (Li and de Muynck, 2021; Wu et al., 2021). The *PPARG* gene may increase the incidence of AD in patients with psoriasis by activating a positive feedback loop leading to excessive inflammation and metabolic disorder (Liu et al., 2022).

However, the relationship of *SUCLA2*, *DLAT*, and *MYC* expression with AD has not been previously reported. The *SUCLA2* gene encodes ATP-specific Succinyl-CoA synthetase (SCS) β subunits, which dimerize with SCS α subunits to form SCS-A, a heterodimeric mitochondrial matrix enzyme, which is an important component of the tricarboxylic acid cycle. By hydrolyzing ATP, SCS-A forms succinic acid and succinyl-CoA. Mutations of *SUCLA2* are one of the causes of myopathic mitochondrial DNA deletion syndrome (Viscomi and Zeviani, 2017). This is somewhat different from our predicted results, and further prospective studies are needed to determine the diagnostic accuracy of *SUCLA2* for AD. The gene *DLAT* encodes the E2 component of the multi-enzyme pyruvate dehydrogenase complex, which is a lipoylated core protein (Carrico et al., 2018). The protein, which is also an antigen of anti-mitochondrial antibody, accepts the acetyl group formed by oxidative decarboxylation of pyruvate and transfers it to coenzyme A. It has been reported that DLAT is the key mediator of cell survival in chronic myeloid leukemia after tyrosine kinase inhibitor-mediated BCR-ABL1 inhibition (Bencomo-Alvarez et al., 2019). It has also been found that SIRT4 can hydrolyze the lipoamide cofactors derived from DLAT, leading to a decrease in pyruvate dehydrogenase activity (Xie et al., 2020). These're not the same as our prediction, and the correlation between *DLAT* expression and AD needs to be thoroughly studied. The proto-oncogene *MYC* encodes a nuclear phosphoprotein that is crucial for the progression of the cell cycle, apoptosis, and transformation of cells (Casey et al., 2018). Its amplification is often observed in human tumors, and many drugs targeting the *MYC* pathway can be used for the treatment of tumors; the therapeutic effect might be related to the ability to restore the immune response (Casey et al., 2018). In addition, *MYC* expression is temporarily upregulated in spinal microglia as a TF after nerve injury to mediate early-phase proliferation of microglia, which is recognized as a hallmark of AD (Tan et al., 2022). The above indirectly reveals the possibility that *MYC* may participate in AD, but the diagnostic value of *MYC* in our research results needs to be further verified.

In this study, the differential expression analysis results of the CDs showed that the expression of *CD44* was highly statistically significant and that of *MYC* was statistically significant between different AD subtypes. In the validation dataset GSE63060, *ITGAX* and *SUCLA2* expression was markedly significantly different between the AD and control groups, whereas *DLAT* expression was significantly different between these two groups. The ROC curves of these three genes in the dataset GSE63060 showed that the expression levels of *DLAT*, *ITGAX*, and *SUCLA2* suggested a low correlation with study group. Thus, we will further explore the biological role of these genes in AD in the future.

In the last few decades, increasingly compelling evidence has emerged showing that AD is associated with immune system imbalance (Heneka et al., 2015; Lewcock et al., 2020). For example, compared with healthy controls, patients with AD have higher numbers of neutrophils, CD4+ T cells, and monocytes in the whole blood (Ferretti et al., 2016; Sommer et al., 2017; Unger et al., 2020). However, there remains a lack of clarity regarding the activation pattern of immune cells in AD. In the current study, an in-depth evaluation of AD immune cell infiltration was conducted using CIBERSORT and ssGSEA to further understand the role of immune responses in AD subtypes. The results of the CIBERSORT analysis showed that the correlation between activated mast cells and regulatory T cells was the highest in subtype A, whereas the correlation between M0 macrophages and neutrophils was the highest in subtype B. Similarly, the results of the ssGSEA showed that MDSCs had the highest correlation with neutrophils, mast cells, and central memory CD8+ T cells in subtype A, whereas the correlation between MDSCs and activated dendritic cells was the highest in subtype B.

In addition, our data mining results further confirmed that mitophagy and immunity may play key roles in the pathogenesis of AD. According to recent research, the cellular components of the immune system that may be modulated by mitophagy include natural killer cells, macrophages, dendritic cells, and T and B lymphocytes (Fang et al., 2019; Xu and Jia, 2021; Xie et al., 2022). Thus, we also analyzed the correlation between the six identified MRHGs (*CD44*, *SUCLA2*, *DLAT*, *ITGAX*, *PPARG*, and *MYC*) and infiltrating immune cells. Our results showed that *DLAT*, *PPARG*, and *SUCLA2* may be significantly correlated with distinct immune cell subsets indicative of different immune responses of AD subtypes. The correlation heatmap of the CIBERSORT analysis showed that *PPARG* expression was significantly positively correlated with follicular helper T cell levels in subtype A, whereas *DLAT* expression was significantly negatively correlated with the levels of activated dendritic cells in subtype A and with those of γδ T cells in subtype B. The correlation heatmap of the ssGSEA showed that *SUCLA2* expression was significantly positively correlated with the levels of effector memory CD4+ T cells and immature dendritic cells and significantly negatively correlated with the levels of activated B cells in subtype A, whereas *DLAT* expression was significantly negatively correlated with activated B cell levels in subtype B.

According to these findings, significant correlations exist between most MRGs and immune cells, which may indicate that mitophagy and immune responses interact in AD. This may further the understanding of the MRG-dependent immune status and microenvironment in AD. However, these assumptions require further studies to clarify the molecular mechanisms of the complex interaction between these genes and immune cells.

Clinically, AD can be divided into familial AD and sporadic AD according to genetic history and into early-onset AD and late-onset AD according to the age of onset. In this study, subtypes were only based on bioinformatics clusters according to the gene expression matrix. No other specific characteristics were taken into consideration, but correlations with clinical AD classifications may exist. In the future, we will aim to specify the degree of correlations and connections. Moreover, we will collect samples from AD patients in our hospital, record their clinical types, and determine whether

clinical classifications are related to subtypes established by bioinformatics approaches.

The biomarkers identified in this study have several advantages. First, it is the first study to comprehensively explain the relationship between biomarkers and AD from the perspective of mitophagy compared with classic genetic biomarkers such as *APP* and *PSEN1*. Second, by combining three datasets, the sample number was sufficient, and the interbatch differences in the datasets were eliminated, avoiding data bias (see Figure 2). Finally, the validation using an external dataset has further consolidated the conclusions of this study.

Our research has some limitations. First, our research was conducted using secondary mining and analysis of previously published datasets. Second, the external validation was only performed on one dataset, which was relatively small, although the development set had sufficient whole-blood samples from patients with AD and healthy controls. Third, although the AUC of the model showed acceptable discrimination, the performance of the model requires improvement. Therefore, it is vital to guarantee a large sample size for independent research to verify and improve the clinical practicability. Finally, the mechanisms and relationships of MRGs are included in gene signatures, which needs further study.

5. Conclusion

We identified six MRHGs that may represent peripheral blood-derived diagnostic biomarkers and may participate in the pathological mechanisms of AD. Furthermore, a diagnostic model of AD based on MRGs was constructed utilizing LASSO and logistic regression, and it exhibited good diagnostic performance in internal and external validation. Moreover, CIBERSORT and ssGSEA were used to analyze the immune cell infiltration in patients with AD, and the correlation analysis showed that mitophagy might modulate the immune response of patients with AD. These findings expand our understanding of the role of MRGs in AD. Our gene signatures may, therefore, provide an accurate and reliable prediction method for the diagnosis of patients with AD.

Data availability statement

The original contributions presented in the study are included in the article/Supplementary material, further inquiries can be directed to the corresponding author.

Author contributions

KZ: study design, data acquisition, analysis, completed drawing, and writing. YiW, DZ, HZ, and JL: data acquisition and analysis, and editing of the manuscript. YuW: data analysis, interpretation, and critical revision of the manuscript. All authors read and approved the final manuscript.

Funding

This work was supported by the research foundation of Affiliated People's Hospital of Jiangsu University (Y2020003-S) and Project 333 of Jiangsu Province (BRA2019231).

Acknowledgments

The authors would like to thank Editage (www.editage.cn) for English language editing.

Conflict of interest

The authors declare that the research was conducted in the absence of any commercial or financial relationships that could be construed as a potential conflict of interest.

Publisher's note

All claims expressed in this article are solely those of the authors and do not necessarily represent those of their affiliated organizations, or those of the publisher, the editors and the reviewers. Any product that may be evaluated in this article, or claim that may be made by its manufacturer, is not guaranteed or endorsed by the publisher.

Supplementary material

The Supplementary material for this article can be found online at: https://www.frontiersin.org/articles/10.3389/fnins.2023.1125281/full#supplementary-material

References

Bencomo-Alvarez, A. E., Rubio, A. J., Gonzalez, M. A., and Eiring, A. M. (2019). Energy metabolism and drug response in myeloid Leukaemic stem cells. *Br. J. Haematol.* 186, 524–537. doi: 10.1111/bjh.16074

Blalock, E. M., Geddes, J. W., Chen, K. C., Porter, N. M., Markesbery, W. R., and Landfield, P. W. (2004). Incipient Alzheimer's disease: microarray correlation analyses reveal major transcriptional and tumor suppressor responses. *Proc. Natl. Acad. Sci. U. S. A.* 101, 2173–2178. doi: 10.1073/pnas.0308512100

Bottero, V., Powers, D., Yalamanchi, A., Quinn, J. P., and Potashkin, J. A. (2021). Key disease mechanisms linked to Alzheimer's disease in the entorhinal cortex. *Int. J. Mol. Sci.* 22:3915. doi: 10.3390/ijms22083915

Butovsky, O., Koronyo-Hamaoui, M., Kunis, G., Ophir, E., Landa, G., Cohen, H., et al. (2006). Glatiramer acetate fights against Alzheimer's disease by inducing dendritic-like microglia expressing insulin-like growth factor 1. *Proc. Natl. Acad. Sci. U. S. A.* 103, 11784–11789. doi: 10.1073/pnas.0604681103

Carrico, C., Meyer, J. G., He, W., Gibson, B. W., and Verdin, E. (2018). The mitochondrial Acylome emerges: proteomics, regulation by Sirtuins, and metabolic and disease implications. *Cell Metab.* 27, 497–512. doi: 10.1016/j.cmet.2018.01.016

Casey, S. C., Baylot, V., and Felsher, D. W. (2018). The MYC oncogene is a global regulator of the immune response. *Blood* 131, 2007–2015. doi: 10.1182/blood-2017-11-742577

Chakravorty, A., Jetto, C. T., and Manjithaya, R. (2019). Dysfunctional mitochondria and Mitophagy as drivers of Alzheimer's disease pathogenesis. *Front. Aging Neurosci.* 11:311. doi: 10.3389/fnagi.2019.00311

Chen, H., Wang, J., Zeng, R., Luo, Y., Guo, K., Wu, H., et al. (2021). Development and validation of a novel Mitophagy-related gene prognostic signature for hepatocellular carcinoma based on Immunoscore classification of tumor. *J. Oncol.* 2021, 5070099–5070016. doi: 10.1155/2021/5070099

Chin, C. H., Chen, S. H., Wu, H. H., Ho, C. W., Ko, M. T., and Lin, C. Y. (2014). Cytohubba: identifying hub objects and sub-networks from complex Interactome. *BMC Syst. Biol.* 8:s11. doi: 10.1186/1752-0509-8-s4-s11

Congdon, E. E., and Sigurdsson, E. M. (2018). Tau-targeting therapies for Alzheimer disease. *Nat. Rev. Neurol.* 14, 399–415. doi: 10.1038/s41582-018-0013-z

Corder, E. H., Saunders, A. M., Strittmatter, W. J., Schmechel, D. E., Gaskell, P. C., Small, G. W., et al. (1993). Gene dose of apolipoprotein E type 4 allele and the risk of Alzheimer's disease in late onset families. *Science* 261, 921–923. doi: 10.1126/science.8346443

Coscia, F., Lengyel, E., Duraiswamy, J., Ashcroft, B., Bassani-Sternberg, M., Wierer, M., et al. (2018). Multi-level proteomics identifies Ct45 as a Chemosensitivity mediator and immunotherapy target in ovarian Cancer. *Cells* 175, 159–70.e16. doi: 10.1016/j.cell.2018.08.065

Davis, S., and Meltzer, P. S. (2007). Geoquery: a bridge between the gene expression omnibus (geo) and Bioconductor. *Bioinformatics* 23, 1846–1847. doi: 10.1093/bioinformatics/btm254

Dumitrescu, L., Mahoney, E. R., Mukherjee, S., Lee, M. L., Bush, W. S., Engelman, C. D., et al. (2020). Genetic variants and functional pathways associated with resilience to Alzheimer's disease. *Brain* 143, 2561–2575. doi: 10.1093/brain/awaa209

Efthymiou, A. G., and Goate, A. M. (2017). Late onset Alzheimer's disease genetics implicates microglial pathways in disease risk. *Mol. Neurodegener.* 12:43. doi: 10.1186/s13024-017-0184-x

Elias-Sonnenschein, L. S., Helisalmi, S., Natunen, T., Hall, A., Paajanen, T., Herukka, S.-K., et al. (2013). Genetic Loci associated with Alzheimer's disease and cerebrospinal fluid biomarkers in a Finnish case-control cohort. *PLoS One* 8:e59676. doi: 10.1371/journal.pone.0059676

Engebretsen, S., and Bohlin, J. (2019). Statistical predictions with glmnet. *Clin. Epigenet.* 11:123. doi: 10.1186/s13148-019-0730-1

Fang, E. F. (2019). Mitophagy and Nad(+) inhibit Alzheimer disease. *Autophagy* 15, 1112–1114. doi: 10.1080/15548627.2019.1596497

Fang, E. F., Hou, Y., Palikaras, K., Adriaanse, B. A., Kerr, J. S., Yang, B., et al. (2019). Mitophagy inhibits amyloid-B and tau pathology and reverses cognitive deficits in models of Alzheimer's disease. *Nat. Neurosci.* 22, 401–412. doi: 10.1038/s41593-018-0332-9

Ferretti, M. T., Merlini, M., Späni, C., Gericke, C., Schweizer, N., Enzmann, G., et al. (2016). T-cell brain infiltration and immature antigen-presenting cells in transgenic models of Alzheimer's disease-like cerebral amyloidosis. *Brain Behav. Immun.* 54, 211–225. doi: 10.1016/j.bbi.2016.02.009

Golinski, M. L., Demeules, M., Derambure, C., Riou, G., Maho-Vaillant, M., Boyer, O., et al. (2020). Cd11c(+) B cells are mainly memory cells, precursors of antibody secreting cells in healthy donors. *Front. Immunol.* 11:32. doi: 10.3389/fimmu.2020.00032

Grimm, A., and Eckert, A. (2017). Brain aging and neurodegeneration: from a mitochondrial point of view. *J. Neurochem.* 143, 418–431. doi: 10.1111/jnc.14037

Heckmann, B. L., Teubner, B. J. W., Boada-Romero, E., Tummers, B., Guy, C., Fitzgerald, P., et al. (2020). Noncanonical function of an autophagy protein prevents spontaneous Alzheimer's disease. *Sci. Adv.* 6:eabb9036. doi: 10.1126/sciadv.abb9036

Heneka, M. T., Carson, M. J., El Khoury, J., Landreth, G. E., Brosseron, F., Feinstein, D. L., et al. (2015). Neuroinflammation in Alzheimer's disease. *Lancet Neurol.* 14, 388–405. doi: 10.1016/s1474-4422(15)70016-5

Jung, H., Lee, S. Y., Lim, S., Choi, H. R., Choi, Y., Kim, M., et al. (2022). Anti-inflammatory clearance of amyloid-B by a chimeric Gas6 fusion protein. *Nat. Med.* 28, 1802–1812. doi: 10.1038/s41591-022-01926-9

Kanehisa, M., and Goto, S. (2000). Kegg: Kyoto encyclopedia of genes and genomes. *Nucleic Acids Res.* 28, 27–30. doi: 10.1093/nar/28.1.27

Kant, S., Stopa, E. G., Johanson, C. E., Baird, A., and Silverberg, G. D. (2018). Choroid plexus genes for Csf production and brain homeostasis are altered in Alzheimer's disease. *Fluids Barriers CNS* 15:34. doi: 10.1186/s12987-018-0120-7

Karch, C. M., and Goate, A. M. (2015). Alzheimer's disease risk genes and mechanisms of disease pathogenesis. *Biol. Psychiatry* 77, 43–51. doi: 10.1016/j.biopsych.2014.05.006

Kerr, J. S., Adriaanse, B. A., Greig, N. H., Mattson, M. P., Cader, M. Z., Bohr, V. A., et al. (2017). Mitophagy and Alzheimer's disease: cellular and molecular mechanisms. *Trends Neurosci.* 40, 151–166. doi: 10.1016/j.tins.2017.01.002

Leek, J. T., Johnson, W. E., Parker, H. S., Jaffe, A. E., and Storey, J. D. (2012). The Sva package for removing batch effects and other unwanted variation in high-throughput experiments. *Bioinformatics* 28, 882–883. doi: 10.1093/bioinformatics/bts034

Lemere, C. A. (2013). Immunotherapy for Alzheimer's disease: hoops and hurdles. *Mol. Neurodegener.* 8:36. doi: 10.1186/1750-1326-8-36

Lewcock, J. W., Schlepckow, K., Di Paolo, G., Tahirovic, S., Monroe, K. M., and Haass, C. (2020). Emerging microglia biology defines novel therapeutic approaches for Alzheimer's disease. *Neuron* 108, 801–821. doi: 10.1016/j.neuron.2020.09.029

Li, Q. S., and de Muynck, L. (2021). Differentially expressed genes in Alzheimer's disease highlighting the roles of microglia genes including OLR1 and astrocyte gene CDK2AP1. *Brain Behavior Immunity Health* 13:100227. doi: 10.1016/j.bbih.2021.100227

Li, J. H., Liu, S., Zhou, H., Qu, L. H., and Yang, J. H. (2014). Starbase V2.0: decoding Mirna-Cerna, Mirna-Ncrna and protein-Rna interaction networks from large-scale clip-Seq data. *Nucleic Acids Res.* 42, D92–D97. doi: 10.1093/nar/gkt1248

Liang, F., Zhang, Y., Hong, W., Dong, Y., Xie, Z., and Quan, Q. (2016). Direct tracking of amyloid and Tu dynamics in neuroblastoma cells using Nanoplasmonic Fiber tip probes. *Nano Lett.* 16, 3989–3994. doi: 10.1021/acs.nanolett.6b00320

Liberzon, A., Subramanian, A., Pinchback, R., Thorvaldsdóttir, H., Tamayo, P., and Mesirov, J. P. (2011). Molecular signatures database (Msigdb) 3.0. *Bioinformatics* 27, 1739–1740. doi: 10.1093/bioinformatics/btr260

Liu, P., Li, H., Liao, C., Tang, Y., Li, M., Wang, Z., et al. (2022). Identification of key genes and biological pathways in Chinese lung Cancer population using bioinformatics analysis. *PeerJ* 10:e12731. doi: 10.7717/peerj.12731

Liu, Z., Li, H., and Pan, S. (2021). Discovery and validation of key biomarkers based on immune infiltrates in Alzheimer's disease. *Front. Genet.* 12:658323. doi: 10.3389/fgene.2021.658323

Liu, S., Yuan, X., Su, H., Liu, F., Zhuang, Z., and Chen, Y. (2022). ZNF384: a potential therapeutic target for psoriasis and Alzheimer's disease through inflammation and metabolism. *Front. Immunol.* 13:892368. doi: 10.3389/fimmu.2022.892368

Lock, E. F., and Dunson, D. B. (2013). Bayesian consensus clustering. *Bioinformatics* 29, 2610–2616. doi: 10.1093/bioinformatics/btt425

Love, M. I., Huber, W., and Anders, S. (2014). Moderated estimation of fold change and dispersion for RNA-seq data with DESeq2. *Genome Biol.* 15:550. doi: 10.1186/s13059-014-0550-8

Mancuso, R., Fryatt, G., Cleal, M., Obst, J., Pipi, E., Monzón-Sandoval, J., et al. (2019). Csf1r inhibitor Jnj-40346527 attenuates microglial proliferation and neurodegeneration in P301s mice. *Brain* 142, 3243–3264. doi: 10.1093/brain/awz241

Mary, A., Eysert, F., Checler, F., and Chami, M. (2023). Mitophagy in Alzheimer's disease: molecular defects and therapeutic approaches. *Mol. Psychiatry* 28, 202–216. doi: 10.1038/s41380-022-01631-6

Mi, H., Muruganujan, A., Ebert, D., Huang, X., and Thomas, P. D. (2019). Panther version 14: more genomes, a new panther Go-slim and improvements in enrichment analysis tools. *Nucleic Acids Res.* 47, D419–D426. doi: 10.1093/nar/gky1038

Moreno-Rodriguez, M., Perez, S. E., Nadeem, M., Malek-Ahmadi, M., and Mufson, E. J. (2020). Frontal cortex Chitinase and Pentraxin neuroinflammatory alterations during the progression of Alzheimer's disease. *J. Neuroinflammation* 17:58. doi: 10.1186/s12974-020-1723-x

Morton, H., Kshirsagar, S., Orlov, E., Bunquin, L. E., Sawant, N., Boleng, L., et al. (2021). Defective Mitophagy and synaptic degeneration in Alzheimer's disease: focus on aging, mitochondria and synapse. *Free Radic. Biol. Med.* 172, 652–667. doi: 10.1016/j.freeradbiomed.2021.07.013

Newman, A. M., Liu, C. L., Green, M. R., Gentles, A. J., Feng, W., Xu, Y., et al. (2015). Robust enumeration of cell subsets from tissue expression profiles. *Nat. Methods* 12, 453–457. doi: 10.1038/nmeth.3337

Pakpian, N., Phopin, K., Kitidee, K., Govitrapong, P., and Wongchitrat, P. (2020). Alterations in mitochondrial dynamic-related genes in the peripheral blood of Alzheimer's disease patients. *Curr. Alzheimer Res.* 17, 616–625. doi: 10.2174/1567205017666201006162538

Park, S. H., Goo, J. M., and Jo, C. H. (2004). Receiver operating characteristic (roc) curve: practical review for radiologists. *Korean J. Radiol.* 5, 11–18. doi: 10.3348/kjr.2004.5.1.11

Poirier, J., Davignon, J., Bouthillier, D., Kogan, S., Bertrand, P., and Gauthier, S. (1993). Apolipoprotein E polymorphism and Alzheimer's disease. *Lancet* 342, 697–699. doi: 10.1016/0140-6736(93)91705-q

Pradeepkiran, J. A., Hindle, A., Kshirsagar, S., and Reddy, P. H. (2022). Are Mitophagy enhancers therapeutic targets for Alzheimer's disease? *Biomed. Pharmacother.* 149:112918. doi: 10.1016/j.biopha.2022.112918

Pradeepkiran, J. A., and Reddy, P. H. (2020). Defective Mitophagy in Alzheimer's disease. *Ageing Res. Rev.* 64:101191. doi: 10.1016/j.arr.2020.101191

Rai, S. N., Singh, C., Singh, A., Singh, M. P., and Singh, B. K. (2020). Mitochondrial dysfunction: a potential therapeutic target to treat Alzheimer's disease. *Mol. Neurobiol.* 57, 3075–3088. doi: 10.1007/s12035-020-01945-y

Ramesha, S., Rayaprolu, S., Bowen, C. A., Giver, C. R., Bitarafan, S., Nguyen, H. M., et al. (2021). Unique molecular characteristics and microglial origin of Kv1.3 channel-positive brain myeloid cells in Alzheimer's disease. *Proc. Natl. Acad. Sci. U. S. A.* 118:e2013545118. doi: 10.1073/pnas.2013545118

Reitz, C., Jun, G., Naj, A., Rajbhandary, R., Vardarajan, B. N., Wang, L. S., et al. (2013). Variants in the Atp-Binding Cassette Transporter (Abca7), Apolipoprotein E ϵ4,and the Risk of Late-Onset Alzheimer Disease in African Americans. *JAMA* 309, 1483–1492. doi: 10.1001/jama.2013.2973

Roussos, P., Katsel, P., Fam, P., Tan, W., Purohit, D. P., and Haroutunian, V. (2015). The triggering receptor expressed on myeloid cells 2 (Trem2) is associated with enhanced inflammation, neuropathological lesions and increased risk for Alzheimer's dementia. *Alzheimers Dement.* 11, 1163–1170. doi: 10.1016/j.jalz.2014.10.013

Ryan, N. S., and Rossor, M. N. (2010). Correlating familial Alzheimer's disease gene mutations with clinical phenotype. *Biomark. Med* 4, 99–112. doi: 10.2217/bmm.09.92

Sevigny, J., Chiao, P., Bussière, T., Weinreb, P. H., Williams, L., Maier, M., et al. (2016). The antibody Aducanumab reduces Aβ plaques in Alzheimer's disease. *Nature* 537, 50–56. doi: 10.1038/nature19323

Shannon, P., Markiel, A., Ozier, O., Baliga, N. S., Wang, J. T., Ramage, D., et al. (2003). Cytoscape: a software environment for integrated models of biomolecular interaction networks. *Genome Res.* 13, 2498–2504. doi: 10.1101/gr.1239303

Sharma, B., Pal, D., Sharma, U., and Kumar, A. (2022). Mitophagy: an emergence of new player in Alzheimer's disease. *Front. Mol. Neurosci.* 15:921908. doi: 10.3389/fnmol.2022.921908

Shigemizu, D., Mori, T., Akiyama, S., Higaki, S., Watanabe, H., Sakurai, T., et al. (2020). Identification of potential blood biomarkers for early diagnosis of Alzheimer's disease through RNA sequencing analysis. *Alzheimers Res. Ther.* 12:87. doi: 10.1186/s13195-020-00654-x

Shim, Y. J., Shin, M. K., Jung, J., Koo, B., and Jang, W. (2022). An in-silico approach to studying a very rare neurodegenerative disease using a disease with higher prevalence with shared pathways and genes: cerebral Adrenoleukodystrophy and Alzheimer's disease. *Front. Mol. Neurosci.* 15:996698. doi: 10.3389/fnmol.2022.996698

Sommer, A., Winner, B., and Prots, I. (2017). The Trojan horse - Neuroinflammatory impact of T cells in neurodegenerative diseases. *Mol. Neurodegener.* 12:78. doi: 10.1186/s13024-017-0222-8

Sood, S., Gallagher, I. J., Lunnon, K., Rullman, E., Keohane, A., Crossland, H., et al. (2015). A novel multi-tissue Rna diagnostic of healthy ageing relates to cognitive health status. *Genome Biol.* 16:185. doi: 10.1186/s13059-015-0750-x

Stelzer, G., Rosen, N., Plaschkes, I., Zimmerman, S., Twik, M., Fishilevich, S., et al. (2016). The Genecards suite: from gene data mining to disease genome sequence analyses. *Curr. Protoc. Bioinformatics* 54, 1.30.1–1.30.33. doi: 10.1002/cpbi.5

Stopa, E. G., Tanis, K. Q., Miller, M. C., Nikonova, E. V., Podtelezhnikov, A. A., Finney, E. M., et al. (2018). Comparative transcriptomics of choroid plexus in Alzheimer's disease, frontotemporal dementia and Huntington's disease: implications for CSF homeostasis. *Fluids Barriers CNS* 15:18. doi: 10.1186/s12987-018-0102-9

Subramanian, A., Tamayo, P., Mootha, V. K., Mukherjee, S., Ebert, B. L., Gillette, M. A., et al. (2005). Gene set enrichment analysis: a knowledge-based approach for interpreting genome-wide expression profiles. *Proc. Natl. Acad. Sci. U. S. A.* 102, 15545–15550. doi: 10.1073/pnas.0506580102

Suh, J., Romano, D. M., Nitschke, L., Herrick, S. P., DiMarzio, B. A., Dzhala, V., et al. (2019). Loss of Ataxin-1 potentiates Alzheimer's pathogenesis by elevating cerebral Bace1 transcription. *Cells* 178, 1159–75.e17. doi: 10.1016/j.cell.2019.07.043

Szklarczyk, D., Gable, A. L., Lyon, D., Junge, A., Wyder, S., Huerta-Cepas, J., et al. (2019). String V11: protein-protein association networks with increased coverage, supporting functional discovery in genome-wide experimental datasets. *Nucleic Acids Res.* 47, D607–D613. oi: 10.1093/nar/gky1131. doi: 10.1093/nar/gky1131

Tan, W., Su, P. P., Leff, J., Gao, X., Chen, J., Guan, A. K., et al. (2022). Distinct phases of adult microglia proliferation: a MYC-mediated early phase and a Tnfaip3-mediated late phase. *Cell Discovery* 8:34. doi: 10.1038/s41421-022-00377-3

Tian, Y., Lu, Y., Cao, Y., Dang, C., Wang, N., Tian, K., et al. (2022). Identification of diagnostic signatures associated with immune infiltration in Alzheimer's disease by integrating Bioinformatic analysis and machine-learning strategies. *Front. Aging Neurosci.* 14:919614. doi: 10.3389/fnagi.2022.919614

Town, T., Laouar, Y., Pittenger, C., Mori, T., Szekely, C. A., Tan, J., et al. (2008). Blocking Tgf-Beta-Smad2/3 innate immune signaling mitigates Alzheimer-like pathology. *Nat. Med.* 14, 681–687. doi: 10.1038/nm1781

Ulrich, J. D., Ulland, T. K., Colonna, M., and Holtzman, D. M. (2017). Elucidating the role of Trem2 in Alzheimer's disease. *Neuron* 94, 237–248. doi: 10.1016/j.neuron.2017.02.042

Unger, M. S., Li, E., Scharnagl, L., Poupardin, R., Altendorfer, B., Mrowetz, H., et al. (2020). Cd8(+) T-cells infiltrate Alzheimer's disease brains and regulate neuronal- and synapse-related gene expression in app-Ps1 transgenic mice. *Brain Behav. Immun.* 89, 67–86. doi: 10.1016/j.bbi.2020.05.070

Van Calster, B., Wynants, L., Verbeek, J. F. M., Verbakel, J. Y., Christodoulou, E., Vickers, A. J., et al. (2018). Reporting and interpreting decision curve analysis: a guide for investigators. *Eur. Urol.* 74, 796–804. doi: 10.1016/j.eururo.2018.08.038

Viejo, L., Noori, A., Merrill, E., Das, S., Hyman, B. T., and Serrano-Pozo, A. (2022). Systematic review of human post-mortem Immunohistochemical studies and bioinformatics analyses unveil the complexity of astrocyte reaction in Alzheimer's disease. *Neuropathol. Appl. Neurobiol.* 48:e12753. doi: 10.1111/nan.12753

Villegas-Llerena, C., Phillips, A., Garcia-Reitboeck, P., Hardy, J., and Pocock, J. M. (2016). Microglial genes regulating Neuroinflammation in the progression of Alzheimer's disease. *Curr. Opin. Neurobiol.* 36, 74–81. doi: 10.1016/j.conb.2015.10.004

Viscomi, C., and Zeviani, M. (2017). Mtdna-maintenance defects: syndromes and genes. *J. Inherit. Metab. Dis.* 40, 587–599. doi: 10.1007/s10545-017-0027-5

Wang, H., Fu, J., Xu, X., Yang, Z., and Zhang, T. (2021). Rapamycin activates Mitophagy and alleviates cognitive and synaptic plasticity deficits in a mouse model of Alzheimer's disease. *J. Gerontol. A Biol. Sci. Med. Sci.* 76, 1707–1713. doi: 10.1093/gerona/glab142

Wang, S., Guan, L., Luo, D., Liu, J., Lin, H., Li, X., et al. (2017). Gene- gene interaction between PPARG and APOE gene on late-onset Alzheimer's disease: a case- control study in Chinese Han population. *J. Nutr. Health Aging* 21, 397–403. doi: 10.1007/s12603-016-0794-y

Wang, Z., Zhao, K., Hackert, T., and Zöller, M. (2018). Cd44/Cd44v6 a reliable companion in Cancer-initiating cell maintenance and tumor progression. *Front. Cell Dev. Biol.* 6:97. doi: 10.3389/fcell.2018.00097

Wilkerson, M. D., and Hayes, D. N. (2010). Consensusclusterplus: a class discovery tool with confidence assessments and item tracking. *Bioinformatics* 26, 1572–1573. doi: 10.1093/bioinformatics/btq170

Williams, R. (2011). Philip Scheltens: friendly face of Alzheimer's disease research. *Lancet Neurol.* 10:208. doi: 10.1016/S1474-4422(11)70032-1

Williams, J. W., Zaitsev, K., Kim, K. W., Ivanov, S., Saunders, B. T., Schrank, P. R., et al. (2020). Limited proliferation capacity of aortic intima resident macrophages requires monocyte recruitment for atherosclerotic plaque progression. *Nat. Immunol.* 21, 1194–1204. doi: 10.1038/s41590-020-0768-4

Wu, Y., Liang, S., Zhu, H., and Zhu, Y. (2021). Analysis of immune-related key genes in Alzheimer's disease. *Bioengineered* 12, 9610–9624. doi: 10.1080/21655979.2021.1999553

Wu, L., Wang, W., Tian, S., Zheng, H., Liu, P., and Wu, W. (2021). Identification of hub genes in patients with Alzheimer disease and obstructive sleep apnea syndrome using integrated bioinformatics analysis. *Int. J. General Med.* 14, 9491–9502. doi: 10.2147/IJGM.S341078

Wu, J., Zhang, H., Li, L., Hu, M., Chen, L., Xu, B., et al. (2020). A nomogram for predicting overall survival in patients with low-grade endometrial stromal sarcoma: a population-based analysis. *Cancer Commun.* 40, 301–312. doi: 10.1002/cac2.12067

Xie, N., Zhang, L., Gao, W., Huang, C., Huber, P. E., Zhou, X., et al. (2020). Nad(+) metabolism: pathophysiologic mechanisms and therapeutic potential. *Signal Transduct. Target. Ther.* 5:227. doi: 10.1038/s41392-020-00311-7

Xie, C., Zhuang, X. X., Niu, Z., Ai, R., Lautrup, S., Zheng, S., et al. (2022). Amelioration of Alzheimer's disease pathology by Mitophagy inducers identified via machine learning and a cross-species workflow. *Nat. Biomed. Eng.* 6, 76–93. doi: 10.1038/s41551-021-00819-5

Xiong, M., Jiang, H., Serrano, J. R., Gonzales, E. R., Wang, C., Gratuze, M., et al. (2021). Apoe immunotherapy reduces cerebral amyloid Angiopathy and amyloid plaques while improving cerebrovascular function. *Sci. Transl. Med.* 13:abd7522. doi: 10.1126/scitranslmed.abd7522

Xu, H., and Jia, J. (2021). Single-cell Rna sequencing of peripheral blood reveals immune cell signatures in Alzheimer's disease. *Front. Immunol.* 12:645666. doi: 10.3389/fimmu.2021.645666

Xu, W., Zhao, D., Huang, X., Zhang, M., Yin, M., Liu, L., et al. (2022). The prognostic value and clinical significance of Mitophagy-related genes in hepatocellular carcinoma. *Front. Genet.* 13:917584. doi: 10.3389/fgene.2022.917584

Xu, J., Zhou, H., and Xiang, G. (2022). Identification of key biomarkers and pathways for maintaining cognitively Normal brain aging based on integrated bioinformatics analysis. *Front. Aging Neurosci.* 14:833402. doi: 10.3389/fnagi.2022.833402

Yang, X., Li, Y., Lv, R., Qian, H., Chen, X., and Yang, C. F. (2019). Study on the multitarget mechanism and key active ingredients of Herba Siegesbeckiae and volatile oil against rheumatoid arthritis based on network pharmacology. *Evid. Based Complement. Alternat. Med.* 2019, 8957245–8957215. doi: 10.1155/2019/8957245

Yu, G., Wang, L. G., Han, Y., and He, Q. Y. (2012). Clusterprofiler: an R package for comparing biological themes among gene clusters. *Omics* 16, 284–287. doi: 10.1089/omi.2011.0118

Zhang, H., Meltzer, P., and Davis, S. (2013). Rcircos: an R package for Circos 2d track plots. *BMC Bioinformatics* 14:244. doi: 10.1186/1471-2105-14-244

Zhao, Y., Zhang, Y., Dai, C., Hong, K., and Guo, Y. (2022). A signature constructed with Mitophagy-related genes to predict the prognosis and therapy response for breast Cancer. *Aging* 14, 6169–6186. doi: 10.18632/aging.204209

Zhao, K., Zhang, H., Wu, Y., Liu, J., Li, X., and Lin, J. (2022). Integrated analysis and identification of hub genes as novel biomarkers for Alzheimer's disease. *Front. Aging Neurosci.* 14:901972. doi: 10.3389/fnagi.2022.901972

Zhou, K. R., Liu, S., Sun, W. J., Zheng, L. L., Zhou, H., Yang, J. H., et al. (2017). Chipbase V2.0: decoding transcriptional regulatory networks of non-coding Rnas and protein-coding genes from Chip-Seq data. *Nucleic Acids Res.* 45, D43–D50. doi: 10.1093/nar/gkw965

Zhuo, Z., Lin, H., Liang, J., Ma, P., Li, J., Huang, L., et al. (2022). Mitophagy-related gene signature for prediction prognosis, immune scenery, mutation, and chemotherapy response in pancreatic Cancer. *Front. Cell Dev. Biol.* 9:802528. doi: 10.3389/fcell.2021.802528

Frontiers in
Aging Neuroscience

Explores the mechanisms of central nervous system aging and age-related neural disease

The third most-cited journal in the field of geriatrics and gerontology, with a focus on understanding the mechanistic processes associated with central nervous system aging.

Discover the latest Research Topics

See more →

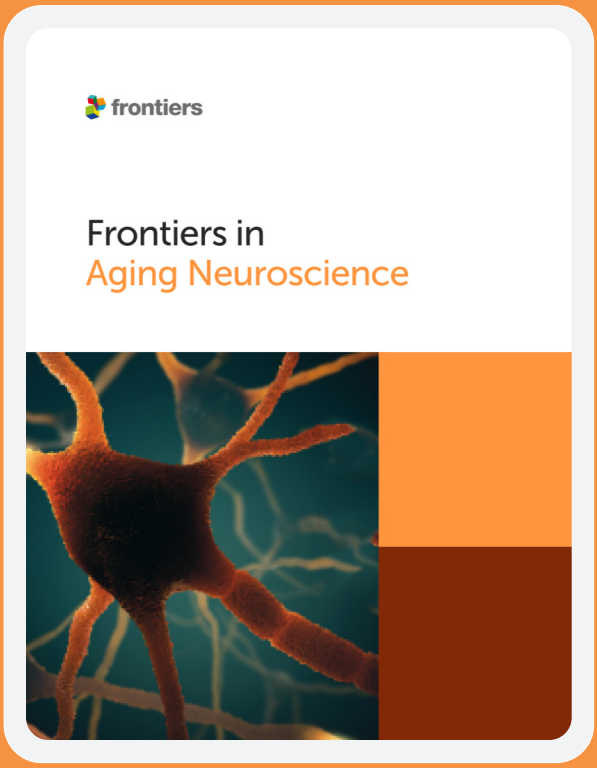

Frontiers

Avenue du Tribunal-Fédéral 34
1005 Lausanne, Switzerland
frontiersin.org

Contact us

+41 (0)21 510 17 00
frontiersin.org/about/contact